La borsa di dottorato è stata cofinanziata con risorse del
Programma Operativo Nazionale Ricerca e Innovazione 2014-202 (CCI 2014IT16M2OP005)
Fondo Sociale Europeo, Azione I.1 "Dottorati Innovativi con caratterizzazione Industriale"





**UNIVERSITA' DELLA CALABRIA**

Dipartimento di CHIMICA E TECNOLOGIE CHIMICHE

**Dottorato di Ricerca in**

SCIENZE DELLA VITA

*Con il contributo di (Ente finanziatore)*

**MIUR**

---

**CICLO**

**XXXIII**

**TITOLO TESI**

# PRODUCTION OF NEW BITUMINOUS MATERIALS (ECOBINDERS) BY RECYCLING WASTE OIL AND RUBBER FROM END-OF-LIFE TIRES ("CRUMB RUBBER")

**Settore Scientifico Disciplinare CHIM02**

**Coordinatore:** Ch.ma Prof. ssa MARIA CARMELA CERRA

Firma _____ Firma oscurata in base alle linee guida del Garante della privacy

**Supervisore/Tutor**: Ch.mo Prof. CESARE OLIVIERO ROSSI

Firma _ Firma oscurata in base alle linee guida del Garante della privacy

**Dottorand**o: Dott. MICHELE PORTO

Firma Firma oscurata in base alle linee guida del Garante della privacy

# Contents

# Abstract

## Chapter 1



**Reference to Chapter 1**

## Chapter 2

**Abstract**

Nowadays the main problems faced by applied research and industry are towards environmental issues such as global warming, carbon footprint, reduction of greenhouse gas emission amongst others. The Kyoto Treaty was developed as a result in 1997 to setting the objective for European countries to develop policies and technologies in order to meet greenhouse gas reduction requirements. In this light, the asphalt industry accordingly implemented measures to facilitate eco-friendly operations. Examples of some of these measures include the introduction of the use of Warm Mix Asphalt (WMA) and Reclaimed Asphalt Pavement (RAP) which reduce production costs and reduce $CO_2$ emissions. Another initiative used to address environmental problems is resource conservation which has made the use, recovery and recycling of resources more practical and effective in not only reducing production costs but also in making a regenerative circular economy. An example of this initiative is an innovation called End of Waste (EoW) product through which waste is converted into a new product and it is proving very practical and effective in recent times. The End of Waste (EoW) criteria means recovery and treatment processes under which waste could be converted in a new potential product. In particular, according to the European normative the main requirements for a given waste - possibly treated by industrial processes - to satisfy the EoW qualification are the following:

a) the substance or object is intended to be used for specific purposes;
b) there is a market or demand for this substance or object;
c) the substance or object meets the technical requirements for the specific purposes and complies with the existing legislation and standards applicable to the products;
d) the use of the substance or object will not lead to overall negative impacts on the environment or human health (in accordance with the Substance of Very High Concern (SVHC) list)

From this perspective, the reuse of opportunely re-refined exhausted oils from automobile and industrial hydraulic applications - that have become unfit for the use for which they were originally intended - completely fulfil the circular economy goals. This PhD thesis deals with the conversion of End of Waste Product (EoW) in the form of Re-refined Engine Oil Bottom (REOB) obtained from exhausted oil regeneration processes – through the addition of recycled industrial waste materials - to high performing bituminous binder suitable for use in asphalt mix production. This can save the asphalt industry an even larger amount of resources if it is normalized to practice using this new potentially revolutionary binder together with Reclaimed Asphalt Pavement (RAP) which reduces the need for virgin aggregates in asphalt mix production. Indeed, in the present work asphalt concrete samples have been obtained by using 100 % Reclaimed Asphalt Pavement (RAP) aggregates. The asphalt concrete samples thus obtained underwent testing in order to study their behaviour with the goal to substitute virgin aggregates that are commonly employed in asphalt pavement. This would allow to reach the standards of most of the European countries where RAP is already used in the range of 70-90%, while up to now in Italy a maximum of 30% of RAP is used in the Hot Mix Asphalt (HMA) and Warm Mix Asphalt (WMA). The aged and more brittle bituminous binder that coats the aggregates limits the use of

RAP material as it stiffens the resulting asphalt mixtures making the pavements more brittle and sometimes more prone to cracking especially at low temperatures. To overcome this problem a rejuvenating agent could be used.

# Chapter 1

## 1. Bitumen generalities

### 1.1. Hystorical Overview

Scientists believes that the term bitumen originated in the ancient and sacred Sanskrit language of Hindus in India, in which jatu means ‘pitch’ and jatu-krit means ‘pitch creating’. These terms referred to the pitch produced by some resinous trees. The historians claimed that the Latin equivalent to be originally gwitu-men (‘pertaining to pitch’) and by others to be pixtu-men (‘bubbling pitch’), which was subsequently shortened to bitumen before passing via French into English. [1]

The use of bitumen by human being dates back 180,000 years ago in the El Kowm Basin in Syria, where it was used as a hafting material applied to stick flint implements to the handles of various tools. [2]. There are several references to bitumen even in the Bible where it is reported as the waterproofing of Noah's arch, of the Babel tower or of the cradle of Moses [1,3]. Medical uses were also reported, with bitumen acting as a remedy for various illnesses as a disinfectant or as an insecticide [2-4.]. Another historical application was for the embalming of mummies by the Egyptians [5]. The ancient uses of natural bitumens continued in those inhabited parts of the world where deposits were readily available. In many countries, none of the present major uses of bitumen were introduced until the end of the nineteenth century.

The use of natural bitumen in road construction was first attributed to Nabopolassar, King of Babylon (625–604 BC): a bitumen-containing mortar cemented both the foundation made of three or more courses of burnt bricks and the stone slabs put on top [3]. The use of natural bitumen in road construction started to decay in the 1910s with the advent of vacuum distillation which made it possible to obtain artificial bitumen from crude oil [6] and nowadays, paving grade bitumen is almost exclusively obtained as the vacuum residue of petroleum distillation.

### 1.2. Bitumen: definition and manufacture

Nowadays, the term bitumen is used to describe the refined product produced by removing the lighter fractions from crude oil during the refining process. Up to the beginning of 20$^{th}$ century bitumen was only recovered from natural sources until modern refining technologies became available for its production [7]. Because there is still a little bit confusion on the terms bitumen and asphalt, it is important to fix the terminology to distinguish them. The term asphalt is used in Europe to identify the mixture obtained from bitumen and aggregates and used for road paving, while in North America the term asphalt is used to identify the bitumen itself and the term asphalt concrete is used to identify the mixture with aggregates for paving. Moreover, no confusion should be made between bitumen and coal derived products such as coal tar or coal tar pitches, which show different physical characteristics respect to bitumen. Similarly, bitumen should not be confused with petroleum pitches which are often aromatic residues, produced by thermal cracking, coking or oxidation from selected petroleum fractions. The composition of petroleum pitches differs significantly from bitumen. Confusion should also be avoided between bitumen and natural or lake asphalt such as Trinidad Lake Asphalt, Gilsonite, rock asphalt

and Selenice [1], that are unrefined products and not produced by refining of crude oil. They often contain a high proportion of mineral matter (up to 37% by weight) and light components, leading to a higher loss of mass when heated. In this thesis the term bitumen is used following the European convention and asphalt indicates the mixture of bitumen and aggregates. In this respect, during past decades a lot of definitions have been proposed and sometimes scientifically incorrect [3,8]. In the current European specifications [9] bitumen is currently defined as: "*a virtually not volatile, adhesive, and waterproofing material derived from crude oil, or present in natural asphalt, which is completely or nearly completely soluble in toluene, and very viscous or nearly solid at ambient temperatures*".Nowadays roads paving involves the use of bitumen obtained from distillation process of crude oil (petroleum). This is a fossil fuel extracted from the ground that was made naturally from decaying plants and animals living millions of years ago [1]. Crude oil sources undergoing topping distillation process [10] (see Figure 1) has a strong influence on the bitumen characteristics [11].

Depending on the extraction sites, crude oils vary in colour, in viscosity - from water-like to almost solid - and chemical composition. From the point of view of the latter, crude oils are complex mixtures of many hydrocarbons composed by chains (linear and branched) and rings all differing in molecular weight and consequently in boiling range. For this reason, crude oils are such a useful starting point for so many different substances. Speaking of which, nowadays, crude oil is separated into various component some of which are further chemically or physically changed. Bitumen is one of the components produced from this process.

The first process in the refining of crude oil is fractional distillation or topping, which physically separates the crude oil into streams varying in boiling point. This is carried out in fractionating or distillation columns. Figure 1 outline a typical atmospheric and a vacuum distillation plant respectively for crude oil and the long residue obtained as sub product. A detailed description of the inside operation of the distillation column as well as the various operating procedures can be found in [12]

Crude oil's lightest fractions leave the top of the distillation column as vapour; heavier fractions are taken off the column as side-streams while the heaviest fractions - also known as long residue - remain as liquids and leave the base of the column. The long residue a is complex mixture of high molecular weight hydrocarbons, and generally requires further processing before it can be used as a feedstock for the manufacture of bitumen. To this respect, the long residue is further distilled in a vacuum distillation column at a temperature of between 350 and 425 °C and at 10–100 mmHg vacuum pressure – to avoid cracking or thermal decomposition - to produce gas oil, distillates fractions and a bottom residue known as short residue (Figure 1 lower panel). Over 20 different grades bitumen are manufactured starting from the short residue. The viscosity and yield of short residue are a function of both the origin of the crude oil, the temperature and pressure in the vacuum column during processing, and these vary significantly from crude oil to crude oil. The blend of crude oil processed - as well as the column conditions are - adjusted to produce a short residue with a penetration grade of 35–300 dmm (decimillimetre)

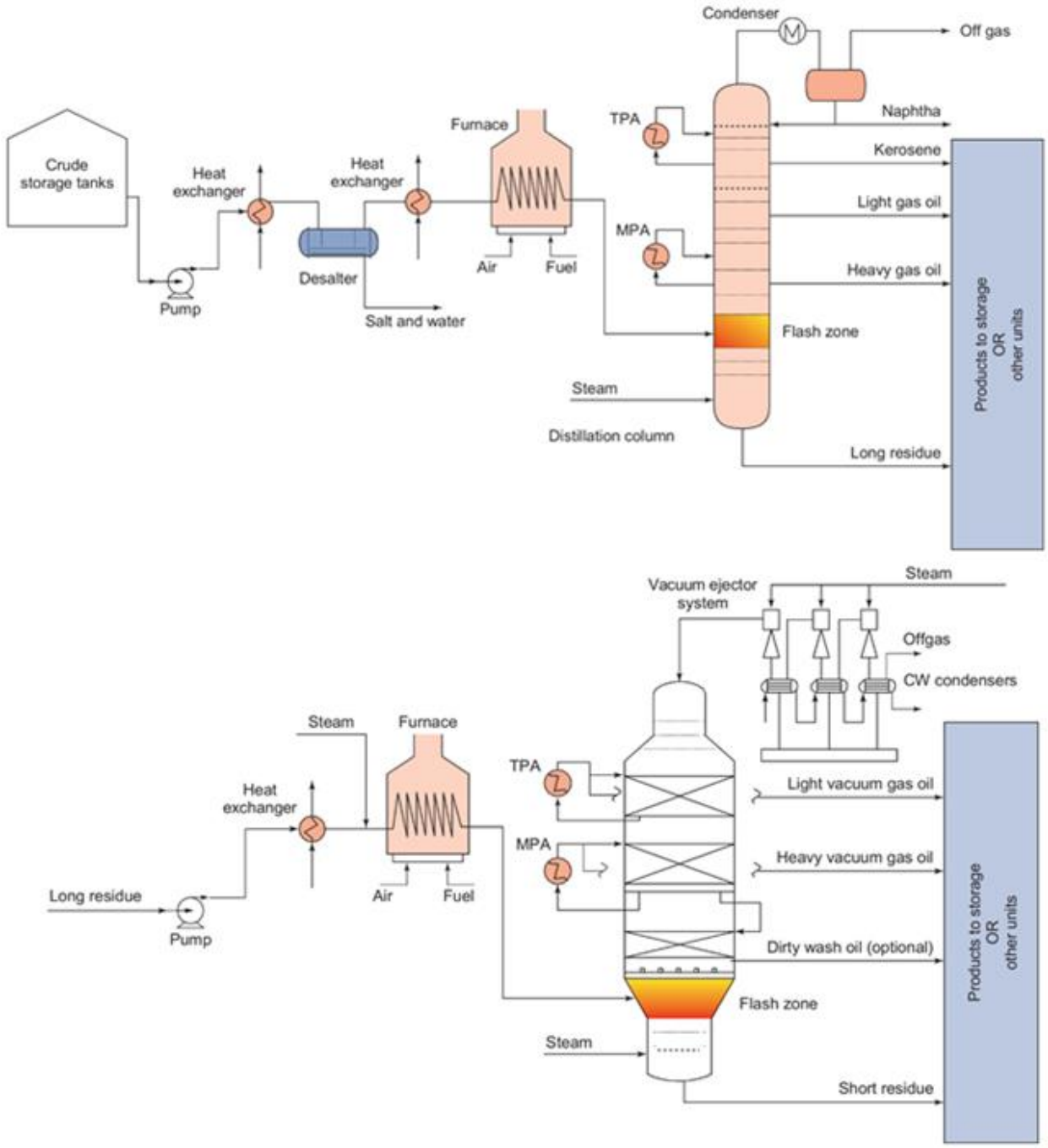


**Figure 1** Atmospheric distillation (upper panel) (MPA, middle pump-around; TPA, top pump-around) and Vacuum distillation (lower panel) (CW, cooling water; MPA, middle pump-around; TPA, top pump-around) [10]

Good crude oils and proper distillation processes can enhance bitumen properties. Generally, heavier crude oil gives higher bitumen yields [13]. Therefore, having a complete knowledge on the bitumen characteristics from different aspects is of paramount importance. Often by the correct selection of the crude oil feed and operating conditions, bitumen with a particular specification can be manufactured directly from the distillation process. Indeed, many crude oils produce bitumen suitable for road construction. However, if a more demanding bitumen's physical properties are required, the short residue can be further modified by 'air blowing'. This is an oxidation process that involves passing air through the short residue at temperature between 240 and 320

°C (Figure 2). The main effect of blowing is that it converts some of the relatively low molecular weight molecules (known as resins) into relatively higher molecular weight ones (known as asphaltenes). The process involves oxidation, dehydrogenation and polymerisation of the lighter molecules of the short residue. It has been found that all the oxygen taken up can be accounted for by the formation of hydroxyl, carbonyl, acid and ester groups; no ether oxygen has been detected, while products like carbon dioxide, water and some light hydrocarbons are considered as side products. Besides carbon–oxygen bonds, carbon–carbon bonds are also formed. Of the functional groups mentioned, the esters are particularly important because they serve as a link up of two different molecules and thus contribute to the formation of material of higher molecular weight. This mechanism results (together with the direct formation of carbon–carbon bonds) in an increase in the high molecular weight molecule content. Ester formation as well as carbon-carbon bond formation are desired reactions; all others are less desirable or even undesirable reactions. As a matter of fact, a decrease of the amount of oxygen used for condensation reactions from 60 to 20%, and an increase of oxygen used for side reactions from 40 to 80% is observed with an increase of temperature from 150 to 350 °C [10].

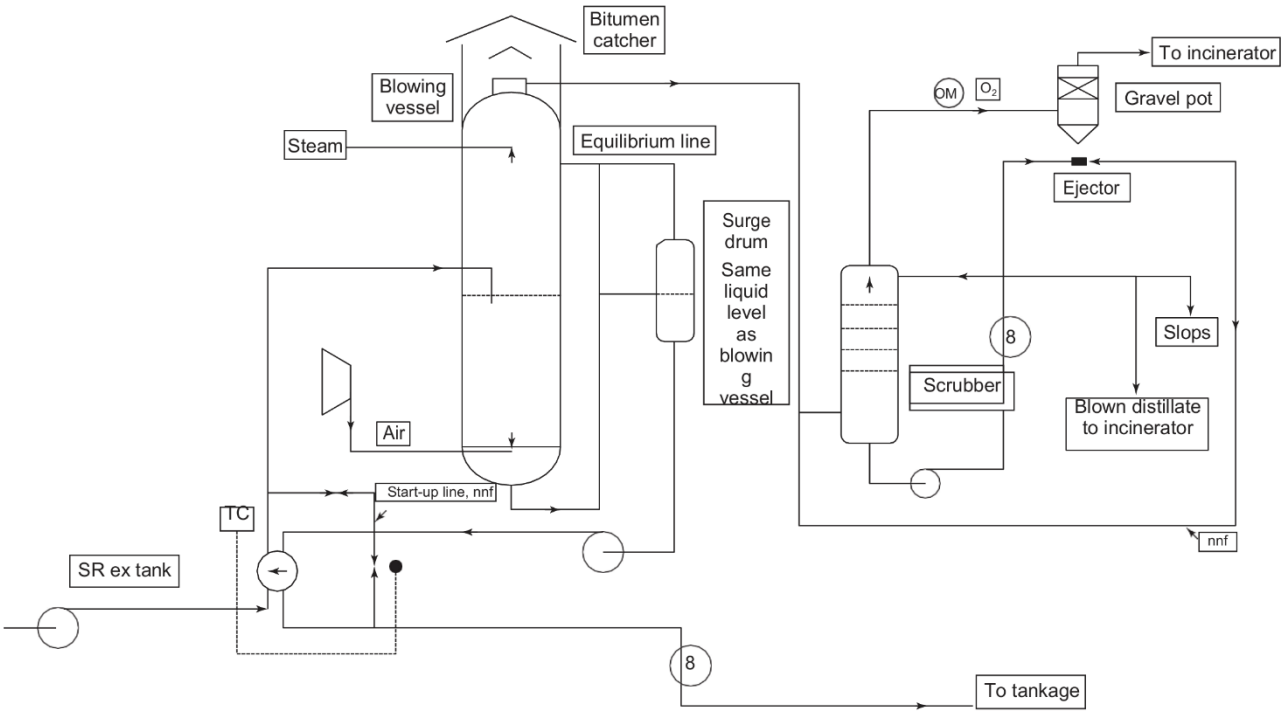


**Figure 2** Simplified diagram of a bitumen blowing unit (Ex, from; nnf, normally no flow; SR, short residue; TC, temperature control; OM, oxygen meter) [10]

### 1.3. Bitumen chemistry: composition and structure

#### 1.3.1 Composition

From a chemical-physics point of view, bitumen can be seen as a viscous viscoelastic liquid (at room temperature) which is totally soluble in toluene, substantially non-volatile, and softens gradually when heated [14]. It comprises a very great number of molecular species that vary widely in polarity and molecular weight [15,16]. Elemental analysis show that bitumen composition is primarily

determined by its crude oil source and it is difficult to give a specific geographical generalization [17,18] (many suppliers also mix bitumen from different sources as well). This has been shown in a wide research by SHRP (Strategic Highway Research: Special Report) [19]. Based on this report, the main constituents of bitumen are carbon, which varies from 80 to 88 wt% and hydrogen ranging from 8 to 11 wt%. In addition, Heteroatoms and transition metal atoms (principally vanadium and nickel) are generally presents: sulfur (0 to 9 wt%), nitrogen (0 to 2 wt%), oxygen (0 to 2%), vanadium up to 2000 ppm, and nickel up to 200 ppm [17,20,21]. A more detailed study on metal content in bitumens, in which other metals (like Chromium, Cobalt, Arsenic, Selenium etc…) are detected, is reported in [22]. Table 1, shows a typical composition of some bitumens from various sources [23]:

**Table 1** Elemental Analysis of bitumen from various sources [23]

| Chemical element | Quantity range | Average value | unit |
|---|---|---|---|
| Carbon | 80.2-84.4 | 82.8 | % *w/w* |
| Hydrogen | 9.8-10.8 | 10.2 | % *w/w* |
| Oxygen | 0.4-1 | 0.7 | % *w/w* |
| Sulfur | 0.9-6.6 | 3.8 | % *w/w* |
| Nitrogen | 0.2-1.2 | 0.7 | % *w/w* |
| Nickel | 10-139 | 83 | ppm |
| Vanadium | 7-1590 | 254 | ppm |
| Iron | 5-147 | 67 | ppm |
| Manganese | 0.1-3.7 | 1.1 | ppm |
| Calcium | 1-335 | 118 | ppm |
| Magnesium | 1-134 | 26 | ppm |
| Sodium | 6-159 | 63 | ppm |

From a molecular point of view, the main compounds of the polar heteroatoms above are: sulphides, thiols and sulfoxides, ketones, phenols and carboxylic acids, pyrrolic and pyridinic compounds, and most metals form complexes such as metalloporphyrins [21]. Molecular weight distribution analysis shows that bitumen is a complex mixture of about 300 to 2000 chemical compounds (medium value 500–700) making a complete chemical characterization very difficult.

For this reason, bitumen is generally fractionated by simple methodology - known as SARA (Saturate, Aromatic, Resin, Asphaltene) analysis - to know its main characteristics. The SARA method is of vital importance because bitumen scientists and technologists usually specify the composition of bitumen in terms of the relative content of these fractions. In addition, the SARA fractions constituted the basis for all early theories on bitumen/polymer interactions and are still used to formulate modern interpretations of the bitumen modification mechanisms [24]. Figure 2 shows a schematic SARA procedure [23]:

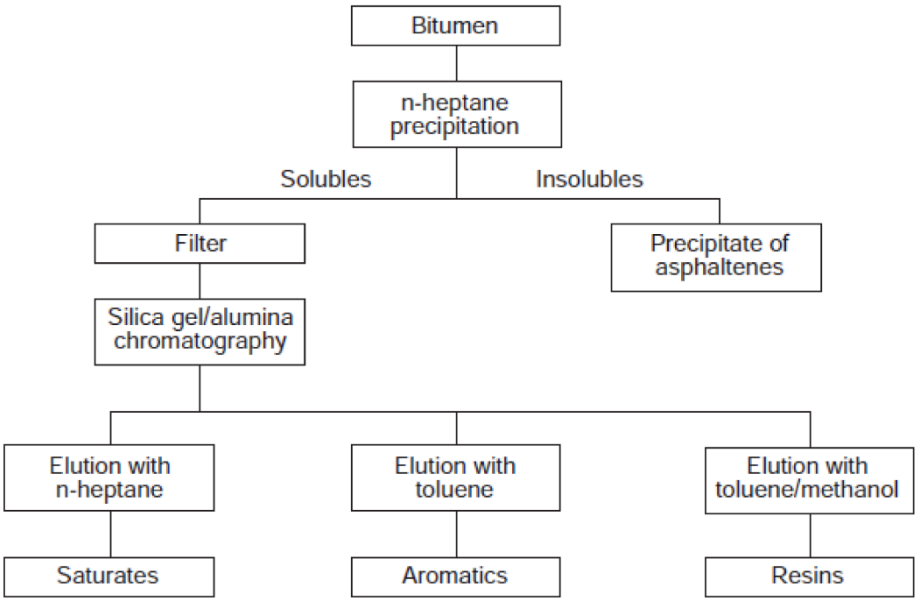


**Figure 3** Schematic of the saturates, aromatics, resins and asphaltenes (SARA) chromatographic method [14]

An in-deep description of the SARA methodology can be found in [24, 25].

The relative abundance of the SARA fractions allows the bitumen chemical composition to be related with its internal structure and some of its macroscopic properties [26]. In a sample of bitumen if the concentration of asphaltenes is kept constant and the other components vary it has been observed that: a) increasing the aromatics content at a constant saturates-to-resins ratio has little effect on the rheology other than a marginal reduction in the shear susceptibility, b) maintaining a constant ratio of resins to aromatics and increasing the saturates content softens the bitumen, c) the addition of resins hardens the bitumen and reduces the penetration index and shear susceptibility, but increases the viscosity. Lin et al [27] has also shown that the rheological properties of bitumen strongly depend on the asphaltenes content. At a constant temperature, the viscosity of a bitumen increases as the concentration of the asphaltenes blended into the parent maltenes is increased. However, the increase in viscosity is substantially greater than would be expected if the asphaltenes were spherical, non-solvated entities. This suggests that the asphaltenes can interact with each other and/or the solvating medium. The marked increase in non-Newtonian behavior as bitumen cools is a consequence of the inter-molecular and intra-molecular attractions between asphaltenes and other entities. Under shear, these extended associations will deform or even dissociate in a way that is not adequately described by classical Newtonian concepts. Consequently, at ambient and intermediate temperatures, it is reasonable to conclude that the rheology of bitumen is dominated by the degree of association of asphaltene particles and the constitution and structure of bitumens relative amount of other species present in the system to stabilize these associations.

#### 1.3.1.1 Asphaltenes

Among the bitumen's SARA fractions, asphaltenes represent the most important one and are connected to the main properties of bitumen. Asphaltenes are the most aromatic of the heaviest components of crude oil, are critical to all aspects of petroleum use, including production, transportation, refining, upgrading, and heavy-end use in paving and coating materials. Indeed, the molecular characterization of asphaltenes is required as well as the detailed understanding of the hierarchical colloidal structures of asphaltenes and petroleum. Their percentage can vary from 5 to 25% and are amorphous brown/black solids at room temperature with particle dimensions between 5–30 μm, insoluble in n-heptane, but soluble in toluene [28,29]. Asphaltenes contain oxygen, nitrogen, sulfur, and heavy metals (V, Ni, etc.) in the form of complexes such as metallo-porphyrins with long aliphatic chains (up to 30 carbon atoms), and pyrrolic and pyridinic rings. As demonstrated by UV-fluorescence spectroscopy [30,31], Fourier Transform Infrared Spectroscopy (FTIR) [31,32], X-ray Raman spectroscopy [33], and NMR spectroscopy [30,34, 35], asphaltene molecules consist of fused aromatic rings, most probably between 4 to 10 units, together with some aliphatic chains as ring substituents. They tend to form small (few nm) stacks stabilized by amphiphilic resins and dispersed in the apolar matrix phase of paraffin and aromatic oils (maltene) [25,36]. Furthermore, by using X-Ray scattering [37] it has been demonstrated that the asphaltenes tend to form clusters organized in hierarchical structures of different length scales (up to hundreds of nanometers and even to micro-scales with the so called "bee-structures" [38]). A more detailed study on the asphaltene nature can be found elsewhere [39]

#### 1.3.1.2. Saturates

The saturated components in bitumen typically are within 0–15%wt. of the overall fractions. From a chemical point of view, saturates are complex mixtures of polyalkyl structures in which straight chains of paraffin prevail as shown by FTIR measures [32]. Saturated fractions of blown bitumens are richer in long-chain paraffins than those of straight-run bitumens [41]. The saturate fraction is a mixture of pure aliphatic (linear and cyclic) [25]. As the content of saturates increases a decrease in the complex shear modulus and an increase in the phase angle of bitumen is expected because the saturate fraction is the lightest part of the maltene phase, whereas the latter is a liquid part of bitumen which is complemented with solid asphaltenes [24].

#### 1.3.1.3 Resins

Resins are dark brown solid (or semi-solid) compounds characterized by particle sizes of 1–5 nm, soluble in n-heptane, and structurally and compositionally similar to asphaltenes, except for a lower molar mass [41]. Resins are present in an amount ranging from 30 to 45%wt. and sometimes can be

more polar than asphaltenes, but with less condensed aromatic rings [28]. Their polar nature enhances the adhesive properties of bitumen, but their principal role is as dispersing agents for the asphaltene macromolecular structures and oils, which are mutually insoluble. When bitumen is oxidized, resins gain oxygen molecules and the similarity of their structure to asphaltenes is enhanced. The bitumen characteristics are determined largely by the resins' asphaltene ratios [42].

#### 1.3.1.4 Aromatics

Aromatic oils are dark brown viscous liquids containing low molecular weight aromatic compounds. They have a slightly aliphatic carbon skeleton with lightly condensed aromatic rings and a molar mass ranging between 300 and 2000 g/mol. Aromatic oils make the highest fraction (40–65%) of bitumen. They have a high solvent power relative to high molecular weight hydrocarbons. Together with saturated oils, they are considered as the plasticizing agents of bitumen [28].

### 1.3.2 Structure

First investigations on bitumen structure dates back to 1914 when Rosinger suggested a colloidal structure for it [43.]. However, only in 1923 Nellensteyn gave a more detailed description of the colloidal structure of bitumen [44] even if Errera also published a discussion on the subject the same year [45]. By studying Tyndall effect of asphaltenes solutions as well as the Brownian motion of asphaltenes in such solutions and the absence of diffusion through membranes Nellensteyn argued that asphaltenes are very close in structure to free carbon and form a colloidal suspension within the maltene phase [46]. Later on, Pfeiffer and coworkers developed a more detailed theory of the colloidal structure of bitumen - what they called sol and gel bitumens (see figure 4) - to explain the difference in rheological properties between various type of bitumen [47,48]. Sol bitumens exhibited Newtonian behaviour, whereas gel bitumens (generally blown ones) were highly non-Newtonian. Between these two extremes, a majority of bitumens was found to have an intermediate behaviour due to a mixed "sol–gel" structure (called in fact "gel–sols" or "elastic sols"). In modern terms, the non-Newtonian behavior would be described as delayed elasticity together with some nonlinearity in the viscoelastic properties [49.].

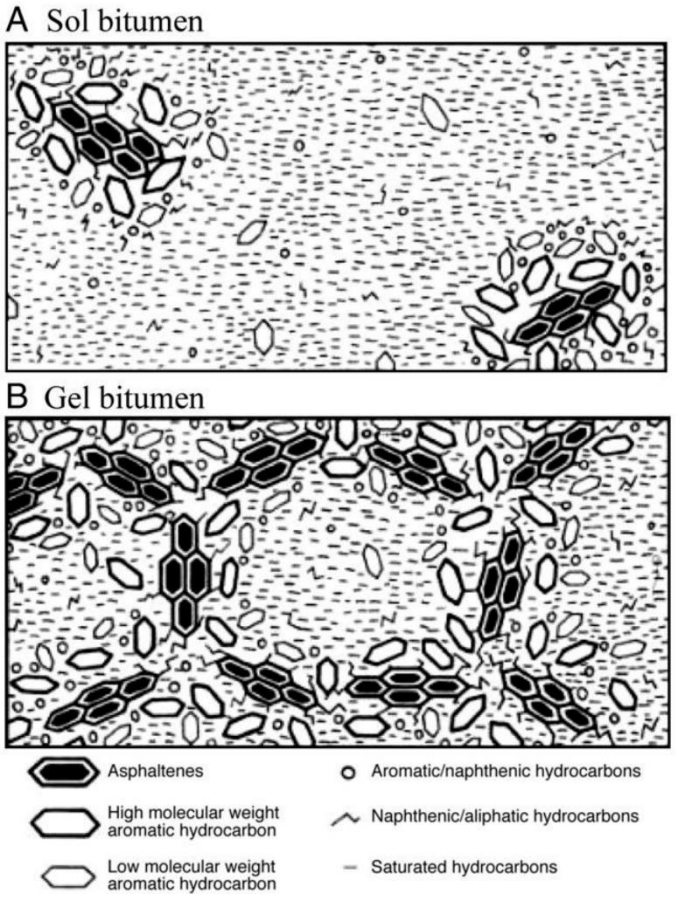


**Figure 4** The original colloidal model: sol and gel bitumens. Reprinted from [47] (courtesy of ACS)

From a structural point of view, the sol type was thought to occur when the asphaltenes micelles were fully dispersed and non-interacting (Fig. 4A - [47]). The non-Newtonian behaviour was thought to originate from a gel structure due to fully interconnecting asphaltenes micelles (Fig. 4B - [47]). The sol–gel structure consisted in the coexistence of sol-type micelles and a gel structure. However, this description proved somewhat incorrect since a gel structure would result in a yield stress or a plateau of modulus versus temperature and frequency [50-52] which have never been observed for paving grade bitumens [53-55.]. Nevertheless, this interpretation was in line with the well-known result that a soft grade differs from a harder grade from the same crude oil by higher asphaltenes content and lower aromatics content with almost unchanged resin and saturate contents [13].

An in deep description of the bitumen structural architecture was provided by Teh Fu Yen who gave a hierarchical picture as reported in figure 5

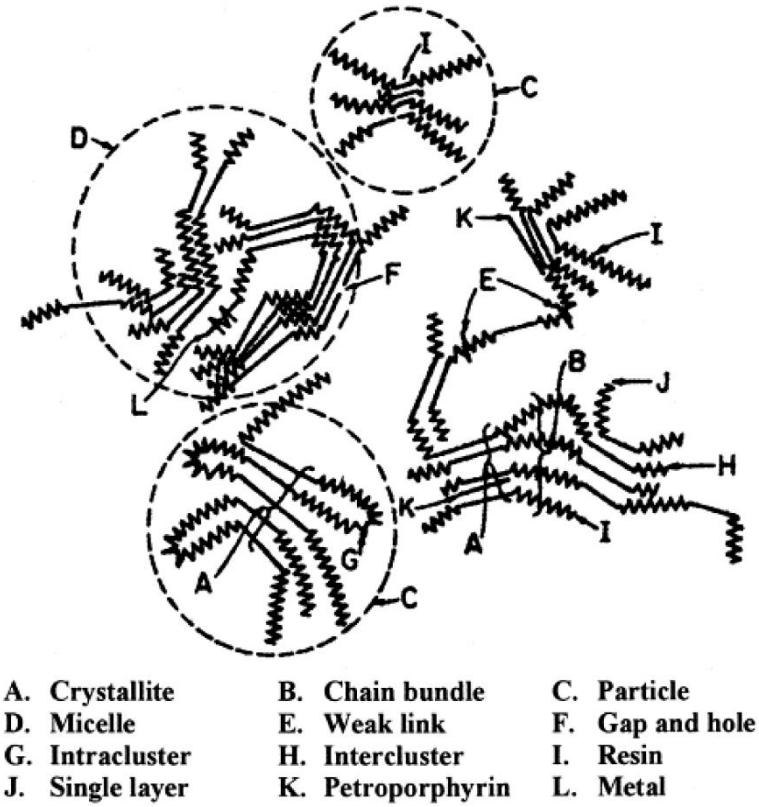


**Figure 5** Yen Model as proposed in 1967 Reprinted from [56] (courtesy of ACS)

The Yen model depicted in figure 5, relates different length scale structures from crystallite to micelle allowing an in deep comprehension of the utility of results within a given length scale. However, the uncertainty in the most basic issue, asphaltene molecular weight, was enormous. Only ten years ago the issue of asphaltene molecular weight was highly debated with only very few who supported the currently accepted value for asphaltene molecular weight. Without resolution of this key molecular attribute, structure-function relationships are precluded and phenomenology prevails. Fortunately, asphaltene science has progressed dramatically in the last 10 years leading to a greater understanding of some topics, some more certainty, while others, less so. Each topic will be treated below to provide a general understanding of the corresponding current status. Following, to start with a description of the modified Yen model is given.

#### 1.3.2.1. Modified Yen Model

The modified Yen model (see figure 6) deals with the hierarchical structures, properties and energies manifested by asphaltenes and their interaction. The model emphasizes the different asphaltene hierarchical structures and show how the hierarchical structures are.

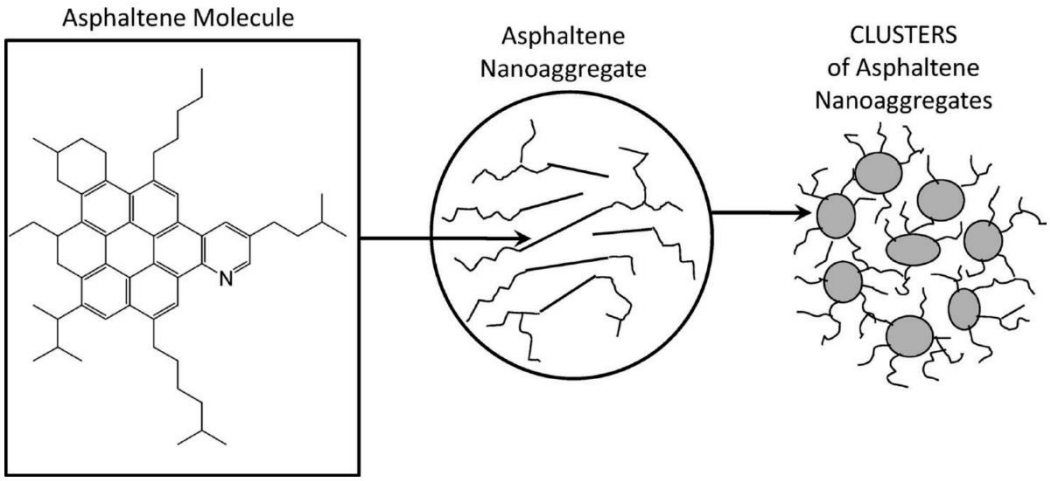


**Figure 6** Modified Yen model. (Left) The predominant asphaltene molecular architecture has a single, moderately large PAH with peripheral alkanes. (Center) Asphaltene molecules form asphaltene nanoaggregates with aggregation numbers of~6 and with a single disordered stack in the interior with peripheral alkane. (Right) Asphaltene nanoaggregates can form clusters with aggregation numbers estimated to be ~8. The modified Yen model provides a framework to treat large numbers of diverse asphaltene studies. Reprinted from [57] (courtesy of ACS)

Figure 6 shows the asphaltene molecular architecture from its single polycyclic aromatic hydrocarbon (PAH) ring system with peripheral alkane substituents to nanoaggregates with a single, disordered stack of PAHs and with aggregation numbers ~6 (the dimension of nanoaggregates is estimated in about 2 nm and with an aggregation energy of few kJ/mol). These nanoaggregates form clusters of nanoaggregates - not much bigger than the nanoaggregates itself - with aggregation numbers estimated to be eight. There is some uncertainty about the size of the clusters. The smallest type observed is of about 6 nm. Larger clusters can form with a length scale of ≥ 10 nm. The cluster's nanoaggregate binding energy is rather small, and can be strongly affected by changing temperature, concentration, and liquid-phase properties. Indeed, asphaltene cluster properties have an enormous influence on the rheological behaviour of bitumen. In figure 6, the grey circles represent the aromatic core of the asphaltene nanoaggregates, while the crooked lines represent the nanoaggregate alkane substituents. The predominant molecular architecture of the Yen model consists of a single, large Polyaromatic Hydrocarbon (PAH). The PAH - due to its polarizability - is the primary site of intermolecular attraction and therefore molecular aggregation. This interaction increases with the number of fused rings and thus is significant for large PAHs structures. In addition, the PAH possesses a degree of charge separation primarily associated with the heteroatoms giving rise to dipole-dipole interactions. The energy of the dipole-dipole interaction and induced dipole-induced dipole interaction decreases with the separation distance as $r^6$ giving rise to a short-range interaction; generally, the PAH structures contains heteroatom such as nitrogen in pyrrolic and to a lesser extent pyridinic structures, sulphur in the form of thiofenic rings, and to a lesser extent oxygen like phenolic rings. Branched - and straight-chain substituents are present as peripheric structures and create steric hindrance, preventing close approach of the attractive PAHs (see Figure 7).

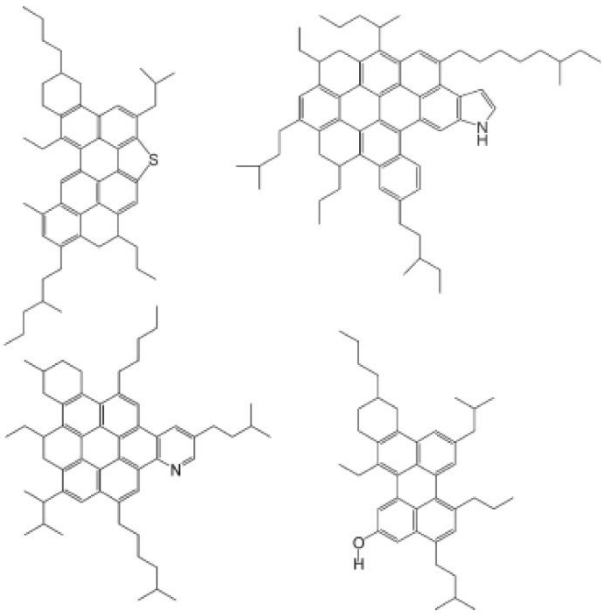


**Figure 7** Proposed asphaltene molecular structures. These structures are consistent with the many molecular constraints that are now known to apply to the asphaltenes. These are the types of molecular structures that dominate asphaltenes. Reprinted from [57] (courtesy of ACS)

After several molecules (nano)- aggregate, their alkanes distort to occupy reduced available volume preventing additional asphaltene molecules to achieve close approach to the interior PAHs. Thus, additional asphaltene molecules form new nanoaggregates of small aggregation numbers and not large nanoaggregates. Critical NanoAggregate Concentration (CNAC) is the physico-chemical parameter generally used to evaluate asphaltene aggregation. It is defined as the concentration at which further nanoaggregate growth stops. It has been observed that asphaltene nanoaggregates are formed when they are placed in toluene in sufficient concentration. So, as a matter of fact they do not need resins to form or to be stably suspended. Very similar nanoaggregates are observed in crude oils. Nevertheless, in crude oils, resins are present but only the heaviest resins participate in the aggregation at a level of ~15% mass fraction. With such small nanoaggregates and relatively small resin fraction, resins do not act as classic surfactants for these asphaltene nanoaggregates.

### 1.3.3. Asphaltene Molecular Architecture

#### 1.3.3.1. Asphaltene Molecular Weight.

Asphaltene molecular weight plays a central role in the modern theory of the modified Yen model and thereby in the structure architecture of crude oil and bitumen. The information that are nowadays acquired have allowed the asphaltene science to not be reduced to a pure phenomenology. About asphaltene molecular weights, only ten years ago there was huge uncertainty and controversy. Long-time debates have been made about this topic for several reasons. Some debates were focused on the molecular asphaltenes polydispersion, causing application of any technique to be somewhat uncertain. Moreover, asphaltenes associate at different concentrations with different binding energies. This caused mistakes and limitations in some methods used to determine the asphaltene molecular weight. Fortunately, the issue of asphaltene molecular weight is now largely resolved.

#### 1.3.3.2 Molecular Diffusion.

One of the techniques that have had a decisive role in resolving the asphaltene's molecular- weight controversy was diffusion. Together with mass spectrometry diffusion, this technique is a primary method used to measure asphaltene molecular weight, because this technique is not affected – unlike other techniques - by the effects of asphaltene aggregation. Time Resolved Fluorescence Depolarization (TRFD). [58-64.] was the first molecular diffusion measurements performed on asphaltenes. This technique employs a polarized laser beam to induce an excited polarized electronic state on the absorber molecules. As the molecule undergoes rotational random walk (rotational diffusion), the polarization direction continuously reorients and decays. The technique measures the rotational correlation time that is the time that it takes for the molecule to reorient on the order of 1 rad. Molecular size and shape influence the rotational correlation time and particularly, for large molecules, internal rotation can yield somewhat shorter correlation times than expected for the molecule as a whole. TRFD is necessarily limited to the fraction of asphaltenes with fluorophores that undergoes fluorescence following the energy gap law as reported in [65]. By selecting specific excitations and emissions the TRFD technique allows sensitive optics to measure very small quantum yield components. In 2002, Wargadalam et al. [66] used Taylor dispersion (TD) – a technique sensitive to translational diffusion and not rotational one – to measure coal-derived asphaltenes molecular weight. Agreement between TRFD and TD data indicates that 1) the fluorescent and nonfluorescent asphaltenes are similar and 2) the TRFD results are not distorted from possible internal rotational effects of molecules. Moreover, Freed and co-workers [67,68] by using Nuclear Magnetic Resonance spectroscopy (NMR) – which is sensitive to asphaltene with hydrogens – have obtained results similar to that of TRFD although the NMR measurements give an average size (diameter) of 2.4 nm slightly higher than those from TRFD. However, as stated by the authors, this could be ascribed to the presence of some di- and trimer concentrations due to the fact that the NMR measurements cannot go to very low concentrations (50 mg/L). Molecular weight measurements have also been made on ultra-dilute solutions of asphaltenes through Fluorescence Correlation Spectroscopy (FCS) [69-71] obtaining results in close agreement with other diffusion measurements. The good agreement of all four molecular diffusion measurements makes it possible to state that asphaltenes are comprised of small molecules. Figure 8

shows typical TRFD data for petroleum asphaltenes. As it can be seen from figure 8 the most probable molecular weight of asphaltenes is 750 Da.

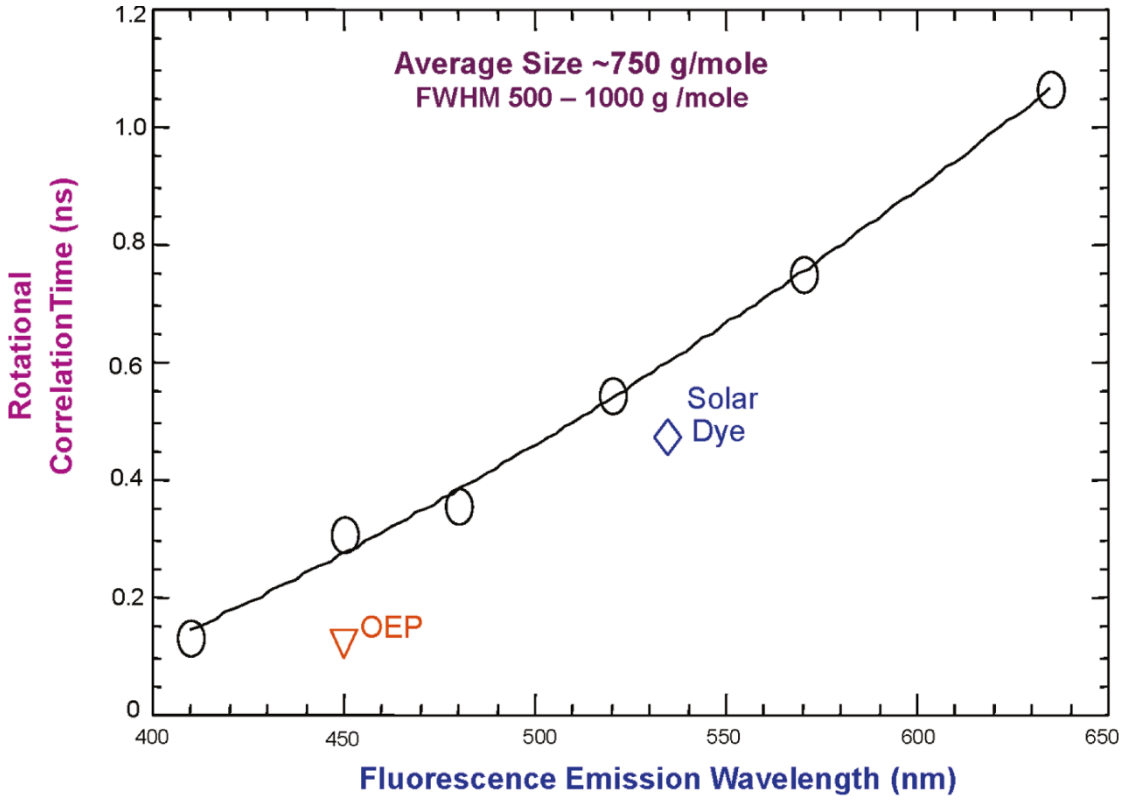


**Figure 8** Rotational correlation times of asphaltene molecules as a function of their PAH fluorescence emission wavelength. Also shown are two model compounds: solar dye with a molecular weight of 755 Da, and octaethylporphine (OEP) with a molecular weight of 535 Da. All correlation times are small, indicating that asphaltene molecules are not large and are comparable to the model compounds. The large wavelength dependence of the correlation times indicates that the fluorophore is a major portion of the asphaltene molecule; thus, there is one PAH per asphaltene molecule. Readapted from [58]. (courtesy of ACS)

#### 1.3.3.3. Mass Spectrometry

Mass Spectrometry (MS) naturally provides essential measurements in any study of molecular weight. However, at early stages the known methods of MS applied to measure asphaltenes molecular weight have given some contradictory results. For example, one of the first MS technique used was field ionization mass spectrometry that gave the most probable molecules weight of about 1000 Da. [72]. However, this result was not generally accepted due to the problems about fragmentation and about not volatilizing the heaviest molecules. Also, some more sophisticated techniques like laser desorption ionization mass spectrometry (LDI-MS) and matrix-assisted laser desorption ionization (MALDI- MS) encounter some problems in obtaining asphaltene molecular weight. A huge problem was for example that different workers obtained very divergent results. For example, different research groups [73,74] used LDI on virgin crude oil asphaltenes obtaining molecular weight that differ of one order of magnitude, i.e. ~1000 Da and ~10 000 Da. The researchers have attributed this discrepancy to the asphaltene aggregation due their high concentration in the plasma. This is in turn dependent on laser power, sample surface concentration, and even timing of ion collection [75-78] Thus, low plasma densities especially at the ion collection times are required to obtain accurate asphaltene molecular

weights. Novel LDI experiments that uses two different lasers - an infrared (IR) laser that desorbs the asphaltene, and a second ultraviolet (UV) laser that performs the ionization step - have shown that most probable asphaltene molecular weights is about 600 Da.

However, the mass spectrometric method applied to asphaltenes that has had perhaps the greatest scrutiny is electrospray ionization Fourier transform ion cyclotron resonance mass spectroscopy (ESI-FT-ICR-MS). [79-83]. Petroleum asphaltene molecular-weight distributions as measured by ESI-FT-ICR-MS are dominated by components in the 400-800 Da range. Moreover, the role of di- and multimers has clearly been delineated by ESI-FT-ICR-MS studies [79].

### 1.4. Type, Size and number of Polyaromatic Hydrocarbons (PAHs) in asphaltene molecules.

#### 1.4.1. Type of Asphaltene PAHs.

The type of PAHs in asphaltenes was at the heart of past longstanding discussions in the asphaltene literature. This discussion has undergone a breakthrough with the incorporation of the Clar representation of PAHs [84] with his "*Aromatic Sextet*" theory. In Clar's representation, no 2 adjacent fused aromatic rings can both be sextets; that is, no two adjacent hexagons can both "have circles" as reported in figure 9.

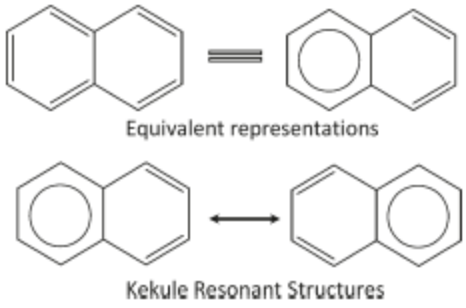


**Figure 9.** Clar's representation of PAHs

Following the Clar's theory the carbon-carbon bond lengths in Polyaromatic compounds are not all equal. Pure sextet compounds, such as benzene, triphenylene, and hexabenzocoronene, are very stable and have blue shifted spectra. Increasing of isolated-double-bond carbon, make PAHs less stable moving towards a red-shifted optical absorption spectra [84-89]. On the basis of geologic time stability of crude oil's asphaltene, and the stability of sextet carbons, many researchers have proposed that the type of carbons found in asphaltenes must be in aromatic-sextet structures and not as isolated-double-bond carbon. The question was experimental addressed by the use of X-ray spectroscopy. The choice of this technique was due to the fact that it relies on exciting empty valence orbitals from inner electron shells instead on valence shell transitions of optical spectroscopy. [90] However, classical X-Ray spectroscopy, although very useful to "discriminate" different chemical identity of compounds, for example, sulphide to sulphate (which differs in a 10 eV shift of the 1s-3p transition in accordance with the formal oxidation state of sulphur) or nitrogen on the basis of peak energy differences for different nitrogen chemical functions, such as pyridinic and pyrrolic nitrogen, which exhibit large 1s-$\pi^*$ peak differences [91-93] can be problematic in asphaltene carbon analysis due to the high concentration of carbon in asphaltenes skeleton. Indeed, it has been observed non-linear effects due to a too much absorption of carbon X-ray bands. On the other hand, X-ray Raman Spectroscopy (XRRS) - due to its

energetics – has proven to be most appropriate for analysis of asphaltene carbon [33,94,95]. The simple idea is that if a PAH is pure aromatic-sextet carbon, the 1s-π* X-ray absorption line will be narrow. The isolated-double-bond carbon has a slightly different 1s-π* line position; thus, for compounds with increasing amounts of isolated-double-bond carbon, the 1s-π* line width for the PAH will increase. On the contrary, compounds with greater aromatic-sextet carbon have smaller line widths. Figure 10 shows the measured asphaltene line of about 1.4 eV. Moreover, figure 10 shows that the Clar description of PAHs matches the 1s-π* line width, as measured by XRRS for a large number of PAHs.

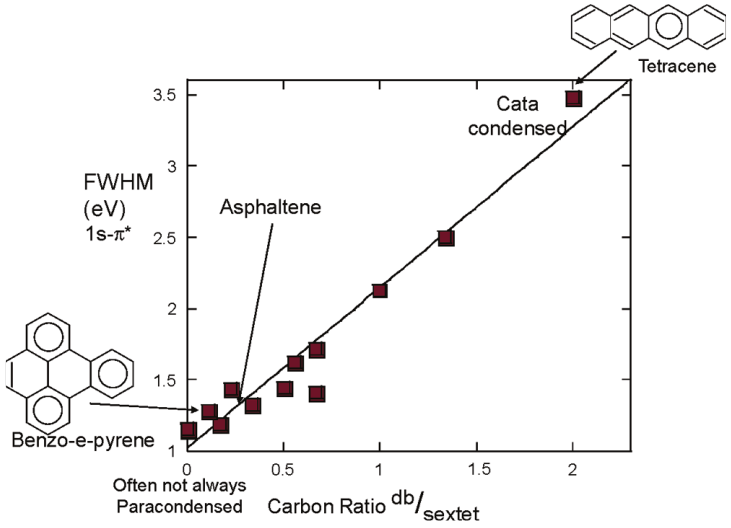


**Figure 10**. 1s-π* line width as determined by XRRS versus the ratio of isolated-double-bond carbon to aromatic-sextet carbon. Readapted from [94] (courtesy of Elsevier). Sextet carbon but not isolated-double-bond carbon dominates asphaltene aromatics. Sextet carbon is known to be more stable and often predominates in pericondensed ring systems. [84,85]

Speaking about the size of PAH, direct molecular imaging acquired using Scanning Tunneling Microscopy (STM) has provided valuable information [96]. From STM data the bulk of the PAHs have a long axis in the range around about 1 nm, which would correspond to roughly 7 fused rings. These results were also supported by high-resolution transmission electron microscopy (HRTEM) [97,98] as well as by Raman spectroscopy from which spectra it has been deduced that the PAHs are roughly 8 fused rings. [99,100] and by $^{13}C$ NMR Distortionless Enhancement by Polarization Transfer (DEPT) spectroscopy [32,101] from which roughly 27 carbons per asphaltene aromatic cluster, corresponding to about 7 fused rings has been found. The different behaviour of electronic structure of isolated versus fused aromatic rings also led to the use of the optical absorption and emission to study the ring size distributions in asphaltenes. The interpretation of asphaltene spectra, is based on the study of the factors that govern the energy of PAH absorption, like transition energies of the π-electron which are mainly governed by the size of the aromatic ring system, and - maybe the most important factor that governs PAH spectral properties - the content of aromatic “sextets” versus the isolated double-bond carbon. As stated above asphaltene PAHs are dominated by aromatic-sextet carbon and not isolated-double-bond carbon, in accordance with the greater stability of aromatic-sextet carbon. Molecular orbital calculations were performed on over 500 candidate asphaltene PAHs to account measured optical

properties of asphaltenes [85-89]. Figure 11 shows the results from molecular orbital calculations of PAHs with different numbers of fused aromatic rings. As it can be seen the red shift increases numbers of fused aromatic rings. Moreover, careful examination of structures in Figure 11 also shows increased red shifts associated with a greater fraction of isolated-double-bond carbon.

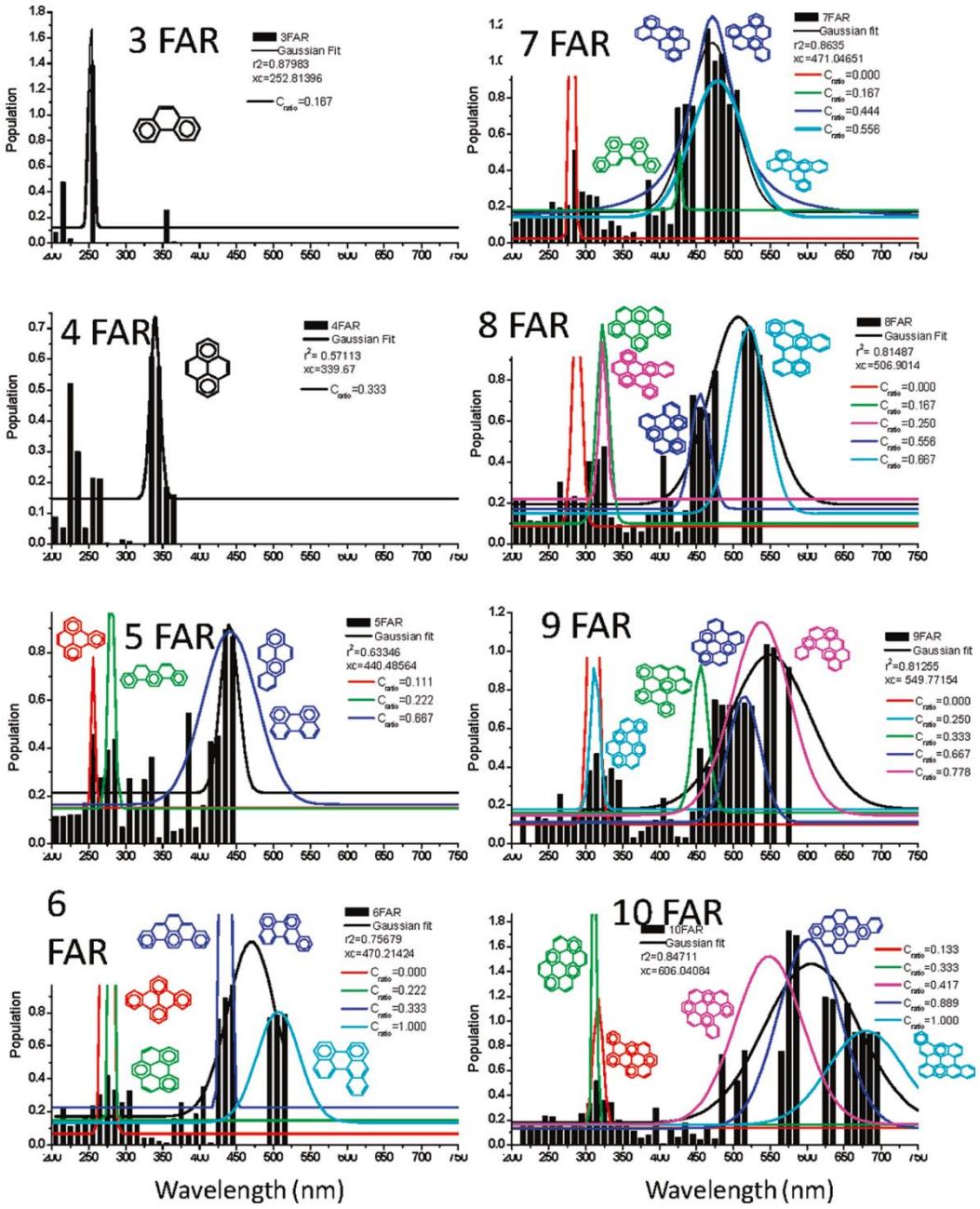


**Figure 11.** Molecular orbital theory predicting optical spectra (absorption and emission) applied to large numbers of candidate asphaltene PAHs. Reprinted from [87]. (Courtesy of ACS)

In 2009, Ruiz-Morales and Mullins [89] calculated a hypothetical absorption spectrum of asphaltene starting from a presumed PAH distribution in asphaltene molecules as reported in figure 12:

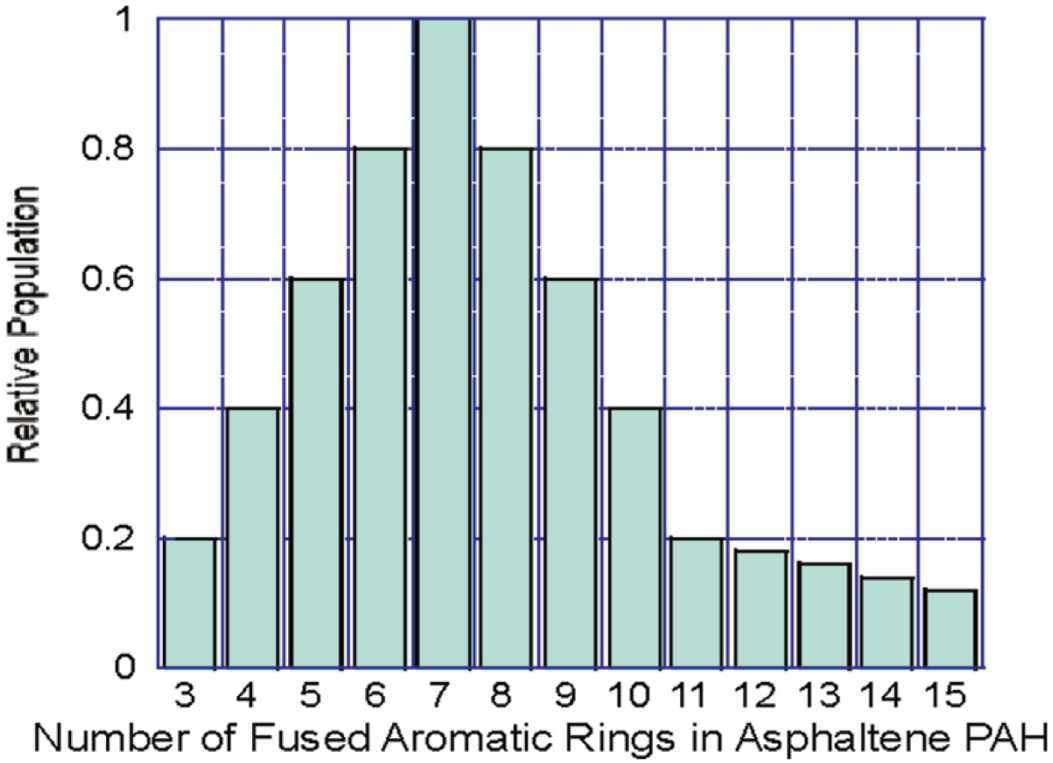


**Figure 12** Presumed asphaltene PAH distribution used to calculate asphaltene optical absorption spectrum (see Figure 13) and fluorescence emission spectrum (see Figure 14). This PAH distribution is in accordance with measured molecular-weight distributions of asphaltenes provided that there is a single PAH per asphaltene molecule. Reprinted from [57]. (courtesy of ACS)

Figure 13 shows a comparison between the experimental and theoretical (calculated) absorption spectra obtained by Ruiz-Morales and Mullins using the distribution in figure 12. As it can be seen spectra closely match. This make it possible to assert that the PAH distribution in Figure 12 appears reasonable. [89]

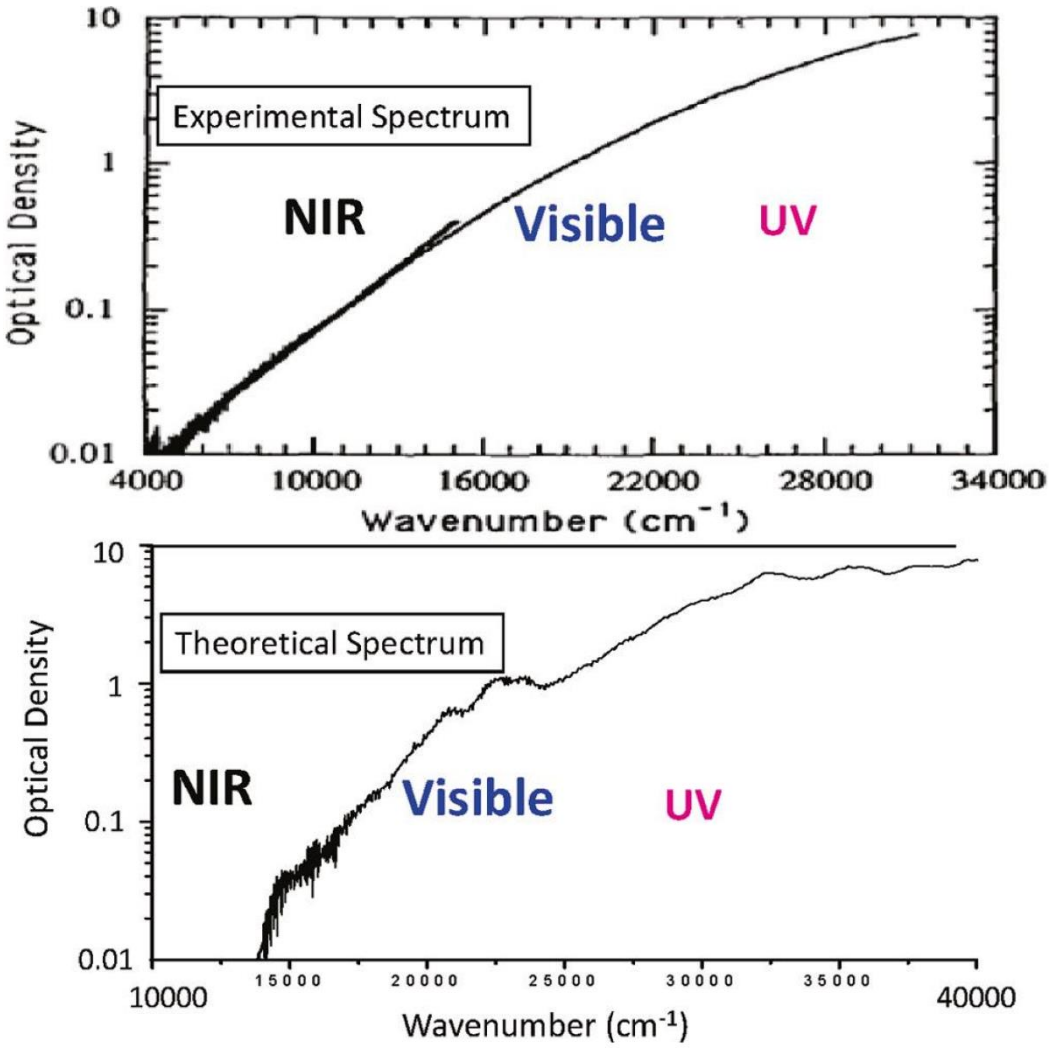


**Figure 13** Experimental spectrum (top) and theoretical spectrum (bottom) for asphaltenes; the theoretical spectrum presumes the PAH distribution shown in Figure 12. There is close agreement between the spectral location of the optical absorption and the magnitude of the increase in optical absorption in going from the near-infrared to the UV. Reprinted from [89]. (Courtesy of ACS)

Moreover, the authors found that a significantly different PAH distributions than that of Figure 12 do not reproduce the proper absorption spectrum for asphaltenes. The authors also used the distribution in figure 12 to predict the asphaltene fluorescence emission spectrum (see Figure 14) [89]

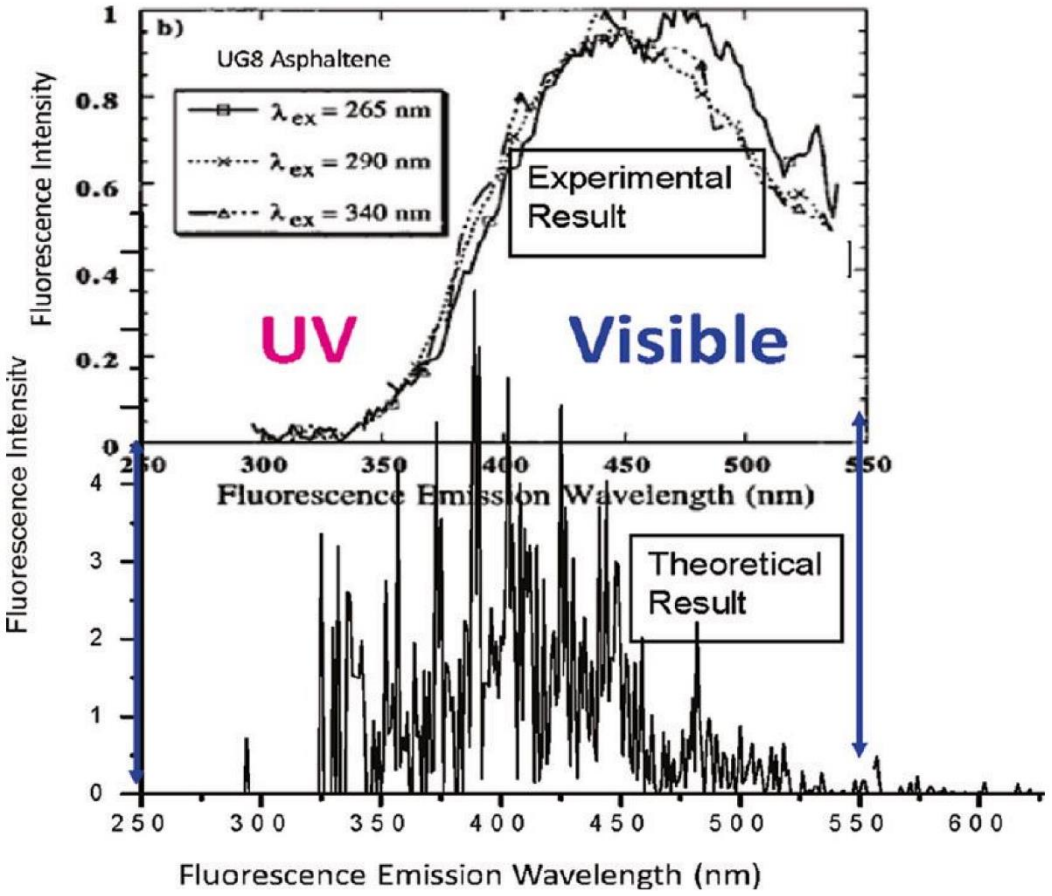


**Figure 14** Experimental and theoretical fluorescence emission spectra of asphaltenes.70 The theoretical curve does not incorporate line broadening that naturally occurs in solution and is found in the experimental spectrum. The close agreement validates the presumed asphaltene PAH distribution shown in Figure 12. Reprinted from [89]. Courtesy of (ACS)

As it can be seen, excellent agreement is obtained (the sharp line nature of the theoretical curve results because no solution line broadening is employed for the theoretical spectrum).

In a preview work Ruiz-Morales, Wu and Mullins, [88] also study the effect of asphaltene aggregation and concentration on the absorption spectra. As it can be seen from figure 15 they found that in the range of the CNAC and the clustering concentration there is no detectable effect of (nanocolloidal) aggregation on asphaltene in the optical absorption spectra.

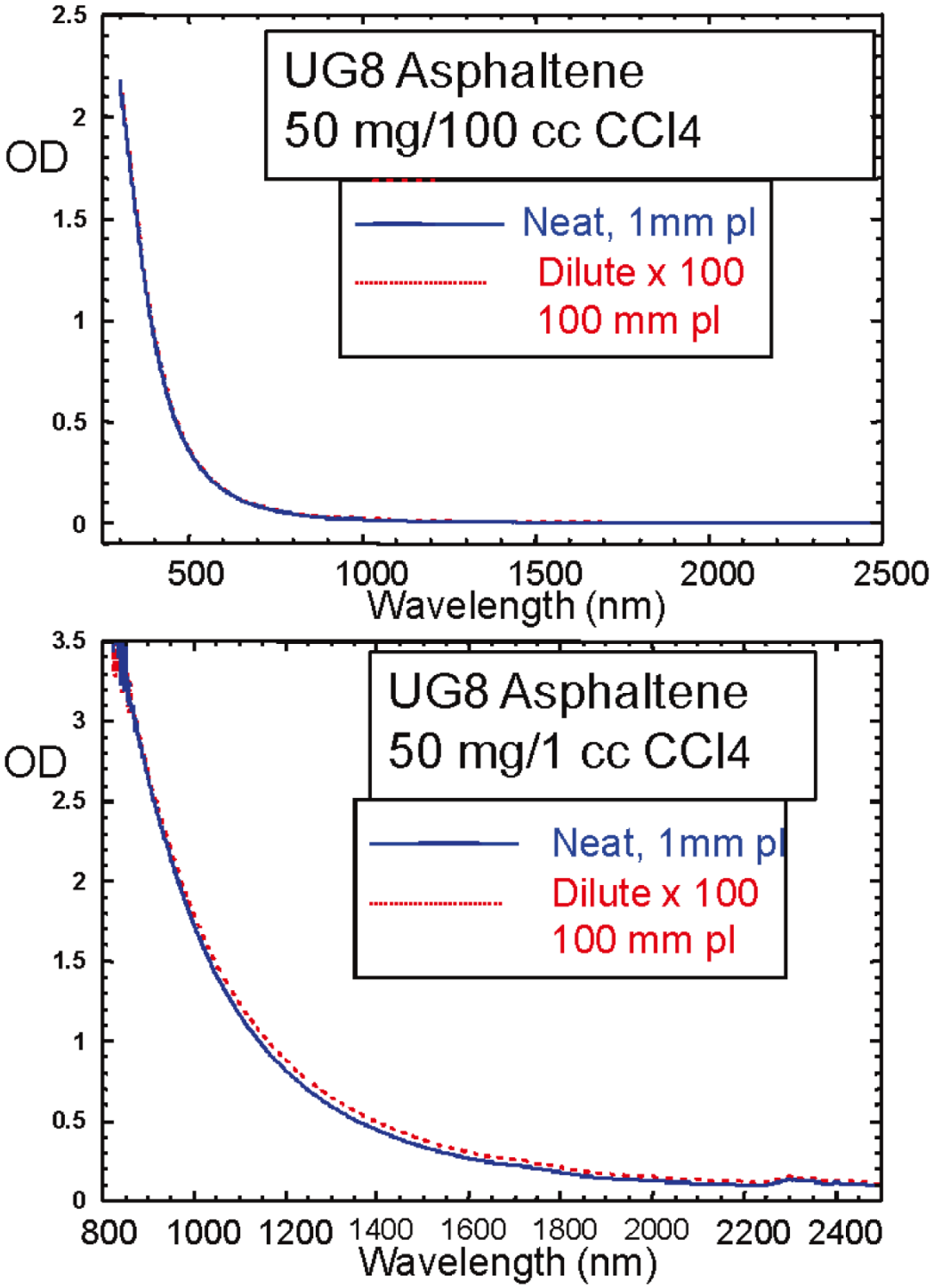


**Figure 15** Optical absorption spectra of asphaltenes versus concentration. (Top blue) Spectrum for 0.5 g/L solution for 1 mm path length (pl) overlays the spectrum for 0.005 g/L solution for 100 mm pl. (Bottom red) Spectrum for 50 g/L for 1mm pl overlays the spectrum for 0.5 g/L for 100 mm pl (minimal differences are attributed to beam walk off in the 100 mm cell). The dilute and concentrated solutions exhibit their absorption edge at the visible and NIR spectra, respectively. There is no nonlinearity in the absorption spectrum of asphaltenes throughout the visible and NIR spectra range. Reprinted from [88] (courtesy of ACS)

That is, asphaltene spectra strictly obey the Lambert-Beer law; the absorption spectra do not exhibit any appreciable nonlinearities because of aggregation. Consequently, the absorption spectra are (incoherent) sums of the absorption spectra of the constituent asphaltene molecules without charge-transfer effects or other concentration-dependent electronic phenomena [88]. In another study, Hammami and Ratulowski [102] found

that if the asphaltenes phase destabilize, forming flocs, then light scattering can become quite strong, contributing to the loss of transmitted light via optical light

### 1.4.2. Number of PAHs per Asphaltene Molecule.

Different and somewhat divergent hypotheses have been made on the number of distinct PAHs that are present in a single asphaltene molecule. On the basis of bulk decomposition studies some researchers proposed a model called “archipelago model” in which PAHs are covalently cross-linked to form the single islands as shown in figure 16.

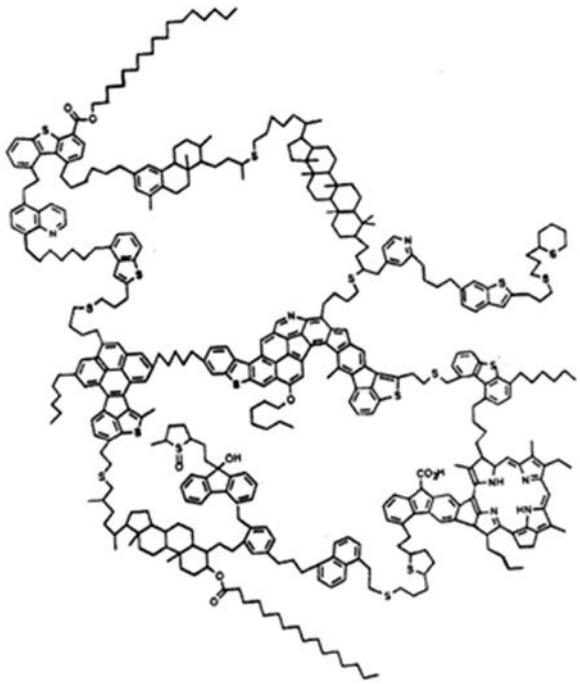

**Figure 16** Asphaltene Archipelago structure Reprinted from [103] (courtesy of ACS)

However, decomposition data are easy to misinterpret unless it is performed under very controlled conditions. More recent data indicates that the predominant asphaltene molecular architecture has a single PAH; this has been termed as “island” model. The island model was firstly supported by TRFD molecular diffusion studies [58-64] as it can be seen from figure 17. From the figure 17 it is possible to observe that for island model small rotational correlation times characterizes all asphaltenes and there is a large differences of correlation times between blue- and red-emitting PAHs. On the contrary, the archipelago model is consistent with large rotational correlation times. In addition, because the blue and red fluorophores are cross-linked, they undergo rotational diffusion with similar correlation times. Finally, well-controlled gas-phase destructive studies, unimolecular decomposition (or equivalently collisionally induced dissociation) have been carried out by the Marshall group at Florida State University [104,105]

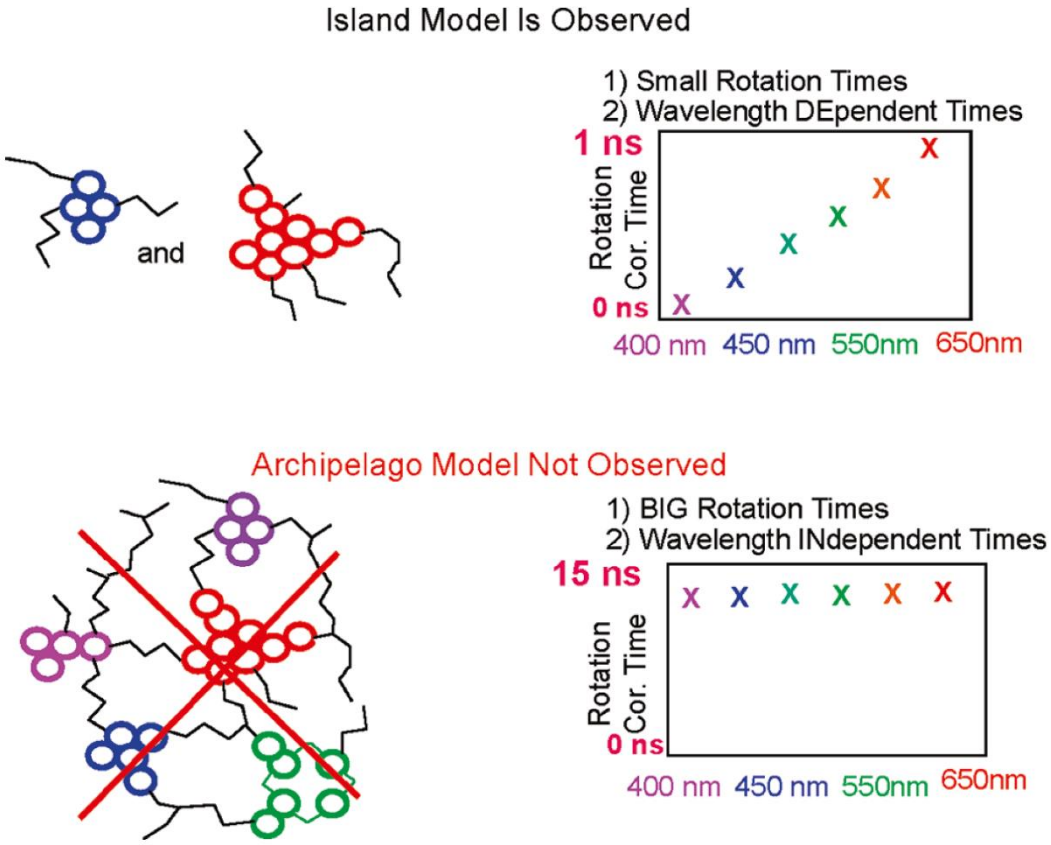


**Figure 17** Color-coded pictorial representation of what the TRFD data should look like for the island versus archipelago molecular architecture for asphaltenes. All measured TRFD data on asphaltenes support the predominance of the "island molecular architecture" for asphaltenes with a single PAH per asphaltene molecule. Reprinted from [57]. (courtesy of ACS)

These studies clearly support the island model as the predominant asphaltene molecular architecture.

### 1.5. Primary Aggregation

#### 1.5.1. Asphaltene Nanoaggregates.

It is now established that asphaltenes have a strong tendency to aggregate. However, to come to such a conclusion a lot of efforts have been made by researchers to shed light on the details of the aggregation processes. In this respect a large number of techniques have been used to investigate asphaltene aggregation, techniques that have provided consistent results. In particular, at least at the beginning, X-ray diffraction, Small-Angle X-ray Scattering (SAXS) and Small-Angle Neutron Scattering (SANS) have been employed to study the asphaltene aggregation. One of the first studies using SAXS techniques date back to 1968 when Dwiggins, Jr. [106], investigated the presence of colloids in crude oil samples using Small Angle X-rays Scattering (SAXS). On the basis of the available ultracentrifuge evidence [107-111] concerning colloids nature in crude oil which are thought to consist largely of asphaltenic molecules, the author asserts that the absence of appreciable scattering intensity for an asphaltenic poor material he analysed, suggested that the colloids being seen in the other samples analysed are largely of an asphaltenic nature. Moreover, to gain further evidence that the colloids being seen by X-ray scattering are the same as the asphaltenic colloids seen in ultracentrifuge experiments, he showed that no appreciable differences in scattering pattern and intensities are obtained after a brief ultracentrifugation, through which clays, wax crystals, water and other potential interfering molecules could be separated (before appreciable asphaltenic molecules could also separate) [108].

In 1988, J. C. Ravey et al. [112], made a new study on the asphaltene macrostructure in liquid dispersion by using a Small Angle Neutron Scattering (SANS) technique. Among other studies on the topic [113,114], this new one was made because, as the authors themselves believe, the Yen proposed structural model [115,116] made of stacks of a few aromatic sheets surrounded by some aliphatic chains was developed using data collected on solid phase compounds, and may be different from their structure in solution. In the liquid phase, there is probably a colloidal polydispersion in both size and shape. Indeed, some of the studies that have been made on this topic are often at odds with Yen's ideas concerning the inference of associated graphite-like aromatic sheets. The authors' choice to use SANS technique to investigate the asphaltene macrostructure in solution was made because as they argued, both light scattering and SAXS shows some technical limits which can cause problems in data acquiring. The authors presented results of SANS analysis on different kinds of asphaltene dispersed samples in different solvents, of which the main one studied was Tetrahydrofuran. To reduce the influence of the polydispersity in the asphaltenes liquid dispersion samples, the asphaltenes obtained from crude oil were further separated by gel permeation chromatography (GPC) and four other asphaltene fractions were obtained (F1, F2, F3, F4). The effects of both concentration and nature of the solvent have been studied by preparing different asphaltene liquid dispersions. A definite particles shapes (i.e. spheroid, disk, sphere, rods ecc…) model was chosen to fit the experimental intensities of SANS scattering signals. From the best fits to the experimental data, the molecular shape parameters, the volume and the 'molecular weight' of the most likely 'average' particle are calculated. The authors found that the best equivalent mean particle which can represent each fraction (F1, F2, F3, F4) is composed of disc-like aggregates, although as they observed, a very flat spheroid could not be excluded. However, the authors believe that the model choice (disk-like or flat

spheroid) does not modify the conclusion that the macrostructure of asphaltenes in solution (Tetrahydrofuran) is that of large and very thin sheet-like particles. Moreover, they state whether the particles are size polydisperse or not since this result was found for any fraction (F). According to the authors, "*hence the asphaltenes in solution may be considered as being essentially bidimensional 'aggregates' or collections of aromatic units*". By studying different crude oil sources, the authors found that although all the corresponding asphaltenes have slightly different compositions, they show a similar macrostructure, and the association of the elementary asphaltene units gives rise to the same overall morphology. Moreover, according to the authors all these results clearly suggest the existence of a colloidal and micellar state for the asphaltene dispersions. Finally, they also studied the effects of different asphaltene solvents (tetrahydrofuran, benzene and pyridine) on the aggregate size of asphaltene systems, finding that the latter are very sensitive to the chemical nature of the liquid medium. Speaking of which, the existence of a correlation between the aggregation rate of 'smaller particles' and the thermodynamic properties of the solvent were found. Based on the SANS data, the authors hypothesized that in the solution state a true thermodynamic equilibrium between 'primary' particles and reversible aggregates exists, whose equilibrium constantly depends on some properties of the solvent. Data also suggest some influence of solvent dielectric constant due to the fact that the larger this constant, the smaller the aggregates. No influence at all on aggregate's thickness was observed but changes in the mean diameter of the particles were spotted. In considering the above results the authors highlighted the important problem of whether one is dealing with primary particles or with reversible aggregates. From the various effects (temperature, concentration, solvent, etc…) they investigated, clear evidence exists that asphaltenes may be involved in 'reversible association'. As an example, they reported the case of the evolution of the heaviest Fl fraction, which retrogrades into the lighter F2 fraction a few hours after the fractionation has been performed: this important point was repeatedly observed. They concluded that the 'primary' particles must be considered as a whole set of size polydisperse sheet-like particles, with diameters in the typical range 2-l0 nm, and for which the average molecular weights range between 3000 – 30000 u.m.a., the (reversible) association between large and small primary particles may be more or less pronounced according to the solvent used, but always leads to very flat aggregates. Later on, E. Y. Sheu et al. [117] studied the structure and polydispersity of asphaltene colloids by Small Angle Neutron Scattering (SANS) measurements on asphaltene solutions in toluene at various temperatures. In this new study, the authors criticized their previous work [118] in which they found an elongated shape for asphaltene aggregates in toluene and the one by J. C. Ravey et al. [119] which, as seen before, proposed a disk-like model for asphaltene aggregates in tetrahydrofuran. According to Sheu and co-workers, the weak point in the previous conclusion was due to the fact that in both studies the SANS data were analysed with the assumption that the asphaltene aggregates are monodisperse, while other techniques [120] showed that the asphaltene aggregates are highly polydispersed. Therefore, according to the authors a rigorous polydispersity treatment of the scattering data to determine structure and size distribution of asphaltene colloids is needed. Contrary to the previous works, this SANS data analysis was performed including the particle size distribution. The authors started by writing the calculated (or theoretical) intensity of the scattered signal for a polydisperse system as [21,121-123]:

$$I(\mathbf{q}) = \langle N_p \rangle \left(\Delta\rho_p\right)^2 \langle V_p^2 \rangle \langle |F(\mathbf{q})|^2 \rangle \quad (1)$$

Where $\langle N_p \rangle, \langle V_p^2 \rangle$ are pre-factors representing respectively the ensembles averages of the particles number density and the particle volume and $\langle |F(Q)|^2 \rangle$ represents the normalized particle form factor, $\Delta\rho_p$ is the particle solvent contrast factor and $\mathbf{q}$ is the scattering vector defined as:

$$\mathbf{q} = \frac{4\pi}{\lambda} \sin\frac{\theta}{2} \quad (2)$$

Where $\lambda$ is the wavelength of the neutrons (or of the X-rays in SAXS) and $\theta$ is the scattering angle measured from the direction of the beam in a vertical plane parallel to the beam and passing through an origin inside the particle.

More specifically $\langle |F(\mathbf{q})|^2 \rangle$ and $\Delta\rho_p$ are defined as follows:

$$\langle |F(\mathbf{q})|^2 \rangle = \frac{\int V_p^2 |F(\mathbf{q})|^2 dV_p}{\int V_p^2 \, dV_p} \quad (3)$$

$$\Delta\rho_p = \left(\frac{b_p}{V_p} - \frac{b_S}{V_S}\right) \quad (4)$$

$b_p$ and $b_S$ are the coherent scattering lengths of the solvent and of the particle, respectively; namely, they are the sum of the scattering length of all the nuclei which constitute this particle also depending on the isotopic nature of the nuclei in the molecules, while $V_p$ and $V_S$ are the volumes of particle and the solvent molecules. In general, by computing each term in equation (1) with a certain number of adjustable parameters, such as the particle radius and so on, SANS data from a polydisperse system can be fitted to the measured *I(***q***)*. Moreover, the $\langle N_p \rangle$ and $\Delta\rho_p$ pre-factors are usually known so the only term involving adjustable parameters is related to the structural parameters through $V_p$ and $F(\mathbf{q})$. However, as can be argued from equation (4) in the case of asphaltene solutions, the contrast term $\Delta\rho_p$, cannot be precisely computed because the detailed molecular structure and the constituents of asphaltene molecules are not well known. Therefore, one more adjustable parameter is usually required to accommodate the amplitude of the scattering intensity. Grouping all the pre-factors equation (1) simplifies as:

$$I(\mathbf{q}) = A \, \langle |F(\mathbf{q})|^2 \rangle \quad (5)$$

Where the parameter dependence is embedded in the *A* factor. SANS data fitting can be achieved through equation (5) by assuming different particle shape and particle size distributions. In order to avoid ambiguous results that sometimes are obtained by using different models which seems to fit both the experimental data, Sheu and co-workers searched for constraints that could be imposed in fitting analysis. In particular, they define a justification parameter α as:

$$\alpha = \frac{A}{\langle N_p \rangle \, \langle V_p^2 \rangle} \quad (6)$$

This $\alpha$ parameter, is the apparent contrast between aggregates and solvent. In a homogeneous colloid, this parameter should be independent of asphaltene concentration at a given temperature if particle size and distribution assumed are correct. So, evaluating the functional behaviour of $\alpha$ with respect to the asphaltene

concentration the authors believe that this parameter could be a good indicator to verify the particle shape and size distribution used to fit the SANS data. To verify their hypotheses, the authors prepared two samples, named as BL1 and BL2, of asphaltenes at different concentrations in toluene. BL1 sample's concentration spanned from 1 % w/w to 20 % w/w and was analysed in the temperature range between 25 °C and 55 °C. BL2 sample's concentration spanned from 0.5 % w/w to 5 % w/w and was analysed in the temperature range between 25 °C and 43 °C. The SANS measures on the BL1 samples were performed just after their preparation, while that on the BL2 samples after an aging of 11 days. The effect of aging was observed on SANS data. The authors reported this effect by showing two intensity spectra of 1% and 5% of the BL1 and BL2 samples at 25 °C. They observed that $I(\mathbf{q})$ from BNL2 measurements increase more rapidly toward small **q** values, but are systematically lower than BNL1 for $\mathbf{q} > 0.03$. This means that, as the samples were prepared, a substantial number of small particles was dispersed in the solution (such as the BNL1 case), but these gradually aggregated to form larger particles at equilibrium (such as in BNL2). According to the authors, a possible justification of this phenomenon is that BNL1 samples were actually undergoing kinetic processes toward more stable thermal equilibrium during SANS measurements. The investigation of the time dependence of $I(\mathbf{q})$ revealed that the thermal equilibrium of BL1 samples is reached after 7 days. Based on this information, since the authors aim was to study the structure and polydispersity of asphaltene aggregates in thermal equilibrium and in one phase state, their successive analyses were concentrated only on the BNL2 samples that were aged for 11 days. Scattering intensity distributions were also recorded as a function of **q** for three asphaltene concentrations, namely 1%, 3% and 5% at 25°C, while $I(\mathbf{q})$ for 1% concentration was investigated at three temperatures, 25 °C, 35 °C and 45 °C. A sharp scattering was observed in the small **q** region in both cases. According to the authors, this implies the existence of disperse phase of different size colloidal particles whit the largest ones as the main contributors of $I(\mathbf{q})$ in the small **q** region. Moreover, the authors observed that the intensity $I(\mathbf{q})$ in the small **q** region decreases substantially as temperature increases, while it appears nearly temperature independent at larger **q**'s. According to the authors, a possible justification could be accounted to a dissociation of larger particles (the main contributors of $I(\mathbf{q})$ in the small **q** region) as the temperature increases. This can be seen as direct evidence that the large particles are aggregates (instead of molecules). However, the authors pointed out that since it is visually difficult to evaluate if there is a change of $I(\mathbf{q})$ in the large **q** region (>0.1 $Å^{-1}$) as temperature increases, it is not possible to argue that the small particles (the main contributors in the large **q** region) are molecules or aggregates of strong intermolecular interactions. Finally, the authors analysed all of the SANS data through various structural models along with several presumed size distributions. Based on the fitting quality and the dependence of the corresponding α value as a function of asphaltene concentration, they concluded that the most appropriate model to describe the asphaltene polydisperse system in toluene is to consider spherical-like asphaltene particles with a size distribution better described by Schultz distribution function, or rather a two-parameter distribution function commonly used for describing polymer systems. Moreover, investigating the size distributions of 1% asphaltene solution as a function of temperature (25°C; 100°C; 167 °C), the authors observed that the temperature increase induces the distribution to evolve from a Schultz-like to a Gaussian-like distribution (see figure 18).

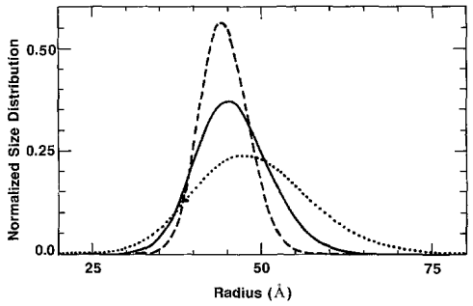


**Figure 18** Size distributions of 1% asphaltene solution as a function of temperature (dotted: 25°C; solid: 100°C; dashed: 167 °C). As temperature increases, the distribution evolves from a Schultz-like (right-hand skewness) to a Gaussian-like distribution, indicating the dissociation of large particles at higher temperature Reproduce from [117] (courtesy of Elsevier)

Moreover, from figure 18 it can be seen that the right-hand skewness of the Schultz-like distribution is reduced as temperature increases and that the particle size gradually evolves to a Gaussian-like distribution. Keeping in mind the inverse correlation between **q** and λ (see eq. 2) (big $\lambda$'s low **q**'s) and that low **q**'s represent the larger particles' scattering. This indicates that as temperature increases, larger asphaltene particles dissociate into smaller ones. The authors also noted that the size distributions for 25 Å < λ ≤ 35 Å vary as temperature increases. However, according to them the particles with sizes in this region require a **q** greater than 0.1 $Å^{-1}$ to resolve. Since the maximum **q** used was approximately 0.1 $Å^{-1}$, the size distribution extracted from analyses for particles of this size range should not be accounted for. Moreover, as authors stated, the larger particles are formed by self-association through some weaker interactions, and are thus easily overcome by dispersion energy (entropic energy). Because of their dissociation, the polydispersity is greatly reduced as temperature increases. On the other hand, as can be seen from figure 1 the particles with size of ~45 Å (the peak position of the distribution) are temperature independent. This indicates that these particles are either in molecular form or are aggregates formed by self-association through a much stronger intermolecular attraction force.

However, despite the good and solid arguments and the clear exposition of the work by Sheu et al., it is necessary to highlight that although the authors moves some critics to the work by Ravey et al. [112] as regards that their disk-like model for asphaltene aggregates in tetrahydrofuran does not consider polydispersity factors, Sheu and co-workers did not propose a counter analysis by investigating the Ravey system applying their model, even more so that the Sheu model is solvent dependent. However, to be exact it has to be said that in [124] an analysis of SANS data (among other investigation techniques used like surface tension, viscosity, dielectric relaxation, conductivity) obtained from samples of different asphaltenes concentration (1%, 2%, 4% and 8% w/w) in various toluene/pyridine solvent ratios was performed to study both the structure and polydispersity dependence on asphaltene concentration and on solvent mix ratio at 22 ° C. There, the authors come to the same conclusion that spherical-like shape particle and Schultz size distribution function represent the best fitting model (although they show only fitting curve of the 8% asphaltene in 30/70 solvent mixture SANS data, as depicted in figure 19, and no supplementary information data about other samples were released), but a study of asphaltenes in pure solvents (i.e. tetrahydrofuran or benzene or other asphaltene "good" solvents) different from toluene or toluene mixes has not been investigated.

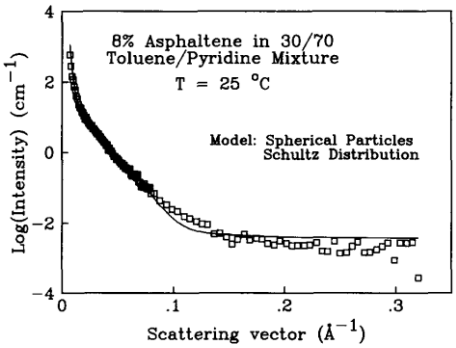


**Figure 19** A typical SANS intensity distribution in logarithmic scale. The solid line is the fit assuming the particle to be spherical with polydispersity following the Schultz distribution. The case depicted is 8% asphaltene in a toluene/pyridine mixture. Reproduced from [124] (courtesy of Elsevier)

Furthermore, in the above-mentioned paper [124] the SANS analyses showed that the average size of the asphaltene aggregates is not concentration dependent, meaning that particle growth is not an energy favourable process. On the contrary, the SANS studies on asphaltene aggregation in previous [118] and successive [117] works by the same authors showed that the association energy between monomers in an aggregate is quite high. To explain the apparent contradiction observed in [124] the authors hypothesized that from the thermodynamic point of view, the free-energy term that prevents growth could be the packing constraint as indicated also in other papers [125,126].

Shape and particle distribution model proposed by Sheu et al. [117] were confirmed by Xu et al. [127] although a SAXS technique was used and a different approach was adopted for data analysis. On the contrary to Sheu et al., the authors preliminary assumed that the particles are monodisperse and the theoretical scattering curve for various shapes, e.g. cylinder, lamella, flat disk of infinitesimal thickness and sphere, was fitted to the experimental results of $I(\mathbf{q})$ for the 5% and 15% asphaltene dispersion. According to authors this range of concentration was chosen to have reasonable SAXS curve within the instrument **q** range. Figure 20 depicts the fitting results for the 5% asphaltene dispersion.

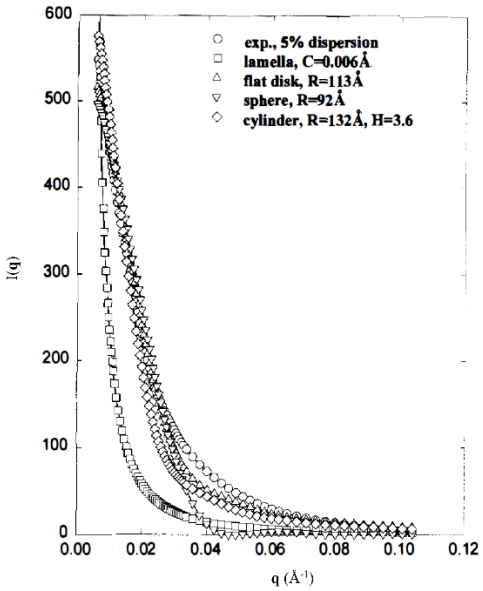


**Figure 20** Smeared SAXS intensity, $I(\mathbf{q})$, for solid asphaltenes and dispersions in toluene, at room temperature, before background correction. Reprinted from [127] (courtesy of Elsevier)

As it can be seen in Figure 20, the flat disk of R = 113 Å and infinite thickness appears showing the closest fit to experimental data but it's definitely not perfect, suggesting polydispersity. By using a distribution function F(***r***), which in turn is related to the correlation function $\gamma(\boldsymbol{r})$ whose trend was evaluated by the authors through the Fourier transformation of the $I(\mathbf{q})$ for the 5% and 15% asphaltene dispersion, they were able to show that colloidal asphaltene particles in the toluene solution could not be properly described by a disk-like model. Moreover, the fact that the main peak in of the F(***r***) function appears almost symmetrical suggests that the particles are essentially spherical. Once the authors have shown that the particle form was probably spherical, the size distribution was calculated from the SAXS intensity curve by a numerical inversion of the equation:

$$I(\boldsymbol{q}) = \int_0^\infty D_n(\boldsymbol{r}) V_p^2(\boldsymbol{r}) P(\boldsymbol{q},\boldsymbol{r}) d\boldsymbol{r} \tag{7}$$

by using Vonk's numerical method [128], where $D_n(\boldsymbol{r})$ is the numerical distribution function, which is proportional to the number of particles defined by the size parameter ***r*** in a unit interval. Plotting the $D_V(\boldsymbol{r})$ function which is the distribution function by volume, namely $D_V(\boldsymbol{r}) = \boldsymbol{r}^3 D_n(\boldsymbol{r})$ the authors observed, in accordance with the data of other researchers [106,117,124,129,130] that the main distribution peak at 33 Å is due to the primary asphaltene particles dispersed in toluene. This peak was skewed to the right, similar to a Schultz distribution at room temperature. Moreover, a second distribution peak at $r = 140$ Å for 5% and $r = 90$ Å for 15%. According to authors, the second peak may be due to coagulated species of the primary particles. However, comparing the two peaks the authors observed that the size of such coagulation species appears to decrease when the concentration of the dispersion increases from 5 to 15%. A possible explanation given by the authors was that the basic assumption, i.e. $S(\mathbf{q}) \cong 1$, is not entirely true and even at 5% some interparticle correlation occurs. It is then quite feasible that such interparticle correlation establishes itself as the second size distribution peak and that the size at this peak, which corresponds to the pair correlation length, decreases on increasing the particle concentration. This in turn may indicate a method of characterizing a colloidal system that is not entirely free from interparticle correlation, by the behaviour of the second size distribution peak. This means that it is almost impossible to rigorously separate $S(\mathbf{q})$ out of the $I(\mathbf{q})$ SAXS data for real colloidal systems, in which monodispersity is never realized.

As it can be seen from the studies discussed above, most of them proposed fitting models of the scattering data concerning dilute dispersed asphaltene systems. Generally, the asphaltene agglomerates or micelles reported have a size of about 2.5-15 nm, depending on the source of the asphaltenes and the solvent. However, as reported by Liu et al. [131], engine deposits from asphaltenes or heavy petroleum components may have very high asphaltene contents. On the basis of different previous studies [124,132,133] where the asphaltene micelles (from various vacuum residue including the Rotawi one analysed by Liu et al.) are polydisperse with a micellar diameter of about 6 nm, it is also known [117] that some asphaltenes tend to cluster even at a concentration lower than 1% w/w. The authors consider it reasonable to assume that asphaltenes would form micellar clusters in the concentration range investigated in their study. Moreover, following the idea of

previous studies on the fractal model applied to asphaltene aggregation in solution [134-136] Liu et al. [131], proposed that a fractal model could be suitable to analyse the SANS data obtained through Ratawi petroleum asphaltenes diluted in toluene in a concentration range from 10% to 80% and aged for two weeks to enable thermodynamic equilibrium. SANS data analysis by Liu et al. was performed by modelling the asphaltene aggregates as polydisperse fractal objects containing *k* monodisperse asphaltene micelles as unit particles. On the basis of a physico-mathematical discussion as well as the help of mathematical formulas in literature, [137-142] they proposed a rather complicated formula in which the intensity of scattering is correlated: 1) to the average number of the unit particles in a cluster through the parameter S, 2) to the degree of polydispersity of the cluster sizes for a given S through the $\tau$ parameter, 3) to the fractal dimension $D_f$ and 4) to the radius of gyration $R_1$ of the elementary unit particle composing clusters, namely $I(S, \tau, D_f, R_1)$. $S, \tau$ and $D_f$ are the adjustable parameters used in the data-fitting. Figure 21 shows the fitting results obtained by Liu et al. [131] for the various samples investigated. According to the authors, although different values of $D_f$ where tested for all SANS data, a unique convergence was found for the fitting curves. However, the authors did not specify if the same phenomenon happened by varying $S, \tau$ parameters.

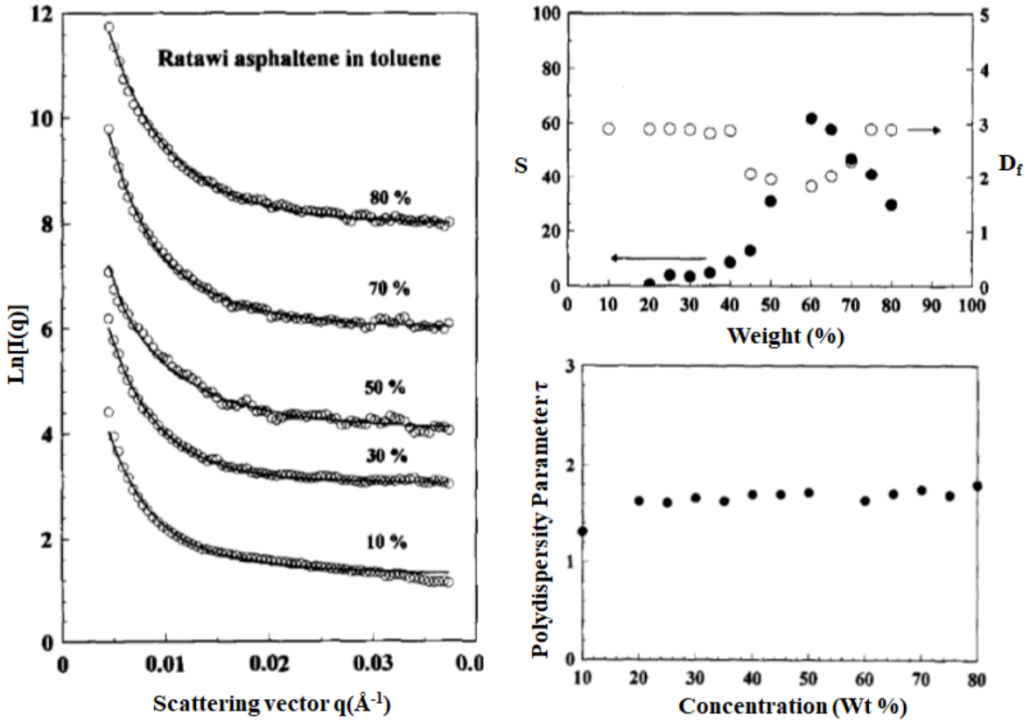


**Figure 21** Panel (a) represents the SANS intensity distributions for asphaltenes in toluene from 10 to 80 wt% concentration. Symbols are experimental data, and solid lines the fitted curves obtained through S, τ and $D_f$ as adjustable free parameters. The five curves are shifted trough an arbitrary constant to allow a better visualization. Panel (b) depicts the trend of S and $D_f$ parameters as a function of asphaltene concentration. Panel (c) depicts the trend of τ parameter as a function of asphaltene concentration Reproduced from [131] (courtesy of Elsevier)

As also noted by the authors some limitation of the model arises due to the fact that the modelled system consists of clusters formed by the linkage (depending in turn on the interactions between the unit particles) of a group of monodisperse unit particles. For example, in the 10% case and at very low **q** values the agreement between data and the calculated $I(\mathbf{q})$ shows a little discrepancy. Author's explanation relies on the fact that

there are practically no clusters in a 10 wt% solution and most of the micelles (the model's unit particles) remain dispersed. Being that the calculated curve is based on the existence of clusters it is expected to observe a discrepancy from the SANS data at this limit. This is particularly true for the low-$q$ region, where the main contribution to the $I(\mathbf{q})$ is given by the large particles. Moreover, the limitation of the model could not led to physically significant parameter values in the extreme cases. However, aside from this limitation, authors believe that their model is flexible because the fractal dimension and the polydispersity $\tau$ of the cluster are explicitly considered in concentration range where cluster formation can happen. According to the authors, the nearly constant low values of the $S$ parameter (see figure 21 panel (b)) in the 10% w/w to about 40%w/w concentration range means that the asphaltene micelles (the unit particles that form clusters) do not seem to form big clusters. On the contrary, as the concentration exceeds the 40 w/w%, large clusters start to form and $S$ increases dramatically reaching a maximum value at 60 %w/w. The behaviour of $S$ implies that the micelles form fractal clusters rapidly when the concentration exceeds 40 %w/w. At the same time, the fractal dimension $D_f$ decreases from ~ 3 (typical of three-dimensional packing) to ~ 1.8 in agreement with the $D_f$ values obtained by Raghunathan et al. [143] through electron paramagnetic resonance (e.p.r), while the polydispersion parameter $\tau$ remain almost constant except for 10% w/w case. From a thermodynamic point of view the fact that the micelles remain dispersed below 40% w/w means that entropic contribution dominates the free energy of the system. As the asphaltene concentration increases more unit particles and small clusters will be created. As a consequence, when the concentration exceeds 40% w/w, the inter-micellar interactions overcome the entropic energy and start to bring the micelles together to form clusters. Furthermore, as it can be observed from panel (b) of figure 21 above the 60% w/w asphaltene concentration the $S$ and $D_f$ parameter start to decrease and increase respectively as if the system becomes dilute again. According to the authors, this behaviour can be explained considering that system reaches its maximum packing fraction at 60% w/w. Above the 60% w/w the above described behaviour of $S$ and $D_f$ is attributed to phase inversion (i.e. toluene becomes the dispersed phase and asphaltenes become the solvent) commonly observed in surfactant systems [144]. Finally, from the constant values of $1.7 \pm 0.1$ of the $\tau$ polydispersity parameter (panel (c) of figure 21) in the 40% to 80% concentration range the authors hypothesize that clusters formation is triggered by a Reaction Limited Aggregation (RLA) mechanism. Indeed, several studies have shown that the RLA mechanism leads to a $\tau$ value of about 1.5. Barré et al. [145] used SAXS and SANS techniques, alongside the Cryo Scanning Electron Microscopy (Cryo-SEM) to investigate and better understand the mechanisms of some problems. These problems result from asphaltene flocculation and deposition which occurs during industrial crude oil production transportation and refining processes such as clogs in the pore pipes in the near wellbore zone, giving rise to a huge product reduction. These mechanisms cannot be explained through the basic information gained about asphaltene chemical composition and their organic structure studies. For example, if crude oils having the same composition can or can't produce deposits. The systems studied by Barré et al. were: 1) asphaltenes or resins in solution with different solvents, 2) several solvents suspensions of asphaltene and resin mixtures and 3) crude oils and heaviest fractions without any prior fractionation; the latter point has been

investigated only in few studies. The size polydispersity and the weight average molecular weight as a function of temperature of these systems was investigated.

SAXS or SANS data analysis was performed in the "classical" way, namely finding an adequate structural model, calculating the scattering curve corresponding to this model and finally fitting the model parameters to the experimental data using for instance, a least-square procedure. Moreover, a lognormal size distribution function was used to take into account the system polydispersity. Table 2 shows the crude oil investigated and their asphaltene chemical composition.

**Table 2** Composition of the various asphaltenes which were investigated and the asphaltene concentration in these crude oils [145] (Open Access)

| Crude oils Asphaltene contents (% w/w) | Asphaltene chemical composition |
|---|---|
| A - 0.6% | $C_{7.27}$ $H_{8.0}$ $N_{0.055}$ $O_{0.2}$ $S_{0.023}$ |
| B - 14% | $C_{6.79}$ $H_{8.02}$ $N_{0.13}$ $O_{0.1}$ $S_{0.215}$ |
| C - 4% | $C_{7.35}$ $H_{8.57}$ $N_{0.112}$ $O_{0.08}$ $S_{0.011}$ |
| D - 1% | $C_{7.36}$ $H_{7.9}$ $N_{0.095}$ $O_{0.13}$ $S_{0.008}$ |
| E - 24% | $C_{6.73}$ $H_{6.88}$ $N_{0.005}$ $O_{0.06}$ $S_{0.357}$ |
| F - 1.5% | $C_{6.96}$ $H_{7.2}$ $N_{0.078}$ $O_{0.07}$ $S_{0.228}$ |
| G - 9% | $C_{6.68}$ $H_{7.69}$ $N_{0.005}$ $O_{0.08}$ $S_{0.337}$ |
| H - 4% | $C_{6.825}$ $H_{6.5}$ $N_{0.093}$ $O_{0.11}$ $S_{0.159}$ |
| Safaniya vacuum residue - 15% | $C_{6.87}$ $H_{7.49}$ $N_{0.072}$ $O_{0.08}$ $S_{0.236}$ |

Particularly interesting is the author's statement that several models to shape the particles (spheres, disks or ellipsoids) tested for the curve fitting of large q-values data can fit experimental data. According to the authors this comparison will probably end the existent debate about the shape of asphaltene molecule [112,130,146].

Tanaka et al. [147] performed SANS measurements on asphaltenes from different crude oils: a Mexican crude oil (Maya), Arabian heavy oil (Khafji), and an Iranian light oil, abbreviated as MY, KF, IL respectively, in three different solvents, deuterated Decalin (Dec), 1-methylnaphthalene (1MN) and quinoline (Qui), in a range of temperatures up to 350 °C in order to better understand the relationship between asphaltene properties and aggregates structures. According to the authors the studies about:1) size and shape of asphaltene aggregates from various crude oils, 2) effects of solvent and temperature condition on size and shape of aggregates, and 3) relationship between molecular structure of asphaltenes and the size and shape of their aggregates are of primary importance even beyond basic scientific interest so as to understand industrial crude oil process problems such as the large amounts of sludge and sediment due to asphaltene aggregation during visbreaking and catalytic hydrocracking [148], due to the flocculation of asphaltenes during processing [149]. Figure 22 shows the SANS spectra obtained by investigating 5% w/w concentration asphaltene dispersion in deuterated Decalin, 1-methylnaphthalene, or quinoline.

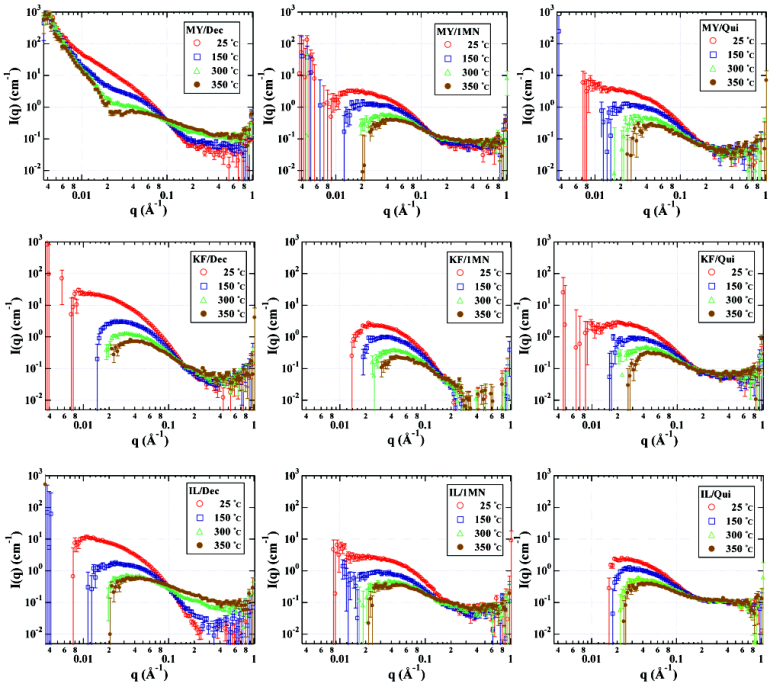


**Figure 22.** Plots of log(I) vs log(q) for the 5 wt % asphaltenes from the three different crude oils sources, in Decalin (Dec), 1-methylnaphthalene (1MN), and quinoline (Qui) at 25, 150, 300, and 350 °C. Reproduced from [147] (courtesy of ACS)

The data in the region of $0.02 < \mathbf{q} < 0.12$ Å$^{-1}$ show the coherent scattering from asphaltene aggregates. With scattering data at this **q** region of coherent scattering, we can get topological information about aggregates within the range of ten to several hundred angstroms. With the data at the lower ***q*** region, information about larger structures can be deduced. Data at a larger **q** region is incoherent scattering, which is determined only by composition of the solutions in the beam path of a neutron, in other words, by concentration of asphaltenes. The analysis of size and shape of aggregates in the various solvents was performed by combining information from the power-law behaviour in the low q region and nonlinear regression analysis using different particle topologies (sphere and ellipsoid) for the form factor $F(\mathbf{q})$. Moreover, to allow the use of the equation proposed to fit the data, a strong assumption that a q-region can be made in which $S(\mathbf{q})$ factor tends to be 1, although said by the authors to be true only at high q-values. According to the authors, to simplify the sample's comparison and to better understand the relationship between the properties of asphaltenes and their aggregation phenomena in the solvents, a monodispersity model was applied as a first approximation to gain the representative values of the aggregates size. However, as authors themselves recognise, polydispersity analysis is also important to understand the distribution of the asphaltene aggregate's size. Fitting analysis results have shown that the shapes of asphaltene aggregates are a prolate ellipsoid with high aspect ratio at low temperature and it becomes a sphere with increasing temperature. Depending on their crude oil sources, solvents and temperature the size of asphaltene aggregates changes. Among the three asphaltene sources, the Mexican (Maya) one, tended to form largest aggregates in any solvents. Moreover, as it can be seen from figure 22, Mexican asphaltene sample in Decalin (MY/Dec) shows intensity data - that persists even at 350 °C - in the region of $\mathbf{q} < 0.01$ Å$^{-1}$ as opposed to all other samples which do not show signal. The author supposed that the neutron scattering in that region is due to a fractal network of asphaltene Mexican asphaltene sample

and hypothesized that it may be due to the high coking tendency of Maya asphaltene. As for the two other asphaltene types, Khafji asphaltene aggregates show the influence of interparticle interactions, while Iranian Light asphaltene precipitates extensively in Decalin at lower temperature owing to its high aromaticity. Later on, Tanaka et al. [150] characterized asphaltene aggregates isolated from the three different crude oils studied in their previous work [147] as well as the vacuum residua - obtained through vacuum distillation of same crude oils - asphaltene aggregates under various conditions through X-ray diffraction (XRD) and Small Angle X-ray Scattering (SAXS). Based on the literature data derived from SANS and SAXS studies and from the XRD and SAXS results obtained in their work, the authors proposed an hypothetical asphaltene aggregation hierarchy – as shown in figure 23 that starts with core aggregates formation, driven mainly by the $\pi - \pi$ stacking of asphaltene molecules (20 Å in size), which in turn form secondary aggregates that result from interactions with media, maltenes, oils, or solvents (50-500 Å) and finally fractal aggregates, that result from diffusion - limited cluster aggregation (DLCA) or reaction-limited cluster aggregation (RLCA), independent of any media (>1000 Å).

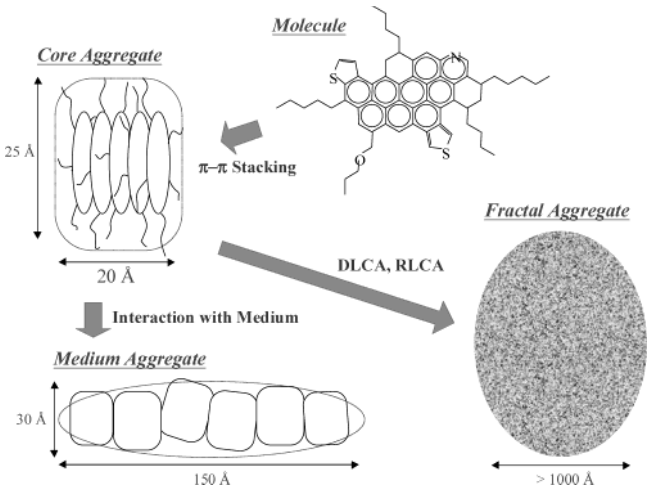


**Figure 23** Hypothetical representation of the hierarchy in asphaltene aggregations based on XRD, SAXS, and SANS data. Reprinted from [150]. (courtesy of ACS)

Spiecker et al. [151] by building solubility curves, using vapor pressure osmometry (VPO) and SANS analysed the characteristics of asphaltene – from four crude oils (Arab Heavy, B6, Canadon Seco, and Hondo) – and their subfractions obtained through dissolution in heptane and toluene mixtures (called heptol). Through asphaltene solubility and aggregate size measurements in different solvents (toluene, 1-methylnaphtalene) and temperature (25 °C, 80 °C), the authors tried to shed light on the complex mechanisms of asphaltenes aggregation. By comparing the data from elemental analysis, VPO, and SANS, the mechanisms that influence the solubility and aggregation of asphaltenes in solution were proposed.

First of all, asphaltenes were isolated from the four crude oil sources, by precipitating them by n-heptane solvent. The four samples obtained were denominated “whole” asphaltene to distinguish them from the various fraction obtained later on. To determine the solubility profile, the authors prepared asphaltene solutions with a concentration of 0.75% w/v or 1 wt% w/v by dissolving the asphaltenes in 15 ml of an heptol solutions of different solvent compositions. The various filtrate and precipitates - the latter dissolved in hot methylene chloride- contain respectively the more soluble asphaltenes and the less soluble in heptol. Small Angle Neutron

Scattering (SANS) was performed on the various samples prepared. Authors also specified that most of the SANS measurements were performed on a spectrometer that allows a measure **q** range extended from 0.0015 $Å^{-1}$ to 0.6 $Å^{-1}$, while the SANS data recorded for the "Whole" Asphaltenes of Hondo crude oil was collected on Small-Angle Neutron Diffractometer (SAND) instrument that allows a **q** range from 0.0035 $Å^{-1}$ to 2 $Å^{-1}$, although they did not specify if there were some technical reasons for that choice. The Ornstein–Zernike formalism was used to describe the correlation between scattering Intensity $I(\mathbf{q})$, scattering vector q and the solute correlation length $\xi$ and the data were fitted through a Lorentzian function using nonlinear least-squares regression to determine the aggregate size and shape. Based on the shape of the neutron scattering curves and according to the authors it is possible to distinguish between solutions of small aggregates from flocculated systems. For example, they described the behaviour of the "Whole" asphaltene sample of B6 crude oil. Figure 24 depicts the trend of B6 asphaltene sample in various heptol solutions.

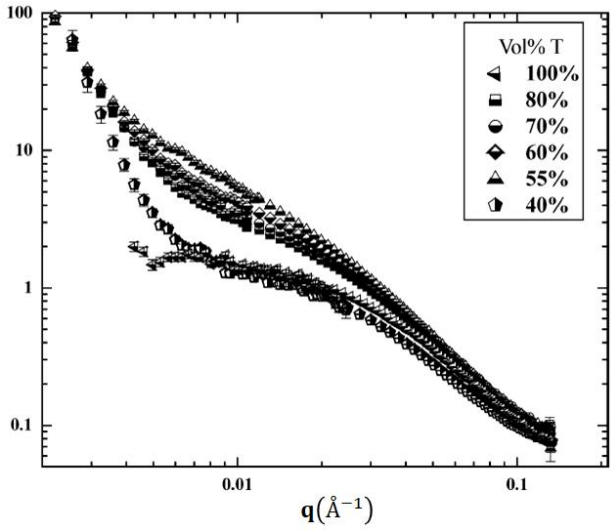


**Figure 24.** Logarithmic plot of SANS curves obtained from a solution at 1% w/w of B6 Whole asphaltenes in mixtures of d-heptane and d-toluene 25 ◦C. Reproduced from [151]. (courtesy of Elsevier)

As discussed by the authors, the low-q plateau in pure toluene indicates that the nanoparticle aggregates present in the solution are soluble and do not undergo flocculation process. The other solvent mixture curves exhibited an intense low-q feature. According to the authors, as the solvent aromaticity reduces, a small fraction of the nanoparticle aggregates form microscale "flocs" that retained their solubility in solution. Moreover, the absence of a plateau region in the lowest q range suggested that the size of these large flocs is greater than the order of $1/q_{min}$ (or >1000 Å). The authors also deduced that the floc size must have been smaller than 1.5 μm, because all solutions above 55% toluene were soluble to filtration. From the intensity trend shown by the various curves in figure 24, it can be guessed that the nanoparticle aggregates were the largest in 55% toluene with aggregate size decreasing as the solvent quality became more aromatic. Furthermore, by recording the SANS spectra at 80 °C, the authors have shown a decrease of the $I(\mathbf{q})$ in the low-q region, while after cooling down the sample at 25 °C similar scattering intensity reappeared. According to the authors, this could suggest that an equilibrium condition is established between the nanoparticle aggregates and microscale aggregates at this temperature. Similar to the Whole asphaltenes, the aggregate sizes of the Soluble asphaltenes decreased

solvent aromaticity increases, while precipitate asphaltenes showed substantial overlap in scattering intensity between large agglomerates and smaller aggregates, and suggested a higher degree of intermolecular association than the Whole and Soluble fractions. Correlation length $\xi$ of "Whole" asphaltenes, soluble asphaltenes and precipitated asphaltene samples at different heptol concentration were deduced from SANS data. Figure 25 shows the trend of correlation length $\xi$ at various heptol concentrations.

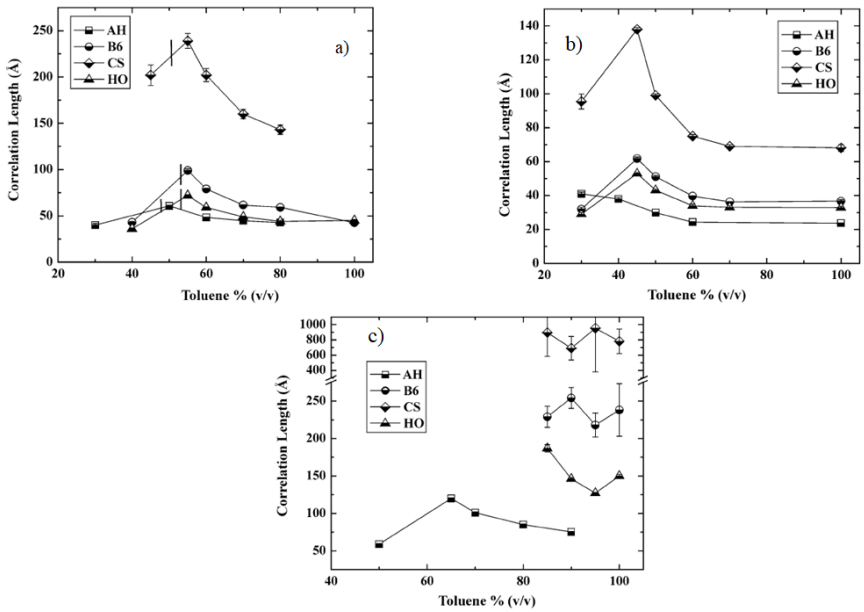


Figure 25. Correlation lengths determined by SANS of a) "Whole" asphaltenes in heptol: 1 wt%, 25 ◦C. The vertical lines represent the solubility limit, b) Soluble asphaltenes in heptol 1 wt%, 25 ◦C and c) Precipitate asphaltenes in heptol 1 wt%, 25 ◦C. Reproduced from [151]. (courtesy of Elsevier)

According to the authors, in the soluble region – i.e. from 100% toluene to the solubility limit indicated by vertical lines - the increase in correlation length for each of the "Whole" asphaltenes as the solvating power of heptol decrease (low percentages of toluene) correlates to an increase of the interaggregate associations. For each of the asphaltenes the correlation length increased with decreasing toluene content within the soluble regime. The maximum correlation length was near the solubility limit of the Whole asphaltenes. Below the solubility limit, precipitation of the largest aggregates lowers the correlation lengths of the asphaltenes, because in this region, correlation length is only a measure of the material remaining in solution. As can be seen from figure 21, the Soluble asphaltene fraction shows a similar trend as the "Whole" ones, although the correlation length is lower. On the contrary, Precipitate asphaltene fraction forms the largest aggregates; it has the highest correlation length. An interesting observation can be made about the Hondo and B6 asphaltene Precipitate fraction. It can be seen as slight, yet reproducible, decrease in aggregate size (correlation length) for solutions in 95% toluene compared to pure toluene. However, further toluene reduction increases the correlation. Similar behaviour was reported also by Fenistein et al. [152] for two chemically different asphaltenes dissolved in toluene. A possible explanation was put forward to a decrease in the intrinsic viscosity that the heptol solution shows below the 15 % v/v of the heptane concentration. Indeed, upon heptane addition, the correlation length and so the aggregate size increases again up to the flocculation threshold. From the SANS studies, the authors

also proved a cooperative interaction between the Soluble and Precipitate asphaltene fractions. Speaking of which they observed that the "Whole" asphaltenes (the show only the case of the Hondo samples) had a lower correlation length than that predicted by the hypothetical recombination of the Soluble and Precipitate fractions. According to the authors, this suggests a cooperative interaction between the two asphaltene fractions. As a result of their investigation, the authors concluded that of four crude oils asphaltenes, Canadon Seco forms the largest aggregates in heptol and that due to the high aromaticity of the Canadon Seco asphaltenes (low H/C ratio) the most plausible mechanism of aggregation appeared to be the aromatic π–π bonding interaction. B6 and Hondo asphaltene aggregates in heptol are smaller than the corresponding Canadon Seco and due to their low aromaticity, the aggregation mechanism is likely driven by polar interactions. Arab Heavy asphaltenes, possess relatively high aromaticities (low H/C ratios) and formed the smallest aggregates. The major difference in the aggregation behaviours of largest Canadon Seco and smallest Arab Heavy aggregates, is the ability of the latter to participate in polar and H-bonding interactions. SANS data also indicate that the less soluble (more polar) asphaltenes contribute the majority of the species responsible for asphaltene aggregation in solution. According to the authors this fraction is the main responsible factor behind the problems encountered in crude oil production.

Later on, Spiecker et al. [153] investigated the effect of the addition of crude oil resins on asphaltene aggregation and on the water-oil emulsion formation and stability. First of all, the authors found that resins appear to enhance the solubility of the polar and aromatic Precipitate asphaltenes more than the Soluble asphaltenes. The latter do not respond as favourably to resins. From SANS data, authors observed that - compared to the spectra with no resins added - a decrease in intensity in low **q** region with increasing resin content. According to them, this could indicate that resins were effective at dissolving the larger flocs into non-interacting aggregates. Figure 26 shows the $I(\mathbf{q})$ trends of resin isolated from B6 crude oil added at various concentration in a Canadon Seco Whole asphaltenes sample.

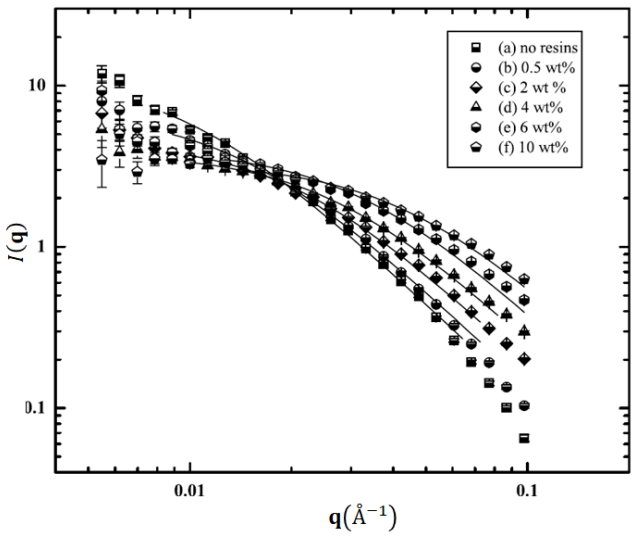


**Figure 26**. SANS fits using Lorentzian function. Canadon Seco Whole asphaltenes at 25 °C in 60% toluene with: (a) No Resins: (b) 0.5 wt.% B6 Resins (c) 2 wt.% B6 Resins (d) 4 wt.% B6 Resins (e) 6 wt.% B6 Resins (f) 10 wt.% B6 Resins. Reproduced from [153] (courtesy of Elsevier)

Moreover, a drastic reduction of the correlation length $\xi$ from 101 Å in the sample with no added resins to 23 Å in the sample with 10% resins was noted. The authors suggest two possible effects to explain this result. One, which they consider trivial, is that with increasing resin concentration the latter form small aggregate on their own and upon mixing to the asphaltene aggregates the average particle size is expected to decrease. On the other hand, the solubility measures done by the authors have shown that resins play a role in enhancing asphaltene solubility in solution so an asphaltene-resin model interaction seems to be more plausible. Bardon et al. arrived at a similar conclusion [154] by comparing the scattering curve of an asphaltene-resin mixture to the sum of the scattering intensities from pure samples. Since the sum of the individual scatterers was larger than the scattering by the mixture, they concluded that asphaltenes were solvated by resins. According to the authors it is not known to what extent the aggregates can be dissociated by resin addition. The presumed minimum would be a single asphaltene monomer solvated completely by resins. The authors have also shown that resins from different sources may be approximately equal in effectiveness at solvating asphaltenic aggregates (see figure 26). Gawrys and Kilpatrick [155] evaluated various mono and polydisperse intra-particle structure factor models as applied to the SANS scattering spectra obtained from asphaltenes isolated from the four crude oils studied in their previous works [151,153] namely, Arab Heavy, B6, Canadon Seco, and Hondo, in mixtures of deuterated solvents like toluene, methanol and heptane. Monodisperse spheres, monodisperse oblate cylinders, monodisperse prolate cylinders, polydisperse spheres, polydisperse length oblate cylinders, and polydisperse radius oblate cylinders assuming a Schultz distribution function of particle sizes were tested. The authors tried three different models to fit the data, namely Guiner approximation [156] from which $I_0$ values (i.e. scattering intensity extrapolated to $\mathbf{q} = 0$) and the radius of gyration $R_G$ - the defined as the root mean squared distance of all atoms from the centre of mass of the particle – are determined, the small-particle mass-fractal model previously discussed and the model based on the introduction of the intraparticle form factor $F(\mathbf{q})$ which we discussed previously. According to the authors, the comparison between the $I_0$ and $R_G$ values obtained from the interparticle model data fitting with those obtained from Guinier suggests that such a form factor model is physically reasonable. Moreover, the authors also determined the reduced $\chi^2$ values for each non-linear least square model fits - for the entire $\mathbf{q}$ range studied - for the scattering intensity distribution to assess the quality of each model respect to the others. Table 3 shows, among the others, the values of $I_0$ $R_G$ and $\chi^2$ for the various models.

**Table 3**. Comparison of fit parameters obtained from the Guinier approximation small-particle mass-fractal models and from various monodisperse and polydisperse form factor models. Reprinted from [155]. (courtesy of Elsevier)

| Asphaltene | Guinier approximation | | | Small-particle mass-fractal | | | | |
|---|---|---|---|---|---|---|---|---|
| | $I_0$ (cm$^{-1}$) | $R_G$ (Å) | $QR_G$ | $I_0$ (cm$^{-1}$) | $\xi$ (Å) | $D$ | $R_G$ (Å) | $\chi^2$ |
| Hondo (90:10 Tol:MeOD) | 1.08 ± 0.03 | 43 ± 3 | 0.986 | 1.07 ± 0.02 | 23.9 ± 0.5 | 2.61 ± 0.02 | 52 ± 2 | 0.8091 |
| Hondo (40:60 H:T) | 4.2 ± 0.2 | 71 ± 5 | 1.005 | 4.15 ± 0.06 | 38.7 ± 0.6 | 2.52 ± 0.02 | 82 ± 2 | 1.6089 |
| Canadon Seco (toluene) | 3.0 ± 0.1 | 58 ± 5 | 0.945 | 3.20 ± 0.05 | 34.3 ± 0.6 | 2.63 ± 0.02 | 75 ± 2 | 1.7325 |
| Arab Heavy (toluene) | 1.48 ± 0.04 | 45 ± 3 | 0.990 | 1.49 ± 0.02 | 22.0 ± 0.5 | 2.76 ± 0.03 | 50 ± 2 | 0.9080 |
| Model fit | $I_0$ (cm$^{-1}$) | $R_{avg}$ (Å) | $\sigma_R$ (Å) | $L_{avg}$ (Å) | $\sigma_L$ (Å) | $\langle R_G^2 \rangle^{1/2}$ (Å) | $\chi^2$ | |
| Hondo asphaltenes (90:10 toluene:methanol) | | | | | | | | |
| Monodisperse spheres | 0.62 ± 0.01 | 35.7 ± 0.1 | – | – | – | 27.7 ± 0.1 | 48.381 | |
| Monodisperse prolate cylinders | 1.12 ± 0.02 | 20.7 ± 0.1 | – | 186 ± 5 | – | 56 ± 2 | 9.5199 | |
| Monodisperse oblate cylinders | 0.88 ± 0.01 | 52.8 ± 0.3 | – | 12.2 ± 0.6 | – | 38 ± 2 | 4.3489 | |
| Schultz polyradius spheres | 0.91 ± 0.01 | 0.69 ± 0.02 | 2.40 ± 0.04 | – | – | 0.68 ± 0.02 | 4.9721 | |
| Schultz polylength oblate cylinders | 0.88 ± 0.01 | 52.7 ± 0.3 | – | 12.1 ± 0.6 | 0.5 | 38 ± 2 | 4.3488 | |
| Schultz polyradius oblate cylinders | 0.98 ± 0.01 | 42.6 ± 0.9 | 13.5 ± 0.3 | 15.1 ± 0.6 | – | 45 ± 4 | 1.3845 | |
| Hondo asphaltenes (40:60 heptane:toluene) | | | | | | | | |
| Monodisperse spheres | 1.61 ± 0.01 | 44.1 ± 0.1 | – | – | – | 34.2 ± 0.1 | 173.7 | |
| Monodisperse prolate cylinders | 179 ± 1 | 7.6 ± 0.2 | – | 11280 ± 50 | – | 3260 ± 30 | 9.5825 | |
| Monodisperse oblate cylinders | 3.29 ± 0.03 | 79.6 ± 0.4 | – | 20.3 ± 0.3 | – | 57 ± 1 | 12.833 | |
| Schultz polyradius spheres | 2.92 ± 0.02 | 0.55 ± 0.04 | 2.52 ± 0.08 | – | – | 0.43 ± 0.03 | 26.086 | |
| Schultz polylength oblate cylinders | 3.29 ± 0.03 | 79.5 ± 0.4 | – | 19.9 ± 0.3 | 2 | 83 ± 2 | 12.830 | |
| Schultz polyradius oblate cylinders | 4.14 ± 0.04 | 69.4 ± 0.7 | 22.3 ± 0.1 | 20.5 ± 0.3 | – | 73 ± 2 | 5.7508 | |
| Canadon Seco asphaltenes (toluene) | | | | | | | | |
| Monodisperse spheres | 1.43 ± 0.01 | 44.8 ± 0.1 | – | – | – | 34.7 ± 0.1 | 125.98 | |
| Monodisperse prolate cylinders | 151 ± 1 | 8.4 ± 0.3 | – | 11260 ± 60 | – | 3300 ± 100 | 8.1415 | |
| Monodisperse oblate cylinders | 2.56 ± 0.02 | 75.3 ± 0.4 | – | 20.5 ± 0.4 | – | 54 ± 1 | 11.548 | |
| Schultz polyradius spheres | 2.48 ± 0.02 | 0.66 ± 0.05 | 2.8 ± 0.1 | – | – | 0.51 ± 0.04 | 13.895 | |
| Schultz polylength oblate cylinders | 2.55 ± 0.02 | 74.7 ± 0.4 | – | 13.7 ± 0.8 | 7 | 53 ± 3 | 11.254 | |
| Schultz polyradius oblate cylinders | 2.84 ± 0.03 | 60 ± 1 | 18.9 ± 0.3 | 25.6 ± 0.4 | – | 58 ± 5 | 2.9527 | |
| Arab Heavy asphaltenes (toluene) | | | | | | | | |
| Monodisperse spheres | 0.88 ± 0.01 | 35.6 ± 0.1 | – | – | – | 27.6 ± 0.1 | 73.381 | |
| Monodisperse prolate cylinders | 1.66 ± 0.03 | 21.2 ± 0.1 | – | 194 ± 5 | – | 58 ± 2 | 12.303 | |
| Monodisperse oblate cylinders | 1.26 ± 0.01 | 52.6 ± 0.3 | – | 17.1 ± 0.4 | – | 38 ± 1 | 6.5966 | |
| Schultz polyradius spheres | 1.33 ± 0.01 | 0.71 ± 0.04 | 2.47 ± 0.07 | – | – | 0.55 ± 0.03 | 4.2643 | |
| Schultz polylength oblate cylinders | 1.26 ± 0.01 | 52.5 ± 0.3 | – | 16.6 ± 0.4 | 2 | 83 ± 2 | 6.5948 | |
| Schultz polyradius oblate cylinders | 1.38 ± 0.01 | 41.4 ± 0.9 | 13.2 ± 0.2 | 20.8 ± 0.7 | – | 45 ± 3 | 1.8979 | |

As a result of their investigation the authors concluded that the asphaltene aggregate structure – regardless the solute chemistry and solvent properties - is best described by a polydisperse oblate cylinder model. In another study, Gawrys et al. [157] investigated the solvation effects within the aggregates of asphaltene samples obtained from the same type of crude oil investigated in their previous studies – which we discussed above. The notion that asphaltenes entrain solvent or are "swelled" by interactions with the surrounding solvent media is known. As an example, Sirota [158] from the analysis of SAXS spectra found a swelling effect of "dry" Cold Lake asphaltenes by increasing dilution by 1-methylnaphthalene solvent. Carbognani et al. [159] through volumetric swelling studies found that the addition of ~1.5 mL of solvent to 300 mg of dry asphaltenes induces an expansion of the packed asphaltene volume from 10% to 70%. Other studies [133,160,161,162] suggested that the solvated volume of the asphaltenic aggregates was 1.7-2.7 times the unsolvated or asphaltene volume, implying a volumetric entrainment of about 40-60%. In [157] Gawrys et al. observed some discrepancies between average aggregate molecular weight values obtained from two different models. According to the authors, these discrepancies suggest the necessity to include the solvation effects in the calculations. The authors found that the solvent entrainment within the aggregates roughly varied from 30 to 50% (v/v) and was consistent with solvation values obtained from viscosity measurements found in the literature.

Headen et al. [163] performed small angle neutron scattering (SANS) and Very Small Angle Neutron Scattering (V-SANS) experiments on two crude oils. The authors investigated the temperature dependence of the size of asphaltene aggregates in their natural crude oil surrounding environment. Moreover, the authors have shown that SANS measurements on crude oils give similar sizes, and temperature-dependence of size, to those found from SANS measurements of asphaltenes redispersed in deuterated toluene. Data analysis was achieved by the fitting of Beaucage functions over two size regimes. Fitting analysis at very low-**q** have shown that the there are two separate species present, namely not all the smaller aggregates are part of the larger aggregates and just 2% of asphaltene molecules are in the larger aggregates large-scale.

Eyssautier et al. [164] compared SANS and SAXS measurements on a large q-scale performed on the same dilute asphaltene-toluene solution. The goal of the work was to give insight into a nanoaggregate structure. According to the authors SANS and SAXS spectra - reported in figure 27 - superimpose at small **q** values meaning that asphaltenes are homogeneous objects at large length scale. However, in the high **q** range, the spectra differ significantly. This discrepancy can be ascribed to the heterogeneities of asphaltene particles at small length scale, which is characteristic of their fine structure.

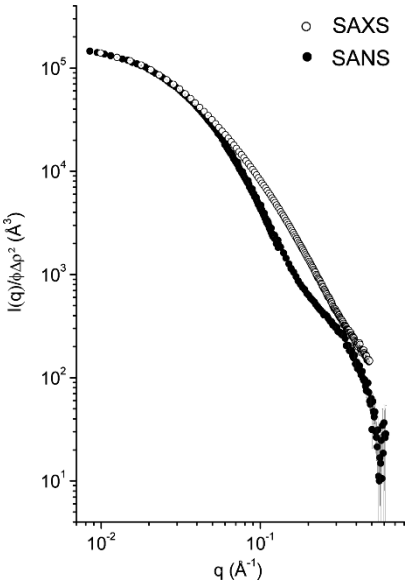


**Figure 27.** SANS and SAXS spectra of a 5 g/L asphaltene solution in deuterated and normal-toluene respectively. Intensities are normalized by the mean contrast term and the asphaltene volume fraction. Reprinted from [164]. (courtesy of ACS)

Direct comparison of neutron and X-ray spectra enables description at high **q** of a fractal organization made from the aggregation of small entities of 16 kDa, exhibiting an internal fine structure. Neutron contrast variation experiments enhance the description of this nanoaggregate in terms of core-shell disk organization, as depicted in figure 28.

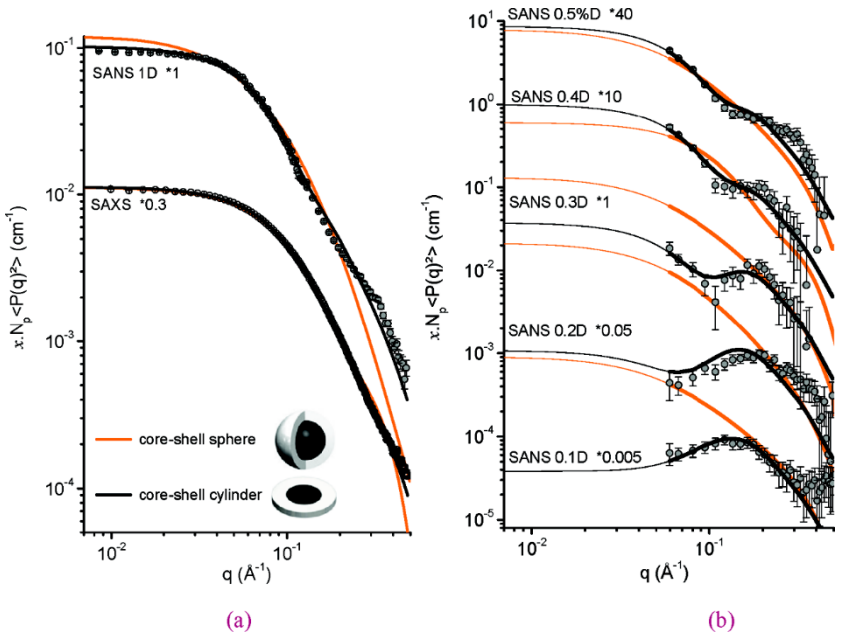


**Figure 28.** Rescaled spectra of (a) SAXS and SANS 100% D (5 g/L in H- and Deuterated (D)-toluene respectively) and (b) SANS contrast variation (50 g/L in toluene at various H/D ratios) asphaltene spectra divided by S(q). Reprinted from [164]. (courtesy of ACS)

The nanoaggregates are best described by a disk of total radius of 32 Å with 30% polydispersity and a height of 6.7 Å. Composition and density calculations show that the core is a dense and aromatic structure, contrary to the shell, which is highly aliphatic. These results show a good agreement with the general view of the Yen model.

However, by considering that the molecular weight of the asphaltene molecule found in literature is around 750 ± 250 g/mol [64] the nanoaggregate found by Eyssautier et al. [164] accounts for about 20 ± 5 elementary molecules, which are in contrast with aggregation numbers – around 8- reported in the literature found by different technique like $^{1}$H NMR, gravitational gradients and conductimetry measurements [67,165,166].

Hoepfner et al. [167] used SANS to study some important items about asphaltene structure and stability of two crude oils (Oil A and oil B) - compared to a "model" oil obtained by dispersing a third type asphaltene in deuterated toluene - after their n-heptane destabilization. The latter was achieved by adding n-heptane at various concentrations and time intervals following the procedure of Maqbool et al. [168]. The instantaneous onset precipitation is the concentration of heptane that produces insoluble asphaltenes that can be observed by optical microscopy after less than 15 min of mixing. Lower precipitant concentrations will require longer destabilization times to detect the asphaltene instability. For Oil A and Oil B and "model" oil, the instantaneous onset heptane concentration was 40 %v/v 50 % v/v and 50 % v/v respectively. On the contrary, the authors called the destabilization time the time that elapses between mixing an oil with precipitant and performing the scattering experiments. Precipitated asphaltenes that can cause significant surface scattering which increases the difficulties of analysis of the nanometre-sized asphaltenes were opportunely centrifugated. Fractal structure of asphaltenes in crude oil-precipitant systems, structural differences between soluble and insoluble asphaltenes, initiation of asphaltene destabilization at dilute precipitant concentrations, and the crude oil fraction(s) that causes small-angle scattering of the crude oils were investigated by the authors. According to

the latter, due to the statistical fluctuations caused by thermal motion, the soluble asphaltene clusters are in a state of complex dynamic equilibrium where different asphaltene nanoaggregates and molecules continuously exchange and rearrange. As the precipitant concentrations grows, the highly unstable asphaltenes tend to precipitate and the asphaltenes that remain dispersed at the nanometre length scale are the most stable ones that also have the smallest fractal clusters. Hoepfner and co-workers also found that – independently from heptane concentration - asphaltenes soluble fraction of crude and "model" oil tends to associate into fractal clusters that have a characteristic fractal dimension that is smaller compared to that of the insoluble asphaltene clusters. Moreover, the observation of fractal dimension changes through transition from soluble to insoluble reveals that the structure of the fractal clusters is modified. The last can be ascribed to a change in the packing organization of individual asphaltene nanoaggregates. According to the authors, the determination of the differences between the interaggregate interactions between soluble versus insoluble asphaltene nanoaggregates may potentially provide the microscopic destabilization mechanism of asphaltenes. It has been observed that the largest fractal clusters are formed by the most unstable asphaltenes, namely the ones that precipitate with the smallest amount of precipitant addition. This asphaltene experience the strongest interaggregate attractions (or weakest repulsion) and will tend to associate preferentially with one another due to the strong interaggregate attractions. Figure 29 depict a schematic precipitation mechanism as proposed by Hoepfner et al. [167]

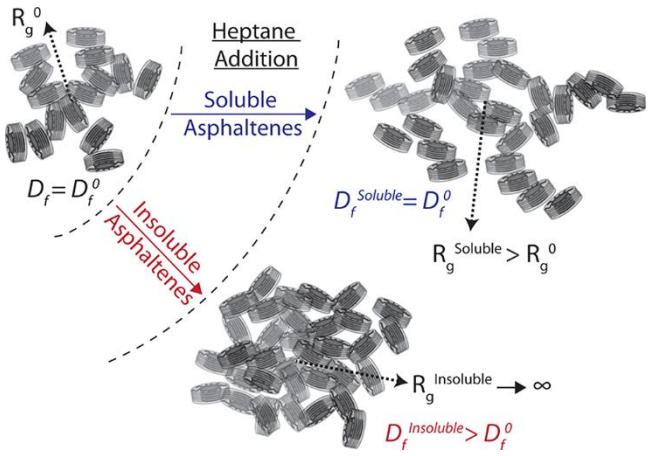


**Figure 29.** Schematic of the proposed asphaltene precipitation mechanism. $R_g^0$ and $D_f^0$ refer to the radius of gyration and fractal dimension, respectively, of the asphaltene fractal clusters in the undiluted crude oil. Reprinted from [167]. (courtesy of ACS)

As it can be seen from figure 29, there is not a well-defined phase envelope for asphaltene stability. Moreover, the polydisperse nature of asphaltenes allows for destabilization of small fractions of asphaltenes at low precipitant concentrations. As a result, the initiation point of asphaltene phase separation as a function temperature, pressure or composition is not an easily determinable parameter. This result questions the experimental validation and basis of many thermodynamic asphaltene stability models that rely on onset points or concentrations.

Barré et al. [169] described a methodology to analyse scattering spectra (neutrons or X-rays) without assumption on particle shape and - more interestingly - investigating higher concentration ranges of asphaltene solutions than those normally discussed in literature. The latter effect is taken into account by considering particle interactions factor $S(\mathbf{q})$ and by manipulating the Zimm equation through a virial expansion. According to the authors, the particle interactions – is therefore described by the expansion's second virial coefficient $A_2$. As a result of their study the authors have shown that the gyration radius $R_g$ the asphaltene's aggregate mass $M_w$ as well as $A_2$ are mutually dependent through a single parameter: the mass fractal dimension $D_f$ of aggregates. The robust method proposed by Barré et al. [169] allows to predict viscosity of a solution at any given asphaltene concentration, adsorption, relative stability of the emulsion and colloidal stability of hydro-conversion effluents.

### 1.5.2. Critical Nanoaggregate Concentration and Aggregation Number

The study of the dynamics of asphaltene aggregation necessarily involves the determination of aggregation as a function of the concentration, in particular, in toluene. Fluorescence quenching studies by Goncalves et al. have shown that asphaltene aggregation occur at low concentrations, about 50 mg/L. [170]. However, as reported by Mullins in [57] the CNAC does not define the onset of aggregation – which can be due to the formation of dimers as well - but rather defines the concentration where further growth of the nanoaggregate shuts off. First studies that correctly determine the CNAC of asphaltenes in toluene used High-Q ultrasonic technique [171,172] that uses the speed of sound u - given by u=(1/Fβ)1/2 where F is the mass density and β is the compressibility - as a function of concentration (see Figure 51)

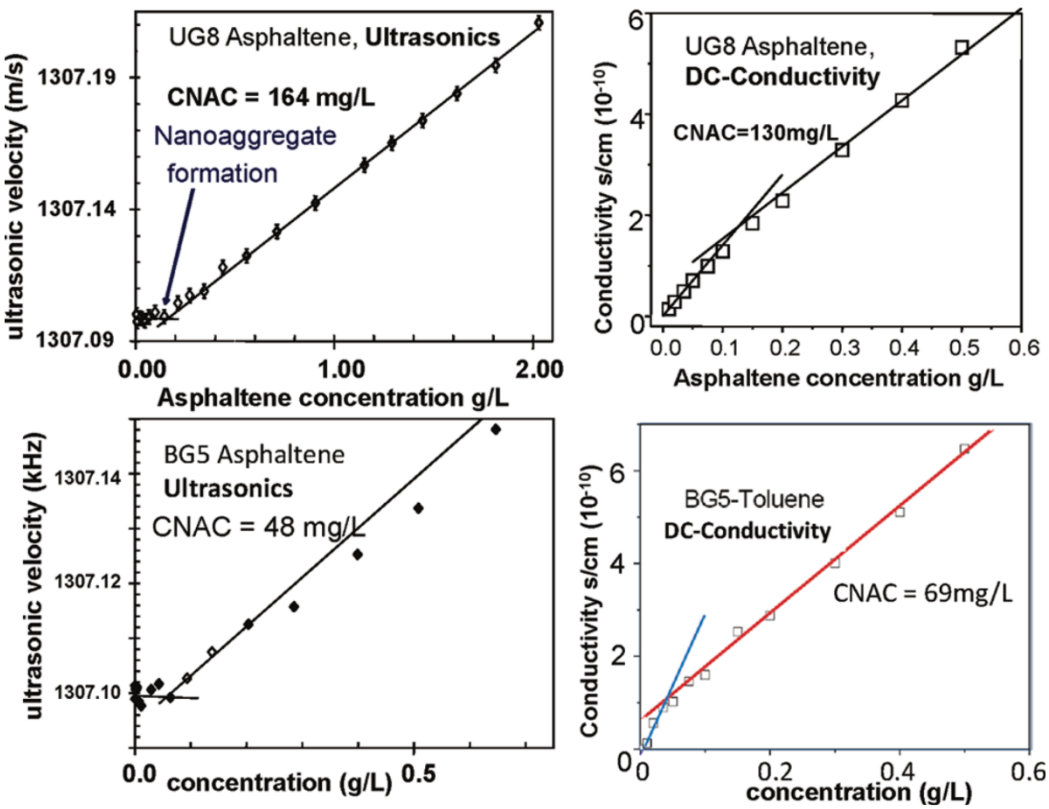


**Figure 51** CNAC of asphaltenes. (Left two panels) High-Q ultrasonics. (Right two panels) Direct-current (DC) conductivity. The break in the ultrasonic-velocity and DC-conductivity curves show the concentration where aggregate growth stops, the CNAC. The straight line of the ultrasonic-velocity and DC-conductivity curves above the CNAC concentration indicates that the nanoaggregate size is independent of the concentration above CNAC. For two different asphaltenes, the CNACs differ somewhat, as shown by consistent high-Q ultrasonics and DC-conductivity data. [172,173] (Courtesy of ACS)

It is worth to notice that the high-Q ultrasonics data show that different asphaltenes have somewhat different values of CNAC. These differences have been confirmed by DC conductivity measurements. Indeed, as it can be seen from figure 51 both high-Q ultrasonics and DC conductivity show that the CNAC for UG8 asphaltene is about 150 mg/L, while for BG5 asphaltene, the CNAC is about 60 mg/L. The significance of these differences is not known. Moreover, there is no obvious relation between the asphaltene chemistry and the CNAC. In this respect, for example Coal-derived asphaltenes with its much different chemical structure has a CNAC determined by high-Q ultrasonics to be 180mg/L, which is close to that of UG8 asphaltene. Interestingly, DC-conductivity measurements show that, for the same crude oil, asphaltenes prepared by n-pentane precipitation have a significantly higher CNAC by 30% or so in concentration than the corresponding asphaltenes prepared by n-heptane precipitation. By using Alternate Current (AC) Sheu et al. obtained similar values of CNAC in agreement with high-Q ultrasonics. [174] Also, DC conductivity measures exhibits similar CNACs values. [165] The DC-conductivity experiments give an aggregation number of about 6. NMR hydrogen index measurements show an aggregation number of about 8. [68]. Motsowfi et al. conducted centrifugation studies through a concentration range from the CNAC and show a dramatically increasing of sedimentation fraction at the CNAC concentration, proving a significant change in aggregation at this concentration (see figure 52) [175]

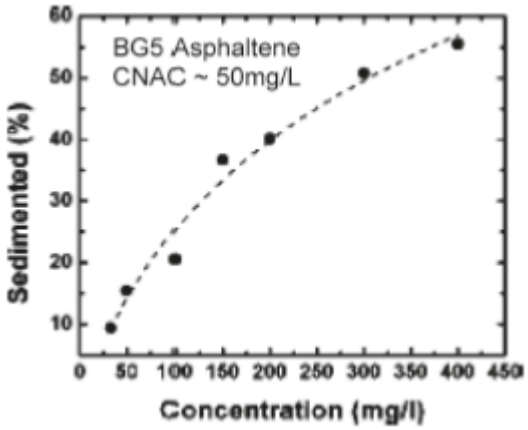


**Figure 52** Percent sedimentation of asphaltenes changes dramatically at the CNAC. While the exact concentration of CNAC is not so evident here, these experiments provide robust proof that the asphaltene aggregation changes significantly in this concentration range. A two-component model, monomer and nanoaggregate, simulates the data. The CNAC for BG5 asphaltene is known from high-Q ultrasonics and DC conductivity. Reprinted from [57] (Courtesy of ACS)

For the particular asphaltene shown in Figure 52, the CNAC was about 50 mg/L as result from high-Q ultrasonics and DC conductivity

### 1.5.3. Asphaltene Aggregation Number and Molecular Architecture

The small aggregation numbers observed for asphaltene nanoaggregates are a consequence of the molecular architecture of asphaltenes. As discussed in the previous sections, asphaltene molecules are formed by a central PAH core, which is polarizable and, thus, the site of intermolecular attraction.

Moreover, all of the nitrogen atoms present in the asphaltene molecules are distributed in the PAH core [93] as pyridinic and pyrrolidynic nitrogen – roughly one per asphaltene molecule – whose chemical nature is opposed: the first one is basic while the second one is acidic. In addition, a high contribution to charge separation comes from the thiofenic function which represents a significant fraction of sulphur present in the asphaltene molecules.

The central PAH core is therefore the site of polarizability and charge separation. The peripheral alkane chains and peripheral fused naphthenic rings yields steric repulsion. However, there must be a balance of attractive forces of the PAHs and repulsive forces of the peripheral alkanes. With attractive forces in the molecular interior and repulsive forces in the molecular exterior, small aggregation numbers follow. After several asphaltene molecules aggregate, a close approach to attractive core is obstructed and additional molecules form new nanoaggregates instead to adhere to existing, fully formed nanoaggregates. Molecular modelling based on these simple molecular forces gives small aggregation numbers [176].

### 1.5.4. surface tension and calorimetry

Isothermal Titration Calorimetry (ITC) is a widely used technique in biochemistry to study ligand-protein interactions [177-179] as well as to measure the changes in enthalpy of a protein solution in a cell following injection of small aliquots of ligand from a syringe. It is also used to study the micellar behaviour of surfactants in water [180,181]. The advantage of ITC above others is that it allows the determination of both the Critical

Micellar Concentration (CMC) and the enthalpy of surfactant micellization in one single experiment. The determination of CMC at several temperatures allows the calculation of the free energy and also the entropy, giving a complete thermodynamic characterization of surfactant micellization. It has also been applied to the study of reversed micelles of AOT in organic solvents [182]. However, Isothermal Titration Calorimetry has never had an extended application into crude oil investigation. To our knowledge, the only examples of ITC application in the crude oil field are given in different papers by Andersen and co-workers [183-187]. In the first work Anderson and Birdi [183] used a microcalorimeter to study the micellization of asphaltenes in solution through the determination of heat of dilution of an asphaltene concentrated solution into a pure solvent. According to the authors – below the Critical Micelle Concentration (CMC) - the heat evolved upon dilution of an asphaltene micelle solution depends upon the total asphaltene concentration of the resulting solution through the equation:

$$\Delta H_{T.D.} = \Delta H_{M.D.} + \Delta H_{Dem.} + \Delta H_{Mon.D.} + Q \quad (8)$$

where the various terms $\Delta H_{T.D.}, \Delta H_{M.D.}, \Delta H_{Dem.}, \Delta H_{Mon.D.}$ stand respectively for Enthalpy variation due to total dilution, Enthalpy variation due to micelle dilution, Enthalpy variation due to de-micellization, Enthalpy variation due to monomer dilution, while $Q$ – which can be minimized although has been found to give a minor contribution - is a heat caused by external influences such as heat from the stirring, frictional effects during liquid injection, as well as minor differences in solvent composition caused by evaporation from the syringe tip. On the contrary, above the CMC the following holds:

$$\Delta H_{T.D.} = \Delta H_{M.D.} + Q \quad (9)$$

as the micelles added to the pure solvent do not dissociate but only their dilution take place. An example of ICT typical experiment result is depicted in Figure 30 in which it can be seen that beyond a certain number of asphaltene solution injections the heat evolved drops as described above.

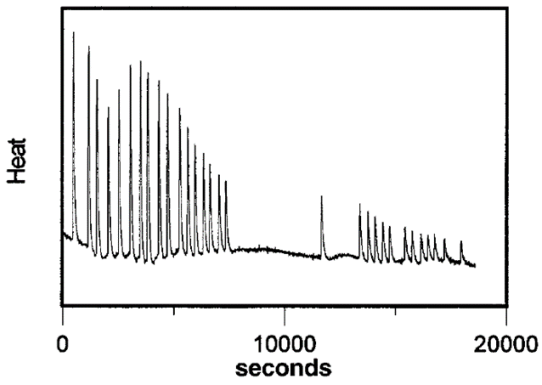


**Figure 30.** Heat of dilution from calorimetric titration of toluene with asphaltenes in solution. Reprinted from [184]. Courtesy of ACS

The change in heat signal as a function of asphaltene concentration has been investigated using two different types of analysis generally used in ITC data treatment. In the first one, the cumulated heat evolved is plotted against the total concentration after each injection. The curve is then approximated by two linear sections, and the intersection of these defines CMC. In the second method the heat/g or mol of asphaltene per injection is plotted versus total concentration after injection, and CMC is taken as the point where a significant drop in

heat/g is observed. However, the authors' data analysis did not detect a clear relation between CMC and asphaltene composition or any obvious relation in the change in CMC as a function of solvent composition. Indeed, as authors themselves noticed, the change in the signal observed during the titration may be interpreted as the presence of a CMC in analogy with similar data of surfactant solutions. or as a result of a stepwise mechanism where a certain average structure is obtained at a certain concentration level. However, in the successive papers [184-187] the authors found that asphaltene aggregation in toluene can occur stepwise in a manner similar to polymerization; that supports the model proposed few years earlier by Agrawala and Yarranton [188]. More literature can be found about the surface tension measurements to study the self-association of asphaltenes. Examples are given by the works of Sheu et al. [132] which made a series of surface tension measurements - as a function of asphaltene concentration - on a lighter (pentane soluble) asphaltene fraction and a heavier (heptane insoluble) asphaltene fraction of a Ratawi crude oil vacuum residue dissolved in two organic solvents: pyridine and nitrobenzene. A distinctive discontinuous point was observed for surface tension. This points out the existence of a critical concentration- similar to surfactant systems - above which self-association occurs. Moreover, in addition to CMC investigation a self-association kinetics was also studied by dynamic surface tension measurements. A simple relation to describe the kinetic data through a parameter that represents the characteristic rate was established to qualitatively evaluate the association kinetics.

Rogel et al. [189] determined the critical micelle concentrations (CMC) of four asphaltenes dissolved in cyclohexane, tetrahydrofuran (THF), toluene, nitrobenzene and carbon tetrachloride by surface tension measurements. The CMC values found ranged from 1 to 30 g/l and depended on the asphaltene and the solvent used. These values were empirically correlated to the Flory–Huggins interaction parameter. According to the authors, this correlation suggests that higher compatibility between asphaltenes and solvent lead to significantly larger CMC in the same solvent. Moreover, the authors tried to find possible correlations among the asphaltene structural parameters – obtained through an NMR analysis - and their self-aggregation behaviour. The authors highlighted that structural and chemical characteristics of the asphaltenes are correlated to their self-aggregation behaviour through the solubility parameter. Furthermore, at the solvent–air interface the same asphaltene shows different molecular areas depending on the solvent. According to the authors, this can be accounted for by two factors: orientation of molecules at the interface and/or preferential adsorption of different molecules. Yarranton et al. [190] investigated the self-association of asphaltenes from Athabasca and Cold Lake bitumens in toluene - at temperatures between 50 and 90 °C - and 1,2-dichlorobenzene at temperatures between 75 and 130 °C. The association appeared to begin at concentrations below 0.5 $kg/m^3$ (0.05%). It has been found that aggregates molar mass was constant at concentrations above 10-20 $kg/m^3$ (1-2 wt %), suggesting that limiting size was reached. The molar mass of these limiting aggregates was measured by Vapor Pressure Osmometry (VPO) and it decreased as the temperature and the polarity of the solvent increased. The average aggregates molar mass was estimated ranging from 4000 to 10 000 g/mol, while the molar mass of an asphaltene "monomer" obtained from VPO measurements has been considered as the value at the intercept (at zero concentration) of a plot of measured molar mass versus asphaltene concentration. Its value was about 1800 g/mol. The VPO results suggest that asphaltenes form aggregates of 2-6 molecules in

aromatic solvents. However, the interfacial tensions measures of asphaltenes in toluene or 1,2-dichlorobenzene at concentrations from 0.3 to 100 kg/m$^3$ has shown that it decreases linearly with concentration, indicating that no micelles are formed. Hence, the aggregation observed with VPO does not appear to be micellization. Monte et al. [191] used surface tension measurements to evaluate molecular weight of asphaltenes - obtained from Brazilian and Venezuelan vacuum residue (VR) - starting from the average radii of the asphaltene molecules adsorbed at the air–solvent interface and hypothesizing a sphere-like shape as indicated by Sheu [192]. They found different molecular areas at the organic solvent–air interface for the same asphaltene, depending on the solubility parameter of the solvent. The molecular weight of asphaltenes, as determined by surface tension measurements with several aromatic solvents, vary and are dependent upon the nature of the solvent. According to the authors as a result of their study it is reasonable to assume that the molecular weights obtained in nitrobenzene are the molecular weights of the individual asphaltene particles.

da Silva Ramos et al. [193] investigated the interfacial and colloidal behaviour of asphaltenes - obtained from Brazilian offshore crude oils - by surface tension measurements of pentane insoluble and heptane insoluble asphaltenes dissolved in toluene, pyridine and nitrobenzene. As it can be seen from figure 31 (toluene solvent), in all cases surface tension measures suggested the occurrence of aggregation phenomena (micelle-like) of asphaltenes in each of the solvents studied.

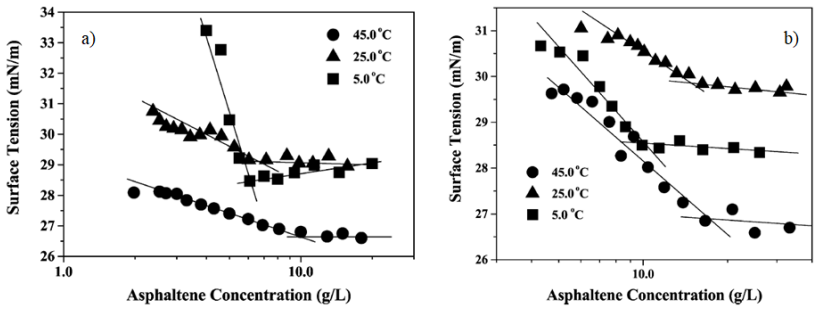


**Figure 31.** Surface Tension trends of: a) heptane insoluble asphaltenes in toluene at 5, 25 and 45 °C and b) pentane insoluble asphaltenes in toluene at 5, 25 and 45 °C. Reprinted from [193]. Courtesy of Elsevier

Similar surface and interfacial tension vs. asphaltene concentration curves were obtained for pyridine and nitrobenzene as solvents at the three different temperatures. From figure 14, one can observe that the critical micelle concentration of asphaltenes in each solvent increase with the temperature increase, revealing the exothermic nature of this self-aggregation phenomenon while, as expected, surface tensions decreases. However, the authors highlight an anomaly which they weren't able to explain, namely the behaviour of the surface tension of the 5 and 25 °C isotherms at concentration beyond the CMC. The authors also observed that in toluene at 25 °C, heptane insoluble asphaltenes were more effective than pentane ones in reducing the solution surface tension, while the opposite happened in pyridine. In nitrobenzene, similar surface activities for these two asphaltene fractions were observed. Finally, by confronting the data reported in literature the authors revealed a lower tendency of asphaltenes used in their study to self-associate.

### 1.5.5. microscopy (optical, AFM, SEM, TEM)

In 2006 a work by Long et al. [194] shed some light on asphaltene aggregation from a completely new perspective. The authors used the single molecule force spectroscopy (SMFS) [195] to investigate the response of single asphaltene aggregates under an external pulling force. The experimental force curve obtained by the authors were well-fitted by the modified worm-like chain model, indicating that those asphaltene aggregates acted like long-chain polymers under pulling by an external force. Acevedo et al. [196] combine freeze fracture-transmission electron microscopy (FFTEM) techniques to study four Venezuelan crude oils and their corresponding maltenes. In all crude oil samples investigated, the authors observed colloidal particles with average diameters in the range of 7-9 nm with maximum diameters of <13 nm and an apparent Gaussian size distribution. Moreover, it has been observed that aggregates of 200 nm in length – also present – are easily broken down to smaller ones or to primary particles by stirring and/or heating the crude oil. This indicates that the binding energy of these aggregates is weak, on the order of kT. Authors also found that a high solvent dilution (in benzene, 80 times) of asphaltene samples, even reducing the particle diameter does not dissolve the colloids completely. On the other hand, the addition of heptane (up to 3 volumes) leads to an increase in diameter. dilution. According to the authors, their experimental observations agree with a previous model for the colloidal particle proposed by Gutiérrez et al. [197] that by fractionating a crude oil asphaltene sample in a low-soluble and a soluble one - named respectively A1 and A2 fraction – and investigating their chemico-physical behaviour proposed a colloidal phase behaviour of asphaltene solutions in aromatic solvents; colloids formed by the low-soluble fraction A1 dispersed by a soluble asphaltene fraction A2 in the maltene phase. Later on, this model was investigated in deeper details by Acevedo et al. [198] by freeze fracture and transmission electron microscopy techniques (FF-TEM) on a solution of asphaltenes in resins at different temperatures from 25 up to 250 °C. As depicted in figure 32 in this temperature range, the mean particle diameters ($D_p$) were found to drop from about 5 to about 3.5 nm. The smallest diameter measured at each temperature ($D_S$) reached a constant value of about to 2.5 nm in the range between 100 and 250 °C.

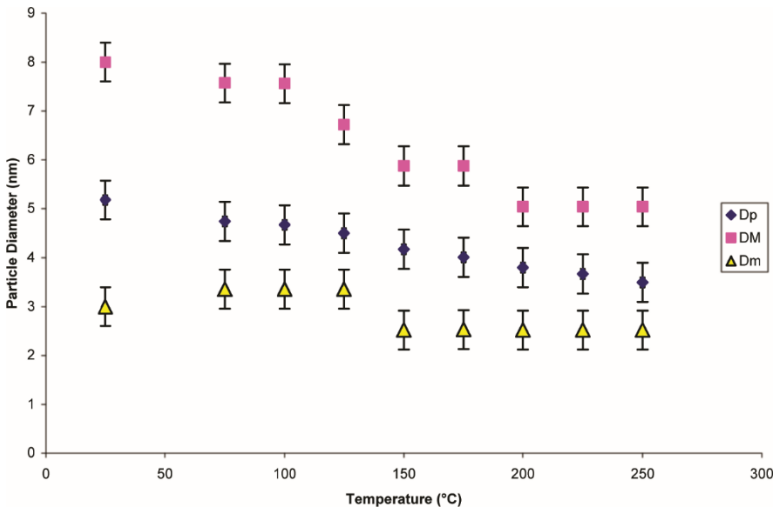


**Figure 32.** Change of particle diameters with temperature, for average (DP), maximum (DM), and minimum (Dm) diameters. Diameter errors are estimated at (0.4 nm. Reprinted from [198]. Courtesy of ACS

Moreover, as it can be seen from figure 32, all frequencies $(f(D))$ (i.e. the number of particles with a specific diameter) except those of $D_S$ tend to decrease above some temperatures values showing that diameters $D > D_S$ correspond to aggregates (Ag).

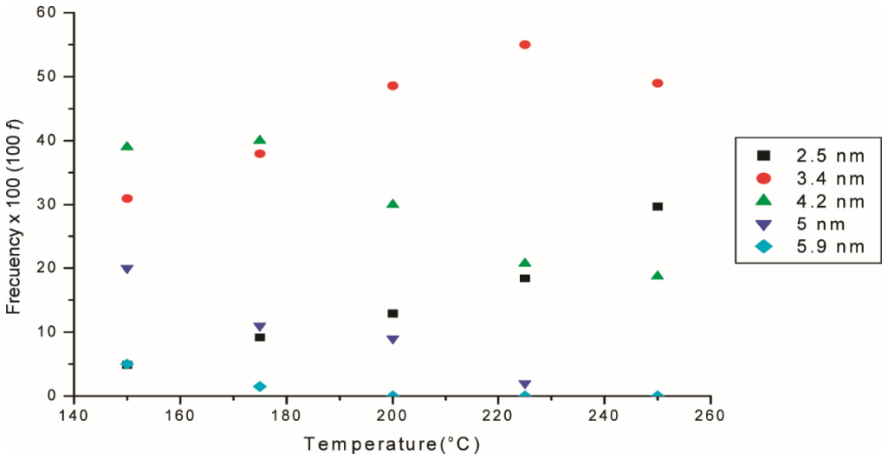


**Figure 32.** Plot of frequencies against temperature for asphaltenes from Furial crude oil. Reprinted from [198]. Courtesy of ACS

More interesting is the fact that during heating, frequencies of big (B) and smallest (S) diameters particles either decrease (big) or increase (S) continuously, while for intermediate (I) diameters maxima were found. According to the authors, this suggests that under the experimental conditions, the conversion from intermediate to smallest diameter particles is hindered by some energy barrier high enough to produce the accumulation of intermediate size diameters. To interpret these observations, the authors proposed a consecutive process model, namely:

$$Ag(B) \overset{k_1}{\rightarrow} Ag(I) \overset{k_2}{\rightarrow} A1M \qquad where\ k_1 > k_2 \tag{10}$$

$Ag(B)$ stands for big aggregates, $Ag(I)$ stands for intermediate medium size aggregates and $A1M$ stands for A1 type molecules fraction, represented by rigid condensed polynuclear systems models with alkyl substituents on the molecule periphery. According to the authors, the above results together with many others in the literature agree with the colloidal, solubility, and aggregates hypothesis related to A1 and A2 fractions of asphaltenes. In 2010 Wang et al. [199] investigated the colloidal interactions between asphaltene (precipitated from a Vacuum distillation feed bitumen sample) surfaces in n-heptane / toluene (heptol) mixtures as a function of the $\Phi_T$ - namely the toluene fraction – parameter by using the atomic force microscopy (AFM) colloidal probe technique. Langmuir-Blodgett upstroke technique was used to deposit asphaltenes on silica wafers and silica spheres. The authors have shown that the magnitude of the interaction forces between asphaltene surfaces can significantly change in function of toluene to heptane ratio. As the experimental results have shown, in pure toluene there is a steric long-range repulsion - observed by the authors in a previous study [200] - which can be well fitted by the scaling theory of polymer brushes. The steric repulsion is somewhat reduced – becoming weakly attractive when $\Phi_T < 0.2$ - as toluene volume fraction gradually decreases from $\Phi_T = 1$ (pure toluene) to $\Phi_T = 0$ as depicted in figure 33.

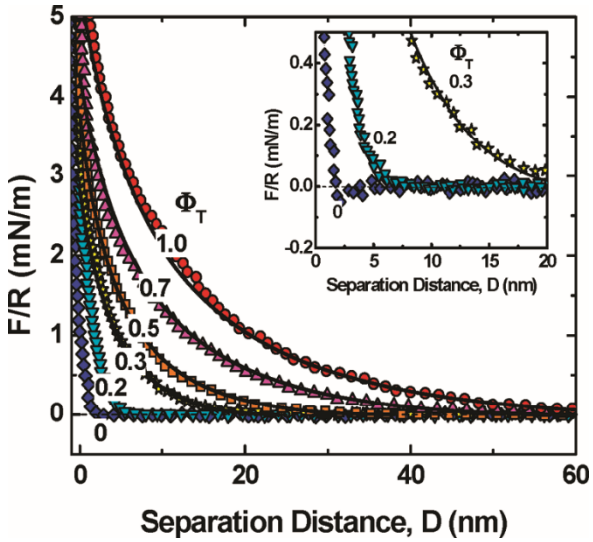


**Figure 33.** AFM experimental data for interaction parameter of asphaltene/heptol as a function of $\Phi_T$. The inset shows the slightly attractive behaviour for $\Phi_T < 0.2$. Solid lines: scaling theory fitting of force curve. Reprinted from [199]. Courtesy of ACS

The attraction in heptane can be fitted by van der Waals forces alone which are thus believed to promote asphaltene aggregation, leading to asphaltene precipitation. According to the authors, the results obtained provide an insight into interactions that determine asphaltene behaviour in an organic medium and hence in crude oils. Essentially similar results were observed by Natarajan et al. [201]

The authors have shown that the repulsive intermolecular forces between asphaltene surfaces in toluene were well-described with the Alexander−de Gennes theory proposed for steric repulsion between polymer layers in good solvents [202-205]. Moreover, according to Natarajan et al. the van der Waals attractive forces were reported as the driving forces for asphaltene aggregation and flocculation in paraffinic solvents.

Burya et al. [206] used light-scattering to investigate the Karazhanbas crude oil's asphaltene colloidal properties and the kinetics of aggregation in hydrocarbon toluene-n-heptane solution and, in three different samples of crude oils: Swanson River, European SkyBlue, Mars A-12. The authors showed that the aggregation of asphaltene particles in hydrocarbon solutions obeys two different kinetics laws: the Diffusion Limited Aggregation (DLA) and the Reaction Limited Aggregation (RLA). Moreover, they observed a crossover between these two regimes when asphaltene solutions have concentrations slightly higher than the CMC threshold and the concentration of the precipitant n-heptane is near the precipitation threshold. According to the authors, their data demonstrate a universal behaviour that may be present in other colloidal systems. Crude oil samples investigation has shown that Swanson River, European SkyBlue oils own an intrinsic colloidal-like structure with particles of approximately 0.02 and 1 mm in diameter but the Mars A-12 sample has no initial colloidal structure, although – as authors highlighted - for Swanson River, this structure is somehow affected by laser radiation. According to the authors the particles observed are asphaltene–resin colloidal particles. Moreover, the stability of crude oil systems against induced (by n-heptane) asphaltene aggregation has been investigated. As a result, Swanson River crude oils exhibits an extremely slow aggregation process. No threshold concentration of the precipitant for this sample has been observed. Fast aggregation was observed for European SkyBlue, whose aggregation lasts a short period of time, with the formation of a colloidal

structure due stable asphaltene aggregates. Mars A-12 crude oil has no initial colloidal structure but it does occur in a solution with 20% n-heptane and remains stable. The addition of more than 60% by volume of precipitant breaks the stability of the structure completely and causes the flocculation of particles into huge clusters, which cannot be measured by the light scattering method. Finally, by comparing DLS data with oil's SARA fraction, the authors concluded that the oils with high aromatic to saturate ratios have a more stable structure and exhibit no slow aggregation, whereas the oil with a much lower ratio is on the edge of stability and shows slow aggregation kinetics.

Confocal Laser Scanning Microscopy (CLSM) was used by Handle et al. [207] to investigate asphaltene behaviour in 50/70, 70/100A, 70/100B and PE1005 (a bitumen precursor, namely a vacuum flashed and cracked vacuum residuum) bitumen samples as well as the bitumen-aggregate interaction. In their work, Handle and co-workers showed that the interpretation of the fluorescent centres in the CLSM as asphaltene micelles is not completely correct as reported in a previous work by Bearsley et al [208]. For this reason, by fractionating bitumen into its main components (SARA fractions) the authors have shown that, the fluorescence capability of the asphaltenes is very low or insignificant Furthermore, the fluorescence analysis of fractions showed clearly that the main source of the fluorescent emissions are aromatic fractions. According to the authors however, by combining this information with the micelle theory it can be argued that the fluorescent signals still originate from asphaltene micelles, but not from the inner core of the asphaltenes themselves but from the stabilizing mantle of declining polarity around the asphaltene agglomerates. These results have been successfully employed in further investigations regarding microstructure and microstructural changes at the ageing of bitumen [209]. Finally, it has been shown that the fluorescent phase was also shown to play no detectable role in the interaction between bitumen and mineral aggregates. This indicates a general lack of interaction on a structural level. In total, this limits the interaction to the molecules in the matrix, indicating that adhesion between minerals and bitumen is mostly based on mechanical phenomenon and perhaps to a lesser extent on van der Waals forces [210]. Castillo et al. [211] investigated the aggregation behaviour of asphaltenes in toluene as a function of asphaltene concentration by studying the nonlinear optical response of the solutions by using the Z-scan technique. The solutions concentration studied by the authors ranges from 10 mg/L to 600 mg/L. It has been observed a strong dependence of the two photon absorption coefficients (β) for concentrated solutions, in contrast to the low values observed at low concentration. According to the authors, this change in (β) occurs as a consequence of aggregation. The results are of importance for the study of dark samples like those relevant for crude oils. The authors' conclusions assert that the changes in the nonlinear optical properties of solutions of asphaltenes in toluene as a function of concentration can be understood in terms of an aggregation model. Anisimov et al. [212] used Dynamic Light Scattering (DLS) to study the effects of resins on the aggregation stability - upon n-heptane addition as precipitant- of 0.1 g/L of Romashkinskaya oil (Tatarstan, Russia) asphaltene in toluene. The authors have shown that the asphaltene aggregate size follows a power law as a function of time with an exponent $\alpha = 0.36 \pm 0.04$ which is related to the fractal dimension $D_f$ of asphaltene aggregates as $\alpha = \frac{1}{(1 + D_f)}$ The authors results have shown a good agreement with that of Haji Akbari et al. [213] namely that despite a considerable variation

of asphaltenes' origin, the evolution of the interaction forces between the asphaltene clusters with a change in the solvent quality seems to be universal. It has been shown that asphaltenes aggregation time decreases exponentially as n-heptane concentration increases but grows linearly upon increase of the resin/asphaltene ratio. This means that resins serve as inhibitors for asphaltene aggregation, shifting the onset of aggregation. However, as noticed by the authors, the dependence of the onset on the concentration of resins tends to saturate. Indeed, the onset of aggregation increases upon the addition of resins but only for limited resins' content. The authors also showed that for all the samples studied (with and without resins) the asphaltene aggregation is controlled by diffusion-limited kinetics. Finally, they note that the observed character of aggregation of real asphaltenes in solution is remarkably similar to that recently found in toluene/heptane mixtures with a single compound hexa-tert-butylhexa-perihexabenzocoronene [214] thus confirming the possibility of modelling the asphaltene aggregation by well-defined compounds.

Yarranton et al. [215] investigated various asphaltene-toluene solutions in order to study the size and distribution of self-associated asphaltenes – extracted from Peace River bitumen and Athabasca bitumen - through a miscellaneous range of techniques. More specifically, the authors used, vapor pressure osmometry (VPO), elemental analysis, Fourier transform-ion cyclotron resonance (FT-ICR) mass spectrometry, and time-resolved fluorescence emission spectra measurements, Small Angle X-ray Scattering (SAXS), Dynamic Light Scattering (DLS), membrane diffusion, Rayleigh scattering and nanofiltration measurements. Molecular and nanoaggregate dimensions were also investigated through a combination of interfacial tension, interfacial adsorption, and surface force measurements. As a result of their study, the authors showed that approximately 90 wt % of the asphaltenes self-associated. Moreover, from ultrahigh resolution spectrometry it has been observed that the non-associated asphaltenes are smaller and more aromatic than the associated ones which lead to the conclusion that the associating species are larger and less aromatic. VPO measurements revealed an average monomer molecular weight of approximately 850 g/mol, while the molecular weight of the nanoaggregates was found to span a range of at least 30000 g/mol with an average on the order of 10000 to 20000 g/mol. On the contrary, SAXS and DLS gave molecular weights 10 times larger. Nanofiltration measurements have shown that the physical dimensions of the nanoaggregates were less than 20 nm, while Rayleigh scattering have shown average diameters of 5 to 9 nm in disagreement with that obtained by SAXS and DLS measurements indicating 14 nm as mean value. Film studies were consistent with the lower molecular weights and dimensions and also demonstrated that asphaltene monolayers swell by a factor of 4 in the presence of a solvent. The most consistent interpretation of the data is that asphaltenes form a highly polydisperse distribution of loosely structured (porous or low fractal dimension) nanoaggregates. However, the discrepancy between VPO and SAXS molecular weights remains unresolved.

Shojaei et al. [216] have studied the asphaltene aggregation kinetics in toluene using dynamic light scattering (DLS) technique. Asphaltene was extracted from dead oil – namely an oil that has lost all its dissolved gases and volatile components – from the Iranian southern oil fields. Asphaltene-toluene solution were made at a concentration of 1 gr/L and then diluted to the desired concentration of 6.25 mg/L and 12.5 mg/L followed by an ultrasonication procedure. From the Dynamic Light Scattering measurements, it has been shown that

sonication time has some influence in asphaltene aggregation. More specifically, high and low sonication times results in monomeric and polymeric forms of asphaltene in solution. Moreover, the authors have shown that the relationship between the amount of sonication energy and the particle size is logarithmic. Deconvolution technique applied to the DLS spectra obtained from the lower sonication solutions revealed four normal distributions, indicating four different clusters in the solution. The authors also evaluated the percentage of nano-aggregates for the lower and the higher concentrations of the asphaltene solutions revealing a distribution between 8%-41% and 4%-51%, respectively. Finally, the authors proposed a coin model to describe asphaltene aggregation kinetics in solution. As it can be seen from figure 34, according to this model it has been assumed the asphaltene molecule to be on a coin-shaped plate and forming a π bond with a minimal coinage overlap.

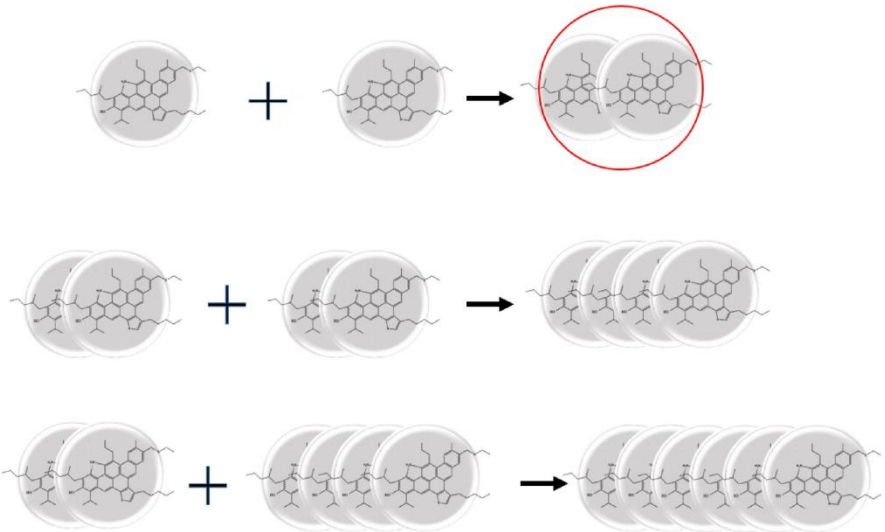

**Figure 34.** coin model of the asphaltene molecules in solution. Reprinted from [216]. (Courtesy of Elsevier)

The concentration of each nano-aggregates in equilibrium in solution is calculated according to the fraction of its presence and the coin model. The authors used these equilibrium concentrations to calculate the equilibrium reaction constants. By combining the coin model and the deconvoluted DLS results the authors have shown that the equilibrium constant as well as the diffusion coefficient of the smaller aggregate is higher than the larger aggregate. Moreover, they showed that the correlation coefficient between the reaction constant and the diffusion coefficient are unique and depend on the nature of the asphaltene. According to the authors, the "coin-like" kinetic model together with the DLS data provided a procedure for calculation of concentration and equilibrium constant of the nano-aggregates in the asphaltene solution. Abbott and Povey [217] used acoustic spectroscopy in the frequency range 2 – 120 MHz to detect the presence of asphaltene aggregates in different crude oil and bitumen samples. Fresh toluene and fresh maltene were used as reference samples. By comparing the results obtained by ultrasound spectroscopy for crude oil and bitumen samples to that of the reference samples, the authors were able to show that aggregation of asphaltenes is taking place in the firsts. Indeed, as depicted in figure 19, both aggregate-free toluene and fresh oil maltenes exhibit a power law dependence which is a function of the continuous phase, while for the whole fresh oil deviances from the normal power law are present, which according to the authors indicates that the fresh crude oil shows clear signs of a changing size of the scattering entities. This is also the case when the crude oil is diluted with toluene.

Indeed, since the data departs from power law dependence this means that – although dilution occurs, - nanoaggregates remain. Moreover, once the diluted fresh crude is stirred sufficiently, the re-suspended asphaltene's spectrum approaches a power law once again. In contrast, the toluene diluted bitumen behaves exactly like the toluene in which the asphaltenes are suspended, indicating that in this case no measurable excess scattering was occurring. According to the authors, with sufficient information it may in future be possible to determine the size of the scattering particles from the acoustic spectrum [218], including the changing size of the asphaltene particles during aggregation.

### 1.5.6. Spectroscopy (NMR, FT-IR, ATR)

Durand et al. [219] performed some Diffusion Order two dimensional NMR Spectroscopy ($^1$H DOSY NMR) experiments to investigate the macrostructure of the asphaltenes extracted from three crude oils: Maya, Athabasca and Buzurgan in deuterated toluene at 20 °C, analysing different solutions in the concentration range from 0.01% w/w to 15% w/w. As it can be seen from figure 35, asphaltenes from different crude oil source exhibit different aggregation behaviours.

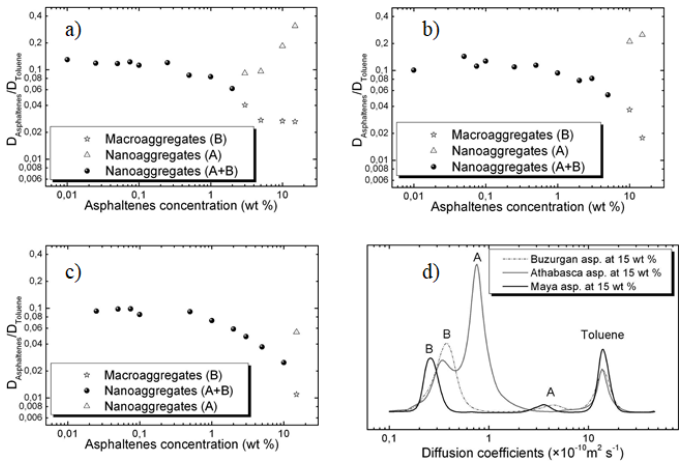


**Figure 35.** Relative diffusivities panel a)-c) and diffusion profiles (arbitrary units on the intensity axis) panel d) of Buzurgan (a)), Maya (b)) and Athabasca (c)) crude oil asphaltenes [219] (Courtesy of ACS)

From figure 35d, according to the authors, peaks A and B are associated with nanoaggregates and macroaggregates, respectively. As seen, the three different asphaltene fractions show a bimodal distribution of aggregates: one diffusing quickly and one diffusing more slowly. The width of the diffusion peaks is due to the polydisperse nature of asphaltene molecules. Indeed, they are composed of thousands of molecules with a wide range of molecular weights and chemical structures. As the diffusion profiles shows, Athabasca asphaltenes are mainly constituted of nanoaggregates (peak A), whereas Buzurgan and Maya asphaltenes are more concentrated in macroaggregates (peak B). These differences in aggregation behaviour are due to selective affinities of organic compounds for toluene. The main point raised from figure 35 is that the chemical behaviour of the three investigated asphaltenes is not the same in toluene-d8, because the aggregation process is strongly dependent on intermolecular interactions. Panel a) to c) of the figure 35 shows the influence of the asphaltene concentrations on their relative diffusivities ($D_{sample}/D_{solvent}$). A strong and nonlinear dependence

of the measured mobility of the solute is noticed on all types of intermolecular interactions: attractive solvent-solute interactions and attractive solute-solute interactions. In fact, there is a continuous decrease in diffusion coefficient beyond 0.5% w/w for Maya and Athabasca asphaltenes and beyond 0.25% w/w for the Buzurgan asphaltenes. Below those concentrations, the solutes are isolated enough so that they are not affected by their chemical environment. In this range of concentrations, solute-solvent interactions are predominant and determine the limiting diffusion coefficient. Buzurgan and Maya asphaltenes show similar self-diffusion in the dilute regime, leading to similar sizes, whereas Athabasca asphaltenes diffuse more slowly. As shown in the various figures, beyond a given concentration (0.25 or 0.5 wt %, depending upon the origin of the sample), there is a semi-dilute regime where more-attractive interactions are involved, leading to an increase in the friction of the solute and, as a result, to a decrease in the mobility of the molecules. There are attractive solute-solute interactions, leading to an aggregation process. For the Buzurgan asphaltenes, both small and large aggregates were detected above 3% w/w, whereas the two aggregates were observed at 10% w/w for the Maya asphaltenes and at 15% w/w for the Athabasca sample. The presence of two different species—one diffusing quickly and one more slowly—suggests a separation of aggregates. At high concentrations, the self-affinity of heavy species increases, which causes an aggregation process. Indeed, the local asphaltenes concentration in the solution varies. The aggregation of asphaltene molecules leads to a local increase of asphaltene concentration, and, consequently, in the vicinity of these aggregates, less asphaltene entities are present and the remaining molecules show a higher mobility. Furthermore, the local concentration of toluene in the mixture varies: it decreases in the neighbourhood of aggregated asphaltene species while the concentration of solvent increases nearby nanoaggregates, leading to an increase of the diffusion properties of these nanoaggregates. Asphaltenes are known to exhibit a large polydispersity, in term of size and molecular weight. Finally, as highlighted by the authors, the experimental results suggest the plausibility to assume that asphaltene mixtures are a continuum of two different types of structure, namely archipelago- and continental. Indeed, according to them, the diffusion results seem to indicate that the interactions involved in the solutions are different, depending on the repartition between the archipelago-and continental-type asphaltenes in the medium. Furthermore, the authors have observed that due to the more favoured π-π interactions continental structures are more aggregated with a high tendency to precipitate in toluene. Experimental data have shown that the Buzurgan asphaltenes are more continental-like than the other crude oil asphaltenes. On the contrary Athabasca asphaltenes have shown a more archipelago-like character. An analogous work was done by da Silva Oliveira et al. [220]. The authors used the Nuclear Magnetic Resonance technique to study the relationship between the structural type (continental or archipelago) and aggregation properties of three different asphaltenes derived from three off-shore Brazilian crude oils. The solutions were prepared dissolving asphaltene samples in a solution of 50 mM of $Cr(acac)_3$ in deuterated chloroform. From $^{1}H$ and $^{13}C$ NMR spectra, the authors deduced that two of the asphaltene samples (Asph_A and asph_C) have around 21% aromatic hydrogens while the sample Asph_B contains only 7%. According to the authors, this indicates that these asphaltenes have highly condensed aromatic molecules, which suggests a continental-type structure for this sample. Asphaltene concentration ranging from 0.01 to 10% in deuterated toluene were used to perform the self-diffusion

measurements of the asphaltene aggregates by Diffusion-Ordered NMR Spectroscopy (DOSY). From the DOSY, the authors observed that for asphaltenes asph_A and asph_C, the formation of macroaggregates occurs only from a concentration of 1%, whereas for asph_B macroaggregates formation starts at concentration of 0.1%. According to them, this is due to the so-called $\pi - \pi$ stacking interaction, which occurs when the structure of the asphaltene is more likely of continental type. For the archipelago model, this interaction is not favourable because of the number of side chains and the also smaller amount of fused aromatic rings. The main difference that can be highlighted comparing the works of da Silva Oliveira and that of Durand et al. is the detection by the first of an intermediary state between the nanoaggregate and macroaggregate states called microaggregate (see figure 36).

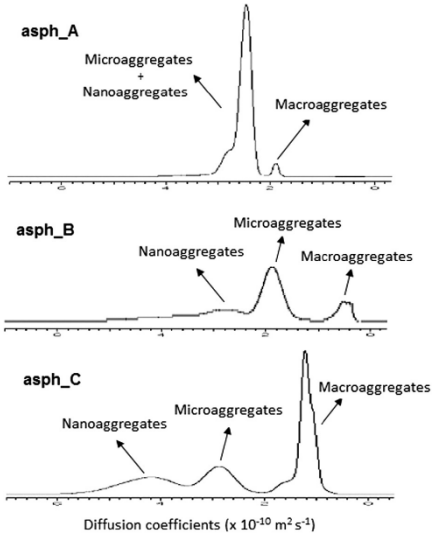


**Figure 36.** Self-diffusion coefficients of the asphaltene aggregates at 8% mass in deuterated toluene. [220]

According to the authors, this intermediary state may be composed of asphaltene molecules forming a middle structure between the higher (macroaggregate) and lower molecular size (nanoaggregate).

Majumdar et al. [221] investigated the solid phase aggregate structure of asphaltenes isolated from a Kuwaiti crude oil (UG8) using various Solid-state $^{1}$H NMR spectroscopy techniques such as the dipolar filter and $^{1}$H Back-to-Back (BABA) recoupling Double Quantum correlation (DQ-MAS). These techniques allowed the authors to get numerous structural information about the asphaltene aggregation structure. For example, they were able to identify skewed π-stacking between the aromatic cores in asphaltenes nanoaggregates, as well as that the nanoaggregates form clusters both through alkyl-alkyl interactions and T-shaped interactions. Furthermore, the authors deduced that the asphaltene monomers participating in aggregate formation are generally larger than simple 3–4 ring polyaromatics (generally peri-condensed of seven or more rings) hydrocarbons. This peri-condensed structure results in the shielding of certain aromatic and aliphatic proton nuclei, lowering their chemical shifts compared to the expected ones. On the basis of the combined results from $T_2$ relaxation results, the dipolar filter and DQ-MAS experiments, the authors proposed a solid-state aggregation model to describe petroleum asphaltenes as presented in figure 37

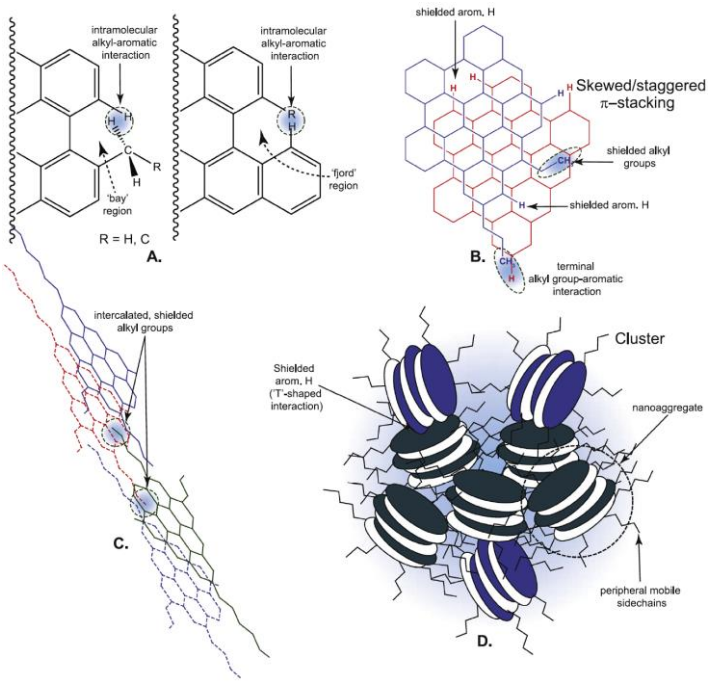


**Figure 37.** Possible modes of aggregation and molecular interactions among asphaltene monomers. (A) Alkyl-aromatic interactions in 'bay' or 'fjord' type regions, (B) possible interactions and shielding regions in a skewed π-stacking conformation of $sp^2$-hybridized aromatic cores molecules, (C) shielding of alkyl groups through intercalation between aromatic sheets, (D) an asphaltene cluster, composed of nanoaggregates. The T-shaped interactions likely play only a small role and are shown for illustration. Also note that the skewed stacking conformation is one of the three possible motifs amenable to shielding of aromatic protons, the others being staggered and twisted hexagonal. Reproduced from [221]. Courtesy of Elsevier

The peri-condensed structure proposed by Majumdar et al. was supported in another study by Wang et al. [222] who used the surface-assisted laser desorption ionization mass spectrometry (SALDI-MS) coupled with laser desorption laser ionization mass spectrometry ($L^2$-MS) to investigate the asphaltene nanoaggregates from three different source materials, namely Coal, Petroleum and Immature Source-Rock. All three types of asphaltenes were found to form nanoaggregates with aggregation numbers close to 7. Furthermore, through Molecular Dynamics calculations, the authors have shown that π-stacking and alkane steric hindrance play an important role in nanoaggregate formation. For example, the authors observed that for Immature Source-Rock asphaltenes, due to their large alkane fraction, π-stacking is almost precluded.

Morozov et al. [223] investigated the dynamics of asphaltene aggregates -isolated from Tatar Republic (Russia) heavy oil - dissolved in chloroform in a wide range of concentrations – 20 to 120 g/L - and at temperatures from 0 to 55 °C using the Pulsed-Field Gradient NMR technique (PFG-NMR) and a multiexponential function to fit the diffusion data. As the authors reported in the 20 g/L to 120 g/L concentration range, a three-parameter function well fit the data, meaning a three-component system: small molecules (asphaltene monomers and possible aggregates with the lowest aggregation numbers), nanoaggregates, and macroaggregates (clusters). Moreover, as expected, the diffusion coefficients of all components grow as the asphaltene concentration decreases, whereas the partial weight of the components attributed to the aggregated structures increases with the increase of the asphaltene concentration. However, as depicted in figure 38a, below 20 g/L concentration (semi-diluted regime) the authors were not able to properly assess components related to the different types of aggregates because both a two component and a three-component function showed a well fit behaviour.

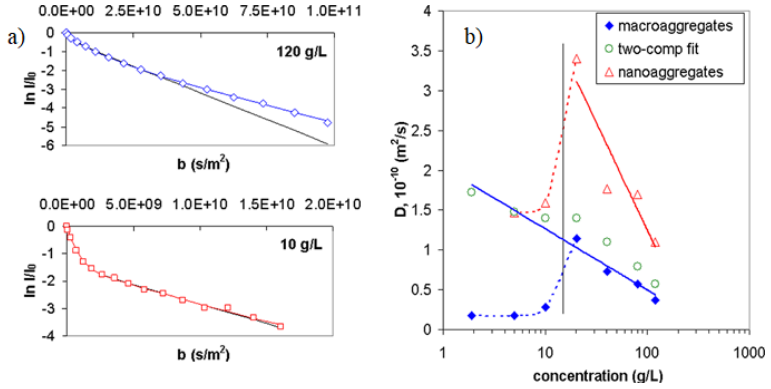


**Figure 38** Panel a): results of two- (black line) and three-component (colour line) fitting used for the simulation of signal decay for the samples with high and low concentrations of asphaltenes. Panel b): concentration dependencies of diffusion coefficients extracted from two- and three-component fitting of the decays of the signal. "Two-comp fit" denotes the second component of two component fitting; black vertical line divides the graph into 1.9−15 g/ L and 15−120 g/L regions just for clarity of visual representation. The first component with $D > 10^{-9}\ m^2/s$ attributed to the smallest species, i.e. small molecules (impurities), asphaltene molecules, and aggregates with the lowest aggregation numbers is not shown in the Figure. Reprinted from [223]. Courtesy of ACS

Figure 38b shows two of the three component exponential analysis – in the concentration range from 20 g/L to 120 g/L - (the one with $D > 10^{-9}\ m^2/s$ is not shown (see the caption of figure 38)) characterized by the diffusion coefficients which differ by two times or more. The component with characteristic $D \approx 1.1 \times 10^{-10} \div 3.4 \times 10^{-10}\ m^2/s$ can be attributed to the nanoaggregates. The slowest component with the characteristic $D \approx 0.3 \times 10^{-11} \div 1.1 \times 10^{-10}\ m^2/s$ is attributed to the macroaggregates (clusters). As it can be seen from the figure 38b at concentrations below 20 g/L the results of two and three-component fitting can no longer be discerned and apparent D values come out of their concentration trends (dotted colour lines). It happens solely due to a mathematical reason: when the third component of the decay is physically absent (i.e., its partial weight is close to zero), the algorithm of the multicomponent analysis provides virtual values for the respective component which have no physical meaning. Consequently, for this concentration range (<20 g/L) the two-component model provides more reliable data and the diffusion coefficients continue following the designated trend. The authors also investigated the effect of the temperature on the asphaltene solutions at various concentration: one in the semi-dilute regime (7g/L), one slightly above the "critical" concentration (24 g/L) and two at higher concentrations (40 g/L and 120 g/L). According to them, the analysis of the echoes decay of samples at 120 g/L is well fitted by a three-component function in the whole range of the temperature investigated (0-55 °C). On the contrary, while the solutions in the dilute regime at ambient temperature did show no differences between two and three-component fitting, as it can be seen from figure 39d differences emerges as the temperature is decreased below the 25 °C. Figure 39a clearly shows that for the 120 g/L solution aside from temperature value three - the first component related to the smallest diffusing species is not shown - separate components with particular diffusion coefficients were clearly resolved. Moreover, the D value for every component increases with the temperature increase, and the data can be approximated with the straight line in the Arrhenius coordinates.

A different behaviour is observed in the semi-diluted regime, as reported in figure 39c. At low temperatures (0 °C to about 25 °C) the diffusion coefficient distributions can be resolved, namely the components associated

with nano- and macroaggregates behave separately. Upon achieving the 25 °C room temperature, the macroaggregates component can no longer be properly distinguished. Indeed, as one can see from figure 39c, above 25 °C the D values of the macroaggregates become physically meaningless being the product of the mathematical fitting procedure: they appear scattered out of any physical trend.

In turn, the nanoaggregates component drops down and continues the dominant trend which came from the macroaggregates component at lower temperatures. Within the temperature range 25−55 °C, both second components coming from two- and three-component fittings are close to each other and behave similarly.

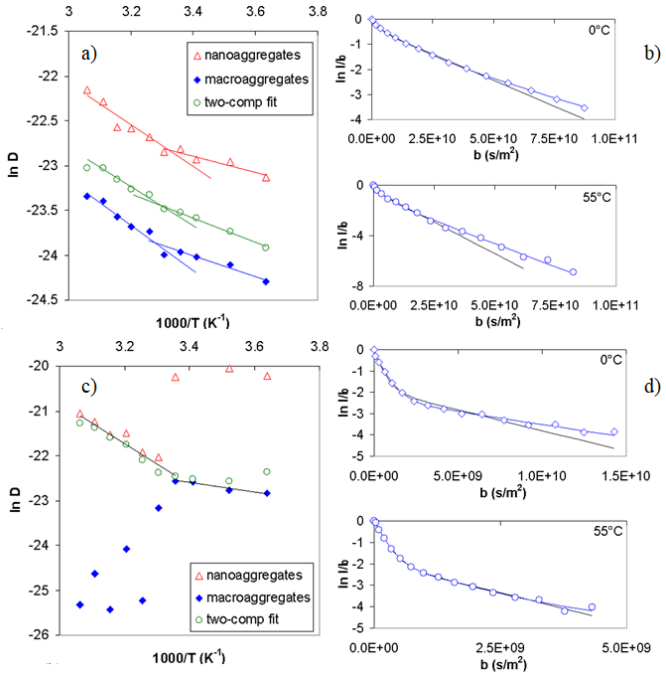


**Figure 39.** Panel a) and c) : Temperature dependencies of diffusion coefficients extracted from two- and three-component fitting of the echoes decays for 120 g/ L (a) and 7 g/L (c) samples within the temperature range of 0 – 55°C. Panel b) and d): results of two- (black line) and three-component (blue line) fitting used for the simulation of signal decay for the 120 g/L solution (b) and for 7 g/L solution (d) at 0 °C and 55 °C Reprinted from [223(ok)] (Courtesy of ACS)

The analysis of the data for the 40 g/L sample revealed a similar behaviour as compared to the samples with higher concentrations (120 g/L). In the case of the 24 g/L sample the diffusion coefficients behave somehow in between: the macroaggregates component behaves like that in Figure 39a whereas the nanoaggregates component is very scattered, dropping down like in Figure 39b upon achieving the room temperature.

Similarly, Kawashima et al. [224] investigated the effects of asphaltene concentration on their aggregate size to elucidate the mechanisms leading to the asphaltene aggregation. The author used asphaltenes isolated from Khafji, Iranian Light, and Maya crude oils vacuum residue (VR) to prepare deuterated chloroform solutions at different concentrations (0.1 g/L to 30 g/L). Diffusion coefficients (D) were determined using Pulsed-Field Gradient Spin-Echo $^{1}$H NMR. According to the authors, the concentration dependency of the D values supports the widely accepted stepwise aggregation mechanism (i.e., monomer < small aggregates < medium-size aggregates < large aggregates (precipitate)). Moreover, in the 0.1 - 1 g/L concentration range, the D values corresponding to the range of small to medium aggregates were observed, and at higher concentrations (10 and 30 g/L), only medium aggregates were detected. Östlund et al [225] used PFG-SE NMR to study the self-

diffusion of asphaltenes in deuterated toluene in a concentration range from 0.044 % w/w to 5 % w/w. The authors have shown that - in the above concentration range - the self-diffusion coefficients D of asphaltenes can be well described by a log–normal distribution function with a width $\sigma$ around 0.65 and independent of the asphaltene concentration in the interval studied. The latter was interpreted by the authors as an evidence of the fact that there is a small self-aggregation between molecules in the concentration range studied. Therefore, they attributed the strong dependence of the diffusion coefficients to the solution concentration - as depicted in figure 40 - to the obstruction effects

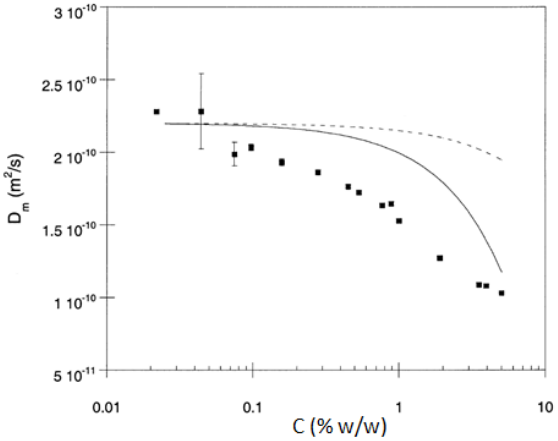


**Figure 40.** Median diffusion coefficient $D_m$ as a function of asphaltene concentration in toluene. The error bars are well represented by the size of the squares except at low concentrations where the signal to noise ratio is low. Also included in the graph are the theoretical curves displaying the obstruction effects for monodisperse spheres (dashed line) and discs with an axial ratio of 20 (full line). Reprinted from [225] (Courtesy of Elsevier)

The authors tried to explain the trend of $D_m$ vs concentration by using a monodisperse model for asphaltene molecules, and tailoring their shape using the oblate disc geometry with an axial ratio of 20, which is in good agreement with that observed in SANS/SAXS experiments. As a comparison term in figure 40, the monodisperse spherical model is also shown. However, as the authors themselves highlighted, it can be seen that the correlation between experiments and theory is not perfect. According to the authors, this discrepancy is due to the fact that there is a large size distribution of asphaltenes, so the monodisperse model is not so appropriate to describe this type of systems. However, as they highlighted the extension of the theory to include polydisperse particles appears to be nontrivial as reported in [226].

Gabrienko et al. [227] used Attenuated Total Reflection Fourier Transform Infrared (ATR-FTIR) spectroscopic imaging approach and the Magnetic Resonance Imaging (MRI) to study - for three crude oil samples – the in situ asphaltene aggregation process induced by n-heptane titration. ATR-FTIR spectroscopic images shown in figure 41 were created using an integrated absorbance of the band at 1650−1550 $cm^{-1}$, which corresponds to the stretching vibration of aromatic C=C bond. Thus, these images represent the spatial distribution of aromatic hydrocarbons (simple and complex).

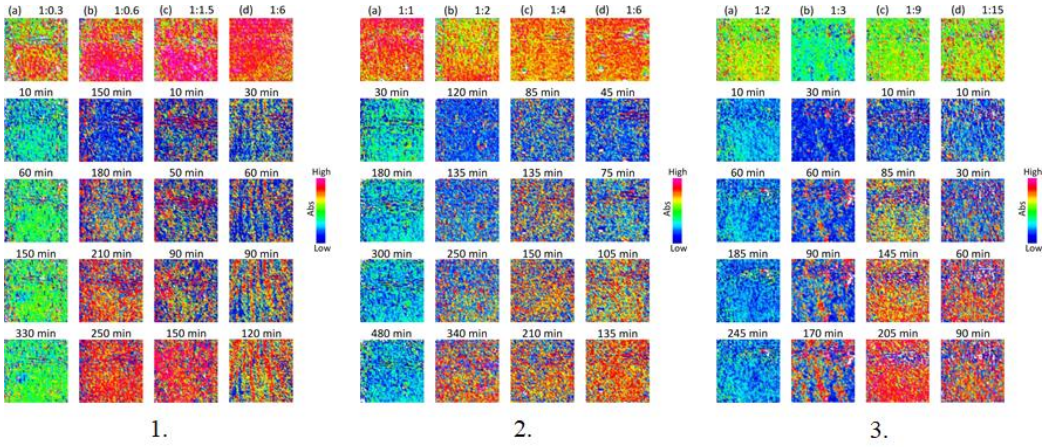


**Figure 41.** In situ macro-ATR-FTIR spectroscopic images of the crude oils: 1. sample 1, 2. Sample 2, 3 sample 3. The first row of images represents crude oil immediately after heptane addition, while The columns show the dynamics of asphaltene precipitation at different crude oil/heptane volume ratios (indicated above the columns) and heptane system. The imaging area is ca. 610 μm × 530 μm. Reprinted from [227] (Courtesy of ACS)

As it can be seen from column a) of figure 41, if the amount of precipitant is not sufficient to induce asphaltene precipitation, no colour change can be observed after the n-heptane addition. This is better shown in picture 3a. where the intense blue colour indicates the very low asphaltene concentration, while in figure 1a the green colour means that a small quantity of asphaltene has been precipitated after n-heptane addition. This led to the conclusion that crude oil sample 3 has a higher stability than the sample 1. On the other hand, if the heptane volume added to crude oil is high enough to destabilize asphaltene molecules the red/yellow isolated spots - which correspond to a relatively high concentration of complex aromatic hydrocarbons, indicating the formation of precipitate particles in particular regions of the measured sample area - followed by bigger patterns appear in the images (columns b-d). Furthermore, the authors selected ATR-FTIR spectra from the ATR-FTIR spectroscopic imaging in order to study the chemistry of the in situ precipitated asphaltenes. Spectra analysis revealed that mixture of various asphaltenes are precipitated by the n-heptane addition with the prevalence of some particular components or functional groups in function of the precipitant amount. For example, the presence of the oxygen-containing species was observed as major heteroatomic constituents in asphaltene molecules precipitated at ratios 1:0.6, 1:2, and 1:3 (and 1:6) for samples 1, 2, and 3, respectively. The precipitation of asphaltenes containing mostly nitrogen heteroatoms has occurred when samples 1, 2, and 3 are diluted with heptane at ratios of 1:1.5 (and 1:3), 1:4, and 1:9, respectively. Moreover, it has been shown that nitrogen atoms are in the form of pyrrole and pyridine groups. It has been shown that the less stable asphaltenes are that containing oxygen and nitrogen heteroatomic functional groups. NMR imaging was used by the authors to study the behaviour of bulk phases formed by aggregated asphaltenes, because ATR-FTIR spectroscopic imaging tests a relatively thin layer (1−5 μm) near the bottom of the sample. Figure 42 shows NMR imaging pictures describing three different cases investigated, namely excess of n-heptane (panel 1 of figure 42) medium n-heptane amount (panel 2 of figure 42) and low amount of n-heptane (panel 3 of figure 42).

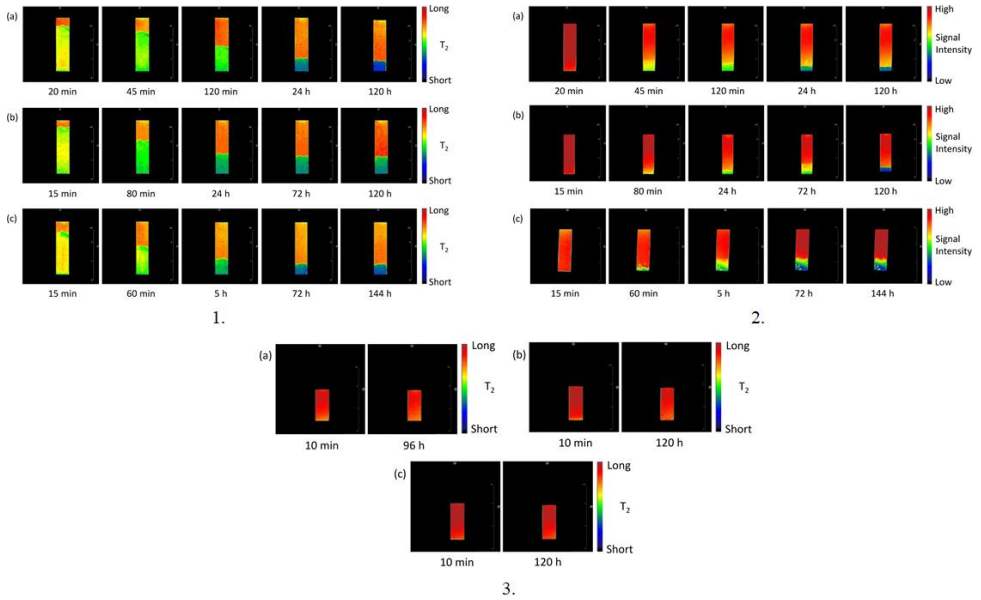


Figure 42 **Panel 1.**: crude oil/n-heptane (volume ratio 1:5). $T_2$ maps of vertical central slices taken during system time evolution. (a) (b), and (c) stand for sample 1, 2 and respectively. The red (orange) domains represent oil/n-heptane blend whereas asphaltenes suspension is represented by yellow and green, slowly transient into blue during the compaction and formation of deposit. **Panel 2**: $T_2$-weighted images of vertical central slices taken during crude oil/n-heptane system evolution: (a) sample 1 (ratio 1:2), (b) sample 2 (ratio 1:1.2), and (c) sample 3 (ratio 1:1). The red domains represent oil/n-heptane blend (top part of the system); yellow and green indicate slow accumulation of settling of asphaltene agglomerates. Blue colour represents the evolution of sediment resulting in deposit formation. **Panel 3:** crude oil/n-heptane (volume ratio 1:0.5). $T_2$-weighted images of vertical central slices taken during system evolution. (a), (b) and (c) stand for sample 1, 2 and 3 respectively. The in-time constant red colour and the same $T_2$ profiles during experiment demonstrate the stability of the system composition. Reprinted from [227] (courtesy of ACS)

As it can be seen from panel 1 of figure 42 the addition of an excess of n-heptane to the systems induces – almost immediately - the formation of two bulk phases (stratification), having remarkably different $T_2$ spin−spin relaxation times. The upper phase is characterized by a relatively and uniform distribution of long $T_2$ relaxation time. According to the authors, this phase is homogeneous and consists of crude oil components dissolved in heptane. The lower phase is characterized by possessing shorter $T_2$ relaxation time with slightly nonuniform initial distribution. The inhomogeneities of this phase represents the aggregates of asphaltenes that form suspension. Panel 2 of figure 42 shows a different behaviour of the system as the n-heptane concentration is lowered. Indeed, as it can be seen from the NMR images, the $T_2$ relaxation time within the sample and the $T_2$ changes near bottom region - where spin−spin relaxation time becomes shorter compared with other parts of the system – indicates that there is a slow formation of a new phase with a diffuse interface near the bottom of a sample. Contrary to the previous case, the formation of the interface in the top part of the samples was not observed. Additionally, the thickness of the deposit in the near bottom region first increases (interface moves upward), but further evolution results in a thickness decrease. During this process, the T2 relaxation time uniformly reduces within the bulk of the deposit (T2-profiles are presented in Figure 43).

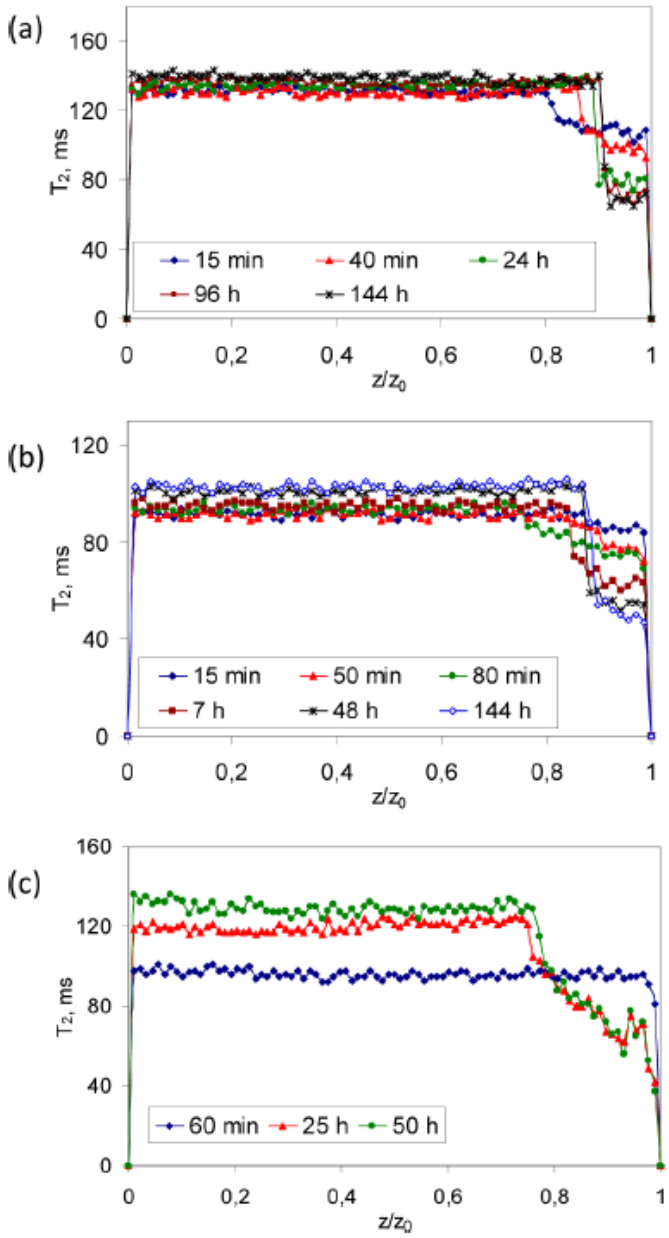


**Figure 43** $T_2$ profiles for crude oil/heptane system evolution: panel a) sample 1 (ratio 1:2), panel b) sample 2 (ratio 1:1.2), panel c) sample 3 (ratio 1:1). Reprinted from [227] (courtesy of ACS)

$T_2$ relaxation time for the upper part shifts to slightly higher values indicating changes of composition or/and structure of the crude oil within this part. Finally, at a very low n-heptane concentration, (panel c of figure 38) no phase separation is observed. Moreover, the corresponding $T_2$ profiles confirm constant and uniform distribution of relaxation times over the sample during the week-long period of experiment. Worthy of notice is the apparent discrepancy about the onset precipitation by n-heptane adding. As reported by the authors, it seems that this differs for the same crude oil sample depending on the method used. For example, the onset of asphaltene precipitation observed with ATR-FTIR spectroscopic imaging is: 1:0.6, 1:2 and 1:3 for sample 1, 2 and 3 respectively. On the contrary, the MRI revealed ratios of: 1:1.5, 1:1.2, 1:1 for sample 1, 2 and 3 respectively. According to the authors, these apparent discrepancies are due to differences in the two experimental methods and conditions used. Indeed, MRI studies the bulk of the sample, while ATR-FTIR spectroscopic imaging focuses only on a thin layer (few micrometres) in the vicinity of the measured surface

of the ATR crystal, namely at the bottom of a miniature container of crude oil. Therefore, it is expected that crude oil or precipitate properties, such as viscosity, rheology, size of agglomerates, density, etc., can influence the ability of spectroscopic methods to detect precipitation at the bottom of the container. Moreover, the MRI method has lower spatial resolution compared to ATR-FTIR chemical imaging, therefore the size of aggregated particles has to be large enough to be detected (basically a separate phase of precipitate should be formed).

### 1.6 Rheology

Nowadays, from a rheological point of view the bitumen can be separated mainly into three regions: the Newtonian at high temperatures, the viscoelastic at intermediate temperatures, and the glassy state at lower temperatures. These corresponds to two distinct relaxation mechanisms, each associated to one phase of the colloid system. [55,228] A transition - above room temperature - from Newtonian behaviour to viscoelastic behaviour (α-relaxation), attributed to the solid phase of the bitumen and a glass transition - in the low temperature region - from viscoelastic to glassy elastic behaviour (β-relaxation). This transition as it can be seen from figure 43 is due to the liquid phase (maltenes) of the bitumen.

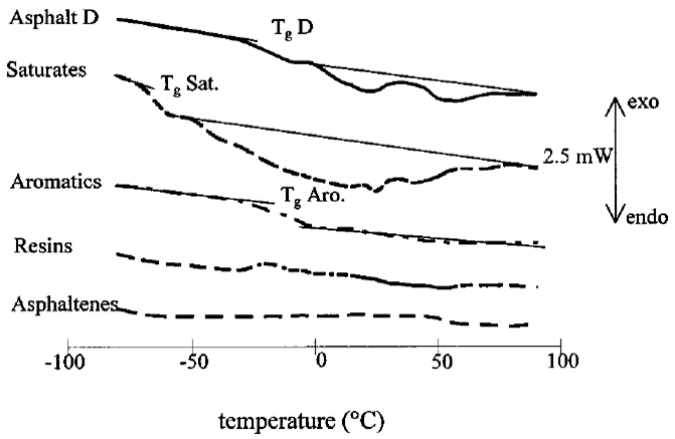


**Figure 43.** DSC thermograms of a bitumen and its SARA fractions. Reprinted from [229] (Courtesy of Taylor and Francis)

On the contrary, as reported by Williams et al. [230] for simple and homogeneous glass forming liquids, viscoelastic behaviour is found in the glass transition region when the glassy material becomes a Newtonian liquid. This results in a single relaxation phenomenon.

As said above at temperatures higher than 60 °C, bitumen is expected to show a Newtonian fluid behaviour, i.e. the zero-shear viscosity and its temperature dependency fully describe the rheological properties of asphalt in this region. Storm and co-workers [231] explain the temperature dependence of bitumen zero-shear viscosity on the basis of their experimental results from 40 to 300 °C by proposing a modified Roscoe–Brinkman equation [232]:

$$\eta_0 = \eta_{0,m}\left(1 - \frac{K\chi_{asph}}{\phi_m}\right)^{-2.5} \quad (11)$$

Where $\eta_{0,m}$ is the zero-shear viscosity of maltene phase, $K$ is the solvation parameter while $\chi_{asph}$ is the asphaltene mass fraction. The term $\frac{K\chi_{asph}}{\phi_m}$ describes the thickness of the solvation shell around the dispersed asphaltene particles, i.e it represents the volume increase due to the solvation shell, and also takes into account compacity effect through the $\phi_m$ parameter. It must be pointed out that $\phi_m$ is highly sensitive to polydispersity, making its theoretical predictions difficult [233-235]

Equation (11) quantifies the viscosity building role of asphaltenes as well as a concentration-viscosity relationship with a limiting compacity $\phi_m$. The Roscoe–Brinkman law was shown to well apply to different tested bitumens (see figure 44).

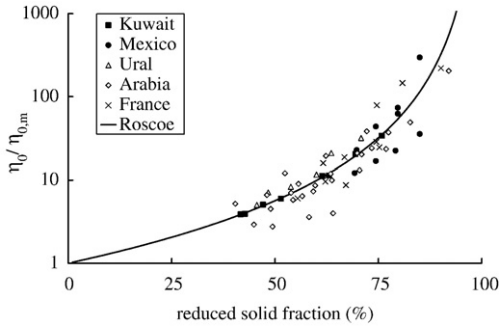


**Figure 44.** The Roscoe law fitting for various bitumens. Reprinted from [25] (courtesy of Elsevier)

As it can be easily seen equation (11) is not linear in $K\chi_{asph}$. This means that hydrodynamic interactions exist between asphaltene particles, i.e., the viscosity ‘‘seen’’ by each asphaltene particle is that of the whole suspension (resembling a Mean-Field theory). Moreover, as pointed out by various researchers [233-235] linearity would indicate a dilute regime where each particle behaves as if no other particle was present. This dilute regime is known to be effective for volume fractions of dispersed particles lower than 10%.

From equation (11), it can be seen that the molecular weight of the components does not appear. This means that no direct proportionality between viscosity and molar mass - such as that found in the polymer literature [51] - apply to bitumen. However, it does not mean that molar mass has no effect on the viscosity. It affects the whole viscosity through its effect on the maltenes viscosity. Then, the shape and chemical nature of the molecules would also be important parameters and makes it therefore very unlikely that a unique molecular indicator such as an average molecular weight, would be sufficient to explain the variability of maltene viscosity among existing bitumens. The main parameters controlling bitumen viscosity are therefore its asphaltenes content, its solvation constant and the maltenes viscosity.

Lowering the temperature, viscoelastic (α-relaxation) and elastic glassy behaviour (β-relaxation) effects appear. Several models were proposed to describe the α- and β-relaxation. The more useful for a close analysis are those by Verney et al. [236] and Lesueur et al. [54] for α-relaxation model, and that of Christensen and Anderson [237] for the β one. These models allow the extraction of the relevant parameters describing the transition, i.e., the Newtonian viscosity and a mean relaxation time $\tau$. The relaxation times $\tau_\alpha$ and $\tau_\beta$ are related

to the viscosity of the material $\eta_0$, to the asphaltenes micelle size $a_0^3$ - as measured by SAXS – and to glassy modulus $G_g$ by [54,228] the following equations:

$$\tau_\alpha = \frac{\eta_0}{\sigma_\alpha} = \frac{6\pi\eta_0 a_0^3}{kT} \quad (\sigma_\alpha = \frac{kT}{6\pi a_0^3}) \tag{12}$$

$$\tau_\beta = \frac{\eta_0}{G_g} \tag{13}$$

Where *k* is the Boltzmann constant *T* the temperature and $\sigma_\alpha$ is the critical stress.

Equations (12) and (13) can be combined in the following one:

$$\tau_\alpha = \frac{6\pi G_g a_0^3}{kT}\tau_\beta \tag{14}$$

From this, and using the typical values of the involved parameters, one shows that the α-relaxation time is about 6 decades higher than the β-relaxation time, explaining the presence of very long relaxation times above the glass transition in bitumen rheology.

The existence of very large relaxation times remained unclear until the last decade. In the light of the colloidal model, long relaxation times occur as a consequence of the presence of asphaltene nanoparticles with a dynamic behaviour coupled to the vitrification of the maltenes through equation (12).

To conclude it can be said that: 1) the bitumen α-relaxation at which viscoelastic effects start to appear is associated to the Brownian motion of the asphaltenes micelles and the relaxation time is proportional to the bitumen viscosity and the cube of the asphaltenes micelle size. The maltene phase is however also directly involved in the phenomenon through the bitumen viscosity and there is therefore a strong coupling between the two phases; 2) the β-relaxation, transition from the viscoelastic to the elastic regime, is a consequence of the vitrification of the maltene phase and the higher the glass transition temperature, the higher the modulus (higher $\tau_\beta$). The asphaltenes still have an influence on the relaxation function, and the higher the asphaltenes content, the smaller the relaxation rate. Thus, just like for the α-relaxation, there is again a coupling between asphaltenes and maltenes at low temperature as well.

### 1.7. Molecular simulations of asphaltene behaviour and interaction between asphaltenes and resins

Studies [41,238,239] have shown that the resin fraction of crude oil stabilizes the asphaltenes. Once the resins are removed, the remaining parts of the crude oil can no longer stabilize the asphaltenes and this leads to aggregate formation- a phenomenon that is responsible for a significant amount of the problems encountered by industries in fractional distillation of crude oil. Resins affect the behaviour of asphaltenes by helping them stay in solution. This characteristic is called the 'peptizing power' of resins. The origin of this peptizing power is still unknown just like the exact nature of asphaltene-resin interactions are still not totally understood [176, 240].

As stated earlier, crude oil can be separated into 4 fractions: Saturates, aromatics, resins and asphaltenes (SARA). This is shown in Figure 45. It is believed that the thermodynamic stability of crude oil largely depends

on the presence and distribution of resins in the crude oil. Studies [145,241-243] have shown that if both asphaltenes and resins are present, resin-asphaltene interactions are preferred over asphaltene-asphaltene interactions and that resins are able to penetrate the structure of solid asphaltenes and break the asphaltene-asphaltene interactions thus facilitating resin-asphaltene interactions. The interplay between asphaltene and resin molecules in the formation of petroleum micelles has been a highly debateable topic in recent years and molecular simulation techniques have been employed by several researchers in order to characterize the interaction between these two groups of molecules using algorithmic tools in a virtual context. The results of molecular modelling of asphaltene-resin complexes can also provide reasonable answers about the homogenous and heterogenous nature of micelles; a topic which has confronted researchers for decades. Molecular simulations also describe π stacking interactions and also the importance of dispersion energy in stabilizing stacked asphaltene dimers. Molecular modelling and molecular dynamics are approaches which effectively characterize several parameters of molecules in general- a huge number of those molecules being biological macromolecules.

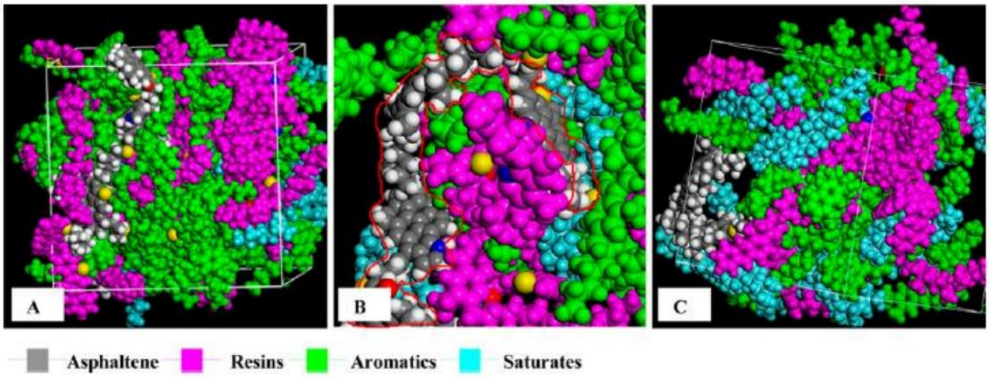


**Figure 45.** Snapshots of asphalt molecular models by MD for the arrangement of SARA fractions. Image A was the whole arrangement of four fractions, while images B and C were the large asphaltene molecular bending. Image B showed the resin molecules inserted into the spaces of bending asphaltenes, and image C also offered the arrangement of resins, aromatics, and saturates [244] (Courtesy of ACS)

Molecular modelling is of paramount importance to characterize structures of molecules of interest. In the case of asphaltenes and resins, molecular modelling is done using two types of software; Structure elucidation programs such as XMOL and SIGNATURE and Molecular simulation programs such as INSIGHT 2 and DISCOVER, MAPS and GROMACS. Structure elucidation programs elaborate the structures of molecular models of interest indicating the positions of atoms and other moieties of the molecule while molecular simulation programs simulate the interactions between molecular models of interest clearly presenting values such as bond length, torsion, bond angle, bond distance and binding energy values. However, before molecular modelling can be done, analytical base data is gathered by atomic analysis and molecular weight measurements in conjuction with molecular analyses of molecules of interest. Molecular mechanics and molecular dynamics are simulation techniques which are both contributively essential to simulating the interactions between these molecules of interest. Molecular mechanics involves the simulation of of atoms and molecules using specific designated force fields and assuming the energies of the molecules are static. This is done by energy minimization of the system which takes the molecules to a relaxed state of the lowest possible energy

conformation. Molecular dynamics on the other hand is the simulation of the motions, trajectories and interactions of molecules within a specific timeframe without depending on force field parameters.

Due to the difficulties involved in characterizing asphaltenes experimentally, computerized molecular simulations offer an effective and powerful tool in characterizing their behaviour. Studies [245] using all atom (AA) molecular dynamics simulations have characterized the nanoaggregation of asphaltenes under various thermodynamic conditions and in various solvents. All Atom (AA) molecular dynamics simulations are atomically detailed and thus are computationally expensive in the sense that they are time consuming and they limit the size and scope of studies to be carried out. Due to the computational expense of AA models, interest in Coarse-Grain (CG) models has risen in recent studies. This model represents systems in reduced detail, simulates longer timescales and larger systems while also generating improved statistics for simulations which have a diverse range of applications on molecules of interest [245]. This study used CG models to simulate and study asphaltene behaviour, some aspects of which are asphaltene phase behaviour and self-assembly processes. The results of their simulations indicated that island-type asphaltenes form nanoaggregates with stacked aromatic cores under conditions that promote aromatic attraction. Interestingly, the threshold for nanoaggregation appears insensitive to the length of the aliphatic tails that surround the aromatic core. This gives further credence to the results of Bhattacharjee et al [246]. Conversely, archipelago asphaltenes do not form prototypical nanoaggregates under any simulated conditions, although they do form large aggregates under conditions that promote strong attraction between either aromatic or aliphatic sites. These results generally agree with the expectations of the Yen-Mullins model [245].

Frigerio and Molinari [247] carried out a simulation of model asphaltenes using the MAPS molecular modelling platform in order to investigate the structure of asphaltene nanoaggregates and the driving force behind their clustering in different solvents. Figure 46 shows the molecular structures of 2 of the asphaltene models used in their study.

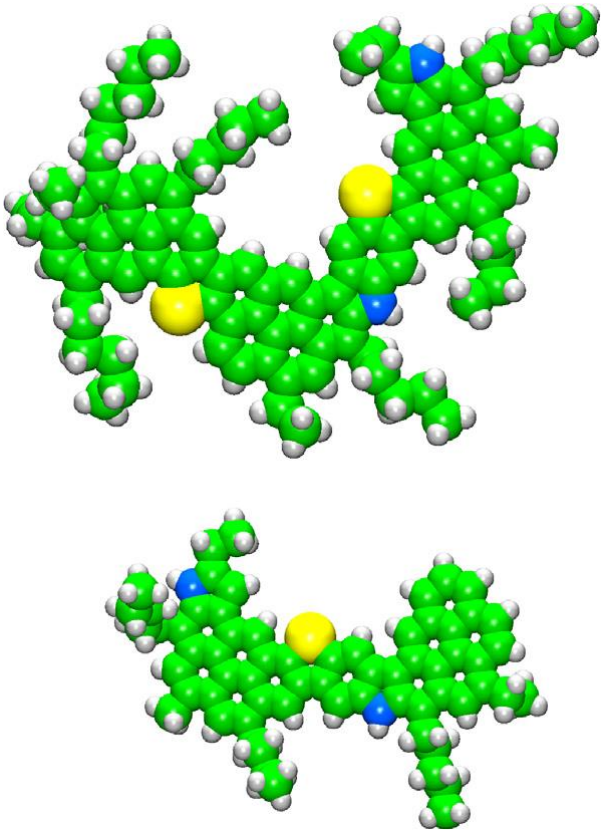

**Figure 46.** Molecular Structures built for some asphaltene models [247] (courtesy of Elsevier)

Molecular weights of all asphaltene structures are usually produced by the molecular modelling software as these values are important in molecular simulation of molecules in order to be able to effectively characterize their behaviour during and even after simulation. Probability distribution function (pdf) curves of intermolecular distance are also usually plotted in order to simulate and characterize the formation of asphaltene clusters obtained in nanoaggregation simulations. C/C distances (all C atoms of the aromatic ring) are suitable for this purpose since their number is large and they are located in the extended planar core of the asphaltenes. These curves are calculated along the Molecular Dynamics (MD) trajectory and generate peaks corresponding to the formation of nanoaggregates derived from trimers, tetramers and so on. This is an effective way to characterize asphaltene nanoaggregation. Figure 47 shows a pdf plot while Figure 48 shows an asphaltene cluster modelled by the molecular simulation of asphaltenes carried out by Frigerio and Molinari [247]

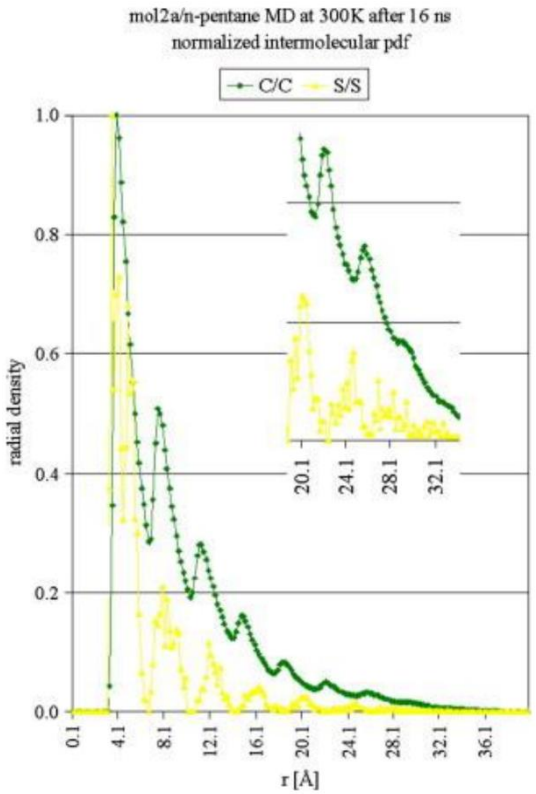


**Figure 47.** pdf plot of model asphaltenes generated along the MD trajectory of molecular simulation [247] (courtesy of Elsevier)

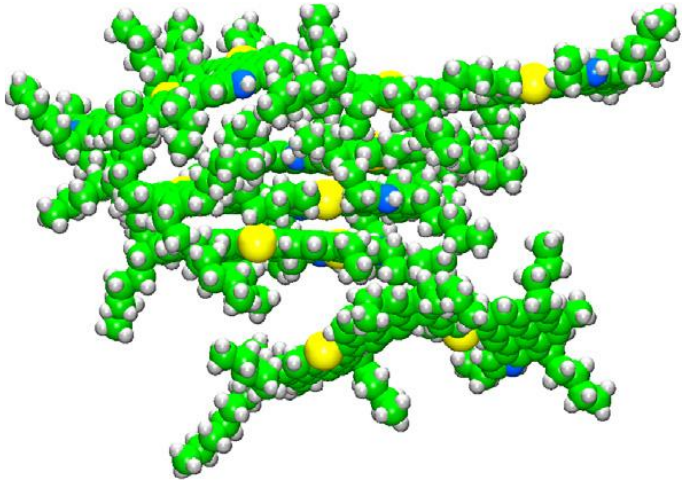

**Figure 48.** Asphaltene cluster obtained during molecular modelling [247] (courtesy of Elsevier)

Similar nanoaggregate clustering was also reported in literature [248,249] and this gives further credence to the data reported by Frigerio and Molinari [247]. Several research groups [246,250-261] have also synthesized several families of asphaltene model molecules that mimic the properties of asphaltenes. Some of these properties include solubility, interfacial properties, surface forces and molecular dynamics simulations. Figure 49 shows the snapshots obtained from molecular dynamics simulations of molecules of families of asphaltene which mimic asphaltenic properties.

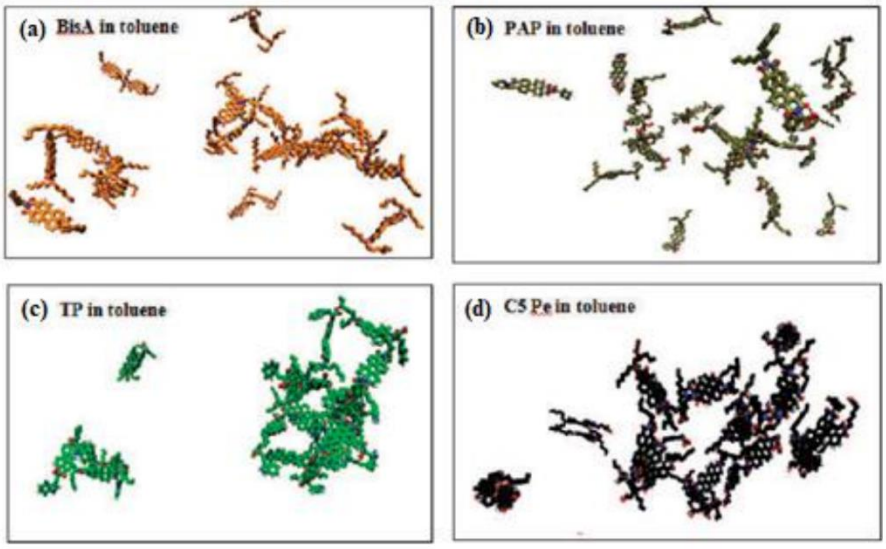


**Figure 49.** Snapshots of molecular configurations of polyaromatic surfactant molecules in toluene after 20 ns simulation time [246] (courtesy of ACS)

Bhattacharjee et al [246] studied the effect of asphaltene side-chains on the self-association properties of molecules similar to Violanthrone VO-79 in water. This is shown in figure 50. They found that the relationship between side-chain length and extent of aggregation is not monotonic. Their results showed that the model molecules wth very short ($C_4$) or very long ($C_{16}$) side chains can form dense aggregates while those with intermediate chain lengths ($C_8$ and $C_{12}$) cannot. This is due to the balance between interactions of polyaromatic cores ($\pi - \pi$) on one hand and between a polyaromatic core and an aliphatic chain ($\pi - \Theta$) or between aliphatic chains ($\Theta$ - $\Theta$).

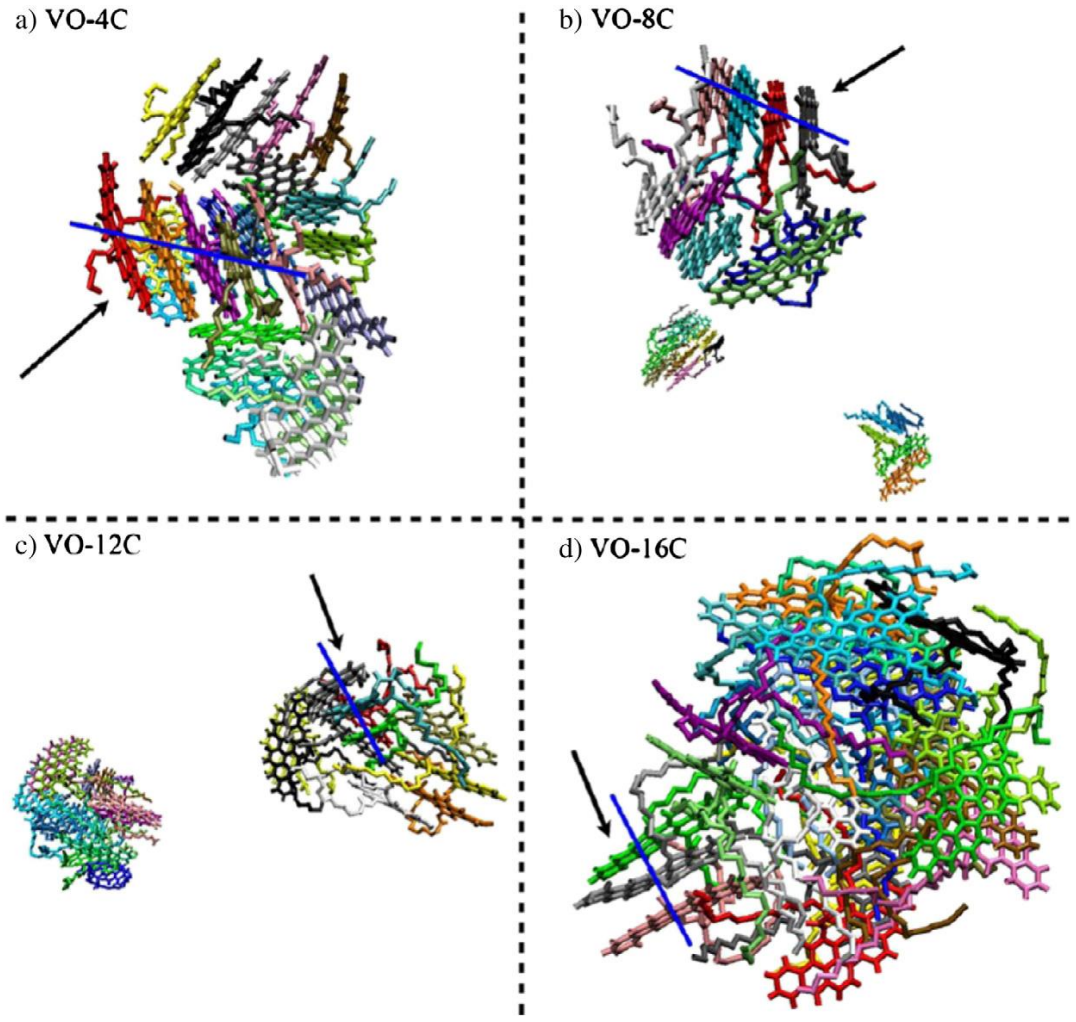


**Figure 50.** Snapshots of 24 asphaltene model molecules in water. The molecules in each system are represented by different colours. Water molecules have been removed for clarity [255] (courtesy of ACS)

H bonding and charge transfer have been initailly cited as the factors responsible for interactions between asphaltenes and resins [21]. Murgich et al however showed that the overall electronic structure of the asphaltene molecule is mainly determined by its much larger hydrocarbon skeleton. They therefore stated that the number of heteroatoms present in asphaltenes and resins (which is less than 5%) suggest that the hydrocarbons are not likely to have a high degree of charge transfer when forming a molecular aggregate. Some molecular simulation studies [262,263] have shown that the minimum energy molecular conformations of asphaltenes and resins prove that these molecules have almost planar aromatic regions. Asphaltenes and resins form parallel stacks in the solid state to maximize the C-C interactions between them and the presence of alkyl and cycloalkyl groups in asphaltene and resin molecules contribute to their molecular recognition mechanism. Cyclic alkyls and the aromatic planes of asphaltene dimers have also been shown to generate around 70% of the total attractive energy of the molecules. The large influence of these carbon atoms on the attraction energy is as a result of the strong ring-ring interactions which exist between aromatic molecules [263]. It is safe to say that the driving force behind the interaction in micelle formation of model asphaltene-resin dimers with aromatic regions is the attraction between the aromatic planes. In the case of an asphaltene-resin trimer or tetramer, the resulting aggregate possesses extra alkyl branches which produce a steric repulsion

which in conjunction with van der Waal forces prevent any further aggregation and thus stops the growth of the micelle [264,265]. The balance between these attractive and repulsive interactions is very likely to be the underlying factor behind the complex colloidal behaviour exhibited by asphaltenes in crude oil.

Using the simple molecular model described above, Rogel [266] developed an analytical expression for the free energy of aggregation of asphaltenes. This analytical expression incorporates 5 contributions due to: (i) transfer of polyaromatic rings from the solvent into the aromatic core (ii) mixing of the aliphatic chain with the solvent (iii) deformation of the aliphatic chains (iv) steric repulsion produced by the aliphatic chains (v) interactions between the aggregate core and the solvent. The analytical expression is:

$$\Delta G^0_{mic}(N, Sh) = \frac{(\mu^0_N - N\mu^0_1)}{N} \tag{15}$$

Where $\mu^0_1$ is the standard chemical potential of an asphaltene molecule free in the solvent, $\mu^0_N$ is the standard chemical potential of an asphaltene aggregate containing N asphaltene molecules and $\Delta G^0_{mic}(N, Sh)$ is the free energy difference. The main goal of any molecular aggregation model is to evaluate this free energy difference.

There is no doubt about the important role played by resins in asphaltene behaviour and stabilization but there are still many questions that baffle researchers about this phenomenon. Molecular simulations, adsorption studies and thermodynamic approaches suggested that either the formation of a steric stabilization layer of resins prevents the flocculation of asphaltene particles or the resins split the asphaltene aggregates into smaller structures to stabilize them [176,240,266]. To explore the mechanism of asphaltene stabilization by resins, Rogel developed a thermodynamic approach to describe the formation of asphaltene-resin aggregates. This work proposed another analytical expression but this time for the free energy of mixed asphaltene-resin aggregates. The development of this expression is based on (i) the transfer of aromatic moieties of resins and asphaltenes from the solvent to the aromatic core (ii)the contribution of the formation of aggregate solvent interface (iii) steric repulsions among the aliphatic chains at the interface between the aromatic core and the shell. The expression goes thus:

$$\Delta G_{agg}(N, \alpha) = \frac{\mu^0_{N,\alpha} - N\alpha\,\mu^0_A - N(1-\alpha)\mu^0_R}{N} \tag{16}$$

Where $\mu^0_{N,\alpha}$ is the standard chemical potential of a mixed aggregate having N molecules and a composition of α while $\mu^0_A$ and $\mu^0_R$ represent the standard chemical potentials of free asphaltene and resin molecules in the solvent. Using this expression, a computational approach was carried out and a new relation for the calculation of aggregate size and composition distribution was developed:

$$X(N, \alpha) = X^{\alpha N}_{A_1} X^{(1-\alpha)N}_{R_1} e^{N\Delta G_{agg}(N,\alpha)} \tag{17}$$

Where $X_{A_1}$ and $X_{R_1}$ are the mole fractions of the singly dispersed asphaltene and resin molecules respectively. In another thermodynamics study, Morgado et al [267] calculated the binding energies of dimer molecules of asphaltenes and resins on the basis of quantum calculations using [268] a density functional theory. The binding energy for the asphaltene-asphaltene dimer was calculated to be 56.5 kJ/mol while that of the asphaltene-resin dimer was 54.4 kJ/mol and that of the resin-resin dimer was calculated to be 23.8 kJ/mol. Morgado et al observed that the binding energies of the asphaltene-asphaltene dimer and asphlatene-resin dimer are very similar. They also observed that due to the significantly lower binding energy of the resin-resin dimer, the resin molecules interact preferentially with the asphaltene molecules rather than with themselves. All these phenomena just go to prove the stabilizing effect resins have on asphaltenes.

### 1.8 Asphaltene-Resin Interaction

One of the key points of the modified Yen model is that it predicts the formation of asphaltene nanoaggregates and nanoaggregate clusters without invoking any resin interaction. Thus, the classic view of the "surfactant resin" for asphaltene nanoaggregates is incompatible with the modified Yen model. When asphaltene science was in its infancy, many researchers have argued that are colloidally suspended in crude oil [47,269], a statement that nowadays has proven to be correct. However, it was also stated without demonstration that asphaltene colloidal particles are stabilized by resin molecules that acts as surfactant for asphaltenes in crude oils. The surfactant role of resins was proposed in similarity with the oil in water emulsion stabilized by charged surfactants whose charged colloidal particles repels each other precluding coalescence. However, the possible role of resin's electric charge was left unaddressed. As indicated by Zeng et al. [270] "*any stabilizing role of resins is unlikely to involve charge because they exhibit less charge than asphaltene*". Moreover, as described in the previous sections different techniques have shown that asphaltene stably suspended in toluene without resins. In addition, the asphaltene nanoaggregates found in crude oil appear similar to those in toluene [271]. However, this not means that there is no interaction between asphaltene and resins. Ultrafiltration studies of very asphaltic systems initially found little evidence of asphaltene-resin interaction [272]. A comprehensive interpretation of all data from the ultrafiltration experiments on very asphaltic systems indicated that the extent of resin interaction with asphaltenes varies with conditions and is on the order of 15% by mass [273]. Microcalorimetry results indicate there is an asphaltene resin interaction and that the strength of interaction is 2-4 kJ/mol and comparable to the asphaltene-asphaltene interaction. [274,275] Other studies have also seen effects from resins on asphaltene aggregation. SANS measurements indicate that asphaltene aggregate sizes decrease in the presence of resins. [153] These data are also consistent with the finding that the more soluble asphaltene fractions are characterized by smaller sized aggregates. [276] The addition of resins to asphaltenes in toluene reduced the interfacial activity of the corresponding solutions. [153] The resins might act to bind high-energy sites that would otherwise be more available to be active at oil-water interfaces. [153] Other measurements also indicate that there are asphaltene-resin interactions, such as the measurement of vapor pressure osmometry. [42] Asphaltenes absorb differently onto quartz crystal microbalances dependent upon

whether resins are present. [277] There is evidently asphaltene-resin interactions. Nevertheless, the interaction is not properly framed within a micelle model.

**References to Chapter 1**


[1] Self A., Introduction. In the Shell Bitumen Handbook, 6th ed.; Hunter, R.N., Self, A., Read, J., Eds.; ICE Publishing: London, UK, 2015; ISBN 978-0727758378

[2] Connan J, Use and trade of bitumen in antiquity and prehistory: molecular archaeology reveals secrets of past civilizations, *Phil Trans R Soc Lond B*, **1999**; 354:33–50

[3] Abraham H. Asphalt and Allied Substances. 6th Ed. New York: Van Nostrand; **1960**

[4] Krishnan M. J, Rajagopal K. R. Review of uses and modelling of bitumen from ancient to modern times. *Appl Mech Rev*, **2003**, 56, 149–214

[5] Barakat A. O, Mostafa A., Qian Y., Kim M., Kennicutt II M.C., Organic geochemistry indicates Gebel El Zeit, Gulf of Suez, is a source of bitumen used in some Egyptian Mummies, *Geoarchaeology*, **2005**, 20, 211–228

[6] Krchma L. C., Gagle D. W., A U.S.A. history of asphalt refined from crude oil and its distribution. *Proc. Assoc. Asphalt Paving Tech.*, **1974**, 43A, 25–88.

[7] Lay M.G., Ways of the World. New Brunswick: Rutgers Univ. Press; **1992**.

[8] Pfeiffer J. P., Introduction. Definitions, nomenclature and concepts. In: Pfeiffer JP, editor. The Properties of Asphaltic Bitumen. Amsterdam: Elsevier; **1950**. p. 1–12

[9] European Committee for Standardization EN 12597: Bitumen and Bituminous Binders-Terminology; European Committee for Standardization: Brussels, Belgium, **2000**.

[10] Petrauskas D.; Ullah S., Manufacture and storage of bitumens. In the Shell Bitumen Handbook, 6th ed.; Hunter, R.N., Self, A., Read, J., Eds.; ICE Publishing: London, UK, **2015**; ISBN 978-0727758378.

[11] Paliukait M.; Vaitkusa A.; Zofkab A., Evaluation of bitumen fractional composition depending on the crude oil type and production technology. In Proceedings of the 9th International Conference "Environmental Engineering" Selected Papers, Vilnius, Lithuania, 22–23 May **2014**

[12] Al-Sahhaf Amal Elkilani M. F. T., Fundamentals of Petroleum Refining 1st Edition, Elsevier Science November **2009** ISBN: 9780444527851

[13] Read J. Witheoak D., The Shell Bitumen Handbook, 5th ed.; Thomas Telford Publishing: London, UK, **2003**.

[14] McNally T. Introduction to polymer modified bitumen (PmB). In Polymer Modified Bitumen Properties and Characterisation, 1st ed.; McNally, T., Ed. Woodhead Publishing: Sawston, UK, **2011**

[15] Lu X., Isacsson U., Ekblad J., Phase Separation of SBS Polymer Modified Bitumens, *J. Mater. Civ. Eng.*, **1999**, 11, 51–57

[16] Petersen J. C. Chemical Composition of Asphalt as Related to Asphalt Durability: State of the Art, *Transp. Res. Rec.*, **1984**, 999, 13–30

[17] Branthaver J. F., Petersen J. C., Robertson, R. E. Duvall, J. J. Kim, S. S., Harnsberger P. M., Mill T., Ensley E. K., Barbour F. A., Schabron J. F., Binder Characterization and Evaluation-vol 2 Chemistry; SHRP Report A-368; National Research Council: Washington, DC, USA, **1994**

[18] Mortazavi M., Moulthrop J. S., SHRP Materials Reference Library; SHRP report A-646; National Research Council: Washington, DC, USA, **1993**

[19] Strategic Highway Research: Special Report 260. Committee for Study for a Future Strategic Highway Research Program, Strategic Highway Research; Transportation Research Board Special Report 260; National Research Council: Washington, DC, USA, **2001**

[20] Jiménez-Mateos J.M., Quintero L.C., Rial C., Characterization of petroleum bitumens and their fractions by thermogravimetric analysis and differential scanning calorimetry, *Fuel*, **1996**, 75, 1691 1700

[21] Speight J. C. The Chemistry and Technology of Petroleum, 3rd ed.; Marcel Dekker: New York, NY, USA, **1999**

[22] Nahar S. N., Schmets A. J. M., Scarpas A., Determining Trace-elements in Bitumen by Neutron Activation Analysis. In proceedings of the 94th Annual Meeting Conference: Transportation Research Board, Washington DC, U.S.A, January **2015**

[23] D'Melo, D., Taylor R., Constitution and Structure of Bitumens. In the Shell Bitumen Handbook, 6th ed.; Hunter, R.N., Self, A., Read, J., Eds.; ICE Publishing: London, UK, **2015**; ISBN 978-0727758378

[24] Polacco G., Filippi, S., Merusi F., Stastna G., A review of the fundamentals of polymer-modified asphalts: Asphalt/polymer interactions and principles of compatibility. *Adv. Colloid Interface Sci.*, **2015**, 224, 72–112

[25] Lesueur D., The Colloidal Structure of Bitumen: Consequences on the Rheology and on the Mechanisms of Bitumen Modification. *Adv. Colloid Interface Sci.*, **2009**, *145*, 42–82

[26] Ashoori S., Sharifi M., Masoumi M., Salehi M.M., The Relationship between SARA Fractions and Crude Oil Stability. *Egypt. J. Pet.*, **2017**, *26*, 209–213

[27] Lin M. S., Chaffin J. M., Liu M., Glover C.J., Davison R.R., Bullin J.A., The effect of asphalt composition on the formation of asphaltenes and their contribution to asphalt viscosity. *Fuel Science and Technology International*, **2006**, *14*(1–2), 139–162

[28] Corbett L. W., Composition of asphalt based on generic fractionation, using solvent deasphaltening, elution-adsorption chromatography and densimetric characterization. *Anal. Chem.*, **1969**, *41*, 576–579.

[29] Speight J.C., Petroleum asphaltenes. Part 1. Asphaltenes, resins and the structure of petroleum. Oil Gas *Sci. Technol.*, **2004**, 59, 467–477

[30] Mullins O., Optical Interrogation of Aromatic Moieties in Crude Oils and Asphaltenes. In Structures and Dynamics of Asphaltenes; Mullins, O., Sheu, E.Y., Eds.; Plenum Press: New York, NY, USA, **1998**; pp. 21–77. ISBN 978-1-4899-1615-0

[31] Piéri N., Etude du Vieillissement Simulé et In-Situ des Bitumens Routiers Par IRTF et Fluorescence UV en Excitation-Emission Synchrones. Ph.D. Thesis, Aix-Marseille University, St-Joseph, France, **1995**

[32] Scotti R., Montanari L., Molecular structure and intermolecular interaction of asphaltenes by FT-IR, NMR, EPR. In Structures and Dynamics of Asphaltenes; Mullins, O., Sheu, E.Y., Eds.; Plenum Press: New York, NY, USA, **1998**; pp. 79–113. ISBN 978-1-4899-1615-0

[33] Bergmann U., Mullins O.C., Cramer S.P., X-Ray Raman spectroscopy of carbon in asphaltene: Light element characterization with bulk sensitivity. *Anal. Chem.*, **2000**, *72*, 2609–2612

[34] Michon L., Didier M., Jean-Pascal P., Bernard H., Estimation of average structural parameters of bitumens by $^{13}C$ Nuclear Magnetic Resonance spectroscopy. *Fuel*, **1997**, 76, 9–15

[35] Sheremata J.M., Gray M.R., Dettman H.D., McCaffrey W.C., Quantitative molecular representation and sequential optimization of Athabasca asphaltenes. *Energy Fuels*, **2004**, 18, 1377–1384

[36] Rozeveld S., Shin, E., Bhurke A., France L., Drzal L., Network morphology of straight and polymer modified asphalt cements. *Microsc. Res. Tech.*, **1997**, 38, 529–543

[37] Calandra P., Caputo P., De Santo M.P., Todaro L., Turco Liveri V., Oliviero Rossi C., Effect of additives on the structural organization of asphaltene aggregates in bitumen. *Constr. Build. Mater.*, **2019**, 199, 288–297

[38] Jager A., Lackner R., Eisenmenger-Sittner C., Blab R., Identification of Microstructural Components of Bitumen by Means of Atomic Force Microscopy (AFM). *Proc. Appl. Math. Mech.*, **2004**, 4, 400–401

[39] Duran J.A., Casas Y., Xiang L., Zhang L., Zeng, H., Yarranton H.W., Nature of Asphaltene Aggregates. *Energy Fuels*, **2019,** *33*, 5, 3694-3710

[40] Gawel I., Czechowski F., Study of saturated components in asphalt., *Pet. Sci. Technol.*, **1997**, 15, 729–742

[41] Koots J. A., Speight J.G., Relation of petroleum resins to asphaltenes, *Fuel*, **1975**, 54, 179–184

[42] Yarranton H.W., Fox W.A., Svrcek W.Y., Effect of Resins on Asphaltene Self-Association and Solubility, *Can. J. Chem. Eng.*, **2007**, 85, 635–642

[43] Rosinger A., Beiträge zur Kolloidchemie des Asphalts. Kolloid-Z, **1914**, 15, 177–9

[44] Nellensteyn F. J., Bereiding en Constitutie van Asphalt, Ph.D. Thesis: Delft University (Netherland), **1923**

[45] Errera J., The sensitiveness to light of asphalt as a function of its degree of dispersion, *Trans Faraday Soc*, **1923**, 19, 314–317

[46] Nellensteyn F. J., The constitution of asphalt, *J Inst Pet Technol*, 1924, 10, 311–325

[47] Pfeiffer J. P, Saal R. N. J., Asphaltic bitumen as colloid systems, *J. Phys. Chem.*, **1940**, 44, 139–149

[48] Saal R. N. J., Physical properties of asphaltic bitumen. 1. Rheological properties. In: Pfeiffer JP, editor. The Properties of Asphaltic Bitumen. Amsterdam: Elsevier; **1950**. p. 50–76

[49] Saal R. N. J., Labout J. W. A., Rheological properties of asphaltic bitumens, *J. Phys. Chem.*, **1940**, 44, 149–165

[50] De Gennes P. G., Scaling Concepts in Polymer Physics. Ithaca: Cornell University Press; **1979**

[51] Ferry J. D., Viscoelastic Properties of Polymers. 3rd Ed. NewYork:Wiley & Sons; **1980**

[52] Russel W. B., Savill D. A., Schowalter W. R., Colloidal Dispersions. London: Cambridge Univ. Press; **1992**

[53] Anderson D. A., et al. Binder Characterization and Evaluation Volume 3: Physical Characterization, SHRP report A- 369.Washington D. C.: National Research Council; **1994**

[54] Lee A. R., Warren J. B., Waters D. B., The flow properties of bituminous materials, *J Inst Pet Technol.*, **1940**, 26, 101–128

[55] Lesueur D., Gérard J. F., Claudy P., Létoffé J. M., Planche J. P., Martin D., A structure related model to describe asphalt linear viscoelasticity, *J. Rheol.*, **1996**, 40, 813–836

[56] Dickie, J. P.; Yen, T. F. Macrostrucutres of asphaltic fractions by various instrumental methods, Anal. Chem., 1967, 39, 1847–1852

[57] Mullins O. C., The Modified Yen Model, *Energy Fuels*, **2010**, 24, 2179–2207

[58] Groenzin H.; Mullins O. C., Asphaltene molecular size and structure, *J. Phys. Chem. A*, **1999**, 103, 11237–11245

[59] Groenzin H., Mullins O. C., Molecular sizes of asphaltenes from different origin, *Energy Fuels*, **2000**, 14, 677

[60] Buenrostro-Gonzalez E., Groenzin H., Lira-Galeana C., Mullins O. C., The overriding chemical principles that define asphaltenes, *Energy Fuels*, **2001**, 15, 972

[61] Groenzin H., Mullins O. C., Eser S., Mathews J., Yang M.-G., Jones D., Asphaltene molecular size for solubility subfractions obtained by fluorescence depolarization, *Energy Fuels*, **2003**, 17, 498

[62] Badre S., Goncalves C. C., Norinaga, K., Gustavson G., Mullins O. C., Molecular size and weight of asphaltene and asphaltene solubility fractions from coals, crude oils and bitumen, *Fuel*, **2006**, 85, 1

[63] Buch L., Groenzin H., Buenrostro-Gonzalez E., Andersen S. I., Lira-Galeana, C., Mullins O. C., Effect of hydrotreatment on asphaltene fractions, *Fuel*, **2003**, 82, 1075

[64] Groenzin H., Mullins O. C., Asphaltene molecular size and weight by time-resolved fluorescence depolarization. In Asphaltenes, Heavy Oils and Petroleomics; Mullins, O. C., Sheu, E. Y., Hammami, A., Marshall, A. G., Eds.; Springer: New York, **2007**, Chapter 2

[65] Turro N. J., Modern Molecular Photochemistry, Benjamin/Cummings: Menlo Park, CA, **1978**

[66] Wargadalam V. J., Norinaga K., Iino M., Size and shape of a coal asphaltene studied by viscosity and diffusion coefficient measurements, *Fuel*, **2002**, 81, 1403–1407

[67] Freed D. E., Lisitza N. V., Sen P. N., Song Y.Q., Asphaltene molecular composition and dynamics from NMR diffusion measurements. In Asphaltenes, Heavy Oils and Petroleomics; Mullins, O. C., Sheu, E. Y., Hammami, A., Marshall, A. G., Eds.; Springer: New York, **2007** Chapter 11

[68] Freed D. E., Lisitza N. V., Sen P. N. Song Y. Q., A study of asphaltene nano-aggregation by NMR, *Energy Fuels*, **2009**, 23, 1189 – 1193

[69] Andrews A. B., Guerra R., Mullins O. C., Sen P. N., Diffusivity of asphaltene molecules by fluorescence correlation spectroscopy, *J. Phys. Chem. A*, **2006**, 110, 8095

[70] Guerra R., Andrews A. B., Mullins O. C., Sen P. N., Diffusivity of coal and petroleum asphaltene monomers by fluorescence correlation spectroscopy, *Fuel*, **2007**, 86, 2016–2020

[71] Schneider M., Andrews A. B., Mitra-Kirtley S., Mullins O. C., Asphaltene molecular size from translational diffusion constant by fluorescence correlation spectroscopy, *Energy Fuels*, **2007**, 21, 2875– 2882
[72] Boduszynski M. M., In Chemistry of Asphaltenes; Bunger, J. W., Li, N. C., Eds.; American Chemical Society: Washington, D.C., **1981**, Chapter 7
[73] Yang M.-G., Eser S., *Prepr. Symp.-Am. Chem. Soc., Div. Fuel Chem*., **1999**, 44, 768
[74] Herod A. A., Bartle K. D., Kandiyoti R., Comment on a paper by Mullins, Martinez-Haya, and Marshall "Contrasting perspective on asphaltene molecular weight. This Comment vs the overview of A. A. Herod, K. D. Bartle, and R. Kandiyoti", *Energy Fuels*, **2008**, 22, 4312–4317
[75] Hortal A. R., Martìnez-Haya B., Lobato M. D., Pedrosa J. M., Lago S., On the determination of molecular weight distributions of asphaltenes and their aggregates in laser desorption ionization experiments. *J. Mass Spectrom*., **2006**, 41, 960
[76] Martıìnez-Haya B., Hortal A. R., Hurtado P. M., Lobato M. D., Pedrosa J. M., Laser desorption/ionization determination of molecular weight distributions of polyaromatic carbonaceous compounds and their aggregates, *J. Mass Spectrom*., **2007**, 42, 701–713
[77] Hortal A. R., Hurtado P. M., Martıìnez-Haya B., Mullins O. C., Molecular weight distributions of coal and petroleum asphaltenes from laser desorption ionization experiments, *Energy Fuels*, **2007**, 21, 2863–2868
[78] Hurtado P., Hortal A. R., Martìnez-Haya B., MALDI detection of carbonaceous compounds in ionic liquid matrices, *Rapid Commun. Mass Spectrom*., **2007**, 21, 3161–3164
[79] Rodgers R. P., Marshall A. G., Petroleomics: Advanced characterization of petroleum derived materials by Fourier transform ion cyclotron resonance mass spectrometry (FT-ICR MS). In Asphaltenes, Heavy Oils and Petroleomics; Mullins, O. C., Sheu, E. Y., Hammami, A., Marshall, A. G., Eds.; Springer: New York, **2007**, Chapter 3
[80] Rodgers R. P., Schaub T. M., Marshall A. G., Petroleomics: Mass spectrometry returns to its roots, *Anal. Chem*., **2005**, 77, 20A–27A
[81] Klein G. C., Kim S., Rodgers R. P., Marshall A. G., Yen A., Asomaning S., Mass spectral analysis of asphaltenes. I. Compositional differences between pressure-drop and solvent-drop asphaltenes determined by electrospray ionization Fourier transform ion cyclotron resonance mass spectrometry, *Energy Fuels*, **2006**, 20, 1965–1972.
[82] Klein G. C., Kim S., Rodgers R. P., Marshall A. G., Yen A., Mass spectral analysis of asphaltenes. II. Detailed compositional comparison of asphaltenes deposit to its crude oil counterpart for two geographically different crude oils by ESI FT-ICR MS, *Energy Fuels*, **2006**, 20, 1973–1979
[83] Hughey C. A., Rodgers R. P., Marshall A. G., Qian K., Robbins W. R., Identification of acidic NSO compounds in crude oils of different geochemical origins by negative ion electrospray Fourier transform ion cyclotron resonance mass spectrometry, *Org. Geochem.*, **2002**, 33, 743–759
[84] Clar E., The Aromatic Sextet; Wiley: London, U.K., **1972**
[85] Ruiz-Morales Y., HOMO-LUMO gap as an index of molecular size and structure for polycyclic aromatic hydrocarbons (PAHs) and asphaltenes: A theoretical study, *J. Phys. Chem. A*, **2002**, 106, 11283

[86] Ruiz-Morales Y., Molecular orbital calculations and optical transitions of PAHs and asphaltenes. In Asphaltene, Heavy Oils and Petroleomics; Mullins, O. C., Sheu, E. Y., Hammami, A., Marshall, A. G., Eds.; Springer: New York, **2007**, Chapter 4

[87] Ruiz-Morales Y., Mullins O. C., Polycyclic aromatic hydrocarbons of asphaltenes analysed by molecular orbital calculations with optical spectroscopy, *Energy Fuels*, **2007**, 21, 256

[88] Ruiz-Morales Y., Wu X., Mullins O. C., Electronic absorption edge of crude oils and asphaltenes analysed by molecular orbital calculations with optical spectroscopy, *Energy Fuels*, **2007**, 21, 944

[89] Ruiz-Morales Y., Mullins O. C., Simulated and measured optical absorption spectra of asphaltenes, *Energy Fuels*, **2009**, 23, 1169–1177

[90] Stohr J., NEXAFS Spectroscopy; Springer-Verlag: Berlin, Germany, **1992**

[91] George G. N., Gorbaty M. L., Sulfur K-edge X-ray absorption spectroscopy of petroleum asphaltenes, *J. Am. Chem. Soc.*, **1989**, 111, 3182

[92] Mitra-Kirtley S., Mullins O. C., Sulfur chemical moieties in carbonaceous materials. In Asphaltene, Heavy Oils and Petroleomics; Mullins, O. C., Sheu, E. Y., Hammami, A., Marshall, A. G., Eds.; Springer: New York, **2007**, Chapter 6

[93] Mitra-Kirtley S., Mullins O. C., Chen J., van Elp J., George S. J., Cramer S. P., Determination of the nitrogen chemical structures in petroleum asphaltenes using XANES spectroscopy, *J. Am. Chem. Soc.*, **1993**, 115, 252

[94] Bergmann U., Groenzin H., Mullins O. C., Glatzel P., Fetzer J., Cramer S. P., Carbon K-edge X-ray Raman spectroscopy supports simple yet powerful description of aromatic hydrocarbons and asphaltenes, *Chem. Phys. Lett.*, **2003**, 369, 184

[95] Bergmann U., Mullins O. C., Carbon X-ray Raman spectroscopy of PAHs and asphaltenes. In Asphaltenes, Heavy Oils and Petroleomics; Mullins, O. C., Sheu, E. Y., Hammami, A., Marshall, A. G., Eds.; Springer: New York, **2007**, Chapter 5

[96] Zajac G. W., Sethi N. K. Joseph J. T., Molecular imaging of asphaltenes by scanning tunneling microscopy: Verification of structure from $^{13}C$ and proton NMR data, *Scanning Microsc.*, **1994**, 8, 463

[97] Sharma A., Groenzin H., Tomita A., Mullins O. C., Probing order in asphaltenes and aromatic ring systems by HRTEM, *Energy Fuels*, **2002**, 16, 490

[98] Sharma A. Mullins O. C., Insights into molecular and aggregate structures of asphaltenes by HRTEM. In Asphaltene, Heavy Oils and Petroleomics; Mullins, O. C., Sheu, E. Y., Hammami, A., Marshall, A. G., Eds.; Springer: New York, **2007**, Chapter 8

[99] Bouhadda Y., Bormann D., Sheu E. Y., Bendedouch D., Krallafa A., Daaou M., Characterization of Algerian Hassi-Messaoud asphaltene structure using Raman spectrometry and X-ray diffraction, *Fuel*, **2007**, 86, 1855–1864

[100] Bouhadda Y., Fergoug T., Sheu E. Y., Bendedouch D., Krallafa A., Bormann D., Boubguira A., Second order Raman spectra of Algerian Hassi-Messaoud asphaltene, *Fuel*, **2008**, 87, 3481–3482

[101] Andrews A. B., Shih W-C., Mullins O. C., Norinaga K., Molecular Size Determination of Coal-Derived Asphaltene by Fluorescence Correlation Spectroscopy, *Applied Spectroscopy*, **2011**, 65(12), 1348-1356

[~~101~~ 102] Hammami A., Ratulowski J., Precipitation and deposition of asphaltenes in production systems: A flow assurance overview. In Asphaltenes, Heavy Oils and Petroleomics; Mullins, O. C., Sheu, E. Y., Hammami, A., Marshall, A. G., Eds.; Springer: New York, **2007**, Chapter 23

[103] Murgich, J.; Abanero, J.; Strausz, O. Molecular Recognition in Aggregates Formed by Asphaltene and Resin Molecules from the Athabasca Oil Sand. Energy Fuels 1999, 13, 278–286

[104] McKenna A. M., Purcell J. M., Rodgers R. P., Marshall A. G., Atmospheric pressure photoionization Fourier transform ion cyclotron resonance mass spectrometry for detailed compositional analysis of petroleum. Proceedings of the 9th International Conference on Petroleum Phase Behaviour and Fouling, Victoria, British Columbia, Canada, June 15-19, **2008**, Abstract 17

[105] McKenna A. M., Purcell J. M., Rodgers R. P., Marshall A. G., Petrophase 10th International Conference on Petroleum Phase Behaviour and Fouling, Rio de Janeiro, Brazil, **2009**

[106] Dwiggins C. W. Jr., A Small Angle X-Ray Scattering Study of the Colloidal Nature of Petroleum, *The Journal of Physical Chemistry*, **1965**, 69(10), 3500

[107] Dwiggins C. W., Dunning H. N., Separation of waxes from petroleum by ultracentrifugation, *J. Phys. Chem.*, **1960**, 64, 377

[108] Eldib I. A., Dunning H. N., Bolen R. J., Nature of Colloidal Materials in Petroleoum, *J. Chem. Eng. Data*, **1960**, 5, 550

[109] Lorenz P. B., Bolen R. J., Dunning H. N., Eldib I. A., Ultracentrifugation and viscosities of crude oils *J. Colloid Sci.*, **1961**, 16, 493

[110] Ray B. P., Witherspoon P. A., Grim R. J., A study of the colloidal characteristics of petroleum using the ultracentrifuge, *J. Phys. Chem.*, **1957**, 61, 1296

[111] Witherspoon P. A., Studies on petroleum with ultracentrifuge, *Illinois State Geol. Surv. Rept. Invest.*, **1958**, 206, 1

[112] Ravey J. C., Ducouret G., Espinat D., Asphalthene Macrostructure by Small Angle Neutron Scattering, *Fuel*, **1988**, 67, 1560-1567

[113] Tchoubar D., Herzog P., Espinat D., Macrostructure of asphaltene dispersions by small-angle X ray scattering, *Fuel*, **1988**, 67, 245

[114] Gourlaouen, C., Ph.D. Thesis- ENSPM, Rueuil Malmaison, France, **1984**

[115] Yen T. F., Erdman J. G., Pollack S. S., Investigation of the Structure of Petroleum Asphaltenes by X-Ray Diffraction, *Anal. Chem.*, **1961**, 33(11), 1581

[116] Dickie J. P., Yen T. F., Macrostructures of the Asphaltic Fractions by Various Instrumental Methods, *Anal. Chem.*, **1961**, 39 (14), 1847

[117] Sheu E. Y., Liang K. S., Sinha S. K.., Overfield R. E., Polydispersity Analysis of Asphaltene Solutions in Toluene, *Journal of Colloid and Interface Science*, **1992**, 153(2), 399

[118] Overfield, B., Sheu, E. Y., Liang, K. S., Sinha, S. K., Sans Study of Asphaltene Aggregation, *Fuel Sci. & Tech. Int.*, **1989**, 7, 611

[119] Ravey J. C., Ducouret G., Espinat D., Asphalthene Macrostructure by Small Angle Neutron Scattering, *Fuel*, **1988**, 67, 1560

[120] Drushel H. V., Schulz W. W., Second Chemical Congress of North America, **1980**,

[121] Speight J. G., Wernick D. L., Could K. A., Overfield R. E., Rao B. M. L., Savage D. W., *Revue de L'institut Français de Petrole*, **1985**, 40, 51

[122] Storm D. A., Decanio S. J., De Tar M. M., Nero V. P., Upper bound on number average molecular weight of asphaltenes, *Fuel*, **1990**, 69, 735

[123] Moschopedis S. E., Fryer J. F., Speight J. G., Investigation of asphaltene molecular weights, *Fuel*, **1976**, 55, 227

[124] Sheu E. Y., Storm D. A., De Tar M. M., Asphaltenes in polar solvents, *Journal of Non-Crystalline Solids*, **1991**, 131-133, 341-347

[125] Israelachvili J. N., Mitchell D. J., Ninham B. W., Theory of self-assembly of hydrocarbon amphiphiles into micelles and bilayers, *Journal of the Chemical Society, Faraday Transactions 2: Molecular and Chemical Physics*, **1976**, 72, 1525-1568

[126] Mitchell D. J., Ninham B. W., Micelles, vesicles and microemulsions, *J. Chem. Soc., Faraday Trans. 2*, **1981**, 77, 601-629

[127] Xu Y., Koga Y., Strausz O. P., Characterization of Athabasca asphaltenes by small-angle X-ray scattering, *Fuel*, **1995**, 74(7) 964

[128] Vonk, C. G., On two methods of determination of particle size distribution functions by means of small-angle X-ray scattering, *J. Appl. Cryst.*, **1976**, 9, 433

[129] Pollack, S. S., Yen T. F., Structural Studies of Asphaltics by X-Ray Small Angle Scattering, *Anal. Chem.*, **1970**, 42, 623

[130] Storm D. A., Sheu E. Y., Detar M. M., Macrostructure of asphaltenes in vacuum residue by small-angle X-ray scattering, *Fuel*, **1993**, 72, 977-981

[131] Liu Y. C., Sheu E. Y., Chent S. H., Storm D. A., Fractal structure of asphaltenes in toluene, *Fuel*, **1995**, 14(9). 1352-1356

[132] Sheu E. Y., de Tar M. M., Storm D. A., DeCanio S. J., Aggregation and kinetics of asphaltenes in organic solvents, *Fuel*, **1992**, 71, 299

[133] Storm D. A., Sheu, E. Y., Rheological studies of Ratawi vacuum residue at 366 K, *Fuel*, **1993**, 72, 233-237

[134] Escobedo J., Mansoori G. A., In Proceedings, SPE International Symposium on Oil Field Chemistry, **1993**, pp. 9-22

[135] Kim S. T., Boudh-Hir M.-E., Mansoori G. A., In SPE Annual Technical Conference and Exhibition **1990**, Part 3, Society of Petroleum Engineers of AIME, pp. 799-809

[136] Park S. J., Mansoori G. A., Aggregation and deposition of heavy organics in petroleum crudes, *Energy Sources*, **1988**, 10, 109

[137] Chen S. H., Teixeira J., Structure and Fractal Dimension of Protein-Detergent Complexes, *J. Phys. Rev. Lett.*, **1986**, 57, 2583

[138] Stauffer D., In:'On Growth and Form' (Eds. H. E. Stanley and N. Ostrowskv). Martinus Niihoff. New York. **1986**

[139] Landau D. P., Family F. (Eds). 'Kinetics of Aggregation and Gelation', North Holland, Amsterdam, **1984**

[140] Pynn R., Skeltorp A. (Eds). 'Scaling Phenomena in Disordered Systems', Plenum, New York, **1986**

[141] Feder J., 'Fractals', Plenum, New York, **1988**

[142] Chen, S. H., Rouch J., Tartaelia P., Light Scattering from Polydispersed Fractal Clusters in Solution, *Croat. Chem. Acta*, **1992**, 65, 353

[143] Raghunathan P., Evidence for fractal dimension in asphaltene polymers from electron-spin-relaxation measurements, *Chem. Phys. Lett.*, **1991**, 182(3-4), 331-335

[144] Ekwall P. In 'Advances in Liquid Crystals' (Ed. G. H. Brown), Vol. 1, Academic Press, New York, **1975**

[145] Barré L., Espinat D., Rosenberg E., Scarsella M., Colloidal Structure of Heavy Crudes and Asphaltene Solutions, *Revue De L'institut Français Du Pétrole*, **1997**, 52 (2)

[146] Thiyagarajan P., Hunt J.E., Winans R.E., Anderson K. B, Miller J.T., Temperature-dependent structural changes of asphaltenes in 1-methylnaphthalene, *Energy and Fuels*, **1995**, 9, 829- 833

[147] Tanaka R., Hunt J. E., Winans R. E., Thiyagarajan P., Sato S., Takanohash T, Aggregates Structure Analysis of Petroleum Asphaltenes with Small-Angle Neutron Scattering, *Energy & Fuels*, **2003**, 17, 127-134

[148] Mushrush G.W., Speight J.G., Petroleum Products: Instability and Incompatibility, Taylor & Francis, Bristol, PA, **1995**

[149] Storm D. A., DeCanio S. J., Sheu E. Y., In: T.F. Yen (Ed.), Asphaltene Particles in Fossil Fuel Exploration, Recovery, Refining, and Production Processes, Plenum, New York, **1994**, 81

[150] Tanaka R., Sato E., Hunt J. E., Winans R. E., Sato S., Takanohashi T., Characterization of Asphaltene Aggregates Using X-ray Diffraction and Small-Angle X-ray Scattering, *Energy & Fuels*, **2004**, 18, 1118-1125

[151] Spiecker P M., Gawrys K. L., Kilpatrick P. K., Aggregation and solubility behaviour of asphaltenes and their subfractions, *Journal of Colloid and Interface Science*, **2003**, 267, 178–193

[152] Fenistein D., Barre L., Broseta,D., Espinat D., Livet A., Roux J.N., Scarsella M., Viscosimetric and Neutron Scattering Study of Asphaltene Aggregates in Mixed Toluene/Heptane Solvents, *Langmuir*, **1998**, 14 (5), 1013

[153] Spiecker P M., Gawrys K. L., Trail C. B., Kilpatrick P. K., Effects of petroleum resins on asphaltene aggregation and water-in-oil emulsion formation, *Colloids and Surfaces A: Physicochem. Eng. Aspects*, **2003**, 220, 9 -27

[154] Bardon C., Barre L., Espinat D., Guille V., Li M.H., Lambard J., Ravey J.C., Rosenberg E., Zemb T., The colloidal structure of crude oils and suspensions of asphaltenes and resins, *Fuel Sci. Technol. Int.*, **1996**, 14(1&2), 203-242

[155] Gawrys K. L., Kilpatrick P. K., Asphaltenic aggregates are polydisperse oblate cylinders, *Journal of Colloid and Interface Science*, **2005**, 288, 325–334

[156] Guinier A., Fournet G., Small Angle Scattering of X-Rays,Wiley, New York, **1955**

[157] Gawrys K. L., Blankenship G. A., Kilpatrick P. K., Solvent Entrainment in and Flocculation of Asphaltenic Aggregates Probed by Small-Angle Neutron Scattering, *Langmuir*, **2006**, 22, 4487-4497

[158] Sirota E. B., Swelling of Asphaltenes, *Pet. Sci. Technol.*, **1998**, 16 (3-4), 415-431

[159] Carbognani L.; Rogel E., Solvent Swelling of Petroleum Asphaltenes, *Energy Fuels*, **2002**, 16 (6), 1348-1358

[160] Takeshige W. J., Hydrodynamic shape and size of Khafji asphaltene in benzene, *Colloid Interface Sci.* **2001**, 234 (2), 261-268

[161] Sheu E. Y., Detar M. M., Storm D. A., Rheological properties of vacuum residue fractions in organic solvents, *Fuel*, **1991**, 70 (10), 1151-1156

[162] Bouhadda Y., Bendedouch D., Sheu E., Krallafa A., Some Preliminary Results on a Physico-Chemical Characterization of a Hassi Messaoud Petroleum Asphaltene, *Energy Fuels*, **2000**, 14 (4), 845-853

[163] Headen T. F., Boek E. S., Stellbrink J., Scheven U. M., Small Angle Neutron Scattering (SANS and V-SANS) Study of Asphaltene Aggregates in Crude Oil, *Langmuir*, **2009**, 25, 422-428

[164] Eyssautier J., Levitz P., Espinat D., Jestin J., Gummel J., Grillo I., Barré L., Insight into Asphaltene Nanoaggregate Structure Inferred by Small Angle Neutron and X-ray Scattering, *J. Phys. Chem. B*, **2011**, 115, 6827–6837

[165] Zeng H., Song Y. Q., Johnson D. L., Mullins O. C., Critical Nanoaggregate Concentration of Asphaltenes by Direct-Current (DC) Electrical Conductivity, *Energy Fuels*, **2009**, 23, 1201–1208

[166] Betancourt S. S., Ventura G. T., Pomerantz A. E., Viloria O., Dubost F. X., Zuo J. L., Monson G., Bustamante D., Purcell J. M., Nelson R. K., Rodgers R. P., Reddy C. M., Marshall A. G., Mullins O. C., Nanoaggregates of Asphaltenes in a Reservoir Crude Oil and Reservoir Connectivity, *Energy Fuels*, **2009**, 23, 1178–1188

[167] Hoepfner M. P., Bôas Fávero C. V., Haji-Akbari N., Fogler H. S., The Fractal Aggregation of Asphaltenes, *Langmuir*, **2013**, 29, 8799−8808

[168] Maqbool T., Balgoa A. T., Fogler H. S., Revisiting Asphaltene Precipitation from Crude Oils: A Case of Neglected Kinetic Effects, *Energy Fuels*, **2009**, 23, 3681−3686

[169] Barré L., Jestin J., Morisset A., Palermo T., Simon S., Relation between Nanoscale Structure of Asphaltene Aggregates and their Macroscopic Solution Properties, *Oil & Gas Science and Technology – Rev. IFP*, **2009**, 64 (5)

[170] Goncalves S., Castillo J., Fernandez A., Hung J., Absorbance and fluorescence spectroscopy on the aggregation of asphaltene toluene solutions, *Fuel*, **2004**, 83, 1823

[171] Andreatta G., Goncalves C. C., Buffin G., Bostrom N., Quintella C. M., Arteaga-Larios F., Perez E., Mullins O. C., Nanoaggregates and structure-function relations in asphaltenes, *Energy Fuels*, **2005**, 19, 1282–1289

[172] Andreatta G., Bostrom N., Mullins O. C., High-Q ultrasonic determination of the critical nanoaggregate concentration of asphaltenes and the critical micelle concentration of standard surfactants, *Langmuir*, **2005**, 21, 2728

[173] Zeng H., Song, Y. Q., Johnson D. L., Mullins O. C., Critical nanoaggregate concentration of asphaltenes by low frequency conductivity, *Energy Fuels*, **2009**, 23, 1201–1208

[174] Sheu E. Y., Long Y., Hamza H., Asphaltene self-association and precipitation in solvents; AC conductivity measurements. In Asphaltene, Heavy Oils and Petroleomics; Mullins, O. C., Sheu, E. Y., Hammami, A., Marshall, A. G., Eds.; Springer: New York, **2007**; Chapter 10

[175] Mostowfi F., Indo K., Mullins O. C., McFarlane R., Asphaltene nanoaggregates and the critical nanoaggregate concentration from centrifugation, *Energy Fuels*, **2009**, 23, 1194–1200

[176] Rogel E., A Molecular Thermodynamic approach to the formation of mixed Asphaltene-resin aggregates. *Energy and Fuels*, **2008**, 22, 3922-3929

[177] Freire E., Mayorga O. L., Straume M., Isothermal Titration, *Analytical chemistry*, 1990, 62(18)

[178] Blandamer M.J., In "Biocalorimetry: Applications of Calorimetry in the Biological Sciences". J.E. Ladbury B.Z. Chowdhry (Editors). John Wiley & Sons Ltd. U, **1998**

[179] Tame J.R.H., O'Brien R., Ladbury J.E., "Biocalorimetry: Applications of Calorimetry in the Biological Sciences". J.E. Ladbury B.Z. Chowdhry (Editors). John Wiley Ltd. UK, **1998**

[180] Majhi P.R., Moulik S.P., Energetics of micellization: reassessment by a high-sensitivity titration microcalorimeter, *Langmuir*, **1998**, 14, 3986-3990

[181] Paula S., Süs W., Tuchtenhagen J., Blume A., Thermodynamics of micelle formation as a function of temperature: a high sensitivity titration calorimetry study, *J. Phys. Chem.*, **1995**, 99, 11742-11751

[182] Majhi P.R., Moulik S.P., Microcalorimetric investigation of AOT self-association in oil and the state of pool water in water/oil microemulsions, *J. Phys. Chem. B*, **1999**, 103, 5977-5983

[183] Andersen S. I., Birdi K. S., Aggregation of Asphaltenes as Determined by Calorimetry, *Journal of Colloid and Interface Science*, **1991**, 142(2)

[184] Andersen S. I., Christensen S. D., The Critical Micelle Concentration of Asphaltenes As Measured by Calorimetry, *Energy & Fuels*, **2000**, 14, 38-42

[185] Merino-Garcia D., Andersen S. I., Isothermal Titration Calorimetry and Fluorescence Spectroscopy Study of Asphaltene Self-Association in Toluene and Interaction with a Model Resin, *Petroleum Science and Technology*, **2003**, 21(3-4), 507-525

[186] Merino-Garcia D., Murgich J., Andersen S. I., Asphaltene Self-Association: Modeling and Effect of Fractionation with A Polar Solvent, *Petroleum Science and Technology*, **2004**, 22(7-8), 735-758

[187] Merino-Garcia D., Murgich J., Andersen S. I., Calorimetric Evidence about the Application of the Concept of CMC to Asphaltene Self-Association, *Journal of Dispersion Science and Technology*, **2005**, 26, 2, 217-225

[188] Agrawala M., Yarranton H. W., An Asphaltene Association Model Analogous to Linear Polymerization, *Ind. Eng. Chem. Res.*, **2001**, 40, 4664-4672

[189] Rogel E., León O., Torres G., Espidel J., Aggregation of asphaltenes in organic solvents using surface tension Measurements, *Fuel*, **2000**, 79, 1389–1394

[190] Yarranton H. W., Alboudwarej H., Jakher R., Investigation of Asphaltene Association with Vapor Pressure Osmometry and Interfacial Tension Measurements, *Ind. Eng. Chem. Res.*, **2000**, 39, 2916-2924

[191] Monte M. B. M., Coelho R. R., Middea A., Investigation of Molecular Weight and Aggregation of Asphaltenes in Organic Solvents Using Surface Tension Measurements, *Petroleum Science and Technology*, **2004**, 22(7 & 8), 991–1001

[192] Sheu E. Y., Physics of asphalthene micelles and microemulsions— theory and experiment, *Journal Physics: Condensated Matter*, **1996**, 8, A125–A141

[193] da Silva Ramos A. C., Haraguchi L., Notrispe F. R., Rahoma W. L., Mohamed S., Interfacial and colloidal behaviour of asphaltenes obtained from Brazilian crude oils, *Journal of Petroleum Science and Engineering*, **2001**, 32, 201– 216

[194] Long J., Xu Z., Masliyah J. H., Single Molecule Force Spectroscopy of Asphaltene Aggregates, *Langmuir*, **2007**, 23, 6182-6190

[195] Hugel, T.; Grosholz, M.; Clausen-Schaumann, H.; Pfau, A.; Gaub, H.; Seitz, M., Elasticity of Single Polyelectrolyte Chains and Their Desorption from Solid Supports Studied by AFM Based Single Molecule Force Spectroscopy, *Macromolecules*, **2001**, 34, 4, 1039–1047

[196] Acevedo S., Rodrìguez Pedro, An Electron Microscopy Study of Crude Oils and Maltenes, *Energy & Fuels*, **2004**, 18, 1757-1763

[197] Gutiérrez L. B., Ranaudo M. A., Méndez B. Acevedo S., Fractionation of Asphaltene by Complex Formation with p-Nitrophenol. A Method for Structural Studies and Stability of Asphaltene Colloids, *Energy & Fuels*, **2001**, 15, 624-628

[198] Acevedo S., Zuloaga C., Rodrìguez P., Aggregation-Dissociation Studies of Asphaltene Solutions in Resins Performed Using the Combined Freeze Fracture-Transmission Electron Microscopy Technique, *Energy & Fuels*, **2008**,22,2332–2340

[199] Wang S., Liu J., Zhang L., Masliyah J., Xu Z., Interaction Forces between Asphaltene Surfaces in Organic Solvents, *Langmuir*, **2010**, 26(1), 183–190

[200] Wang S., Liu J., Zhang L., Xu Z., Masliyah J., Colloidal Interactions between Asphaltene Surfaces in Toluene, *Energy & Fuels*, **2009**, 23, 862–869

[201] Natarajan A., Xie J., Wang S., Liu Q., Masliyah J., Zeng H., Xu Z., Understanding Molecular Interactions of Asphaltenes in Organic Solvents Using a Surface Force Apparatus, *J. Phys. Chem. C*, **2011**, 115,16043–16051

[202] deGennes, P. G., Polymers at an interface; a simplified view, *Adv. Colloid Interface Sci.*, **1987**, 27, 189–209

[203] Kuhl T. L., Leckband D. E., Lasic D. D., Israelachvili J. N., Modulation of interaction forces between bilayers exposing short-chained ethylene oxide headgroups, *Biophys. J.*, **1994**, 66, 1479–1488

[204] Efremora N. V., Bondurant B., O'Brien D. F., Leckband D. E., Measurements of Interbilayer Forces and Protein Adsorption on Uncharged Lipid Bilayers Displaying Poly(ethylene glycol) Chains, *Biochemistry*, **2000**, 39, 3441–3451

[205] Butt H. J., Kappl M., Mueller H., Raiteri R., Meyer W., Ruhe J., Steric forces measured with the atomic force microscope at various temperatures, *Langmuir*, **1999**, 15, 2559–2565

[206] Burya Y. G., Yudin I. K., Dechabo V. A., Kosov V. I., Anisimov M. A., Light-scattering study of petroleum asphaltene aggregation, *Applied Optics*, **2001**, 40(24), 4028-4035

[207] Handle F., Füssl J., Neudl S., Grossegger D., Eberhardsteiner L., Hofko B., Hospodka M., Blab R., Grothe H., The bitumen microstructure: a fluorescent approach, *Mater Struct*, **2016**, 49, 167–180

[208] Bearsley S., Forbes A., Haverkamp R. G., Direct observation of the asphaltene structure in paving-grade bitumen using confocal laser-scanning microscopy, *Journal of Microscopy*, **2004**, 215(2), 149–155

[209] Eberhardsteiner L, Füssl J, Hofko B, Handle F, Hospodka M, Blab R, Grothe H, Influence of asphaltene content on mechanical bitumen behavior—experimental investigation and micromechanical modelling, *Materials and Structures*, **2015**, 48, 3099–3112

[210] Lyne Å L, Birgisson B, Redelius P () Interaction forces between mineral aggregates and bitumen calculated using the Hamaker constant, *Road Materials and Pavement Design*, 2011, 11(sup1), 305-323

[211] Castillo J., Hung J., Fernández A., Mujica V., Non-Linear Optical evidences of aggregation in asphaltene-toluene solution, *Fuel*, **2001**, 80, 1239-1243

[212] Anisimov M. A., Ganeeva Y. M., Gorodetskii E. E., Deshabo V. A., Kosov V. I., Kuryakov V. N, Yudin D. I., Yudin I. K., Effects of Resins on Aggregation and Stability of Asphaltenes, *Energy Fuels*, **2014**, 28, 6200−6209

[213] Haji-Akbari N.; Teeraphapkul P., Fogler H. S., Effect of Asphaltene Concentration on the Aggregation and Precipitation Tendency of Asphaltenes, *Energy Fuels*, **2014**, 28, 909−919

[214] Breure B., Subramanian D., Leys J., Peters C. J., Anisimov M. A., Modeling Asphaltene Aggregation with a single compound, *Energy Fuels*, **2013**, 27, 172−176

[215] Yarranton H. W., Ortiz D. P., Barrera D. M., Baydak E. N., Barré L., Frot D., Eyssautier J., Zeng H., Xu Z., Dechaine G., Becerra M., Shaw J. M., McKenna A. M., Mapolelo M. M., Bohne C., Yang Z., Oake J., On the Size Distribution of Self-Associated Asphaltenes, *Energy Fuels*, **2013**, 27, 5083−5106

[216] Abdollah S. S., Osfouri S., Azin R., Dehghani S. A. M., Kinetic modeling of asphaltene nano-aggregates formation using dynamic light scattering technique, *Journal of Petroleum Science and Engineering*, **2020**, 192, 107293

[217] Abbott G. D., Povey M. J. W., The acoustic spectroscopy of asphaltene aggregation in petroleum, *IOP Conf. Ser.: Mater. Sci. Eng.*, **2012**, 42, 012022

[218] Povey M. J. W., Ultrasound Techniques for Fluids Characterization (London: Academic Press), **1997**
[219] Durand E., Clemancey M., Lancelin J.-M., Verstraete J., Espinat D., Quoineaud A.-A., Effect of Chemical Composition on Asphaltenes Aggregation, *Energy Fuels*, **2010**, 24, 1051–1062
[220] da Silva Oliveira E. C., Neto Á. C., Lacerda V. Jr, de Castro E. V. R., de Menezes S. M. C., Study of Brazilian asphaltene aggregation by Nuclear Magnetic Resonance spectroscopy, *Fuel*, **2014**, 117, 146–151
[221] Majumdar R. D., Montina T., Mullins O.C., Gerken M., Hazendonk P., Insights into asphaltene aggregate structure using ultrafast MAS solid-state $^{1}$H NMR spectroscopy, *Fuel*, **2017**, 193, 359–368
[222] Wang W., Taylor C., Hu H., Humphries K. L., Jaini A., Kitimet M., Scott T., Stewart Z., Ulep K. J., Houck S., Luxon A., Zhang B., Miller B., Parish C. A., Pomerantz A. E., Mullins O. C., Zare R. N., Nanoaggregates of Diverse Asphaltenes by Mass Spectrometry and Molecular Dynamics, *Energy Fuels*, **2017**, 31, 9140−9151
[223] Morozov E. V., Yushmanov P. V., Martyanov O. N., Temperature-Triggered Rearrangement of Asphaltene Aggregates as Revealed by Pulsed-Field Gradient NMR, *Energy Fuels*, **2019**, 33, 6934−6945
[224] Kawashima H., Takanohashi T., Iino M., Matsukawa S., Determining Asphaltene Aggregation in Solution from Diffusion Coefficients as Determined by Pulsed-Field Gradient Spin-Echo $^{1}$H NMR, *Energy & Fuels*, **2008**, 22, 3989–3993
[225] Östlund J.-A., Andersson S.-I., Nydén M., Studies of asphaltenes by the use of pulsed-field gradient spin echo NMR, *Fuel*, **2001**, 80(11), 1529-1533
[226] Jonstromer M., Jonsson B., Lindman B., Self-Diffusion in Nonionic Surfactant-Water Systems, *J. Phys. Chem.*, **1991**, 95, 3293-3300
[227] Gabrienko A. A., Morozov E. V., Subramani V., Martyanov O. N., Kazarian S. G., Chemical Visualization of Asphaltenes Aggregation Processes Studied in Situ with ATR-FTIR Spectroscopic Imaging and NMR Imaging, *J. Phys. Chem. C*, **2015**, 119 (5), 2646−2660
[228] Lesueur D, Gérard J F, Claudy P, Létoffé J M, Planche J P, Martin D. Relationships between the structure and the mechanical properties of paving grade asphalt cements, *J Assoc Asphalt Paving Techn*, **1997**, 66, 486–507
[229] Claudy P., Létoffé J.-M., King G. N., Planche J.-P., Brûlé B., Characterization of paving asphalts by differential scanning calorimetry, *Fuel Sci. Technol. Int.*, **1991**, 9, 71–92
[230] Williams M. L., Landel R. F., Ferry J. D., The temperature dependence of relaxation mechanisms in amorphous polymers and other glass forming liquids, *J. Am. Chem. Soc.*, **1955**, 77, 3701–3707
[231] Storm D A, Barresi R J, Sheu E Y., Rheological study of Ratawi vacuum residue in the 298–673 K temperature range, *Energy Fuels*, **1995**, 9, 168–76
[232] Roscoe R., The viscosity of suspensions of rigid spheres, *Brit. J. Appl. Phys.*, **1952**, 3, 267–269; Brinkman H. C., The viscosity of concentrated suspensions and solutions, *J. Chem. Phys.*, **1952**, 20, 571
[233] Metzner A. B., Rheology of suspensions in polymeric liquids, *J. Rheol.*, **1985**, 29, 739–775
[234] Carreau P. J., Comportement rhéologique de suspensions dans les liquides polymèriques, *Proceedings Rhéologie des Suspensions* (27éme Colloque du GFR), Grenoble, **1992**, pp. 3–15

[235] Sudduth R. D., A generalized model to predict the viscosity of solutions with suspended particles, *J. Appl. Polym. Sci.*, **1993**, 48, 25–36

[236] Verney V., Michel A, Planche J. P., Brûlé B., Influence de la température sur la viscosité complexe d'un bitume routier, *Cahiers Rhéol*, **1990**, 41, 811–9

[237] Christensen D. W., Anderson D. A., Interpretation of dynamic mechanical test data for paving grade asphalt cements, *J Assoc Asphalt Paving Techn*., **1992**; 61, 67–98

[238] Taylor S. E., Use of surface tension measurements to evaluate aggregation of asphaltenes in organic solvents, *Fuel*, **1992**, 71, 1338

[239] Galoppini M., Tambini M., SPE European Production Operations Conference and Exhibition, Aberdeen, U.K. SPE 27622, **1994**

[240] Andersen S. I., Speight J. G., Petroleum resins: separation, character, and role in petroleum, *Pet. Sci. Technol.* **2001**, 19, 1

[241] Leòn O., Contreras E., Rogel E., Dambakli G., Acevedo S., Carbognani L., Espidel J., Adsorption of native resins on asphaltene particles: a correlation between adsorption and activity, *Langmuir*, **2002**, 18, 5106

[242] Andersen S. I., Birdi K. S., Aggregation of asphaltenes as determined by calorimetry, *J. Colloid Interface Sci.*, **1991**, 142, 497

[243] Gawrys K. L., Spiecker P. M., Kilpatrick P. K., The role of asphaltene solubility and chemical composition on asphaltene aggregation, *Pet. Sci. Technol.*, **2003**, 21, 461

[244] Wang P., Dong Z., Tan Y., Liu Z., Investigating the Interactions of the SARA four fractions in asphalt binders by molecular simulations, *Energy and Fuels*, **2015**, 29, 112-121

[245] Dunn N.J., Gutama B., Noid W.G., Simple Simulation model for exploring the effects of solvent and structure for asphaltene aggregation, *J. Phys. Chem. B*, **2019**, 123, 6111−6122

[246] Teklebrhan R. B., Ge L., Bhattacharjee S., Xu Z., Sjöblom J., Probing structure nano-aggregation relations of polyaromatic surfactants: a molecular dynamics simulation and dynamic light scattering study, *J Phys Chem B*, **2012**, 116(20), 5907–18

[247] Frigerio F., Molinari D., A multiscale approach to the simulation of asphaltenes, *Computational and Theoretical Chemistry*, **2011**, 975, 76–82

[248] Boek E.S., Yakovlev D.S., Headen T.F., Quantitative molecular representation of asphaltenes and molecular dynamics simulation of their aggregation, *Energy & Fuels*, **2009**, 23, 1209–1219

[249] Headen T.F., Boek E.S., Skipper N.T., Evidence for asphaltene nano-aggregation in toluene and heptane from molecular dynamics simulations, *Energy & Fuels*, **2009**, 23 1220–1229

[250] Akbarzadeh K. et al. Association behavior of pyrene compounds as models for asphaltenes, *Energy Fuels*, **2005**, 19(4), 1268–71

[251] Rakotondradany F., Fenniri H., Rahimi P., Gawrys K. L., Kilpatrick P. K., Gray M. R., Hexabenzocoronene model compounds for asphaltene fractions: synthesis & characterization, *Energy Fuels*, **2006**, 20(6), 2439–47

[252] Tan X., Fenniri H., Gray M. R., Pyrene derivatives of 2,2′-bipyridine as models for asphaltenes: synthesis, characterization, and supramolecular organization, *Energy Fuel*, **2007**, 22(2), 715–20
[253] Kuznicki T., Masliyah J. H., Bhattacharje S., Molecular dynamics study of model molecules resembling asphaltene-like structures in aqueous organic solvent systems, *Energy Fuels*, **2008**, 22, 2379–89
[254] Kuznicki T., Masliyah J. H., Bhattacharjee S., Aggregation and partitioning of model asphaltenes at toluene–water interfaces: molecular dynamics simulations, *Energy Fuel*, **2009**, 23(10), 5027–35
[255] Jian C., Tang T., Bhattacharjee S., Probing the effect of side-chain length on the aggregation of a model asphaltene using molecular dynamics simulations, *Energy Fuel*, **2013**, 27(4), 2057–67
[256] Alshareef A. H., et al. Effect of chemical structure on the cracking and coking of archipelago model compounds representative of asphaltenes, *Energy Fuel*, **2012**, 26(3), 1828–43
[257] Alshareef A. H., Scherer A., Stryker J. M., Tykwinski R. R., Gray M. R., Thermal cracking of substituted cholestane–benzoquinoline asphaltene model compounds, *Energy Fuel*, **2012**, 26(6), 3592–3603
[258] Nordgård E. L., Landsem E., Sjöblom J., Langmuir films of asphaltene model compounds and their fluorescent properties, *Langmuir*, **2008**, 24(16), 8742–51
[259] Nordgård E. L., Sjöblom J., Model compounds for asphaltenes and C80 isoprenoid tetraacids. Part I: synthesis and interfacial activities, *J Dispers Sci Technol.*, **2008**, 29(8), 1114–22
[260] Nordgård E. L., Sørland G., Sjöblom J., Behavior of asphaltene model compounds at w/o interfaces, *Langmuir*, **2009**, 26(4), 2352–60
[261] Teklebrhan R. B., Ge L., Bhattacharjee S., Xu Z., Sjöblom J., Initial partition and aggregation of uncharged polyaromatic molecules at the oil–water interface: a molecular dynamics simulation Study, *J Phys Chem B*, **2014**, 118(4), 1040–51
[262] Gavezzotti A., Crystal packing of hydrocarbons. Effects of molecular size, shape and stoichiometry, *Acta Crystallogr*., **1990**, B46, 275-283
[263] Murgich J., Rodriguez M. J., Aray Y., Molecular Recognition and mechanics of micelles of some model asphaltenes and resins, *Energy and Fuels*, **1996**, 10, 68-76
[264] Carnaham N. F., Quintero L., Pfund, D. M., Fulton J. L., Smith R. D., Capel, M., Leontaritis K., A small angle X-ray scattering study of the effect of pressure on the aggregation of asphaltene fractions in petroleum fluids under near-critical solvent conditions, *Langmuir*, **1993**, 9, 2035-2044
[265] Yen T. F., The colloidal aspect of a macrostructure of petroleum asphalt, *Fuel Sci*. *Technol*. *Int*., **1992**, 10, 723-733
[266] Rogel E., Thermodynamic modelling of Asphaltene aggregation, *Langmuir*, **2004**, 20, 1003-1012
[267] Morgado J., Aquinos-Olivos M. A., Martinez-Hernandez R., Grolier J. P., del Rio J. M., Thermodynamics of Interactions at infinite dilution between asphaltenes and surfactants, *Energy & Fuels*, **2009**, 23, 2581–2591
[268] Alvarez-Ramirez F., Ramìrez-Jaramillo E., Ruiz-Morales Y., Calculation of the interaction potential curve between asphaltene − asphaltene, asphaltene − resin, and resin − resin systems using density functional theory, *Energy Fuel*, **2006**, 20, 195

[269] Nellensteyn F. I., In the Science of Petroleum; Dunstan, A. E., Ed.; Oxford University Press: London, U.K., **1938**; Vol. 4

[270] Zeng, H.; Song, Y. Q.; Johnson, D. L.; Mullins, O. C. Critical nanoaggregate concentration of asphaltenes by low frequency conductivity, *Energy Fuels*, **2009**, 23, 1201–1208.

[271] Aske N., Kallevik H., Johnsen E. E., Sjoblom J., Asphaltene aggregation from crude oils and model systems studied by high-pressure NIR spectroscopy, *Energy Fuels*, **2002**, 16, 1287–1295

[272] Zhao B., Shaw J. S., Composition and size distribution of coherent nanostructures in Athabasca bitumen and Maya crude oil, *Energy Fuels*, **2007**, 21, 2795–2804

[273] Zhao B., Becerra M., Shaw J. M., On asphaltene and resin association in Athabasca bitumen and Maya crude oil, *Energy Fuels*, **2009**, 23, 4431–4437

[274] Merino-Garcia D., Andersen S. I., Application of isothermal titration calorimetry in the investigation of asphaltene association. In Asphaltenes, Heavy Oils and Petroleomics; Mullins, O. C., Sheu, E. Y., Hammami, A., Marshall, A. G., Eds.; Springer: New York, **2007**; Chapter 13

[275] Merino-Garcia D., Andersen S. I., Thermodynamic characterization of asphaltene-resin interaction by microcalorimetry, *Langmuir*, **2004**, 20, 4559–4565

[276] Fossen M., Kallevik H., Knudsen, K. D., Sjöblom J., Asphaltenes precipitated by a two-step precipitation procedure. 1. Interfacial tension and solvent properties, *Energy Fuels*, **2007**, 21, 1030–1037

[277] Ekholm P., Blomberg E., Claesson P., Auflem I. H., Sjöblom J., Kornfeldt A., A quartz crystal microbalance study of the adsorption of asphaltenes and resins onto a hydrophilic surface, J. *Colloid Interface Sci.*, **2002**, 247, 342–350

# Chapter 2

## 2. Recycled materials and by-products as an alternative to non-renewable resources

Every year, the European Union (EU) produces around 15 million tons of bitumen [1]. Most of this is mixed with aggregates to create asphalt concrete for roads paving. Approximately, 90% of all paved roads are surfaced with bituminous materials. Annually, the EU produces more than 200 million tons of bituminous materials for maintenance operations of the existing asphalt pavements and for paving new transportation infrastructures [2]. However, the bitumen used as well as the virgin aggregates are not renewable resources. This led the researchers to look for alternative binders (or eco-binders) to reduce the consumption of petroleum bitumen and for recycled aggregates to substitute the virgin ones in the asphalt mixture skeleton. On one hand, the employment of recycled aggregates is becoming a consolidated practice in the production of asphalt concretes especially in terms of RAP material as previously mentioned, and the use of recycled asphalt mixture with high or very high content of RAP is becoming feasible [3,4]. On the other hand, the partial substitution of neat bitumen with recycled materials and/or by-products is still a challenge. The possible substitutes of neat bitumen can either come from recycled materials of non-renewable resources such as REOBs or come from renewable resources as wood or vegetable waste oils for instance. The bituminous binders that partially consists of the latter products are referred as bio-binders [5,6], which is an eco-friendly alternative for bitumen obtained from non-petroleum-based renewable resources. The chemical composition of the majority of these alternative binders are similar to those of a traditional bitumen, which includes resins, saturates, aromatics and asphaltenes [7]. Regardless of the origin of the bitumen substitutes, i.e. renewable and non-renewable resources, the waste and/or recycled products can partially replace neat bitumen. In general, the substitutes can be introduced in neat bitumen in four different ways based on the type and quantity of waste materials and/or by-products are used, and they are referred as [8]:

i. Bitumen modifier (<10%wt.);
ii. Bitumen fluxes (7-15%wt.);
iii. Bitumen extender (25-75%wt.);
iv. Alternative binders (>75%wt.).

So far, the bitumen modifiers, fluxes and extenders are the most used solutions to add waste materials and/or by-products in the bituminous binders for the production of asphalt mixtures. Nonetheless, the use of alternative binders to partially and/or completely replace the bitumen in the new asphalt formulations is the final goal of the research nowadays inspired by the circular economy concept. Up to date, different alternative binders have been studied, including engine oil residue, soybean oil, palm oil, fossil fuel, swine waste, and materials from pyrolysis [9]. Different vegetable oils have been investigated in recent times to determine their physical and chemical properties and to evaluate their applicability as bio-binders in the pavement industry [10-12]. Bio-oils are produced from plant matter and residues, such as municipal wastes, agricultural crops, and by-products from agricultural and forestry. Other biomass sources include molasses and rice, sugar, potato

starches and corn, gum resins and natural tree, vegetable oils and natural latex rubber, cellulose, lignin, waste oil of palm, peanut oil waste, coconut waste, potato starch, canola oil waste, dried sewerage effluent, and others [7]. Rauf and Williams [13] have conducted a study about bio-oils. They have produced different bio-oils from different sources, i.e. oakwood, switch grass and corn stover, which exhibited similar behaviour of neat bitumen. Fini et al [14] produced a bio-oil from swine manure and used it as a partial replacement of bitumen. This recycled product was a promising candidate for partial replacement for standard bitumen. In particular, this bio-binder will improve the low temperature properties of the petroleum-based binder while reducing asphalt pavement construction costs. A Dutch study is testing asphalt roads and cycle paths paved with a bitumen-like product made from the natural binder lignin [15]. Lignin is a structural polymer in plants and trees that is released as a waste product from a number of industrial processes. The used lignin from various sources including different types of paper pulp production and a bio-refinery that produces cellulosic ethanol from straw. On the demonstration roads, the material appears to be performing in a similar way to a standard bitumen and a slight noise reduction has been observed. In 2018, Yang et al. developed a process to break down the organic part of household waste, e.g. food waste, plastic, paper and textiles, to produce a sticky, gloopy black liquid that is very similar to bitumen [16]. The bio-bitumen was produced by pyrolysis. By changing the processing parameters, such as temperature, processing time and product collection strategy, the research team was able to alter the characteristics and quantities of the final bitumen-like substance.

### 2.1. The Itelyum Re-Refining used oils Process

Figure 1 below shows a general scheme of the oil refining process adopted by the Itelyum company in the industrial site of Pieve Fissiraga (LO).

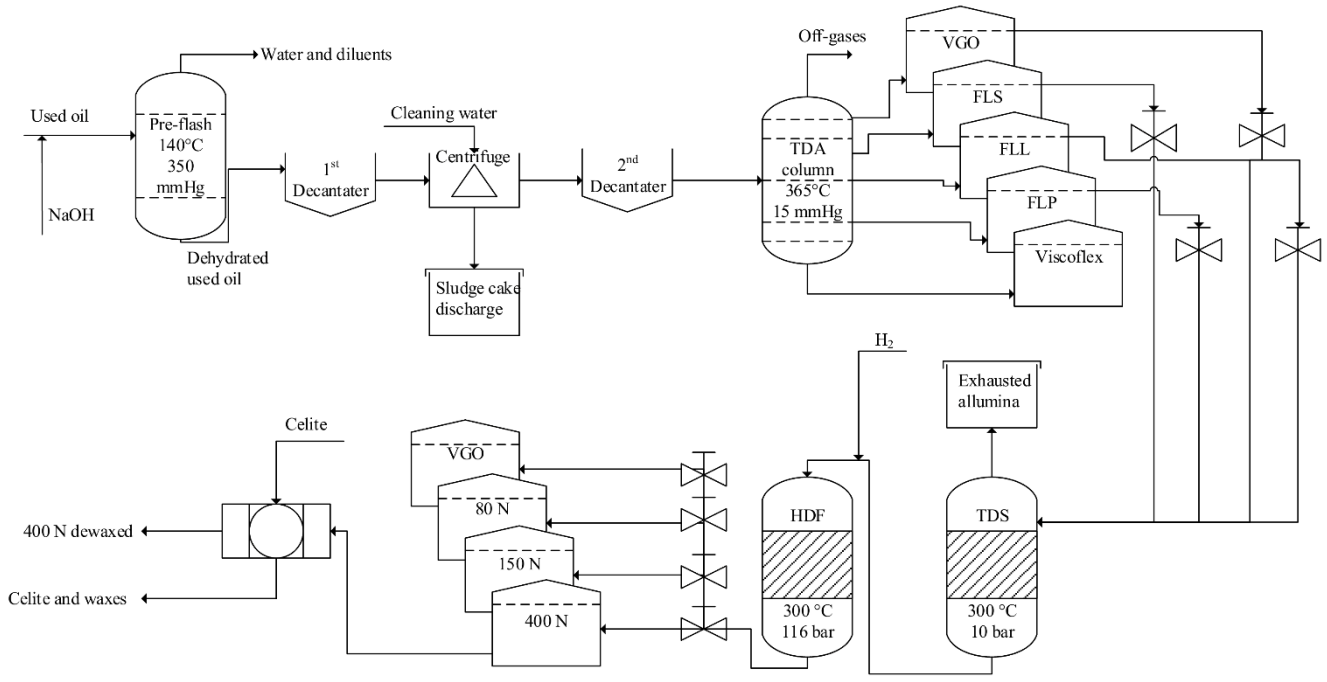


**Figure 1** Simplified scheme of the mineral oil regeneration of the Itelyum company plant located in Pieve Fissiraga (LO)

The lube oils that undergoes to the regeneration process are constantly analysed as they arrive to the plant in order to check their quality and that all parameters follow in the Italian normative ranges. The oils are mainly composed by aliphatic hydrocarbons (mainly $C_{10-40}$ chain) a small amount of aromatic hydrocarbons, low quantity of phenols, organic pollutants (POP's), organic acids and solvents, metallic ions, inorganic acids and water. As it can be seen from figure xxxx, the used lube oil is treated with sodium hydroxide (1% m/m) in order to saponify the organic acids and phenols (typically saponification number 11 mg/g). The so treated oil undergoes to a pre-Flash treatment in a Colum operating at 140 °C and 350 mmHg pressure. From the top of the column a mixture of water and small amount of organic and inorganic molecules is obtained. From the bottom of the column instead, a mixture of mainly aliphatic hydrocarbons, aromatic hydrocarbons, organic solvents (less percentage), metallic ions, organic salts and a minimum percentage of water is obtained. This mixture is sent to decanter tank (first decanter in figure 1) where it remains for two days. Here, after the decantation process, a biphasic system is formed. This consists of a top phase composed mainly by hydrocarbons and solvents and a minimum percentage of organic and inorganic salts, metal ion and water. The bottom phase is composed of organic and inorganic salts, metal ions and a small percentage of aliphatic and aromatic hydrocarbons and water. The upper phase is sent to centrifugation process (at about 6000 rpm) to obtain a dehydrated hydrocarbon phase (that contain little percentages of organic solvents, organic and inorganic salts). The dehydrated hydrocarbon phase is then sent to a second decanter tank to finalize the separation of the organic solvents, organic and inorganic salts residua. The centrifuge depot is washed every 15 minutes with a high-pressure water jet at 110 °C and collected underneath the centrifuge (the sludge cake in figure 1). The second thank dehydrated hydrocarbon phase is then sent to a pre-heater furnace at 340 °C and to the Thermodeaspahalting colums (TDA) working at 365 °C and 15 mmHg. After the TDA process three different oils, a vacuum gas oil and Re-refined Engine Oil Bottom (REOB) (commercialized as viscoflex 1000 ®) - whose physical aspect is shown in figure 2 - are obtained:

1) Vacuum Gas Oil (VGO)
2) Spindle lubricating fraction (SLF)
3) Light lubricating fraction (LLF)
4) Heavy lubricating fraction (HLF)
5) Re-refined Engine Oil Bottom (REOB)

**Figure 2.** REOB (Viscoflex 1000®) at 160 °C

The 2-4 TDA fractions undergoes (in turn) to a thermo desiloxanation (TDS) process at 300 °C and 10 bar through a catalytic reaction over an alumina ($\gamma - Al_2O_3$) bed (alumina granules of 1.5-2 mm diameter) in order to remove the silica traces (if any as polysiloxanes). The exhausted alumina is collected and subsequently disposed.

After the TDS process each oily fraction is sent to a Hydrofinishing (HDF) column where it is treated with gaseous Hydrogen with the aid of a specific (and patented) catalytic bed at 300 °C and 116 bar. After the HDF treatment three different oil type are obtained: 80N, 150N, 400N (N stands for neutral). The 80N and 150N undergoes daily to a qualitative check and stored in 150 $m^3$ tanks. The 400N fraction undergoes to a dewaxing process using the Fundabac technology, that uses a diatomaceous earth (Celite) as filtrating agent. From this treatment a 400N deparaffined lube oil is obtained. Exhausted celite is opportunely disposed.

## 2.2. Materials and methods

### 2.2.1. Materials

Various recycled materials and/or by-products were used to define alternative binders intended to fully replace neat bitumen for the production of more sustainable asphalt mixtures. The main constituents of alternative binders are REOBs that have been modified by specific additives to obtain a material similar to the standard bitumen.

### 2.2.2 REOBs

Two different REOBs were supplied by Itelyum Regeneration s.r.l, Lodi (LO), Italy. The by-products were produced in two distinct refinery plants of the same company and are marketed as Viscoflex 1000® (V1) and Viscoflex 2000® (V2TQ). The by-product V2 is usually fluxed with low molecular weight oils—in a quantity equal to 20 or 30%wt.—to facilitate materials handling. In particular, the fluxed REOB with 20%wt. and 30%wt. of the low molecular oil are referred to hereafter as V2F (F stands for fluid) and V2D (D stands for dense), respectively. The two petroleum-based by-products are viscous liquids at room temperature and are obtained by different processes. The V1 is the heavier fraction, obtained in a distillation column working at 365 °C and 15 mmHg; while the V2 is obtained through a propane de-asphalting process. Table 1 reports the main physico-chemical characteristics of both products.

**Table 1**. Main physical and chemical characteristics of V1 and V2F.

| Property | Standard | Results | |
|---|---|---|---|
| | | V1 | V2F |
| Needle Penetration Test | EN 1462 | / | >500 (0.1 mm) |
| Softening Point | UNI EN 1427 | / | <4 °C |
| Density at 15 °C | ASTM D70 | 1003 kg/m$^3$ | 0.975 kg/m$^3$ |
| Kinematic Viscosity at 100 °C | ISO 3104 | Not determinable | 580 mm$^2$/s |
| Kinematic Viscosity at 135 °C | ISO 3104 | 110.0 mm$^2$/s | / |
| Dynamic Viscosity at 60 °C | EN 13702 | 25.13 Pa s | 0.380 Pa s |
| Pour Point | ASTM D97 | > 50 °C | / |
| Insoluble Matter | ASTM D 2042 | 14% w/w | / |
| Soluble Matter | ASTM D 2042 | 86.10 % w/w | / |
| Water Content | ASTM D6304 (Procedure C) | 290 mg/kg | / |
| Sulphur | ISO 8754 | 1.13 % w/w | / |
| Nitrogen Content | ASTM D3228 | 0.32 % w/w | / |
| Gasoline Fuel | ASTM D3525 | < 0.01 % w/w | / |
| Gasoline Diluent | ASTM D322 | < 0.1% V/V | / |
| Diesel Fuel | ASTM D3524 | < 0.1 % w/w | / |
| Ash | ASTM D482 | 8.089 % w/w | / |
| Conradson Carbon Residue | ASTM D189 | 19.2 % w/w | / |
| TSE Remark | ISO 10307-1 | Filtration Time exceeds 25 min | / |
| Saturates | IP 469 | 32.9 % w/w | 37.0 % w/w |
| Aromatics | | 0 % w/w | 1.6 % w/w |
| Polars (I) | | 19.6 % w/w | 18.1 % w/w |
| Polars (II) | | 47.5 % w/w | 43.3 % w/w |
| Asphaltene | IP 143 | 16.6 % w/w | 3.7 % w/w |

| | | | |
|---|---|---|---|
| Pensky–Martens Flash Point (Closed Cup) Procedure B | ASTM D93/IP34/EN ISO 2719 | 270 °C | / |
| Cleveland Flash Point (Open Cup) | ASTM D92/EN ISO 2592 | 284 °C | 180 °C |
| PCB Content | EN 12766-3 | < 4 mg /kg | / |
| PCT | EN 12766-3 | < 10 mg /kg | / |

With the aim of replacing neat bitumen mainly with REOBs, the two available REOBs were preliminarily characterized by the use of spectroscopic analysis in order to identify the possible similarities of these materials with a standard 50/70 penetration grade bitumen (Pen 50/70). The Pen 50/70 was considered as the reference bituminous binder throughout the present study. The REOBs were firstly characterized through high-resolution 1H-NMR spectroscopy. In Figure 3, the 1H-NMR spectra of (a) Pen 50/70, (b) V2TQ, (c) V1, (d) V2D, and (e) V2F are reported. As can be seen from Figure 3, all samples are characterized by a rich aliphatic part (0.8 to 2.5 ppm). The areas under the curves for the aliphatic part are of the same order of magnitude for the 50/70 reference bitumen as well as for all REOBs samples. From this point of view, it can be said that REOBs and classic bitumen are very similar., On the other hand, it can be seen from the integral of the aromatic region that the various REOBs have a total aromatic content (asphaltene plus aromatic molecules) about one order of magnitude lower than Pen 50/70. This is in accordance with the results of the analysis shown in Table 1.

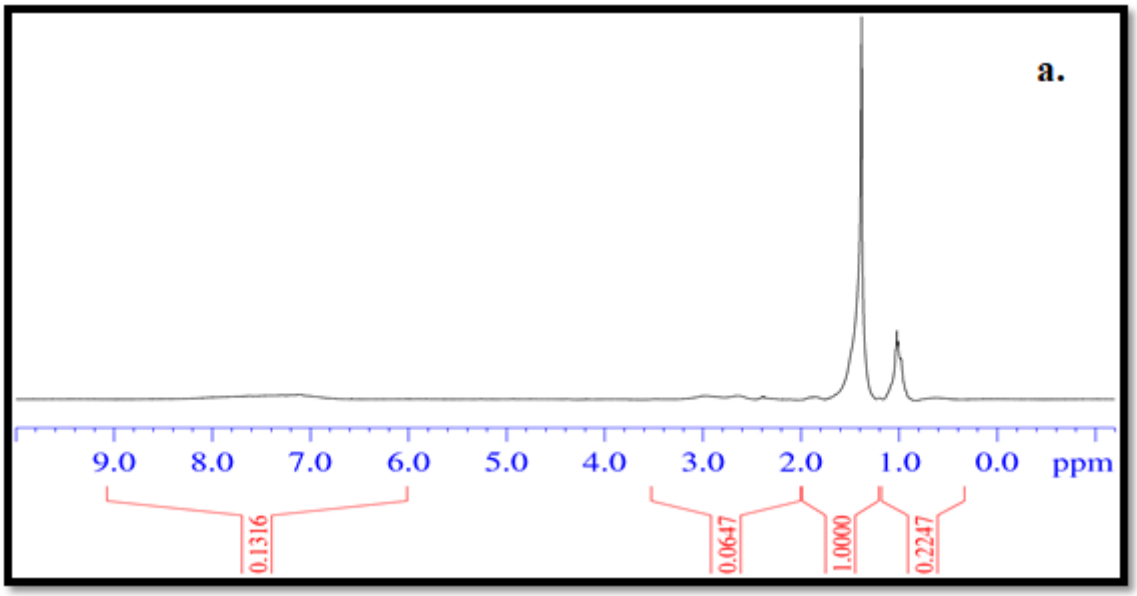

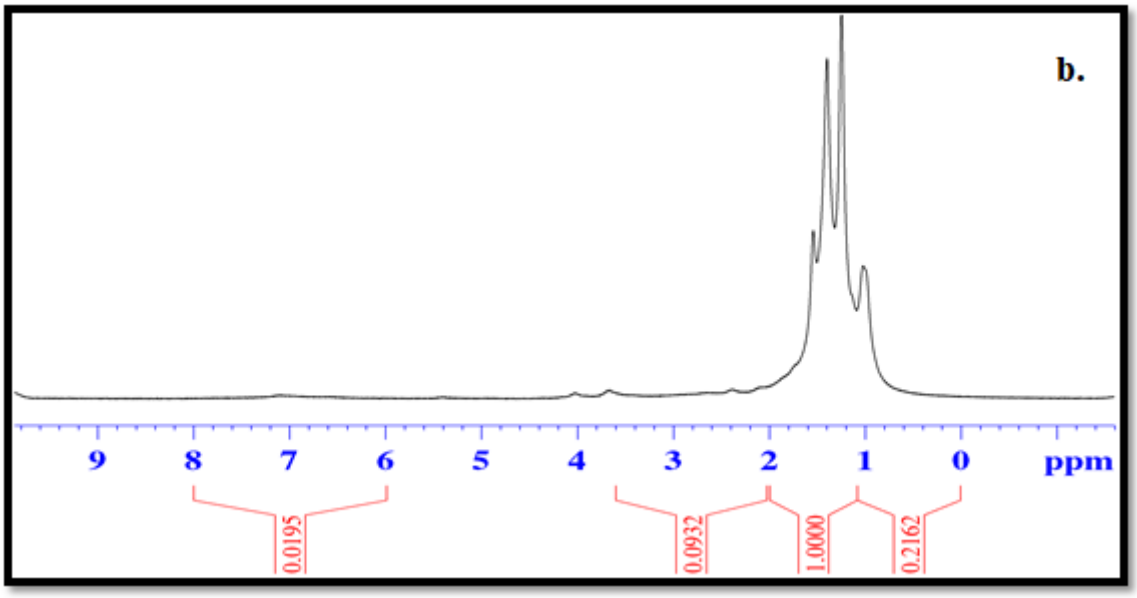
b.
9 8 7 6 5 4 3 2 1 0 ppm
0.0195
0.0932
1.0000
0.2162

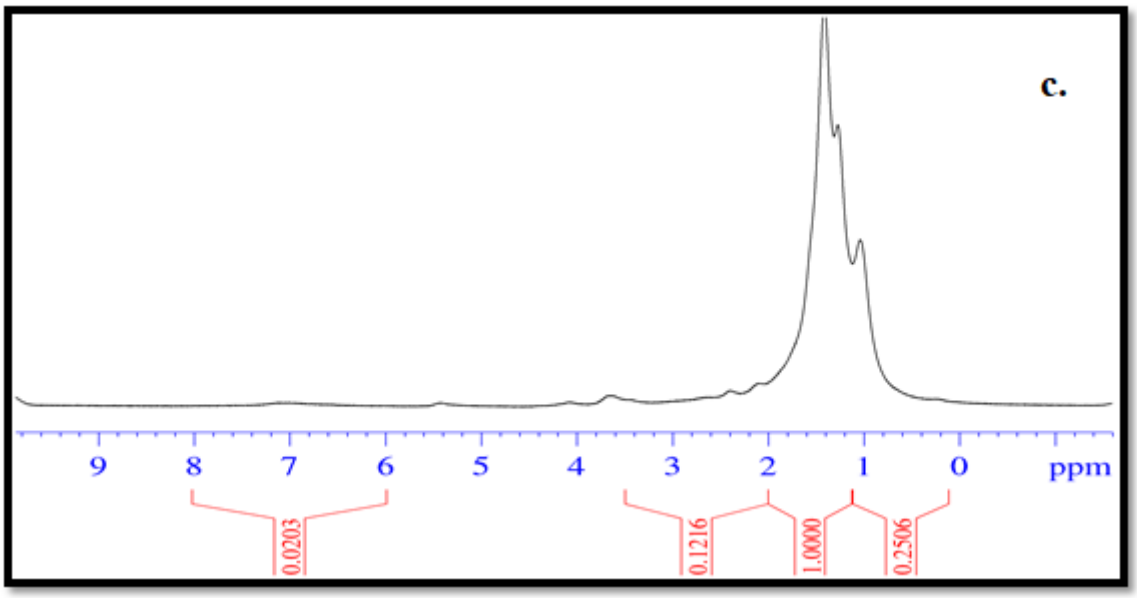
c.
9 8 7 6 5 4 3 2 1 0 ppm
0.0203
0.1216
1.0000
0.2506

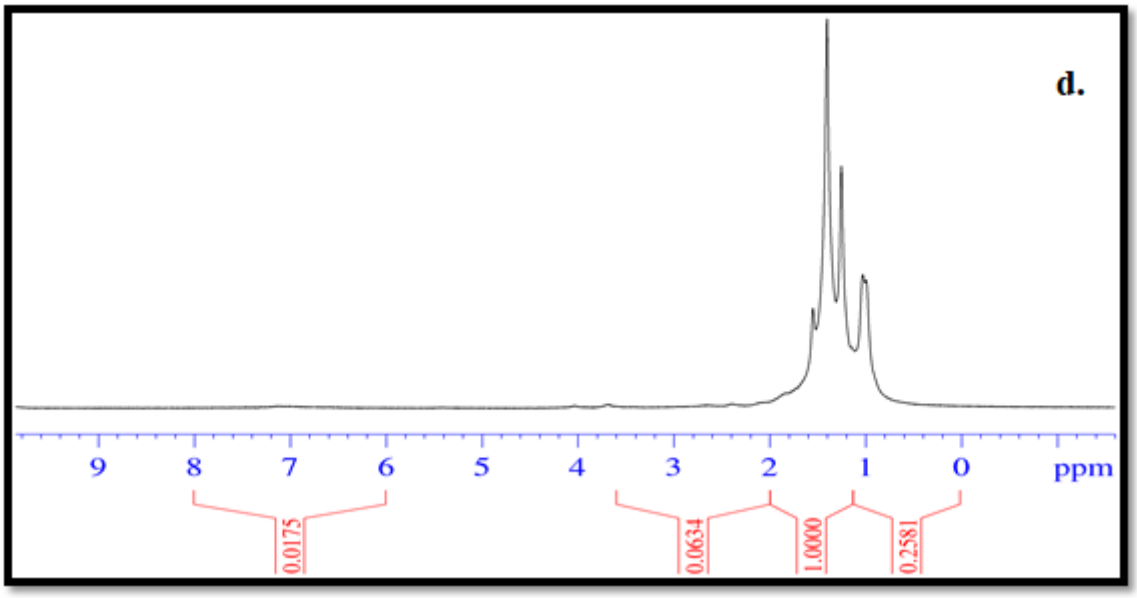
d.
9 8 7 6 5 4 3 2 1 0 ppm
0.0175
0.0634
1.0000
0.2581

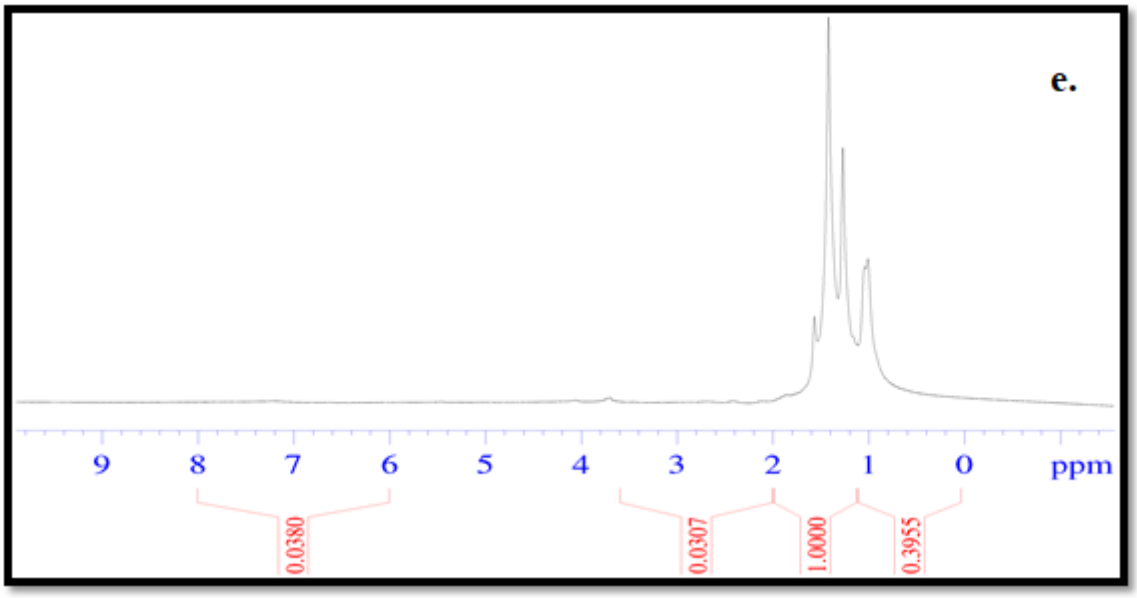


**Figure 3.** $^{1}$H-NMR spectra of (**a**) Pen 50/70 (**b**) V2TQ, (**c**) V1, (**d**) V2D, (**e**) V2F.

### 2.2.3 Additives

The polymers were introduced in the composition of the alternative binders to improve the elastic response of the final formulations. The powdered rubber from ELTs was supplied by Ecopneus s.c.p.a. The product is a black powder with a maximum size dimension of about 42 μm. Moreover, the introduction of SBS polymer has been considered, since this elastomeric polymer is commonly used in the road sector for the production of modified bitumens. In this study, the amount of SBS used was limited to a maximum of 2% in order to reduce the production costs of the final blends. In addition, it is well-known that SBS polymers work well in combination with rubber from ELTs [17,18]. The SBS polymer was supplied by Kraton Polymers LLC. In order to improve the adhesion of REOBs to the lithic skeleton, an adhesion promoter (AP) has been employed, since it was proven to be effective [19,20]. To modulate the viscosity, various cellulose polysaccharides were used as viscosifier: P2, nano-fibrillated cellulose (CNF), and nanocrystalline cellulose (CNC) [21]. Additionally, to ensure a good workability of the asphalt mix at high temperatures, waxes with melting points of about 100 °C were used, which are commonly used for the production of WMA mixtures [22,23]. In particular, Sasobit waxes (Sb) were employed in this study. Some other issues observed during the blend preparation and analysis have been solved by the aid of other additives such as pine resins (PR) [24,25], which improve the cohesive properties of the REOBs; thickening agents such as Lithium salt (LiS) and nanotubes (Nt) have been used to take advantages of their gelling properties (widely employed in industrial grease production). The PR, AP, and P2 were supplied by Kimical s.r.l. The lithium salt (LiS) was supplied by Sigma Aldrich, while the nanotubes (Nt) were produced in laboratories of the University of Calabria. The nano-fibrillated cellulose (CNF) was supplied by Nanografi Co. Inc., while nano-crystalline cellulose (CNC) was obtained in the laboratories of the University of Calabria from waste papers following the methods reported in the reference [26]. All the supplied products were used without any further treatment. The mean cost of the blends, considering the various additives' prices and percentages used in our blend preparation, is about 350–

400 €/ton.

### 2.2.4. Alternative Binders

The additives that were used allowed for the definition of final alternative binders similar to the traditional bitumen used for paving. In total, 18 alternative binders were defined and then characterized at the binder and the asphalt mixture levels, which are listed in Table 2. Each alternative binder description consists of all materials that were used in quantity greater than 0%. Hence, each line of Table 2 represents the recipe of one alternative binder.

Prior to samples preparation, the various additives underwent thermogravimetric analysis in order to check their stability at the high temperature, i.e., 160 °C. No additives showed considerable weight loss and, consequently, no additives degradation would occur during mixing process.

The preparation of alternative binders required the preliminary heating phase of each specific REOB (V1, V2TQ, V2F and V2D) at about 160 ± 5 °C. Then, the quantity of the chosen additives was gradually added to the warmed REOB (1 g/min). The additives were incorporated at room temperature. All constituents were mixed by means of high-shear mixer (IKA model) with an average speed of about 1400–1600 rpm. Each blend was mixed at 160 °C for 60 min to guarantee an essentially homogenous sample.

**Table 2.** Type and percentage of constituent materials of the 18 alternative binders.

| Blend | V1 | V2TQ | V2F | V2D | PFU | Sb | SBS | AP | P2 | CNC | CNF | PR | Nt | LiS |
|---|---|---|---|---|---|---|---|---|---|---|---|---|---|---|
| B23 CNC | - | - | 60 | - | 15 | 10 | - | 0.3 | - | 14.7 | - | - | - | - |
| B26 | - | - | 40 | - | 10 | 10 | - | - | 20 | - | - | 40 | - | - |
| B27 | - | - | 60 | - | 5 | 10 | - | - | 15 | - | - | 10 | - | - |
| B29 | - | - | 40 | - | 10 | 10 | - | - | - | - | - | 40 | - | - |
| B29V1 | 40 | - | - | - | 10 | 10 | - | - | - | - | - | 40 | - | - |
| B30 | - | - | 40 | - | - | 8 | - | - | 14.9 | - | - | 27 | 0.1 | 10 |
| B26D | - | - | - | 40 | 10 | 10 | - | - | 20 | - | - | 20 | - | - |
| B27D | - | - | - | 60 | 5 | 10 | - | - | 15 | - | - | 10 | - | - |
| B29D | - | - | - | 40 | 10 | 10 | - | - | - | - | - | 40 | - | - |
| B30D | - | - | - | 40 | - | 8 | - | - | 14.9 | - | - | 27 | 0.1 | 10 |
| B26-1 | - | - | 60 | - | 10 | 10 | 1 | 0.3 | 8.7 | - | - | 10 | - | - |
| B27-1 | - | - | 60 | - | 5 | 10 | 1 | 0.3 | 13.7 | - | - | 10 | - | - |
| B29-1 | - | - | 50 | - | 10 | 10 | 0.5 | 0.3 | - | - | - | 29.2 | - | - |
| B31 | - | - | 60 | - | 15 | 10 | 2 | 0.3 | 7.7 | - | - | 5 | - | - |
| B31V1 | 60 | - | - | - | 15 | 10 | 2 | 0.3 | 7.7 | - | - | 5 | - | - |
| B32 | - | - | 60 | - | 15 | 5 | - | 0.3 | - | - | 14.7 | 5 | - | - |
| B32V1 | 60 | - | - | - | 15 | 5 | - | 0.3 | - | - | 14.7 | 5 | - | - |
| B33TQ | - | 60 | - | - | 19.7 | 13 | 2 | 0.3 | - | - | - | 5 | - | - |

### 2.2.5 Asphalt Mixtures

The asphalt mixes with the alternative binders were produced using RAP aggregates only. The recycled aggregates consisted of milled asphalt concrete from existing pavements of highways. The grading distribution and the binder content were designed in order to produce a traditional wearing course asphalt mixture. The grading distribution of the RAP aggregates met the Italian technical specifications. Based on the aged bituminous binder content already present in the recycled aggregates and on previous studies based on

Cantabro test (EN 12697-17) [27], the optimum binder content was selected as equal to 2.5% of the total weight of aggregates. The innovative asphalt mixtures were compared with samples of a traditional wearing course layer made of 90% virgin aggregates and 10% RAP and Pen 50/70, which was considered as a reference mix, and a mix consisting of 100% RAP aggregate and Pen 50/70. Moreover, the limits of the Italian technical specifications for wearing course layers were considered as reference for comparisons.

All alternative binders were used for producing 18 different asphalt mixtures. Per each asphalt concrete mix, three samples were manufactured. The cylindrical samples had diameter of 100 mm and were 55 mm tall, approximately. The correct amount of recycled aggregates and the alternative binders were preliminarily heated in an air-forced oven before being mixed and compacted. Per each asphalt mix, 3000 g of RAP aggregates were heated at 150 °C for 2 h and 75 g of the prepared blends (i.e., 2.5%wt.) at 150 °C for a minimum of 1 h. The samples underwent compaction by means of a gyratory compactor applying 100 gyrations at 600 kPa [28].

### 2.2.6 Test Methods

In order to preliminarily assess the feasibility of using alternative binders for road construction materials, the 18 new binders underwent rheological analysis. Then, the mechanical response of all asphalt mixtures, those containing an alternative binder and the reference mixes, were investigated. Since these were binders without bitumen as the main constituent, the basic tests were planned with the aim of assessing a possible relationship, if any, between the behaviour of binders and that of mixtures as they exist for traditional bituminous materials.

### 2.2.7. Rheological Measurements

A dynamic shear rheometer (SR5000, Rheometric Scientific, Piscataway, NY, USA) was used to perform the rheological tests on the various alternative binders. The controlled shear stress rheometer was used in a plate–plate configuration. Plate tools of $\phi$ = 25 mm diameter were used for testing in the temperature range of 25–120 °C. The gap was set equal to 2 mm. A Peltier system (±0.1 °C) controlled the test temperature. The rheological responses of Pen 50/70 and alternative binders were determined under the kinematics of both steady and oscillatory simple shears. In steady-shear experiments, the viscosity of blend samples was determined from the ratio of measured shear stress to applied shear rate, as a function of shear rate that varied from 1 to 100 s−1. Steady states were previously checked by transient experiments (step-rate test). For all samples, it was observed that 10 s was a sufficient scanning time to ensure the steady-state condition. All samples showed a Newtonian behaviour in the investigated shear rate range. Dynamic tests were carried out in conditions of linear viscoelastic (LVE) region, where measured material features do not depend on the amplitude of applied load and are related to materials microstructure only. With the aim of investigating the material viscoelastic phase transition, dynamic temperature ramp tests (DTRT) were performed both at 1 Hz and temperature rate of 1 °C/min from 25 °C to 120 °C by applying the proper stress values—previously determined by stress sweep tests—to guarantee linear viscoelastic conditions at all tested temperatures.

### 2.2.8 Mechanical Analysis

The resulting 18 asphalt mixtures were subjected to dynamic and static mechanical characterizations. The asphalt concrete samples underwent mechanical tests after being cured for a minimum of 24 h. Dynamic tests were used to determine the Indirect Tensile Stiffness Modulus (ITSM) at 20 °C of all samples by using a servo-pneumatic testing machine. The ITSM values were determined according to EN 12697-26 standard [29], in the indirect tensile configuration (IT-CY). A pulse loading was applied with a 124 ms rise-time to generate a horizontal deformation of 5 ± 2 μm. Two static mechanical characterizations were used to measure the Indirect Tensile Strength (ITS) and the Indirect Tensile Strength Ratio (ITSR) of all mixes according to the EN 12697-23 [30] and EN 12697-12 [31] standards, respectively. The tensile resistance of asphalt concretes was determined by applying a compression load with a constant speed rate of 51 mm/min. The ITS test was performed at 25 °C. The latest characterization, i.e., the ITSR ratio, aimed to assess the durability of the wearing course samples, as it determines the effect of water conditioning. This investigation quantifies the ratio between the ITS values of an asphalt mix after water conditioning and those of dry specimen. According to standard method A, the samples were saturated while stored in a water bath at 40 °C for three days. Successively, the samples were removed, dried, and conditioned at 25 °C in a climate chamber to further undergo ITS testing. The two static characterizations applied a load until failure; hence, two samples were used to evaluate the average ITS values, while the third specimen of each asphalt mix was used to determine the corresponding ITSR value. Before being tested, all samples were kept in a climate chamber at the test temperature for at least 4 h.

## 2.3 Results and Discussion

### 2.3.1. Rheological Analysis

Figure 4 shows the results of the DTRT obtained from the blends B26-1, B27-1, B29-1, and B32V1. Among all alternative binders, these four blends were selected because they exhibit good rheological and mechanical responses, as can be seen by comparing the DTRT of our blends with that of a 50/70 bitumen reported in Figure 5. The remaining blends that were prepared show good rheological behaviour, but they do not behave as expected from a mechanical point of view. The DTRT of virgin REOBs (V2F, V1, V2D, V2TQ) are reported in Figure 5. Figures 4 and 5 shows that alternative binders strongly enhance the rheological properties of both REOBs and bitumen. Moreover, by comparing the DTRT of the alternative binders—even those reported in the Supplementary Information—with that of an SBS-modified bitumen (PmB) reported in Figure 6, it can be concluded that the alternative binders resemble the behaviour of a polymer-modified bitumen.

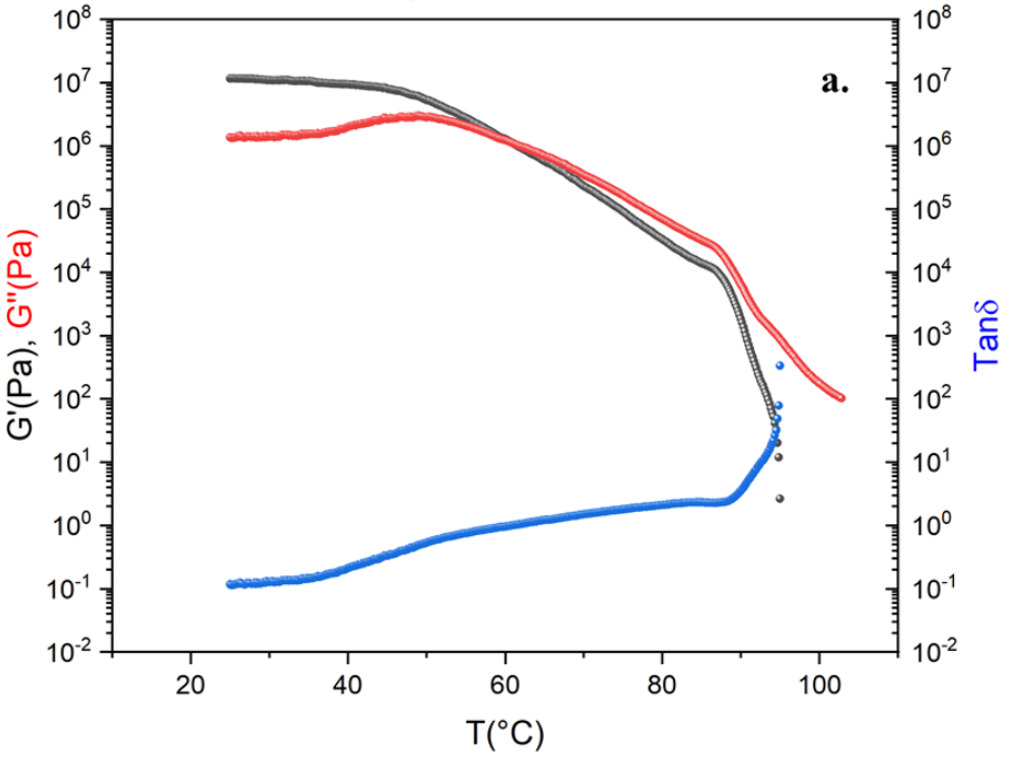
a.
G'(Pa), G"(Pa)
Tanδ
T(°C)
20
40
60
80
100

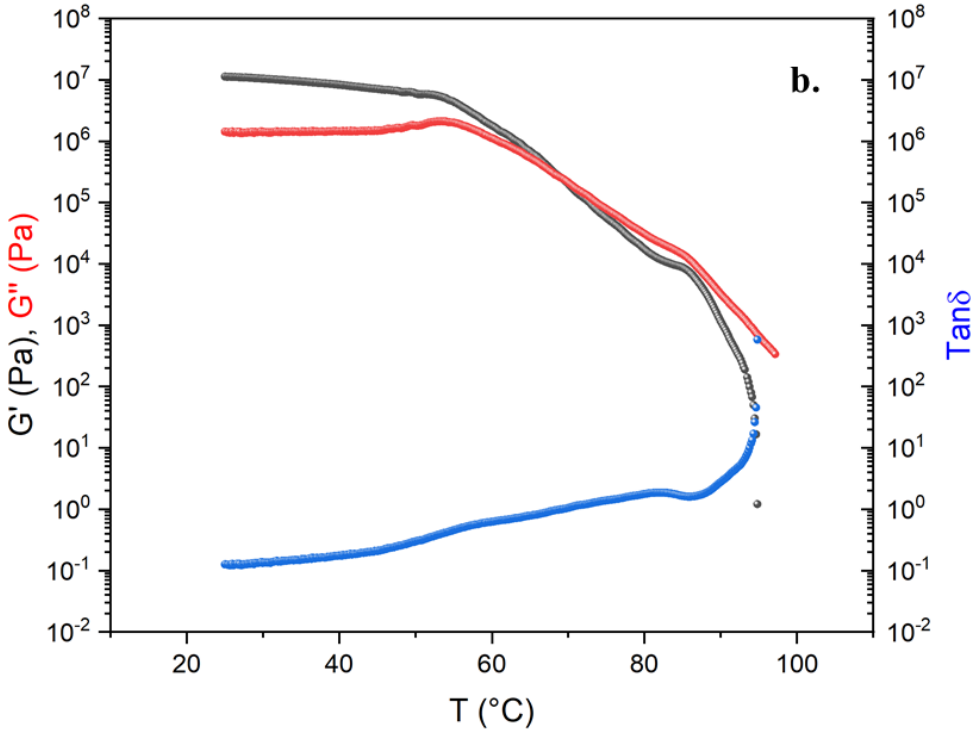
b.
G' (Pa), G" (Pa)
Tanδ
T (°C)
20
40
60
80
100

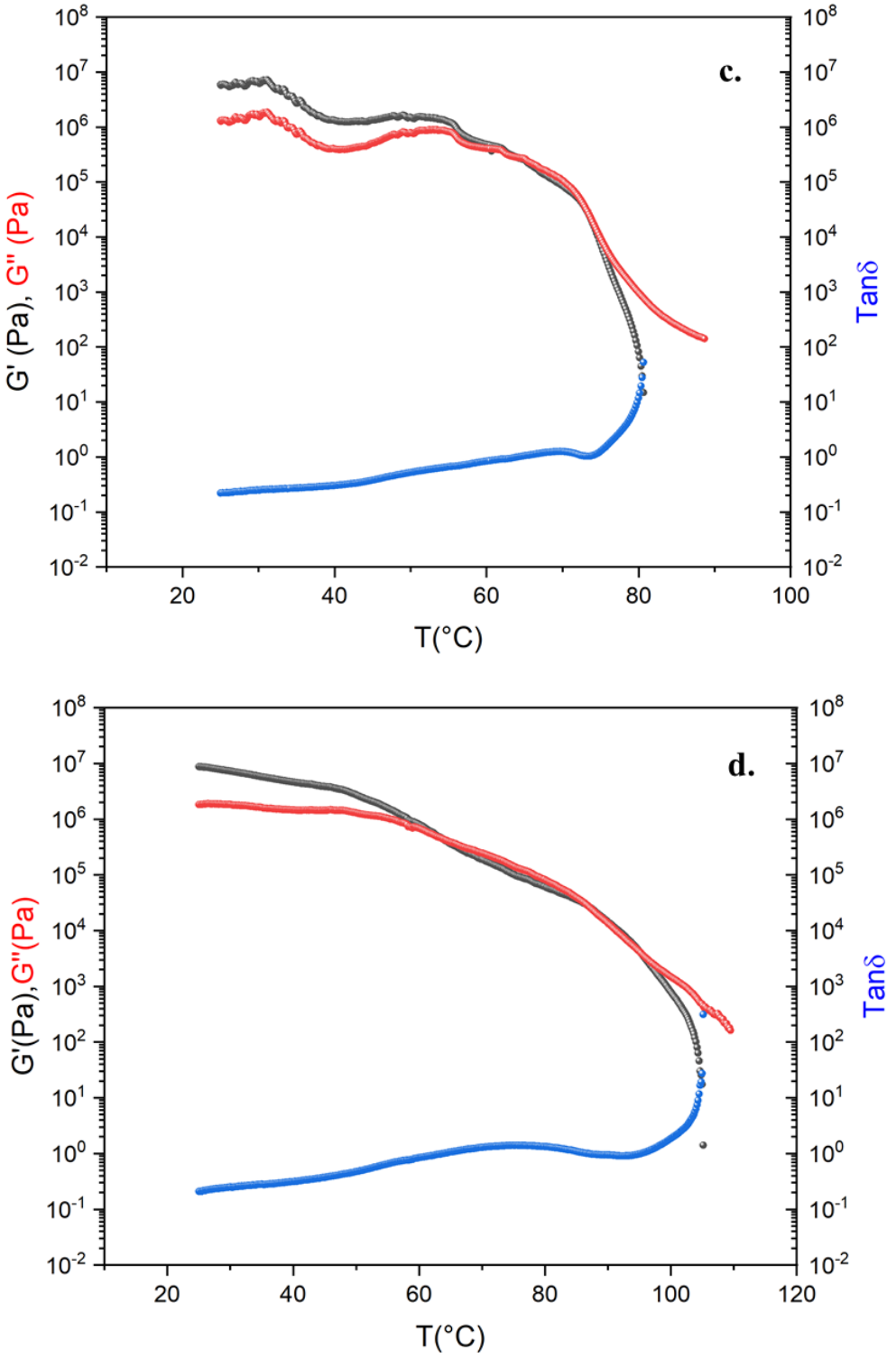


**Figure 4.** Dynamic Temperature Ramp Test (DTRT) of (**a**) blend 26-1, (**b**) blend 29-1, (**c**) blend 27-1, (**d**) blend 32V1.

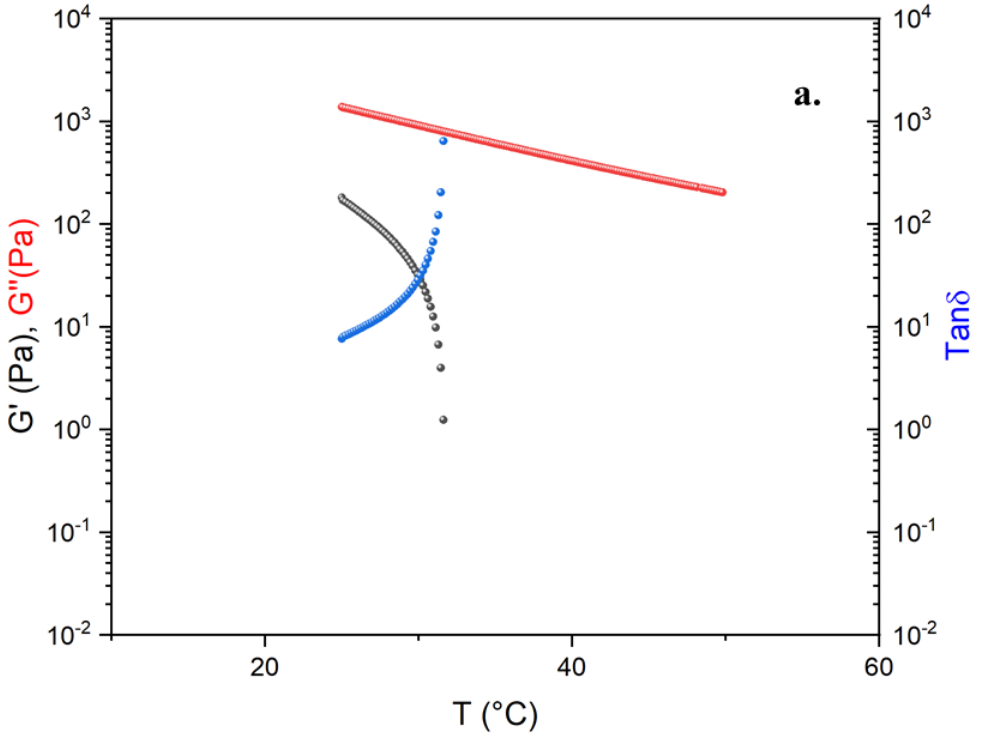
a.
G' (Pa), G''(Pa)
Tanδ
T (°C)
10^4
10^3
10^2
10^1
10^0
10^-1
10^-2
20
40
60

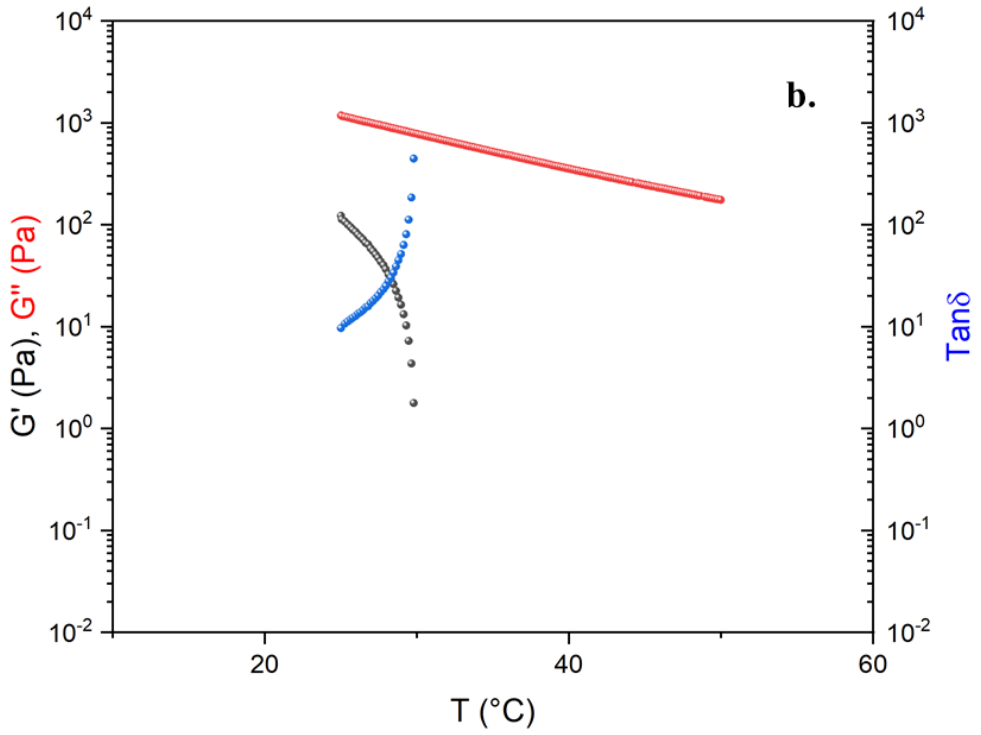
b.
G' (Pa), G'' (Pa)
Tanδ
T (°C)
10^4
10^3
10^2
10^1
10^0
10^-1
10^-2
20
40
60

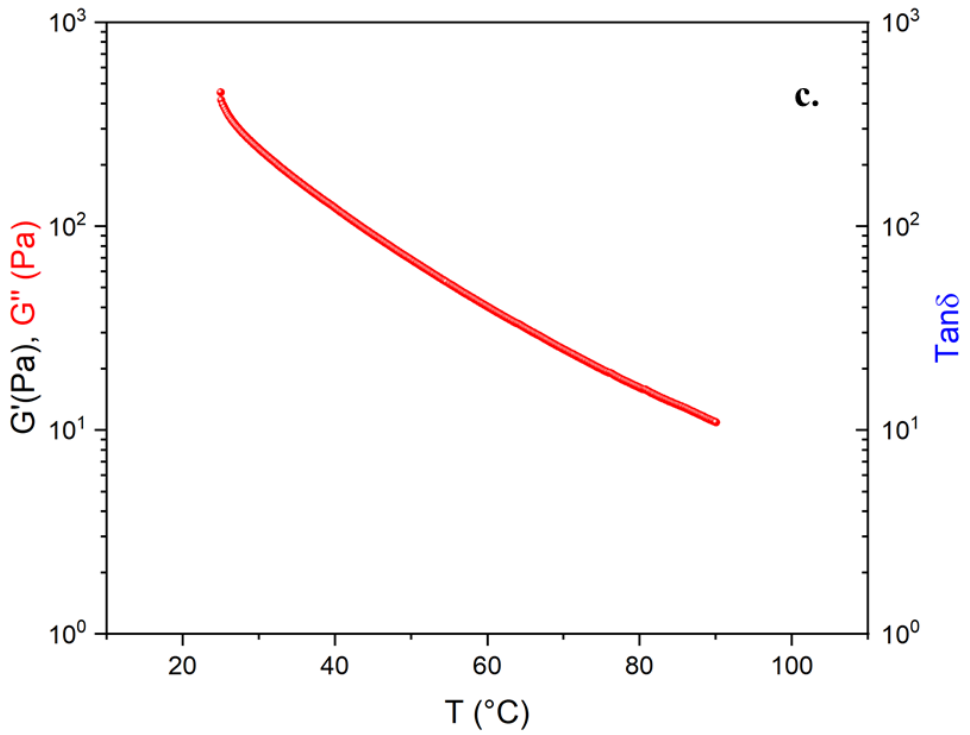
c.
G'(Pa), G'' (Pa)
Tanδ
T (°C)
10^3
10^2
10^1
10^0
20
40
60
80
100

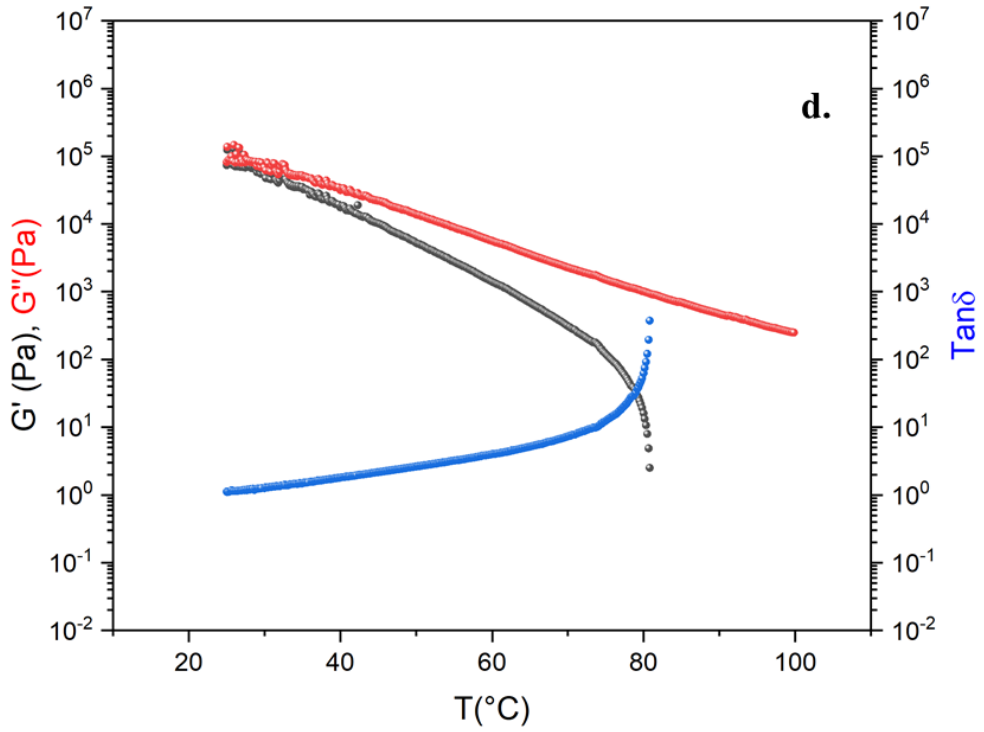
d.
G' (Pa), G''(Pa)
Tanδ
T(°C)
10^7
10^6
10^5
10^4
10^3
10^2
10^1
10^0
10^-1
10^-2
20
40
60
80
100

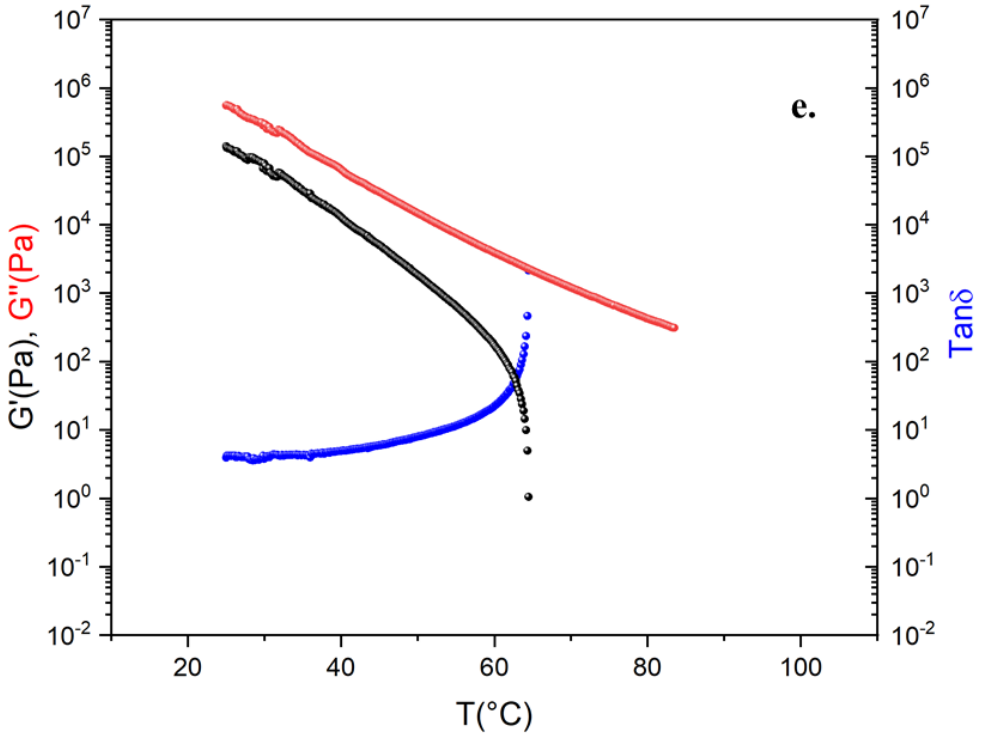


**Figure 5.** Dynamic Temperature Ramp Test of (**a**) V2F, (**b**) V2D, (**c**) V1, (**d**) V2TQ, (**e**) Pen 50/70.

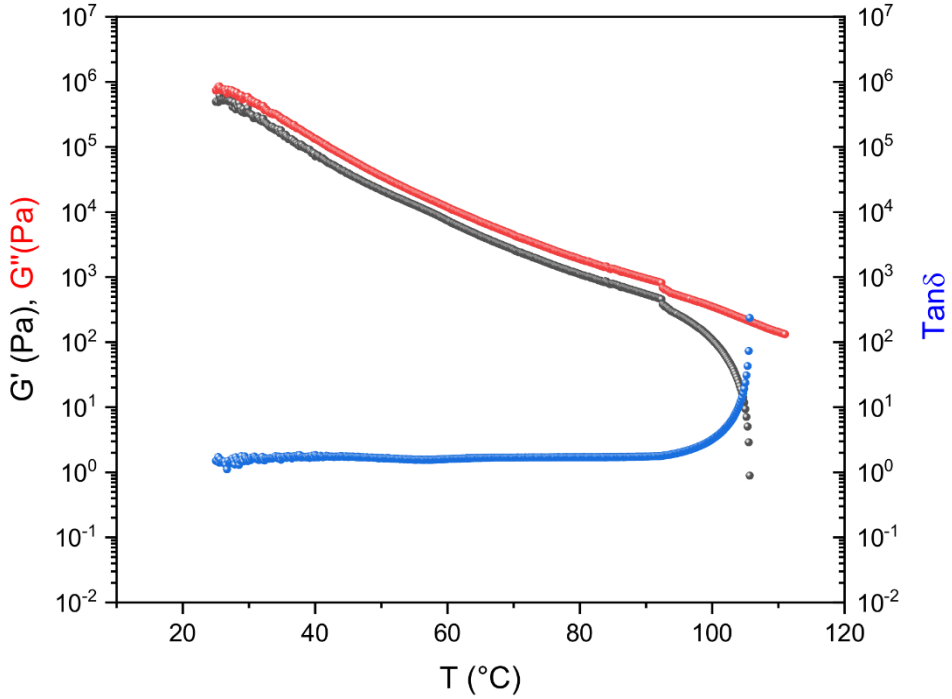


**Figure 6.** Dynamic Temperature Ramp Test of an SBS-modified bitumen (Pen 50/70 + 3% SBS).

### 2.3.2. Mechanical Analysis

The dynamic mechanical characterization of the asphalt mixtures manufactured with the 18 alternative binders and Pen 50/70 is reported in Figure 7. The asphalt mixes exhibit high variability in the ITSM results, which can be ascribed to the constituent materials used. The mixture with B23CNC shows the lowest stiffness modulus, while the mixture containing B29D has the highest stiffness. In general, the asphalt mixes containing the V2D show higher stiffness than the corresponding asphalt concrete mixtures with V2F. The higher presence

of low-molecular-weight oil in the alternative binders lead to soften the final materials as expected. Hence, the type of REOB affects the final ITSM values. Additionally, the combination of specific additives permits alternatively increasing or decreasing the stiffness modulus of the corresponding asphalt mixture. In fact, the B33TQ mix has lower ITSM value than the B29D asphalt concrete. In general, the minimum ITSM values at 20 °C of a traditional wearing course layer made with virgin materials only are 3000 MPa and 3500 MPa for samples produced with unmodified and polymer-modified bitumens, respectively. Previous studies on the reference mix that contains 10% of RAP and Pen 50/70 have assessed an average ITSM value equal to 5500 MPa at 20 °C, which can be used for comparing the stiffness modulus of the innovative asphalt mixtures with the alternative binders. Among all tested asphalt materials, the mixtures manufactured with B26-1, B27, B27-1, B31, B31V1, B32, and B32V1 have similar stiffness to the reference mixture that mainly contains virgin materials. Most of the recycled asphalt mixtures with alternative binders have higher stiffness than the samples of the reference mix, which can be mainly related to the presence of RAP and to the addition of PR. In general, the use of recycled aggregates has been found to stiffen the final asphalt concretes; indeed, the mixture with 100% RAP and Pen 50/70 is stiffer than the reference one. The introduction of PR in the bituminous binders improve the cohesion properties, which turn in higher ITSM values. Indeed, the alternative binders with a high content of PR are very stiff. However, the use of asphalt mixtures with a very high stiffness is disadvantageous, as the resulting asphalt pavement may be more prone to fatigue and thermal cracking.

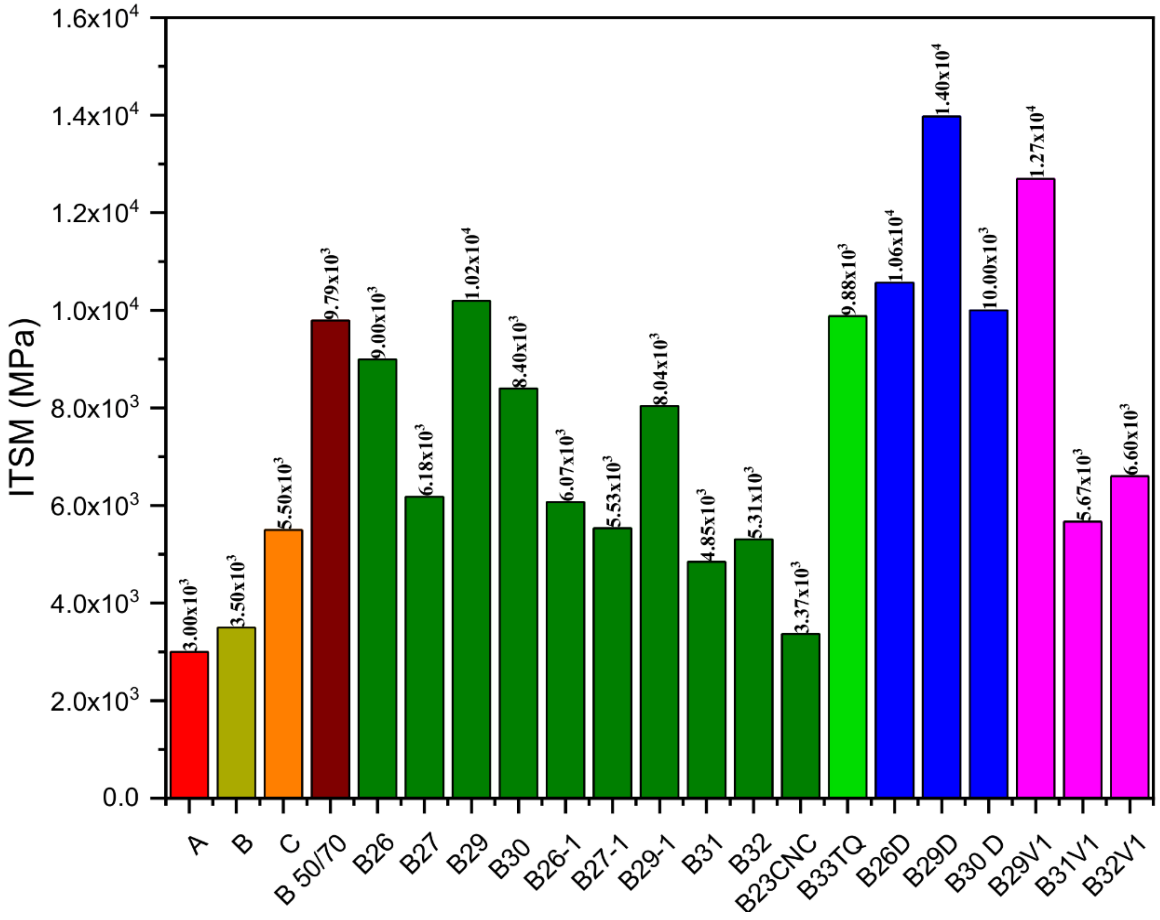


Figure 7 . Results of the ITSM values at 20 °C for the recycled asphalt mixtures produced with 100% RAP and the alternative binders. Legend: Asphalt concrete with virgin bitumen and aggregates (A); Asphalt concrete with virgin polymer-modified bitumen and aggregates (B); Reference mix (C); 100% RAP asphalt concrete with Pen 50/70; 100% RAP asphalt concrete with alternative binders containing V2F; 100% RAP asphalt concrete with B33TQ; 100% RAP asphalt concrete with alternative binders containing V2D; 100% RAP asphalt concrete with alternative binders containing V1

Figure 8 shows the indirect tensile resistance of the innovative asphalt mixtures produced with RAP and alternative binders. The Italian technical specifications require a minimum ITS value equal to 0.72 or 0.95 MPa for asphalt concrete with unmodified and polymer-modified bitumens, respectively. Almost all innovative mixtures meet the requirement; only the innovative mixtures with B23CNC, B27-1, and B29-1 show insufficient tensile resistance. The recycled mix with Pen 50/70 exhibits the highest tensile resistance. For bituminous materials, the tensile resistance and stiffness values are directly related to each other, and this correlation is also confirmed in the present study. The innovative asphalt mixes with the highest ITSM values exhibit the highest ITS results. However, the ITS values close to or higher than 2.0 MPa may reflect a very high stiffness, which may turn into brittle asphalt pavements. As a consequence, the Italian technical specifications limit the tensile resistance of the asphalt mixes, and the ITS values of the asphalt mixtures with neat and polymer-modified bitumen have to be lower than 1.60 and 1.90 MPa, respectively. In this regard, the samples manufactured with B26, B26D, B26-1, B27, B27-1, B29V1, B29-1, B30, B30D, B31, B32, and B32V1 meet the required specifications for mixtures with unmodified bituminous binders. These innovative

mixes have a similar response to the reference mix with virgin materials, as their ITS values are equal to 1.2 MPa on average.

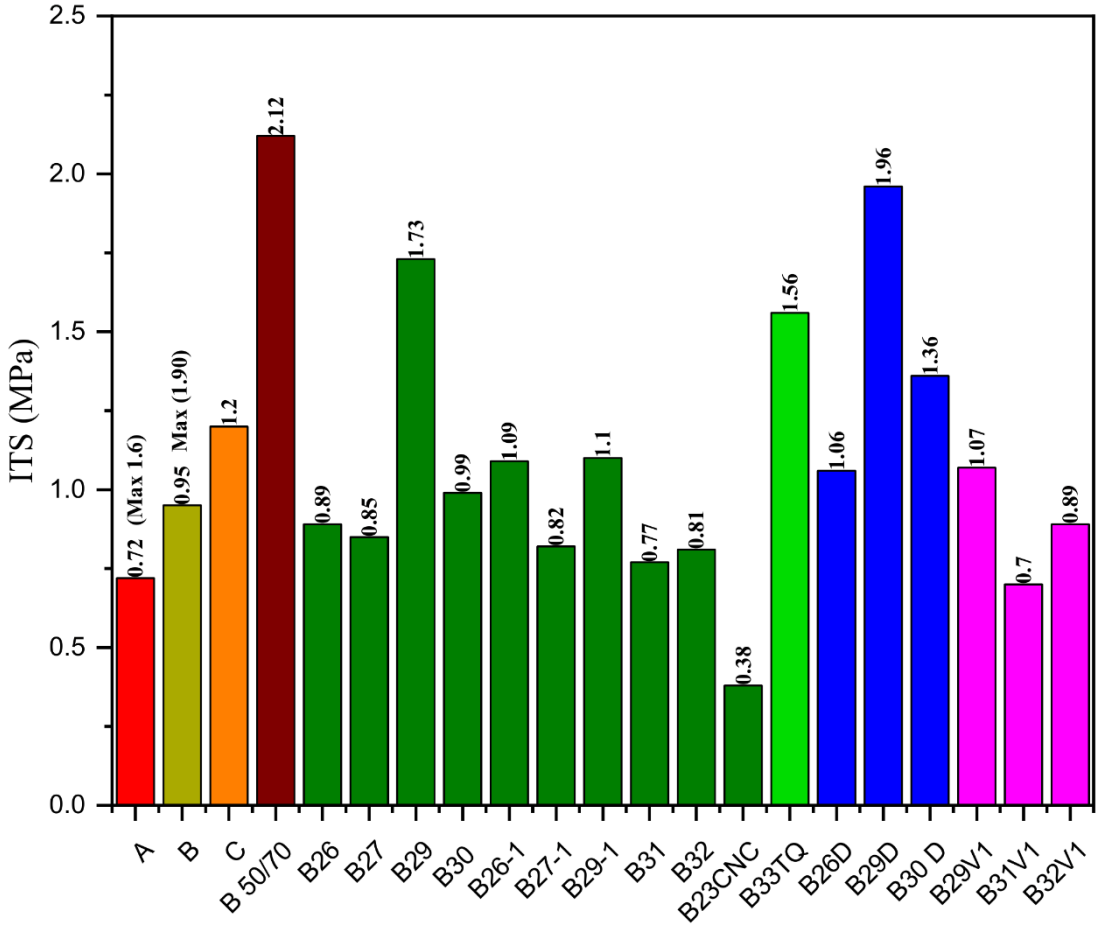


Figure 8 . Results of the ITSM values at 20 °C for the recycled asphalt mixtures produced with 100% RAP and the alternative binders. Legend: Asphalt concrete with virgin bitumen and aggregates (A); Asphalt concrete with virgin polymer-modified bitumen and aggregates (B); Reference mix (C); 100% RAP asphalt concrete with Pen 50/70; 100% RAP asphalt concrete with alternative binders containing V2F; 100% RAP asphalt concrete with B33TQ; 100% RAP asphalt concrete with alternative binders containing V2D; 100% RAP asphalt concrete with alternative binders containing V1

The results of measuring the water susceptibility for the innovative asphalt mixtures are reported in Figure 9. The type of REOB significantly affect the resistance of asphalt concrete, as the use of V1 decreases the water damage resistance of the mixes when compared to the corresponding mixtures with one of the V2s. The minimum ITSR value required by the Italian technical specifications is about 90% when unmodified bitumens are used. Among the innovative asphalt mixtures, almost all mixes that contain V2F (except for B26 and B23CNC) and the mixtures made with B33TQ, B29D, B30D, and B32V1 show good resistance against water damage, or they do not even show any water susceptibility, as the ITSR results are greater than 100%. This behaviour can be ascribed to the presence of a very high quantity of RAP aggregates. The abovementioned asphalt concrete mixes behave similarly to the reference mix mainly produced with virgin aggregates. On the other hand, the ITS value of the 100% RAP mix with Pen 50/70 is considerably reduced after water conditioning, and its ITSR ratio is about 89%.

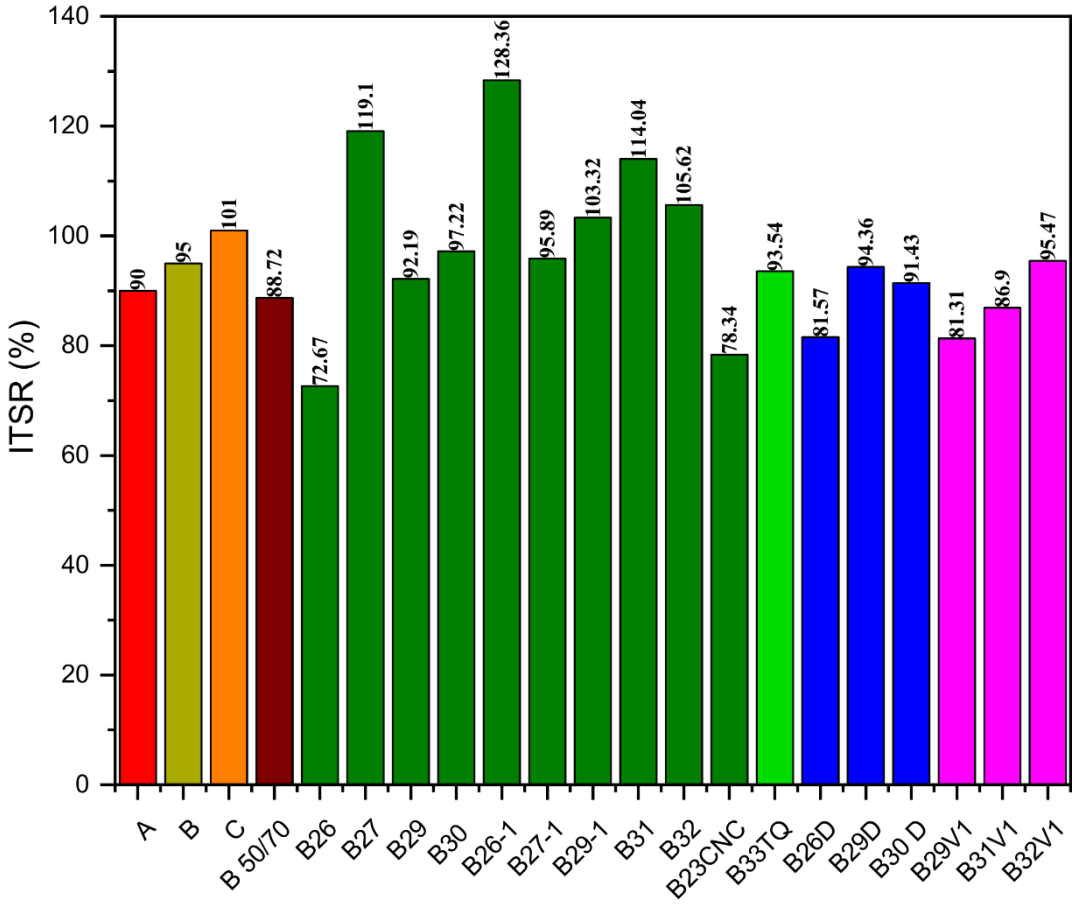


Figure 9 . Results of the ITSM values at 20 °C for the recycled asphalt mixtures produced with 100% RAP and the alternative binders. Legend: Asphalt concrete with virgin bitumen and aggregates (A); Asphalt concrete with virgin polymer-modified bitumen and aggregates (B); Reference mix (C); 100% RAP asphalt concrete with Pen 50/70; 100% RAP asphalt concrete with alternative binders containing V2F; 100% RAP asphalt concrete with B33TQ; 100% RAP asphalt concrete with alternative binders containing V2D; 100% RAP asphalt concrete with alternative binders containing V1

Among all analysed asphalt mixtures, those containing the blends B26-1, B27, B27-1, B31, B32, and B32 V1 exhibit good mechanical properties in terms of stiffness, tensile resistance, and water susceptibility. Although the results obtained with the alternative binders are promising, further specific rheological and mechanical tests have to be carried out in order to assess the feasibility and the durability of these road materials that do not contain standard bitumen. For instance, testing fatigue (mechanical), ageing susceptibility (rheological and mechanical), and low-temperature behaviour of the final alternative binders and asphalt mix will be crucial to establish the performances of these innovative asphalt products. In particular, the ageing tendency of the alternative binders, and consequently of asphalt concrete, has to be evaluated, since an aged material is used, i.e., REOB. Some of the abovementioned tests are ongoing and are showing promising results.

### 2.4. Conclusions

In this work, the potential reuse of waste products that were opportunely treated to produce new possible petroleum-based binders starting from REOBs is proposed. In addition, the use of 100% recycled aggregates (RAP) together with alternative binders can represent a good alternative to the current use of virgin materials at the binder and asphalt mixture levels. During this study, rheological and mechanical tests were carried out

to preliminarily assess the mechanical properties of these innovative binders. From a rheological point of view, the alternative binders exhibit similar behaviour to polymer-modified bitumen (3%wt. of SBS). The type of REOB, the chosen additives, and the combination of constituent materials are found to be crucial to the final responses of the innovative petroleum-based binders and asphalt mixes. In particular, the introduction of low-molecular-weight oils by REOB products softens the resulting alternative binders and, consequently, the asphalt mixtures, resulting in lower ITSM and ITS values. In addition, the use of recycled mixture with 100% of RAP and alternative binders confers good water damage resistance to the corresponding asphalt mix. In general, various eco-friendly asphalt mixtures show promising results in terms of stiffness, tensile resistance, and water susceptibility. In detail, among all tested materials, the asphalt concretes that contained the alternative binders B26-1, B27, B27-1, B31, B32, and B32V1 meet the requirements of the Italian technical specifications for wearing course samples produced with virgin materials. Hence, these innovative mixtures satisfy the basic mechanical performances. However, limited recipe adjustment may allow the stiffness reduction of the abovementioned asphalt mixtures without compromising the cohesion and water sensitivity of the final road materials. Even though the results of the present study are promising, they represent a preliminary evaluation of the performances of the alternative binders, and further rheological and mechanical analyses are necessary. In particular, the durability of the asphalt concrete has to be investigated, considering the natural ageing process of petroleum-based product and the use of an aged material for the production of the alternative binders (i.e., REOB). The determination of eco-friendly road materials is still ongoing, and the responses of the low-temperature DTRT and fatigue tests are under investigation.

**Reference Chapter 2**


[1] https://www.eurobitume.eu/bitumen/industry/

[2] https://eapa.org/eapa-asphalt-in-figures-2017/

[3] del Barco-Carrión A. J., Pérez-Martínez M., Themeli A., Lo Presti D., Marsac P., Pouget S., Hammoum F., Chailleux E., Airey G. D., Evaluation of bio-materials' rejuvenating effect on binders for high-reclaimed asphalt content mixtures, *Materiales de Construcción*, **2017**, 67, 1-11

[4] Zaumanis M., Mallick R., Frank R., 100% recycled hot mix asphalt: A review and analysis, *Resour. Conserv. Recycl.*, **2014**, 92, 230-245

[5] Walters R. C., Fini E. H., Abu-Lebdeh T., Enhancing asphalt rheological behaviour and aging susceptibility using bio-char and nano-clay, *American Journal of Engineering & Applied Sciences*, **2014**, 7(1), 66-76

[6] Ingrassia L. P., Lu X., Ferrotti G., Canestrari F., Renewable materials in bituminous binders and mixtures: Speculative pretext or reliable opportunity?, *Resour. Conserv. Recycl.*, **2019**, 144, 209-222

[7] Raouf M. A., Williams R. C., Temperature Susceptibility of Non-petroleum Binders Derived from Bio-oils. In The 7th Asia Pacific Conference on Transportation and the Environment, **2010**, Semarang, Indonesia

[8] Airey G. D., "Rheological and fracture characterization of sustainable bio-binders and rejuvenators for virgin and recycled asphalt mixtures". Proceedings of the 1st Winter School 'Advanced in Sustainable Asphalt Pavements', **2017**, Modena, Italy

[9] Yang X., You X., Dai Q., Performance evaluation of asphalt binder modified by bio-oil generated from waste wood resources, *International Journal of Pavement Research and Technology*, **2013**, 6(4), 431-439
[10] Airey G. D., Mohammed M. H., Rheological properties of polyacrylates used as synthetic road binders, *Rheologica Acta*, **2008**, 47, 751-763
[11] Shields J., Adhesives Handbook, 2nd ed, Butterworth-Heinemann, London, **1976**
[12] Tan C. P., Che Man Y. B., Comparative differential scanning calorimetric analysis of vegetable oils: Effects of heating rate variation, *Phytochemical Analysis*, **2002**, 13, 129-141
[12] Abd Eltawab Abd El-latief R., Asphalt Modified with Biomaterials as Eco-Friendly and Sustainable Modifiers, http://dx.doi.org/10.5772/intechopen.76832
[13] Fini E. H, Kalberer E. W., Shahbazi A., Basti M., You Z., Ozer H., Aurangzeb Q., Chemical characterization of bio-binder from swine manure: Sustainable modifier for asphalt binder, *Journal of Materials in Civil Engineering*, **2011**, 23(11), 1506-1513
[16] Yang Y., Zhang Y., Omairey E., Cai J., Gu F., Bridgwater A. V., Intermediate pyrolysis of organic fraction of municipal solid waste and rheological study of the pyrolysis oil for potential use as bio-bitumen, *Journal of Cleaner Production*, **2018**, 187, 390-399
[17] Caputo, P.; Porto, M.; Loise, V.; Teltayev, B.; Rossi, C.O. Analysis of mechanical performance of bitumen modified with waste plastic and rubber (SBR) additives by rheology and PGSE NMR experiments. *Eurasian Chem. Technol. J.*, **2019**, 21, 235–239.
[18] Adedeji, A.; Grunfelder, T.; Bates, F.S.; Macosko, C.W. Asphalt Modified by SBS Triblock Copolymer: Structures and Properties. *Polym. Eng. Sci.*, **1996**, 36, 1707–1723.
[19] Cui, S.; Blackman, B.R.K.; Kinloch, A.J.; Taylor, A.C. Durability of asphalt mixtures: Effect of aggregate type and adhesion promoters International. *J. Adhes. Adhes.*, **2014**, 54, 100–111.
[20] Rossi, C.O.; Caputo, P.; Baldino, N.; Szerb, E.I.I.; Teltayev, B. Quantitative evaluation of organosilane-based adhesion promoter effect on bitumen-aggregate bond by contact angle test. *Int. J. Adhes. Adhes.*, **2017**, 72, 117–122.
[21] Porto, M.; Caputo, P.; Loise, V.; de Filpo, G.; Rossi, C.O.; Calandra, P. Polysaccharides-Reinforced Bitumens: Specificities and Universality of Rheological Behavior. *Appl. Sci.*, **2019**, 9, 5564
[22] Gui-juan, Z.; Ping, G.Workability of Sasobit Warm Mixture Asphalt. *Energy Procedia*, **2012**, 16, 1230–1236.
[23] Caputo, P.; Abe, A.A.; Loise, V.; Porto, M.; Calandra, P.; Angelico, R.; Rossi, C.O. The role of additives in warm mix asphalt technology: An insight into their mechanisms of improving an emerging technology. *Nanomaterials*, **2020**, 10, 1202.
[24] El-latief, R.A.E.A. Asphalt Modified with Biomaterials as Eco-Friendly and Sustainable Modifiers; *IntechOpen*, **2018**.
[25] Verma, T.; Chauhan, H. Replacement of Bitumen with Pine Resin a Project Report; Jaypee University of Information Technology: Waknaghat, Solan—173234, Himachal Pradesh, India, **2019**
[26] De Souza, A.G.; Kano, F.S.; Bonvent, J.; Rosa, D.S. Cellulose Nanostructures Obtained from Waste Paper

Industry: A Comparison of Acid and Mechanical Isolation Methods. *Mater. Res.*, **2017**, 20 (Suppl. S2), 209–214.

[27] EN 12697-17. Bituminous Mixtures—Test Methods—Part 17: Particle Loss of Porous Asphalt Specimens; British Standards Institution: London, UK, **2017**.

[28] EN 12697-31. Bituminous Mixtures. Test Methods. Specimen Preparation by Gyratory Compactor; British Standards Institution: London, UK, **2019**.

[29] UNI EN 12697-26. Bituminous Mixtures—Test Methods—Part 26: Stiffness; British Standards Institution: London, UK, **2018**.

[30] UNI EN 12697-23. Bituminous Mixtures—Test Methods—Part 23: Determination of the Indirect Tensile Strength of Bituminous Specimens; British Standards Institution: London, UK, **2018**

[31] EN 12697-12. Bituminous Mixtures—Test Methods—Part 12: Determination of the Water Sensitivity of Bituminous Specimens; British Standards Institution: London, UK, **2020**.

molecules

MDPI

*Article*

# Preliminary Study on New Alternative Binders through Re-Refined Engine Oil Bottoms (REOBs) and Industrial By-Product Additives

**Michele Porto [1], Paolino Caputo [1,*], Valeria Loise [1,*], Abraham A. Abe [1], Giulia Tarsi [2], Cesare Sangiorgi [2], Francesco Gallo [3] and Cesare Oliviero Rossi [1]**

[1] Department of Chemistry and Chemical Technologies, University of Calabria, Via P. Bucci, Cubo 14/D, 87036 Rende, Italy; michele.porto@unical.it (M.P.); abraham.abe@unical.it (A.A.A.); cesare.oliviero@unical.it (C.O.R.)
[2] Department of Civil, Chemical, Environmental and Materials Engineering, Viale del Risorgimento 2, 40136 Bologna, Italy; giulia.tarsi2@unibo.it (G.T.); cesare.sangiorgi4@unibo.it (C.S.)
[3] Itelyum Regeneration Srl, Via Tavernelle 19, Pieve Fissiraga, 26900 Lodi, Italy; francesco.gallo@itelyum.it
* Correspondence: paolino.caputo@unical.it (P.C.); valeria.loise@unical.it (V.L.); Tel.: +39-0984-492033 (P.C.); +39-0984-492045 (V.L.)

**Abstract:** Recent studies have worked towards addressing environmental issues such as global warming and greenhouse gas emissions due to the increasing awareness of the depletion of natural resources. The asphalt industry is seeking to implement measures to reduce its carbon footprint and to promote sustainable operations. The reuse of several wastes and by-products is an example of a more eco-friendly activity that fulfils the circular economy principle. Among all possible solutions, the road pavement sector encourages, on one hand, the use of recycled materials as a partial replacement of the virgin lithic skeleton; on the other hand, it promotes the use of recycled materials to substituting for a portion of the petroleum bituminous binder. This study aims to use Re-refined Engine Oil Bottoms (REOBs) as a main substitute and additives from various industrial by-products as a full replacement for virgin bitumen, producing high-performing alternative binders. The REOBs have been improved by utilizing additives in an attempt to improve their specific properties and thus to bridge the gap between REOBs and traditional bituminous binders. An even larger amount of virgin and non-renewable resources can be saved using these new potential alternative binders together with the RAP aggregates. Thus, the reduction in the use of virgin materials is applied at the binder and the asphalt mixture levels. Rheological, spectroscopic, thermogravimetric, and mechanical analysis were used to characterize the properties, composition, and characteristics of the REOBs, REOB-modified binders, and asphalt mixes. Thanks to the rheological investigations of possible alternative binders, 18 blends were selected, since they behaved like an SBS-modified bitumen, and then they were used for producing the corresponding asphalt mixtures. The preliminary mechanical analysis of the asphalt mixtures shows that six mixes have promising responses in terms of stiffness, tensile resistance, and water susceptibility. Nevertheless, the high variability of recycled materials and by-products has to be taken into consideration during the definition of alternative binders and recycled asphalt mixtures. In fact, this study highlights the crucial effects of the chemical composition of the constituents and their compatibility on the behaviour of the final product. This preliminary study represents a first attempt to define alternative binders, which can be used in combination with recycled aggregates for producing more sustainable road materials. However, further analysis is necessary in order to assess the durability and the ageing tendency of the materials.

**Keywords:** circular economy; waste materials; REOB; alternative binders; asphalt mixture

check for updates

**Citation:** Porto, M.; Caputo, P.; Loise, V.; Abe, A.A.; Tarsi, G.; Sangiorgi, C.; Gallo, F.; Oliviero Rossi, C. Preliminary Study on New Alternative Binders through Re-Refined Engine Oil Bottoms (REOBs) and Industrial By-Product Additives. *Molecules* **2021**, *26*, 7269. https://doi.org/10.3390/molecules26237269

Academic Editor: Antonio Zuorro

Received: 28 October 2021
Accepted: 26 November 2021
Published: 30 November 2021

**Publisher's Note:** MDPI stays neutral with regard to jurisdictional claims in published maps and institutional affiliations.

**Copyright:** © 2021 by the authors. Licensee MDPI, Basel, Switzerland. This article is an open access article distributed under the terms and conditions of the Creative Commons Attribution (CC BY) license (https://creativecommons.org/licenses/by/4.0/).

## 1. Introduction

An ever-increasing pressure for resources conservation and environmental protection—e.g., $CO_2$ reduction [1]—has led to a systemic change in the use and recovery

of resources towards a clear transition to a regenerative circular economy [2,3]. This has been done by creating a closed-loop system, minimizing the use of resource inputs and the creation of wastes, pollution, and carbon emissions [3]. New potential pathways in innovation and investment, reducing wastes and promoting the continual use of resources, have therefore been proposed [4,5]. Considering this aspect, waste ceases to be waste and acquires the status of End of Waste product (EoW). The End of Waste (EoW) criteria include recovery and treatment processes under which waste could be converted in a new potential product. In particular, according to the European standards [6], the main requirements to satisfy the EoW criteria for a given waste (possibly treated by industrial processes) are: (a) the substance or object is intended to be used for specific purposes; (b) there is a market or demand for this substance or object; (c) the substance or object meets the technical requirements for the specific purposes and complies with the existing legislation and standards applicable to the products; (d) the use of the substance or object will not lead to overall negative impacts on the environment or human health (in accordance with the Substance of Very High Concern (SVHC) list [7]).

From this perspective, the reuse of re-refined exhausted oils from vehicles and industrial hydraulic applications [4,5] that have become unfit for the use for which they were originally intended completely fulfils circular economy goals. In the view of a circular economy and considering the opportunity to reduce as much as possible the extraction of crude oil, a study has been started between universities and industries [8–11] that aims to produce new potential alternative binders (or eco-binders) by using recycled materials and/or by-products. In detail, the present research used Re-refined Engine Oil Bottoms (REOBs) to obtain suitable petroleum-based binders, enhancing the properties of these by-products, which are mainly used as bitumen-like product or bituminous membrane additive. The physical properties of the REOBs were enhanced by using a set of synthetic and/or natural additives such as powdered rubber from End-of-Life Tyres (ELTs) or other waste polymers [12], cellulose from waste paper or from olive pomace wastes, other suitable wastes or industrial by-products, and cheap chemical products. The incorporation of additives into REOBs aims to create alternative binders that could be used for producing asphalt concretes whose mechanical properties satisfy the technical requirements. Moreover, Reclaimed Asphalt Pavement (RAP) aggregates were used to obtain the asphalt concrete samples that underwent testing in order to study their behaviour with the goal of substituting the virgin aggregates, which are commonly employed in asphalt pavement. This would allow for meeting the standards of many European countries where RAP is already re-introduced in Hot Mix Asphalt (HMA) and Warm Mix Asphalt (WMA) mixes in the range of 70–90% by the total weight of available RAP material [13]. In Italy, an average RAP content of 20–30%wt. is usually introduced in WMA and HMA mixes, alternatively [13,14]. The aged and more brittle bituminous binder that coats the recycled aggregates limits the use of RAP material, as it stiffens the final asphalt mixtures, making the pavements more brittle and sometimes more prone to cracking, especially at low temperatures. To overcome this problem, a rejuvenating agent could be used [15,16].

Every year, the European Union (EU) produces around 15 million tons of bitumen [17]. Most of this amount is mixed with aggregates to create asphalt concrete for roads paving. Approximately 90% of all paved roads are surfaced with bituminous materials. Annually, the EU produces more than 200 million tons of bituminous materials for maintenance operations on the existing asphalt pavements and for paving new transportation infrastructure [18]. However, the bitumen used and the virgin aggregates are non-renewable resources. This has led researchers to look for alternative binders (or eco-binders) to reduce the consumption of petroleum bitumen and for recycled aggregates to substitute the virgin ones in the asphalt mixture skeleton. On one hand, the employment of recycled aggregates is becoming a consolidated practice in the production of asphalt concretes, especially in terms of RAP material as previously mentioned, and the use of recycled asphalt mixture with high or very high content of RAP is becoming feasible [19,20]. On the other hand, the partial substitution of neat bitumen with recycled materials and/or by-products is

still a challenge. The possible substitutes for neat bitumen can either come from recycled materials from non-renewable resources such as REOBs or come from renewable resources such as wood or vegetable waste oils. The bituminous binders that partially consist of the latter products are referred as bio-binders [21,22], which are an eco-friendly alternative to bitumen obtained from non-petroleum-based renewable resources. The chemical composition of the majority of these alternative binders is similar to that of a traditional bitumen, which includes resins, saturates, aromatics, and asphaltenes [23]. Regardless of the origin of the bitumen substitutes, i.e., renewable or non-renewable resources, the waste and/or recycled products can partially replace neat bitumen. In general, substitutes can be introduced in neat bitumen in four different ways based on the type and quantity of waste materials and/or by-products used, and they are referred to as [24]: (a) Bitumen modifier (<10%wt.); (b) Bitumen fluxes (7–15%wt.); (c) Bitumen extender (25–75%wt.); (d) Alternative binders (>75%wt.). Currently, the bitumen modifiers, fluxes, and extenders are the most-used solutions to add waste materials and/or by-products to bituminous binders for the production of asphalt mixtures. Nonetheless, the use of alternative binders to partially and/or completely replace the bitumen in new asphalt formulations is the final goal of the current research inspired by the circular economy concept. Up to date, several different alternative binders have been studied, including engine oil residue, soybean oil, palm oil, fossil fuel, swine waste, and materials from pyrolysis [25]. Different vegetable oils have been investigated in recent times to determine their physical and chemical properties and to evaluate their applicability as bio-binders in the pavement industry [26–28]. Bio-oils are produced from plant matter and residues, such as municipal wastes, agricultural crops, and by-products from agriculture and forestry. Other biomass sources include molasses, rice, sugar, potato starches, corn, gum resins and natural tree resins, vegetable oils, natural latex rubber, cellulose, lignin, palm oil waste, peanut oil waste, coconut waste, potato starch, canola oil waste, dried sewerage effluent, and others [29]. Rauf and Williams [23] have conducted a study about bio-oils. They have produced different bio-oils from different sources, i.e., oakwood, switch grass, and corn stover, which exhibited similar behaviour to neat bitumen. Fini et al. [30] produced bio-oil from swine manure and used it as a partial replacement of bitumen. This recycled product was a promising candidate for partial replacement for standard bitumen. In particular, this bio-binder would improve the low-temperature properties of a petroleum-based binder while reducing asphalt pavement construction costs. A Dutch study tested asphalt roads and cycle paths paved with a bitumen-like product made from the natural binder lignin [31]. Lignin is a structural polymer in plants and trees that is released as a waste product from a number of industrial processes. The used lignin came from various sources including different types of paper pulp production and a bio-refinery that produces cellulosic ethanol from straw. On the demonstration roads, the material appeared to be performing in a similar way to a standard bitumen, and a slight noise reduction was observed. In 2018, Yang et al. developed a process to break down the organic parts of household waste, e.g., food waste, plastic, paper, and textiles, to produce a sticky, gloopy black liquid that is very similar to bitumen [32]. The bio-bitumen was produced by pyrolysis. By changing the processing parameters, such as temperature, processing time, and product collection strategy, the research team was able to alter the characteristics and quantities of the final bitumen-like substance. In conclusion, this preliminary study on alternative binders tried to fulfil circular economy goals by identifying suitable additives, coming from recycled materials and industrial by-products, in order to modify REOBs and to achieve the minimum rheo-mechanical performance required for bituminous binders and mixtures. Thus, the new alternative binders underwent rheological and mechanical analysis to measure some of the parameters required for road construction materials. Nevertheless, beyond this preliminary research, additional investigations are needed in order to fully characterize the rheo-mechanical performances and durability of the binders and the corresponding asphalt mix.

## 2. Materials

Various recycled materials and/or by-products were used to define alternative binders intended to fully replace neat bitumen for the production of more sustainable asphalt mixtures. The main constituents of alternative binders are REOBs that have been modified by specific additives to obtain a material similar to the standard bitumen.

### *2.1. REOBs*

Two different REOBs were supplied by Itelyum Regeneration s.r.l, Lodi (LO), Italy. The by-products were produced in two distinct refinery plants of the same company and are marketed as Viscoflex 1000® (V1) and Viscoflex 2000® (V2TQ). The by-product V2 is usually fluxed with low molecular weight oils—in a quantity equal to 20 or 30%wt.—to facilitate materials handling. In particular, the fluxed REOB with 20%wt. and 30%wt. of the low molecular oil are referred to hereafter as V2F (F stands for fluid) and V2D (D stands for dense), respectively. The two petroleum-based by-products are viscous liquids at room temperature and are obtained by different processes. The V1 is the heavier fraction, obtained in a distillation column working at 365 °C and 15 mmHg; while the V2 is obtained through a propane de-asphalting process. Table 1 reports the main physico-chemical characteristics of both products.

**Table 1.** Main physical and chemical characteristics of V1 and V2F.

| Property | Standard | Results | |
|---|---|---|---|
| | | **V1** | **V2F** |
| Needle Penetration Test | EN 1462 | / | >500 (0.1 mm) |
| Softening Point | UNI EN 1427 | / | <4 °C |
| Density at 15 °C | ASTM D70 | 1003 kg/m$^3$ | 0.975 kg/m$^3$ |
| Kinematic Viscosity at 100 °C | ISO 3104 | Not determinable | 580 mm$^2$/s |
| Kinematic Viscosity at 135 °C | ISO 3104 | 110.0 mm$^2$/s | / |
| Dynamic Viscosity at 60 °C | EN 13702 | 25.13 Pa s | 0.380 Pa s |
| Pour Point | ASTM D97 | >50 °C | / |
| Insoluble Matter | ASTM D 2042 | 14% *w*/*w* | / |
| Soluble Matter | ASTM D 2042 | 86.10% *w*/*w* | / |
| Water Content | ASTM D6304 (Procedure C) | 290 mg/kg | / |
| Sulphur | ISO 8754 | 1.13% *w*/*w* | / |
| Nitrogen Content | ASTM D3228 | 0.32% *w*/*w* | / |
| Gasoline Fuel | ASTM D3525 | <0.01% *w*/*w* | / |
| Gasoline Diluent | ASTM D322 | <0.1% *v*/*v* | / |
| Diesel Fuel | ASTM D3524 | <0.1% *w*/*w* | / |
| Ash | ASTM D482 | 8.089% *w*/*w* | / |
| Conradson Carbon Residue | ASTM D189 | 19.2% *w*/*w* | / |
| TSE Remark | ISO 10307-1 | Filtration Time exceeds 25 min | / |
| Saturates | IP 469 | 32.9% *w*/*w* | 37.0% *w*/*w* |
| Aromatics | | 0% *w*/*w* | 1.6% *w*/*w* |
| Polars (I) | | 19.6% *w*/*w* | 18.1% *w*/*w* |
| Polars (II) | | 47.5% *w*/*w* | 43.3% *w*/*w* |

**Table 1.** *Cont.*

| Property | Standard | Results | |
|---|---|---|---|
| | | V1 | V2F |
| Asphaltene | IP 143 | 16.6% *w*/*w* | 3.7% *w*/*w* |
| Pensky–Martens Flash Point (Closed Cup) Procedure B | ASTM D93/IP34/EN ISO 2719 | 270 °C | / |
| Cleveland Flash Point (Open Cup) | ASTM D92/EN ISO 2592 | 284 °C | 180 °C |
| PCB Content | EN 12766-3 | <4 mg /kg | / |
| PCT | EN 12766-3 | <10 mg /kg | / |

With the aim of replacing neat bitumen mainly with REOBs, the two available REOBs were preliminarily characterized by the use of spectroscopic analysis in order to identify the possible similarities of these materials with a standard 50/70 penetration grade bitumen (Pen 50/70). The Pen 50/70 was considered as the reference bituminous binder throughout the present study. The REOBs were firstly characterized through high-resolution 1H-NMR spectroscopy. In Figure 1, the 1H-NMR spectra of (a) Pen 50/70, (b) V2TQ, (c) V1, (d) V2D, and (e) V2F are reported. As can be seen from Figure 1, all samples are characterized by a rich aliphatic part (0.8 to 2.5 ppm). The areas under the curves for the aliphatic part are of the same order of magnitude for the 50/70 reference bitumen as well as for all REOBs samples. From this point of view, it can be said that REOBs and classic bitumen are very similar., On the other hand, it can be seen from the integral of the aromatic region that the various REOBs have a total aromatic content (asphaltene plus aromatic molecules) about one order of magnitude lower than Pen 50/70. This is in accordance with the results of the analysis shown in Table 1.

### *2.2. Additives*

The polymers were introduced in the composition of the alternative binders to improve the elastic response of the final formulations. The powdered rubber from ELTs was supplied by Ecopneus s.c.p.a. The product is a black powder with a maximum size dimension of about 42 µm. Moreover, the introduction of SBS polymer has been considered, since this elastomeric polymer is commonly used in the road sector for the production of modified bitumens. In this study, the amount of SBS used was limited to a maximum of 2% in order to reduce the production costs of the final blends. In addition, it is well-known that SBS polymers work well in combination with rubber from ELTs [12,33]. The SBS polymer was supplied by Kraton Polymers LLC. In order to improve the adhesion of REOBs to the lithic skeleton, an adhesion promoter (AP) has been employed, since it was proven to be effective [34,35]. To modulate the viscosity, various cellulose polysaccharides were used as viscosifier: P2, nano-fibrillated cellulose (CNF), and nanocrystalline cellulose (CNC) [36]. Additionally, to ensure a good workability of the asphalt mix at high temperatures, waxes with melting points of about 100 °C were used, which are commonly used for the production of WMA mixtures [37,38]. In particular, Sasobit waxes (Sb) were employed in this study. Some other issues observed during the blend preparation and analysis have been solved by the aid of other additives such as pine resins (PR) [29,39], which improve the cohesive properties of the REOBs; thickening agents such as Lithium salt (LiS) and nanotubes (Nt) have been used to take advantages of their gelling properties (widely employed in industrial grease production). The PR, AP, and P2 were supplied by Kimical s.r.l. The lithium salt (LiS) was supplied by Sigma Aldrich, while the nanotubes (Nt) were produced in laboratories of the University of Calabria. The nano-fibrillated cellulose (CNF) was supplied by Nanografi Co. Inc., while nano-crystalline cellulose (CNC) was obtained in the laboratories of the University of Calabria from waste papers following the methods

reported in the reference [40]. All the supplied products were used without any further treatment. The mean cost of the blends, considering the various additives' prices and percentages used in our blend preparation, is about 350–400 €/ton.

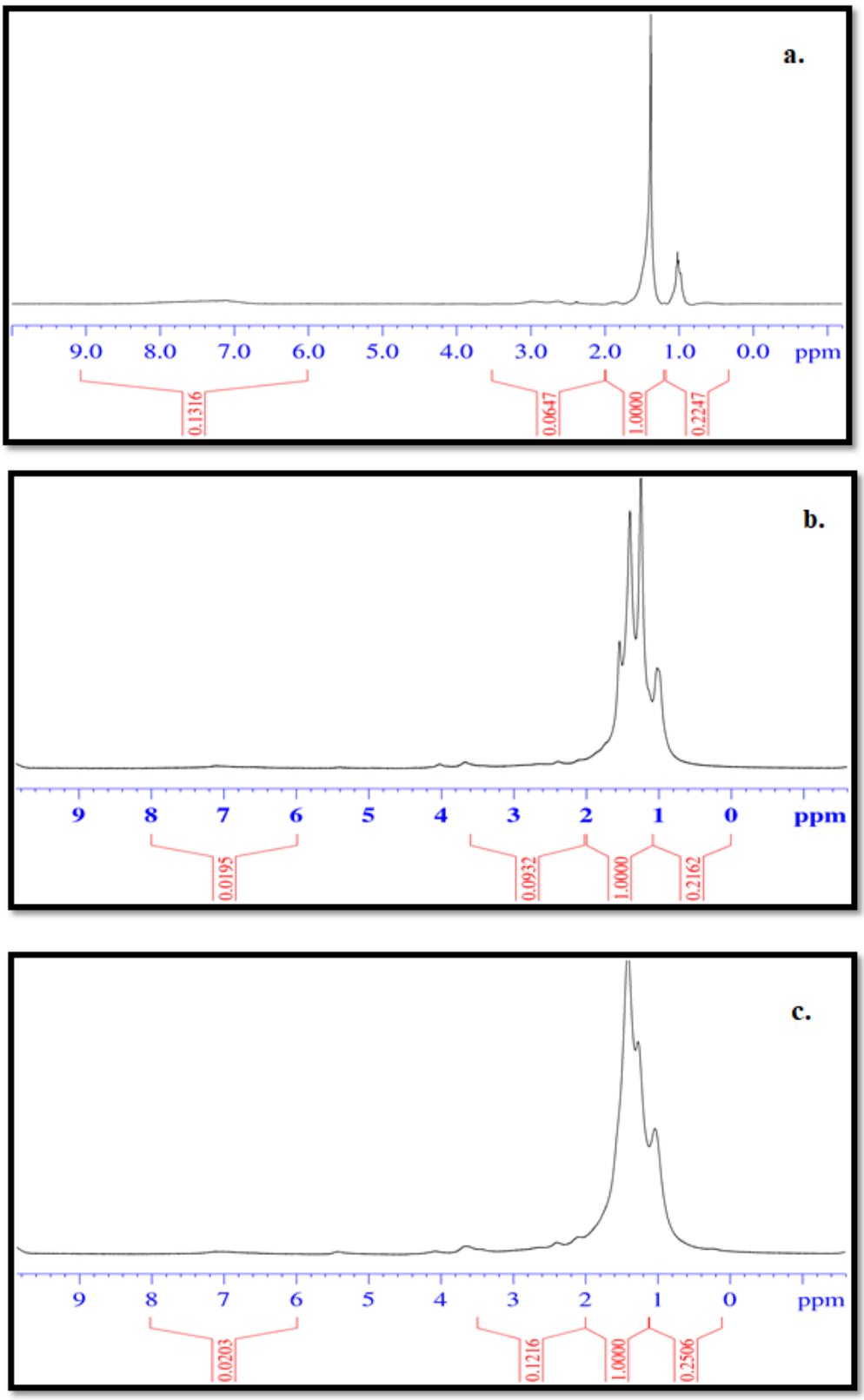


**Figure 1.** *Cont.*

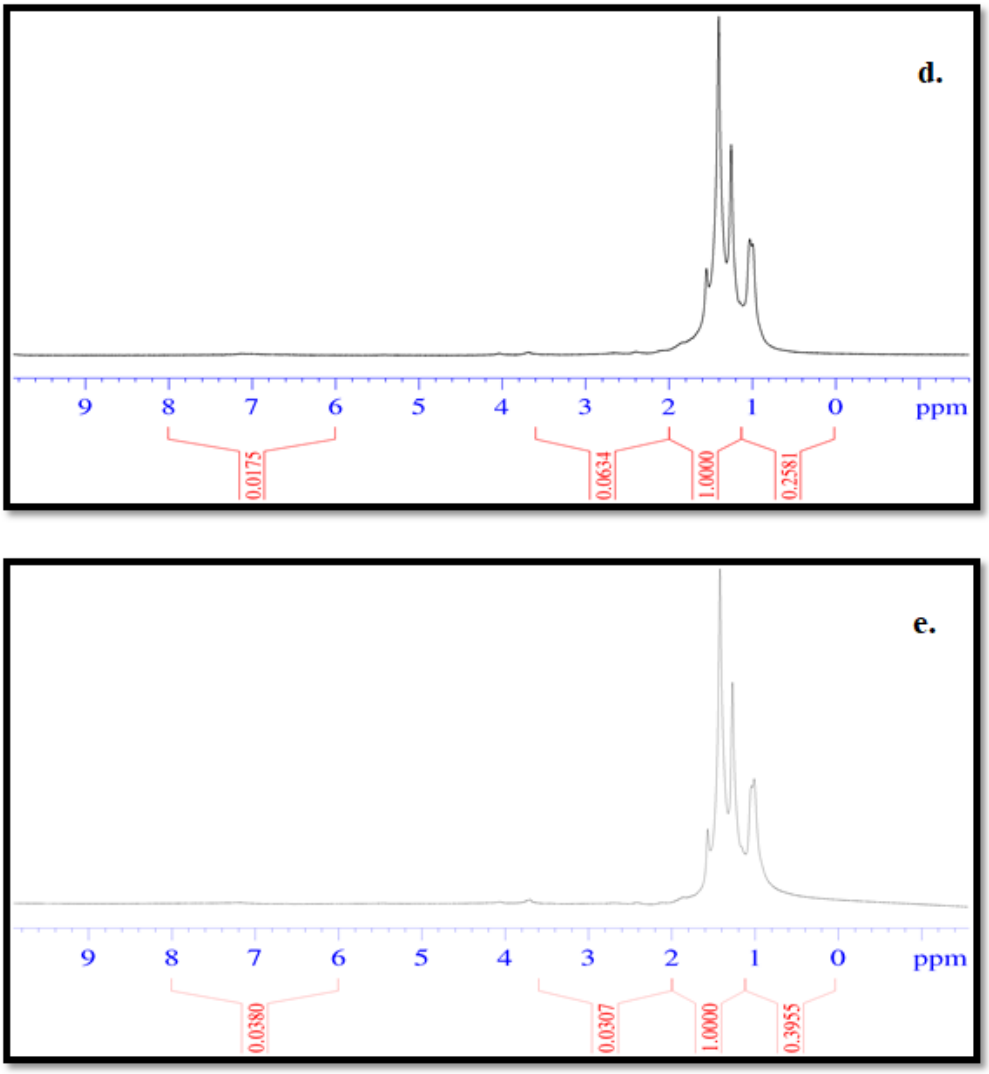


**Figure 1.** $^{1}$H-NMR spectra of (**a**) Pen 50/70 (**b**) V2TQ, (**c**) V1, (**d**) V2D, (**e**) V2F.

### *2.3. Alternative Binders*

The additives that were used allowed for the definition of final alternative binders similar to the traditional bitumen used for paving. In total, 18 alternative binders were defined and then characterized at the binder and the asphalt mixture levels, which are listed in Table 2. Each alternative binder description consists of all materials that were used in quantity greater than 0%. Hence, each line of Table 2 represents the recipe of one alternative binder.

Prior to samples preparation, the various additives underwent thermogravimetric analysis in order to check their stability at the high temperature, i.e., 160 °C. No additives showed considerable weight loss and, consequently, no additives degradation would occur during mixing process.

The preparation of alternative binders required the preliminary heating phase of each specific REOB (V1, V2TQ, V2F and V2D) at about 160 ± 5 °C. Then, the quantity of the chosen additives was gradually added to the warmed REOB (1 g/min). The additives were incorporated at room temperature. All constituents were mixed by means of high-shear mixer (IKA model) with an average speed of about 1400–1600 rpm. Each blend was mixed at 160 °C for 60 min to guarantee an essentially homogenous sample.

**Table 2.** Type and percentage of constituent materials of the 18 alternative binders.

| Blend | V1 | V2TQ | V2F | V2D | PFU | Sb | SBS | AP | P2 | CNC | CNF | PR | Nt | LiS |
|---|---|---|---|---|---|---|---|---|---|---|---|---|---|---|
| B23 CNC | - | - | 60 | - | 15 | 10 | - | 0.3 | - | 14.7 | - | - | - | - |
| B26 | - | - | 40 | - | 10 | 10 | - | - | 20 | - | - | 40 | - | - |
| B27 | - | - | 60 | - | 5 | 10 | - | - | 15 | - | - | 10 | - | - |
| B29 | - | - | 40 | - | 10 | 10 | - | - | - | - | - | 40 | - | - |
| B29V1 | 40 | - | - | - | 10 | 10 | - | - | - | - | - | 40 | - | - |
| B30 | - | - | 40 | - | - | 8 | - | - | 14.9 | - | - | 27 | 0.1 | 10 |
| B26D | - | - | - | 40 | 10 | 10 | - | - | 20 | - | - | 20 | - | - |
| B27D | - | - | - | 60 | 5 | 10 | - | - | 15 | - | - | 10 | - | - |
| B29D | - | - | - | 40 | 10 | 10 | - | - | - | - | - | 40 | - | - |
| B30D | - | - | - | 40 | - | 8 | - | - | 14.9 | - | - | 27 | 0.1 | 10 |
| B26-1 | - | - | 60 | - | 10 | 10 | 1 | 0.3 | 8.7 | - | - | 10 | - | - |
| B27-1 | - | - | 60 | - | 5 | 10 | 1 | 0.3 | 13.7 | - | - | 10 | - | - |
| B29-1 | - | - | 50 | - | 10 | 10 | 0.5 | 0.3 | - | - | - | 29.2 | - | - |
| B31 | - | - | 60 | - | 15 | 10 | 2 | 0.3 | 7.7 | - | - | 5 | - | - |
| B31V1 | 60 | - | - | - | 15 | 10 | 2 | 0.3 | 7.7 | - | - | 5 | - | - |
| B32 | - | - | 60 | - | 15 | 5 | - | 0.3 | - | - | 14.7 | 5 | - | - |
| B32V1 | 60 | - | - | - | 15 | 5 | - | 0.3 | - | - | 14.7 | 5 | - | - |
| B33TQ | - | 60 | - | - | 19.7 | 13 | 2 | 0.3 | - | - | - | 5 | - | - |

### *2.4. Asphalt Mixtures*

The asphalt mixes with the alternative binders were produced using RAP aggregates only. The recycled aggregates consisted of milled asphalt concrete from existing pavements of highways. The grading distribution and the binder content were designed in order to produce a traditional wearing course asphalt mixture. The grading distribution of the RAP aggregates met the Italian technical specifications. Based on the aged bituminous binder content already present in the recycled aggregates and on previous studies based on Cantabro test (EN 12697-17) [41], the optimum binder content was selected as equal to 2.5% of the total weight of aggregates. The innovative asphalt mixtures were compared with samples of a traditional wearing course layer made of 90% virgin aggregates and 10% RAP and Pen 50/70, which was considered as a reference mix, and a mix consisting of 100% RAP aggregate and Pen 50/70. Moreover, the limits of the Italian technical specifications for wearing course layers were considered as reference for comparisons.

All alternative binders were used for producing 18 different asphalt mixtures. Per each asphalt concrete mix, three samples were manufactured. The cylindrical samples had diameter of 100 mm and were 55 mm tall, approximately. The correct amount of recycled aggregates and the alternative binders were preliminarily heated in an air-forced oven before being mixed and compacted. Per each asphalt mix, 3000 g of RAP aggregates were heated at 150 °C for 2 h and 75 g of the prepared blends (i.e., 2.5%wt.) at 150 °C for a minimum of 1 h. The samples underwent compaction by means of a gyratory compactor applying 100 gyrations at 600 kPa [42].

## 3. Test Methods

In order to preliminarily assess the feasibility of using alternative binders for road construction materials, the 18 new binders underwent rheological analysis. Then, the mechanical response of all asphalt mixtures, those containing an alternative binder and the reference mixes, were investigated. Since these were binders without bitumen as the main

constituent, the basic tests were planned with the aim of assessing a possible relationship, if any, between the behaviour of binders and that of mixtures as they exist for traditional bituminous materials.

### *3.1. Rheological Measurements*

A dynamic shear rheometer (SR5000, Rheometric Scientific, Piscataway, NY, USA) was used to perform the rheological tests on the various alternative binders. The controlled shear stress rheometer was used in a plate–plate configuration. Plate tools of $\phi$ = 25 mm diameter were used for testing in the temperature range of 25–120 °C. The gap was set equal to 2 mm. A Peltier system (±0.1 °C) controlled the test temperature. The rheological responses of Pen 50/70 and alternative binders were determined under the kinematics of both steady and oscillatory simple shears. In steady-shear experiments, the viscosity of blend samples was determined from the ratio of measured shear stress to applied shear rate, as a function of shear rate that varied from 1 to 100 $s^{-1}$. Steady states were previously checked by transient experiments (step-rate test). For all samples, it was observed that 10 s was a sufficient scanning time to ensure the steady-state condition. All samples showed a Newtonian behaviour in the investigated shear rate range. Dynamic tests were carried out in conditions of linear viscoelastic (LVE) region, where measured material features do not depend on the amplitude of applied load and are related to materials microstructure only. With the aim of investigating the material viscoelastic phase transition, dynamic temperature ramp tests (DTRT) were performed both at 1 Hz and temperature rate of 1 °C/min from 25 °C to 120 °C by applying the proper stress values—previously determined by stress sweep tests—to guarantee linear viscoelastic conditions at all tested temperatures.

### *3.2. Mechanical Analysis*

The resulting 18 asphalt mixtures were subjected to dynamic and static mechanical characterizations. The asphalt concrete samples underwent mechanical tests after being cured for a minimum of 24 h. Dynamic tests were used to determine the Indirect Tensile Stiffness Modulus (ITSM) at 20 °C of all samples by using a servo-pneumatic testing machine. The ITSM values were determined according to EN 12697-26 standard [43], in the indirect tensile configuration (IT-CY). A pulse loading was applied with a 124 ms rise-time to generate a horizontal deformation of 5 ± 2 μm. Two static mechanical characterizations were used to measure the Indirect Tensile Strength (ITS) and the Indirect Tensile Strength Ratio (ITSR) of all mixes according to the EN 12697-23 [44] and EN 12697-12 [45] standards, respectively. The tensile resistance of asphalt concretes was determined by applying a compression load with a constant speed rate of 51 mm/min. The ITS test was performed at 25 °C. The latest characterization, i.e., the ITSR ratio, aimed to assess the durability of the wearing course samples, as it determines the effect of water conditioning. This investigation quantifies the ratio between the ITS values of an asphalt mix after water conditioning and those of dry specimen. According to standard method A, the samples were saturated while stored in a water bath at 40 °C for three days. Successively, the samples were removed, dried, and conditioned at 25 °C in a climate chamber to further undergo ITS testing. The two static characterizations applied a load until failure; hence, two samples were used to evaluate the average ITS values, while the third specimen of each asphalt mix was used to determine the corresponding ITSR value. Before being tested, all samples were kept in a climate chamber at the test temperature for at least 4 h.

## 4. Results and Discussion

### *4.1. Rheological Analysis*

Figure 2 shows the results of the DTRT obtained from the blends B26-1, B27-1, B29-1, and B32V1. Among all alternative binders, these four blends were selected because they exhibit good rheological and mechanical responses, as can be seen by comparing the DTRT of our blends with that of a 50/70 bitumen reported in Figure 3. The remaining

blends that were prepared show good rheological behaviour, but they do not behave as expected from a mechanical point of view (the DTRT of the other blends can be found in the Supplementary Information Figure S1). The DTRT of virgin REOBs (V2F, V1, V2D, V2TQ) are reported in Figure 3. Figures 2 and 3 shows that alternative binders strongly enhance the rheological properties of both REOBs and bitumen. Moreover, by comparing the DTRT of the alternative binders—even those reported in the Supplementary Information—with that of an SBS-modified bitumen (PmB) reported in Figure 4, it can be concluded that the alternative binders resemble the behaviour of a polymer-modified bitumen.

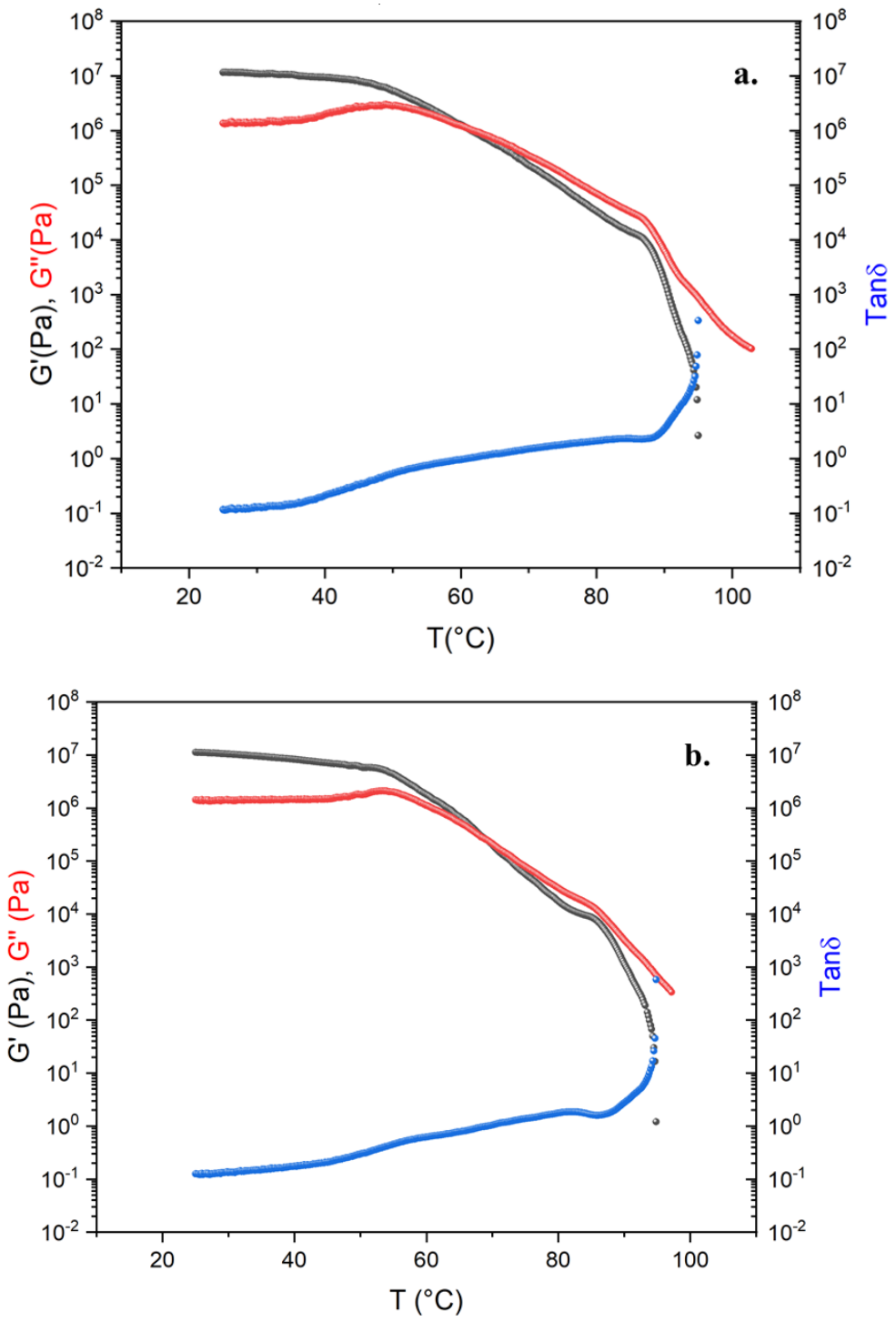


**Figure 2.** *Cont.*

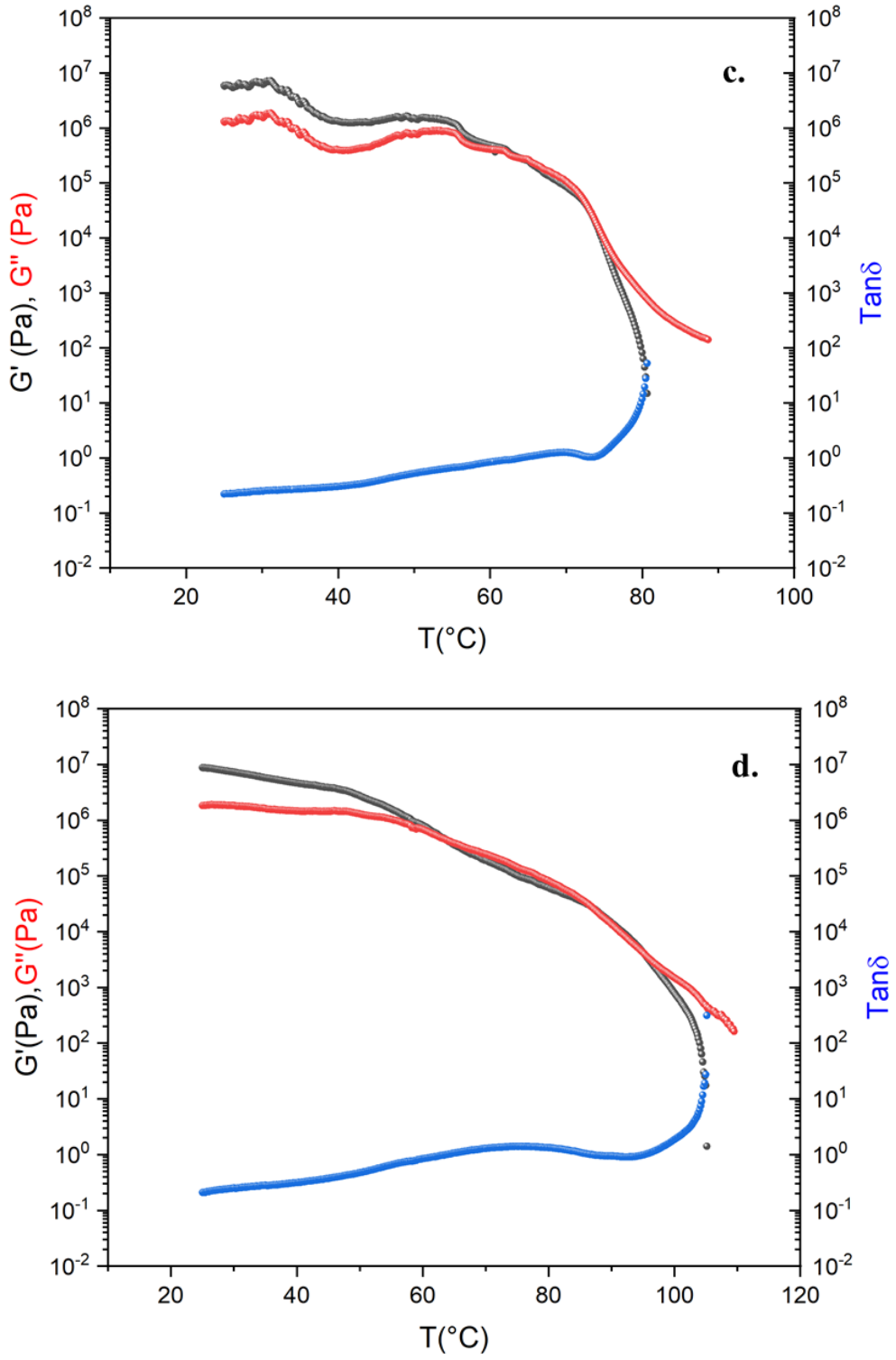


**Figure 2.** Dynamic Temperature Ramp Test (DTRT) of (**a**) blend 26-1, (**b**) blend 29-1, (**c**) blend 27-1, (**d**) blend 32V1.

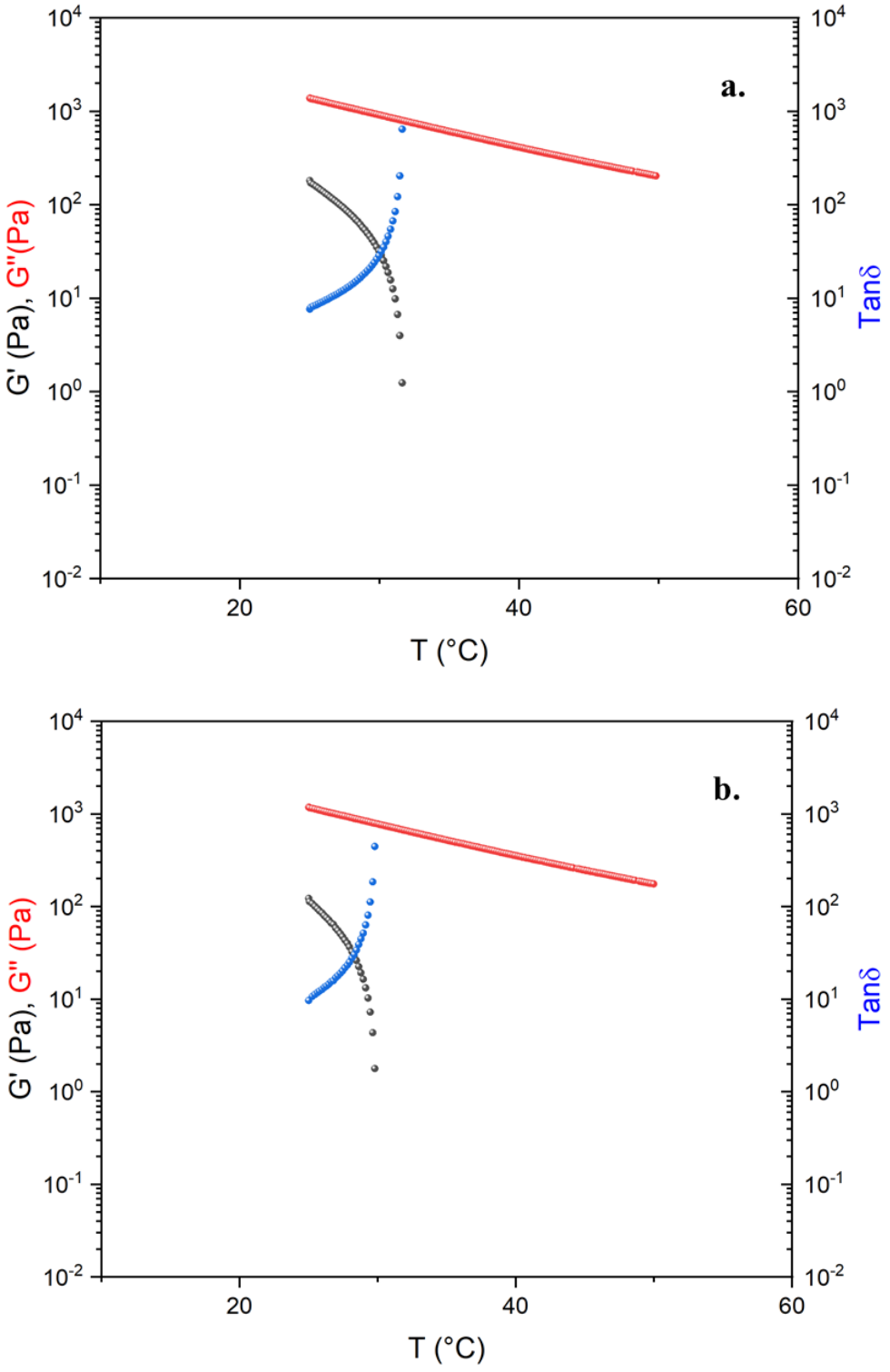


**Figure 3.** *Cont*.

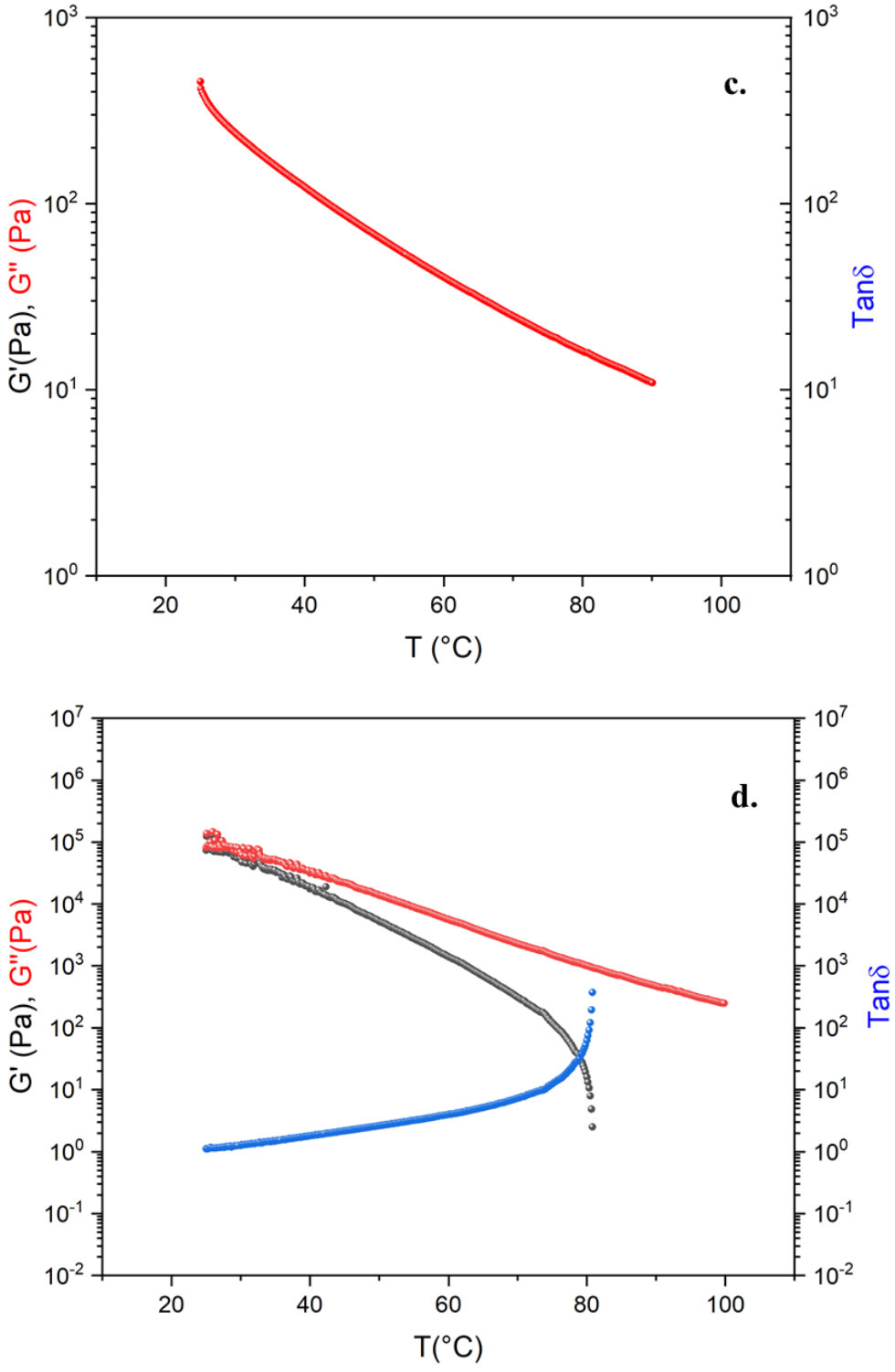


**Figure 3.** *Cont*.

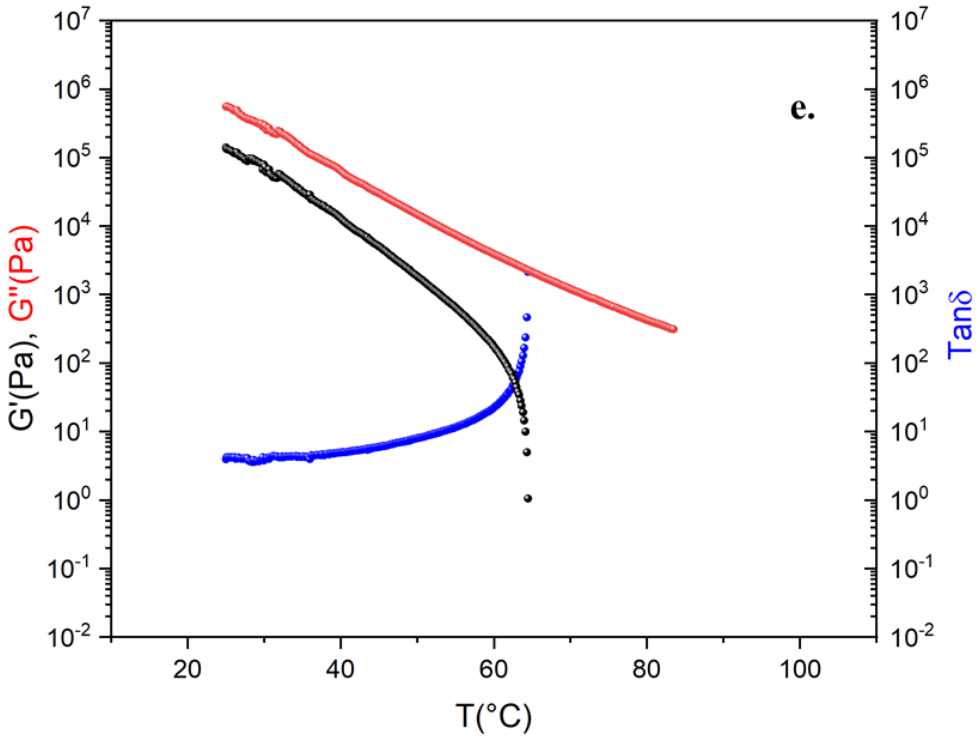


**Figure 3.** Dynamic Temperature Ramp Test of (**a**) V2F, (**b**) V2D, (**c**) V1, (**d**) V2TQ, (**e**) Pen 50/70.

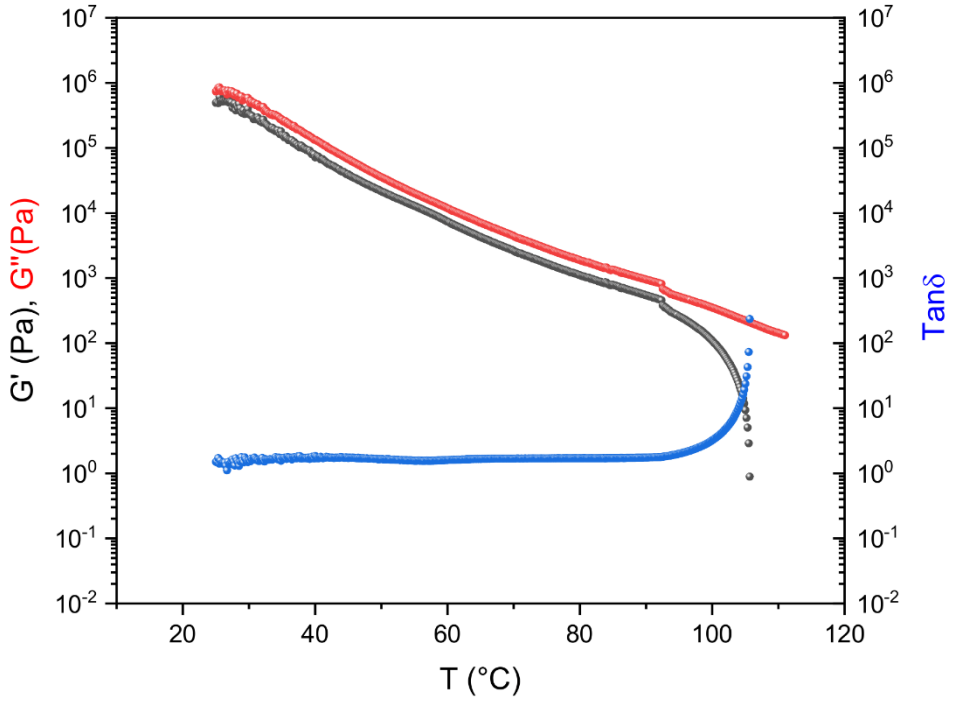


**Figure 4.** Dynamic Temperature Ramp Test of an SBS-modified bitumen (Pen 50/70 + 3% SBS).

### *4.2. Mechanical Analysis*

The dynamic mechanical characterization of the asphalt mixtures manufactured with the 18 alternative binders and Pen 50/70 is reported in Figure 5. The asphalt mixes exhibit high variability in the ITSM results, which can be ascribed to the constituent materials used. The mixture with B23CNC shows the lowest stiffness modulus, while the mixture containing B29D has the highest stiffness. In general, the asphalt mixes containing the V2D show higher stiffness than the corresponding asphalt concrete mixtures with V2F.

The higher presence of low-molecular-weight oil in the alternative binders lead to soften the final materials as expected. Hence, the type of REOB affects the final ITSM values. Additionally, the combination of specific additives permits alternatively increasing or decreasing the stiffness modulus of the corresponding asphalt mixture. In fact, the B33TQ mix has lower ITSM value than the B29D asphalt concrete. In general, the minimum ITSM values at 20 °C of a traditional wearing course layer made with virgin materials only are 3000 MPa and 3500 MPa for samples produced with unmodified and polymer-modified bitumens, respectively. Previous studies on the reference mix that contains 10% of RAP and Pen 50/70 have assessed an average ITSM value equal to 5500 MPa at 20 °C, which can be used for comparing the stiffness modulus of the innovative asphalt mixtures with the alternative binders. Among all tested asphalt materials, the mixtures manufactured with B26-1, B27, B27-1, B31, B31V1, B32, and B32V1 have similar stiffness to the reference mixture that mainly contains virgin materials. Most of the recycled asphalt mixtures with alternative binders have higher stiffness than the samples of the reference mix, which can be mainly related to the presence of RAP and to the addition of PR. In general, the use of recycled aggregates has been found to stiffen the final asphalt concretes; indeed, the mixture with 100% RAP and Pen 50/70 is stiffer than the reference one. The introduction of PR in the bituminous binders improve the cohesion properties, which turn in higher ITSM values. Indeed, the alternative binders with a high content of PR are very stiff. However, the use of asphalt mixtures with a very high stiffness is disadvantageous, as the resulting asphalt pavement may be more prone to fatigue and thermal cracking.

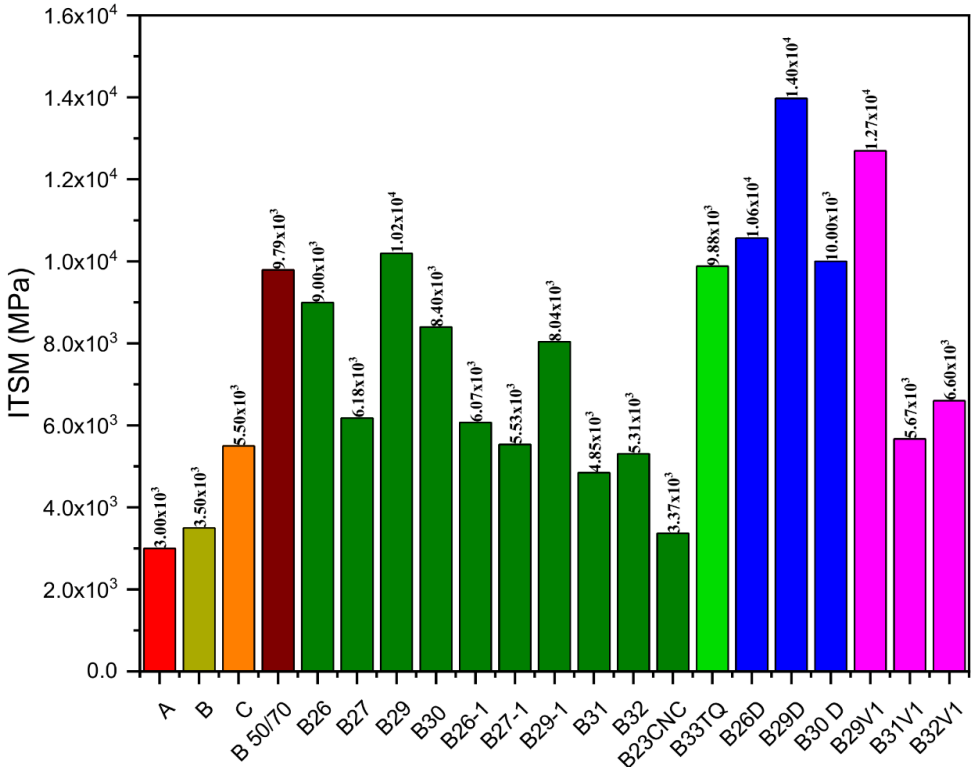


**Figure 5.** Results of the ITSM values at 20 °C for the recycled asphalt mixtures produced with 100% RAP and the alternative binders. Legend: Asphalt concrete with virgin bitumen and aggregates (A); Asphalt concrete with virgin polymer-modified bitumen and aggregates (B); Reference mix (C); 100% RAP asphalt concrete with Pen 50/70; 100% RAP asphalt concrete with alternative binders containing V2F; 100% RAP asphalt concrete with B33TQ; 100% RAP asphalt concrete with alternative binders containing V2D; 100% RAP asphalt concrete with alternative binders containing V1.

Figure 6 shows the indirect tensile resistance of the innovative asphalt mixtures produced with RAP and alternative binders. The Italian technical specifications require a minimum ITS value equal to 0.72 or 0.95 MPa for asphalt concrete with unmodified and polymer-modified bitumens, respectively. Almost all innovative mixtures meet the requirement; only the innovative mixtures with B23CNC, B27-1, and B29-1 show insufficient tensile resistance. The recycled mix with Pen 50/70 exhibits the highest tensile resistance. For bituminous materials, the tensile resistance and stiffness values are directly related to each other, and this correlation is also confirmed in the present study. The innovative asphalt mixes with the highest ITSM values exhibit the highest ITS results. However, the ITS values close to or higher than 2.0 MPa may reflect a very high stiffness, which may turn into brittle asphalt pavements. As a consequence, the Italian technical specifications limit the tensile resistance of the asphalt mixes, and the ITS values of the asphalt mixtures with neat and polymer-modified bitumen have to be lower than 1.60 and 1.90 MPa, respectively. In this regard, the samples manufactured with B26, B26D, B26-1, B27, B27-1, B29V1, B29-1, B30, B30D, B31, B32, and B32V1 meet the required specifications for mixtures with unmodified bituminous binders. These innovative mixes have a similar response to the reference mix with virgin materials, as their ITS values are equal to 1.2 MPa on average.

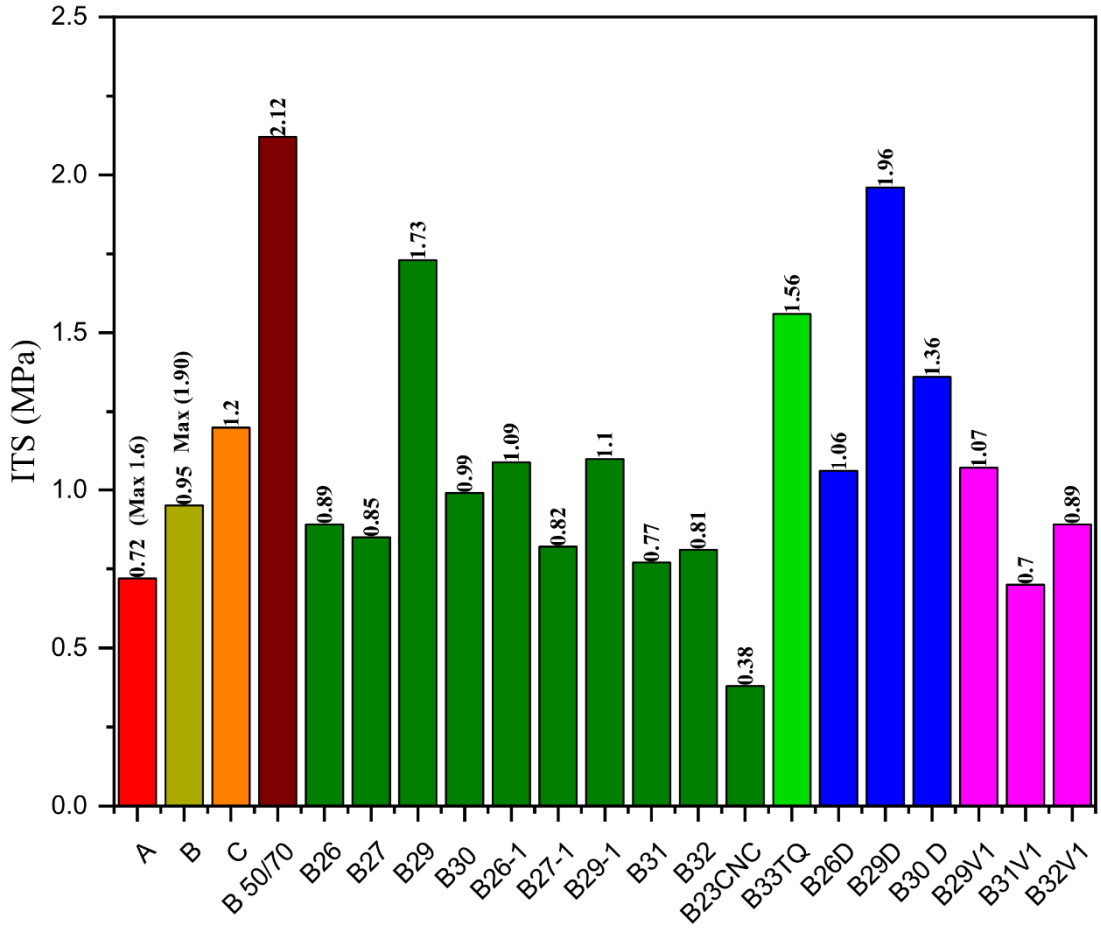


**Figure 6.** Results of the ITS values at 20 °C for the recycled asphalt mixtures produced with 100% RAP and the alternative binders. Legend: Asphalt concrete with virgin bitumen and aggregates (A); Asphalt concrete with virgin polymer-modified bitumen and aggregates (B); Reference mix (C); 100% RAP asphalt concrete with Pen 50/70; 100% RAP asphalt concrete with alternative binders containing V2F; 100% RAP asphalt concrete with B33TQ; 100% RAP asphalt concrete with alternative binders containing V2D; 100% RAP asphalt concrete with alternative binders containing V1.

The results of measuring the water susceptibility for the innovative asphalt mixtures are reported in Figure 7. The type of REOB significantly affect the resistance of asphalt

concrete, as the use of V1 decreases the water damage resistance of the mixes when compared to the corresponding mixtures with one of the V2s. The minimum ITSR value required by the Italian technical specifications is about 90% when unmodified bitumens are used. Among the innovative asphalt mixtures, almost all mixes that contain V2F (except for B26 and B23CNC) and the mixtures made with B33TQ, B29D, B30D, and B32V1 show good resistance against water damage, or they do not even show any water susceptibility, as the ITSR results are greater than 100%. This behaviour can be ascribed to the presence of a very high quantity of RAP aggregates. The abovementioned asphalt concrete mixes behave similarly to the reference mix mainly produced with virgin aggregates. On the other hand, the ITS value of the 100% RAP mix with Pen 50/70 is considerably reduced after water conditioning, and its ITSR ratio is about 89%.

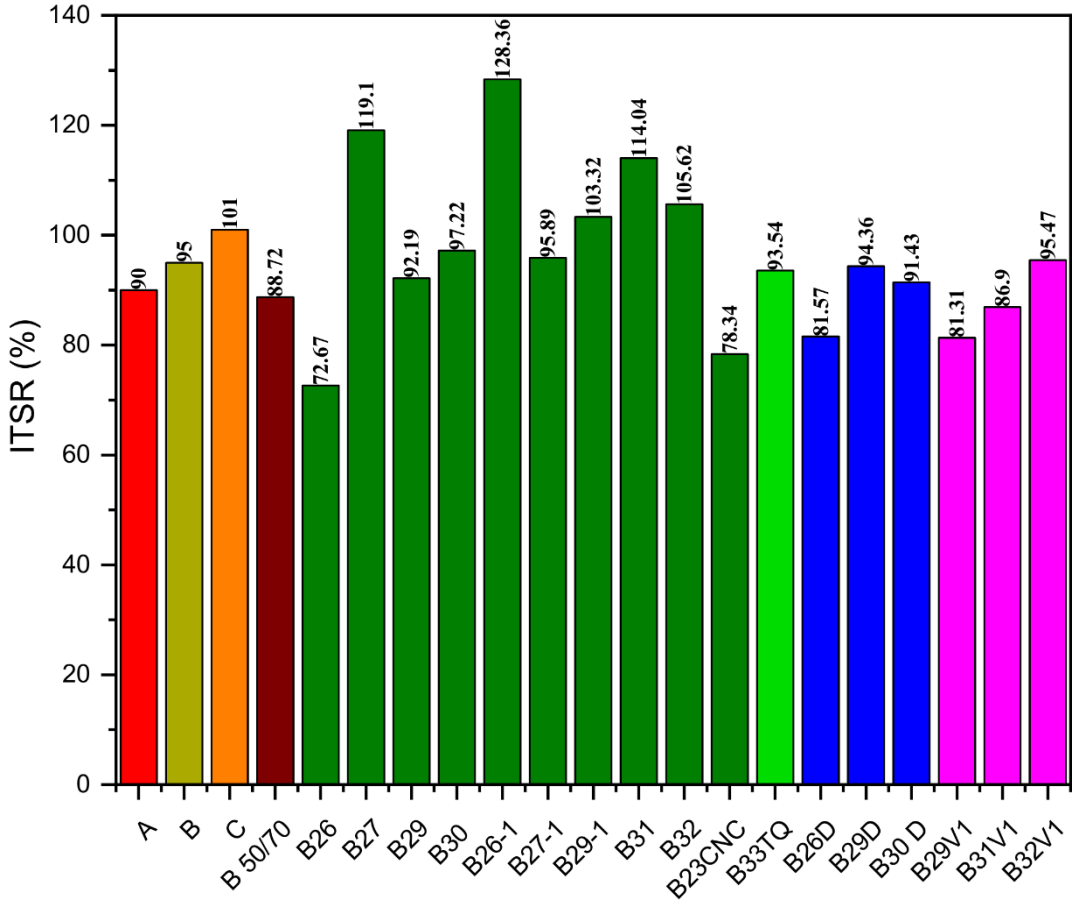


**Figure 7.** Results of the ITSR values at 20 °C of the recycled asphalt mixtures produced with 100% RAP and the alternative binders. Legend: Asphalt concrete with virgin bitumen and aggregates (A); Asphalt concrete with virgin polymer-modified bitumen and aggregates (B); Reference mix (C); 100% RAP asphalt concrete with Pen 50/70; 100% RAP asphalt concrete with alternative binders containing V2F; 100% RAP asphalt concrete with B33TQ; 100% RAP asphalt concrete with alternative binders containing V2D; 100% RAP asphalt concrete with alternative binders containing V1.

Among all analysed asphalt mixtures, those containing the blends B26-1, B27, B27-1, B31, B32, and B32 V1 exhibit good mechanical properties in terms of stiffness, tensile resistance, and water susceptibility. Although the results obtained with the alternative binders are promising, further specific rheological and mechanical tests have to be carried out in order to assess the feasibility and the durability of these road materials that do not contain standard bitumen. For instance, testing fatigue (mechanical), ageing susceptibility (rheological and mechanical), and low-temperature behaviour of the final alternative binders and asphalt mix will be crucial to establish the performances of these innovative asphalt products. In particular, the ageing tendency of the alternative binders, and consequently of

asphalt concrete, has to be evaluated, since an aged material is used, i.e., REOB. Some of the abovementioned tests are ongoing and are showing promising results.

## 5. Conclusions

In this work, the potential reuse of waste products that were opportunely treated to produce new possible petroleum-based binders starting from REOBs is proposed. In addition, the use of 100% recycled aggregates (RAP) together with alternative binders can represent a good alternative to the current use of virgin materials at the binder and asphalt mixture levels. During this study, rheological and mechanical tests were carried out to preliminarily assess the mechanical properties of these innovative binders. From a rheological point of view, the alternative binders exhibit similar behaviour to polymer-modified bitumen (3%wt. of SBS). The type of REOB, the chosen additives, and the combination of constituent materials are found to be crucial to the final responses of the innovative petroleum-based binders and asphalt mixes. In particular, the introduction of low-molecular-weight oils by REOB products softens the resulting alternative binders and, consequently, the asphalt mixtures, resulting in lower ITSM and ITS values. In addition, the use of recycled mixture with 100% of RAP and alternative binders confers good water damage resistance to the corresponding asphalt mix. In general, various eco-friendly asphalt mixtures show promising results in terms of stiffness, tensile resistance, and water susceptibility. In detail, among all tested materials, the asphalt concretes that contained the alternative binders B26-1, B27, B27-1, B31, B32, and B32V1 meet the requirements of the Italian technical specifications for wearing course samples produced with virgin materials. Hence, these innovative mixtures satisfy the basic mechanical performances. However, limited recipe adjustment may allow the stiffness reduction of the abovementioned asphalt mixtures without compromising the cohesion and water sensitivity of the final road materials. Even though the results of the present study are promising, they represent a preliminary evaluation of the performances of the alternative binders, and further rheological and mechanical analyses are necessary. In particular, the durability of the asphalt concrete has to be investigated, considering the natural ageing process of petroleum-based product and the use of an aged material for the production of the alternative binders (i.e., REOB). The determination of eco-friendly road materials is still ongoing, and the responses of the low-temperature DTRT and fatigue tests are under investigation.

**Supplementary Materials:** The following are available online. Figure S1: Dynamic Temperature Ramp Test of B26 V2000F; Figure S2: Dynamic Temperature Ramp Test of B26 V2000D; Figure S3: Dynamic Temperature Ramp Test of B27 V2000D; Figure S4: Dynamic Temperature Ramp Test of B27 V2000F; Figure S5: Dynamic Temperature Ramp Test of B29 V1000; Figure S6: Dynamic Temperature Ramp Test of B29 V2000D; Figure S7: Dynamic Temperature Ramp Test of B29 V2000F; Figure S8: Dynamic Temperature Ramp Test of B30 V2000D; Figure S9: Temperature Ramp Test of B30 V2000F; Figure S10: Dynamic Temperature Ramp Test of B31 V2000F; Figure S11: Dynamic Temperature Ramp Test of B31 V1000; Figure S12: Dynamic Temperature Ramp Test of B32; Figure S13: Dynamic Temperature Ramp Test of B33.

**Author Contributions:** M.P. investigation, methodology, and writing; P.C. conceptualization; V.L. conceptualization; A.A.A. writing—reviewing; G.T. investigation, methodology, and writing; F.G. resources; C.S. supervision; C.O.R. conceptualization and supervision. All authors have read and agreed to the published version of the manuscript.

**Funding:** This research received no external funding: National Operational Program Research And Innovation 2014–2020 (Cci 2014it16m2op005), and the European Social Fund, Action I.1 "Innovative Doctorates With Industrial Characterization".

**Institutional Review Board Statement:** Not Applicable.

**Informed Consent Statement:** Not Applicable.

**Data Availability Statement:** The data presented in this study is available upon request from the corresponding author.

**Acknowledgments:** Authors are thankful to Itelyum Regeneration s.r.l. and Ecopneus s.c.p.a for the raw material supplied and for their support during research, the National Operational Program Research And Innovation 2014–2020 (Cci 2014it16m2op005), and the European Social Fund, Action I.1 "Innovative Doctorates With Industrial Characterization".

**Conflicts of Interest:** The authors declare no conflict of interest.

**Sample Availability:** Samples of the compounds are not available from the authors.

## References

1. Gudde, N.; Larivé, J.-F.; Yugo, M. *$CO_2$ Reduction Technologies. Opportunities within the EU refining system (2030/2050) Concawe Special Task Force Refinery 2050 (STF-2) Report n° 8/19*; Concawe: Brussels, Belgium, 2019.
2. Available online: https://ec.europa.eu/commission/presscorner/detail/en/MEMO_12_989 (accessed on 9 November 2021).
3. Geissdoerfer, M.; Savaget, P.; Bocken, N.M.P.; Hultink, E. The Circular Economy—A new sustainability paradigm? *J. Clean. Prod.* **2017**, *143*, 757–768. [CrossRef]
4. Available online: https://eur-lex.europa.eu/legal-content/EN/TXT/?uri=CELEX:32008L0098 (accessed on 9 November 2021).
5. Abdalla, N.; Fehrenbach, H. *LCA for Regeneration of Waste Oil to Base Oil: Updating the Study Ecological and Energetic Assessment of Re-Refining Waste Oils to Base Oils—Substitution of Primarily Produced Base Oils Including Semi-Synthetic and Synthetic Compounds*; Institut für Energie- und Umweltforschung: Heidelberg, Germany, 2018.
6. Available online: https://ec.europa.eu/environment/waste/framework/end_of_waste.htm (accessed on 9 November 2021).
7. Available online: https://echa.europa.eu/it/candidate-list-table (accessed on 9 November 2021).
8. Chemical and Chemical Technology (CTC) Department. Available online: https://www.unical.it/portale/strutture/dipartimenti_240/ctc/ (accessed on 9 November 2021).
9. Available online: https://www.unibo.it (accessed on 9 November 2021).
10. Itelyum Regeneration Srl, via Tavernelle 19, Pieve Fissiraga, Lodi (LO). Available online: http://www.itelyum-regeneration.com/it/ (accessed on 9 November 2021).
11. Available online: https://www.ecopneus.it/ (accessed on 9 November 2021).
12. Caputo, P.; Porto, M.; Loise, V.; Teltayev, B.; Rossi, C.O. Analysis of mechanical performance of bitumen modified with waste plastic and rubber (SBR) additives by rheology and PGSE NMR experiments. *Eurasian Chem. Technol. J.* **2019**, *21*, 235–239. [CrossRef]
13. Available online: https://eapa.org/wp-content/uploads/2020/02/Asphalt-in-figures_2018.pdf (accessed on 9 November 2021).
14. Tarsi, G.; Tataranni, P.; Sangiorgi, C. The challenges of using reclaimed asphalt pavement for new asphalt mixtures: A review. *J. Mater.* **2020**, *13*, 4052. [CrossRef]
15. Caputo, P.; Loise, V.; Ashimova, S.; Teltayev, B.; Vaiana, R.; Rossi, C.O. Inverse Laplace Transform (ILT)NMR: A powerful tool to differentiate a real rejuvenator and a softener of aged bitumen. *Colloids Surf. A* **2019**, *574*, 154–161. [CrossRef]
16. Caputo, P.; Loise, V.; Crispini, A.; Sangiorgi, C.; Scarpelli, F.; Rossi, C.O. The efficiency of bitumen rejuvenator investigated through Powder X-ray Diffraction (PXRD) analysis and T2-NMR spectroscopy. *Colloids Surf. A* **2019**, *571*, 50–54. [CrossRef]
17. Available online: https://www.eurobitume.eu/bitumen/industry/ (accessed on 9 November 2021).
18. Available online: https://eapa.org/eapa-asphalt-in-figures-2017/ (accessed on 9 November 2021).
19. Del Barco-Carrión, A.J.; Pérez-Martínez, M.; Themeli, A.; Presti, D.L.; Marsacb, P.; Pouget, S.; Hammoum, F.; Chailleux, E.; Airey, G.D. Evaluation of bio-materials' rejuvenating effect on binders for high-reclaimed asphalt content mixtures. *Mater. Construcción* **2017**, *67*, 1–11. [CrossRef]
20. Zaumanis, M.; Mallick, R.; Frank, R. 100% recycled hot mix asphalt: A review and analysis. *Resour. Conserv. Recycl.* **2014**, *92*, 230–245. [CrossRef]
21. Walters, R.C.; Fini, E.H.; Abu-Lebdeh, T. Enhancing asphalt rheological behaviour and aging susceptibility using bio-char and nano-clay. *Am. J. Eng. Appl. Sci.* **2014**, *7*, 66–76. [CrossRef]
22. Ingrassia, L.P.; Lu, X.; Ferrotti, G.; Canestrari, F. Renewable materials in bituminous binders and mixtures: Speculative pretext or reliable opportunity? *Resour. Conserv. Recycl.* **2019**, *144*, 209–222. [CrossRef]
23. Raouf, M.A.; Williams, R.C. Temperature Susceptibility of Non-petroleum Binders Derived from Bio-oils. In Proceedings of the 7th Asia Pacific Conference on Transportation and the Environment, Semarang, Indonesia, 3–5 June 2010.
24. Airey, G.D. Rheological and fracture characterization of sustainable bio-binders and rejuvenators for virgin and recycled asphalt mixtures. In Proceedings of the 1st Winter School 'Advanced in Sustainable Asphalt Pavements', Modena, Italy, 17–20 December 2017.
25. Yang, X.; You, X.; Dai, Q. Performance evaluation of asphalt binder modified by bio-oil generated from waste wood resources. *Int. J. Pavement Res. Technol.* **2013**, *6*, 431–439. [CrossRef]
26. Airey, G.D.; Mohammed, M.H. Rheological properties of polyacrylates used as synthetic road binders. *Rheol. Acta* **2008**, *47*, 751–763. [CrossRef]
27. Shields, J. *Adhesives Handbook*, 2nd ed.; Butterworth-Heinemann: London, UK, 1976.
28. Tan, C.P.; Man, Y.B.C. Comparative differential scanning calorimetric analysis of vegetable oils: Effects of heating rate variation. *Phytochem. Anal.* **2002**, *13*, 129–141. [CrossRef]

29. El-latief, R.A.E.A. *Asphalt Modified with Biomaterials as Eco-Friendly and Sustainable Modifiers*; IntechOpen, 2018. [CrossRef]
30. Fini, E.H.; Kalberer, E.W.; Shahbazi, A.; Basti, M.; You, Z.; Ozer, H.; Aurangzeb, Q. Chemical characterization of biobinder from swine manure: Sustainable modifier for asphalt binder. *J. Mater. Civ. Eng.* **2011**, *23*, 1506–1513. [CrossRef]
31. Available online: https://www.greencarcongress.com/2019/07/20190708-lignin.html (accessed on 9 November 2021).
32. Yang, Y.; Zhang, Y.; Omairey, E.; Cai, J.; Gu, F.; Bridgwater, A.V. Intermediate pyrolysis of organic fraction of municipal solid waste and rheological study of the pyrolysis oil for potential use as bio-bitumen. *J. Clean. Prod.* **2018**, *187*, 390–399. [CrossRef]
33. Adedeji, A.; Grunfelder, T.; Bates, F.S.; Macosko, C.W. Asphalt Modified by SBS Triblock Copolymer: Structures and Properties. *Polym. Eng. Sci.* **1996**, *36*, 1707–1723. [CrossRef]
34. Cui, S.; Blackman, B.R.K.; Kinloch, A.J.; Taylor, A.C. Durability of asphalt mixtures: Effect of aggregate type and adhesion promoters International. *J. Adhes. Adhes.* **2014**, *54*, 100–111. [CrossRef]
35. Rossi, C.O.; Caputo, P.; Baldino, N.; Szerb, E.I.I.; Teltayev, B. Quantitative evaluation of organosilane-based adhesion promoter effect on bitumen-aggregate bond by contact angle test. *Int. J. Adhes. Adhes.* **2017**, *72*, 117–122. [CrossRef]
36. Porto, M.; Caputo, P.; Loise, V.; de Filpo, G.; Rossi, C.O.; Calandra, P. Polysaccharides-Reinforced Bitumens: Specificities and Universality of Rheological Behavior. *Appl. Sci.* **2019**, *9*, 5564. [CrossRef]
37. Gui-juan, Z.; Ping, G. Workability of Sasobit Warm Mixture Asphalt. *Energy Procedia* **2012**, *16*, 1230–1236. [CrossRef]
38. Caputo, P.; Abe, A.A.; Loise, V.; Porto, M.; Calandra, P.; Angelico, R.; Rossi, C.O. The role of additives in warm mix asphalt technology: An insight into their mechanisms of improving an emerging technology. *Nanomaterials* **2020**, *10*, 1202. [CrossRef]
39. Verma, T.; Chauhan, H. *Replacement of Bitumen with Pine Resin a Project Report*; Jaypee University of Information Technology: Waknaghat, Solan—173234, Himachal Pradesh, India, 2019.
40. De Souza, A.G.; Kano, F.S.; Bonvent, J.; Rosa, D.S. Cellulose Nanostructures Obtained from Waste Paper Industry: A Comparison of Acid and Mechanical Isolation Methods. *Mater. Res.* **2017**, *20* (Suppl. S2), 209–214. [CrossRef]
41. EN 12697-17. *Bituminous Mixtures—Test Methods—Part 17: Particle Loss of Porous Asphalt Specimens*; British Standards Institution: London, UK, 2017.
42. EN 12697-31. *Bituminous Mixtures. Test Methods. Specimen Preparation by Gyratory Compactor*; British Standards Institution: London, UK, 2019.
43. UNI EN 12697-26. *Bituminous Mixtures—Test Methods—Part 26: Stiffness*; British Standards Institution: London, UK, 2018.
44. UNI EN 12697-23. *Bituminous Mixtures—Test Methods—Part 23: Determination of the Indirect Tensile Strength of Bituminous Specimens*; British Standards Institution: London, UK, 2018.
45. EN 12697-12. *Bituminous Mixtures—Test Methods—Part 12: Determination of the Water Sensitivity of Bituminous Specimens*; British Standards Institution: London, UK, 2020.

Journal of Molecular Liquids 248 (2017) 847–853

Contents lists available at ScienceDirect

Journal of Molecular Liquids

journal homepage: www.elsevier.com/locate/molliq

# Extensive molecular field theoretical investigation of thermotropic biaxial nematics composed of board-like ($D_{2h}$) molecules in the partially repulsive regime of orientational interactions

G. Celebre *, C. D'Urso, M. Porto

*Dipartimento di Chimica e Tecnologie Chimiche, Università della Calabria, v. P. Bucci, I-87036 Rende (CS), Italy*

ARTICLE INFO

*Article history:*
Received 8 September 2017
Received in revised form 16 October 2017
Accepted 19 October 2017
Available online 21 October 2017

*Keywords:*
Liquid crystals
Thermotropic biaxial nematics with $D_{2h}$ symmetry
Partially repulsive orientational interactions

ABSTRACT

A recently proposed molecular-field approach, based on the formulation of an approximate, analytical orientational partition function to describe the thermodynamic properties of $D_{2h}$ thermotropic biaxial nematics governed by fully attractive orientational interactions (G. Celebre, J. Mol. Liq. 209 (2015) 104–114), has now been extended to treat also the partially repulsive regime of orientational interactions. This has been made by the implementation of a Minimax algorithm to locate the stationary, stable points of the Helmholtz Free Energy for the studied systems. The developed tool paved the way to new interesting (and intriguing) scenarios, allowing us to virtually explore a wide range of cases, where the features determining the existence of possible stable biaxial nematic mesophases were basically dictated by the geometric parameters characterizing the single $D_{2h}$ mesogenic particles. Many cases have been revisited to validate the method (starting from the pioneering work of Straley), and also new simulated and experimental (goethite) cases have been addressed. Particular attention has been paid to the physical meaning of the two biaxiality parameters (called $\gamma$ and $\lambda$), weighting the biaxial extra-terms in the molecular-field expression of the mean-torque potential. Moreover, an explicit mathematical relation has been found between the parameter $\lambda$, ruling the dominant biaxial interaction, and the ratio of the biaxial-to-uniaxial and uniaxial-to-isotropic transition temperatures, whereas a substantial uncorrelation amongst the transition temperatures $T_{NB\text{-}NU}$ and the other biaxiality parameter, $\gamma$, has been verified.

© 2017 Elsevier B.V. All rights reserved.

## 1. Introduction

The dream of every physical chemist (especially in the research field of innovative materials) is probably to find a certain way to link molecular and macroscopic properties, in order to design/predict materials endowed with specific interesting features, starting from the physico-chemical characteristics of the constituent molecules. This is the reason why the physical chemists often work alongside organic chemists, able to synthesize new molecules, so giving concreteness to some possible good idea about new/smart materials. Unfortunately, due to many different reasons, it is usually a very complicated (when not impossible) problem to predict exactly in which way the molecular properties transfer to the macroscopic piece of material. This is particularly true in the field of liquid crystals (see, for example, [1]) and, especially, in the case of thermotropic biaxial nematics (an exhaustive survey on this topic can be found in [2] and refs. therein). The latter represents an elusive state of matter for which the efforts to create and isolate it, starting from seemingly suitable constituent molecules (*i.e.*, molecules with the presumably required structural/geometrical/symmetry features, the simplest ones being hard rectangular $D_{2h}$ blocks [3]), often (almost always) failed (at least, until today). In spite of this, the studies, both experimental and theoretical, about this topic continue, because there are still many things to understand and it is well-known that also the failures often help in understanding. Computer simulation techniques (see, *e.g.*, chap. 6 of [2] and refs. therein) and molecular field models (see, *e.g.*, chap. 3 of [2] and refs. therein), in particular, are the most common theoretical approaches to treat these systems. The latter are appealing due to their conceptual simplicity (even though the mathematical details and the calculations are often rather complicated and difficult to understand for non-specialists); anyway, a cost to be paid for their simplicity is that often, in the models, *ad hoc* phenomenological parameters are introduced, whose molecular meaning (or, at least, a possible interpretation of them at a molecular level) remains usually quite obscure. This is the case of the $\gamma$ and $\lambda$ biaxiality parameters, appearing in the formulation of the orientational (or mean-torque) potential $U$ for $D_{2h}$ particles (possibly giving rise to $D_{2h}$ biaxial nematic mesophases), within the frame of purely quadrupolar molecular interactions [4–6]:

$$U = -u_0\{\boldsymbol{q}\cdot\boldsymbol{Q} + \gamma(\boldsymbol{q}\cdot\boldsymbol{B} + \boldsymbol{b}\cdot\boldsymbol{Q}) + \lambda\,(\boldsymbol{b}\cdot\boldsymbol{B})\} \tag{1}$$

* Corresponding author.
*E-mail addresses:* giorgio.celebre@unical.it (G. Celebre), christian.durso@unical.it (C. D'Urso), m_porto24@yahoo.it (M. Porto).

https://doi.org/10.1016/j.molliq.2017.10.093
0167-7322/© 2017 Elsevier B.V. All rights reserved.

In this expression, $u_0$ is a positive parameter useful to scale the absolute temperature $T$, and the **q** and **b** tensors are defined as follows:

$$\mathbf{q} = \boldsymbol{e_z}\otimes\boldsymbol{e_z} - \frac{1}{3}\mathbf{I} \tag{2}$$

$$\mathbf{b} = \boldsymbol{e_x}\otimes\boldsymbol{e_x} - \boldsymbol{e_y}\otimes\boldsymbol{e_y} \tag{3}$$

where **I** is the identity tensor and $\{\boldsymbol{e}_x, \boldsymbol{e}_y, \boldsymbol{e}_z\}$ are the orthonormal unit vectors of the molecular symmetry axes. Moreover, the following relations hold:

$$\mathbf{Q} = \langle \boldsymbol{q} \rangle = S\left(\boldsymbol{e_Z}\otimes\boldsymbol{e_Z} - \frac{1}{3}\boldsymbol{I}\right) + \frac{1}{3}P(\boldsymbol{e_X}\otimes\boldsymbol{e_X} - \boldsymbol{e_Y}\otimes\boldsymbol{e_Y}) \tag{4}$$

$$\mathbf{B} = \langle \boldsymbol{b} \rangle = D\left(\boldsymbol{e_Z}\otimes\boldsymbol{e_Z} - \frac{1}{3}\boldsymbol{I}\right) + \frac{1}{3}C(\boldsymbol{e_X}\otimes\boldsymbol{e_X} - \boldsymbol{e_Y}\otimes\boldsymbol{e_Y}) \tag{5}$$

where $\{\boldsymbol{e}_X, \boldsymbol{e}_Y, \boldsymbol{e}_Z\}$ is the triad of unit vectors representing the laboratory Principal Axis System (PAS) shared by **Q** and **B** tensors, and the order parameters $S$, $D$, $P$, $C$ are so defined:

$$S = \frac{1}{2}\ \langle 3\ \cos^2\theta_{Z,z} - 1 \rangle \tag{6}$$

$$D = \frac{3}{2}\ \langle (\cos^2\theta_{Z,x} - \cos^2\theta_{Z,y}) \rangle \tag{7}$$

$$P = \frac{3}{2}\ \langle (\cos^2\theta_{X,z} - \cos^2\theta_{Y,z}) \rangle \tag{8}$$

$$C = \frac{3}{2}\ \langle (\cos^2\theta_{X,x} - \cos^2\theta_{X,y}) - (\cos^2\theta_{Y,x} - \cos^2\theta_{Y,y}) \rangle \tag{9}$$

where the uppercase subscripts denote the axes of the PAS of the Lab, whereas the lowercase subscripts indicate the axes of the molecular PAS. All four order parameters $S$, $D$, $P$ and $C$ (with $-1/2 \le S \le 1$; $-(1-S) \le D \le (1-S)$; $-(1-S) \le P \le (1-S)$ and $-3 \le C \le 3$)) are nonzero in the biaxial phase, whereas only the order parameters $S$ and $D$ survive in the uniaxial nematic mesophase [2]. The potential $U$ given in Eq. (1) is, essentially, an extension of that proposed by Maier-Saupe [7], through the addition of the terms in $\gamma$ and $\lambda$. It must be emphasized that, following this model, the orientational intermolecular interactions promoting the alignment of the particles side by side are globally attractive; anyway, these interactions are fully attractive when $\lambda \ge \gamma^2$ whereas they are partially repulsive when $\lambda > 0$ AND $\lambda < \gamma^2$ AND $\lambda - |2\gamma| + 1 > 0$ (see [8] for more details); moreover, to avoid redundancies, the $\gamma$ and $\lambda$ values are chosen within a so-called "essential triangle", where $0 \le \gamma \le 1/2$ and $0 \le \lambda \le 1/3$ (for more explanations about the essential triangle, see [6,9] and refs. therein). Even though, as said above, the molecular nature of $\gamma$ and $\lambda$ is rather unspecified, a way can be tried to link their values to expressions where the geometry of the molecules (crudely described as hard parallelepipeds of length $L$, breadth $B$ and thickness (width) $W$; see Scheme 1) appears.

The expressions, based on the modellization of excluded-volume interactions [10,11], can be written as follows:

$$\lambda = \frac{L\left[(B-W)^2\right]}{\left[2\left(B\left(W^2+L^2\right) + W\left(B^2+L^2\right)\right) - \left(L\left(W^2+B^2\right) + 6LBW\right)\right]} \tag{10}$$

$$\gamma = \frac{\left(L^2 - WB\right)(B-W)}{\left[2\left(B\left(W^2+L^2\right) + W\left(B^2+L^2\right)\right) - \left(L\left(W^2+B^2\right) + 6LBW\right)\right]} \tag{11}$$

Note that in Eqs. (10) and (11) the Straley convention [3] $L > B > W$ (Scheme 1) has been used, unlike ref. [10], where the Authors call $L$ the longest molecular axis and $B$ (instead of $W$) the shortest one. The $\gamma$ and

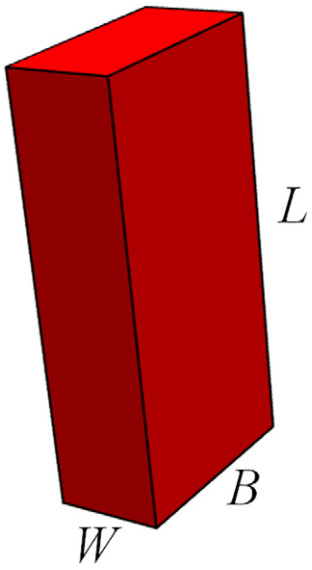


**Scheme 1.** Schematic representation of the $D_{2h}$ particle as a hard rectangular box of length $L$, breadth $B$ and thickness (width) $W$.

$\lambda$ values predicted by Eqs. (10) and (11) for $D_{2h}$ particles fall into the partially repulsive orientational regime (see above). This fact has an important implication about the theoretical search of stationary points of the Helmholtz Free Energy $F$ for the studied systems. As a matter of fact, for fully attractive orientational interactions, the stable points of the phase can be found by minimizing $F$ as a function of the four order parameters at each temperature. This has been already done by one of the Authors for a number of cases of study [12], by means of a recently suggested approach where the use of an analytical, effective (even though approximate) orientational partition function made it possible to carry out, very quickly and easily, a large set of reliable simulations of different systems and scenarios. For partially repulsive orientational interactions, on the contrary, a Minimax algorithm for the search of equilibrium states of the free energy is required [8,5,13,14]. In the present work, the previously presented approach [12] has been then upgraded by the implementation of the Minimax algorithm (where, thanks to the analytical form of the partition function, given in Eqs. (15)–(19) of ref. [12], the derivatives $\frac{\partial \mathcal{F}}{\partial S}$, $\frac{\partial \mathcal{F}}{\partial D}$, $\frac{\partial \mathcal{F}}{\partial P}$ and $\frac{\partial \mathcal{F}}{\partial C}$ ($\frac{\partial \mathcal{F}}{\partial S} = 0, \frac{\partial \mathcal{F}}{\partial D} = 0, \frac{\partial \mathcal{F}}{\partial P} = 0, \frac{\partial \mathcal{F}}{\partial C} = 0$) can be calculated analytically and instantaneously; for more technical details about the implemented algorithm, see Appendix A, where its flow-chart is shown). The new code is now able to treat also the partially repulsive cases, and this allowed us to explore a series of $\gamma$ and $\lambda$ values, virtually corresponding to different geometries of particles described as hard rectangular blocks. In the following sections, we will discuss a large set of our tests and the corresponding results. All the calculations of this study have been carried out by *Mathematica 11* [29].

## 2. Sampling the partially repulsive region of the essential triangle

### 2.1. The "Straley" trajectory

In Fig. 1, the partially repulsive region of the essential triangle (in white) is shown, where the internal points, representing the tested cases, correspond to ($\lambda$,$\gamma$) couples of coordinates obtained by Eqs. (10) and (11) according to different choices of $L$, $B$ and $W$ molecular dimensions.

First of all, to test the reliability of our approach, we walked the "Straley trajectory" (corresponding to the black points in Fig. 1), in order to compare our results with those given in [3]. In that work,

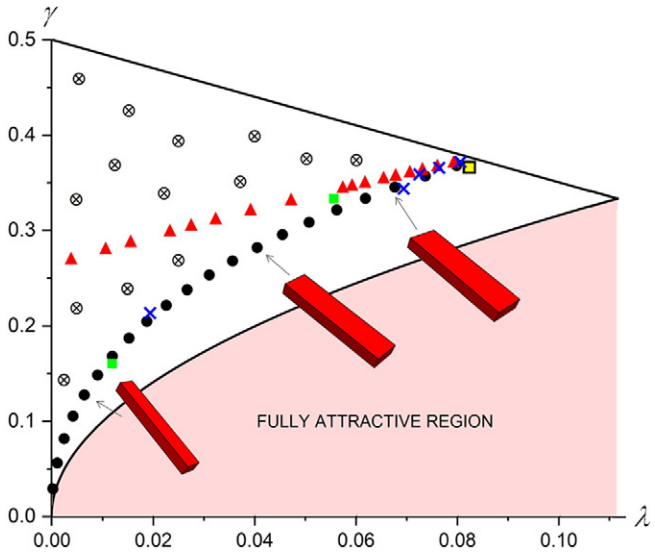


**Fig. 1.** Different points, investigated by our approach, in the partially repulsive region (in white) of the essential triangle (the fully attractive region, exhaustively explored in ref. [12], is also shown in pink). In the figure: (a) the black circles (●) represent the points described in the Straley work [3] (see Section 2.1 of this work); (b) the red triangles (▲) sample the region lying between L/W > 9 and 2.6 < B/W < 3.73, where, following MC computer simulations [19], it is predicted to have the highest possibility to find a biaxial nematic phase (see Section 2.2); (c) the blue crosses (×) compare with the MC simulations carried out in [18] (see Section 2.2); (d) the green squares (■) compare with the Molecular Field studies carried out in [13] (see Section 2.3); (e) the yellow square (□) is the goethite point (see Section 2.4); (f) the circled crosses (⊗) represent 14 new treated cases to investigate the dependence of the transition temperature $T_{NB\text{-}NU}$ on **λ** and **γ** (see Section 2.5). The shapes of particles corresponding to some points are also shown.

following the conceptual line of Onsager's theory for a gas of hard rods [15], and some seminal ideas of Alben and Shih [16,17], a molecular field model of interaction was suggested, involving the mutually excluded volumes (and, consequently, the dimensions $L$, $B$ and $W$) of pairs of $D_{2h}$ hard block particles characterized by different orientations. At the end of the work, a phase diagram was shown (fig. 2 of [3]), for blocks of varying breadth $B$, very similar to that we have found by using our model (see Fig. 2).

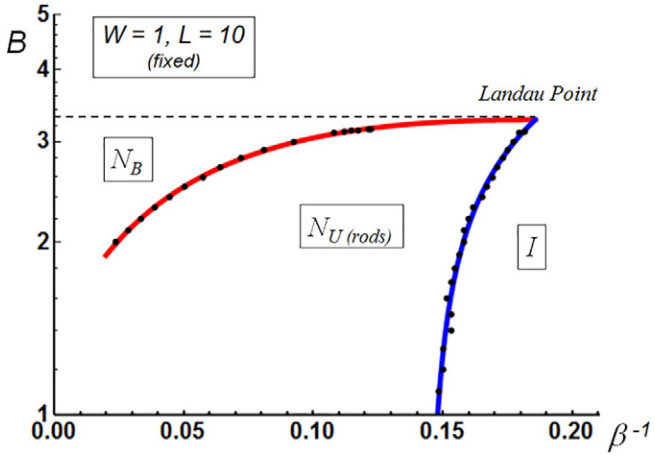


**Fig. 2.** Phase diagram (*à la* Straley) *versus* $\beta^{-1} = (k_B T/u_0)$ for $D_{2h}$ hard block particles in the regime of partially repulsive orientational interactions. The plot is obtained from the black point data of Fig. 1: the dimension $B$ was changed, whereas $W = 1$ and $L = 10$ were kept fixed. The Isotropic ($I$), Uniaxial Nematic ($N_U$) and Biaxial Nematic ($N_B$) regions are shown (note that the $B$ scale is logarithmic, as in ref. [3]).

### 2.2. Comparisons with Monte Carlo computer simulations: investigating the "aspect ratio difference"

It is clear, from the previous section, that the shape anisotropy is a key requirement for the emergence of orientational biaxiality from partially repulsive interactions.

Often, especially in computer simulations [18,19], the shape anisotropy is quantified by the so-called aspect ratio difference $\nu$, defined as [18–20,3]:

$$\nu = \frac{L}{B} - \frac{B}{W} \tag{12}$$

Several aspect ratio differences, corresponding to the cases treated in [18,19] and represented by the red triangles and the blue crosses shown in Fig. 1, have been investigated by us. In particular, the red triangles of Fig. 1 sample the region lying between $L/W > 9$ and $2.6 < B/W < 3.73$, where there is the highest possibility to find a biaxial nematic phase (on the basis of the salient features of the phase diagram given in fig. 2 of ref. [19]). By our approach, we obtained the phase diagram shown in Fig. 3, where the biaxial nematic phase clearly emerges, as expected, in the regions predicted by the MC simulations; moreover, the width of the range of thermodynamic stability of the uniaxial region increases, as expected, with the aspect ratio difference. About the blue cross symbols shown in Fig. 1, our results regarding the three crosses at $\lambda > 0.07$ agree with Monte Carlo computer simulations [see ref. 18 and its Supplementary Information] in finding biaxial ordering of the phase in some interval of temperature. *Vice versa*, unlike the MC simulated results, we have found phase biaxiality, as expected, also for the blue cross at $\lambda = 0.07$ (see also the corresponding molecular shape represented in Fig. 1). It seems very strange that MC simulations fail in finding biaxiality in that point: in our opinion, this could be due to some kind of computational anomaly in that specific simulated case. On the contrary, both the approaches (the MC and the present one) indicate the absence of phase biaxiality for the point represented by the blue cross at $\lambda \sim 0.02$.

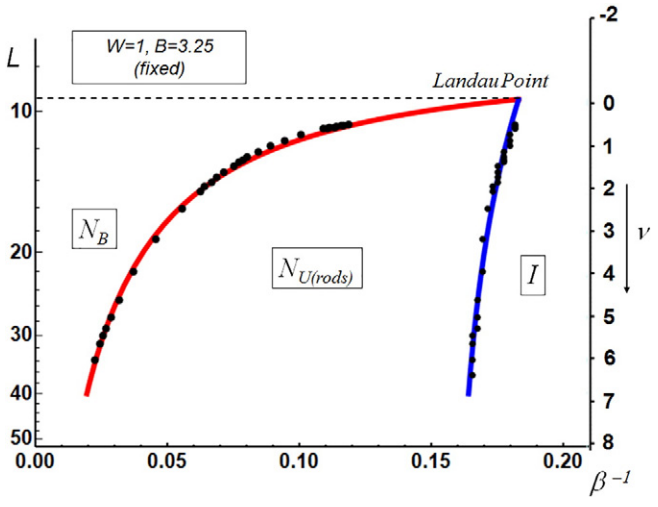


**Fig. 3.** Phase diagram *versus* $\beta^{-1} \propto T$, obtained from the red triangle data of Fig. 1. In particular, different aspect ratios $\nu$ have been explored in the region comprised between $L/W > 9$ and $2.6 < B/W < 3.73$ (by changing the dimension $L > 9$, whereas $W = 1$ and $B = 3.25$ were kept fixed), corresponding to the zone where the highest possibility to find a biaxial nematic phase is predicted by MC computer simulations [19] (see text for more details). The Isotropic ($I$), Uniaxial Nematic ($N_U$) and Biaxial Nematic ($N_B$) regions are also clearly labelled in the figure (note that the $L$ scale is logarithmic and increases downwards).

### 2.3. Comparisons with a well-established numerical molecular field approach [13]

Another important test of our methodology has been carried out by comparing our results with those obtained by Bisi, Romano and Virga (BRV) in ref. [13], based on a MF approach where the $Z$ partition function and its derivatives with respect to the order parameters are numerically evaluated (see Eqs. (18)–(20) of ref. [13]). In that work, the Authors decided to investigate, in particular, two points (called G and R; see fig. 2 of [13]) in the partially repulsive region of the essential triangle: the studied cases are represented by the green squares in our Fig. 1. For the point G, characterized by $\lambda = 1/18 \cong 0.056$ and $\gamma = 1/3 \cong 0.33$ (virtually corresponding to a parallelepiped of dimensions $L = 12.2$, $B = 3$ and $W = 1$), the behavior of the order parameters $S$, $D$, $P$, $C$ *vs* the reduced temperature $T_{red} = T/T_{NU\text{-}I}$ obtained by our approach is shown in Fig. 4.

The trends of the order parameters are very similar to those shown in figs. 3-6 of ref. [13] (note that, in [13], the ensemble average of the Wigner functions are used as order parameters, the relations being the following: $S = \langle R^2_{00} \rangle$ ; $D = \sqrt{6}\langle R^2_{02} \rangle$ ; $P = \sqrt{6}\langle R^2_{20} \rangle$ ; $C = 6\langle R^2_{22} \rangle$ ); moreover, the transition temperature $T_{NB\text{-}NU}$, occurring at $T_{red} = 0.38$, is perfectly reproduced by us. Only the value of our $C$ order parameter, for $T_{red} \to 0$, is underestimated, but we are aware of this flaw suffered by our model, due to the approximations adopted in obtaining the closed, analytical form of the orientational Partition Function (about this, the reader is referred to [12] for more details regarding the mathematical derivation). Also the so-called *uniaxial rebound* phenomenon [13] at the nematic biaxial transition is observed for our $D$ order parameter (see Fig. 5), even though the magnitude of the effect is less enhanced than in ref. [13]. About the point R of [13], represented by the green square on the left in our Fig. 1 (characterized by $\lambda = (\frac{7}{6} - \frac{2\sqrt{3}}{3}) \cong 0.012$ and $\gamma = (\frac{\sqrt{3}}{3} - \frac{5}{12}) \cong 0.160$ and virtually corresponding to a parallelepiped of dimensions $L = 8.6$, $B = 1.6$ and $W = 1$) the order parameter profiles are shown in Fig. 6. Also in this case, the order parameters calculated by us show trends similar to those reported in [13], and the values of $T_{NB\text{-}NU}$ once again match very well (0.08 in this work, against 0.089 for the study [13]). The good agreement of our results with the results produced by a different MF approach corroborated the reliability of our method, so that we proceeded by addressing new cases never treated before.

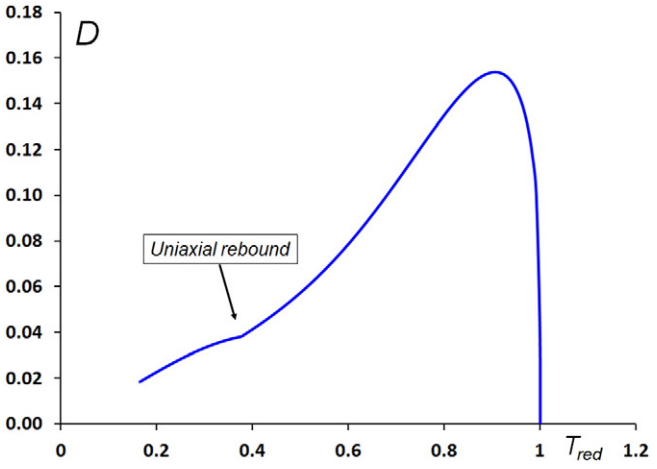


**Fig. 5.** The observed phenomenon of *uniaxial rebound* at the nematic biaxial transition [13] for the $D$ order parameter of the $\boldsymbol{\lambda} = 1/18$ and $\boldsymbol{\gamma} = 1/3$ treated case (see text for more details).

### 2.4. Investigation of a virtual mesophase composed of goethite-shaped particles

Mineral liquid crystals (MLCs) ([21] and refs. therein) and, in particular, biaxial phases in MLC [22–24], have recently received considerable attention since, unlike thermotropic biaxial phases (still debated), there are experimental unquestionable evidences of the existence of biaxial orientational ordering [22]. Actually, the MLCs are made by colloidal particles dispersed in a surrounding liquid (technically speaking, they are colloidal suspensions [25,26]); then, they should be called *colloidal LC* and should be classified as lyotropic phases [24]. Nonetheless, the geometric features of board-like colloidal particles, as goethite [25,26], play a decisive role in generating or not the biaxiality of the phase [22, 23]; so, we decided to study by our method a virtual mesophase composed of particles characterized exactly by the same molecular dimensions exhibited by the goethite [23], namely: $L = 254$ nm, $B = 83$ nm and $W = 28$ nm (a similar conceptual approach has been used in [27], to study the phase stability of a fluid of hard board-like particles by using density functional theory). This case is represented by the point

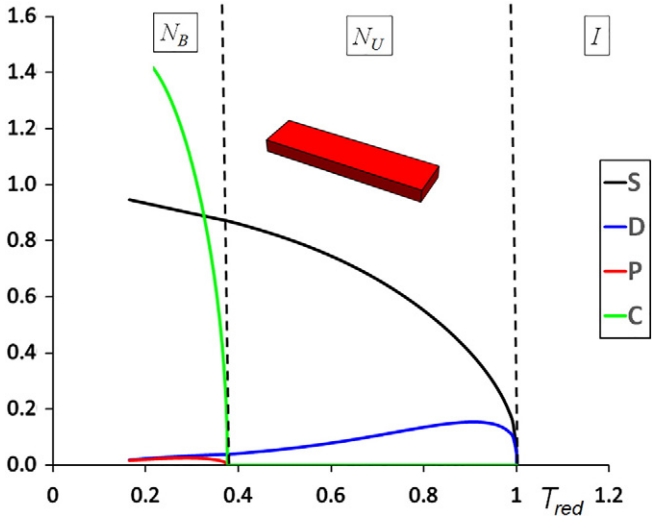


**Fig. 4.** The behavior of order parameters $S$, $D$, $P$ and $C$ as a function of the reduced temperature $T_{red}$, $= T/T_{NU\text{-}I}$ for $D_{2h}$ hard block particles in the regime of partially repulsive orientational interactions, when $\boldsymbol{\lambda} = 1/18$ and $\boldsymbol{\gamma} = 1/3$ (point G of ref. [13]).

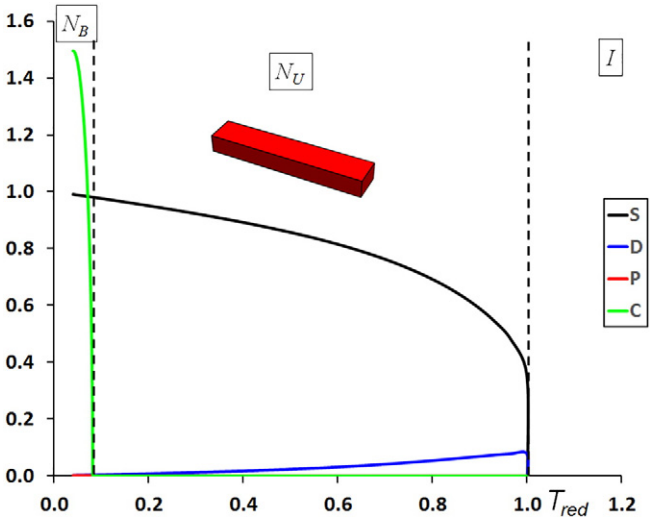


**Fig. 6.** The behavior of order parameters $S$, $D$, $P$ and $C$ as a function of the reduced temperature $T_{red}$ for $\boldsymbol{\lambda} = (\frac{7}{6} - \frac{2\sqrt{3}}{3})$ and $\boldsymbol{\gamma} = (\frac{\sqrt{3}}{3} - \frac{5}{12})$ (point R of ref. [13]).

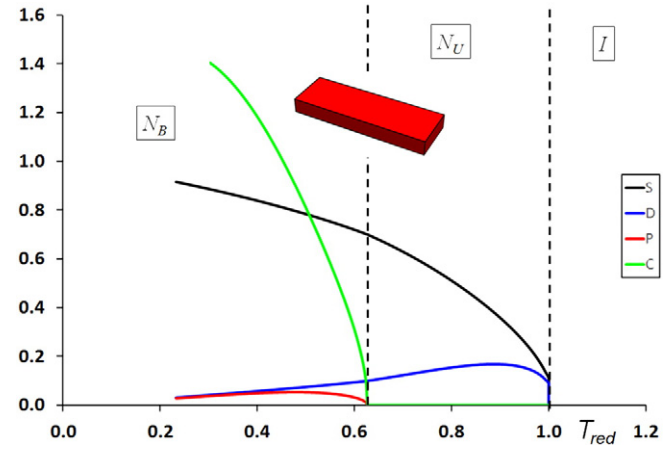


**Fig. 7.** The behavior of order parameters *S*, *D*, *P* and *C* as a function of the reduced temperature $T_{red}$, for $D_{2h}$ hard block units representing goethite particles in the regime of partially repulsive orientational interactions ($\boldsymbol{\lambda} = 0.082$ and $\boldsymbol{\gamma} = 0.366$).

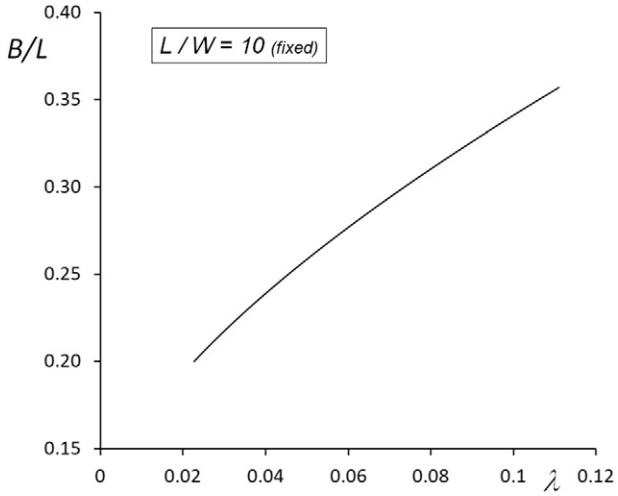


**Fig. 9.** The relative flatness *B*/*L* of the particle increases with **λ**.

given as a yellow square in Fig. 1, whose biaxiality parameters λ and γ, calculated by Eqs. (10) and (11), are, respectively, 0.082 and 0.366. The order parameters corresponding to this virtual goethite-mesophase are shown in Fig. 7. Interestingly, the existence of both uniaxial and biaxial nematic regions is predicted by our calculations, even though the *L*/*B* and *B*/*W* dimension ratios of goethite are not far from those characterizing the so-called *dual-shape* [18] (or *self-dual* [3,28]) situation, where $L/B \approx B/W$ ($\approx 3$ for goethite) and the *aspect ratio difference* $\nu$ is $\approx 0$ (corresponding to the so-called *Landau point*, shown in the figures), so that a direct transition $N_B$-*I* should be detected. Actually, this is what is observed experimentally [22], even though it should not forgotten that the real system is a lyotropic nematic mesophase (and not a thermotropic one).

### 2.5. Systematic exploration of the dependence of the transition temperature $T_{NB\text{-}NU}$ on λ and γ: 14 new treated cases

It is known [6] that the dominant biaxial contribution for a mean-torque potential *U* written as in Eq. (1), is that ruled by λ with respect to that depending on γ. On the other hand, here we have a way to directly relate the λ parameter to the shape of the particles composing the mesophase; then, by a systematic investigation of these relations, we can hope to find a direct, quantitative relation between the shape features of the mesogenic particles and the onset of the phase biaxiality, going beyond the intuitive deductions that it is possible and reasonable to formulate. To do this, we decided to treat many cases (represented by the circled crosses in Fig. 1) covering in practice all the still unexplored partially repulsive region. First of all, we treated four cases (on the extreme left in the Fig. 1) all corresponding to a very small λ value (~0.005) and a variable γ going from ~0.145 to ~0.46. The shapes representing the particles predicted for these cases are shown in Fig. 8(a).

It is interesting to observe that, for this fixed very small value of λ, the breadth *B* and thickness *W* of the particle are really tiny with respect to *L* and become even more negligible as the parameter γ increases, till the particle becomes a sort of noodle when γ ~0.46. This means that the already slight biaxial anisometric features of the particles decrease and are finally lost as γ increases. Actually, our calculations do not predict the existence of stable biaxial nematic regions for virtual mesophases formed by such particles. The things start to change by increasing λ:

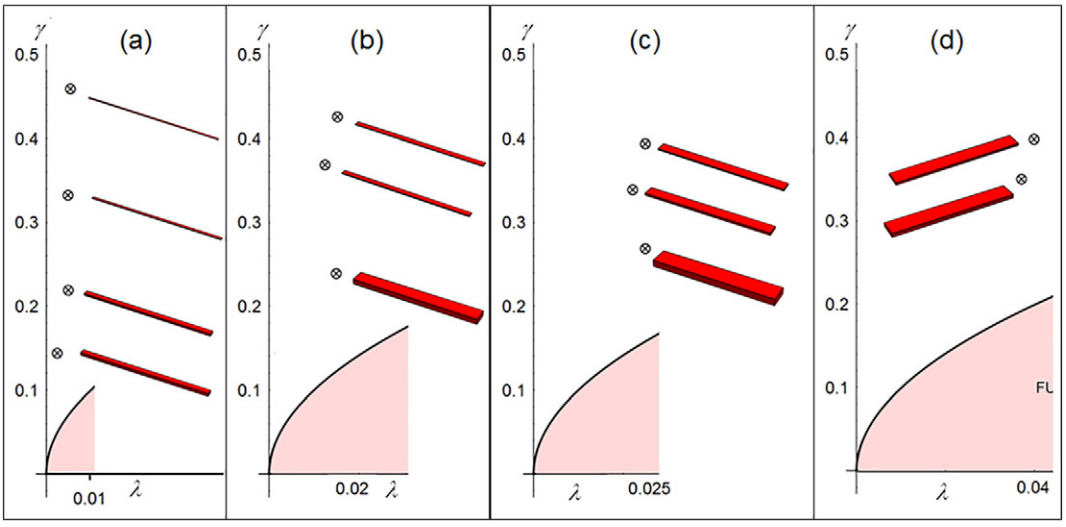


**Fig. 8.** The shapes of particles corresponding to the circled crossed points of Fig. 1, characterized by: (a) **λ** ~0.005 and **γ** going from ~0.145 to ~0.46; (b) **λ** ~0.015 and **γ** going from ~0.24 to ~0.43; (c) **λ** ~0.025 and **γ** going from ~0.27 to ~0.40; (d) **λ** ~0.04 and **γ** going from ~0.35 to ~0.40.

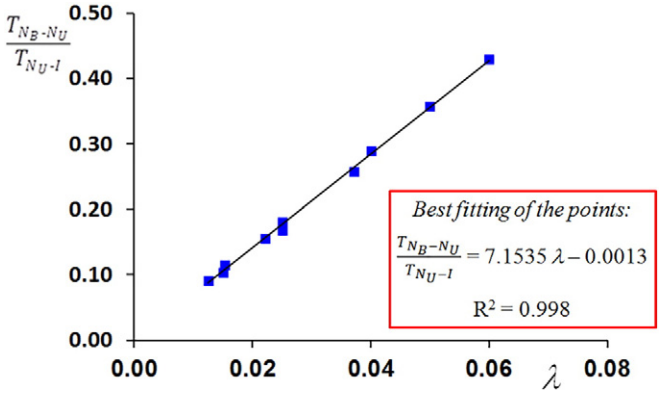


**Fig. 10.** The transition temperature $T_{NB\text{-}NU}$ (in $T_{red}$ units) *versus* **λ** exhibits a perfectly linear trend.

concerning the three circled crosses at λ ~0.015 and γ going from ~ 0.24 to ~ 0.43 (Fig. 8(b)), the biaxial nematic phase emerges for values of the transition temperature $T_{NB\text{-}NU}$ of about 0.1 (in $T_{red}$ units); moreover, also in these cases there is a clear trend of the relative thickness *W*/*L* of the particle to decrease by increasing γ. Three more points were investigated for λ ~0.025 and γ going from ~0.27 to ~0.40 (see Fig. 8(c) for the shapes): the biaxial phase appears for values of $T_{NB\text{-}NU}$ of about 0.16–0.18 $T_{NU\text{-}I}$, and a significantly decrease of *W*/*L vs* γ is still evident, whereas the relative breadth *B*/*L* of the particle is no longer negligible. This behavior is even more evident also for the two points at λ ~0.04 and γ ~0.35 and γ ~ 0.40 (Fig. 8(d)), where the flatness of the particle become significant and the biaxial phase occurs for values of $\frac{T_{N_B-N_U}}{T_{N_U-I}}$ of about 0.26–0.29. Finally, two more points at (λ ~0.05, γ ~0.38) and (λ ~0.06, γ ~0.37) were investigated: the $N_B$-$N_U$ phase transition was predicted for values of $T_{red}$ of, respectively, about 0.36 and 0.43. What described above allowed us to conclude that, on the whole, a λ value sufficiently large (≳0.01) basically means a significant flatness *B*/*L* of the particle and good possibilities to virtually observe the existence of the biaxial nematic phase when partially repulsive orientational interactions are involved (see Fig. 9, where the behavior of the relative flatness of the mesogenic particle *vs* λ, for a arbitrarily fixed $L/W = 10$ ratio, is shown; the figure has been obtained from Eq. (10), by inverting the monotonic functional dependence).

On the contrary, large γ values are basically representative of very thin particles, where *W*/*L*≲0.1. Since, following our convention (see Scheme 1), the *B* geometric parameter (*i.e.*, the molecular flatness) is more important than *W* in dictating the phase biaxiality, then λ confirms to be more important than γ as dominant biaxial parameter, also for partially repulsive orientational interactions, as already found for fully attractive interactions [6]. Now, if we plot the values of $\frac{T_{N_B-N_U}}{T_{N_U-I}}$ *versus* λ for the cases just discussed above, we obtain the behavior shown Fig. 10, where it is immediate to recognize a perfect linear dependence of the transition temperature $\frac{T_{N_B-N_U}}{T_{N_U-I}}$ on λ.

The best fitting of the points (reported in the red inset of Fig. 10) is indeed given by the linear expression of Eq. (13):

$$\frac{T_{N_B-N_U}}{T_{N_U-I}} = 7.1535\,\lambda - 0.0013 \tag{13}$$

Since the intercept of Eq. (13) is basically 0, we can interestingly conclude that, for partially repulsive orientational interactions of $D_{2h}$ hard block particles, $\frac{T_{N_B-N_U}}{T_{N_U-I}}$ is simply directly proportional to λ; *i.e.*:

$$\frac{T_{N_B-N_U}}{T_{N_U-I}} \propto \lambda \tag{14}$$

The results reported in Eqs. (13)–(14) confirm, in a quantitative way and for partially repulsive orientational interactions, what only qualitatively suggested in [6] for fully attractive orientational interactions. In our knowledge, these outcomes have never been recognized before in this quantitative form. On passing to the other biaxiality parameter, if we plot the $\frac{T_{N_B-N_U}}{T_{N_U-I}}$ values against γ, we obtain a distribution represented by the randomly scattered points shown in Fig. 11, where it is evident that there is no correlation (then, no physical relationship) amongst the $N_B$-$N_U$ transition temperatures and this specific biaxial contribution. Also in this case, our result is similar to that qualitatively suggested for fully attractive orientational interactions in [6].

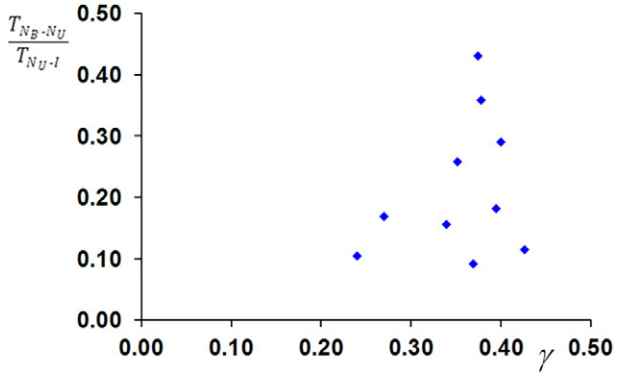


**Fig. 11.** Random distribution of the transition temperature $T_{NB\text{-}NU}$ (in $T_{red}$ units) *versus* **γ**.

## 3. Conclusions

In this work, on the basis of a recently proposed molecular-field approach making use of a closed approximate form of the orientational Partition Function [12], we implemented the Minimax algorithm [8,5,13,14] within an in-house *Mathematica 11* [29] computer code, in order to carry out statistical thermodynamics simulations of virtual thermotropic biaxial nematics in the regime of partially repulsive orientational interactions. Many tests have been carried out to validate the reliability of the present upgraded code, with excellent results. This allowed us to extensively investigate biaxial systems constituted by board-like $D_{2h}$ particles. In particular, we were interested in shedding more light on the physical meaning of the γ and λ biaxiality parameters (weighting the biaxial extra-terms in the expression of the mean-torque potential) and their relationships, at a molecular level, with the geometrical parameters of the mesogenic particles. A significant, unequivocal correlation between the λ parameter and the relative flatness *B*/*L* of the mesogenic molecules emerged, whereas γ seems to be mainly related to the relative thickness *W*/*L* of the particles. Then, since the molecular flatness is more important than the thickness as a possible cause of phase biaxiality, λ confirmed to be dominant with respect γ in inducing the biaxial ordering, also for partially repulsive orientational interactions, as already recognized for fully attractive interactions [6]. Finally, last but not least, an explicit, quantitative linear dependence between the ratio of the $N_B$-$N_U$ and the $N_U$-*I* transition temperatures and the λ parameter has been found, whereas no physical dependence amongst the transition temperatures $T_{NB\text{-}NU}$ and the γ biaxiality parameter has been detected.

## Acknowledgments

The authors thank University of Calabria for financial support.

## Appendix A. Research and Classification of *Helmoltz Free Energy* (F) critical points in the Partially Repulsive Region of the Essential Triangle

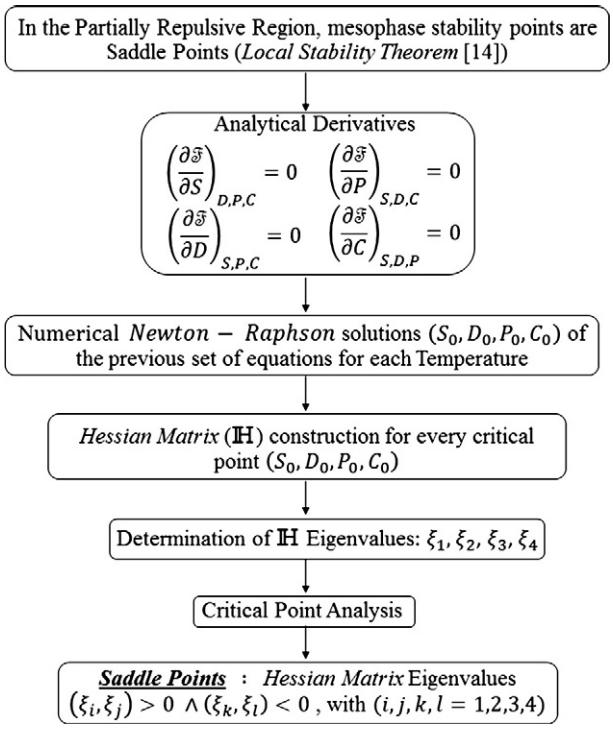


**Fig. A1.** Flow-chart describing the implemented Minimax algorithm for the search of Helmholtz Free Energy (F) stable points for partially repulsive orientational interactions.

## References


[1] W.H. De Jeu, Liquid crystalline materials: physical properties and intermolecular interactions, Phil. Trans. R. Soc. Lond. A 309 (1983) 217–229.
[2] G.R. Luckhurst, T.J. Sluckin (Eds.), Biaxial Nematic Liquid Crystals, J. Wiley & Sons Chichester, UK, 2015.
[3] J.P. Straley, Ordered phases of a liquid of biaxial particles, Phys. Rev. A 10 (1974) 1881–1887.
[4] A.M. Sonnet, E.G. Virga, G.E. Durand, Dielectric shape dispersion and biaxial transitions in nematic liquid crystals, Phys. Rev. E 67 (2003) 061701.
[5] G. De Matteis, F. Bisi, E.G. Virga, Constrained stability for biaxial nematic phases, Contin. Mech. Thermodyn. 19 (2007) 1–23.
[6] F. Bisi, G.R. Luckhurst, E.G. Virga, Dominant biaxial quadrupolar contribution to the nematic potential of mean torque, Phys. Rev. E 78 (2008) 021710.
[7] W. Maier, A. Saupe, A simple molecular theory of the nematic liquid-crystalline state, Z. Naturforsch. A 13 (1958) 564–566.
[8] F. Bisi, E.G. Virga, E.C. Gartland Jr., G. De Matteis, A.M. Sonnet, G.E. Durand, Universal mean-field phase diagram for biaxial nematics obtained from a minimax principle, Phys. Rev. E 73 (2006) 051709.
[9] S.S. Turzi, T.J. Sluckin, Symmetry adapted molecular-field theory for thermotropic biaxial nematic liquid crystals and its expansion at low temperature, SIAM J. Appl. Math. 73 (2013) 1139–1163.
[10] R. Rosso, E.G. Virga, Quadrupolar projection of excluded-volume interactions in biaxial nematic liquid crystals, Phys. Rev. E 74 (2006) 021712.
[11] B.M. Mulder, The excluded volume of hard sphero-zonotopes, Mol. Phys. 103 (2005) 1411–1424.
[12] G. Celebre, Statistical thermodynamics of thermotropic biaxial nematic liquid crystals: an effective, molecular-field based theoretical description by means of a closed approximate form of the orientational partition function, J. Mol. Liq. 209 (2015) 104–114.
[13] F. Bisi, S. Romano, E.G. Virga, Uniaxial rebound at the nematic biaxial transition, Phys. Rev. E 75 (2007) 041705.
[14] E.C. Gartland, E.G. Virga, Minimum principle for indefinite mean-field energies, Arch. Ration. Mech. Anal. 196 (2010) 143–189.
[15] L. Onsager, The effects of shape on the interaction of colloidal particles, Ann. N. Y. Acad. Sci. 51 (1949) 627–659.
[16] C.S. Shih, R. Alben, Lattice model for biaxial liquid crystals, J. Chem. Phys. 57 (1972) 3055–3061.
[17] R. Alben, Phase transitions in a fluid of biaxial particles, Phys. Rev. Lett. 30 (1973) 778–781.
[18] S.D. Peroukidis, A.G. Vanakaras, D.J. Photinos, Supramolecular nature of the nematic-nematic phase transition of hard boardlike molecules, Phys. Rev. E 88 (2013) 062508.
[19] S.D. Peroukidis, A.G. Vanakaras, Phase diagram of hard board-like colloids from computer simulations, Soft Matter 9 (2013) 7419–7423.
[20] B. Mulder, Isotropic-symmetry-breaking bifurcations in a class of liquid-crystal models, Phys. Rev. A 39 (1989) 360–370.
[21] H.N.W. Lekkerkerker, G.J. Vroege, Liquid crystal phase transitions in suspensions of mineral colloids: new life from old roots, Phil. Trans. R. Soc. A 371 (2013) (20120263 and refs. therein).
[22] E. Van den Pol, A.V. Petukhov, D.M.E. Thies-Weesie, D.V. Byelov, G.J. Vroege, Experimental realization of biaxial liquid crystal phases in colloidal dispersions of board-like particles, Phys. Rev. Lett. 103 (2009) 258301.
[23] E. Van den Pol, D.M.E. Thies-Weesie, A.V. Petukhov, D.V. Byelov, G.J. Vroege, Uniaxial and biaxial liquid crystal phases in colloidal dispersions of board-like particles, Liq. Cryst. 37 (2010) 641–651.
[24] G.J. Vroege, Biaxial phases in mineral liquid crystals, Liq. Cryst. 41 (2014) 342–352.
[25] B.J. Lemaire, et al., Physical properties of aqueous suspensions of goethite (α-FeOOH) nanorods (part I), Eur. Phys. J. E 13 (2004) 291–308.
[26] B.J. Lemaire, et al., Physical properties of aqueous suspensions of goethite (α-FeOOH) nanorods (part II), Eur. Phys. J. E 13 (2004) 309–319.
[27] Y. Martínez-Ratón, S. Varga, E. Velasco, Biaxial nematic phases in fluids of hard-boardlike particles, Phys. Chem. Chem. Phys. 13 (2011) 13247–13254.
[28] F. Biscarini, C. Chiccoli, P. Pasini, F. Semeria, C. Zannoni, Phase diagram and orientational order in a biaxial lattice model: a Monte Carlo study, Phys. Rev. Lett. 75 (1995) 1803–1806.
[29] Mathematica® Is a trademark of Wolfram Research, Inc.

Molecular Crystals and Liquid Crystals

ISSN: 1542-1406 (Print) 1563-5287 (Online) Journal homepage: https://www.tandfonline.com/loi/gmcl20

# Effect of epoxidized soybean oil on mechanical properties of bitumen and aged bitumen

Paolino Caputo, Michele Porto, Pietro Calandra, Maria Penelope De Santo & Cesare Oliviero Rossi

**To cite this article:** Paolino Caputo, Michele Porto, Pietro Calandra, Maria Penelope De Santo & Cesare Oliviero Rossi (2018) Effect of epoxidized soybean oil on mechanical properties of bitumen and aged bitumen, Molecular Crystals and Liquid Crystals, 675:1, 68-74, DOI: 10.1080/15421406.2019.1606979

**To link to this article:** https://doi.org/10.1080/15421406.2019.1606979

Published online: 27 Jun 2019.

Submit your article to this journal

Article views: 16

View Crossmark data

Full Terms & Conditions of access and use can be found at
https://www.tandfonline.com/action/journalInformation?journalCode=gmcl20

MOLECULAR CRYSTALS AND LIQUID CRYSTALS
2018, VOL. 675, NO. 1, 68–74
https://doi.org/10.1080/15421406.2019.1606979

Taylor & Francis
Taylor & Francis Group

Check for updates

# Effect of epoxidized soybean oil on mechanical properties of bitumen and aged bitumen

Paolino Caputo[a], Michele Porto[a], Pietro Calandra[b], Maria Penelope De Santo[c], and Cesare Oliviero Rossi[a]

[a]Department of Chemistry and Chemical Technologies, University of Calabria, 87036 Arcavacata di Rende (CS), Italy; [b]CNR-ISMN, National Council of Research, Institute for the Study of Nanostructured Materials, Via Salaria km 29.300, Monterotondo Stazione (RM), Italy; [c]Department of Physics and CNR-Nanotec, University of Calabria, via Bucci 31C, 87036 Rende (CS), Italy

**ABSTRACT**

Tuning the rheological properties of bitumens is extremely important for applicative purposes. This can be achieved by the use of chemical additives tuning the asphaltene-asphaltene and asphaltene-maltene interactions. We propose the use of an epoxy-resin to give more rigid and thermally stable bitumens on the basis of its tendency to form polymeric networks which would bridge asphaltene clusters. Rheometry confirmed this hypothesis and showed that a load of epoxy-resin as low as 0.1% gives the highest rigidity. Atomic Force Microscopy highlighted the structural changes at the basis of the observed effects.

The small amount of epoxy resin needed and its low-cost are elements deserving monitoring.

**KEYWORDS**

bitumen; additives; AFM; rheometry; epoxy-resin; asphaltene

## 1. Introduction

The use of asphalt for road pavement is well known throughout the world. Chemically, this material is made of macro-meter sized inorganic particles (93-96% w/w) hold together by an organic plastic binding agent, the bitumen, which confers to the overall asphalt the desired properties of plasticity, rigidity and stability. It is possible to improve these characteristics by the use of opportune additives interfering to the microstructure generally characterized by nano-meter sized aggregates of polar molecules (asphaltenes) organized in hierarchical structures[1], stabilized by resins and dispersed in an apolar phase of paraffins and aromatic oils[2,3]. For example, an additive tuning the red-ox state of the polar molecules can hinder oxidation-induced degradation, an adhesion promotion (acting on the inorganic/organic interfacial tension) can better disperse the inorganic particles among the bitumen matrix, an amphiphilic additive like lecithin can help in stabilizing the asphaltene clusters avoiding ageing[4]. In this ambit, we have recently observed that some additives can form a polymeric network (e.g. poly phosphoric acid) increasing the rigidity[5].

For this reason, in the light of the recent progresses in the field of intermolecular self-assembly in amphiphile-based and complex systems[6], we wanted to use a unique

CONTACT Pietro Calandra pietro.calandra@cnr.it; Michele Porto michele.porto@unical.it
© 2019 Taylor & Francis Group, LLC

additive to synergically stabilize the asphaltene clusters through strong additive-cluster chemical bonds and to form a polymeric network through additive reticulation. A soybean oil opportunely epoxidized has been therefore chosen as prototypal high-availability and low-cost additive fulfilling the desired requirements: its chemical structure suggests both strong chemical binding with asphaltenes and possibility to polymerize/reticulate. This strategy will turn out to be successful opening new possibilities in the realization of bitumens with desired properties.

## 2. Experimental part

### 2.1. Materials

The bitumen, kindly supplied by Loprete Costruzioni Stradali - Terranova Sappo Minulio - Calabria - Italy, had penetration grade, measured by the usual standardized procedure (ASTM D946)[7], (50/70). By the S.A.R.A. method[8], the concentrations (w/w %) of the four different portions (Saturates, Aromatics, Resins and Asphaltenes)[9] were found to be 3.8, 51.3, 21.5 and 23.4 respectively. The asphaltenes amount is typical of 50/70 grade bitumens.

The additive was an epoxidized soybean oil (EPOXOL D65) supplied by FACI S.p.a. (Carasco (GE) - Italy)

For the preparation of additive-containing bitumens, the epoxidized soy oil was added to a fully flowing hot bitumen ($150 \pm 10\,^{\circ}C$) at a desired content and stirred at 500–700 rpm by a mechanical stirrer (IKA RW20, Königswinter, Germany) for 30 min at the same temperature to allow homogenization. After that, cooling down was allowed.

Additive was also added, in various amounts, to bitumens aged through the Rolling Thin-Film Oven Test (RTFOT) method according to ASTM D2872-04, where aging is carried out by heating a moving film of bitumen in an oven for 85 min at $163\,^{\circ}C$. In this article, time aging was lengthened up to 225 min to emphasize aging effect.

### 2.2. Rheological Tests

The complex shear modulus $G^* = G' + i\,G''$ was measured in the regime of small-amplitude oscillatory shear at 1Hz as a function of temperature (temperature controlled by a Peltier element, uncertainty $\pm 0.1\,^{\circ}C$) by dynamic stress-controlled rheometer (SR5, Rheometric Scientific, Piscataway, NJ, USA) equipped with a parallel plate geometry (gap 2 mm, diameter 25 mm). Conditions were chosen after preliminary stress-sweep tests to guarantee linear viscoelastic conditions in all measurements. The real and imaginary parts define the in-phase (storage, measure of the reversible elastic energy) and the out-of-phase (loss, irreversible viscous dissipation of the mechanical energy) moduli, respectively. Their ratio is related to the phase angle $\delta$ according to $\tan\,\delta = G''/G'$.

### 2.3. AFM

Atomic Force Microscopy (AFM) was carried out by a Nanoscope VIII, Bruker microscope operating in tapping mode (150kHz). When the tip is brought close to the

surface, the vibration of the cantilever is influenced by the tip–sample interaction: shifts in the phase angle of vibration of the cantilever, implying energy dissipation in the tip-sample ensemble, are due to the specific mechanical properties of the sample. Cantilever with nominal tip radius of curvature 10 nm were used. Both topographic and phase images were recorded and they usually match.

## 3. Results and discussion

### 3.1. Rheology

The temperature dependence of the G′ and G″ measured at 1Hz (shown in Fig. 1a) can give several information. It can be seen that when temperature is increased all the samples are progressively softened (see the progressive decrease of G′). At a certain point G′ drops causing divergence in tan $\delta$. It must be noted that in this temperature range both G′ and G″ have a decreasing trend since the explored temperature window is on the high temperature side of the glass transition expected for these materials ($\leq$-4 °C [1]). In these conditions G″>G′ so it can be concluded that the samples behave as pseudo-plastic fluids.

From these rheological curves we have extracted:

1. the value of G′ at 50 °C (G′ @50 °C). This can be seen as an indicator of the mechanical property (rigidity) of the material under usage conditions;

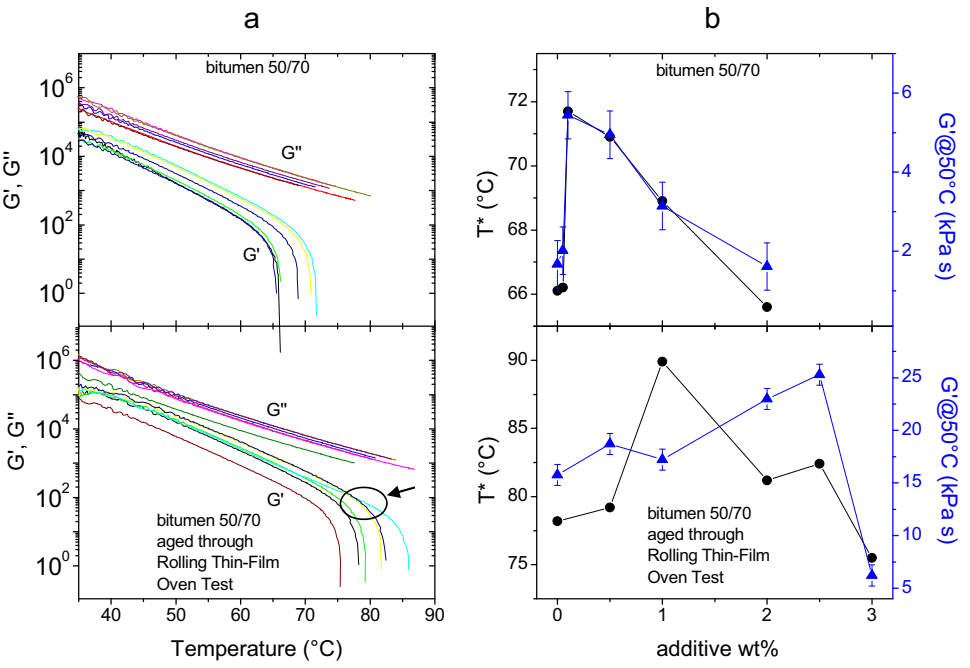


Figure 1. a) G′ and G″ as a function of temperature (top panel: bitumen 50/70; bottom panel: bitumen 50/70 aged); b) T* and G′@50 °C of pristine bitumens (top panel) and of aged bitumen (bottom panels) as a function of additive wt%

2. the temperature at which G′ drops (T*), which is the temperature at which the thermal motion is high enough to completely destroy the bitumen structure so that no elastic energy storage under mechanical stress is any more possible.

The values of T* and G′@50 °C are reported in Figure 1b. All the values change according to the additive amount.

Let's focus attention on the neat 50/70 bitumen (upper panels in Fig. 1). It can be noted that the addition of epoxidized soybean oil in small amounts (≈0.1% wt/wt) gives already increased rigidity. This also, confers to the bitumen increased thermal stability at higher temperatures, as resulting from the increased T* value of the sample with 0.1% wt/wt additive. Chemical arguments lead to the hypothesis that the epoxy-resin can bind asphaltenes through their polar functional groups. So, the increased overall rigidity and resistance to heating are consequence of the polymeric networks that epoxy-resins are expected to form and bridge the asphaltene clusters. An amount of epoxy-resin higher than that needed to saturate all the asphaltene polar functional groups and to form the polymeric network exert a detriment effect destabilizing the network so a drop in rigidity and T* takes place at additive content high enough (2% wt/wt in pristine bitumens). To test this hypothesis, the same experiments were carried out also on bitumens artificially aged through Rolling Thin-Film Oven Test (RTFOT, according to ASTM D2872-04, see experimental part), hereafter labeled as "aged" bitumens. After aging, asphaltene clusters are richer in polar functional groups thus offering more sites for additive binding. Therefore the additive was added in various amounts to such aged bitumens and the results are also reported in Figure 1 for comparison (lower panels). First of all, aged samples are obviously stiffer: T* values of aged bitumens are shifted to higher temperatures with respect to those of pristine 50/70 bitumens containing the same amount of additive. This is the result of the aging effect and the same consideration can be made by looking at G′@50 °C: the value is higher for aged bitumens than for pristine bitumens. Interestingly, it can be seen that also for aged samples a maximum exists, both for G′@50 °C and T*, but it is located at higher additive contents: the maximum in T* takes place at additive content of 1% wt/wt and the maximum in G′@50 °C takes place at additive content of 2.5% wt/wt. This confirms that the aging process, causing an increase in the number of polar chemical groups in asphaltenes, allows an increased number of additive molecules to bind asphaltenes thus further reinforcing the overall structure. As a result, the maximum in rigidity and T* occurs at higher additive content and the materials are generally more rigid and more resistant to temperature increase. Similarly to pristine bitumens, also in aged bitumens at additive amount higher enough a drop in G′@50 °C and T* takes place.

It deserves to be noticed that in pristine 50/70 bitumens maxima in T* and G′@50 °C are located at the same additive content, where in aged bitumens the two maxima are located at different additive contents. This comes from the different slope of G′ vs. temperature of the various aged samples (see Fig. 1a lower panel). Indeed, the sample at 1% wt/wt shows a discrete (but not the highest) rigidity at 50 °C but the best resistance to temperature increase. This causes the crossing of the curve belonging to 1% wt/wt composition with those belonging to 2% and 2.5% wt/wt. The crossing point has been marked in Figure 1 by a pointing arrow.

The additive therefore affects the bitumen rigidity differently according to the number of oxidized (aged) asphaltenes and this is consistent with our hypothesis of a network built by the additive and bridging the asphaltene molecules via direct interactions involving the polar groups.

### 3.2. Atomic Force Microscopy (AFM)

Atomic Force Microscopy has been used to analyze the topographical structure of the samples. Representative phase images are shown in Figure 2. In the unaged 50/70 bitumen (left panel) elongated clusters of 2 $\mu$m, with a rippled interior conferring the typical "bee" structure[10] dispersed in a quite uniform matrix, can be clearly seen. These aggregates are made of asphaltene clusters at different levels of aggregation, in accordance with a recent investigation[1]. In phase images darker regions are characterized by a lower rigidity. Asphaltene clusters shows the highest rigidity tuned accordingly to the rippled interior structure and the peripheral regions. The continuous medium (the so-called maltene) shows the lowest rigidity. By addition of additive at low content (see additive 0.1% panel) the size of asphaltene clusters is lowered and the bee structure reduced: this

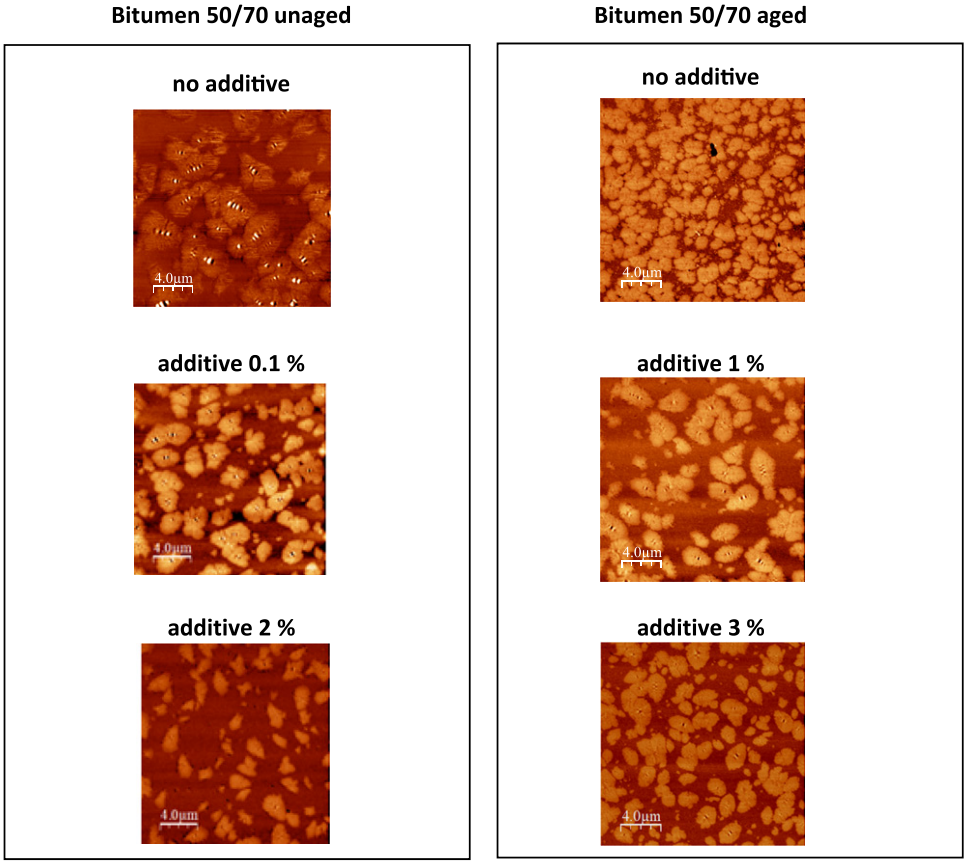


Figure 2. representative AFM phase images of the sample under investigation. For each sample the topographic and phase images usually match.

is a strong evidence of the fact that the epoxy-resin influences the morphology and structure of asphaltene clusters. Moreover, asphaltene clusters appear more rigid (see phase image) and forming a network. Taking into account for the fact that asphaltene clusters, usually of nano-meter size, form hierarchical self-assembled aggregates from nano- to meso- to micro- scale[1], the observed behavior means that the epoxy-resin is able to modify the aggregation pattern at the micro scale. A direct interaction between the epoxy-resin and the asphaltene clusters is therefore confirmed. At higher addition of additive (additive 2%) the asphaltene clusters rigidity looks decreased, the asphaltene "bee" structure is completely lost, the size of the clusters is further reduced and their "dilution" in maltene is observed. As a consequence, at this epoxy-resin amount, the overall rigidity is reduced. This behavior is in full accordance with the rheological data.

As for the aged bitumens (right panel), the neat bitumen shows already abundance of rigid asphaltene clusters as a consequence of the RTFOT aging procedure. The additive therefore exerts its effect by making asphaltene clusters even more rigid (see additive 1% panel) thus increasing the overall rigidity: in this situation an interplay of effects in rigidity (G′) and resistance to temperature (T*) characterize the samples, as a consequence of the fact that the additive affects the bitumen rigidity differently according to the number of oxidized (aged) asphaltenes (see discussion of rheological data). At higher additive content (see additive 3% panel), again, a lowering of asphaltene rigidity is observed. This is self-consistent with the unaged samples and again confirms rheological data.

## 4. Conclusions

We showed that an epoxidized soybean oil (epoxy-resin) can be used as additive to increase the rigidity in bitumens. This takes place thanks to the direct interactions between the epoxy-resin and the asphaltene clusters jointly to the inherent epoxy-resin tendency to form polymeric network. Rheological properties of bitumens containing various additive amounts showed that the optimal load of epoxy-resin is around 0.1% wt/wt: at this amount, maxima in rigidity (G′ at 50 °C) and resistance to temperature (temperature at which the bitumen starts flowing, T*) take place. Amount of additive higher than this has a detrimental effect as a consequence of the saturation of the asphaltene sites available for additive binding and their consequent dilution effect into the maltene phase which destructures the overall structure. Atomic Force Microscopy highlighted the additive effect to the asphaltene clusters which even lose their classical "bee" structure with a parallel increase in rigidity and formation of a network. The mechanism is confirmed by performing the additivation to bitumens which were previously aged by the Rolling Thin-Film Oven Test (RTFOT) method: aged bitumens, having more numerous polar functional groups, offer an increased number of sites for additive binding so they require a higher amount of epoxy-resin to maximize the rigidity (1% wt/wt) and resistance to temperature (2.5% wt/wt). The small amount of needed additive (less than half of the amount typically required in traditional additivation of 50/70 bitumens) and its low-cost are elements to be monitored for the future design of high-performances bitumens.

## References

[1] Pietro Calandra, Paolino Caputo, Maria Penelope Santo, Lorena Todaro, Vincenzo Turco Liveri, Cesare Oliviero Rossi. Effect of additives on the structural organization of asphaltene aggregates in bitumen, Constr. Build. Mater. 2018 in press.

[2] Rozeveld, S.; Shin, E.; Bhurke, A.; France, L.; Drzal, L. Network morphology of straight and polymer modified asphalt cements. *Microsc. Res.Tech.* 1997, *38*, 529–43.

[3] Lesueur D. The colloidal structure of bitumen: Consequences on the rheology and on the mechanisms of bitumen modification. *Adv. Colloid. Interface Sci.* 2009, *145*, 42–82.

[4] Oliviero Rossi, C.; Ashimova, S.; Calandra, P.; De Santo, M. P., Angelico, R. Mechanical Resilience of Modified Bitumen at Different Cooling Rates: A Rheological and Atomic Force Microscopy Investigation *Applied Science* 2017, *7(8),* a.n. 779; doi:10.3390/app7080779

[5] Gentile, L.; Filippelli, L.; Oliviero Rossi, C.; Baldino, N.; Ranieri, G. A. Rheological and H-NMR spin–spin relaxation time for the evaluation of the effects of PPA addition on bitumen. *Molecular Crystals and Liquid Crystals* 2012, *558(*1*)*, 54–63.

[6] Calandra, P.; Caschera, D.; Turco Liveri, V.; Lombardo, D. How self-assembly of amphiphilic molecules can generate complexity in the nanoscale. *Colloids and Surfaces A: Physicochemical and Engineering Aspects* 2015, 484, 164–183.

[7] Read, J.; Whiteoak, D. The Shell Bitumen Handbook, 5th ed.; Hunter, R.N., Ed.; Thomas Telford Publishing: London, UK, 2003

[8] Yoon, S.; Durgashanker Bhatt, S.; Lee, W.; Lee, H. Y.; Jeong, S.Y.; Baeg, J.-O.; Wee Lee, C. Separation and characterization of bitumen from Athabasca oil sand. *Korean J. Chem. Eng.* 2009, *26*, 64–71.

[9] Sheu, E. Y., Storm, D. A. Colloidal properties of asphaltenes in organic solvents. *Asphaltenes: Fundamentals and Applications*, E.Y. Sheu, O.C. Mullins (Eds), Plenum Press, New York City 1995, Chap.1

[10] Identification of Microstructural Components of Bitumen by Means of Atomic Force Microscopy (AFM) Andreas Jager , Roman Lackner , Christoph Eisenmenger-Sittner and Ronald Blab, Proc. Appl. Math. Mech. 4, 400–401 (2004). DOI 10.1002/pamm.200410181

applied sciences

MDPI

*Review*

# Bitumen and Bitumen Modification: A Review on Latest Advances

**Michele Porto [1,*], Paolino Caputo [1], Valeria Loise [1], Shahin Eskandarsefat [2], Bagdat Teltayev [3] and Cesare Oliviero Rossi [1,*]**

1 Department of Chemistry and Chemical Technologies, University of Calabria, Via P. Bucci, Cubo 14/D, 87036 Rende (CS), Italy; paolino.caputo@unical.it (P.C.); valeria.loise@unical.it (V.L.)
2 Department of Civil, Chemical, Environmental and Materials Engineering, University of Bologna, V.le Risorgimento 2, 40136 Bologna, Italy; shahin.eskandarsefat@unibo.it
3 Kazakistan Highway Research Institute, Nurpeisova Str., 2A, Almaty 050061, Kazakistan; bagdatbt@yahoo.com
* Correspondence: michele.porto@unical.it (M.P.); cesare.oliviero@unical.it (C.O.R.); Tel.: +39 0984492045 (C.O.R.)

Received: 21 December 2018; Accepted: 17 February 2019; Published: 20 February 2019


**Abstract:** This synthesis explores the state-of-the-knowledge and state-of-the-practice regarding the latest updates on polymer-modified bitumens (PmBs). The information in this study was gathered from a thorough review of the latest papers in the literatures related to modified bituminous materials, technologies, and advances. For this purpose, the paper is presented in two principle sections. In the first part, the bitumen itself is investigated in terms of chemical structure and microstructural systems. In the second part, the paper focuses on bitumen modification from different aspects for assessing the effectiveness of the introduced additives and polymers for enhancing the engineering properties of bitumen in both paving and industrial applications. In conclusion, the knowledge obtained in this study has revealed the importance of the chemical composition of base bitumen for its modification. It can be declared that while some polymers/additives can improve one or some aspects of neat bitumen properties, they can lead to compatibility problems in storage and production. In this respect, several studies showed the effectiveness of waxes for improving the compatibility of polymers with bitumen in addition to some benefits regarding warm mix asphalt (WMA) production.

**Keywords:** polymer-modified bitumens (PmBs); chemical structure; microstructural systems; spectroscopy; compatibility

## 1. Introduction

### *1.1. Bitumen Functionality*

According to the European specification (EN 12597), bitumen is defined as a virtually involatile, adhesive, and waterproofing material derived from crude oil, or present in natural asphalt, which is completely or nearly completely soluble in toluene, and very viscous or nearly solid at ambient temperatures [1]. It is well-accepted that the original characteristics of bitumen are highly dependent on its production and processing procedure, as well as bitumen crude oil characteristics [2]. Good crude oils and proper distillation processes can enhance bitumen properties. Generally, heavier crude oil gives higher bitumen yields [3]. Therefore, having a complete knowledge on the bitumen characteristics from different aspects is of paramount importance. This knowledge proves to be more important when, for some bitumen applications, some difficulties such as discontinuity in phase, mal-dispersion, and instability with polymers/additives make it challenging in the production and application of bituminous materials.

From a commercial point of view bitumen is a low-cost thermoplastic material that has been widely used in roofing and pavement application, paving mixtures, and industrial products for a long time. In both paving and industrial applications, the bitumen should be resistant to climate and more demanding traffic loads, for which reason rheological properties play a key role in different aspects [4–6]. From a functional point of view, the bitumen has to be fluid enough at high temperature (≈160 °C) to be pumpable and workable to allow for a homogeneous coating of aggregate upon mixing. Moreover, it has to be stiff enough at high temperatures to resist rutting (according to the local temperatures, ≈60 °C). Finally, it must remain soft and elastic enough at low temperatures to resist thermal cracking [4]. All the mentioned requirements are almost opposite, and most of the available neat bitumens would not provide all the needed characteristics together. Moreover, in some applications, the performance of conventional neat bitumens may not be satisfactory considering the required engineering properties because it is brittle in a cold environment and softens readily in a warm environment. This limited performance temperature range is the main drawback to neat bitumen, limiting its use for both roofing and road paving applications. In addition, as the traffic speed and load has dramatically increased, unplanned overloading has notably shortened the life of asphalt pavements, increasing its costs of maintenance and risks to users. Hence in order to enhance the performance properties of neat bitumen, to date, a variety of additives have been introduced and some have been used successfully for many applications. Modifiers and additives have been used to boost bitumen performance include: polymers, chemical modifiers, extenders, oxidants and antioxidants, hydrocarbons, and anti-stripping additives. The following sections are dedicated to the discussion about bitumen chemistry composition in order to describe the main features and mainly to describe the additives used over the last few decades of research, providing a comprehensive and in-depth coverage of the science and technology of bitumen modifiers.

### *1.2. Bitumen Chemistry*

From a chemical point of view, bitumen is defined as a viscous viscoelastic liquid (at room temperature) consisting essentially of hydrocarbons and their derivatives, which is totally soluble in toluene, substantially non-volatile, and softens gradually when heated [7]. It comprises a very great number of molecular species that vary widely in polarity and molecular weight [8,9]. Elemental analysis show that bitumen composition is primarily determined by its crude oil source and it is difficult to give a specific geographical generalization [10,11] (many suppliers also mix bitumen from different sources as well). This has been shown in a wide research by SHRP (Strategic Highway Research: Special Report) [12]. Based on this report, the main constituents of bitumen are carbon, which varies from 80 to 88 wt% and hydrogen ranging from 8 to 11 wt%. In addition, Heteroatoms and transition metal atoms (principally vanadium and nickel) are generally presents: sulfur (0 to 9 wt%), nitrogen (0 to 2 wt%), oxygen (0 to 2%), vanadium up to 2000 ppm, and nickel up to 200 ppm [10,13,14].

From a molecular point of view, the main compounds of the polar heteroatoms above are: sulphides, thiols and sulfoxides, ketones, phenols and carboxylic acids, pyrrolic and pyridinic compounds, and most metals form complexes such as metalloporphyrins [14]. Molecular weight distribution analysis shows that bitumen is a complex mixture of about 300 to 2000 chemical compounds (medium value 500–700) making a complete chemical characterization very difficult. For this reason, bitumen is generally fractionated by simpler methodologies, which allow two principal constituents to be identified:

I Asphaltenes
II Malthenes (also called petrolenes)

Maltenes are then classified into saturate, aromatic, and resin, which together with asphaltene are known as the bitumen SARA (Saturate, Aromatic, Resin, Asphaltene) fraction. The relative abundance of the SARA fractions allows the bitumen chemical composition to be related with its internal structure and some of its macroscopic properties [15]. However, it should be noted that

changes in experimental conditions (especially eluent nature) significantly affect the proportion of every bitumen fraction [10,16]. It is, therefore, important to specify the experimental setup condition for comparing the various chemical compositions of bitumen, even though they show some common features and overall properties that remain substantially unchanged.

#### 1.2.1. Asphaltenes

Asphaltenes, whose percentage in bitumen varies from 5 to 25% are amorphous brown/black solids at room temperature with particle dimensions between 5–30 μm, insoluble in n-heptane, but soluble in toluene [17,18]. Asphaltene contains oxygen, nitrogen, sulfur, and heavy metals (V, Ni, etc.) in the form of complexes such as metallo-porphyrins with long aliphatic chains (up to 30 carbon atoms), and pyrrolic and pyridinic rings. As demonstrated by UV-fluorescence spectroscopy [19,20], Fourier transform infrared spectroscopy (FTIR) [20,21], X-ray raman spectroscopy [22], and NMR spectroscopy [20,23,24], asphaltene molecules consists of fused aromatic rings, most probably between 4 to 10 units, together with some aliphatic chains as ring substituents, as shown in Figure 1.

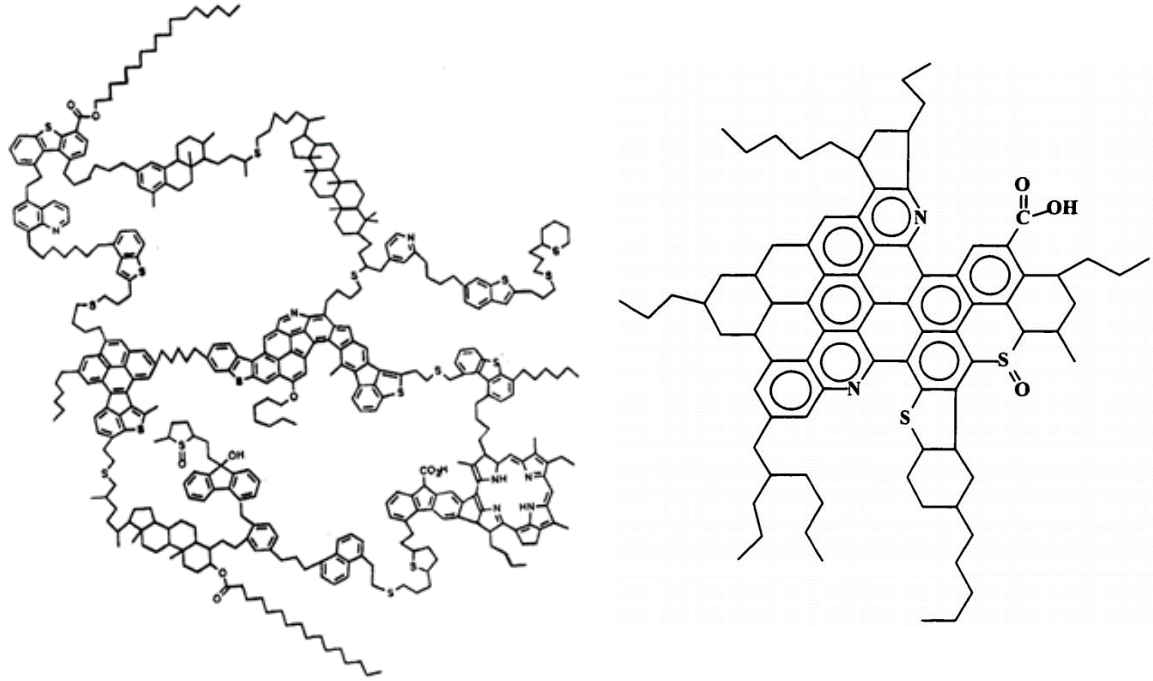


**Figure 1.** Asphaltene hypothetical structure: (**a**) Archipelago structure, and (**b**) continent structure (reprinted from [25,26] with the permission of the American Chemical Society and OnePetro).

Owing to the presence of many condensed aromatic rings, asphaltenes form an almost planar structure that can associate by π–π bonding interaction to form graphite like structures (see Figure 2) [21,27].

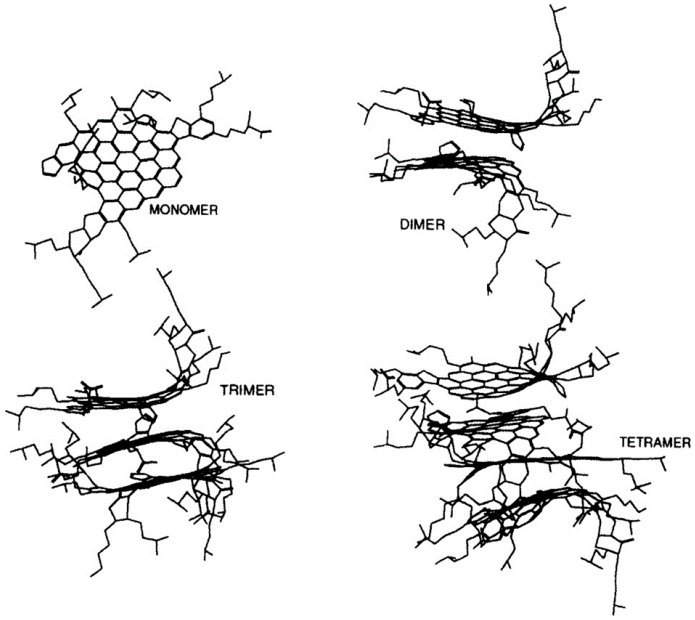


**Figure 2.** Monomeric, dimeric, trimeric, and tetrameric structure of a Venezuelian asphaltene molecule (reprinted from [28] with permission of the American Chemical Society).

X-ray diffraction spectra of solid asphaltenes [29–31] have shown two main peaks: one amorphous at a $2\theta = 19^{\circ}$, mainly due to the aliphatic structures of the molecules, and a very wide diffraction peak at $2\theta = 26^{\circ}$, corresponding to the Bragg angle scattering of the (0,0,2) planes of graphite, meaning that the graphite-like crystals of asphaltene aggregates are very small [4]. As reported by Yen et al. [30] based on the half-width of the diffraction peak, they estimate the graphite-like structure size in the order of 2–5 nm with an average of five-unit sheets (see Figure 3).

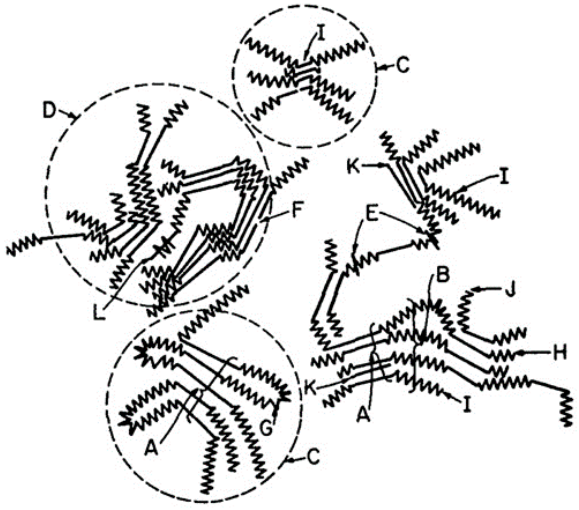


**Figure 3.** Yen model of solid asphaltenes (reprinted from [28], with permission of the American Chemical Society).

Asphaltene aggregation is still maintained in solvent, where they associate to form the so-called "micelles" [14,32–35] whose size is principally determined by the solvent nature, asphaltene content, and temperature [28,29,35]. Asphaltene graphite-like stacking of the molecules has as consequences a

high degree of electron delocalization, giving an overall negative charge [27,36] a permanent electrical charge [37], and a dielectric constant between 5 and 7 [38–40]. Finally, asphaltene association also has particular effects on the rheological behavior of bitumen [41–43]. A more detailed study on the asphaltene nature can be found in [44].

#### 1.2.2. Saturates

The saturated components in bitumen typically are within 0–15 wt% of the overall fraction. From a chemical point of view, saturates are complex mixtures of polyalkyl structures in which straight chain paraffins prevail as shown by FTIR measures [21]. Saturated fractions from blown bitumen are richer in long-chain paraffins than those from straight-run bitumen [45]. The saturate fraction is a mixture of pure aliphatics (linear and cyclic) [4]. As the content of saturates increases a decrease in the complex shear modulus and an increase in the phase angle of bitumen is expected because the saturate fraction is the lightest part of the maltenes, whereas the latter are a liquid part of bitumen which is complemented with solid asphaltenes [45,46].

#### 1.2.3. Resins

Resins are dark brown solid (or semi-solid) compounds characterized by particle sizes of 1–5 nm, soluble in n-heptane, and structurally and compositionally similar to asphaltenes, except for a lower molar mass [47]. Resins are present in an amount ranging from 30 to 45 wt% and sometimes can be more polar than asphaltenes, but with less condensed aromatic rings [17]. Their polar nature enhances the adhesive properties of bitumen, but their principal role is as dispersing agents for the asphaltene macromolecular structures and oils, which are mutually insoluble. When bitumen is oxidized, resins gain oxygen molecules and the similarity of their structure to asphaltenes is enhanced. The bitumen characteristics are determined largely by the resins' asphaltene ratios [48].

#### 1.2.4. Aromatics

Aromatic oils are dark brown viscous liquids containing low molecular weight aromatic compounds. They have a slightly aliphatic carbon skeleton with lightly condensed aromatic rings and a molar mass ranging between 300 and 2000 g/mol. Aromatic oils make the highest fraction (40–65%) of bitumen. They have a high solvent power relative to high molecular weight hydrocarbons. Together with saturated oils they are considered as the plasticizing agents of bitumen [17].

## 2. Bitumen Polymers

Polymers are macromolecules synthesized through chemical reaction between smaller molecules (monomers) to form long chains. The physical properties of the resulting polymer are determined by the chemical structure of the monomers and by their sequence inside the polymer. A combination of two different monomers that can be in a random or block arrangement gives a so-called copolymer. Polymers include a broad range of modifiers with elastomers and plastomers being the most commonly-used types. Polymer-modified bitumens (PmBs) are produced by the mechanical mixing or chemical reactions of a bitumen and one or more polymer in a percentage usually ranging from 3% to 10%, relatively to the weight of bitumen. In the first case, the mixtures are said to be simple, because no chemical reactions occur between the two partners in the system. In this case, the polymer is considered as a filler which gives specific properties to the mixture. In the second case, the mixtures are said to be complex, because chemical reactions or some other interaction occurs between the two partners in the system [49].

Modified bitumens are characterized as a two-phase system: bituminous, prevalently as asphaltenic matrix, and polymeric matrix, which has been investigated from two different points of view.: (1) the complex interaction mechanism between bitumen and additive and (2) the influence of different type of bitumen modifiers aiming to study the rheological performance

characteristics, temperature sensitivity, morphology, thermal behavior storage stability, and aging of the resulting PmBs.

From a bitumen/polymer interaction mechanism point of view, according to Polacco et al. [50], polymer modification results in a thermodynamically unstable but kinetically stable system in which the polymer is partially swollen by the light bitumen components (maltenes) and can swell up to nine times its initial volume [51]. Competing for bitumen's light fractions, polymers tend to induce the micelles aggregation of the asphaltenes or to increase their degree of association, according to the nature of the original bitumen. At high temperatures, a relatively low viscosity of the melted micro-heterogeneous polymer-modified bitumen allows the substances with similar structure and polarity to form their domains: the swollen polymers and the asphaltenes. However, the thermodynamic instability of this system induces a phase separation (or sedimentation) under the influence of the gravitational field. Therefore, associated asphaltene micelles can settle to the bottom of the blend during static hot storage. According to this mechanism, the degree of phase separation of polymer modified binders can be influenced by storage conditions such as temperature and time. As shown by Lu et al., the phase separation will mainly be governed by the nature of the base bitumen and the characteristics and content of the polymer [8]. To date, different types of additives and polymers have been used for bitumen modification [52]. Table 1 summarizes the most common types of additives used as bitumen modifiers.

**Table 1.** Examples of additives used to modify bitumen (reconstructed from [52] with the permission of Thomas Telford).

| Type of Modifier | Examples | Abbreviation |
|---|---|---|
| thermoplastic elastomers | Styrene–butadiene elastomer | SBE |
| | Styrene–butadiene–styrene elastomer (linear or radial) | SBS |
| | Styrene–ISOPRENE–STYRENE elastomer | SIS |
| | Styrene–ethylene–butadiene–Styrene elastomer | SEBS |
| | Ethylene-propylene-diene terpolymer | |
| | Isobutene–isoprene random copolymer | IIR |
| | Polyisobutene | PIB |
| | Polybutadiene | PBD |
| | Polyisoprene | PI |
| latex | Natural rubber | NR |
| thermoplastic polymers | Ethylene–vinyl acetate | EVA |
| | Ethylene–methyl acrylate | EMA |
| | Ethylene–butyl acrylate | EBA |
| | Atactic polypropylene | APP |
| | Polyethylene | PE |
| | Polypropylene | PP |
| | Polyvinyl chloride | PVC |
| | Polystyrene | PS |
| thermosetting polymers | Epoxy resin | |
| | Polyurethane resin | PU |
| | Acrylic resin | |
| | Phenolic resin | |
| chemical modifiers | Organometallic compounds | |
| | Sulfur | S |
| | Phosphoric acid, polyphosphoric acid | PA, PPA |
| | Sulfonic acid, sulfuric acid | |
| | Carboxylic anhydrides or acid esters | |
| | Dibenzoyl peroxide | |
| | Silanes | |
| | Organic or inorganic sulfides | |
| | Urea | |
| recycled materials | Crumb rubber, plastics | |
| fibers | Lignin | |
| | Cellulose | |
| | Alumino-magnesium silicate | |
| | Glass fibers | |
| | Asbestos | |
| | Polyester | |
| | Polypropylene | PP |
| adhesion improvers | Organic amines | |
| | Amides | |
| anti-oxidants | Phenols | |
| | Organo-zinc or organo-lead compounds | |
| natural asphalts | Trinidad Lake Asphalt | LA |
| | Gilsonite | |
| | Rock asphalt | |

In Table 2 are summarized the most common used modifiers found in the literature, which are discussed in this paper.

**Table 2.** Different categories of polymers mainly used in bitumen modification.

| | |
|---|---|
| **Thermoplastics Polymers (see Section 2.1)** | Polyethylene (PE)<br>Polypropylene (PP)<br>Ethylene-Vinyl-Acetate (EVA)<br>PVC<br>EBA |
| **Thermoplastic Elastomers (see Section 2.2)** | Styrene-Butadiene-Styrenhe-Block copolymers (SBS)<br>Styrene-Isoprene-Styrene-Block copolymers (SIS) |
| **Thermosets (see Section 2.3)** | Epoxy resin<br>Polyurethane resin<br>Acrylic resin<br>Phenolic resin |
| **Natural and Synthetic Rubbers (see Section 2.4)** | Styrene-Butadiene rubber (SBR)<br>Natural rubber<br>Polydiolefins<br>Reclaimed Tire rubber |
| **Bitumen Chemical Modifier (see Section 3)** | Sulphur (S)<br>Polyphosphoric acid (PPA)<br>Reactive Polymers<br>Maleic Anhydride (MAH)<br>Nanocomposite Modifiers |
| **Warm Mix Asphalt methodology (see Section 4)** | |

Each of these groups associate with different pros and cons as a bitumen additive. In addition to the large group of polymers, other bitumen modifiers, such as polyphosphoric acid (PPA), sulfur, maleic anhydride, and different kinds of clays, have been introduced and experienced, in this respect, some success.

### *2.1. Thermoplastics Polymers*

Polyolefinic plastomers, also known as thermoplastics, whose category includes: Polyethylene (PE), polypropylene (PP), ethylene vinyl acetate (EVA), ethylene butyl acrylate (EBA), and polyvinyl chloride (PVC). Polyethylene which can be found in in three forms; low-density polyethylene (LDPE), high-density polyethylene (HDPE), and linear low-density polyethylene (LLDPE) are the most common plastomers. The use of plastomers as polymers to obtain PmBs arose as a consequence of the high costs of the styrenic polymers and the degradation phenomena due to their unsaturations. On the contrary, polyolefinic plastomers have a low cost and high availability presenting also higher stability than styrenic ones. Polyolefin polymers addition generally increases the bitumen stiffness and a good rutting resistance [53,54]. For these reasons plastomers play a leading role in PmBs in which they represent about 15% of the reference market. Reclaimed polyethylene is recovered from low-density domestic waste PE carry bags. Punith and Veeraragavan investigated an 80/100 paving-grade bitumen with different PE ratios [55]. The blends were tested using Hamburg wheel track tests, resilient modulus tests, an indirect tensile test, and an unconfined dynamic creep test. The results analysis showed that the PE-modified asphalt mixtures exhibited better performance characteristics than conventional mixtures. Even though polyethylene and polypropylene are the most common plastomers used, their non-polar nature results in compatibility problems with bitumen also sharpened by their tendency to crystallize which deeply restricts the interaction with bitumen [4,56]. In addition to compatibility problems of thermoplastics, these kinds of polymers also failed to increase the bitumen elasticity [53]. In an attempt to avoid the problems of compatibility and crystallization, other kinds of thermoplastics have been introduced. Principally, these modified polymers are obtained by inserting acetate groups, producing ethylene vinyl acetate (EVA) with vinyl acetate group content higher than 14%, ethylene methyl

acrylate (EMA), and ethylene butyl acrylate (EBA). Esters groups of these polymers have the double advantage of increasing the polarity and reducing their crystallization tendency, disrupting the closely packed crystalline microstructure [50]. Both factors increase the bitumen compatibility and storage stability of the blend. In general, relative to the compatibility of plastomers with the bituminous matrix, it is believed that the higher the ester fraction is, a lower crystallinity is achieved. However, the crystallinity degree must be carefully balanced. If the crystallinity degree is to low, the lattice formed tends to be disrupted early after the crystals are interlocked with the bituminous fraction. In the EVA case, the optimal crystallinity degree is obtained using vinyl-acetate percentage ranging from 14% to 28%. However, despite the enhanced properties obtained by using EVA and other similar polymers, like compatibility, the problem of elastic recovery of polymer-added bitumen still remains [50,53,57]. Furthermore, the glass transition temperature of EVA which is dependent on the acetate content is not low enough to improve significantly the low-temperature properties of bitumen [58]. In this respect, Ameri et al. demonstrated that bitumen resistance to low-temperatures cracking can be increased by an amount of added EVA ranging between 2% to 4%, whereas it is decreased adding about 6% of EVA [59].

### *2.2. Thermoplastic Elastomers Modified Bitumen*

Thermoplastic elastomers can resist permanent deformation over stretching, and elastically recovers once the load is removed [53,60]. Generally, thermoplastic elastomers used as modifiers are block copolymers of mono- or di-olefins. As mono-olefin unit the styrene molecule is used as mesomer, whereas as diolefin the butadiene or isoprene unit are normally used. The corresponding elastomers are called styrene butadiene styrene (SBS), styrene isoprene styrene (SIS), styrene-ethylene/butylene-styrene (SEBS).

Thermoplastic elastomer structure is generally linear and is characterized by weak inter-chain linkage. However, radial SBS copolymer are widely used as a bitumen modifier. Figure 4 represents the linear and radial SBS structures.

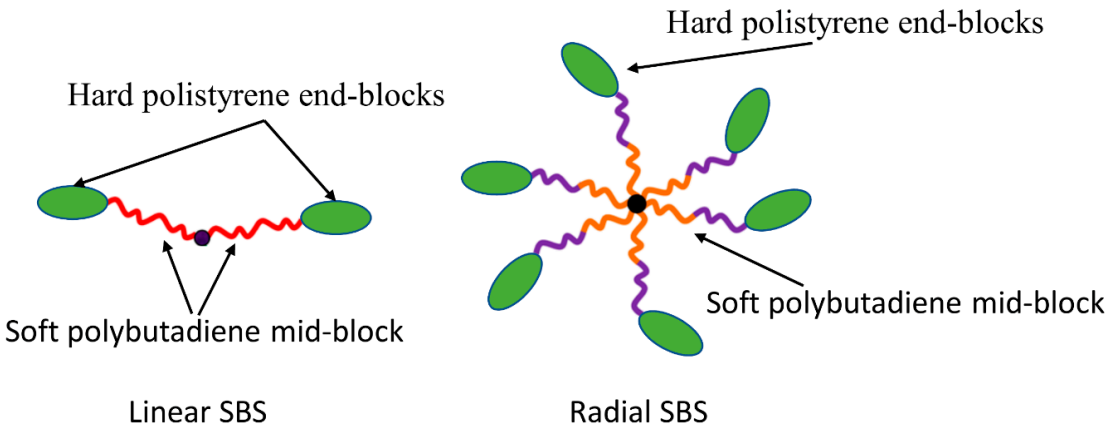


**Figure 4.** Representation of linear and radial SBS (reconstructed from [61] open access).

As can be seen in Figure 4 the linear polymer is characterized by two polystyrenic blocks linked to a two-polybutadiene block, while in the radial structure polystyrene blocks make a radial configuration around the polybutadiene block. This structure distinction is decisive because it characterizes the final performances of the blend. It has been noted that radial structure offers a higher system stability and a better redistribution of the elastic and viscous components of bitumen. The elastic and sturdiness feature of styrenic elastomers are due to a three-dimensional lattice formed by the physical interlocking of the molecules. The three-dimensional vertexes of the lattice are formed by polystyrenic blocks, which form separated domains in a rubber matrix formed by polybutadiene units. A schematic representation is shown in Figure 5.

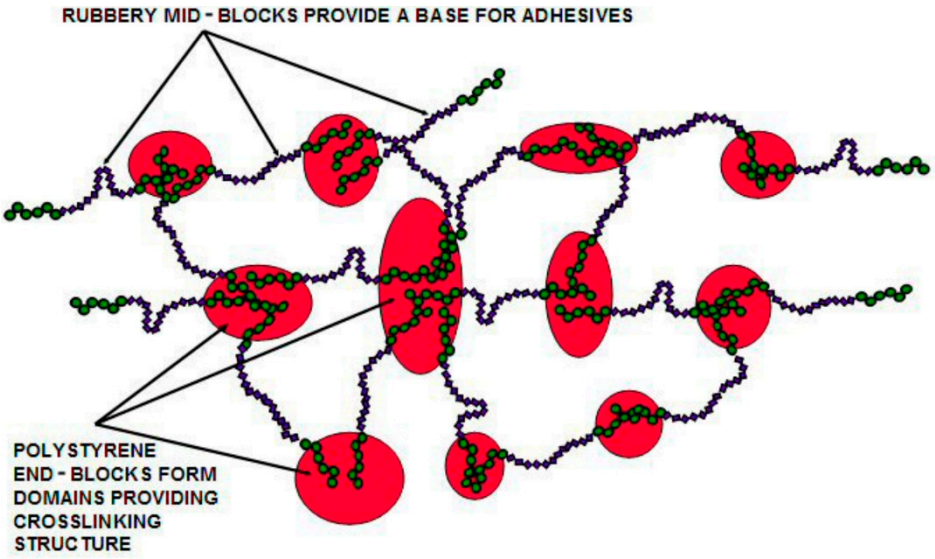


**Figure 5.** Schematic representation of styrene-butadiene block copolymer morphology (reprinted from [62]).

Polystyrenic blocks are responsible for the sturdiness of the polymers while polybutadiene blocks give elasticity. At temperatures above the glass transition of polystyrene (Tg = 100 °C) the latter softens with a consequent weakness of the PS domains. This allows an easier bitumen treatment. Upon cooling to room temperature, styrenic blocks reaggregate to re-form rigid domains restoring sturdiness and elasticity. Once SBS polymer is added, some interactions happen between the bitumen and SBS. Polystyrene blocks swell by absorbing light components of bitumen, which causes the hardening of the bitumen [63,64].

The repeatedly reported excellent properties, relatively good dispersibility in bitumen (dependent on the base bitumen composition), and acceptable cost have made SBS popular as a bitumen modifier. Many studies showed that the addition of SBS to the bitumen increases the softening point, decreases the penetration slightly, lessens the thermal susceptibility, increases the viscosity and decreases the Frass breaking point. It has also been observed that SBS moderates the increasing of stiffness due to the oxidation process simulated by short and long-term aging maintaining almost unaltered virgin bitumen properties also following RTFOT (Running Thin Film Oven Test) treatments.

The SBS concentration plays a fundamental role in polymer-added bitumen properties. Bitumen modification can be done by adding up to 7% of elastomers and, in some cases, different polymers can be used contemporarily. For soft and medium modifications polymer quantities are less than 4.5% (about 3% for soft modification and 4.2% for medium modification). For hard modifications added quantities are higher than 5%, while at low concentrations, SBS is dispersed as a discrete phase in bitumen, increasing the SBS concentration results in a phase inversion and two interlocked continuous phases are obtained: the bitumen rich phase and SBS rich phase typically shown in Figure 6. The latter is characterized by two sub-phases: one formed by a swollen polybutadiene matrix and polystyrene domains [63].

In spite of many proven benefits regarding the use of SBS copolymers for bitumen modification, they are still far from perfect. For example, the compatibility between bitumen and SBS is not always that good and storage instability of SBS modified bitumen was reported even for bitumens containing a low quantity of polymer [66–68]. In other words, the same level of compatibility may not be obtained with different base bitumen as in the example shown in Figure 7. In this respect, Airey has observed a competition between thermoplastic elastomers and asphaltenes to absorb the light components of bitumen in SBS/bitumen blends [64]. An insufficient amount of light components induces phase separation in modified bitumen. It was also noted that to produce a compatible and stable SBS modified bitumen a high aromatic content in the latter could be helpful [69]. In this respect, it has been

observed that an improvement in compatibility between SBS and some bitumens with low aromatic content could be achieved by the addition of aromatic oils [65]. However, too high an aromatic content (70–80%) in modified bitumen can lead to swelling and anti-plasticization (i.e., an increase in its glass transition temperature) of some polystyrene blocks [70], which is not good for the resulting properties of the modified bitumen. Lu et al. concluded that for the bitumens containing 50–60% of aromatic components, blends with linear SBS provide greater stability than those with radial SBS copolymer [71].

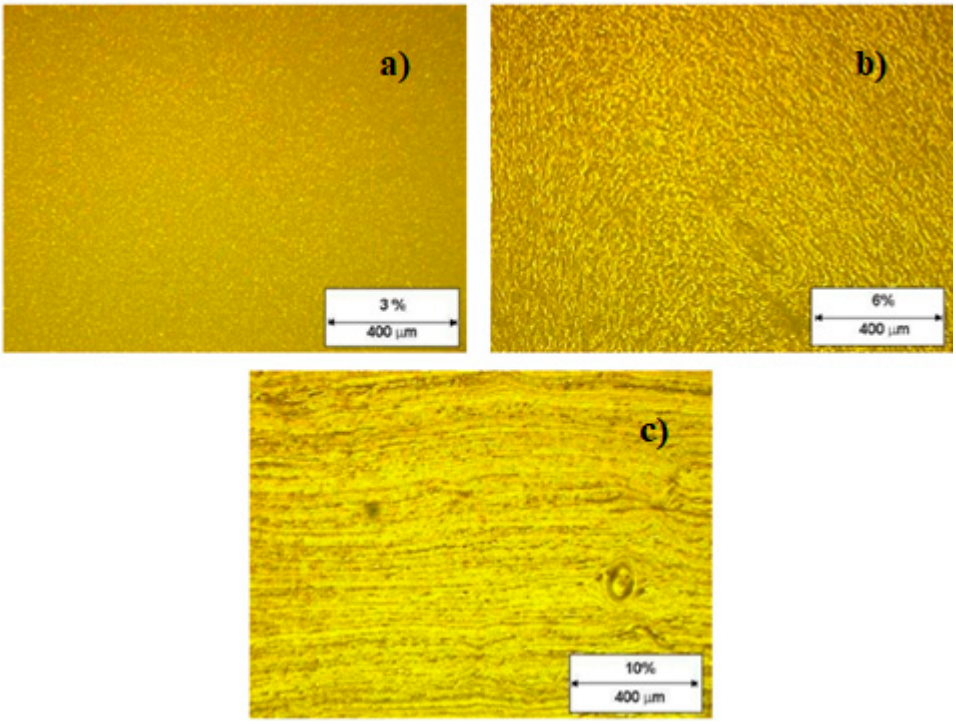


**Figure 6.** Dispersion of: (**a**) 3%, (**b**) 6%, and (**c**) 10% (*w*/*w*) of linear SBS obtained by fluorescence microscopy (reprinted from [65] with the permission of the American Chemical Society).

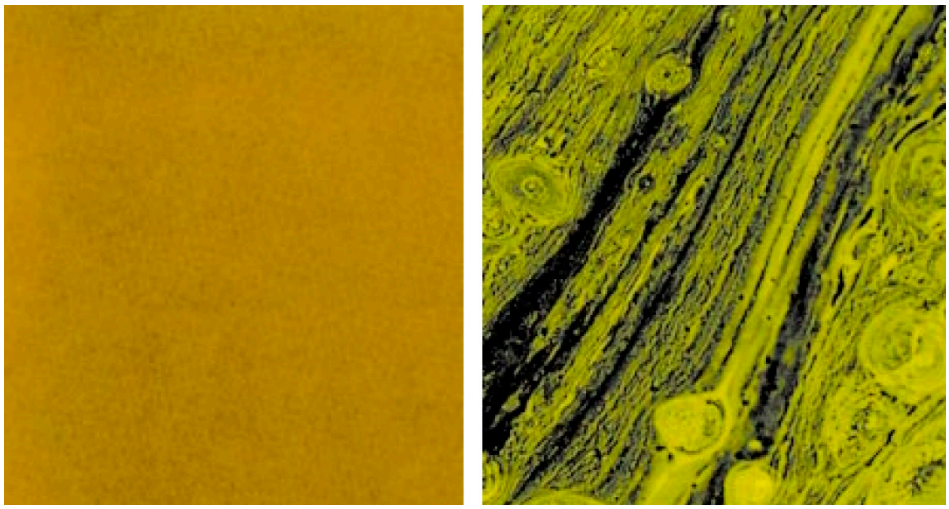

(**a**) (**b**)

**Figure 7.** (**a**) A compatible system with 4% SBS and (**b**) an incompatible system with 4% of SBS content (reprinted from the Shell Bitumen Industrial Handbook with permission of SHELL Publisher).

In addition to polymer chemical structure and concentration, it has been shown that the molecular weight of the polymer is also of paramount importance to bitumen/polymer compatibility. It has been

shown that, an increase in molecular weight decreases entropy and blend stability. In this respect, linear and radial SBSs with similar S/B ratios were used by Lu et al. to study their respective blend stability. It has been observed that the use of the linear SBS produces a higher-stability blend than the radial one. This was ascribed to the lower molecular weight of the linear SBS used than the branched one. However, as Polacco et al. declares it is doubtful that a significant difference would have been observed if the linear and branched copolymers had similar molecular weights due to differences in molecular structure [46].

### 2.3. Thermosets

Thermosetting plastics (TP)—two liquid compounds (resin and hardener) — are first blended together and then with the bitumen a few seconds before application as surface coating/surface dressing (main use) or before mixing with aggregates for the production of hot asphalts (occasional use) [72]. Thermosetting plastics are polymers that turn into a solid state while heated or impose hardness. Before hardening, TP molecules have a linear structure, the same as thermoplastics molecules, but the size of their molecules is significantly smaller. TP molecules are chemically active. They contain either double (unsaturated) bonds or other chemically active groups. Therefore, under certain conditions (at heating, irradiation, or adding hardeners) thermosetting molecules react with each other and form a continuous network. Epoxy, phenol-formaldehyde, carbamide, polyester, silicone, and other resins belong to TP [73]. It has been shown that when epoxy thermosets polymers are blended with bitumen the modified bitumen displays the properties of the epoxy rather than those of the bitumen [74]. Since the epoxy bitumen presents the properties of the thermosetting polymer, the available time to use the modified bitumen is limited and is determined to a great extent by the mixing temperature. The higher the temperature, the shorter is the time of use. After producing, the thermosetting bitumen begins to 'cure' and increase its strength (hardens) once it is applied. The curing time is according to ambient temperatures. The higher the ambient temperature, the longer is the curing time. Once curing is completed, future temperature increase, which would soften the conventional bitumen, does not affect the hardness of the thermosetting bitumen at all. The completely cured bitumen is designated as an elastic material having no viscous behavior. Even though the PmBs with thermosetting plastics have relatively high adhesion to the mineral particles and great strength they are not common for paving applications. This is because firstly, when entering these polymers, owing to the imposed hardening, the technological properties of PmB are almost immediately deteriorated; secondly, the rigidity of the PmB is increased at low temperatures, which results in increased thermal sensitivity; thirdly, the use of TP complicates the system and raises its price; and finally, the effectiveness of thermosetting plastics appears usually at their large quantities in bitumen (more than 10 wt%). Asphalt mixtures produced with thermosetting polymer-modified bitumen have excellent adhesive ability, excellent resistance to deformation, excellent fatigue performance, and high stiffness modulus.

### 2.4. Natural and Synthetic Rubber

#### 2.4.1. Natural Rubber

Natural rubber polymer could be easily synthesized through the chemical reaction of isoprene molecules. The resulting compound, the cis-1,4-polyisoprene with a chemical formula of $(C_5H_8)_n$ with high molecular weight is analogous to natural rubber [75,76]. In each repeated unit of polyisoprene, the double bond presence makes the polymer easily undergo a vulcanization process. This consists in the addition of sulfur to change the properties of natural rubber into a thermoset [77]. From a physical point of view, the presence of complex molecular chains of polyisoprene gives natural rubber a large elasticity and resilience characteristics [78]. For practical application of natural rubber, vulcanization is needed. However, in this process rubber creates disulfide bonds between chains, limiting its degree of freedom and the chains speedily tighten. Thus, the rubber is harder and less extensible because of an increasing in elastic force [79].

Natural rubber latex has been applied in the bitumen industry for over 30 years and is perceived to have potential for improving bitumen binder performance by improving thermal sensitivity, flexibility, stability, and stripping. In terms of thermal sensitivity, while at low temperatures it helps to dissipate the developed stress, preventing asphalt concrete cracking, at high temperatures it acts as a membrane, controls the asphalt flow, enhancing shear resistance [80]. In addition, its inherent elastomer properties proved that natural rubber latex has great potential for improving the long-term pavement performance of asphalt concrete [81].

It has been found that rubberizing asphalt concrete not only increases the rut resistance, but also enhances fatigue life with the increase in resilient modulus [82,83]. In addition to improving the mechanical and performance properties of asphalt concrete, in a study using both the Marshall method and a gyratory compacter it has been shown that natural rubber decreases the optimum binder content in asphalt concretes, increasing its density and stability [84]. From another point of view, liquid natural rubber (LNR) was found to be more efficient than latex for the aim of modifying bitumen binders. This is mainly because LNR blends easier with a binder, which results in a homogeneous binder [85]. In this form, natural rubber has more benefits compared to its conventional form, and the properties of the blend are comparable to those produced with synthetic rubbers.

Despite the benefits regarding the use of natural rubber in bitumen binder modification, there are some drawbacks that limit its use on a large industrial scale. Natural rubber is a highly valuable biomaterial compared to other biopolymers, hence natural rubber has been commercialized into synthetic rubber. This is mainly because of the huge difference between the available produced amount and the demand. From another point of view, even if several studies showed some benefits about the bitumen binders modified with natural rubbers for paving applications, there are still some doubts regarding to asphalt concrete performance and mechanical properties throughout the performance temperature range [86,87].

#### 2.4.2. Synthetic Rubber

Synthetic rubber is a man-made rubber which is produced in manufacturing plants by synthesizing it from petroleum and other minerals. Synthetic rubber is basically a polymer or an artificial polymer. It has the property of undergoing elastic stretch ability or deformation under stress, but can also return to its previous size without permanent deformation. Styrene butadiene rubber (SBR), polyisoprene, and polybutadiene, polychloroprene, and tire rubber are some of the synthetic rubbers commonly used today. From the mentioned categories, synthetic rubber obtained from end-of-life tires (ELTs) are common for producing rubberized bitumen binders for both paving and industrial application. To date many studies have investigated synthetic rubbers from different points of view. From these studies, it can be concluded that many factors can influence the performance and mechanical properties of rubberized binders including: the size and content of rubber [88–90], the chemical structure [91,92], particles surface properties (ambient granulating or cryogenically crushed tire rubber) [93], blend production method and temperature [94,95].

Among the aforementioned factors, probably the most important one is the optimum percentage of rubber in the binder. Many research works have been conducted comparing the performance and mechanical properties of mixtures containing different amounts of rubber. However, it greatly depends on the application method (dry or wet), when it is used in asphalt mixtures and the characteristics of the base binder. Regarding rubberized bitumen, ASTM D6114 defines asphalt rubber (rubberized bitumen) as material consisting of the virgin binder and a minimum of 15% crumb rubber (by the weight of total blend) [96]. In addition, many studies concluded that while a low rubber content, around 4% (to the weight of bitumen), has almost no effect, or at least no significant effects on the performance and mechanical properties of the binder, more than 20% was found to be unsuitable.

## 3. Bitumen Chemical Modifiers

Systematic investigation of mechanical, rheological, and aging properties, temperature sensitivity, morphology, and thermal behavior of different PmBs has shown some advantages and drawbacks [6,97–111]. First of all, it has been shown that polymer modification improves some of the properties of bitumen, such as better elastic recovery, higher cracking resistance at low temperatures, and higher rutting resistance at high temperatures [96,97,102]. Secondly, some drawbacks have been observed, such as thermal instability and PmB's phase separation problems [68,79]. The first attempts to overcome the PmB's drawbacks were started in the early 1990s, when Giavarini et al. claimed that PmBs could be stabilized by adding polyphosphoric acid (PPA) [112]. They also believe that PPA could help to improve storage stability of polypropylene-modified bitumens by changing the bitumen structure from sol to gel. From then, various attempts have been made to remove the drawbacks of the PmBs. In addition to physical blends of bitumens and polymers, another way to improve the binder properties is through chemical modification, which uses the chemical agent as an additive to modify the characteristics of pure bitumen.

To date many chemical agents have been introduced for the target of bitumen modification, such as: organo-metallic compounds [113,114], sulfur (S) [66,115–121], polyphosphoric acid (PPA) [122–124], sulfonic acid [125], carboxylic anhydrides [126–128], silanes [129,130], thiourea dioxide [131], nanocomposite-modified bitumen [132–140], and reactive polymers [141–155]. However, from the above-mentioned chemical compounds only a few of them have been used practically. Sulfur (S), polyphosphoric acid (PPA), reactive polymers, maleic anhydride (MAH), and polymer/clay or polymer/layered silicate (PLS) nanocomposites are the most common chemical agents.

### *3.1. Sulfur Modifier*

The early applications of sulfur as a modifier involve its use in large quantities without other materials, such as polymers [115,116]. Some commercial products, named as "sulfur extended bitumen" (e.g., Shell Thiopave®, Shell Brands International AG, Baar, Switzerland [52]) are obtained using this methodology, in which many parameters should be considered. Among the factors that control the reaction between sulfur and bitumen, the mixing temperature plays a determinant role. Below 140 °C sulfur can be incorporated into the bitumen molecules or can form hydrogen sulfide via dehydrogenation reaction. Higher temperatures allow C–S bond formation promoting a dynamic vulcanization of bitumen. It induces bridge formation within aromatic and naphthenic components modifying the chemical composition and colloidal structure of bitumen. Some authors also suggested that sulfur could self-polymerize when added to the binder [156]. However, nowadays, sulfur is added in very small quantities to bitumen where the polymers are the main modifiers. Some studies [120,121] have also shown that sulfur vulcanization made the PmBs more susceptible to oxidative aging and concluded that it is not a good idea to use sulfur as a sole additional modifier.

The first studies that used a small quantity of sulfur to increase the polymer/bitumen interaction date from the early 1970s when Petrossi proposed a method for preparing a rubber-modified bitumen. He blends bitumen with rubber (natural or synthetic) at 145 to 185 °C and after slightly reducing the temperature (125 to 160 °C) added 0.3 to 0.9% (by the weight of rubber) of sulfur. A free-radical vulcanization accelerator is also added to aid vulcanization [157]. Later on, Maldonado [158] proposed a different procedure starting with the preparation of a homogeneous PmB by stirring bitumen and SBS for 2 h at 130 to 230 °C and then adding 0.1 to 3 w/w% of sulfur and stirring for another 20–60 min. However, the exact reaction of sulfur-polymer-bitumen system is not completely clear. It was supposed that sulfur crosslinks the polymer molecules and links polymer and bitumen through sulfide and/or polysulfide chemical bonds. This assumption comes from the well-known process of vulcanization of unsaturated rubbers.

Further investigation on this topic was carried out by Wen et al. [117,118]. They prepared a low-viscosity homogeneous bitumen/SBS/sulfur blend by heating it to a temperature of 120 °C. This limits the occurrence of reactions between bitumen and sulfur or the vulcanization of SBS. Finally,

an increase in the temperature in the range of 150 to 180 °C allow these reactions to start. Possible evidence of this fact is that, unlike the two binary systems, an increase of the torque to maintain a constant rpm for the ternary bitumen/SBS/sulfur blend was necessary. The authors also hypothesized a vulcanization of both the unsaturated rubber and the functionalized bitumen components by the aid of sulfur, which creates interconnections between the polymer and bitumen. It has been claimed that these connections increase blend storage-stability by linking the polymer with the bitumen components through covalent chemical bonds. Later, Martınez-Estrada et al. [159] reported more indirect evidence for vulcanization. In this study a detailed rheological characterization of bitumen/SBS/sulfur and bitumen/SB/sulfur blends was performed. The importance of the homogeneity of the blend before sulfur addition has been also highlighted. In this respect a fast vulcanization, and consequently a useless material, could be observed if a too early sulfur addition is carried out. An appropriate sulfur bridge distribution is also important for a good chemical compatibility. To avoid freezing the blend's morphology at an earlier stage, good polymer dispersion and swelling must be achieved before network formation. Finally, the risk of gelation must be avoided. An "anti-gelling" adjuvant with the formula R-X, where R is a $C_{2–50}$ monovalent organic radical and X is an acidic function (carboxylic, sulfonic, phosphoric) has been used. Other solutions were proposed by Chevillard et al. and Ho et al. [160,161].

Many studies have shown that the use of sulfur as modifier improves the properties of some PmBs. In this respect it has been shown that sulfur enhances the storage stability, the elasticity, the deformation resistance, and some rheological properties of the PmBs [66,119,162]. From the rheological point of view, PmBs added with sulfur show a "more elastic" behavior compared to the ones without sulfur [66,118,163]. However, the use of sulfur as a chemical modifier has shown some drawbacks. First of all, the reaction of sulfur with polymer modifiers is based on the chemical reactions between sulfur and the double bonds of the polymer, so the use of sulfur is limited to PmBs modified by unsaturated polymers. The risk of obtaining nonhomogeneous PmBs during the polymer and sulfur addition into bitumen, is due to the difficulty of distributing the sulfur throughout the mixture. Moreover, local over-vulcanization of the polymer was detected. Replacing elemental sulfur with a more bitumen soluble polysulfide like di-hydrocarbyl polysulfide, represents a possible solution to this problem [164]. However, the emission of the hazardous health gas hydrogen sulfide during preparation of the bitumen/polymer mixes is the main drawback to the use of elemental sulfur. Hydrogen sulfide could be generated during sulfur vulcanization through the abstraction of hydrogen atoms in both bitumen and polymer modifiers, especially at high temperatures [165–167]. Some researchers argued that the gaseous emission is relatively small and most manufacturers know how to deal with the associated risks and dangers. The use of other sulfur-based agents as alternatives to elemental sulfur was introduced to eliminate, or at least reduce, such emissions. Compounds like benzothiazole sulfonamides, di-thiocarbamates, thiuram sulfates, morpholine sulfates, and caprolactam sulfates. Zinc mercaptobenzothiazole, zinc oxide, and dithiodimorpholine, as well as compositions without elemental sulfur, such as mercaptobenzothiazole, zinc oxide, mixed polythiomorpholine zinc 2-mercaptobenzothiazole, and dithiodimorpholine, were reported [168–170]. Nevertheless, the undesired formation of hazardous hydrogen sulfide has been observed also using this sulfur source. Shell Oil Company [171] used a disulfide that does not release sulfur at high temperature mixing. It has been claimed that the disulfide, instead of a conventional source of free sulfur, enhances compatibility between the polymer and bitumen. Diaryl disulfides were firstly proposed. However, all these additives are so expensive that they have not, in general, been used commercially. Finally, the poor recyclability of sulfur PmBs is another problem with sulfur vulcanization. All these drawbacks limit the application of sulfur vulcanization in PmB.

### *3.2. PPA-Based Techniques*

Among the different acids that can be used to improve bitumen properties through chemical modification, polyphosphoric acid (PPA) has been studied in numerous papers and patent

publications [172–185]. From a chemical point of view PPA is an oligomer of phosphoric acid ($H_3PO_4$), with no free water, which may have more than 10 repeating units [122].

The bitumen modification of PPA appears to be a complex physico chemical process, and the resulting properties may be strongly dependent on the bitumen nature. The difficult investigation of the reactions between the bitumen molecules and PPA is due to the large number of molecules with different chemical structures and their possible interactions. In this respect, an NMR investigation has shown that PPA tends to revert to orthophosphoric acid after mixing with bitumen [123]. Orange et al. claim that PPA neutralizes polar interactions between the asphaltene molecules, by protonation of basic sites or through esterification [186]. Co-polymerization, alkyl aromatization of saturates, and so on are other classes of reactions that have been proposed. A more detailed description can be found in [4,122,186]. From a thermal and rheological point of view bitumen/PPA blends [185–188] have shown an increased high-temperature performance with no significant changes in the low-temperature ones. It has been also found that PPA can improve the storage stability of PmBs. Giavarini et al. [112] used three ethylene–propylene copolymers of different molecular weights (MWs) and crystallinity to modify four different bitumens. In all cases, at a minimum amount of 3 %wt. of PPA added polymer segregation showed a remarkable reduction.

However, it should be noted that this improvement could be dependent on many factors, like polymer type and the quantity of PPA, as shown recently by Zhang and Hu [189].

### 3.3. Reactive Polymer Modifiers

Reactive polymers, also known as reactive ethylene terpolymers (RET) because of their ethylene-based structure, are polymer-based compounds grafted with reactive groups derived from, glycidyl methacrylate (GMA), acrylic acid, etc. The use of these types of polymer has been introduced to increase the compatibility between polyolefin (e.g., PE, PP, etc.) and bitumen by creating covalent linkages. Polymer grafting is a good solution and often simple to realize because it involves a single-step melt process. However, a possible drawback is the uncontrolled and undesired crosslinking of unsaturated polymers because of the radical mechanism of the grafting. Therefore, saturated polymers, such as styrene-ethylene-butylene-styrene (SEBS), PE, PP, etc., are more suitable for this process.

Owing to acrylic functionalization, the use of reactive polymers showed some advantages, like increased polarity and reactivity. However, higher costs compared to the other types of polymers and gelation problems due to the rather high number of reactive groups on a single macromolecule are the mainly-reported disadvantages that have been observed. To overcame these drawbacks, the amount of RET that could be used is around 2 to 2.5% and, in many cases, is even lower than 1% by weight [143]. Owing to these problems RETs are not ideal as bitumen modifiers, because the overall effect on the performances can be quite poor [143,190,191]. Therefore, their use could be mainly for increasing the compatibility between bitumen and other polyolefins, as shown by Yeh et al [144]. In this respect, using differential scanning calorimetry (DSC), they demonstrated an improvement in the bitumen/polymer interactions relative to unfunctionalized PP. Recently, two poly(ethylenebutylacrylate-glycidylmethacrylate), known as Elvaloy®AM and Elvaloy®4170 (produced by DuPont, Wilmington, DE, USA), were blended with neat bitumen in order to study the blend storage stability [192]. After high-temperature storage a complete homogeneity of all the samples was observed. This indicates the use of RET basically guarantees the storage stability, although under severe conditions of temperature and storage time another study has shown the instability of the blend [193]. Low-density polyethylene (LDPE) was used to compare the storage stability properties of blends prepared by using LDPE before and after grafting with GMA [148]. As can be observed from Figure 8 the use of GMA-grafted LDPE shows a higher stabilizing effect than LDPE.

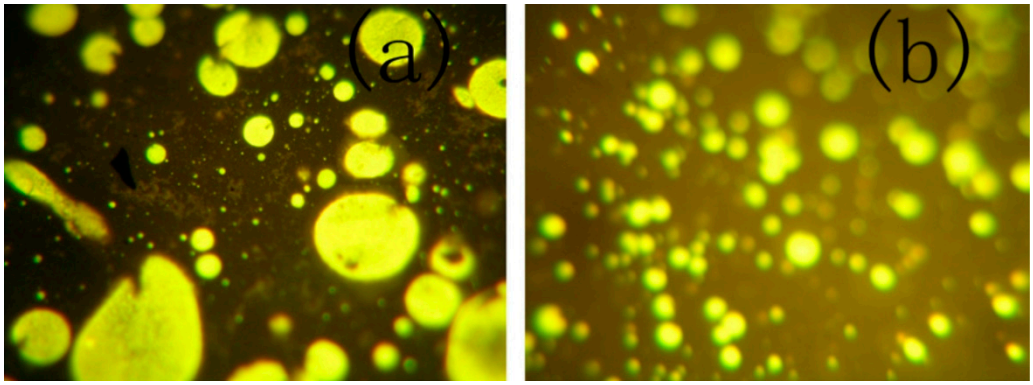


**Figure 8.** Fluorescence microscopy images showing the morphology of: (**a**) the LDPE and (**b**) GMA-g-LDPE blends (reprinted from [148] with permission of Elsevier).

Finally, a particular mention goes to silicon-based polymers like polyoxyalkylene with reactive silicon groups which form siloxane bonds by the silanol condensation reaction [194].

### *3.4. Maleic Anhydride*

Maleic anhydride (MAH) is an unsaturated cyclic (five atom ring) compound with molecular formula $C_4H_2O_3$. It has been widely used as a bitumen modifier and bitumen-polymer compatibilizer. MAH-bitumen interaction is characterized by complex mechanisms (copolymerization with bitumen molecules [126] or Diels-Alder reactions [195,196]). Nevertheless, it has been shown that meaningful physical properties change of bitumen are induced by MAH. In this respect Nadkarni et al. [197] studied a bitumen containing different amounts of MAH in terms of dynamic mechanical analysis (DMA), melt viscosity, and softening point. The results have shown that the chemical modification of bitumen with MAH improves the cracking resistance at low temperature and cohesive strength at high temperature.

Chemical reactions between MAH and bitumens were also investigated by comparing the effects of MAH and the related di-acids and anhydrides such as succinic anhydrides (SAH). The results of FTIR and gas chromatography-mass spectroscopy analysis showed the presence of two acid groups (-COOH) for both MAH and SAH. This leads to the conclusion that the two anhydrides undergo ring opening to give the corresponding di-acid. Moreover, in the case of MAH, the disappearance of the double IR bond signal was noticed. This fact could be explained by its reaction (or coordination) with bitumen molecules [126].

From another point of view, several studies have shown that the rheological properties of the blends obtained by adding to a bitumen MAH, SAH and different di-acids follow the order: MAH > SAH ~ dicarboxylic acids > monocarboxylic acid.

These results suggest the hypotheses that the two carboxylic acid groups are able to link two bitumen molecules. The better result obtained by adding MAH to the bitumen was hypothesized to be due to the double bond of MAH that interacts by coordination or other bonding mechanism to the bitumen molecules creating an additional linking. However, a recent study has shown controversial results about the MAH-bitumen reaction. In this respect, new FTIR analysis has shown that the IR band due to the MAH ring was retained during the MAH-bitumen reaction [127]. This observation, leads to the hypotheses that both Diels–Alder and π–π charge-transfer mechanism are involved instead of a ring opening process. The π–π charge-transfer process was possible because of the polynuclear aromatic nature of asphaltenes which act as donors in the charge-transfer processes. However, although the high reactivity of MAH could be used to improve the bitumen properties by promoting its interactions with polymers, this high reactivity raises drawbacks related to its handling and storage. A solution to these problems is achieved by synthesizing a polymer–MAH in advance and then modifying the

bitumen with this modified polymer, namely creating a reactive polymer (see Section 3.3). However, a further purification step is needed to eliminate unreacted MAH monomers, increasing the costs.

Recently Becker et al. [198], compared storage stability of PmBs prepared using SBS, SEBS, and two commercial SEBS-grafted MAH with different MAH content. SEBS-grafted MAH showed the best storage stability, although it did not improve significantly the rheological behavior of the binder.

### *3.5. Nanocomposite Modifiers*

Polymer/layered silicate nanocomposite (PLS) (aka polymer/clay nanocomposites) has been, and are still, widely used in polymer science research. Layered silicate can improve the polymer properties, such as mechanical properties, heat resistance, decreasing gas permeability and flammability, and increasing biodegradability [199–201]. The most commonly used silicates for preparation of PLS nanocomposites are hectorite ($M_x(Mg_{6-x}Li_x)Si_8O_{20}(OH)_4$) and montmorillonite (MMT; $M_x(Al_{4-x}Mg_x)Si_8O_{20}(OH)_4$) that belong to the same general family of phyllosilicates. As shown in Figure 9 they have a crystal structure made up of layers composed of two tetrahedrally-coordinated silicon atoms fused to an edge-shared octahedral sheet of either aluminum or magnesium hydroxide. The layer thickness is around 1 nm, and the lateral dimensions of these layers may vary from 30 nm to several microns or larger, depending on the particular layered silicate.

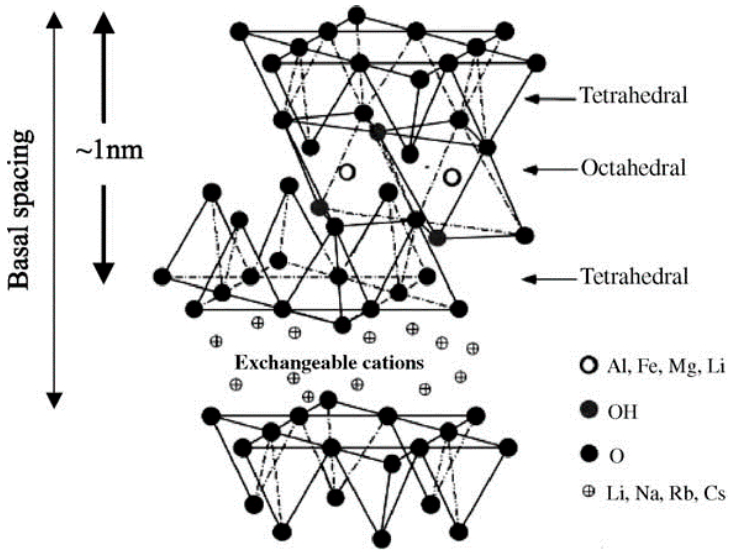


**Figure 9.** Structure of a 2:1 phyllosilicate (reprinted from [199] with the permission of Elsevier).

Due to the hydrophilic nature of layered silicates, it is very difficult to disperse them into polymer matrix and in most cases separation into two discrete phases takes place. The most common way to overcome this problem is to replace the interlayer cations ($Na^+$, $K^+$, etc.) with cationic surfactants, such as alkyl ammonium or phosphonium, preferably with long alkyl chains. The surfactants have a double role: (1) reducing the surface energy of the inorganic host and (2) improving the wetting characteristics of the polymer matrix. Additionally, their functional groups can react with the polymer matrix, and in some cases initiate the polymerization of monomers to improve the strength of the interface between the inorganic and the polymer matrix [202,203]. Increasing interactions between the polymer and the layered silicate in PLS nanocomposites led to the dispersion at the nanometer level of organic and inorganic phases. As a result, nanocomposites exhibit unique properties not shared by their micro counterparts or conventionally-filled polymers.

Furthermore, depending on the strength of interfacial interactions between the polymer matrix and layered silicate, three different types of PLS nanocomposites are thermodynamically achievable (see Figure 10):

I Intercalated nanocomposites: these are obtained by the insertion of few molecular layers of polymer into the layered silicate structure. From the crystallographic point of view this insertion occurs in a regular way.

II Flocculated nanocomposites: conceptually, this is the same as intercalated nanocomposites. However, silicate layers are sometimes flocculated due to hydroxylated edge–edge interaction of the silicate layers.

III Exfoliated nanocomposites: in these compounds the individual clay layers are separated in a continuous polymer matrix by an average distance that depends on clay loading.

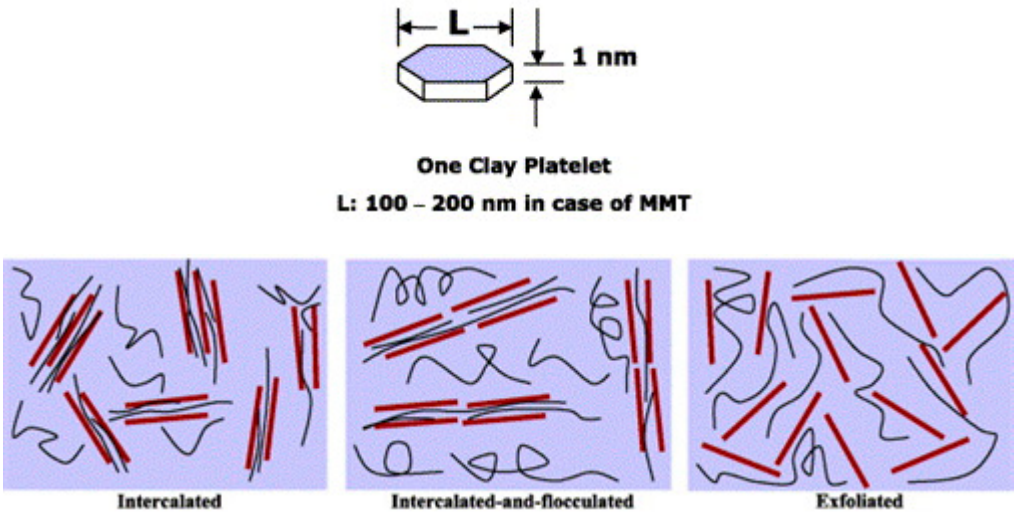


**Figure 10.** Illustration of three different types of polymer/layered silicate nanocomposites (reprinted from [199] with the permission of Elsevier).

The preparative methods of PLS can be divided into three main groups according to the starting materials and processing techniques. 1) From solution: the layered silicate is first swollen in a solvent of the polymer, such as water, chloroform, or toluene. When the polymer and layered silicate solutions are mixed, the polymer chains intercalate and displace the solvent within the interlayer of the silicate. Upon solvent removal, the intercalated structure remains, resulting in PLS nanocomposite. 2) In situ polymerization: the layered silicate is swollen within the liquid monomer or a monomer solution so the polymer formation can occur between the intercalated sheets. Polymerization can be initiated either by heat or radiation, by the diffusion of a suitable initiator, or by an organic initiator or catalyst fixed through cation exchange inside the interlayer before the swelling step. 3) Melt intercalation method: this involves an annealing process, statically or under shear, of a mixture of the polymer and an organically-modified layer silicate (OMLS) above the softening point of the polymer. This method has great advantages over the other two. First, it is environmentally benign due to the absence of organic solvents. Second, it is compatible with current industrial process. The melt intercalation method allows the use of polymers which were previously not suitable for in situ polymerization or solution intercalation.

In several studies, clays were used as compatibilizer agents in polymer blends. In this respect, clay localizes at the interfacial bitumen-polymer region reducing the interfacial tension. As a consequence, the "minor phase-dispersed" particles lose the typical rounded shape they possess in the pure polymer blends, and a finer dispersion is obtained [204–213]. Based on this fact, the studies have been focused mainly on their effects on the compatibility between bitumen and polymers. As the results have shown a considerable increase in the bitumen/polymer compatibility, it has been suggested that using ternary bitumen/polymer/clay (BPC) systems, the PmB's performances may be improved. In particular it has been claimed that the use of PLS in PmBs has mainly two effects: (1) improving the aging resistance of PmB with barrier properties of the dispersed clay platelets and (2)

enhancing the storage stability of PmB by decreasing the density difference between polymer modifiers and bitumen [68].

The Bitumen–Polymer–Clay Ternary System

Among the three preparatory methods of PLS described above, melt intercalation is the one that can be easily applied to bitumen modification due to its compatibility with current industrial processes and with all types of thermoplastic polymers. Bitumen, polymer, and clay can be mixed in a single step known as physical mix (PM) (see Figure 11). Otherwise, two consecutive steps could be employed: (1) nano-composite preparation and (2) addition to a bitumen. Globally, the process is known as master batch (MB). The use of one (PM) or the other (MB) method is very important and can give different results.

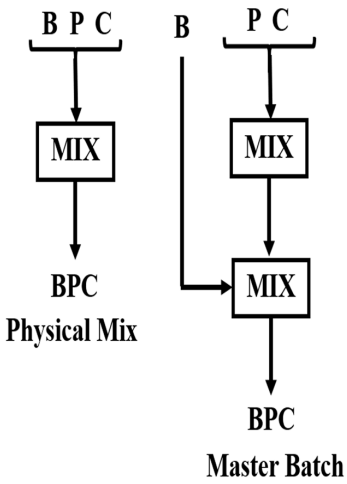


**Figure 11.** Schematic representation of the two mixing processes: physical mix and master batch (reprinted from [46] with the permission of Elsevier).

These two methods were applied and studied in different research works, in which different polymers and clays were reported for the production of bitumen/polymer/composites (BPC). SBS and kaolinite [132], SBS and organobentonite [214], poly(styrene-b-ethylene-b-butene-b-styrene) (SEBS) and kaolinite [133], and LDPE or EPDM and silica [134] were the primary compounds which have been studied. In all the previously reported cases, different ratios of polymer-clay nanocomposites were firstly prepared and successively added to bitumen. Storage stability, blend morphology, and mechanical and rheological properties of the BPCs were characterized. Tube tests to evaluate the storage stability of the blend were made. In all cases, storage stability was observed. To justify these results, it has been hypothesized that clays tend to reduce the density gap between the polymer rich phase (PRP) and bitumen asphaltene rich phase (ARP) by locating themselves preferentially in the PRP phase. However, this was not directly supported by experimental evidence.

In this respect, the recorded values of softening points are certainly consistent with this interpretation being considered as evidence. Ouyang et al. [133] lists the softening points of the top and bottom sections of the tube test for the bitumen/SEBS/kaolinite mixes (see Table 3).

As can be seen from Table 3, for a given SEBS content, the ΔS parameter whose magnitude is indicative of the blend stability (higher magnitude equals lower stability), decreases as clay content increases. Moreover, for the sample of 4% SEBS this difference become negative indicating that the Polymer Rich Phase (PRP) migrates toward the bottom of the tube. At high clay contents, negative values for the ΔS were obtained. This could be explained by considering that the polymeric rich phases become heavier than the asphaltenic rich phase (ARP). A balance of PRP and ARP densities obtained at well-defined clay amounts, inducing a storage stability. An LDPE-modified bitumen also has shown a similar effect [134]. However, storage stability is not simply due to a decrease in density difference

between the PRP and ARP phases. Several studies have shown that compatibility between bitumen and polymer also plays a fundamental role [215]. Therefore, the improved storage stability can be ascribed mainly to two factors: decrease in density difference between the PRP and ARP phases and, to a greater extent, to a real bitumen/polymer compatibilizing effect. Furthermore, the preparation procedure also plays an important role. As can be seen from Table 3, the only mix found unstable during the high-temperature storage was prepared using the PM method. This, in accordance with the idea that the clay resides preferentially in the PRP leads to a conclusion that only with a pre-formed nanocomposite storage stabilization could it be achieved.

**Table 3.** SEBS/KC-modified bitumen storage stabilities at high-temperature (from Table 4 of [133] with the permission of Elsevier).

| **Formulation** | | **S (°C)** | | |
|---|---|---|---|---|
| SEBS %(w/w) | SEBS/KC (w/w) | Top ($S_t$) | Bottom ($S_b$) | ΔS |
| 3 | 100/0 | 53.0 | 50.0 | 3.0 |
| 3 | 100/50 | 52.5 | 52.8 | −0.3 |
| 4 | 100/0 | 57.0 | 53.8 | 3.2 |
| 4 | 100/10 | 56.5 | 50.8 | 5.7 |
| 4 | 100/30 | 55.0 | 52.0 | 3.0 |
| 4 | 100/50 | 55.5 | 55.8 | −0.3 |
| 4 | 100/50 [a] | 59.0 | 52.0 | 7.0 |
| 4 | 100/70 | 52 | 52.5 | −0.5 |
| 5 | 100/0 | 70.5 | 58.0 | 12.5 |
| 5 | 100/50 | 57.0 | 58.0 | −1.0 |
| 6 | 100/0 | 85.0 | 67.5 | 17.5 |
| 6 | 100/50 | 59 | 60.5 | −0.5 |

[a] Mix prepared using PM. $\Delta S = S_t - S_b$.

This point was confirmed by other researchers who studied different systems, such as a styrene-butadiene rubber (SBR) with a palygorskite- and organo-modified palygorskite clays [216]. This paper studied the storage stability of the blends and the importance of the preparation procedure. Polacco et al. [136] investigated the internal structure and nanocomposite nature of the blends. In this research a neat bitumen (NB) and SBS were modified with OMMT (Cloisite 20A, referred to simply as 20A) through melt mixing, obtaining two blends of bitumen/clay and polymer/clay: (1) SBS/20A, (2) NB/20A. Ternary blends were then prepared using both PM and MB methods: (3) NB/SBS/20A PM, and (4) NB/SBS/20A MB. Figure 12 reports the X-ray diffractometry (XRD) characterization, which was performed on virgin materials (bitumen, polymer, and clay) and blends. A comparison between the binary blend NB/20A and the 20A alone shows that the clay's interlayer spacing almost doubled. This was attributed to bitumen intercalation. A partial exfoliation of the stacks can also be seen. Moreover, storage tests showed the absence of phase separation, confirming a high degree of interaction between NB and 20A.

As shown by the XRD pattern, intercalated nanocomposites were also obtained in the SBS/20A binary blends. The interlayer spacing was found to be independent of the clay quantity, but it was lower than that of NB/20A blends. This suggests that the clay had higher compatibility with the bitumen compared to the polymer. Regarding ternary blends, XRD patterns show that both mixing processes (PM, MB) give intercalation with interlayer spacing equal to that obtained by mixing bitumen and clay without the polymer. This may indicate that the degree of intercalation is substantially determined by the bitumen molecules and is independent of the mixing sequence. This could be explained by considering that the polymer chains are present in a very small amount compared to the bitumen molecules and they interact with a limited amount of clay stacks. Therefore, polymer chains, even if already intercalated between some of the clay platelets, are not expected to inhibit the interactions between clay and the small and abundant bitumen molecules. On the contrary, the ability of the

polymer molecules to intercalate the clay stacks is strongly influenced by the mixing sequence. Finally, once the clay-polymer interactions are established, bitumen molecules are not necessarily expected to substitute the polymer chains in clay interlayers. For these reasons the similarity in the XRD spectra does not necessarily mean a similarity in the internal structure of PM and MB mixes.

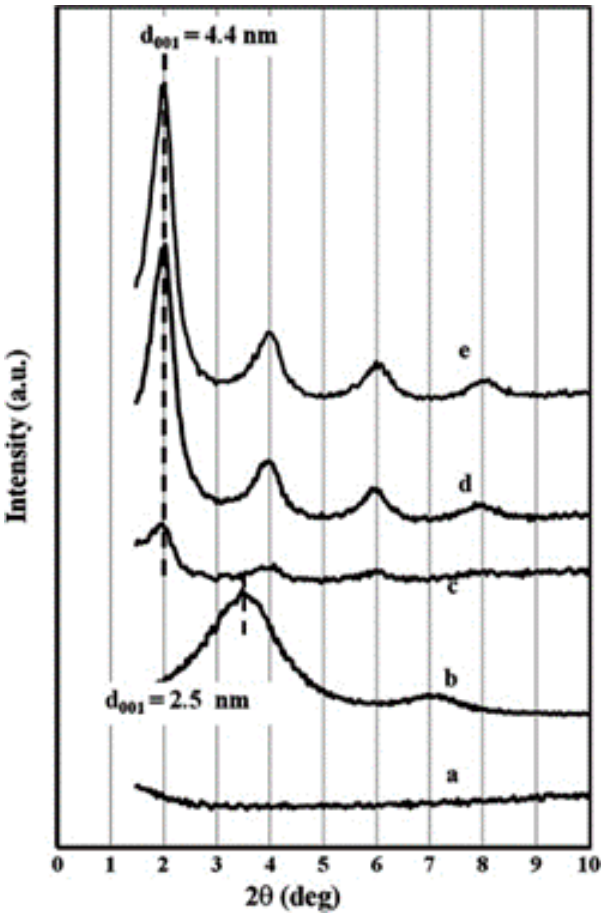


**Figure 12.** XRD pattern of neat bitumen, Closite 20A, SBS/20A, B/20A, B/SBS/20A (PM) and B/SBS/20A (MB) (reprinted from [136] with the permission of Elsevier).

From a morphological point of view, Figure 13 shows three different systems: (a) the binary NB/SBS blend, (b) NB/SBS/clay PM blend, and (c) NB/SBS/clay MB blend. As can be seen NB/SBS blend is characterized by a biphasic morphology, which results in high-temperature storage instability. The NB/SBS/clay PM blend still shows a biphasic pattern, but the smaller microdomains indicate an improved compatibility and stability of the system. A further improvement of the morphology is observed for the NB/SBS/clay MB blend, which has the canonical aspect of a perfectly compatible PmB pattern. In addition, Figure 13a,b show the important role of clay, which favors the contact between the polymer chains and those bitumen molecules that would otherwise be confined in the ARP. Clays acts as the substrate where polymer and asphaltene molecules come into contact, reducing the differences in composition between the PRP and ARP phases.

Later, Sureshkumar et al. [217,218] prepared different PmBs using EVA as a polymer and studied the effect of two different organoclays: 20A and another OMMT known as Dellite 43B (namely referred to as 43B). Figure 14 shows the fluorescence microscopy images of the blends studied.

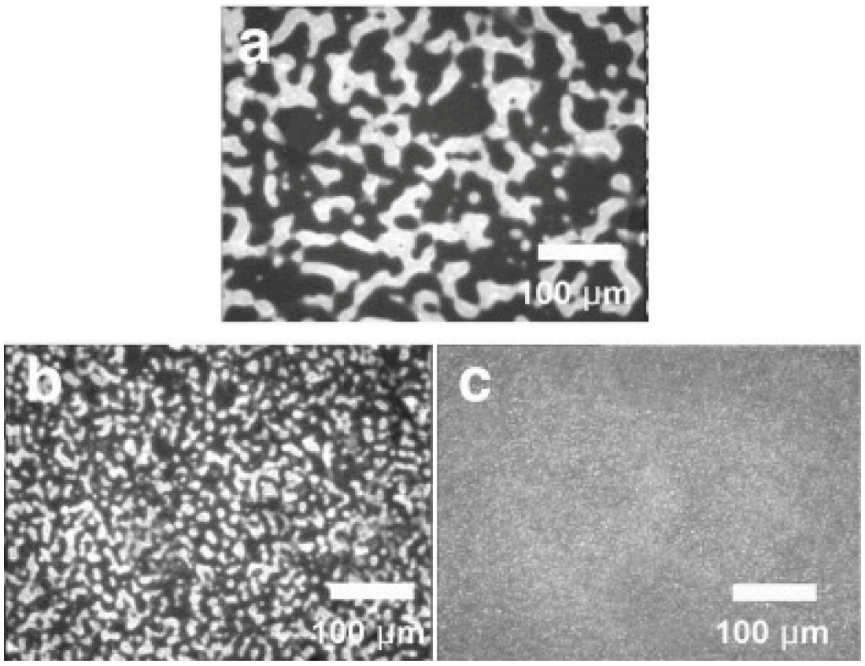


**Figure 13.** Fluorescence Images of (**a**) BA/SBS, (**b**) BA/SBS/20A PM, and (**c**) BA/SBS/20A MB (reprinted from [46] reprinted with the permission of Elsevier).

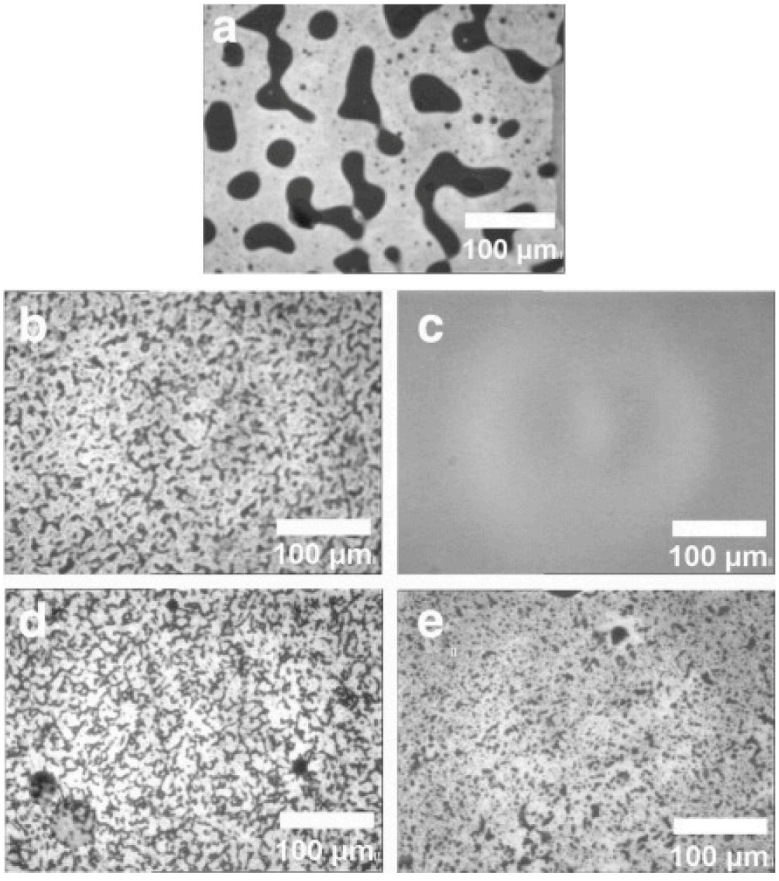


**Figure 14.** Fluorescence images of (**a**) BA/EVA, (**b**) BA/EVA/20A PM, (**c**) BA/EVA/20A MB, (**d**) BA/EVA/43B (PM), and (**e**) BA/EVA/43B (MB) (reprinted from Figure 1 of [217] with the permission of Elsevier).

The pictures show results similar to those described for SBS. However, clay 43B has a compatibilizing effect less pronounced than 20A. The differences observed among the blends prepared using PM or MB are reflected in the macroscopic behavior. Rheological tests have shown an improvement in thermo-mechanical properties of the ternary blend prepared using MB. Therefore, the MB procedure is preferable to the PM since it guarantees better homogeneity, stability, and mixture performance. However, the PM has the advantage of being simpler from a practical point of view because it involves a single step using classic paving equipment.

## 4. PmBs in Warm Mix Asphalt (WMA) Technology

A new kind of polymer-modified bitumen technology has been introduced in recent years. It combines the classic ones (PmB) with the warm mix asphalt technique (WMA). One of the methodologies employed to shift from hot mix asphalts to warm ones is based on the use of waxes. This is due to the fact that above their melting temperature, they act as plasticizers, while at low temperatures they crystallize and act as fillers [4,219,220]. While the PmB is well consolidated the WMA is relatively new, but rapidly growing, due to its economic and environmental advantages. Compared with classic hot mix asphalts (HMA), warm mix ones, in general, are characterized by lower fuel consumption and costs, lower production of greenhouse gases, fumes, and odors, which improve the environmental impact and working conditions, extension of haul distances, and good workability during laying and compaction [219]. Although naturally present as constitutive components of all crude oil products [221,222] and studied in the technical literature, where bitumen wax content [223–225], crystallization properties [226], chemical structure [227,228], and influences on bitumen and bitumen mixture properties [220,223,229–234] were analyzed, waxes affect the binder performances. For example, wax melting can soften bitumen at high service temperature, reducing rutting resistance of the pavement, while at low temperatures wax crystallization can increase stiffness and sensitivity to fatigue and thermal cracking [219,223,234]. Nowadays there is an increase development about warm polymer modified bitumen which can maintain the advantages of both technologies (WMA and PMB) although this is not an easy task because waxes used as warm modifiers reduce the high temperature viscosity while increasing the low temperature stiffness and polymers do basically the contrary [219]; simply adding the two modifiers does not guarantee the enhancement of bitumen properties like those obtained by adding single ones. For example, a ternary mixture bitumen/polymer/wax has significantly different properties (like viscoelasticity) from those predictable by superposing the effect of wax and polymer only and the final warm effect and performances of the binder will be determined by the interactions between the three components. Scientific studies on this ternary mixture are still limited. Edwards et al. [235] for example, studied the addition of paraffinic waxes to a polymer-modified mastic bitumen, showing that a 4% wax addition improves workability of the mastic bitumen without affecting its performances. Kim et al. [236,237] studied the artificial long- and short-term aging of a PmB mixed with wax additives. Other studies analyzed the properties and pavement performance, compacting temperatures, long-term performance [238], fatigue characteristics [4], thermo-mechanical properties [239], and viscosity and rheological properties [240]. Rossi et al. [219] conducted a preliminary investigation by mixing bitumen, SBS, and three typologies of wax chosen among the three categories: paraffinic (obtained by Fischer-Tropsch process), partially oxidized and maleic anhydride functionalized. By morphological and calorimetric analyses and solubility tests they were able to characterize blend behavior related to wax type. In particular, they found that paraffinic waxes preferentially reside in the polymer-rich phase and slightly enhance the bitumen polymer compatibility. Partial oxidation tends to aggregate with the asphaltene rich phase reducing compatibility with the polymer, while functionalized wax, although not clear where they are located, has a considerable compatibilizing effect strongly altering the colloidal equilibrium of the bitumen polymer blend.

## 5. Concluding Remarks

This paper summarizes the findings obtained from an extensive literature review focused on the basic aspects related to different types of bitumens, processing technologies and polymers, chemical and nanocomposite-modified bitumen characterizations' pros and cons, as well as identifying corresponding areas of study for future perspectives. The comprehensive review implies that the relative abundance of the bitumen SARA fractions results in significant differences in bitumen chemical composition and further mechanical properties. It is evident that different types of processing of crude oil result in bitumens with different chemical compositions. This also has a great influence on the compatibility with any polymer through polymer modification.

The author believes that the widespread use of the PmB technologies within the road pavement industry is advisable considering the genuine shortcomings of neat bitumens and the heavy-duty pavements of current transportation networks.

The review conducted on the different kinds of PmBs can be concluded as the follows:

- While plastomer-modified bitumens are suitable for improving the permanent deformation resistance of the bituminous compounds and asphalt concrete mixtures over high stresses, the absence of elasticity at low temperature limited the application of these bitumins.
- The field recorded data, as well as experimental works, showed that plastomer-modified bitumens, such as polyethylene and polypropylene, are the most common plastomers resulting in compatibility problems. This is due to their non-polar chemical nature.
- Despite the thermal and aging stability of plastomer-modified bitumens due to the absence of double bonds, the main problem resides in the stability of the blend (polymer + bitumen) during storage and difficulties to disperse them homogenously in the bitumen matrix.
- Thermoplastic elastomer copolymers, owing to their elastic component, are usually more effective than plastomers for bitumen modification in pavement applications. The modification ranges from low-modified containing 3% polymer to a high level with polymer content of 7%.
- Bitumen modification via styrene butadiene styrene (SBS) as the most commonly used elastomer has numerous benefits, including the improved thermal susceptibility, increased softening point, and slight decrease of penetration value at 25 °C. In addition, it has been observed that SBS can moderate the increase of stiffness due to oxidation processes.
- Bitumens modified with thermosetting polymers show a high elasticity and no viscous behavior. Asphalt mixtures produced with thermosetting polymer-modified bitumen have excellent adhesive ability, excellent resistance to deformation, excellent fatigue performance, and high stiffness modulus. Even though the PmBs with thermosetting plastics have relatively high adhesion to the mineral particles and high strength they are not common for paving applications. This is because the technological properties of PmB are almost immediately deteriorated by these polymers due to their hardening properties; secondly, the rigidity of the PmB is increased at low temperatures, which results in increased thermal sensitivity; thirdly, the use of TP complicates the system and raises its price; and, finally, the effectiveness of thermosetting plastics usually appears due to their large quantities in bitumen (more than 10 wt%)
- Natural rubber latex has potential for improving bitumen binder performance by enhancing the thermal sensitivity, flexibility, stability, and stripping. In addition, its inherent elastomeric properties proved its high potential in improving long-term pavement performance of asphalt concrete by increasing rutting resistance, fatigue life, etc. Natural rubber also decreases the optimum binder content in asphalt concretes, increasing its density and stability. However, natural rubber is a highly valuable biomaterial compared to other biopolymers, hence natural rubber has been commercialized into synthetic rubber. This is mainly because of the very large difference between the available produced amount and the demand. Still, there are some doubts regarding asphalt concrete performance and mechanical properties throughout the performance temperature range

- The synthetic rubber/bitumen system was investigated from a different point of view. It can be concluded that many factors can influence the performance and mechanical properties of rubberized binders including: the size and content of rubber, the chemical structure, particles surface properties (ambient granulating or cryogenically crushed tire rubber), blend production method, and temperature. A low content of rubber, around 4% (to the weight of bitumen) has almost no effect, or at least no significant effects, on the performance and mechanical properties of the binder, while more than 20% was found to be unsuitable.
- In spite of the proven advantages regarding the use of polymers in bitumen modification systems, several research works showed the difficulties regarding the incompatibility with the bitumen. Phase separation could occur in such modified bitumen.
- Several research works showed that the stability of the PmBs is highly dependent on the asphaltene and aromatic content of base bitumen: the less asphaltene, the more stable the modified compound that can be expected. However, polymer chemical structure and reactivity are also of paramount importance in bitumen/polymer system compatibility.
- Various solutions to remove drawbacks to currently used polymer modifiers, among which the use of chemical modifiers received great attention, have been employed in the last few decades. These solutions overcome some disadvantages of PmBs, but most cause some new problems. Thus, more research needs to be carried out in the future to solve these problems and find new ways to modify bitumen effectively and cheaply.
- Finally, few research works showed the effectiveness of waxes in improving some of the characteristics of base bitumens and modified bitumens. In addition, the presence of a determined amount of wax could improve the polymer compatibility.

Considering the variety of the conclusions, especially regarding the bitumen chemical characteristics and related engineering properties, further studies are required to be able to fully integrate the aspects related to bitumen functionality and obtain conclusions concerning many challenges on this topic.

**Author Contributions:** M.P. conceptualization, methodology and writing, P.C. conceptualization; V.L. conceptualization, S.E. writing, B.T. conceptualization and C.O.R. conceptualization and supervision.

**Funding:** This research received no external funding.

**Conflicts of Interest:** The authors declare no conflict of interest.

## References

1. *European Committee for Standardization EN 12597: Bitumen and Bituminous Binders-Terminology*; European Committee for Standardization: Brussels, Belgium, 2000.
2. Paliukait, M.; Vaitkusa, A.; Zofkab, A. Evaluation of bitumen fractional composition depending on the crude oil type and production technology. In Proceedings of the 9th International Conference "Environmental Engineering" Selected Papers, Vilnius, Lithuania, 22–23 May 2014.
3. Read, J.; Witheoak, D. *The Shell Bitumen Handbook*, 5th ed.; Thomas Telford Publishing: London, UK, 2003.
4. Lesueur, D. The Colloidal Structure of Bitumen: Consequences on the Rheology and on the Mechanisms of Bitumen Modification. *Adv. Colloid Interface Sci.* **2009**, *145*, 42–82. [CrossRef] [PubMed]
5. Olli-Ville, L. Low-Temperature Rheology of Bitumen and Its Relationships with Chemical and Thermal Properties. Ph.D. Thesis, School of Engineering, Aalto University, Espoo, Finland, 2015.
6. D'Melo, D.; Taylor, R. Constitution and Structure of Bitumens. In *The Shell Bitumen Handbook*, 6th ed.; Hunter, R.N., Self, A., Read, J., Eds.; ICE Publishing: London, UK, 2015; ISBN 978-0727758378.
7. McNally, T. Introduction to polymer modified bitumen (PmB). In *Polymer Modified Bitumen Properties and Characterisation*, 1st ed.; McNally, T., Ed.; Woodhead Publishing: Sawston, UK, 2011.
8. Lu, X.; Isacsson, U.; Ekblad, J. Phase Separation of SBS Polymer Modified Bitumens. *J. Mater. Civ. Eng.* **1999**, *11*, 51–57. [CrossRef]

9. Petersen, J.C. Chemical Composition of Asphalt as Related to Asphalt Durability: State of the Art. *Transp. Res. Rec.* **1984**, *999*, 13–30.
10. Branthaver, J.F.; Petersen, J.C.; Robertson, R.E.; Duvall, J.J.; Kim, S.S.; Harnsberger, P.M.; Mill, T.; Ensley, E.K.; Barbour, F.A.; Schabron, J.F. *Binder Characterization and Evaluation-vol 2 Chemistry*; SHRP Report A-368; National Research Council: Washington, DC, USA, 1994.
11. Mortazavi, M.; Moulthrop, J.S. *SHRP Materials Reference Library*; SHRP report A-646; National Research Council: Washington, DC, USA, 1993.
12. *Strategic Highway Research: Special Report 260. Committee for Study for a Future Strategic Highway Research Program, Strategic Highway Research*; Transportation Research Board Special Report 260; National Research Council: Washington, DC, USA, 2001.
13. Jiménez-Mateos, J.M.; Quintero, L.C.; Rial, C. Characterization of petroleum bitumens and their fractions by thermogravimetric analysis and differential scanning calorimetry. *Fuel* **1996**, *75*, 1691–1700. [CrossRef]
14. Speight, J.C. *The Chemistry and Technology of Petroleum*, 3rd ed.; Marcel Dekker: New York, NY, USA, 1999.
15. Ashoori, S.; Sharifi, M.; Masoumi, M.; Salehi, M.M. The Relationship between SARA Fractions and Crude Oil Stability. *Egypt. J. Pet.* **2017**, *26*, 209–213. [CrossRef]
16. Rostler, F.S. *Fractional Composition: Analytical and Functional Significance*; Hoiberg, A.J., Robert, E., Eds.; Krieger Publishing Company, Huntington: New York, NY, USA, 1979; Volume 2, pp. 151–222.
17. Corbett, L.W. Composition of asphalt based on generic fractionation, using solvent deasphaltening, elution-adsorption chromatography and densimetric characterization. *Anal. Chem.* **1969**, *41*, 576–579. [CrossRef]
18. Speight, J.C. Petroleum asphaltenes. Part 1. Asphaltenes, resins and the structure of petroleum. *Oil Gas Sci. Technol.* **2004**, *59*, 467–477. [CrossRef]
19. Mullins, O. Optical Interrogation of Aromatic Moieties in Crude Oils and Asphaltenes. In *Structures and Dynamics of Asphaltenes*; Mullins, O., Sheu, E.Y., Eds.; Plenum Press: New York, NY, USA, 1998; pp. 21–77. ISBN 978-1-4899-1615-0.
20. Piéri, N. Etude du Vieillissement Simulé et In-Situ des Bitumens Routiers Par IRTF et Fluorescence UV en Excitation-Emission Synchrones. Ph.D. Thesis, Aix-Marseille University, St-Joseph, France, 1995.
21. Scotti, R.; Montanari, L. Molecular structure and intermolecular interaction of asphaltenes by FT-IR, NMR, EPR. In *Structures and Dynamics of Asphaltenes*; Mullins, O., Sheu, E.Y., Eds.; Plenum Press: New York, NY, USA, 1998; pp. 79–113. ISBN 978-1-4899-1615-0.
22. Bergmann, U.; Mullins, O.C.; Cramer, S.P. X-Ray Raman spectroscopy of carbon in asphaltene: Light element characterization with bulk sensitivity. *Anal. Chem.* **2000**, *72*, 2609–2612. [CrossRef]
23. Michon, L.; Didier, M.; Jean-Pascal, P.; Bernard, H. Estimation of average structural parameters of bitumens by $^{13}$C Nuclear Magnetic Resonance spectroscopy. *Fuel* **1997**, *76*, 9–15. [CrossRef]
24. Sheremata, J.M.; Gray, M.R.; Dettman, H.D.; McCaffrey, W.C. Quantitative molecular representation and sequential optimization of Athabasca asphaltenes. *Energy Fuels* **2004**, *18*, 1377–1384. [CrossRef]
25. Murgich, J.; Abanero, J.; Strausz, O. Molecular Recognition in Aggregates Formed by Asphaltene and Resin Molecules from the Athabasca Oil Sand. *Energy Fuels* **1999**, *13*, 278–286. [CrossRef]
26. Mullins, O. Review of the Molecular Structure and Aggregation of Asphaltenes and Petroleomics. *Spe J.* **2008**, *13*, 48–57. [CrossRef]
27. Becker, J.R. *Crude Oil Waxes, Emulsiones and Asphaltenes*; PennWell: Tulsa, OK, USA, 1997.
28. Dickie, J.P.; Yen, T.F. Macrostructures of the Asphaltic Fractions by Variuos Instrumental Methods. *Anal. Chem.* **1967**, *5213*, 1963–1968.
29. Speight, J.C. Molecular Models for Petroleum Asphaltenes and Implication for Asphalt Science and Technology. In Proceedings of the International Symposium on the Chemistry of Bitumens, Rome, Italy, 5–8 June 1991; pp. 154–207.
30. Yen, T.F.; Erdman, J.G.; Pollack, S.S. Investigation of the Structure of Petroleum Asphaltenes by X-Ray Diffraction. *Anal. Chem.* **1961**, *33*, 1587–1594. [CrossRef]
31. Sadeghi, M.A.; Chilingarian, G.V.; Yen, T.F. X-Ray Diffraction of Asphaltenes. *Energy Sources* **1986**, *8*, 99–123. [CrossRef]
32. Sheu, E.Y.; De Tar, M.M.; Storm, D.A. Surface activity and dynamics of asphaltenes. In *Asphaltene Particles in Fossil Fuel Exploration, Recovery, Refilling and Production*; Sharma, M.K., Yen, T.F., Eds.; Plenum Press: New York, NY, USA, 1994; pp. 115–121.

33. Roux, J.N.; Broseta, D.; Demésans, B. Study of asphaltene aggregation: Concentration and solvent quality effects. *Langmuir* **2001**, *17*, 5085–5092. [CrossRef]
34. Pryanto, S.; Mansoori, G.A.; Suwono, A. Measurement of property relationships of nano-structure micelles and coacervates of asphaltene in a pure solvent. *Chem. Eng. Sci.* **2001**, *56*, 6933–6939. [CrossRef]
35. Mullins, O. *Structures and Dynamics of Asphaltenes*; Mullins, O., Sheu, E.Y., Eds.; Plenum Press: New York, NY, USA, 1998; ISBN 978-1-4899-1615-0.
36. Fotland, P.; Anfindsen, H. Conductivity of asphaltenes. In *Structures and Dynamics of Asphaltenes*; Mullins, O., Sheu, E.Y., Eds.; Plenum Press: New York, NY, USA, 1998; pp. 247–266.
37. Taylor, S.E. The electrodeposition of asphaltenes and implication for asphaltene structure and stability in crude and residual oils. *Fuels* **1998**, *77*, 821–828. [CrossRef]
38. Swanson, J.M. A contribution to the physical chemistry of the asphalts. *J. Phys. Chem.* **1942**, *46*, 141–150. [CrossRef]
39. Marruska, S.; Rao, B.M.L. The role of polar species in the aggregation of asphaltenes. *Fuel Sci. Technol. Int.* **1987**, *5*, 119–168. [CrossRef]
40. Fotland, P.; Anfidsen, H.; Fadnes, F.H. Detection of asphaltene precipitation and amounts precipitated by measurement of electrical conductivity. *Fluid Phase Equilib.* **1993**, *82*, 157–164. [CrossRef]
41. Mozaffari, S.; Tchoukov, P.; Atias, J.; Czarnecki, J.; Nazemifard, N. Effect of Asphaltene Aggregation on Rheological Properties of Diluted Athabasca Bitumen. *Energy Fuels* **2015**, *29*, 5595–5599. [CrossRef]
42. Mozaffari, S.; Tchoukov, P.; Mozaffari, A.; Atias, J.; Czarnecki, J.; Nazemifarda, N. Capillary driven flow in nanochannels—Application to heavy oil rheology studies. *Colloids Surf. A Physicochem. Eng. Asp.* **2017**, *513*, 178–187. [CrossRef]
43. Fang, L.; Shaghayegh, D.; Nelya, A.; Charles, M.; Sanjoy, B.; Pauchard, V. Mixture Effect on the Dilatation Rheology of Asphaltenes-Laden Interfaces. *Langmuir* **2017**, *33*, 1927–1942.
44. Duran, J.A.; Casas, Y.; Xiang, L.; Zhang, L.; Zeng, H.; Yarranton, H.W. Nature of Asphaltene Aggregates. *Energy Fuels* **2018**, *1*. [CrossRef]
45. Gawel, I.; Czechowski, F. Study of saturated components in asphalt. *Pet. Sci. Technol.* **1997**, *15*, 729–742. [CrossRef]
46. Polacco, G.; Filippi, S.; Merusi, F.; Stastna, G. A review of the fundamentals of polymer-modified asphalts: Asphalt/polymer interactions and principles of compatibility. *Adv. Colloid Interface Sci.* **2015**, *224*, 72–112. [CrossRef] [PubMed]
47. Koots, J.A.; Speight, J.G. Relation of petroleum resins to asphaltenes. *Fuel* **1975**, *54*, 179–184. [CrossRef]
48. Yarranton, H.W.; Fox, W.A.; Svrcek, W.Y. Effect of Resins on Asphaltene Self-Association and Solubility. *Can. J. Chem. Eng.* **2007**, *85*, 635–642. [CrossRef]
49. Boutevin, B.; Pietrasanta, Y.; Robin, J.J. Bitumen-Polymer Blends for Coatings Applied to Roads and Public Constructions. *Prog. Org. Coat.* **1989**, *17*, 221–249. [CrossRef]
50. Polacco, G.; Stastna, J.; Biondi, D.; Zanzotto, L. Relation Between Polymer Architecture and Nonlinear Viscoelastic Behaviour of Modified Asphalts. *Curr. Opin. Colloid Interface Sci.* **2006**, *11*, 230–245. [CrossRef]
51. Walkering, C.P.; Vonk, W.C.; Whiteoak, C.D. Improved Asphalt Properties Using SBS modified Bitumens. *Shell Bitum. Rev.* **1992**, *66*, 9–11.
52. Rodrigues, C.; Hanumanthgari, R. Polymer modified bitumens and other modified binders. In *The Shell Bitumen Handbook*, 6th ed.; Hunter, R.N., Self, A., Read, J., Eds.; ICE Publishing: London, UK, 2015; ISBN 978-0727758378.
53. Becker, Y.; Méndez, M.P.; Rodríguez, Y. Polymer Modified Asphalt. *Vis. Tecnol.* **2001**, *9*, 39–50.
54. Polacco, G.; Berlincioni, S.; Biondi, D.; Stastna, J.; Zanzotto, L. Asphalt Modification with Different Polyethylene-Based Polymers. *Eur. Polym. J.* **2005**, *41*, 2831–2844. [CrossRef]
55. Punith, V.S.; Veeraragavan, A. Behaviour of asphalt concrete mixtures with reclaimed poly ethylene as additive. *J. Mater. Civ. Eng.* **2007**, *19*, 500–507. [CrossRef]
56. Lesueur, D.; Gérard, J.-F. Polymer modified Asphalts as Viscoelastic Emulsions. *J. Rheol.* **1998**, *42*, 1059–1074. [CrossRef]
57. Isacsson, U.; Lu, X. Testing and Appraisal of Polymer Modified Road Bitumens-State of the Art. *Mater. Struct.* **1995**, *28*, 139–159. [CrossRef]
58. Stastna, J.; Zanzotto, L.; Vacin, O.J. Viscosity Function in Polymer-modified Asphalts. *J. Colloid Interface Sci.* **2003**, *259*, 200–207. [CrossRef]

59. Ameri, M.; Mansourian, A.; Sheikhmotevali, A.H. Investigating Effects of Ethylene Vinyl Acetate and Gilsonite Modifiers Upon Performance of Base Bitumen Using Superpave Tests Methodology. *Constr. Build. Mater.* **2012**, *36*, 1001–1007. [CrossRef]
60. Stroup-Gardiner, M.; Newcomb, D.E. *Polymer Literature Review*; September. Report N°: MN/RC-95/27; Minnesota Department of Transportation: Saint Paul, MN, USA, 1995.
61. Iatridi, Z.; Tsitsilianis, C. Water-Soluble Stimuli Responsive Star-Shaped Segmented Macromolecules. *Polymers* **2011**, *3*, 1911–1933. [CrossRef]
62. Available online: https://www.eastman.com/Markets/Tackifier_Center/Pages/Block_Copolymer.aspx (accessed on 3 July 2018).
63. Chen, J.S.; Liao, M.C.; Shiah, M.S. Asphalt Modified by Styrene-Butadiene-Styrene Triblock Copolymer: Morphology and Model. *J. Mater. Civ. Eng.* **2002**, *14*, 224–229. [CrossRef]
64. Airey, G.D. Rheological Properties of Styrene Butadiene Styrene Polymer Modified Road Bitumens. *Fuel* **2003**, *82*, 1709–1719. [CrossRef]
65. Masson, J.F.; Collins, P.; Robertson, G.; Woods, J.R.; Margeson, J. Thermodynamics Phase Diagrams and Stability of Bitumen-Polymer Blends. *Energy Fuels* **2003**, *17*, 714–724. [CrossRef]
66. Wen, G.; Zhang, Y.; Zhang, Y.; Fan, Y. Rheological Characterization of Storage-Stable SBS-Modified Asphalts. *Polym. Test.* **2002**, *21*, 295–302. [CrossRef]
67. Wang, T.; Yi, T.; Yuzhen, Z. Compatibility of SBS-modified Asphalt. *Pet. Sci. Technol.* **2010**, *28*, 764–772. [CrossRef]
68. Galooyak, S.S.; Dabir, B.; Nazarbeygi, A.E.; Moeini, A. Rheological Properties and Storage Stability of Bitumen/SBS/Montmorillonite Composites. *Constr. Build. Mater.* **2010**, *24*, 300–307. [CrossRef]
69. Krauss, G. Modification of Asphalt by Block Polymers of Butadiene and Styrene. *Rubber Chem. Technol.* **1982**, *55*, 1389–1402. [CrossRef]
70. Wloczysiak, P.; Vidal, A.; Papirer, E.; Gauvin, P. Relationships Between Rheological Properties, Morphological Characteristics and Composition of Bitumen-Styrene Butadiene Styrene Copolymers Mixes. I. A Three Phase System. *J. Appl. Polym. Sci.* **1998**, *65*, 1595–1607. [CrossRef]
71. Lu, X.; Isacsson, U. Compatibility and Storage Stability of Styrene-Butadiene-Styrene Copolymer Modified Bitumens. *Mater. Struct.* **1997**, *30*, 618–626. [CrossRef]
72. Nikolaides, A. *Highway Engineering Pavements, Materials and Control of Quality*, 1st ed.; CRC Press Taylor & Francis: Boca Raton, FL, USA, 2014; ISBN 9781466579972.
73. Pyshyev, S.; Gunka, V.; Grytsenko, Y.; Bratychack, M. Polymer modified bitumen: Review. *Chem. Chem. Technol.* **2016**, *10*, 631–636. [CrossRef]
74. Dinnen, A. Epoxy bitumen binders for critical road conditions. In Proceedings of the 2nd Eurobitume, Cannes, France, 7–9 October 1981; p. 294.
75. Chan, C.H.; Sabu, T.; Pothan, L.A.; Maria, H.J. Composites and Nanocomposites. In *Natural Rubber Materials (Vol. 2)*; Royal Society of Chemistry: Cambridge, UK, 2013; ISBN 978-1-84973-631-2.
76. Kohjiya, S. *Chemistry, Manufacture and Applications of Natural Rubber*, 1st ed.; Woodhead Publishing Limited: Cambridge, UK, 2014; ISBN 9780857096838.
77. Van Krevelen, D.W.; Te Nijenhuis, K. *Properties of Polymers: Their Correlation with Chemical Structure; Their Numerical Estimation and Prediction from Additive Group Contributions*, 4th ed.; Elsevier: Oxford, UK, 2009; ISBN 9780080548197.
78. Mark, J.E. (Ed.) *Physical Properties of Polymers Handbook*, 2nd ed.; Springer-Verlag: New York, NY, USA, 1996; ISBN 978-0-387-31235-4.
79. Studebaker, M.L. Effect of Curing Systems on Selected Physical Properties of Natural Rubber Vulcanizates. *Rubber Chem. Technol.* **1966**, *39*, 1359–1381. [CrossRef]
80. Wen, Y.; Wang, Y.; Zhao, K.; Sumalee, A. The use of natural rubber latex as a renewable and sustainable modifier of asphalt binder. *Int. J. Pavement Eng.* **2017**, *8*, 547–559. [CrossRef]
81. Shaffie, E.; Ahmad, J.; Arshad, A.K.; Kamarudin, F. Stripping Performance and Volumetric Properties Evaluation of Hot Mix Asphalt (HMA) Mix Design Using Natural Rubber Latex Polymer Modified Binder (NRMB). In *INCIEC*; Springer: Singapore, 2014.
82. Saad, A.A.; Yusof, I.B.; Hermadi, M.; Marwan, B.S.; Alfergani, M.B.S. Pavement Performance with Carbon Black and Natural Rubber (Latex). *Int. J. Eng. Adv. Technol.* **2013**, *2*, 124–129.

83. Krishnapriya, M.G. Performance Evaluation of Natural Rubber Modified Bituminous Mixes. *Int. J. Civ. Struct. Environ. Infrastruct. Eng. Res. Dev.* **2015**, *5*, 121–134.
84. Nrachai, T.; Chayatan, P.; Direk, L. The modification of asphalt with natural rubber latex. *Proc. East. Asia Soc. Transp. Stud.* **2005**, *5*, 679–694.
85. Okieimen, F.E.; Akinlabi, A.K. Processing characteristics and physico-mechanical properties of natural rubber and liquid natural rubber blends. *J. Appl. Polym. Sci.* **2002**, *85*, 1070–1076. [CrossRef]
86. Ibeagi, U.M.; Okereke, S.; Okpareke, O.C.; Ukoha, P.O. Studies on the Modifications of Asphalt Binder Using Some Selected Polymers. *Int. J. Chem. Sci.* **2012**, *10*, 2048–2056.
87. Azahar, N.B.M.; Hassan, N.A.; Jaya, R.P.; Mahmud, M.Z.H. An overview on natural rubber application for asphalt modification. *Int. J. Agric. For. Plant.* **2016**, *2*, 212–218.
88. Vural Kök, B.; Çolak, H. Laboratory comparison of crumb rubber and SBS modified bitumen and hot mix asphalt. *Constr. Build. Mater.* **2011**, *25*, 3204–3212.
89. Wang, H.; You, Z.; Mills-Bealeb, J.; Haoa, P. Laboratory evaluation on high temperature viscosity and low temperature stiffness of asphalt binder with high percent scrap tire rubber. *Constr. Build. Mater.* **2012**, *26*, 583–590. [CrossRef]
90. Mashaan, N.S.; Karim, M.R. Waste tyre rubber in asphalt pavement modification. *Mater. Res. Innov.* **2014**, *18* (Suppl. 6), S6–S9. [CrossRef]
91. Grechanovskii, V.A.; Ya Poddubnyi, I.; Ivanova, L.S. Molecular Structure and Macroscopic Properties of Synthetic Cis-Poly(Isoprene). *Rubber Chem. Technol.* **1974**, *47*, 342–356. [CrossRef]
92. Flory, P.J. Effects of Molecular Structure on Physical Properties of Butyl Rubber. *Rubber Chem. Technol.* **1946**, *19*, 552–598. [CrossRef]
93. Olivares, H.F.; Schultz, W.B.; Fernández, A.M.; Moro, B.C. Rubber-modified Hot Mix Asphalt Pavement by Dry Process. *Int. J. Pavement Eng.* **2009**, *10*, 277–288. [CrossRef]
94. Hassan, N.A.; Airey, G.D.; Jaya, R.P.; Mashros, N.; Aziz, M.M. A Review of Crumb Rubber Modification in Dry Mixed Rubberised Asphalt Mixtures. *J. Teknol.* **2014**, *70*, 127–134.
95. Lo Presti, D. Recycled Tyre Rubber Modified Bitumens for road asphalt mixtures: A literature review. *Constr. Build. Mater.* **2013**, *49*, 863–881. [CrossRef]
96. *Standard Specification for Asphalt-Rubber Binder, D 6114–97*; ASTM: West Conshohocken, PA, USA, 2002.
97. Valkering, C.P.; Vonk, W. Thermoplastic rubbers for the modification of bitumens: Improved elastic recovery for high deformation resistance of asphalt mixes. In Proceedings of the 15th Australian Road Research Board (ARRB) Conference, Darwin, Australia, 26–31 August 1999; pp. 1–19.
98. Krutz, N.C.; Siddharthan, R.; Stroup-Gardiner, M. Investigation of rutting potential using static creep testing on polymer-modified asphalt concrete mixtures. *Transp. Res. Rec.* **1991**, *1317*, 100–118.
99. Collins, J.H.; Bouldin, M.G.; Gelles, R.; Berker, A. Improved performance of paving asphalts by polymer modification (with discussion). In Proceedings of the Association of Asphalt Paving Technologists Technical Sessions, Seattle, DC, USA, 4–6 March 1991; pp. 43–79.
100. Bouldin, M.G.; Collins, J.H.; Berker, A. Rheology and microstructure of polymer/asphalt blends. *Rubber Chem. Technol.* **1991**, *64*, 577–600. [CrossRef]
101. Wardlaw, K.R.; Shuler, S. (Eds.) *Polymer Modified Asphalt Binders*; ASTM: West Conshohocken, PA, USA, 1992; ISBN 0-8031-1413-3.
102. Stock, A.F.; Arand, W. Low temperature cracking in polymer modified binders. In Proceedings of the Asphalt Paving Technology, Austin, TX, USA, 22–24 March 1993; pp. 23–53.
103. Aglan, H. Polymeric additives and their role in asphaltic pavements. Part I: Effect of additive type on the fracture and fatigue behavior. *J. Elastomers Plast.* **1993**, *25*, 307–321. [CrossRef]
104. Bahia, H.U.; Anderson, D.A. Glass transition behavior and physical hardening of asphalt binders (with discussion). In Proceedings of the Asphalt Paving Technology, Austin, TX, USA, 22–24 March 1993; pp. 93–129.
105. Elmore, W.E.; Thomas, W.K.; Mansour, S.; Bolzan, P. *Long-Term Performance Evaluation of Polymer-Modified Asphalt Concrete Pavements*; Report No.: FHWA-TX-94+1306-1F; Federal Highway Administration: Washington, DC, USA, 1993.
106. Bonemazzi, F.; Braga, V.; Corrieri, R.; Giavarini, C. Characteristics of polymers and polymer-modified binders. *Transp. Res. Rec.* **1996**, *1535*, 36–47. [CrossRef]

107. Brulè, B. Polymer-modified asphalt cements used in the road construction industry: Basic principles. *Transp. Res. Rec.* **1996**, *1535*, 48–53. [CrossRef]
108. Adedeji, A.; Grünfelder, T.; Bates, F.S.; Macosko, C.W.; Stroup-Gardiner, M.; Newcomb, D.E. Asphalt modified by SBS triblock copolymer: Structures and properties. *Polym. Eng. Sci.* **1996**, *36*, 1707–1723. [CrossRef]
109. Shin, E.E.; Bhurke, A.; Edward, S.; Rozeveld, S.; Drzal, L.T. Microstructure, morphology, and failure modes of polymer-modified asphalts. *Transp. Res. Rec.* **1996**, *1535*, 61–73. [CrossRef]
110. Loeber, L.; Durand, A.; Muller, G.; Morel, J.; Sutton, O.; Bargiacchi, M. New investigations on the mechanism of polymer–bitumen interaction and their practical application for binder formulation. In Proceedings of the 1st Eurasphalt & Eurobitume Congress, Congress Paper No. 5115, Strasbourg, France, 7–10 May 1996.
111. Gahvari, F. Effects of thermoplastic block copolymers on rheology of asphalt. *J. Mater. Civ. Eng.* **1997**, *9*, 111–116. [CrossRef]
112. Giavarini, C.; De Filippis, P.; Santarelli, M.L.; Scarsella, M. Production of stable polypropylene-modified bitumens. *Fuel* **1996**, *75*, 681–686. [CrossRef]
113. Rojo, E.; Fernàndez, M.; Peña, J.J.; Peña, B. Rheological aspects of blends of metallocene-catalysed atactic polypropylenes with bitumen. *Polym. Eng. Sci.* **2004**, *44*, 1792–1799. [CrossRef]
114. González, O.; Muñoz, M.E.; Santamaría, A. Bitumen/polyethylene blends: Using m-LLDPEs to improve stability and viscoelastic properties. *Rheol. Acta* **2006**, *45*, 603–610. [CrossRef]
115. Henderson, G. Bituminous Binders and Process of Making Same from Coal-Tar Pitch. U.S. Patent 1264932, 30 July 1917.
116. Gagle, D.W.; Draper, H.L. High Ductility Asphalt. U.S. Patent 4130516, 12 April 1976.
117. Wen, G.; Zhang, Y.; Zhang, Y.; Sun, K.; Chen, Z. Vulcanization characteristics of asphalt/SBS blends in the presence of sulphur. *J. Appl. Polym. Sci.* **2001**, *82*, 989–996. [CrossRef]
118. Wen, G.; Zhang, Y.; Zhang, Y.; Sun, K. Improved properties of SBS modified asphalt with dynamic vulcanization. *Polym. Eng. Sci.* **2002**, *42*, 1070–1081. [CrossRef]
119. Chen, J.S.; Huang, C.C. Fundamental characterization of SBS-modified asphalt mixed with sulphur. *J. Appl. Polym. Sci.* **2006**, *103*, 2817–2825. [CrossRef]
120. Zhang, F.; Yu, J.; Wu, S. Effect of ageing on rheological properties of storage-stable SBS/sulphur-modified asphalts. *J. Hazard Mater.* **2010**, *182*, 507–517. [CrossRef] [PubMed]
121. Zhang, F.; Yu, J.; Han, J. Effects of thermal oxidative ageing on dynamic viscosity, TG/DTG, DTA and FTIR of SBS-and SBS/sulphur-modified asphalts. *Constr. Build. Mater.* **2011**, *25*, 129–137. [CrossRef]
122. Masson, J.-F.; Gagné, M. Polyphosphoric Acid (PPA)-Modified Bitumen: Disruption of the Asphaltenes Network Based on the Reaction of Non-basic Nitrogen with PPA. *Energy Fuels* **2008**, *22*, 3402–3406. [CrossRef]
123. Miknis, F.P.; Thomas, K.P. NMR Analysis of Polyphosphoric Acid-modified Bitumens. *Road Mater. Pavement Des.* **2008**, *9*, 59–72. [CrossRef]
124. Jaroszek, H. Polyphosphoric acid (PPA) in road asphalts modification. *CHEMIK* **2012**, *66*, 1340–1345.
125. García-Morales, M. Dodecylbenzenesulfonic Acid as a Bitumen Modifier: A Novel Approach to Enhance Rheological Properties of Bitumen. *Energy Fuels* **2017**, *31*, 5003–5010.
126. Herrington, P.R.; Wu, Y.; Forbes, M.C. Rheological modification of bitumen with maleic anhydride and dicarboxylic acids. *Fuel* **1999**, *78*, 101–110. [CrossRef]
127. Kang, Y.; Wang, F.; Chen, Z. Reaction of asphalt and maleic anhydride: Kinetics and mechanism. *Chem. Eng. J.* **2010**, *164*, 230–237. [CrossRef]
128. Cong, P.; Chen, S.; Chen, H. Preparation and properties of bitumen modified with the maleic anhydride grafted styrene-butadiene-styrene triblock copolymer. *Polym. Eng. Sci.* **2011**, *51*, 1273–1279. [CrossRef]
129. Marzocchi, A.; Roberts, M.G.; Bolen, C.E. Asphalt Compositions Modified with Organo-Silane Compounds. U.S. Patent US4292371A, 24 March 1980.
130. Peng, C.; Chen, P.; You, Z.; Lv, S.; Zhang, R.; Xu, F.; Zhang, H.; Chen, H. Effect of silane coupling agent on improving the adhesive properties between asphalt binder and aggregates. *Constr. Build. Mater.* **2018**, *169*, 591–600. [CrossRef]
131. Cuadri, A.A.; Partal, P.; Navarro, F.J.; García-Morales, M.; Gallegos, C. Bitumen chemical modification by thiourea dioxide. *Fuel* **2011**, *90*, 2294–2300. [CrossRef]

132. Ouyang, C.; Wang, S.; Zhang, Y.; Zhang, Y. Preparation and properties of styrene–butadiene–styrene copolymer/kaolinite clay compound and asphalt modified with the compound. *Polym. Degrad. Stab.* **2005**, *87*, 309–317. [CrossRef]
133. Ouyang, C.; Wang, S.; Zhang, Y.; Zhang, Y. Thermo-rheological properties and storage stability of SEBS/kaolinite clay compound modified asphalts. *Eur. Polym. J.* **2006**, *42*, 446–457. [CrossRef]
134. Ouyang, C.; Wang, S.; Zhang, Y.; Zhang, Y. Low-density polyethylene/silica compound modified asphalts with high-temperature storage stability. *J. Appl. Polym. Sci.* **2006**, *101*, 472–479. [CrossRef]
135. Yu, J.; Wang, L.; Zeng, X.; Wu, S.; Li, B. Effect of montmorillonite on properties of styrene–butadiene–styrene copolymer modified bitumen. *Polym. Eng. Sci.* **2007**, *47*, 1289–1295. [CrossRef]
136. Polacco, G.; Kříž, P.; Filippi, S.; Stastna, J.; Biondi, D.; Zanzotto, L. Rheological properties of asphalt/SBS/clay blends. *Eur. Polym. J.* **2008**, *44*, 3512–3521. [CrossRef]
137. Zhang, B.; Xi, M.; Zhang, D.; Zhang, H.; Zhang, B. The effect of styrene-butadiene-rubber/montmorillonite modification on the characteristics and properties of asphalt. *Constr. Build. Mater.* **2009**, *23*, 3112–3117. [CrossRef]
138. Golestani, B.; Nejad, F.M.; Galooyak, S.S. Performance evaluation of linear and nonlinear nanocomposite modified asphalts. *Constr. Build. Mater.* **2012**, *35*, 197–203. [CrossRef]
139. Jasso, M.; Bakos, D.; MacLeod, D.; Zanzotto, L. Preparation and properties of conventional asphalt modified by physical mixtures of linear SBS and montmorillonite clay. *Constr. Build. Mater.* **2013**, *38*, 759–765. [CrossRef]
140. Zhang, H.; Yu, J.; Wang, H.; Xue, L. Investigation of microstructures and ultraviolet aging properties of organo-montmorillonite/SBS modified bitumen. *Mater. Chem. Phys.* **2011**, *129*, 769–776. [CrossRef]
141. Zanzotto, L.; Stastna, J.; Vacin, O. Thermomechanical properties of several polymer modified asphalts. *Appl. Rheol.* **2000**, *10*, 134–144.
142. Hesp, S.; Hoare, T.R.; Roy, S.D. Low-temperature fracture in reactive ethylene-terpolymer-modified asphalt binders. *Int. J. Pavement Eng.* **2002**, *3*, 153–159. [CrossRef]
143. Polacco, G.; Stastna, J.; Biondi, D.; Antonelli, F.; Vlachovicova, Z.; Zanzotto, L. Rheology of asphalts modified with glycidylmethacrylate functionalized polymers. *J. Colloid Interface Sci.* **2004**, *280*, 366–373. [CrossRef] [PubMed]
144. Yeh, P.H.; Nien, Y.-H.; Chen, J.-H.; Chen, W.-C.; Chen, J.-S. Thermal and rheological properties of maleated polypropylene modified asphalt. *Polym. Eng. Sci.* **2005**, *45*, 1152–1158. [CrossRef]
145. Fu, H.; Xie, L.; Dou, D.; Li, L.; Yu, M.; Yao, S. Storage stability and compatibility of asphalt binder modified by SBS graft copolymer. *Constr. Build. Mater.* **2007**, *21*, 1528–1533. [CrossRef]
146. Wang, Q.; Liao, M.; Wang, Y.; Ren, Y. Characterization of end functionalized styrene butadiene–styrene copolymers and their application in modified asphalt. *J. Appl. Polym. Sci.* **2007**, *103*, 8–16. [CrossRef]
147. Navarro, F.J.; Partal, P.; García-Morales, M.; Martinez-Boza, F.J.; Gallegos, C. Bitumen modification with a low-molecular-weight reactive isocyanate-terminated polymer. *Fuel* **2007**, *86*, 2291–2299. [CrossRef]
148. Li, J.; Zhang, Y.; Zhang, Y. The research of GMA-g-LDPE modified Qinhuangdao bitumen. *Constr. Build. Mater.* **2008**, *22*, 1067–1073.
149. Martin-Alfonso, M.J.; Partal, P.; Navarro, F.J.; García-Morales, M.; Gallegos, C. Use of an MDI functionalized reactive polymer for the manufacture of modified bitumen with enhanced properties for roofing applications. *Eur. Polym. J.* **2008**, *44*, 1451–1461. [CrossRef]
150. Martin-Alfonso, M.J.; Partal, P.; Navarro, F.J.; García-Morales, M.; Gallegos, C. Role of water in the development of new isocyanate-based bituminous products. *Ind. Eng. Chem. Res.* **2008**, *47*, 6933–6940. [CrossRef]
151. Martin-Alfonso, M.J.; Partal, P.; Navarro, F.J.; García-Morales, M.; Bordado, J.C.M.; Diogo, A.C. Effect of processing temperature on the bitumen/ MDI–PEG reactivity. *Fuel Process. Technol.* **2009**, *90*, 525–530. [CrossRef]
152. Navarro, F.J.; Partal, P.; García-Morales, M.; Martín-Alfonso, M.J.; Martínez-Boza, F.; Gallegos, C.; Bordado, J.C.M.; Diogo, A.C. Bitumen modification with reactive and non-reactive (virgin and recycled) polymers: A comparative analysis. *J. Ind. Eng. Chem.* **2009**, *15*, 458–464. [CrossRef]
153. Carrera, V.; Partal, P.; García-Morales, M.; Gallegos, C.; Páez, A. Influence of bitumen colloidal nature on the design of isocyanate-based bituminous products with enhanced rheological properties. *Ind. Eng. Chem. Res.* **2009**, *48*, 8464–8470. [CrossRef]

154. Carrera, V.; Garcia-Morales, M.; Partal, P.; Gallegos, C. Novel bitumen/isocyanate-based reactive polymer formulations for the paving industry. *Rheol. Acta* **2010**, *49*, 563–572. [CrossRef]
155. Shivokhin, M.; Garcia-Morales, M.; Partal, P.; Cuadri, A.A. Rheological behaviour of polymer-modified bituminous mastics: A comparative analysis between physical and chemical modification. *Constr. Build. Mater.* **2012**, *27*, 234–240. [CrossRef]
156. Syroezhko, A.M.; Begak, O.Y.; Fedorov, V.V.; Gusarova, E.N. Modification of paving asphalts with sulphur. *Russ. J. Appl. Chem.* **2003**, *76*, 491–496. [CrossRef]
157. Petrossi, U. Modifizierte Bitumen und Verahren zu Ihrer Herstellung. U.S. Patent 3803066, 22 February 1971.
158. Maldonado, P.; Mas, J.; Phung, T.K. Process for Preparing Bitumen-Polymer Compositions. U.S. Patent 4145322, 20 March 1979.
159. Martınez-Estrada, A.; Chávez-Castellanos, A.E.; Herrera-Alonso, M.; Herrera-Najera, R. Comparative study of the effect of sulphur on the morphology and rheological properties of SB- and SBS-modified asphalt. *J. Appl. Polym. Sci.* **2010**, *115*, 3409–3422. [CrossRef]
160. Chevillard, C.; Buras, P.; Kelly, K.P.; Butler, J.R. Method for Preparation of Stable Bitumen Polymer Compositions. U.S. Patent 6441065, 27 July 2004.
161. Ho, S.; MacLeod, D.; Brown, J.; Gee, L.; Zanzotto, L. Process of Polymer Modified Asphalt Preparation. U.S. Patent 0118395 A1, 14 January 2014.
162. Sun, D.; Ye, F.; Shi, F.; Lu, W. Storage stability of SBS-modified road asphalt: Preparation, morphology, and rheological properties. *Pet. Sci. Technol.* **2006**, *24*, 1067–1077. [CrossRef]
163. Gedik, A.; Lav, A.H. Analytical, morphological, and rheological behavior of sulfur-extended-binder. *Can. J. Civ. Eng.* **2016**, *43*, 532–541. [CrossRef]
164. Hagenbach, G.; Maldonado, P.; Maurice, J. Process for Preparing Bitumen-Polymer Compositions, Application to These Compositions of the Obtention of Coverings and Mother Solution of Polymers Usable for the Obtention of the Said Compositions. U.S. Patent 4554313A, 9 June 1983.
165. Lee, D. Modification of asphalt and asphalt paving mixtures by sulfur additives. *Ind. Eng. Chem. Prod. Res. Dev.* **1975**, *14*, 171–177. [CrossRef]
166. De Filippis, P.; Giavarini, C.; Santarelli, M.L. Reaction of visbreaker bitumens with sulfur. *Pet. Sci. Technol.* **1997**, *15*, 743–753. [CrossRef]
167. De Filippis, P.; Giavarini, C.; Santarelli, M.L. Sulphur-extended asphalt: Reaction kinetics of $H_2S$ evolution. *Fuel* **1998**, *77*, 459–463. [CrossRef]
168. Kelly, K.P.; Butler, J.R. Method for Preparation of Stable Bitumen Polymer Compositions. U.S. Patent 6180697 Bl, 5 July 2002.
169. Butler, J.R.; Kelly, K.P. Method for Preparing Asphalt and Polymer Compositions Incorporating Multi-Component Crosslinking Agents. U.S. Patent 6,407,152 Bl, 28 November 2000.
170. Butler, J.R.; Kelly, K.P.; Buras, P. Method for Preparation of Stable Bitumen Polymer Compositions. U.S. Patent 0073761A1, 4 September 1999.
171. Schermer, W.E.M.; Steernberg, K. Preparation Process for Polymer-Modified Bitumen. U.S. Patent 5719216A, 21 September 1996.
172. Kodrat, I.; Sohn, D.; Hesp, S.A.M. Comparison of polyphosphoric acid-modified asphalt binders with straight and polymer-modified materials. *Transp. Res. Rec.* **2007**, *1998*, 47–55. [CrossRef]
173. Ashry, E.S.H.; Awad, L.; El Zaher, M.A.; Elkharashe, E.; Bkheat, A.A. Modification of asphalt properties. *Prog. Rubber Plast. Recycl. Technol.* **2008**, *24*, 273–285. [CrossRef]
174. Huang, S.C.; Turner, T.; Miknis, F.; Thomas, K. Long-term aging characteristics of polyphosphoric acid-modified asphalts. *Transp. Res. Rec.* **2008**, *2051*, 1–7. [CrossRef]
175. Masson, J.F.; Collins, P.; Woods, J.R.; Bundalo-Perc, S.; Margeson, J. Chemistry and effects of polyphosphoric acid on the microstructure, molecular mass, glass transition temperatures and performance grades of asphalts. *J. Assoc. Asph. Paving Technol.* **2009**, *78*, 403–430.
176. Baumgardner, G.L. Why and how of polyphosphoric acid modification—An industry perspective. *J. Assoc. Asph. Paving Technol.* **2010**, *79*, 663–678.
177. Bennert, T.; Martin, J.V. Polyphosphoric acid in combination with styrene butadiene styrene block copolymer-laboratory mixture evaluation. *J. Assoc. Asph. Paving Technol.* **2010**, *79*, 773–791.
178. D'Angelo, J.A. Effect of poly phosphoric acid on asphalt binder properties. *J. Assoc. Asph. Paving Technol.* **2010**, *79*, 679–693.

179. McGennis, R.B. Case study: Implementation of polyphosphoric acid modification of asphalt binders and related experience. *J. Assoc. Asph. Paving Technol.* **2010**, *79*, 793–816.
180. Romagosa, E.E.; Maldonado, R.; Fee, D.; Dongre, R. Polyphosphoric acid binder modification. *J. Assoc. Asph. Paving Technol.* **2010**, *79*, 743–771.
181. Li, X.; Clyne, T.; Reinke, G.; Johnson, E.N. Laboratory evaluation of asphalt binders and mixtures containing polyphosphoric acid. *Transp. Res. Rec.* **2011**, *2210*, 47–56. [CrossRef]
182. Huang, S.C.; Miknis, F.P.; Schuster, W.; Salmans, S.; Farrar, M.; Boysen, R. Rheological and chemical properties of hydrated lime and polyphosphoric acid-modified asphalts with long-term aging. *J. Mater. Civ. Eng.* **2011**, *23*, 628–637. [CrossRef]
183. De Fatima, A.A.M.; de Freitas, V.C.L.; Pasa, V.M.D.; Leite, L.F.M. Weathering aging of modified asphalt binders. *Fuel Process. Technol.* **2013**, *115*, 19–25.
184. Zhang, F.; Hu, C. Influence of aging on thermal behaviour and characterization of SBR compound-modified asphalt. *J. Anal. Calorim.* **2014**, *115*, 1211–1218. [CrossRef]
185. Orange, G.; Jean-Valery, M.; Menapace, A.; Hemsley, M.; Baumgardner, G.L. Rutting and moisture resistance of asphalt mixtures containing polymer and polyphosphoric acid modified bitumen. *Road Mater. Pavement Des.* **2004**, *5*, 323–354. [CrossRef]
186. Baumgardner, G.L.; Masson, J.-F.; Hardee, J.R.; Menapace, A.M.; William, A.G. Polyphosphoric acid modified asphalt: Proposed mechanisms. *J. Assoc. Asph. Paving Technol.* **2005**, *74*, 283–305.
187. Thomas, K.P.; Turner, T.F. Polyphosphoric-acid modification of asphalt binders—Impact on rheological and thermal properties. *Road Mater. Pavement Des.* **2008**, *9*, 181–205. [CrossRef]
188. Oliviero Rossi, C.; Spadafora, A.; Teltayev, B.; Izmailova, G.; Amerbayev, Y.; Bortolotti, V. Polymer modified bitumen: Rheological properties and structural characterization. *Colloids Surf. A Physicochem. Eng. Asp.* **2015**, *480*, 390–397. [CrossRef]
189. Zhang, F.; Hu, C. The research for SBS and SBR compound modified asphalts with polyphosphoric acid and sulphur. *Constr. Build. Mater.* **2013**, *43*, 461–468. [CrossRef]
190. Selvavathi, V.; Sekar, V.A.V.; Sriram, V.; Sairam, B. Modifications of bitumen by elastomer and reactive polymer—A comparative study. *Pet. Sci. Technol.* **2002**, *20*, 535–547. [CrossRef]
191. Pérez-Lepe, A.; Martınez-Boza, F.J.; Attane, P.; Gallegos, C. Destabilization mechanism of polyethylene-modified bitumen. *J. Appl. Polym. Sci.* **2006**, *100*, 260–267. [CrossRef]
192. Bulatović, V.O.; Rek, V.; Markovic, J. Rheological properties of bitumen modified with ethylene butylacrylate glycidylmethacrylate. *Polym. Eng. Sci.* **2014**, *54*, 1056–1065. [CrossRef]
193. Perez-Lepe, A.; Martínez-Boza, F.J.; Gallegos, C. High temperature stability of different polymer-modified bitumens: A rheological evaluation. *J. Appl. Polym. Sci.* **2007**, *103*, 1166–1174. [CrossRef]
194. Kawakami, A.; Ando, K. Curable Composition. U.S. Patent 7452930B2, 24 October 2006.
195. Duty, R.C.; Liu, H.F. Study of the reaction of maleic anhydride with Illinois bituminous coal. *Fuel* **1980**, *59*, 546–550. [CrossRef]
196. Zher'akova, G.; Kochkan'an, R. Reactivity and structure investigation of coals in reaction with dienophiles. *Fuel* **1990**, *69*, 898–901. [CrossRef]
197. Nadkarni, V.M.; Shenoy, A.V.; Mathew, J. Thermomechanical behaviour of modified asphalts. *J. Ind. Eng. Chem. Prod. Res. Dev.* **1985**, *24*, 478–484. [CrossRef]
198. Becker, Y.M.; Muller, A.J.; Rodriguez, Y. Use of rheological compatibility criteria to study SBS modified asphalts. *J. Appl. Polym. Sci.* **2003**, *90*, 1772–1782.
199. Ray, S.S.; Okamoto, M. Polymer/layered silicate nanocomposites: A review from preparation to processing. *Prog. Polym. Sci.* **2003**, *28*, 1539–1641.
200. Alexandre, M.; Dubois, P. Polymer-layered silicate nanocomposites: Preparation, properties and uses of a new class of materials. *Mater. Sci. Eng.* **2000**, *28*, 1–63. [CrossRef]
201. Paul, D.R.; Robeson, L.M. Polymer nanotechnology: Nanocomposites. *Polymer* **2008**, *49*, 3187–3204. [CrossRef]
202. Blumstein, A. Polymerization of adsorbed monolayers: II. Thermal degradation of the inserted polymers. *J. Polym. Sci. A* **1965**, *3*, 2665–2673. [CrossRef]
203. Krishnamoorti, R.; Vaia, R.A.; Giannelis, E.P. Structure and dynamics of polymer-layered silicate nanocomposites. *Chem. Mater.* **1996**, *8*, 1728–1734. [CrossRef]

204. Liu, X.; Wu, Q.; Berglund, L.; Jiaqi, F. Polyamide 6-clay nanocomposites/polypropylene-grafted-maleic anhydride alloys. *Polymer* **2001**, *42*, 8235–8239. [CrossRef]
205. Tjong, S.C.; Bao, S.P. Impact fracture toughness of polyamide-6/montmorillonite nanocomposites toughened with a maleated styrene/ethylene butylene/styrene elastomer. *J. Polym. Sci. Part B Polym. Phys.* **2005**, *43*, 585–595. [CrossRef]
206. González, I.; Eguiazábal, J.I.; Nazábal, J. Nanocomposites based on a polyamide 6/maleated styrene-butylene-co-ethylene-styrene blend: Effects of clay loading on morphology and mechanical properties. *Eur. Polym. J.* **2006**, *42*, 2905–2913. [CrossRef]
207. Wang, H.; Zeng, C.; Elkovitch, M.; Lee, L.J.; Koelling, K.W. Processing and properties of polymeric nano-composites. *Polym. Eng. Sci.* **2001**, *41*, 2036–2046. [CrossRef]
208. Yurekli, K.; Karim, A.; Amis, E.J.; Krishnamoorti, R. Influence of layered silicates on the phase-separated morphology of PS—PVME Blends. *Macromolecules* **2003**, *36*, 7256–7267. [CrossRef]
209. Si, M.; Araki, T.; Ade, H.; Kilcoyne, A.L.D.; Fisher, R.; Sokolov, J.C.; Rafailovich, M.H. Compatibilizing bulk polymer blends by using organoclays. *Macromolecules* **2006**, *39*, 4793–47801. [CrossRef]
210. Vo, L.T.; Giannelis, E.P. Compatibilizing poly(vinylidene fluoride)/Nylon-6 blends with nanoclay. *Macromolecules* **2007**, *40*, 8271–8276. [CrossRef]
211. Chow, W.S.; MohdIshak, Z.A.; Karger-Kocsis, J. Morphological and rheological properties of polyamide 6/poly(propylene)/organoclay nanocomposites. *Macromol. Mater. Eng.* **2005**, *290*, 122–127. [CrossRef]
212. Fang, Z.; Xu, Y.; Tong, L. Free-volume hole properties of two kinds thermoplastic nanocomposites based on polymer blends probed by positron annihilation lifetime spectroscopy. *J. Appl. Polym. Sci.* **2006**, *102*, 2463–2469. [CrossRef]
213. Filippi, S. Effects of organoclay on morphology and properties of nanocomposites based on LDPE/PA-6 Blends without and with SEBS-g-MA compatibilizer. *Polym. Eng. Sci.* **2009**, *49*, 1187–1197. [CrossRef]
214. Wang, Y.P.; Liu, D.J.; Li, Y.F.; Gao, J.M. Preparation and properties of asphalts modified with SBS/organobentonite blends. *Polym. Polym. Compos.* **2006**, *14*, 403–411. [CrossRef]
215. Merusi, F.; Giuliani, F.; Filippi, S.; Polacco, G. A model combining structure and properties of a 160/220 bituminous binder modified with polymer/clay nanocomposites. A rheological and morphological study. *Mater. Struct.* **2013**, *47*, 819–838. [CrossRef]
216. Zhang, J.; Wang, J.; Wu, Y.; Sun, W.; Wang, Y. Investigation on thermo-rheological properties and stability of SBR modified asphalts containing palygorskite clay. *J. Appl. Polym. Sci.* **2009**, *113*, 2524–2535. [CrossRef]
217. Sureshkumar, M.S.; Filippi, S.; Polacco, G.; Kazatchkov, I.; Stastna, J.; Zanzotto, L. Internal structure and linear viscoelastic properties of EVA/asphalt nanocomposites. *Eur. Polym. J.* **2010**, *46*, 621–633. [CrossRef]
218. Sureshkumar, M.S.; Stastna, J.; Polacco, G.; Filippi, S.; Kazatchkov, I.; Zanzotto, L. Rheology of bitumen modified by EVA—Organoclay nanocomposites. *J. Appl. Polym. Sci.* **2010**, *118*, 557–565.
219. Rossi, D.; Filippi, S.; Merusi, F.; Giuliani, F.; Polacco, G. Internal Structure of Bitumen/Polymer/Wax Ternary Mixtures for Warm Mix Asphalt. *J. Appl. Polym. Sci.* **2013**, *129*, 3341–3354. [CrossRef]
220. Edwards, Y.; Redelius, P. Rheological Effects of Waxes in Bitumen. *Energy Fuels* **2003**, *17*, 511–520. [CrossRef]
221. Warth, A.B. *The Chemistry and Technology of Waxes*; Reinhold: Waldwick, NJ, USA, 1956.
222. Thanh, N.X.; Hsieh, M.; Philip, R.P. Waxes and Asphaltenes in Crude Oils. *Org. Geochem.* **1999**, *30*, 119–132. [CrossRef]
223. Edwards, Y.; Isacsson, U. Wax in Bitumen, Part 1-Classifications and General Aspects. *Road Mater. Pavement Des.* **2005**, *6*, 281–309. [CrossRef]
224. Edwards, Y.; Isacsson, U. Wax in Bitumen, Part 2-Characterization and Effects. *Road Mater. Pavement Des.* **2005**, *6*, 439–468. [CrossRef]
225. Lu, X.; Kalman, B.; Redelius, P. A New Test Method for Determination of Wax Content in Crude Oils, Residues and Bitumen. *Fuel* **2008**, *87*, 1543–1551. [CrossRef]
226. Lu, X.; Langton, M.; Olofsson, P.; Redelius, P. Wax Morphology in Bitumen. *J. Mater. Sci.* **2005**, *40*, 1893–1900. [CrossRef]
227. Michon, L.C.; Netzel, D.A.T.; Turner, F.; Martin, D.; Planche, J.P. A $^{13}C$ NMR and DSC Study of the Amorphous and Crystalline Phases in Asphalts. *Energy Fuels* **1999**, *13*, 603–610. [CrossRef]
228. Lu, X.; Redelius, P. Compositional and Structural Characterization of Waxes Isolated from Bitumens. *Energy Fuels* **2006**, *20*, 653–660. [CrossRef]

229. Lu, X.; Redelius, P. Effect of Bitumen Wax on Asphalt Mixture Performance. *Constr. Build. Mater.* **2007**, *21*, 1961–1970. [CrossRef]
230. Lee, H.; Wong, W. Effect of wax on basic and rheological properties of bitumen with similar Penetration-grades. *Constr. Build Mater.* **2009**, *23*, 507–514. [CrossRef]
231. Wong, W.; Li, G. Analysis of the effect of wax content on bitumen under performance grade classification. *Constr. Build. Mater.* **2009**, *23*, 2504–2510. [CrossRef]
232. Giuliani, F.; Merusi, F. Flow Characteristics and Viscosity Functions in Asphalt Binders Modified by Wax. *Int. J. Pavement Res. Technol.* **2009**, *2*, 51–60.
233. Merusi, F.; Caruso, A.; Roncella, R.; Giuliani, F. Moisture Susceptibility and Stripping Resistance of Asphalt Mixture Modified with Different Synthetic Waxes. *Transp. Res. Rec.* **2010**, *2180*, 110–120. [CrossRef]
234. Merusi, F.; Giuliani, F. Rheological Characterization of Wax-Modified Asphalt Binders at High Service Temperatures. *Mater. Struct.* **2011**, *44*, 1809–1820. [CrossRef]
235. Edwards, Y.; Tasdemir, Y.; Butt, A. An Energy Saving and Environmental Friendly Wax Concept for Polymer Modified Mastic Asphalt. *Mater. Struct.* **2010**, *43*, 123–131. [CrossRef]
236. Kim, H.; Lee, S.J.; Amirkhasian, S.N. Effects of Warm Mix Asphalts Additives on Performance Properties of Polymer Modified Asphalt Binders. *Can. J. Civ. Eng.* **2010**, *37*, 17–24. [CrossRef]
237. Kim, H.; Lee, S.J.; Amirkhasian, S.N. Performance Evaluation of Recycled PMA Binders Containing Warm Mix Asphalt Additives. *J. Test. Eval.* **2011**, *39*, 728–734.
238. Akisetty, C.K.; Lee, S.J.; Amirkhanian, S.N. Laboratory Investigation of the Influence of Warm Asphalt Additives on Long-Term Performance Properties of CRM Binders. *Int. J. Pavement Eng.* **2011**, *11*, 153–160. [CrossRef]
239. Gonzalez, V.; Martinez-Boza, F.J.; Navarro, F.J.; Gallegos, C.; Perez-Lepe, A.; Paez, A. Thermomechanical Properties of Bitumen Modified with Crumb Rubber and Polymeric Additives. *Fuel Process. Technol.* **2010**, *91*, 1033–1039. [CrossRef]
240. Akisetty, C.K.; Gandhi, T.; Lee, S.J.; Amirkhanian, S.N. Analysis of Rheological Properties of Rubberized Binders Containing Warm Asphalt Additives. *Can. J. Civ. Eng.* **2010**, *37*, 763–771. [CrossRef]


© 2019 by the authors. Licensee MDPI, Basel, Switzerland. This article is an open access article distributed under the terms and conditions of the Creative Commons Attribution (CC BY) license (http://creativecommons.org/licenses/by/4.0/).

applied sciences

MDPI

*Review*

# A Review on Bitumen Rejuvenation: Mechanisms, Materials, Methods and Perspectives

**Valeria Loise [1], Paolino Caputo [1,*], Michele Porto [1], Pietro Calandra [2,*], Ruggero Angelico [3] and Cesare Oliviero Rossi [1]**

[1] Department of Chemistry and Chemical Technologies, University of Calabria, Via P. Bucci, Cubo 14/D, 87036 Rende (CS), Italy; valeria.loise@unical.it (V.L.); michele.porto@unical.it (M.P.); cesare.oliviero@unical.it (C.O.R.)

[2] CNR-ISMN, National Council of Research, Institute for the Study of Nanostructured Materials, Via Salaria km 29.300, 00015 Monterotondo Stazione (RM), Italy

[3] Department of Agricultural, Environmental and Food Sciences (DAAA), University of Molise, Via De Sanctis, 86100 Campobasso (CB), Italy; angelico@unimol.it

* Correspondence: paolino.caputo@unical.it (P.C.); pietro.calandra@ismn.cnr.it (P.C.); Tel.: +39-0984-493381 (P.C.); +39-0690-672409 (P.C.)

Received: 12 September 2019; Accepted: 7 October 2019; Published: 14 October 2019


**Abstract:** This review aims to explore the state of the knowledge and the state-of-the-art regarding bitumen rejuvenation. In particular, attention was paid to clear things up about the rejuvenator mechanism of action. Frequently, the terms rejuvenator and flux oil, or oil (i.e., softening agent) are used as if they were synonymous. According to our knowledge, these two terms refer to substances producing different modifications to the aged bitumen: they can decrease the viscosity (softening agents), or, in addition to this, restore the original microstructure (real rejuvenators). In order to deal with the argument in its entirety, the bitumen is investigated in terms of chemical structure and microstructural features. Proper investigating tools are, therefore, needed to distinguish the different mechanisms of action of the various types of bitumen, so attention is focused on recent research and the use of different investigation techniques to distinguish between various additives. Methods based on organic synthesis can also be used to prepare ad-hoc rejuvenating molecules with higher performances. The interplay of chemical interaction, structural changes and overall effect of the additive is then presented in terms of the modern concepts of complex systems, which furnishes valid arguments to suggest X-ray scattering and Nuclear Magnetic Resonance relaxometry experiments as vanguard and forefront tools to study bitumen. Far from being a standard review, this work represents a critical analysis of the state-of-the-art taking into account for the molecular basis at the origin of the observed behavior. Furnishing a novel viewpoint for the study of bitumen based on the concepts of the complex systems in physics, it constitutes a novel approach for the study of these systems.

**Keywords:** Bitumen; rejuvenator; oils; flux agents; physical chemistry techniques; structure; RAP

## 1. Introduction to Bitumen and Ageing

Asphalts are well-known materials used for road pavement throughout the world. They are heterogeneous systems where one phase is constituted by macro-meter sized inorganic particles called aggregates, and the other one is the binding agent (bitumen). The latter, in turn, is a micro heterogeneous complex viscous fluid constituted by nano-meter sized aggregates of polar molecules (asphaltenes) hierarchically organized with different levels of aggregations [1], and dispersed in a more apolar continuous phase of saturated paraffins, aromatic oils and resins called maltene [2,3].

Asphalts are, therefore, biphasic systems, with the predominant phase (93–96%, *w*/*w*) made by the macro-meter sized inorganic aggregates (size from microns to millimeters) hold together by small amounts of binding bitumen which constitutes the second phase. Although the bitumen constitutes the minor part of the asphalt, it however plays the most important role, giving consistency to the overall material, which is necessary for practical purposes: even slight changes in the bitumen will affect the overall properties of asphalt. Even the usability of asphalt can be traced back to the properties of its bitumen. This work will focus the attention on bitumen as a key ingredient in asphalt. Where necessary, however, some extensions will cover asphalt and related aspects. The aggression of chemicals normally presents in the environment, or ageing can oxidize some of the organic components in the bitumen so that the increase in polar functional groups can cause immobilization of an excessive number of macromolecules and ultimately bitumen embrittlement and asphalt cracks. Other processes causing ageing are loss of volatiles and changes in a molecular organization driven by the spontaneous tendency to reach a stable (equilibrium) thermodynamic state, which obviously depends on the conditions [4]. As a consequence of the mentioned processes taking place in bitumen, the final asphalt is susceptible to fracturing or cracking in thermal or mechanical stresses. Ageing of bitumen, therefore, constitutes a serious problem. Aged asphalt can be re-used in mixtures with new binders, answering the economic need for low-cost production and fully facing obvious environmental concerns. Therefore, recent research has been focused on reclaimed asphalt pavements (RAPs), which really are environmentally friendly alternatives and constitute an economically viable way to afford the costs of binder and aggregates. However, their use is still limited (less than 20% in the new mixtures), due to their low rheological performances (high stiffness and low stress relaxation ability [5] which can cause unexpected premature failure [6]. To overcome these problems, opportune actions must be taken to improve the mechanical and chemical properties of aged bitumen or RAP/bitumen mixtures. The addition of opportune additives is certainly one of the most effective. For example, a compound able to tune the red-ox state of the polar molecules contained in the bitumen can avoid the degrading process. The restoring of a favorable asphaltene/maltene relative ratio by providing more maltene is another solution, since the viscosity of bitumen is related to the fraction of asphaltene [7]. Another strategy can be directed to the stabilization of the supramolecular aggregates mainly made by asphaltene formed in the maltene phase [8,9] acting on their interfacial tension and consequently better dispersing them. In all these cases, a rejuvenator is usually dealt with. With this work, the recent studies carried out in this field will be highlighted in order to shed light on the possible mechanisms of actions of a rejuvenator and to furnish a panoramic view considering both theoretical considerations and applicative aspects. This works will show the state-of-the-art in the use of rejuvenators in bitumen, taking care to highlight also some applications to the rejuvenation of recycled asphalt for a more complete view of the problematics. Differently from standard review papers, this work, prior to presenting all the state-of-the-art works dealing with rejuvenators (Section 4), it proposes a clear, new and marked distinction between different "rejuvenators" according to their effect and influence at the microscopic length-scale individuating techniques and methods of analysis for their distinction (Section 3 "mechanisms of ageing and rejuvenating" and sub-paragraphs). Then, the work will show methods for the synthesis of ever more performing rejuvenators (Section 5) and suggest vanguard techniques of investigation (Section 6).

## 2. Methods for Bitumen Characterizations

The characteristics of bitumen are not trivial at all: it is an organic high-viscosity viscoelastic binding agent which is itself a composite system constituted by nano-meter sized aggregates of polar molecules (asphaltenes) dispersed in a more apolar continuous phase of saturated paraffins, aromatic oils and resins called maltene [2,3]. Usually, these fractions can be determined by the so-called S.A.R.A. determination (Saturates, Aromatics, Resins and Asphaltenes) [10]. In this method, the sample of bitumen is dissolved in peroxide-free tetrahydrofuran solvent (usually to reach a 2% (*w*/*v*) solution). Saturated components of the sample are developed in *n*-heptane solvent while the aromatics in a 4:1

mixture of toluene and *n*-heptane. Afterwards, the rods are dipped into a third tank, (usually 95 to 5% mixture of dichloromethane and methanol). This organic medium proved suitable to develop the resin fraction, whereas, the asphaltene fraction is left on the lower end of the rods. However, it must also be pointed out that asphaltenes are not classified using their molecular structure, but they are defined traditionally on the basis of the procedure required to extract them from heavy oils [11]. Bitumen are a not well-defined mixture of constituents so different methods of analysis exist where solvents are added to bitumen to determine its chemical properties. For example, Zenke [12] offered a method for not only determining the number of maltenes and asphaltenes of bitumen, but also distinguishing light-, middle-, and high-solubility of asphaltenes. However, for an effective study, the general viewpoint of their overall assembly becomes more important than the detailed chemical speciation of the various molecules involved. Based on this, a testing method for determination of the quality of bitumen, called "simplified laboratory method", was developed in order to gain fast and easy information. S.A.R.A. determination and the attempts by Zenke are examples of this approach to gain chemical information. Bitumen are also regarded in terms of their performances, for which a rheological description of the materials is often given. Empirical approaches are always followed to determine the performances within a chosen temperature range [13,14] for convenient use [15,16]. Due to the general description of the bitumen performances in rheological terms (penetration index, softening point, ductility, viscosity), and due to the need of quick, easy and low-cost methods to characterize the bitumen, the lack of detailed knowledge of the supramolecular assembly characterizing the bitumen structure at the various levels of complexity caused the fact that a rational correlation of the bitumen structure with its performances is actually missing. Attempts at more sophisticated investigative tools are present. Scattering experiments, and in particular X-ray scattering ones, would be advisable to probe the structure from the Å to the meso-scale. As a matter of fact, remarkable attempts have been made since the '60s [17], but the bitumen complex organization has hindered the development of such structural study in details. The structural investigation has been, therefore, generally carried out by Atomic Force Microscopy (AFM) [18], by Confocal Laser Scanning Microscopy [19], by Optical Microscopy [20], and Fluorescence Microscopy [21], but all these methods were used to probe the micro-scale (not going deeper to the nano-scale) and the surface. Attempts at gaining information on the nano-scale structure of the bulk have been limited, and the results remained quite hypothetical [22]. Even the "colloidal structure" is just empirically derived by the contents of aromatics, resins, asphaltenes and saturates [23]. This is probably due, in our opinion, to the always-urgent need of improving performances for applicative purposes so that basic research, highlighting the specific intermolecular interactions and the molecular organization at the base of the observed behavior has been sometimes overlooked. Therefore, there is still a lack of information on how many additives affect the supra-molecular structure and the distribution of aggregates within the bituminous colloidal network and how this can reflect on the overall material properties. This makes the relationship between molecular interactions and the final material structure/properties (which is ultimately the final objective of physical chemistry) still quite vague. This problem was already faced recognizing that bitumen are characterized by intermolecular associations at different length-scales: asphaltene molecules are aggregated to form stacks by self-interactions and these aggregates are stabilized by polar resins, due to their amphiphilic chemical nature and the overall structures are then dispersed in a paraffin-like apolar matrix. These characteristics render the material a truly complex system, so an approach based on the complex systems theory is, therefore, necessary foreseeing different levels of complexity, each of them potentially showing emerging properties arising from the opportune organization of the molecules. It has been, in fact, recently highlighted that asphaltenes tend to form stacks of about 18 Å, organized at higher levels of complexity in anisotropic aggregates of about 200 Å × 28 Å, which, again, are assembled to form micrometer-size elongated aggregates characterized by the so-called "bee-structure" [24]. However, asphaltenes are unable to create a continuous network [25]. These recent findings opened the door to a better comprehension of the bitumen structure from X-ray scattering data, making this technique a method of election [26] for the structural investigation of such systems. In this context, it was shown

that the influence of additives is exerted by their preferential localization in the maltene phase or close to the asphaltene clusters, depending on the additive chemical characteristics, thus, finally affecting the overall rheological properties. An additive can play, therefore, important roles: it can exert its effect at the inorganic/organic interface, or, at a lower level of complexity, within the maltene/asphaltene aggregates, whereas, a redox additive works at the chemical state of the single polar molecules, i.e., at an even lower level of complexity. Another mechanism exerted by the additive is the formation of a network inside the maltene giving elasticity to the bitumen [27] or a simple change of physical phase transition with fluxing at a higher temperature while conferring rigidity at lower ones [28]. The so-called "antistripping agents" act by stabilization of eventual supramolecular asphaltene aggregates in the maltene phase [8,9]. As regards the additive chemical nature, selected polymers have been used (low-density polyethylene, ethylene-vinyl-acetate, SBS-polyphosphoric acid (PPA), Elvaloy, etc.) [29], as well as smaller molecules falling in the categories of organosilane and phospholipids [30] or paraffinic synthetic waxes, derivate of fatty amines and surfactants [31], antioxidants [32], etc. Once introduced the chemical and the structural characteristics of a bitumen, the next paragraphs will highlight the modifications taking place during ageing and how the original state can be restored by the introduction of the concept of rejuvenator.

## 3. Mechanisms of Ageing and Rejuvenating

### *3.1. Ageing*

Due to the ageing process of bitumen and its corresponding increase in viscosity, the stiffness of asphalt pavement increases during its lifetime. The general, zero-order, description of aging is given in terms of an overall mechanism where some of the maltene medium is transformed into the asphaltene phase, resulting in higher asphaltene and lower maltene contents. This leads to a higher viscosity and lower ductility, due to the stronger polar-polar interactions between asphaltenes. In simpler words, "when the asphaltene micelles are not sufficiently mobile to flow past one another under the applied stress, the resistance of asphalt binder to cracking or fracture is decreased" as beautifully depicted by J. Petersen [4]. However, ageing is a more complex process involving different sub-mechanisms usually taking place in different time-scales. It can already take place during asphalt construction through volatilization of light components in the maltene. Then, long-term aging occurs in the field as a consequence of different processes:

1. Oxidative, due to changes in composition through a reaction between bitumen constituents and atmospheric oxygen;
2. Evaporative, due to the evaporation of low-molecular weight components in the maltene. These compounds have higher vapor pressure and are somehow volatile so they can escape the maltene phase causing not only a change of its composition, but also an overall reduction of its amount in the bitumen;
3. Structural ageing, by a chemical reaction between molecular components causing polymerization with consequent formation of a structure within the bitumen (thixotropy) [33].

The processes involved are schematically depicted in Figure 1.

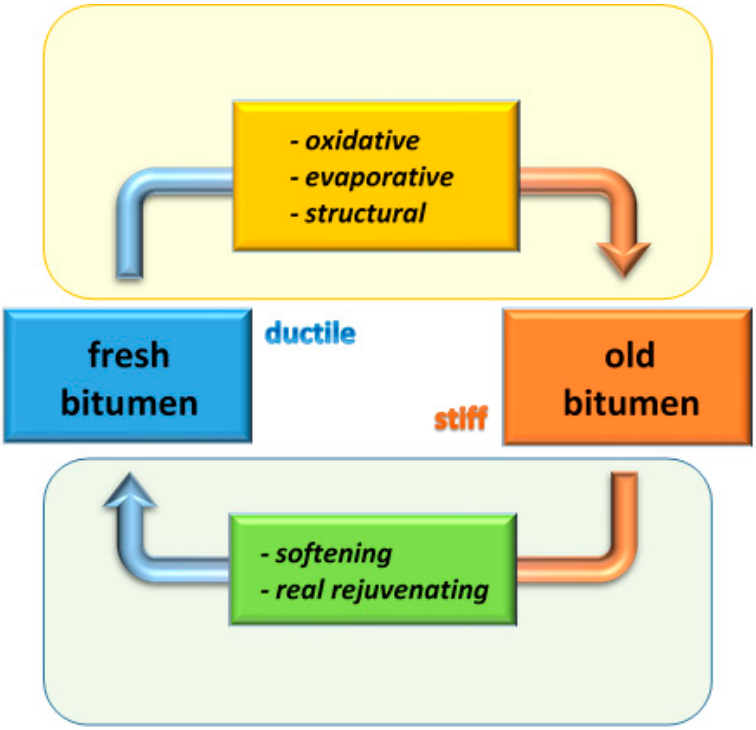


**Figure 1.** Scheme showing the main processes involved in bitumen ageing and its rejuvenation.

### *3.2. Rejuvenation*

A rejuvenator has been defined as that agent capable of restoring the original rheological properties of a bitumen. Therefore, it is assumed that the primary action of a rejuvenator should be to bring the bitumen to lower stiffness and viscosity and higher ductility. Despite the above description of bitumen ageing showing different and somehow interconnected mechanisms, taking place, simultaneously, the very first action to restore the original bitumen rheological properties is to shift back the ratio between solid asphaltenes and fluid maltenes to higher maltene contents. However, a rheological rejuvenating agent can exert its action in different sub-mechanisms (see the schematic diagram of Figure 1):

1. Softening (usually called fluxing) agent: flux oil, lube stock, slurry oil, etc. can lower the viscosity of the aged binder;
2. Real rejuvenator: it helps to restore the physical and chemical properties [33].

As it will be seen (see Section 4), literature does not make a clear distinction among the types of mechanism exerted by the specific rejuvenator: this name is usually given to any king of additive, which allows a certain restoring of the original rheological properties, no matter the effective mechanism involved. Instead, we are keen on making a clear distinction: given the aim of this contribution to go deeper into the details and to make clear all the aspects involved, it will be now defined a rheological rejuvenator as any type of additive causing a certain restoring of the rheological characteristics. In the specific, if the rejuvenator is also able to restore even the bitumen inner structure, then it will be defined as a real rejuvenator. If, on the other hand, the rheological rejuvenator makes the bitumen more ductile and less viscous/brittle by simply furnishing oily components to maltene without restoring the original complex structure (hierarchical structures of asphaltenes), then it will be called as softening (more often fluxing) agent. It can be seen that in this distinction, the term "rheological rejuvenator" has a more general sense and is associated with the concept of "rejuvenator" usually present in the literature. For this reason, in the following, when simply naming "rejuvenator" it will be referred to rheological rejuvenator, to resemble the classical meaning of rejuvenator usually adopted. Instead, when dealing with real rejuvenator effect, the terminology "real rejuvenator" will be stressed. Rheological rejuvenators are, however, usually based on oils: lubricating oil extracts and extender

oils. They contain an adequate amount of maltene constituents, naphthenic or polar aromatic fractions, which re-balance the composition of the aged binder in favour of such compounds or those usually lost during construction and service. Rejuvenator must fulfil two requirements:

1. They should have a high proportion of aromatics, which are necessary to keep the asphaltenes dispersed;
2. They should contain a low content of saturates, which are highly incompatible with the asphaltenes.

#### 3.2.1. Down to the Nano-Scale

Of course, the effectiveness of a rejuvenation action depends on the uniform dispersion of the rejuvenator within the bitumen. In fact, after its mixing with aged bitumen and the obvious homogenization, diffusional processes taking place at longer times and shorter length-scales must complete the job. This aspect was first faced by Lee et al. in 1983 [34] who mixed a dye with the rejuvenator to estimate the homogenization of the overall product by visual inspection. The authors concluded that mechanical mixing could give a uniform distribution of the rejuvenators within the bitumen. However, our perplexity holds in the fact that visual inspection cannot probe the uniformity of dispersion at the sub-micro scale, which instead is the final goal of an efficient mixing allowing complete rejuvenator action. According to a work by Carpenter and Wolosick [35] published few years before, the diffusion of a rejuvenator into an aged binder is a complex, multi-step mechanism consisting of four steps (the curious reader is redirected to the reading of that article for details), but basically the requirement of a complete homogenization of the rejuvenator down to the nano-scale was already pointed out. However, their results were later confirmed by Noureldin and Wood [36], and Huang et al. [37]. The complete homogenization, down to the sub-micro scale cannot happen without being diffusion-driven and diffusion-limited—a dynamical process whose rate is given by the viscosity of the medium. This indeed, has been shown by Karlsson and Isacsson [38], who highlighted that the diffusion rate is governed by the viscosity of the maltene phase rather than the viscosity of the recycled binder as a whole, an aspect which was somehow observed previously by Oliver [39] who had suggested that the diffusion could be sped up by diluent oil fractions addition and/or raising the temperatures.

#### 3.2.2. Distinguishing Softening Agents and Real Rejuvenators

From the point of view of the physical performances, softening (fluxing) and real rejuvenating, which constitute two different mechanisms, can be distinguished experimentally. Whereas, the stiffness or rigidity of a bitumen, usually empirically determined by simplified and fast methods generally by immediate techniques developed for characterizing mechanical and rheological properties and used especially in the field of engineering [40], the distinction of the two effects of fluxing and real rejuvenating needs the exploitation of methods with a substantial physical basis. In this ambit, small amplitude oscillatory rheometry is a useful technique using specific specimen geometries and mathematical interpretation of the data to achieve physical quantities: the complex modulus $G^*$. $G^*$ is a measure of the total energy required to deform the specimen and is defined as:

$$|G^*|^2 = (G')^2 + (G'')^2 \quad (1)$$

where $G'$ is the elastic modulus (or storage modulus), a measure of the energy stored in the material during oscillation, and $G''$ is the viscous modulus (or loss modulus), a measure of the energy dissipated as heat. Martin Radenberg et al. [41] highlighted the difference between a "rejuvenating" (here associated with our conception of real rejuvenating) effect and a "fluxing" agent from a rheological perspective using the so-called black diagrams, which depict the magnitude of the complex modulus $G^*$ versus the phase angle ($\delta$, defined as $\tan \delta = G''/G'$) obtained from the dynamic tests. In black diagrams, frequency and temperature are eliminated. This method was previously suggested by Airey and Brown [42] to assess and compare the rheological properties of bitumen. The characterization of

the two different actions of rejuvenator has been recently carried out by NMR. Although bitumen is a complex material, ambitious studies are facing structural characterization by probing relaxation times. Application of Low-Field NMR has been used for the determination of physical properties of petroleum fractions [43,44], and the Inverse Laplace Transform (ILT) analysis of the NMR echo signal decay gives the $T_2$ relaxation time which can be connected to different domains characterized by different rigidities [45]. The chemical reasoning for this lies on the molecular constraint, causing dynamic hindrance and lowering $T_2$, an effect that can be considered quite general and already found also in different systems [46]. These attempts have given interesting and encouraging results, which deserve to be tailored. We support efforts in this direction since the comprehension of the microscopic/molecular processes at the basis of the observed behavior of a material is of fundamental importance for the improvement of materials characteristics in specific applications.

## 4. The State-Of-The-Art

### *4.1. General Requirements*

As a general requirement, additives should be non-hazardous and stable over a wide range of temperatures, from production to application. In addition, they must not experience any exudation or evaporation, in order to ensure good performance over the designed lifetime of the asphalt pavement. Further specific requirements depend on the local country specification. Bocci et al. for example [47], focus on the use of a specific bio-based rejuvenator to produce asphalt concrete using a high amount of RAP without scarifying the mix performance and complying with the Italian specifications. In particular, the paper presents the results from a trial section on a highway connecting Ancona to Perugia, in the center of Italy.

In any case the use of "forbidden" chemicals should not be the goal of the work: for example, Tine et al. [48] take care in clarifying that the additives they studied in their work (a liquid process oil with a typical viscosity at 40 °C of 700 $mm^2/s$) conform to all current Registration, Evaluation, Authorisation and restriction of Chemicals, (REACH) and Polycyclic Aromatic Hydrocarbons (PAHs) limits. Another additive they used (a tall oil distillate originating from pine trees) is "not classified as dangerous according to Directive 67/548/EEC and its amendments and according to EU legislation". In our opinion, any work should clarify the environmental/safety/legal issues connected to the additives presented.

In this sense, Król et al. [49], and Somé et al. [50] show that the addition of some particular bio-additives has a large potential application as reversible fluxing agents in bitumen industry, RAP technology and Warm Mix Asphalt (WMA). They used vegetable oil produced using various raw materials (Rapeseed oils, Soybean oil, Sunflower oil, Linseed oil, etc.) and combined in bituminous binders generally as a modifier/additive (up to 10%). Interestingly, not only they used vegetable oils, but they also perform chemical action to prepare other additives (they use methyl esters of fatty acid obtained by transesterification of vegetable oils). The aspect of a couple the use of raw/cheap materials with chemical actions to increase their performances is intriguing and promising. The chemical actions that can be performed for the optimization of additive performances will be discussed in Section 5.

The rejuvenating benefits can be utilized to allow for higher RAP addition using traditional hot mix asphalt (HMA) configuration or in the warm mix asphalt (WMA) technology since the additives, changing the viscosity of the binder, allow for the lowering of the asphalt mixture production temperature. Critical issue related to the application of the additive fluxing of the bitumen is the final viscosity of the bitumen and stiffness of the mixture placed in the pavement. In fact, while fluxing is desired during mixture production, placement and compaction, it is no longer appreciated once the road is open to traffic. Considering the examples of Król et al. [49], and Somé et al. [50], the suitability criterion for vegetable oils and the corresponding methyl esters for obtaining environment-friendly bitumen fluxes is their reactivity to the oxypolymerization reaction, which raises the viscosity of the stock, thus, contributing to its hardening and drying. The efficiency of polymerization depends on the

number of double bonds and their position in the aliphatic chain of fatty acid. Oxypolymerization of the fatty acids present in the vegetable stocks is a multistage process and leads to the crosslinking of their structural units. The principle of using additives susceptible to oxypolimerization has been recently exploited for preparing additives, increasing the bitumen viscosity [51].

This paragraph, from the next sub-paragraph on, is devoted to showing the works involving rejuvenators as additives in bitumen. Some applications to the rejuvenation of partly recycled asphalt will also be shown for a more complete view of the problematics also because for practical uses sometimes rejuvenation must be exerted on recycled asphalt (RAP, reclaimed asphalt pavement). They have been grouped according to the experimental methods that can be used for the rejuvenation evaluation. In addition, particular care has been taken in using the same names and formalisms used by the various Authors, for a better comparison with the original works.

### 4.2. Rejuvenation Probed by IR

Zargar et al. in 2012 [52] explored the possibility of using a waste cooking oil (WCO) as rejuvenator in the aged bitumen, in order to reduce the expense of highway renovation. They added various amounts of a WCO mainly composed by Oleic acid (C18:2n9c, 43.7%), Palmitic acid (C16:0, 38.4%) and Linoleic acid (C18:2n6c, 11.4%) to an aged bitumen monitoring the changes in standard parameters like penetration index, softening point, Brookfield viscosity and dynamic shear viscosity. The comparison among pristine, aged and rejuvenated bitumen gave self-consistent results furnishing clear clues: the aged bitumen, which is stiffer than the virgin one as result of oxidation processes, can be substantially driven to the performances typical of the virgin bitumen by progressive addition of waste cooking oil. The restoring of the virgin performances takes place at WCO content of 3%, but they can even be improved (n penetration index, softening point and viscosity) by further addition of WCO up to 5%. See, for example, Figure 2 where the penetration value versus various rejuvenator amounts is reported. These results were interpreted at the molecular basis with the aid of Fourier transform infrared spectroscopy (FT-IR) which probes the amount of oxidized functional groups, and specifically C=O and S=O. The increase of polar functional group signal intensity, and specifically C=O and S=O ones, in FT-IR spectra when the bitumen is aged correlates with its stiffness increase. This suggests that the loss in bitumen performances is due to the oxidation process. Even, this increase correlates with an increase in asphaltenes fraction, i.e., the most polar component of the bitumen. On the other hand, the addition of WCO implies a substantial restoring of the pristine C=O and S=O signal, together with the pristine asphaltene/maltene ratio, although the process seems not to be complete/quantitative. Typical IR spectra, together with the most important band attributions, are reported in Figure 3. In conclusion, WCO appears to have a rejuvenating effect because it reduces the oxidation (asphaltene content) compared to an aged bitumen, even if it is not capable of restoring the correct ratio maltene asphaltenes. However, it is interesting to point out that the rejuvenated bitumen has less tendency to ageing compared to original bitumen and has lower volatility than the virgin bitumen reasonably, due to the lower volatility of bio-oil as a consequence of its high content in saturated hydrocarbons. Unfortunately, the Authors do not give details on the FT-IR experiments.

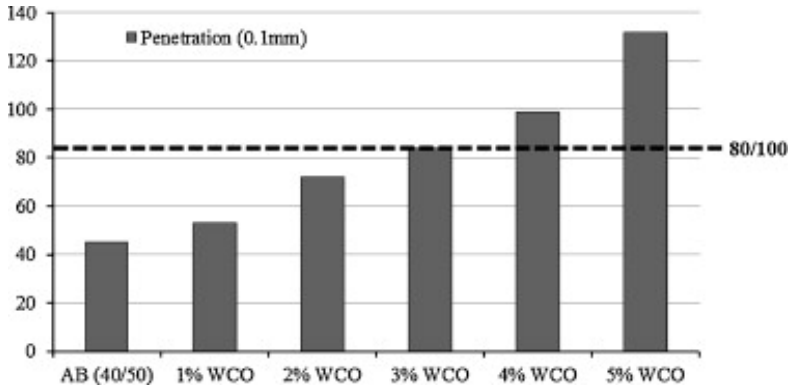


**Figure 2.** Penetration value versus different rejuvenated waste cooking oil (WCO) bitumen's (AB, aged bitumen) (reprinted from Reference [52] with the permission of Elsevier).

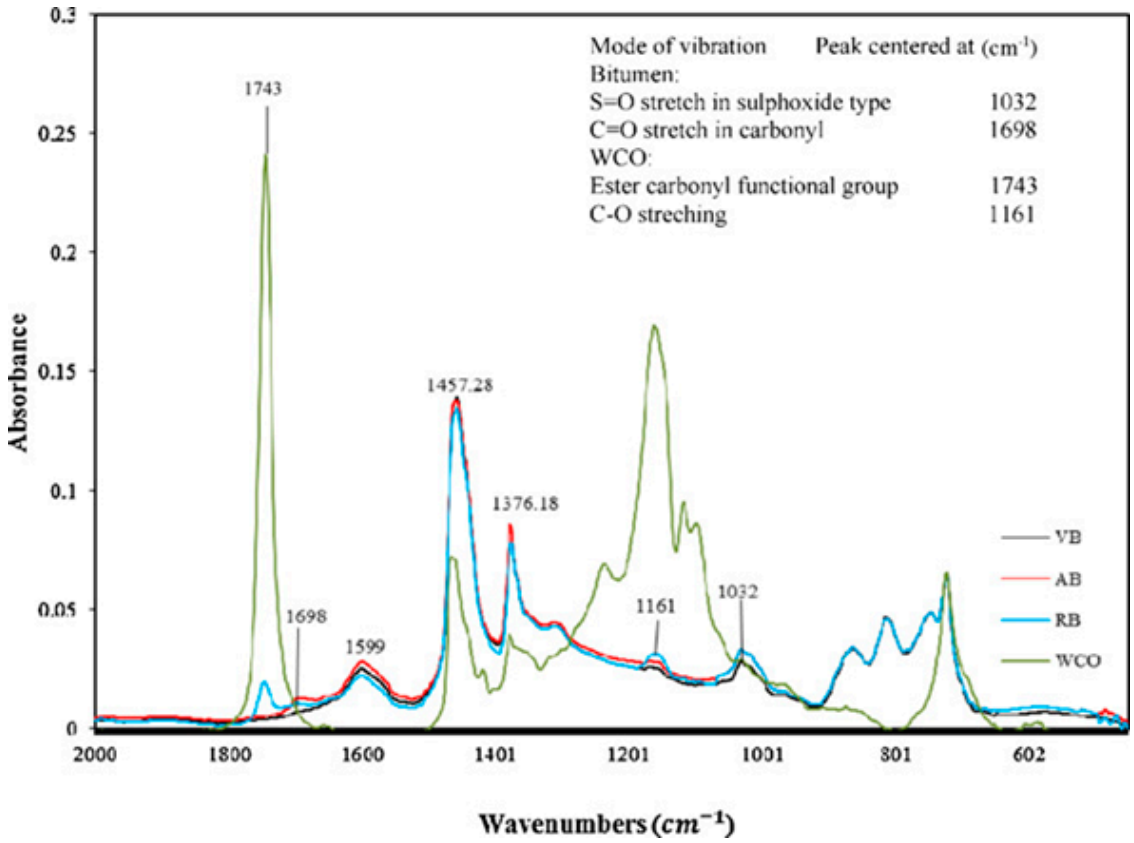


**Figure 3.** FTIR analysis of virgin aged and rejuvenated bitumen (VB, virgin bitumen; AB, aged bitumen; RB, rejuvenated bitumen) (reprinted from Reference [52] with the permission of Elsevier).

To avoid FT-IR artefacts, due to differences in the optical path (different thickness of samples) or in experimental procedures, Nayak and Sahoo [53] wisely consider the relative amount of ketonic bond with respect to the signals of functional groups which are not expected to change, like the bending of C–H bonds. This peak is pointed out in Figure 4.

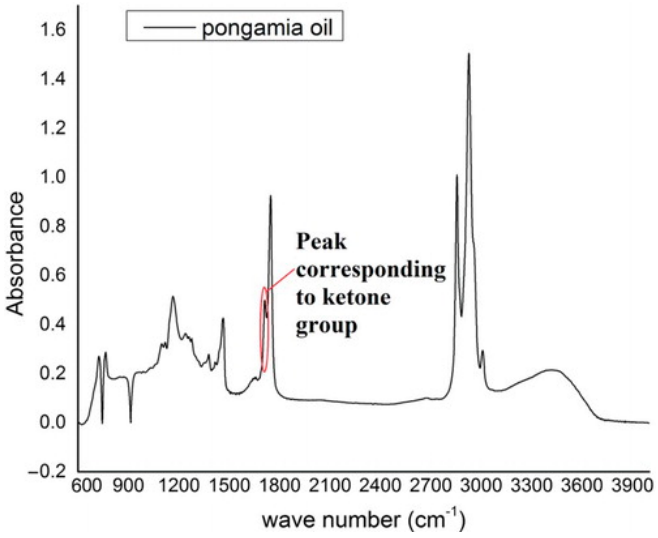


**Figure 4.** FTIR spectrum for pongamia oil (reprinted from Reference [53] with the permission of Taylor and Francis).

This criterion of using a relative intensity was proposed by De la Roche et al. [54], but the use of the relative area is consistent with the consideration by Lamontagne et al. [55].

In any case, Nayak and Sahoo studied the rejuvenating effect of two different types of oils (the pongamia oil and a composite castor oil made of 70% castor oil and 30% coke-oven gas condensate). The results confirm the clues by Zargar et al. showing an increase of the C=O relative signal when the bitumen is aged. Moreover, they found that the C=O relative signal slightly tends to decrease when the composite oil is added, but more markedly increases when pongamia oil is added. The reason lies in the fact that the ketone group is present in pongamia oil itself, and therefore, it is not necessarily due to ageing process. This result should be interpreted as an invitation in being prudent when performing FT-IR experiments and when interpreting its results.

### *4.3. Thermal Stability Helps in Probing Rejuvenation*

By monitoring viscoelasticity, creep and response, FT-IR, Thermogravimetric Analysis (TGA) and Differential Scanning Calorimetry (DSC), Nayak and Sahoo proved that successful rejuvenation takes place when these oils are added to the bitumen. It is interesting to notice that both oils have good thermostability performances. The virgin binder showed a visible mass loss at temperatures below 200 °C; instead, all the rejuvenated binders along with aged binder showed significant mass loss beyond 200 °C, but such temperatures are much higher than those typically adopted in hot mix asphalt preparation, rendering this difference not significant for practical purposes.

Also, Elkashef et al. [56] used thermal stability analysis to evaluate the effect of rejuvenating soybean oil on reclaimed asphalt pavement (RAP). Acknowledging the importance of studying thermal stability of rejuvenated binders to assure that eventual loss of rejuvenating additive (typically characterized by low molecular mass) does not modify asphalt performance, they carried out thermogravimetric analysis on the RAP, on the blend made by RAP and the pristine bitumen (PG58-28), and finally, on the mixture formed by RAP, soybean oil (12%) and the pristine bitumen. Coupled to Thermogravimetry (TG), an FT-IR spectrometric investigation on the gases produced by heating was also carried out. The Authors' results obtained by Thermogravimetry (TG) can be summarized in Table 1.

**Table 1.** TG results of the studied asphalt binders (reprinted from Reference [56] with the permission of Springer Nature).

| Sample | IDT (°C) | Char Yield (%) | Residue (%) |
|---|---|---|---|
| RAP | 316 | 30 | 7 |
| RAP + PG58-28 | 309 | 26 | 6 |
| RAP + 12% Mod PG58-28 | 309 | 26 | 6 |

This table shows the Initial Decomposition Temperature (IDT), defined as the temperature where 2% mass loss occurs; the char yield percentage is the mass remaining at the temperature of 550 °C, and the percentage residue is the remaining percentage of asphalt material at the end of the analysis. From this table it is clear that the RAP binder shows the highest thermal stability, confirming that the stiffness is due to asphaltene amount that is more thermally stable, whereas, the other two binders show the same behavior, having an IDT few degrees lower. Elkashef et al. also compared the spectra (at a temperature of 390 °C) of the gases evolved from the three different binders, taking into account for the blank constituted by the bare soybean oil. It turned out that the spectrum of the binder containing the rejuvenator shows a relatively intense peak typical of the rejuvenator itself. Although this observation can be thought as trivial, a pseudo-quantitative analysis, carried out at different temperatures by normalizing the FT-IR spectra at the same C-H stretching peak height (2930 $cm^{-1}$), allowed the Authors to conclude that FT-IR spectrometry can be used as a tool to probe the rate of mass loss of the rejuvenator. In fact, a higher mass loss triggered by a temperature increase implies higher relative intensities of the characteristic functional groups of the rejuvenator itself (C=O stretching at 1736 $cm^{-1}$ and the two C-O stretching at 1015 and 1153 $cm^{-1}$).

### *4.4. Rejuvenation May Be Uncorrelated with IR Functional Groups: Need of Chromatography*

Cavalli et al. [57] found an interesting aspect. In fact, these Authors pointed out that, despite the addition of rejuvenators, the bitumen physico-chemical oxidation did not reverse: mechanical changes were not caused by chemical changes at functional groups level, but by a rearrangement of polar/nonpolar components. They took into account for three different commercial bio-based rejuvenators: a natural seed oil (called rejuvenator "A"), a cashew nut shell oil (called rejuvenator "B") and a rejuvenator based on tall oil (rejuvenator "C"). After highlighting by FT-IR that rejuvenator A and C have a rather similar chemical nature (see Figure 5 which reports the FT-IR spectra of the bare three rejuvenators), they performed FT-IR spectra on samples of RAP containing 5% of each rejuvenating and compared them to the spectrum of a virgin bitumen 50/70. The results are shown in Figure 6: the peaks corresponding to the ageing of binders, due to oxidation do not disappear although rejuvenators were added to the RAP binder. Chemical structures of RAP +5% C and RAP +5% A were found to be similar, suggesting that the chemical effect of rejuvenator C and A on RAP binder is similar.

The Authors also determined the chemical ageing index (CAI). This is given by the sum of carbonyl index (CI) and sulfoxide index (SI) defined, as suggested in Marsac et al. [58], as the area of the carbonyl and sulphoxide signal, respectively, normalized, to the peaks related to the asymmetric vibration of $CH_2$ and $CH_3$ (around 1455 $cm^{-1}$) and to the symmetric deformation vibration of $CH_3$ (around 1376 $cm^{-1}$) as the latter areas do not change significantly. It must be noted that here the Authors use the same indices as Nayak and Sahoo, by considering the area of the FT-IR signals (and not the bare intensities) and normalizing them to signals related to the C-H functional group since they are expected to be hardly sensitive to the chemical environment.

By using these indices, the Authors found that the unaged binders RAP + 5% A and RAP + 5% C have a higher CAI index than the plain RAP. Most probably due to the fact that seed oil and tall oil themselves contain carboxylic groups C=O, they found the same clues derived by Nayak and Sahoo who found that the ketone group is present in their rejuvenator (pongamia oil) itself.

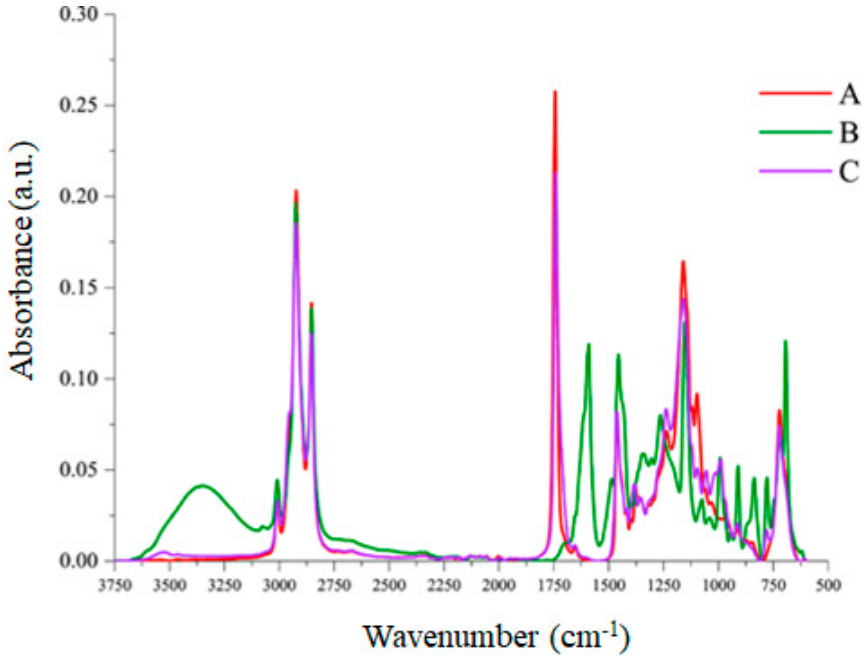


**Figure 5.** ATR-FT-IR spectra of the plain rejuvenators A, B and C before ageing) (reprinted from Reference [57] with the permission of Elsevier).

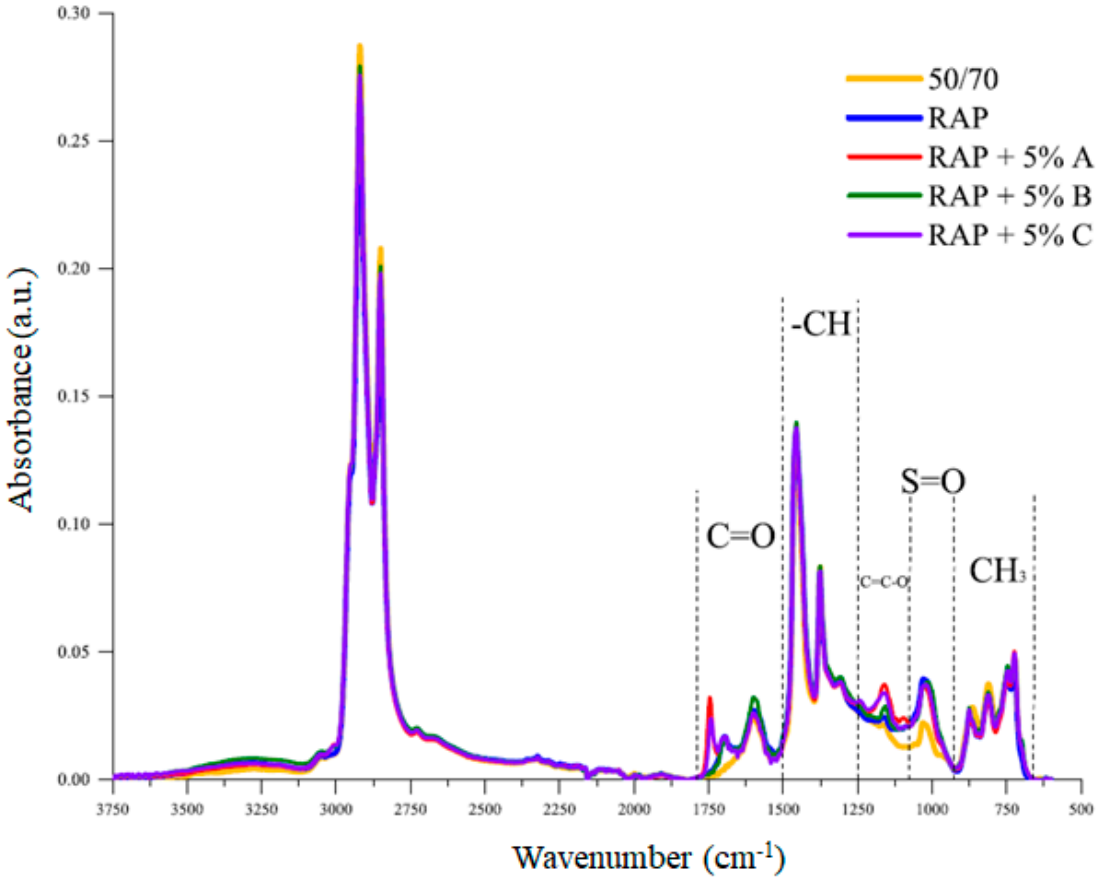


**Figure 6.** ATR-FTIR spectra of the virgin binder 50/70, the RAP binder and the RAP binders with rejuvenators A, B and C (5% by mass of RAP binder each) (reprinted from Reference [57] with the permission of Elsevier).

Elkashef et al. [59] also used the FT-IR-ATR analysis to explore the effect of soybean-derived rejuvenator on two different kinds of performance grade bitumen. The types of bitumen, PG 64-28 and PG 58-28, were aged by Rolling Thin Film Oven Test (RTFOT, similar but slightly different in parameters values from TFOT technique) and pressure-aging-vessel (PAV) methods, and then they were doped with 0.75% of soybean-derived rejuvenator.

Figure 7a shows the increase in the carbonyl index with ageing. The soybean additive does not influence the ageing behavior of the binder. Regarding the sulfoxide index, (shown in Figure 7b) it increases with the aging of PG 58-28. On the contrary, it decreases dramatically to the last step of PG 64-28 ageing (PAV). The drop is also present for the aged doped binder. Ageing was probed by FT-IR-ATR in both the control and modified asphalt binders. As a result, the carbonyl and sulfoxide functional groups increase with ageing. The time evolution of these two functional groups, leads to the conclusion that the modification does not cause any significant influence on the ageing behavior of the asphalt binders. Cavalli et al. also investigated the molecular size distribution with Gel Permeation Chromatography (GPC) in order to evaluate if the rejuvenator modified molecular properties of RAP binder. They used two kinds of detector: one is the refractive index (RI) detector, and the second one is a variable wavelength detector with UV signal (UV). From RI detector, RAP + 5% A and RAP + 5% C (see Figure 8) displayed a shift from the large to the middle size as compared to RAP binder.

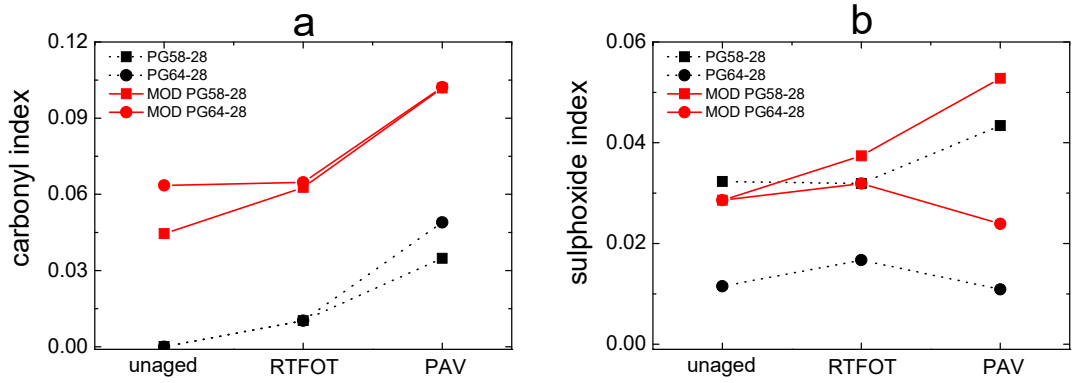


**Figure 7.** Carbonyl index (**a**) and sulfoxide index (**b**) (data taken from Reference [59]).

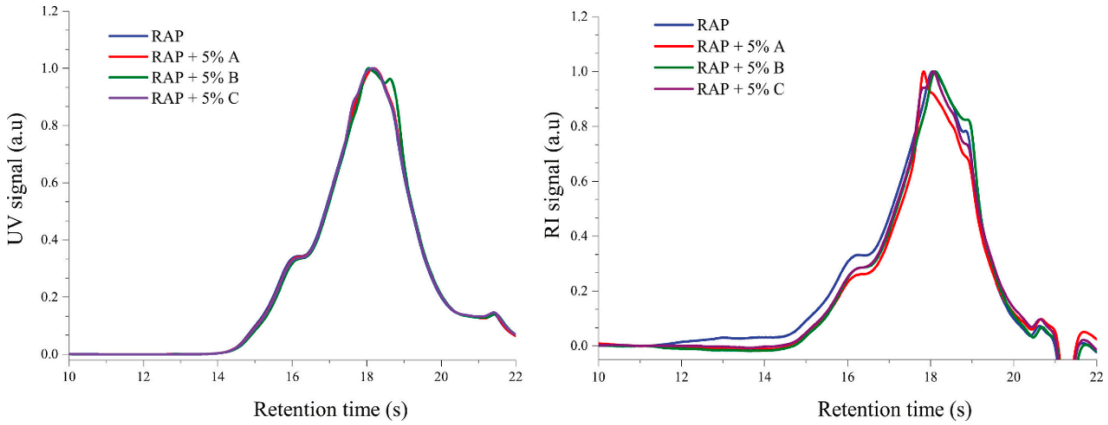


**Figure 8.** GPC spectra with UV (**left**) and RI-signals (**right**) of the RAP binder and the RAP binder with rejuvenator A, B and C (5% by mass of RAP binder each) (reprinted from Reference [57] with the permission of Elsevier).

Comparing the FT-IR spectra and the results obtained with GPC they hypothesized the presence of an ether group (C-O-C) in the RAP modified with A and C, whereas, from UV detector a shift towards the smaller molecular sizes has been observed in RAP + 5% B. In summary rejuvenators could partially change the molecular size distribution of the RAP binders.

The idea of combining FT-IR to obtain information on functional groups and GPC test to obtain information on molecular weight distribution was also exploited by Zhu et al. [60] who studied the effect of a bio-rejuvenator made by a by-product in cotton-oil production and dibutyl phthalate (7.5 wt% in the bio-rejuvenator) as plasticizer. In fact, they carried out a comparison between the FT-IR spectra of pure bio-rejuvenator; pristine bitumen; bitumen aged by Thin Film Oven Test (TFOT - 5 h, 163 °C) followed by a pressure-aging-vessel (PAV) test (aging temperature in the PAV test 90 °C, pressure 2.1 MPa, duration of the test 20 h); PAV was added with 5% or 10% bio-rejuvenator. Moreover, they carried out FT-IR spectra on an asphalt modified with styrene-butadiene-styrene (SBS); SBS-modified PAV, and 5% or 10% bio-rejuvenator on SBS-modified PAV. The peak-area intensity of the oxygenated groups (CO and SO) was used to probe the degree of aging and rejuvenation of the asphalt. Here, again, the Authors calculated the $I_{co}$ and the $I_{so}$ indexes. As expected, for pristine bitumen and SBS-modified asphalt, the carbonyl and sulfoxide indexes increase after aging. As it can be seen by a perusal of Figure 9, both indexes decrease with the addition of the bio-rejuvenator.

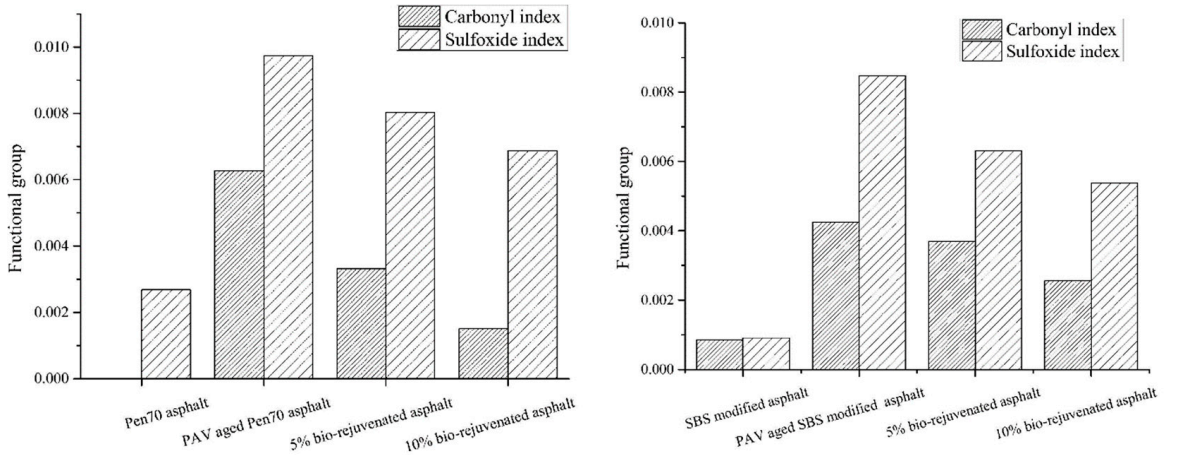


**Figure 9.** Carbonyl and sulfoxide indexes of virgin, aged, and bio-rejuvenated asphalt (reprinted from Reference [60] with the permission of Elsevier).

However, the carbonyl and sulfoxide indexes of the PAV-aged asphalt cannot be restored to their original levels. The Authors applied the GPC to the system under consideration to shed light on the effect of the rejuvenator on the molecular size distribution. The chromatogram reported in Figure 10a shows that the dw/dlogM versus Mw (weight-average molecular weight) curves for the bio-rejuvenator. Mw of the bio-rejuvenator is about 1000 g/mol, and the narrow and sharp peak indicates that the molecular-distribution dispersity of the bio-rejuvenator is low.

Figure 10b shows that the PAV-aging process causes a decrease in the low and medium-weight molecular content of the pristine bitumen while increasing its high-weight molecular content. Adding the rejuvenator helps in improving the properties of the PAV-aged bitumen by increasing the medium-weight molecular content and decreasing the low-weight molecular content. Figure 10c shows a similar phenomenon with the single-peak in the PAV-aged SBS-modified asphalt splitting into two peaks after bio-rejuvenation. In order to characterize the molecular mass distribution, the Authors used analysis of polydispersity, defined as the Mw-to-Mn ratio (Mw, weight average molecular weight; Mn, number-average molecular weight). The results are reported in Figure 11. Both Mw and polydispersity of the virgin asphalt were found to increase after PAV ageing, due to the various chemical reactions in the asphalt/polymer. On the other hand, the values of the PAV-aged virgin and SBS-modified bitumen show that the rejuvenation effect can be primarily attributed to the changes in the molecular polydispersity of the asphalt.

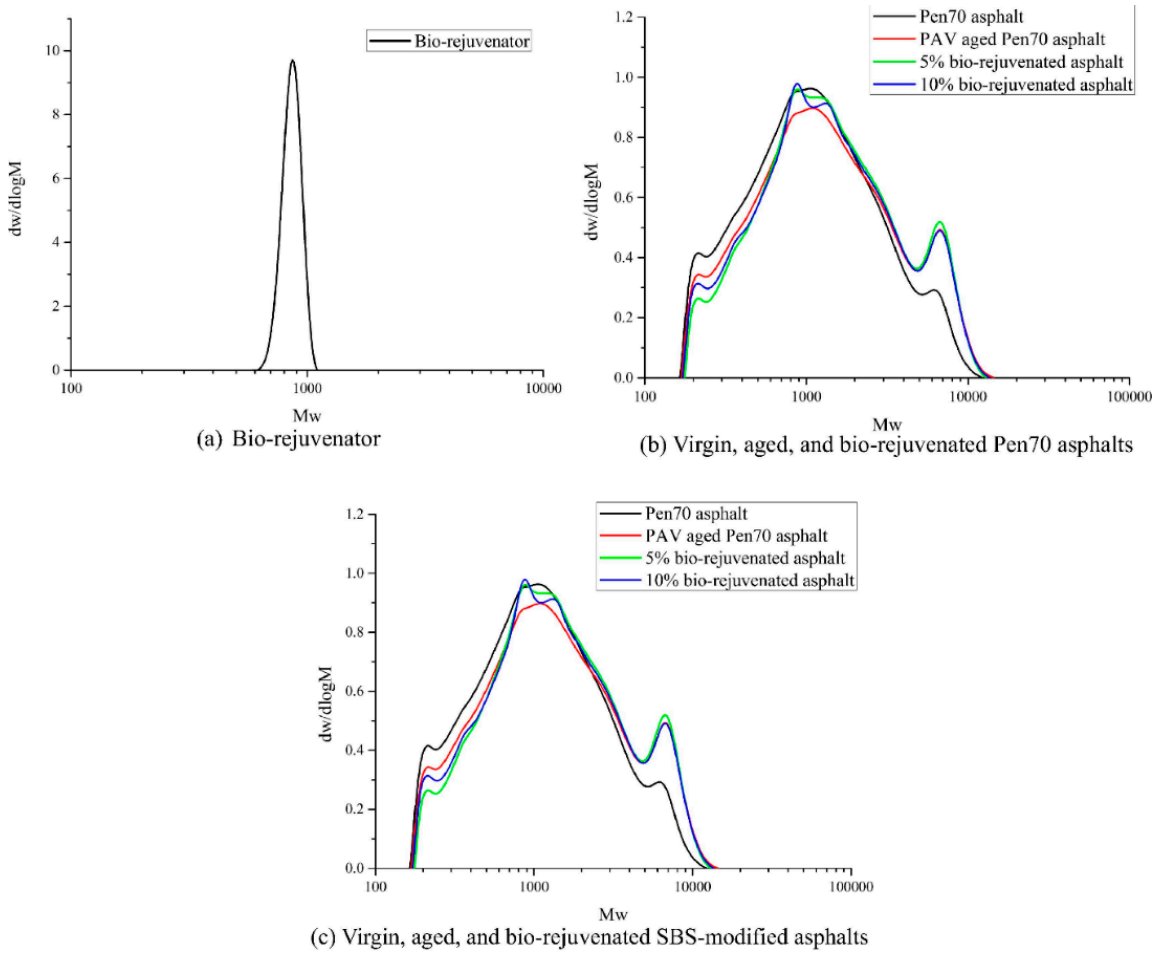


**Figure 10.** GPC curves of bio-rejuvenator and virgin, aged, and bio-rejuvenated asphalt (reprinted from Reference [60] with the permission of Elsevier).

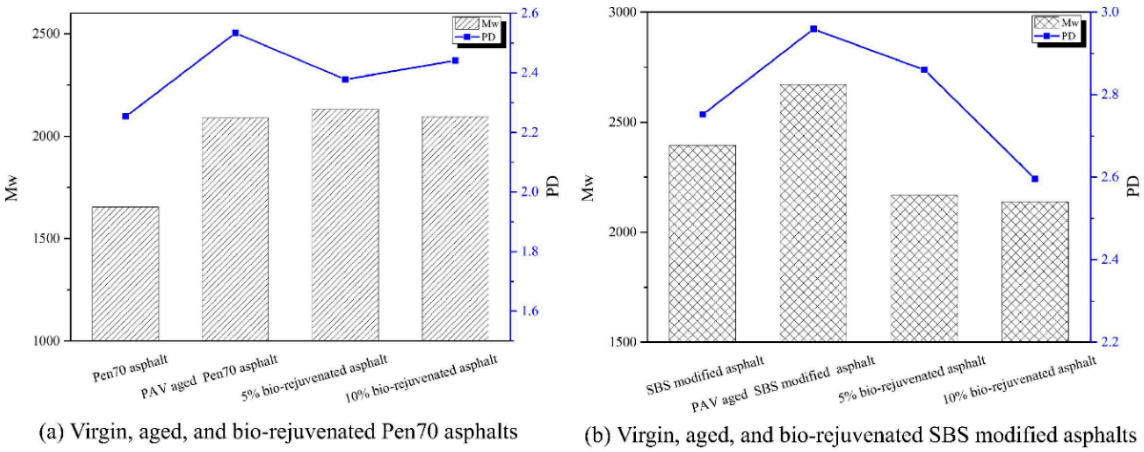


**Figure 11.** GPC Mw and PD results of virgin, aged, and bio-rejuvenated asphalt (for bio-rejuvenator: Mw = 861, PD = 1.0082) (reprinted from Reference [60] with the permission of Elsevier).

Conversely, for the PAV-aged SBS-modified asphalt, Mw decreases with the increase in the dosage of the bio-rejuvenator from 0 to 10%. Both the 5% and 10%-bio-rejuvenated asphalt exhibit lower PDs than the PAV-aged SBS-modified asphalt. However, there is no clear difference between the Mw values of the 5% and 10%-bio-rejuvenated asphalt.

In order to understand the role played by the rejuvenator on the RAP bitumen, Elkashef et al. [61] used the GC-MS (Gas Chromatography-Mass Spectroscopy). They considered a rejuvenator produced from soybean oil, but they did not furnish further details. First, they analyzed the pure rejuvenator: its total ion chromatogram (see Figure 12a) shows five distinct and well-resolved peaks. The pure rejuvenator was then subjected to RTFOT-aging and PAV-aging following the same protocol as that used for asphalt binders aging to assess the chemical stability of the rejuvenator with aging. The total ion chromatogram for the RTFOT-aged and PAV-aged rejuvenator samples are shown in Figure 12 (panels b and c, respectively): they clearly show that the aged rejuvenator gives the same peaks at the same retention times and with similar relative intensity as the unaged rejuvenator. This indicates that the chemical composition of the rejuvenator is preserved during aging.

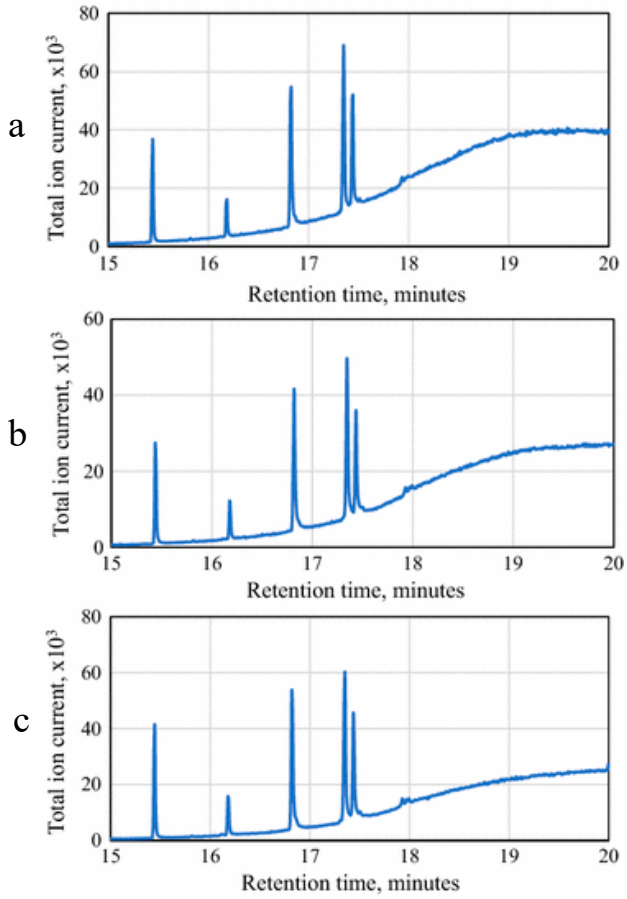


**Figure 12.** Total ion chromatogram for the used rejuvenator (**a**), the RTFOT-aged rejuvenator (**b**) and the pressure-aging-vessel (PAV)-aged rejuvenator (**c**) (reprinted from Reference [61] with the permission of Elsevier).

Subsequently, they submitted rejuvenated RAP (unaged, RTFOT-aged and PAV-aged) to pyrolysis to analyze the evolved gases using Gas Chromatography coupled with Mass Spectrometry (GC-MS) (see Figure 13). The total ion chromatogram of the unaged rejuvenated binder shows the rejuvenator's peaks in addition to other smaller peaks attributed to the binder itself. However, the structure of the rejuvenator added to the binder appears to change with aging.

It is, therefore, clear that the rejuvenator interacts with the RAP binder, with the consequent structure modification of the rejuvenator itself. Strikingly, the two peaks at 17.3 and 17.4 min are reduced in intensity with aging, and they entirely disappear in the PAV-aged binder.

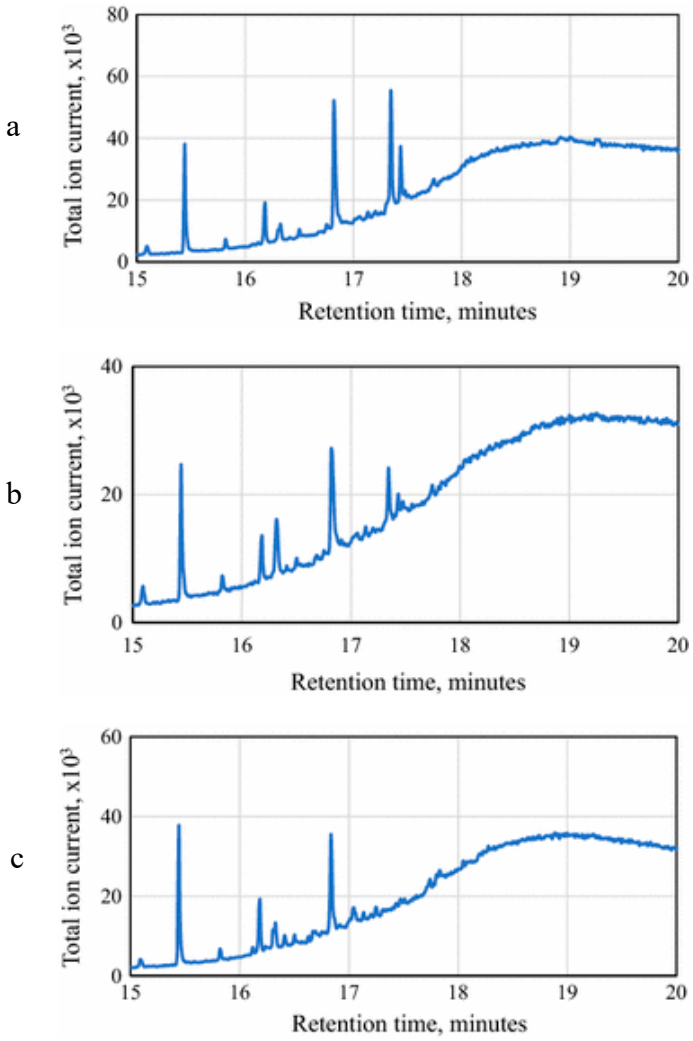


**Figure 13.** Total ion chromatogram for (**a**) unaged, (**b**) RTFOT-aged and (**c**) PAV-aged rejuvenated RAP (reprinted from Reference [61] with the permission of Elsevier).

### *4.5. Images Techniques as Useful Complementary Tools*

Mokhtari et al. [62] have exploited the potential of FT-IR to investigate the effect of two different rejuvenators: a petroleum oil (called "A"), and a product derived from refined tall oil (called "B"). Rejuvenator "A" was added to 15% or 30% by weight on PAV, while the rejuvenator "B" was added to 10% or 20% by weight on PAV. These two dosage rates are the lower and upper limits of each rejuvenator type. Once the spectra were acquired, in order to determine if the use of the rejuvenators minimizes the oxidation, the $I_{co}$ and $I_{so}$ indices were calculated although the normalization seems to us to take place only over the C-H signal at 1459 $cm^{-1}$. As expected, PAV-aged samples show an increase in the $I_{so}$ value, as well as in the $I_{co}$ index.

On the contrary, by perusal of Figure 14 it can be seen that both rejuvenators at both concentrations show a significant decrease in $I_{so}$ values, while the decrease with respect to the $I_{co}$ index is moderate. However, both additives have proved to be effective in counteracting the oxidation of the carbonyl groups, as well as the sulfoxide groups. The Authors also thought to compare the FT-IR results with a Cryo-Scanning Electron Microscopy (Cryo-SEM) investigation for evaluating fracture surface properties of rejuvenator-restored through a digital image processing technique to quantify cracks developed on the fractured surface, due to the aging process. The choice of this technique comes from the Authors' consideration that the evaluation of the microstructural assessment of asphalt with SEM would not be confident, due to presence of volatile components in asphalt and its susceptibility

to electron beam damage. Instead, the use of Cryo attachment to SEM, implying a lowering of the samples' temperature well below the glass point, allows observing samples with greater beam and lower temperature sensitivity. They have acquired images with varying magnifications in different parts of the samples, to indicate the fracture surface characteristics of each sample. It is possible to notice that the asphalt sample has a rough and fractured surface with many fragments, due to the high stiffness caused by the aging process. Rejuvenator "A" makes the fracture surface of aged asphalt smoother with some remaining minor cracks or fragments. However, no further improvement of the surface texture can be observed when rejuvenator "A" amount was increased from 15 to 30%. Even adding rejuvenator "B" (10%) makes the fracture surface smoother, although at a minor extent, since significant amounts of fragments still holds. Instead, increasing the rejuvenator "B" amount from 10 to 20%, results in a significant improvement of the surface.

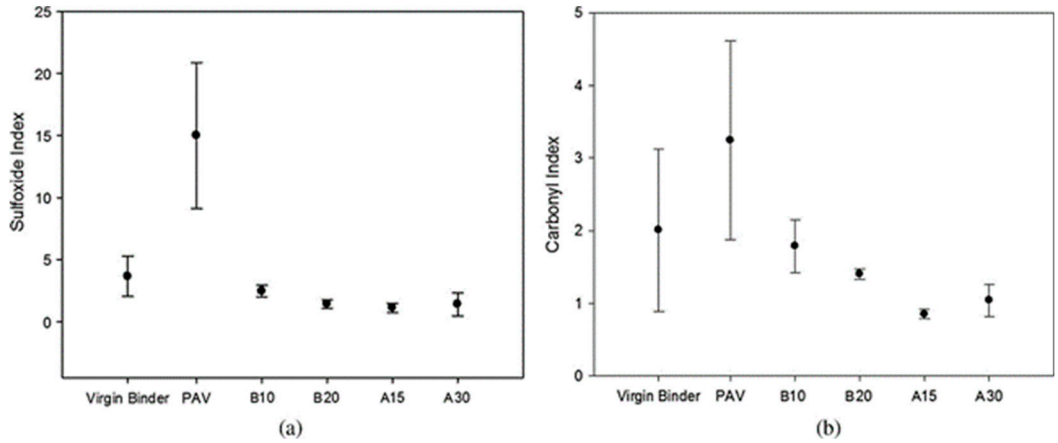


**Figure 14.** Calculated index values for various asphalt types (**a**) sulfoxide index, (**b**) carbonyl index (reprinted from Reference [62] with the permission of Elsevier).

An interesting aspect can be found in the work of Mokhtari et al., who notes that in order to identify the length and the gravity of the cracks, a digital analysis of the images was carried out using an edge detection technique. Briefly, various algorithms developed using MATLAB software DIP image toolbox were used to generate fracture models, including the crack propagation throughout the samples. Comparison with real samples allowed the selection of the best algorithm and a Fracture Index (F.I.) was defined in order to quantify the fracture capability of aged and restored asphalt samples.

As expected, as it can be seen from Figure 15, PAV-aged asphalt has the highest F.I., confirming more pronounced brittleness of the aged asphalt with respect to the aged asphalt with rejuvenators.

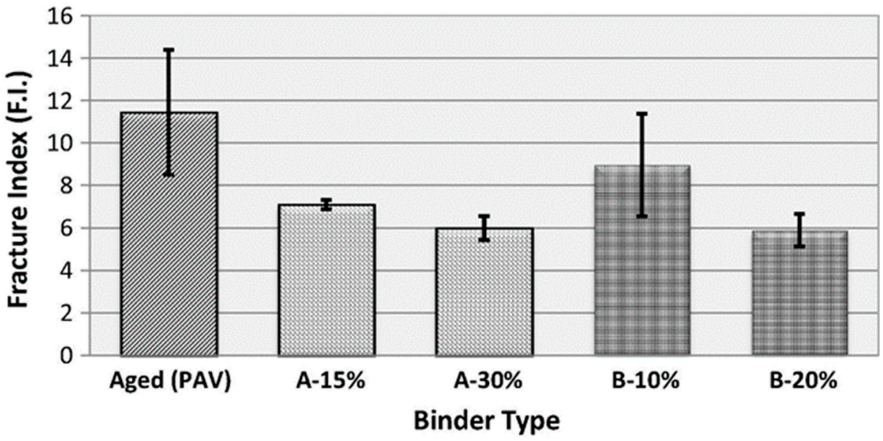


**Figure 15.** The comparative plot of fracture index for various asphalt types (reprinted from Reference [62] with the permission of Elsevier).

Figure 15 shows that the addition of 10% of the rejuvenator "B" could not significantly soften the aged asphalt. However, although 10% of the rejuvenator "B" was not completely effective in softening the PAV-aged asphalt, 20% of that rejuvenator shows the highest efficiency in preventing undesirable cracks at low temperatures. Moreover, both A-15% and A-30% asphalts were soft enough to prevent surface fractures.

Other authors have also focused their attention on the use of image techniques to better understand the structural changes induced by the use of rejuvenators. Indeed, Yu et al. [5] have used the AFM technique to analyze the materials' surface morphology. They have investigated two types of bitumen which are called by the Authors as asphalt binders, named AAD (PG 58–28) and ABD (PG 58–10), and two types of rejuvenators: one comes from fast and convenience food frying oil, here named WV oil, the other is an aromatic extract containing approximately 75% of aromatic oil and resin compounds with small amount of saturate oil. AFM images are shown in Figure 16.

The two virgin binders displayed different morphologies: virgin ABD has a dispersed phase with flake-like structures (with an average size of fewer than 2 μm in diameter) spreading over a smooth matrix continuous phase; virgin AAD, instead, clearly shows the elliptical domains with "bee-structures" (with axes of a few microns). The Authors attribute these differences to the chemical composition of the two samples, in particular, worth of note is the high wax content of the bitumen AAD (1.94%) with respect to the ABD bitumen (0.81%). Upon aging, in ABD, the size of the flake-like microstructures decreased while the quantity increased; on the other hand, in AAD, the "bee-structures" are still present with no obvious morphological changes. The addition of the aromatic extract in the aged ABD bitumen, instead, produces marked changes, giving elliptical domains with "bee-structures" at the middle of the domains. On the other hand, the use of the aromatic extract in the aged bitumen AAD gives smaller-sized "bee-structures". Even, the less noticeable contrast between the 'bee-structures' and the matrix suggests that the amplitude of the undulated "bee-structures" is smaller than that of the virgin and aged ones. On the contrary, the addition of WV oil in both aged binders do not produce a significant morphological modification.

The Authors conclude that the addition of the rejuvenator can cause big morphological changes, even bigger than those coming from the aging; however, this behavior is not general, depending on the specific rejuvenator. This because the asphalt binders' effect depends on its chemical behavior, and therefore, on the complicated molecular interactions which can establish with the other chemical species in the bitumen (and also the eventual inorganic particles). This is generally true for any additive. This conclusion is in accordance with the clues of a recent paper by Calandra et al. [1] which highlights the physical and chemical reasons for this. In this work, the Authors carried out a deep structural investigation by X-ray scattering on bare and additivated bitumen and found that asphaltene clusters hierarchically self-assemble to form aggregates at various levels of complexity, with different sizes up to the micrometer-sized domains dispersed in the maltene, and hold up by interactions of different strengths. The eventual presence of an additive triggers the formation of further intermolecular interaction in competition with those responsible for this self-assembly, causing a change of the size and shape of these aggregates.

The potential of the AFM has been exploited by Kuang et al. [23] to discriminate the effect of Dodecyl Benzene Sulfonic Acid (DBSA) as a solubilizer together with conventional rejuvenator (a blend of fluid catalytic cracking slurry—FCC—and bitumen with penetration of 70 grade) in two different aged (TFOT and PAV) bitumen.

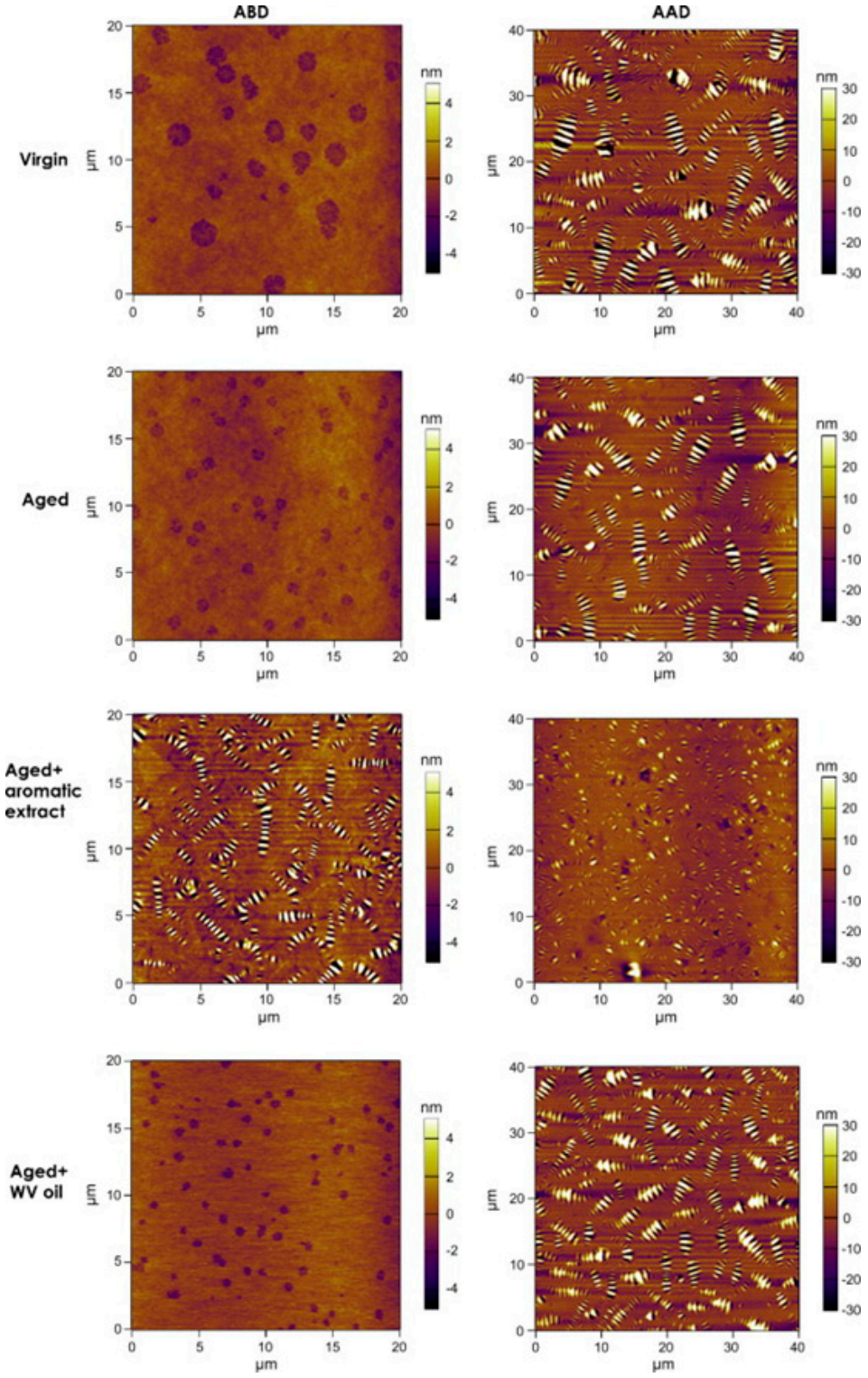


**Figure 16.** Topographic images of virgin (**top row**), aged (**2nd row**), aromatic extract (**3rd row**), and WV oil rejuvenated (**4th row**) ABD (left, 20 × 20 µm$^2$) and AAD (right, 40 × 40 µm$^2$) measured at room temperature (~20 °C). The colour scales range over 10 nm and 60 nm for ABD and AAD based samples, respectively (reprinted from Reference [5] with the permission of Elsevier).

Kuang et al. compared first the effect of aging on the virgin bitumen, whose clues are reported in Figure 17. This figure shows the AFM images of virgin bitumen, Thin Film Oven Test (TFOT) aged bitumen and PAV aged bitumen. The Authors have observed that the aging of the bitumen leads

to a change in the colloidal structure, and differently from Yu et al., an increase in the size of the bee-structures (see Figure 17). Then, they compared the effect of adding the conventional rejuvenating (CR) and the solubilised rejuvenating (SR) on the aged bitumen TFOT and PAV. The comparison in TFOT-aged bitumen and PAV-aged bitumen are reported in Figure 17. They found that in any case the surface of both TFOT and PAV bitumen become smoother with the introduction of CR or SR. However, in the case of TFOT there is no evident difference between the effect of CR and SR showing that, in this case, DBSA does not affect much the surface smoothing action exerted by the rejuvenator. On the other hand, an evident effect can be detected in the case of PAV. By inspection of Figure 18 (lower panel) and comparison with Figure 17, it is possible to notice how the addition of CR on the aged PAV bitumen does not bring marked morphological changes, just a slight reduction in the size of the bee-structures. On the contrary, the addition of SR helps asphaltenes of PAV aged bitumen to be re-dispersed, and this contributes to the performance improvement.

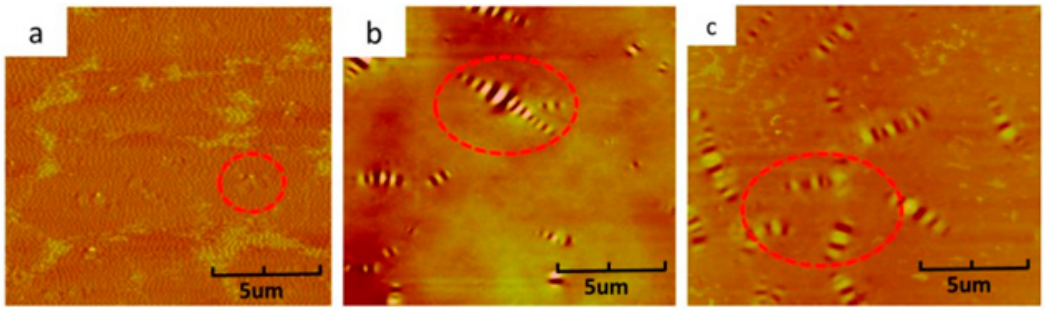


**Figure 17.** Atomic Force Microscopy (AFM) images of virgin bitumen, TFOT aged bitumen and PAV aged bitumen: (**a**) Virgin bitumen, (**b**) TFOT aged bitumen, (**c**) PAV aged bitumen (reprinted from Reference [23] with the permission of MDPI open access journal).

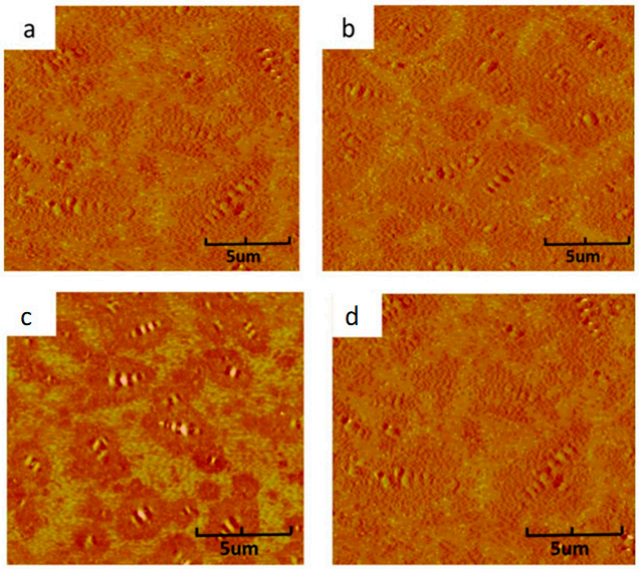


**Figure 18.** Upper panel: (**a**) Regenerated TFOT aged bitumen with 10 wt% CR, (**b**) regenerated TFOT aged bitumen with 10 wt% SR; lower panel: (**c**) Regenerated PAV aged bitumen with 10 wt% CR, (**d**) regenerated PAV aged bitumen with 10 wt% SR (reprinted from Reference [23] with the permission of MDPI open access journal).

For the Authors DBSA (1.5% by weight of rejuvenator) can react with asphaltenes via its sulfonic group to form a solvation layer covering on the surface of asphaltenes clusters, thus, interfering with the colloidal structure transformation of aged bitumen. Therefore, PAV aged bitumen can be recovered

from Gel to Sol-Gel by 10 wt% SR, and the dimension of a bee-like structure formed by asphaltenes can be approximately that of virgin bitumen.

Also, Nahar et al. [63] have explored the potentiality of AFM techniques to investigate the effect of rejuvenator on the aged bitumen. They used a bitumen aged through Rotational Cylinder Ageing Tester (RCAT) for testing two types of rejuvenators, namely, BM1 and CM1. They analyzed the pristine, aged and doped aged bitumen by means rheology and AFM.

From the rheological analysis, they were able to observe that the aged bitumen P1 shows higher complex shear modulus and lower phase angle compared to the pristine bitumen. Obviously, ageing makes the bitumen stiffer (Figure 19a) and less viscous (Figure 19b). The neat rejuvenators show very distinct behaviors. In fact, the rheology of the BM1 rejuvenator shows a lower viscosity compared to bitumen, while CM1 rejuvenator has different rheological characteristics. Indeed, it displays a much lower shear modulus at low frequencies. There is even a behavior of dilatant fluid or shear thickening at a frequency of about 3–5 Hz. The Authors thought that this was due to the presence of suspended particles like structures in rejuvenator CM1 or the formation of such structures at higher shear rates. However, the addition of rejuvenator BM1 into the aged bitumen causes a decreasing of the complex shear modulus, while the phase angle increases to the value of the virgin bitumen. CM1 rejuvenator on the aged bitumen leads to a lower complex shear modulus than pristine bitumen for both the concentrations tested. On the contrary, as expected, the phase angle is almost equal to (10% *w*/*w* CM1) or higher than the pristine bitumen (25% *w*/*w* CM1). It is worth noting that in a blend with aged bitumen any signature of the dilatant nature of the pure rejuvenator CM1 is completely lost.

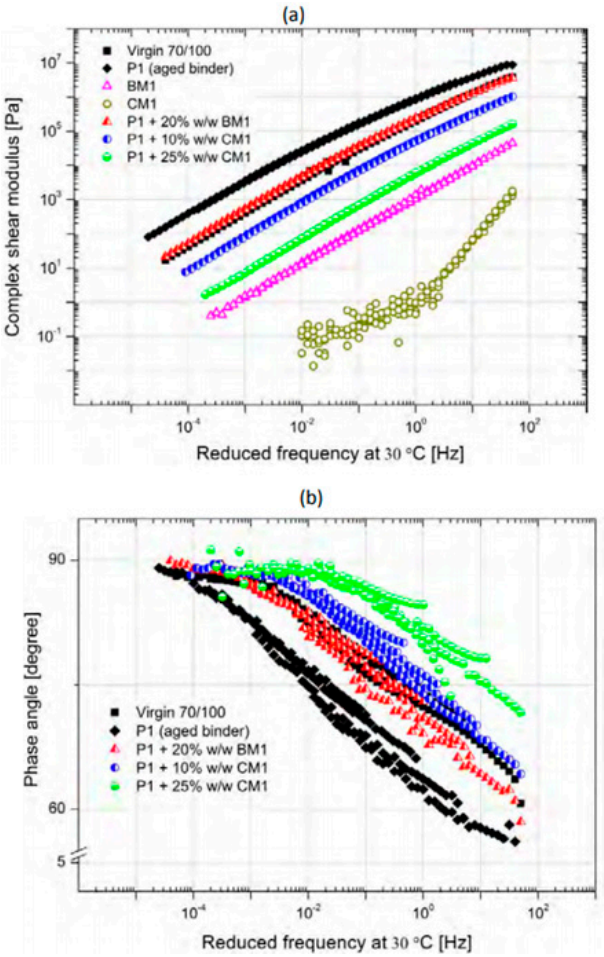


**Figure 19.** (**a**) Complex shear modulus of pristine, aged, doped aged and rejuvenator; (**b**) phase angle of pristine, aged and doped aged bitumen (reprinted from Reference [63] with the permission of SAGE Publications).

In our opinion, the AFM analysis conducted by Nahar et al. is commendable. To our eyes, it seems to be almost the most complete job among all the AFM-based works we have examined. In fact, the authors were not limited to the identification of domains and bee structures, having identified new types of structures (e.g., tertiary and quaternary) providing an accurate description. Figure 20(ai) shows the AFM phase image for the pristine bitumen. It is possible to estimate the length of the domains long axes which falls into the range 2–6 µm. The topography images show "wrinkling" in the middle of the domain. Finally, the domains result to be buried about 2–5 nm with respect to the average height of the continuous phase. On the contrary, the aged bitumen is very different from the pristine one. Figure 21 shows the same elliptical domain (i) and matrix (ii) of pristine bitumen. Moreover, it is possible to observe the tertiary phase, which consists of fine dark arcs and spots dispersed throughout the matrix (iii). This tertiary phase displays the lowest phase shift, and it is the softest phase. From the topography (shown in Figure 20 (ii)), it turns out that the elliptical domains are 5–8 nm lower (buried) the matrix surface, on average, while the tertiary phase protrudes above the matrix phase by 3–5 nm.

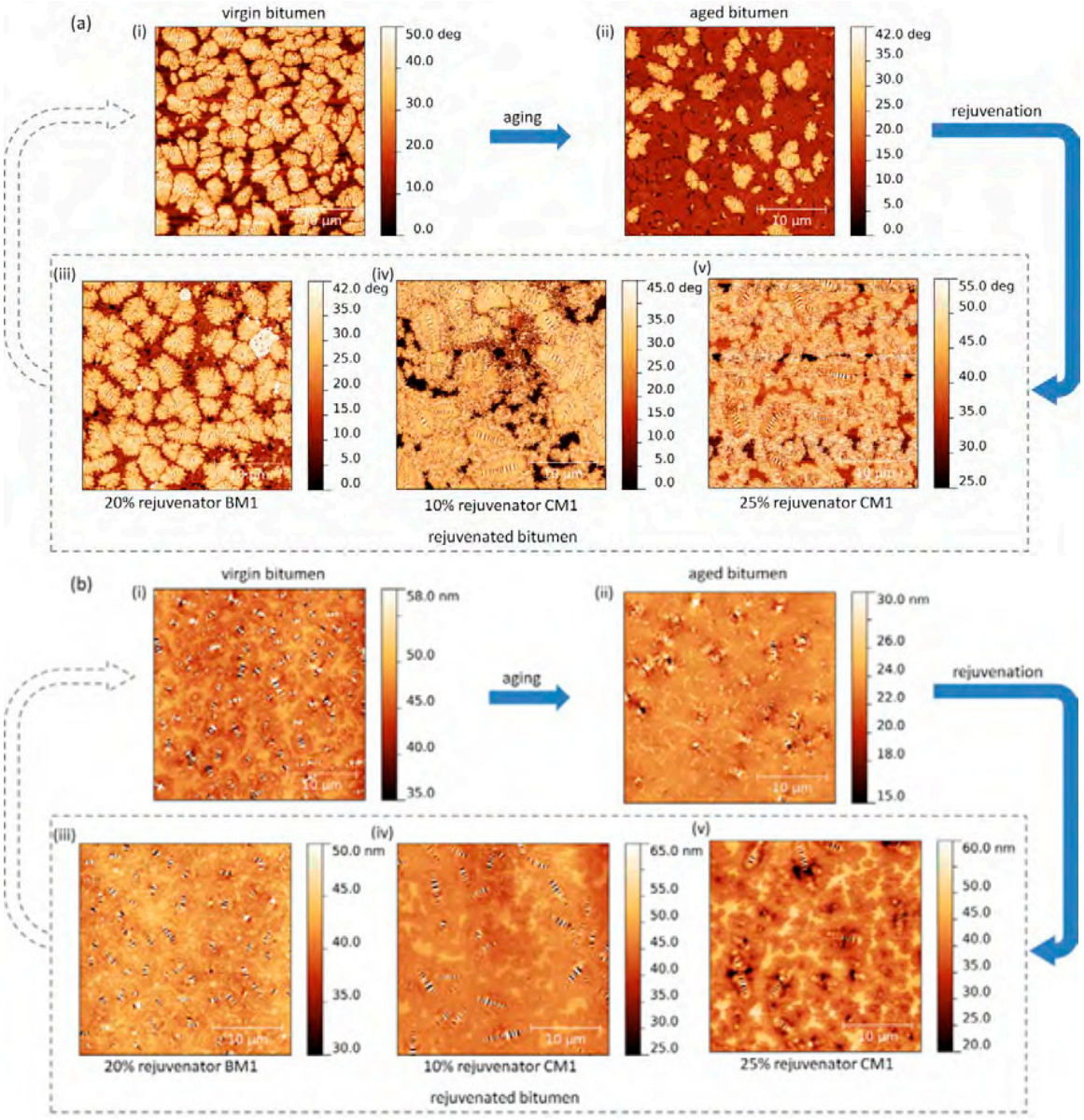


**Figure 20.** AFM (**a**) phase images, (**b**) topography images of pristine, aged and doped aged bitumen (reprinted from Reference [63] with the permission of SAGE Publications).

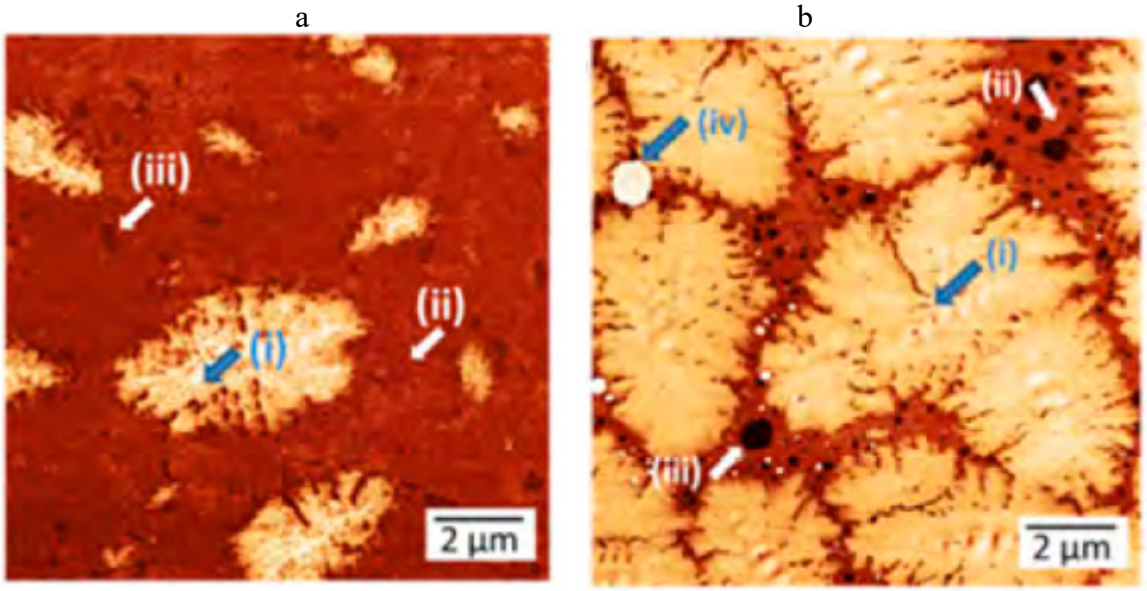


**Figure 21.** AFM phase image of aged bitumen (**a**) and aged bitumen doped with 20% of BM1 (**b**) with (i) elliptical domains, (ii) matrix, (iii) tertiary phase and (iv) quaternary phase (adapted from Reference [63]).

From Figure 20(aiii), it is possible to notice that the addition of 20% of BM1 to aged bitumen restores the microstructure. However, now it is possible to distinguish a new phase at the boundary of the domains and at the interstitial spaces of consecutive domains. A new quaternary phase is found, see Figure 21(biv). This new phase has the highest phase shift (highest stiffness), and it appears in almost circular shapes with sizes in the range 15.2–4 µm.

As it can be seen from Figure 20 (iv) and (v), the addition of the CM1 additive at both concentrations causes a change in morphology: needle-like particles, 20–90 nm wide and 50–250 nm long, appear. The network becomes the main phase at a microstructural level at the increasing of CM1 concentration.

In order to understand if the microstructure evolves with time, the Authors analyzed the samples, again, after seven days. The aged bitumen and the aged doped with 20% BM1 did not show any change over time. On the contrary, the aged bitumen doped with 10 and 25% of CM1 evolve over time (see Figure 22). The biggest change can be observed for the blend with the lower (10%) concentration of CM1 rejuvenator (see Figure 22(aii)). Over time, some effects can be highlighted: needles are expelled from the matrix phase, disconnected domains only comprising the network phase are born, and the wrinkling in the elliptical domains tends to decrease. The network phase, in this period, has formed a kind of bilayer around the elliptical domains, consisting of 200–300 nm stiffer layer (higher phase shift, light colour in Figure 22(bii)), surrounded by a 1 µm somewhat softer layer. Both layers display the typical pattern of randomly oriented needles, typical of the network phase. The higher stiffness layer may be just a denser packed region of the network phase. On the contrary, for the higher concentration of CM1 rejuvenator (25%) the effect of the time on microstructure is less obvious. Indeed, it is possible to notice islands solely consisting of the needle network, as well as the bilayer of 15 needles surrounding the elliptical domains. It is noticeable that, here, the stiffer (white) region of the needle network phase is the more prominent phase. Also, at a 25% concentration of CM1, the wrinkling in the elliptical domains remains over time, though the oscillation amplitude has decreased.

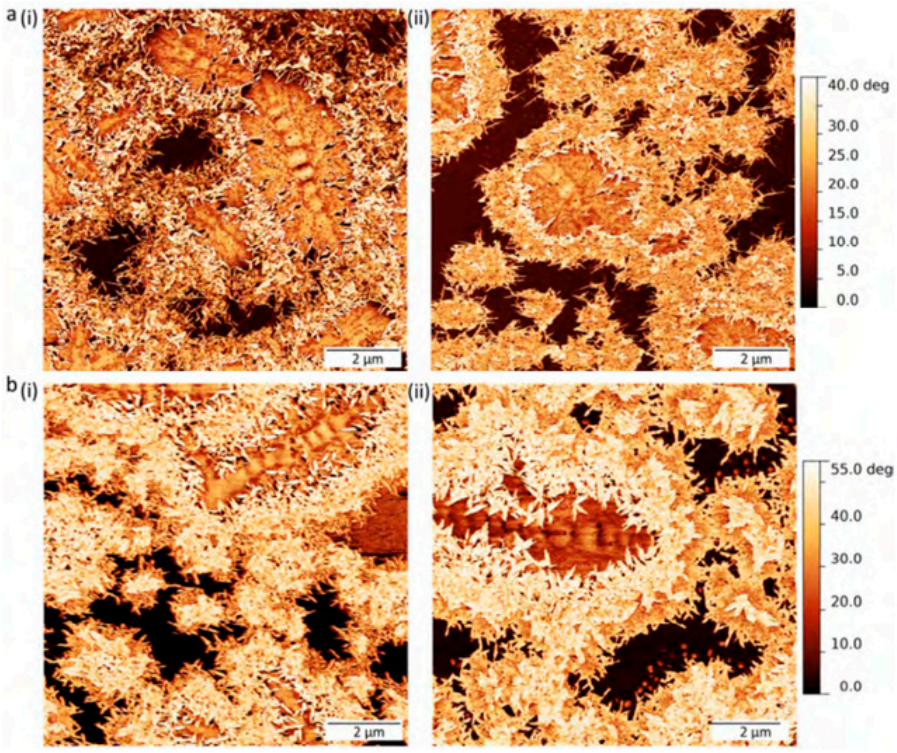


**Figure 22.** Time evolution of microstructure of aged bitumen doped with CM1. AFM phase images; (**a**) 10% CM1 and (**b**) 25% CM1, (i) after preparation (ii) after seven days (reprinted from Reference [63] with the permission of SAGE Publications).

Kuang et al. [64] evaluated the effect of composite rejuvenator in comparison with a common rejuvenator by means of dynamic shear rheometer (DSR) and atomic force microscopy (AFM). The composite rejuvenator, named RRA, was laboratory-prepared by blending the light weight oil rich in aromatics with a chemical compound containing polar group. The common rejuvenator, denoted as CRA, was also prepared in a laboratory. They used for these researches the bitumen SK-70, whose physical properties are listed in Table 2.

**Table 2.** Physical properties of SK-70 bitumen (reprinted from Reference [64] with the permission of Springer Nature).

| Index | Value |
|---|---|
| Penetration (25 °C, dmm) | 73 |
| Ductility (15 °C, cm) | >150 |
| Softening point/°C | 45.2 |
| Viscosity (135 °C, Pa·s) | 0.6 |

The aged binder was prepared through the aging of SK-70 by Thin Film Oven Test (TFOT). Aged bitumen was doped with 4; 6; 8 and 10 wt% of the two kinds of rejuvenator.

The results are shown in Figure 23: the composite rejuvenator (RRA) has a greater effect with respect to the common rejuvenator (CRA). When the content of RRA is 10 wt%, the values of penetration, ductility, softening point and viscosity are very close to the values of pristine SK-70. Therefore, the Authors believe that the rejuvenator RRA is able to restore the colloidal structure by increasing the aromatics content. In addition, the polar groups of RRA can react with the asphaltene in aged bitumen, decreasing the asphaltenes content themselves. On the contrary, according to them, chemical reactions between the common rejuvenator and asphaltenes molecules do not take place, due to the lack of polar groups in common rejuvenator.

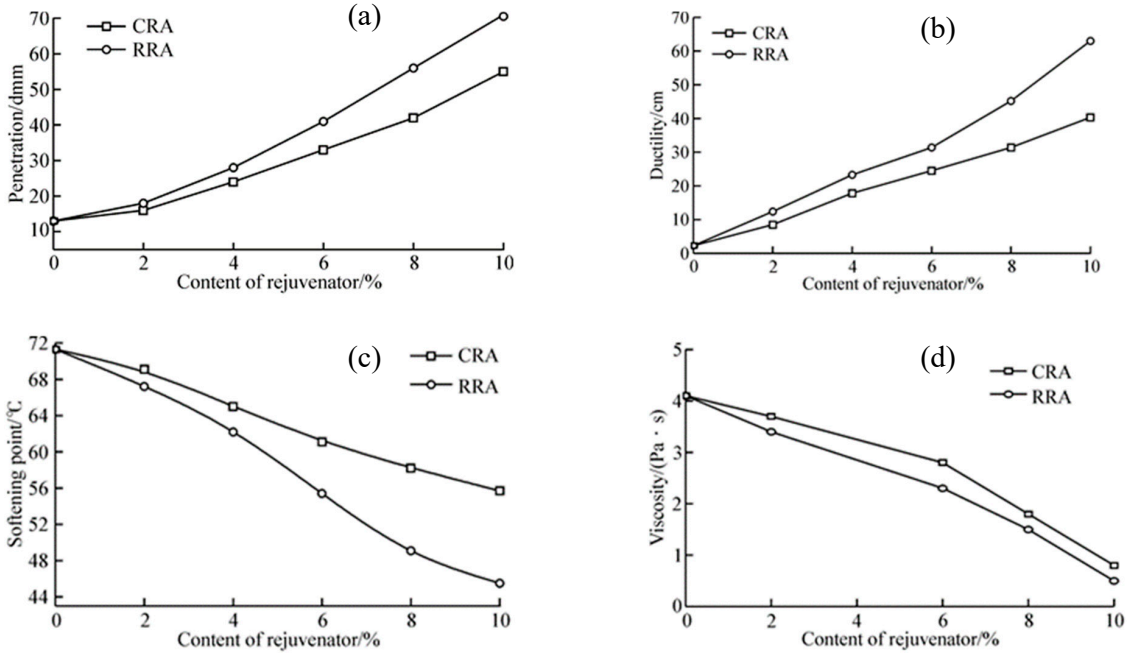


**Figure 23.** Effect of rejuvenators on penetration (**a**), ductility (**b**), softening point (**c**) and viscosity (**d**) (reprinted from Reference [64] with the permission of Springer Nature).

From the rheological analysis, it results that the rutting factor, shown in Figure 24a as a function of temperature, of the aged binder is greater than the virgin one. The addition of 10 wt% of RRA and CRA causes a decrease in the rutting factor, but sample with RRA gives a trend similar to the pristine one. Obviously, the aged bitumen is very brittle and easy to crack under load at low temperature, in fact, has a high fatigue factor (see Figure 24b) compared to virgin bitumen. The poor regenerative power of CRA is evident. Aged asphalt with 10 wt% CRA and aged asphalt shows similar fatigue factor curves. Nevertheless, the addition of 10 wt% of RRA improves the fatigue resistance considerably, being the fatigue factor trend close to that of virgin bitumen. In order to evaluate the effect of rejuvenators on the bitumen structure, the Authors carried out AFM analysis. From topographic images, the virgin asphalt (see Figure 25a) seems to be rather smooth; instead, the aged asphalt, (see Figure 25b) appears to be more wrinkled. Even, the surface of aged asphalt doped with 10 wt% of CRA seems to be rougher with flocculated structure just like that of the aged asphalt, see Figure 25c. The addition of RRA restores a smooth surface like that of virgin asphalt, Figure 25d. The disappearance of the flocculated structure is due to the dissolution of asphaltenes. Therefore, it can be concluded that aged asphalt can experience good recover of its original microstructure by means of the composite rejuvenator: an effective rejuvenation of the aged asphalt performance can be claimed.

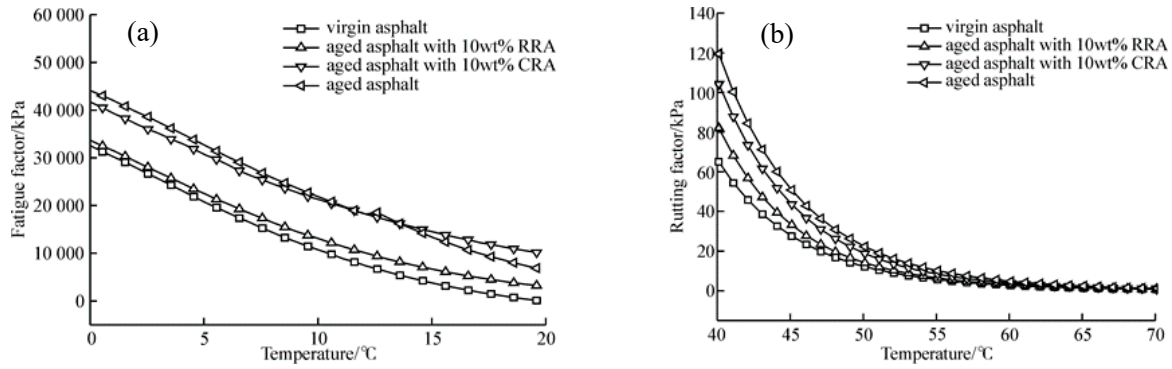


**Figure 24.** Effect of the rejuvenators on the Rutting factor (**a**) and on the Fatigue factor (**b**) (reprinted from Reference [64] with the permission of Springer Nature).

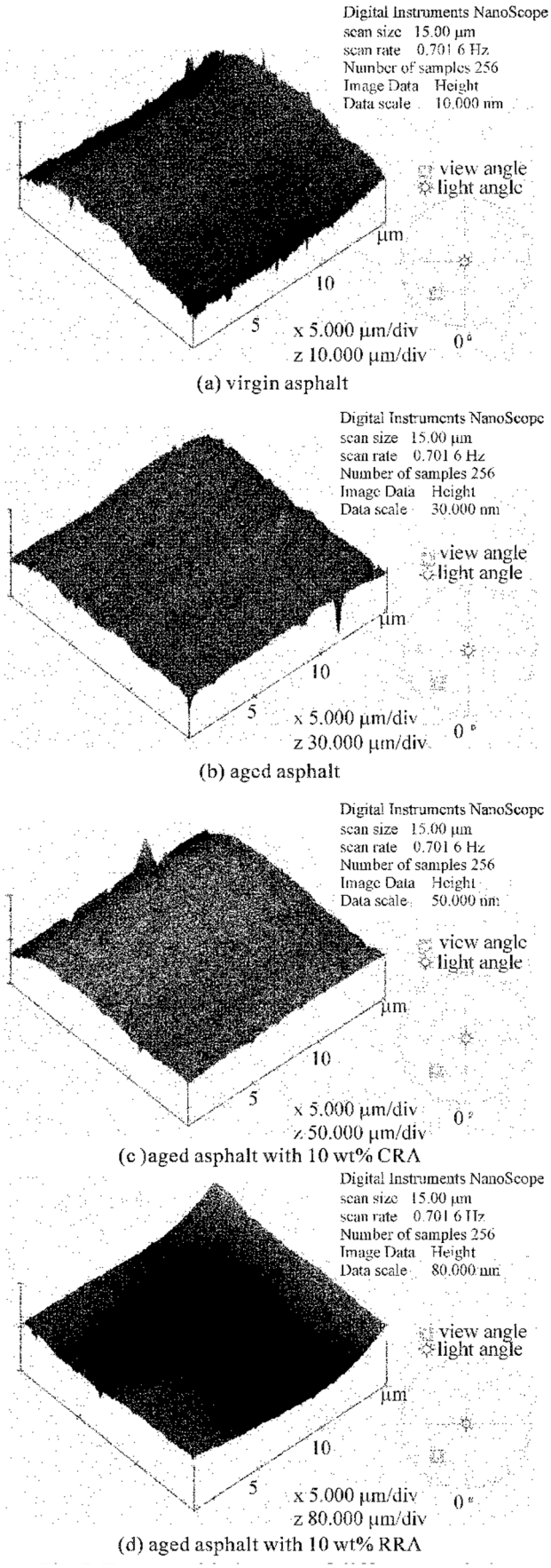


**Figure 25.** Topographic AFM images of samples (reprinted from Reference [64] with the permission of Springer Nature).

## 5. Perspectives

### *5.1. Improving Rejuvenators Characteristics*

As already discussed above, a rejuvenator is commonly made by simple oil waste for their low-cost and obvious environmental concerns. In fact, oil waste is the by-product of edible oils surely more produced in the world. Therefore, its re-utilization may provide a feasible method to minimize the amount of generated waste, providing a positive environmental impact. From a chemical point of view, the oil subjected to elevated temperature changes its chemical composition, producing molecules with high anti-oxidant properties, which are certainly advantageous, for example, in the exhausted oil utilization as rejuvenating of bitumen. However, the waste oils have some disadvantageous, such as poor low temperature fluid properties, a propensity to oxidative degradation, a susceptibility to hydrolysis in acid media, which limits its application. For this reason, it is actually of greatest interest the proposal of chemical modifications of their structure to improve its physicochemical properties. In particular, if search should be narrowed only to vegetable oil waste (i.e., Waste Cooking Oils (WCO), then soybean oil, canola oil, coconut oil, castor oil, etc.), esterification, [65] hydrogenation [66], epoxidation [67], acylation [24] are only some examples of adopted chemical transformations to enhance the performance of these oils. In fact, the major components of vegetable oil waste are triglycerides esters of glycerol with saturated and unsaturated long-chain fatty acids, therefore, the transesterification reaction may represent the most valid method to change their properties, and it progresses through hydrolysis and successive esterification of the hydrolyzed products as schematically shown in Scheme 1.

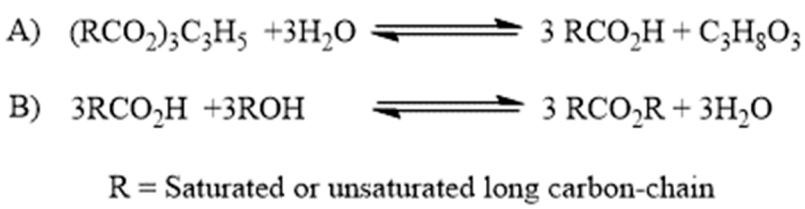


**Scheme 1.** (A) Hydrolysis reaction to form long-chain fatty acids; (B) esterification reaction to produce esters of long carbon-chain fatty acids.

This procedure paves the way to subsequent chemical modifications. An example is reported from Xiang et al. [68] that carried out the transesterification reaction by the treatment of exhausted oils with NaOH in $CH_3OH$ to obtain methyl esters of fatty acids. The latter were transformed in variously substituted triester derivatives by the first epoxidation of unsaturated bounds present on of carbon backbone of R and a subsequent opening of oxirane ring to produce a final matrix with increased physicochemical properties, (i.e., better anti-wear ability, improved oxidation stability, etc.). However, it is evident that in proposing new synthetic methodologies of structural transformations, the chemists should take into account cheap and eco-friendly procedures. For this reason new perspectives on this typology of reaction may be, for example, the introduction of low-cost catalysts (i.e., Lanthanide salts, Fe salts, Zn salts, Cu salts, etc.), which are known to be employed in many chemical manipulations [69,70] in combination with green solvents, such as ionic liquid, Deep Eutectic Solvents (generally named DES) or water or Microwave irradiation [71,72]. For example, in order to transform oil waste into more performing products, it is possible to suggest a synthesis process to open oxirane rings, formed on the unsaturated bounds of R chain, in mild conditions, introducing transformable functional groups, such as nitriles or nitro that may be subsequently oxidized in environmentally friendly solvents. Another suggested modification may be the introduction of acyl groups with alkyl or aromatic chains on the unsaturated scaffold of the carbon-chain [73–75]. The presence of alkyl or aromatic groups could lead to forming secondary interaction, such as Wan der Waals or π-π interactions that may confer to the modified oils a major branched substructure, varying the physicochemical characteristics, increasing the chemical stability of the substrates and obtaining their better performance.

An alternative to the chemical catalysts could be the enzymatic catalysis, as proposed by Avisha and co-workers [76]. Candida rugosa lipase was used to hydrolyze oil wastes in a water solution with successive esterification by Amberlyst 15(H) resin catalyst. In addition, orange lipase deriving from waste was used from Okino-Delgado et al. in transesterification reaction, realizing remediated oils with higher performance profile [77]. However, the enzymatic catalysis through the commercial and the homemade lipase is considerably less convenient than the chemical one, because of higher reaction costs, specific reaction conditions, less manageability, the greater facility of degradation. On the other hand, the negative impact of oil waste on the environment and humans directs the scientists to propose its re-use to reduce the produced amount. Then, the chemical manipulation of the exhausted oils fits perfectly in the contest of its recycling. Obviously, it is important to always make a cost/benefit ratio. In fact, it is correct to think that chemical modification of an oil matrix has a major cost than its use as such, but it is equally true that with a view to having products, such as bitumen rejuvenating ones with enhanced physicochemical properties, the future of research in this field is to invest in rebirth of oil waste by innovative synthetic methods.

### 5.2. New/Novel Rejuvenators

The overall characteristics of a bitumen are, as a matter of fact, the consequence of its complex structure. The term "complex" does not refer to "complicated" or "hard to describe" but, instead, the term is used on a physical basis. The peculiar aspect involved in this topic will be better clarified in the next paragraph. Aging perturbs and changes the complex organization of a bitumen through various mechanisms whose consequence is to change the overall complex organization of the material and not, strictly speaking, one single specific aspect of the molecular organization of the bitumen. That is why, if only one specific structural feature is looked at, it may not correlate the dynamic behavior. In this respect, novel rejuvenators can be thought of. A typical class of molecule usually related to complex behavior is that of surfactant, and more generally that of amphiphiles. Amphiphiles, simultaneously possessing polar and apolar moieties within their molecular architecture, can give a wide scenario of possible intermolecular interactions: polar–polar, polar–apolar, apolar–apolar interactions, eventual directional H-bonds, steric hindrance, etc. For this reason, some of them are a surfactant, i.e., surface-active agents, when dissolved in water: they expose to the air their apolar part while binding water through their polar head, thus, decreasing the surface tension [78,79]. The same principle holds when trying to mix polar and apolar substances. Bypassing their natural tendency to remain separated, they actually can be effectively mixed if an amphiphile is present. Thanks to its capability to simultaneously linking both the polar and the apolar phases, the amphiphile act as a bridging molecule between the two. The two phases can be, therefore, homogenized to such an extent that the system can become homogeneous at the macro-scale although heterogeneous at the nano-scale, with the formation of local domain of one phase stabilized by one or more layers of opportunely oriented amphiphilic molecules and dispersed in the other phase [80]. Micelles, vesicles, bicontinuous structures and liquid crystals are only examples of stabilization of the systems through the formation of local intermolecular assemblies. This principle can be used, in our opinion, to the bitumen cases also. Let us consider that, in the micellar model, the bitumen is constituted by polar aggregates stabilized by polar resins and dispersed in a more apolar matrix. In this case, an amphiphilic molecule can bind on a side the asphaltene cluster, and on the other side, the apolar maltene phase. The overall outcome of these simultaneous interactions would be to disperse the asphaltene clusters contrasting aging better, or even, drawing back to rejuvenation. On the other hand, it must be admitted that the general mechanism of action shown by amphiphiles is already well-known and used for several issues in various fields: amphiphiles have been proved to be effective in stabilizing organic molecule clusters within an apolar solvent [81,82], as well as metal clusters [83], nanoparticles [84], and ionic clusters [85], so in our opinion their direct application to bitumen represents an obvious and immediate step. This idea has been recently tested in preliminary works where the surfactants have been successfully used to prepare warm mix asphalt binders. The results showed that the use of the

surfactant-based additive reduces surface free energy. It increases after short-term (Rolling Thin Film Oven) and reduces after long-term (Pressure Aging Vessel) aging [86]. Moreover, the addition of DBSA (Dodecylbenzosulfonic acid) based surfactant enhanced viscoelastic response of bitumen and reduced glass transition temperatures since it promotes the association of asphaltene molecules/aggregates into larger clusters in bitumen [87].

## 6. Forefront/Vanguard Techniques Facing Complexity in Bitumen

### 6.1. Complexity

The aim of this last paragraph is to furnish some hints on the future developments of new techniques for the investigation of bitumen. To do so, it is advisable first to clarify the exact nature of such systems, so it is needed to shed light on what is meant with the concept of "complex systems". Complexity is based on a hierarchical relationship between constituents and objects. Just to introduce the topic by an example, elementary particles are somehow assembled to form atoms, atoms are assembled to form molecules, molecules can assemble to form living cell, opportunely organized living cells can constitute tissues, and insisting with such a kind of reasoning, tissues, organs, human beings, society, etc., can be consecutively considered in an escalation within the principle a high number of levels. What is called "constituents" can be assembled together to form a complex object which, in turn, can be one of the "constituents" making an even bigger (i.e., more complex) object. So, what are called "constituents" belong to a specific "level", but when they are assembled to form a "bigger" object, a successive level is reached. These are what are called levels of complexity, and it can be misleading to deal with "bigger" or "smaller" systems, because it is not a matter of size: it is correct to deal with different levels of complexity. The peculiar features possessed by the elements belonging to each level of complexity are the consequence of novel emerging and unexpected properties that can arise when passing from a level to the successive. Since constituents are interacting, in fact, the complex system is not the mere collection of its building blocks so that the overall properties cannot be obtained by simple extrapolation of the characteristics of their constituents. Interestingly, novel and unexpected emerging properties can arise when passing from a level to the successive. Complex materials exhibit, therefore, spatial correlations between their constituents at different scales.

### 6.2. Probing Complexity

Bitumen is certainly a complex system, due to the asphaltene aggregation taking place at different length-scales, and due to the specific molecular aggregation involving different chemical species (see Sections 1 and 2). As in micellar systems, there are structures living for milliseconds (micelles) which can also be spatially correlated at high concentrations, in a similar way the same can be expected for bitumen. The term "structure", obviously crucial for an adequate description of a complex system is to be intended as strictly related to the spatial correlation between the constituents of the system. On the other hand, it cannot be neglected that for applicative purposes, the study of material must advisably involve non-invasive techniques. This is exactly what scattering techniques probe. The structure factor is inherently contained in the output of a scattering experiment. Scattering techniques not only give direct information on the structure possessed by the system, but also give its synthetic fingerprint. Such information (characterization of the constituents and their correlation to longer scales) are crucial in order to establish the proper connection between nanoscale morphology and bulk properties in complex systems. Here we want to emphasize that the "structure" involved in complexity is exactly defined in terms of the direct observable through scattering techniques, i.e., the existence of preferred distances (spatial correlations) among specific constituents of the system and taking place at different length-scales [88] so will give, in the following paragraphs, some hints on the theoretical background at the basis of this technique. Of course, other methods, especially microscopy-based, are available, i.e., Atomic Force Microscopy (AFM), Scanning Electron Microscopy (SEM) and Fluorescence Microscopy were used to investigate bitumen doped by polymers. The AFM and SEM have been used in order to

study the structure of asphalt while Fluorescence Microscopy was used to aid in understanding the structural changes occurring when polymers are added to the asphalt. The Atomic Force Microscopy was able to study the only structures of the asphaltenes. On the contrary, the Fluorescence Microscopy can only reveal the presence of fluorescing molecules. Oil exhibits autofluorescence when irradiated with shorter wavelength light, such as UV light, but for bitumen, there is very little fluorescent light emission because the oil phase is mixed with an asphaltene and a resin phase which do not exhibit any autofluorescence [89]. Performances and rheological behavior of a bitumen, however, is also a consequence of the dynamics involved at the molecular basis. Whereas, the above-cited techniques essentially probe the structure, a vanguard method to probe the dynamics fit for accurate bitumen characterization must also be individuated. Therefore, after a presentation of the scattering techniques, it will be shown another vanguard technology that can be used to deeply analyze the bitumen dynamics: the Relaxometry NMR, consisting in the measurement of the $^{1}$H-NMR relaxation times of bitumen at low magnetic fields.

#### 6.2.1. Scattering Theory

Apart from the development of scattering techniques at the large-scale facilities, recent improvements in lab instrumentation and the related beam intensities have greatly enhanced the importance of scattering methods in the structural characterization of complex materials. The quality of the recorded spectra is becoming adequate to extract information even from complex systems as bitumen is. The fundamentals of scattering techniques are, therefore, now given with the only scope to show how they are able to furnish the synthetic view of the material structure [90] of any nature [88]. A typical scattering geometry is reported in Figure 26: an incident (monochromatic or monochromatized) beam from a given source (e.g., Neutrons, X-rays, visible light, electrons, etc.) with incident wavevector ($k_0$) impinges on the material system under investigation. The scattered radiation intensity $I$ is collected by a detector at a given scattering angle $2\theta$ with respect to the incident radiation direction. The difference between the scattered ($k_F$) and incident ($k_0$) wavevectors furnishes the scattering wavevector $q = |k_F - k_0| = (4\pi n/\lambda)\sin(\theta)$ (where n is the index of refraction of the medium and $\lambda$ is the wavelength of the employed radiation). For light n = 1.33 for a water medium, whereas, for X-rays and neutron n is very close to unit. It is worth noticing that a scattering experiment furnishes information over distances that are of the same order, or bigger, than the wavelength $\lambda$ of the source radiation. The scattering is generally described as arising from the constructive interference coming from objects that are embedded in a continuum medium (treated as constant background). The interaction of radiations with materials is characterized then by a scattering length $b_i$, and its scattering length density (SLD) which is given by $\rho(\boldsymbol{r}) = \sum_i \rho_i(\boldsymbol{r}) b_i$ where $\rho_i(\boldsymbol{r})$ is the local density of scatters of type $i$ [91,92].

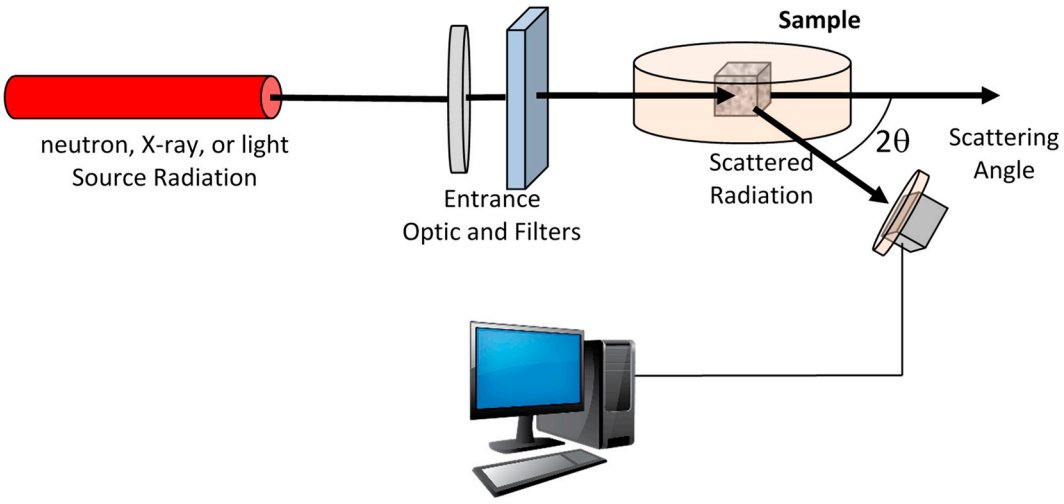


**Figure 26.** Schematic setup of a scattering experiment.

So, for example:

(i) neutron scattering arises through (short-range) nuclear interactions (or magnetically, if atoms have unpaired electron spins), while the scattering length depends on the nature of the nuclei of the reference atoms.
(ii) X-rays scattering comes from the interactions among all the electrons in the material under investigation. In this case, the scattering density can be traced back to the electron density.
(iii) In the case of Light photons, which have lower energy than X-rays ones, are scattered only by the outer part of the electronic cloud of an atom. In this case, the scattering length density is proportional to the polarizability of the materials.

Of course, different radiation (particle) sources give different sub-techniques. However, in the following, the different information that can be derived from the various scattering angle ranges, which in turn give different methods of analysis, will be shown.

6.2.2. Scattering of Neutrons (SANS), X-rays (SAXS) and Light

Scattering probes the statistical ensemble of the nano-structures and deals with the diffusion of electromagnetic (or particle) waves by heterogeneities in material systems [93]. At small angles 2θ, the (coherent) scattering intensity in the so-called "static approximation" is given by:

$$\boldsymbol{I}(\boldsymbol{q}) \propto \left[\sum_{\boldsymbol{i}} \boldsymbol{b_i}\, \boldsymbol{e}^{\boldsymbol{iqR}}\right]^2 \tag{2}$$

where $b_i$ is the scattering length of the particle (chemical species) that occupy the position $\boldsymbol{R}$ in the material system. For SANS experiments the scattering length density $\rho(\boldsymbol{r})$ of the sample is defined as $\rho(\boldsymbol{r}) = \sum_i n_i(\boldsymbol{r}) b_i$, where $b_i$ is the scattering length of the nucleus of type $i$, while $n_i(\boldsymbol{r})$ is the corresponding number density of such nuclei. For X-ray scattering $\rho(\boldsymbol{r}) = \left(\frac{e^2}{mc^2}\right) n_{el}(\boldsymbol{r})$, where $\left(\frac{e^2}{mc^2}\right)$ is the Thompson scattering length of the electron, and $n_{el}(\boldsymbol{r})$ is the electron number density.

By replacing $b_i$ by a locally averaged scattering length density $\rho_i(\boldsymbol{r})$, (where $r$ is a variable position vector), it is possible to perform an integration over the sample volume, V:

$$I(\boldsymbol{q}) \propto \left[\int_V \rho(\boldsymbol{r}) e^{i\boldsymbol{qR}} d^3\boldsymbol{r}\right]^2 \tag{3}$$

If isotropic samples are considered (i.e., where the orientation effects are averaged, due to the radial symmetry), the scattering intensity $I(q)$ can be expressed as:

$$I(q) \propto \int_0^\infty (\rho(r))^2 \frac{\sin qr}{qr} 4\pi r^2 dr \tag{4}$$

Very often, it is not immediate from the experimental Small Angle Scattering (SAS) intensity profile to obtaining direct information about the $\rho(\boldsymbol{r})$ function by inverse transform methods. In this case, SAS interpretation is based on the choice of suitable models expressed in terms of specified functions, which are capable of furnishing information on specific parameters connected to particular properties of the material system under consideration. The name of the technique is then further characterized by the probe which is used: if the probe is made of X-rays, then SAXS is considered; if the probe is a flux of neutrons, then SANS holds, etc. If the source is light, then it will obviously deal with light scattering. However, it must be noticed that, when dealing with light scattering, another technique, called dynamic light scattering (DLS) also known as photon correlation spectroscopy (PCS), is usually referred to. In such a method, time fluctuations of the scattering intensity as a consequence

of the Brownian motion of nano-scatters in a solution are recorded. Then, a time-dependent scattering function is derived to the diffusion coefficient of the particles (the scatters) dispersed in the liquid phase [94,95]. In contrast to this (more widely known) technique, the static light scattering (SLS) configuration resembles the typical scattering apparatus.

In the case of wide-angle scattering, higher $\boldsymbol{q}$ values are considered, which means that shorter distances are explored. In a typical Wide-Angle Scattering experiment, which can use in principle the same sources as small-angle, usually, the scatters are the atoms themselves. Typical interatomic distances are, therefore, probed: in the case of pure crystals, where positional order is dominant, this gives the famous Bragg law:

$$2\boldsymbol{d}\ \mathbf{sin}\boldsymbol{\theta} = \boldsymbol{n\lambda} \tag{5}$$

where $n$ is an integer and $d$ is the characteristic distance of reticular planes.

However, when the order is weak, the principle still holds, and wide-angle scattering can also be used for amorphous materials as in the case of bitumen. In this case, typical interatomic distances are unveiled: the interatomic first shell (which is often associated to the interatomic spacing typical of the liquid phase [96]) and other eventual longer-range peaks sometimes occurring as a consequence of intermolecular interactions [97]. In this situation, no sharp peak is observed, due to the disordered nature of the system. This disorder can be due to two effects:

(i) a polydispersion of the value of the interatomic distance represented by the peak. The intrinsically-disordered nature of the system (fluid) gives a peak broadening whose width gives the distance polydispersion. The order is partially lost at any distance.

(ii) Reduced size of the domain. The band broadening is due to the fact that the specific interatomic distance is only help at a certain length, called the correlation length. The order is lost beyond this length. The scattering domain size can be derived by the full width at half maximum (FWHM) of the band through the Debye-Sherrer formula:

$$\boldsymbol{\Delta} = \frac{\mathbf{K\lambda}}{\mathbf{FWHM\ cos\theta}} \tag{6}$$

where Δ is the average scattering domain size θ is the Bragg angle, λ is the wavelength of the incident beam, the FWHM (is expressed in radians and must be corrected for instrumental broadening, and K is a factor, approximately equal to unity, related to the domain shape [98].

This approach has proved to be effective in the structural analysis of structured molecular fluids [99,100], even in ionic liquids [101], and recently also in bitumen [1]

#### 6.2.3. Applications of Scattering Techniques to Bitumen

Due to the high diffusion of X-ray scattering techniques and the development of lab-scale instrumentation giving adequate data quality, X-ray scattering was used for the analysis of bitumen even in the '60 [17]. Of course, when exploring the structure, taking into account values of typical length scales longer than a few nm small-angle scattering is best suitable [102]. However, in the wide angle range, the spectrum gives already a significant amount of information: it will be now briefly shown how to interpret it taking as an example of the representative spectrum, reported in Figure 27, as a function of a scattering vector $\boldsymbol{q}$ ($\boldsymbol{q}$ = (4π/λ) sinθ).

Let us pay attention to the following features:

1. A prominent broad band centered around 1.3 $Å^{-1}$ dominates the spectrum;
2. A weak and broad band around 3 $Å^{-1}$;
3. There is a tiny, but sharp, peak around 0.5 $Å^{-1}$, not always present;

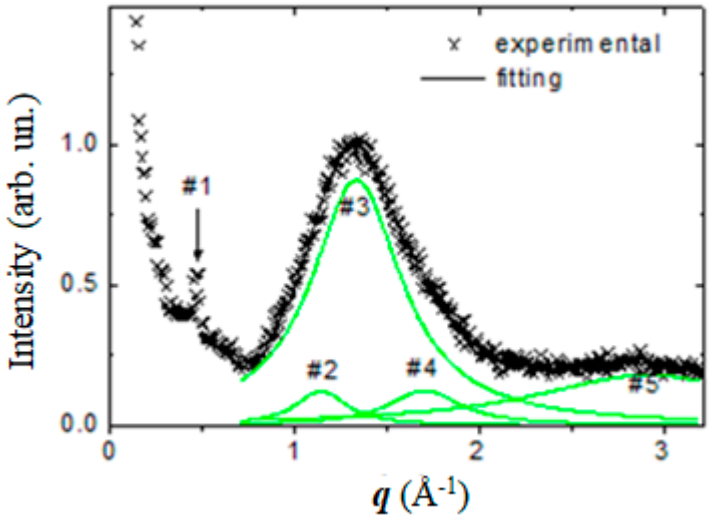


**Figure 27.** A typical X-ray scattering spectrum together with the Lorentzian deconvolution.

Different peaks (in Figure 27 indicated with progressive numbers) indicate that there are different characteristic distances belonging to various atomic and molecular organizations of different levels of complexity. The position of the center of each peak gives the characteristic distance (d), according to the Bragg law (Equation (7)) which, readapted, gives the following:

$$d = \frac{n\lambda}{2\sin\theta}. \quad (7)$$

As above, $d$ is the interplanar distance, $\theta$ is the scattering angle, and $\lambda$ is the wavelength of the incident radiation. Table 3 resembles the peculiarities and meaning of the peaks.

**Table 3.** Bands in the WAXS profile with the corresponding characteristics.

| Position ($Å^{-1}$) | Features | Characteristic Distance (Å) | Meaning |
|---|---|---|---|
| 1.3 | Dominant and broad | ~4.7 | combination of various intermolecular distances between alkyl and aromatic parts: See text |
| 2.9 | Broad and weak | 2.2 | interatomic distance within asphaltene; |
| ~0.5, varying | Not always present usually tiny | ~13 | supra-molecular aggregation: Repetition distance of aggregates of local asphaltene aggregates |

The most prominent band centered at around 1.3 $Å^{-1}$ deserves some attention. In alkyl-based fluids, this band has been attributed to a characteristic intermolecular lateral distance of 4.4–4.7 Å [96,100,103] usually present in the conventional liquid (disordered) state [96,97,99–105]. Aromatic compounds are characterized by shorter distances, due to their tendency to form stacks, so they give the so-called graphene band (the lateral distance of about 3.6 Å) [22]. Due to the simultaneous presence of both aliphatic and aromatic compounds in the bitumen, it is reasonable to treat this band as a not-resolved superposition of these two contributions. Deconvolution in terms of bell-shaped curves is sometimes necessary to discriminate all the signals. Two noteworthy observations are due:

1. The fitting procedure will also help in analyzing the weaker band at higher angles (around 2.9 $Å^{-1}$ and which is a characteristic distance $d$ of about 2.2 Å) which is sometimes partially overlapped;
2. The fitting allows to derive, from each curve, also the Full Width at Half Maximum (FWHM)

The shorter distance, of about 2.2 Å, can be surely attributed to some particular interatomic distance. The value is in the range of the typical distance between non-adjacent carbons reported for polycyclic aromatic compounds [106] so such attribution can be safely hypothesized. In the range

0.3–0.8 $Å^{-1}$ it can be present at a tiny peak. This would reveal the occurrence of a supra-molecular aggregation and would be, therefore, associated to a repetition distance between one asphaltene local aggregate and its neighboring one [22], suggesting the presence of aggregates of asphaltene aggregates, in accordance with a model of a complex system with different levels of complexity. Finally, in the low-angles range of the WAXS spectrum ($q < 0.3$ $Å^{-1}$), the fractal aggregation of the supra-aggregates of asphaltene clusters can be explored. The presence of self-similar, fractal structures, in fact, can be in principle possible in bitumen: in these cases, interfacial boundary is not sharp, and a scaling law between the mass M (or particle number N) and the enclosed volume is established, which furnishing an indication of how efficiently the particles are packed [107]. For a porous fractal cluster containing N identical primary units this scaling law is expressed as $N \sim R^{Df}$, were the fractal dimension $D_f$ is connected with the involved aggregation mechanism. Since 1984 scattering techniques have been widely used for characterization of materials having fractal microstructures. The fractal dimension of a particle can be determined by analyzing the power-law regime of the scattered intensity $I(q) \sim q^{-\alpha}$, where the exponent $\alpha$ is related to the fractal dimension $D_f$ of the scattering structures. For a mass fractal, it is possible to show that $\alpha = D_m$ and $1 < \alpha < 3$ in a three-dimensional space. In contrast, $\alpha = 6 - D_s$ for surface fractals. If $D_s = 2$ the well-known Porod's law $I(q) \sim q^{-4}$ for non-fractal structures with smooth interfaces is obtained.

So, the slope $\alpha$ can be, therefore, derived by linear fit, in an adequate region of the spectrum (see Figure 28 as reference), using the equation:

$$I(q) \propto q^{-\alpha} \tag{8}$$

However, self-similar hierarchical structures are seldom present or rarely probed in the literature, and, due to diversity of bitumen origin, chemical composition and age, this feature of the structure can change dramatically. Additives can change (i) the fractal structure, if present (ii) the band around 1.3 $Å^{-1}$ and (iii) the peak around 0.5 $Å^{-1}$, if present, but not the higher angle band around 2.2 $Å^{-1}$ because this distance refers to an intra-molecular distance, and it is not expected, therefore, to be changed by the presence of an additive.

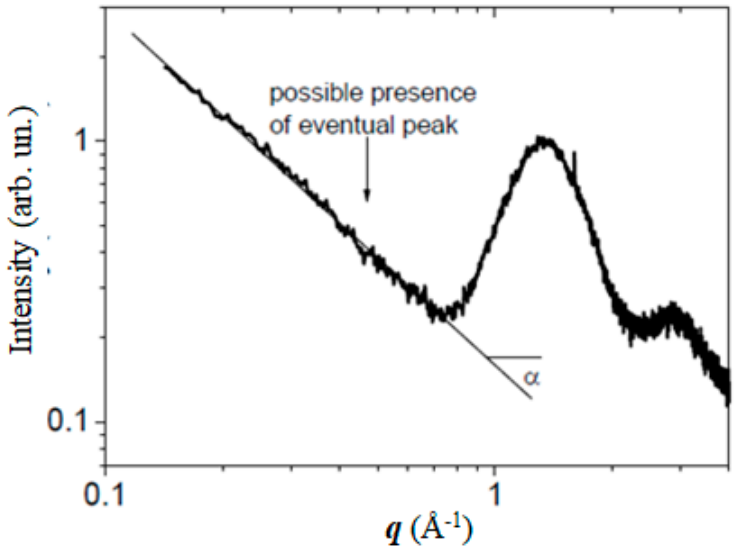


**Figure 28.** X-ray scattering spectrum of a bitumen showing fractal-like structure (see text for details).

### 6.2.4. Relaxometry Nuclear Magnetic Resonance Theory

The second vanguard technology that can be used to analyze the bitumen is the Relaxometry NMR. This method probes dynamic features and consists of measuring the $^1$H-NMR relaxation times of bitumen at the low magnetic field. In the current high-resolution NMR technique, it is not

possible to obtain high resolution spectra because of their highly heterogeneous and low magnetic field strengths. In a basic NMR concept, at equilibrium, protons nuclei are distributed among the energy levels according to a Boltzmann distribution. Following any process that disrupts this distribution (e.g., absorption of radio frequency energy), the nuclear spin system returns to equilibrium with its surroundings (the "lattice") by a first-order relaxation process characterized by a time $T_1$ called the spin−lattice relaxation time. To account for processes that cause the nuclear spins to come to equilibrium with each other, a second time $T_2$ is required. $T_2$ is called the spin−spin relaxation time, because the relaxation is concerned with the exchange of energy between spins via a flip-flop type mechanism. In a perfectly homogeneous field, the NMR time constant of the decay would be $T_2$, but, in fact, the signal decays in a time $T_2$* that often is determined primarily by field inhomogeneity, since nuclei in different parts of the field precess at slightly different frequencies, and hence, quickly get out of phase with each other. Thus, the signal decays with a characteristic time $T_2$*. This decay directly measures the decrease in the transverse magnetization $M_{xy}$. The contribution of the magnetic field inhomogeneity to the free induction decay precludes the use of this decay time, $T_2$* as a measure of $T_2$. A method for overcoming the inhomogeneity problem is to apply the Carr−Purcell technique (CP) [108]. This method may be described as a 90°, τ, 180°, 2τ, 180°, 2τ, 180°, 2τ, ... pulse sequence. In Figure 29, experimental steps of bitumen, NMR Relaxometry are shown. Four hundred echoes have been obtained by Carr−Purcell sequence and analyzed by Inverse Laplace Transform (ILT).

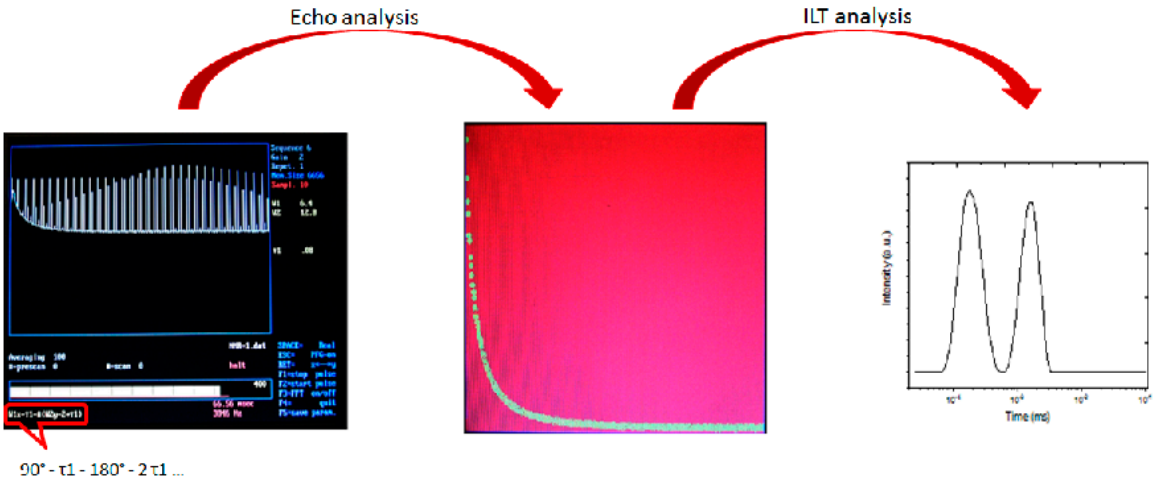


**Figure 29.** Schematic sequence of Echo and Inverse Laplace Transform (ILT) analysis in NMR Relaxometry.

The 180° pulses are applied at 90° phase difference relative to the initial 90° pulse, and the τ time delay was 0.05 ms. The main advantage of such a multiple echo technique is its quickness compared with other techniques based on single echoes. Consequently, it allows multiple accumulations of the echo train signal, which is an important issue in low-field experiments where the detection sensitivity is strongly reduced relative to the high-field experiments. If the CP envelope has a mono-exponential decay, the relaxation time $T_2$ of the sample can be obtained by fitting the $n$ data to the following equation:

$$A_n = A_0 e^{-\frac{2n\tau}{T_2}} \quad (9)$$

where $A_n$ is the amplitude of the $n$th echo in the echo train and $A_0$ is a constant depending on the sample magnetization, filling factor, and other experimental parameters. Usually, the $T_2$ relaxation time varies all over the sample because of the sample heterogeneity or surface relaxation differences; then a multiexponential attenuation of the CP envelope should be observed. Hence, if inside the sample, a continuous distribution of relaxation times exists, the amplitude of the $n$th echo in the echo train is given by:

$$A_n = A_0 \int_0^\infty P(T_2) e^{-\frac{2\pi\tau}{T_2}} dT_2, \tag{10}$$

where $P(T_2)$ is the $T_2$ relaxation time probability density.

Equation (10) suggests that the analysis of the experimental data using an inverse Laplace transform (ILT) might provide the relaxation time probability function. The ILT is a well-known mathematical tool, where it needs to face the inverse problem of estimating the desired function from the noisy measurements of experimental data. For convenience, the definition of the problem will be shortly recalled. Let $f(t)$ be a function defined for $t \geq 0$; the function $F(s)$ introduced by means of the expression:

$$F(s) = L\{f(t)\} = \int_0^\infty f(t) e^{-st} dt \tag{11}$$

is the real Laplace transform of $f(t)$. The inverse process, indicated by the notation $f(t) = L^{-1}[F(s)]$, is termed the inverse Laplace transform (ILT). $P(T_2)$ is the ILT of the unknown function that fit the echo amplitude curve. Hence, $P(T_2)$ can be understood as a distribution of rate (inverse of time) constants, strictly speaking, a Probability Density Function (PDF) that, among other things, could account for the different macro-structures that compose the bitumen binder [109]. This technique allows finding the PDF distribution, which associates with relaxation times that correspond to unrelated molecular aggregates inside the bitumen.

#### 6.2.5. Applications of Relaxometry Nuclear Magnetic Resonance to Bitumen

Generally, regarding types of bitumen, the $T_2$ relaxation time distribution exhibits two peaks. Direct correlation can be made between $T_2$ and the rigidity of structures in these materials [43], as well as the molecular constraint, which causes dynamic hindrance [46]. The shorter $T_2$ times (around 10 ms) reasonably corresponds, therefore, to more rigid supra-molecular aggregates; hence, they are attributed to asphaltenes. Conversely, high $T_2$ times (around 100 ms) can be attributed to low intra-molecular interactions; they can be referred to the maltene fraction of the sample under examination. This finding supports the colloidal model of the bitumen. In fact, if the polar fluid model suggested by Christensen [110] were applicable to our system, the ILT result would demonstrate a sole broad peak referred to as a continuous $T_2$ time. Figure 30 shows a typical Probability Density Function obtained through an ILT transform of $T_2$ relaxation time data determined by analyzing neat and modified 100/130 penetration grade bitumen supplied by Highway Research Institute (Almaty, Kazakhstan) [111]. The measures of $T_2$ were made at a temperature 15 °C lower than transition temperature (solid-liquid) measured by dynamic temperature ramp test experiment. In Figure 30 the panels refer to the following samples: SD refers to PAV bitumen + 2 wt% HR (the green rejuvenator), SC refers to PAV bitumen + 2 wt% VO (Vegetable Flux Oil), SB PAV bitumen, SA Neat Bitumen.

The $T_2$ relaxation time distribution can be considered a structural fingerprint of the bitumen where changes in the $T_2$ relaxation times evidence modification in the structure of colloidal binder. In particular, the powerful ILT, applied to the echo decay, can be used to verify the effectiveness of the real rejuvenator. The same or better similar profile of $T_2$ relaxation times prove that the structure of aged bitumen has been regenerated reorganizing the same distribution of asphaltene micelles in the maltene phase. In general, by ILT NMR relaxometry it is possible to follow the structural evolution of bitumen when additives (polymer surfactants, etc.) are added, in fact, the relaxation distribution is strongly affected by the supramolecular organizations present in the colloids.

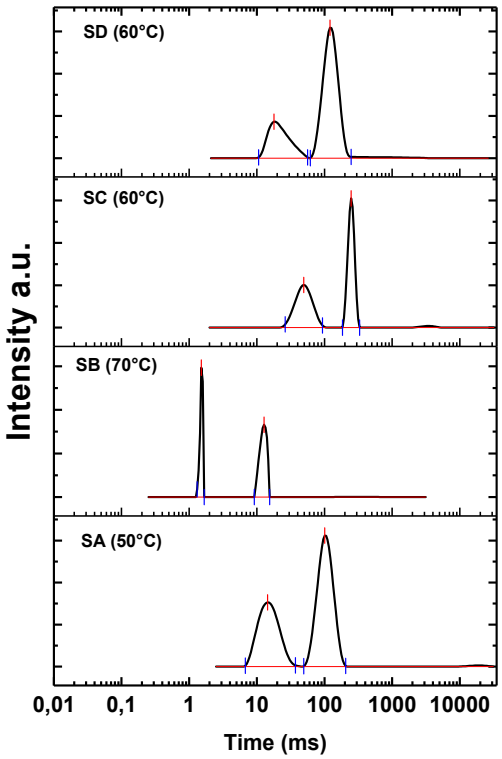


**Figure 30.** Inverse Laplace Transform (ILT) showing the Probability Density Function (PDF) of asphaltene and maltene aggregates of bitumen samples.

## 7. Concluding Remarks

1. Many materials are used for rejuvenating bitumen by lowering viscosity and stiffness. Since different physico-chemical mechanisms are involved in bitumen ageing (oxidation, evaporation, structural changes), different mechanisms of actions can be consequently exerted by the various rejuvenators (softening/fluxing, restoration of the pristine structure/properties). The distinction of the various mechanisms has been highlighted. These aspects have been shown in Sections 1–3.
2. The state-of-the-art constituted by the works carried out by several researchers in this field has been shown. Low-cost oils are generally added to increase the maltene fraction, but it should be noticed that an additive having complete rejuvenating function should also induce a reorganization of the chemical structure of asphaltenes and their assemblies. The restoring of the aged bitumen structure to the original conditions is not trivial, due to its complex organization at the supra-molecular scale. This has been extensively shown in Section 4.
3. Taking into account the complex chemistry involved in the bitumen rejuvenation, the additive performances can be improved by chemical manipulation/modification (paragraph 5.1). Some perspectives have been also presented (Section 5.2) considering for the complexity of the systems and suggesting the use of amphiphilic species as promising rejuvenator thanks to their simultaneous presence, within their molecular architecture of both polar and apolar moieties which permits their simultaneous interactions with polar (asphaltene clusters), apolar (maltene) and amphiphilic (resins) species of the bitumen.
4. Scattering techniques and nuclear magnetic relaxometry have been presented as vanguard and promising techniques deserving attention for deeper analyses in bitumen. In fact, they can probe the effectiveness of a rejuvenator in restoring the microstructure of bitumen after the aging process, whereas, mechanical properties, on their own, are not enough for investigating this aspect. A clear introduction to the physics of the techniques and applications to the study of bitumen has been presented.

5. With this work, we would like to share with the reader our belief that the detailed analysis of the physics of bitumen at the molecular basis extends the information taken from the commonly used empirical and quick tools. This allows to better understand the phenomena taking place in bitumen furnishing new tools for the piloted design of new and ever-performing rejuvenators.
6. We wanted to furnish a novel viewpoint for the study of bitumen based on the concepts of the complex systems in physics. According to this approach, the final behavior of the material is not only dictated by specific interactions, as usually assumed in most of the research papers, but also by collective contributions of many molecules interacting and aggregating themselves usually at different length scales in hierarchical structures generating emerging properties. We hope that this study can constitute a novel approach for the investigation of bitumen, and the improvements of its performances.

**Author Contributions:** P.C. (Pietro Calandra) conceptualization methodology and writing, P.C. (Paolino Caputo) conceptualization; M.P. editing correction and writing, V.L. conceptualization and research, R.A. conceptualization, and C.O.R. conceptualization and supervision.

**Funding:** This research received no external funding.

**Conflicts of Interest:** The authors declare no conflict of interest.

## References

1. Calandra, P.; Caputo, P.; De Santo, M.P.; Todaro, L.; Turco Liveri, V.; Oliviero Rossi, C. Effect of additives on the structural organization of asphaltene aggregates in bitumen. *Constr. Build. Mater.* **2019**, *199*, 288–297. [CrossRef]
2. Rozeveld, S.; Shin, E.; Bhurke, A.; France, L.; Drzal, L. Network morphology of straight and polymer modified asphalt cements. *Microsc. Res. Technol.* **1997**, *38*, 529–543. [CrossRef]
3. Lesueur, D. The colloidal structure of bitumen: Consequences on the rheology and on the mechanisms of bitumen modification. *Adv. Colloid Interface Sci.* **2009**, *145*, 42–82. [CrossRef] [PubMed]
4. Petersen, J.C. Chemical composition of asphalt as related to asphalt durability: State of the art Transport. *Transp. Res. Rec.* **1984**, *999*, 13–30.
5. Yu, X.; Zaumanis, M.; dos Santos, S.; Poulikakos, L.D. Rheological, microscopic, and chemical characterization of the rejuvenating effect on asphalt binders. *Fuel* **2014**, *135*, 162–171. [CrossRef]
6. Copeland, A. Reclaimed asphalt pavement in asphalt mixtures: State of the practice. In *Report No. FHWA-HRT-11-021*; Federal Highway Administratio: McLean, WV, USA, 2011.
7. Firoozifar, H.; Foroutan, S.; Foroutan, S. The effect of asphaltene on thermal properties of bitumen. *Chem. Eng. Res. Des.* **2011**, *89*, 2044–2048. [CrossRef]
8. Filippelli, L.; Gentile, L.; Oliviero Rossi, C.; Ranieri, G.A.; Antunes, F.E. Structural change of bitumen in the recycling process by using rheology and NMR. *Indus. Eng. Chem. Res.* **2012**, *51*, 16346–16353. [CrossRef]
9. Gentile, L.; Filippelli, L.; Oliviero Rossi, C.; Baldino, N.; Ranieri, G.A. Rheological and H-NMR spin–spin relaxation time for the evaluation of the effects of PPA addition on bitumen. *Mol. Cryst. Liq. Cryst.* **2012**, *558*, 54–63. [CrossRef]
10. Yoon, S.; Durgashanker Bhatt, S.; Lee, W.; Lee, H.Y.; Jeong, S.Y.; Baeg, J.O.; Wee Lee, C. Separation and characterization of bitumen from Athabasca oil sand. *Korean J. Chem. Eng.* **2009**, *26*, 64–71. [CrossRef]
11. Altgelt, K.H.; Boduszynski, M.M. Compositional Analysis: Dream and Reality. In *Composition and Analysis of Heavy Petroleum Fractions*; Marcel Dekker: New York, NY, USA, 1994; pp. 9–39.
12. Zenke, G. Zum Löseverhalten von "Asphaltenen": Anwendung von Löslichkeitsparameter-Konzepten auf Kolloidfraktionen Schwerer Erdöl Produkte. Ph.D. Thesis, Technical University of Clausthal, German State, Germany, 1989.
13. Hurley, G.C.; Prowell, B.D. Evaluation of potential processes for use in warm mix asphalt. *J. Assoc. Asph. Paving Technol.* **2006**, *75*, 41–90.
14. Silva, H.M.R.D.; Oliveira, J.R.M.; Ferreira, C.I.G.; Pereira, P.A.A. Assessment of the performance of warm mix asphalts in road pavements. *Int. J. Pavement Res. Technol.* **2010**, *3*, 119–127.

15. Hakseo, K.; Soon-Jae, L. Rheology of warm mix asphalt binders with aged binders. *Constr. Build. Mater.* **2011**, *25*, 183–189.
16. Jamshidia, A.; Hamzaha, M.O. Performance of warm mix asphalt containing Sasobit®: State of the art. *Constr. Build. Mater.* **2013**, *38*, 530–553. [CrossRef]
17. Yen, T.F.; Erdman, J.G.; Pollak, S.S. Investigation of the Structure of Petroleum Asphaltenes by X-Ray Diffraction. *Anal. Chem.* **1961**, *33*, 1587–1594. [CrossRef]
18. Jäger, A.; Lackner, R.; Eisenmenger-Sittner, C.; Blab, R. Identification of Microstructural components of bitumen by means of Atomic Force microscopy (AFM). *Proc. PAMM Appl. Math. Mech.* **2004**, *4*, 400–401. [CrossRef]
19. Handle, F.; Füssl, J.; Neudl, S.; Grossegger, D.; Eberhardsteiner, L.; Hofko, B.; Hospodka, M.; Blab, R.; Grothe, H. The bitumen microstructure: A fluorescent approach. *Mater. Struct.* **2016**, *49*, 167–180. [CrossRef]
20. Zhang, F.; Hu, C.; Zhang, Y. Influence of poly (phosphoric acid) on the properties and structure of ethylene-vinyl acetate-modified bitumen. *J. Appl. Polym. Sci.* **2018**, *135*, 46553. [CrossRef]
21. Xu, X.; Yu, J.; Xue, L.; Zhang, C.; He, B.; Wu, M. Structure and performance evaluation on aged SBS modified bitumen with bi- or tri- epoxy reactive rejuvenating system. *Constr. Build. Mater.* **2017**, *151*, 479–486. [CrossRef]
22. Tanaka, R.; Sato, E.; Hunt, J.E.; Winans, R.E.; Sato, S.; Takanohashi, T. Characterization of Asphaltene Aggregates Using X-ray Diffraction and Small-Angle X-ray Scattering. *Energy Fuels* **2004**, *18*, 1118–1125. [CrossRef]
23. Kuang, D.; Ye, Z.; Yang, L.; Iu, N.; Lu, Z.; Che, H. Effect of Rejuvenator Containing Dodecyl Benzene Sulfonic Acid (DBSA) on Physical Properties, Chemical Components, Colloidal Structure and Micro-Morphology of Aged Bitumen. *Materials* **2018**, *11*, 1476. [CrossRef]
24. Sharma, B.K.; Adhavaryu, A.; Liu, Z.; Erhan, S.Z. Chemical modification of vegetable oils for lubrificant application. *J. Am. Oil Chem. Soc.* **2006**, *83*, 129–136. [CrossRef]
25. Thyrion, F. Asphalt Oxidation. In *Asphaltenes and Asphalts: Development in Petroleum Science 2000*; Elsevier: New York, NY, USA, 2000; pp. 445–474.
26. Calandra, P.; Turco Liveri, V.; Caputo, P.; Teltayev, B.; Oliviero Rossi, C. Wide Angle X-Ray Scattering as a Technique of Choice to Probe Asphaltene Hierarchical structures. *J. Nanosci. Nanotechnol.*. in press.
27. Lu, I.; Isacsson, U. Influence of styrene-butadiene-styrene polymer modification on bitumen viscosity. *Fuel* **1997**, *76*, 1353–1359. [CrossRef]
28. Edwards, Y. Influence of Waxes on Bitumen and Asphalt Concrete Mixture Performance. *Road Mater. Pavement Des.* **2009**, *10*, 313–335. [CrossRef]
29. Senise, S.; Carrera, V.; Navarro, F.J.; Partal, P. Thermomechanical and microstructural evaluation of hybrid rubberised bitumen containing a thermoplastic polymer. *Constr. Build. Mater.* **2017**, *157*, 873–884. [CrossRef]
30. Oliviero Rossi, C.; Ashimova, S.; Calandra, P.; De Santo, M.P.; Angelico, R. Mechanical Resilience of Modified Bitumen at Different Cooling Rates: A Rheological and Atomic Force Microscopy Investigation. *Appl. Sci.* **2017**, *7*, 779. [CrossRef]
31. Remišová, E.; Holý, M. Changes of Properties of Bitumen Binders by Additives Application. *IOP Conf. Ser. Mater. Sci. Eng.* **2017**, *245*, 032003. [CrossRef]
32. Abdullin, A.I.; Idrisov, M.R.; Emelyanycheva, E. Improvement of thermal-oxidative stability of petroleum bitumen using "overoxidation-dilution" technology and introduction of antioxidant additives. *Pet. Sci. Technol.* **2017**, *35*, 1859–1865. [CrossRef]
33. Roberts, F.L.; Kandhal, P.S.; Brown, E.R.; Lee, D.Y.; Kennedy, T.W. *Hot Mix Asphalt Materials, Mixture Design and Construction*, 2nd ed.; NAPA: Lanham, MD, USA, 1996; p. 576.
34. Lee, C.; Terrel, R.; Mahoney, J. Test for Efficiency of Mixing of Recycled Asphalt Paving Mixtures. In *Proceedings of the Transportation Research Record 911*; TRB: Washington, DC, USA, 1983.
35. Carpenter, S.; Wolosick, J. Modifier Influence in the Characterization of Hot-Mix Recycled Material. In *Proceedings of Transportation Research Record 777*; TRB: Washington, DC, USA, 1980.
36. Noureldin, S.; Wood, L. Rejuvenator Diffusion in Binder Film for Hot-Mix Recycled Asphalt Pavement. In *Proceeding of Transportation Research Record 1115*; TRB: Washington, DC, USA, 1987.
37. Huang, B.; Li, G.; Vukosavljevic, D.; Shu, X.; Egan, B. Laboratory Investigation of Mixing Hot-Mix Asphalt with Reclaimed Asphalt Pavement. In *Proceedings of Transportation Research Record 1929*; TRB: Washington, DC, USA, 2005.

38. Karlsson, R.; Isacsson, U. Investigations on Bitumen Rejuvenator Diffusion and Structural Stability. *J. Assoc. Asph. Paving Technol.* **2003**, *72*, 463–501.
39. Oliver, J. *Diffusion of Oils in Asphalts*; Report No. 9; Proceedings of Australian Road Research Board: Vermont South, Victoria, Australia, 1975.
40. Yousefi, A.A. Rubber-Modified Bitumens. *Iran. Polym. J.* **2002**, *11*, 303–309.
41. Radenberg, M.; Boetcher, S.; Sedaghat, N. Effect and efficiency of rejuvenators on aged asphalt binder—German experiences. In Proceedings of the 6th Eurasphalt & Eurobitume Congress, Prague, Czech Republic, 1–3 June 2016.
42. Airey, G.D.; Brown, S.F. Rheological Performance of Aged Polymer Modified Bitumens. *J. Assoc. Asph. Paving Technol.* **1998**, *67*, 66–100.
43. Barbosa, L.L.; Kock, F.V.C.; Silva, R.C.; Freitas, J.C.C.; Lacerda Jr, V.; Castro, E.V.R. Application of low-field NMR for the determination of physical properties of petroleum fractions. *Energy Fuels* **2013**, *27*, 673–679. [CrossRef]
44. Oliviero Rossi, C.; Caputo, P.; De Luca, G.; Maiuolo, L.; Eskandarsefat, S.; Sangiorgi, C. $^{1}$H-NMR Spectroscopy: A Possible Approach to Advanced Bitumen Characterization for Industrial and Paving Applications. *Appl. Sci.* **2018**, *8*, 229. [CrossRef]
45. Caputo, P.; Loise, V.; Crispini, A.; Sangiorgi, C.; Scarpelli, F.; Oliviero Rossi, C. The efficiency of bitumen rejuvenator investigated through Powder X-ray Diffraction (PXRD) analysis and $T_2$ -NMR spectroscopy. *Colloids Surf. A Physicochem. Eng. Esp.* **2019**, *571*, 50–54. [CrossRef]
46. Osman, K.S.; Taylor, S.E. Insight into Liquid Interactions with Fibrous Absorbent Filter Media Using Low-Field NMR Relaxometry. Prospective Application to Water/Jet Fuel Filter−Coalescence. *Ind. Eng. Chem. Res.* **2017**, *56*, 14651–14661. [CrossRef]
47. Bocci, E.; Grilli, A.; Bocci, M.; Gomes, V. Recycling of high percentage of reclaimed asphalt using bio-rejuvenator—A case study. In Proceedings of the 6th Eurasphalt & Eurobitume Congress, Prague, Czech Republic, 1–3 June 2016.
48. Tine, T.; Lemoine, G.; Nösler, I.; Kloet, B. Influence of rejuvenating additives on recycled asphalt (RAP) properties. In Proceedings of the 5th Eurasphalt & Eurobitume Congress, Istanbul, Turkey, 13–15 June 2012.
49. Król, J.B.; Kowalski, K.J.; Niczke, L.; Radziszewski, P. Effect of bitumen fluxing using a bio-origin additive. *Constr. Build. Mater.* **2016**, *114*, 194–203. [CrossRef]
50. Somé, C.; Pavoine, A.; Chailleux, E.; Andrieux, L.; DeMArco, L.; Philippe Da, S.; Stephan, B. Rheological behaviour of vegetable oil-modified asphaltite binders and mixes. In Proceedings of the 6th Eurasphalt & Eurobitume Congress, Prague, Czech Republic, 1–3 June 2016.
51. Caputo, P.; Porto, M.; Calandra, P.; De Santo, M.P.; Oliviero Rossi, C. Effect of epoxidized soybean oil on mechanical properties of bitumen and aged bitumen. *Mol. Cryst. Liq. Cryst.* **2018**, *675*, 68–74. [CrossRef]
52. Zargar, M.; Ahmadinia, E.; Asli, H.; Karim, M.R. Investigation of the possibility of using waste cooking oil as a rejuvenating agent for aged bitumen. *J. Hazard. Mater.* **2012**, *233*, 254–258. [CrossRef]
53. Nayak, P.; Sahoo, U.C. Rheological, chemical and thermal investigations on an aged binder rejuvenated with two nonedible oils. *Road Mater. Pavement Des.* **2016**, *18*, 612–629. [CrossRef]
54. De la Roche, C.; Van de Ven, M.; Van den bergh, W.; Gabet, T.; Dubois, V.; Grenfell, J.; Porot, L. Development of a laboratory bituminous mixtures ageing protocol. In *Advanced Testing and Characterization of Bituminous Materials*, 1st ed.; Loizos, A., Partl, M.N., Scarpas, T., Al-Qadi, I.L., Eds.; CRC Press: AK Leiden, The Netherlands, 2009; Volume 1, pp. 331–345.
55. Lamontagne, J.; Dumas, P.; Mouillet, V.; Kister, J. Comparison by Fourier transform infrared (FTIR) spectroscopy of different ageing techniques: Application to road bitumens. *Fuel* **2001**, *80*, 483–488. [CrossRef]
56. Elkashef, M.; Williams, R.C.; Cochran, E. Thermal stability and evolved gas analysis of rejuvenated reclaimed asphalt pavement (RAP) bitumen using thermogravimetric analysis–Fourier transform infrared (TG–FTIR). *J. Anal. Calorim.* **2018**, *131*, 865–871. [CrossRef]
57. Cavalli, M.C.; Zaumanis, M.; Mazza, M.; Partl, M.N.; Poulikakos, L.D. Effect of ageing on the mechanical and chemical properties of binder from RAP treated with bio-based rejuvenators. *Compos. Part B Eng.* **2018**, *141*, 174–181. [CrossRef]
58. Marsac, P.; Piérard, N.; Porot, L.; Van den bergh, W.; Grenfell, J.; Mouillet, V.; Pouget, S.; Besamusca, J.; Farcas, F.; Gabet, T.; et al. Potential and limits of FTIR methods for reclaimed asphalt characterisation. *Mater. Struct.* **2014**, *47*, 1273–1286. [CrossRef]

59. Elkashef, M.; Podolsky, J.; Williams, R.C.; Cochran, E.W. Introducing a soybean oil-derived material as a potential rejuvenator of asphalt through rheology, mix characterisation and Fourier Transform Infrared analysis. *Road Mater. Pavement Des.* **2017**, *19*, 1750–1770. [CrossRef]
60. Zhu, H.; Xu, G.; Gong, M.; Yang, J. Recycling long-term-aged asphalts using bio-binder/plasticizer-based rejuvenator. *Constr. Build. Mater.* **2017**, *147*, 117–129. [CrossRef]
61. Elkashef, M.; Williams, R.C.; Cochran, E.W. Physical and chemical characterization of rejuvenated reclaimed asphalt pavement (RAP) binders using rheology testing and pyrolysis gas chromatography-mass spectrometry. *Mater. Struct.* **2018**, *51*, 12. [CrossRef]
62. Mokhtari, A.; Lee, H.D.; Williams, R.C.; Guymon, C.A.; Scholte, J.P.; Schram, S. A novel approach to evaluate fracture surfaces of aged and rejuvenator-restored asphalt using cryo-SEM and image analysis techniques. *Constr. Build. Mater.* **2017**, *133*, 301–313. [CrossRef]
63. Nahar, S.; Qiu, J.; Schmets, A.; Schlangen, E.; Shirazi, M.; van de Ven, M.; Schitter, G.; Scarpas, A. Turning Back Time: Rheological and Microstructural Assessment of Rejuvenated Bitumen. In Proceedings of the 93th Annual Meeting of the Transportation Research Board, Washington, DC, USA, 12–16 January 2014.
64. Kuang, D.; Yu, J.; Chen, H.; Feng, Z.; Li, R.; Yang, H. Effect of Rejuvenators on Performance and Microstructure of Aged Asphalt. *J. Wuhan Univ. Technol.* **2014**, *29*, 341–345. [CrossRef]
65. Sharma, B.K.; Doll, K.M.; Erhan, S.Z. Ester hydroxyl derivatives of methyl oleate. Tribological, oxidation and low temperature properties. *Bioresour. Technol.* **2008**, *99*, 7333–7340. [CrossRef]
66. King, J.W.; Holliday, R.L.; List, G.R.; Snyder, J.M. Hydrogenation of vegetable oils using mixture of supercritical carbon dioxide and hydrogen. *J. Am. Oil Chem. Soc.* **2001**, *78*, 107–113. [CrossRef]
67. Campanella, A.; Baltanas, M.A.; Capel-Sanchez, M.C.; Campos-Martin, J.M.; Fierro, J.L.G. Soybean oil epoxidation with hydrogen peroxide using an amorphous Ti/SiO2 catalyst. *Green Chem.* **2004**, *6*, 330–334. [CrossRef]
68. Xiang, S.; Chen, L.; Yang, X.; Zhang, P.; Zhu, L. Physiochemical and Tribological Properties of Triester Derivatives from Chemically Modified Waste Cooking Oil. *Biotechnology* **2015**, *141*, 1–8.
69. Maiuolo, L.; De Nino, A.; Merino, P.; Russo, B.; Stabile, G.; Nardi, M.; D'Agostino, N.; Bernardi, T. Rapid, efficient and solvent free microwave mediated synthesis of aldo- and ketonitrones. *Arab. J. Chem.* **2016**, *9*, 25–31. [CrossRef]
70. Bortolini, O.; Mulani, I.; De Nino, A.; Maiuolo, L.; Melicchio, A.; Russo, B.; Granchi, D. Synthesis of a novel class of gem-phosphonate-phosphates by reductive cleavage of the isoxazolidine ring. *Curr. Org. Synth.* **2014**, *11*, 461–465. [CrossRef]
71. Nardi, M.; Costanzo, P.; De Nino, A.; Di Gioia, M.L.; Olivito, F.; Sindona, G.; Procopio, A. Water excellent solvent for the synthesis of bifunctionalized cyclopentenones from furfural. *Green Chem.* **2017**, *19*, 5403–5411. [CrossRef]
72. Di Gioia, M.L.; Nardi, M.; Costanzo, P.; De Nino, A.; Maiuolo, L.; Oliverio, M.; Procopio, A. Biorenewable deep eutectic solvent for selective and scalable conversion of furfural into cyclopentenone derivatives. *Molecules* **2018**, *23*, 1891. [CrossRef] [PubMed]
73. Procopio, A.; Costanzo, P.; Dalpozzo, R.; Maiuolo, L.; Nardi, M.; Oliverio, M. Efficient ring opening of epoxides with trimethylsilyl azide and cyanide catalyzed by erbium(III) triflate. *Tetrahedron Lett.* **2010**, *51*, 5150–5153. [CrossRef]
74. Bortolini, O.; De Nino, A.; Garofalo, A.; Maiuolo, L.; Russo, B. Mild oxidative conversion of nitroalkanes into carbonyl compounds in ionic liquids. *Synth. Commun.* **2010**, *40*, 2483–2487. [CrossRef]
75. Nardi, M.; Di Gioia, M.L.; Costanzo, P.; De Nino, A.; Maiuolo, L.; Oliverio, M.; Olivito, F.; Procopio, A. Selective Acetylation of Small Biomolecules and Their Derivatives Catalyzed by Er(OTf)3. *Catalysts* **2017**, *7*, 269. [CrossRef]
76. Avisha, C.; Debarati, M.; Dipa, B. Biolubricant synthesis from waste cooking oil via enzymatic hydrolysis followed by chemical esterification. *J. Chem. Technol. Biotechnol.* **2013**, *88*, 139–144.
77. Okino-Delgad, C.H.; Zanoni do Prado, D.; Facanali, R.; Marques, M.M.O.; Nascimento, A.S.; da Costa Fernandes, C.J.; Zambuzzi, W.F.; Fleuri, L.F. Bioremediation of cooking oil waste using lipases from wastes. *PLoS ONE* **2017**, *12*, 1–17. [CrossRef] [PubMed]
78. Atkins, P.W.; de Paula, J.; Keeler, J. *Physical Chemistry*, 14th ed.; Oxford Press: Oxford, UK, 2011.
79. De Giorgio, V.; Corti, M. *Physics of Amphiphiles: Micelles*; Vesicles and Microemulsions: North-Holland, The Netherlands, 1985.

80. Lombardo, D.; Kiselev, M.A.; Magazù, S.; Calandra, P. Amphiphiles Self-Assembly: Basic Concepts and Future Perspectives of Supramolecular Approaches. *Adv. Condens. Matter Phys.* **2015**, *11*, 1–22. [CrossRef]
81. Calandra, P.; Longo, A.; Ruggirello, A.; Turco Liveri, V. Physico-Chemical Investigation of the State of Cyanamide Confined in AOT and Lecithin Reversed Micelles. *J. Phys. Chem. B* **2004**, *108*, 8260–8268. [CrossRef]
82. Calandra, P.; Giordano, C.; Ruggirello, A.; Turco Liveri, V. Physicochemical investigation of acrylamide solubilization in sodium bis(2-ethylhexyl)sulfosuccinate and lecithin reversed micelles. *J. Colloid Interface Sci.* **2004**, *277*, 206–214. [CrossRef]
83. Longo, A.; Calandra, P.; Casaletto, M.P.; Giordano, C.; Venezia, A.; Turco Liveri, V. Synthesis and physico-chemical characterization of gold nanoparticles softly coated by AOT. *Mater. Chem. Phys.* **2006**, *96*, 66–72. [CrossRef]
84. Calandra, P.; Giordano, C.; Longo, A.; Turco Liveri, V. Physicochemical investigation of surfactant-coated gold nanoparticles synthesized in the confined space of dry reversed micelles. *Mater. Chem. Phys.* **2006**, *98*, 494–499. [CrossRef]
85. Calandra, P.; Di Marco, G.; Ruggirello, A.; Turco Liveri, V. Physico-chemical investigation of nanostructures in liquid phases: Nickel chloride ionic clusters confined in sodium bis(2-ethylhexyl) sulfosuccinate reverse micelles. *J. Colloid Interface Sci.* **2009**, *336*, 176–182. [CrossRef]
86. Kakar, M.R.; Hamzah, M.O.; Akhtar, M.N. Surface free energy and moisture susceptibility evaluation of asphalt binders modified with surfactant-based chemical additive. *J. Clean. Prod.* **2016**, *112*, 2342–2353. [CrossRef]
87. Ortega, F.J.; Navarro, F.J.; García-Morales, M. Dodecylbenzenesulfonic Acid as a Bitumen Modifier: A Novel Approach to Enhance Rheological Properties of Bitumen. *Energy Fuels* **2017**, *31*, 5003–5010. [CrossRef]
88. Glatter, O.; Kratky, O. *Small-Angle X-ray Scattering*; Academic Press: London, UK, 1982.
89. Shirzad, S.; Hassan, M.M.; Aguirre, M.A.; Mohammad, L.N. Evaluation of Sunflower Oil as a Rejuvenator and Its Microencapsulation as a Healing Agent. *J. Mater. Civ. Eng.* **2016**, *28*. [CrossRef]
90. Fitter, J.; Gutberlet, T.; Katsaras, J. *Neutron Scattering in Biology Techniques and Applications*; Springer: Berlin, Germany, 2006; p. 560.
91. Zemb, T.; Lindner, P. *Neutron, X-rays and Light Scattering Methods Applied to Soft Condensed Matter*, 1st ed.; North-Holland (publisher): Amsterdam, The Netherlands, 2002; p. 552.
92. Feigin, L.A.; Svergun, D.I. *Structure Analysis by Small-Angle X-Ray and Neutron Scattering*, 1st ed.; Plenum Press: New York, NY, USA; London, UK, 1987; p. 335.
93. Magazù, S.; Migliardo, F.; Benedetto, A. Elastic incoherent neutron scattering operating by varying instrumental energy resolution: Principle, simulations, and experiments of the resolution elastic neutron scattering (RENS). *Rev. Sci. Instrum.* **2011**, *82*, 105115. [CrossRef] [PubMed]
94. Berne, B.J.; Pecora, R. *Dynamic Light Scattering*, 1st ed.; Wiley-Interscience: New York, NY, USA, 1976; p. 376.
95. Brown, W. *Light Scattering: Principles and Development*, 1st ed.; Clarendon: Oxford, UK, 1996; p. 544.
96. Nagana Gowda, G.A.; Chen, H.; Khetrapal, C.L.; Weiss, R.G. Amphotropic ionic liquid crystals with low order parameters. *Chem. Mater.* **2004**, *16*, 2101–2106. [CrossRef]
97. Calandra, P.; Ruggirello, A.; Mele, A.; Turco Liveri, V. Self-assembly in surfactant-based liquid mixtures: Bis(2-ethylhexyl)phosphoric acid/bis(2-ethylhexyl)amine systems. *J. Colloid Interface Sci.* **2010**, *348*, 183–188. [CrossRef] [PubMed]
98. Kumar, A.; Kuneida, H.; Vazquez, C.; Lopez-Quintela, M.A. Studies of domain size of hexagonal liquid crystals in C 12 EO 8 /water/alcohol systems. *Langmuir* **2001**, *17*, 7245–7250. [CrossRef]
99. Calandra, P.; Turco Liveri, V.; Ruggirello, A.; Licciardi, M.; Lombardo, D.; Mandanici, A. Anti-Arrhenian behaviour of conductivity in octanoic acid–bis(2-ethylhexyl)amine systems: A physico-chemical study. *J. Mater. Chem. C* **2015**, *3*, 3198–3210. [CrossRef]
100. Calandra, P.; Turco Liveri, V.; Riello, P.; Freris, I.; Mandanici, A. Self-assembly in surfactant-based liquid mixtures: Octanoic acid/Bis(2-ethylhexyl)amine systems. *J. Colloid Interface Sci.* **2012**, *367*, 280–285. [CrossRef]
101. Turco Liveri, V.; Lombardo, D.; Pochylski, M.; Calandra, P. Molecular association of small amphiphiles: Origin of ionic liquid properties in dibutyl phosphate/propylamine binary mixtures. *J. Mol. Liq.* **2018**, *263*, 274–281. [CrossRef]
102. Dickie, J.P.; Yen, T.F. Macrostructures of the Asphaltic Fractions by Various Instrumental Methods. *Anal. Chem.* **1967**, *39*, 1847–1852. [CrossRef]

103. Calandra, P.; Mandanici, A.; Turco Liveri, V. Self-assembly in surfactant-based mixtures driven by acid–base reactions: Bis(2-ethylhexyl) phosphoric acid–n-octylamine systems. *RSC Adv.* **2013**, *3*, 5148–5155. [CrossRef]
104. Calandra, P.; de Caro, T.; Caschera, D.; Lombardo, D.; Todaro, L.; Turco Liveri, V. Spectroscopic and structural characterization of pure and $FeCl_3$-containing tri-n-butyl phosphate. *Colloid Polym. Sci.* **2014**, *293*, 597–603. [CrossRef]
105. Cui, S.; de Almeida, V.F.; Hay, B.P.; Ye, X.; Khomami, B. Molecular dynamics simulation of Tri-n-butyl-phosphate liquid: A force field comparative study. *J. Phys. Chem. B* **2012**, *116*, 305–313. [CrossRef] [PubMed]
106. Charlesby, A.; Finch, G.I.; Wilman, H. The diffraction of electrons by anthracene. *Proc. Phys. Soc.* **1939**, *51*, 479–528. [CrossRef]
107. Bale, H.D.; Schmidt, P.W. Small-Angle X-Ray-Scattering Investigation of Submicroscopic Porosity with Fractal Properties. *Phys. Rev. Lett.* **1984**, *53*, 596–599. [CrossRef]
108. Carr, H.Y.; Purcell, E.M. Effects of Diffusion on Free Precession in Nuclear Magnetic Resonance Experiments. *Phys. Rev.* **1954**, *94*, 630. [CrossRef]
109. Oliviero Rossi, C.; Spadafora, A.; Teltayev, B.; Izmailova, G.; Amerbayev, Y.; Bortolotti, V. Polymer modified bitumen: Rheological properties and structural characterization. *Coll. Surf. A* **2015**, *480*, 390–397. [CrossRef]
110. Christensen, D.W.; Anderson, D.A. Rheological evidence concerning the molecular architecture of asphalt cements. *Proc. Chem. Bitum.* **1991**, *2*, 568–595.
111. Oliviero Rossi, C.; Caputo, P.; Loise, V.; Ashimova, S.; Teltayev, T.; Sangiorgi, C. A New Green Rejuvenator: Evaluation of Structural Changes of Aged and Recycled Bitumens by Means of Rheology and NMR. In *RILEM 252-CMB Symposium*; RILEM 252-CMB 2018; Poulikakos, L., Cannone Falchetto, A., Wistuba, M., Hofko, B., Porot, L., Di Benedetto, H., Eds.; Springer: Cham, Switzerland, 2018; Volume 20.


© 2019 by the authors. Licensee MDPI, Basel, Switzerland. This article is an open access article distributed under the terms and conditions of the Creative Commons Attribution (CC BY) license (http://creativecommons.org/licenses/by/4.0/).

https://doi.org/10.18321/ectj864

# Analysis of Mechanical Performance of Bitumen Modified with Waste Plastic and Rubber Additives by Rheology and Self Diffusion NMR Experiments

**P. Caputo, M. Porto[1]*, V. Loise[1], B. Teltayev[2], C. Oliviero Rossi[1]***

[1]University of Calabria, Via P. Bucci, 87036 Arcavacata di Rende (CS), Italy
[2]Kazakhstan Highway Research Institute, 2A Nurpeisova Str., 050061, Almaty, Kazakhstan

**Article info**

*Received:*
18 April 2019

*Received in revised form:*
9 June 2019

*Accepted:*
2 August 2019

**Keywords:**
Waste plastic
Bitumen
Stability
Plastic waste
Rheology

**Abstract**

In this study, the mechanical and physico-chemical properties of a new kind of modified bitumen are presented. The bituminous binders have been modified in order to understand the effect on the structural properties of several compounds such as a Polymer elastomer as Styrene Butadiene Rubber (SBR), Polymer thermoplastic polypropylene (PP) and a waste plastic (Waste PP). Laboratory tests have been focused on the characterization of bitumen modified with single product and their binary combinations compared with pristine binder as a reference. Characterization has been conducted by using conventional as well as advanced methods on bitumens. Fundamental rheological tests, based on dynamic shear rheometer in the temperature range from -30 °C to +160 °C have been performed and the structure of a bitumens and modified bitumens has been analysed by the mobility of the oily maltene by self-diffusion Pulsed field gradient spin-echo (PGSE) FT-NMR experiments.

## 1. Introduction

Bituminous binders are organic materials whose binding and hardening properties are caused by the temperature-related change of adhesion and cohesion of their molecules [1, 2]. Bitumen is commonly modelled as a colloid, with maltenes as the continuous phase and micelles of asphaltenes stabilized by associated resins as the dispersed phase [3, 4]. Following the analogy with reversed micelles in water-oil microemulsions where the stabilization of the polar domains is of pivotal importance for determining both the structure and the properties of the overall aggregates [5, 6, 7], in the same way in bitumens the composition and the colloidal structure [8] influence its physical and rheological properties [9, 10, 11]. These binders are commonly used in the pavement constructions to meet the raising requirements of the surface durability of the roads. A wide range in viscoelasticity values is essential to achieve long-lasting road surface, as it ensures consistency of rheological state of bitumen in extreme service temperatures [12]. The rheological weakness of the conventional bitumen has generated an increasing interest in the use of polymer modified binders to enhance the conventional bitumen properties [13]. A limited number of polymers has been used as modifying agents due to their high cost. In fact, due to the high cost of these polymers the amount needed to improve pavement performance should be as small as possible. The main modifiers applied to improve the viscoelasticity of bitumen are long chained hydrocarbon polymers. Moreover, elastomers increase the elasticity of the bitumen at high temperature and reduce the stiffness at low temperature. Linear and radial styrene–butadiene–styrene (SBS) copolymers are the most used ones. In the bitumen, SBS forms a highly elastic network that disappears above 100 °C and reforms when cooled.

Nowadays the use of polymers reclaimed from waste plastic (bottles, glasses, etc…) is one of the hot topics in the field of bitumen modification.

*Corresponding authors.
E-mail: michele.porto@unical.it
cesare.oliviero@unical.it

© 2019 Eurasian Chemico-Technological Journal.
This is an open access article under the CC BY license (http://creativecommons.org/licenses/by/4.0/).

In this regard waste plastic represents the biggest polymer sources. As reported in [14] 8300 million of Metric Tons (MT) of virgin plastic have been produced to date. Approximatively 6300 MT had been generated in 2015, around 9% of which had been recycled, 12% was incinerated and 79% was accumulated in landfills or in the natural environment. The use of recycled plastic is the only way to avoid environmental pollution which is, together with climate changes, the biggest problem that human being has to overcome.

In this work a Polypropylene, abbreviated as PP, polymer obtained from waste plastic was used as a bitumen modifier in comparison with a typically used polymer styrene-butadiene-rubber (SBR).

PP is a recyclable thermoplastic polymer widely used in many different products. PP is rugged and resistant to different chemical solvents, acids, and bases. PP's resin identification code is 5, and it is recyclable.

## *2. Materials*

The bitumen used in this study has been produced in Kazakhstan and it was supplied by Kazakhstan Highway Research Institute (Almaty, Kazakhstan). It has a 50/70 penetration grade. The bitumen was modified with Polymer elastomer (SBR), Polymer thermoplastic (PP) and a Waste polypropylene plastic (WPP).

SBR: Styrene/Butadiene-rubber was furnished by CMS SPA (Mangone, Italy);

PP: Polypropylene was furnished by Sigma Aldrich (Mangone, Italy);

WPP: waste Polypropylene was furnished by Calabria Maceri (Rende Italy), label WPP;

Waste PP was pulverized by milling in order to homogenize the sample.

### *2.1. Sample preparation*

The first step was to prepare the polymer modified bitumen, by using a high shear mixing homogenizer (IKEA model). Firstly, bitumen was heated up to 180±5 °C until it fully flowed and then three blends with SBR (0.5% of the weight of the base bitumen, wt.%), WPP and PP (1% of the weight of the base bitumen) were prepared gradually added the polymers to the melted bitumen under a speed shear mixer of 600 to 800 rpm. The mixtures were stirred by a mechanical stirrer at 180 °C for 1 h while the rotation speed was 600 rpm so that the blends became essentially homogenous.

**Table 1**
Sample Labels

| Sample | Sample ID |
|---|---|
| Pristine Bitumen | PB |
| Bit. + 0.5% SBR | SBR |
| Bit. + 1% Waste PP | WPP |
| Bit. + 1% PP | PP |
| Bit. + 1% WPP + 0.5% SBR | WPP/SBR |
| Bit. + 1% PP + 0.5% SBR | PP/SBR |

The PP/SBR WPP/SBR modified bitumens were prepared adding 0.5 wt.% of SBR and 1wt.% of Polypropylene by using the same procedure for the bitumen modified by single polymer. After mixing, the resulting blends were poured into a small sealed can and then stored in a dark chamber at a constant temperature of 25 °C to retain the obtained morphology.

All the prepared mixtures are listed and labelled in Table 1. The following labels will be adopted for the samples throughout the text.

### *2.2. Rheological measurement*

Rheological measurement has been conducted using a shear stress-controlled rheometer SR5000 (Rheometrics, USA) equipped with a plate geometry (gap 2 mm, diameter 25 mm). The temperature has been controlled by Peltier system (±0.1 °C).

All the experiments have been performed during heating. The rheological behaviour at different temperatures has been investigated by a time cure test at 1 Hz with a heating ramp rate of 1 °C/min. The small amplitude dynamic tests provided information on the linear viscoelastic behaviour of materials through the determination of the complex shear modulus [15].

$$G^*(\omega) = G'(\omega) + iG''(\omega)$$

or in terms of complex viscosity,

$$\eta^* = \frac{G^*(\omega)}{\omega}$$

where $G'(\omega)$ is the in phase (or storage) component, $G''(\omega)$ is the out-of-phase (or loss) component, and i is the imaginary unit of the complex number. $G'(\omega)$ is a measure of the reversible, elastic energy, while $G''(\omega)$ represents the irreversible viscous dissipation of the mechanical energy.

The dependence of these quantities on the oscillating frequency gives rise to the so-called mechanical spectrum, allowing the quantitative rheological characterization of studied materials. The applied stress amplitude for the viscoelastic measurements has been reduced until the linear response regime has been reached. This analysis has been made by performing stress sweep tests in all investigated temperature range.

### *2.3. Nuclear Magnetic Resonance (NMR) characterization*

NMR spectroscopy is one of efficient and reliable technique for the characterization of complex materials such as bitumen. $^{1}H$ and $^{13}C$ NMR spectra are commonly used in solution for the characterization of synthetic/natural products, while the use of anisotropic media allows to investigate the structural and conformational behaviour of flexible molecules [16, 17, 18].

Dynamic NMR measurements like determination of self-diffusion coefficients provide information about molecular dynamics and spatial dimensions of aggregates and cavities. In this work, measurements of the self-diffusion coefficients were carried out on the samples analysed to investigate their mobility and microstructure.

NMR measurements were carried out using a Bruker 300 spectrometer under certain operating conditions, in particular in a temperature. The NMR spectra were derived from Free Induction Decay (FID) through the Fourier transform. In the pulsed NMR experiment the pulse width was equal to π/2 while the number of scans used was equal to 8. Experimental measurements of the self-diffusion coefficient (D) directly were made using a Diff30 NMR probe. The sequence that was used is the PFG-STE (Pulsed Field Gradient Stimulated-Echo) because the transverse relaxation time ($T_2$) is much shorter than the longitudinal relaxation time ($T_1$) [19, 20]. This sequence consists of three pulses 90 rf ($\pi/2$-$\tau_1$-$\pi/2$-$\tau_m$-$\pi/2$) and two gradient pulses which are applied after the first and third pulse rf. The echo was identified at time $\tau = 2\tau_1 + \tau_m$, while the amplitude attenuation of the ECO was decrypted from the following equation:

$$I(2\tau_1 + \tau_m) = I_0 e^{-\left[\frac{\tau_m}{T_1} + \frac{2\tau_1}{T_2} + (\gamma g \delta)^2 D\left(\Delta - \frac{\delta}{3}\right)\right]}$$

where D is the self-diffusion coefficient. The experimental NMR parameters that were used to study the samples are: the gradient length pulse, δ, diffusion delay time, Δ, while the gradient amplitude, g. The number of scans is 8, this increases as the number of repetitions increases. The standard deviation of the fitting is very low and on the repeatability of measurements, the uncertainties in D fall within ~3%.

## 3. Results and discussion

In the present work, 50/70 penetration grade bitumen was modified by Polymer thermoplastic (PP), Plastic waste (waste PP) and SBR. Firstly, the penetration depth (PN) and the softening point (R&B) were determined with standardized tests (Table 2).

A good correlation exists between bitumen hardness and polymer content for each of the investigated bitumen. As can be seen from Table 2 all the additives induce a shifting in the viscoelastic-sol transition temperature (TR) of about 20 °C higher than the neat bitumen. In particular, the best polymer modification was observed in presence of SBR. Temperature-sweep experiments have also been exploited to have some information on the structural changes induced by temperature, trying to better define a TR range. In fact, in this experiment, the evolution of the storage modulus is continuously monitored during a temperature ramp, at a constant heating rate (1 °C/min) and at a frequency of 1 Hz.

In Fig. 1 the Dynamic Temperature Ramp Test of all investigated blends are shown in the temperature range 25–100 °C. At high temperatures the elastic modulus *G′(ω)* have a non-linear behaviour approaching to the viscoelastic to liquid transition (60 and 80 °C for neat and modified bitumens respectively). The starting point of the non-linear region of *G′(ω)* can be considered as the beginning of the TR region. The whole transition process from viscoelastic to liquid regime ends when *G′(ω)* modulus is no longer detectable and consequently the loss tangent tan δ diverges at about 80 °C for the polymer modified bitumens. Tan δ increases with increasing temperature, evidencing a reduction in material consistency. In fact, the prevalent liquid-like behaviour is enhanced by the temperature increase. In Fig. 2 the tan δ of the investigated blends are shown at low temperatures. Phase angle values at low temperature are quite scattered, due to instrumental problems related to the high material consistency.

**Table 2**
Penetration depth (PN) Softening point and Transition temperature of prepared blends

| Sample ID | PN (1/10 mm) | R&B (°C) | Transition temperature (°C) |
|---|---|---|---|
| PB | 64 | 47.2 | 65.9 |
| SBR | 48 | 63.6 | 88.7 |
| WPP | 53 | 56.4 | 81.5 |
| PP | 51 | 59.4 | 84.5 |
| WPP/SBR | 55 | 58.6 | 83.5 |
| PP/SBR | 54 | 57.2 | 82.2 |

In principle, to prevent the cracking phenomena, a system is required to keep a viscous character. Herein, it is worth to note that between 0 °C and 30 °C, the tan δ trends of WPP, WPP/SBR, PP/SBR and SBR overlap. The pure bitumen (B) shows higher tan δ values, while PP has a more rigid behaviour (lowest tan δ). These results are interesting in terms of mechanical properties because:

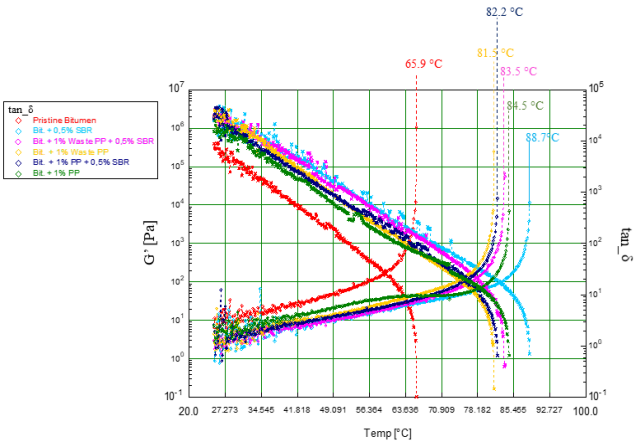


Fig. 1. Dynamic temperature ramp test (TimeCure) at high temperature (25 to 130 °C).

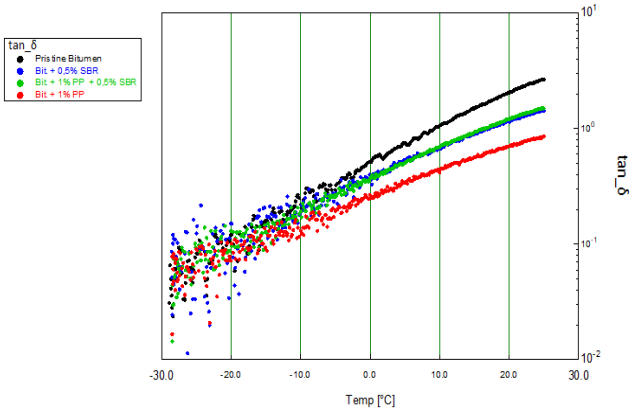


Fig. 2. Dynamic temperature ramp test (TimeCure) at low temperature (-30 °C to 25 °C).

a) it is evident that even only WPP polymer improves the rheological properties at low temperatures limiting the "solid effect".

b) the PP modified bitumen show higher rigidity of the system exposing the binder to possible cracking phenomena.

Fourier transform NMR self-diffusion provides insight into the bitumen microstructure by determining the long-range mobility of the mixture components. Detection of motion over long distances, compared with typical micelles (some nm), provides a sensitive probe for the aggregate state [20, 21]. Unfortunately, because of the short transverse relaxation times of asphaltenes protons, asphaltenes molecules self-diffusion values cannot be detected and consequently the measured self-diffusion coefficients can be related to the maltenes phase. Here self-diffusion coefficients of oil protons at 100 and 120 °C are reported in Figs. 3 and 4 respectively.

The self-diffusion is due to the mobility of the observed molecules and is hindered by the obstruction they meet during their motion. The data can be considered as a fingerprint of the structure where the motion occurs. The observed data are really interesting. The highest self-diffusion values are found for the PP and PB bitumens. The WPP, SBR WPP/SBR PP/SBR affect the mobility of the maltene reducing the diffusion. The data confirm what observed by rheology where PP modified bitumen shows a mechanical behaviour different from the bitumens doped by the other polymers. WPP, SBR WPP/SBR PP/SBR seem to absorb the light part of the maltenes trapping them in their network. As a consequence, maltenes phase is enriched by the heavy oil part. The mobility is therefore reduced. The PP does not interact with oily part of the maltenes and consequently the self-diffusion is comparable to the pure bitumen. This analysis takes into account that the percentage of asphaltenes is the same and therefore the obstruction factor can be neglected for all samples.

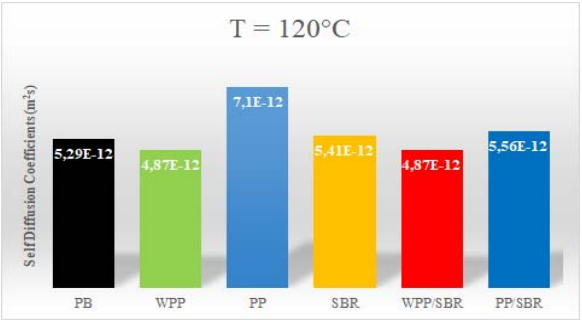


Fig. 3. NMR characterization at 120 °C.

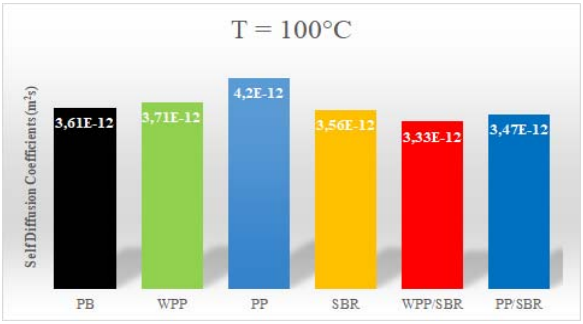


Fig. 4. NMR characterization at 100 °C.

## 4. Conclusions

A bitumen system modified with waste plastic (WPP) was investigated and compared to other polymer modifiers. It has been shown that the addition of WPP enhances bitumen mechanical performance at high and low temperatures. This investigation also showed that the WPP can be considered a useful polymer in the road construction. In fact, even though the pure reference has lightly higher temperature transition, WPP shows similar values. Additionally, the effects at low temperature are practically equal confirming the goodness of its use as polymer for the bitumen modification.

## References

[1]. C. Oliviero Rossi, P. Caputo, N. Baldino, F.R. Lupi, D. Miriello, R. Angelico, *Int. J. Adhes. Adhes.* 70 (2016) 297–303. DOI: 10.1016/j.ijadhadh.2016.07.013

[2]. C. Oliviero Rossi, P. Caputo, N. Baldino, E.I. Szerb, B. Teltayev, *Int. J. Adhes. Adhes.* 72 (2017) 117–122. DOI: 10.1016/j.ijadhadh.2016.10.015

[3]. D. Lesueur, *Adv. Colloid Interfac.* 145 (2009) 42–82. DOI: 10.1016/j.cis.2008.08.011

[4]. C. Oliviero Rossi, P. Caputo, G. De Luca, L. Maiuolo, S. Eskandarsefat, C. Sangiorgi, *Appl. Sci.* 8 (2018) 229. DOI: 10.3390/app8020229

[5]. P. Calandra, G. Di Marco, A. Ruggirello, V. Turco Liveri, *J. Colloid Interf. Sci.* 336 (2009) 176–182. DOI: 10.1016/j.jcis.2009.03.066

[6]. P. Calandra, C. Giordano, A. Ruggirello, V. Turco Liveri, *J. Colloid Interf. Sci.* 277 (2004) 206–214. DOI: 10.1016/j.jcis.2004.04.021

[7]. A. Longo, P. Calandra, M.P. Casaletto, C. Giordano, A.M. Venezia, V. Turco Liveri, *Mater. Chem. Phys.* 96 (2006) 66–72. DOI: 10.1016/j.matchemphys.2005.06.043

[8]. P. Calandra, P. Caputo, M.P. De Santo, L. Todaro, V. Turco Liveri, C. Oliviero, *Constr. Build. Mater.* 199 (2019) 288–297. DOI: 10.1016/j.conbuildmat.2018.11.277

[9]. N. Baldino, D. Gabriele, C. Oliviero Rossi, L. Seta, F. R. Lupi, P. Caputo, T. Falvo, *Constr. Build. Mater.* 40 (2013) 397–404. DOI: 10.1016/j.conbuildmat.2012.11.001

[10]. N. Baldino, D. Gabriele, C. Oliviero Rossi, L. Seta, F. R. Lupi, P. Caputo, *Constr. Build. Mater.* 36 (2012) 592–596. DOI: 10.1016/j.conbuildmat.2012.06.011

[11]. C. Oliviero Rossi, P. Caputo, S. Ashimova, A. Fabozzi, G. D'Errico, R. Angelico, *Appl. Sci.* 8 (2018) 1405. DOI: 10.3390/app8081405

[12]. C. Oliviero Rossi, P. Caputo, V. Loise, D. Miriello, B. Teltayev, R. Angelico, *Colloid. Surface. A* 532 (2017) 618–624. DOI: 10.1016/j.colsurfa.2017.01.025

[13]. M. Porto, P. Caputo, V. Loise, S. Eskandarsefat, B. Teltayev, C. Oliviero Rossi, *Appl. Sci.* 9 (2019) 742. DOI: 10.3390/app9040742

[14]. R. Geyer, J.R. Jambeck, K.L. Law, *Science Advanced* 3 (2017) e1700782. DOI: 10.1126/sciadv.1700782

[15]. J.C Jansen, M MacChione, C. Oliviero Rossi, R. Mendichi, G. A. Ranieri, E. Drioli, *Polymer* 46 (2005) 11366–11379. DOI: 10.1016/j.polymer.2005.10.041

[16]. C. Aroulanda, G. Celebre, G. De Luca, M. Longeri, *J. Phys. Chem. B* 110 (2006) 10485–10496. DOI: 10.1021/jp061345s

[17]. G. Celebre, M. Concistrè, G. De Luca, M. Longeri, G. Pileio, *ChemPhysChem* 7 (2006) 1930–1943. DOI: 10.1002/cphc.200600220

[18]. M.E. Di Pietro, C. Aroulanda, D. Merlet, G. Celebre, G. De Luca, *J Phys. Chem. B* 118 (2014) 9007–9016. DOI: 10.1021/jp505084g

[19]. J.E. Tanner, *J. Phys. Chem.* 52 (1970) 2523–2526. DOI: 10.1063/1.1673336

[20]. L. Coppola, C. Oliviero Rossi, U. Olsson, G.A. Ranieri, *Langmuir* 16 (2000) 4180–4184. DOI: 10.1021/la991458lL.

[21]. Coppola, C. Oliviero, L. Pogliani, G.A. Ranieri, M. Terenzi, *Colloid Polymer Sci.* 278 (2000) 434–442. DOI: 10.1007/s003960050536

applied sciences

MDPI

Article

# Polysaccharides-Reinforced Bitumens: Specificities and Universality of Rheological Behavior

**Michele Porto [1], Paolino Caputo [1], Valeria Loise [1], Giovanni De Filpo [1], Cesare Oliviero Rossi [1,*] and Pietro Calandra [2,*]**

[1] Department of Chemistry and Chemical Technologies, University of Calabria, 87036 Arcavacata di Rende (CS), Italy; michele.porto@unical.it (M.P.); paolino.caputo@unical.it (P.C.); valeria.loise@unical.it (V.L.); giovanni.defilpo@unical.it (G.D.F.)

[2] CNR-ISMN, National Council of Research, Institute for the Study of Nanostructured Materials, Via Salaria km, 29300 Monterotondo Stazione (RM), Italy

* Correspondence: cesare.oliviero@unical.it (C.O.R); pietro.calandra@cnr.it (P.C.); Tel.: +39-0984-492-045 (C.O.R.); +39-06-90-672-409 (P.C.)

Received: 25 November 2019; Accepted: 13 December 2019; Published: 17 December 2019

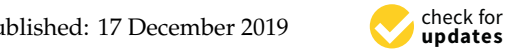


**Abstract:** The rheological properties of bitumens can be modified by the addition of specific chemical additives. Taking into account the molecular complex aggregation pattern, we hypothesized that macromolecules characterized by long, flexible, and hydrophilic chains can establish soft bridges connecting the different polar aggregates of asphaltenes, strengthening their overall hierarchical supra-structures, and consequently increasing rheological performance at higher temperatures. Here, we propose the use of low cost and high availability polysaccharides as chemical additives to improve the rheological characteristics of a bitumen and to strengthen its thermal resistance. Fourteen different low-cost and high-availability polysaccharides, (flours, gums, and extracts from vegetable products) have been tested. While alghae *euchemae* have proved to be the most effective additive, corn and 00 flours are the least effective. Attempts to explain their differences have been made considering their chemical interactions with the polar molecules of asphaltenes within the complex framework of their supramolecular hierarchical structures. Through Arrhenius analysis, a correlation between activation energy and preexponential factor has been found, which can be useful for practical purposes, together with an unexpected consistency with the behavior of simple liquids, despite the striking differences in structure. Furthermore, a qualitative model has been suggested. The added value of this work is the focus on polysaccharides constituting low-cost, high availability materials which are sometimes even found as waste in industrial processes, all factors which, together with the environmental issues connected with their use, can be considered for large-scale applications.

**Keywords:** bitumen; asphaltene; network; polysaccharides; Arrhenius; viscosity

## 1. Introduction

Asphalts are used throughout the world for road pavement. They are biphasic materials with the major phase made by macro-meter sized inorganic particles (93–96% *w/w*) held together by the minor phase, an organic high viscosity viscoelastic material called bitumen, which acts as the binding agent among the inorganic particles, thus conferring to the final material the required plasticity, rigidity, and stability. Despite its minor presence in the overall material, bitumen plays a pivotal role in determining rheological characteristics, which must fulfill the desired need for ductility, resistance to stress, and thermal stability.

The properties of a bitumen are the overall consequence of its structure: it is characterized by the presence of assemblies of small (few nm) stacks of polar molecules (asphaltenes) stabilized by

amphiphilic resins and dispersed in the apolar matrix phase of paraffins and aromatic oils (maltene) [1,2]. Recently, it has been unveiled by X-Ray scattering [3] that the structure is even more complex, with the asphaltene clusters organized in hierarchical structures of different length scales (up to hundreds of nanometers and even to micro-scales with the so called "bee-structures" [4]).

In this framework, an additive can therefore exert its action through various mechanisms: for example, an additive tuning the red-ox state of the polar molecules can hinder oxidation-induced degradation, an adhesion promotion (acting on the inorganic/organic interfacial tension) can better disperse the inorganic particles among the bitumen matrix, and an amphiphilic additive like lecithin can help in avoiding ageing [5] stabilizing the asphaltene clusters due to their well-known capability of keeping dispersed nanoparticles of polar substances, both organic [6,7] and inorganic [8,9]. In this ambit, it has been recently observed that some additives can form a polymeric network (e.g., poly phosphoric acid) increasing the rigidity [10]. Furthermore, additives with rejuvenating actions (reducing viscosity and restoring the plastic behavior of a freshly prepared bitumen) have been discovered [11].

In evaluating the rheological performances of such a complex material, an empirical approach is always followed within a chosen temperature range [12,13] for convenient use [14,15]. Among the various methods for bitumen characterization [16], however, small amplitude oscillatory rheometry is considered one of the most effective. It uses specific specimen geometries and instruments and allows systematic and mathematical interpretation of the results. Moreover, rheometry, as a scientifically rigorous (non-empirical) method, has the advantage to give data that can be rationalized in terms of the real complex structure possessed by the bitumen. A review offering perspectives of bitumen characterization is the recent review by Loise et al. [11].

Then, the scientific idea behind this work takes into account for the spatial distribution of the asphaltene-based polar domains, and the microscopic mechanism of viscosity involved in such systems: to use a soft (i.e. flexible) and long molecule characterized by hydrophilic functional groups which can bridge the different polar stacks/aggregates of asphaltenes by formation of a network connecting them and reinforncing the overall structure. The idea is somehow not new: Król et al. [17] and Somé et al. [18], used vegetable oils and the corresponding methyl esters for obtaining environment-friendly bitumen fluxes by oxypolymerization-based polymerization, which crosslinks the structural units. This allowed for the viscosity increase of the stock, and contributed to its hardening and drying. The principle of using additives susceptible to oxypolimerization has been recently exploited to prepare additives able to increase the bitumen viscosity [19] and resembles the well-known effect of poly-phosphoric acid of stiffening the bitumen [20]. However, here the scientific idea is more articulated: given the complex framework of asphaltene stacks hierarchically organized in assembles with different length-scales, it can be reasonably hypothesized that the interactions at longer length scales must be of lower intensity than those at shorter length-scales. Therefore, in order to better accommodate both (i) small and strongly interacting asphaltene stacks, and (ii) bigger and less interacting asphaltene assemblies of clusters, "softer", long and flexible molecules with interacting polar groups disseminated along their chain would be needed.

The flexibility would allow for the additive to better adapt its conformational state to the long-range structure, whereas the presence of polar functional groups along the chain, together with its length, can allow for effective and disseminated interactions. The mutual interactions between the additive molecules (polysaccharides are well known in increasing the viscosity even at low concentrations) should complete the job. The additive can therefore be considered as a "softly interacting" species, not establishing a rigid network, which would bring brittleness, but, rather the high number of soft interactions would allow for a marked final effect in increasing the viscosity without causing brittleness. To test this hypothesis several polysaccharides have been used as additives in comparable conditions (same concentrations, same operating temperatures) and the data of small amplitude oscillatory rheometry have been used to gain insight on their effects. It must be noted that the choice of polysaccharides has been dictated by the will of exploring highly commercially available, low-cost, and environmentally friendly chemicals, which are aspects worthy of attention for large-scale applications.

This constitutes, besides the original scientific idea connected to the hypothesized mechanism, further added value of this work. Finally, an unexpected behavior upon temperature change, resembling that of simple liquids, will be found, and a qualitative model will be suggested.

## 2. Experimental Part

### *2.1. Materials*

The bitumen, kindly supplied by Loprete Costruzioni Stradali—Terranova Sappo Minulio—Calabria—Italy, had penetration grade, measured by the usual standardized procedure (ASTM D946) [21], (50/70). By the S.A.R.A. method [22], the concentrations (*w/w* %) of the four different portions (Saturates, Aromatics, Resins and Asphaltenes) [23] were found to be 3.8, 51.3, 21.5, and 23.4 respectively. The asphaltenes amount is typical of 50/70 grade bitumens. It is called hereafter "ref" (standing for "reference").

The additives were collected in powder form from the local supermarket given the applicative purpose of the work. They were: algae *euchemae*, carob seeds flour, orange skin, 00 flour, agar, carragenine, carboxymethylcellulose (CMC), pectin, arabic gum, cellulose, corn flour, starch, guar gum, xantam gum. The particle size in all the powders was characterized by optical microscopy and the analysis is reported in Supplementary Table S1. The small size of the particles (micrometer range) and the thermal treatment required for sample preparation (see below) allow for complete additive/bitumen homogenization.

### *2.2. Methods*

A weighted amount of additive (1 g of additive in 20 g of bitumen, giving a final content of 4.76% *w/w*), was added separately to a fully flowing hot bitumen (150 ± 10 °C) and stirred at 500–700 rpm by a mechanical stirrer (IKA RW20, Königswinter, Germany) for 30 min at the same temperature to allow homogenization of the blend. Our previous studies showed that such conditions assure the preparation of homogeneous samples: at lower rpm, sample homogenization is not effective, while above 700 rpm the bitumen can become oxidized with a consequent change in the rheological properties. This method is quite standard and also other authors use analogous procedure [24].

After mixing, the resulting bitumen was poured into a small sealed can and then stored in a dark chamber at 25 °C to retain the desired morphology. Due to the sensitivity of such kinds of material to the annealing time [5], and due to the comparative spirit of our work, we took care that all our samples had the same temperature cooling rate (5 °C $min^{-1}$) and annealing time (15 min).

A standard additive-free bitumen sample was used as a reference, hereafter labeled as "ref".

### *2.3. Rheological Tests*

The complex shear modulus $G^* = G' + i \cdot G''$ was measured in the regime of small-amplitude oscillatory shear at 1Hz as a function of temperature (temperature controlled by a Peltier element, uncertainty ±0.1 °C) by dynamic stress-controlled rheometer (SR5, Rheometric Scientific, Piscataway, NJ, USA) equipped with a parallel plate geometry (gap 2 mm, diameter 25 mm). Conditions were chosen after preliminary stress-sweep tests to guarantee linear viscoelastic conditions in all measurements. The real and imaginary parts define the in-phase (storage, measure of the reversible elastic energy) and the out-of-phase (loss, irreversible viscous dissipation of the mechanical energy) moduli, respectively. Their ratio is related to the phase angle δ according to $\tan \delta = G''/G'$.

## 3. Results and Discussion

The data obtained during a small amplitude oscillatory rheometry test include the complex modulus $G^*$, which is a measure of the total energy required to deform the specimen, and is defined as:

$$|G^*|^2 = G'^2 + G''^2 \quad (1)$$

where $G'$ is the elastic modulus (or storage modulus), a measure of the energy stored in the material during an oscillation, and $G''$ is the viscous modulus (or loss modulus), a measure of the energy dissipated as heat.

The temperature dependence of the experimental $G'$ and $G''$ measured at 1 Hz can give several information.

### 3.1. G'@50 °C and T*

First of all, the value of $G'$ at 50°C ($G'$@50 °C) can be immediately derived and is representative of the mechanical property (rigidity) of the material. The temperature of 50 °C was chosen as representative of the normal temperature under usage conditions. On the other hand, the idea of considering the rigidity at temperatures higher than room temperature is sometimes adopted in the literature so the use of $G'$ at 50 °C in the present work allows comparison with those papers [18]. The value of $G'$@50 °C is expected to change in the presence of additives as a consequence of the additive (reinforcing) effect on the bitumen microstructure.

The effect of temperature is reported in Figure 1 where the behavior of $G'$ and $G''$ as a function of temperature is shown for the neat bitumen chosen as representative. When temperature is increased, the material becomes progressively softer with $G'$ monotonously decreasing.

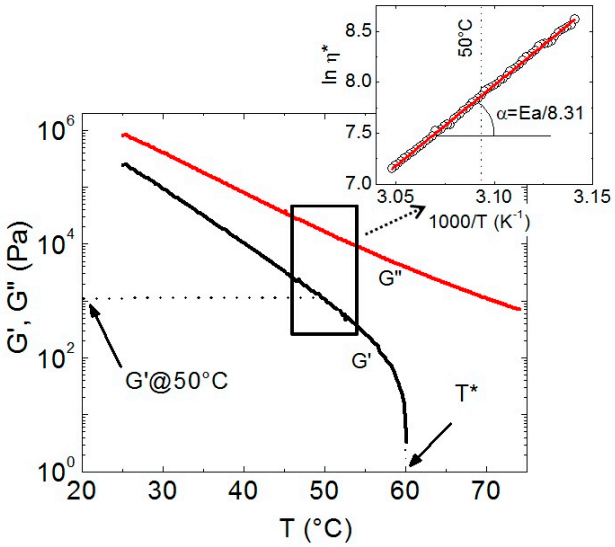


**Figure 1.** Plot of $G'$ and $G''$ as a function of temperature for a representative sample (neat bitumen). The meaning of the extracted values of $G'$@50 °C and T* is shown by the pointing arrows. From the values of $G'$ and $G''$ around 50 °C the Arrhenius plot of $\eta^*$ is built and reported in the inset which also shows how to extract the activation energy (Ea). In the inset the red line is the linear regression of the experimental data (circles).

This fact, together with the fact that $G' < G''$ always holds, shows that the samples have a pseudoplastic fluid behavior and allows to consider that the investigated temperatures are all at higher values than the glass temperature, usually slightly below 0 °C [3], at which $G''$ should have a maximum.

Upon increasing temperature, at a certain point, $G'$ suddenly drops. The temperature at which $G'$ drops (T*) is taken as that temperature at which $G''/G' > 1000$. T* has the meaning of being that temperature at which the binder can be considered almost as a Newtonian fluid. From the microscopic point of view, it can be intended as the temperature at which the thermal motion is sufficiently high to completely destroy the interacting network made by the above described complex structure. Consequently, at T* no storage of energy can be afforded by the sample so the storage modulus $G'$ drops. The sudden drop of $G'$ is shown in the same Figure 1 together with the easy way to extract the

corresponding T*. Like *G'*@50 °C, and for the same reason, T* is also expected to change according to the additive added to the bitumen.

The values of *G'*@50 °C and T* are reported in Table 1 for the various samples.

**Table 1.** *G'*@50 °C, T* and Ea values for bitumen modified with various additives.

| Additive | *G'*@50 °C (kPa) | T* (°C) | Ea (kJ/mol) |
|---|---|---|---|
| ref | 1.0 | 60.2 | 132 |
| Algae *euchemae* | 13.0 | 75.0 | 130 |
| carobs | 10.5 | 72.0 | 139 |
| orange skin | 5.4 | 68.5 | 123 |
| flour 00 | 1.4 | 61.8 | 132 |
| agar | 1.9 | 63.2 | 132 |
| carragenine | 6.0 | 70.3 | 127 |
| carboxymethylcellulose | 7.8 | 70.5 | 140 |
| pectin | 1.7 | 62.7 | 139 |
| arabic gum | 1.4 | 62.2 | 131 |
| cellulose | 1.7 | 63.1 | 133 |
| Corn flour | 1.1 | 60.4 | 134 |
| starch | 1.6 | 62.6 | 131 |
| guar gum | 5.3 | 68.4 | 135 |
| xantam gum | 2.4 | 64.2 | 138 |

It is interesting to notice that the *G'*@50 °C is correlated with T* as shown in Figure 2. The goodness of this result is supported by the observed R-squared value (0.985). Although this may be expectable, it must be noticed that *G'*@50 °C refers to the Y-value of the *G'* plot in Figure 1, whereas T* refers to the X-value at which the curve drops, i.e., two independent, in principle, parameters. The observed correlation therefore confirms that the reinforcing effect caused by the network-type interactions between the additive and the asphaltene clusters and their aggregates takes place at all temperatures shifting T* to higher values: this means that the rigidity at temperatures under usage conditions and the maximum possible operational temperatures can be seen as different aspects of the same microscopic phenomenon. This observation is in accordance with that observed by Oliviero Rossi et al. [3], who investigated the rheological effect of some additives. They found in that paper that some additives with almost apolar nature, like organosilane, oleic acid, and octadecylamine, are preferentially solubilized within the maltene phase, giving weak interactions with asphaltenes and their cluster, and consequently not being able to reinforce the overall structure. In this situation, T* decreases, as well as *G'*@50 °C, which seemed correlated. On the contrary, a more polar additive like polyphosphoric acid was able to reinforce the structure, stiffening the bitumen, and increasing T*.

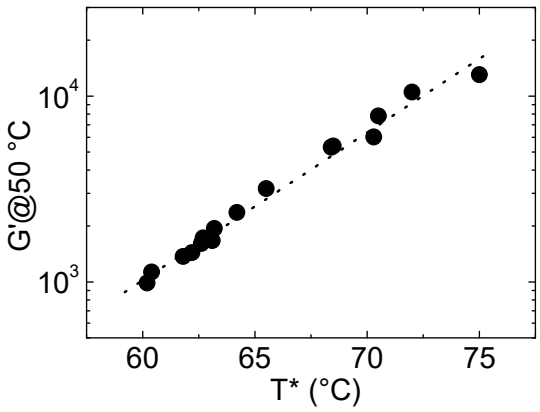


**Figure 2.** Correlation between the values of *G'*@50 °C and T*. The dotted line is a guide for the eye.

In our case, the additives are long molecules/polymers characterized by the presence of numerous polar groups. They would be able, in fact, to establish interactions with the asphaltene molecules and their clusters and this is confirmed by the fact that all additives tend to bring both *G*'@50 °C and T* to higher values. This can be ascribed by the presence of numerous polar groups that are able to establish interactions with the asphaltene molecules and their clusters. There are some differences among the various polysaccharides in the extent of *G*'@50 °C and T* increase: the most prominent effect is exerted by algae *euchemae*, followed by carob seeds flour, with the least effect by 00 and corn flours. These differences can be ascribed to their specific molecular structure. The most soluble additives, like those rich in starch, i.e., 00 and potato flours, have little influence on the bitumen properties. They can bind asphaltenes but are not of sufficient length or strength to connect the hierarchical structures made of asphaltenes clusters at longer length scales. Fibers instead, (recognizable by their lower solubility in water) like carboxymetylcellulose or algae *euchemae*, have the proper characteristics to do this. The remaining small differences among the various polysaccharides should be interpreted going deeper into their specific interactions with all the molecules involved in such complex systems, for which more challenging experiment would be required. The present data however, represent a good starting point for experimentalists and theoreticians.

### 3.2. Viscosity ($\eta$) as a Function of Temperature (T)—Arrhenius Model

The temperature dependence of both *G*' and *G*'' allows further analysis. To do so, a more synthetic indicator has been derived: the complex viscosity ($\eta^*$). It is the ratio of *G** to angular frequency $\omega$, i.e., [25]:

$$\eta^* = \frac{G^*}{\omega} = \frac{\sqrt{G'^2 + G''^2}}{\omega} \quad (2)$$

Here, $\eta^*$ has been considered because it is a synthetic indicator. In fact, differently from *G*' and *G*'', which give separate information on the energy absorbed by the system in elastic (*G*') and dissipating (*G*'') form, $\eta^*$ instead synthetically yields information on the *total* amount of energy that the system absorbs. In addition, besides being more synthetic, $\eta^*$ has the physical meaning of representing the resistance to flow under oscillatory shear conditions.

The temperature dependence of $\eta^*$ is reported in the inset of Figure 1 as ln $\eta^*$ vs. 1000/T (Arrhenius plot).

The choice of the Arrhenius plot, far from following usual habits to show the temperature dependence of viscosity, is instead the result of our approach based on the molecular interpretation of the macroscopic properties (an approach we are keen on) which lead to the following observations and considerations. From the microscopic point of view, in fact, the complex viscosity modulus is determined ultimately by the force field between the molecules, i.e., the strength of the interactions involved in the intermolecular network in bitumen. The theoretical description is quite complex [26], and several approaches have been developed, both theoretical [27–29] and numerical as based on molecular dynamic simulations [30]. On the other hand, for a simple analytical description of the temperature dependence of viscosity, several forms have been derived. The most common is the Arrhenius model, but other models are also present, like the Vogel-Tamman-Fulcher (VTF) equation, the polynomial expansion [31] and other formulas taking into account for eventual tunneling [32]. These forms are nicely commented in [30] and [31]. Basically, as some authors shown [31], the main distinction lies on the linearity of the ln $\eta^*$ vs. 1/T trend (Arrhenian behavior). The trend is usually linear for simple liquids, which follows the basic two-wells potential model. If the trend is not linear then other equations must be used according to the reason of non-linearity: if cooperative effects are present, as occurring for example for strongly interacting fluids like ionic liquids, heavy oils and fuels, polymers, melting salts, and glasses, then, the VTF can be used. It is usually used, indeed, for glass, with the phenomenological description of the glass forming behavior close to Tg. If tunneling is present, then the Nakamura-Takayanagi-Sato (NTS) or Aquilanti-Sanches-Coutinho-Carvalho (ASCC) formulas can be considered. Other approaches, like a polynomial expansion, with interpolation of

experimental data, can be used. Further details of these aspects can be found in many academic and specialized textbooks so the eager reader is redirected to those readings. Here, this preliminary distinction will be used to justify the choice of Arrhenius model. As can be seen by the Arrhenius plot (inset in Figure 1), the linear trend of the data is pretty well observed in an adequate interval around the temperature chosen as representative of the working condition (50 °C). It has been also observed that:

1. this behavior is observed for all the investigated samples;
2. the same linear trend is observed also in a wider interval including lower temperatures;
3. the effect of network breakdown at higher temperatures (*G*' drop at T = T*), which represents however a strong structural modification, does not exert its effects in the temperature range considered, preserving the linear trend in the Arrhenius plot.

These observations suggest that the choice the Arrhenius model is the most adequate. There is no reason, in fact, to use the VTF equation since the temperatures considered are significantly higher than the Tg (in this case the VTS would reduce to the Arrhenius giving $T_0 = 0$) and since a polynomial expression would get rid of the physics behind the Arrhenius model (see later) to simply take into account for the numerical interpolation of experimental data. In fact, although the Arrhenius model has been derived from the reaction kinetics in the gas phase, a favored theoretical base for the interpretation of viscosity has been provided by the application of the transition-state-theory [33] (TST) by Eyring of Arrhenius chemical kinetics to transport phenomena [34]. In this framework, Ea represents the activation energy to overcome for flowing to occur. It can be easily derived from the slope of the best fit line in the Arrhenius plot (as shown in the inset of Figure 1) according to the logarithmic form

$$\ln \eta * (T) = \ln As + \frac{Ea}{R} \cdot \frac{1}{T} \quad (3)$$

where $\eta$* is the complex viscosity (Equation (2)), R is the gas constant, 8.314 J $K^{-1}$ $mol^{-1}$ and As is the pre-exponential (entropic) factor.

In the same framework, the logarithm of pre-exponential factor (ln *As*) can be derived as the intercept of the best fit linear regression of the experimental data. *As* has been generally dealt with a "frequency factor", representing the fraction of effective collisions which are able to turn into the flow process. In the context of TST, ln *As* represents the entropic change when passing from the initial state to the transition state typically formed during the hopping between one potential well to the other in the shearing process.

Let's now use these physical quantities to interpret the observed data (reported in Table 1). The Ea values are consistent with the value observed for other additivated bitumens [3] lying in the range 120–140 kJ/mol. In addition, while all additives cause a more or less marked increase in the *G*'@50 °C, they do not uniquely affect Ea. Some additives in fact cause an increase in Ea, like carob seeds flour, xanthan gum, pectin and carboxymethylcellulose, whereas some other compounds affect the bitumen in the opposite way causing a decrease of Ea, like oranges skins and carragenines. This observation suggests prudence in interpreting the two parameters (rigidity—or *G*'—and Ea) in the same terms. They should be treated, instead, as independent and sometimes different aspects of the phenomenon. Indeed, as shown in Figure 3, lack of correlation has been found between Ea and *G*'@50 °C (or T*, given the correlation between T* and *G*'@50 °C shown in Figure 2). Similar behavior has been found in other papers as, for example, the polyphosphoric acid-additivated bitumen in [31], which showed higher rigidity with respect to the neat bitumen but lower activation energy of the viscosity.

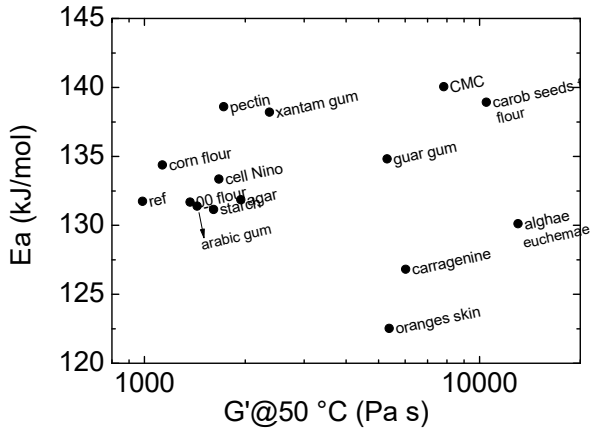


**Figure 3.** Plot of Ea vs. *G*′@50 °C showing lack of correlation.

As for the pre-exponential factor, it can be observed that ln As is always negative, independently of the additive used. Remaining in the same theoretical model considering the formation of a transition state during flow (TST model), this would indicate a positive entropy of formation of the activated state during flow. This means that the mechanism of flowing is mediated by the formation of a *disaggregated* transition state. This is typical for viscosity, since during flow the chemical species must find the room for their sliding one over the other: they must somehow pass over a situation where some displacement is required in order to make locally room for a chemical species to be able to finally slip over the remaining neighbors thus determining the flow. We like the description given by Byran et al. [35] so we report their own words: "For any one molecule to move, other surrounding molecules must first give way and move into vacant lattice sites or "holes" to create a space for the molecule to enter". Beyond the TST theory, and considering *As* as a frequency factor, its low value would indicate a low number of effective molecular collisions which are able to turn into the flowing process, in agreement with the complex structure of the bitumen, the presence of high molecular mass molecules, and the low viscosity.

When considering the effect of temperature, the microscopic interpretation becomes more complex since the various additives differently affect the force field among the molecules in the systems. In our opinion, during bitumen flowing, the disaggregative step bringing to the intermediate step ("activated complex") must be affected by the conformational re-adaptability of the additive connecting the various asphaltene clusters and their clusters. However, further investigations, both theoretical and experimental, are needed to validate this hypothesis.

### *3.3. Correlation between Activation Energy (Ea) and Pre-Exponential Factor (As)*

Before rationalizing the specific effect of the various additives on the activation energy and the pre-exponential factor, it must be unveiled another interesting observation: the activation energies are correlated with the pre-exponential factors (Figure 4). The goodness of this result is supported by the observed R-squared value (0.93) and the mean squared errors (MES) value of less than 0.2. Although the R-squared value may seem to be not strikingly high, it must be considered that the pre-exponential factor, as derived by the Arrhenius model, is an extrapolation to the *Y*-axis of the data in the Arrhenius plot, i.e., at infinite temperature, which is an un-physical situation. Moreover, it must be considered that the determination of viscosity in bitumens is problematic for several reasons. As an example, it can be considered that measurements from different laboratories on carefully collected samples of the same bitumen have given values differing even of a factor of two [36]. After these considerations, and given the statistically significant number of the samples (fifteen samples, including the reference) of the present work, in our opinion the correlation seems safe and deserves attention.

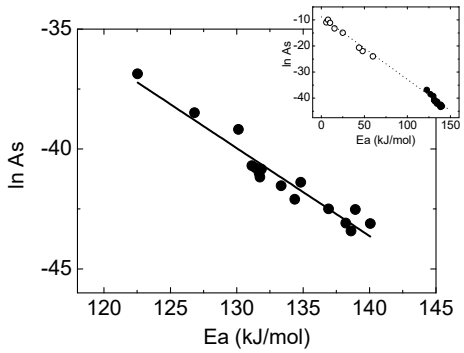


**Figure 4.** Correlation between the pre-exponential factor A and the activation energy Ea. The line is the linear regression of the experimental data. In the inset the data of the present paper (closed symbols) are shown together with those taken from biography (open symbols). In the inset the dotted line is only a guide for the eye.

The correlation between Ea and ln As has been already observed for simple liquids [31]. This is an important aspect also for applicative purposes. In fact, if this correlation holds, then the temperature dependence of the viscosity of liquids can be expressed through one parameter only (the only one known, Ea or As). This would have the advantage to allow for the viscosity description even if only one parameter is known, since the other can be derived from it. Although there is not a theory explaining such correlation [31] this can be helpful for practical uses. The data presented in that paper are reported in the inset of Figure 4 (open circles) together with the data of the present work. It must be noted that the viscosity calculated for our data refers to a region quite far from the Tg (generally occurring around 0 °C) and where the contribution of the elastic response is negligible ($G'$ is lower than $G''$ by two orders of magnitude) so it can be approximated to the zero-shear viscosity. For this reason, the comparison with the literature data shown in the inset of Figure 4 can be considered at first approximation as safe. Interestingly, we found a nice consistency between the two sets of data, despite they greatly differ in:

I. viscosity (the viscosity of our samples is several orders of magnitudes higher);
II. activation energies (Ea of our samples is from 2 to 20 times higher);
III. pre-exponential factor (our samples have pre-exponential factors several orders of magnitude lower);
IV. structure (bitumens are highly complex materials—see introduction - contrasting the structure of simple liquids).

The data in the present work, despite these big differences, extend the number and types of systems for which this linear correlation holds, suggesting a quite universal behavior although some difference in the slope is still (reasonably) present. The data of the present paper open a door for a more general view of fluids, based on a deeper understanding of the key ingredients dictating their behavior. For this reason, we hope that our data can be precious for further theoretical investigation in order to model such a universal behavior.

This correlation lets us to schematically depict the additive effect on the microstructure as a more or less pronounced "shrinking" or "stretching" of the structure and, consequently, of the microscopic energetic landscape that the system has to explore in the flowing process. This principle is represented in Scheme 1. If the additive gets closer the microscopic molecular structures involved in the flowing, then the energetic landscape is shrunk, and so the two potential wells are shrunk and brought closer. So, a more pronounced overlap of the two potential curves can be expected. This would result in a lowering of the activation energy as well as a neat increase of the entropy change during the disaggregative formation of the activated state. This makes sense, since in a compressed and tighter structure an increased entropy change is expected to pull away a chemical species from its original location. On the contrary, if the additive stretched the two-potential well landscapes, the opposite effect is observed. Of course this hypothesis needs to be verified with further experiments and investigations.

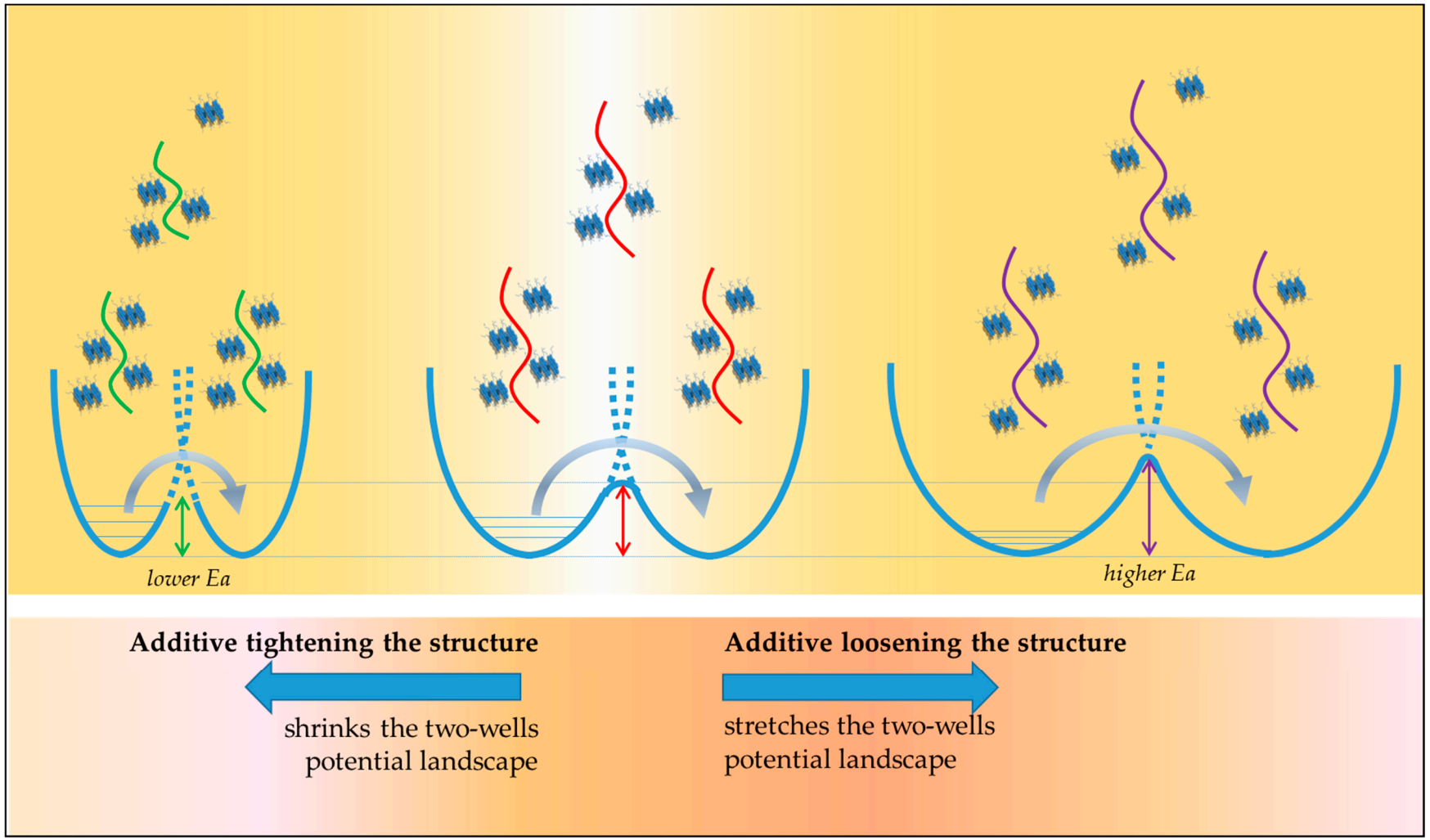


**Scheme 1.** Scheme of the additive hypothesized effect on the microscopic structure of a bitumen with consequent modification of the two wells potential.

## 4. Conclusions

We showed that the addition of commercially available polysaccharides can increase the rigidity in bitumens and their resistance to temperatures. This has been attributed to the high number of polar groups able to bind the polar clusters of asphaltene and their supra assembled aggregates, forming an interconnected network. Algae *euchemae* and carob seeds flour exert a more marked effect. Viscosity follows an Arrhenian behavior, showing, despite what one would expect, an activation energy uncorrelated with the rigidity. Interestingly, the activation energy is correlated with the pre-exponential factor, an effect already observed in simple liquids/solvents. An interpretation of the Arrhenius model in terms of Eyring transition state theory (TST) highlights a disaggregative process as the necessary step in allowing the hopping from one potential well to the successive for flowing to occurs.

The effect of the additive has been therefore interpreted in terms of shrinking or stretching of the structure and consequently of the microscopic energetic landscape that the system has to explore in the flowing process. The low cost and availability of the additive used, their big rheological effect, and their eco-friendly nature, make their use of added value. The rheological characteristics of bitumens reinforced with those materials have been shown. The observed correlation between activation energy and pre-exponential factor deserves attention for practical purposes since it allows for the description of the rheological behavior from only one of these two parameters, since the other can be derived. Finally, the microscopic interpretation of the observed outcome presents new opportunities in the comprehension of the rheological effect of additives for the future piloted design of ever performing additives.

**Supplementary Materials:** The following are available online at http://www.mdpi.com/2076-3417/9/24/5564/s1, Table S1: range size (min-max) and average size of the grains making the additives.

**Author Contributions:** M.P. investigation; P.C. (Paolino Caputo) investigation; V.L. investigation; G.D.F. investigation, C.O.R. methodology; supervision; P.C. (Pietro Calandra) funding acquisition, data curation, writing.

**Funding:** CNR-PAN bilateral project 2017–2019 (prot. n. 0033107/2017).

**Acknowledgments:** The Authors want to acknowledge Vincenzo Turco Liveri (retired professor from University of Palermo, Italy) for fruitful discussions. His experience in surfactant-base systems allowed the arising of interesting chemical reasoning useful for the interpretation of the observed behavior. Financial support from the CNR-PAN bilateral project 2017–2019 (prot. n. 0033107/2017) is acknowledged. It permitted a fruitful discussion on the data with Mikolaj Pochylski and Jacek Gapinski (Adam Mickiewicz University in Poznan, Poland) who are also gratefully acknowledged.

**Conflicts of Interest:** The authors declare no conflict of interest.

## References

1. Rozeveld, S.; Shin, E.; Bhurke, A.; France, L.; Drzal, L. Network morphology of straight and polymer modified asphalt cements. *Microsc. Res. Tech.* **1997**, *38*, 529–543. [CrossRef]
2. Lesueur, D. The colloidal structure of bitumen: Consequences on the rheology and on the mechanisms of bitumen modification. *Adv. Colloid. Interface Sci.* **2009**, *145*, 42–82. [CrossRef] [PubMed]
3. Calandra, P.; Caputo, P.; De Santo, M.P.; Todaro, L.; Turco Liveri, V.; Oliviero Rossi, C. Effect of additives on the structural organization of asphaltene aggregates in bitumen. *Constr. Build. Mater.* **2019**, *199*, 288–297. [CrossRef]
4. Jager, A.; Lackner, R.; Eisenmenger-Sittner, C.; Blab, R. Identification of Microstructural Components of Bitumen by Means of Atomic Force Microscopy (AFM). *Proc. Appl. Math. Mech.* **2004**, *4*, 400–401. [CrossRef]
5. Oliviero Rossi, C.; Ashimova, S.; Calandra, P.; De Santo, M.P.; Angelico, R. Mechanical Resilience of Modified Bitumen at Different Cooling Rates: A Rheological and Atomic Force Microscopy Investigation. *Appl. Sci.* **2017**, *7*, 779. [CrossRef]
6. Calandra, P.; Longo, A.; Ruggirello, A.; Turco Liveri, V. Physico-Chemical Investigation of the State of Cyanamide Confined in AOT and Lecithin Reversed Micelles. *J. Phys. Chem. B* **2004**, *108*, 8260–8268. [CrossRef]

7. Calandra, P.; Giordano, C.; Ruggirello, A.; Turco Liveri, V. Physicochemical investigation of acrylamide solubilization in sodium bis(2-ethylhexyl)sulfosuccinate and lecithin reversed micelles. *J. Coll. Interf. Sci.* **2004**, *277*, 206–214. [CrossRef]
8. Calandra, P.; Ruggirello, A.; Pistone, A.; Turco Liveri, V. Structural and Optical Properties of Novel Surfactant Coated $TiO_2$-Ag Based Nanoparticles. *J. Clust. Sci.* **2010**, *21*, 767–778. [CrossRef]
9. Calandra, P.; Di Marco, G.; Ruggirello, A.; Turco Liveri, V. Physico-chemical investigation of nanostructures in liquid phases: Nickel chloride ionic clusters confined in sodium bis(2-ethylhexyl) sulfosuccinate reverse micelles. *J. Colloid Interface Sci.* **2009**, *336*, 176–182. [CrossRef]
10. Gentile, L.; Filippelli, L.; Oliviero Rossi, C.; Baldino, N.; Ranieri, G.A. Rheological and H-NMR spin–spin relaxation time for the evaluation of the effects of PPA addition on bitumen. *Mol. Cryst. Liq. Cryst.* **2012**, *558*, 54–63. [CrossRef]
11. Radenberg, M.; Boetcher, S.; Sedaghat, N. Effect and efficiency of rejuvenators on aged asphalt binder—German experiences. In Proceedings of the 6th Eurasphalt & Eurobitume Congress, Prague, Czech Republic, 1–3 June 2016.
12. Hurley, G.C.; Prowell, B.D. Evaluation of potential processes for use in warm mix asphalt. *J. Assoc. Asph. Paving Technol.* **2006**, *75*, 41–90.
13. Silva, H.M.R.D.; Oliveira, J.R.M.; Ferreira, C.I.G.; Pereira, P.A.A. Assessment of the performance of warm mix asphalts in road pavements. *Int. J. Pavement Res. Technol.* **2010**, *3*, 119–127.
14. Hakseo, K.; Soon-Jae, L. Rheology of warm mix asphalt binders with aged binders. *Constr. Build. Mat.* **2011**, *25*, 183–189.
15. Jamshidia, A.; Hamzaha, M.O. Performance of warm mix asphalt containing Sasobit®: State-of-the-art. *Constr. Build. Mater.* **2013**, *38*, 530–553. [CrossRef]
16. Yousefi, A.A. Rubber-Modified Bitumens. *Iran. Polym. J.* **2002**, *11*, 303–309.
17. Król, J.B.; Kowalski, K.J.; Niczke, L.; Radziszewski, P. Effect of bitumen fluxing using a bio-origin additive. *Constr. Build. Mat.* **2016**, *114*, 194–203. [CrossRef]
18. Somé, C.; Pavoine, A.; Chailleux, E.; Andrieux, L.; DeMArco, L.; Philippe, D.-S.; Stephan, B. Rheological behaviour of vegetable oil-modified asphaltite binders and mixes. In Proceedings of the 6th Eurasphalt & Eurobitume Congress, Prague, Czech Republic, 1–3 June 2016; p. 222.
19. Caputo, P.; Porto, M.; Calandra, P.; De Santo, M.P.; Oliviero Rossi, C. Effect of epoxidized soybean oil on mechanical properties of bitumen and aged bitumen. *Mol. Cryst. Liq. Cryst.* **2018**, *675*, 68–74. [CrossRef]
20. Edwards, Y.; Tasdemir, Y.; Isacssonc, U. Rheological effects of commercial waxes and polyphosphoric acid in bitumen 160/220—Low temperature performance. *Fuel* **2006**, *85*, 989–997. [CrossRef]
21. Read, J.; Whiteoak, D. *The Shell Bitumen Handbook*, 5th ed.; Hunter, R.N., Ed.; Thomas Telford Publishing: London, UK, 2003.
22. Yoon, S.; Durgashanker Bhatt, S.; Lee, W.; Lee, H.Y.; Jeong, S.Y.; Baeg, J.-O.; Wee Lee, C. Separation and characterization of bitumen from Athabasca oil sand. *Korean J. Chem. Eng.* **2009**, *26*, 64–71. [CrossRef]
23. Sheu, E.Y.; Storm, D.A. Colloidal properties of asphaltenes in organic solvents. In *Asphaltenes: Fundamentals and Applications*; Chap.1; Sheu, E.Y., Mullins, O.C., Eds.; Plenum Press: New York, NY, USA, 1995.
24. Shaffie, E.; Arshad, A.K.; Alisibramulisi, A.; Ahmad, J.; Hashim, W.; Abd Rahman, Z.; Jaya, R.P. Effect of mixing variables on physical properties of modified bitumen using natural rubber latex. *Int. J. Civ. Eng. Technol.* **2018**, *9*, 1812–1821.
25. Macosko, C.W. *Rheology: Principles, Measurements, and Applications*; Wiley Publishing: Hoboken, NJ, USA, 1994; ISBN 978-0-471-18575-8.
26. Haj-Kacem, R.B.; Ouerfelli, N.; Herráez, J.; Guettari, M.; Hamda, H.; Dallel, M. Contribution to modeling the viscosity Arrhenius-type equation for some solvents by statistical correlations analysis. *Fluid Phase Equilib.* **2014**, *383*, 11–20. [CrossRef]
27. Kirkwood, J.G.; Buff, F.P.; Green, M.S. The statistical mechanical theory of transport processes. III. The coefficients of shear and bulk viscosity of liquids. *J. Chem. Phys.* **1949**, *17*, 988–994. [CrossRef]
28. Eyring, H. Viscosity, plasticity, and diffusion as examples of absolute reaction rates. *J. Chem. Phys.* **1936**, *4*, 283–291. [CrossRef]
29. Eyring, H.; John, M.S. *Significant Liquid Structure*; Wiley: New York, NY, USA, 1969.
30. Cummings, P.T.; Evans, D.J. Nonequilibrium molecular dynamics approaches to transport properties and non-Newtonian fluid rheology. *Ind. Eng. Chem. Res.* **1992**, *31*, 1237–1252. [CrossRef]

31. Messaâdi, A.; Dhouibi, N.; Hamda, H.; Belgacem, F.B.M.; Adbelkader, Y.H.; Ouerfelli, N.; Hamzaoui, A.H. A New Equation Relating the Viscosity Arrhenius Temperature and the Activation Energy for Some Newtonian Classical Solvents. *J. Chem.* **2015**, *2015*, 163262. [CrossRef]
32. Carvalho-Silva, V.H.; Coutinho, N.D.; Aquilanti, V. Temperature Dependence of Rate Processes Beyond Arrhenius and Eyring: Activation and Transitivity. *Front. Chem.* **2019**, *7*, 380. [CrossRef] [PubMed]
33. Eyring, H. The activated complex in chemical reactions. *J. Chem Phys.* **1935**, *3*, 107–115. [CrossRef]
34. Tyrrell, H.J.V.; Harris, K.R. *Diffusion in Liquids*; Butterworths: London, UK, 1984.
35. Byran, J.; Kantzas, A.; Bellehumer, C. Oil-viscosity predictions from low-field NMR measurements. *SPE Reserv. Eval. Eng.* **2005**, *8*, 44–52. [CrossRef]
36. Rabbani, A.; Schmitt, D.R. Ultrasonic shear wave reflectometry applied to the determination of the shear moduli and viscosity of a viscoelastic bitumen. *Fuel* **2018**, *232*, 506–518. [CrossRef]


© 2019 by the authors. Licensee MDPI, Basel, Switzerland. This article is an open access article distributed under the terms and conditions of the Creative Commons Attribution (CC BY) license (http://creativecommons.org/licenses/by/4.0/).

ISSN 2518-170X (Online),
ISSN 2224-5278 (Print)

ҚАЗАҚСТАН РЕСПУБЛИКАСЫ
ҰЛТТЫҚ ҒЫЛЫМ АКАДЕМИЯСЫНЫҢ
Қ. И. Сәтпаев атындағы Қазақ ұлттық техникалық зерттеу университеті

# Х А Б А Р Л А Р Ы

# ИЗВЕСТИЯ

НАЦИОНАЛЬНОЙ АКАДЕМИИ НАУК
РЕСПУБЛИКИ КАЗАХСТАН
Казахский национальный исследовательский
технический университет им. К. И. Сатпаева

# N E W S

OF THE ACADEMY OF SCIENCES
OF THE REPUBLIC OF KAZAKHSTAN
Kazakh national research technical university
named after K. I. Satpayev

## SERIES
## OF GEOLOGY AND TECHNICAL SCIENCES

**6 (438)**

**NOVEMBER – DECEMBER 2019**

THE JOURNAL WAS FOUNDED IN 1940

PUBLISHED 6 TIMES A YEAR

ALMATY, NAS RK

*NAS RK is pleased to announce that News of NAS RK. Series of geology and technical sciences scientific journal has been accepted for indexing in the Emerging Sources Citation Index, a new edition of Web of Science. Content in this index is under consideration by Clarivate Analytics to be accepted in the Science Citation Index Expanded, the Social Sciences Citation Index, and the Arts & Humanities Citation Index. The quality and depth of content Web of Science offers to researchers, authors, publishers, and institutions sets it apart from other research databases. The inclusion of News of NAS RK. Series of geology and technical sciences in the Emerging Sources Citation Index demonstrates our dedication to providing the most relevant and influential content of geology and engineering sciences to our community.*

*Қазақстан Республикасы Ұлттық ғылым академиясы "ҚР ҰҒА Хабарлары. Геология және техникалық ғылымдар сериясы" ғылыми журналының Web of Science-тің жаңаланған нұсқасы Emerging Sources Citation Index-те индекстелуге қабылданғанын хабарлайды. Бұл индекстелу барысында Clarivate Analytics компаниясы журналды одан әрі the Science Citation Index Expanded, the Social Sciences Citation Index және the Arts & Humanities Citation Index-ке қабылдау мәселесін қарастыруда. Webof Science зерттеушілер, авторлар, баспашылар мен мекемелерге контент тереңдігі мен сапасын ұсынады. ҚР ҰҒА Хабарлары. Геология және техникалық ғылымдар сериясы Emerging Sources Citation Index-ке енуі біздің қоғамдастық үшін ең өзекті және беделді геология және техникалық ғылымдар бойынша контентке адалдығымызды білдіреді.*

*НАН РК сообщает, что научный журнал «Известия НАН РК. Серия геологии и технических наук» был принят для индексирования в Emerging Sources Citation Index, обновленной версии Web of Science. Содержание в этом индексировании находится в стадии рассмотрения компанией Clarivate Analytics для дальнейшего принятия журнала в the Science Citation Index Expanded, the Social Sciences Citation Index и the Arts & Humanities Citation Index. Web of Science предлагает качество и глубину контента для исследователей, авторов, издателей и учреждений. Включение Известия НАН РК. Серия геологии и технических наук в Emerging Sources Citation Index демонстрирует нашу приверженность к наиболее актуальному и влиятельному контенту по геологии и техническим наукам для нашего сообщества.*

Б а с р е д а к т о р ы

э. ғ. д., профессор, ҚР ҰҒА академигі

**И.К. Бейсембетов**

Бас редакторының орынбасары

**Жолтаев Г.Ж.** проф., геол.-мин. ғ. докторы

Р е д а к ц и я а л қ а с ы:

**Абаканов Т.Д.** проф. (Қазақстан)
**Абишева З.С.** проф., академик (Қазақстан)
**Агабеков В.Е.** академик (Беларусь)
**Алиев Т.** проф., академик (Әзірбайжан)
**Бакиров А.Б.** проф., (Қырғыстан)
**Беспаев Х.А.** проф. (Қазақстан)
**Бишимбаев В.К.** проф., академик (Қазақстан)
**Буктуков Н.С.** проф., академик (Қазақстан)
**Булат А.Ф.** проф., академик (Украина)
**Ганиев И.Н.** проф., академик (Тәжікстан)
**Грэвис Р.М.** проф. (АҚШ)
**Ерғалиев Г.К.** проф., академик (Қазақстан)
**Жуков Н.М.** проф. (Қазақстан)
**Қожахметов С.М.** проф., академик (Казахстан)
**Конторович А.Э.** проф., академик (Ресей)
**Курскеев А.К.** проф., академик (Қазақстан)
**Курчавов А.М.** проф., (Ресей)
**Медеу А.Р.** проф., академик (Қазақстан)
**Мұхамеджанов М.А.** проф., корр.-мүшесі (Қазақстан)
**Нигматова С.А.** проф. (Қазақстан)
**Оздоев С.М.** проф., академик (Қазақстан)
**Постолатий В.** проф., академик (Молдова)
**Ракишев Б.Р.** проф., академик (Қазақстан)
**Сейтов Н.С.** проф., корр.-мүшесі (Қазақстан)
**Сейтмуратова Э.Ю.** проф., корр.-мүшесі (Қазақстан)
**Степанец В.Г.** проф., (Германия)
**Хамфери Дж.Д**. проф. (АҚШ)
**Штейнер М.** проф. (Германия)

**«ҚР ҰҒА Хабарлары. Геология мен техникалық ғылымдар сериясы».**
**ISSN 2518-170X (Online),**
**ISSN 2224-5278 (Print)**
Меншіктенуші: «Қазақстан Республикасының Ұлттық ғылым академиясы» РҚБ (Алматы қ.).
Қазақстан республикасының Мәдениет пен ақпарат министрлігінің Ақпарат және мұрағат комитетінде 30.04.2010 ж. берілген **№10892-Ж** мерзімдік басылым тіркеуіне қойылу туралы куәлік.

Мерзімділігі: жылына 6 рет.
Тиражы: 300 дана.

Редакцияның мекенжайы: 050010, Алматы қ., Шевченко көш., 28, 219 бөл., 220, тел.: 272-13-19, 272-13-18,
http://www.geolog-technical.kz/index.php/en/

---

© Қазақстан Республикасының Ұлттық ғылым академиясы, 2019

Редакцияның мекенжайы: Қазақстан, 050010, Алматы қ., Қабанбай батыра көш., 69а.
Қ. И. Сәтбаев атындағы геология ғылымдар институты, 334 бөлме. Тел.: 291-59-38.

Типографияның мекенжайы: «Аруна» ЖК, Алматы қ., Муратбаева көш., 75.

Главный редактор

д. э. н., профессор, академик НАН РК

**И. К. Бейсембетов**

Заместитель главного редактора

**Жолтаев Г.Ж.** проф., доктор геол.-мин. наук

Редакционная коллегия:

**Абаканов Т.Д.** проф. (Казахстан)
**Абишева З.С.** проф., академик (Казахстан)
**Агабеков В.Е.** академик (Беларусь)
**Алиев Т.** проф., академик (Азербайджан)
**Бакиров А.Б.** проф., (Кыргызстан)
**Беспаев Х.А.** проф. (Казахстан)
**Бишимбаев В.К.** проф., академик (Казахстан)
**Буктуков Н.С.** проф., академик (Казахстан)
**Булат А.Ф.** проф., академик (Украина)
**Ганиев И.Н.** проф., академик (Таджикистан)
**Грэвис Р.М.** проф. (США)
**Ергалиев Г.К.** проф., академик (Казахстан)
**Жуков Н.М.** проф. (Казахстан)
**Кожахметов С.М.** проф., академик (Казахстан)
**Конторович А.Э.** проф., академик (Россия)
**Курскеев А.К.** проф., академик (Казахстан)
**Курчавов А.М.** проф., (Россия)
**Медеу А.Р.** проф., академик (Казахстан)
**Мухамеджанов М.А.** проф., чл.-корр. (Казахстан)
**Нигматова С.А.** проф. (Казахстан)
**Оздоев С.М.** проф., академик (Казахстан)
**Постолатий В.** проф., академик (Молдова)
**Ракишев Б.Р.** проф., академик (Казахстан)
**Сеитов Н.С.** проф., чл.-корр. (Казахстан)
**Сейтмуратова Э.Ю.** проф., чл.-корр. (Казахстан)
**Степанец В.Г.** проф., (Германия)
**Хамфери Дж.Д**. проф. (США)
**Штейнер М.** проф. (Германия)

**«Известия НАН РК. Серия геологии и технических наук».**
**ISSN 2518-170X (Online),**
**ISSN 2224-5278 (Print)**
Собственник: Республиканское общественное объединение «Национальная академия наук Республики Казахстан (г. Алматы)
Свидетельство о постановке на учет периодического печатного издания в Комитете информации и архивов Министерства культуры и информации Республики Казахстан **№10892-Ж,** выданное 30.04.2010 г.

Периодичность: 6 раз в год
Тираж: 300 экземпляров

Адрес редакции: 050010, г. Алматы, ул. Шевченко, 28, ком. 219, 220, тел.: 272-13-19, 272-13-18,
http://nauka-nanrk.kz /geology-technical.kz

---

© Национальная академия наук Республики Казахстан, 2019

Адрес редакции: Казахстан, 050010, г. Алматы, ул. Кабанбай батыра, 69а.
Институт геологических наук им. К. И. Сатпаева, комната 334. Тел.: 291-59-38.

Адрес типографии: ИП «Аруна», г. Алматы, ул. Муратбаева, 75

E d i t o r i n c h i e f

doctor of Economics, professor, academician of NAS RK

**I. K. Beisembetov**

Deputy editor in chief

**Zholtayev G.Zh.** prof., dr. geol-min. sc.

E d i t o r i a l b o a r d:

**Abakanov T.D.** prof. (Kazakhstan)
**Abisheva Z.S.** prof., academician (Kazakhstan)
**Agabekov V.Ye.** academician (Belarus)
**Aliyev T.** prof., academician (Azerbaijan)
**Bakirov A.B.** prof., (Kyrgyzstan)
**Bespayev Kh.A.** prof. (Kazakhstan)
**Bishimbayev V.K.** prof., academician (Kazakhstan)
**Buktukov N.S.** prof., academician (Kazakhstan)
**Bulat A.F.** prof., academician (Ukraine)
**Ganiyev I.N.** prof., academician (Tadjikistan)
**Gravis R.M.** prof. (USA)
**Yergaliev G.K.** prof., academician (Kazakhstan)
**Zhukov N.M.** prof. (Kazakhstan)
**Kozhakhmetov S.M.** prof., academician (Kazakhstan)
**Kontorovich A.Ye.** prof., academician (Russia)
**Kurskeyev A.K.** prof., academician (Kazakhstan)
**Kurchavov A.M.** prof., (Russia)
**Medeu A.R.** prof., academician (Kazakhstan)
**Muhamedzhanov M.A.** prof., corr. member. (Kazakhstan)
**Nigmatova S.A.** prof. (Kazakhstan)
**Ozdoyev S.M.** prof., academician (Kazakhstan)
**Postolatii V.** prof., academician (Moldova)
**Rakishev B.R.** prof., academician (Kazakhstan)
**Seitov N.S.** prof., corr. member. (Kazakhstan)
**Seitmuratova Ye.U.** prof., corr. member. (Kazakhstan)
**Stepanets V.G.** prof., (Germany)
**Humphery G.D**. prof. (USA)
**Steiner M.** prof. (Germany)

**News of the National Academy of Sciences of the Republic of Kazakhstan. Series of geology and technology sciences.**
**ISSN 2518-170X (Online),**
**ISSN 2224-5278 (Print)**
Owner: RPA "National Academy of Sciences of the Republic of Kazakhstan" (Almaty)
The certificate of registration of a periodic printed publication in the Committee of information and archives of the Ministry of culture and information of the Republic of Kazakhstan N 10892-Ж, issued 30.04.2010

Periodicity: 6 times a year
Circulation: 300 copies

Editorial address: 28, Shevchenko str., of. 219, 220, Almaty, 050010, tel. 272-13-19, 272-13-18,
http://nauka-nanrk.kz/geology-technical.kz

---

© National Academy of Sciences of the Republic of Kazakhstan, 2019

Editorial address: Institute of Geological Sciences named after K.I. Satpayev
69a, Kabanbai batyr str., of. 334, Almaty, 050010, Kazakhstan, tel.: 291-59-38.

Address of printing house: ST "Aruna", 75, Muratbayev str, Almaty

**N E W S**
OF THE NATIONAL ACADEMY OF SCIENCES OF THE REPUBLIC OF KAZAKHSTAN
**SERIES OF GEOLOGY AND TECHNICAL SCIENCES**
ISSN 2224-5278
Volume 6, Number 438 (2019), 295 – 301 **https://doi.org/10.32014/2019.2518-170X.181**

UDC 691.16:625.7/.8

**M. Porto[1], P. Caputo[1], V. Loise[1], B. Teltayev[2], R. Angelico[3], P. Calandra[4], C. Oliviero Rossi[1]**

[1]Department of Chemistry and Chemical Technologies of University of Calabria,
Via P. Bucci, Cubo 14/D, 87036 Rende (CS) Italy,
[2]Kazakhstan Highway Research Institute, Almaty, Kazakhstan,
[3]Department of Agricultural, Environmental and Food Sciences (DIAAA), University of Molise,
Via De Sanctis, 86100 Campobasso (CB), Italy,
[4]CNR-ISMN, National Council of Research, Via Salaria km 29.300, 00015 Monterotondo Stazione (RM), Italy.
E-mail: michele.parto@unical.it, paolino.caputo@unical.it, valeria.loise@unical.it,
bagdatbt@yahoo.com, angelico@unimol.it, pietro.calandra@ismn.cnr.it, cesare.oliviero@unical.it

# NEW EXPERIMENTAL APPROACHES TO ANALYSE THE SUPRAMOLECULAR STRUCTURE OF REJUVENATED AGED BITUMENS

**Abstract.** Bitumen aging occurs through volatilization, oxidation and supramolecular assembly variations involving drastic changes in the structure of the material. Due to the ageing process of bitumen and its corresponding increase in viscosity, the stiffness of asphalt pavement is increased during its lifetime. Chemically, the relative content between asphaltenes and maltenes in the bitumen shifts towards a lower maltene fraction. Therefore, addition of high amounts of Reclaimed Asphalt Pavement (RAP) in asphalt mixtures may negatively affect the quality and performance of the final mix design. Rejuvenating agents can assist in this process by decreasing the aged bitumen's viscosity and restoring its original properties. An efficient rejuvenating agent favors there organization of the colloidal structure of the oxidized bitumen, thus recreating a supramolecular structure similar to fresh bitumen. Then, novel experimental approaches are needed to evaluate the efficiency of rejuvenators as well as the effect such additives have on aged bitumen properties. To achieve the aforementioned purpose, two advanced experimental approaches able to provide detailed information on bitumen microstructure are examined here. The essential concepts underlying the scattering and NMR techniques will be reviewed and the results of some recent applications of these methods in the evaluation of the effectiveness of the RAP rejuvenation will be synthetically illustrated.

**Key words:** rejuvenators, bitumen, aging, scattering, PXRD, NMR, relaxometry.

**Introduction.** Many important physical, mechanical, rheological and other characteristics of asphalt concretes depend considerably on bitumen properties [1-6]. But bituminous materials are easily subject to oxidative aging during pavement service life, especially in conditions of thermal and / or ultraviolet radiation [7, 8]. It is well assessed that oxidized bitumen is characterized by reprocessing temperatures higher than fresh one, because most of the condensed aromatic components and resins, which are responsible for a certain grade of mobility, are converted into highly oxygenated polar and more saturated compounds (asphaltenes and saturates), [9]. Indeed, the depletion of polycyclic aromatic compounds with amphiphilic activity and acting as supramolecular cage surrounding the polar asphaltenes, may lead to an increase of average colloidal sizes dispersed in the continuous a polar maltene phase. This phenomenon in turn gives rise to loss of elasticity and predisposition to material failure. Thus, once removed and processed, the bituminous layers can be recycled as reclaimed asphalt pavements (RAPs), even though their reuse is still limited (less than 20% in the mix design) due to their poor bulk mechanical properties (complex modulus and viscosity), which can cause premature cracking failures. The RAP performances as asphalt binders may be partially restored towards their original state upon addition of several classes of compounds called rejuvenators [10-12]. In particular, at least two classes of rejuvenators can be

distinguished on the basis of the mechanism by which they exert their respective regenerating action, namely, softening agents (usually called flux oils, lube stock, slurry oils etc.) able to decrease the viscosity of the aged binder, and real rejuvenators capable to restore the physicochemical properties of bitumen whose virgin microstructure has been altered by volatilization and oxidative processes [13]. To the former type belong the rheological rejuvenators (commonly taken from vegetable oil wastes), which should replenish the volatiles and light chemical fractions that have been lost during aging of asphalts, and rebalance the asphaltene/maltene ratio typical of fresh bitumen. The latter category comprises novel rejuvenators related to the general class of surfactants. Indeed, thanks to its capability to lower the interfacial energy between two immiscible phases, an amphiphilic molecule can bind on a side the polar phase and on the other side the a polar one, due to the simultaneous presence within its molecular architecture of both polar and non-polar moieties. The overall result of these simultaneous interactions proved to be effective in the stabilization of clusters of polar molecules dispersed in polar solvents [14, 15].

Therefore, amphiphilic molecules are expected to work similarly well in improving the dispersion of asphaltene clusters in the maltene phase, and consequently counteracting the aging process and reverting to rejuvenation eventually [16, 17].

The efficient and targeted use of additives with documented rejuvenating action on RAPs employed in the road paving industry must be based primarily on a rigorous experimental investigation of their effect exerted on the colloidal microstructure of bitumen. However, although these additives play an important role in bitumen recycling methods, their impact on the bitumen supramolecular structure arrangement has not yet been fully investigated in depth. The purpose of the present contribution is to emphasize the potentialities of advanced experimental methods such as scattering techniques and nuclear magnetic relaxometry, which can be considered promising techniques in the elucidation of the dynamics of the complex microstructure in bitumen. In fact, unlike the results acquired through the analysis of the mechanical bulk properties, scattering (in particular X-ray scattering) and NMR experiments can probe from nano- to mesoscale level the effectiveness of a rejuvenator in restoring the microstructure of bitumen subjected to the drastic action of aging processes [18, 19]. This work underlines that the detailed analysis of the microstructural dynamics of bitumen, extending the information taken from commonly used empirical and rapid methods, allows us to better understand the phenomena that occur in such complex materials, providing new tools for the piloted design of ever-performing rejuvenations.

**Experimental methods.** Information on how rejuvenators can affect the supramolecular structure and distribution of aggregates within the bituminous colloidal network and how this may affect the overall material properties can be achieved from careful analyses of Powder X-Ray Diffraction (PXRD) data and NMR measurements performed at low magnetic fields ($^1$H-NMR Relaxometry), making these techniques very powerful methods to carry out structural investigation in such complex systems [18, 20].

*Application of X-ray scattering techniques for the analysis of bitumen.* X-ray scattering techniques represent non-destructive analytical methods able to reveal information about the crystallographic structure, chemical composition, and physical properties of materials and thin films. These techniques are based on observing the scattered intensity of an X-ray beam hitting a sample as a function of incident and scattered angle, polarization, and wavelength or energy [21]. The PXRD spectrum provides the nanostructural information as well as the crystallite parameter of the molecules that are associated with the asphaltene aggregates [22-24]. For structure investigations on length scales longer than a few nm, Small-Angle X-ray Scattering (SAXS) is best suitable, whereas in the wide angle range (WAXS) the spectrum furnishes precious indications about characteristic distances belonging to various atomic and molecular organizations of different levels of complexity.

*Application of Nuclear Magnetic Resonance techniques for the analysis of bitumen*. Nuclear Magnetic Resonance (NMR) spectroscopy has been recently found to be an efficient and powerful technique for the characterization of complex materials such as bitumen [25]. One of the advantages of this technique is the ability to simultaneously identify several components of the mixture with the acquisition of a single high resolution$^1$H-NMR spectrum and, consequently, to evaluate the relative amount of the aliphatic and aromatic hydrogens portion in the complex system. In particular, dynamics information can be obtained from $^1$H spin−spin relaxation time ($T_2$) measurements according to the Carr-Purcell-Meiboom-Gill (CPMG) pulse sequence (NMR Relaxometry) [26, 27]. Usually the $T_2$ varies all over the sample because

of the sample heterogeneity or surface relaxation differences; then a multi-exponential attenuation of the NMR spin echo envelope should be observed. The relaxation time probability distribution function can be obtained by applying an inverse Laplace transform (ILT) to the experimental data [28]. The $T_2$ relaxation time distribution can be considered a structural fingerprint of the bitumen in which the changes in relaxation times reflect the changes that occur in the structure of the colloidal binder. In general, by ILT NMR relaxometry one can monitor the structural evolution of bitumen when additives (polymers, surfactants and so on) are added, since the relaxation distribution is strongly affected by the supramolecular organisation present in the colloids. In particular, the powerful ILT method applied to the experimental NMR echo decay can be exploited to test the effectiveness of the real rejuvenator. Indeed, direct correlation can be made between $T_2$ and the rigidity of structures in these materials as well as the molecular constrain causing dynamic hindrance [29].

**Results and discussion.** The bulk mechanical properties of bituminous materials such as, e.g., ductility and rigidity, are empirically determined by the amplitude oscillatory rheometry through the measurement of the complex modulus $G^*$consisting in its real (elastic modulus G′) and imaginary (viscous modulus G″) components [30-33]. However, more sophisticated experimental investigations such as NMR relaxometry and X-ray scattering are being proposed as emerging methods for the comprehension of the microscopic/molecular processes underneath the observed behaviour of a bituminous material subjected to both physical and chemical treatments. Indeed, the application of low-field NMR spectroscopy has been used for the determination of physical properties of petroleum fractions [25, 29] and the Inverse Laplace Transform analysis of the NMR echo signal decay gives the transverse (or spin-spin) relaxation time $T_2$ that can be connected to different domains characterized by different rigidities [20]. The chemical reasoning for this lies on the molecular constrain causing dynamic hindrance and lowering $T_2$, an effect that can be considered quite general and already found also in different systems [34-36]. In bitumen, the $T_2$ relaxation time distribution profile is usually characterized by two distinct peaks.

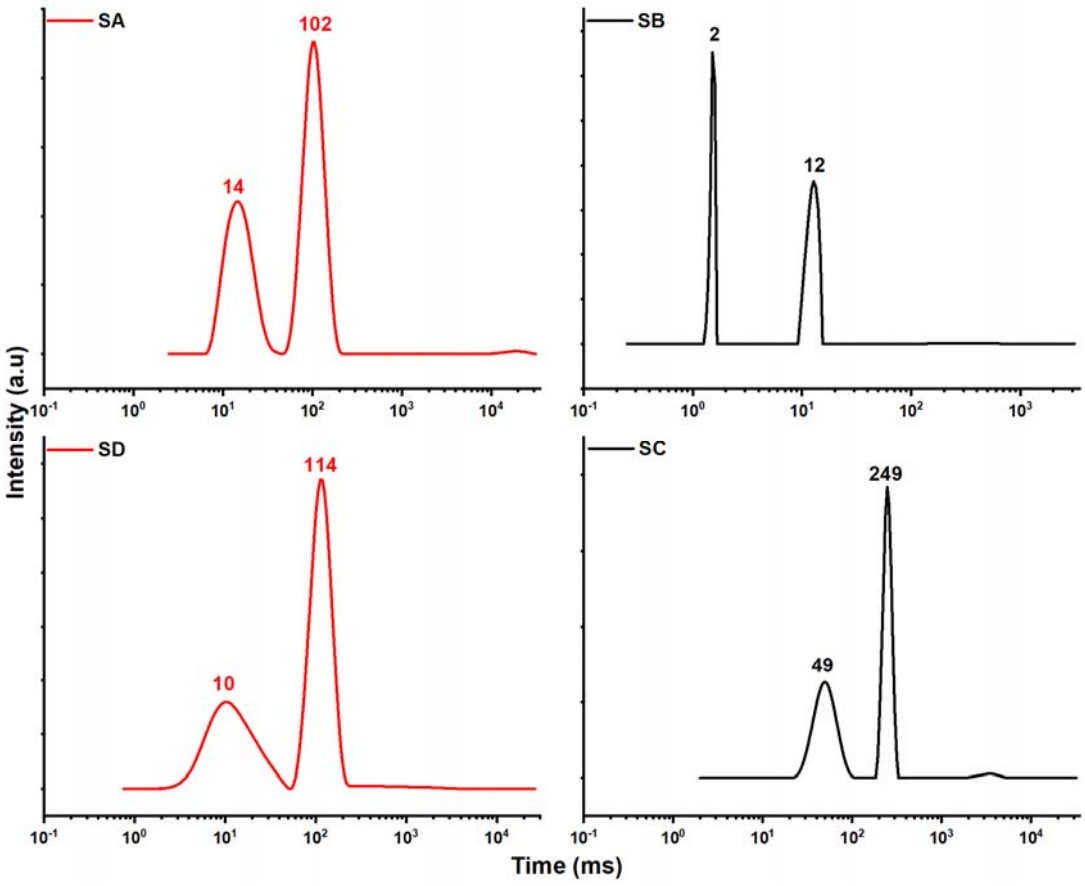


Figure 1 - $T_2$ relaxation time distribution functions obtained for pristine bitumen (SA) at 50°C, PAV bitumen (SB) at 70°C, PAV bitumen + 2 wt% vegetable flux oil (SC)at 60°C and PAV bitumen + 2 wt% green rejuvenator (SD) at 60 °C

The short $T_2$ times (around 10 ms) arise from slow tumbling of more rigid supra-molecular aggregates; hence they can be reasonably attributed to the dynamics of asphaltenes. Conversely, long $T_2$ times (around 100 ms) connected to low intra-molecular interactions can be referred to the maltene fraction of the sample under examination. The $T_2$ profiles illustrated in figure 1 provide an example of the application of the ILT method in the choice of the right rejuvenator through a quick comparison of the $T_2$ distributions for different treatments subjected to the same bituminous matrix. Indeed, one can easily verify that the addition of a green rejuvenator to the oxidized bitumen (PAV bitumen), has the effect of restoring the original probability density function compatible with fresh pristine bitumen (compare SA with SD). On the other hands, the pattern is only partially recovered when a flux oil (a softening agent) is used (compare SA with SC).

Structural features of the asphaltene clusters self-aggregated in the maltene phase can be also investigated by the X-ray scattering technique in order to gain new results on the role played by some additives in the rejuvenation action of bitumen whose colloidal structure has been seriously compromised by the aging processes. Indeed, the eventual presence of an additive triggers the formation of further intermolecular interaction in competition with those responsible for this self-assembly, causing a change of the size and shape of these aggregates. A representative X-Ray scattering spectrum of bitumen together with the Lorentzian deconvolution reported in figure 2 as a function of scattering vector $q = 4\pi \sin\theta / \lambda$, illustrates several important features.

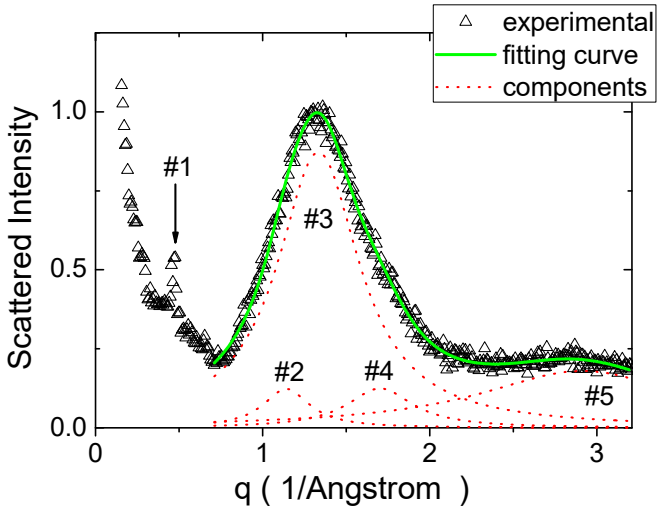


Figure 2 – Typical Wide AngleX-Ray diffraction pattern of asphalt binder with peak profile analysis

The most prominent band centred at around 1.3 $Å^{-1}$gives a characteristic of 4.4-4.7 Å, which can be attributed to the typical intermolecular lateral distance commonly present in disordered fluids. This length parameter results to be slightly higher than that identified from the band of graphene (lateral distance of about 3.6 Å) and coming from the stacks in the aromatic compounds. However, owing to the coexistence of aliphatic components in the bitumen it is reasonable to treat this band as an unresolved superposition of these two contributions. Therefore, deconvolution procedures in terms of bell-shaped curves are necessary to discriminate all the signals. Besides, an eventual low-intensity reflection in the range 0.3-0.8 $Å^{-1}$ can be attributed to the occurrence of a supra-molecular aggregation and would be therefore associated to a repetition distance between one asphaltene local aggregate and its neighbouring one, in accordance with a model of a complex system with different levels of complexity. Finally, for $q<0.3$ $Å^{-1}$ the fractal aggregation generated by an ensemble of asphaltene clusters can be examined. In principle, the formation of self-similar, fractal structures in bituminous materials cannot be excluded. In such case, the interfacial boundary is not sharp and a scaling law between the mass M (or particle number N) and the enclosed volume is established, which can provide an indication of how efficiently the particles are packed. The presence of additives may modify not only the fractal structure but also the intermolecular assembly as probed by the band centred at 1.3 $Å^{-1}$ and the peak around 0.5 $Å^{-1}$.

**Conclusion.** The restoring of the aged bitumen structure to the original conditions is a challenging task due to its complex organization at the supra-molecular scale. It has been emphasized that scattering techniques and nuclear magnetic relaxometry represent promising methods of investigation that deserve attention for a deeper analysis of bituminous materials. In fact, they can probe the effectiveness of a rejuvenator in restoring the bitumen microstructure after the aging process, while the mechanical properties alone do not allow reaching this degree of microstructural knowledge. In conclusion, we want to bring to the attention the fact that the detailed analysis of the physics of molecular bitumens allows us to better understand the phenomena that occur in bitumen, providing new tools for the piloted design of new rejuvenators with ad-hoc performances.

**М. Порто[1], П. Капуто[1], В. Лоиз[1], Б. Телтаев[2], Р. Агенлико[3], П. Каландра[4], Ч. Оливиеро Росси[1]**

[1]Калабрия Университеті Химия және Химия Технологиялары кафедрасы, Италия,
[2]Қазақстан Жол Ғылыми-Зерттеу институты, Алматы, Қазақстан,
[3]Ауыл шаруашылығы, Экология және Тағам Ғылымдары кафедрасы (DIAAA), Молиз Университеті, Италия,
[4]CNR-ISMN, Ұлттық Ғылыми Зерттеулер Кеңесі, Италия

## ЖАСАРТЫЛҒАН ЕСКІРГЕН БИТУМДАРДЫҢ МОЛЕКУЛАЛЫҚ ҚҰРЫЛЫМЫН ТАЛДАУҒА АРНАЛҒАН ЖАҢА ТӘЖІРИБЕЛІК ТӘСІЛДЕР

**Аннотация.** Битумның ескіруі материал құрылымындағы өзгерістермен байланысты болатын булану, тотығу және молекулалық қосылыстардағы өзгерістердің нәтижесінде орын алады. Битумның ескіру үдерісіне және оның тұтқырлығының артуына байланысты асфальтбетон жамылғысының қаттылығы пайдалану кезінде арта түседі. Химиялық тұрғыдан түсіндіргенде, битумдағы асфальтендер пен мальтендердің салыстырмалы үлесі мальтендердің төмен құрамына қарай жылжиды. Сондықтан, қайта қалпына келтірілген асфальт жамылғысын (ҚАЖ) асфальт қоспаларына көп мөлшерде қосу асфальтбетон жамылғысының сипаттамасына теріс әсер етуі мүмкін. Жасартқыш реагенттер ескірген битумның тұтқырлығын азайту және оның бастапқы қасиеттерін қалпына келтурі арқылы осы үдерісті жақсартуы мүмкін. Тиімді жасартқыш реагент тотыққан битумның коллоидті құрылымының ұйымдасуына қолайлы жағдай туғызып, жаңадан дайындалған битумның молекулалы құрылымын қалпына келтіреді. Одан басқа, жаңа тәжірибелік тәсілдер жасартқыш реагенттердің тиімділігі мен мұндай қоспалардың ескірген битумның қасиеттеріне ықпалын бағалау үшін қажет. Жоғарыда аталған мақсаттарға қол жеткізу үшін, осы мақалада битумның микроқұрылымы туралы толық ақпарат беретін неғұрлым перспективалық тәсілдер қарастырылады. Сейілу және ЯМР әдістерінің негізі болған басты тұжырымдамалар қарастырылады, сондай-ақ ҚАЖ жасартудың тиімділігін бағалауда осы әдістерді синтетикалық пайдалану нәтижелері көрсетілді.

**Түйін сөздер:** жасартқыш реагенттер, битум, ескіру, сейілу, рентген дифракциясы (ҰРД), ядролық-магниттік резонанс (ЯМР), релаксометрия.

**М. Порто[1], П. Капуто[1], В. Лоиз[1], Б. Телтаев[2], Р. Агенлико[3], П. Каландра[4], Ч. Оливиеро Росси[1]**

[1]Кафедра Химии и химических технологий университета Калабрии, Италия,
[2]Казахстанский дорожный научно-исследовательский институт, Алматы, Казахстан,
[3]Кафедра Сельскохозяйственных, экологических и пищевых наук (DIAAA), Университет Молиз, Италия,
[4]CNR-ISMN, Национальный совет научных исследований, Италия

## НОВЫЕ ЭКСПЕРИМЕНТАЛЬНЫЕ ПОДХОДЫ К АНАЛИЗУ НАДМОЛЕКУЛЯРНОЙ СТРУКТУРЫ ОМОЛОЖЕННЫХ СОСТАРЕННЫХ БИТУМОВ

**Аннотация.** Старение битума происходит из-за выпаривания, окисления и изменений в надмолекулярных соединениях, связанных со значительными изменениями в структуре материала. В связи с процессом старения битума и соответствующего увеличения его вязкости, жесткость асфальтобетонного покрытия увеличивается во время эксплуатации. В химическом смысле относительное содержание между асфальтенами и мальтенами в битуме сдвигается в сторону более низкого содержания мальтенов. Поэтому добавление большого количества регенерированного асфальтового покрытия (РАП) в асфальтовые смеси может отрицательно повлиять на качество и характеристики окончательного состава смеси. Омолаживающие реагенты

могут поспособствовать улучшению данного процесса путем уменьшения вязкости состаренного битума и восстановления его первоначальных свойств. Эффективный омолаживающий реагент благоприятствует организации коллоидной структуры окисленного битума, тем самым восстанавливая надмолекулярную структуру свежеприготовленного битума. Затем, новые экспериментальные подходы необходимы для оценки эффективности омолаживающих реагентов, а также какое влияние оказывают такие добавки на свойства состаренного битума. Чтобы достичь вышеуказанной цели, в данной статье рассматриваются два наиболее перспективных подхода, способные предоставить подробную информацию о микроструктуре битума. Будут рассмотрены основополагающие концепции, лежащие в основе методик рассеивания и ЯМР, а также будут проиллюстрированы результаты некоторых недавних синтетических применений этих методов в оценке эффективности омолаживания РАП.

**Ключевые слова:** омолаживающие реагенты, битум, старение, рассеивание, рентгеновская дифракция (ПРД), ядерно-магнитный резонанс (ЯМР), релаксометрия.

**Information about authors:**

Porto Michele, PhD Student “Life Science”, Department of Chemistry and Chemical Technologies of University of Calabria, Italy; michele.parto@unical.it; https://orcid.org/0000-0001-6019-1089

Caputo Paolino, Research fellow Department of Chemistry and Chemical Technologies of University of Calabria, Italy; paolino.caputo@unical.it; https://orcid.org/0000-0003-3472-7710

Loise Valeria, PhD Student “Life Science”, Department of Chemistry and Chemical Technologies of University of Calabria, Italy; valeria.loise@unical.it; https://orcid.org/0000-0001-5156-5077

Teltayev Bagdat Burkhanbaiuly, Doctor of Technical Sciences, President of JSC “Kazakhstan Highway Research Institute”, Almaty, Kazakhstan; bagdatbt@yahoo.com; https://orcid.org/ 0000-0002-8463-9965

Angelico Ruggero, PhD, Senior researcher in chemistry and physics of soft and hard matter, Department of Agricultural, Environmental and Food Sciences (DIAAA), University of Molise, Campobasso (CB), Italy; angelico@unimol.it; https://orcid.org/0000-0002-0769-5680

Calandra Pietro, Researcher CNR-ISMN, National Council of Research, Monterotondo Stazione (RM), Italy; pietro.calandra@ismn.cnr.it; https://orcid.org/0000-0002-4479-4311

Oliviero Rossi Cesare, Professor of physical chemistry, President of the spin-off “Kimical” at University of Calabria, Department of Chemistry and Chemical Technologies of University of Calabria, Italy; cesare.oliviero@unical.it; https://orcid.org/0000-0003-4406-7824

**REFERENCES**

[1] Iskakbayev A.I., Teltayev B.B., Rossi C.O. Deformation and strength of asphalt concrete under static and step loadings // Transport Infrastructure and Systems – Proceedings of the AIIT International Congress on Transport Infrastructure and Systems, TIS. 2017. P. 3-8 (in Eng.).

[2] Teltayev B.B., Amirbayev Y.D. Experimental evaluation of strength for asphalt and polymer modified asphalt concretes at low temperatures // News of the National academy of sciences of the Republic of Kazakhstan. Series of Geology and Technical Sciences. 2017. 1 (421). P. 167-176 (in Eng.).

[3] Iskakbayev A.I., Teltayev B.B., Rossi C.O. Steady-state creep of asphalt concrete // Applied Sciences. 2017. 7(2) 142 (in Eng.).

[4] Iskakbayev A.I., Teltayev B.B., Rossi C.O., Yensebayeva G.M. Experimental investigation of an asphalt concrete deformation under cyclic loading // News of the National academy of sciences of the Republic of Kazakhstan. Series of Geology and Technical Sciences. 2018. 2 (428). P. 104-111 (in Eng.).

[5] Iskakbayev A.I., Teltayev B.B., Rossi C.O., Estayev K. A new simple damage accumulation model for predicting of an asphalt concrete cyclic strength // News of the National academy of sciences of the Republic of Kazakhstan. Series of Geology and Technical Sciences. 2018. 5 (431). P. 38-47. doi.org/10.32014/2018.2518-170X.8 (in Eng.).

[6] Iskakbayev A.I., Teltayev B.B., Yensebayeva G.M., Kutimov K.S. Computer modelling of creep for hereditary materials by Abel’s kernel // News of the National academy of sciences of the Republic of Kazakhstan. Series of Geology and Technical Sciences. 2018. 6(432). P. 66-76. doi.org/10.32014/2018.2518-170X.36 (in Eng.).

[7] Oliviero Rossi C., Caputo B., Baldino N., Szerb E.I., Teltayev B. Quantitative evaluation of organosilane-based adhesion promoter effect on bitumen-aggregate bond by contact angle test // International Journal of Adhesion and Adhesives. 1 January 2017. Vol. 72. P. 117-122 (in Eng.).

[8] Oliviero Rossi C., Caputo P., Ashimova S., Fabozzi A., D’Errico G., Angelico R. Effects of natural antioxidant agents on the bitumen aging process: an EPR and rheological investigation // Appl. Sci. 2018. N 8. P. 1405-1418 (in Eng.).

[9] Handle F., Harir M., Füssl J., Koyun A.N., Grossegger D., Hertkorn N., Eberhardsteiner L., Hofko B., Hospodka M., Blab R., Schmitt-Kopplin P., Grothe H. Tracking aging of bitumen and its saturate, aromatic, resin, and asphaltene fractions using high-field Fourier transform ion cyclotron resonance mass spectrometry // Energy Fuels. 2017. N 31. P. 4771-4779 (in Eng.).

[10] Zaumanis M., Mallick R.B., Poulikakos L., Frank R. Influence of six rejuvenators on the performance properties of Reclaimed Asphalt Pavement (RAP) binder and 100% recycled asphalt mixtures // Constr. Build. Mater. 2014. N 71. P. 538-550 (in Eng.).

[11] Ashouri Taziani E., Toraldo E., Crispino M., Giustozzi F. Application of rejuvenators and virgin bitumen to restore physical and rheological properties of RAP binder // Aust. J. Civil Eng. 2017. N 15. P. 73-79 (in Eng.).

[12] Oliviero Rossi C., Caputo P., Loise V., Ashimova S., Teltayev B., Sangiorgi C. A new green rejuvenator: Evaluation of structural changes of aged and recycled bitumens by means of rheology and NMR // In: Poulikakos L., Cannone Falchetto A., Wistuba M., Hofko B., Porot L., Di Benedetto H. (Eds) RILEM 252-CMB Symposium. 2018. RILEM Book Series. Vol. 20. Springer, Cham. (in Eng.).

[13] Roberts F.L., Kandhal P.S., Brown E.R., Lee D.Y., Kennedy T.W. Hot Mix Asphalt Materials, Mixture Design and Construction / 2nd ed. NAPA, Lanham, MD. 1996. 576 p. (in Eng.).

[14] Calandra P., Longo A., Ruggirello A., Turco Liveri V. Physico-Chemical Investigation of the State of Cyanamide Confined in AOT and Lecithin Reversed Micelles // Journal of Physical Chemistry B. 2004. 108, 8260-8268. DOI: 10.1021/jp0492422 (in Eng.).

[15] Calandra P., Giordano C., Ruggirello A., Turco Liveri V. Physicochemical investigation of acrylamide solubilization in sodium bis (2-ethylhexyl) sulfosuccinate and lecithin reversed micelles // Journal of Colloid and Interface Science. 2004. 277, 206-214 DOI: 10.1016/j.jcis.2004.04.021 (in Eng.).

[16] Kakar M.R., Hamzah M.O., Akhtar M.N. Surface free energy and moisture susceptibility evaluation of asphalt binders modified with surfactant-based chemical additive // J. of Cleaner Prod. 2016. N 112. P. 2342-2353 (in Eng.).

[17] Caputo P., Porto M., Calandra P., De Santo M.P., Oliviero Rossi C. Effect of epoxidized soybean oil on mechanical properties of bitumen and aged bitumen // Mol. Cryst. Liq. Cryst. 2018. N 675. P. 68-74 (in Eng.).

[18] Loise V., Caputo P., Porto M., Calandra P., Angelico R., Oliviero Rossi C. A review on bitumen rejuvenation: mechanisms, materials, methods and perspectives // Appl. Sci. 2019. N 9. P. 4316-4359 (in Eng.).

[19] Szerb E.I., Nicotera I., Teltayev B., Vaiana R., Rossi C.O. Highly stable surfactant-crumb rubber-modified bitumen: NMR and rheological investigation // Road Materials and Pavement Design. 4 July 2018. Vol. 19, Issue 5. P. 1192-1202 (in Eng.).

[20] Caputo P., Loise V., Crispini A., Sangiorgi C., Scarpelli F., Oliviero Rossi C. The efficiency of bitumen rejuvenator investigated through Powder X-ray Diffraction (PXRD) analysis and $T_2$-NMR spectroscopy // Colloid Surface A. 2019. N 571. P. 50-54 (in Eng.).

[21] Zemb T., Lindner P. Neutron, X-rays and Light Scattering Methods Applied to Soft Condensed Matter, 1st edition, North Holland, Amsterdam, Netherlands. 2002. 552 p. (in Eng.).

[22] Trejo F., Ancheyta J., Morgan T.J., Herod A.A., Kandiyoti R. Characterization of Asphaltene from Hydrotreated Products by SEC, LDMS, LAMDI, NMR, and XRD // Energy Fuels. 2007. N 21. P. 2121-2128 (in Eng.).

[23] Calandra P., Caputo P., De Santo M.P., Todaro L., Turco Liveri V., Oliviero Rossi C. Effect of additives on the structural organization of asphaltene aggregates in bitumen // Constr. Build. Mater. 2019. N 199. P. 288-297 (in Eng.).

[24] Tanaka R., Sato E., Hunt J.E., Winans R.E., Sato S., Takanohashi T. Characterization of Asphaltene Aggregates Using X-ray Diffraction and Small-Angle X-ray Scattering // Energy Fuels. 2004. N 18. P. 1118-1125 (in Eng.).

[25] Oliviero Rossi C., Caputo P., De Luca G., Maiuolo L., Eskandarsefat S., Sangiorgi C.$^1$H-NMR spectroscopy: a possible approach to advanced bitumen characterization for industrial and paving applications // Appl. Sci. 2018. N 8. P. 229-242 (in Eng.).

[26] Angelico R., Ceglie A., Olsson U., Palazzo G., Ambrosone L. Anomalous surfactant diffusion in a living polymer system // Physical Review E. 2006. N 74. P. 031403-031410 (in Eng.).

[27] Angelico R., Murgia S., Palazzo G. Reverse wormlike micelles: a special focus on Nuclear Magnetic Resonance investigations // RSC Soft Matter. 2017. N 6. P. 31-62 (in Eng.).

[28] Caputo P., Loise V., Ashimova S., Teltayev B., Vaiana R., Oliviero Rossi C. Inverse Laplace Transform (ILT) NMR: A powerful tool to differentiate a real rejuvenator and a softener of aged bitumen // Colloid Surface A. 2019. N 574. P. 154-161 (in Eng.).

[29] Barbosa L.L., Kock F.V.C., Silva R.C., Freitas J.C.C., Lacerda Jr V., Castro E.V.R. Application of low-field NMR for the determination of physical properties of petroleum fractions // Energy Fuels. 2013. N 27. P. 673-679 (in Eng.).

[30] Filippelli L., Gentile L.Oliviero Rossi C., Ranieri G.A., Antunes F.E. Structural Change of Bitumen in the Recycling Process by Using Rheology and NMR // Ind. Eng. Chem. Res. 2012. N 51. P. 16346-16353 (in Eng.).

[31] Yu X., Zaumanis M., dos Santos S., Poulikakos L.D. Rheological, microscopic, and chemical characterization of the rejuvenating effect on asphalt binders // Fuel. 2014. N 135. P. 162-171 (in Eng.).

[32] Oliviero Rossi C., Caputo P., Loise V., Miriello D., Teltayev B., Angelico R. Role of a food grade additive in the high temperature performance of modified bitumens // Colloid Surface A. 2017. N 532. P. 618-624 (in Eng.).

[33] Oliviero Rossi C., Ashimova S., Calandra P., De Santo M.P., Angelico R. Mechanical resilience of modified bitumen at different cooling rates: A rheological and atomic force microscopy investigation // Appl. Sci. 2017. N 7. P. 779-789 (in Eng.).

[34] Olsson U., Börjesson J., Angelico R., Ceglie A., Palazzo G. Slow dynamics of wormlike micelles // Soft Matter. 2010. N 6. P. 1769-1777 (in Eng.).

[35] Angelico R., Gentile L., Ranieri G. A., Oliviero Rossi C. Flow induced structures observed in a viscoelastic reverse wormlike micellar system by Magnetic Resonance Imaging and NMR velocimetry // RSC Advances. 2016. N 6. P. 33339-33347 (in Eng.).

[36] Osman K.S., Taylor S.E. Insight into Liquid Interactions with Fibrous Absorbent Filter Media Using Low-Field NMR Relaxometry. Prospective Application to Water/Jet Fuel Filter-Coalescence // Ind. Eng. Chem. Res. 2017. N 56. P. 14651-14661 (in Eng.).

**Publication Ethics and Publication Malpractice**
**in the journals of the National Academy of Sciences of the Republic of Kazakhstan**

For information on Ethics in publishing and Ethical guidelines for journal publication see http://www.elsevier.com/publishingethics and http://www.elsevier.com/journal-authors/ethics.

Submission of an article to the National Academy of Sciences of the Republic of Kazakhstan implies that the described work has not been published previously (except in the form of an abstract or as part of a published lecture or academic thesis or as an electronic preprint, see http://www.elsevier.com/postingpolicy), that it is not under consideration for publication elsewhere, that its publication is approved by all authors and tacitly or explicitly by the responsible authorities where the work was carried out, and that, if accepted, it will not be published elsewhere in the same form, in English or in any other language, including electronically without the written consent of the copyright-holder. In particular, translations into English of papers already published in another language are not accepted.

No other forms of scientific misconduct are allowed, such as plagiarism, falsification, fraudulent data, incorrect interpretation of other works, incorrect citations, etc. The National Academy of Sciences of the Republic of Kazakhstan follows the Code of Conduct of the Committee on Publication Ethics (COPE), and follows the COPE Flowcharts for Resolving Cases of Suspected Misconduct (http://publicationethics.org/files/u2/New_Code.pdf). To verify originality, your article may be checked by the Cross Check originality detection service http://www.elsevier.com/editors/plagdetect.

The authors are obliged to participate in peer review process and be ready to provide corrections, clarifications, retractions and apologies when needed. All authors of a paper should have significantly contributed to the research.

The reviewers should provide objective judgments and should point out relevant published works which are not yet cited. Reviewed articles should be treated confidentially. The reviewers will be chosen in such a way that there is no conflict of interests with respect to the research, the authors and/or the research funders.

The editors have complete responsibility and authority to reject or accept a paper, and they will only accept a paper when reasonably certain. They will preserve anonymity of reviewers and promote publication of corrections, clarifications, retractions and apologies when needed. The acceptance of a paper automatically implies the copyright transfer to the National Academy of Sciences of the Republic of Kazakhstan.

The Editorial Board of the National Academy of Sciences of the Republic of Kazakhstan will monitor and safeguard publishing ethics.

Правила оформления статьи для публикации в журнале смотреть на сайте:

www:nauka-nanrk.kz

**ISSN 2518-170X (Online), ISSN 2224-5278 (Print)**

http://www.geolog-technical.kz/index.php/en/

Верстка *Д. Н. Калкабековой*

Подписано в печать 15.11.2019.
Формат 70x881/8. Бумага офсетная. Печать – ризограф.
19,7 п.л. Тираж 300. Заказ 6.

*Национальная академия наук РК*
*050010, Алматы, ул. Шевченко 28, т. 272-13-19, 272-13-18*

Colloids and Surfaces A 603 (2020) 125182

Contents lists available at ScienceDirect

Colloids and Surfaces A

journal homepage: www.elsevier.com/locate/colsurfa

# Unravelling the role of a green rejuvenator agent in contrasting the aging effect on bitumen: A dynamics rheology, nuclear magnetic relaxometry and self-diffusion study

Valeria Loise[a], Paolino Caputo[a,*], Michele Porto[a,*], Bagdat Teltayev[b], Ruggero Angelico[c], Cesare Oliviero Rossi[a]

[a] Department of Chemistry and Chemical Technologies, University of Calabria, 87036, Arcavacata Di Rende, CS, Italy
[b] Kazakhstan Highway Research Institute, Nurpeisova Str., 2A, Almaty, 050061, Kazakhstan
[c] Department of Agricultural, Environmental and Food Sciences (DIAAA), University of Molise, Via De Sanctis 86100, Campobasso, CB, Italy

## GRAPHICAL ABSTRACT

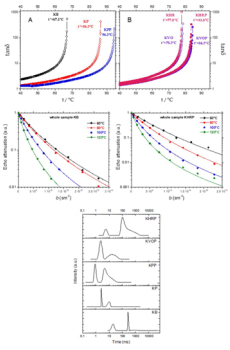

## ARTICLE INFO

*Keywords:*
Recycled aged bitumen
Rejuvenator
Physical chemistry techniques
Reuse waste bituminous materials
RAP

## ABSTRACT

This paper evaluated the potentialities of a green and biocompatible rejuvenator agent (HR) in conferring an appreciable resistance against the effects caused by artificial aging on a given bitumen. Both neat and aged bitumens were analyzed and compared to analogous samples modified with HR. Control samples containing a vegetable oil as softening agent were also tested for comparison. The tested samples were subjected to a second aging cycle. Structural differences between the samples were carried out through an inverse Laplace transform of the NMR spin-echo decay ($T_2$) and self-diffusion measurements by pulsed gradient spin echo nuclear magnetic resonance (PGSE-NMR) spectroscopy. In addition, dynamic rheological analyses were conducted to determine the dependence of the gel-sol transition temperature on both the type of additive and ageing process. The present study clearly highlighted the fact that artificial ageing, realized here by the rolling thin film oven test (RTFOT) and the pressure ageing vessel (PAV) test, induced important structural modifications. The analysis of relaxation times and self-diffusion coefficients indicated that ageing promoted the formation of molecular populations characterized by a shift of the distribution toward higher molecular weights compared to unaged bitumen. Diffusion data showed also an Arrhenius-like temperature dependence. A correlation between all the data was

* Corresponding authors.
*E-mail addresses:* paolino.caputo@unical.it (P. Caputo), michele.porto@unical.it (M. Porto).

https://doi.org/10.1016/j.colsurfa.2020.125182
Received 20 April 2020; Received in revised form 13 June 2020; Accepted 15 June 2020
Available online 16 June 2020
0927-7757/ © 2020 Elsevier B.V. All rights reserved.

attempted to understand the role of the investigated additives. The eco-friendly biocompatible rejuvenator helped not only to restore the structure of the aged bitumen, but even slowed down the processes of a second aging (aiming at the first aged sample).

## 1. Introduction

One of the phenomena most responsible for the deterioration of the performance of road surfaces in the bituminous conglomerate is the oxidation of the binder, which occurs both during installation and throughout the lifetime of the road pavement [1]. Furthermore, in recent decades, the increase in traffic and the need to economically and ecologically dispose of material from old road pavements have led to searching for new materials and methods for recycle the road surface. Nowadays, one of the most important concern is the production of waste. The scientific community is working to make waste products recirculated. When aging, wear and adverse climatic events make the asphalts no longer safe, so the pavement must be replaced after a certain time in use [2]. The scarifying of the road surface produces the reclaimed asphalt binder, which is often regarded as a waste to dispose of. Fortunately, the waste asphalt mixture still contains valuable asphalt binder. The aged bitumen from this reclaimed asphalt pavement (RAP), has a lower penetration degree and is more viscous than when all pristine components are used [3]. However, the effect of aging can be delayed by using rejuvenating agents that have a distinct role from common softening agents [4]. Indeed, it is known by now that it is possible to exploit RAP using a rejuvenator capable to reduce stiffness, viscosity, brittleness, and restore the right balance between asphaltenes and maltenes characteristic of unaged bitumen.

Considering the accelerated aging methods, by aging thin films of bitumen in an oven at 163 °C, the rolling thin film oven test (RTFOT) simulates short-term aging in the laboratory that represents aging before the material is placed in the road [5]. The pressure aging vessel (PAV) uses temperature of 90–110 °C and a pressure 2.10 MPa to simulate long-term aging in the laboratory [6].

According to the classical colloidal model of bitumen, its general composition can be broadly subdivided into higher molecular weight asphaltenes dispersed in lower molecular weight maltenes, the latter being the n-heptane soluble part of bitumen, sometimes called deasphaltened bitumen [7]. Those class of compounds, collectively indicated as SARA (saturates, aromatics, resins and asphaltenes) fractions, are characterized by different sizes, aromaticity, and polarity, which can be hardly analysed individually [8]. Asphaltenes form a black powder and decompose when heated above 350 °C. The asphaltene fraction consists of large molecules containing hetero atoms like oxygen, nitrogen, sulphur and metal atoms. Resins are a black solid at room temperature and liquefy at higher temperature whereas saturates are a colourless viscous liquid, the amount of which (5 − 20 wt%) is not altered during ageing. Aromatics or naphthene aromatics appear yellow to dark brown, they constitute 30 − 60 wt% of bitumen and are more viscous than saturates. Their average molecular weight is of the order of a few thousands of Da and the averaged structure is composed by lightly condensed aromatic and naphthenic rings with side chains. All these ingredients are organized in supra-molecular assemblies whose structure resembles that of reversed micelles: clusters of asphaltene molecules piled in stacks (polar domains) are stabilized by resins (amphiphilic part) and dispersed in saturates and aromatics (apolar matrix). The role of resin is essential in the delicate equilibrium of intermolecular interactions (polar-polar, polar-apolar and van deer Waals interactions) which holds up the overall structure, since amphiphilic molecules are well-known to bind from a side the polar molecules clusters and from the other side the apolar phase [9,10].

In this framework, the chemical reactivity towards oxidation processes and loss of volatile hydrocarbons activated by heat, lead to a significant change in composition within the SARA fractions characterized by an increasing content of asphaltenes and decreasing content of aromatics during ageing, [11–14]. Moreover, due to oxidative aging, the molecular interactions change as well. The combined effect of these two processes affects the mechanical performances of bitumen and asphalt mixture behaviour [15]. As a consequence, insights on the microstructure evolution over the strength of oxidative treatment (steric hardening) could be monitored by measuring molecular dynamic properties such as NMR relaxation times and self-diffusion coefficients [16–18]. On the other hands, changes in bulk rheological properties, such as viscosity and sol-gel transition temperature turn to be useful for verifying the effect of age hardening and for controlling the rejuvenating action of specific additives [19,20].

The present paper aims to investigate the ability of the green rejuvenator HR, developed by the academic Spin-Off Kimical SRL (University of Calabria, Italy), to compensate for the microstructural deterioration effects observed in a bitumen subjected to multiple artificial aging processes. This study is important to understand the rejuvenating effect of a green additive specially designed to reduce the disposal of aged asphalt and promote sustainable practices for the recycling of reclaimed asphalt binder. Therefore, the potential use of HR in increasing the useful life cycle of the RAP is deeply described.

To highlight the real rejuvenating effect, control samples containing a vegetable oil (flux oil) were also tested.

All the bitumens were characterized by rheological time cure tests and NMR techniques such as proton relaxometry and measurements of self-diffusion coefficients. The inverse Laplace transform to the spin-echo decay ($T_2$) was carried out.

## 2. Experimental

### 2.1. Chemicals and materials

A pristine bitumen with a penetration grade 100/130 produced in Kazakhstan and supplied by Kazakhstan Highway Research Institute (Almaty, Kazakhstan) has been tested in this work. The vegetable oil VO and the rejuvenator eco-friendly additive HR were provided by Kimical SRL (Rende, Italy). HR was prepared by a direct reaction between low cost and green materials such as oleic acid and urea [21].

### 2.2. Sample preparations

Samples with differently ageing treatments, with or without VO and HR additives, were produced to allow a direct comparison of results. The analysed samples were initially subjected to artificial aging consisting of RTFOT + PAV according, respectively, to the standard methods ASTM D2872-04 and AASTHO/ASTM T179. Subsequently, the bitumen thus obtained was heated and mixed with the selected additives for 10 min under mechanical stirring. Finally, the samples were subjected to a further PAV aging cycle. For various states and aging conditions KB means virgin bitumen; KP and KPP mean, respectively, bitumen aged with the first treatment of RTFOT + PAV and subsequently subjected to a second PAV aging; KVO and KVOP mean, respectively, bitumen modified with VO (2 wt%) after being aged with RTFOT + PAV, and subjected to a second PAV treatment; KHR and KHRP mean, respectively, bitumen modified with HR (2 wt%) after being aged with RTFOT + PAV, and subjected to a second PAV treatment. A second series of samples consisted of maltene fractions (deasphaltened bitumens) extracted from the correspondent whole samples. In the text $(KB)^M$ means the maltene fraction extracted from KB sample; $(KP)^M$ and $(KPP)^M$ mean the maltene fractions extracted from samples

KP and KPP, respectively, and so on. The dosage of 2 wt% of additive was chosen according the literature data. In fact, it is a typical percentage for the modification of the bitumen [22]

#### 2.2.1. Aging

The bitumen samples were artificially aged by means of the Rolling Thin Film Oven Test (RTFOT) according to ASTM D1754 with thermal treatment for 5 h at 163 °C, followed by 20 h of a pressure aging vessel PAV test according to ASTM D6521 (at 100 °C, 2.1 MPa). Details of the RTFOT and PAV method of aging is based on a previous research work done by the authors [21]. This procedure should mimic the aging process that would take place during the hot mixing of asphalt binder with aggregates, followed by the pavement construction phase and then the in-service life of asphalt pavement.

### 2.3. Empirical characterization

The bitumen softening temperature (R&B T, ring and ball temperature) is determined with the ring and ball test (ASTM Standard D36).

The bitumen consistency was evaluated by measuring the penetration depth (of a stainless-steel needle of standard dimensions under determinate charge conditions (100 g), time (5 s) and temperature (25 °C), according to the standard procedure (ASTM D946).

### 2.4. Rheological characterization

Temperature sweep (time cure) rheological characterization of the samples was performed by means of sinusoidal oscillatory experiments conducted through a controlled shear stress rheometer (SR5, Rheometric Scientific, USA) equipped with a parallel plate geometry (gap 2 mm, ø = 25 mm) and a Peltier system ( ± 0.1 °C) for temperature control. In a temperature sweep test, the frequency and the oscillation amplitude were kept constant, while the temperature was increased in some progression. The analysis of the mechanical behaviour of the selected binders was carried out within the Linear Visco-Elastic (LVE) region by measuring the complex modulus G* and viscosity η* and phase angle δ as a function of the temperature in the range 25–120 °C with a ramp of 1 °C/min and constant frequency of 1 Hz.

### 2.5. NMR measurement and inverse laplace transform (ILT)

The method is based on the application of the Carr-Purcell-Meiboom-Gill (CPMG) spin-echo pulse sequence as described in ref. [23]. $^{1}$H NMR relaxation experiments were conducted at 15 and 30 °C both below and above the gel-sol the transition temperature (t*) determined for each sample through dynamic temperature ramp tests. Relaxation experiments were carried out by means of a custom-built NMR instrument that operates at a proton frequency of 15 MHz. In general, two peaks corresponding to $T_2$ relaxation time distribution can be observed, one peak at shorter $T_2$ times corresponding to the more rigid (asphaltenes), while other one at longer $T_2$ times corresponding to the maltene fraction. This finding has been proved in several research works. All details of the experimental procedure can be found in the following references [24–26].

### 2.6. PGSE NMR self-diffusion

The Pulsed Gradient Spin Echo (PGSE) NMR experiments performed on a Bruker 300 spectrometer have been described in detail elsewhere. The magnetic field gradient unit is electronically controlled and produces gradients $g$ between 0 and 10 $T{\cdot}m^{-1}$ (0 and 1000 $G{\cdot}cm^{-1}$) with typical duration δ of 2 − 4 ms, and a diffusion observation time Δ typically of 20 − 30 ms. Experimental measurements of the self-diffusion coefficient ($D$) directly were made using a Diff30 NMR probe. The experiments were run in the PFG-STE (Pulsed Field Gradient Stimulated-Echo) echo version, using three 90° radio frequency pulses [17], because the transverse relaxation time ($T_2$) was much shorter than the longitudinal relaxation time ($T_1$). In an experimental run, δ and δ are kept constant and $g$ is varied. Sixteen different values for $g$ give 10 signal intensities measured as the area, after Fourier transformation of the free induction decay (FID) that are fit to the Eq. (4) to determine the mean self-diffusion coefficient, $\langle D \rangle$.

## 3. Results and discussion

### 3.1. Mechanical behaviour

The aging of the bitumen leads to an embrittlement of the binder, making it susceptible to fractures or cracking. From a microscopic point of view, the aging process leads to a loss of oily bitumen components,

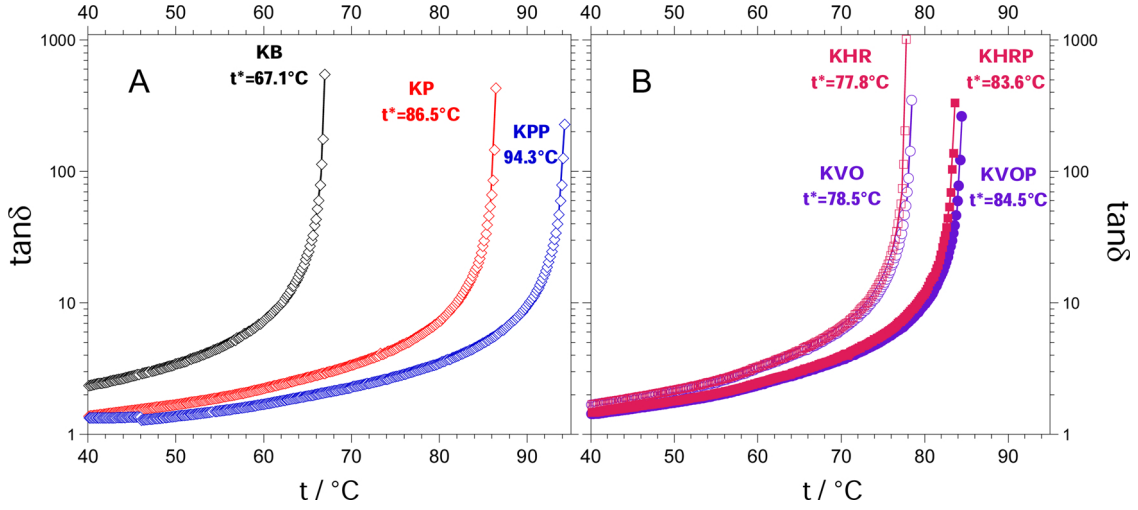


**Fig. 1. (A)** Temperature sweep (time cure) tests performed on the pristine bitumen (KB) and on the same sample after a first (KP) and second cycle (KPP) of artificial aging. The gel-sol transition temperature t*, estimated from the asymptotic value of the tangent of phase angle δ, is reported close to each curve. **(B)** Time cure tests for bitumens modified with 2 wt% of rejuvenating HR (hollow and full squares for KHR and KHRP, respectively) and softening VO (hollow and full circles for KVO and KVOP, respectively) additives. Hollow symbols indicate samples subjected to RTFOT + PAV aging whereas full symbols refer to the subsequent second PAV treatment. The gel-sol transition temperature t* is reported close to each curve.

due to the volatility or absorption by the porous aggregates. In addition, polar compounds increase due to polar groups containing oxygen. This is the cause of a loss of mobility on the part of molecules or molecular aggregates, which are no longer free to flow one on top of the other [27]. From the macroscopic point of view, a decrease in penetration depth is observed, while the softening point increases [28]. Moreover, the viscoelastic-liquid transition temperature increases with the aging process. In this research the dynamic material properties of bitumen samples have been tested through dynamic shear rheometer (DSR) analysis. The response to a mechanical stress-strain on materials such as bitumen are characterized by their elastic (G') and viscous (G") moduli. The loss factor tanδ is defined as the ratio between the viscous G" and elastic moduli G'. All these parameters depend on the temperature, in fact as the temperature increases tanδ increases too and diverges upon reaching a certain critical temperature value, called gel-sol transition temperature t*. This trend is due to the loss of the elastic component G' by the system, and consequently the viscous component G" becomes predominant. Fig. 1A and B show the time cure tests of the investigated samples in which the dependence of tanδ on the temperature is evident. In particular, t* shifts towards higher values along the sequence: untreated bitumen, bitumen aged by the first heating treatment (RTFOT + PAV) and bitumen aged by the second heating treatment PAV. Resins can be more polar than asphaltenes and govern the rheological properties together with asphaltenes [29]. Therefore, upon ageing, the bitumen is oxidized and as a consequence the polarity of the medium increases leading to increased interaction forces between the molecules. These conditions would favour the aggregation of asphaltenes by forming large molecular structures and causing a considerable hardening of the binder. As illustrated in Fig. 1A for bitumen not modified with additives, ageing causes a shift of t* towards higher temperatures, indicating a change in rheological behaviour which consists in a stiffness increase accompanied by an enhancement of elastic response (see the sequence KB→KP→KPP).

In Fig. 1B, the time cure tests for KHR and KHRP bitumens mixed with HR additive are compared to those modified with the softening agent VO (KVO and KVOP) at same 2 wt% dosage.

It is evident that both the one-step (KHR and KVO) and second-step (KHRP and KVOP) ageing treatments yield a similar rejuvenating effect since both additives are able to reduce t* by 8 − 9 °C and 10 − 11 °C in relation to the first (KP) and second (KPP) aging step, respectively.

### 3.2. NMR study

#### 3.2.1. Diffusion coefficient

PGSE NMR self-diffusion measurements have been carried out for both the series of whole samples and maltene fractions, after one- and two-steps oxidative artificial treatments, to evaluate the effect of a rejuvenator additive on the observed molecular translational motion. We premise that the molecular species that contribute to the observed average self-diffusion coefficients and transversal relaxation times should be identified in the lighter components of the maltene fraction [30]. Previous studies have reported that a significant amount of the latter class of compounds tends to decrease with aging, converting to more polar and heavier molecules such as resins and asphaltenes [12,14,31]. Other works have revealed that after short- and long-term aging the content of resins in the bitumen remained practically constant whereas the oil content reduced up to 7 wt% and concomitantly the increase in asphaltenes content could reach about 6 wt% [32]. Therefore, the contribution to the observed translational diffusion can be reasonably attributed to the mobility of the oil components of maltene, namely, saturates and aromatics, which are liquid at the experimental temperatures in the range 60 − 120 °C whereas resins and asphaltenes constitute solid nuclei embedded in the oil. Owing to the molecular complexity of maltene, the correspondent NMR echo attenuation cannot be described by a single exponential function. Indeed, an exact explicit solution of the Bloch-Torrey equation is only available for unrestricted diffusion in the whole space for which the echo attenuation NMR signal *S(b)* takes the classical mono-exponential form [33]:

$$S(b) = S_0 e^{-bD} \tag{1}$$

where $S_0$ is the reference signal (without diffusion-weighting gradient), and the *b*-value is defined as $b = (\gamma g \delta)^2(\Delta - \delta/3)$ according to the Stejskal-Tanner profile, where $\Delta - \delta/3$ is the observation time. Varying either the gradient pulse strength (g) or pulse duration (δ) or Δ, one can access the diffusion coefficient *D* of freely diffusing molecules from the slope of a semi-logarithmic representation of Eq. (1). Any deviation from the mono-exponential decay of *S(b)* may be interpreted in terms of a phenomenological anomalous diffusion model [34]. Generally, the echo attenuation shows non-linear behaviour for molecules with a large degree of polydispersity. For polydisperse species which cannot be resolved due to their chemical shift, it is assumed that the signal attenuation is multi-exponential as a result of the mass-weighted distribution of diffusion coefficients.

Here, we apply a model where the *D*-values are distributed according to the following probability density function:

$$P_{\Gamma}(D, \kappa, \theta) = \frac{D^{\kappa-1}}{\theta^{\kappa}\Gamma(\kappa)} e^{-\frac{D}{\theta}} \tag{2}$$

where κ and θ are, respectively, the shape and scaling parameters and Γ is the Gamma function. Previous works [35,36] have discussed the usefulness of the Gamma model with regard to performance and consistency for the analysis of PFG NMR data, in comparison to more established approaches based on the stretched exponential and the log-normal distribution model. Assuming that *S(b)* can be described by an integral over a multi-exponential decay with self-diffusion coefficients *D* that respect the probability distribution of Eq. (2), one would have the following:

$$S(b, \kappa, \theta) = S_0 \int_0^{\infty} P_{\Gamma}(D, \kappa, \theta) e^{-bD} dD \tag{3}$$

where $S_0$ is the signal intensity for $b = 0$. As described in details in ref. [35], the analytical expression of the NMR signal attenuation can be obtained in a closed form to be used directly in a non-linear best-fitting

**Table 1**
Mean self-diffusion coefficient $\langle D \rangle_{t°C}$ and standard deviation $\sigma_{t°C}$ for whole samples at various temperatures, calculated from non-linear fits of the NMR echo decays (see Eq. (4)) according to the gamma distribution model. Data are expressed in $10^{-10}$ units. The last column shows the transition temperatures derived from rheological time cure tests. Legend: KB = pristine bitumen; KP = RTFOT + PAV bitumen; KVO = KP + VO (2 wt%); KHR = KP + HR (2 wt%); KPP = RTFOT + PAV aging, followed by a second PAV treatment; KVOP = KVO subjected by a second PAV; KHRP = KHR subjected by a second PAV.

| whole sample | $\langle D \rangle_{60°C}/\sigma_{60°C}$ | $\langle D \rangle_{80°C}/\sigma_{80°C}$ | $\langle D \rangle_{100°C}/\sigma_{100°C}$ | $\langle D \rangle_{120°C}/\sigma_{120°C}$ | $t_{gel \rightarrow sol}$ (°C) |
|---|---|---|---|---|---|
| KB | 2.3 / 1.0 | 2.5 / 1.1 | 4.0 / 2.0 | 7.1 / 3.8 | 67.1 (0.1) |
| KP | – | 2.0 / 1.1 | 3.5 / 2.0 | 6.5 / 3.9 | 86.5 (0.1) |
| KVO | – | 1.7 / 1.2 | 3.7 / 2.2 | 7.1 / 4.5 | 78.5 (0.1) |
| KHR | – | 2.4 / 1.1 | 4.0 / 2.1 | 7.5 / 4.5 | 77.8 (0.1) |
| KPP | 2.5 / 1.1 | 3.8 / 1.5 | 5.9 / 2.6 | – | 94.3 (0.1) |
| KVOP | 1.0 / 0.7 | 1.7 / 1.2 | 3.6 / 5.2 | 9.1 / 12 | 84.5 (0.1) |
| KHRP | 2.1 / 0.8 | 3.1 / 1.3 | 5.3 / 2.6 | 8.9 / 4.9 | 83.6 (0.1) |

procedure with respect to the experimental data:

$$S(b, \kappa, \theta) = \frac{S_0}{(1 + \theta b)^{\kappa}} \quad (4)$$

Then, from the calculated best-fit parameters, namely, κ (dimensionless) and θ ($m^2s^{-1}$), the mean self-diffusion coefficient $\langle D \rangle = \kappa\theta$ and the distribution width or standard deviation $\sigma = \theta\sqrt{\kappa}$ can be obtained. Tables 1 and 2 collect both $\langle D \rangle$ and $\sigma$ at various temperatures and referred, respectively, to the whole samples and to their correspondent maltene fractions. In Supporting Material, several plots showing the temperature dependence of $\langle D \rangle$ together with error bars correspondent to the width of distributions $\sigma$, have been collected for a better comparison between diffusion data illustrated in Tables 1 and 2.

Regarding the analysis of the echo attenuations, typical examples of the good agreement between NMR PFG signals and Gamma diffusion model are illustrated in Fig. 2 (whole samples) and Fig. 3 (maltene fractions), respectively. By comparing the data shown in Table 1 with the ones in Table 2, it is found that $\langle D \rangle < \langle D \rangle^M$ for all the samples at each explored temperature, with the exception of KHRP and $(KHRP)^M$ at t = 60 °C. This is the evidence that the molecular transport of oil within the whole bituminous samples is more hindered than the diffusive transport that occurs in the corresponding maltene fractions. It is plausible, in fact, that the diffusivity decreases through more restrictive structural regions such as the large supramolecular aggregates of asphaltenes and resins, which are instead absent in the maltene fractions.

From the analysis of diffusion data within the series of whole samples without additives, it can be noted that the datasets of both the unaged bitumen (KB) and bitumen subjected to one-step aging treatment (KP) match substantially the same $\langle D \rangle$ values when considering the width of the respective distributions as error bars ($\sigma_{t°C}$) (see Fig. S1A in Supporting Material). Besides, $\langle D \rangle$ for KPP appear shifted towards higher values with respect to both KB and KPP samples. The latter effect can be explained considering first that with aging, there is a drastic variation in the chemical composition and colloidal structure of the bitumen attributed to an increase in the content of asphaltenes, which in turn is a consequence of the conversion of polar aromatic molecules. During the oxidative ageing process, the concentration of polar functional groups increases, resulting in an immobilisation of large asphaltene molecules through intermolecular association. As it has been described before, this association promotes the formation of much larger molecular agglomerates and significantly increase the apparent molecular weight leading to higher viscosity. Besides, the high molecular weight populations increase slightly after RTFOT and significantly after PAV ageing. This behaviour is confirmed by the probability density profiles of the relaxation time distributions illustrated in the next Fig. 5 (see 3.3.1 NMR relaxometry), where the samples KP and KPP show two peaks shifted toward shorter times, the displacement of the peaks being greater with increasing the aging treatment. This behaviour indicates a gradually rise of the materials rigidity with the on-going of the oxidation process. Therefore, according to the above description, it can be argued that after the second accelerated aging treatment (KPP), the only species that possess high translational mobility and contribute most to the observed molecular transport should be low MW saturated compounds, which are inert to oxidation. However, in both KB and KP (mild aged) samples, the contribution of a significant fraction of larger molecules to the observed diffusional process is not negligible and causes a lowering of the mean diffusion coefficients.

The effect of type of additive on the artificially aged whole samples, can be inferred by comparing the diffusion data of Table 1 as well as by checking the graphical trends as a function of temperature (see Figs. S2A–S3A in Supporting Material). As far as VO additive is concerned, while no appreciable differences can be revealed between KVO, KP and KB, the two-step aging results to a decrease of diffusion data for KVOP sample with respect to the reference KB, especially at relatively low temperatures (KVOP < KB for both $\langle D \rangle_{60°C}$ and $\langle D \rangle_{80°C}$). This fact could indicate a substantial difference between the microstructures of both unaged KB and double-aged KVOP samples. Therefore, VO could not be classified as a real rejuvenating additive.

Different trends are observed for the samples modified with HR (KHR and KHRP) whose diffusion data as a function of temperature are also plotted together with those of virgin bitumen and bitumen aged without additive (KB, KP and KPP) as illustrated in Fig. S3A of Supporting Material. Here, the data for KHR match with those of KB while $\langle D \rangle$ values of KHRP are closer to KB data (compare $\langle D \rangle_{80°C}$ values in Table 1) than the sample without additives and subjected to same aging treatment (KPP). This evidence is consistent with a rejuvenating action exerted by the additive HR, which is able to disperse the large molecular agglomerations produced with the two-step aging, making the colloidal microstructure similar to that of virgin bitumen. Concerning the maltene fractions, data shown in Table 2 (see also the graphs illustrated in Figs. S2B–S3B in Supporting Material), reveal that $\langle D \rangle^M$ values obtained in presence of either VO or HR and relating to both stages of aging, coincide with those of the KP sample. On the other hands, the most evident differences are found for the maltene fractions derived from samples in absence of additives, where the diffusion data follow the sequence KB > KPP > KP (see also Fig. S1B in Supporting Material).

As a final observation, from the calculated standard deviations $\sigma_{t°C}$ of the correspondent Gamma distributions, it is observed that each whole sample shows an amplitude of the dispersion of $\langle D \rangle$ which widens with increasing temperature (see Table 1). A similar behaviour is reflected for $\langle D \rangle^M$ as well (see Table 2).

### 3.3. Temperature dependence

It is evident that the mean self-diffusion coefficients increase with increasing temperature as expected by the temperature dependence of diffusion described by the Arrhenius model. The Arrhenius equation expressed in its logarithmic form is:

$$ln\langle D \rangle = lnA - \frac{E_A}{RT} \quad (5)$$

where $A$ is a pre-exponential factor assumed to be independent of absolute temperature $T$, $E_A$ is the activation energy and $R$ is the gas constant. The agreement to the Arrhenius behaviour within the explored range of temperatures is verified by analysing the semi-log plots of $\langle D \rangle$ *vs* $T^{-1}$ as in Fig. 4A (whole samples) or $\langle D \rangle^M$ *vs* $T^{-1}$ as in Fig. 4B (maltene fraction), respectively.

Due to the multicomponent origin of the self-diffusion coefficients determined for our samples, only mean activation energies $\langle E_A \rangle$ could be calculated from the slope of each Arrhenius plot. In the present context, $\langle E_A \rangle$ may be defined as the energy barrier that should be overcome when the oil component of bitumen (saturates and aromatics) moves from one surrounding environment to the another.

For the whole samples, $\langle E_A \rangle$ varies between 23 and 53 KJ·mol$^{-1}$ whereas for the maltene fractions an average value of 40 ± 2 KJ·mol$^{-1}$

**Table 2**
Mean self-diffusion coefficient $\langle D \rangle^M_{t°C}$ and standard deviation $\sigma^M_{t°C}$ for maltene samples at various temperatures, calculated from non-linear fits of the NMR echo decays (see Eq. (4)) according to the gamma distribution model. Data are expressed in $10^{-10}$ units. Legend: each label identifies the maltene fraction extracted from the correspondent sample.

| maltene fraction | $\langle D \rangle^M_{60°C}/\sigma^M_{60°C}$ | $\langle D \rangle^M_{80°C}/\sigma^M_{80°C}$ | $\langle D \rangle^M_{100°C}/\sigma^M_{100°C}$ | $\langle D \rangle^M_{120°C}/\sigma^M_{120°C}$ |
|---|---|---|---|---|
| $(KB)^M$ | 9.4 / 5.5 | 18 / 9.5 | 29 / 15 | 40 / 20 |
| $(KP)^M$ | 2.0 / 1.8 | 3.7 / 2.5 | 7.9 / 5.2 | 16 / 11 |
| $(KVO)^M$ | 1.7 / 1.5 | 4.5 / 4.0 | – | 16 / 12 |
| $(KHR)^M$ | 2.5 / 2.2 | 4.2 / 2.8 | 8.8 / 6.0 | 17 / 12 |
| $(KPP)^M$ | 3.3 / 2.1 | 7.8 / 4.7 | 15 / 8.2 | 28 / 14 |
| $(KVOP)^M$ | 1.9 / 1.1 | 4.0 / 2.2 | 8.1 / 4.4 | 17 / 8.4 |
| $(KHRP)^M$ | 1.6 / 0.9 | 4.7 / 2.1 | 9.8 / 4.9 | 19 / 8.9 |

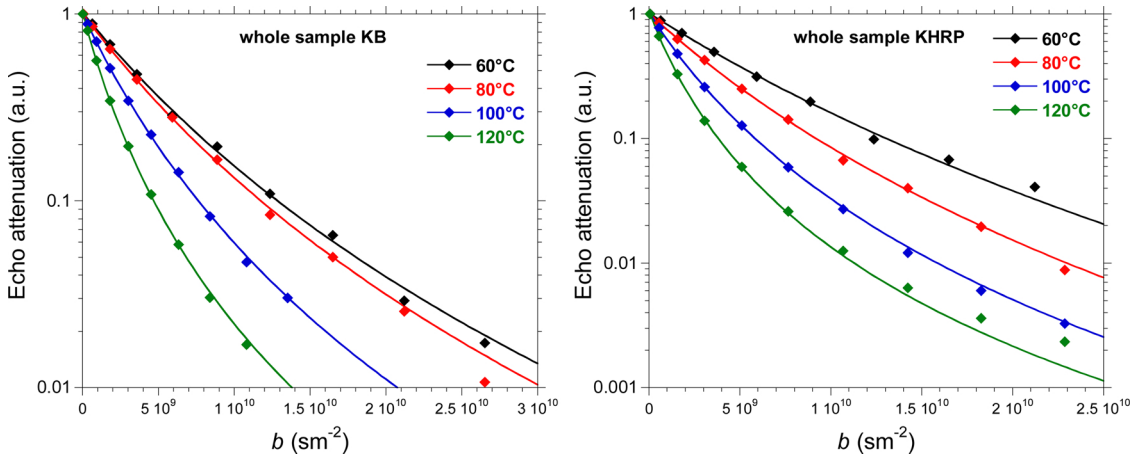


**Fig. 2.** Examples of semi-logarithmic plots of normalized experimental NMR PFG echo attenuations *vs* $b = (\gamma g \delta)^2(\Delta - \delta/3)$, acquired at various temperatures from the whole samples, respectively, KB (left) and KHRP (right). Solid lines represent non-linear best fits ($R^2 > 0.999$) using the Gamma distribution model (see Eq. (4)).

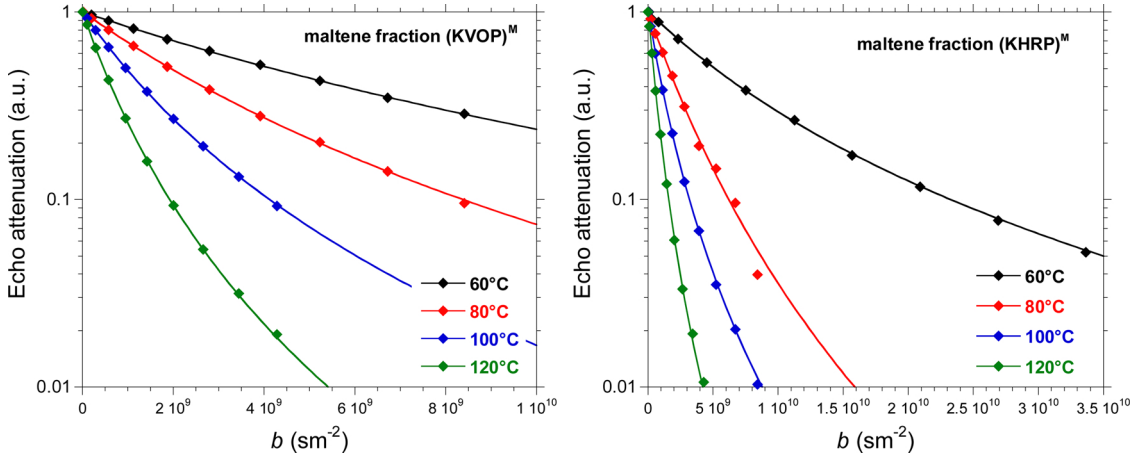


**Fig. 3.** Examples of semi-logarithmic plots of normalized experimental NMR PFG echo attenuations *vs* $b = (\gamma g \delta)^2(\Delta - \delta/3)$, acquired at various temperatures from the maltene fractions, respectively, $(KVOP)^M$ (left) and $(KHRP)^M$ (right). Solid lines represent non-linear best fits ($R^2 > 0.999$) using the Gamma distribution model (see Eq. (4)).

is estimated between all the values except that calculated for the original KB sample, as shown graphically in Fig. 4B by the parallelism of the straight lines. Since the fractions of maltene are devoid of the heavier molecular components, such as resins and mainly asphaltenes, it can be argued that the marked variability of $\langle E_A \rangle$ observed for the whole samples (Fig. 4A) may be attributable to the asphaltene/oil interactions, regarded as the major factor dictating the energy barrier of the diffusion. The rejuvenating effect promoted by the HR additive can

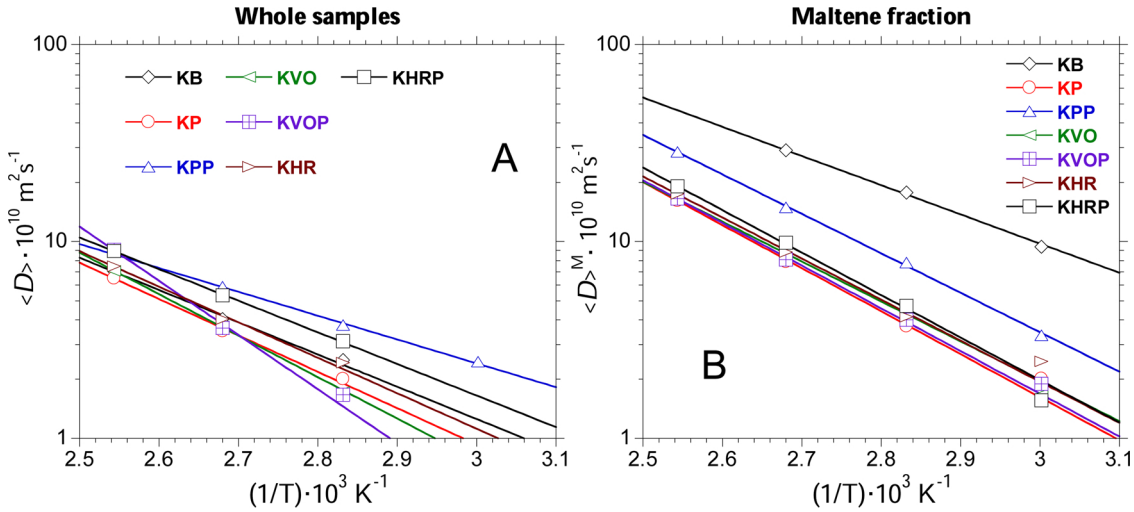


**Fig. 4.** Plot of the logarithm of the mean self-diffusion coefficients *vs.* the reciprocal of the absolute temperature for whole samples **(A)** and maltene fractions **(B)**, respectively. The straight lines were obtained from the Arrhenius fit with Eq. (5) and the mean activation energies were calculated from the respective slopes.

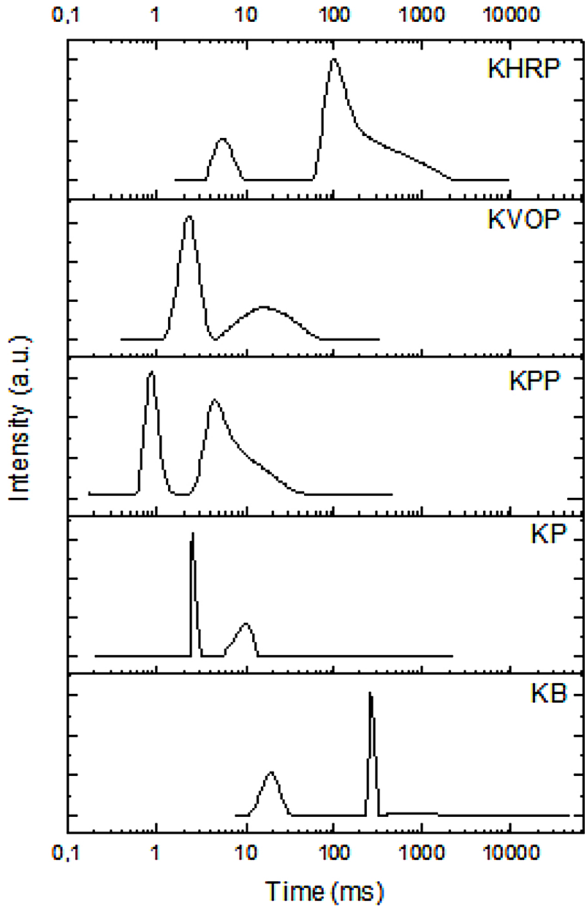


**Fig. 5.** Probability Density Function (PDF) distributions of $T_2$ relaxation times for the whole samples KB, KP, KPP, KVOP and KHRP determined at t* + 15 °C (**C**) where t* is the gel-sol the transition temperature for each sample.

be checked by comparing $\langle E_A \rangle$ of the pristine bitumen KB (31 ± 2 KJ·mol$^{-1}$) with those determined, respectively, for the KHR sample after the first RTFOT + PAV aging (34 ± 3 KJ mol$^{-1}$) and KHRP sample after the second PAV aging process (31 ± 1 KJ mol$^{-1}$). This means that upon artificial oxidation, HR is capable to restore in some way the interactions between the asphaltenic and maltenic phase typical of the unaged bitumen, confirming the clues derived from the diffusion coefficient data. In contrast, bitumen samples modified with the softening agent VO gave 40 ± 1 and 53 ± 4 KJ mol$^{-1}$, after the first RTFOT + PAV (KHR) and second PAV (KHRP) aging treatments, respectively.

In the light of all these results, it can be stated that the effective rejuvenating action exerted by HR with respect to the flux oil, can be interpreted as a consequence of the chemical nature of HR. Thanks to its complex/amphiphilic characteristic, HR would tend to reduce the associative interactions between the asphaltene particles by interposing itself between the asphaltenes and the maltenes. Such phenomenon can be considered similar to that exerted by the rheological modifier polyphosphoric acid (PPA), which has been found able to stabilize the hydrophobic interactions between asphaltene molecules, leading to a reduction of the macro-aggregate sizes [27].

It can be argued, taking for example the self-assembly properties of amphiphilic molecules, that the additive can effectively interact with the resins, competing with them for the interactions with asphaltenes and maltenes. Specific interactions between surfactants can in fact bring to peculiar self-assembly processes [37,38] giving extended amphiphilic network [39,40], which could help in dispersing/stabilizing asphaltene clusters restoring their original distribution.

### 3.3.1. NMR relaxometry

By applying the $^1$H NMR relaxometry technique, the transverse ($T_2$) relaxation times have been determined for the whole bitumen samples subjected to the second PAV ageing treatment (KPP, KVOP and KHRP) as well as for the native bitumen and for the first RTFOT + PAV ageing treatment (KB, KP). In fluid systems, $T_2$ is dominated by molecular rotations and is sensitive to the local dynamics of the molecule that the proton is attached to (spin-spin interactions) and therefore reveals inhomogeneities in the system [41]. For our systems, the NMR echo decays are characterized by a multi-exponential behaviour and have been analysed by applying the Inverse Laplace Transform (ILT) to derive the $T_2$ distributions directly from the experimental signals. Fig. 5 collects the calculated Probability Density Function (PDF) distributions as a function of $T_2$ at a reference temperature characteristic for each of investigated samples, namely, at 15 °C above the gel-sol transition temperature t*.

Almost all the $T_2$ distributions exhibited two variously narrow or wide peaks, which could be ascribed to the more or less rigidity of supramolecular aggregates as well as to the molecular constrain causing dynamic hindrance [42]. In bitumen, supramolecular aggregates of asphaltene and resins possess average sizes of a few nanometers, as observed by several small-angle neutron and X-ray scattering measurements [43,44]. Therefore, the shorter $T_2$ may be reasonably attributed to the rigid supra-molecular aggregates constituted by asphaltenes and resins, while longer $T_2$ could be referred to the rotational dynamics of the lighter components of maltene fraction (saturates and aromatics) [23].

Since the aging process is responsible for shifting the distributions towards higher molecular weights and, that is, towards shorter relaxation times, bitumen modified with the HR agent appeared to benefit from its rejuvenating effect. At higher temperatures above the gel-sol transitions the samples are outside the viscoelastic region of the material and present various structural heterogeneities giving rise to more complicated $T_2$-distribution patterns.

The PDF distribution of the aged bitumens (KP and KPP) shows two peaks shifted toward shorter times, the displacement of the peaks being greater with increasing the aging process. This behaviour indicates a gradually rise of the materials rigidity with the on-going of the oxidation process.

The effect exerted by the two additives, VO and HR, is to move the peaks towards $T_2$ values higher than those of aged bitumens. In more details, the peak attributable to the asphaltenes of the KVOP sample is considerably more intense than that one referred to the maltenes and it is centred on asphaltenic peak of the KP sample. This indicates a softening effect of VO but no rejuvenating action occurs since the huge asphaltene peak does not change. On the other hand, KHRP and KB bitumen have similar distribution profiles. This indicate a sort of antioxidant effect of HR additives.

## 4. Conclusions

In this paper, the dynamic properties of bitumen samples subjected to different artificial aging processes have been tested through dynamic shear rheometer (DSR) analysis, NMR relaxometry and NMR diffusion measurements. The aim of this study was to develop a fundamental understanding on the role played by a rejuvenating green additive (HR) to compensate for the microstructural deterioration effects observed in a bitumen subjected to multiple artificial aging processes. Analogous control samples containing a softening agent (VO) were also tested as term of comparison between the performances exhibited by both the additives. The measurements of bulk rheological properties, such as viscosity and sol-gel transition temperature, were not sufficient to identify the real functionality of an additive. In fact, according to the rheological profiles, both the tested additives were found equally capable of counteracting the bitumen hardening induced by ageing processes.

NMR methodologies employed for investigating translational diffusion coefficients and relaxation times have been found useful to differentiate between the rejuvenating and antioxidant effect of HR compared to the mere fluxing effect of VO. Indeed, the analysis of the temperature dependence of diffusion data gave the indication that in response to artificial oxidation, HR was capable to restore somehow the interactions between the polar asphaltene molecules and maltene phase, typical of the unaged bitumen. As a consequence, a more efficient dispersion of large macro-molecular aggregates produced during the aging treatments was achieved for bitumen mixed with HR rather than VO. That property was confirmed by analysing the Probability Density Function (PDF) distributions acquired through Inverse Laplace Transform, as a function of relaxation times $T_2$ at a reference temperature above the gel-sol transition temperature t* characteristic for each of investigated samples. Indeed, the presence of HR in aged bitumen promoted a certain downsizing effect of the asphaltenes aggregates, identified by an evident shift of relaxation times to longer values. Such effect was not detected in the profile of the relaxation time distributions for aged samples in presence of VO, indicating the inability of VO to restore the initial colloidal distribution of bitumen. Overall, the results of the present work reinforce the potential use of the green rejuvenator HR in increasing the useful life cycle of the reclaimed asphalt pavement (RAP) and furnish more reliable and rigorous methodological approaches as useful tools for a correct interpretation of the effective action exerted by this important class of additives for asphalt binders.

## CRediT authorship contribution statement

**Valeria Loise:** Investigation, Conceptualization. **Paolino Caputo:** Data curation, Methodology. **Michele Porto:** Data curation, Methodology. **Bagdat Teltayev:** Supervision. **Ruggero Angelico:** Writing - original draft. **Cesare Oliviero Rossi:** Supervision.

## Declaration of Competing Interest

No affiliations with or involvement in any organization or entity with any financial interest (such as honoraria; educational grants; participation in speakers' bureaus; membership, employment, consultancies, stock ownership, or other equity interest; and expert testimony or patent-licensing arrangements), or non-financial interest (such as personal or professional relationships, affiliations, knowledge or beliefs) in the subject matter or materials discussed in this manuscript.

## Appendix A. Supplementary data

Supplementary material related to this article can be found, in the online version, at doi:https://doi.org/10.1016/j.colsurfa.2020.125182.

## References


[1] O. Sirin, D.K. Paul, E. Kassem, State of the art study on aging of asphalt mixtures and use of antioxidant additives, Adv. Civ. Eng. (2018), https://doi.org/10.1155/2018/3428961.

[2] M.F.C. Van De Ven, K.J. Jenkins, J.L.M. Voskuilen, R. Van Den Beemt, Development of (half-) warm foamed bitumen mixes: state of the art, Int. J. Pavement Eng. (2007), https://doi.org/10.1080/10298430601149635.

[3] M.C. Cavalli, M.N. Partl, L.D. Poulikakos, Measuring the binder film residues on black rock in mixtures with high amounts of reclaimed asphalt, J. Clean. Prod. (2017), https://doi.org/10.1016/j.jclepro.2017.02.055.

[4] V. Loise, P. Caputo, M. Porto, P. Calandra, R. Angelico, C.O. Rossi, A review on Bitumen Rejuvenation: mechanisms, materials, methods and perspectives, Appl. Sci. (Switzerland) 9 (2019), https://doi.org/10.3390/app9204316.

[5] ASTM, Effect of heat and air on a moving film of asphalt (rolling thin-film oven test), Standard Test Method for Effect of Heat and Air on a Moving Film of Asphalt (Rolling Thin-Film Oven Test), (2004), https://doi.org/10.1520/D2872.

[6] ASTM D6521, Standard practice for accelerated ageing of asphalt binder using a pressurized ageing vessel (PAV), Annual Book of American Society for Testing Materials Standards, (2008), https://doi.org/10.1520/D6521-08.Copyright.

[7] D. Lesueur, The colloidal structure of bitumen: consequences on the rheology and on the mechanisms of bitumen modification, Adv. Colloid Interface Sci. (2009), https://doi.org/10.1016/j.cis.2008.08.011.

[8] J.G. Speight, The Chemistry and Technology of Petroleum, (2006), https://doi.org/10.1201/9781420008388.

[9] P. Calandra, A. Longo, A. Ruggirello, V.T. Liveri, Physico-chemical investigation of the state of cyanamide confined in AOT and lecithin reversed micelles, J. Phys. Chem. B (2004), https://doi.org/10.1021/jp0492422.

[10] P. Calandra, C. Giordano, A. Ruggirello, V.T. Liveri, Physicochemical investigation of acrylamide solubilization in sodium bis(2-ethylhexyl)sulfosuccinate and lecithin reversed micelles, J. Colloid Interface Sci. (2004), https://doi.org/10.1016/j.jcis.2004.04.021.

[11] X. Lu, U. Isacsson, Effect of ageing on bitumen chemistry and rheology, Constr. Build. Mater. (2002), https://doi.org/10.1016/S0950-0618(01)00033-2.

[12] M. Paliukaitė, A. Vaitkus, A. Zofka, Influence of bitumen chemical composition and ageing on pavement performance, Balt. J. Road Bridge Eng. (2015), https://doi.org/10.3846/bjrbe.2015.12.

[13] S. Dessouky, C. Reyes, M. Ilias, D. Contreras, A.T. Papagiannakis, Effect of preheating duration and temperature conditioning on the rheological properties of bitumen, Constr. Build. Mater. (2011), https://doi.org/10.1016/j.conbuildmat.2010.12.058.

[14] V. Mouillet, F. Farcas, E. Chailleux, Physico-chemical techniques for analysing the ageing of polymer modified bitumen, Polymer Modif. Bitumen (2011), https://doi.org/10.1016/B978-0-85709-048-5.50012-2.

[15] J.C. Petersen, A review of the fundamentals of asphalt oxidation (E-C140), Transp. Res. Rec.: J. Transp. Res. Board (2009).

[16] W.S. Price, NMR Studies of Translational Motion, (2009), https://doi.org/10.1017/CBO9780511770487.

[17] R. Angelico, S. Murgia, G. Palazzo, Reverse wormlike micelles: a special focus on nuclear magnetic resonance investigations, RSC Soft Matter (2017), https://doi.org/10.1039/9781782629788-00031.

[18] M. Porto, P. Caputo, V. Loise, B. Teltayev, R. Angelico, P. Calandra, C.O. Rossi, New experimental approaches to analyse the supramolecular structure of rejuvenated aged bitumens, News of the National Academy of Sciences of the Republic of Kazakhstan, Ser. Geol. Tech. Sci. 6 (2019), https://doi.org/10.32014/2019.2518-170X.181.

[19] C.O. Rossi, S. Ashimova, P. Calandra, M.P. De Santo, R. Angelico, Mechanical resilience of modified bitumen at different cooling rates: a rheological and atomic force microscopy investigation, Appl. Sci. (Switzerland) (2017), https://doi.org/10.3390/app7080779.

[20] C.O. Rossi, P. Caputo, S. Ashimova, A. Fabozzi, G. D'Errico, R. Angelico, Effects of natural antioxidant agents on the bitumen aging process: an EPR and rheological investigation, Appl. Sci. (Switzerland) (2018), https://doi.org/10.3390/app8081405.

[21] H. Cui, S. Siva, L. Lin, Ultrasound processed cuminaldehyde/2-hydroxypropyl-β-cyclodextrin inclusion complex: Preparation, characterization and antibacterial activity, Ultrason. Sonochem. (2019), https://doi.org/10.1016/j.ultsonch.2019.04.001.

[22] C. Oliviero Rossi, P. Caputo, V. Loise, S. Ashimova, B. Teltayev, C. Sangiorgi, A new green rejuvenator: evaluation of structural changes of aged and recycled bitumens by means of rheology and NMR, © RILEM (2019), https://doi.org/10.1007/978-3-030-00476-7_28 L. D. Poulikakos et al. (Eds.): RILEM 252-CMB 2018, RILEM Bookseries 20, pp. 177–182, 2019.

[23] P. Caputo, V. Loise, S. Ashimova, B. Teltayev, R. Vaiana, C.O. Rossi, Inverse Laplace Transform (ILT)NMR: a powerful tool to differentiate a real rejuvenator and a softener of aged bitumen, Colloids Surf. A Physicochem. Eng. Asp. (2019), https://doi.org/10.1016/j.colsurfa.2019.04.080.

[24] A. Muhammad, R.B.D.V. Azeredo, $^{1}$H NMR spectroscopy and low-field relaxometry for predicting viscosity and API gravity of Brazilian crude oils – a comparative study, Fuel (2014), https://doi.org/10.1016/j.fuel.2014.04.026.

[25] L. Gentile, L. Filippelli, C.O. Rossi, N. Baldino, G.A. Ranieri, Rheological and H-NMR spin-spin relaxation time for the evaluation of the effects of PPA addition on bitumen Mol, Cryst. Liq. Cryst. (2012), https://doi.org/10.1080/15421406.2011.653679.

[26] P. Caputo, V. Loise, A. Crispini, C. Sangiorgi, F. Scarpelli, C.O. Rossi, The Efficiency of Bitumen Rejuvenator Investigated Through Powder X-ray Diffraction (PXRD) Analysis and $T_2$-NMR Spectroscopy Colloids and Surfaces a: Physicochemical and Engineering Aspects, (2019), https://doi.org/10.1016/j.colsurfa.2019.03.059.

[27] C.O. Rossi, A. Spadafora, B. Teltayev, G. Izmailova, Y. Amerbayev, V. Bortolotti, Polymer modified bitumen: rheological properties and structural characterization, Colloids Surf. A Physicochem. Eng. Asp. (2015), https://doi.org/10.1016/j.colsurfa.2015.02.048.

[28] S. Saoula, K. Soudani, S. Haddadi, M.E. Munoz, A. Santamaria, Analysis of the rheological behavior of aging bitumen and predicting the risk of permanent deformation of asphalt, Mater. Sci. Appl. (2013), https://doi.org/10.4236/msa.2013.45040.

[29] P. Redelius, H. Soenen, Relation between bitumen chemistry and performance, Fuel (2015), https://doi.org/10.1016/j.fuel.2014.09.044.

[30] P. Caputo, M. Porto, V. Loise, B. Teltayev, C.O. Rossi, Analysis of mechanical performance of bitumen modified with waste plastic and rubber (SBR) additives by rheology and PGSE NMR experiments, Eurasian Chem. J. 21 (2019), https://doi.org/10.18321/ectj864.

[31] M. Le Guern, E. Chailleux, F. Farcas, S. Dreessen, I. Mabille, Physico-chemical analysis of five hard bitumens: identification of chemical species and molecular organization before and after artificial aging, Fuel (2010), https://doi.org/10.1016/j.fuel.2010.04.035.

[32] A.A.A. Molenaar, E.T. Hagos, M.F.C. van de Ven, Effects of aging on the mechanical

characteristics of bituminous binders in PAC, J. Mater. Civ. Eng. (2010), https://doi.org/10.1061/(ASCE)MT.1943-5533.0000021.
[33] G.H. Sørland, Dynamic pulsed-field-Gradient NMR, Springer Ser. Chem. Phys. (2014), https://doi.org/10.1007/978-3-662-44500-6.
[34] R. Angelico, A. Ceglie, U. Olsson, G. Palazzo, L. Ambrosone, Anomalous surfactant diffusion in a living polymer system, Phys. Revi. E - Stat. Nonlinear Soft Matter Phys. (2006), https://doi.org/10.1103/PhysRevE.74.031403.
[35] M. Röding, D. Bernin, J. Jonasson, A. Särkkä, D. Topgaard, M. Rudemo, M. Nydén, The gamma distribution model for pulsed-field gradient NMR studies of molecular-weight distributions of polymers, J. Magn. Reson. (2012), https://doi.org/10.1016/j.jmr.2012.07.005.
[36] N.H. Williamson, M. Nydén, M. Röding, The lognormal and gamma distribution models for estimating molecular weight distributions of polymers using PGSE NMR, J. Magn. Reson. (2016), https://doi.org/10.1016/j.jmr.2016.04.007.
[37] P. Calandra, A. Ruggirello, A. Mele, V.T. Liveri, Self-assembly in surfactant-based liquid mixtures: Bis(2-ethylhexyl)phosphoric acid/bis(2-ethylhexyl)amine systems, J. Colloid Interface Sci. 348 (2010) 183–188, https://doi.org/10.1016/j.jcis.2010.04.031.
[38] P. Calandra, V.T. Liveri, P. Riello, I. Freris, A. Mandanici, Self-assembly in surfactant-based liquid mixtures: Octanoic acid/Bis(2-ethylhexyl)amine systems, J. Colloid Interface Sci. 367 (2012) 280–285, https://doi.org/10.1016/j.jcis.2011.10.015.
[39] P. Calandra, A. Mandanici, V.T. Liveri, Self-assembly in surfactant-based mixtures driven by acid-base reactions: Bis(2-ethylhexyl) phosphoric acid-n-octylamine systems, RSC Adv. 3 (2013) 5148–5155, https://doi.org/10.1039/c3ra23295f.
[40] P. Calandra, I. Nicotera, C.O. Rossi, V.T. Liveri, Dynamical properties of self-assembled surfactant-based mixtures: triggering of one-dimensional anomalous diffusion in Bis(2-ethylhexyl)phosphoric acid/ n -octylamine systems, Langmuir (2013), https://doi.org/10.1021/la403522q.
[41] W.S. Price, Spin Dynamics: Basics of Nuclear Magnetic Resonance, 2nd ed., Concepts in Magnetic Resonance Part A, 2009, https://doi.org/10.1002/cmr.a.20130.
[42] L.L. Barbosa, F.V.C. Kock, R.C. Silva, J.C.C. Freitas, V. Lacerda, E.V.R. Castro, Application of low-field NMR for the determination of physical properties of petroleum fractions, Energy Fuels (2013), https://doi.org/10.1021/ef301588r.
[43] J. Eyssautier, P. Levitz, D. Espinat, J. Jestin, J. Gummel, I. Grillo, L. Barré, Insight into asphaltene nanoaggregate structure inferred by small angle neutron and X-ray scattering, J. Phys. Chem. B (2011), https://doi.org/10.1021/jp111468d.
[44] M.P. Hoepfner, H.S. Fogler, Multiscale scattering investigations of asphaltene cluster breakup, nanoaggregate dissociation, and molecular ordering, Langmuir (2013), https://doi.org/10.1021/la403531w.

applied sciences

MDPI

Article

# NMR Diffusiometry Spectroscopy, a Novel Technique for Monitoring the Micro-Modifications in Bitumen Ageing

**Paolino Caputo [1], Dlshad Shaikhah [2,3], Michele Porto [1,*], Valeria Loise [1,*], Maria Penelope De Santo [4] and Cesare Oliviero Rossi [1]**

1 Department of Chemistry and Chemical Technologies, University of Calabria, 87036 Arcavacata di Rende (CS), Italy; paolino.caputo@unical.it (P.C.); cesare.oliviero@unical.it (C.O.R.)
2 Institute of Functional Surfaces, School of Mechanical Engineering, University of Leeds, Woodhouse Lane LS2 9JT, UK; D.M.Shaikhah@leeds.ac.uk
3 Department of Chemistry, College of Science, Salahaddin University-Erbil, Erbil 44002, Kurdistan
4 Department of Physics and CNR-Nanotec, University of Calabria, via Bucci 31C, 87036 Arcavacata di Rende (CS), Italy; maria.desanto@fis.unical.it
* Correspondence: michele.porto@unical.it (M.P.); valeria.loise@unical.it (V.L.); Tel./Fax: +39-0984492045

Received: 9 July 2020; Accepted: 29 July 2020; Published: 5 August 2020


**Abstract:** In the past three decades, several conventional methods have been employed for characterizing the bitumen ageing phenomenon, such as rheological testing, ultraviolet testing, gel permeation chromatography (GPC), gas chromatography (GC), atomic force microscopy (AFM), X-ray scattering, and Fourier transform infrared spectroscopy (FTIR). Nevertheless, these techniques can provide only limited observations of the structural micro-modifications occurring during bitumen ageing. In this study, Fourier transform nuclear magnetic resonance self-diffusion coefficient (FT-NMR-SDC) spectroscopy, as a novel method, was employed to investigate and compare the microstructural changes between virgin bitumen (pristine bitumen) and aged bitumen. The virgin bitumen was aged artificially using two standard ageing tests: Rolling Thin-Film Oven Test (RTFOT) and Pressure Ageing Vessel (PAV). For a comprehensive comparison and an assessment of the validity of this method, the generated samples were studied using various methods: rheological test, atomic force microscopy, and optical microscopy. Significant differences were obtained between the structure and ageing patterns of virgin and aged bitumen. The results indicate that the modification of maltenes to asphaltenes is responsible for the ageing character. When compared with the other methods' findings, FT-NMR-SDC observations confirm that the asphaltene content increases during ageing processes.

**Keywords:** aged bitumen; NMR diffusiometry; rheology; AFM

## 1. Introduction

The most widely used road material in the world is asphalt. As this product possesses the desired industrial characteristics (waterproof and excellent thermoplasticity), it is widely employed in the construction industry, mainly in road construction and other paved areas [1]. From the chemical point of view, an asphalt is defined as a heterogenous system consisting of macro-meter-sized inorganic particles, known as aggregates, and a binder material called bitumen [2]. Bitumen is a heavy hydrocarbon material, and it is the by-product of the fractural refinement process of crude oil, which removes the lighter fractions (i.e., liquid petroleum gas, gasoline, and diesel) [3].

Traditionally, bitumen is defined as a colloidal system consisting of micelles of high polarity and molecular mass known as asphaltene; these are the solid particles behaving as adhesive aggregates.

Richardson defined the asphaltenes as insoluble in naphtha but soluble in carbon tetrachloride and also introduced the term "carbenes" for the fraction insoluble in carbon tetrachloride but soluble in carbon disulphide [4]. The word "carboids" for the part insoluble in carbon disulphide is also seldom used [5] (although not used by Richardson [4]). In all cases, these two additional fractions are present in very limited amounts in paving-grade bitumen [6] and are generally not mentioned in the road industry. Asphaltene aggregates remain in an oily apolar environment of lower molecular weight, known as maltenes, granting fluidity [7]. The apolar maltene phase, in turn, is composed of saturated paraffins, aromatic oils, and resins. Figure 1 shows a schematic splitting of bitumen into its main components. The proposed model of bitumen in the literature is that the asphaltene, in the form of polar nano-aggregates, remains dispersed as a peninsula or group of peninsulas within a more apolar continuous maltene phase [8]. In the conventional colloidal model, the resins-to-asphaltenes ratio characterizes the bitumen behavior to a specific path if the bitumen is in solution (sol). Sol bitumen is due to a high maltene concentration that leads to rapid relaxation modes (a liquid-like system), while the bitumen is gelatinous (gel) when the asphaltene concentration is dominant, resulting in slow relaxation modes [9].

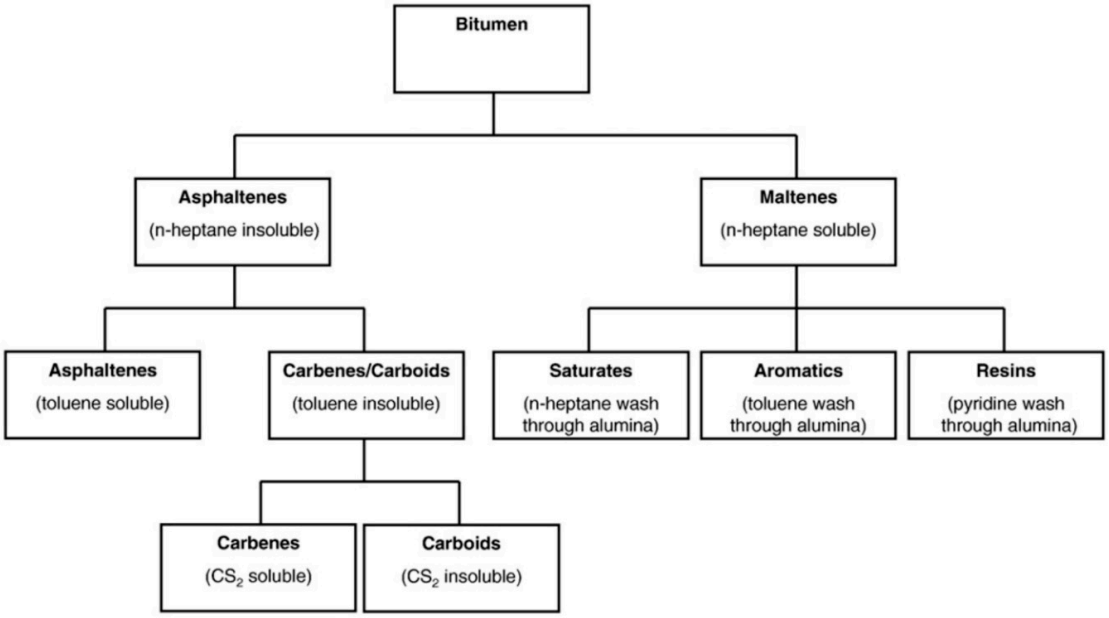


**Figure 1.** Bitumen separation into its various constituents, highlighting the SARA (saturates, aromatics, resins, asphaltenes) distribution, reproduced from [10], Copyright Elsevier, 2020.

In bitumen, resins are the dispersing agents for asphaltene molecules, combining them with aromatics and saturates; this produces the conditions for asphaltic flow. In fact, the chemistry of bitumen is the key element to defining its physical properties: following the analogy with reversed micelles in water-in-oil microemulsions [11], the stabilization of the polar domains is of pivotal importance for determining both the structure and the properties of the overall aggregates of organic-based materials [12,13], even if, it must be pointed out, the stabilization mechanism is quite general, spanning from organic materials to inorganic complexes [14] and even nanoparticles [15]. Due to these strict relationships between intermolecular interactions, the aggregates' structure, and their dynamic properties, the rheology (ductility at a given temperature/frequency) and behavior of bitumen are dependent not only on its structure, but also on the maltene's glass transition temperature and the effective asphaltene content [10].

When it comes to the bitumen structure, the microstructural model offers a typical point of view. It describes the system as a complex solution of evenly distributed molecules, classifying them according to their molecular weight and polarity; these behaviors are the key to grasping whether

the bitumen is modified. As there are millions of such constituents within the bitumen, its chemical analysis is usually performed based on the molecular structure type, not by studying the constituents individually [16]. Any technique, therefore, that differentiates the types of molecules or fractions within narrower properties would be a more effective form of analysis.

The stiffness and viscosity of asphalt pavement and its corresponding bitumen increase with time while it is in service; this is called the ageing phenomenon. As this phenomenon is responsible for the chemical modifications occurring in each fraction of bitumen, it is one of the most important factors impacting the bitumen structure. Asphalt research is currently directed towards the construction of new road pavements using milled reclaimed asphalt pavement (RAP) with consequent advantages both economically and environmentally. To use RAP in a bituminous conglomerate, it is necessary to add additives termed "Rejuvenating". The search for these additives is simply based on the evaluation of their effect on the mechanical performance of the final conglomerate. Having more information on the effect of the bitumen ageing process will make it possible to design these additives by identifying molecules containing functional groups which can interact in a targeted manner with aged bitumen components, thus regenerating them.

Generally, the ageing process is divided into two stages: short-term ageing and long-term ageing [17]. The former results from the loss of volatile components from the bitumen's maltene due to mixing at high temperature in the pristine paving process or during asphalt construction. The latter, in turn, occurs in the field, owing to the following factors: oxidation of bitumen components by atmospheric oxygen, evaporation of low-molecular-weight components of maltene, and polymerization between the bitumen's components. These processes induce greater stiffness and viscosity of the bitumen, which ultimately hardens the material, causing potential cracking and loss of its binding efficiency [16].

In the laboratory, different artificial standard methods for simulating the ageing phenomenon have been introduced. The Rolling Thin-Film Oven Test (RTFOT) and Thin-Film Oven Test (TFOT) techniques are considered short-term ageing as they simulate bitumen ageing during storage, mixing, transport, and placing as pavement. Meanwhile, to simulate long-term ageing, ultraviolet testing (UV) and Pressure Ageing Vessel (PAV) are employed. In this study, RTFOT and PAV are used as short- and long-term ageing simulation techniques, respectively [18].

As the outcome of ageing is crucial, a vast number of studies, using various perspectives and theories, have explored a range of parameters or factors relating to this phenomenon. Different in situ techniques have been used in the laboratory to evaluate, analyze, and identify what actually occurs inside bitumen during the ageing process [9]. These studies or techniques, however, are mainly measuring a specific factor of a material; this raises a challenge to identify all the feasible variables and forms of the material to study the bitumen ageing process, for either short-term ageing or long-term ageing.

The ageing phenomenon impacts not only the rheology of binders but also the structural chemistry; thus, there are numerous techniques to characterize this phenomenon, such as softening point (EN 1427 [19]), penetration test (EN 1426 [20]), and viscosity (EN 13302 [21]). As explained above, the process of ageing causes an increase in stiffness and viscosity but reduces the bitumen penetration grade. Thus, from this point of view, it is feasible to establish an ageing index by measuring the variation of the abovementioned physical properties (before and after ageing). This parameter has proven to be the most exemplary measure with regard to the results observed in the field [22].

It is important to note that assessing bitumen's physical and mechanical properties allows indirect macro-structural analysis of the binder. To measure these properties, the most commonly used techniques are dynamic shear rheology (DSR), softening point test, penetration test, and Brookfield or rotational viscosity determination [9]. Additionally, a variety of perspectives are utilized through a range of evaluation techniques to explain changes in asphalt materials after ageing. These techniques include Fourier transform infrared spectroscopy (FTIR) [23], spectrophotometry [24], X-ray scattering spectroscopy [25,26], gel permeation chromatography (GPC) [27], thin-layer chromatography with

flame ionization detection (TLC-FID) [28], atomic force spectroscopy (AFM) [29] and self-diffusion Pulsed Field Gradient Spin-Echo (PGSE) nuclear magnetic resonance (NMR) [30]. NMR spectroscopy is one of the most authentic and efficient techniques used to characterize complex materials i.e., bitumen. It is a conventional tool in the characterization of synthetic and natural products, wherein the structural and conformational behavior of their flexible molecules are investigated using anisotropic media [31]. In dynamic NMR characterization, the determination of self-diffusion coefficients can provide data about self-assembly [32,33], molecular dynamics, and spatial dimensions of cavities [34] and aggregates [35–38].

In this study, Fourier transform (FT) NMR self-diffusion coefficient measurements were performed on bitumen samples in order to have a better understanding of their molecular mobility and microstructure modification due to ageing; then, the measurements were compared with the results of rheological testing, AFM, and optical microscopy for validation. Ultimately, obtaining more information on the ageing process will provide consequent advantages in the design of rejuvenating additives and in understanding the structural organization of aged bitumen.

## 2. Materials

The pristine bitumen (PB) was kindly supplied by Total Italia S.p.A. (Italy) and produced in Saudi Arabia. It was used as a fresh standard with penetration grade 50/70 as measured by the usual standardized procedure [39]. Essentially, the standard needle is loaded with a weight of 100 g, and the length travelled into the bitumen specimen is measured in tenths of a millimeter for a known time, at a fixed temperature.

The chemical composition of the bitumen in terms of saturates, aromatics, resins, and asphaltenes (SARA) is reported in Table 1.

**Table 1.** Group composition of pristine bitumen.

| Sample | % *w/w* |
|---|---|
| Saturates | 4 |
| Aromatics | 51 |
| Resins | 22 |
| Asphaltenes | 23 |

### 2.1. Sample Preparation

In order to produce simulated short-term and long-term ageing samples, pristine bitumen (PB) was aged artificially via two conventional techniques: Rolling Thin-Film Oven Test (RTFOT) and Pressure Ageing Vessel (PAV). The RTFOT simulation was used for three ageing terms (75 min, 150 min, and 225 min) as per ASTM D2872, whereas the PAV simulation was performed on the virgin binder for a long term as specified in ASTM D6521. The sample IDs of RTFOT-aged binders were adopted based on their ageing time (BRTFOT-75, BRTFOT-150, and BRTFOT-225), while the PAV-aged binder was named BPAV.

### 2.2. Asphaltene and Maltene Separation (Modified Conventional Method)

To perform optical microscopy measurements, asphaltenes were isolated from the bitumen in the manner described elsewhere [40]. Chloroform and n-pentane were used as solvents to separate the maltenes and the asphaltenes.

## 3. Methodology

### 3.1. Rheological Characterization

The performance grades of the binders were determined using a dynamic shear rheometer (DSR) to quantify the viscoelastic properties in the temperature range 25–100 °C. The rheological

measurements were performed by utilizing a shear-stress-controlled rheometer (DSR5000, Rheometrics Scientific, Piscataway, USA), set up with a plate geometry (gap = 2 mm and diameter ∅ = 25 mm). The temperature of the system was controlled by a Peltier system (±1 °C).

Temperature sweep (time cure) rheological tests were performed to analyze the mechanical response of modified bitumens versus temperature. Bitumen exhibits aspects of both elastic and viscous behaviors and is thus classified as a viscoelastic material [41,42]. DSR is a common and standard technique used to study the rheology of asphalt binders at high and intermediate temperatures [43,44].

Operatively, a bitumen sample was sandwiched between two parallel plates, one standing and one oscillatory. The oscillating plate was rotated accordingly with the sample and the resulting shear stress was measured.

During the tests, a periodic sinusoidal stress at constant frequency of 1 Hz was applied to the sample, and the resulting sinusoidal strain was measured in terms of amplitude and phase angle as the loss tangent (tan $\delta$).

All experiments were conducted during the heating of the bitumen sample. The study of rheological characteristics, complex shear modulus, and phase angle was performed in a time cure test (1 Hz) with a heating ramp rate of 1 °C/min. Information on the linear viscoelastic character of materials was provided by small-amplitude dynamic tests through characterization of the complex shear modulus [45]:

$$G^*(\omega) = G'(\omega) + iG''(\omega) \quad (1)$$

where $G^*(\omega)$ is the complex shear modulus, $G'(\omega)$ is the storage (in-phase) component (Pascal, Pa), $G''(\omega)$ is the loss (out-of-phase) component (Pascal, Pa), and $i$ is the imaginary parameter of the complex number. The definitions of the parameters are as follows:

- $G'(\omega)$ represents elastic and reversible energy;
- $G''(\omega)$ represents irreversible viscous dissipation of mechanical energy.

The linear response regime was acquired by reducing the applied stress amplitude for the viscoelastic measurements. All rheological analyses were achieved by applying stress within the viscoelastic region.

### 3.2. Optical Microscopy

A polarized Leica Digital Microscope Light Polarized (DMLP) Research Microscope equipped with a Leica DFC280 digital camera was utilized to track the melting behaviors and morphologies of the asphaltenes. A Mettler FP82 HThot stage with a Mettler FP90 temperature controller was applied to control the temperature profile. The sample was kept at constant temperature, for each investigated temperature, for 10 min before taking images.

### 3.3. Nuclear Magnetic Resonance (NMR) Characterization

NMR characterization was conducted using a Bruker 300 spectrometer. A range of temperatures—from 90 to 130 °C in 10 °C increments—was chosen to conduct NMR experiments to determine the self-diffusion coefficient (D) for each binder.

Using Fourier transform, the acquired NMR spectra were derived from the free induction decay (FID). In Figure 2, a typical $^1$H-NMR spectrum of the bitumen is presented. The number of scans used in the pulsed NMR experiment was 8 with pulse width equal to $\pi/2$. The measurements of D were conducted using a Diff30 NMR probe. As the transverse relaxation time ($T_2$) is much shorter than the longitudinal relaxation time ($T_1$), the Pulsed Gradient Stimulated Spin Echo (PFG-STE) sequence was utilized [46,47]. This sequence comprises three radiofrequency (RF) pulses of 90 ($\pi/2$-$\tau_1$-$\pi/2$-$\tau_m$-$\pi/2$) and two gradient pulses that are performed after the first and third pulse RF. $\tau_1$ and $\tau_m$ are the time

intervals between RF pulses (milliseconds). The echo appears at $2\tau_1 + \tau_m$, and the ECHO amplitude attenuation was derived from the equation below:

$$I\,(2\tau_1 + \tau_m) = I_0 e^{-\left[\frac{\tau_m}{T_1} + \frac{3\tau_1}{T_2} + (\gamma g \delta)^2\ \mathrm{D}(\Delta - \frac{\delta}{3})\right]} \quad (2)$$

where D is the self-diffusion coefficient, and $I$ and $I_0$ are the signal intensities in the presence and absence of gradient pulses. The NMR characterization parameters applied in the experiments to investigate the samples were as follows: $\delta$ (2 ms), the gradient length pulse; $\Delta$, diffusion delay time (30 ms); and $g$, the gradient amplitude (from 100 to 900 gauss/cm). The number of scans increased due to an increment in the number of repetitions. This NMR has a very low fitting standard deviation and good reproducibility of measurements, where the uncertainty of D is approximately 3%.

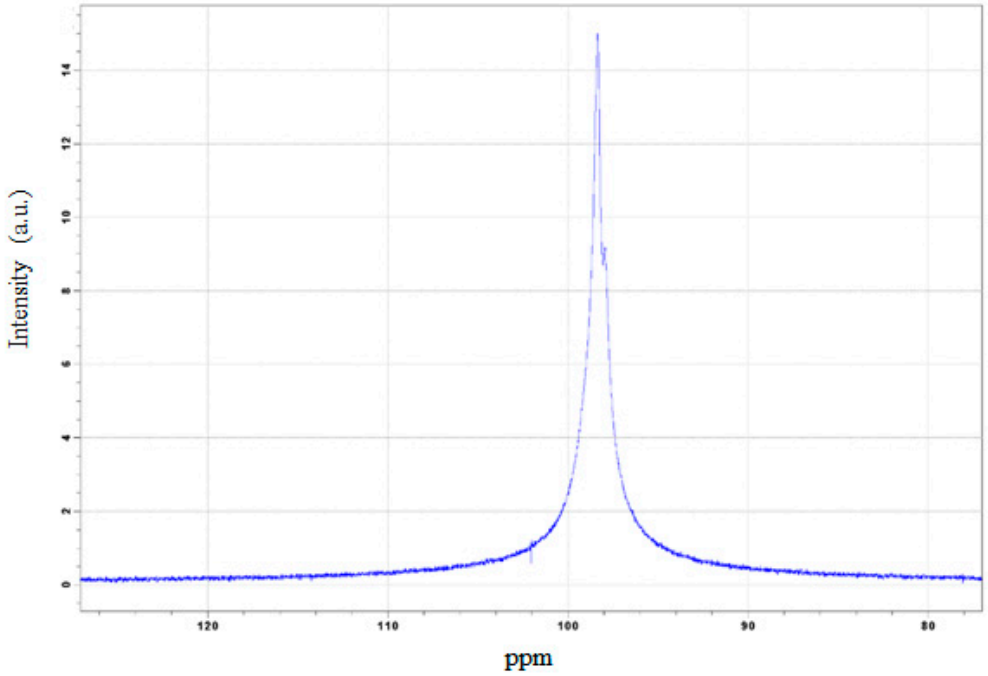


**Figure 2.** FT-NMR spin echo spectrum for the virgin bitumen.

According to the colloidal model, bitumen is generally composed of two principal constituents: asphaltene and maltene. The asphaltene is the rigid and polar part, which is characterized by high melting points. The maltene, in turn, is the soft and oily part that disperses the asphaltenes. Considering the low $T_2$ relaxation times of the asphaltenes [48], the self-diffusion coefficients can be attributed to the oily part of the bitumen; in fact, the NMR signal of asphaltenes relaxes during the pulse's application [49].

### *3.4. Atomic Force Microscopy (AFM)*

Atomic force microscopy (AFM) was carried out using a Nanoscope VIII Bruker microscope which was operated in tapping mode. In this mode, the cantilever oscillates close to its resonance frequency (150 kHz) [50]. Since the cantilever oscillates up and down, the tip is in contact with the sample surface intermittently. When the tip is brought close to the surface, the vibration of the cantilever is influenced by the tip–sample interaction. The shift in the phase angle of the cantilever vibration implies energy dissipation in the tip–sample ensemble, so it depends upon the specific mechanical properties of the sample underlying the tip. For the measurements, cantilevers with elastic constants of 5 N/m and 42 N/m were used. Antimony-doped silicon probes (TAP150A, TESPA-V2, Bruker) with resonance

frequencies 150 kHz and 320 kHz, respectively, and nominal tip radius of curvature 10 nm were used. Phase images were acquired simultaneously with the topography.

## 4. Results and Discussion

### *4.1. Rheology*

The below rheological plots illustrate consistent viscoelastic transition temperature (TR) trends among the binders (see Figures 3 and 4). It is worth noting that at low temperatures, PB shows a higher phase angle value when compared with aged samples; this indicates that PB has lower rigidity. The TR for each of the studied aged binders increased with ageing, which implies an increase in hardness. The effect of ageing on pristine bitumen shifted the TR depending on the duration of ageing; for instance, the TR values of the most-aged binders, BRTFOT-225 and BPAV, increased by approximately 25 °C in comparison with the neat bitumen. The phase angle, tan $\delta$, increased with temperature, signalling a reduction in material consistency, which means that the prevalent liquid-like character is inclined with temperature [41]. In order to have a clearer image of the bitumen TR range and the structural modifications, temperature-sweep experiments were plotted in terms of the elastic modulus $G'$. This experiment was conducted at a frequency of 1 Hz and at a constant heating rate (1 °C/min). The binder's elastic modulus was observed continuously during a temperature ramp.

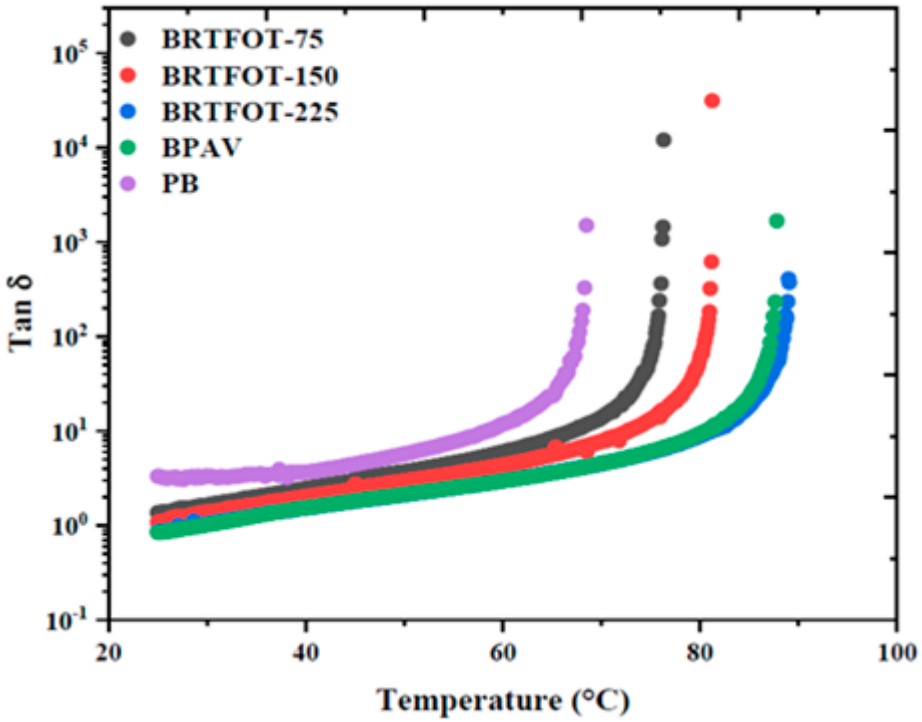


**Figure 3.** Temperature dependence (in the range 25 to 100 °C) of the loss tangent for pristine (PB) and aged bitumen samples (BRTFOT-75; BRTFOT-15; BRTFOT-225 and BPAV).

Figure 4 depicts the elastic modulus $G'(\omega)$ against temperature for all studied samples, in the temperature range 25 to 100 °C. In the temperature range 25–45 °C, the BRTFOT-75 and BRTFOT-150 binders had overlapped $G'(\omega)$ values, meaning their rigidity character is similar. At elevated temperatures, however, the aged binders showed higher $G'(\omega)$ values depending on their degree of ageing. For instance, PB had the lowest $G'(\omega)$ value in correlation with its tan $\delta$ value. After 60 °C for virgin bitumen and after 70 °C for aged binders, nonlinearity tended to appear in the trends, indicating the starting point of the TR region. When the elastic modulus is no longer detected, the transition

process from viscoelastic to a liquid regime can be considered complete, and this proves that the liquid-like behavior increases with temperature.

Interestingly, the viscoelastic responses of the PAV and RTFOT binders show similar rheological behavior. This analysis should prompt thinking that the two kinds of ageing processes (RTFOT 225 and PAV) could have similar effects on the structure and self-assembling properties of the binder.

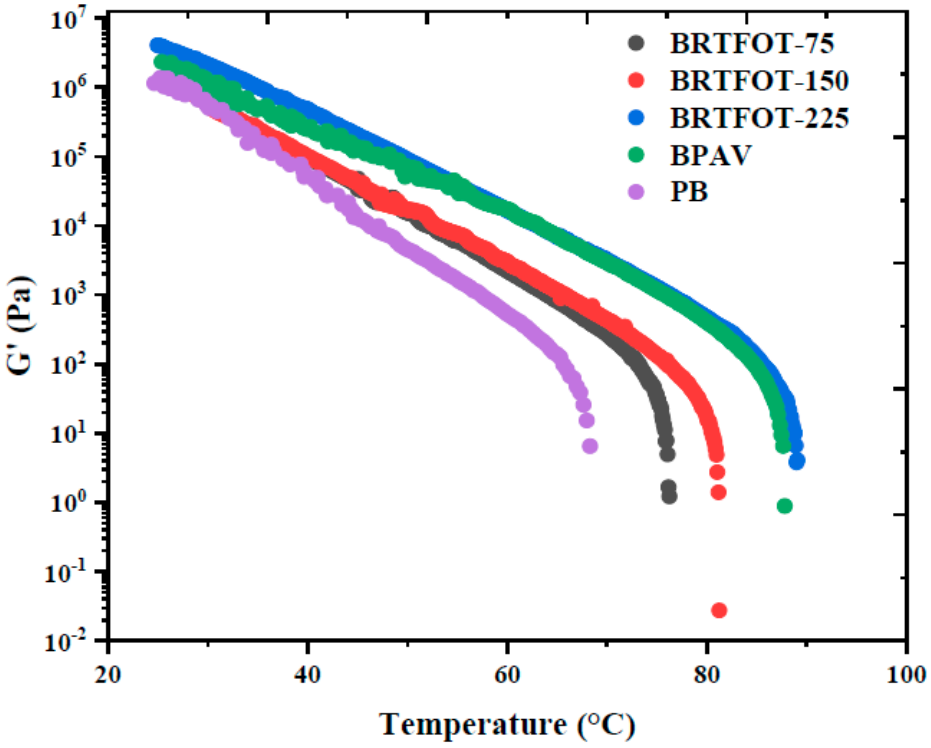


**Figure 4.** Temperature dependence (in the range 25 to 100 °C) of the elastic modulus for pristine and aged bitumen samples.

### *4.2. Optical Microscopy*

The PB and BPAV samples were studied under optical microscopy since they were the softest and hardest samples among the investigated samples. In Figure 5, images of the PB and PAV asphaltenes are presented. The results imply that the BPAV binder is harder than the PB binder due to a higher concentration of asphaltenes.

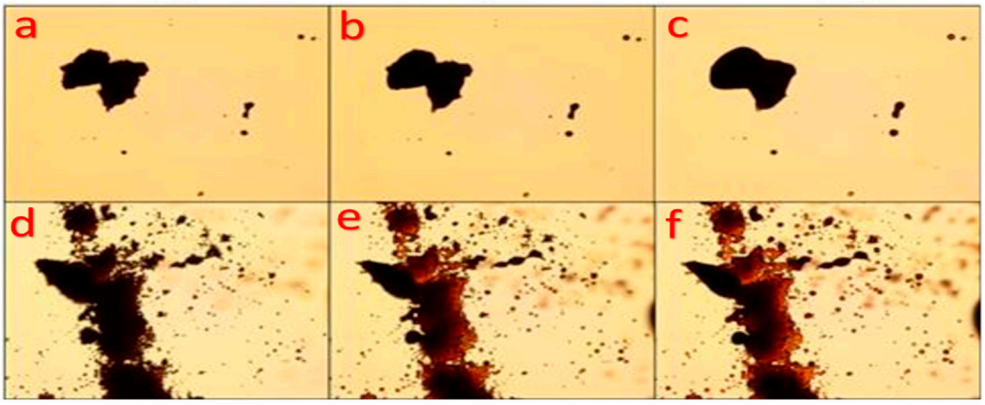


**Figure 5.** Optical microscopy (20×) images of PB (**a**–**c**) and PAV (**d**–**f**) asphaltenes at high temperature.

These images, obtained at 150 (a and d), 160 (b and e), and 165 °C (c and f), show the materials at different crystallization stages. The high-temperature stage of the experiment also shows the melting point of the crystallized material near 160 °C for the PB asphaltenes, while the material is partially melted at 165 °C for the BPAV sample, where the crystals are almost lost.

These novel results reveal two crucial points: First, the asphaltenes are solid at temperatures lower than 150 °C. Secondly, the asphaltene phase of virgin bitumen holds a different assembling structure to aged bitumen.

### 4.3. Fourier Transform NMR Self-Diffusion Coefficient Test

An advanced molecular investigation was conducted using NMR in order to analyze the chemical ageing processes and microstructural modification. As previously mentioned, Fourier transform (FT) NMR self-diffusion coefficient (SDC) allows insight into the bitumen microstructure by detecting the long-range mobility of the mixture constituents. The determination of motion over long distances, in comparison with ideal micelles, provides a sensitive probe for the state of aggregates [47,51]. It is crucial to note that the SDC values of asphaltene molecules cannot be detected owing to the short transverse relaxation times of their protons; so, hereafter, the measured SDC values are related to the maltene phase.

The observation of self-diffusion is based on the mobility of molecules. The motion of these molecules can be hindered due to the obstruction they face during their mobility in media. These typical data, observed where the motion occurs, can be considered as a fingerprint of the microstructural behavior.

In this study, the SDC data for each sample were investigated within the temperature range of 90–130 °C, increasing in increments of 10 °C at a time, as per Figure 6. The SDC data are related to the maltene part since at this temperature the asphaltenes are solid, meaning that their signals are not visible on the NMR spectrum after a spin echo sequence. According to this chart, the SDC values for binders decreased with ageing at each specific temperature. This effect is due to the stronger rigidity in aged bitumen which unavoidably involves stronger intermolecular connectivity when compared to the less dense network of the virgin bitumen, where the asphaltene domains are poorly connected to each other. As a result of this aggregation-based process/modification, a progressive shift from the viscoelastic toward the liquid regime dominating the highest temperatures occurs. In this picture, the resin molecules, due to their amphiphilic nature, will tend to reduce the associative interactions between the asphaltene particles by interposing themselves between the asphaltenes and the maltenes. This phenomenon might be like that found in the deactivation of hydrophobic cross-links in hydrophobically modified polymers by surfactants [43].

The interaction of the apolar part of the resin (its apolar moiety) with the maltene phase drags the latter to more-hindered dynamics typical of the stiffened asphaltene-dominated structure. Another mechanism concurrently present may be the formation of direct interactions between the surfactant polar headgroup and polar parts of asphaltene. In fact, it has been recently highlighted that, in addition to polar and apolar interactions, further specific interactions between surfactants themselves with consequent peculiar self-assembly processes [52,53] dictate the final overall aggregation pattern [54] and the (usually slowed-down) dynamics [55,56]. As an overall result of the two processes above described, maltene molecules in aged binders showed lower SDC values. What remains to be seen is the reproducibility of this gradual difference between virgin and aged binders at even higher temperatures in future experiments. It is worth noting that the BPAV bitumen's SDC value is a little bit higher than that of BRTFOT-225. This result could be due to the different dimensions of the asphaltenes or different structural network morphology. The BRTFOT-225 asphaltenes are expected to be bigger and to provide a strong obstruction to the maltene molecules' mobility. This difference in behavior is also visible in both ageing techniques (RTFOT and PAV). This is an interesting finding, and it could be hypothesized that the FT-NMR-SDC technique can be used to investigate the effects induced by the ageing phenomenon in bitumen. In order to confirm this hypothesis, AFM morphological images

were employed. By raising the temperature, we also observed upward trends in SDC values for all binders; this can be attributed to the incremental liquefying (melting) of the solid constituents, which inclines the motion of molecular protons. Although there was a steady rise in SDC measurements by a degree for each 10 °C increment, they increased dramatically at 130 °C, reaching twice the values of the respective binders at 120 °C. The results mentioned above are the most relevant findings and perhaps the most significant, confirming that the FT-NMR-SDC technique can be utilized as a fingerprint for the characterization of microstructural behaviors of bitumen.

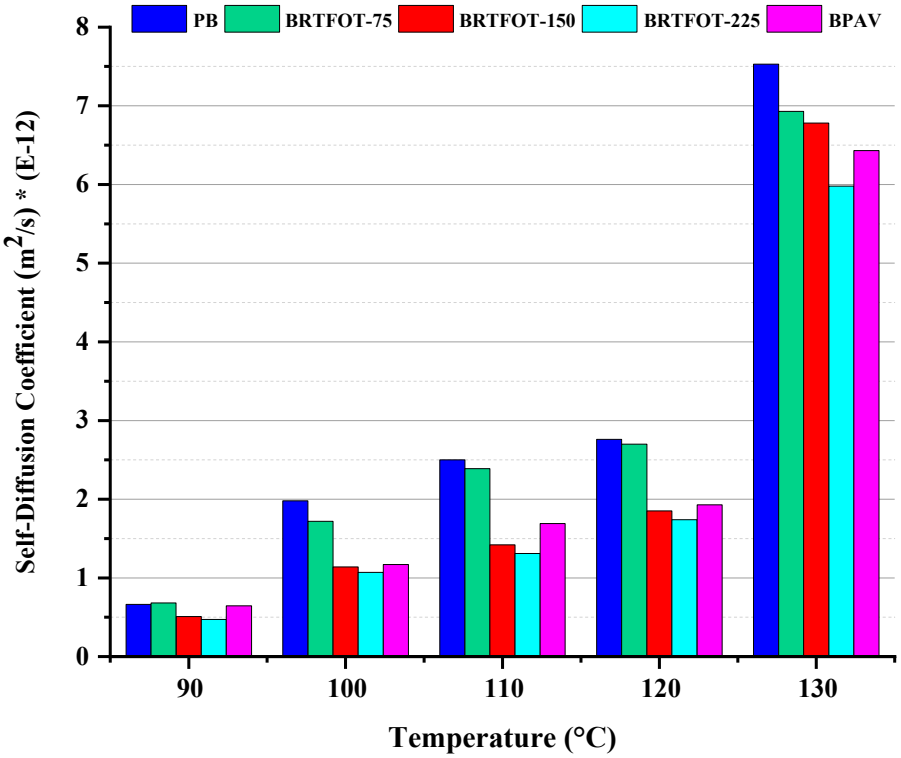


**Figure 6.** NMR self-diffusion coefficient characterization in the temperature range 90–130 °C for the different samples (PB, BRTFOT-75, BRTFOT-150, BRTFOT-225, and BPAV).

### *4.4. Atomic Force Microscopy (AFM)*

AFM has been found to be a useful technique in bitumen microscopic analysis. In this work, we aimed to analyze the AFM images regardless of the correlations between the bitumen structures at different ageing processes in AFM images.

AFM characterization was performed in tapping mode at room temperature in air on a Multimode 8. The AFM system equipped with a Nanoscope V controller (Bruker) provided simultaneous topography and phase imaging of the sample. The measurements of bitumen were performed using probes with a conical tip of nominal end radius 10 nm and a resonance frequency of 150 kHz.

Phase images can show the sample's viscoelastic properties and are useful for bitumen microscopic analysis because materials with different viscoelasticity are clearly distinguishable: soft domains appear dark, while the hard ones appear bright.

The AFM measurements in Figure 7 show that with increasing exposure time (RTFOT), the morphological structure of asphaltenes changes. More specifically, in the aged samples, we note the arising of progressively more oscillations in the AFM signal within each single cluster, a feature which is known as "bee structure" [57] and which denotes structuring of asphaltene clusters at the micrometer-length scale [50]. Moreover, the asphaltene domain size increased with ageing time. For instance, at BRTFOT-225, the domains were about 10 microns in length and 5 microns in width;

the AFM image of PAV bitumen instead revealed asphaltene domains smaller than those observed in BRTFOT-225, homogeneously dispersed on the sample surface.

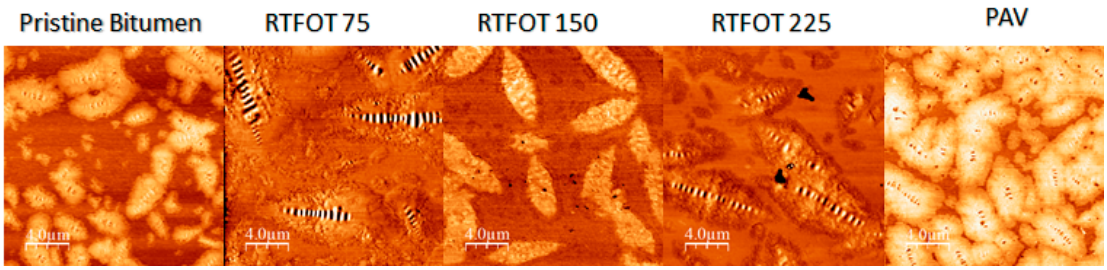


**Figure 7.** AFM phase images of PB, BRTFOT-75, BRTFOT-150, BRTFOT-225, and BPAV.

It must be pointed out that asphaltene clusters as they are seen by optical microscopy (length scales of micrometers) are the overall, long-range result of asphaltene molecules' hierarchical aggregation occurring at different length scales [50], for which different kinds of intermolecular interactions, from strong and short-range to weak and long-range, are involved. Among these, however, polar–polar interactions are expected to play the major role, since amphiphilic molecules can effectively bind, through their polar moiety, the polar groups of the dispersed molecules or the interfacial polar groups if the molecules are dispersed as clusters, as in the case of asphaltenes in the bitumen. So, a change of the cluster structure can be expected if the polar interactions are strong enough to trigger competition between asphaltene–asphaltene interactions and asphaltene–additive interactions, competition which has been found to be typical at the nanoscale in complex systems [58]. In light of this observation, atomic force microscopy can be seen additionally as a technique to indirectly probe the interactions taking place at shorter length scales, allowing us to explain, in the present work, the trends observed by FT-NMR-SDC. AFM images show the structural morphology of the bitumen, and they allow us to understand where maltene molecular mobility occurs. Considering the RTFOT ageing, the decrease in self-diffusion coefficients at all temperatures is apparently due to an increase in the size of asphaltenes, while the BPAV image clearly shows a different structural morphology from that in the image of BRTFOT-225.

## 5. Conclusions

In summary, ageing produces fundamental modifications in the colloidal structure of bitumen. Ageing also causes oxidation of bitumens and, consequently, increases the content of large molecules and the bitumen's molecular weight; these changes increase with ageing time. The two conventional ageing processes (RTFOT and PAV) modified the colloidal system of the bitumen, and both showed a certain level of asphaltene content. The RTFOT ageing, for different exposure times, changed the asphaltene structure in a consistent way, while the PAV ageing created a new colloid structural network. From the tangent loss and elastic modulus results, the rheological properties of the aged binders were found to be dependent on bitumen oxidation and changes in microstructures. The impact of these varies with the amount of ageing.

From the optical microscopy results, we concluded that the microstructural assembly of asphaltenes in unaged and aged bitumen is different, which is consistent with our FT-NMR-SDC observations. The core of this investigation was focused on using FT-NMR-SDC to track changes in the chemical functionalities of an unmodified binder and four types of aged binders manufactured with the same bitumen subjected to RTFOT/PAV ageing conditions. Most interestingly, this technique showed strong ability to monitor the ageing processes and to highlight the structural differences induced during ageing. The AFM results indirectly confirmed what was obtained via the FT-NMR-SDC technique by showing that the size of asphaltenes in aged bitumens is increased when compared with the size of asphaltenes in unaged bitumen.

The latter results provide new information in addition to that already present in the scientific literature regarding the subject, providing a more complete picture of the ageing process, in particular, on how the ageing techniques used in the laboratory affect the chemical structure of bitumen. This new information can be used in future research for the creation of new rejuvenating additives that are even higher performance than those currently on the market.

**Author Contributions:** Conceptualization, M.P. and C.O.R.; Writing-Original draft preparation P.C. and D.S.; Writing-review and Editing M.P.; Formal analysis V.L. and M.P.D.S.; Investigation P.C. and M.P.D.S.; Supervision C.O.R. All authors have read and agreed to the published version of the manuscript.

**Funding:** This research received no external founding.

**Conflicts of Interest:** The authors declare no conflicts of interest.

## References

1. Huang, S.C.; Di Benedetto, H. *Advances in Asphalt Materials*; Elsevier: Dordrecht, The Netherlands, 2015. [CrossRef]
2. Speight, J.G. *Asphalt Materials Science and Technology*; Elsevier: Dordrecht, The Netherlands, 2016. [CrossRef]
3. Fahim, M.A.; Alsahhaf, T.A.; Elkilani, A. *Fundamentals of Petroleum Refining*; Elsevier: Dordrecht, The Netherlands, 2010. [CrossRef]
4. TH, B. The modern asphalt pavement. *Nature* **1905**, *72*, 316. [CrossRef]
5. Speight, J.G. *The Chemistry and Technology of Petroleum*; CRC Press: Boca Raton, FL, USA, 2014. [CrossRef]
6. Fischer, K.A.; Schram, A. The constitution of asphaltic bitumen. In Proceedings of the 5th World Petroleum Congress, New York, NY, USA, 30 May–5 June 1959; pp. 259–271.
7. Thurston, R.R.; Knowles, E.C. Asphalt and Its constituents. Oxidation at service temperatures. *Ind. Eng. Chem.* **1941**, *33*, 320–324. [CrossRef]
8. Loise, V.; Caputo, P.; Porto, M.; Calandra, P.; Angelico, R.; Oliviero Rossi, C. A Review on bitumen rejuvenation: Mechanisms, materials, methods and perspectives. *Appl. Sci.* **2019**, *9*, 4316. [CrossRef]
9. Tauste, R.; Moreno-Navarro, F.; Sol-Sánchez, M.; Rubio-Gámez, M.C. Understanding the bitumen ageing phenomenon: A review. *Constr. Build. Mater.* **2018**, *192*, 593–609. [CrossRef]
10. Lesueur, D. The colloidal structure of bitumen: Consequences on the rheology and on the mechanisms of bitumen modification. *Adv. Colloid Interface Sci.* **2009**, *145*, 42–82. [CrossRef] [PubMed]
11. Cautela, J.; Giustini, M.; Pavel, N.V.; Palazzo, G.; Galantini, L. Wormlike reverse micelles in lecithin/bile salt/water mixtures in oil. *Colloids Surf. A Physicochem. Eng. Asp.* **2017**, *532*, 411–419. [CrossRef]
12. Calandra, P.; Giordano, C.; Ruggirello, A.; Turco Liveri, V. Physicochemical investigation of acrylamide solubilization in sodium bis(2-ethylhexyl)sulfosuccinate and lecithin reversed micelles. *J. Colloid Interface Sci.* **2004**, *277*, 206–214. [CrossRef]
13. Calandra, P.; Longo, A.; Ruggirello, A.; Turco Liveri, V. Physico-chemical investigation of the state of cyanamide confined in AOT and lecithin reversed micelles. *J. Phys. Chem. B* **2004**, *108*, 8260–8268. [CrossRef]
14. Calandra, P.; Di Marco, G.; Ruggirello, A.; Liveri, V.T. Physico-chemical investigation of nanostructures in liquid phases: Nickel chloride ionic clusters confined in sodium bis(2-ethylhexyl) sulfosuccinate reverse micelles. *J. Colloid Interface Sci.* **2009**, *336*, 176–182. [CrossRef]
15. Longo, A.; Calandra, P.; Casaletto, M.P.; Giordano, C.; Venezia, A.M.; Liveri, V.T. Synthesis and physico-chemical characterization of gold nanoparticles softly coated by AOT. *Mater. Chem. Phys.* **2006**, *96*, 66–72. [CrossRef]
16. Petersen, J.C. *A Review of the Fundamentals of Asphalt Oxidation: Chemical, Physicochemical, Physical Property, and Durability Relationships*; Transportation Research Board: Washington, DC, USA, 2009. [CrossRef]
17. Ashimova, S.; Teltayev, B.; Oliviero Rossi, C.; Caputo, P.; Eskandarsefat, S. Organic-based recycling agents for road paving applications in cold-climate regions. *Int. J. Pavement Eng.* **2020**, 1–9. [CrossRef]
18. Caputo, P.; Loise, V.; Ashimova, S.; Teltayev, B.; Vaiana, R.; Oliviero Rossi, C. Inverse laplace transform (ILT) NMR: A powerful tool to differentiate a real rejuvenator and a softener of aged bitumen. *Colloids Surf. A Physicochem. Eng. Asp.* **2019**, *574*, 154–161. [CrossRef]

19. European Committee for Standardization. *EN 1427, Bitumen and Bituminous Binders—Determination of the Softening Point—Ring and Ball Method*; European Committee for Standardization: Brussels, Belgium, 2015; p. 18.
20. European Committee for Standardization. *EN 1426, Bitumen and Bituminous Binders—Determination of Needle Penetration*; European Committee for Standardization: Brussels, Belgium, 2007.
21. European Committee for Standardization. *EN 13302, Bitumen and Bituminous Binders—Determination of Dynamic Viscosity of Bituminous Binder Using a Rotating Spindle Apparatus*; European Committee for Standardization: Brussels, Belgium, 2010; p. 16.
22. Lin, J.; Hong, J.; Liu, J.; Wu, S. Investigation on physical and chemical parameters to predict long-term aging of asphalt binder. *Constr. Build. Mater.* **2016**, *122*, 753–759. [CrossRef]
23. Yao, H.; Dai, Q.; You, Z. Fourier transform infrared spectroscopy characterization of aging-related properties of original and nano-modified asphalt binders. *Constr. Build. Mater.* **2015**, *101*, 1078–1087. [CrossRef]
24. Hou, X.; Xiao, F.; Wang, J.; Amirkhanian, S. Identification of asphalt aging characterization by spectrophotometry technique. *Fuel* **2018**, *226*, 230–239. [CrossRef]
25. Tanaka, R.; Sato, E.; Hunt, J.E.; Winans, R.E.; Sato, S.; Takanohashi, T. Characterization of asphaltene aggregates using X-ray diffraction and small-angle X-ray scattering. *Energy Fuels* **2004**, *18*, 1118–1125. [CrossRef]
26. Caputo, P.; Loise, V.; Crispini, A.; Sangiorgi, C.; Scarpelli, F.; Oliviero Rossi, C. The efficiency of bitumen rejuvenator investigated through Powder X-ray Diffraction (PXRD) analysis and T2-NMR spectroscopy. *Colloids Surfaces A Physicochem. Eng. Asp.* **2019**, *571*, 50–54. [CrossRef]
27. Lee, S.-J.; Amirkhanian, S.N.; Shatanawi, K.; Kim, K.W. Short-term aging characterization of asphalt binders using gel permeation chromatography and selected Superpave binder tests. *Constr. Build. Mater.* **2008**, *22*, 2220–2227. [CrossRef]
28. Masson, J.-F.; Price, T.; Collins, P. Dynamics of bitumen fractions by thin layer chromatography/flame ionization detection. *Energy Fuels* **2001**, *15*, 955–960. [CrossRef]
29. Allen, R.G.; Little, D.N.; Bhasin, A. Structural characterization of micromechanical properties in asphalt using atomic force microscopy. *J. Mater. Civ. Eng.* **2012**, *24*, 1317–1327. [CrossRef]
30. Menapace, I.; Masad, E.; Papavassiliou, G.; Kassem, E. Evaluation of ageing in asphalt cores using low-field nuclear magnetic resonance. *Int. J. Pavement Eng.* **2016**, *17*, 847–860. [CrossRef]
31. Pauli, G.F.; Jaki, B.U.; Lankin, D.C. Quantitative 1 H NMR: Development and potential of a method for natural products analysis §. *J. Nat. Prod.* **2005**, *68*, 133–149. [CrossRef] [PubMed]
32. Cozzolino, S.; Galantini, L.; Leggio, C.; Pavel, N.V. Correlation between small-angle X-ray scattering spectra and apparent diffusion coefficients in the study of structure and interaction of sodium taurodeoxycholate micelles. *J. Phys. Chem. B* **2005**, *109*, 6111–6120. [CrossRef] [PubMed]
33. Galantini, L.; Giglio, E.; Leonelli, A.; Pavel, N.V. An integrated study of small-Angle X-ray scattering and dynamic light scattering on cylindrical micelles of sodium glycodeoxycholate. *J. Phys. Chem. B* **2004**, *108*, 3078–3085. [CrossRef]
34. Corain, B.; D'Archivio, A.A.; Galantini, L.; Lora, S.; Isse, A.A.; Maran, F. Electrochemical, pulsed-field-gradient spin-echo NMR spectroscopic, and ESR spectroscopic study of the diffusivity of molecular probes inside gel-type cross-linked polymers. *Chem. A Eur. J.* **2007**, *13*, 2392–2401. [CrossRef]
35. Aroulanda, C.; Celebre, G.; De Luca, G.; Longeri, M. Molecular ordering and structure of quasi-spherical solutes by liquid crystal NMR and Monte Carlo simulations: The case of norbornadiene. *J. Phys. Chem. B* **2006**. [CrossRef]
36. Celebre, G.; Concistré, M.; De Luca, G.; Longeri, M.; Pileio, G. Intrinsic information content of NMR dipolar couplings: A conformational investigation of 1,3-Butadiene in a nematic phase. *ChemPhysChem* **2006**, *7*, 1930–1943. [CrossRef]
37. Di Pietro, M.E.; Aroulanda, C.; Merlet, D.; Celebre, G.; De Luca, G. Conformational investigation in solution of a fluorinated anti-inflammatory drug by NMR spectroscopy in weakly ordering media. *J. Phys. Chem. B* **2014**, *118*, 9007–9016. [CrossRef]
38. Angelico, R.; Ceglie, A.; Olsson, U.; Palazzo, G.; Ambrosone, L. Anomalous surfactant diffusion in a living polymer system. *Phys. Rev. E* **2006**, *74*, 031403. [CrossRef]
39. Read, J.; Whiteoak, D.; Hunter, R.N. *The Shell Bitumen Handbook*, 5th ed.; Thomas Telford Ltd.: London, UK, 2003. [CrossRef]

40. Oliviero Rossi, C.; Caputo, P.; De Luca, G.; Maiuolo, L.; Eskandarsefat, S.; Sangiorgi, C. 1H-NMR spectroscopy: A possible approach to advanced bitumen characterization for industrial and paving applications. *Appl. Sci.* **2018**, *8*, 229. [CrossRef]
41. Barnes, H.A.; Hutton, J.F.; Walters, K. *An Introduction to Rheology*; Elsevier: Dordrecht, The Netherlands, 1989; Volume 3.
42. Olsson, U.; Börjesson, J.; Angelico, R.; Ceglie, A.; Palazzo, G. Slow dynamics of wormlike micelles. *Soft Matter* **2010**, *6*, 1769–1777. [CrossRef]
43. Oliviero Rossi, C.; Spadafora, A.; Teltayev, B.; Izmailova, G.; Amerbayev, Y.; Bortolotti, V. Polymer modified bitumen: Rheological properties and structural characterization. *Colloids Surf. A Physicochem. Eng. Asp.* **2015**, *480*, 390–397. [CrossRef]
44. Oliviero Rossi, C.; Caputo, P.; Loise, V.; Miriello, D.; Teltayev, B.; Angelico, R. Role of a food grade additive in the high temperature performance of modified bitumens. *Colloids Surf. A Physicochem. Eng. Asp.* **2017**, *532*, 618–624. [CrossRef]
45. Jansen, J.C.; Macchione, M.; Oliviero, C.; Mendichi, R.; Ranieri, G.A.; Drioli, E. Rheological evaluation of the influence of polymer concentration and molar mass distribution on the formation and performance of asymmetric gas separation membranes prepared by dry phase inversion. *Polymer* **2005**, *46*, 11366–11379. [CrossRef]
46. Stejskal, E.O.; Tanner, J.E. Spin diffusion measurements: Spin echoes in the presence of a time-dependent field Gradient. *J. Chem. Phys.* **1965**, *42*, 288–292. [CrossRef]
47. Coppola, L.; Oliviero, C.; Olsson, U.; Ranieri, G.A. Characterization of a reverse hexagonal lyomesophase by a PGSE NMR water self-diffusion study. *Langmuir* **2000**, *16*, 4180–4184. [CrossRef]
48. Filippelli, L.; Gentile, L.; Rossi, C.O.; Ranieri, G.A.; Antunes, F.E. Structural change of bitumen in the recycling process by using rheology and NMR. *Ind. Eng. Chem. Res.* **2012**, *51*, 16346–16353. [CrossRef]
49. Chidichimo, D.; De Fazio, G.A.; Ranieri, M.; Terenzi, M. Self-diffusion of water in a lamellar lyotropic liquid crystal: A study by pulsed field gradient NMR. *Chem. Phys. Lett.* **1985**, *117*, 514–517. [CrossRef]
50. Calandra, P.; Caputo, P.; De Santo, M.P.; Todaro, L.; Turco Liveri, V.; Oliviero Rossi, C. Effect of additives on the structural organization of asphaltene aggregates in bitumen. *Constr. Build. Mater.* **2019**, *199*, 288–297. [CrossRef]
51. Coppola, L.; Oliviero, C.; Pogliani, L.; Ranieri, G.A.; Terenzi, M. A self-diffusion study in aqueous solution and lyotropic mesophases of amphiphilic block copolymers. *Colloid Polym. Sci.* **2000**, *278*, 434–442. [CrossRef]
52. Calandra, P.; Ruggirello, A.; Mele, A.; Liveri, V.T. Self-assembly in surfactant-based liquid mixtures: Bis(2-ethylhexyl)phosphoric acid/bis(2-ethylhexyl)amine systems. *J. Colloid Interface Sci.* **2010**, *348*, 183–188. [CrossRef] [PubMed]
53. Calandra, P.; Turco Liveri, V.; Riello, P.; Freris, I.; Mandanici, A. Self-assembly in surfactant-based liquid mixtures: Octanoic acid/Bis(2-ethylhexyl)amine systems. *J. Colloid Interface Sci.* **2012**, *367*, 280–285. [CrossRef] [PubMed]
54. Calandra, P.; Mandanici, A.; Liveri, V.T. Self-assembly in surfactant-based mixtures driven by acid–base reactions: Bis(2-ethylhexyl) phosphoric acid–n-octylamine systems. *RSC Adv.* **2013**, *3*, 5148. [CrossRef]
55. Calandra, P.; Mandanici, A.; Turco Liveri, V.; Pochylski, M.; Aliotta, F. Emerging dynamics in surfactant-based liquid mixtures: Octanoic acid/bis(2-ethylhexyl) amine systems. *J. Chem. Phys.* **2012**, *136*, 064515. [CrossRef]
56. Calandra, P.; Mandanici, A.; Liveri, V.T. Dynamical properties of self-assembled surfactant-based mixtures: Triggering of one-dimensional anomalous diffusion in bis(2-ethylhexyl)phosphoric acid/ n -octylamine systems. *Langmuir* **2013**, *29*, 14848–14854. [CrossRef]
57. Jäger, A.; Lackner, R.; Eisenmenger-Sittner, C.; Blab, R. Identification of microstructural components of bitumen by means of atomic force microscopy (AFM). *PAMM* **2004**, *4*, 400–401. [CrossRef]
58. Calandra, P.; Caschera, D.; Turco Liveri, V.; Lombardo, D. How self-assembly of amphiphilic molecules can generate complexity in the nanoscale. *Colloids Surf. A Physicochem. Eng. Asp.* **2015**, *484*, 164–183. [CrossRef]


© 2020 by the authors. Licensee MDPI, Basel, Switzerland. This article is an open access article distributed under the terms and conditions of the Creative Commons Attribution (CC BY) license (http://creativecommons.org/licenses/by/4.0/).

applied sciences

MDPI

*Commentary*

# Exploiting Nanoparticles to Improve the Properties of Bitumens and Asphalts: At What Extent Is It Really Worth It?

**Pietro Calandra [1,*], Valeria Loise [2,*], Michele Porto [2], Cesare Oliviero Rossi [2], Domenico Lombardo [3] and Paolino Caputo [2]**

1 CNR-ISMN, National Research Council—Institute for the Study of Nanostructured Materials, Via Salaria km 29.300, 00015 Monterotondo Stazione (RM), Italy
2 Department of Chemistry and Chemical Technologies, University of Calabria, 87036 Arcavacata di Rende (CS), Italy; michele.porto@unical.it (M.P.); cesare.oliviero@unical.it (C.O.R.); paolino.caputo@unical.it (P.C.)
3 CNR-IPCF, National Research Council—Institute for the Physico-Chemical Processes—Viale Ferdinando Stagno d'Acontres, 98158 Messina, Italy; lombardo@ipcf.cnr.it
* Correspondence: pietro.calandra@cnr.it (P.C.); valeria.loise@unical.it (V.L.)

Received: 18 June 2020; Accepted: 25 July 2020; Published: 29 July 2020


**Abstract:** Asphalt concretes are materials used worldwide. It is well-known that in such materials the minor component, the *bitumen*, plays the most important role since it binds the high fraction (>95%) of inorganic macrometer-sized particles ensuring a coherent material fit for uses in road pavement. Additives can be used to increase the overall rheological properties, with high benefits in terms of resistance to mechanical stress and to ageing. Among these, nanoparticles have recently been considered as very effective additives in increasing the overall performance, increasing the viscosity, the rutting parameter and the recovery from deformation. However, they are expensive, so a delicate equilibrium between costs and benefits must be found for large-scale uses. In this framework, we furnish our critical analysis of the state-of-the art technologies used for improving the bitumen performances by means of nanoparticles with an eye to eventual added-values (like anti-oxidant effect, antistripping properties, or UV radiation screening which avoids radiation-induced ageing . . . ). We will critically consider the costs involved in their use and we will give our opinion about vanguard techniques which can be fit for the analysis of nanoparticles-containing bitumens and asphalts. Interesting perspectives will be also given for future research and applications.

**Keywords:** nanoparticles; bitumen; asphalts; surface functionalization

## 1. Aim of the Work

This work is far from being a review of the state-of-the art technologies, methods and materials used for using nanoparticles-containing bitumens and asphalts. For this, specialised textbooks, good reviews, and interesting research articles are present. They can furnish all the necessary information. This work is, instead, a critical presentation of this field, introducing the reader to the properties of nanoparticles and their use to improve the properties of bitumens and asphalt concretes. For this purpose, the various kinds of nanoparticles (nanosilica, nanoceramics, nanoclays, and even organic nanoparticles or inorganic nanoparticles surface-functionalised) used in this field will be rationally classified and presented. The added-value properties they confer to bituminous materials will be critically discussed, highlighting at the same time both positive and negative aspects, costs included. The purpose is to furnish useful and critic comparisons, suggestions and perspectives. This work is therefore a thought commentary on all the aspects involved in this topic, from the physical origin of

the emergence of novel properties, to the principles to be followed to choose the most appropriate technique of investigation, according to the complex nature of the material involved and according to the specific chemical aspect needing investigation. The aim of the work is then to provide a panoramic view of the state-of-the art, making useful criticisms and giving comments and suggestions, to make researchers conscious of several hidden aspects that can be hardly found in standard research articles (for instance how to analyse IR spectra, how to improve the excitonic absorption to make bitumens resistant to UV radiation, how to investigate the distribution of nanoparticles in the bulk state rather than in the surface as usually done by standard microscopies, the eternal costs/benefits struggle, need of interdisciplinary works etc.). To do so, the work will follow this logical scheme: we first show (Sections 2 and 3) the peculiar properties of bitumens and how they can be improved by the use of nanoparticles and why; then we present the problems to be faced: the issue of nanoparticle stabilization and the cost involved. To show how to face these problems, we will present the possible solutions to obtain a reasonable cost/benefit equilibrium, in order, from the cheapest solution (use of inorganic nanoparticles), gradually moving to surface-functionalized nanoparticles up to the use of organic nanostructures (Sections 4–6). Then, we will comment the added values conferred by the nanoparticles (Section 7) and the experimental methods for a proper characterization (Section 8), to finally conclude with future perspectives as we see them (Section 9).

It is our conviction that literature is quite rich in experimental works related to the use of nanoparticles in bitumens, but it is still relatively poor in works critically commenting the state-of-the art and offering different points of view especially on the basis of the fascinating fields of molecular physics and the physics of complex systems. We hope that this contribution could finally tickle researchers' curiosity and stimulate their imagination in the piloted design of material for road pavements with ever-increasing performances.

## 2. An Introduction to the Problematics

### 2.1. Bitumen and Asphalt Generalities

Bitumen is an involatile, adhesive, waterproofing, highly viscous viscoelastic fluid derived from the crude oil topping distillation process or present in natural sources [1]. Its composition and physicochemical properties depend on the crude oil sources undergoing the distillation process [2,3]. However, the molecules present in a bitumen are not uniquely defined so the bitumen is classified according to the relative amounts of four classes of molecules (Saturates, Aromatics, Resins and Asphaltenes), never by the definition of the millions of constituents individually [4].

A typical composition is reported in the top panel of Figure 1. However, the exact relative fractions of any specific bitumen can be determined by the S.A.R.A. method [5], usually following the ASTM D4124-09(2018) procedure.

Bitumen viscoelastic properties allow its use as binder for the inorganic particles used in road paving. In this use, it is heated so that its viscosity decreases sufficiently [6] to allow it to be properly mixed with the aggregates; after cooling down to ambient temperature, the bitumen will act as a viscous binder of the aggregates.

Bitumen has a very complex structure consisting of polar asphaltene stacks of aggregates stabilized by resins and dispersed in apolar components (saturates and aromatics). The similarity with micellar systems gives this picture the name of "micellar model", but the structures turn out to be more complex since asphaltene clusters are organized in complex way at various hierarchical levels of different length-scales [7].

The complexity of this system is even higher if we consider that both the composition and (therefore) the structure changes with time, since ageing takes place with various mechanisms leading to brittleness with time [8,9].

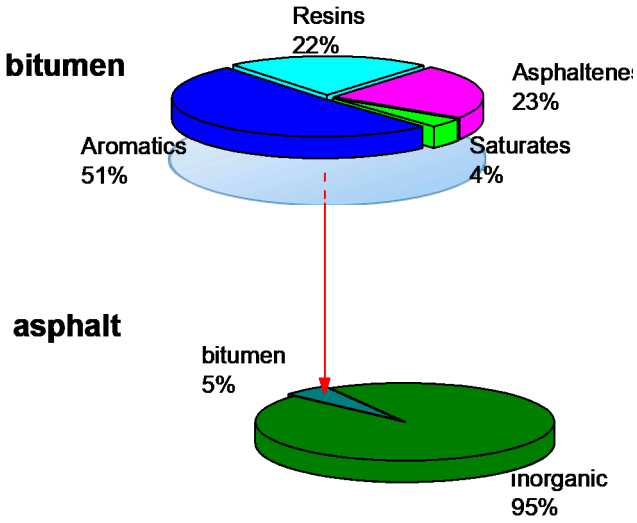


**Figure 1.** Typical compositions of asphalts and bitumens.

### *2.2. Our Opinion on The Role of Resins and Amphiphiles*

The maltene glass transition temperature is certainly an important factor governing the rheological properties [6], but effective asphaltene content and their aggregation state is practically the most important factor dictating properties of the bitumen and resulting asphalt [10].

For this reason, we want to emphasize the role of resins. To do so we can present chemical reasoning applying to bitumens what is known about colloidal systems: the stabilization of the polar domains is of pivotal importance for determining both the structure and the properties of the overall aggregates.

It is therefore clear that resins are the stabilizing agents that actually hold up the overall structure of the system. This peculiar characteristic is given by their amphiphilic properties, i.e., the molecules have both polar and apolar parts within their molecular architecture. So, at their polar end they can bind the polar clusters of asphaltenes, and at the apolar one, they can bind the maltene, acting as a bridge between the polar and apolar domains which, in absence of such molecules, would be unstable towards segregation/separation/ sedimentation. Without going deeper into details, it is important to point out that their role in the overall self-assembly and dynamics is complex. Besides simple polar and apolar interactions, further specific interactions between amphiphiles themselves can in principle take place.

It has been recently highlighted that the mutual interactions between amphiphiles lead to peculiar self-assembly processes [11,12] sometimes with extended molecular networks, dictating the final overall aggregation pattern [13] and the (usually slowed-down) dynamics [14,15]. In any case, the bottom-up self-assembly of organic-based complex materials is sometimes a very complicated issue [16].

Given the extreme sensitivity of the aggregation pattern to the presence of other amphiphiles, our opinion is that amphiphiles can be considered as one of the most promising and effective classes of substances which can be used for improving the properties of bitumens and asphalts. It is not a case if the most effective and important additives are amphiphilic substances: since resins influence the asphaltene dispersion within the matrix avoiding their aggregation, they promote structural stability hindering the deterioration of the rheological performances [17].

In the context of nanoparticle-containing bitmens and asphalts, the role of resins is even more important, since they must stabilize also the nanoparticles in the apolar maltenic matrix typical of the bitumens.

Amphiphilic compounds have proven in fact to be effective in stabilizing organic-based materials [18,19], inorganic complexes [20,21] and above all inorganic nanoparticles dispersed in the apolar phase [22–24], even under drastic conditions [25,26]. Since aggregation is usually a

thermodynamically favored process, the effect of resins is therefore also important in contrasting ageing effects, thus increasing the service life of the asphalt [27].

### *2.3. From Macro Aggregates to Nanoparticles: Size Matters*

A recent definition of nanomaterial concisely given by the European Commission is: "A natural, incidental or manufactured material containing particles, in an unbounded state or as an aggregate or as an agglomerate and where, for 50% or more of the particles in the size distribution, one or more external dimension is in the size range 1–100 nm" [28].

It has been understood that nanometer-sized particles have unique properties which cannot be found in their relative bulk counterparts. Their use in asphalt production is then becoming more and more appealing: nanoparticles can give increased pavement load and decrease its cracks due to fatigue during the operational life, they boost asphalt concrete pavement long-term performance, they give better resistance to traffic and environmental loads or mitigate the incompatibility between some natural aggregates and the bitumen binder, enabling more sustainable and durable pavement solutions [29]. The origin of this interest can be traced back to the enhanced surface to volume ratio [30]. In Figure 2 it is shown the fraction of surface atoms with respect to the total amount of atoms, making part of a model cubic sample made of atoms arranged in a primitive cubic lattice of lattice spacing $L_0$.

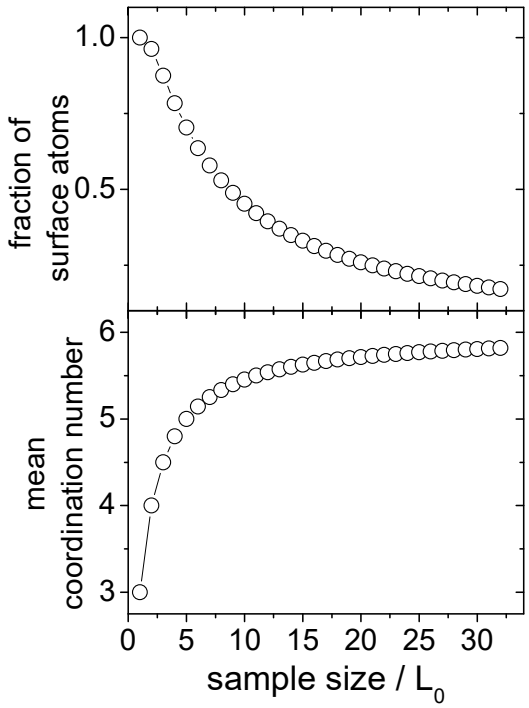


**Figure 2.** Fraction of surface atoms and mean coordination number in a primitive cubic sample ($L_0$ is the atom bond distance, see text for comments).

It can be seen that, with decreasing size, the fraction of surface atoms increases as well as the fraction of low-coordination number atoms (atoms at the edges and at corners). Such atoms have dangling bonds which need to be saturated by bonds with other chemical species and therefore they have peculiar properties and a certain reactivity.

The use of nanosized particles has given rise to a modern technological field: nanotechnology. Many different aspects are included [31]: Nano- and quantum electronics, nanostructured materials, scanning probe microscopy, molecular materials for electronics, molecular technology, computer modelling, cluster and mesoscopic science and technology and supramolecular chemistry, which have all become part of nanotechnology since the late nineties, are to be taken into account. Finally, this new field is nowadays involved in construction and road pavement materials [32–34].

Figure 3, inspired from a work by Sobolev and Ferrada-Gutiérrez [35], shows how the use of nanoparticles with sizes down to the nanometer range can be used in various bitumen and asphalt technologies.

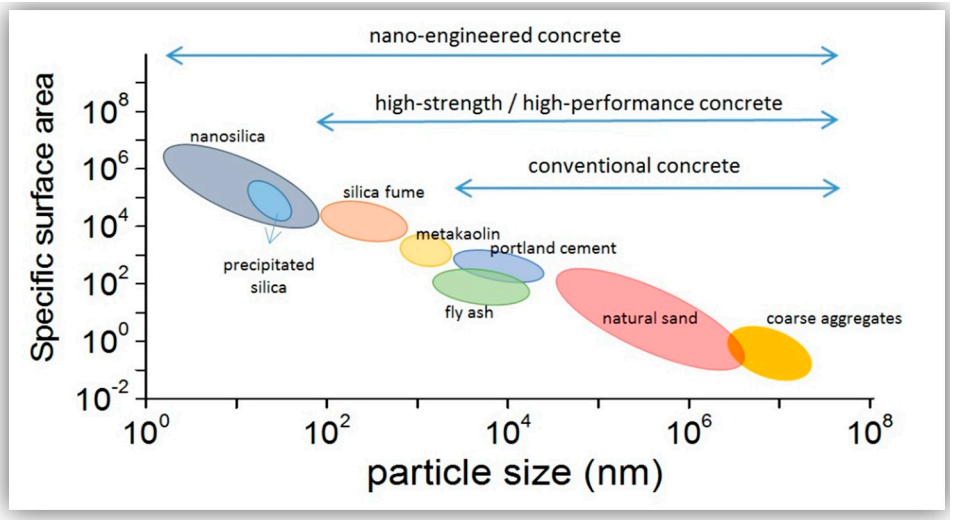


**Figure 3.** Some kinds of differently-sized particles used for asphalt concrete production.

If Portland cement aggregates, fly ashes, natural sands and coarse aggregates are involved in conventional asphalt concretes, more finely-subdivided particles (size 10 nm and above) like metakaolin, finely ground mineral additives and silica fumes are employed in the production of high strength/high performance concrete. Recently, even smaller particles (down to 1 nm) and mesoporous materials with large surface area (5–100 $m^2/g$), have been employed in nano-engineered asphalt concretes.

Since there are clear differences among all the disciplines involved in the study of nanostructured materials, it is evident that nanotechnology applied to bitumens is a complex structure of interconnected research areas. It follows, and we strongly support this, that synergic co-operation among researchers with different skills is to be considered pivotal making nanosciences definitely multidisciplinary, an aspect which cannot be absent in modern research in general [36].

### *2.4. A Problem Arises: Nanoparticles Tend to Aggregate*

The use of nanoparticles poses however a problem. Due to the general incompatibility between the chemical nature of the bitumen and that of the inorganic particles, a tendency of nanoparticle aggregation/separation is observed. This will be seen afterwards, when the solution to functionalize nanoparticle surface will be discussed in Section 5 entitled "An expensive solution: organic-modification of inorganic nanoparticle surfaces".

Although detailed discussions on the possible mechanisms of nanoparticle growth/aggregation can be found in the literature [37,38], it is important to simply point out here is that the driving force of any growth process is the attempt of surface atoms to form bonds to complete their coordination structure so it can be expected that the more efficient is the saturation of surface dangling bonds by growing, the more powerful the driving force is. The variation of the number of surface atoms with increasing the particles size is then represented by the size derivative of the fraction of surface atoms, reported in Figure 2, upper panel.

This force diminishes very rapidly with size but, increasing the nanoparticle size, their peculiar characteristics are progressively lost. It is now obvious that the use of nanoparticles in bitumen technology must involve the size control. This is, indeed, what is generally done by the functionalization of nanoparticle surface.

Thus, not only must the method for nanoparticle preparation take into account the final nanoparticle size, but also a method for their stabilization should be taken into account, thus involving an obvious

cost increase. The costs to improve bitumens properties with the addition of nanoparticles are not trivial at all, and can make the difference between an affordable method or not. Some comments about the costs are therefore the topic of the following section.

## 3. The Main Drawback: the Costs

This is a crucial point: at what extent a given technological field can bear the costs of reducing the size? Each size regime has specific properties and can give application-specific added-value, so it is not true that smaller means better. There is a delicate equilibrium among properties, costs and added value to be taken into account.

At current prices, for the nanomodifications to be cost effective, a significant improvement in durability has to be attained. It is expected that the production of nanoparticles in bulk quantity and the use of alternative sources will significantly reduce the costs. For example, rice husk, an abundant waste biomass with high content of silica was identified as a potential low-cost resource for the production of nanosilica particles [39]. Therefore, it is necessary to carry out economic, ecological and environmental evaluations of nanomodified asphalt before a large-scale application in practical engineering.

The use of nanoparticles implies costs which make nanoparticles-additivated bitumens and asphalts much more expensive. The costs involved in bitumen and asphalt productions depend on different factors as depicted by Martinho et al. [40]. However, they are of the order of 3–350 (€/ton) for common bitumens/asphalts as listed in Table 1

**Table 1.** Cost evaluation of typical asphalt mixtures.

| Materials | Average Unit Prices (€/ton) |
|---|---|
| Bitumen 35/50 | 350 |
| Natural aggregates | 10 |
| Electric arc furnace steel slag aggregates | 3 |
| Reclaimed asphalt pavement aggregates | 5 |
| Recycled concrete aggregate | 5 |

In comparison to this, the cost of nanomaterials to be used as asphalt additives is much higher. This is due to the use of expensive equipment and technology and the highly qualified personal involved and so on.

Products with high purity and narrow size range and high specific surface may demand higher processing efforts, higher complexity of the apparata involved and higher skills of the people involved, thus implying higher final costs. For this reason, it is not possible to define a cost for a given nanomaterial, but only a rough range. Mind that the prices for nanoparticles are not given in €/ton like for bitumens, but in €/kg or even in €/g! Let us examine Table 2, which reports some indicative ranges for nanoparticle costs, for some comments. From a perusal of Table 2 it can be seen that the cheapest material is nanosilica, which can cost down to 80 €/kg (see 0.08 €/g, first entry in the table). However, its surface modification to increase its compatibility with the apolar nature of the bitumen increases the cost a lot, so a silane-modified nanosilica cost between 180 €/kg to 450 €/kg. If organic particles are used the cost increases severely: the most expensive family of such nanomaterials is that of single walled nanotubes, whose cost can span from 65 €/g to about 200 €/g. Multiwalled carbon nanotubes (MWCNTs) are cheaper, ranging from about 2 €/g up to 40 €/g. Among the organic carbon nanostructures, however, carbon nanofibers and nanoplatelets are the most affordable solutions, since their cost hardly exceeds 15 €/g [41].

Of course, specialized technology development and the increasing market of carbon and graphene families will cause a decrease in their price, probably making such kind of materials more appealing for bitumen and asphalt modification. However, at the moment, the use of inorganic nanoparticles is still the most affordable solution.

**Table 2.** Costs of inorganic and organic nanoparticles used as additive in bitumens and asphalt concrets; (a) Laser Synthesized; (b) from [42]; (c) from [43].

| | Materials | Unit Price (€/g) |
|---|---|---|
| Inorganic nanoparticles | Nano $SiO_2$ | 40 (a)<br>0.08–0.15 (b)<br>1.6–6.5 (c) |
| | Nano Iron | 4.8–17<br>0.1–2.6 (b) |
| | $Fe_2O_3$ | 3.4<br>0.1–0.3 (b)<br>4.42–11.5 (c) |
| | Nano ZnO | 1.48<br>1.23–1.94 (c) |
| | Nano CuO | 2–7.2<br>1.24–9.8 (c) |
| | Nano $Al_2O_3$ | 1.8–9<br>1.3–6.9 (c) |
| | Nanoclay (800 nm) | 1.16 |
| Organic nanoparticles | Single Walled CNT (SWCNT) | 65–195<br>54.7–263 (c) |
| | Double Walled CNT (DWCNT) | 43<br>51.21 (c) |
| | Multiwalled CNT (MWCNT) | 1.5–33<br>30.9–34.4 (c) |
| | Graphene Nanoplatelets (GNP) | 6–11<br>15–114 (c) |
| | Graphene Oxide (GO) | 68–165<br>172 (c) |
| | Reduced Graphene Oxide (rGO) | 48 |
| | Carbon Nanofibers (CNF) | 14<br>65 (c) |

## 4. A Cheap Solution: The Use of Inorganic Nanoparticles to Improve Mechanical Properties

Nanosilica is probably one of the cheapest materials among all the nano-sized ones, and this renders its use quite affordable, due to its high stability, ability to disperse, filler effect and its pozzolanic reactivity [44,45]. Besides, the rutting resistance, fatigue cracking and anti-stripping properties are enhanced [46].

Several authors have added nano-$SiO_2$ to a bare bitumen to demonstrate enhancement of performance (softening point increases according to the nanosilica content, while penetration decreases) as well as a clear improvement in storage stability [47]. Zghair et al. [48] self-consistently found that the penetration value and the ductility decrease with the amount of nanosilica whereas the softening temperature and rotational viscosity increase.

The effect of silica is clear also in the increase of the Marshall stability and of resistance against rutting at loading conditions, as well as the fatigue life of warm mix asphalts as found by Galooyak et al. [49], They conclude that increasing mixing times would positively affect the properties of the binder, because, obviously, longer times can guarantee a better dispersion. However, as the authors correctly point out, this would increase the energy consumption and consequently the costs.

As Crucho et al. themselves admit [50], nanosilicas are the most studied materials as asphalt binder modifiers. This is unavoidable, in our opinion, due to the low cost and the ease of supply. Despite the wide use of nanosilica, however, comparative studies among different kinds of nanoparticles are also

important: thanks to comparative studies, in fact, it was found that nano-$TiO_2$ has more problems than nano-$SiO_2$ in chemical compatibility with the apolar bitumen [51] while hydrophilic bentonite and Zero-valent nano-iron have better affinity with bitumens [50].

Specific influences of nano- $TiO_2$, ZnO, $Al_2O_3$ and $Fe_2O_3$ in the creep rate and strain modulus of hot mix asphalt have been also highlighted [52]. Nano-CuO was, instead, found to enhance resistance to rutting deformations of bitumens and aged bitumens but only at temperatures lower than 64 °C [53]. The authors also found that the addition of nano-CuO to bitumen enhances its fatigue cracking, while other authors have found that nano-CuO can be used as phase change material to increase thermal properties (glass transition temperature, melting peak temperature, specific heat capacity) [54].

Nazari and other co-workers [55] explored the potential of $CaCO_3$ nanoparticles, besides those of $SiO_2$ and $TiO_2$. Confirming that silica are the particles giving greatest fatigue resistance, the authors detected a possible antioxidant effect of nano-$TiO_2$ and nano-$CaCO_3$.

A similar comparative study among $SiO_2$, $TiO_2$ and $CaCO_3$ nanoparticles was conducted with F.M. Nejad [52] who confirmed that the major effect was found with nanosilica, probably due to its higher specific surface and lower density (which probably gives a higher volume fraction in the bitumen at parity of *w*/*w*%).

In this scenario, an interesting class of nanosilicates is surely nanoclays. They are hydrated silicates with a sheet-like geometry. For this reason, such hydrated silicates are generally known as phyllosilicates [56] (from the Greek *phillon*, leaf). Phyllosilicate sheets are made up of repeating units of six-membered rings, in turn made up of the $SiO_4$ tetrahedral units. Each ring is shared with the other three oxygen atoms [57].

It is a low-cost material, in fact easily available as residual clay (originated from the surface erosion of rocks or sedimentary rocks) or as transported clay (that is, due to atmospheric agents, removed from the original deposit site and transported far away) [56]. For this reason, clay has always been one of the most used materials in construction. In this context, it was found that bitumen can be reinforced with nanoclay particles since they confer increased stiffness and resistance against aging as well as improved elastic properties [58].

Due to the generally high costs involved in the use of nanoparticles, a brilliant idea is that of Hussein et al. [59], who wanted to reuse the waste from the ceramic material industries as possible modifiers for bitumen. They crushed the powder, sieved it at 75 μm, and heated it for 30 min at 130 °C for water elimination, and finally grounded it using a milling bowl. Consistently with other authors, they found that the presence of nanoparticles caused a decrease in penetration, an increase in softening temperature and an improvement in resistance to rutting. However, due to the nanoparticles' high surface energy, the authors found that their agglomeration is favoured. This aspect has been shown from a theoretical point of view, using simple chemical reasoning, in Section 2.4 entitled "A Problem Arises: Nanoparticles Tend to Aggregate".

## 5. An Expensive Solution: Organic-Modification of Inorganic Nanoparticle Surface

As the eager reader has probably already observed, some authors have reported problems in the chemical compatibility of the nanoparticles [51] and nanoparticles' tendency to agglomerate due to the high surface energy [59]. To solve this problem, an expensive but effective solution is represented by functionalization of the nanoparticle surface to change its chemical nature, making it more compatible with the apolar nature of the host matrix (bitumen, asphalt) thus avoiding instability problems.

The role of aluminium oxide nanoparticles in the rheological properties of bitumen modified with acrylonitrile styrene acrylate (ASA) polymer was investigated by Mubaraki et al. [60]. An increase in viscosity, softening point temperatures and in storage stability and resistance against rutting were found. Nano-montmorillonite (size 1–2 nm), after organomodification to make it organophilic for a better dispersion in bitumen, was tested by Sedaghat et al. [61].

The functionalization of silica nanoparticles with (3-aminopropyl) triethoxysilane (APTES) can favour their dispersion (probed by SEM) within the bituminous matrix, and consequently improve their

performance (reduction of the chemical aging index—CAI—for carbonyl and sulfoxide groups, higher rutting parameter and lower cracking parameter) [62]. The same authors explored the possibility to combine different coupling agents to minimize nanoparticle agglomeration [63].

Effectiveness of surface functionalization was confirmed by Li et al. [64] who found that a better dispersion of the nano-ZnO inside the bitumen is achieved if nanoparticles are silano-modified at the surface (FT-IR checks if the silano-modification is effective). Surface treatment of nano-$SiO_2$, nano-$TiO_2$ and nano-ZnO with γ-(2,3-epoxypropoxy) propyltrimethoxysilane as silane coupling agent to modify the nanoparticles' surfaces was performed by Zhang et al. [65]. Similar clues were found by Chen et al. in 2015 [66].

In general, it is now quite clear that the surface modification improves the dispersion. A worth of note is the work by Sun et al. [67], who used modified nanoparticles (seven different nanoparticles: $SiO_2$; $CaCO_3$; montmorillonite; $TiO_2$; $Fe_2O_3$; ZnO and bentonite with size in the range 15–30 nm functionalized with silane stearic acid or polyethylenimmine). They demonstrated how modification can give better performances (softening point and viscosity general increase, parallel to decrease in ductility) especially at high temperatures. It is important to note, in our opinion, how the authors are convinced about the importance of the surface modification to influence the final material properties. Probably for this reason, in fact, these authors improved the methodology for surface modification of nanoparticles. The previous procedure involved dosing the coupling agents on the amount of bitumen; instead, in their new procedure the percentage by weight of coupling agents is calculated with respect to the quantity of nano-$SiO_2$. In doing so, they discovered the optimal amount of coupling agent with consequent benefits procedure efficiency.

## 6. Novel Materials: Organic Nanoparticles

The problem of chemical compatibility between nanoparticles and the bitumen/asphalt can be solved also if organic nanoparticles are used. This is in our opinion a brilliant solution since in this way the cost of the surface functionalization of inorganic nanoparticles is also avoided.

Chen et al. [66] found that organic expanded vermiculite compounds (OEVMT) give better resistance to fatigue and higher thermal stability with respect to nano-$TiO_2$ and nano-ZnO modified on the surface by ϒ-(2,3-epoxypropoxy)propyltrimethoxysilane, even if inorganic nanoparticles nano-$TiO_2$ showed better resistance to photo-oxidation and, consequently, better anti-aging effect due to their semiconductor nature. However, for further comments on the photo-protection effect given by nanoparticles see below the section about "Added-Values Given by the Use of Nanoparticles". In similar way, Zhang et al. [68] found that OEVMT, treated with star quaternary alkylammonium chloride to modify its interlayers from hydrophilic to lipophilic, can contrast the thermo-oxidative aging. Another interesting class of organic nanoparticles is that of carbon nanostructures: graphenes, nanotubes and nanofibers. Such nanostructures are schematically depicted in Figure 4. Their main use is in electronics-related applications like in flexible electronic and optoelectronic devices [69] or as electrodes and buffer layers component in polymer solar cells (PSCs) [70], but they were found to behave like reinforcing fillers in composites, photochemical cells, etc. [71]. This "filling" behavior can be transferred from to the fields of construction materials [72–75].

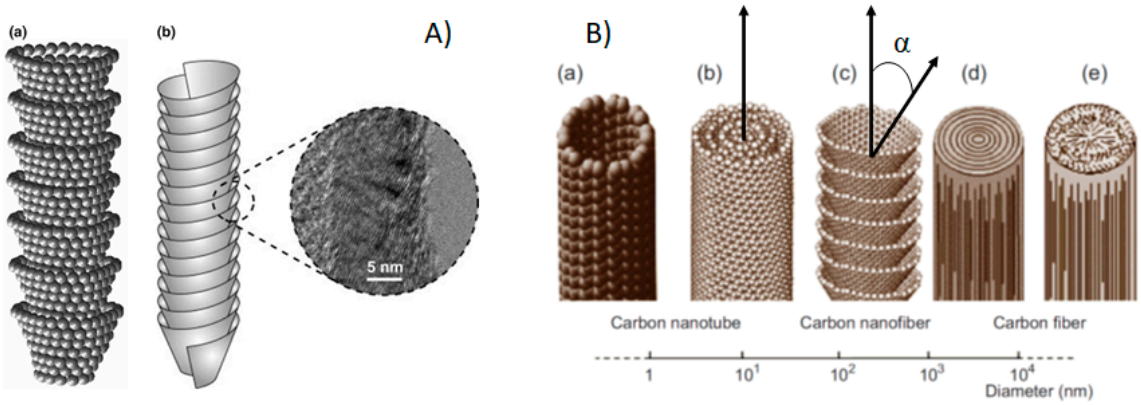


**Figure 4.** Panel (**A**): (a) 3D representation of cup-stacked graphene layers in a single CNF, and (b) Simplified schematic of stacked-cup carbon nanofiber helical structure with inset showing TEM image of inclined orientation of grapheme planes along the side of structure with respect to nanofiber axis. Image taken from [76]. Courtesy of Elsevier. Panel (**B**): Schematic of size and morphology distribution of various nanotubular structures that shows the main difference in the structure between carbon nanofibers and carbon nanotubes. (a) single wall carbon nanotube, (b) multi walled carbon nanotube, (c) carbon nanofiber, (d,e) carbon fibers of different complexity. Reprinted from [68].

Generally, the use of nanostructured carbon materials gives more durable substrates [77], so, for example, graphene was used as modifier in bitumens [78,79] conferring increased stiffness and improving elastic behavior. However, the main drawback of the use of graphene as a bitumen modifier—and more generally as an element to improve the mechanical performances of construction materials—is its high production cost. For this reason, the studies on grapheme are very few and have been shifted toward graphene-derived nanomaterials like graphene oxide (GO) [80], and graphene nanoplatelets (GNPs) [81,82] or some cheap carbon nanotubes and carbon nanofibers. The general structure of carbon nanotubes and carbon nanofibers is shown in Figure 4A. Carbon nanotubes were found to give stiffness increase and strain decrease regardless of the stress applied [83] improving also the mechanical performance of hot mix asphalt (HMA). Multi-walled carbon nanotubes (MWNTs) were used by Loise et al. to improve the rheological properties of bitumen [84]. In this case, the authors hypothesize that higher defectiveness in MWNTs gives better improvement of the rheological properties, due to a probable formation of networks bridged by MWNTs defects. Finally, an increase by a factor of 2–3 in the fatigue life of bitumens modified with carbon nanofibers and improved characteristics of hot mix asphalts were found by Khattak et al. [85] who, highlighting the actual requirement of huge amounts of solvents to disperse CNFs, advise of the need to explore more eco-friendly mixing techniques to use lower amounts of solvents.

In conclusion, there is no doubt that organic nanoparticles have a chemical nature intrinsically compatible with that of bituminous materials, and that their use avoids the costs of further steps consisting in the chemical modification of nanoparticle surface, like in the case of inorganic nanoparticles. However, their cost is still high in some cases (graphenes, nanotubes). The increasing market of carbon and graphene families and the technology development specialized in the production of such kind of materials will cause a decrease in their price, probably making carbon nanostructures more appealing for large-scale applications like in bitumen and asphalt modification.

## 7. Added-Values Given by the Use of Nanoparticles

There are numerous examples showing that the addition of nanoparticles within the bitumens or asphalts confers specific properties of certain added values. For example, hot mix asphalt mixtures modified with carbon nanofibers can give piezoresistive responses [86].

Modification of bitumens with nanoclays (montmorillonite) reduces their flammability. In this way, bitumen can move from a "fuel" classification to a "self-extinguishing" classification [87]. The proposed

mechanism of action is interesting: nanoclays can catalyse char-forming reactions producing charred residues which are able to delay the escape of volatile products and the penetration of oxygen thus hindering combustion.

Nano-zinc oxide can also behave like an antistripping agent in hot mix asphalt (HMA) with limestone and granite as aggregates [88]. It was found, in fact, that nano-ZnO decreases the acidity of the bitumen thus favouring the adhesion between the bitumen itself and acid aggregates, such as granite. In this way, nano-ZnO improves the adhesion between the bitumen and the aggregates, especially in the case of moisture-conditioned samples.

Another very interesting added value provided by the addition of nanoparticles is the protection against aging. Aging effect, indeed, is particularly severe in surface layers that are exposed to environmental conditions such as UV radiation, moisture, oxygen, and temperature changes [89]. In this ambience, even if there are examples of uses of very expensive materials like silver nanoparticles [90] to contrast oxidative aging, nano-$TiO_2$ and nano-$CaCO_3$ were found to have a possible antioxidant action [55]. However, another interesting effect is that provided by semiconductor nanoparticles in the screening of UV-radiation. Thus, nano-ZnO was found to give good resistance of modified bitumens to the UV aging, although Du et al. [91] found that their effect depends on the bitumen nature. The potential of ZnO nanoparticles to increase the resistance of bitumen to ultraviolet aging was also studied by Li et al. [64] and Zhang et al. [65].

Since some semiconductor nanoparticles have some problems in chemical compatibility with the apolar bitumen [51], other authors modified their surface to better disperse nanoparticles within the bituminous matrix [65,67].

The problems of obtaining a better distribution of nanoparticles come above all from the chemical reasoning that asphalt concretes are heterogeneous materials: there are composed of aggregates, nanoparticles, bitumen and pores; sometimes there are also networks, so the mechanical properties depend also on the form and the distribution of the aggregates. Some more comments are given below, in Section 8.2 entitled "How to Probe the Distribution of Nanoparticles: Nanotomography as One of the Techniques of Election".

However, in the case of semiconductor nanoparticles, we want to stress another aspect which in our opinion has to be taken into account for. Semiconductor nanoparticles have basically two effects whose relative contributions are in complex competition: (i) their semiconductor nature allows absorption of those radiations whose energies are above the energy gap value and (ii) the size in the nano-regime allows radiation scattering within the sample.

Our opinion is supported by the observation, made by Chen et al. [65], that 3% *w*/*w* of nanoparticles is the optimum amount of nanoparticles in giving resistance to photo-oxidation, but 1% of nanoparticles gives worse behaviour even with respect to the reference bitumen. This is consistent with the competition of two opposite effects.

We think that at low nanoparticle concentration a detriment effect can arise as a result of the scattering contribution of the nanosized particles which helps in diffusing the radiation within the sample. This effect is not counterbalanced enough by the absorption contribution of such nanoparticles which would help in depleting radiation. So, at nanoparticles concentrations higher enough, the absorption effect can overcome the scattering contribution and so effective photo-screening and protection of the matrix can take place.

It is obvious that the capability of nanoparticles to absorb photons must be exactly determined for a wisely-designed bitumen, and this requires suitable techniques for nanoparticle characterization. For this aspect we will give some hints, comments and perspectives in Section 8.3 entitled "UV-Vis absorption for probing bitumen screening towards UV radiation". A scheme of the techniques used with the corresponding references is reported in Table 3.

**Table 3.** A panoramic view of the techniques used for investigating nanoparticles-containing bitumens and asphalts.

| Techniques | Authors | Bitumen Matrix | Nano-Materials |
|---|---|---|---|
| X-Ray Diffraction (XRD) | Jahromi et al. (2009) [58] | Fresh, short-term aged, long-term aged | Clay (closite and nanofil) |
| | Wu et al. (2009) [87] | Fresh, short-term aged, long-term aged | Clay (montmorillonite) |
| | Zhang et al. (2015) [67] | Fresh, long-term aged, UV aged | ZnO |
| | Chen et al. (2015) [66] | Fresh, short-term aged, long-term aged, UV aged | $SiO_2$, $TiO_2$, ZnO |
| | Nazari et al. (2018) [55] | Fresh, short-term aged, long-term aged | $SiO_2$, $TiO_2$, $CaCO_3$ |
| | Loise et al. (2019) [84] | Fresh | Carbon nanotubes |
| | Sedaghat et al. (2020) [61] | Fresh, short-term aged, long-term aged | Clay (montmorillonite) |
| | Hussein et al. (2017) [59] | Fresh | Ceramic powder |
| | Li et al. (2018) [92] | Fresh, SBS modified | Graphene oxide |
| Fourier-Trasform Infra-Red Spectroscopy (FTIR) | Zhang et al. (2015) [68] | Fresh, long-term aged, UV aged | ZnO |
| | Du et al. (2015) [91] | Fresh, short-term aged, UV-aged | ZnO |
| | Li et al. (2015) [64] | Fresh, short-term aged, UV-aged | ZnO |
| | Ali et al. (2017) [93] | Fresh | $Al_2O_3$ |
| | Sun et al. (2017) [67] | Fresh, asphalt mixture | $SiO_2$, $TiO_2$, $CaCO_3$, ZnO, montmorillonite, bentonite, $Fe_2O_3$ |
| | Hussein et al. (2017) [59] | Fresh | Ceramic powder |
| | Olabemiwo et al. [90] | Fresh | Ag |
| | Amini and Hayati (2020) [54] | Fresh, short and long term aged | CuO, carbon nanotubes |
| | Li et al. (2018) [92] | Fresh, SBS modified | Graphene oxide |
| | Nazari et al. (2018) [55] | Fresh, short-term aged, long-term aged | $SiO_2$, $TiO_2$, $CaCO_3$ |
| | Liu et al. (2018) [94] | Fresh, WMA, HMA | Graphene oxide |
| Atomic Force Microscopy (AFM) | Karnati et al. (2019) [62] | Fresh, long-term aged | $SiO_2$ |
| | Karnati et al. (2020) [63] | Fresh, aged | $SiO_2$ |
| | Zhang et al. (2015) [65] | Fresh, long-term aged, UV aged | ZnO |
| | Du et al. (2015) [91] | Fresh, short-term aged, UV-aged | ZnO |
| | Hussein et al. (2017) [53] | Fresh | Ceramic powders |
| | Arabani et al. (2015) [83] | HMA | Carbon nanotubes |
| | Taherkani et al. (2016) [87] | Fresh | $SiO_2$ |
| | Nejad et al. (2016) [95] | Fresh, HMA | $TiO_2$, ZnO, $Al_2O_3$, $Fe_2O_3$ |
| Scanning Electron Microscopy (SEM) | Shafabakhsh et al. (2018) [53] | Fresh, short-term aged, long-term aged | CuO |
| | Nazari et al. (2018) [55] | Fresh, short-term aged, long-term aged | $SiO_2$, $TiO_2$, $CaCO_3$ |
| | Yang et al. (2020) [96] | Fresh | Carbon nanotube sponges |
| | Amini and Hayati (2020) [54] | Fresh, short and long term aged | CuO, carbon nanotubes |
| | Ali et al. (2017) [93] | Fresh | $Al_2O_3$ |
| | Karnati et al. (2019) [62] | Fresh, long-term aged | $SiO_2$ |
| | Karnati et al. (2020) [63] | Fresh, aged | $SiO_2$ |
| | Li et al. (2015) [64] | Fresh, short-term aged, UV aged | ZnO |
| | Sun et al. (2017) [67] | Fresh, asphalt mixture | $SiO_2$, $TiO_2$, $CaCO_3$, ZnO, montmorillonite, bentonite, $Fe_2O_3$ |

**Table 3.** *Cont.*

| Techniques | Authors | Bitumen Matrix | Nano-Materials |
|---|---|---|---|
| UV spectroscopy | Zhang et al. (2015) [68] | Fresh, long-term aged, UV aged | ZnO |
| | Amini and Hayati (2020) [54] | Fresh, short and long term aged | CuO, Carbon nanotubes |
| | Li et al. (2015) [64] | Fresh, short-term aged, UV aged | ZnO |
| Rotational viscosity | Zhang et al. (2015) [68] | Fresh, UV aged | $SiO_2$, $TiO_2$, ZnO |
| | Zhang et al. (2015) [68] | Fresh, long-term aged, UV aged | ZnO |
| | Du et al. (2015) [91] | Fresh, short-term aged, UV-aged | ZnO |
| | Li et al. (2015) [58] | Fresh, short-term aged, UV aged | ZnO |
| | Nejad et al. (2016) [95] | Fresh, HMA | $TiO_2$, ZnO, $Al_2O_3$, $Fe_2O_3$ |
| | Mubaraki et al. (2016) [60] | Fresh | $Al_2O_3$ |
| | Ali et al. (2017) [93] | Fresh | $Al_2O_3$ |
| | Liu et al. (2018) [94] | Fresh, WMA, HMA | Graphene oxide |
| | Karnati et al. (2019) [62] | Fresh, long-term aged | $SiO_2$ |
| | Karnati et al. (2020) [63] | Fresh, aged | $SiO_2$ |
| | Zghair et al. (2020) [48] | Fresh | $SiO_2$ |
| | Sedaghat et al. (2020) [61] | Fresh, short-term aged, long-term aged | Clay (montmorillonite) |
| | Li et al. (2018) [92] | Fresh, SBS modified | Graphene oxide |
| RAMAN Spectroscopy | Moreno-Navarro et al. (2018) [78] | Fresh | Graphene |
| | Loise et al. (2019) [84] | Fresh | Carbon nanotubes |
| Limiting oxygen index methods | Wu et al. (2009) [87] | Fresh, short-term aged, long-term aged | Clay (montmorillonite) |
| | Wu et al. (2009) [87] | Fresh, short-term aged, long-term aged | Clay (montmorillonite) |
| Differential Scanning Calorimetry (DSC) | Sun et al. (2017) [67] | Fresh, asphalt mixture | $SiO_2$, $TiO_2$, $CaCO_3$, ZnO, Montmorillonite, bentonite, $Fe_2O_3$ |
| | Nejad et al. (2017) [52] | Fresh | $SiO_2$, $TiO_2$, $CaCO_3$ |
| | Amini and Hayati (2020) [54] | Fresh, short and long term aged | CuO, Carbon nanotubes |
| | Liu et al. (2018) [94] | Fresh, WMA, HMA | Graphene oxide |
| | Yang et al. (2020) [96] | Fresh | Carbon nanotube sponges |
| Indirect Tensile Stress (ITS) | Ghasemi et al. (2012) [47] | Fresh, HMA | $SiO_2$, |
| | Galooyak et al. (2015) [49] | Fresh, WMA | $SiO_2$, |
| | Amini and Hayati (2020) [54] | Fresh, short and long term aged | CuO, carbon nanotubes |
| | Hamedi et al. (2016) [88] | Fresh, HMA | ZnO |
| | Crucho et al. (2018) [50] | Fresh, asphalt mixture | $SiO_2$, zero-valent iron, clay |
| Performance grade (PG) | Brcic (2016) [97] | Fresh, short-term aged, long-term aged | Graphene |
| | Sedaghat et al. (2020) [61] | Fresh, short-term aged, long-term aged | Clay (montmorillonite) |
| Thermo Gravimetric Analysis (TGA) | Loise et al. (2019) [84] | Fresh | Carbon nanotubes |
| | Yang et al. (2020) [96] | Fresh | Carbon nanotube sponges |
| | Li et al. (2018) [92] | Fresh, SBS modified | Graphene oxide |

**Table 3.** *Cont.*

| Techniques | Authors | Bitumen Matrix | Nano-Materials |
|---|---|---|---|
| Storage stability | Zhang et al. (2015) [65] | Fresh, UV aged | $SiO_2$, $TiO_2$, ZnO |
| | Mubaraki et al. (2016) [60] | Fresh | $Al_2O_3$ |
| | Ali et al. (2017) [93] | Fresh | $Al_2O_3$ |
| Transmission Electron Microscopy (TEM) | Hussein et al. (2017) [59] | Fresh | Ceramic powders |
| | Loise et al. (2019) [84] | Fresh | Carbon nanotubes |
| Indirect Tensile Stiffness Modulus (ITSM) | Ghasemi et al. (2012) [47] | Fresh, HMA | $SiO_2$ |
| | Arabani et al. (2015) [83] | HMA | Carbon nanotubes |
| X-Ray Fluorescence (XRF) | Hussein et al. (2017) [59] | Fresh | Ceramic powders |
| Flash point | Nejad et al. (2016) [95] | Fresh, HMA | $TiO_2$, ZnO, $Al_2O_3$, $Fe_2O_3$ |
| | Olabemiwo et al. [90] | Fresh | Ag |
| Kinematic viscosity | Sadeghnejad et al. (2017) [51] | Fresh | $SiO_2$, $TiO_2$ |
| | Sedaghat et al. (2020) [61] | Fresh, short-term aged, long-term aged | Clay (montmorillonite) |
| | Olabemiwo et al. [90] | Fresh | Ag |
| Pyrolysis-gas Chromatography test | Zeng et al. (2017) [98] | Fresh, short-term aged, long-term aged | Graphene oxide |
| Rheology (performed by means of Dynamic Shear Rheometer) | Jahromi et al. (2009) [58] | Fresh, short-term aged, long-term aged | Clay (closite and nanofil) |
| | Wu et al. (2009) [87] | Fresh, short-term aged, long-term aged | Clay (montmorillonite) |
| | Du et al. (2015) [91] | Fresh, short-term aged, UV-aged | ZnO |
| | Galooyak et al. (2015) [49] | Fresh, WMA | $SiO_2$ |
| | Chen et al. (2015) [66] | Fresh, short-term aged, long-term aged | $SiO_2$, $TiO_2$, ZnO, EVMT |
| | Le et al. (2016) [82] | Fresh, short-term aged, long-term aged, asphalt mixture | Graphene |
| | Brcic (2016) [97] | Fresh, short-term aged, long-term aged | Graphene |
| | Mubaraki et al. (2016) [60] | Fresh | $Al_2O_3$ |
| | Zeng et al. (2017) [98] | Fresh, short-term aged, long-term aged | Graphene oxide |
| | Ali et al. (2017) [93] | Fresh | $Al_2O_3$ |
| | Sun et al. (2017) [67] | Fresh, asphalt mixture | $SiO_2$, $TiO_2$, $CaCO_3$, ZnO, montmorillonite, bentonite, $Fe_2O_3$ |
| | Nejad et al. (2017) [52] | Fresh | $SiO_2$, $TiO_2$, $CaCO_3$ |
| | Sadeghnejad et al. (2017) [51] | Fresh | $SiO_2$, $TiO_2$ |
| | Hussein et al. (2017) [59] | Fresh | Ceramic powders |
| | Shafabakhsh et al. (2018) [53] | Fresh, short-term aged, long-term aged | CuO |
| | Amini and Hayati (2020) [54] | Fresh, short and long term aged | CuO, Carbon nanotubes |
| | Li et al. (2018) [92] | Fresh, SBS modified | Graphene oxide |
| | Nazari et al. (2018) [55] | Fresh, short-term aged, long-term aged | $SiO_2$, $TiO_2$, $CaCO_3$ |
| | Olabemiwo et al. [90] | Fresh | Ag |
| | Liu et al. (2018) [94] | Fresh, WMA, HMA | Graphene oxide |
| | Moreno-Navarro et al. (2018) [78] | Fresh | Graphene |
| | Loise et al. (2019) [84] | Fresh | Carbon nanotubes |
| | Karnati et al. (2019) [62] | Fresh, long-term aged | $SiO_2$ |
| | Karnati et al. (2020) [63] | Fresh, aged | $SiO_2$ |
| | Yang et al. (2020) [96] | Fresh | Carbon nanotube sponges |

**Table 3.** *Cont.*

| Techniques | Authors | Bitumen Matrix | Nano-Materials |
|---|---|---|---|
| Rheology (performed by means of bending beam rheometer) | Le et al. (2016) [82] | Fresh, short-term aged, long-term aged, asphalt mixture | Graphene |
| | Sun et al. (2017) [67] | Fresh, asphalt mixture | $SiO_2$, $TiO_2$, $CaCO_3$, ZnO, montmorillonite, bentonite, $fe_2o_3$ |
| | Shafabakhsh et al. (2018) [53] | Fresh, short-term aged, long-term aged | CuO |
| | Amini and Hayati (2020) [54] | Fresh, short- and long-term aged | CuO, carbon nanotubes |
| | Sedaghat et al. (2020) [61] | Fresh, short-term aged, long-term aged | Clay (montmorillonite) |
| Gel-Permeation Chromatography (GPC) | Sun et al. (2017) [67] | Fresh, asphalt mixture | $SiO_2$, $TiO_2$, $CaCO_3$, ZnO, montmorillonite, bentonite, $Fe_2O_3$ |
| Gas Cromatography - Mass spectrometry (GC-MS) | Li et al. (2018) [92] | Fresh, SBS modified | Graphene oxide |
| Surface free energy | Hamedi et al. (2016) [88] | Fresh, HMA | ZnO |
| Repeated load axial test | Arabani et al. (2015) [83] | HMA | Carbon nanotubes |
| Zeta potential | Karnati et al. (2019) [62] | Fresh, long-term aged | $SiO_2$ |
| | Karnati et al. (2020) [63] | Fresh, aged | $SiO_2$ |
| Hydrodynamic diameter | Karnati et al. (2019) [62] | Fresh, long-term aged | $SiO_2$ |
| | Karnati et al. (2020) [63] | Fresh, aged | $SiO_2$ |
| Physical characterization (Softening point, Ductility, Penetration) | Jahromi et al. (2009) [58] | Fresh, short-term aged, long-term aged | Clay (closite and nanofil) |
| | Wu et al. (2009) [87] | Fresh, short-term aged, long-term aged | Clay (montmorillonite) |
| | Ghasemi et al. (2012) [47] | Fresh, HMA | $SiO_2$ |
| | Zhang et al. (2015) [68] | Fresh, long-term aged, UV aged | ZnO |
| | Olabemiwo et al. [90] | Fresh | Ag |
| | Du et al. (2015) [91] | Fresh, short-term aged, UV aged | ZnO |
| | Li et al. (2015) [64] | Fresh, short-term aged, UV aged | ZnO |
| | Zhang et al. (2015) [65] | Fresh, UV aged | $SiO_2$, $TiO_2$, ZnO |
| | Galooyak et al. (2015) [49] | Fresh, WMA | $SiO_2$ |
| | Taherkani et al. (2016) [99] | Fresh | $SiO_2$ |
| | Nejad et al. (2016) [95] | Fresh, HMA | $TiO_2$, ZnO, $Al_2O_3$, $Fe_2O_3$ |
| | Zeng et al. (2017) [98] | Fresh, short-term aged, long-term aged | Graphene oxide |
| | Ali et al. (2017) [93] | Fresh | $Al_2O_3$ |
| | Sun et al. (2017) [67] | Fresh, asphalt mixture | $SiO_2$, $TiO_2$, $CaCO_3$, ZnO, montmorillonite, bentonite, $Fe_2O_3$ |
| | Sadeghnejad et al. (2017) [51] | Fresh | $SiO_2$, $TiO_2$ |
| | Hussein et al. (2017) [59] | Fresh | Ceramic powders |
| | Li et al. (2018) [92] | Fresh, SBS modified | Graphene oxide |
| | Zghair et al. (2020) [48] | Fresh | $SiO_2$ |
| | Sedaghat et al. (2020) [61] | Fresh, short-term aged, long-term aged | Clay (montmorillonite) |
| ITF | Arabani et al. (2015) [83] | HMA | Carbon nanotubes |
| Compatibility test | Li et al. (2015) [64] | Fresh, short-term aged, UV aged | ZnO |
| TCLP | Hussein et al. (2017) [59] | Fresh | Ceramic powders |
| Static creep test | Nejad et al. (2016) [95] | Fresh, HMA | $TiO_2$, ZnO, $Al_2O_3$, $Fe_2O_3$ |
| MSCR | Liu et al. (2018) [94] | Fresh, HMA, WMA | Graphene oxide |

**Table 3.** *Cont.*

| Techniques | Authors | Bitumen Matrix | Nano-Materials |
|---|---|---|---|
| Direct tension test | Karnati et al. (2019) [62] | Fresh, long-term aged | $SiO_2$ |
| | Karnati et al. (2020) [63] | Fresh, aged | $SiO_2$ |
| Thermal conductivity | Moreno-Navarro et al. (2018) [78] | Fresh | Graphene |
| X-ray Photoelectron Spectroscopy (XPS) | Moreno-Navarro et al. (2018) [78] | Fresh | Graphene |
| Optical microscopy | Moreno-Navarro et al. (2018) [78] | Fresh | Graphene |
| Softening point test | Moreno-Navarro et al. (2018) [78] | Fresh | Graphene |
| Wheel tracking | Galooyak et al. (2015) [49] | Fresh, WMA | $SiO_2$ |
| | Crucho et al. (2018) [50] | Fresh, asphalt mixture | $SiO_2$, zero-valent iron, clay |
| Flow test | Ghasemi et al. (2012) [47] | Fresh, HMA | $SiO_2$ |
| Marshall stability | Ghasemi et al. (2012) [47] | Fresh, HMA | $SiO_2$ |
| Affinity test | Crucho et al. (2018) [50] | Fresh, asphalt mixture | $SiO_2$, zero-valent iron, clay |
| Stiffness test | Crucho et al. (2018) [50] | Fresh, asphalt mixture | $SiO_2$, zero-valent iron, clay |
| Fatigue test | Crucho et al. (2018) [50] | Fresh, asphalt mixture | $SiO_2$, zero-valent iron, clay |

## 8. A Critical Discussion on the Techniques of Characterization

Generally, the most common techniques described in literature that are used to study bitumen modification involves rheology measurements [100,101]. However, recently, more sophisticated techniques are also being used. Among these, nuclear magnetic resonance techniques have proven to be able to give detailed information both from the structural and from the dynamical point of views [102–105].

Another important technique is the X-ray scattering/diffraction. This can probe the structure at the nanoscale in soft and hard condensed matter.

In particular, small-angle X-ray scattering (SAXS), ultra-small angle x-rays scattering (USAXS) and wide-angle x-rays scattering (WAXS) are among the most employed experimental techniques for the investigation, in non-invasive way, of the structural properties of materials and complex self-assembly processes in a large variety of environments [106].

This non-destructive method efficiently evidences the formation of different nanostructures and morphologies thus highlighting the important role of the relevant molecular conformations in many different processes in the field on nanomaterials science [106].

More specifically the employment of synchrotron-based (multi-scale) X-ray scattering techniques allows advanced characterization of nano-structural properties and structural time evolution in large variety of materials systems including polymeric systems [107–112] organic structures including bio-materials and bio-(macro)molecules, [112–116] zeolites [117–119], alloys, ceramics and composite materials [119,120].

Their enormous potentialities and how they can be successfully applied to bitumens and asphalts, have been already discussed in some recent papers [121,122].

However, the reader may surely agree with us that the synergistic use of different techniques can give an even better comprehension of the complex physico-chemistry involved in these materials [123].

Due to the complexity of nanoparticles-containing bitumens and asphalts, it is clear that different techniques can probe different things, giving therefore different information. Due to the same complexity of the material under study, different questions now arise. Let's address each of them in the following subsections.

### *8.1. How to Probe the Presence of Nanoparticles by FT-IR*

We have shown how functionalization of inorganic nanoparticles is an emerging way to improve nanoparticle dispersion within the bituminous matrix. Such expensive methods require a technique to easily, and possibly cheaply, observe if the surface functionalization has taken place and to what extent.

Usually FT-IR has been used for this purpose. For example, the antioxidant effect of the two inorganic nanoparticles was deepened by FTIR by Nazari et al. [55]. However, also Hussein et al. [59], Li et al. [64], Karnati et al. [62] cited in the present work, have used FT-IR spectroscopy, as it can be seen by perusal of Table 3, which gives a panoramic view of the techniques used for investigating the properties of nanoparticles containing bitumens and asphalts.

Some comments are now due. Taking the work by Ali et al. [93] as a representative example, the authors, suspecting an irregular dispersion of the nanoparticles in binder, carried out a FT-IR investigation. In their work, the IR peak shifts were individuated as indicators of the coupling agent binding to the nanoparticle surface. We reproduce their key figure in Figure 5

In their work, tiny shifts of the peaks were interpreted as the consequence that asphalt is subjected to no obvious changes during modification. This was interpreted as that modification of asphalt with $Al_2O_3$ nanoparticles is merely a physical process.

We want to take inspiration from this conclusion to warn that in infra-red spectroscopy even small shifts in the absorption peaks can reveal interesting changes in the vibrational states of the functional groups. This can actually unveil real changes in interactions, which can be effectively treated through proper analysis [124]. An effective analysis must pass, in our opinion, through the separate analysis of the various IR ranges in which the functional groups absorb [125].

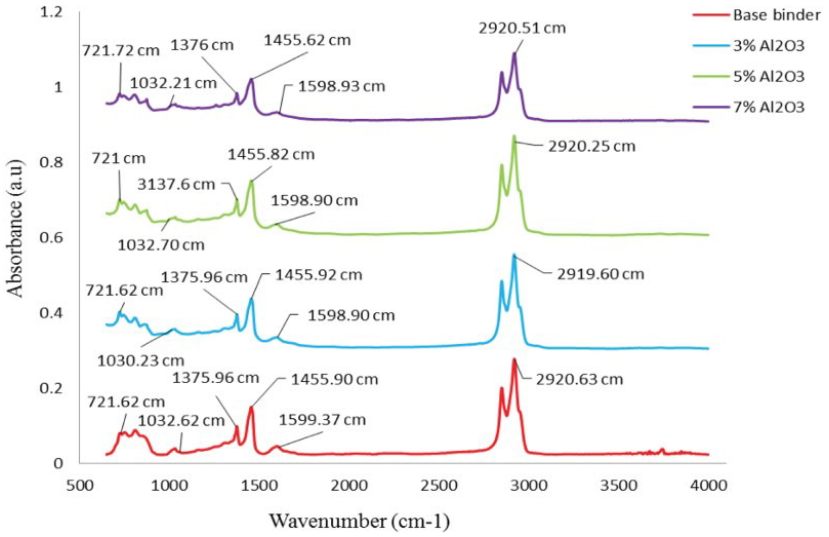


**Figure 5.** Spectra of the neat and $Al_2O_3$-modified bitumens studied by Ali et al. [93].

For example, it has been seen that the frequency of C-H stretching are usually quite robust but the relative intensities of the $CH_2$ and $CH_3$ symmetric and antisymmetric contributions are not, so they are usually indicated as interesting indicators of the chain packing [11,126].

*8.2. How to Probe the Distribution of Nanoparticles: Nanotomography as One of the Techniques of Election*

If nanoparticle-containing bitumens are studied, a specific aspect must be faced: the spatial distribution and organization of the nanoparticles within the bituminous matrix. It is obvious, in fact, that the nanoparticle distribution is of pivotal importance in the final properties.

From the structural point of view, being asphalt concretes heterogeneous materials, composed of aggregates, bitumen and porous networks, their mechanical properties depend on many factors such as the form and the distribution of the aggregate, the asphalt content, the pore content, pore distribution, and so on.

To face this problem, usually researchers probe the dispersion of nanoparticles within the bitumen or asphalts by microscopies, essentially scanning electron microscopy (SEM). Table 3 reports as summary of the techniques used by various authors, from which those who used SEM can be easily extracted.

As a representative example only, Taherkhani and Afroozi [99] in 2016 used SEM to probe the dispersion of the nanoparticles in the binder. Although they were able to find some nanoparticle tendency in aggregation and their tendency to form a network of aggregates responsible for the mechanical properties of the modified binder, it must be said that SEM is a surface method and it is not fit for probing the inner part of the material.

The problem is therefore twofold:

(1) On the one hand side, the technique must be able to probe the nanoparticles, differentiating their signal from that of the rest of the material.
(2) On the other hand, the technique must be able to also probe the inner part of the sample.

None of the above cited techniques can solve these two problems simultaneously.

For this reason, we want to point out the emergence of an interesting method for nanoparticles-containing matrices: nanotomography. It is a non-destructive technique which—like its related modalities tomography and microtomography—uses x-rays to create cross-sections from a 3D-object that later can be used to recreate a virtual model. However, unlike the classical tomography in the nano case the pixel sizes of the cross-sections are in the nanometer range. More common applications of micro- and nano-tomography can be found in many areas of research and development like: materials science, geology, biomedical engineering, dentistry, bio-engineering, building engineering. In all

these fields, the X-ray computed tomography (XCT) deals with materials of which the fine internal structure or the changes within the material are of outmost importance to understand the behavior of the material or to have insights in the processes going on. The interested reader can find more information in [127]. In the field of bitumen nanotomography technique was used by different authors to analyze and reconstruct the 3D structure of bitumen modified with different nanomaterials.

For example, nano-computed tomography (n-CT) was used to investigate the distribution of montmorillonite nanoparticles in the asphalt system [128]. Figure 6 shows the 3D distribution image of sodium montmorillonite nanoparticles in the bitumen at the maximum resolution (about 1μm) of the CT scanning equipment as obtained by those authors.

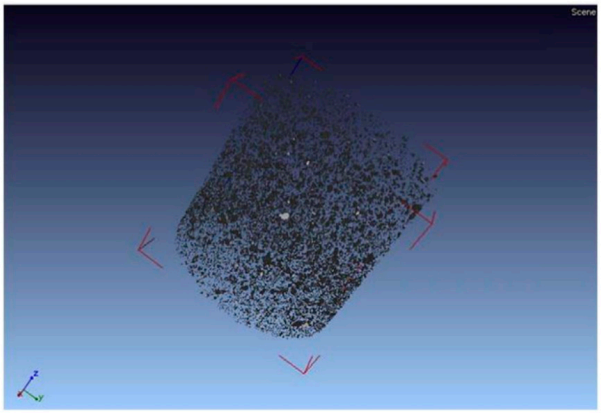

**Figure 6.** 3D distribution image of $Na^+$ montmorillonite particles in the bitumen.

Mohajeri et al. used the XCT technique visualize the interface between bitumen binder present in a reclaimed asphalt pavement (RAP) and a virgin bitumen used to blend it for new pavement surfacing [129]. XCT can also study the voids or to know the exact distribution of certain compounds to understand their effective layer-to-layer distribution inside the asphalt concrete as depicted in Figure 7 [130].

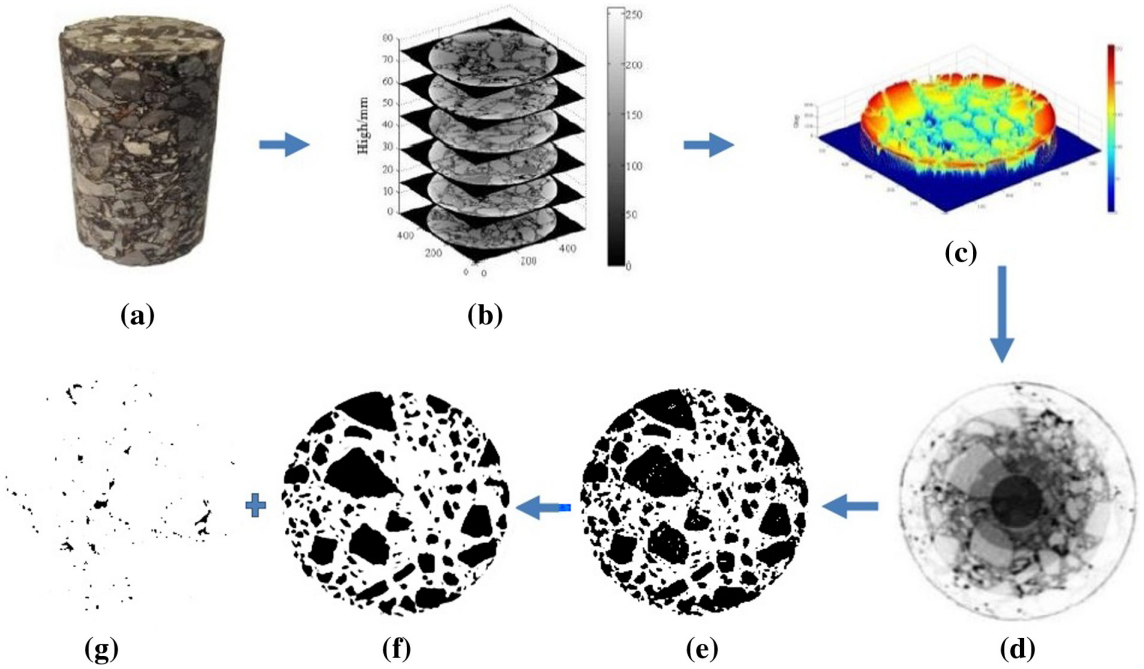


**Figure 7.** Extraction of the area of interest using CT scan technology [130]. (**a**) Asphalt concrete, (**b**) tomographic images, (**c**) gray distribution, (**d**) are of interest divided by annular masks, (**e**) initial binary image, (**f**) aggregate particles (>2.36 mm), (**g**) air-voids.

Another example of the successful application of the CT scan can be found in [131], where the authors used small quantities of $TiO_2$ as tracing agents of the virgin bitumen. In this way the blending between a virgin bitumen and a reclaimed asphalt pavement (RAP) could be studied.

Figure 8 shows 3D images of the cylinder-like sample of an asphalt concrete, in which the spatial distribution of the large virgin (shown in red, characterized by the presence of the tracing nanoparticles) and small RAP aggregates (shown in green) are evidenced inside the sample.

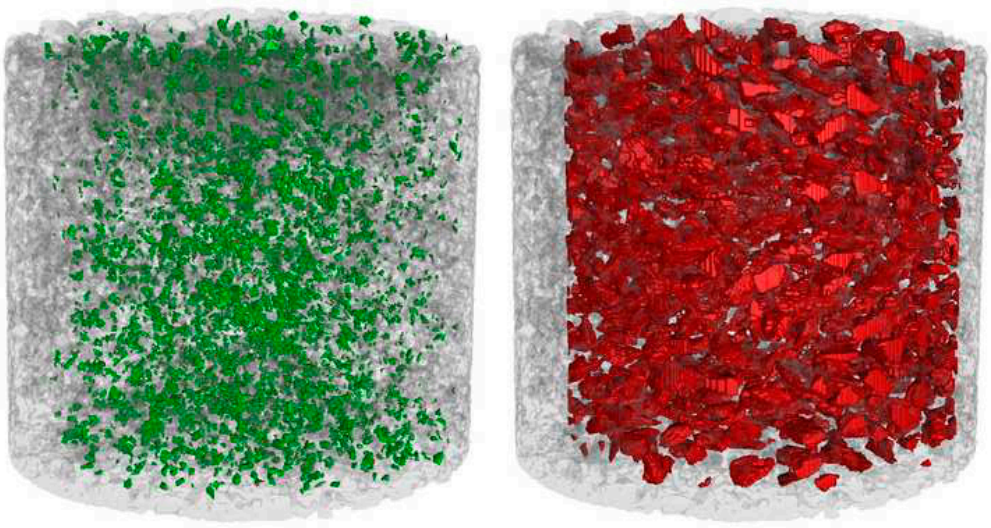

**Figure 8.** 3D images of the whole cylinder, as discussed in the text. The spatial distribution inside the sample of the large virgin and small RAP aggregates is shown with different colors (red and green, respectively).

### *8.3. UV-Vis Absorption for Probing Bitumen Screening towards UV Radiation*

Some nanoparticles, due to their semiconductor nature, can absorb radiations whose energies are above the semiconductor energy gap. This energy threshold of absorption can be changed by changing the type of nanoparticles: for example, as expected, the widely-used nano-$SiO_2$ cannot counteract the effect of photo-oxidation due to UV aging [66] since its energy gap is too high (7.5–9.6 eV [132,133]). It is, indeed, considered more as an insulator rather than a semiconductor.

The energy threshold of absorption can also be changed by changing nanoparticle size and the efficiency of absorption by the inner structure governing the physical nature (direct or indirect) of the photon absorption [134]. This actually provides researchers with a further method to tune the absorption of radiation. For this reason, the capability of nanoparticles to absorb photons must be exactly determined for a wise design of a performing bitumen, and this requires suitable techniques for nanoparticle characterization.

This aspect can be in-depth explored by a simple UV-Vis spectroscopy technique, which can probe the photophysical behaviour through very simple data analysis, allowing the determination of both the energy gap and the efficiency of absorption. [26,135].

The possibility to tune the probability of photon absorption by changing the nanoparticle structural characteristics could be, in our opinion, a powerful way to further enhance the resistance of a nanoparticle-modified bitumen to the photo-induced ageing, which deserves much attention. For examples, the presence in traces of a metal within nanoparticles can induce a lowering of the nanoparticle energy gap (sensitization) thus extending the wavelength range of the photons which are absorbed. [26,135]. More absorbed photons means that the resulting nanoparticle-containing bitumen can be more resistant to photo-induced ageing. Here the same consideration on costs holds: it is obvious that obtaining nanoparticles with enhanced photophysical properties involves huge costs, but progresses in specialized technologies for their productions and an eventual increasing market can

make, with time, the use of such kind of nanoparticles affordable, with unprecedented benefits, in our opinion, in terms of durability of bituminous materials.

## 9. Conclusions and Perspectives

Nanoparticles have unique properties. Recent progress in nanotechnology has allowed their preparation and modification with control even at the atomic level. Two approaches for nanoparticle production can be followed: they are top-down and bottom up. The former starts from bulk materials to obtain nano-sized particles through mainly physical processes. Ball milling is, for example, a cheap and quick such method. On the other hand, bottom-up approaches obtain nanoparticles from atomic and molecular precursors by self-assembly. The use of nanoparticles in bitumens must be scalable and cheap, so the former are preferred.

Recent works show that the nanoparticle surface has a pivotal importance in their embedding into the bitumen matrix. In this context we want to point out that the specific surface can be greatly enhanced if zeolites are used: modern protocols [136] individuate different stages in their growth so different morphologies can be obtained. In addition, surface manipulation allows the functionalization of certain nanoparticles with clear benefits in terms of increased affinity towards the bitumen apolar nature. The proper engineering of the bitumen addition with nanoparticles implies higher costs, obviously, but on the other hand it is clear that presence of nanoparticles can greatly enhance the mechanical properties of bitumens, potentially conferring also other new/novel important properties. Among these, the resistance to UV radiation is the most appealing to our eyes, granting higher stability over long times. Exploiting this possibility requires skills in photophysics, which widens the competencies required for research in this field and clearly indicating that multidisciplinarity is necessary. In any case, all this can be studied within the framework of the physics of complex systems, where the simultaneous presence of different chemical ingredients can give sometimes unexpected, but advanced, characteristics thanks to synergistic/cooperative effects among them, which are worth tailoring for specific applications [137].

All this has a cost, not only economic but also in the general sense of resources (time, availability of instruments, know-how ... ). Apart from some brilliant solutions to reuse nanoparticles from wastes, like that of Hussein et al. [59], which is a strategy we strongly support for environmental concerns and for sustainable economy, at the moment the costs are generally high and affect negatively the affordability of nanoparticle use in bitumens and asphalt addition, but in our opinion, the high costs are due to the fact that the use of nanoparticles in bitumens is still quite recent, so we are confident that with the development of technology the costs will lower and demand will increase. We believe that the discoveries in nanotechnology field, which have been always confined to small-quantities applications, can also be beneficial in large-scale applications like road pavement, in the next future. This is probably the biggest challenge in modern technology but we hope that it will be achieved soon in the field of bitumen, since the intelligent incorporation of nanoparticles can give, as it has been shown, novel properties of extreme added-value.

**Author Contributions:** Writing—Original Draft Preparation, P.C. (Pietro Calandra) and V.L.; Writing—Review & Editing, P.C. (Pietro Calandra); Conceptualization, M.P. and D.L.; Investigation, V.L. and M.P.; Conceptualization and Supervision, P.C. (Paolino Caputo) and C.O.R. All authors have read and agreed to the published version of the manuscript.

**Funding:** This research received no external funding.

**Conflicts of Interest:** The author declares no conflict of interest.

## References

1. Petrauskas, D.; Saleem, U. The Shell bitumen handbook. In *The Shell Bitumen Handbook*; Read, J., Whiteoak, D., Eds.; Thomas Telford: London, UK, 2003; p. 29. ISBN 072773220X.

2. Paliukaitė, M.; Vaitkus, A.; Zofka, A. Evaluation of bitumen fractional composition depending on the crude oil type and production technology. In Proceedings of the 9th International Conference on Environmental Engineering, Vilnius, Lithuania, 22–24 May 2014.
3. Porto, M.; Caputo, P.; Loise, V.; Eskandarsefat, S.; Teltayev, B.; Rossi, C.O. Bitumen and bitumen modification: A review on latest advances. *Appl. Sci.* **2019**, *9*, 742. [CrossRef]
4. *EN 12597 Bitumen and Bituminous Binders-Terminology*; European Commetee for Standardization: Brussels, Belgium, 2000.
5. Yoon, S.; Bhatt, S.D.; Lee, W.; Lee, H.Y.; Jeong, S.Y.; Baeg, J.-O.; Lee, C.W. Separation and characterization of bitumen from Athabasca oil sand. *Korean J. Chem. Eng.* **2009**, *26*, 64–71. [CrossRef]
6. Lesueur, D. The colloidal structure of bitumen: Consequences on the rheology and on the mechanisms of bitumen modification. *Adv. Colloid Interface Sci.* **2009**, *145*, 42–82. [CrossRef] [PubMed]
7. Calandra, P.; Caputo, P.; De Santo, M.P.; Todaro, L.; Turco Liveri, V.; Oliviero Rossi, C. Effect of additives on the structural organization of asphaltene aggregates in bitumen. *Constr. Build. Mater.* **2019**, *199*, 288–297. [CrossRef]
8. Loise, V.; Caputo, P.; Porto, M.; Calandra, P.; Angelico, R.; Rossi, C.O. A review on Bitumen Rejuvenation: Mechanisms, materials, methods and perspectives. *Appl. Sci.* **2019**, *9*, 4316. [CrossRef]
9. Hunter, R.; Self, A.; Read, J. *The Shell Bitumen Handbook*, 6th ed.; Hunter, R., Ed.; ICE Publishing: London, UK, 2015; ISBN 0727758373.
10. Firoozifar, S.H.; Foroutan, S.; Foroutan, S. The effect of asphaltene on thermal properties of bitumen. *Chem. Eng. Res. Des.* **2011**, *89*, 2044–2048. [CrossRef]
11. Calandra, P.; Ruggirello, A.; Mele, A.; Liveri, V.T. Self-assembly in surfactant-based liquid mixtures: Bis(2-ethylhexyl)phosphoric acid/bis(2-ethylhexyl)amine systems. *J. Colloid Interface Sci.* **2010**, *348*, 183–188. [CrossRef]
12. Calandra, P.; Turco Liveri, V.; Riello, P.; Freris, I.; Mandanici, A. Self-assembly in surfactant-based liquid mixtures: Octanoic acid/Bis(2-ethylhexyl)amine systems. *J. Colloid Interface Sci.* **2012**, *367*, 280–285. [CrossRef]
13. Calandra, P.; Mandanici, A.; Liveri, V.T. Self-assembly in surfactant-based mixtures driven by acid–base reactions: Bis(2-ethylhexyl) phosphoric acid–n-octylamine systems. *RSC Adv.* **2013**, *3*, 5148–5155. [CrossRef]
14. Calandra, P.; Mandanici, A.; Turco Liveri, V.; Pochylski, M.; Aliotta, F. Emerging dynamics in surfactant-based liquid mixtures: Octanoic acid/bis(2-ethylhexyl) amine systems. *J. Chem. Phys.* **2012**, *136*, 064515. [CrossRef]
15. Calandra, P.; Nicotera, I.; Rossi, C.O.; Liveri, V.T. Dynamical properties of self-assembled surfactant-based mixtures: Triggering of one-dimensional anomalous diffusion in bis(2-ethylhexyl)phosphoric acid/n-octylamine systems. *Langmuir* **2013**, *29*, 14848–14854. [CrossRef] [PubMed]
16. Lombardo, D.; Calandra, P.; Pasqua, L.; Magazù, S. Self-assembly of Organic Nanomaterials and Biomaterials: The Bottom-Up Approach for Functional Nanostructures Formation and Advanced Applications. *Materials* **2020**, *13*, 1048. [CrossRef] [PubMed]
17. Oliviero Rossi, C.; Ashimova, S.; Calandra, P.; De Santo, M.P.; Ruggero, A. Mechanical resilience of modified bitumen at different cooling rates: A rheological and atomic force microscopy investigation. *Appl. Sci.* **2017**, *7*, 779. [CrossRef]
18. Calandra, P.; Longo, A.; Ruggirello, A.; Turco Liveri, V. Physico-Chemical Investigation of the State of Cyanamide Confined in AOT and Lecithin Reversed Micelles. *J. Phys. Chem. B* **2004**, *108*, 8260–8268. [CrossRef]
19. Calandra, P.; Giordano, C.; Ruggirello, A.; Turco Liveri, V. Physicochemical investigation of acrylamide solubilization in sodium bis(2-ethylhexyl)sulfosuccinate and lecithin reversed micelles. *J. Colloid Interface Sci.* **2004**, *277*, 206–214. [CrossRef]
20. Calandra, P.; Marco, G.D.; Ruggirello, A.; Liveri, V.T. Physico-chemical investigation of nanostructures in liquid phases: Nickel chloride ionic clusters confined in sodium bis(2-ethylhexyl) sulfosuccinate reverse micelles. *J. Colloid Interface Sci.* **2009**, *336*, 176–182. [CrossRef]
21. Longo, A.; Banerjee, D.; Hermida-Merino, D.; Portale, G.; Calandra, P.; Turco Liveri, V. Induced Chirality in Confined Space on Halogen Gold Complexes. *J. Phys. Chem. C* **2015**, *119*, 18798–18807. [CrossRef]
22. Longo, A.; Calandra, P.; Casaletto, M.P.; Giordano, C.; Venezia, A.M.; Liveri, V.T. Synthesis and physico-chemical characterization of gold nanoparticles softly coated by AOT. *Mater. Chem. Phys.* **2006**, *96*, 66–72. [CrossRef]

23. Calandra, P.; Giordano, C.; Longo, A.; Liveri, V.T. Physicochemical investigation of surfactant-coated gold nanoparticles synthesized in the confined space of dry reversed micelles. *Mater. Chem. Phys.* **2006**, *98*, 494–499. [CrossRef]
24. Calandra, P. Synthesis of Ni nanoparticles by reduction of NiCl2 ionic clusters in the confined space of AOT reversed micelles. *Mater. Lett.* **2009**, *63*, 2416–2418. [CrossRef]
25. Calandra, P.; Lombardo, D.; Neri, F.; Ruggirello, A.; Trusso, S.; Liveri, V.T. Synthesis of Yb nanoparticles by laser ablation of ytterbium target in sodium bis(2-ethylhexyl)sulfosuccinate reverse micellar solution. *Mater. Lett.* **2010**, *64*, 576–579. [CrossRef]
26. Calandra, P.; Lombardo, D.; Pistone, A.; Liveri, V.; Trusso, S. Structural and optical properties of novel surfactant-coated Yb@TiO2 nanoparticles. *J. Nanopart. Res.* **2011**, *13*, 5833–5839. [CrossRef]
27. Apostolidis, P.; Liu, X.; Kasbergen, C.; Scarpas, A.T. Synthesis of asphalt binder aging and the state of the art of antiaging technologies. *Transp. Res. Rec.* **2017**, *2633*, 147–153. [CrossRef]
28. European Commission. European Commission Recommendation of 18 October 2011 on the definition of nanomaterial, 2011/696/EU. *Off. J. Eur. Union* **2011**, *275*, 38–40.
29. Steyn, W. Applications of Nanotechnology in Road Pavement Engineering. In *Nanotechnology in Civil Infrastructure—A Paradigm Shift*; Springer: Berlin/Heidelberg, Germany, 2011; pp. 49–84. ISBN 978-3-642-16656-3.
30. Donegà, C. The Nanoscience Paradigm: "Size Matters!". In *Nanoparticles: Workhorses of Nanoscience*; Donega, C.d.M., Ed.; Springer: Berlin/Heidelberg, Germany, 2014; pp. 1–12.
31. Malsch, I. Nanotechnology in Europe: Scientific trends and organizational dynamics. *Nanotechnology* **1999**, *10*, 1–7. [CrossRef]
32. Zhu, W.; Bartos, P.; Porro, A. Application of nanotechnology in construction. *Mater. Struct.* **2004**, *37*, 649–658. [CrossRef]
33. Roduner, E. *Nanoscopic Materials Size-Dependent Phenomena*, 1st ed.; RSC: Cambridge, UK, 2006; ISBN 10: 085404857X.
34. Pacheco-Torgal, F.; Jalali, S. Nanotechnology: Advantages and drawbacks in the field of construction and building materials. *Constr. Build. Mater.* **2011**, *25*, 582–590. [CrossRef]
35. Sobolev, K.; Gutierrez, M.F. How Nanotechnology Can Change The Concrete World Part 1. *Am. Ceram. Soc. Bull.* **2005**, *84*, 14–17.
36. Correia, A. PHANTOMS: Nanotechnology network for information processing and storage. *Nanotechnology* **2001**, *12*, 89–90. [CrossRef]
37. Sohnel, O.; Garside, J. *Precipitation: Basic Principles and Industrial Applications*; Butterworth-Heinemann: Oxford, UK, 1992; ISBN 0750611073.
38. Ludwig, F.P.; Schmelzer, J. Cluster Formation and Growth in Segregation Processes with Constant Rates of Supply of Monomers. *Z. Phys. Chem.* **1995**, *192*, 155–167. [CrossRef]
39. Karahancer, S.; Saltan, M.; Morova, N.; Serin, S.; Terzi, S. Evaluation of rice husk ash as filler in hot mix asphalt concrete. *Constr. Build. Mater.* **2013**, *48*, 390–397.
40. Martinho, F.; Picado-Santos, L.; Capitão, S. Feasibility Assessment of the Use of Recycled Aggregates for Asphalt Mixtures. *Sustainability* **2018**, *10*, 1737. [CrossRef]
41. Filonzi, A.; Sabaraya, I.V.; Hajj, R.; Das, D.; Saleh, N.B.; Bhasin, A. *Evaluating the Use of Nanomaterials to Enhance Properties of Asphalt Binders and Mixtures*; Technical report 0-6854-1; University of Texas—Center for Trasportation Research: Austin, TX, USA, 2017.
42. Crucho, J.; Picado-Santos, L.; Neves, J.; Capitão, S. A review of nanomaterials' effect on mechanical performance and aging of asphalt mixtures. *Applied. Sci.* **2019**, *9*, 3657. [CrossRef]
43. $Fe_2O_3$ Iron Oxide Nanoparticles/Nanopowder (Alpha, 99.9%, 5nm, Red). Available online: https://www.us-nano.com/inc/sdetail/50544 (accessed on 10 June 2020).
44. Singh, L.P.; Karade, S.R.; Bhattacharyya, S.K.; Yousuf, M.M.; Ahalawat, S. Beneficial role of nanosilica in cement based materials—A review. *Constr. Build. Mater.* **2013**, *47*, 1069–1077. [CrossRef]
45. Li, R.; Xiao, F.; Amirkhanian, S.; You, Z.; Huang, J. Developments of nano materials and technologies on asphalt materials—A review. *Constr. Build. Mater.* **2017**, *143*, 633–648. [CrossRef]
46. Yang, J.; Tighe, S. A Review of Advances of Nanotechnology in Asphalt Mixtures. *Procedia–Soc. Behav. Sci.* **2013**, *96*, 1269–1276. [CrossRef]

47. Ghasemi, M.; Marandi, M.; Tahmooresi, M.; Jalal kamali, R.; Taherzade, R. Modification of Stone Matrix Asphalt with Nano-$SiO_2$. *J. Basic Appl. Sci. Res.* **2012**, *2*, 1338–1344.
48. Zghair, H.H.; Jony, H.; Hassan, M. Rheological Characteristics of Nano Silica Modified Asphalt Binder Material. In Proceedings of the 2019 International Engineering Conference (IEC), Erbil, Iraqi Kurdistan, 23–24 April 2019; pp. 79–84.
49. Galooyak, S.S.; Palassi, M.; Goli, A.; Farahani, H.Z. Performance Evaluation of Nano-silica Modified Bitumen. *Int. J. Transp. Eng.* **2015**, *3*, 55–66.
50. Crucho, J.M.L.; das Neves, J.M.C.; Capitão, S.D.; de Picado-Santos, L.G. Mechanical performance of asphalt concrete modified with nanoparticles: Nanosilica, zero-valent iron and nanoclay. *Constr. Build. Mater.* **2018**, *181*, 309–318. [CrossRef]
51. Sadeghnejad, M.; Shafabakhsh, G. Experimental Study on the Physical and Rheological Properties of Bitumen Modified with Different Nano Materials (Nano $SiO_2$ & Nano $TiO_2$). *Int. J. Nanosci. Nanotechnol.* **2017**, *13*, 253–263.
52. Nejad, F.M.; Nazari, H.; Naderi, K.; Karimiyan Khosroshahi, F.; Hatefi Oskuei, M. Thermal and rheological properties of nanoparticle modified asphalt binder at low and intermediate temperature range. *Pet. Sci. Technol.* **2017**, *35*, 641–646. [CrossRef]
53. Shafabakhsh, G.H.; Sajadib, S.R. Evaluation of rheological behavior of bitumen modified with Nano Copper Oxide. *Int. J. Eng. Technol.* **2018**, *7*, 13–18. [CrossRef]
54. Amini, N.; Hayati, P. Effects of CuO nanoparticles as phase change material on chemical, thermal and mechanical properties of asphalt binder and mixture. *Constr. Build. Mater.* **2020**, *251*, 118996. [CrossRef]
55. Nazari, H.; Naderi, K.; Moghadas Nejad, F. Improving aging resistance and fatigue performance of asphalt binders using inorganic nanoparticles. *Constr. Build. Mater.* **2018**, *170*, 591–602. [CrossRef]
56. Uddin, F. Clays, Nanoclays, and Montmorillonite Minerals. *Metall. Mater. Trans. A* **2008**, *39*, 2804–2814. [CrossRef]
57. Phyllosilicates (Micas, Chlorite, Talc, & Serpentine). Available online: Tulane.edu/~{}sanelson/eens211/phyllosilicates.htm. (accessed on 10 June 2020).
58. Jahromi, S.G.; Khodaii, A. Effects of nanoclay on rheological properties of bitumen binder. *Constr. Build. Mater.* **2009**, *23*, 2894–2904. [CrossRef]
59. Hussein, A.A.; Jaya, R.P.; Abdul Hassan, N.; Yaacob, H.; Huseien, G.F.; Ibrahim, M.H.W. Performance of nanoceramic powder on the chemical and physical properties of bitumen. *Constr. Build. Mater.* **2017**, *156*, 496–505. [CrossRef]
60. Mubaraki, M.; Ali, S.I.A.; Ismail, A.; Yusoff, N.I.M. Rheological Evaluation of Asphalt Cements Modified with ASA Polymer and $Al_2O_3$ Nanoparticles. *Procedia Eng.* **2016**, *143*, 1276–1284. [CrossRef]
61. Sedaghat, B.; Taherrian, R.; Hosseini, S.A.; Mojtaba Mousavi, S. Rheological properties of bitumen containing nanoclay and organic warm-mix asphalt additives. *Constr. Build. Mater.* **2020**, *243*, 118092. [CrossRef]
62. Karnati, S.R.; Oldham, D.; Fini, E.H.; Zhang, L. Surface functionalization of silica nanoparticles to enhance aging resistance of asphalt binder. *Constr. Build. Mater.* **2019**, *211*, 1065–1072. [CrossRef]
63. Karnati, S.R.; Oldham, D.; Fini, E.H.; Zhang, L. Application of surface-modified silica nanoparticles with dual silane coupling agents in bitumen for performance enhancement. *Constr. Build. Mater.* **2020**, *244*, 118324. [CrossRef]
64. Li, R.; Pei, J.; Sun, C. Effect of nano-ZnO with modified surface on properties of bitumen. *Constr. Build. Mater.* **2015**, *98*, 656–661. [CrossRef]
65. Zhang, H.; Zhu, C.; Yu, J.; Shi, C.; Zhang, D. Influence of surface modification on physical and ultraviolet aging resistance of bitumen containing inorganic nanoparticles. *Constr. Build. Mater.* **2015**, *98*, 735–740. [CrossRef]
66. Chen, Z.; Zhang, H.; Zhu, C.; Zhao, B. Rheological examination of aging in bitumen with inorganic nanoparticles and organic expanded vermiculite. *Constr. Build. Mater.* **2015**, *101*, 884–891. [CrossRef]
67. Sun, L.; Xin, X.; Ren, J. Inorganic nanoparticle-modified asphalt with enhanced performance at high temperature. *J. Mater. Civ. Eng.* **2017**, *29*, 1–9. [CrossRef]
68. Zhang, H.B.; Zhang, H.L.; Ke, N.X.; Huang, J.H.; Zhu, C.Z. The effect of different nanomaterials on the long-term aging properties of bitumen. *Pet. Sci. Technol.* **2015**, *33*, 388–396. [CrossRef]
69. Han, T.-H.; Kim, H.; Kwon, S.-J.; Lee, T.-W. Graphene-based flexible electronic devices. *Mater. Sci. Eng. R Rep.* **2017**, *118*, 1–43. [CrossRef]

70. Nguyen, T.P.; Nguyen, D.L.T.; Nguyen, V.H.; Le, T.H.; Vo, D.V.N.; Ly, Q.V.; Kim, S.Y.; Van Le, Q. Recent progress in carbon-based buffer layers for polymer solar cells. *Polymers* **2019**, *11*, 1858. [CrossRef]
71. Vajtai, R. (Ed.) *Springer Handbook of Nanomaterials*, 1st ed.; Springer: Berlin/Heidelberg, Germany, 2013; ISBN 978-3-642-20594-1.
72. Young, R.J.; Kinloch, I.A.; Gong, L.; Novoselov, K.S. The mechanics of graphene nanocomposites: A review. *Compos. Sci. Technol.* **2012**, *72*, 1459–1476. [CrossRef]
73. Le, J.-L.; Du, H.; Pang, S.D. Use of 2D Graphene Nanoplatelets (GNP) in cement composites for structural health evaluation. *Compos. Part B Eng.* **2014**, *67*, 555–563. [CrossRef]
74. Du, H.; Pang, S.D. Enhancement of barrier properties of cement mortar with graphene nanoplatelet. *Cem. Concr. Res.* **2015**, *76*, 10–19. [CrossRef]
75. Du, H.; Pang, S.D. *Mechanical Response and Strain Sensing of Cement Composites Added with Graphene Nanoplatelet under Tension BT—Nanotechnology in Construction*; Sobolev, K., Shah, S.P., Eds.; Springer International Publishing: Cham, Switzerland, 2015; pp. 377–382.
76. Palmeri, M.J.; Putz, K.W.; Ramanathan, T.; Brinson, L.C. Multi-scale reinforcement of CFRPs using carbon nanofibers. *Compos. Sci. Technol.* **2011**, *71*, 79–86. [CrossRef]
77. Lu, S.-N.; Xie, N.; Feng, L.-C.; Zhong, J. Applications of Nanostructured Carbon Materials in Constructions: The State of the Art. *J. Nanomater.* **2015**, *2015*, 807416. [CrossRef]
78. Moreno-Navarro, F.; Sol-Sánchez, M.; Gamiz, F.; Gámez, M. Mechanical and thermal properties of graphene modified asphalt binders. *Constr. Build. Mater.* **2018**, *180*, 265–274. [CrossRef]
79. Aravind, S.; Isac, A.J.; Aparajith, S. Construction of porous asphalt pavement using graphene. *Int. J. Recent Trends Eng. Res.* **2018**, *4*, 475–481.
80. Habib, N.; Ng, C.; Zoorob, S.; Lee, P. Use of Graphene Oxide as a Bitumen Modifier: An Innovative Process Optimization Study. *Adv. Mater. Res.* **2015**, *1105*, 365–369. [CrossRef]
81. Cataldi, P.; Athanassiou, A.; Bayer, I. Graphene Nanoplatelets-Based Advanced Materials and Recent Progress in Sustainable Applications. *Appl. Sci.* **2018**, *8*, 1438. [CrossRef]
82. Le, J.; Marasteanu, M.; Turos, M. *Graphene Nanoplatelet (GNP) Reinforced Asphalt Mixtures: A Novel Multifunctional Pavement Material*. IDEA Program Final Report NCHRP 173. 2016, pp. 1–28. Available online: http://onlinepubs.trb.org/onlinepubs/IDEA/FinalReports/Highway/NCHRP173_Final_Report.pdf (accessed on 28 July 2020).
83. Arabani, M.; Faramarzi, M. Characterization of CNTs-modified HMA's mechanical properties. *Constr. Build. Mater.* **2015**, *83*, 207–215. [CrossRef]
84. Loise, V.; Vuono, D.; Policicchio, A.; Teltayev, B.; Gnisci, A.; Messina, G.; Oliviero Rossi, C. The effect of multiwalled carbon nanotubes on the rheological behaviour of bitumen. *Colloids Surf. A Physicochem. Eng. Asp.* **2019**, *566*, 113–119. [CrossRef]
85. Khattak, M.J.; Khattab, A.; Rizvi, H.R.; Zhang, P. The impact of carbon nano-fiber modification on asphalt binder rheology. *Constr. Build. Mater.* **2012**, *30*, 257–264. [CrossRef]
86. Rizvi, H.R.; Khattak, M.J.; Madani, M.; Khattab, A. Piezoresistive response of conductive Hot Mix Asphalt mixtures modified with carbon nanofibers. *Constr. Build. Mater.* **2016**, *106*, 618–631. [CrossRef]
87. Wu, S.; Zhang, Y.; Wang, J. A novel potential flame-retarded bitumen nanoclay modified bitumen. *Road Mater. Pavement Des.* **2009**, *10*, 115–128. [CrossRef]
88. Hamedi, G.H.; Nejad, F.M.; Oveisi, K. Estimating the moisture damage of asphalt mixture modified with nano zinc oxide. *Mater. Struct.* **2016**, *49*, 1165–1174. [CrossRef]
89. Erkens, S.; Porot, L.; Glaser, R.; Glover, C.J. Aging of Bitumen and Asphalt Concrete: Comparing State of the Practice and Ongoing Developments in the United States and Europe. In Proceedings of the Transportation Research Board 95th Annual Meeting, Washington, DC, USA, 10–14 January 2016.
90. Olabemiwo, O.M.; Lateef, A.; Agunbiade, F.O.; Akanji, S.B.; Bakare, H.O. The effects on oxidative aging, physical and flow properties of Agbabu natural bitumen modified with silver nanoparticles. *Heliyon* **2020**, *6*, e04164. [CrossRef] [PubMed]
91. Du, P.; Ke, N.; Zhang, H. Effect of Nano-zinc Oxide on the Morphology and Ultraviolet Aging Properties of Various Bitumens. *Pet. Sci. Technol.* **2015**, *33*, 1110–1117. [CrossRef]
92. Li, Y.; Wu, S.; Amirkhanian, S. Investigation of the graphene oxide and asphalt interaction and its effect on asphalt pavement performance. *Constr. Build. Mater.* **2018**, *165*, 572–584. [CrossRef]

93. Ali, S.I.A.; Ismail, A.; Karim, M.R.; Yusoff, N.I.M.; Al-Mansob, R.A.; Aburkaba, E. Performance evaluation of Al 2 O 3 nanoparticle-modified asphalt binder. *Road Mater. Pavement Des.* **2017**, *18*, 1251–1268. [CrossRef]
94. Liu, K.; Zhang, K.; Wu, J.; Muhunthan, B.; Shi, X. Evaluation of mechanical performance and modification mechanism of asphalt modified with graphene oxide and warm mix additives. *J. Clean. Prod.* **2018**, *193*, 87–96. [CrossRef]
95. Nejad, F.M.; Tanzadeh, R.; Tanzadeh, J.; Hamedi, G.H. Investigating the effect of nanoparticles on the rutting behaviour of hot-mix asphalt. *Int. J. Pavement Eng.* **2016**, *17*, 353–362. [CrossRef]
96. Yang, Q.; Li, X.; Zhang, L.; Qian, Y.; Qi, Y.; Kouhestani, H.S.; Shi, X.; Gui, X.; Wang, D.; Zhong, J. Performance evaluation of bitumen with a homogeneous dispersion of carbon nanotubes. *Carbon* **2020**, *158*, 465–471. [CrossRef]
97. Brcic, H. Investigation of the Rheological Properties of Asphalt Binder Containing Graphene Nanoplatelets. Master's Thesis, Norwegian University of Science and Technology, Norway, Norway, 2016.
98. Zeng, W.; Wu, S.; Pang, L.; Sun, Y.; Chen, Z. The Utilization of Graphene Oxide in Traditional Construction Materials: Asphalt. *Materials* **2017**, *10*, 48. [CrossRef]
99. Taherkhani, H.; Afroozi, S. The properties of nanosilica-modified asphalt cement. *Pet. Sci. Technol.* **2016**, *34*, 1381–1386. [CrossRef]
100. Porto, M.; Caputo, P.; Loise, V.; De Filpo, G.; Rossi, C.O.; Calandra, P. Polysaccharides-reinforced bitumens: Specificities and universality of rheological behavior. *Appl. Sci.* **2019**, *9*, 5564. [CrossRef]
101. Caputo, P.; Porto, M.; Calandra, P.; De Santo, M.P.; Oliviero Rossi, C. Effect of epoxidized soybean oil on mechanical properties of bitumen and aged bitumen. *Mol. Cryst. Liq. Cryst.* **2018**, *675*, 68–74. [CrossRef]
102. Caputo, P.; Porto, M.; Loise, V.; Teltayev, B.; Rossi, C.O. Analysis of mechanical performance of bitumen modified with waste plastic and rubber (SBR) additives by rheology and PGSE NMR experiments. *Eurasian Chem. J.* **2019**, *21*, 235–239. [CrossRef]
103. Caputo, P.; Loise, V.; Ashimova, S.; Teltayev, B.; Vaiana, R.; Oliviero Rossi, C. Inverse Laplace Transform (ILT)NMR: A powerful tool to differentiate a real rejuvenator and a softener of aged bitumen. *Colloids Surf. A Physicochem. Eng. Asp.* **2019**, *574*, 154–161. [CrossRef]
104. Rossi, C.O.; Caputo, P.; Loise, V.; Ashimova, S.; Teltayev, B.; Sangiorgi, C. A new green rejuvenator: Evaluation of structural changes of aged and recycled bitumens by means of rheology and NMR. In *RILEM 252-CMB-Symposium on Chemo Mechanical Characterization of Bituminous Materials*; Springer: Cham, Switzerland, 2018; Volume 20, pp. 177–182.
105. Oliviero, C.; Caputo, P.; Ashimova, S.; Fabozzi, A.; D'Errico, G.; Angelico, R. Effects of Natural Antioxidant Agents on the Bitumen Aging Process: An EPR and Rheological Investigation. *Appl. Sci.* **2018**, *8*, 1405. [CrossRef]
106. Walenta, E. Small angle X-ray scattering. Von O. GLATTER und O. KRATKY. London: Academic Press Inc. Ltd. 1982. ISBN 0-12-286280-5. X, 515 Seiten, geb. £ 43,60; US $ 81.00. *Acta Polym.* **1985**, *36*, 296. [CrossRef]
107. Chu, B.; Hsiao, B.S. Small-Angle X-ray Scattering of Polymers. *Chem. Rev.* **2001**, *101*, 1727–1762. [CrossRef]
108. Nozue, Y.; Shinohara, Y.; Amemiya, Y. Application of Microbeam Small- and Wide-angle X-ray Scattering to Polymeric Material Characterization. *Polym. J.* **2007**, *39*, 1221–1237. [CrossRef]
109. Calandra, P.; Turco Liveri, V.; Ruggirello, A.M.; Licciardi, M.; Lombardo, D.; Mandanici, A. Anti-Arrhenian behaviour of conductivity in octanoic acid–bis(2-ethylhexyl)amine systems: A physico-chemical study. *J. Mater. Chem. C* **2015**, *3*, 3198–3210. [CrossRef]
110. Lombardo, D.; Munaò, G.; Calandra, P.; Pasqua, L.; Caccamo, M.T. Evidence of pre-micellar aggregates in aqueous solution of amphiphilic PDMS–PEO block copolymer. *Phys. Chem. Chem. Phys.* **2019**, *21*, 11983–11991. [CrossRef] [PubMed]
111. Turco Liveri, V.; Lombardo, D.; Pochylski, M.; Calandra, P. Molecular association of small amphiphiles: Origin of ionic liquid properties in dibutyl phosphate/propylamine binary mixtures. *J. Mol. Liq.* **2018**, *263*, 274–281. [CrossRef]
112. Hyland, L.L.; Taraban, M.B.; Yu, Y.B. Using small-angle scattering techniques to understand mechanical properties of biopolymer-based biomaterials. *Soft Matter* **2013**, *9*, 10218–10228. [CrossRef]
113. Ochbaum, G.; Bitton, R. Using small-angle X-ray scattering (SAXS) to study the structure of self-assembling biomaterials. In *Self-Assembling Biomaterials*; Azevedo, H.S., Silva, R.M.P., Eds.; Woodhead Publishing Series in Biomaterials; Woodhead Publishing: Cambridge, UK, 2018; pp. 291–304. ISBN 978-0-08-102015-9.

114. Kiselev, M.A.; Lombardo, D. Structural characterization in mixed lipid membrane systems by neutron and X-ray scattering. *Biochim. Biophys. Acta—Gen. Subj.* **2017**, *1861*, 3700–3717. [CrossRef]
115. Lombardo, D.; Calandra, P.; Magazù, S.; Wanderlingh, U.; Barreca, D.; Pasqua, L.; Kiselev, M.A. Soft nanoparticles charge expression within lipid membranes: The case of amino terminated dendrimers in bilayers vesicles. *Colloids Surf. B Biointerfaces* **2018**, *170*, 609–616. [CrossRef]
116. Lombardo, D.; Calandra, P.; Bellocco, E.; Laganà, G.; Barreca, D.; Magazù, S.; Wanderlingh, U.; Kiselev, M.A. Effect of anionic and cationic polyamidoamine (PAMAM) dendrimers on a model lipid membrane. *Biochim. Biophys. Acta* **2016**, *1858*, 2769–2777. [CrossRef]
117. de Moor, P.-P.E.A.; Beelen, T.P.M.; van Santen, R.A.; Tsuji, K.; Davis, M.E. SAXS and USAXS Investigation on Nanometer-Scaled Precursors in Organic-Mediated Zeolite Crystallization from Gelating Systems. *Chem. Mater.* **1999**, *11*, 36–43. [CrossRef]
118. Bonaccorsi, L.; Calandra, P.; Kiselev, M.A.; Amenitsch, H.; Proverbio, E.; Lombardo, D. Self-assembly in poly(dimethylsiloxane)-poly(ethylene oxide) block copolymer template directed synthesis of Linde type A zeolite. *Langmuir* **2013**, *29*, 7079–7086. [CrossRef]
119. Ingham, B. X-ray scattering characterisation of nanoparticles. *Crystallogr. Rev.* **2015**, *21*, 229–303. [CrossRef]
120. Fratzl, P. Small-angle scattering in materials science - a short review of applications in alloys, ceramics and composite materials. *J. Appl. Crystallogr.* **2003**, *36*, 397–404. [CrossRef]
121. Rossi, C.O.; Caputo, P.; De Luca, G.; Maiuolo, L.; Eskandarsefat, S.; Sangiorgi, C. 1H-NMR spectroscopy: A possible approach to advanced bitumen characterization for industrial and paving applications. *Appl. Sci.* **2018**, *8*, 229.
122. Calandra, P.; Liveri, V.T.; Caputo, P.; Teltayev, B.; Rossi, C.O. Wide Angle X-ray Scattering as a Technique of Choice to Probe Asphaltene Hierarchical Structures. *J. Nanosci. Nanotechnol.* **2020**, *20*, 4574–4579. [CrossRef]
123. Caputo, P.; Loise, V.; Crispini, A.; Sangiorgi, C.; Scarpelli, F.; Oliviero Rossi, C. The efficiency of bitumen rejuvenator investigated through Powder X-ray Diffraction (PXRD) analysis and T2-NMR spectroscopy. *Colloids Surf. A Physicochem. Eng. Asp.* **2019**, *571*, 50–54. [CrossRef]
124. Bartolotta, A.; Calandra, P. Indication of Local Phase Separation in Polyimide/Silica Hybrid Polymers. *Macromol. Chem. Phys.* **2010**, *211*, 1784–1792. [CrossRef]
125. Pochylski, M.; Oliviero, C.; Nicotera, I.; Liveri, V.; Calandra, P. Nano-demixing as a novel strategy for magnetic field responsive systems: The case of Dibutyl phosphate/bis(2-ethylhexyl) amine systems. *RSC Adv.* **2016**, *6*, 26696–26708. [CrossRef]
126. Calandra, P.; Caponetti, E.; Chillura Martino, D.; D'Angelo, P.; Minore, A.; Turco Liveri, V. FT-IR and dielectric study of water/AOT liquid crystals. *J. Mol. Struct.* **2000**, *522*, 165–178. [CrossRef]
127. Midgley, P.A.; Ward, E.P.W.; Hungría, A.B.; Thomas, J.M. Nanotomography in the chemical, biological and materials sciences. *Chem. Soc. Rev.* **2007**, *36*, 1477–1494. [CrossRef]
128. Liu, G.; Wu, S.; Ven, M.; Yu, J.; Molenaar, A. Influence of sodium and organo-montmorillonites on the properties of bitumen. *Appl. Clay Sci.* **2010**, *49*, 69–73. [CrossRef]
129. Mohajeri, M.; Molenaar, A.A.A.; Van de Ven, M.F.C. Experimental study into the fundamental understanding of blending between reclaimed asphalt binder and virgin bitumen using nanoindentation and nano-computed tomography. *Road Mater. Pavement Des.* **2014**, *15*, 372–384. [CrossRef]
130. Hu, J.; Qian, Z.; Wang, D.; Oeser, M. Influence of aggregate particles on mastic and air-voids in asphalt concrete. *Constr. Build. Mater.* **2015**, *93*, 1–9. [CrossRef]
131. Rinaldini, E.; Schuetz, P.; Partl, M.; Tebaldi, G.; Poulikakos, L. Investigating the blending of reclaimed asphalt with virgin materials using rheology, electron microscopy and computer tomography. *Compos. Part B Eng.* **2014**, *67*, 579–587. [CrossRef]
132. Tan, G.-L.; Lemon, M.F.; French, R.H. Optical Properties and London Dispersion Forces of Amorphous Silica Determined by Vacuum Ultraviolet Spectroscopy and Spectroscopic Ellipsometry. *J. Am. Ceram. Soc.* **2003**, *86*, 1885–1892. [CrossRef]
133. Ravindra, N.M.; Narayan, J. Optical properties of amorphous silicon and silicon dioxide. *J. Appl. Phys.* **1986**, *60*, 1139–1146. [CrossRef]
134. Serpone, N.; Lawless, D.; Khairutdinov, R. Size Effects on the Photophysical Properties of Colloidal Anatase TiO2 Particles: Size Quantization versus Direct Transitions in This Indirect Semiconductor? *J. Phys. Chem.* **1995**, *99*, 16646–16654. [CrossRef]

135. Calandra, P.; Ruggirello, A.; Pistone, A.; Turco Liveri, V. Structural and Optical Properties of Novel Surfactant Coated TiO2–Ag Based Nanoparticles. *J. Clust. Sci.* **2010**, *21*, 767–778. [CrossRef]
136. Bonaccorsi, L.; Calandra, P.; Amenitsch, H.; Proverbio, E.; Lombardo, D. Growth of fractal aggregates during template directed SAPO-34 zeolite formation. *Microporous Mesoporous Mater.* **2013**, *167*, 3–9. [CrossRef]
137. Calandra, P.; Caschera, D.; Liveri, V.T.; Lombardo, D. How self-assembly of amphiphilic molecules can generate complexity in the nanoscale. *Colloids Surf. A Physicochem. Eng. Asp.* **2015**, *484*, 164–183. [CrossRef]

© 2020 by the authors. Licensee MDPI, Basel, Switzerland. This article is an open access article distributed under the terms and conditions of the Creative Commons Attribution (CC BY) license (http://creativecommons.org/licenses/by/4.0/).

nanomaterials

MDPI

*Review*

# The Role of Additives in Warm Mix Asphalt Technology: An Insight into Their Mechanisms of Improving an Emerging Technology

**Paolino Caputo [1], Abraham A. Abe [1], Valeria Loise [1], Michele Porto [1], Pietro Calandra [2], Ruggero Angelico [3,*] and Cesare Oliviero Rossi [1,*]**

[1] Department of Chemistry and Chemical Technologies, University of Calabria, 87036 Arcavacata di Rende (CS), Italy; paolino.caputo@unical.it (P.C.); abraham.abe@unical.it (A.A.A.); valeria.loise@unical.it (V.L.); michele.porto@unical.it (M.P.)

[2] CNR-ISMN, National Research Council, Institute for the Study of Nanostructured Materials, Via Salaria km 29.300, 00015 Monterotondo Stazione (RM), Italy; pietro.calandra@cnr.it

[3] Department of Agricultural, Environmental and Food Sciences (DIAAA), University of Molise, Via De Sanctis, 86100 Campobasso (CB), Italy

* Correspondence: angelico@unimol.it (R.A.); cesare.oliviero@unical.it (C.O.R.); Tel.: +39-0874-404649 (R.A.); +39 0984-492045 (C.O.R.)

Received: 30 May 2020; Accepted: 17 June 2020; Published: 19 June 2020

**Abstract:** The asphalt industry's incentive to reduce greenhouse gas emissions has increased since the 1990s due to growing concerns on environmental issues such as global warming and carbon footprint. This has stimulated the introduction of Warm Mix Asphalt (WMA) and its technologies which serve the purpose of reducing greenhouse gas emissions by reducing the mixing and compaction temperatures of asphalt mix. WMA gained popularity due to the environmental benefit it offers without compromising the properties, performance and quality of the asphalt mix. WMA is produced at significantly lower temperatures (slightly above 100 °C) and thus results in less energy consumption, fewer emissions, reduced ageing, lower mixing and compaction temperatures, cool weather paving and better workability of the mix. The latter of these benefits is attributed to the incorporation of additives into WMA. These additives can also confer even better performance of WMA in comparison to conventional Hot Mix Asphalt (HMA) methods. Even though there are recommended dosages of several WMA additives, there is no general standardized mixture design procedure and this makes it challenging to characterize the mechanism(s) of action of these additives in the warm mix. The effects of the addition of additives into WMA are known to a reasonable extent but not so much is known about the underlying interactions and phenomena which bring about the mechanism(s) by which these additives confer beneficial features into the warm mix. Additives in a certain way are being used to bridge the gap and minimize or even nullify the effect of the mixing temperature deficit involved in WMA processes while improving the general properties of the mix. This review presents WMA technologies such as wax, chemical additives and foaming processes and the mechanisms by which they function to confer desired characteristics and improve the durability of the mix. Hybrid techniques are also briefly mentioned in this paper in addition to a detailed description of the specific modes of action of popular WMA technologies such as Sasobit, Evotherm and Advera. This paper highlights the environmental and technical advantages of WMA over the conventional HMA methods and also comprehensively analyzes the mechanism(s) of action of additives in conferring desirable characteristics on WMA, which ultimately improves its durability.

**Keywords:** warm mix asphalt; binder; surface free energy; wax; emulsifiers; surfactants; zeolites; contact angle; bitumen; aggregates; WMA; viscosity

## 1. Introduction

Since the 1900s, Hot Mix Asphalt (HMA) has been the most common and generally accepted technology for asphalt pavement construction. Road pavements are made up of over 93% stones with less than 7% of bitumen functioning as a binder. Bitumen is a soft material made up of several components and is a by-product of petroleum industry processes. Its chemical composition is complex and it can be characterized using special methods [1]. In order to ensure proper coating of aggregates and provide sufficient workability of HMA, both asphalt binder and aggregates are heated up to high temperatures between 150 °C and 180 °C. This results in high energy costs and the emission of several greenhouse gases (mainly $CO_2$). The Kyoto Treaty was developed as a result in 1997, thus setting the objective for European countries to develop policies and technologies in order to meet greenhouse gas reduction requirements [2]. Warm Mix Asphalt (WMA) technologies were developed to produce asphalt at temperatures slightly above 100 °C, with performances and characteristics equivalent to or even sometimes better than that of conventional HMA. WMA technologies mostly focus on the binder (bitumen) by adding different additives to improve its properties [3–7]. These technologies, which produce asphalt between 110 °C and 140 °C, facilitate proper coating of the aggregates and hence the workability and compactibility of the mix while also reducing production and compaction temperatures by 20–40 °C. This reduces energy consumption, minimizes fume and odor emissions and also creates a cooler working environment for asphalt workers [8]. Figure 1 shows the position of WMA among the different techniques ranging from cold to hot mixes.

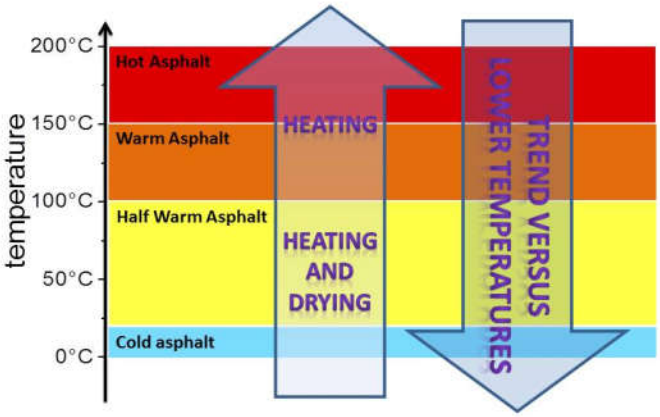


**Figure 1.** Classification by temperature range.

Several techniques exist for the production of WMA. The three generally most accepted are those using (i) *organic additives*; (ii) *chemical additives*; and, (iii) *foaming techniques* [9]. Organic additives are usually waxes and fatty amides, which are able to reduce the viscosity of the binder above the melting point of the binder. Common waxes used in the production of WMA are Sasobit® and Asphaltan B®. On the other hand, chemical additives are usually emulsifiers and surfactants that do not reduce the binder viscosity but improve the coating of aggregates by reducing the surface energy of the aggregate/binder interface and/or the inner friction. Products such as Rediset® and Evotherm® are often used [10]. Foaming techniques function by reducing the viscosity of the binder, just like organic additive techniques, but only for a short period of time. This is achieved by introducing small amounts of water in the hot binder (bitumen), causing expansion of the bitumen and the formation of a large quantity of foam. Foaming techniques are subcategorized into (i) *water-based processes*, which entail the use of injection foaming nozzles; and, (ii) *water-bearing additives*, which involve the use of minerals in the form of zeolites [8,11].

Aside from the aforementioned WMA techniques, there are also several combined technologies and products used to produce WMA, like zeolites or fibers with organic additives or pallets with

fibers. These are called *hybrid techniques*. Hybrid techniques involve a combination of two or more technologies and are used less often. Examples of hybrid techniques are Low Energy Asphalt (LEA) and the Tri-Mix Warm Mix Injection system, which are both technologies that combine chemical and water-based techniques to achieve the required results [2,12,13]. In addition to all of the commonly known techniques for WMA production, an uncommon technique that uses emulsions to pre-coat aggregates is sometimes used. This technique involves the use of stabilized bituminous emulsion to pre-coat aggregates before the main mixing procedure with asphalt binder. Due to the absence of hazardous additives in this specialized emulsion technique, it is designed to produce a more environmentally friendly and cost-effective procedure [14].

Just like any new technology, WMA needs a lot of further research and study. A few concerns like finding a mix design strategy and the need for a comprehensive specification have been identified thus far. Previous research [15,16] confirms that the lack of standardized mixture design procedure of WMA makes it important to identify the mechanism(s) of action of additives. The wide range of mechanisms through which several WMA additives act also provides a wide range of WMA additive product options when deciding how to formulate warm mixes. In addition, since the set of instrumentation, machinery and apparatus available for WMA production contribute to determine the technique to be used, a good knowledge of how and why the additives work gives a realistic evaluation of methods and techniques to be used for future WMA technology. Table 1 shows the range of additives used in warm mix technologies.

**Table 1.** Products used in Warm Mix technology. Reprinted with permission from [9]. Copyright (2011), with permission from Elsevier.

| WMA processes | Product | Company | Description | Dosage of Additive | Country where technology is used | Production temp. (or reduction range) °C |
|---|---|---|---|---|---|---|
| ***Organic additives*** | | | | | | |
| FT Wax | Sasobit® | Sasol | Fischer-Tropsch Wax | 1.0–2.5% by weight of binder | Worldwide | (20–30 °C) |
| Montan Wax | Asphaltan B | Romonta GmbH | Montan Wax with fatty acid amide | 2.0–4.0% by mass of bitumen | Germany | (20–30 °C) |
| Fatty Acid Amides | Licomont BS | Clariant | Fatty acid amide | 3.0% by mass of bitumen | Germany | (20–30 °C) |
| Wax | 3E LT or Ecoflex | Colas | Proprietary | Not specified | France | (20–30 °C) |
| ***Chemical additives*** | | | | | | |
| Emulsion | Evotherm® technologies | MeadWestvaco | Chemical packages with or without water | 0.5–0.7% by mass of bitumen | USA, worldwide | 85–115 °C |
| Surfactant | Rediset | Akzo Nobel | Cationic surfactants & organic additive | 1.5–2.0% by weight of bitumen | USA, Norway | (30 °C) |
| Surfactant | Cecabase RT | CECA | Chemical package | 0.2–0.4% by mixture weight | USA, Norway | (30 °C) |
| Liquid Chemical | Iterlow | IterChimica | | 0.3–0.5% by mass of bitumen | Italy | 120 °C |
| ***Foaming Processes*** | | | | | | |

| | | | | | | |
|---|---|---|---|---|---|---|
| Water-containing | Aspha-Min® | Eurovia and MHI | Water-containing technology using zeolites | 0.3% by total weight of mix | Worldwide | (20–30 °C) |
| Water-containing | Advera® | PQ Corp. | Water-containing technology using zeolites | 0.25% by total weight of mix | USA | (10–30 °C) |
| Water-based | WAM Foam | Shell and Kolo-Veidekke | Foamed binder | 2–5% water by mass of binder | Worldwide | 100–200 °C |

Substantial information is known about the effects of additives on warm mix, but the precise mechanism of how these additives work to confer the desired characteristics on WMA is still unclear. The main goal of this paper is to review the most relevant works appearing in the literature on the subject to highlight the mechanism(s) of action of additives and relate them to the effects observed in the WMA technology.

## 2. Organic Additives

Organic WMA additives are known to reduce the bitumen viscosity in order to improve workability. These organic additives are mainly waxes (natural or synthetic) and fatty amides, and they are added to warm mix to lower the viscosity of the asphalt binder at temperatures slightly above 90 °C and to improve lubrication. The reduction in viscosity translates to an increase in stiffness by solidifying into microscopic particles which are distributed uniformly in the mix when it cools [9]. The underlying concept is the fact that waxes suitable for this technique have melting points below the conventional HMA production temperatures, hence they become dispersible in the mix during the WMA production process [11]. They are expected to feed the maltene phase due to their apolar nature. In doing so, their effect would be to better disperse asphaltene clusters at their various levels of aggregation, thus reducing viscosity [17]. At high temperatures, the viscosity of the asphalt binder is an important property because it directly reflects the ability of the binder to be pumped through an asphalt plant, to accurately coat the aggregate in the asphalt concrete mixture and to be compacted to form a new pavement surface [18].

An important fact to consider is that the type of additive must be carefully selected so that its melting point is higher than the expected Warm Mix in-service temperatures. This is done in order to prevent deformation and embrittlement of the asphalt at low temperatures [8].

Paraffin waxes are the ideal and most commonly used additives for enhancing binder flow and quality. Paraffin waxes are of two types: (i) naturally occurring bituminous waxes and (ii) synthetic waxes. Wax manufacturers emphasize the difference between naturally occurring bituminous wax and synthetic wax in terms of their physical properties and structure. The differences are due to the longer carbon chain lengths and the finer crystalline structures of industrially synthesized waxes. An example of an industrially synthesized wax which is known to be very effective in WMA is Sasobit, which has a hydrocarbon chain length in the range of 40 to 115 carbon atoms. Naturally occurring bituminous wax has a hydrocarbon chain length of about 22 to 45 carbon atoms [19].

### *2.1. Sasobit*

Sasobit is a fine crystalline, long chain aliphatic hydrocarbon produced from coal gasification using the Fischer-Tropsch (FT) process and is otherwise known as an FT paraffin wax. It is generally added in a 3% to 4% proportion with respect to the total asphalt weight. Several studies have reported an increase in the resistance to permanent deformation of WMA mixtures produced with asphalt modified with Sasobit [20,21]. Sasobit acts as a flow modifier in the mix which facilitates the aggregates free movement and coating by the asphalt binder. As Sasobit melts over a temperature range between 85 and 115 °C, it is more dispersible in asphalt binder at temperatures above 115°C

and thus lowers the viscosity of the binder at mixing temperatures [11]. During the cooling process (see Figure 2), Sasobit starts to crystallize at approximately 90 °C and forms a microscopic crystal lattice structure in the bitumen which confers the stiffening effect, and this is responsible for the deformation resistance of the so-modified bitumen [22]. Recent speculation about this phenomenon is that waxes having long hydrocarbon chains (like Sasobit) combine with the binder (bitumen) and alter the hydrocarbon chain length of the binder, thus altering the physical properties of the binder, like stiffness and viscosity [13].

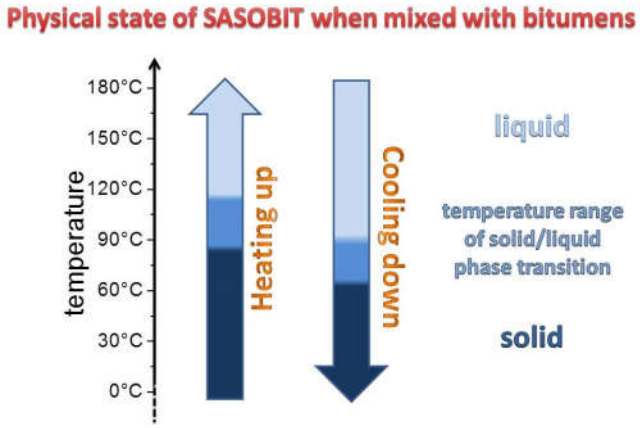


**Figure 2.** Phase transition mechanism of Sasobit in bitumen binder.

Another contributing factor to the stiffness of the binder is the interaction of long hydrocarbon chains of the waxes with the N-Alkane-rich crystallizing material in asphalt mix [23–25]. The small crystalline structure of the Fischer-Tropsch wax molecules reduces brittleness of the paved asphalt road at low temperatures due to the formation of a lattice structure of microscopic particles in the modified binder. Another important feature of the asphalt binder that changes due to the addition of the wax is the number and size of air voids present in the mix. The number and size of air voids is reduced due to the improved flow of the modified bitumen during mixing and compaction procedures. Less air voids result in a greater resistance to ruts induced by traffic demands on the paved asphalt [26].

Several modifications of Sasobit technology profit from its formation of lattice structures in the binder and combine this feature with the introduction of polymers into the wax to achieve target specifications. An example of this is the creation of an additive called Sasoflex which is a compound of a plastomer (Sasobit) combined with an elastomer (styrene-butadiene-styrene) by using a proprietary chemical cross-linking agent (sasolink). The plastomer (Sasobit) fraction reduces the viscosity of the mix at paving temperatures and stiffens the binder at in-service pavement temperatures while the elastomer (SBS) fraction maintains the flexibility at low temperatures [26,27]. Sasobit REDUX is another modification of Sasobit technology, which consists of Fischer-Tropsch synthetic wax (Sasobit) and other petroleum-based waxes. This product has a congealing point of between 72 and 83 °C, thus making it softer than Sasobit. Sasobit REDUX functions using the same lattice-forming mechanism but effectively reducing production and compaction temperatures due to its lower melting point [28].

### *2.2. Licomont 100*

Other organic additives like Licomont BS 100 also function with the same mechanism of a viscosity reduction of the binder. Licomont BS 100 is a fatty acid amide which acts as a viscosity enhancer with a mechanism quite similar to that of Sasobit. Its physical properties are slightly different from that of Sasobit as it melts over the temperature range between 140 and 145 °C, and thus one requires production and compaction temperatures slightly higher than Sasobit-modified bitumen [11,29].

### *2.3. Asphaltan B*

Asphaltan B, a blend of wax obtained by solvent extraction from lignite and fatty acid amides, is another commercially available wax with the mechanism to facilitate the production of WMA similar to that of Sasobit. The dynamics of the viscosity reduction in Asphaltan B-modified asphalt binder is similar to that of Sasobit-modified asphalt [30].

## 3. Chemical Additives

Chemical additives are some of the most recent emerging WMA technologies. They contribute to improving the ability of the asphalt binder to coat the aggregate particles rather than reducing the viscosity of the binder [31]. Chemical additives have a more diverse range of mechanisms through which they exert their function compared to other categories.

Chemical additives exist in the form of emulsions and surfactants, which work at the microscopic interface of the binder and aggregates to regulate and reduce the frictional forces at that interface within a range of temperatures (typically between 85 and 140 °C). The reduction and regulation of the frictional forces facilitate lubrication between the binder and aggregate during mixing and compaction, and this accounts for the improvement in adhesion obtained after the addition of chemical additives.

In the same way as waxes, some chemical additives (generally surfactants such as Rediset and Cecabase) reduce the binder viscosity while the emulsifying chemical additives (like Evotherm) improve lubrication in the aggregate/binder interface by altering some other parameters such as the surface free energy of the mix [32,33] thanks to their amphiphilic (surfactant) nature. This improvement in lubrication accounts for the asphalt mix particles moving over each other more easily which in turn lowers the mixing and compaction energy levels at lower temperatures [11].

It can be expected that another mechanism is concurrently present, i.e., the competitive interactions between the amphiphilic additive and the amphiphilic resins pre-existent in bitumen. In fact, it has been recently highlighted that, in addition to polar and apolar interactions, further specific interactions between surfactants themselves can trigger peculiar self-assembly processes [34,35] dictating the final overall aggregation pattern and the peculiar dynamics and transport processes [36,37]. There are several approaches that can be used to evaluate the durability of asphalt pavements and the moisture-induced damage potential of WMA. Two of the most viable and mechanistic approaches are the Surface Free Energy (SFE) approach and the Contact angle approach. Arabani et al. [38] reported a strong correlation between the moisture-induced damage potential of WMA mixes based on the SFE of asphalt mixes. Bhasin et al. [39,40] also suggested different combinations of SFE parameters such as the Work of Adhesion, Work of Debonding and Work of Cohesion also known as Cohesion Energy of aggregates to describe the moisture susceptibility of an asphalt binder–aggregate system as a single value.

The SFE of a material is the work required to create a unit area of a new surface in a vacuum. Hence, a high value is desirable for the durability and effectiveness of paved asphalt [41]. The total SFE ($\gamma_{total}$) comprises three components, $\gamma^{LW}$, $\gamma^{+}$ and $\gamma^{-}$, respectively, the non-polar Lifshitz van der Waals (LW), Lewis acid and Lewis base components. Depending on the state of the material, these components combined in different ratios produce the $\gamma_{total}$ of the material [42]. The variability of these components defines the SFE parameters such as cohesion energy, work of adhesion, work of debonding and energy ratio. These parameters define the variable combination of the SFE of asphalt binder with that of the aggregates to give a durable pavement.

Previous research [41] has shown that the elemental composition (Carbon, Nitrogen, Hydrogen and Sulphur) of an asphalt binder is correlated to SFE parameters. Since additives in general alter the structure and physical properties of binders, it is necessary to study the effect that above all the chemical additives exert on the SFE parameters of both the binder and the aggregates.

The use of chemical additives has been proven to alter several parameters and their components, such as SFE, its components and contact angle parameters e [41,43], which will all be discussed later in this paper. The two most important SFE parameters which are altered by the application of chemical additives are work of adhesion and work of debonding. The former is defined as the work

required to detach asphalt binder coating from aggregate surface in a dry state in their interface in vacuum [42]. It is also known as the *dry adhesion energy* and it is a parameter frequently measured to determine the effectiveness of warm mix. A high work of adhesion value implies a strong bond between the components of the warm mix, leading to a more durable and less moisture-susceptible warm mix. The work of debonding, also known as the *wet adhesion energy*, is another important parameter linked the reduction of system energy when the binder separates from the aggregate in the presence of water in a phenomenon called *stripping*. A high value of this parameter implies a higher thermodynamic potential for stripping to occur in the presence of water, hence a low value of this parameter is desired [43]. The $\gamma_{total}$, the work of adhesion and the work of debonding are the most important energy parameters used to evaluate the durability and stability of warm mix asphalt. Several studies [41,43] have shown that the use of chemical additives in WMA have resulted in higher SFE values, higher work of adhesion values and lower work of debonding values.

### *3.1. Evotherm*

One of the most commonly researched and used chemical additives is Evotherm®. Hurley and Prowell [44] demonstrated that, at a given compaction temperature, the addition of Evotherm to asphalt binder increases the resilient modulus of an asphalt mix compared to control mixtures having the same performance-graded (PG) binder. The first generation of Evotherm® technology is a high residue emulsion known as Evotherm ET (Emulsion Technology). MeadWestvaco then introduced a second generation Evotherm technology where the chemical additives are injected as a solution into the asphalt line at the plant known as Evotherm DAT (Dispersed Additive Technology).

The latest and most recently emerging Evotherm Technology known as Evotherm 3G (3rd Generation) is a water-free WMA technology which allows the additive to be mixed with the binder at a terminal [15]. Evotherm 3G and Evotherm DAT have made Evotherm ET obsolete due to the convenience with which they can be incorporated into WMA. Evotherm ET is a binder-rich, water-based emulsion that contains about 70% asphalt binder. The water in the emulsion turns into steam when mixed with hot aggregates, thus facilitating better mixing and compaction.

The emulsifiers in the Evotherm® are adsorbed onto the aggregate surface with a long hydrocarbon tail extending beyond the aggregate surface, which promotes interfacial adhesion between binder-aggregate interface surfaces [11,45]. It is highly possible that in Evotherm the long hydrocarbon tails of the emulsifiers extending beyond the aggregate surface, are responsible for the higher SFE values of the binder–aggregates interface.

The pH compatibility of binder and aggregates is also an important factor that influences the level of bonding in the warm mix. Since most asphalt binders are more acidic than basic [43], it is highly recommended to be careful using acidic aggregates such as granite with an asphalt binder which is also acidic in nature, as this may result in a weak bond between asphalt binder and aggregate, which will result in high value of work of debonding and, consequently, a higher susceptibility of the mix to moisture-induced damage [46]. It must be pointed out that the pH and the presence of acidic or basic species is a delicate matter, since they can greatly influence the intermolecular aggregation pattern giving sometimes unexpected structural and dynamic properties [47]. Several previous studies [43,48,49] have proven that the incorporation of Evotherm into WMA resulted in higher asphalt–aggregate interfacial SFE values whether applied to the binder or into the mix at the plant.

Ghabchi et al. [43] estimated $\gamma_{total}$, work of adhesion, work of debonding and energy ratios to assess the moisture-induced damage potential of combinations of neat and Evotherm® asphalt binders and different aggregates. They also measured and compared contact angle values of Evotherm-modified asphalt binder and unmodified neat asphalt binder.

Their results (reported in Table 2) indicated that the addition of 0.5% and 0.7% Evotherm® resulted in an increase in both $\gamma_{total}$ and work of adhesion and a reduction in work of debonding, implying a better aggregate–binder bond and thus lower moisture susceptibility potential. Their results also showed that the use of Evotherm® resulted in reduced contact angles compared to those of unmodified asphalt binder. Yu et al. [50] carried out a study in which they combined two

generations of Evotherm technology (Evotherm DAT and Evotherm 3G) to evaluate the WMA effect on the mechanical resistance of the binder. In the base sample, Evotherm DAT and Evotherm 3G were added in the proportions of 5% and 0.5% of the total weight, respectively. The results of the study showed improved fatigue resistance, moisture damage resistance and better workability.

**Table 2.** SFE components of PG64-22 asphalt binder modified with Evotherm® and aggregates (Reprinted with permission from [43]. Copyright (2013), with permission from Elsevier.). $\gamma^{LW}$: LW component. $\gamma^-$: Lewis base component. $\gamma^+$: Lewis acid component. $\gamma^{+-} = 2\sqrt{\gamma^+\gamma^-}$ : acid–base component. $\gamma_{total}$: total surface free energy of the material.

| Material type | additive (%) | Surface Free Energy Components (mJ/m²) | | | | | |
|---|---|---|---|---|---|---|---|
| | | $\gamma^{LW}$ | $\gamma^-$ | $\gamma^+$ | $\gamma^{+-}$ | $\gamma_{total}$ | $\gamma^+/\gamma^-$ |
| *PG64-22 Binder with different % additive* | | | | | | | |
| Neat | 0% | 9.44 | 0.93 | 1.22 | 2.13 | 11.57 | 1.30 |
| Evotherm® | 0.25% | 6.84 | 1.24 | 3.45 | 4.14 | 10.99 | 2.77 |
| | 0.50% | 6.74 | 2.50 | 3.03 | 5.50 | 12.24 | 1.21 |
| | 0.75% | 9.17 | 3.03 | 5.50 | 4.52 | 13.69 | 1.82 |
| *Aggregates from Testing and Literature* | | | | | | | |
| Limestone (Tested) | - | 51.4 | 741.4 | 17.5 | 227.8 | 279.2 | 0.024 |
| Granite [1] | - | 133.2 | 96 | 24.1 | 96.2 | 229.4 | 0.251 |
| Basalt [1] | - | 52.3 | 164 | 0.6 | 19.8 | 72.1 | 0.004 |

In general, when the contact angle value of the binder and aggregate sample is ≥ 90°, it indicates low wettability, and the binder is unable to wet and coat the surface of the aggregate. When contact angles are < 90°, there is some adhesion and the binder is able to wet the surface of the aggregate. For contact angle values ≈ 0°, spreading of the binder around the surface of the aggregate can occur and there is a strong adhesion. This parameter is what translates to the extent of coating of the aggregate by the asphalt binder. The implications of variations in contact angle on the properties of asphalt binder are expected to influence the SFE components and energy parameters such as moisture susceptibility potential and work of adhesion and debonding [41,43].

In addition to the effect of chemical additives, anti-stripping agents are also incorporated into WMA to improve its durability. They decrease the moisture susceptibility of warm mix asphalt by reducing the potential of moisture to disrupt the adhesive bond between binder and aggregate. Hydrated lime is a model anti-stripping agent and it has been proven to be highly effective in strengthening the adhesion between the asphalt binder and aggregates [51]. Some researchers attribute the increase in adhesive strength to changes in the surface chemistry or molecular polarity of the aggregate surface. This consequently leads to a stronger bond at the binder–aggregate interface [52,53]. Since hydrated lime is basic in nature, it is believed that its application in WMA increases the base component of the SFE of aggregates thus increasing the overall SFE value. These changes in aggregate SFE components lead to a significant improvement in adhesion between an asphalt binder and acidic aggregate that is more sensitive to moisture damage. The use of hydrated lime has also been proven to decrease aggregate polarity, thus decreasing the affinity of aggregate surface, which has polar molecules, to water [52]. Apart from the treatment of WMA with anti-stripping agents, the type of stones used as aggregate has to be carefully chosen. This is because different stones have different polarities and SFE parameters which leads to a variability in adhesion potential when incorporated into the warm mix. Hesami et al. [52] proved that the free energy of adhesion between water and granite aggregate is much greater than that between water and limestone aggregate, indicating that the affinity of granite to water is higher compared to limestone.

### *3.2. Rediset*

Rediset is another chemical additive produced by Akzo Nobel that contains cationic surfactants and rheology modifiers (of organic nature). It is a polyfunctional additive based on fatty amine surfactants and olyethylenes [54]. This additive contains a long chain aliphatic hydrocarbon structure

and an $-NH_3^+$ group, which reacts chemically with aggregate surfaces [55]. Rediset has a slightly different mechanism compared to other chemical additives because it contains in-built anti-stripping agents, which reduce susceptibility to moisture damage [56]. Rediset is regarded as a polyfunctional additive because it functions by reducing the interfacial friction between thin films of the asphalt binder and the coated aggregates, while also improving workability by increasing lubrication and allowing mixing and compaction at reduced temperatures [11]. The surfactant part of this product (similar to chemical additives) decreases the surface tension of asphalt binder and improves the wettability of the aggregate by using an asphalt binder [56]. The organic part reduces the viscosity of the asphalt binder and provides a lubricating effect for easier coating and compaction [32]. It has also been reported that Rediset positively changes kinematic and dynamic viscosity as well. Studies in the literature [57,58] showed that Rediset decreases the kinematic viscosity of asphalt binder at 135°C. Van de Ven et al. [59] also demonstrated that Rediset has a strong effect on the dynamic viscosity at 110°C for a hard asphalt binder using Dynamic Shear Rheology results with a cone and plate device. The use of Rediset has also been shown to have similar effects on the SFE parameters, as was observed with the use of Evotherm [60]. Cecabase RT is another chemical additive produced by CECA (France), which has the same hypothesized mechanism to produce WMA as that of surfactants such as Rediset [11].

### *3.3. Iterlow*

Iterlow is a liquid chemical additive produced by Iterchimica (Italy) which, when added to the asphalt binder, allows for the production of WMA at temperatures above 120 °C. According to Hill et al. [61], liquid chemical additives generally act as emulsifying agents and contain amine groups that can improve the cracking resistance at low service temperatures and the resistance to moisture damage. Just like other chemical additives, Iterlow improves the workability of the mix and facilitates paving and mixing at lower temperatures (between 90 °C and 120 °C) depending on the type of bitumen. Iterlow has little or no effect on the bitumen grade [60].

## 4. Foaming Technologies

Foaming technologies involve the introduction of small amounts of water which are delivered into the binder using different methods. Although the method of water delivery is different, foaming processes generally conform to one underlying concept, which is the expansion factor of water after transition from liquid to vapor state. The expansivity of water by a factor of about 1700 when it is converted into steam is the mechanism behind the effectiveness of foaming technologies in general [62]. The latent steam in the form of foam causes an overall reduction in the viscosity of the asphalt binder which is facilitated by an increase in volume and surface area of the binder and this results in improved aggregate coating and easier compaction of the asphalt mix at lower temperatures [11]. As mentioned earlier in this review, foaming technologies are divided into two processes, namely, *water-bearing* and *water-based* processes. Water-bearing processes involve the use of water-containing technologies which combine water foaming and additive (zeolites) dosage. These processes involve the incorporation of hydro-thermally crystalized minerals called zeolites into asphalt binder. Upon contact of the zeolite with hot binder, water is released from the zeolite's crystal structure without changing the volume and structure of the crystal. The released water changes to water vapor and causes foaming. There are two groups of zeolites namely; synthetic zeolites which are produced from chemical reactions, and natural zeolites which are formed by naturally occurring geological processes [63–66]. Water-based processes, on the other hand, do not actually involve the use of additives but involve the direct injection of water into a binder, which generates microscopic bubbles and thus causes foaming in the binder [11,67]. Water-based processes involve the injection of pressurized cold water into hot asphalt using specially designed injection nozzles. These processes do not chemically modify the asphalt binder during the production of foam resulting from the addition of water. The foaming only occurs in order to enable for easier aggregate coating. Water-based processes eliminate the need for expensive additives due to its general technique of directly injecting small amounts of water (generally with a mass ratio of between 1% and 5% to the mass of binder) into the hot binder

to form microscopic bubbles (which creates the foam) in the continuous phase. These processes rely solely on the foaming action of steam when water is injected into hot asphalt. WAM Foam (Warm Asphalt Mix Foam) and Double barrel green are examples of water-based processes [11]. Unlike organic additive techniques, the reduction in viscosity of binder caused by foaming processes is temporary and only for a short time usually during mixing and compaction of the asphalt mix after which the foam collapses and the asphalt binder reverts to its normal binder state. This technology reduces WMA production temperatures by between 20 and 30 °C.

### *4.1. Water-Bearing Processes*

The main foaming technologies that concern this review are the water-bearing processes. These processes involve the use of porous, hydrated aluminosilicate minerals called zeolites. Zeolites have a general formula of $M_{x/m}[(AlO_2)_x(SiO_{2y})]$. H2O, where the $M_{x/m}$ unit constitutes ion-exchangeable cations, and the $[(AlO_2)_x(SiO_{2y})]$ unit is the zeolite crystalline framework. The apices of the $SiO_4$ and $AlO_4$ tetrahedrons are connected by oxygen atoms creating a three-dimensional spatial network in which voids are formed in the form channels and chambers. This defines the crystallinity of these aluminosilicates. The Si/Al ratio in the crystalline framework determines factors such as the mineralogical composition of the zeolite, size of channels and chambers, ion-exchangeable capabilities and hydrophilic–hydrophobic properties [64]. In addition to these features, water molecules are bound to the zeolite crystals and are released when subjected to high temperatures without changing the zeolite structure. Zeolites are either naturally occurring or synthetic although the synthetic zeolites are the most commonly used group of zeolites for WMA. Natural zeolites are microporous, hydrated aluminosilicates, which are generally used as commercial adsorbents [67,68]. The most common, naturally occurring zeolites are Clinoptilolite and Phillipsite. Clinoptilolite is a common natural zeolite and comprises of microporous tetrahedral arrangements of silica and alumina [69]. It is used in the production of cement, concrete and asphalt due to its large distribution of micropore spaces and high resistance to extreme temperatures [70].

Synthetic zeolites are finely powdered hydrated sodium aluminosilicates, which have been usually hydro-thermally crystallized. They have a complex structure, usually with a porous morphology [71] and sometimes with fractal arrangement conferring high surface-to-volume ratio [72]. Common examples of synthetic zeolites are sodium silicates ($Na_2SiO_3$) and sodium aluminates ($NaAlO_2$) each of which are categorized into types. The most common types are ZSM-5, X, Y, A, and NaP1 types [65,66]. Synthetic zeolite technologies such as Aspha-min and Advera belong to the same group of Linde A (LTA) structure-type synthetic zeolites and are the most commonly used zeolites for WMA. Advera® which is an additive produced by PQ Corporation is a new generation of the Aspha-min technology. These additives contain between 18% and 22% of water by mass which is released at higher temperatures facilitated by the mixing and compaction processes [11,32,73]. The recommended dosage of Advera in the Warm Mix is 0.25% by weight of the mix. During the mixing process, due to the elevated temperature, the water contained in the zeolite is released into the binder and foaming occurs. As a result of this, a reduction of binder viscosity and increase in workability are observed. Previous research studies have suggested that water released from Advera condenses and is reabsorbed by the zeolite which reduces moisture susceptibility [73–75]. This in-built anti-stripping feature of Advera makes it more commonly used in the asphalt industry because foaming technologies in general must introduce enough water into the binder to cause foaming without adding so much to induce stripping. Aspha-min works in a mechanism very similar to Advera. Aspha-min is a sodium aluminosilicate produced by Eurovia GmbH, (Germany) who recommend that the dosage of Aspha-min should be 0.3% by weight of mix. This additive releases water at a temperature range of 85–180°C. During the mixing process, both the additive and binder are added simultaneously to the aggregates. The water trapped inside the additive is released and this expands the volume of the binder while foaming occurs. This facilitates aggregate coating of the mixture at lower temperatures [76,77].

Advera and Aspha-min have similar effects on WMA due to the similarities in their chemical compositions and mechanism of action. The only slight difference is the anti-stripping characteristic

that Advera possesses. This feature is absent in Aspha-min, thus anti-stripping agents are recommended to be used in combination with Aspha-min [78]. In the National Center for Asphalt Technology (NCAT) report [76], it was pointed out that the moisture susceptibility and stripping potential were decreased upon addition of an anti-stripping agent (1.5% hydrated lime) to the foamed mix. Another notable observation about WMA foaming processes is that, since the introduction of water into the binder only brings about a temporary reduction in viscosity, it is highly preferable to introduce water into the binder in steps. This stepwise addition of water ensures consistent workability for longer periods. Barthel et al. [79] proved that a stepwise release of water creates a controlled foaming effect and prolongs the timeframe in which there is an improved workability of the mix. This facilitates better coating of aggregates by the binder. In water-based processes, the entire water content of the zeolite mineral is not released into the warm mix. This is due to the fact that zeolites can continuously release water while being subjected to temperatures as high as 400 °C. The lower processing temperature of Warm Mix Asphalt means that the zeolites still retain some of the water in their structures. The amount of released zeolite water at WMA production temperatures can be estimated by thermal analysis [80].

## 5. Super-Stabilized Emulsions and other WMA Techniques

Several other techniques exist for producing WMA, which involve methodologies slightly different from the generally accepted techniques. Hybrid WMA technologies such as Tri-Mix Warm Mix Injection System and Low Energy Asphalt, constitute some of these techniques. One less common technique for WMA production is the use of stabilized emulsion to produce Warm Mix. As mentioned earlier, this procedure is even more environmentally friendly and is also very cost effective because it does not really involve the use of additives in the form of products. Instead, it utilizes chemically stabilized bituminous emulsions systematically added into the mix to improve its quality and durability. In this process, the aggregates are first pre-coated with the emulsion before the binder is added to the mix, and sometimes the binder is foamed before being added to the mix, making it a hybrid technology [81]. The combination of these processes most likely increases workability of the mix because of the reduced viscosity of the binder and also the adhesion parameters like SFE of the aggregates, which have been favorably changed due to the pre-coating of aggregates by the stabilized emulsion. Since an emulsion consists of a dispersion of small droplets of one liquid in another liquid, stabilized emulsions have three important components: water, bitumen and an emulsifying agent (surfactant) which is chemically composed of large molecules and functions to reduce interfacial tension in the mix [14]. Chemically stabilized (non-traditional) bituminous emulsions have better characteristics in WMA compared to traditional bituminous emulsions. Prowell [82] found it worthy to note that non-traditional bitumen emulsions have been developed for the production of WMA. The main advantage of stabilized emulsion over traditional emulsion is that, upon mixing, most of the water evaporates and surfactants converge to form inverse groups of molecules or micelles (shown in Figure 3b), which is not the case with traditional emulsion (shown in Figure 3a).

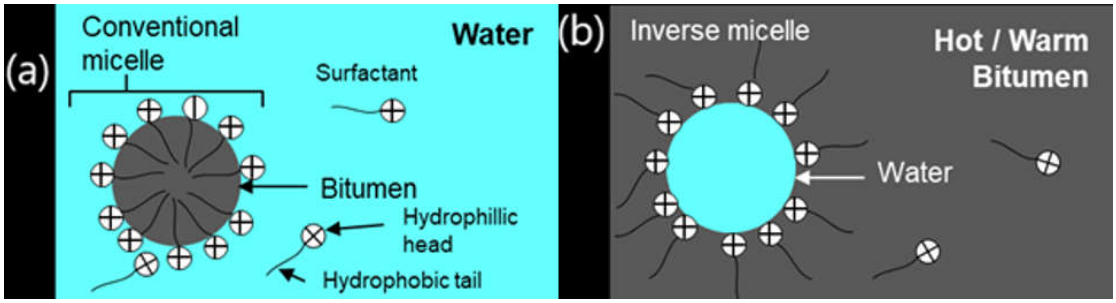


**Figure 3. (a)** Traditional bitumen emulsion. **(b)** Stabilized bitumen emulsion. Reprinted with permission from [81]. Copyright (2019), with permission from Elsevier.

The inverse micelles prevent evaporation of the remaining water and forms a thin film of water between the aggregates, improving the workability and compaction of the mixture. Once the aggregate and bitumen have been mixed and compacted, the remaining water evaporates by chemical reactions that are designed during emulsion formulation [81,83]. Chemical additives which are emulsion-based exist and are also used for WMA production, although these products cost more. An example of a super-stabilized emulsion is Evotherm® and has been described in Section 3.1. These are emulsions that have been stabilized and additive technology has been added to the formulation. These emulsion-based products are called *super-stabilized emulsions*. This stability is achieved by a special formulation of the liquid phase containing additives, which impart higher stability to the emulsion [81]. The combination of these stabilized emulsions with surfactants or polymers can improve mixture workability, coating properties and result in more effective compaction at lower temperatures [84].

## 6. Conclusions

Increasing concern regarding environmental issues is the most stimulating factor behind the drift of the asphalt industry towards Warm Mix Asphalt (WMA). WMA is a new, fast emerging technology and the validation of facts about this technology will contribute to its widespread acceptance. The lack of a standardized WMA mix design increases the need for an understanding of the underlying mechanisms of action of additives in the mix. Lack of knowledge on the potential and dynamics of WMA in several parts of the world where the technology discoveries are not widespread is a limiting factor on the growth of this technology. This is partly due to the limited knowledge on WMA additives which does not encourage proficiency with WMA techniques on the part of industry personnel. The discussions presented in this paper, fostered by a review of previous research and studies, highlight the following points about WMA additives and technology:

1. Organic additives in the form of waxes and fatty amides act as flow modifiers by melting below the melting point of the binder, thus reducing its viscosity during mixing which improves the coating and workability of the mix.
2. During the cooling phase of the mix, waxes such as Sasobit start to crystallize and form a microscopic lattice structure in the binder which results in the increased stiffness of the asphalt pavement. This is responsible for the deformation resistance and reduction in the amount of air voids observed in wax-treated WMA. It is speculated that the stiffness observed in the improved mix results from the alteration of binder hydrocarbon chain length by organic additives which are hydrocarbon-rich in nature.
3. Chemical additives in the form of emulsions and surfactants function at the microscopic interface of the binder and aggregates to regulate and reduce the frictional forces at that interface. This improves lubrication between the binder and aggregates.
4. Emulsifying agents such as Evotherm generally improve lubrication of the mix by altering Surface Free Energy components and parameters. This is responsible for asphalt mix particles moving more easily over each other in the mix which in turn translates to better coating of aggregates caused by an improved contact angle. Liquid chemical additives like Iterlow also act as emulsifying agents which contain amine groups and improves cracking resistance of the mix at low temperatures.
5. Surfactants such as Rediset generally reduce surface tension of asphalt binder to improve wettability of aggregates. They also function in a similar fashion as the organic additives by reducing the viscosity of the binder to improve workability of the mix.
6. Foaming technologies in the form of Zeolites (aluminosilicates) and water-based processes (injection nozzles) generally reduce binder viscosity temporarily. This improves coating and mix workability. These processes are more susceptible to moisture damage due to the involvement of water in the foaming process thus anti-stripping agents are often added to the mix if it is not already contained in the product.
7. Hybrid techniques such as Sasoflex and Tri-Mix Warm Mix Injection system combine different categories of additives with specific desirable features to synthesize additives with versatile functions. This might be the future of WMA technology.

Each category of additive is characterized by specific mechanism(s) of action in Warm Mix Asphalt. Some additives combine several mechanisms such as conjoining improved lubrication with reduced viscosity while altering several adhesion and cohesion parameters of the mix. The ability of additives to exploit several mechanisms to improve Warm Mix is a characteristic that can be better exploited in the asphalt industry to produce high-performance WMA. The establishment of facts regarding mechanism of action of additives is key to formulating a standard design mix procedure and the advancement of asphalt production technologies in general.

**Author Contributions:** All authors contributed equally to this work. All authors have read and agreed to the published version of the manuscript.

**Funding:** This work has been partially supported by "Loprete Costruzioni Stradali SRL (Italy)". It also supplied the asphalt materials needed for our research projects on the bitumen modifications.

**Conflicts of Interest:** The authors do not endorse any proprietary products or technologies referred to in this paper. Any product name mentioned in this paper appears only because it is considered essential to research and the objectives of this review.

## References

1. Rossi, C.O.; Caputo, P.; De Luca, G.; Maiuolo, L.; Eskandarsefat, S.; Sangiorgi, C. 1H-NMR spectroscopy: A possible approach to advanced bitumen characterization for industrial and paving applications. *Appl. Sci.* **2018**, *8*, 229, doi:10.3390/app8020229.
2. Prowell, B.D.; Hurley, G.C.; Frank, B. *Warm-Mix Asphalt: Best Practices*, 2nd ed.; Quality Improvement Publication: (NAPA) Lanham, MD, USA, 2011.
3. Rossi, C.O.; Caputo, P.; Baldino, N.; Lupi, F.R.; Miriello, D.; Angelico, R. Effects of adhesion promoters on the contact angle of bitumen-aggregate interface. *Int. J. Adhes. Adhes.* **2016**, *70*, 297–303, doi:10.1016/j.ijadhadh.2016.07.013.
4. Baldino, N.; Gabriele, D.; Lupi, F.R.; Rossi, C.O.; Caputo, P.; Falvo, T. Rheological effects on bitumen of polyphosphoric acid (PPA) addition. *Constr. Build. Mater.* **2013**, *40*, 397–404, doi:10.1016/j.conbuildmat.2012.11.001.
5. Caputo, P.; Porto, M.; Calandra, P.; De Santo, M.P.; Rossi, C.O. Effect of epoxidized soybean oil on mechanical properties of bitumen and aged bitumen. *Mol. Cryst. Liq. Cryst.* **2018**, *675*, 68–74, doi:10.1080/15421406.2019.1606979.
6. Rossi, C.O.; Caputo, P.; Ashimova, S.; Fabozzi, A.; D'Errico, G.; Angelico, R. Effects of natural antioxidant agents on the bitumen aging process: An EPR and rheological investigation. *Appl. Sci.* **2018**, *8*, 1405, doi:10.3390/app8081405.
7. Porto, M.; Caputo, P.; Loise, V.; De Filpo, G.; Rossi, C.O.; Calandra, P. Polysaccharides-reinforced bitumens: Specificities and universality of rheological behavior. *Appl. Sci.* **2019**, *9*, 5564, doi:10.3390/app9245564.
8. European Asphalt Pavement Association (EAPA). *The Use of Warm Mix Asphalt-EAPA Position Paper*; EAPA: Brussels, Belgium, 2014.
9. Rubio, M.C.; Martínez, G.; Baena, L.; Moreno, F. Warm mix asphalt: An overview. *J. Clean. Prod.* **2012**, *24*, 76–84, doi:10.1016/j.jclepro.2011.11.053.
10. Pereira, R.; Almeida-Costa, A.; Duarte, C.; Benta, A. Warm mix asphalt: Chemical additives' effects on bitumen properties and limestone aggregates mixture compactibility. *Int. J. Pavement Res. Technol.* **2018**, *11*, 285–299, doi:10.1016/j.ijprt.2017.10.005.
11. Diab, A.; Sangiorgi, C.; Ghabchi, R.; Zaman, M.; Wahaballa, A.M.; Lee, Y.-H.; Chou, N.N.; He, J.; Qian, G.; Zhu, J.; et al. Warm mix asphalt (WMA) technologies: Benefits and drawbacks—A literature review. In Proceedings of the Functional Pavement Design, Delft, The Netherland, 29 June–1 July 2016.
12. Romier, A.; Audeon, M.; David, J.; Martineau, Y.; Olard, F. Low energy asphalt with performance of hot mix asphalt. *Transp. Res. Rec.* **2006**, *1962*, 101–112.
13. Srikanth, G.; Kumar, R.; Vasudeva, R. A Review on Warm Mix Asphalt. In Proceedings of National Conference: Advanced Structures, Materials and Methodology in Civil Engineering (ASMMCE–2018), NIT Jalandhar, India, 3–4 November 2018.
14. Panda, M.; Padhi, M.M.; Giri, J.P. Use of emulsion for warm mix asphalt. *Int. J. Transp. Sci. Technol.* **2017**, *6*, 78–85, doi:10.1016/j.ijtst.2017.04.001.
15. Bonaquist, R. *Mix Design Practices for Warm-Mix Asphalt*; Transportation Research Board: Washington, DC, USA, 2011.

16. Hamzah, M.O.; Golchin, B.; Tye, C.T. Determination of the optimum binder content of warm mix asphalt incorporating rediset using response surface method. *Constr. Build. Mater.* **2013**, *47*, 1328–1336, doi:10.1016/j.conbuildmat.2013.06.023.
17. Calandra, P.; Caputo, P.; De Santo, M.P.; Todaro, L.; Liveri, V.T.; Rossi, C.O. Effect of additives on the structural organization of asphaltene aggregates in bitumen. *Constr. Build. Mater.* **2019**, *199*, 288–297, doi:10.1016/j.conbuildmat.2018.11.277.
18. Asphalt Institute. *Performance Graded Asphalt Binder Specification and Testing*; Asphalt Institute: Lexington, KY, USA, 2003.
19. Corrigan, M. Warm Mix Asphalt Technologies and Research. Every Day Counts, US Department of Transportation Federal Highway Administration Factsheet. Available online: https://www.fhwa.dot.gov/pavement/asphalt/wma.cfm (accessed on 6 April 2020).
20. Biro, S.; Gandhi, T.; Amirkhanian, S. Midrange temperature rheological properties of warm asphalt binders. *J. Mater. Civ. Eng.* **2009**, *21*, 316–323, doi:10.1061/(asce)0899-1561(2009)21:7(316).
21. Capitão, S.D.; Picado-Santos, L.G.; Martinho, F. Pavement engineering materials: Review on the use of warm-mix asphalt. *Constr. Build. Mater.* **2012**, *36*, 1016–1024, doi:10.1016/j.conbuildmat.2012.06.038.
22. Sasol Wax Sasobit Factsheet. 2008. Available online: https://www.sasolwax.com/fileadmin/sasolwax/documents/Asphalt%20Additives/SASOBIT.pdf (accessed on 11 April 2020)
23. Kvasnak, A.N.; West, R.C. Case study of warm-mix asphalt moisture susceptibility in Birmingham, Alabama. In Proceedings of the Transportation Research Board 88th Annual Meeting, Washington, DC, USA, 11–15 January 2009.
24. Stimilli, A.; Virgili, A.; Canestrari, F. Warm recycling of flexible pavements: Effectiveness of warm mix asphalt additives on modified bitumen and mixture performance. *J. Clean. Prod.* **2017**, *156*, 911–922, doi:10.1016/j.jclepro.2017.03.235.
25. Arabali, P.; Sakhaeifar, M.S.; Freeman, T.; Wilson, B.; Borowiec, J.D. Decision-making guideline for preservation of flexible pavements in general aviation airport management. *J. Transp. Eng. B Pavements* **2017**, *143*, 04017006, doi:10.1061/jpeodx.0000002.
26. Hurley, G.; Prowell, B. Evaluation of Sasobit for use in warm mix asphalt. *NCAT Rep.* **2005**, *5*, 1–27.
27. Caputo, P.; Porto, M.; Loise, V.; Teltayev, B.; Rossi, C.O. Analysis of mechanical performance of bitumen modified with waste plastic and rubber additives by rheology and self diffusion NMR experiments. *Eurasian Chem. Technol. J.* **2019**, *21*, 235–239, doi:10.18321/ectj864.
28. Sasol Wax Sasobit REDUX Factsheet, 2016. Available online: https://www.sasolwax.com/fileadmin/sasolwax/documents/Asphalt%20Additives/Asphalt_Additive_Sasobit_REDUX.pdf. (accessed on 11 April 2020)
29. D'Angelo, J.A.; Harm, E.; Bartoszek, J.; Baumgardner, G.; Corrigan, M.; Cowsert, J.; Harman, T.; Jamshidi, M.; Jones, W.; Newcomb, D.; et al. *Warm-Mix Asphalt: European Practice*; American Trade Initiatives: Alexandria, VA, USA, 2008.
30. Rowe, G.M.; Baumgardner, G.L.; Reinke, G.; D'Angelo, J.; Anderson, D.A. Evaluation of the BBR test with mixtures containing waxes. In Proceedings of the Binder Expert Task Group Meeting, San Antonio, TX, USA, 14–15 September 2009.
31. Li, X.; Wang, H.; Zhang, C.; Diab, A.; You, Z. Characteristics of a surfactant produced warm mix asphalt binder and workability of the mixture. *J. Test. Eval.* **2015**, *44*, 2219–2230, doi:10.1520/jte20140447.
32. Kheradmand, B.; Muniandy, R.; Hua, L.T.; Yunus, R.; Solouki, A. An overview of the emerging warm mix asphalt technology. *Int. J. Pavement Eng.* **2013**, *15*, 79–94, doi:10.1080/10298436.2013.839791.
33. Kakar, M.R.; Hamzah, M.O.; Akhtar, M.N.; Woodward, D. Surface free energy and moisture susceptibility evaluation of asphalt binders modified with surfactant-based chemical additive. *J. Clean. Prod.* **2016**, *112*, 2342–2353, doi:10.1016/j.jclepro.2015.10.101.
34. Calandra, P.; Ruggirello, A.; Mele, A.; Liveri, V.T. Self-assembly in surfactant-based liquid mixtures: Bis(2-ethylhexyl)phosphoric acid/bis(2-ethylhexyl)amine systems. *J. Colloid Interface Sci.* **2010**, *348*, 183–188, doi:10.1016/j.jcis.2010.04.031.
35. Calandra, P.; Liveri, V.T.; Riello, P.; Freris, I.; Mandanici, A. Self-assembly in surfactant-based liquid mixtures: Octanoic acid/Bis(2-ethylhexyl)amine systems. *J. Colloid Interface Sci.* **2012**, *367*, 280–285, doi:10.1016/j.jcis.2011.10.015.
36. Calandra, P.; Mandanici, A.; Liveri, V.T.; Pochylski, M.; Aliotta, F. Emerging dynamics in surfactant-based liquid mixtures: Octanoic acid/bis(2-ethylhexyl) amine systems. *J. Chem. Phys.* **2012**, *136*, 064515, doi:10.1063/1.3684713.
37. Calandra, P.; Nicotera, I.; Rossi, C.O.; Liveri, V.T. Dynamical properties of self-assembled surfactant-based mixtures: Triggering of one-dimensional anomalous diffusion in bis(2-ethylhexyl)phosphoric acid/n-octylamine systems. *Langmuir* **2013**, *29*, 14848–14854, doi:10.1021/la403522q.

38. Arabani, M.; Roshani, H.; Hamedi, G.H. Estimating moisture sensitivity of warm mix asphalt modified with zycosoil as an antistrip agent using surface free energy method. *J. Mater. Civ. Eng.* **2012**, *24*, 889–897, doi:10.1061/(asce)mt.1943-5533.0000455.
39. Bhasin, A.; Masad, E.; Little, D.; Lytton, R.; Information, R. Limits on adhesive bond energy for improved resistance of hot-mix asphalt to moisture damage. *Transp. Res. Rec. J. Transp. Res. Board* **2006**, *1970*, 3–13, doi:10.3141/1970-03.
40. Bhasin, A.; Little, D.N.; Vasconcelos, K.L.; Masad, E. Surface free energy to identify moisture sensitivity of materials for asphalt mixes. *Transp. Res. Rec. J. Transp. Res. Board* **2007**, *2001*, 37–45, doi:10.3141/2001-05.
41. Habal, A.; Singh, D. Moisture damage resistance of GTR-modified asphalt binders containing WMA additives using the surface free energy approach. *J. Perform. Constr. Facil.* **2017**, *31*, 04017006, doi:10.1061/(asce)cf.1943-5509.0000995.
42. Little, D.N.; Bhasin, A. *Using Surface Energy Measurements to Select Materials for Asphalt Pavement*; Transportation Research Board: Washington, DC, USA, 2006.
43. Ghabchi, R.; Singh, D.; Zaman, M.; Tian, Q. Application of asphalt-aggregates interfacial energies to evaluate moisture-induced damage of warm mix asphalt. *Procedia Soc. Behav. Sci.* **2013**, *104*, 29–38, doi:10.1016/j.sbspro.2013.11.095.
44. Hurley, G.C.; Prowell, B.D. Evaluation of evotherm for use in warm mix asphalt. *NCAT Rep*. **2006**, *2*, 15–35.
45. Chowdhury, A.; Button, J.W. *A Review of Warm Mix Asphalt*; Texas Transportation Institute: College Station, TX, USA, 2008.
46. Arabani, M.; Hamedi, G.H. Using the surface free energy method to evaluate the effects of polymeric aggregate treatment on moisture damage in hot-mix asphalt. *J. Mater. Civ. Eng.* **2011**, *23*, 802–811, doi:10.1061/(asce)mt.1943-5533.0000228.
47. Calandra, P.; Mandanici, A.; Liveri, V.T. Self-assembly in surfactant-based mixtures driven by acid–base reactions: Bis(2-ethylhexyl) phosphoric acid–n-octylamine systems. *RSC Adv.* **2013**, *3*, 5148, doi:10.1039/c3ra23295f.
48. Sanchez-Alonso, E.; Vega-Zamanillo, A.; Castro-Fresno, D.; DelRio-Prat, M. Evaluation of compactability and mechanical properties of bituminous mixes with warm additives. *Constr. Build. Mater.* **2011**, *25*, 2304–2311, doi:10.1016/j.conbuildmat.2010.11.024.
49. Cheng, D.; Little, D.N.; Lytton, R.L.; Holste, J.C. Use of surface free energy of asphalt-aggregate system to predict moisture damage potential. *J. Assoc. Asph. Paving Technol.* **2002**, *71*, 59–88.
50. Yu, H.; Leng, Z.; Dong, Z.; Tan, Z.; Guo, F.; Yan, J. Workability and mechanical property characterization of asphalt rubber mixtures modified with various warm mix asphalt additives. *Constr. Build. Mater.* **2018**, *175*, 392–401, doi:10.1016/j.conbuildmat.2018.04.218.
51. Little, D.N.; Epps, J.A.; Sebaaly, P.E. The benefits of hydrated lime in hot-mix asphalt. Arlington (Virginia, USA): National Lime Association, April 2006 (<https://www.lime.org/documents/publications/free_downloads/benefits-hydrated-lime2006.pdf>).
52. Hesami, S.; Roshani, H.; Hamedi, G.H.; Azarhoosh, A. Evaluate the mechanism of the effect of hydrated lime on moisture damage of warm mix asphalt. *Constr. Build. Mater.* **2013**, *47*, 935–941, doi:10.1016/j.conbuildmat.2013.05.079.
53. McCann, M.; Sebaaly, P.E. Evaluation of moisture sensitivity and performance of lime in hot-mix asphalt: Resilient modulus, tensile strength, and simple shear tests. *Transp. Res. Rec.* **2003**, *1832*, 9–16, doi:10.3141/1832-02.
54. Smiljanic, M.; Pap, I.; Tatic, U.; Strbic, M.; Milinski, S.; Markovic, B. Potentials of using the polyfunctional additive "Rediset wmx" for asphalt mixtures. In Proceedings of the 5th International Conference Bituminous Mixtures and Pavements, Thessaloniki, Greece, 1–3 June 2011.
55. Syroezhko, A.M.; Baranov, M.A.; Ivanov, S.N.; Maidanova, N.V. Influence of natural additives and those synthesized by the Fischer-Tropsch method on the properties of petroleum bitumen and quality of floated asphalt. *Coke Chem.* **2011**, *54*, 26–31, doi:10.3103/s1068364x11010066.
56. Banerjee, A.; Smit, A.D.F.; A. Prozzi, J. The effect of long-term aging on the rheology of warm mix asphalt binders. *Fuel* **2012**, *97*, 603–611, doi:10.1016/j.fuel.2012.01.072.
57. Shi, P.C.; Xie, Z.X.; Fan, W.Z.; Wang, L.L.; Shen, J.N. Selecting warm mix asphalt (WMA) additives by the properties of WMA binders. *Adv. Mater. Res.* **2013**, *753*, 585–590, doi:10.4028/www.scientific.net/amr.753-755.585.
58. Zaumanis, M.; Haritonovs, V. Research on properties of warm mix asphalt. *Sci. J. Riga Tech. Univ.* **2010**, *11*, 77–84.
59. Zhang, J.Z.; Wu, S.P.; Van De Ven, M.; Chen, F. Dynamic viscosity analysis of base bitumen with the addition of rediset. *Adv. Mater. Res.* **2012**, *476*, 1621–1625, doi:10.4028/www.scientific.net/amr.476-478.1621.

60. Estakhri, C.; Button, J.; Alvarez, A.E. *Field and Laboratory Investigation of Warm Mix Asphalt in Texas*; Texas Transportation Institute: College Station, TX, USA, 2010.
61. Hill, B.; Behnia, B.; Buttlar, W.G.; Reis, H. Evaluation of warm mix asphalt mixtures containing reclaimed asphalt pavement through mechanical performance tests and an acoustic emission approach. *J. Mater. Civ. Eng.* **2013**, *25*, 1887–1897, doi:10.1061/(asce)mt.1943-5533.0000757.
62. James, R. Metering of steam-water two-phase flow by sharp-edged orifices. *Proc. Inst. Mech. Eng.* **1965**, *180*, 549–572, doi:10.1243/pime_proc_1965_180_038_02.
63. Grela, A. The mineral composition and textural properties of zeolites with metakaolin Skład mineralny i właściwości teksturalne zeolitów z metakaolinu. *Przem. Chem.* **2015**, *1*, 193–196, doi:10.15199/62.2015.4.24.
64. Breck, D.W. *Zeolite Molecular Sieves, Structure, Chemistry, and Use*; John Wiley & Sons: New York, NY, USA, 1974.
65. Franus, W.; Wdowin, M.; Franus, M. Synthesis and characterization of zeolites prepared from industrial fly ash. *Environ. Monit. Assess.* **2014**, *186*, 5721–5729, doi:10.1007/s10661-014-3815-5.
66. Franus, M.; Wdowin, M.; Bandura, L.; Franus, W. Removal of environmental pollutions using zeolites from fly ash: A review. *Fresenius Environ. Bull*. **2015**, *24*, 854–866.
67. Sengoz, B.; Topal, A.; Gorkem, C. Evaluation of natural zeolite as warm mix asphalt additive and its comparison with other warm mix additives. *Constr. Build. Mater.* **2013**, *43*, 242–252, doi:10.1016/j.conbuildmat.2013.02.026.
68. Grace, W.R. Web Site of Grace Co. Zeolite Structure. Available online: http://www.grace.com/EngineeredMaterials/MaterialSciences/Zeolites/ZeoliteS tructure.aspx (accessed on 28 May 2020)
69. Clinoptilolite. The Mineral and Locality Database. Available online: http://www.mindat.org/min-1082.html (accessed on 28 May 2020).
70. Sengoz, B.; Topal, A.; Gorkem, C. Evaluation of moisture characteristics of warm mix asphalt involving natural zeolite. *Road Mater. Pavement Des.* **2013**, *14*, 933–945, doi:10.1080/14680629.2013.817352.
71. Bonaccorsi, L.; Calandra, P.; Kiselev, M.A.; Amenitsch, H.; Proverbio, E.; Lombardo, D. Self-assembly in poly(dimethylsiloxane)–poly(ethylene oxide) block copolymer template directed synthesis of linde type A zeolite. *Langmuir* **2013**, *29*, 7079–7086, doi:10.1021/la400951s.
72. Bonaccorsi, L.; Calandra, P.; Amenitsch, H.; Proverbio, E.; Lombardo, D. Growth of fractal aggregates during template directed SAPO-34 zeolite formation. *Microporous Mesoporous Mater.* **2013**, *167*, 3–9, doi:10.1016/j.micromeso.2012.10.024.
73. PQ-Corporations, 2010. Adveraw WMA Aluminosilicate. Available online: http://www.pqcorp.com/msds/advera_wma_ansi_msds.pdf (accessed on 30 May 2020)
74. Zhang, J. Effects of warm-mix asphalt additives on asphalt mixture characteristics and pavement performance. *Civ. Eviron. Eng. Theses* **2010**, *12*, 89.
75. Goh, S.W.; You, Z. Evaluation of warm mix asphalt produced at various temperatures through dynamic modulus testing and four point beam fatigue testing. *Pavements Mater.* **2011**, 123–130, doi:10.1061/47623(402)15.
76. Hurley, G.C.; Prowell, B.D. Evaluation of aspha-min zeolite for use in warm mix asphalt. In *NCAT Report*; National Center for Asphalt Technology: Auburn, AL, USA, 2005.
77. Kristjansdottir, O. Warm mix asphalt technology adoption. In Proceedings of the NVF 33 Annual Meeting, Trondheim, Norway, June 2007.
78. Mitchell, M.R.; Link, R.E.; Buddhala, A.; Hossain, Z.; Wasiuddin, N.M.; Zaman, M.; O'Rear, E.A. Effects of an amine anti-stripping agent on moisture susceptibility of sasobit and aspha-min mixes by surface free energy analysis. *J. Test. Eval.* **2012**, *40*, 91–99, doi:10.1520/jte103618.
79. Barthel, W.; Marchand, J.P.; von Devivere, M.V. Warm asphalt mixes by adding a synthetic zeolite. In Proceedings of the 3rd Eurasphalt & Eurobitume Congress, Vienna, Austria, 12–14 May 2004.
80. Woszuk, A.; Zofka, A.; Bandura, L.; Franus, W. Effect of zeolite properties on asphalt foaming. *Constr. Build. Mater.* **2017**, *139*, 247–255, doi:10.1016/j.conbuildmat.2017.02.054.
81. López, C.; González, Á.; Thenoux, G.; Sandoval, G.; Marcobal, J. Stabilized emulsions to produce warm asphalt mixtures with reclaimed asphalt pavements. *J. Clean. Prod.* **2019**, *209*, 1461–1472, doi:10.1016/j.jclepro.2018.11.138.
82. Prowell, B.D. *Warm Mix Asphalt, The International Technology Scanning Program*; American Trade Initiatives: Alexandria, VA, USA, 11 July 2007.

83. Rashwan, M.H. Characterization of Warm Mix Asphalt (WMA) Performance in Different Asphalt Applications. Ph.D. Thesis, Iowa State University, Ames, IA, USA, 2018.
84. Cheraghian, G.; Falchetto, A.C.; You, Z.; Chen, S.; Kim, Y.S.; Westerhoff, J.; Moon, K.H.; Wistuba, M.P. Warm mix asphalt technology: An up to date review. *J. Clean. Prod.* **2020**, *268*, doi:10.1016/j.jclepro.2020.122128.

© 2020 by the authors. Licensee MDPI, Basel, Switzerland. This article is an open access article distributed under the terms and conditions of the Creative Commons Attribution (CC BY) license (http://creativecommons.org/licenses/by/4.0/).

applied sciences

MDPI

Article

# A Study of Rubber-REOB Extender to Produce Sustainable Modified Bitumens

**Giulia Tarsi [1], Paolino Caputo [2], Michele Porto [2,*] and Cesare Sangiorgi [1]**

[1] Department of Civil, Chemical, Environmental and Materials Engineering–University of Bologna, 40131 Bologna, Italy; giulia.tarsi2@unibo.it (G.T.); cesare.sangiorgi4@unibo.it (C.S.)
[2] Department of Chemistry and Chemical Technologies–University of Calabria, 87036 Arcavacata di Rende, Italy; paolino.caputo@unical.it
* Correspondence: michele.porto@unical.it

Received: 31 December 2019; Accepted: 7 February 2020; Published: 11 February 2020


**Abstract:** Thanks to greater attention to the environment and the depletion of non-renewable resources, the sustainability and the circular economy have become crucial topics. The current trend of pavement engineering is to reduce the use of standard bitumen by replacing it with more sustainable materials such as industrial residues and by-products. In this regard, the present study aims to characterize innovative extended bitumen using recycled materials. Due to promising preliminary results as bitumen modifiers, the powdered rubber from end-of-life tires and the re-refined engine oil bottom (REOB) have been investigated as feasible components of bitumen extenders. Nevertheless, several variables strongly affect the performance of the resulting binder, which cannot be neglected. Hence, this research focuses on the rubber–REOB interaction in order to evaluate their optimum ratio, which may maximize the use and advantages of both recycled materials as suitable partial replacements for bitumen. Various rubber–REOB ratios were considered and investigated by means of low and high frequency nuclear magnetic resonance (NMR) spectrometers and scanning electron microscope (SEM).

**Keywords:** powdered rubber; re-refined engine oil bottom; bitumen extender; NMR analysis; SEM analysis; bitumen

## 1. Introduction

The production and construction of road pavements need a substantial amount of energy and non-renewable materials. Therefore, the use of recycled materials and/or by-products seems to be necessary to create a more sustainable future for asphalt mixtures. The recycled materials and by-products that come from construction and demolition waste or urban and industrial waste can be introduced in asphalt mixes as recycled aggregates (e.g., RAP, steel slag, ceramics) instead of only using mineral aggregates [1]; on the other hand, waste polymers and oils can be used at the binder level as additives or modifiers of bitumen. Since the binder has a significant effect on asphalt mixture performances, the modification of bituminous binders has become the mainstream of research in recent decades [2].

Practical experiences and research have shown that rubber from end-of-life tires (ELTs) may be successfully used as bitumen modifiers to improve the binder response over a wide range of temperatures [3]. Without neglecting the several parameters that influence the physico-chemical properties of modified binders such as type, quantity, and characteristics of constituent materials, some studies have highlighted the feasible replacement for styrene-butadiene-styrene (SBS) polymers with recycled rubber [4,5]. The rubberized binder shows good resistance to permanent deformations that turns into a high rutting resistance, which has been evaluated by the use of dynamic shear

rheometer (DSR) device [4,6]. Although, the SBS modified binder has the best resistance to crack, the binder that contains rubber shows the best anti-fatigue response [4]. In addition, based on rheological data, both virgin and waste polymers can decrease the brittleness of modified binders at intermediate temperature, and reduce the resulting stiffness at low temperatures [7]. However, the use of rubber has a disadvantageous aspect which is the overall increase in binder viscosity. This feature is important for pumpability and workability of modified binder [8]. The new candidates to improve low temperature properties and reduce the viscosity of the rubberized binders are oils that can have various origins (i.e., petroleum or bio-based oils, waste or refined used oils) [9]. Previous studies have highlighted the mitigation effect of oil when added to a modified binder regardless of its nature [10–12]. The oil modification alters the rheological and thermal behavior of bitumen, which has been observed through dynamic shear rheometer (DSR) and bending beam rheometer (BBR) analysis [9]. The introduction of oil leads to a decrease in the stiffness of binders, sometimes with adverse effects at high service temperature if overdosed. In detail, the study of [13] regarding the use of re-refined engine oil bottom (REOB) revealed that a limited concentration of the oil unaffected the thermal cracking performance of binders at low temperature and their fatigue cracking resistance at intermediate temperature. However, by increasing the concentration of REOB up to 15%, the binder strength and strain tolerance at intermediate temperature could be significantly influenced. Moreover, a large amount of oil may jeopardize the thermal cracking performance of binders [13]. Another study observed that blending standard bitumen with REOB at a rate of 9% did not compromise asphalt mixture stiffness and ageing [14]. On the other hand, a non-similar ageing susceptibility of fluxed and standard bitumens has been demonstrated, and the different binder responses were attributed to the composition of the various oils [9]. Therefore, the influence of oil has to be investigated deeply to minimize the related risks considering the maximum level that can be used and the variability of oil residues. Both wastes, ELTs and REOB, are engineering materials that represent a resource for further civil engineering applications. The compound of rubber particles and oil may represent a sustainable extender that is able to replace a certain quantity of standard bitumen without compromising the performances of the resulting binder, since they can mitigate their each other drawbacks.

As previously mentioned, the effect of rubber and oil modifications is strictly dependent on the constituent materials [9,15]. As a consequence, the complete characterization of modified binders requires the investigation of the components' interactions themselves. The rubberized binder is produced with the so-called wet process, during which the rubber particles are thoroughly mixed with bitumen to obtain a ductile and elastic modified bitumen. The interaction of components is made up of two simultaneous phenomena: the partial digestion of the rubber particles into the bituminous matrix and the absorption of the aromatic fraction available in this latter within the rubber itself [16,17]. The absorption of the aromatic fraction from the bitumen into the rubber's polymer chains is a physical interaction mainly controlled by the rubber particles' shape and size that causes the rubber to swell and soften [18]. Therefore, during the reaction there is a simultaneous reduction in the oily fraction and the expansion of rubber particles forming a gel-like surface coating [16]. In this form, the particles of rubber are still visible (granular-like appearance) in the composite binder, even if the distance between the particles themselves decreases. If curing is carried out at an excessive temperature and/or for a too long period, the degradation phenomenon becomes prevalent and the rubber particles are totally digested in the bitumen [3].

Based on the promising results obtained so far, the present research pushes for a greater use of recycled materials in bituminous binders with the aim of using rubber and REOB as substitutes for bitumen, and not only as bitumen modifiers. The final objective of this study is the definition of a proper rubber-REOB compound that can replace the 25% by weight of standard bitumen obtaining an extended bitumen. Since the oil used is a petroleum-based material mainly constituted of oily fractions, it was assumed that rubber particles might absorb REOB as they absorb bitumen; this assumption has been used to define the optimum weight proportion of products to produce the extenders. Hence, to maximize the presence of both recycled materials, their interaction was investigated and various

extenders have been produced. Finally, the feasibility of using the selected extenders was evaluated by mixing them with a standard neat bitumen and assessing the rheological responses of the resulting extended bitumens.

## 2. Materials and Methods

In this study, two recycled materials (i.e., the powdered rubber from ELTs and the re-refined engine oil bottom (REOB)) were used to produce bitumen extenders that were able to replace a specific amount of petroleum bitumen obtaining extended bitumens.

The 50/70 penetration grade bitumen (B-50/70) was used as the reference material and base constituent of the extended bitumen. The powdered rubber (R) was produced from the trituration processes at an ambient temperature of waste tires from cars and trucks after the separation phase of textile and metallic parts of the tires themselves. The maximum dimension of rubber particles was 0.40 mm, while the density was 1.01 g/cm$^3$. The Italian consortium, Ecopneus Scpa, to promote the recycle and the reuse of waste tires, provided the material. The REOB is the by-product of a vacuum tower in a re-refinery plant of exhausted engine oil supplied by Itelyum Srl. This research used and compared two recycled oils (hereinafter called O1 and O2, or Ox if both or one of them were considered alternatively) that were produced in two distinct refinery plants of the same company. Both REOBs had a density approximately equal to 1.00 g/cm$^3$.

Five mixes were prepared per each REOB (i.e., O1 and O2) by varying the mass of each recycled materials. In particular, the considered R-REOB ratios were:

1. R:Ox = 3:1
2. R:Ox = 2:1
3. R:Ox = 1:1
4. R:Ox = 1:2
5. R:Ox = 1:3

All extenders were prepared by mixing the pre-heated materials. The first step consisted of warming up both materials at 130 °C in the oven; the Ox for at least 1 h 30', while R for 15'. Then, the Ox was added to the R portion and the recycled materials were mixed by the use of a propeller mixer at a rate of about 600 ÷ 650 rpm for 15'. The mixing phase was performed at a temperature equal to 130 °C. In order to keep the blend at a constant temperature during the mixing process, the container was immersed in a glycerine bath, which was continuously warmed up by a heating plate.

The resulting blends underwent nuclear magnetic resonance (NMR) and scanning electron microscopy (SEM) analysis to establish the optimum R–REOB ratio, which has been considered as the maximum amount of REOB that can be absorbed by R. The optimal proportion aims to maximize the use of both recycled materials. The spectroscopic analysis was carried out by two NMR instruments that operated at two different proton frequencies: a low resolution NMR (L-NMR) at 15 MHz and high resolution NMR (H-NMR) at 300 MHz [19]. The L-NMR is a homemade instrument, which has been used to perform relaxation experiments at ambient temperature; while, the H-NMR is a Bruker Avance 300 (Germany) that allowed the analysis of diffusion. Thanks to the software Mathematica, the collected data were post-processed and the spin–spin relaxation time ($T_2$) of all extenders were determined by fitting with an exponential equation. This relaxation time is concerned with the exchange of energy among spins without being affected by the surrounding environment [20]. The H-NMR spectra and diffusion properties of all samples were evaluated at the production temperature of 130 °C. The specimens do not need any specific conditioning before performing the tests. The scanning electron microscope (SEM, JEOL JXA-8230, Japan) allowed the investigation of the R–REOB blends' morphological structure. The tests were run in vacuum mode on the pre-conditioned samples, which were sputter coated with a thin film of graphite. Various magnifications were considered to collect the images of all specimens.

Thanks to the definition of the optima R–REOB ratios (that is 1:1 and 1:2), the extenders were used to produce four extended bitumens replacing 25% by the total weight of the binder, and their rheological response was investigated. The list of constituents of the four extended bitumens and their percentages are reported in Table 1. The conditions of the extenders' production have been defined in preliminary studies that have taken into consideration the optimal mixing temperature. The production of extended bitumens requires the pre-heating of constituents before mixing them. Both materials (i.e., optima extenders and bitumen) were warmed up at 160 °C, the R–REOB blends for more than 1 h and bitumen for more than 1 h 30'. They were mixed by the use of a propeller mixer at a constant rate of 800 rpm for 1 h. During the mixing phase, the materials were kept warm by the use of a heating plate.

**Table 1.** Percentage of extended bitumens' constituents.

| Extended Bitumen | Percentage of Constituent Materials | | |
|---|---|---|---|
| | B | R | O1/O2 |
| BRO1_1:1 | 75.0 | 12.5 | 12.5 |
| BRO2_1:1 | 75.0 | 12.5 | 12.5 |
| BRO1_1:2 | 75.0 | 8.3 | 16.7 |
| BRO2_1:2 | 75.0 | 8.3 | 16.7 |

The rheological analyses were carried out using a dynamic shear rheometer (DSR, Anton Paar MCR 302, Austria). This instrument has been used to investigate the extended bitumens' behavior over a wide range of frequencies and temperatures thanks to the amplitude sweep and frequency sweep tests. The amplitude sweep test allows the definition of the linear visco-elastic (LVE) range of each extended bitumen, which is one of the input data to perform the frequency sweep test. During the amplitude sweep test, all samples were subjected to a variable strain that increased in a logarithmic manner from 0.1% to 15%, while the frequency was constant and equal to 1.59 Hz. The test was carried out at three temperatures (10, 30, and 60 °C) to define the most restrictive non-destructive deformation range. Thereafter, the extended bitumens underwent the frequency sweep test. Each specimen was subjected to the corresponding maximum deformation (LVE range) applied at different angular frequencies that logarithmically increased from 0.1 Hz to 10 Hz. The tests were performed at six temperatures: 10, 20, 30, 40, 50, and 60 °C. Following the standard EN 14770, the rheological analysis was carried out using the plate–plate configuration; plates with a diameter of 8 mm and a gap equal to 2 mm were chosen to perform all tests.

## 3. Results and Discussion

### *3.1. Nuclear Magnetic Resonance Measurements—$T_2$ Relaxation Time and Diffusion Coefficient*

The basic of spectroscopic analysis is the evaluation of the nuclei behavior that underwent an inhomogeneous external field, which perturbs the equilibrium in a steady uniform magnetic field. In fact, at equilibrium, nuclei are distributed among the energy levels according to the Boltzmann distribution with a specific net magnetization vector, but this state can be disrupted by the absorption of radio-frequency energy such as that caused by a NMR instrument [21]. After the removal of the disruption field, the nuclear spin system returns to its equilibrium state and the transverse component of the magnetization vector exponentially decays. The time constant $T_2$ characterizes the signal decay, which is called spin–spin relaxation time because it is related to the exchange of energy between spins via flip-flop mechanisms [22]. Usually, the collected signal decay is an envelope of multi-exponential attenuation since the relaxation time varies in the sample due to the heterogeneity or surface relaxation differences [23].

In this study, the relaxation time $T_2$ of pure oils and extenders was evaluated by the use of the L-NMR device [24]. The trend of spin–spin relaxation time and the resulting $T_2$ value of both pure

oils and extenders are reported in Figure 1 and Table 2, respectively. In general, a short $T_2$ time corresponds to more rigid supra-molecular particles; while, higher $T_2$ times refer to low intra-molecular interactions [25]. The pure oils show the highest relaxation time over the corresponding extenders made with themselves, and it means a lower intra-molecular interactions of Ox. The introduction of rubber particles into Ox leads to a decrease in the $T_2$ values. The oil absorption by the rubber limits the mobility of the oil's molecules, therefore the $T_2$ relaxation times, which reflects a more rapid relaxation decay. This trend is more evident in the extenders made with O1, which means a higher compatibility between the rubber and O1 than the R-O2 compounds. The relaxation time of the O1-extenders was reduced from $5.39\times10^{-3}$ s for O1 to about $4.00\times10^{-3}$ s for those extenders with an R content up to 50% by total weight. Then, more changes in the $T_2$ value can be observed in samples with a higher quantity of R than O1. In fact, their curves almost overlapped each other. On the other hand, the samples of R:O2 = 1:3 and R:O2 = 1:2 and pure O2 had similar $T_2$, as shown by the overlapping curves (see Figure 1). The amount of R in these two extenders does not seem to affect their relaxation time more than the reference one of pure O2. When the quantity of R is equal or higher than 50%, the reduction in $T_2$ values can be observed. Based on the collected data, the R-REOB ratios 1:1 and 1:2 represent the latest ratios after which some changes occurred in the relaxation time. Therefore, these two R-REOB proportions were defined as optimal.

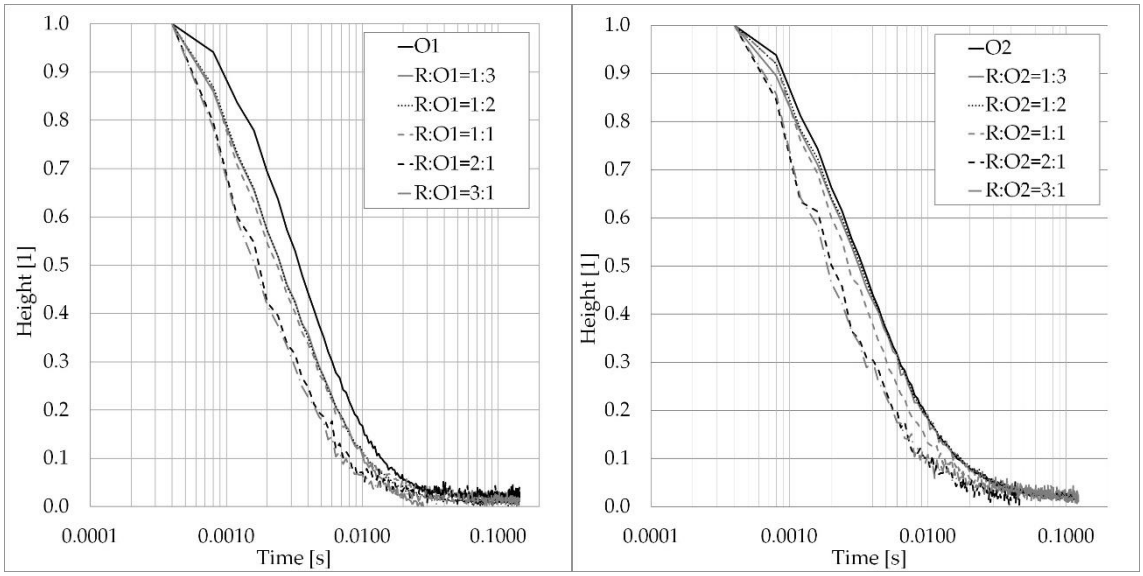


(**a**) (**b**)

**Figure 1.** Trend of spin–spin relaxation time of oils and extenders: (**a**) O1 and O1-R blends; (**b**) O2 and O2-R blends.

**Table 2.** $T_2$ relaxation time of the O1, O2, and extenders.

| Samples | Relaxation Time $T_2$ [s] | |
|---|---|---|
| | **O1** | **O2** |
| Ox | $5.39\times10^{-3}$ | $6.49\times10^{-3}$ |
| R:Ox = 3:1 | $2.71\times10^{-3}$ | $3.59\times10^{-3}$ |
| R:Ox = 2:1 | $3.00\times10^{-3}$ | $3.69\times10^{-3}$ |
| R:Ox = 1:1 | $4.22\times10^{-3}$ | $4.90\times10^{-3}$ |
| R:Ox = 1:2 | $4.21\times10^{-3}$ | $6.33\times10^{-3}$ |
| R:Ox = 1:3 | $4.07\times10^{-3}$ | $6.38\times10^{-3}$ |

The NMR measurements with the self-diffusion H-NMR probe allowed the evaluation of the self-diffusion coefficient (D) of oil into the extenders. The present measurements provide information

concerning the molecular dynamics and spatial dimensions of the particles and cavities in order to establish the particles' mobility and the microstructures of the samples [26]. The NMR spectra were obtained from Free Induction Decay by means of the Fourier transform. Path widths equal to $\pi/2$ and 16 scans were used to perform all of the NMR tests. The self-diffusion coefficient was determined directly by the use of a standard pulsed gradient stimulated echo (PGStE) sequence with a mono-exponential fitting [27]. The self-diffusion coefficient can be ascribed to the average diffusion phenomena of oil onto (external) and into (internal) the R particles. The self-diffusion coefficients of the extenders are shown in Figure 2. In theory, the self-diffusion coefficients should decrease with the addition of R because it reduces the particles' mobility. In fact, the extenders at ratios equal to 2:1 and 3:1 showed low values of the self-diffusion coefficient for both O1 and O2 samples. The oil self-diffusion coefficient jumped at the ratio of 1:1. Hence, the behavior was in agreement with the higher mobility of the oil when the maximum absorption was reached.

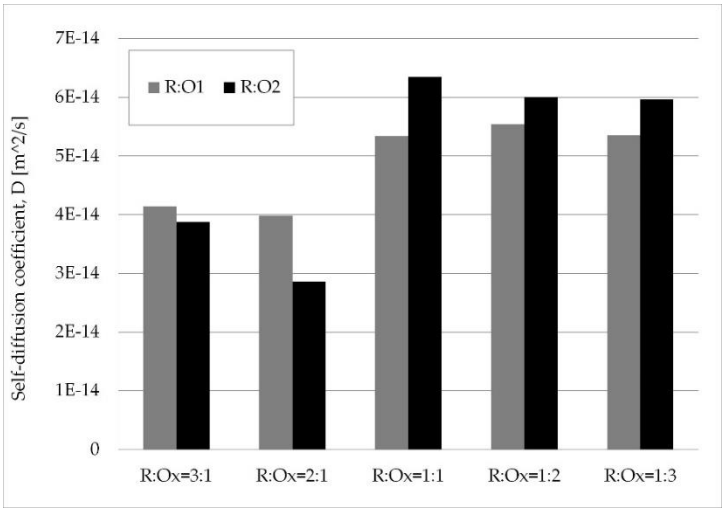


**Figure 2.** Self-diffusion coefficients (D) of the bitumen extenders.

### *3.2. Scanning Electron Microscopy Analysis—Morphological Structure*

The R and extenders underwent SEM analysis to evaluate their morphological structures. The images of the samples are shown in Figure 3. The increasing amount of oil in the samples is clearly visible moving from Figure 3a, that is, rubber particles without any oil, to Figure 3j,k, which contain a triple quantity of Ox than R. The sequence of images shows how the rubber may first absorb Ox; then, the amount of oil became high and started covering the R particles. Since the optimum R–REOB ratio is defined as the maximum amount of oil that can be absorbed by R, the extenders R:Ox = 1:1 and R:Ox = 1:2 can be identified as the optimal. The visual investigation of the morphological structures of samples confirmed the results obtained from spectroscopic analysis.

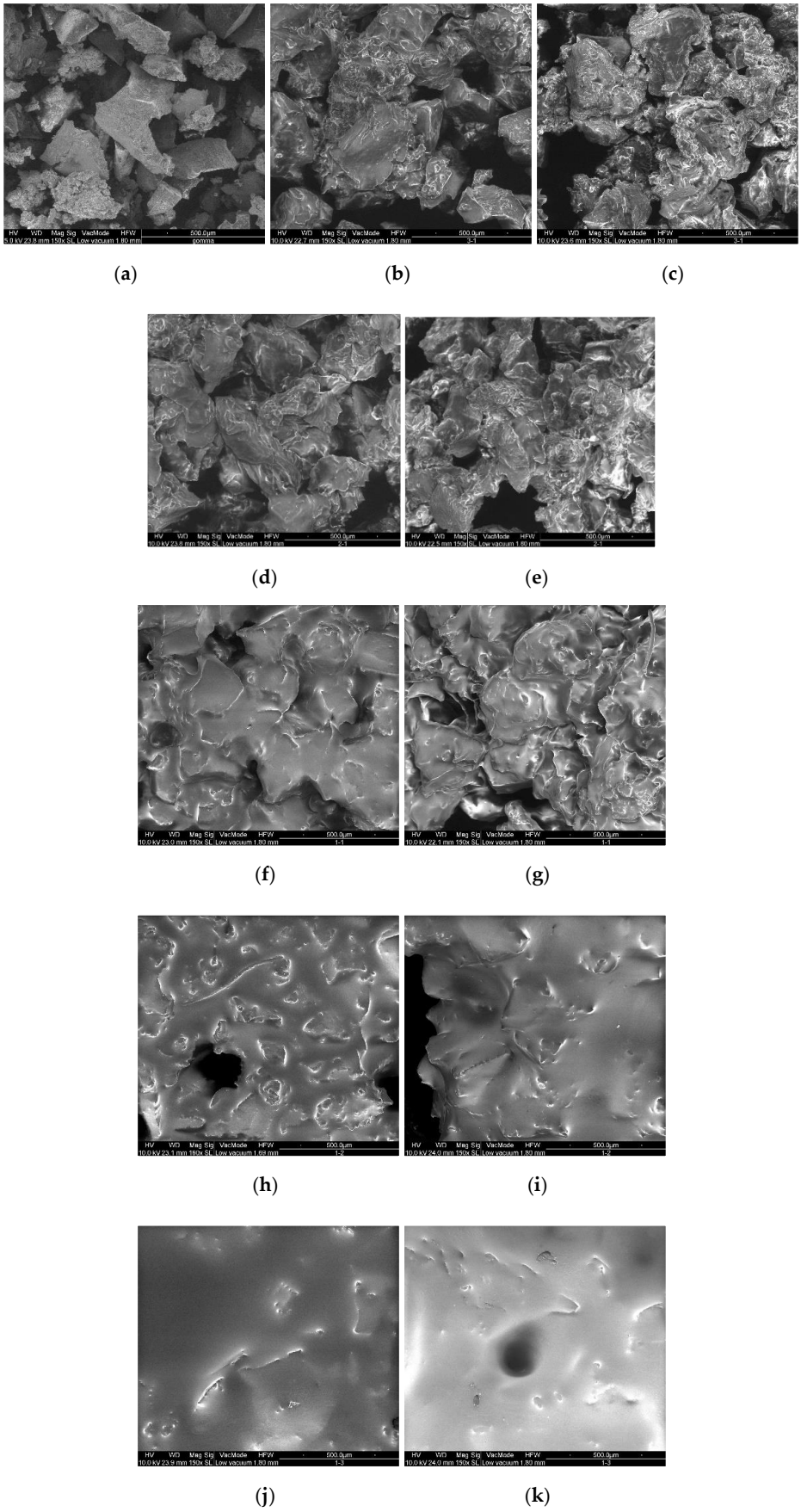

**Figure 3.** Rubber and extenders images acquired by scanning electron microscope with a magnitude of about 150x. (**a**) R; (**b**) R:O1 = 3:1; (**c**) R:O2 = 3:1; (**d**) R:O1 = 2:1; (**e**) R:O2 = 2:1; (**f**) R:O1 = 1:1; (**g**) R:O2 = 1:1; (**h**) R:O1 = 1:2; (**i**) R:O2 = 1:2; (**j**) R:O1 = 1:3; (**k**) R:O2 = 1:3.

### *3.3. Dynamic Shear Rheometer Investigation—Rheological Behavior*

The rheological responses of extended bitumens were investigated and compared with the behavior of the reference material in order to verify the possibility of using the extenders as a replacement for neat bitumen. Hence, we checked that the extended bitumens did not show performance degradations at the binder level.

At first, the amplitude sweep test was carried out to define the linear visco-elastic (LVE) range of neat and extended bitumens, and the most restrictive ranges were defined at 10 °C. The limits of samples non-destructive deformation that corresponded to the 95% of initial storage modulus were:

1. $\gamma$ BRO1_1:1 = 1.61%
2. $\gamma$ BRO2_1:1 = 1.51%
3. $\gamma$ BRO1_1:2 = 1.46%
4. $\gamma$ BRO2_1:1 = 1.14%
5. $\gamma$ B-50/70 = 1.61%

The B-50/70 and BRO1_1:1 had the same LVE limit; it seems that the substitution of standard bitumen with the compound O1-R in the proportion 1:1 does not weaken the resulting binder while the same extender made with O2 reduced the LVE limit of the binder, leading it to withstand a lower deformation until structural changes occur. Regarding the effect of different R–REOB ratios, double the amount of REOB than R into the extender strongly influences the response of binders, and the results confirmed the more detrimental effect of O2 than O1.

The complex shear modulus (G*) and phase angle (δ) master curves obtained from the frequency sweep tests are shown in Figure 4. Concerning the complex shear modulus master curves, all extended bitumens showed a stiffness reduction with respect to B-50/70 at high frequencies that corresponded to low temperatures. Lower values of G* may turn into a greater thermal cracking resistance, which may be related to the addition of REOB. At intermediate conditions, the G* values of extended bitumens were still lower than B-50/70; however, the differences between the binders decreased. By decreasing the frequencies, an inverted trend could be observed in the G* master curves. About all of the extended bitumens showed a greater complex modulus than neat bitumen at low frequencies or high temperatures; only the BRO1_1:1 sample had a similar response of B-50/70 and their master curves overlapped. The higher values of G* at low frequencies means that almost all extended bitumens can better withstand permanent deformations. This improvement may be ascribed to the presence of R; as a matter of fact, the binders made with R–REOB ratio equal to 1:1 had a greater stiffness than those made with a ratio 1:2 over all tested frequencies. Nevertheless, the samples BRO1_1:1 and BRO1_1:2 showed the opposite behavior at low frequencies/high temperature, which could be related to the production and/or test issues (e.g., non-well homogenization of components or the sample is not representative). On the other hand, the phase angle master curves of the extended bitumens showed lower values than that of neat bitumen, especially at low frequencies or high temperature. The introduction of R particles improves the elastic response of all bituminous binders. Moreover, the addition of a polymer (i.e., R) leads to changes in the shape of the binders' phase angle master curves. The curves of the extended binders showed two different slopes, while the curve of the neat bitumen was continuous.

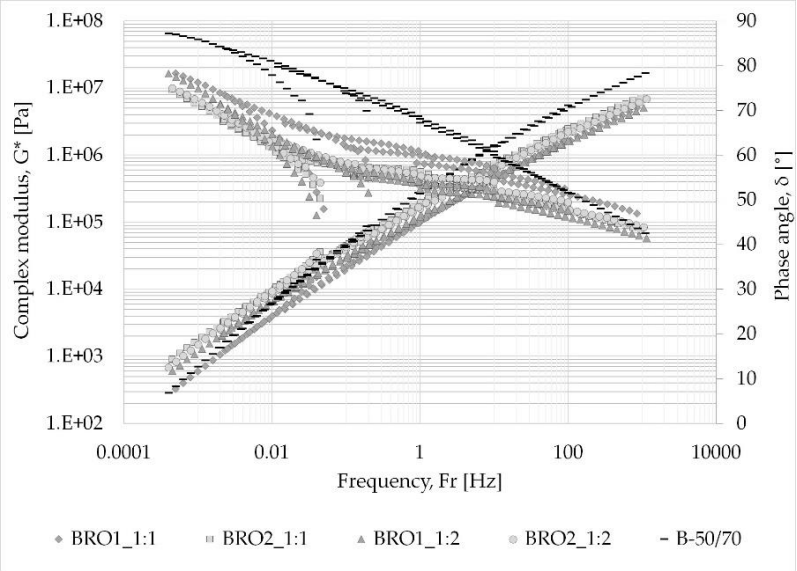


**Figure 4.** G* and δ master curves of the neat and extended bitumens.

## 4. Conclusions

This research aimed to define suitable bitumen extenders by the use of rubber from ELTs and REOB maximizing the quantity of both recycled materials used. Furthermore, the feasibility of using these materials as bitumen extenders, replacing 25% by weight of bitumen itself, has been studied.

Thanks to the NMR and SEM measurements, the optimum proportion of the two recycled materials was determined; both spectroscopic and imaging investigations confirmed the ratios R:Ox = 1:1 and R:Ox = 1:2 as the optimal to maximize the quantities of both recycled materials. Hence, the NMR and SEM measurements were found to be useful to study the R–REOB interactions.

The rheological results of extended bitumens by means of DSR are promising. The partial substitution of standard bitumen by the use of R–REOB blends can improve the performance of binders at low temperature; most probably the addition of REOB, which is a softening agent, leads to an enhancement of their thermal cracking resistance. The extended bitumens have acquired a greater elasticity at all tested conditions, which can be related to the introduction of rubber. In addition, the waste polymers may improve the binder responses at high temperature; however, one extended bitumen did not show greater resistance to permanent deformation.

Due to the variability of the components used and the complexity of interactions that takes place between constituent materials, further studies are necessary to fully understand the effect of each added product and ensure good performances of the resulting extended bitumen. Furthermore, other materials can be used as constituents of the bituminous binders, which should be investigated.

**Author Contributions:** Conceptualization, C.S. and G.T.; Software, M.P.; Validation, M.P., P.C., and G.T.; Formal analysis, M.P.; Investigation, G.T. and M.P.; Resources, G.T. and M.P.; Data curation, G.T. and M.P.; Writing—original draft preparation, G.T.; Writing—review and editing, M.P., P.C., and C.S.; Visualization, G.T.; Supervision, C.S.; Project administration, C.S.; Funding acquisition, C.S. All authors have read and agreed to the published version of the manuscript.

**Funding:** This research was funded by ECOPNEUS Scpa, Italy.

**Acknowledgments:** The authors would like to acknowledge ITELYUM Regeneration Srl for providing the REOBs.

**Conflicts of Interest:** The authors declare no conflict of interest. The funders had no role in the design of the study; in the collection, analyses, or interpretation of data; in the writing of the manuscript, or in the decision to publish the results.

## References


1. Ossa, A.; García, J.L.; Botero, E. Use of recycled construction and demolition waste (CDW) aggregates: A sustainable alternative for the pavement construction industry. *J. Clean. Prod.* **2016**, *135*, 379–386. [CrossRef]
2. Pouranian, M.R.; Shishehbor, M. Sustainability assessment of green asphalt mixtures: A review. *Environments* **2019**, *6*, 73. [CrossRef]
3. Zanetti, M.C.; Fiore, S.; Ruffino, B.; Santagata, E.; Dalmazzo, D.; Lanotte, M. Characterization of crumb rubber from end-of-life tyres for paving applications. *Waste Manag.* **2015**, *45*, 161–170. [CrossRef] [PubMed]
4. Ding, X.; Ma, T.; Zhang, W.; Zhang, D. Experimental study of stable crumb rubber asphalt and asphalt mixture. *Constr. Build. Mater.* **2017**, *157*, 975–981. [CrossRef]
5. Ziari, H.; Goli, A.; Amini, A. Effect of crumb rubber modifier on the performance properties of rubberized binders. *J. Mater. Civ. Eng.* **2016**, *28*, 04016156. [CrossRef]
6. Behnood, A.; Olek, J. Stress-dependent behavior and rutting resistance of modified asphalt binders: An MSCR approach. *Constr. Build. Mater.* **2017**, *157*, 635–646. [CrossRef]
7. Behnood, A.; Olek, J. Rheological properties of asphalt binders modified with styrene-butadiene-styrene (SBS), ground tire rubber (GTR), or polyphosphoric acid (PPA). *Constr. Build. Mater.* **2017**, *151*, 464–478. [CrossRef]
8. Subhy, A.; Presti, D.L.; Airey, G. An investigation on using pre-treated tyre rubber as a replacement of synthetic polymers for bitumen modification. *Road Mater. Pavement Des.* **2015**, *16*, 245–264. [CrossRef]
9. Golalipour, A.; Bahia, H. Evaluation of Oil Modification Effect on Asphalt Binder Thermal Cracking and Aging Properties. In Proceedings of the 59th Annual Meeting of the Canadian Technical Asphalt Association, Victoria, BC, Canada, 16–19 November 2014; pp. 345–374.
10. Amini, A.; Imaninasab, R. Investigating the effectiveness of Vacuum Tower Bottoms for Asphalt Rubber Binder based on performance properties and statistical analysis. *J. Clean. Prod.* **2018**, *171*, 1101–1110. [CrossRef]
11. Fini, E.H.; Hosseinnezhad, S.; Oldham, D.; Mclaughlin, Z.; Alavi, Z.; Harvey, J. Bio-modification of rubberised asphalt binder to enhance its performance. *Int. J. Pavement Eng.* **2019**, *20*, 1216–1225. [CrossRef]
12. Tarsi, G.; Mazzotta, F.; Sangiorgi, C. Rheo-mechanical analysis of bitumens produced with green binder extenders. In Proceedings of the 7th International Conference Bituminous Mixtures and Pavements (7ICONFBMP), Thessaloniki, Greece, 12–14 June 2019; pp. 81–87.
13. Li, X.; Gibson, N.; Andriescu, A.; Arnold, T.S. Performance evaluation of REOB-modified asphalt binders and mixtures. *Road Mater. Pavement Des.* **2017**, *18*, 128–153. [CrossRef]
14. Wielinski, J.; Kriech, A.; Huber, G.; Horton, A.; Osborn, L. Analysis of vacuum tower asphalt extender and effect on bitumen and asphalt properties. *Road Mater. Pavement Des.* **2015**, *16*, 90–110. [CrossRef]
15. Lei, Z.; Chao, X.; Fei, G.; Tian-Shuai, L.; Yi-qiu, T. Using DSR and MSCR tests to characterize high temperature performance of different rubber modified asphalt. *Constr. Build. Mater.* **2016**, *127*, 466–474.
16. Way, G.B.; Kaloush, K.E.; Biligiri, K.P. *Asphalt Rubber Standard Practice Guide*; Rubber Pavements Association: Tempe, AZ, USA, 2011.
17. Szerb, E.I.; Nicotera, I.; Teltayev, B.; Vaiana, R.; Rossi, C.O. Highly stable surfactant-crumb rubber-modified bitumen: NMR and rheological investigation. *Road Mater. Pavement Des.* **2018**, *19*, 1192–1202. [CrossRef]
18. Hosseinnezhad, S.; Holmes, D.; Fini, E.H. Decoupling the physical filler effect and the time dependent dissolution effect of crumb rubber on asphalt matrix rheology. In Proceedings of the Transportation Research Board 93rd Annual Meeting, Washington, DC, USA, 12–16 January 2014.
19. Coppola, L.; Gentile, L.; Nicotera, I.; Rossi, C.O.; Ranieri, G.A. Evidence of formation of ammonium perfluorononanoate/2H 2O multilamellar vesicles: Morphological analysis by rheology and Rheo-2H NMR experiments. *Langmuir* **2010**, *26*, 19060–19065. [CrossRef]
20. Rossi, C.O.; Spadafora, A.; Teltayev, B.; Izmailova, G.; Amerbayev, Y.; Bortolotti, V. Polymer modified bitumen: Rheological properties and structural characterization. *Colloids Surfaces A Physicochem. Eng. Asp.* **2015**, *480*, 390–397. [CrossRef]
21. Leggio, A.; Belsito, E.L.; De Luca, G.; Di Gioia, M.L.; Leotta, V.; Romio, E.; Siciliano, C.; Liguori, A. One-pot synthesis of amides from carboxylic acids activated using thionyl chloride. *RSC Adv.* **2016**, *6*, 34468–34475. [CrossRef]

22. Filippelli, L.; de Santo, M.P.; Gentile, L.; Rossi, C.O. Quantitative evaluation of the restructuring effect of a warm mix additive on bitumen recycling production. *Road Mater. Pavement Des.* **2015**, *16*, 741–749. [CrossRef]
23. Carr, H.Y.; Purcell, E.M. Effects of diffusion on free precession in nuclear magnetic resonance experiments. *Phys. Rev.* **1954**, *94*, 630–638. [CrossRef]
24. Filippelli, L.; Gentile, L.; Rossi, C.O.; Ranieri, G.A.; Antunes, F. Structural change of bitumen in the recycling process by using rheology and NMR. *Ind. Eng. Chem. Res.* **2012**, *51*, 16346–16353. [CrossRef]
25. Filippelli, L.; Rossi, C.O.; Carini, M.; Chiaravallotti, F.; Gentile, L. Structural characterization of bitumen system by Prony-like method applied to NMR and rheological relaxation data. *Mol. Cryst. Liq. Cryst.* **2013**, *572*, 50–58. [CrossRef]
26. Caputo, P.; Porto, M.; Loise, V.; Teltayev, B.; Rossi, C.O. Analysis of mechanical performance of bitumen modified with waste plastic and rubber (SBR) additives by rheology and PGSE NMR experiments. *Eurasian Chem. J.* **2019**, *21*, 235–239. [CrossRef]
27. Calandra, P.; Nicotera, I.; Rossi, C.O.; Liveri, V.T. Dynamical properties of self-assembled surfactant-based mixtures: Triggering of one-dimensional anomalous diffusion in Bis(2-ethylhexyl)phosphoric acid/n-octylamine systems. *Langmuir* **2013**, *29*, 14848–14854. [CrossRef] [PubMed]


© 2020 by the authors. Licensee MDPI, Basel, Switzerland. This article is an open access article distributed under the terms and conditions of the Creative Commons Attribution (CC BY) license (http://creativecommons.org/licenses/by/4.0/).

Advances in Colloid and Interface Science 285 (2020) 102283

Contents lists available at ScienceDirect

Advances in Colloid and Interface Science

journal homepage: www.elsevier.com/locate/cis

Historical Perspective

# Bitumen and asphalt concrete modified by nanometer-sized particles: Basic concepts, the state of the art and future perspectives of the nanoscale approach

Paolino Caputo [a], Michele Porto [a], Ruggero Angelico [b], Valeria Loise [a,*], Pietro Calandra [c,*], Cesare Oliviero Rossi [a]

[a] Department of Chemistry and Chemical Technologies, University of Calabria, 87036 Arcavacata di Rende, CS, Italy
[b] Department of Agricultural, Environmental and Food Sciences (DIAAA), University of Molise, Via De Sanctis, 86100 Campobasso, CB, Italy
[c] CNR-ISMN, National Research Council – Institute for the Study of Nanostructured Materials, Via Salaria km 29.300, 00015 Monterotondo, Stazione (RM), Italy

ARTICLE INFO

*Article history:*
5 October 2020
Available online 15 October 2020

*Keywords:*
Bitumen
Nanoparticles
Rheology
Asphalt concrete

ABSTRACT

Asphalt concretes are biphasic systems, with a predominant phase (c.a. 93–96% *w*/w) made by the macro-meter sized inorganic aggregates hold together by small amounts of a viscoelastic binding bitumen (c.a. 5%). Even if the bitumen is in minor amount, it plays an important role dictating all the desired properties: rheological performances, resistance to aging etc. What happens if nanoparticles are used as additive in such materials? They usually confer enhanced resistance under mechanical stress and give sometimes interesting added-values properties so, despite the high costs of their production, nanoparticles are interesting materials which are being monitored for large scales applications. This work introduces the reader to the properties of nanoparticles in an easy to review their use in bitumen and asphalt preparation. Silica, ceramic, clay, other oxides and inorganic nanoparticles are presented and critically discussed in the framework of their use in bitumen and asphalt preparation for various scopes. Organic and functionalized nanoparticles are likewise discussed. Perspectives and cost analysis are also given for a more complete view of the problematic, hoping this could help researchers in their piloted design of material for road pavements with ever-increasing performances.

© 2020 Elsevier B.V. All rights reserved.

**Contents**



* Corresponding authors.
*E-mail addresses:* valeria.loise@unical.it (V. Loise), pietro.calandra@cnr.it (P. Calandra).

https://doi.org/10.1016/j.cis.2020.102283
0001-8686/© 2020 Elsevier B.V. All rights reserved.

## 1. Bitumen and asphalt generalities

Bitumen can be defined as high viscous visco-elastic liquids at ambient temperatures. At high temperatures (typically above its softening temperature, that is above 60 °C), bitumen is a viscous Newtonian liquid characterized by a temperature-dependent viscosity [1]. It is a virtually non-volatile, adhesive, and waterproofing material, derived from crude oil distillation process or present in natural sources, which is completely or nearly completely soluble in toluene [2]. Bitumen physico-chemical characteristics strongly depend on crude oil sources undergoing topping distillation process [3–5]. Bitumen viscoelastic properties allow its use as binder, for roofing, industrial applications and mainly for asphalt concrete production for road paving through the world. For the latter application, bitumen is heated to be properly mixed with the aggregates (whose mixing follows well defined granulometric curves) and, finally, after the compaction process and cooling to ambient temperature, the bitumen will act as the binder of the aggregates. Asphalt concretes are, therefore, biphasic systems, with the predominant phase (c.a. 93–96% *w*/w) made by the macro-meter sized inorganic aggregates (size from microns to millimeters) hold together by small amounts of binding bitumen (c.a. 5%) which constitutes the second phase. See Fig. 1 left panel. Bitumen is in turn a complex mixture of Saturates, Aromatics, Resins and Asphaltenes, whose typical relative fractions are reported in Fig. 1 right panel.

Bitumen has a very complex structure which is usually described in terms of colloidal facets. The dispersed phase is made up of micelles of high polarity and molecular mass made by asphaltenes stacks, behaving as solid and adhesive particles. These colloidal aggregates, are dispersed in the dispersing phase, an oily apolar environment of lower molecular weight known as maltene, granting fluidity [6].The apolar maltene phase, in turn, is composed of saturated paraffins, aromatic oils and resins, as schematically depicted in Fig. 1. The proposed model of bitumen is called colloidal model: the asphaltene, in the form of polar nano-aggregates, are stabilized by resins which behave as the dispersing agents for asphaltene molecules combining them with aromatics and saturates; however asphaltenes have the tendency to self-assemble into hierarchical structures of different length-scales [7] .

The delicate equilibrium among all the interactions among all these components and all these structures produces the conditions for asphaltic flow, which is susceptible to change upon aging [8] or addition of other chemical species.

It must be pointed out that the chemistry of bitumen is the key element to define its physical properties: following the analogy with the micellar model, and borrowing the information known for reversed micelles in water-in-oil microemulsions (polar micelles dispersed in apolar matrix, like in bitumen), the stabilization of the polar domains is of pivotal importance for determining both the structure and the properties of the overall aggregates of organic-based materials [9,10], being the stabilization mechanism (it must be pointed out) quite general, spanning from organic materials to inorganic complexes [11] and even nanoparticles [12].

As a consequence of these strict relationships between intermolecular interactions, aggregates structures and their dynamic properties, the rheology (ductility at a given temperature/frequency) and behaviour of bitumen are dependent not only on its structure, but also on the maltene's glass transition temperature and the effective asphaltene content [1].

When it comes to the bitumen structure, molecules are not uniquely defined, so bitumen is classified according to the molecular weight and polarity of its components. Since there are millions of such constituents within the bitumen, the bitumen chemical analysis is usually performed based on the molecular structure class, not by studying the molecular species individually [13].

We believe in fact that any technique differentiating the types of molecules or fractions within narrower properties would be a more effective form of analysis, although of hard practical use.

A final comment is due to the role of resins, because, being the stabilizing agents actually hold up the overall structure of the system. This peculiar characteristic is given by their amphiphilic properties, i.e. such substances possess both polar and apolar parts within their

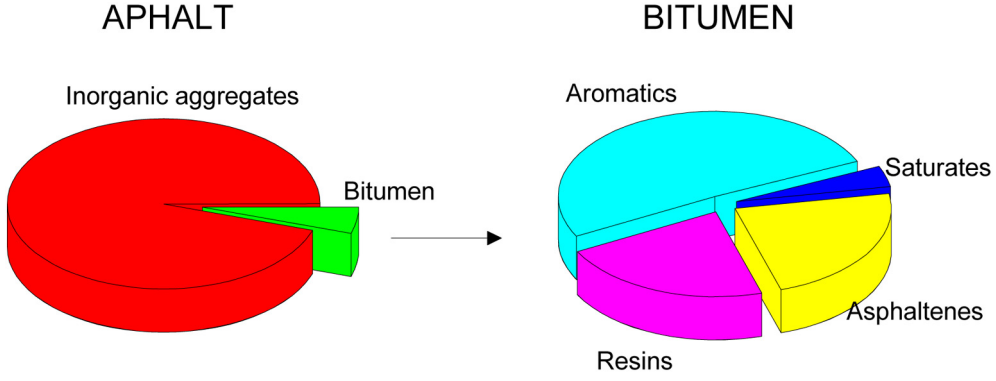


**Fig. 1.** Asphalt and bitumen composition.

molecular architecture. So, at their polar side they can bind the polar clusters of asphaltenes, and at the apolar one, they can bind the maltene, acting as a bridge between polar and apolar domains which, in absence of such molecules, would be unstable towards segregation/separation/sedimentation. Without going deep into details, it is important to point out here their complex role in the overall self-assembly and dynamics.

In fact, it has been recently highlighted that, in addition to polar and apolar interactions, further specific interactions between amphiphiles themselves with consequent peculiar mutual interactions and self-assembly processes [14,15] of extended molecular network, dictating the final overall aggregation pattern [16] and the (usually slowed-down) dynamics [17,18]. The latter, in particular, must be taken into account when considering the dynamical properties (see next paragraph).

## 2. Bitumen properties

In both paving and industrial applications, the bitumen should be resistant to climate and more demanding traffic loads, for which reason rheological properties play a key role in different aspects [1,19,20]. From a functional point of view, the bitumen has to be fluid enough at high temperature (c.a.160 °C) to be pumpable and workable to allow a homogeneous coating of the mineral aggregates upon mixing. Moreover, it has to be stiff enough at working temperatures (according to the local temperatures, c.a.60 °C) to resist rutting. Finally, it must remain soft and elastic enough at low temperatures to resist thermal cracking [1]. All the mentioned requirements are almost opposite, and most of the available neat bitumens would not provide all the needed characteristics together. Moreover, in some applications, the performance of conventional neat bitumens may not be satisfactory considering the required engineering properties because it is brittle in a cold environment and softens readily in a warm environment. This limited performance temperature range is the main drawback of neat bitumen, limiting its use in particular for road paving applications. In addition, as the traffic speed and load has dramatically increased, unplanned overloading has notably shortened the life of asphalt pavements, increasing its costs of maintenance and risks to users. In addition, the bitumen is a material sensitive to aging, and its properties deteriorate over the service life [8]. Bitumen become stiffer and more brittle with time, so the performance of the asphalt mixture is affected. Aging effect is particularly severe in surface layers that are exposed to environmental conditions such as UV radiation, moisture, oxygen, and temperature changes [21]. Thus, the service life of the asphalt concrete is dependent of its aging resistance [22]. Hence in order to enhance the performance properties of neat bitumen, to date, a variety of additives have been introduced and some have been used successfully for many applications. Modifiers and additives that have been used to boost bitumen performance include: polymers, chemical modifiers, extenders, oxidants and antioxidants, hydrocarbons, and anti-stripping additives, adhesion improvers, fibers etc. [5,23].

## 3. Nanomaterials as additives for improving bitumen properties

Recently, researchers are turning to nanotechnology as a novel methodology to improve bitumen properties. Both theoretical and experimental studies on this topic have shown that several appealing characteristics of nanoparticles (size, distribution, constitution, phase, etc.), their small size (1–100 nm) and consequently their large surface area-to-volume ratio, can have significant effects on development of rheological properties of bitumen and asphalt pavement, also when are added in few percent as modifiers to bitumen [24] (Nanomaterial can increase the capacity of the pavement load and decrease cracks due to fatigue during the operation life of the pavement. Thanks to their high efficiency in increasing the long-term performance of asphalt concrete pavement, the use of nanomaterials has therefore gained considerable popularity. However, some limitations encountered in dispersion of nanoparticles and chemical compatibility with bitumen matrix have affected the development of bitumen nanocomposite materials.

What is important here is to point out that nanomaterials can play a significant role in enhancing the rheological characteristic of the existing materials by providing better performances, like increased resistance to traffic and environmental loads. Nanoparticles can mitigate incompatibility between some natural aggregates and bitumen binder, enabling more sustainable and durable pavement solutions [25]. Other application are represented by specific properties conferred by nanoparticles: nanoparticles can have anti-oxidant effects (section 6.2) or reduce the photo-induced aging (see section 6.6.1), they can reduce asphalt flammability (section 6.4) and can also behave like a antistripping agent or promote adhesion between bitumen and acid aggregates like granite (section 6.5.1).

Fig. 2 illustrates, respectively, the evolution of length scales of flexible pavement material in macro-scale to quantum-scales and particle sizes and specific surface area related to concrete materials.

It can be seen that different particle sizes are used for different purposes. Macro-scale particles are used for pavement preparation, as already evidenced in section 1. Smaller particles falling within the range $10^{-5}$–$10^{-2}$ m (micro-scale) are used for conventional concretes giving large air voids [27–29]. Particles with size in the range $10^{-5}$-$10^{-8}$ m are used for high-strength and high performance concrete [30,31]. An important role is exerted by the so-called fillers, i.e. those particles with size <75 μm, thus falling in between the micro- and the meso- scale, which are used in blends with neat bitumens to enhance adhesion and the overall bitumen properties in road pavements [27,32]. It can be expected that the chemical nature of the filler can influence the filler-bitumen interaction giving, in accordance, different types of bonds/strengths. However, it has been concluded by some authors that the adsorption of the bitumen elements is proportional to the surface area of the filler and it is not affected by the chemical composition [33].

As it can be seen from Fig. 3, different kinds of particles with dimensions ranging from few nanometres to centimetres can be used for asphalt concrete production. For example, conventional concrete production generally uses particle size spanning from few microns to centimetres. Normally, a mixture of different kinds of materials like Portland cement aggregates, fly ashes, natural sands and coarse aggregate are employed. In addition to these, the use of aggregates with particle size ranging from tenth of nanometres to centimetres such as metakaolin, finely ground mineral additives and silica fumes (also known as micro silica) is involved in the high strength/high performance concrete production. More recently, the field of nano-engineered concretes has prominence in asphalt concrete production. For the latter in addition to the previous materials, aggregates of nanometres dimension (typically from 1 nm to few microns) like nanosilica particles or precipitated silica, a type of mesoporous material, which has large and controllable surface area (5–100 $m^2/g$), pore size (5–100 nm with agglomerate size between 1 and 40 μm) with high density of silanol groups on the surface, are commonly employed.

This review explores the state-of-the-knowledge and state-of-the-practice regarding the latest updates on bitumen modified by nanomaterials. The information in this study was gathered from a thorough review of the recent studies carried out in the field of nanomaterial modification of bituminous binder in order to give a comprehensive view considering both theoretical considerations and applicative aspects. In the following sections, some historical information about nanotechnology and nanomaterials (section 4) and the properties of nanoparticles (section 5), are briefly reviewed. Then, we will present several types of nanomaterials for specific uses in asphalts and bitumens (section 6), some perspectives on vanguard techniques and side considerations on the costs (section 7) and, finally, the conclusions (section 8).

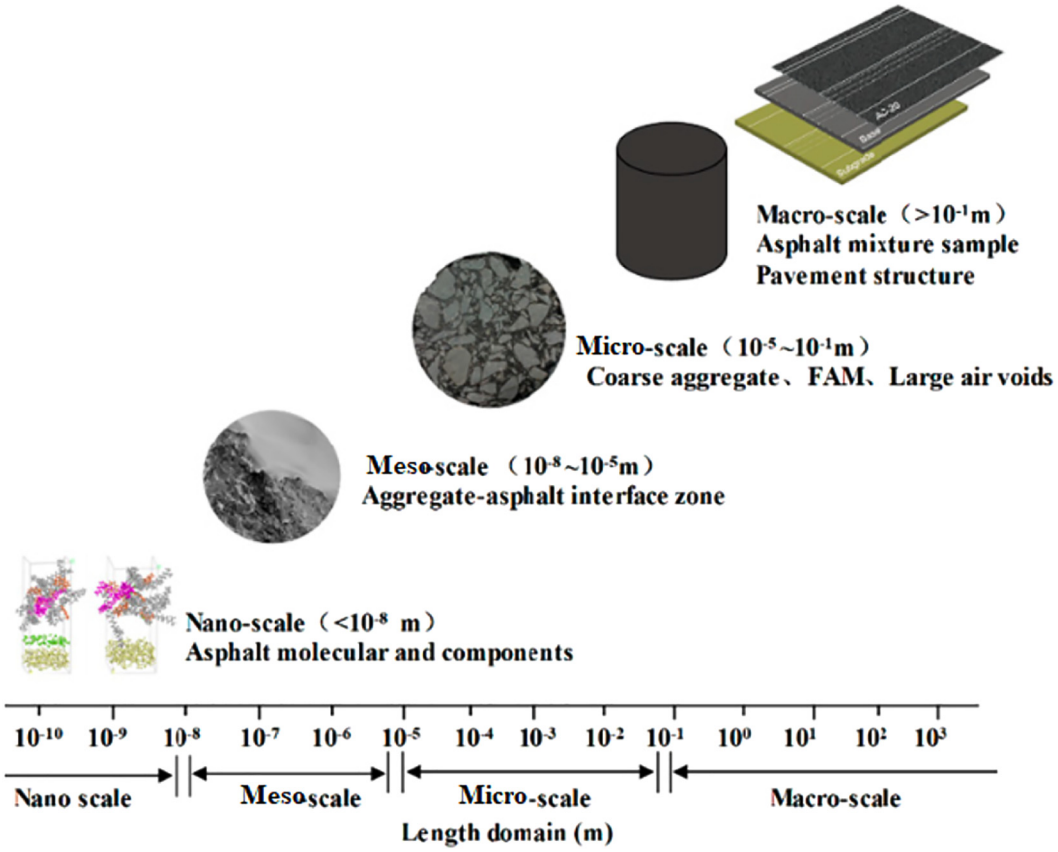


**Fig. 2.** Adapted from [26].

## 4. Nanomaterials

### 4.1. Historical background

*Nano- (from the Ancient Greek νάνος, nanos, "dwarf")* is unit prefix name, represented by the letter *n* and means "one billionth". The S.I. unit *nm* corresponds therefore to a one billionth of meter, i.e. 1 $nm = 10^{-9}m$. This length-scale seeded all the world of nanotechnology, a concept first discussed in 1959 by physicist Richard Feynman in his talk *There's Plenty of Room at the Bottom* [34], where he described the possibility of synthesis via direct manipulation of atoms. For that time this concept was probably pioneering, since the technologies going beyond controlling materials and engineering on the micrometer scale were discussed in 1974 by Norio Taniguchi who also used (for the first time) the term nanotechnology [35]. Few years later, in 1981, Drexler [36] pointed out a new approach which is more related to the meaning of today applications. It corresponds to the atom-by-atom manipulative, "hardtech" processing methodology [37–45]. Nowadays, nanotechnology can be defined as the science and engineering involved in the design, synthesis, characterization and application of materials and

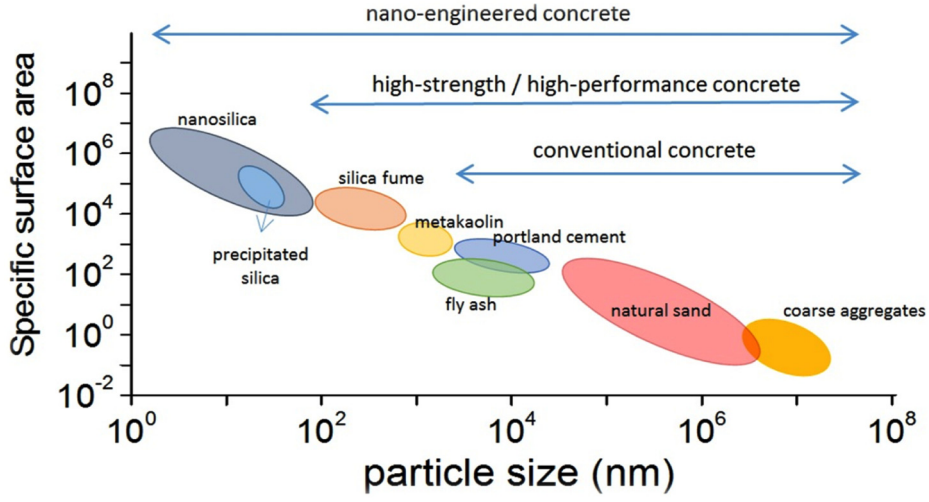


**Fig. 3.** Some kinds of differently-sized particles used for asphalt concrete production (image taken from ref. 76).

devices which smallest functional organisation in at least one dimension is on the nanometer scale. The emergence of nanotechnology as a field in the 1980s occurred through convergence of Drexler's theoretical and public work, the invention of the scanning tunnelling microscope by IBM Zurich Research Laboratory which provided unprecedented visualization of individual atoms and bonds and was successfully used to manipulate individual atoms, and the synthesis of Fullerene ($C_{60}$) by Harry Kroto et al. [46]. The term nanomaterial can be referred to a wide variety of different materials (e.g. nanoparticles, nanorods, nanotubes, nanowires, nanoplatelets, nanoporous, nanofibers and so on) that have their dimension ranging in the scale of 1–100 nm.

In this realm, many different aspects are included: Malsch for instance already in1999 [47] reported the results of a survey in which 22 experts working in different research areas were asked to indicate what they saw as nanotechnology. It turned out that there was no 100% consensus and many different fields were considered as part of nanotechnology. In particular, nano- and quantum electronics, nanostructured materials and scanning probe microscopy were the most cited fields, being quoted by more than 17 researchers. Molecular materials for electronics and molecular nanotechnology were also considered as part of nanotechnology for 16 of the 22 experts: interestingly this field was taken into account by most workers in inorganic materials and excluded by those working in organic ones. However, also computer modelling, cluster and mesoscopic science and technology and supramolecular chemistry were taken into account. Since there are clear differences among all these disciplines, it was evident already in that pioneering work that it was better to think of nanotechnology not as a unique field but just as a complex structure of interconnected research areas. It followed that synergic co-operation among researchers with different skills was to be considered pivotal making nanosciences definitely multidisciplinary.

We want to stress here the pivotal aspect of multidisciplinarity: interdisciplinary works are actually so important that already in 2001 Correia [48] pointed out the important actions taken by the European Commission (IST programme) who funded the PHANTOMS network. That network, noticeable for that time, involved 38 partners from 12 European countries. Members come from governments, industries and universities with the objective to stimulate nanoelectronics research for developments in information technology (IT) and microelectronics. The aim of that network was to make European science and research more competitive to become a reference point on nanotechnology and nanoelectronics although industrial participation (only 13%, with the rest composed by public institutions) was still low.

The European Commission Recommendation itself, gives recently a more concise definition of nanomaterial. It defines a nanomaterial as "*a natural, incidental or manufactured material containing particles, in an unbounded state or as an aggregate or as an agglomerate and where, for 50% or more of the particles in the size distribution, one or more external dimension is in the size range 1-100 nm*" [49].

The advances and refinements of knowledge about manipulation of materials on the nanometer scale in order to obtain characteristics which could not otherwise be achieved growth the interest in nanostructured materials. By pushing the surface to volume ratio (specific surface area) to high value and consequently the spatial confinement to nanoscale, one allows the material to behave differently than its macroscopic counterpart [50]. Some basic observation will show, in the following paragraph, the reasons.

### *4.2. Some techniques usually exploited for nanostructure characterization in bituminous materials*

Generally, the most common techniques to study bitumen modification involve rheology measurements. They directly probe their behaviour under mechanical stress. However, more sophisticated techniques probing the inner structure, which is starting to be correlated to the overall performance, can be used. Recently, nuclear magnetic resonance techniques have proven to be able to give detailed information both from the structural and from the dynamical point of views [51–54]. In addition, X-ray scattering/diffraction are also non-invasive methods which proved to be effective for investigating the structural properties of materials especially in nanomaterials science [55]. The advances obtained by the use of synchrotron-based (multi-scale) X-ray scattering radiations allowed detailed characterizations of a wide range of materials, from polymeric systems [56–61] and organic structures including bio-materials and bio-(macro)molecules [61–65], to zeolites [66–68], alloys, ceramics and composite materials [68,69]. Applications to bitumens and asphalts cannot be an exception, as it has been already discussed in some recent papers [70,71]. Due to the complexity of nanoparticles-containing bitumens and asphalts, it is clear that different techniques can probe different things, giving therefore different information, so, as the reader may surely agree, the synergistic use of different techniques can give a better comprehension of the complex physico-chemistry involved in these materials [72].

Besides such expensive techniques, a cheap and easy way to observe the presence of certain materials by probing the typical frequencies of their atomic vibrations, is FT-IR This can be used for recognizing the presence of both inorganic and organic materials. Frequency shifts (usually red shifts) can also be used to highlight eventual interactions with other species (for example when an organic molecule bind a nanoparticle surface, as it will be shown in section 6.7). In this ambit, eventual interactions between the amphiphilic species present in the bitumen and the metal atoms of certain nanoparticles must also be taken into consideration [73]. However, a careful analysis of FT-IR spectra need to be taken into account [74], which must pass, in our opinion, through the analysis of the individual IR ranges where the various functional groups absorb [75], as also shown in ref. [76] where some comments are devoted to bituminous materials.

For having a "vision" of the material, microscopies are the most suitable techniques. A pivotal role is exerted by scanning electron microscopy (SEM) and atomic force microscopy (AFM), although it must be pointed out that they are essentially surface methods and therefore they are not fit for probing the inner part of the material. A useful method to characterize the degree of subdivision of a powder which will be inserted into a bitumen, is the evaluation of its specific surface. This can be done by routine methods like nitrogen adsorption (BET). The specific area is, in our opinion, an important parameter to be measured, since the surface atoms of (nano)particles are those which interact with the matrix: uneven surface can, in principle, offer more interfacial atoms, in comparison with a flat interface, for interactions with the matrix.

More sophisticated methods like nanotomography can simultaneously

1. probe the nanoparticles, as distinct objects different from rest of the (bituminous) material and
2. probe the inner part of the sample, differently from microscopies.

But a dedicated paragraph (section 7.1) will be devoted to the discussions of such technique.

## 5. Reducing the size to nano-scale: nanoparticle peculiarities and their tendency to agglomerate

Indeed, the specific surface area increases as the particle size decreases, becoming significantly large in the nanoscale. For example, in the case of a single spherical particle the surface-to-volume ratio is 3 $mm^{-1}$, $3 \cdot 10^3$ $mm^{-1}$, and $3 \cdot 10^6$ $mm^{-1}$, for the sphere radius of 1 mm, 1 μm, and 1 nm, respectively. Thus, considering the same volume unit, the use of nanoparticles instead of microparticles will allow a much larger available surface area. In reality, when dealing with aggregates made by a relatively small number of atoms, it is not plausible any more the treatment in terms of model sphere, since the individuality of the atoms as discrete entities must be taken into account for.

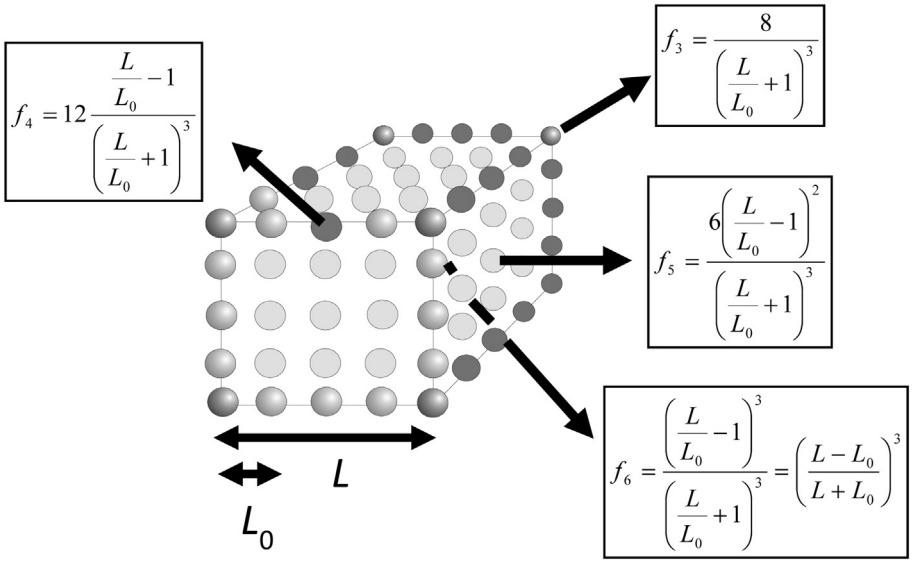


**Fig. 4.** A model of cubically packed spheres to estimate the fraction of species at the flat surfaces ($f_5$), at the edges ($f_4$) and at the corners ($f_3$). The subscript indicates the coordination number. See text for details and discussion.

Referring to a model ideal primitive cubic arrangement of size L composed by atoms at distance size $L_0$ from one another in the vacuum, as that depicted in Fig. 4, some simple geometrical considerations can be done.

It is obvious that in this model bulk atoms have a coordination number (c.n.) of six and surface atoms can be divided into three groups according to their c.n.. So, there are:

- Bulk atoms with c.n. = 6 and zero dangling bonds;
- Atoms at flat surfaces with c.n. = 5 and one dangling bond;
- Atoms at edges with c.n. = 4 and 2 dangling bonds;
- Atoms at corners with c.n. = 3 and 3 dangling bonds.

Being $f_6$, $f_5$, $f_4$ and $f_3$ the fractions of atoms with number of coordination of 6, 5, 4 and 3, respectively, from simple geometrical considerations it follows that their values are those reported in Fig. 4.

The size dependence is shown in Fig. 5. where the fraction of total surface atoms $f_{sur}$

$$f_{sur} = f_5 + f_4 + f_3 \tag{1}$$

together with the single contributes $f_5$, $f_4$, $f_3$ is shown.

It can be seen that the surface atom fraction is negligible for cluster bigger than 100 nm but it increases for smaller clusters. When the particle size approaches to the critical size of few nanometres sudden changes occur: the surface atoms start to be a consistent fraction of the total number of atoms and they are mostly atoms at faces, i.e. with c.n. = 5. When the size is further reduced to few times the atomic

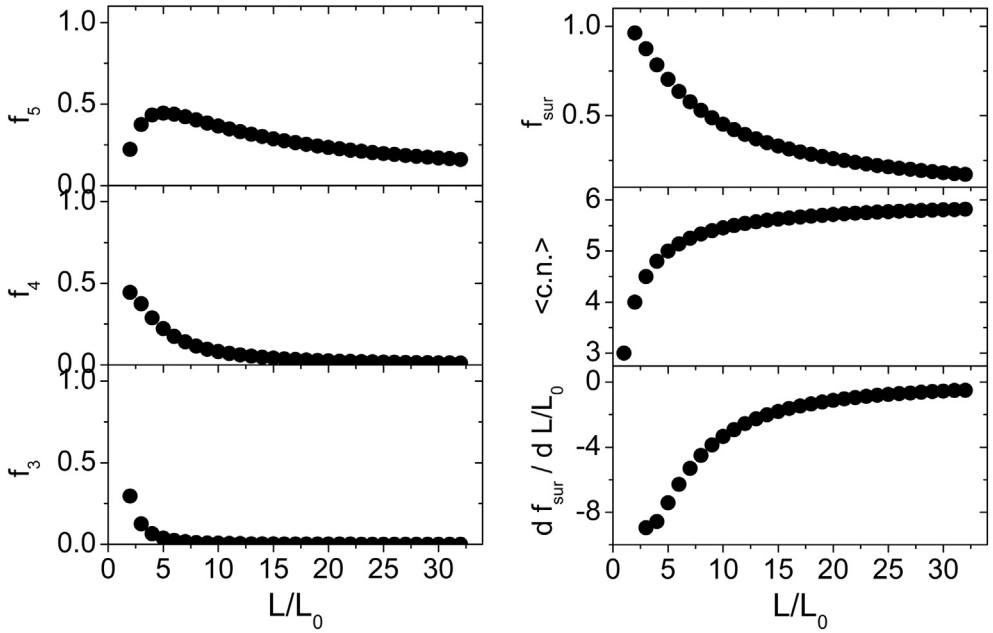


**Fig. 5.** Size dependence of: a, surface-to-volume ratio (S/V); b, fraction of surface atoms ($f_{sur}$); c, mean coordination number (<c.n.>); d, $df_{sur}/d(L/L_0)$ see text for details.

scale, other changes take place, because the number of atoms with c.n. = 5 drops in favour of atoms with lower c.n. Actually smallest nanoparticles are mainly made up of atoms with low c.n. and so it would be expected that they possess exotic properties just because they are made of atoms with lower c.n.. This is clearly shown in Fig. 4c, where the average coordination number ⟨c.n.⟩ worked out as

$$\langle c.n. \rangle = 6f_6 + 5f_5 + 4f_4 + 3f_3 \quad (2)$$

is reported as a function of size.

These argumentations are based on the assumption of perfectly cubic nanoparticles but of course this is not generally true in reality: it is argued that nanoparticle surface is not generally smooth possessing a fractal-like structure. The presence of irregularities makes the surface-to-volume ratio higher but also give nanoparticles more exotic properties. Surface species, and in particular surface defects, can in fact play a different role from that shown so far and, as it will be shown, further modify the nanoparticle structure thus further contributing to exotic and enhanced nanoparticle properties.

It is expected for example that surface species can adsorption of chemical species at the surface, so further interesting considerations can be achieved by thermodynamics.

The free energy (G) of a phase depends, at constant pressure and temperature, on the surface A through the surface tension γ:

$$dG = \gamma dA \quad (3)$$

Now, γ is usually positive, reflecting the fact that the surface atoms are in a high-energy state, so nanoparticles have the natural tendency to reduce this contribution by minimizing the surface-to-volume ratio. Nanoparticles tend, in fact, to grow with no limits and this can take place through several different mechanisms. Detailed discussions on the possible mechanisms of nanoparticle growth can be found in the literature [77,78].

However, what is important to point out here is that the driving force of any growth process is the attempt of surface atoms to form bonds to complete their coordination structure so it can be expected that the more efficient is the saturation of surface dangling bonds by growing, the more powerful is the driving force. The variation of the number of surface atoms with increasing the particles size is then represented by the derivative of the eq. 1, i.e. $df_{sur}/d\left(L/L_0\right)_{sur}$.

This curve is shown in Fig. 5 and it clearly shows that the driving force diminishes very rapidly with size. It is now obvious that a synthetic protocol should inhibit nanoparticle growth thus allowing the size control in the nanosize regime. This can be achieved by:

1) compartmentalization in distinct domains so nanoparticles cannot come into contact to aggregate
2) charging of particles, so charged nanoparticles cannot aggregate owing to the repulsive inter-particle forces
3) adsorption of suitable molecules at the nanoparticle surface. The role of such molecules is twofold: first, they act as surface-active molecules reducing the nanoparticle interfacial energy, and, secondly, they coat the nanoparticle with a protective shell preventing them from all those mechanisms that tend to increase nanoparticle size: ripening (in solutions), aggregation, coalescence.

However, an important factor to be taken into account for is that nanoparticles must diffuse to come into contact for aggregation to occur. So, in the case of bitumens, the high viscosity limits unavoidably at some extent such motions, leaving the problems generally in such stages where the different condition (bitumen homogenization at high temperature, for example) allows nanoparticle diffusion. Another point deserving attention is that the aforementioned actions are needed only when the substance-specific thermodynamic tendency to the growth, i.e. the reduced nanoparticle size, poses the problem. This happens, as shown in Fig. 5, usually for smaller particles, which may not be necessarily used in bitumens applications.

So, the choice of the method for nanoparticle preparation must take into account for the final nanoparticle size, jointly to its inherent drawbacks, and be therefore finalised to the subsequent use of such particles.

This is a crucial point: at what extent a given technological field can bear the costs of reducing the size? Each size regime, as shown in Fig. 5, has specific properties and can give application-specific added-value. So, it is not true that smaller means better. There is a delicate equilibrium among properties, costs and added value to be taken into account.

The case of bitumen and asphalts, is not of course an exception, so a final paragraph reporting consideration in this sense will be finally provided.

## 6. State of the art in the use of nanoparticles in bitumens and asphalts

### 6.1. Nano-$SiO_2$

The most common material used as nanoparticles added to bitumens is certainly silica. In our discussion, therefore, we cannot but considering them as a starting point. Silica is the name usually used to depict silicon dioxide. It is a covalent solid with the chemical formula $(SiO_2)_n$. The silicon atom is located in the centre of a tetrahedron and is covalently linked to four oxygen atoms. Silica exists both in crystalline forms, such as quartz, and in amorphous forms, such as silica glass [79]. Due to its low-cost production, it is used in many areas such as medicine, drug delivery and agriculture. Nevertheless, it is used in particular in the production of cement and concrete, due to its high stability, ability to disperse, filler effect and its pozzolanic reactivity [,80,81]. Silica nanoparticles are often used in the construction of asphalt concrete thanks to its properties: it causes a significant viscosity increase which usually decreases with increasing temperature [82].

Lower viscosity means lower compaction temperature. Besides, the rutting resistance, fatigue cracking and anti-stripping properties are enhanced [83]. Ghasemi et al. [84] have added nano-$SiO_2$ to a bare bitumen to demonstrate enhancement of performances. The bare bitumen properties are listed in Table 1 as well as the code for the test method. Such bitumen was then modified with a mixture of SBS (styrene-butadiene-styrene) at a fixed amount of 5% and nanosilica at five different amounts. The diameter of the nanosilica used for this research was 15 ± 3 nm.

The bitumens physical properties after modification are reported in Table 2: it is possible to note that the softening point increases according to the nanosilica content, while penetration decrease. Some differences have been found if the analysis was conducted at the top or at the bottom of a sample opportunely prepared to test storage stability. The difference between the ring and ball temperatures of the upper and lower part is indicative of the stability and it was found to decrease in presence of nanoparticles. This indicates a clear improvement in storage stability.

The authors also performed mechanical tests on the asphalt concrete. The Marshall stabilities and flows, reported in Table 3, reveal a stability increase due to the presence of nanosilica, in fact the values increase as the nano-$SiO_2$ increases. This result is consistent with the

**Table 1**
Properties of the bitumen studied by Ghasemi et al. [84].

| Physical properties | Test Method | Measured values |
|---|---|---|
| Penetration at 25 °C, 100 g, 5 s (deci-millimetere, d-mm) | ASTM D-5 | 64 |
| Softening point, ring and ball (°C) | ASTM D36 | 48 |
| Ductility at 25 °C at 5 cm/min (cm) | ASTM D-113 | 100+ |
| Flash Point, Cleveland open cup (°C) | ASTM D-92 | 284 |
| Specific gravity at 25 °C (gr/cm$^3$) | ASTM D-70 | 1.021 |
| Loss on heating, wt (%) | ASTM D-6 | 0.06 |

**Table 2**
properties of SBS/nanosilica modified asphalt binders tested by Ghasemi et al. [84].

| Properties | 5%SBS + 0.0%nano | 5%SBS+0.5%nano | 5%SBS+1.0%nano | 5%SBS+1.5%nano | 5%SBS+2.0%nano |
|---|---|---|---|---|---|
| Penetration (d-mm) | 55 | 54 | 51 | 48 | 46 |
| Ductility (cm) | 100+ | 100+ | 100+ | 100+ | 100+ |
| Top ring and ball (°C) | 54.4 | 54.7 | 56.7 | 58.9 | 59.0 |
| Bottom ring and ball (°C) | 51.5 | 53.5 | 55.6 | 58.0 | 58.3 |
| Difference | 2.9 | 1.2 | 1.1 | 0.9 | 0.7 |

**Table 3**
Marshall test results of reference and SBS/nanosilica asphalt mixtures tested by Ghasemi et al. [84].

| Sample | Stability (kN) | Flow (mm) |
|---|---|---|
| Bare bitumen | 6.42 | 3.4 |
| bitumen +5%SBS + 0.0%nano | 7.00 | 3.13 |
| bitumen +5%SBS + 0.5%nano | 8.86 | 3.33 |
| bitumen +5%SBS + 1.0%nano | 10.13 | 2.90 |
| bitumen +5%SBS + 1.5%nano | 11.20 | 3.35 |
| bitumen +5%SBS + 2.0%nano | 11.74 | 2.85 |

research conducted later by Crucho et al. [85]. Ghasemi et al. evaluated that the Marshall stability increase by 83% adding nano-$SiO_2$.

Interestingly, the value of ITS (indirect tensile strength) progressively increases as a function of added silica, from a minimum of 680 kPa for the asphalt concrete made by neat bitumen, to a maximum of 890 kPa for the asphalt concrete made by bitumen with 2% nanoparticle. This behaviour shows that the cohesion and adhesion of the binder is improved with the addition of SBS and nanosilica. On the other hand, the TSR (tensile strength ratio), after one freeze-thaw cycle, had values comprised between 0.7 and 0.91 obtained for the highest content in nanoparticles showing that nanosilica is effective in counteracting moisture damage.

Self-consistently, the indirect tensile stiffness modulus increases as the nano-$SiO_2$ content increases, from 811 MPa for the bare bitumen up to 1830 MPa for the nanoparticle content of 2% whereas the addition of SBS only can cause an increase in stiffness modulus by about 53% compared to the neat sample.

Galooyak et al. [86], three years later, analysed a 60/70 pen binder modified with 2% of Sasobit and variable percentages of nano-$SiO_2$ (from 2 to 6% wt). The nanosilica used was 20–30 nm and the physical properties of the bitumen are listed in Table 4.

The physical properties after modification are reported in Table 5, which shows a self-consistent decrease in penetration and ductility and an increase in softening point with the nanoparticle content increase.

Also, the complex modulus, $G^*$, analysed as a function of frequency through frequency sweep between 0.1 and 700 rad/s, at 10 and 50 °C increases as nanosilica content increases, especially at low frequency. It can be concluded that the modified bitumen has better resistance against rutting at heavy loading condition. Interestingly the authors found that the high temperature (50 °C) enhances nanosilica dispersion, so the difference between the complex modulus with and without nanoparticles is higher than that at low temperature (10 °C).

**Table 4**
Physical properties of bitumen studied by Galooyak et al. [86].

| Physical properties | Measured values |
|---|---|
| Penetration (25 °C, 0.1 mm) | 68 |
| Softening point (°C) | 51 |
| Ductility (25 °C, cm) | +100 |
| Penetration Index (PI) | −0.20 |

**Table 5**
Physical properties of modified bitumen studied by Galooyak et al. [86].

| Test | Base Binder | Nano-silica content with 2% Sasobit | | | |
|---|---|---|---|---|---|
| | | 0% wt | 2% wt | 4% wt | 6% wt |
| Penetration (25 °C, 0.1 mm) | 68 | 62 | 60 | 56 | 54 |
| Softening point (°C) | 51 | 54 | 55 | 57 | 58 |
| Ductility (25 °C, cm) | +100 | 92 | 88 | 83 | 81 |

We would like to point out that the same authors correctly pointed out that attention must be paid to the elastic and viscous behaviour of bitumen, because this affects service temperatures. For this reason, they also analysed the phase angle, pointing out that an ideal bitumen should show a plateau, in the complex module and in the phase angle, with varying frequency, in accordance with Oliviero Rossi et al. who, two years later, have described the latter behaviour as a sort of buffer effect [87].

It must be pointed out that Galooyak et al. carried out also tests on WMA (Warm Mix Asphalt). From these tests we report the essential clues. The Authors estimating the asphalt concrete response to traffic loading, showed that the resilient modulus (the ratio between applied stress and recoverable part of strain), increases as a function of the nanosilica content. Moreover, there is a direct relationship between the nanosilica content and the number of loading cycles (25 ms loading and 125 ms resting time) required for cracking (see Fig. 6). The fatigue life of the WMA is higher for samples containing nanoparticles than for the unmodified sample. Moreover, the modified 6% sample has the lowest cracking depth. According to the authors, nanosilica reduces air voids, which, in turn, increases the fatigue life. The mechanism linking nanosilica presence to air void reduction, can be, in our opinion, traced back to the tendency of smaller particles (nanosilica, size 20–30 nm) to fill bigger cavities (air voids, typically μm-mm size) [29].

The dispersion of nanoparticles within the bitumen matrix can be probed by microscopy. In the study carried out by Taherkhani and Afroozi [88] in 2016, the dispersion of the nanoparticles in the binder was analysed through Scanning Electron Microscopy (SEM). The binder used had a penetration grade 60/70, and the size of the nanosilica was 11–13 nm. From their SEM images it is possible to observe how some nanoparticles are separated in the mass of the binder while others are aggregated in small groups. However, this implies a strong tendency to form a network of aggregates responsible for the mechanical properties of the modified binder.

In another research conducted four years later, Zghair et al. [89] analysed the physical properties of 60/70 penetration grade bitumen modified with various percentages of nanosilica (size between 11 and 12 nm).

Two different types of samples modified with nanosilica were prepared by varying the mixing time between binder/nanoparticles (30 or 60 min). The clues are synthetically reported in Fig. 7: the penetration value and the ductility decrease with the amount of nanosilica. The reduced penetration value is due to the higher stiffness of the modified binder. According to the Authors, the decrease in penetration is a consequence of the adsorption, by nanosilica, of the lighter maltenic fractions. The subtraction, in the maltene phase, of lighter components, causes an

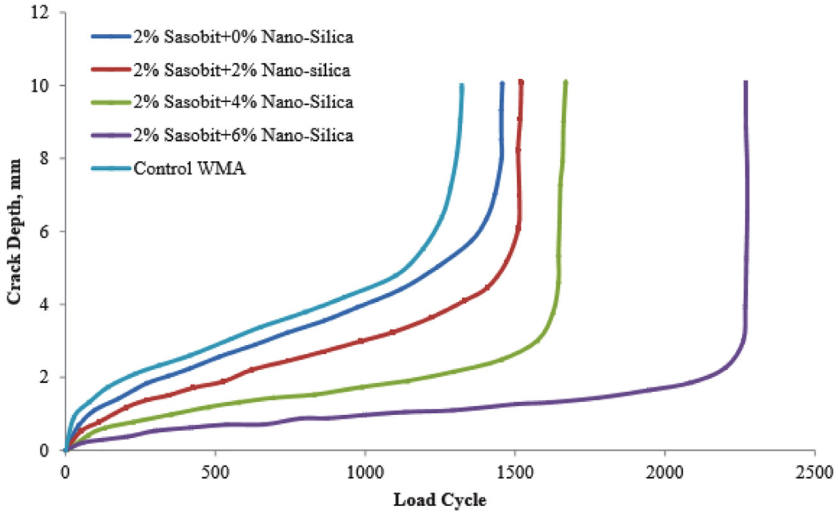


**Fig. 6.** Crack depth vs number of load cycles for reference and modified asphalt mixture analysed by Galooyak et al. [86].

increase in asphaltene concentration and, consequently, a stiffness increase. The ductility decrease has been rationalized in terms of increase in the silica agglomeration. On the other hand, the softening temperature and rotational viscosity increase with the nanosilica content. The softening temperature increase is due to the absorption of asphalt light volatiles by the nanoparticles; consequently, the resin is transformed in asphaltene. The rotation viscosity test, useful for determining the workability of the material at high temperatures, highlights the rotation viscosity increase, in accordance to the increase in stiffness, because of the absorption and diffusion of the nanosilica inside the binder.

As regards the mixing times, it is evident that with increasing times the properties of the binder improve. Certainly, longer times can guarantee a better dispersion but, as the authors correctly point out, this would increase the energy consumption and consequently the costs.

In contrast, surprisingly, the penetration index (PI) seemed to be not correlated with the nanosilica content. The author point out how the penetration index is an estimate of the thermal susceptibility of a bitumen, textually writing: "*The lower the PI value, the higher the bitumen temperature susceptibility. For example, bitumen with a PI below −2 is highly temperature susceptible, usually exhibit brittleness at low temperatures, and are very prone to transverse cracking in cold climates*", although it can be controversial if the proper parameter to be considered is penetration index or simply penetration. However, bitumens that exhibit high PI values are called soft and are used mainly in areas with cold climate; on the contrary bitumen that exhibit low PI values are called hard and are used mainly in areas with hot climate [90]. In any case, Zghair et al. comment that the addition of nanosilica has a negative effect on temperature sensitivity of binder. However, we have noticed that, in both mixing times, nanoparticles at the amount of 4% cause a general improvement compared to the neat bitumen. In our opinion, therefore, it would be interesting to investigate this sample further, probably also by exploring slightly different concentrations within the range 2–6%

### 6.2. Comparison between nanosilica and other inorganic nanoparticles

In this paragraph we report the studies comparing the results coming from the use of nanosilica and from the use of other inorganic nanoparticles. Such kind of works is very useful in our opinion, since it opens the way to explore the chemical features of the nanoparticles, besides the bare morphological (basically the size) ones. Such works are, also, quite recent. For example, Sadeghnejhad et al. [91] evaluate physical and rheological properties of modified bitumen with nanosilica and nanotitanium. Table 6 shows bitumen and nanoparticles characteristics, respectively.

It must be noticed that it is quite peculiar that the smaller $TiO_2$ particles (size 30 nm) as compared to $SiO_2$ (size 80 nm) can give markedly lower surface-to-volume ratio (60 $m^2/g$ for $TiO_2$, as compared to 160 $m^2/g$ for $SiO_2$). This is quite in opposition to the general increase in specific area with the degree of subdivision of a given material. However, the authors show that adding 1.2% of Nano Silica gives the most intense effect in decreasing the penetration grade and increasing the softening point. However, 0.9% of nanotitanium oxide into bitumen gives an interesting effect, the highest effect possible that can be given by nanotitanium oxide in these conditions. The trends are reported in Fig. 8.

The improved penetration is an indication of harder bitumen and possibly suggests increase in the strength of the asphalt mixtures against rutting. On the other hand, the bitumen hardness can cause more fragility and there is more possibility of the fatigue phenomenon to be overcome in the high number of loadings. However, it should be noted that the degree of hardness improvement was not that high to make the bitumen more fragile. Therefore, the increased hardness can be considered as a positive characteristic for the bitumen. Also the observed 16% increase in the softening point with addition of nano $SiO_2$ can decrease the bitumen specification due to the temperature changes, because the sensitivity of the modified bitumen to the temperature changes is declined.

In this study, the complex modulus, $G^*$, was obtained for the unmodified and modified bitumens at the different temperatures. The data show, self-consistently with the previously cited works, that addition of different percentages of nano $SiO_2$ and nano $TiO_2$, causes $G^*$ increase, an effect due to the improved bitumen elastic and viscoelastic behaviour at different temperatures with addition of nanomaterial different percentages. In this manuscript, however, the authors furnish an interesting explanation. In fact, the addition of nano $SiO_2$ and nano $TiO_2$ particles (with high surface to volume ratio) to the bitumen strengthens the bonds between bitumen particles and create an appropriate cover. The cover can prevent the viscous nature of bitumen at high temperatures and delay the withdrawal from the elastic behaviour to the viscous area. According to the results, the increasing amount of $G^*$ in all the nano $SiO_2$ percentages used by Sadeghnejhad et al. is maintained and shows that the compatibility between nano $SiO_2$ particles and bitumen with the increased percentages has been still maintained and its addition would improve the bitumen rheology.

This is not true for nano $TiO_2$ added in amount of 1.2% which causes a decrease in $G^*$. This is an exception in the general trend already seen for the penetration grade and softening point, justified by the Authors assuming that the compatibility between nano $TiO_2$ particles and bitumen decreases as the concentration of nano $TiO_2$ increases over a certain

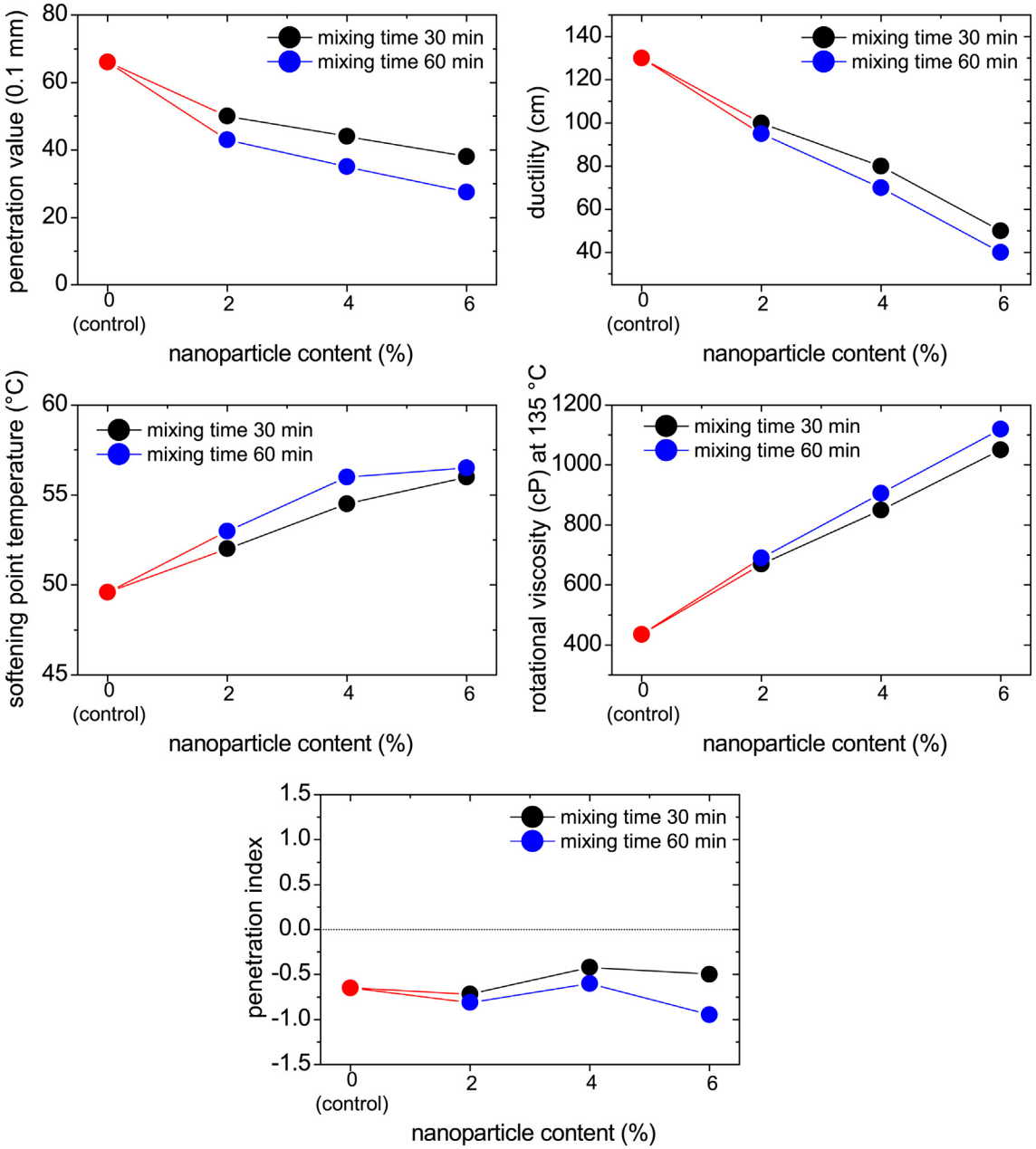


**Fig. 7.** Penetration value, ductility, softening point, rotational viscosity and penetration index of neat (control, red points) and modified asphalt after 30 min (black points) and 60 min (blue points) mixing time. Data taken from Zghair et al. [89].

**Table 6**
Physical properties of bitumen and nanoparticles studied by Sadeghnejhad et al. [91] .

| Test | Standard | Values |
|---|---|---|
| Penetration (100 g, 5 s, 25 °C), 0.1 mm | ASTM D5-73 | 68 |
| Ductility (25 °C, 5 cm/min), cm | ASTM D113-79 | 112 |
| Kinematic Viscosity at 135 °C, C.st | ASTM D-2170 | 355 |
| Kinematic Viscosity at 150 °C, C.st | ASTM D-2170 | 205 |
| Solubility in trichloroethylene, % | ASTM D2042-76 | 99.5 |
| Softening point, °C | ASTM D36-76 | 51 |
| Flash point, °C | ASTM D92-78 | 250 |
| Loss of heating, % | ASTM D1754-78 | 0.2 |
| Nanoparticles | $SiO_2$ | $TiO_2$ |
| Purity % | 99.9 | 99.9 |
| Surface volume ratio $m^2/g$ | 160 | 60 |
| Diameter nm | 80 | 30 |
| Density $g/cm^3$ | 2.40 | 4.23 |

value changing the nature of bitumen and its rheological behaviour. It must be noticed, in our opinion that the volume fraction of nano-$SiO_2$ is quite different from that of $TiO_2$ due to their different densities (which are reported by the authors themselves, see Table 7). In fact, according to the densities, same weight percentage implies that $TiO_2$ has a volume fraction 2.4/4.23 (which is the $SiO_2$-to-$TiO_2$ density ratio) times that of $SiO_2$, i.e. about a half. The deviation observed by $TiO_2$ at higher contents, could indicate the marked incompatibility with the bitumen claimed by the authors, which can be in our opinion, related to the markedly lower surface-to-volume ratio of these nanoparticles (see Table 7) which could offer fewer surface atoms for stabilizing interactions with bitumen. As a result, it is predicted that among the percentages used, 1.2% for nano $SiO_2$ and 0.9% for nano $TiO_2$ create the best performance.

Another conclusion is the high impact of temperature on the normal and modified bitumen performance. The temperature has great impact

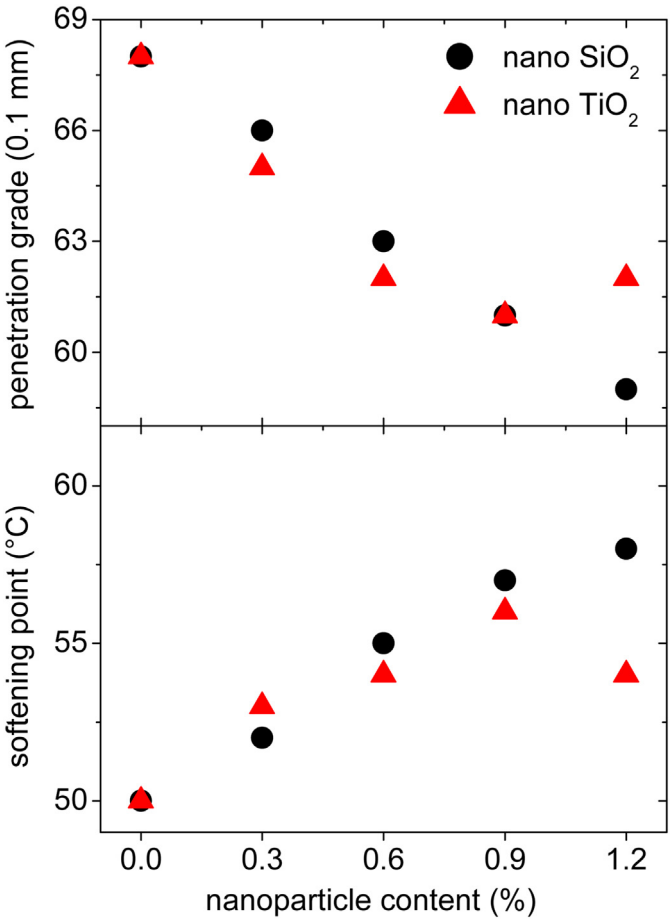


**Fig. 8.** Effect of different percentage of nanoparticles on the penetration grade and softening point.

on the physical and rheological properties of bitumen and many asphalt pavements damages will happen more intensely with the increased temperature. The increased temperature breaks the bond between particles and leads to the separation between the constituent particles. As shown, the addition of nano $SiO_2$ and nano $TiO_2$ particles to bitumen decreases the thermal sensitivity of bitumen and improves the rheological behaviour even in the high temperatures.

Also Nazari et al. [92] explored the potential of $SiO_2$, $TiO_2$ and $CaCO_3$ nanoparticles, investigating the chemical and microstructural properties by X-ray diffraction (XRD) and SEM (Scanning Electron Microscopy). Compared to the studies so far considered, they have carried out a more detailed investigation of the mechanical properties of bitumen modified with nanoparticles. As usual, the properties of neat bitumen and inorganic nanoparticles are summarized in Table 7.

The samples were prepared by mixing the hot bitumen with 2 and 4% by weight of the three different types of nanoparticles. Here again, the differences in densities are clearly shown and it can be also noted that nano-$SiO_2$ has a much higher surface-to-volume ratio with respect to nano-$TiO_2$ and nano- ($CaCO_3$)

XRD analysis identifies a peak at $2\theta = 18°$ attributable to the asphaltenes structures (in accordance to literature studies [93], although the aggregation state of asphaltene molecules is quite complex) [94] and the nature of the dispersed nanoparticles (quite amorphous silica, rutile phase $TiO_2$, quite crystalline calcite $CaCO_3$). By XRD data, the authors claim a correct dispersion of the inorganic nanoparticles inside the bitumen. They also speculate that peak intensity may be related to the amount of nanoparticles present. Unfortunately, however, the study through XRD was conducted only on 4% modified samples, so this remains only a hypothesis.

**Table 7**
Physical properties of base bitumen and nanoparticles studied by Nazari et al. [92].

| TEST | Standard | Unit | Result |
|---|---|---|---|
| Penetration | ASTM D5 | 0.1 mm | 70 |
| Softening Point | ASTM D36 | °C | 50.4 |
| PI | – | – | −0.268 |
| Viscosity@135 °C | ASTM D4402 | cP | 315 |
| Ductility | ASTM D113 | cm | 126 |
| Flash Point | ASTM D92 | °C | 275 |
| Nanoparticles | $SiO_2$ | $TiO_2$ | $CaCO_3$ |
| Specific surface area ($m^2/g$) | 180–600 | 35–60 | 30–60 |
| Average particle size (nm) | 20–30 | 30 | 10–45 |
| Bulk Density (g/ml) | <0.10 | 0.25 | 0.68 |
| True Density ($g/cm^3$) | 2.4 | 4.23 | 2.93 |

SEM investigation confirms good uniformity in the morphological phases for the sample containing $SiO_2$, with the creation of a network, although with some agglomerations in sample modified with calcium carbonate.

In parallel with the structural characterization of the bitumens, Nazari et al. carried out also a study on the mechanical properties of bitumen modified with 2 or 4% of the inorganic nanoparticles in order to evaluate the fatigue performance. It is shown that content of nanoparticles plays an important role on the lifespan of fatigue life in the case of nano-$TiO_2$ and nano-$CaCO_3$. Although, the authors do not comment on this data, from the acquired curves it would seem that the samples containing nano-$SiO_2$ are less affected by the content of nanocomposite, than those containing the other two types of nanoparticles. However, in general, the samples containing silica, at both assays, are those with the greatest fatigue resistance. They hypothesized that the addition of nanosilica could improve the recovery ability of binder. So, by addition of nano-silica, both the mechanical performances and the cracking resistance were improved.

Interestingly, the authors in their study used linear amplitude sweep test, with the VECD (viscoelastic continuum damage) theory. As shown in the data reported in Table 8, the samples modified at 2% have higher maximum stress values than the neat bitumen. In this way they are more resistant to micro cracks nucleation. Moreover, it should be noted that the increase in the concentration of nanoparticles does not lead to any improvement, indeed the maximum stress values decrease. However, the effect of nanoparticles is greater on maximum stress than on failure strain. In fact, the failure strain values drop from 7% to 6% with the passage of the concentration of the nanoparticles from 2% to 4%, except for nano-$SiO_2$, which shows the same failure strain values at both concentrations.

The authors also focused on the effects of RTFOT (Rolling Thin Film Oven Test) and PAV (Pressure Aging Vessel) aging on the samples under examination. The aging procedures were in accordance with AASTHO T240 and R28 for RTFOT and PAV respectively. They observed an increase in the complex modulus in the nanoparticle-containing samples, and the reaching of a constant value of the modulus at high frequencies, indicating a lower influence of the nanoparticles. The greatest effects on the complex module and on the phase angle are visible for the sample modified with nano-$SiO_2$. From the analysis of master curves constructed

**Table 8**
Maximum stress and failure strain values of neat and modified bitumen analysed by Nazari et al. [92].

| Samples | Shear stress (kPa) | Strain (%) |
|---|---|---|
| Neat | 468 | 6 |
| 2% SiO2 | 554 | 7 |
| 4% SiO2 | 509 | 7 |
| 2% CaCO3 | 550 | 7 |
| 4% CaCO3 | 503 | 6 |
| 2% TiO2 | 530 | 7 |
| 4% TiO2 | 524 | 6 |

by the model of Christensen and Anderson, the authors hypothesize a possible antioxidant effect of attributing to nano-$TiO_2$ and nano-$CaCO_3$.

The antioxidant effect of the two inorganic nanoparticles was deepened by FTIR. A quantitative comparison was made by estimating the aging indices, carbonyl index ($I_{C=O}$) and sulfoxide index ($I_{S=O}$) (eq. 4 and 5 respectively)

$$I_{C=O} = {}^{A_{1700}}\Big/_{\sum A} \tag{4}$$

$$I_{S=O} = {}^{A_{1080}}\Big/_{\sum A} \tag{5}$$

Where $A_{1700}$ and $A_{1030}$ indicate the area under the curve centred at the wavelengths 1700 and 1030 $cm^{-1}$, respectively. The latter are precisely the wavelengths of the carbonyl group and the sulfoxide group. Obviously, an increase in the indices is observed as oxidative aging increases. The way of determine the aging index is discussed in [8].

The authors estimated the relationship between the aging indices, at the RTFOT and PAV steps, and the neat bitumen indices, in order to evaluate how much oxidative aging affects the indices and found that the ratio of the indexes decreases considerably in the case of titanium dioxide and calcium carbonate. This behaviour would confirm the antioxidant effect of the two types of nanoparticles.

Also Nejad et all. [95] tested $SiO_2$, $TiO_2$ and $CaCO_3$ nanoparticles as additives to counteract fatigue and low-temperature cracking. The nanoparticles used for this study had the same dimensions as those used for the previously mentioned study (see Table 7); even the bitumen had the same physical characteristics (see Table 7). Both the samples and the neat bitumen were prepared by mixing them for 60 min at 160 °C and at 6000 rpm. Obviously, according to Nazari et al. [92], also in this case the rheological analyses show the lowering of the phase angle of the modified samples with respect to the neat bitumen (Fig. 9), due to an increase in the elastic component. This effect is most pronounced in samples containing 4% of nanoparticles. Nejad and others also found that at low temperatures the phase angle values were higher. Clearly, this trend is due to a lower elasticity of the analysed samples. In order to evaluate the effect of nanoparticles on fatigue properties, authors measured the Superpave fatigue parameter ($G^* \cdot sin\delta$) on a single loading cycle. The parameter was also found to be dependent on the concentration of nanoparticles. As the concentration of nanoparticles increases, the Superpave parameter values increase. Analyses show that the modification disadvantages fatigue cracking resistance. According to the authors, higher stiffness values of the nanoparticles compared to neat bitumen cause an increase in the value of the complex module. Analysing Fig. 9, which reports the phase angle and the fatigue parameter of neat and nano-particle modified asphalt binders, it is observed that the samples modified with silicon dioxide are those with the lowest phase angle and highest Superpave parameter values, although this nanoparticle is not the hardest among those used. In fact, nano-$TiO_2$ is the hardest nanoparticle (Shear Modulus ≈115GPa) among those used, but the large specific surface area and the good dispersion of nano-$SiO_2$ make it the one with the most significant effect on bitumen, albeit negatively.

In addition, Nejad et al. studied the thermal behaviour of samples treated with 4% nanoparticles via Differential Scanning Calorimeter (DSC) in nitrogen inert atmosphere. The transition glass temperatures are reported in table below (Table 9).

It is clear that the addition of nanoparticles causes an increase in the transition glass temperature. In agreement with the observed mechanical behaviours, the authors hypothesize that the increase in the glass transition temperature is indicative of a decrease in the flexibility and therefore in the mobility of the bitumen molecules near the interface of the particles. In fact, the greatest increase occurs in the case of modification with silicon dioxide nanoparticles. This behaviour is justified by the high specific area and the lower molecular weight of the nano-$SiO_2$.

As Crucho et al. [85] report, and as can be easily seen from the studies up to now updated, nanosilica are the most studied materials as asphalt binder modifiers. In fact, these same authors have carried out a study on the effect of nanosilica, of nanoclay and of zero-valent iron on the mechanical performance of asphalt concrete. The binder used for this research was with a penetration grade 35/50, the properties of the neat binder, modified binder, and nanoparticles are listed below (Table 10). It is important to consider that nanosilica is mainly made up of silicon dioxide, $SiO_2$, while nanoclay, $H_2Al_2O_6Si$, is hydrophilic bentonite. The reader can consider the paragraph 6.4, which is dedicated to nanoclays,

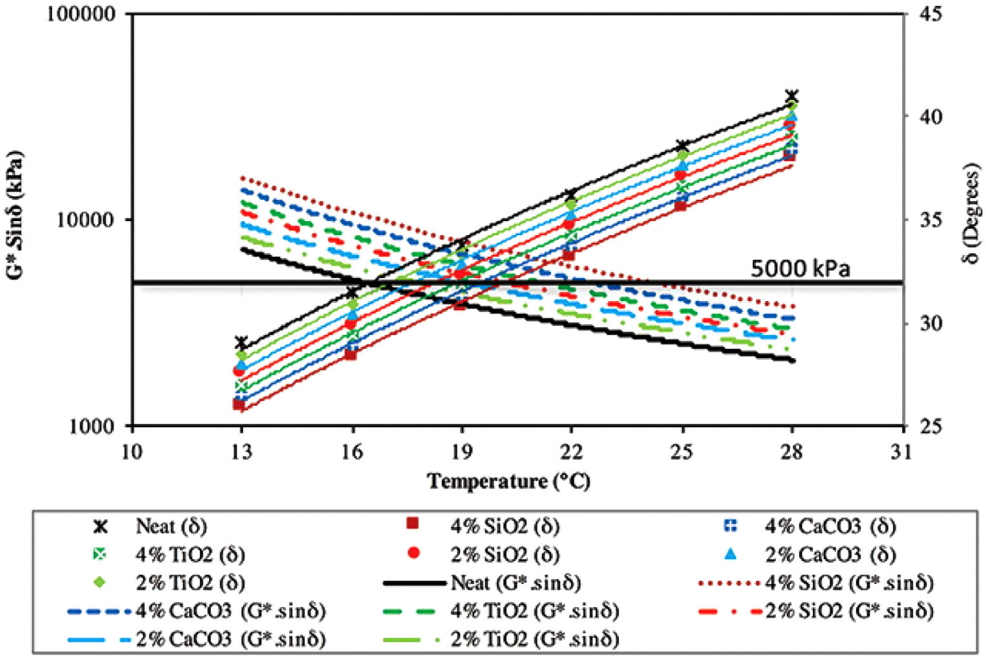


**Fig. 9.** Plot of phase angle and Superpave fatigue parameter as function of temperatures investigated by Nejad et al. [95].

**Table 9**
Transition temperatures for samples analysed by Nejad et al. [95].

| Samples | Temperature (°C) |
|---|---|
| Neat bitumen | −33.61 |
| 4% nano-$SiO_2$ modified binder | −8.94 |
| 4% nano-$TiO_2$ modified binder | −19.88 |
| 4% nano-$CaCO_3$ modified binder | −28.31 |

for further details on this class of substances. Finally, the composition of Zero-valent nano-iron (ZVI) is Fe (65–80%), FeO and $Fe_3O_4$ (20–35%).

Contrary to what has been seen in the studies reported so far, the authors carried out tests on asphalt concrete. The asphalt mixture was made with granitic aggregates and limestone filler. The mixing and compaction temperatures were 164 and 154 °C respectively. In order to compare all the mixtures analysed, the same mixing and compaction temperatures were used. According to Marshall methodology the determined optimum binder content was 4.5%. All the produced mixtures presented similar properties: bulk density of 2.390 Mg/m3, porosity of 3.6% and voids in mineral aggregate (VMA) of 14%.

In this study, the authors accurately described the mixing methodology of the nanoparticles and the binder: to obtain the modified binder, the nanoparticles are added to the binder heated to 160° C, the mixture is stirred at 2000 rpm for 60 min. The choice is justified by the geometry of the head which allows to prevent the vortex effect on the surface of the mixture, preventing the creation of a vortex which, trapping air bubbles, would cause accelerated oxidation of the binder. Subsequently, the modified binder is used for the production of concrete. According to the authors, nanoparticles have limited mobility due to their small size, they assume a terminal settling velocity probably below 0.1 mm per day.

In a preliminary test, the authors evaluated the affinity between bitumen and aggregates. Fig. 10 shows the results of the affinity test (EN12697-11, — bituminous mixtures - test methods for hot mix asphalt - part 11: determination of the affinity between aggregate and bitumen) exploiting the measure of the coverage. There is a clear lack of affinity between the granite aggregates and the neat bitumen (Neat AC), at both observation times. The best results are found in samples modified with ZVI and nanoclay Bent. The results of these two samples after 24 h are very similar to each other, the authors note that this value is almost equivalent to that of the sample with Neat AC after 6 h.

They also carried out stiffness measurements (EN12697-26) on the asphalt mixture at a temperature of 20 and 30 °C, in a frequency range of 1 to 30 Hz. The authors then obtained the master curve, based on the principle of time-temperature superposition, taking 20 °C as the reference temperature. The sample modified with silica shows the higher stiffness while the sample added with ZVI shows the lower stiffness (see Fig. 11). Instead, the sample containing 4% nanoclay (Bent, see Table 10) has higher and lower stiffness value at low frequency and high frequency respectively. According to the authors, this behaviour indicates better high and low temperature susceptibility.

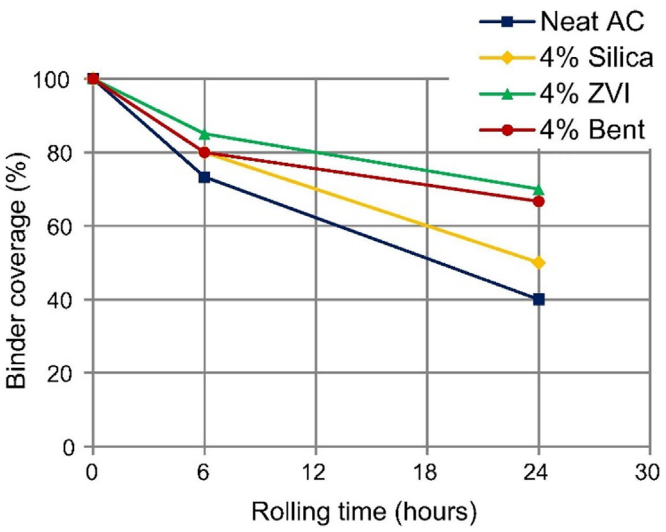


**Fig. 10.** Binder coverage of aggregates analysed by Crucho et al. [85] .

### 6.3. Ceramic nano-powder

A study published in 2017, which in our opinion deserves to be analysed to introduce the use of ceramic nano-powder in bitumens, is that conducted by Hussein et al. [96]. Their goal was to reuse the waste from ceramic materials industries as possible modifiers for bitumen. For this purpose, the authors used a waste ceramic powder from a factory (their chemical composition was analysed through X-ray Fluorescence). At the beginning the powder was crushed and subsequently, after sieving at 75 μm, it was heated for 30 min at 130 °C for water elimination. Lastly, it was ground for 5, 10 and 15 h using a milling bowl to determine the best grinding time. Using a 60/70 bitumen the control sample and the samples modified with 2, 4 and 6% of NCP (nanoceramic powder) were prepared.

Through transmission electron microscopy (TEM) the authors analysed the morphology of the NCPs (NCP some ellipsoidal shapes, average nanocrystallite size around 16 nm) concluding that high surface energy and strong surface tension of ultrafine nanoparticles favour the agglomeration of nanoparticles. This matches our simple geometrical considerations (see paragraph 5).

By X-ray diffraction (XRD) it was also possible to evaluate the influence of ceramic grinding on the size of the nanocrystallite grains and on the reticular structure of the product obtained [72]. The authors used

**Table 10**
Physical properties of neat and modified binder, and analysed samples, studied by Crucho et al. [85].

| Binder | Penetration 25 °C (0.1 mm) | Softening point (°C) | Dynamic viscosity (mPa.s) 135 °C | 160 °C | Density ($Kg/m^3$) |
|---|---|---|---|---|---|
| Neat AC | 41.3 | 55.7 | 665 | 174 | 1034 |
| 4% Silica | 25.0 | 59.3 | 1009 | 242 | 1041 |
| 4% ZVI | 35.7 | 56.2 | 764 | 186 | 1039 |
| 4% Bent | 40.1 | 57.7 | 704 | 189 | 1038 |

| Nanoparticles | Nanosilica | Zero-valent nano-iron (ZVI) | Nanoclay (Bent) |
|---|---|---|---|
| Average particle size (nm) | 70 | 50 | 1–2 (thickness of the silicate layer) |
| Specific surface ($m^2/g$) | 64 | >25 | – |
| Bulk density ($kg/m^3$) | 2200 to 2600 | 2900 to 3000 | 2400 |

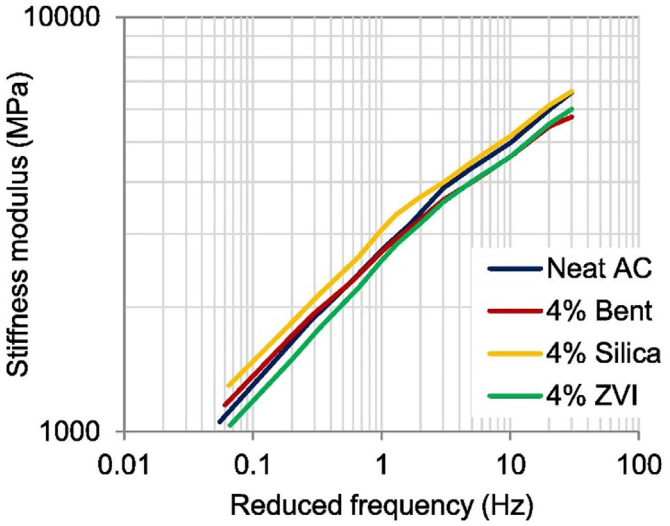


**Fig. 11.** Master curves of the samples analysed by Crucho et al. [85].

the Debye-Scherrer to correlate FWHM (full width at half maximum) with $D$ (nanocristallite size):

$$D = \left(k\lambda/\beta\right)cos\theta;$$

where $k$ is a constant taken as 0.89, λ is the wavelength of the X-ray radiation, $\theta$ is the diffraction angle (also known as Bragg angle of the reflection peak) and $\beta$ is the FWHM. The widening of the peaks is therefore due to a decrease in the nanocrystallites size [97]. The $\beta$ value gives the microstrain ($\varepsilon, \varepsilon = \beta \cdot 4tan\theta$)d it is reported, together with the nanocristallite size D in Fig. 12.

On the basis of XRD data, the authors claim a plausible modification of the asphaltenes sheets by the crystallite nanoparticles.

The authors used also FTIR to probe the chemical bonds and functional groups and highlighted a probable fusion of the aromatic rings with the nanoparticle content which led to the formation of further asphaltenic sheets with formation of strong interactions, contributing to the improvement of the elastic properties of the modified binder.

However, a chemical characterization was completed by a TCLP analysis, carried out according to EPA SW846-1311, USA, to quantify the hazardous elements present in the leachate. The test was carried out for the asphalt mix sample with 6% NCP and all elements have lower values than the limits set.

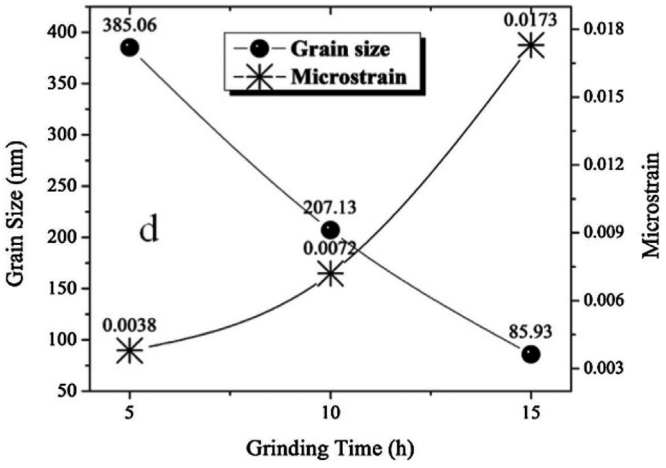


**Fig. 12.** Grinding duration dependence of grain size and microstrain in NCP, analysed by Hussein et al. [96] .

As regards the mechanical properties of the samples under examination, it was clearly seen, again, that the decrease in penetration and the increase in softening temperature is correlated to the increase in the NCP content. It was also observed an improvement in the resistance to rutting from the neat binder to the modified one, obtaining the maximum values with the maximum loaded NPC. The improvement is less marked at high temperatures.

Finally, Atomic Force Microscopy (AFM) analysis is shown in Fig. 13. The images show the three common phases for binder: catana, *peri* and para phase. The bee structures are surrounded by the peri phase, the most scattered one, and by the para phase, the flowing matrix. The addition of NCP on the bitumen has led to a redistribution of the bee structures, which are more numerous and larger. NCP modified bitumen with a high concentration of silica (more than 70%) improves the adhesive and cohesive properties of the binder. In fact, the peri phase, which affects the adhesive/cohesive properties of the bitumen, is more uniform in the treated bitumen than in the neat one. Furthermore, an extensive biphasic microstructure in the bitumen containing NCP is evident, which further contributes to the improvement of the properties of the binder.

### 6.4. Nano clays

A large class of hydrated silicates is clay. Clay-based minerals are interesting materials since they have a sheet-like atomic arrangement. For this reason, hydrated silicates are generally known as phyllosilicates [98] (from the Greek *Phillon*, leaf). The phyllosilicate sheets are made up of repeating units of six-membered rings, in turn made up of the $SiO_4$ tetrahedral unit. Each ring shares with the three first neighbouring ones, three oxygen atoms, one for each of them [99]. Clay has always been one of the most used materials in construction, being a low cost material, in fact it is easily available as residual clay (originated from the surface erosion of rocks or sedimentary rocks) or as transported clay (that is, due to atmospheric agents, removed from the original deposit site and transported far away) [98]. The clay has been widely used in the modification of polymeric matrix, thanks to the high specific surface, and they are capable of forming an intercalation and exfoliation layers. This allows to improve the thermal and mechanical properties, as well as the barrier properties [100]. In this perspective Jahromi's research is worth of note [101]. He and his collaborators conducted some experiments on bitumen samples reinforced with nano-clays particles. Such samples showed increased stiffness and resistance against aging as well as improved elastic properties. In particular, we want to report the study carried out on a 60/70 penetration grade bitumen (AC-10) and two types of common nanoclays: cloisite-15A and nanofil-15. The properties of bitumen and nanoclays are reported in Tables 11 and 12, respectively:

All tests were performed on virgin and unmodified (un-aged), short term aged and long-term aged samples of the modified and unmodified bitumen. Short term and long-term aging were carried out with the Rotating Cylindrical Aging Tester (RCAT) [50]. The authors used an X-ray diffraction (XRD) technique to study the intercalated or exfoliated nanostructure of the nanomaterial modified bitumen by analysing the position, shape, and intensity of basal reflections of XRD patterns of the materials. They observed the disappearance of any coherent XRD in an exfoliated nanocomposite whereas in an intercalated nanocomposite the appearance of a new basal reflection due to the finite layer expansion was observed. Fig. 14 shows X-ray diffraction results on modified bitumen samples.

These figures show that, the addition of nanoclay content, results in a shift upwards of the spectrum. All of the reported curves indicate a complete exfoliation of the nanoclay in the bitumen matrix because of the absence of any main peak.

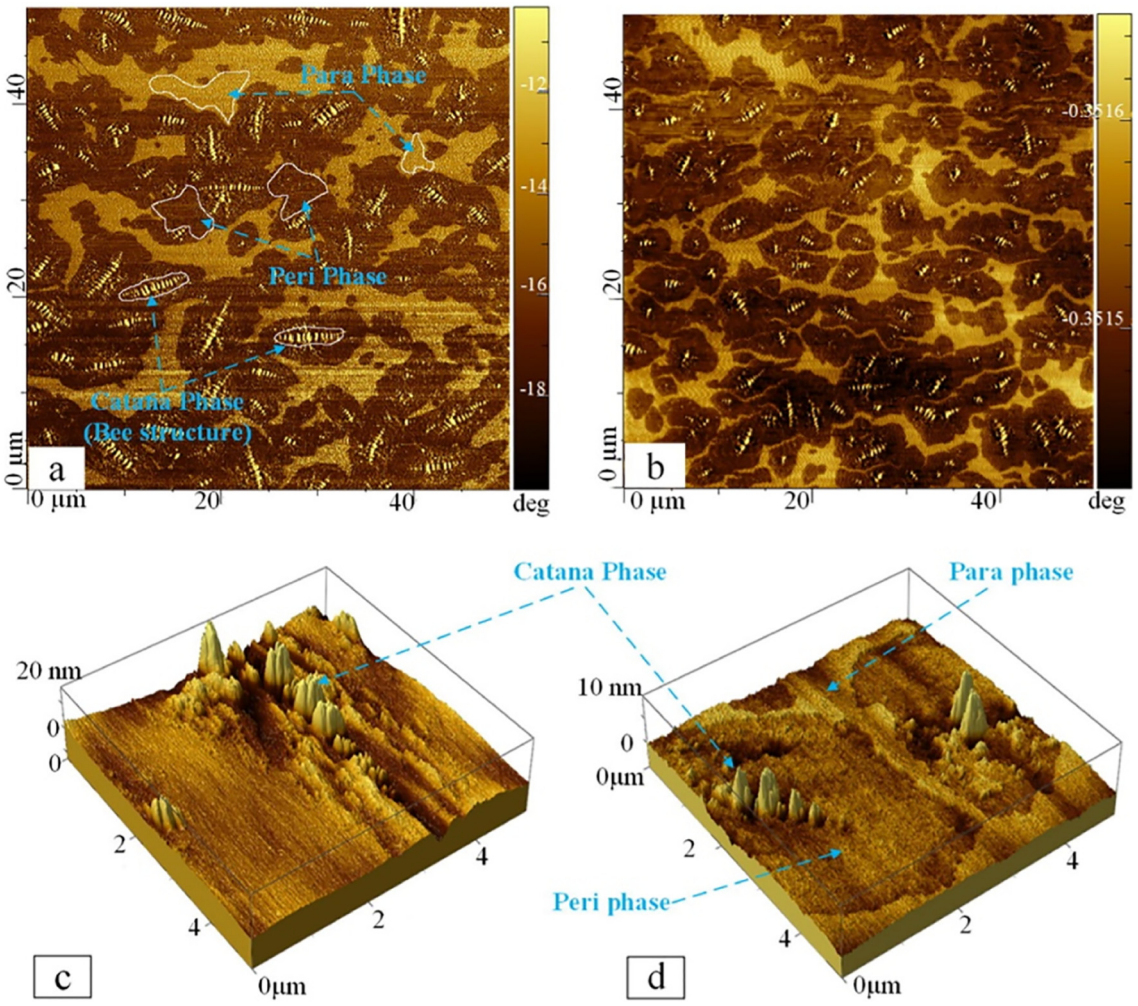


**Fig. 13.** AFM images of unmodified sample (a and c) and of modified sample (b and d) acquired by Hussein et al. [96].

The authors also investigated the rheological properties on two types of modified bitumen i.e. 7% nanofil and 7% cloisite. Rheological measurements were done over a wide range of temperature varying between −15 and 100 °C. In particular, the authors studied the stiffness and phase angle values of the unmodified and nanofil modified bitumen for a wide range of frequencies.

It is found that the nanofil modification increases the stiffness of bitumen to some degree.

Regarding the short- term aging for the unmodified bitumen, the authors found an obvious increase in the stiffness value at low frequencies (increase in the stiffness value to about 40% and 85% at 0 Hz and $10^{-3}$ Hz, respectively). Interestingly, parallel to this, the authors also found that the nanofil-modified bitumen is characterized by a (small) *reduction* of stiffness when subjected to aging in a quite large frequency range ($10^{-3}$-100 Hz).). So, it can be concluded that nanofil modification

**Table 11**
Physical properties of bitumen studied by Jahromi et al. [101].

| Softening point | 54 °C |
|---|---|
| Penetration at 25 °C | 6.3 mm |
| Flash point | 243 °C |
| Penetration index | +0.4 |
| Ductility at 25 °C | >100 cm |
| Fraass braking point | 14 °C |
| Loss of heating | 0.05% |
| Density | 1.035 |
| Maltens | 75% |
| Asphaltenes | 27.2% |

**Table 12**
Properties of nanoparticles studied by Jahromi et al. [101] .

| Treatment/properties | *Cloisite*-15A | Nanofil-15 |
|---|---|---|
| Organic modifier | MT2ETOH (methyl, tallow, bis-2-hydroxyethyl, quaternary ammonium) | Nanodispers layered silicate, long chain hydrocarbon |
| Base | Montmorillonite | Montmorillonite |
| Modifier concentration | 90 meq/100 g clay | 75 meq/100 g clay |
| Moisture | <2% | <3% |
| Weight loss on ignition | 43% | 35% |
| Anion | Chloride | Ammonium chloride |
| Particle size | | |
| 10% less than | 2 µm | 5 µm |
| 50% less than | 6 µm | 15 µm |
| 90% less than | 13 µm | 25 µm |
| Color | Off white | Cream |
| Loose bulk | 230 kg/m$^3$ | 190 |
| Packed bulk | 364 kg/m$^3$ | 480 |
| Density | 1.66 g/cc | 1.88 |
| X-ray results | $d_{001}$ = 31.5 Å | $d_{001}$ = 28 Å |
| Plastic index | 88% | 85% |

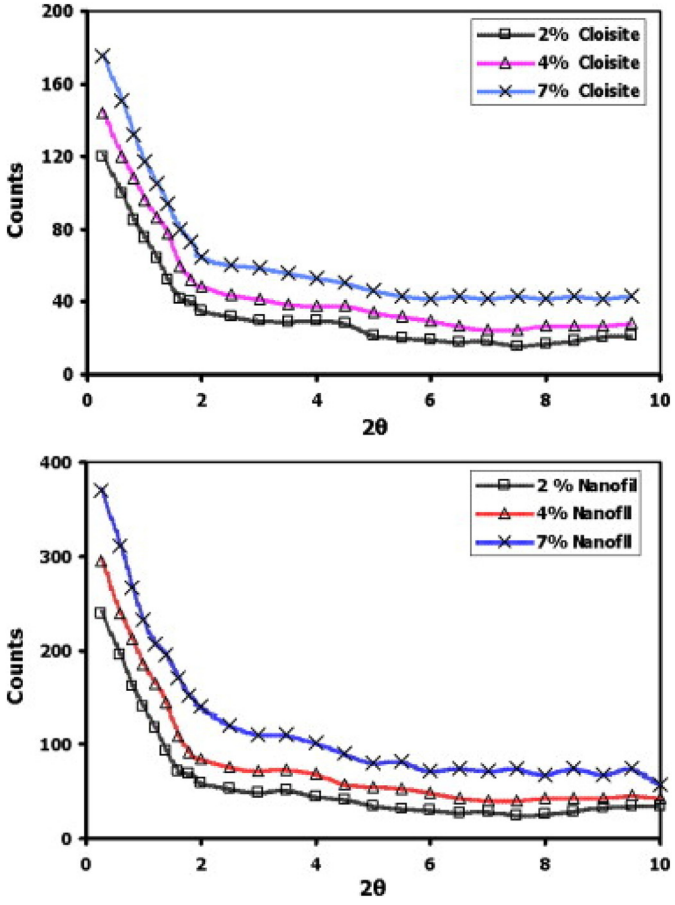


**Fig. 14.** Diffraction pattern of cloisite (top) and nanofil (bottom) modified samples analysed by Jahromi et al. [101].

gives remarkable reduction in aging effect and, even if the reported effects are not evident in the whole (broad) frequency range of the master curves (but only in parts of it), they can be nevertheless considered as worth of note.

Further analysis of the phase angle allowed the authors to conclude that the nanofil modification helps reducing the aging effect of the bitumen to some degree.

Regarding the long-term aging, the stiffness of the unmodified bitumen and modified bitumen increases by about 225% and 110%, respectively, in comparison to their original values. After a study similar to that carried out for short-term aging, the authors concluded that the modification helps in improving resistance to aging of bitumen to some degree.

On the other hand, cloisite modification increases the stiffness of unmodified bitumen and decreases the phase angle of the unmodified bitumen. After short-term aging authors concluded that cloisite modification helped in slightly reducing the aging effect.

As for the long-term aging on unmodified and cloisite-modified bitumen, the stiffness of the unmodified bitumen and the cloisite modified bitumen increases about 320% and 220%, respectively, compared to their original values. This shows lack of improvement in long term aging resistance due to cloisite modification compared to nanofil. Phase angle analysis confirms that the closite modification hardly increases the resistance to aging. Finally, it can be concluded that nanoclay modification increases the stiffness of bitumen and decreases the phase angle compared to unmodified bitumen; hence, this can reduce aging effect on bitumen too.

In a very recent study Sedaghat et al. [102] tested Sasobit as a warm mix asphalt (WMA) additive and nano-clay based on nano-montmorillonite (with particle size 1–2 nm) as a bitumen modifier, to improve resistance to traffic load.

According to the authors, a preliminary modification of the nano-montmorillonite is necessary to obtain an organo-modified (organophilic) nano-montmorillonite (nano-montmorillonite k10). The process ensures that the polymer chains enter into the nanoclay sheets and therefore depends on the basal spacing of the nanoclay.

Then, the authors used a 60/70 (B1) and a 40/50 (B2) penetration grade bitumens, modified with different percentage of Sasobit and nano-montorillonite k10.

X-ray spectra (XRD) have been acquired with the aim of verifying the insertion of the polymer between the nanosheets. In fact, the XRD spectra of the modified bitumen does not show peaks such as those present in the spectrum of the nano-clay powder, ensuring a correct intercalation of the polymer. In order to evaluate the synergistic action of Sasobit and nano-montmorillonite k10, the authors analysed the effect of each additive on the two bitumen separately, comparing the results with those obtained for the neat bitumen. The viscosity of both bitumens decreases with the addition of Sasobit or nano-montmorillonite k10. The decrease in viscosity is greater if Sasobit is added. Instead, the ductility values underwent an increase due to the addition of the nano-montmorillonite k10 and a decrease due to the effect of the Sasobit. In addition, the authors carried out an accurate rheological characterization.

The authors showed that the $G^*/\sin\delta$ parameter (rutting parameter) increases with increasing Sasobit concentration. Samples containing Sasobit and nano-clay also showed an increase in the rutting parameter, although the increase is smaller than samples containing only Sasobit. This demonstrates a positive effect of both Sasobit and nano-montmorillonite k10 on resistance to rutting. Rheological characterization was also carried out on short and long-term aged samples. The addition of Sasobit in aged samples via roll thin film oven test (RTFOT) has led to an increase in rutting resistance. It has been observed that the $G^*/\sin\delta$ parameter increased with the Sasobit concentration, but decreased with the increase in temperature. Once more there is an improvement in the rutting parameter of the samples containing Sasobit and nano-clay, which increase with the concentration of nano-montmorillonite k10.

As for the microscopic interpretation, according to the authors in the samples containing Sasobit, a crystalline network would form at temperatures lower than the melting temperature of Sasobit, which would guarantee improved performance. Interestingly, from the rheological analyses on samples unaged and aged by RTFOT it also emerges that the tests carried out at 76 °C have a lower rutting parameter than that required by the Superpave system (1 kPa for samples with aged and 2.2 kPa for samples aged with RTFOT). In our opinion this data would confirm the microscopic interpretation furnished by the authors, since the minimum melting point temperature of the Sasobit is 75 °C according to Jamshidi et al. [103].

As regards samples aged through pressure aging vessels (PAV), the authors monitored the variation in the fatigue cracking values, $G^* \cdot sin\delta$. The addition of Sasobit to the two PAV aged bitumen samples leads to a lower resistance of the sample to fatigue cracking at all the temperatures tested. The addition of nano-clay instead has an opposite effect. Its addition decreases the values of $G^* \cdot sin\delta$, thus improving the resistance to fatigue cracking. According to the authors this improvement is due to the ability of the nano-montmorillonite k10 to create smaller barriers that change the direction of the crack from direct to zig-zag state.

Wu et al. [104] used nano-clay not only to improve the rheological properties of bitumen, but also to reduce its flammability. For the purpose of this research the authors used bitumen with penetration 84.3 ± 0.1 mm (SB), montmorillonite (MMT) and organically modified montmorillonite (OMMT) with average crystal thickness less than 25 nm. Wu et al. acquired X-ray diffraction (XRD) spectra in order to verify that intercalation has taken place by investigating the structure

of nanoclays. In fact, when the intercalation takes place there is a shift of the peak referable to the nanoclays towards smaller angles, consequently the interlayers distance increases [103,104]. Actually, it is possible to observe an increase in the interlayers distance from MMT to OMMT. Therefore, bitumen appears to be intercalated between OMMT's plans.

As far as rheological characterization is concerned, penetration and softening point of the neat and modified with 3% and 5% of OMMT bitumen were evaluated. Each sample was then subjected to short-term aging (through rotating cylindrical aging tester) and long-term aging (via pressure aging vessel) and the rheological properties were reassessed. Analyses show a substantial decrease in penetration and an increase in the softening point with increasing OMMT concentration. The variation of these parameters suggests a better resistance of the modified samples to permanent deformation. However, despite the authors' hypothesis, it must be pointed out that there is hardly any mixture testing available to directly confirm the improvement of the permanent deformation behaviour.

In our opinion, it is very interesting the possibility of using nanoclays as flame retardancy in bitumen. For this purpose, the authors estimated the limiting oxygen index (LOI). This index was used for the first time in 1966 by Fenimore and Martin [105], it indicates the minimum concentration of oxygen in a mixture of oxygen and nitrogen that is needed to support the flaming combustion of a material. For LOI values lower than 21% the material is considered combustible, for higher values the material can be classified as self-extinguishing [106]. From Fig. 15 it is clear that with increasing OMMT concentration, the tendency to burn decreases. In fact, the neat bitumen has a LOI value of 19.8, while the bitumen modified with 7% of OMMT has a LOI value of 24.4. Demonstrating that adding nanoclay can move from a "fuel" classification to a "self-extinguishing" classification. Moreover, the authors also reported that the treated bitumen produced less smoke than the neat bitumen while burning.

By differential scanning calorimetry (DSC) some interesting information have been found helping in the interpretation of the observed phenomenon: the samples containing OMMT show

a. slower heat release rates
b. peaks located at higher temperatures as the OMMT concentration increases in bitumens.

According to the authors, nanoclays can catalyse char-forming reactions producing charred residues able to intercalating with the silica layers to form a carbonaceous silicate structure, delaying the escape of volatile products and the penetration of oxygen.

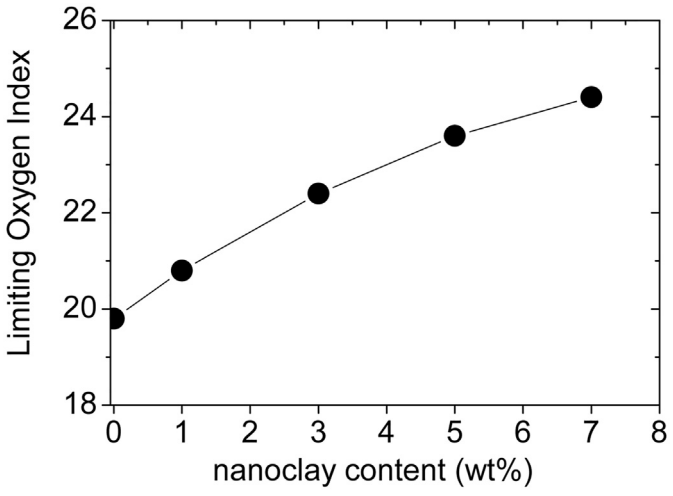


**Fig. 15.** Trend of the Limiting Oxygen Index (LOI) value compared to the OMMT nanoclay content, studied by Wu et al. [104].

### 6.5. Simple metal oxides nanoparticles - miscellaneous

Many studies have made no use of nanosilica as reference nanoparticles. Before going into details of specific materials, an interesting study by Nejad et al. [107] compare different inorganic nanoparticles: These have been used as modifiers on Hot Mix Asphalt (HMA) in order to decrease the rutting potential. The characteristics of nanoparticles are listed in the Table 13. The HMA was prepared mixing a 77 penetration grade bitumen and granite stones.

The samples were prepared with three different contents (2%; 4% and 6%) of $TiO_2$, ZnO, $Al_2O_3$ and $Fe_2O_3$ Then, the modified asphalt binder was used in preparing the asphalt concrete samples, according to Marshal ASTM D6926. These latter samples were analysed to determine their resistance to permanent deformation, at two stress levels of 150 and 300 kPa, through creep measurements. Creep measurements express the time-dependent deformation due to the application of constant stress, thus it can be explained as a rate process [108].

At 150 kPa ZnO nanoparticle had maximum strain modulus, whereas at 300 kPa, the asphalt binder sample modified by nano-$Fe_2O_3$ has the maximum value of the deformation (nano-$Al_2O_3$ had minimum creep). However, $TiO_2$ nanoparticles demonstrated minimum strain during a short period from the loading.

#### 6.5.1. Nano-ZnO

Li et al. [109] exploited the potential of ZnO nanoparticles to increase the resistance of bitumen to ultraviolet aging. This study was carried out both on samples containing the nanoparticles as such, and on samples containing nanoparticles modified on the surface. The physical properties of the analysed bitumen are shown in Table 14:

For their surface-modification the authors used methacryloxy propyl trimethoxy silane (KH-570), as silane coupling agent, to give nano-ZnO (SMN-ZnO). The interested reader is referred to the original paper for details in the chemical modification of the surface. Here, it is enough to point out that the authors took care in treating the pristine bitumen in the same way as the modified bitumen in order to be able to consider it as a true reference. The real modification of the nano-ZnO surface was probed by Fourier Transform Infrared spectra (FTIR) although, in our opinion, this technique can give structural information which can be only indirectly used to provide useful information on the mechanism of action of nanoparticles on bitumen. Indeed, the authors themselves merely comment that the addition of nanoparticles does not generate new absorption peaks.

Certainly, more interesting are the SEM (Scanning Electron Microscope) images, which clearly show a better dispersion of the modified nanoparticles (Fig. 16b as compared to Fig. 16a).

The surface of the SMN-ZnO covered with nano-silica reacts with bitumen, which causes the dimensions of the nanoparticles to decrease. However, to carry out the compatibility test between bitumen and nanoparticles, the authors prepared an aluminium tube with the same procedure used by Zhang et al. [110]. The difference in softening point ($\Delta S$) between the upper and lower part of the aluminium tube increases as long as the concentration of nano-ZnO increases, as reported in Fig. 17. This figure shows that the increase in the concentration of

**Table 13**
Properties of nanoparticles studied by Nejad et al. [107].

| Nano | Purity grade (%) | Specific surface area ($m^2/g$) | Average particle size (nm) |
|---|---|---|---|
| $TiO_2$ | 99 | 200–240 | 10–25 |
| ZnO | 99 | 20–60 | 10–30 |
| $Al_2O_3$ | 99 | >138 | 20 |
| $Fe_2O_3$ | 99 | >60 | 40 |

**Table 14**
Physical characterization of bitumen studied by Li et al. [109].

| Physical properties | Measured values |
|---|---|
| Penetration (25 °C, 0.1 mm) | 72 |
| Softening point (°C) | 48.5 |
| Ductility (15 °C/10 °C, cm) | 140.0/15.9 |
| Viscosity (60 °C, Pa s) | 256 |
| Viscosity (135 °C, Pa s) | 0.52 |

nanoparticles is detrimental to compatibility. However, the same Fig. 15 shows that there is a big difference between samples modified with nano-ZnO than those modified with methacryloxy propyl trimethoxy silane (KH-570).

Interestingly, from the upper and lower part of the tube the authors are also able to determine the content of nano-ZnO.

These results confirm the data obtained from the SEM images, which showed a better dispersion of the modified nanoparticles inside the bitumen.

Li et al. tested both nanoparticles also on the aged bitumen. Aging was carried out for 5 h at 163 °C through TFOT (Thin Film Oven Test), and then the bitumen was placed under a UV light source for 10 days at 60 °C. Fig. 18 show the values of viscosity aging index (VAI index) for the aged bitumen modified with the two nanoparticles. The VAI index was calculated according to:

$$VAI = \left(Agedviscosityvalue - Unagedviscosityvalue / Unagedviscosityvalue\right) x100 \quad (6)$$

Again, it is possible to notice a better shielding of UV radiation by SMN-ZnO modified bitumens, with increasing concentration, due to the presence of nano-silica on the surface. Evidently, the best dispersion of the modified nanoparticles is fundamental to create a "shield" of protection for UV aging.

Hamedi et al. [111] conducted another interesting study using nano-ZnO as antistripping agent to estimate the moisture damage on asphalt. For this purpose, they designed two types of hot mix asphalt (HMA), using the same bitumen (penetration grade 60/70) and two different types of aggregates, namely limestone and granite. The nanoparticles, with an average grain size of about 20 nm, were added to the bitumen at two different concentrations: 2 and 4% by weight with respect to the binder. In order to evaluate the cohesive strength of the bitumen and the bond strength at the bitumen/aggregate interface the authors carried out indirect tensile strength (ITS) measurements. HMA can experience fatigue cracking both due to excessive moisture and due to the load due to heavy traffic [112]. ITS measurements can be used to estimate the potential damage due to moisture, if they are conducted on

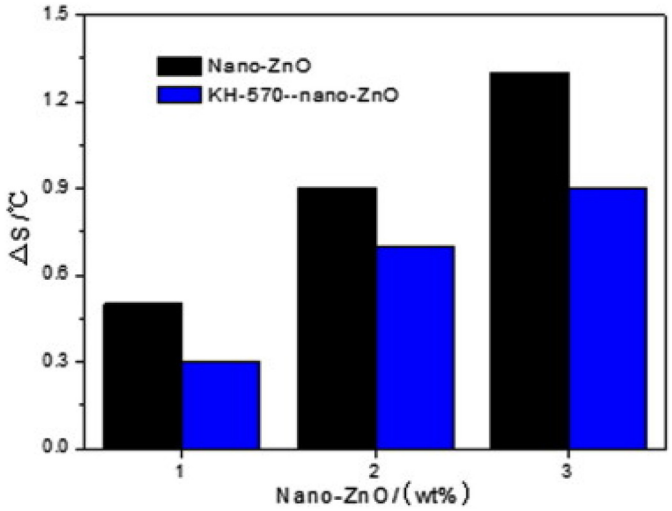


**Fig. 17.** Difference in softening point in modified bitumen treated with unmodified and modified nanoparticles, analysed by Li et al. [109].

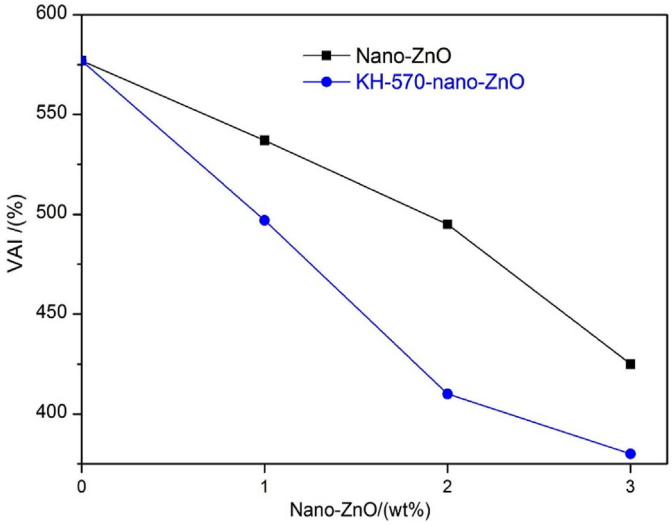


**Fig. 18.** Effect of modified and unmodified nanoparticles content on VAI after UV aging, analysed by Li et al. [109].

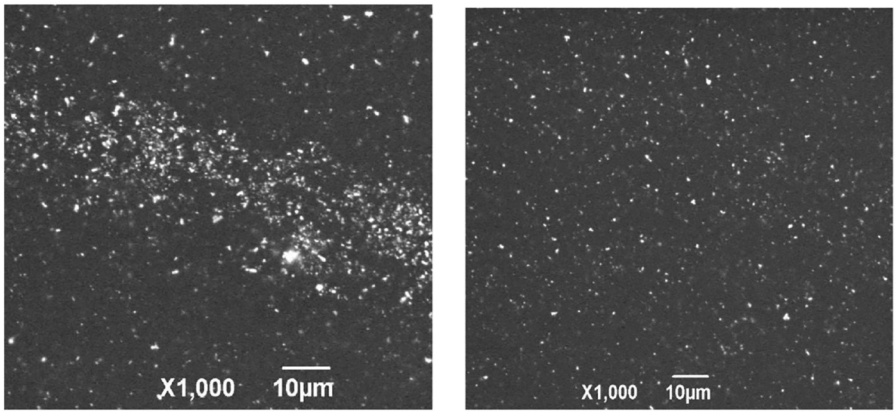


(a) Unmodified nano-ZnO modified asphalt (b) SMN-ZnO modified asphalt(3wt%)

**Fig. 16.** SEM images of bitumen treated with unmodified and modified nanoparticles acquired by Li et al. [109].

both dry and moisture conditioned samples [113]. The ITS measurements were carried out on both dry (unconditioned) and moisture-conditioned samples, showing, obviously, that the wet samples had ITS values lower than the dry ones, both in the case of HMA containing limestone and granite. Nevertheless, conditioned samples modified with nano-ZnO exhibit higher ITS values than the unmodified conditioned sample. Moreover, the values increase with increasing concentration of nanoparticles. Therefore, these data demonstrate that the use of nano-ZnO improves the adhesion between bitumen and aggregates, especially in the case of moisture-conditioned samples.

In addition, the authors evaluated the tensile strength ratio (TSR) defined as

$$TSR = \left({ITS_{cond}}/{ITS_{uncond}}\right) \times 100 \quad (7)$$

Where $ITS_{cond}$ and $ITS_{uncond}$ are the indirect tensile strength ratio for moisture-conditioned and for dry samples, respectively, noting that TSR for HMA-limestone is greater than HMA-granite. Hamedi et al. hypothesized that there could be a weakening in the bond between bitumen and aggregates, considering that limestone is poorer in $SiO_2$ than granite. Moreover, the effect of nano-ZnO was better on granite than on limestone. According to the authors, the nanoparticles decrease the acidity of the bitumen, favouring the adhesion between the bitumen itself and acid aggregates, such as granite. For this reason, Hamedi et al. estimated the surface free energy (SFE) [114] components of the unmodified and nano-ZnO modified bitumen through Wilhelmy Plate method [115] finding useful correlations with the concentration of nano-ZnO, of basic components and on acidic ones. This in our opinion deserves attention since sheds light on how the chemical nature of the bitumens can influence its performances. We believe that such approach should be followed in the rational design of new pavements and waterproof membranes

Du et al. [116] investigated the effect of nano-ZnO on the morphology and ultraviolet (UV) aging on two bitumens. The bitumens had 73 and 92 mm penetration values at 25 °C, and they are labelled B1 and B2 respectively. Regards nano zinc oxide (with particle size 15–25 nm), it has been modified with ϒ-(2,3-epoxypropoxy) propyltrimethoxysilane. Henceforth, we will write nano-ZnO, meaning its modified form. Topographic images (Fig. 19) were acquired thought atomic force microscopy (AFM) in order to evaluate the change in morphology between the unmodified and nano-ZnO modified bitumens. Sample B1 shows the typical bee structures (Fig. 19a), which instead seem to be absent in sample B2 (Fig. 19c). The effect due to the addition of nano-ZnO on B1 is to decrease the dimension of the bee-structure, which are also dispersed more homogeneously (Fig. 19b). On the contrary, in B2 the bee-like structures with small dimensions appear after modification (Fig. 19d). Although the response to the modification with the nano-ZnO is different in samples B1 and B2, the reasons for these behaviours are the same. Therefore, the nanoparticles act as nucleation agents, favouring the heterogeneous nucleation crystallization of asphaltenes.

In order to obtain a UV aging modified and unmodified bitumen, the thin film oven test (TFOT) bitumens were exposed to the action of a 500 W UV lamp inside a draft oven ($T = 60$ °C) for a period of time ranging from 0 to 24 days. Besides an increased viscosity, a good resistance of modified bitumens to the UV aging was detected. For bitumen B1 a greater decrease is observed than for bitumen B2. The authors also provided a rheological characterization thought rheological aging index (RAI). The RAI is defined as:

$$RAI = {G^*_{aged}}/{G^*_{unaged}} \quad (8)$$

Also, in this case bitumen B1 shows a better resistance against UV aging. RAI index highlighted how the B1 is better than B2 even in its unmodified state. This behaviour implies that the effect of nano-ZnO depends on the bitumen nature. Moreover, the B1 modified bitumen shows a greater decrement respect B2 modified bitumen.

*6.5.2. Nano-$Al_2O_3$*

The role of Aluminium Oxide nanoparticles in the rheological properties of bitumen modified with Acrylonitrile Styrene Acrylate (ASA) polymer was investigated by Mubaraki et al. [117]. Chemical and physical characteristics of the base product are highlighted in Table 15:

The authors investigated the effect on the storage stability, viscosity, frequency sweep and multiple stress creep and recovery (MSRC) test of the 60/70 bitumen modified with 3, 5 and 7% of each modifier. The nano-$Al_2O_3$ used for this research has a size of 13 nm, while the ASA has a size of 2 nm. The viscosity measurements carried out at 135 and 165 °C have shown an increase in the values as the concentration of modifier increases, regardless of its nature. Worth of note is that the viscosity values of the samples containing the inorganic nanoparticles are higher than those of the samples containing ASA, with the same concentration.

The authors also studied the storage stability of the base bitumen, ASA polymer and $Al_2O_3$ nanoparticles modified bitumen. Storage stability is a fundamental parameter that estimates how stable a bitumen is during the storage period, i.e. it does not give rise to phenomena such as phase separation. Often the modified bitumen is stored in special tank and subjected to continuous stirring. Thus, an improvement in storage stability as well as ensuring a more uniform product ensures a reduction in costs for the bitumen industry [118]. For this test they poured the samples in an aluminium tube with a height of 16 cm and diameter of 3 cm. Then, the tubes underwent the same treatment described by Zhang et al. [110]. This analysis revealed a general increase in softening point temperatures in the upper and lower samples of the tube. This demonstrates a gradual hardening of the modified samples with respect to the basic bitumen. In fact, the maximum softening point difference between the basic bitumen and the bitumen modified with 7% ASA is 12 °C. This also demonstrates a phase segregation between the base bitumen and the ASA, when this is added at high concentrations. This latter behaviour is not present in samples modified with nano-Al2O3. In conclusion, samples containing inorganic nanoparticles have greater storage stability.

Finally, the results of rheological tests (reported in Fig. 20) pointed out that base bitumen had the lowest $G^*$ and $G^*/\sin\delta$ compared with modified bitumen and also that the modified bitumen with 5% of Nano Aluminium Oxide had the best functionality of resistance against rutting among all modified samples.

It can be concluded that the use of Aluminium Oxide nanoparticles generally displayed better results compared to using ASA polymer.

Ali et al. [119] conducted, in our opinion, a very accurate study on the effects of $Al_2O_3$ nanoparticles on bitumen. The properties of the binder and of the nanoparticles are listed in Table 16. The base binder has been added with 3, 5 or 7% nano-$Al_2O_3$ and it has been melted for 90 min at 5000 rpm.

After that, the physical properties of the sample were re-evaluated. The Penetration index (PI) is a useful property for determining the temperature susceptibility of the binder. It is defined as:

$$PI = {1952 - 500\log(pen) - 20\ softeningpoint}/{50\log(pen) - softeningpoint - 12} \quad (9,)$$

where *pen* is the values of penetration calculated at 25 °C and reported in mm (see the original work for details);

Table 17 reports the derived data. According to the Table, penetration decreases and softening point increases when the nanoparticles are added to bitumen. Also, the PI index is influenced. In fact, higher PI values are found for modified samples; this behaviour is due to an increase in stiffness indicating an improvement in thermal susceptibility. It is important to note that the sample containing 7% $Al_2O_3$, has a different trend compared to the others (higher penetration value, lower

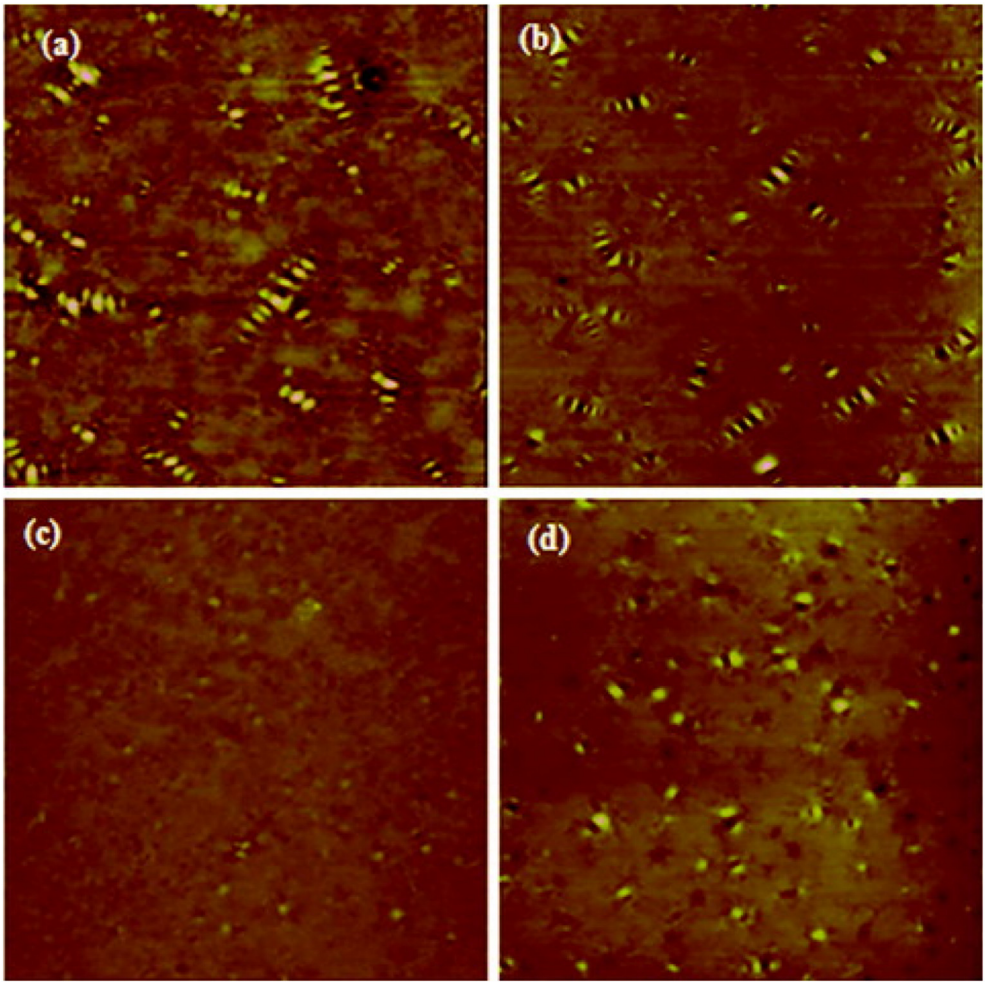


**Fig. 19.** Topographic images of (a) B1, (b) nano-ZnO/B1, (c) B2, and (d) nano-ZnO/B2. See text for discussion. Images show 15 μm × 15 μm areas, acquired by Du et al. [116].

**Table 15**
Physical characterization of the bitumen, ASA and $Al_2O_3$, studied by Mubaraki et al. [117].

| Material | Properties | Test Method | Value |
|---|---|---|---|
| Bitumen 60/70 | Specific Gravity | ASTM D70 | 1.03 |
| | Penetration @ 25 °C | ASTM D5 | 70 |
| | Softening Point (°C) | ASTM D36 | 46.0 |
| | Viscosity @ 135 °C (Pa s) | ASTM D4402 | 0.5 |
| | Ductility (cm) @ 25 °C | ASTM D113 | ≥125 |
| Acrylonitrile Styrene Acrylate (ASA) | Specific Gravity | – | 0.30 |
| | Size nm | – | 2 |
| Nano $Al_2O_3$ | Size nm | – | 13 |

softening point value), the authors attribute this behaviour to irregular dispersion of the nanoparticles in binder.

The Fourier Transform Infrared (FTIR) analysis was performed in order to evaluate the change in the structural and chemical composition of the modified binders compared to unmodified one Figure 21. The most important data that emerge from the analysis of the spectra is that the positions of the peaks are very similar, indicating in the authors' opinion, that there has been no structural change of the base ligands with the addition of the nanoparticles. The authors indeed textually report "The results show that asphalt has no obvious changes before and after modification, which indicates that modification of asphalt with Al2O3 nanoparticles is merely a physical process." We do not agree with the authors' comment, since small shift in the IR absorption peaks can reveal interesting changes in the vibrational states of the functional groups as a consequence of changes in interactions. These small changes can be effectively unveiled and quantitatively treated through proper analysis [74,75], which must pass through the separate analysis of the various IR ranges in which the functional groups absorb.

For example, it has been seen that the frequency of C—H stretching are usually quite robust but the relative intensities of the $CH_2$ and $CH_3$ symmetric and antisimmetric contributions are not, so they are usually indicated as interesting indicators of the chain packing [15,120].

Other authors have used IR spectroscopy: the antioxidant effect of the two inorganic nanoparticles was deepened by FTIR by Nazari et al. and also Hussein et al. [96] and Li et al. [109], Karnati et al. [121] cited in the present work, have used FT-IR spectroscopy.

To better evaluate the structure of the binders analysed, the authors acquired X-ray diffraction (XRD) spectra. From acquired spectra both neat binder and $Al_2O_3$ nanoparticles turned out to be amorphous. Meanwhile, all modified samples show no new crystalline phase.

Regarding to the rheological properties, Ali et al. noted that the viscosity in general decreases with increasing temperature and that it increases with increasing the $Al_2O_3$ concentration. In any case, at a temperature of 135 °C, the viscosity values were below 3 Pa·s (Superpave specification).

Meanwhile, the storage stability tests highlight a pretty good stability during high temperature storage. In fact, the difference in softening point between the upper and lower sections were less than 2.5 °C for all binders.

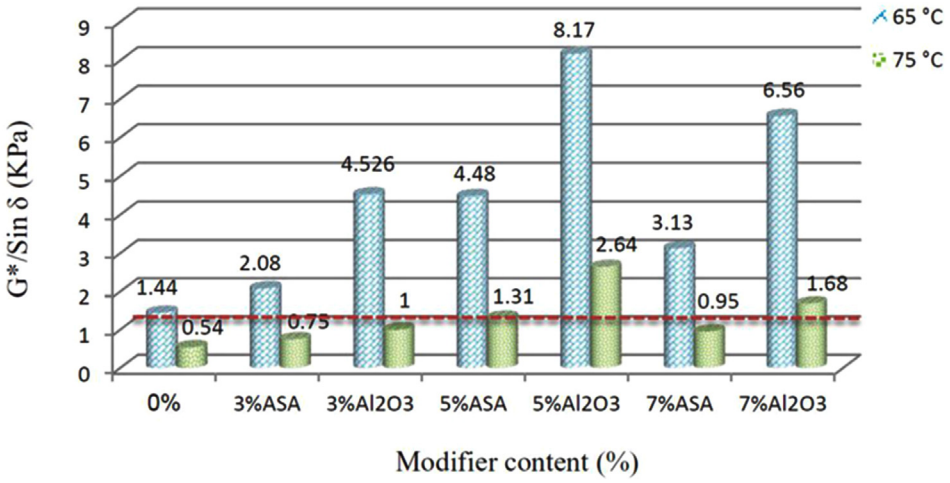


**Fig. 20.** Rutting Parameter of neat, ASA Polymer and nano-Al2O3 modified bitumen, analysed by Mubaraki et al. [117].

In addition, the authors constructed the master curve for the complex modulus ($G^*$) and for the phase angle (δ), in order to evaluate viscoelastic properties over a large range of loading times. This has been reported in Fig. 22. It is possible to note an increase in the value of complex modulus, going from the base binder to the sample containing 5% of nanoparticles. But, instead, the samples modified with 7% of $Al_2O_3$ shows a decline in the complex modulus values. Regarding the phase angle, it shows a decrease as the content of nanoparticles increase. This behaviour mainly concerns the 5% modified sample, indicating a better elastic recovery.

For the purpose of a complete rheological characterization of the binders analysed, Ali et al. measured also the failure temperature. This parameter is defined as the point at which the factor of $G^*/\sin\delta$ alls below 1 kPa, according to Superpave binder grade specifications. The neat bitumen has the lowest failure temperature, instead, the modified samples have higher failure temperature, especially the sample 5% $Al_2O_3$.

The $G^*/\sin\delta$ parameter was also used to describe the resistance to rutting. Superpave standards require that an aged binder has a minimum rutting parameter of 1 kPa. The rutting parameters of the samples reveals that the base binder has a lower value, of course, conversely the addition of nanoparticles increase the $G^*/\sin\delta$ clues. 5% $Al_2O_3$ has the higher rutting parameter. This trend indicates that 5% $Al_2O_3$ exhibits the best resistance to permanent deformation. On the contrary, to obtain the fatigue parameter the product $G^* \cdot sin\delta$ is used, which, according to the Superpave standards, must be maximum 5000 kPa. It was shown that the addition of nanoparticles causes a decreasing of the value.

Finally, the authors argue that with the repeated creep and recovery test it is possible to obtain an estimate of the permanent deformation of the binder after applying a stress [122].

The authors performed the tests at a temperature of 64 °C and at two different applied stresses, 100 and 3200 Pa (maximum and minimum level of traffic stress), according to ASTM D7405. The sample with the best resistance to permanent deformation, with both stresses applied, was 5% $Al_2O_3$, showing a marked improvement over the base binder. It showed a marked decrease of the compliance (total load strain per unit of stress [123]): in the case of bitumen modified with the 5% of nano-$Al_2O_3$ it showed a decrease of a factor of about four with respect to the basic bitumen both at 100 Pa and at 3200 Pa. This showed the important role exerted by the nanoparticles in improving the mechanical characteristics.

*6.5.3. Nano-CuO*

nano-CuO was the material used in the work by Shafabakhsh et al. [124]. The authors conducted a study on rheological properties of virgin, Rolling Thin Film Oven Test (RTFOT) and Pressure Aging Vessel (PAV) aged PG 64–16 bitumen, modified by nano-CuO in 2, 3.5 and 5% by high shear mixer. To evaluate the modified bitumen properties, Dynamic Shear Rheometer (DSR) and Bending Beam Rheometer (BBR) were used. After deriving the complex modulus $G^*$ and phase angle δ from DSR measurements, the authors investigated the tendency to rutting deformation of the virgin and modified (both unaged and aged) bitumen by evaluating the trend of $G^*/\sin\delta$ parameter at 64 °C and 70 °C. In particular, according to Superpave Binder Specification the above-mentioned parameter has to be greater than 1 kPa for unaged bitumen samples and greater than 2.2 KPa for aged ones.

The authors found that at 64 °C the addition of nano-CuO to bitumen produces an increase of the $G^*/\sin\delta$ above the required limit value of 1 kPa, and consequently it enhances the bitumen resistance to rutting deformations. In particular the authors found that the higher increase in the $G^*/\sin\delta$ parameter is obtained in the 2% modified sample, namely 2.1 kPa compared to the 1.15 kPa of the unmodified sample. Moreover, although the $G^*/\sin\delta$ values at 3.5 and 5% are lower than that at 2% modified sample, their $G^*/\sin\delta$ values are higher than the corresponding unmodified sample. On the contrary, they observed that the $G^*/\sin\delta$

**Table 16**
Physical characterization of neat bitumen and nano-$Al_2O_3$ studied by Ali et al. [119].

| Material | Properties | Unit | Limts | Value |
|---|---|---|---|---|
| Asphalt 60/70 | Specific gravity | – | 1.00–1.05 | 1.03 |
| | Penetration @ 25 °C | mm | 60–70 | 70 |
| | Softening point | °C | 47 Minimum | 47.0 |
| | Viscosity @ 135 °C | Pa s | 3 Max | 0.5 |
| | Ductility (cm) @25 °C | cm | 100 Minimum | ≥100 |
| Nano $Al_2O_3$ | Size | nm | – | 13 |
| | Specific gravity | – | – | – |

**Table 17**
Physical characterization of unmodified and modified bitumens, analysed by Ali et al. [119].

| Asphalt cement | Penetration @ 25 °C (dmm) | Softening point | PI | Ductility (cm) @25 °C |
|---|---|---|---|---|
| Base binder | 70.0 | 46 | −1.48 | >100 |
| 3% $Al_2O_3$ | 27.64 | 51 | −2.14 | 95 |
| 5% $Al_2O_3$ | 25.45 | 53 | −1.84 | 62 |
| 7% $Al_2O_3$ | 38.18 | 51 | −1.54 | 91 |

parameter at 70 °C is lower than 1.0 kPa. On the base of these results the authors concluded that adding nano-CuO to bitumen cannot develop the rutting performance of bitumen at temperatures higher than 64 °C. Rutting resistance of modified bitumen has also been investigated on RTFOT aged samples used to study the effect of short-term aging. The $G^*/\sin\delta$ values for RTFOT samples reveals that this parameter for modified bitumen at 64 °C is above the required limit value of 2.2 kPa. However, at 70 °C the results fall again below the limit value of 2.2 kPa. Based on these results for unaged and RTFOT-aged modified bitumen the authors concluded that in the limit temperature of 64 °C, modified bitumen with nano-CuO develops a higher rutting resistance compared to pure bitumen PG 64–16, but it has no effect at higher temperature limit (70 °C).

Finally, in order to evaluate the dynamic viscoelastic properties for the samples after PAV (Pressure Aging Vessel) treatment, Shafabakhsh et al. investigates the fatigue cracking, due to long term aging effects and loads of vehicle transit. Fatigue cracking, generally, is one of the important pavement damages in moderate temperatures ranges. To evaluate its effects the authors used the parameter $G^* \cdot \sin\delta$ and performed DSR tests at 19, 22 and 25 °C and 28 °C. According to AASHTO M 320–10 this parameter should be ≤5000 kPa at 28 °C for a Performance grade (PG) bitumen. The authors found that at 28 °C the value of $G^* \cdot \sin\delta$ was smaller than the limit value of 5000 kPa, and also smaller than virgin PG 64–16 bitumen used as a reference. This indicates that the nano-CuO modification enhances the fatigue cracking of the virgin bitumen. Moreover, as can be seen from Fig. 23, the authors found that this result holds also at 25 °C for all nano-CuO contents and for 5% nano content it holds even at 22 °C but not at 19 °C in which maybe a higher concentration is needed. However, the authors believe that going beyond the 5% value of additive could be economically expensive. Considerations on the costs constitute the body of the paragraph 7.2 "Cost Evaluation".

#### 6.5.4. Nano-FexOy

Recent studies have shown that iron oxide nanoparticles (Nano-$Fe_xO_y$) can become very promising materials in the road pavement industry. Anhydrous iron oxide minerals are a result of aqueous reactions under various temperature, redox and pH conditions [125–127]. They have the basic composition of $Fe_xO_y$, but differ in the valency of iron and overall crystal structure. Some of the important polymorphs are magnetite ($Fe_3O_4$), maghemite ($\gamma$-$Fe_2O_3$), and hematite ($\alpha$-$Fe_2O_3$). These are very versatile nanomaterials that find applications in magnetic data storage, biosensing, drug-delivery, electrochemistry, and many others. Their widespread use is due to many advantageous properties, such as superparamagnetism, high values of saturation magnetization, easy control by low intensity magnetic fields, as well as non-toxicity, biodegradability and biocompatibility [128]. The magnetic properties of Nano-$Fe_xO_y$ in combination to the thermoplastic nature of bitumen can prove useful for repairing micro- and macro-scale cracks that are generated in the asphalt during the service life of the road pavement. Crack-healing can be defined as the capability of a material to recover the original mechanical properties either autonomously [129] or by applying an external stimulus [130] due to its thermoplastic property, a potential strategy to promote crack-healing in bituminous materials would be to reduce the viscosity of bitumen by increasing the temperature or through the release of bitumen-miscible diluting agents. Hence, Jeoffroy et al. exploited the ability of $Fe_3O_4$ and $\gamma$-$Fe_2O_3$ magnetic nanoparticles to locally heating the surrounding medium when exposed to a high-frequency oscillating magnetic field (hyperthermia) [131]. The process investigated by the authors and sketched in Fig. 24, effectively triggers a rapid decrease of bitumen viscosity by means of pre-embedded iron oxide nanoparticles, previously coated with oleic acid to prevent the formation of particle clusters and agglomerates larger than 1 μm.

The most pronounced effect on thermal response was achieved by incorporating into bitumen 1 vol% of $\gamma$-$Fe_2O_3$ nanoparticles with mean size of 50 nm, showing the strongest local heating effect of 50 °C in about 8 s under an alternating magnetic field with an amplitude of 30 mT. Other studies have focused on the rheological characterization of heavy and extra-heavy oils containing Nano-$Fe_xO_y$ of different chemical nature, particle size, surface acidity, and concentration of nanoparticles. Taborda et al. have conducted a theoretical and experimental investigation on the effect played by certain types of nanoparticles including Nano-$Fe_3O_4$ as viscosity reducers for bituminous materials [24]. In particular, the inclusion of Nano-$Fe_3O_4$ into bitumen can lead both to adsorption of asphaltenes onto nanoparticles and a reduction of their mean aggregate size [132]. The results of this research on the phenomenological behaviour of the rheological properties of crude oil in the presence of nanoparticles, could prove useful in the industrial applications related to the mobility of heavy and extra heavy crude oil. Other tests have been carried out to investigate the capability of Nano-$Fe_2O_3$ as well as other types on nanoparticles to decrease the rutting potential of hot-mix asphalt. SEM images of asphalt binder modified by the nanoparticles demonstrated that the nanomaterial was properly distributed into the binder matrix and provided a positive effect on the rutting performance of the asphalt mixes.

### 6.6. Organic nanostructures: a solution to increase nanoparticles-bitumen affinity

In order to avoid nanoparticle agglomeration, the use of organic nanoparticles, granting higher compatibility between the matrix and the modifier, can be explored. The aim would be then to exploit the hydrophobicity typical of organic nanoparticles for obtaining a match with that of maltene phase. We will show some materials used for this purpose.

#### 6.6.1. Organic expanded vermiculite (OEVM)

Chen et al. [133] conducted a worth-of-note study on the effects of nanoparticles used to counteract bitumen aging: they used organic expanded vermiculite compounds (OEVMT) as well as three different kind of nanoparticles: nano-$TiO_2$; nano-ZnO and nano-$SiO_2$. The base bitumen used has a penetration grade 60/80, hereinafter referred to as SK-70.

The three different inorganic nanoparticles, with dimension in the range 15–20 nm, have been modified on the surface by ϒ-(2,3-epoxypropoxy) propyltrimethoxysilane.

Their preparation is quite complex so (see the original paper for the details) the final vermiculite microstructure was firstly analysed by X-ray. Interesting difference was observed in the spectra from the bare OEVMT and that extracted from the modified bitumen: in the OEVMT extracted from the modified bitumen the diffraction peak characteristic of bare OEVMT was absent, indicating that the silicate layer was shrugged off during the bitumen modification process.

As for the mechanical properties, the evolution of the phase angle ($\delta$) and the complex modulus ($G^*$) in the temperature range 40–80 °C was observed. It was concluded that the modified samples have better resistance to fatigue indicated by greater stiffness and elasticity, compared to pristine bitumen. Moreover, the additives samples have a higher thermal stability when compared to untreated bitumen. Increasing the concentration of nano-$TiO_2$ improves the mechanical properties, indeed the best results are for SK-70 + 1% OEVMT + 3% Nano-$TiO_2$. According to the authors, these behaviours are due in part to the nano-$TiO_2$ that reduces

**Table 18**
Properties of bitumen studied by Zhang et al. [137].

| Penetration (25 °C) | 75 dmm |
|---|---|
| Softening point | 49.5 °C |
| Viscosity (135 °C) | 0.58 Pa s |
| Viscosity (60 °C) | 259 Pa s |
| Ductility (15 °C) | 150 cm |

the flow, and therefore the deformation, of the bitumen because it limits its movements. Similar role is exerted by silicate layers, hindering the movement of molecular chains of bitumen at high temperatures. Comparison among the rheological properties of the samples modified with 3% of nano-ZnO, nano-SiO2 and nano-TiO2 shows that the sample modified with nano-$SiO_2$ has the highest values of complex modulus and phase angle, while the sample modified with nano-ZnO has the lowest values.

In this study, the three different inorganic nanoparticles were also tested on bitumen subjected to short and long-term thermal oxidation aging. Short-term aging was carried out by TFOT (Thin Film Oven Test) for 5 h at 163 °C. The bitumen thus obtained was subjected to UV aging for 6 days in a draft oven equipped with an UV lamp of 500 W. Instead, long-term aging was carried out by PAV (Pressure Aging Vessel) for 20 h at 100 °C. The resistance of the samples to aging was assessed through two parameters: phase angle aging index and complex modulus aging index. These two parameters can be obtained from the following ratios:

$$Phaseangleagingindex = {}^{agedphaseangle}/_{unagedpahseangle} \quad (10,)$$

$$Complexmodulusagingindex = {}^{agedcomplexmodulus}/_{unagedcomplexmodulus} \quad (11)$$

Comparing the action of nano-$TiO_2$, at a dosage of 3%, with that of the other nanoparticles, at the same dosage, it is observed that up to 50 °C nano-$TiO_2$ gives the better resistance against short-term aging. But, between 50 and 80 °C, the sample containing nano-ZnO shows the best anti-aging effect for short-term aging. Furthermore, the latter sample was also the best in counteracting long-term aging. On the contrary, the sample containing nano-SiO2 showed the worst effects at both aging steps.

Lastly, Chen et al. tested the nanoparticles on the samples subjected to photo oxidation process. It was found that nano-$TiO_2$ has an antiaging effect even in the case of photo oxidation, however, this effect is highly dependent on concentration. This fact can be rationalized in our opinion by considering that nano-$TiO_2$ has a twofold effect whose relative contributions are in complex competition: i) its semiconductor nature allows the absorption of those radiations whose energies are above the energy gap value and ii) the size in the nanoregime allows radiation scattering within the sample. In fact, the sample with 3% nano-$TiO_2$ turns out to be the best, as already seen for aging via TFOT and PAV. While the sample with 1% of nanoparticles is worse than the reference aged bitumen. In our opinion this detriment effect is the result of the scattering contribution of the nanosized particles which helps in diffusing the radiation within the sample. This effect is not counterbalanced enough by the absorption contribution of such nanoparticles which would help in depleting radiation. At the same time, however, by comparing the three types of nanoparticles also nano-ZnO has a good anti-aging effect, enough to have the lowest complex modulus aging index of the sample with nano-$TiO_2$. This is due to the fact that nano-ZnO has semiconductor nature, too. As expected, instead nano-$SiO_2$ cannot counteract the effect of photo oxidation due to UV aging since its energy gap is too high so it is considered more an insulator rather than a semiconductor. These effects are, indeed, commented by the authors: nano-TiO2 (and nano-ZnO) is able to reflect and absorb UV light. This phenomenon, in addition to the ability of OEVMT to increase the average path length of the oxygen molecules inside the bitumen, could act as a barrier against aging. It must be noted, however, that due to the nanosize regime of $TiO_2$ which breaks the crystal periodicity at relatively short range, the physical nature (direct or indirect) of the photon absorption is still under discussion [134].

**Table 19**
Properties of the bitumen studied by Zhang et al. [110].

| Physical properties | Measured values |
|---|---|
| Penetration (25 °C, 0.1 mm) | 73 |
| Softening point (°C) | 48.5 |
| Ductility (15 °C/10 °C, cm) | 145.0/16.0 |
| Viscosity (60 °C, Pa s) | 258 |

2% by weight of nanoparticles was added to the bitumen.

Indeed, some studies point out the possibility of occurrence of both transitions with different probabilities also taking into account the materials in contact with the nanoparticles and/or their inherent structure (polycrystalline or not) [135,136].

The possibility to tune the probability of photon absorption by changing the nanoparticle structural characteristics could be, in our opinion, a powerful way to further enhance the resistance of a nanoparticle-modified bitumen to the photo-induced aging, which deserves much attention. For examples, the presence in traces of a metal within nanoparticles can induce a lowering of the nanoparticle energy gap (sensitization) thus extending the wavelength range of the photons which are absorbed [135,136]. More absorbed photon means that resulting nanoparticle-containing bitumen can be more resistant to photo-induced aging.

In similar way, Zhang et all. [137] tested nano-ZnO in combination with organic expanded vermiculite (OEVMT), using 3-aminopropyltriethoxysilane, analytically pure, to modify the nano-zinc oxide (15–25 nm) surface, and star quaternary alkylammonium chloride, to modify the interlayers of expanded vermiculite (EVMt, 300 mesh) from hydrophilic to lipophilic. Then, the modified EVMt were marked to obtain organic expanded vermiculite (OEVMt). Table 18 lists the physical properties of the bitumen used in this investigation.

The samples were obtained by mixing 3% by weight of nanomaterials with hot bitumen (150 °C for 60 min at 5000 rpm and then for another 90 min at 2000 rpm). The reference bitumen was mixed itself in the same way for effective comparison purpose.

Initially the authors analysed the structure of vermiculite through X-ray diffraction (XRD).

The organic modification of EVMt shifts the peak towards higher interlayer spacing value, from d = 1.42 nm to d = 6.44 nm. This has been attributed to the effect of the star quaternary alkylammonium chloride that is placed in the interlayer of EVMt. Furthermore, the analysis shows how an exfoliated structure is obtained for bitumen modified with OEVMt. In fact, the OEVMt, extracted from bitumen, does not show peaks due to the interlayer spacing above angles equal to $2\theta = 0.5°$.

Clues AFM images are reported in Fig. 25. Panel a show the topography of the unmodified sample, in which the so-called bee structures are clearly visible. They are micrometer sized structures with a rippled interior with few nanometres edges and dispersed in a quite uniform matrix. Such structures, have been observed by several authors [138] and can be considered to be made of asphaltene clusters at different levels of aggregation, in accordance with previous observations [93].

According to the authors, who also refer to their previous study [139], the presence of bee structures is due to the crystallization of the microcrystalline waxes of asphaltenes. In our opinion this attribution is only in part contradicting the previously reported one, because, since asphaltenes are arranged in clusters and hierarchical suprastructure of higher levels of complexity of various length scales [94], the presence of wax, at least within all these clusters and aggregates, is obvious. In any case, it seems that the structure at the meso-scale (bee-structures) is somehow correlated to that at the nano-scale (molecules and their aggregates).

However, the sample modified with OEVMt is shown in Fig. 25 panel b. The modification causes the bee structures to be diluted in the matrix. The effect of OEVMt is to reduce the size of the microcrystalline structures because their crystallization is inhibited during cooling from high to test temperatures. The sample containing nano-ZnO has more bee structures (Fig. 25c), even if smaller than the unmodified bitumen. Zhang et all. Attribute a nucleating function to inorganic nanoparticles, which would favour a heterogeneous nucleation crystallization of asphaltenes.

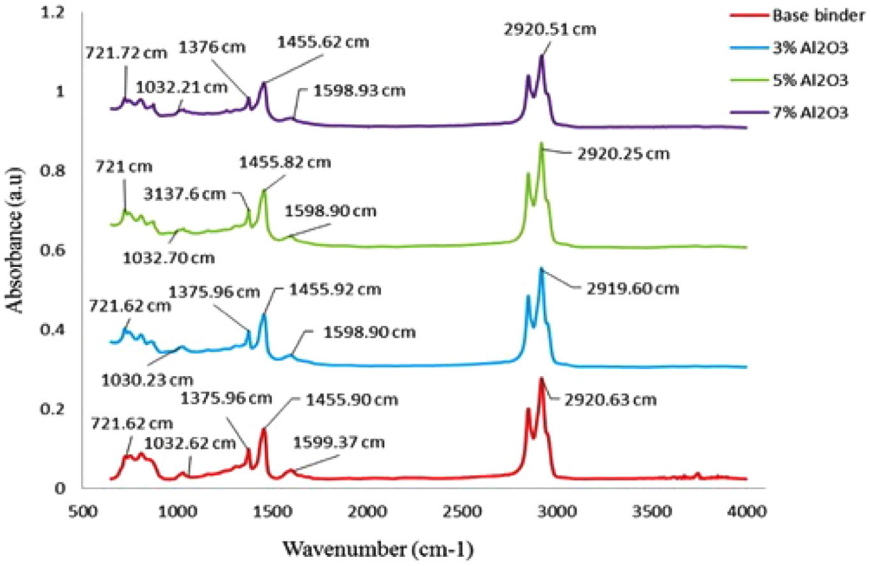


**Fig. 21.** spectra of the neat and $Al_2O_3$-modified bitumens studied by Ali et al. [119]

In this research the degree of aging of the bitumen was also evaluated by comparing the VAI indices (see eq. 6). The samples that had already undergone an aging process by TFOT (Thin Film Oven Test) were treated by PAV (in accordance with ASTM D6521); by in situ thermal aging (a 3.2 mm thick sample was kept in the oven for 30 days at 70 °C); photo-oxidative aging (in a draft oven with UV lamp of 500 W for 12 days at 70 °C). A substantial decrease in the VAI indices is easily noted for the samples treated with OEVMt, both in the case of PAV aging and in the case of in situ thermal aging. Aging is countered by the formation of exfoliated nanostructure due to the effect of EVMt. On the contrary, nano-ZnO appears to have only a weak effect on thermo-oxidative aging, in fact its VAI values are slightly lower than those of the two aged reference bitumens. Instead, there is an opposite situation in the case of photo-oxidative aging. In fact, inorganic nanoparticles are very effective in counteracting UV aging, thanks to their good ability to screen UV radiation. Rightly, since there are no absorption peaks of the UV radiation to be attributed to OEVMt, its effect in counteracting aging is minimal.

### 6.6.2. Carbon nanostructures

*6.6.2.1. Graphenes.* Since its emergence in 2004 [140], graphene has opened up a number of new research lines in the field of construction engineering. It is an allotrope of carbon in the form of a single layer of atoms in a two-dimensional hexagonal lattice in which one atom (with $sp^2$ hybridization) forms each vertex. It can be considered as an indefinitely large aromatic molecule, the ultimate case of the family of flat polycyclic aromatic hydrocarbons (PAH). Fig. 26 highlights the structure and some remarkable physical properties.

Its use as nano-modifier in the improvement of the mechanical properties of bituminous materials is one of the most interestingly studied solutions. On the other hand, its use in construction materials for the improvement of the mechanical performance of matrixes such as polymers or other composites is well-known [142], as well as its role in controlling some functional properties like electrical conductivity, gas barrier behaviour, thermal conductivity, expansion, and stability.

For example, graphene can enhance the electrical conductivity of cement mortars [143], as well as their stiffness, tensile strength, and durability [144,145]. Similarly, the use of graphene has been regarded as a potential modifier in bitumens that could help to achieve more durable substrates. The hydrophobic nature of graphene sheets can also facilitate interactions with the non-polar groups of bitumen binder to form stable nanocomposites. In such situation, it can be expected that a continuous transition of stress from the bitumen binder to the graphene particle holds. In addition, the presence of graphene sheets could modify the thermal conductivity of bitumen binders as well as the lubricant

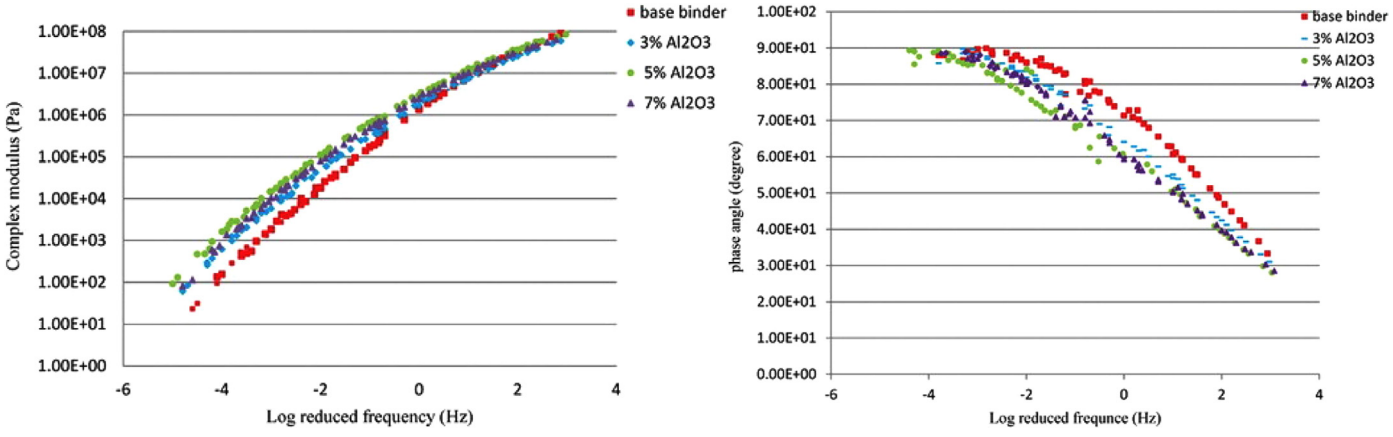


**Fig. 22.** Master curves of complex modulus (left) and phase angle (right) for samples studied by Ali et al. [119].

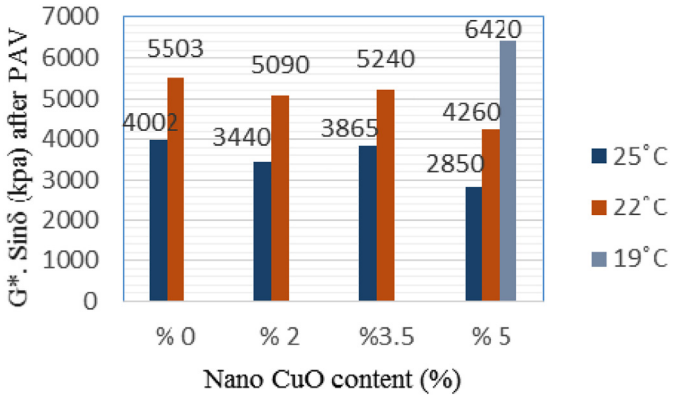


**Fig. 23.** Values of fatigue parameter versus percentage of Nano Copper Oxide in modified bitumen with long term aging, studied by Shafabakhsh et al. [124].

effect on the material which could improve asphalt concrete workability [146]. Nonetheless, its use as a modifier in bitumen technology is still relatively recent and rather limited [147]. Moreover, due to pure graphene high production costs, most of the studies have been made by using graphene oxide (GO) or graphene nanoplatelets (GnPs), the latter being composed of single /few graphene layers mixed with thicker graphite (structurally they are in between graphene and graphite, i.e. from 0.34 to 100 nm [141]. Among the very few articles present in the literature, worthy of note are that by Moreno-Navarro et al. [148] and that by Aravind et al. [149].

In the study by Moreno-Navarro et al. the interest is directed to the rheological, and thermal properties of the resulting blends. The authors evaluated the mechanical and thermal properties of graphene modified binders, by studying a B 50/70 bitumen binder blended with 0.1%, 0.5%, and 1% (*w*/w) of graphene, selected in order to find the most effective range of added material that could induce a desired modification of the binder. The graphene material used in this study was obtained by a thermal reduction of graphene oxide in $H_2$ ambient. Fig. 27 shows images from the optical microscopy of the neat binder and the 1% graphene modified binder taken by the authors.

The typical "bee" structure is found in the neat binder (panel a) of Fig. 27 while panel b shows the presence of graphene sheets of different sizes. In addition, the authors observed that the shape of the "bee" structure found in the modified bitumen differs from that shown by the virgin one, which could be due to a reaction between some of the graphene sheets with the non-polar phase of the bitumen (aromatics). This could indicate that the effect of graphene as a bitumen modifier could be influenced by the chemical composition of the binder (polar/non-polar phase ratio). The authors also investigated the mechanical performances of the bitumen through frequency and temperature sweep tests and the Multiple Stress Creep and Recovery Test (MSCRT). The latter was used to determine the resistance to deformation at high temperatures (45 and 64 °C) and the delayed elastic response of the binders during recovery periods. Creep Compliance was measured as indicative parameter of residual strain after repeated creep and recovery to evaluate the resistance to permanent deformations of the asphalt binders at the two stress levels. The elastic recovery (%) in each stress level was measured to gain information about the capacity of the sample to return to its initial shape during the recovery time after each load cycle. It has been observed that the presence of graphene tends to produce a slight increment in the degree of recovery of the binders as well as a minor increment in their resistance to permanent deformations (non-recoverable creep compliance). However, the improvement detected in the elastic response of the binder is much lower than that produced when other commonly used modifiers such as SBS polymers are applied (which produce a considerable increment in the degree of recovery and a high increment in the resistance to permanent deformations). The authors also pointed out that the test temperature plays an important role in the mechanical response of the materials. Speaking of which, the increase of temperature decreases the recovery capacity of the binder. The values of Jnr decrease as the graphene content increases, regardless of the test temperature and shear stress. The authors concluded that when graphene is used to modify asphalt binders it renders these materials stiffer at any given temperature, whilst improving their elastic behaviour as temperature and shear stress decrease.

Dynamic Shear Rheometer showed that the addition of graphene to the bitumen increases their complex modulus and elasticity (decreases their phase angle) at any given temperature and that the optimum graphene content could be between 0.5% and 1%.

Also, it appeared that bitumen binders could offer a lower sensitivity to temperature changes during their service life due to the presence of this modifier. It is worth of note that traditional bitumen modifiers (such us polyethylene or SBS) can give similar effect only at much higher concentrations (from 3 to 5%).

Observation of the $G^*/\sin\delta$ value showed also that all the modified binders have higher values than the neat binder at any temperature, which indicates that graphene-modified bitumens are more resistant to suffering plastic deformations,

It appears that graphene-modified binders could offer better performance against plastic deformations on roads that are required to withstand higher temperatures. Unfortunately, the work of Moreno-Navarro et al. is the only one, in our opinion, offering a complete characterization of rheological (and thermal) properties of a bitumen modified by graphene.

The work of Aravind et al. [149] on the other hand, deals with the study of mechanical properties of asphalt concretes obtained by using a different bitumen-graphene blend, so it is difficult to make a comparison between the two works.

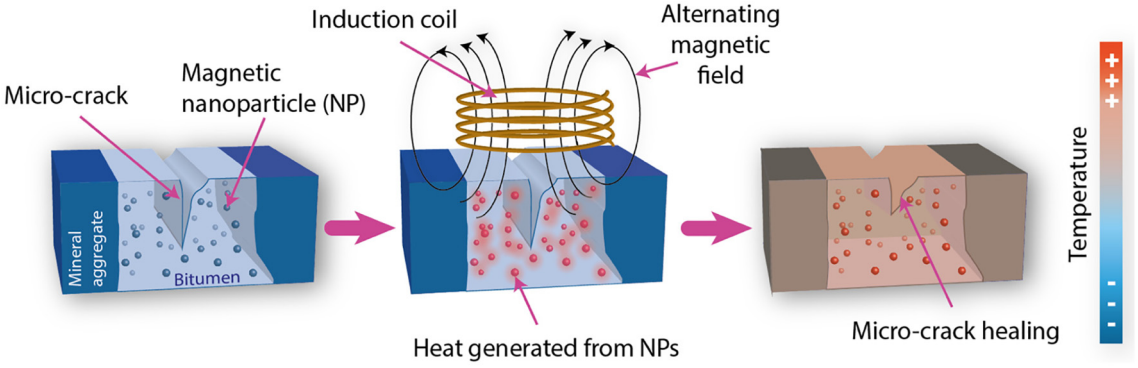


**Fig. 24.** Cartoon illustrating the crack healing method for bituminous materials using magnetic nanoparticles embedded in bitumen. Reprinted from Jeoffroy et al. [131].

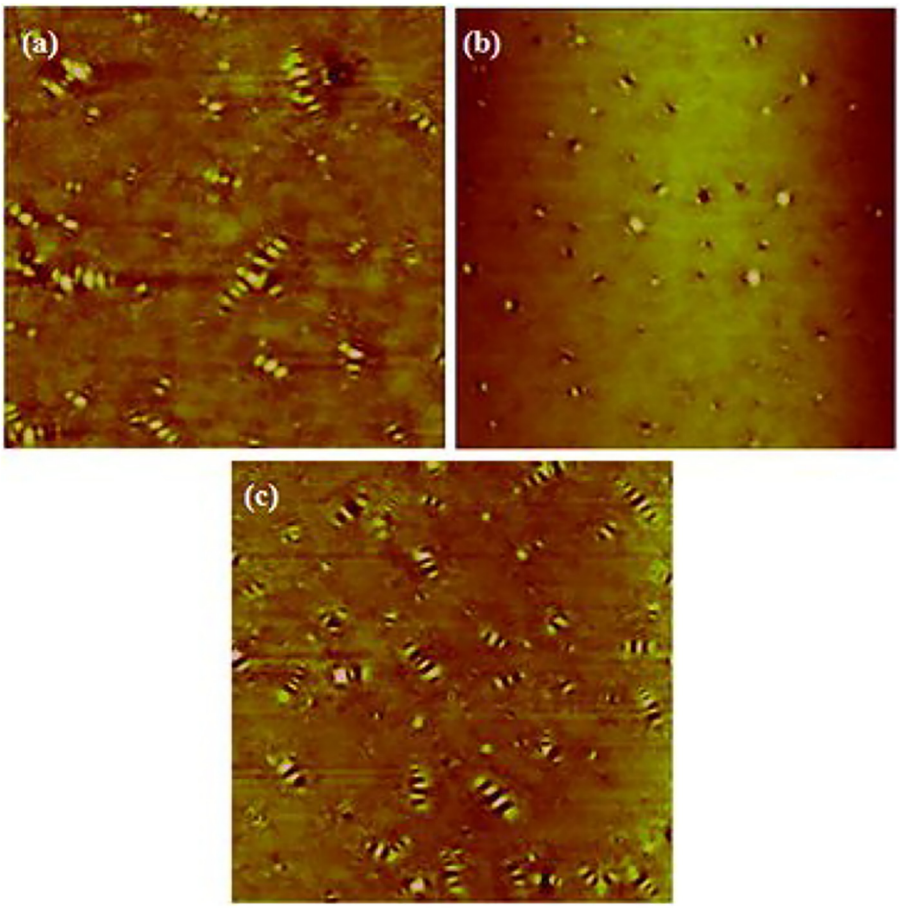


**Fig. 25.** AFM images of (a) unmodified bitumen, (b) OEVMt modified bitumen, and (c) nano-ZnO modified bitumen on a scale of 15 × 15 μm, acquired by Zhang et al. [137].

As for graphene oxide and graphene nanoplatelets (GNPs) Le et al. [146,150] evaluated the rheological properties of bitumen binders obtained from of an unmodified PG 52–34 binder and a SBS modified PG 64–34 binder producing different blends by using three types of Graphene Nanoplatelets: M750, M850, and 4827, at a dosage of 3% and 6% over the total weight of the binder.

Each blend was first short-term aged using a rolling thin film oven test (RTFOT) and then a long-term aging treatment was done using a pressure aging vessel (PAV).

The authors observed that the addition of GNPs materials does not result in significant changes in the rheological properties of the binders and that only a moderate increase (5–15%) in creep stiffness holds.

However, the addition of GNPs leads to a remarkable improvement in flexural strength at low temperatures. For both plain and SBS-modified asphalt binders, a moderate addition of GNPs, from 3% to 6% *w*/w could result in a 130% increase in flexural strength. Such an increase has never been observed in other binder modifiers.

On the contrary, Brcic [151] concluded that GNPs compromises thermal cracking resistance of asphalt binder at low temperatures. To conclude this section, Table 22 summarizes the main studies that have done on graphene oxide modification of bitumen and compare the effects of Graphene Oxide (GO) on the various bitumen tested.

*6.6.2.2. Carbon nanotubes.* The history of the discovery of carbon nanotubes (CNTs) starts from afar, in fact the first to observe an image of carbon nanotubes with a diameter of 50 nm were in 1952 Radushkevich and Lukyanovich [152]. However, 1991 was a very important year for the scientific community, in fact, a research by S. Iijima appeared in Nature which developed the synthesis to obtain a large quantity of nanotubes, observed through the high resolution transmission electron (HRTEM) [153]. Thereafter, the study and use of CNTs has affected

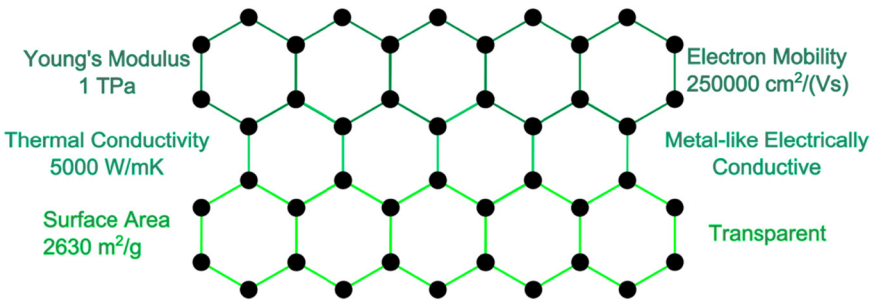


**Fig. 26.** Graphene hexagonal honeycomb chemical structure and its remarkable physical properties. The black dots are carbon atoms [141].

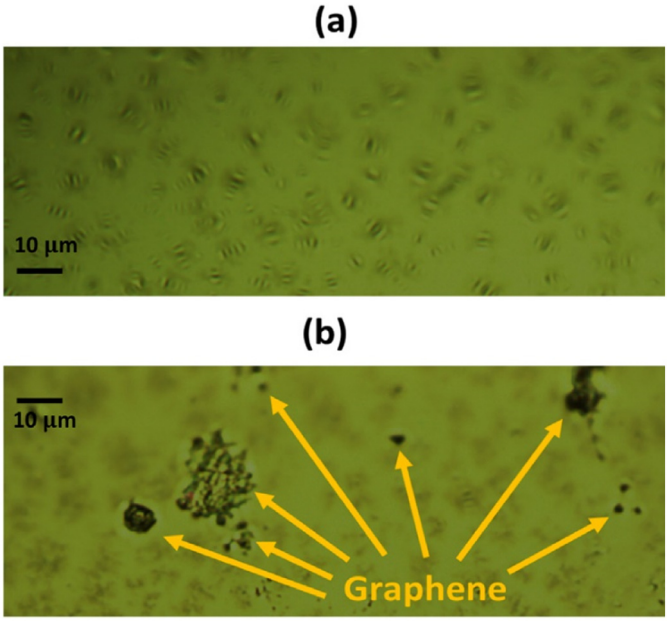


**Fig. 27.** Optical microscopy of the neat binder and the 1% graphene modified binder.

many scientific sectors, thanks to their extraordinary properties. It has been estimated, for example, through TEM and AFM measurements, that their Young modulus is of the order of 1 TPa. CNTs have also proved to be excellent conductors, both thermal and electrical, in fact the current density reaches up to $10^{11}$ $Am^{-2}$ [154]. From a structural point of view, it is possible to have single-walled or multi-walled carbon nanotubes, according to the number of graphene layer. Therefore, when a single layer of graphene is ideally rolled on itself a one-dimensional system is obtained (SWNTs). See Fig. 28 for a vision of the process

In the event that three or more layers of graphene are rolled on themselves concentrically, the multi-walled nanotubes (MWNTs) will be obtained [156]. Arabani et al. [157] investigated the use of carbon nanotubes to improve the mechanical performance of the hot mix asphalt (HMA). For this purpose, the authors used a 60/70 bitumen modified with different percentage of commercial multiwalled carbon nanotubes, made by chemical vapor deposition, with an external diameter between 10 and 20 nm. The aggregates used to obtain HMA were in agreement with continuous type IV scale of the AASHTO standard.

In order to evaluate the effect of CNTs content, the authors prepared samples containing different percentages of CNTs by mixing the bitumen / CNTs mixture for 40 min at 160 °C. To rule out the possibility that the experimental conditions required for bitumen modification with CNTs (160 °C for 40 min) could give rise to short-term aging phenomena, a reference sample containing only neat bitumen was also prepared, under the same conditions as the modified ones.

Indirect tensile resilient modulus tests were performed to characterize the stiffness of the samples, giving an estimate of a material's ability to absorb loads without permanently deforming itself (the higher the resilient modulus, the higher the elastic modulus of that material will have) [158]. The highest modulus of resilience values is obtained for the sample modified with 1% of CNTs. A certain modulus decrease was observed with increasing the temperature.

According to the authors at high temperatures, bitumen / CNTs interactions weaken, making HMA more susceptible to stress. To have an estimate of the permanent deformation (rutting) that the samples may undergo, Arabani et al. performed repeated load axial tests (RLA). The samples are subjected to cyclic loads and the variation in height of the samples is measured, as final strain at different stresses and temperatures [159]. Fatigue cracking was assessed through the indirect tensile fatigue test (ASTM D4123) in controlled stress mode. The measurements were carried out at two applied stress levels, 100 and 300 kPa, each at the temperature of 5, 25 and 40 °C. Tests have shown that the strain increases with increasing temperatures, and that the lower strain values are obtained for the sample modified with 1% of CNTs, regardless of the stress applied. The effect of the modification with nanotubes is remarkable even at lower concentrations, in fact for example the sample containing 0.5% of CNTs has a 180% increase in fatigue life at 100 kPa and 5 °C, compared to the sample containing neat bitumen.

MWNTs were used by Loise et al. to improve the rheological properties of bitumen [160]. The authors used two different types of

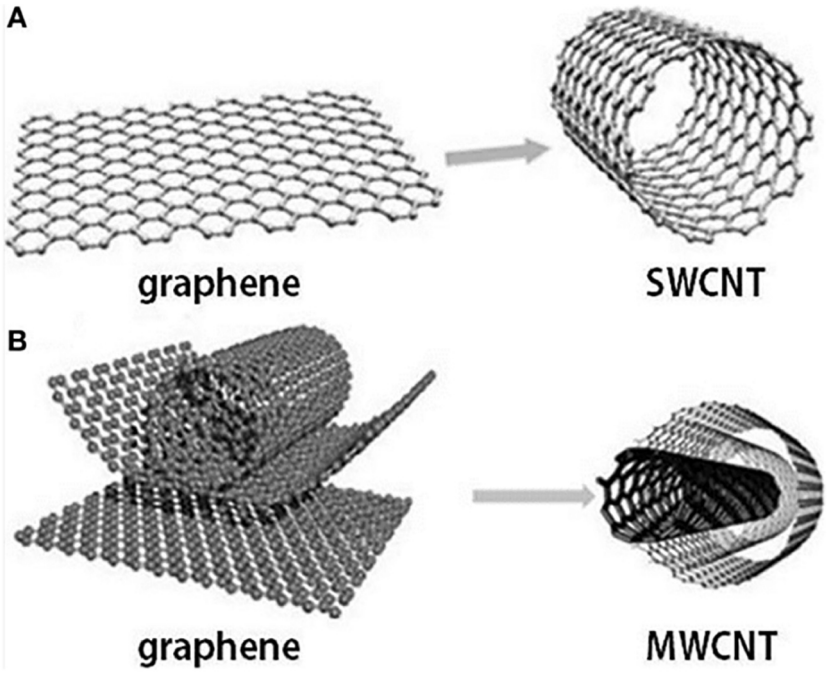


**Fig. 28.** Graphene and carbon nanotubes as (A) single wall carbon nanotube (SWCNT) and (B) multi-wall carbon nanotube (MWCNT) structures. Reproduced from [155].

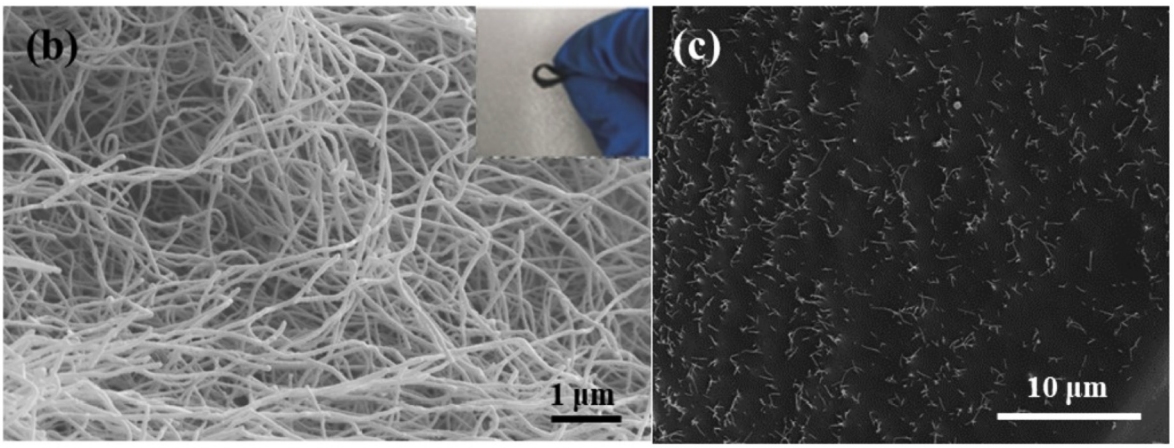


**Fig. 29.** b) self-assembled and randomly distributed porous CNT skeletons, c) CNT sponge/bitumen matrix, studied by Yang et al. [162].

nanotubes, one was a commercial product (diameter between 50 and 120 nm), the other (diameter between 17 and 20 nm) was a product obtained by catalytic chemical vapor deposition (CCVD), hereinafter referred as MWNTs/CCVD. They concluded that the MWNTs characterized by the greatest defectiveness were the best in improving the rheological properties of bitumen. The presence of defects was assessed through micro-Raman spectroscopy and thermogravimetric analysis (TGA). From the micro-Raman spectroscopy, Loise et al. used the intensities ratio of D and G peaks as an indicator of defect density [161], noting that this ratio was higher (greater defectiveness) for the MWNTs/CCVD, a characteristic correlated with the thermal stability, as evidenced by TGA.

Rheological patterns show an increase in sol-transition temperature as the concentration of MWNTs increases. The greatest increase is

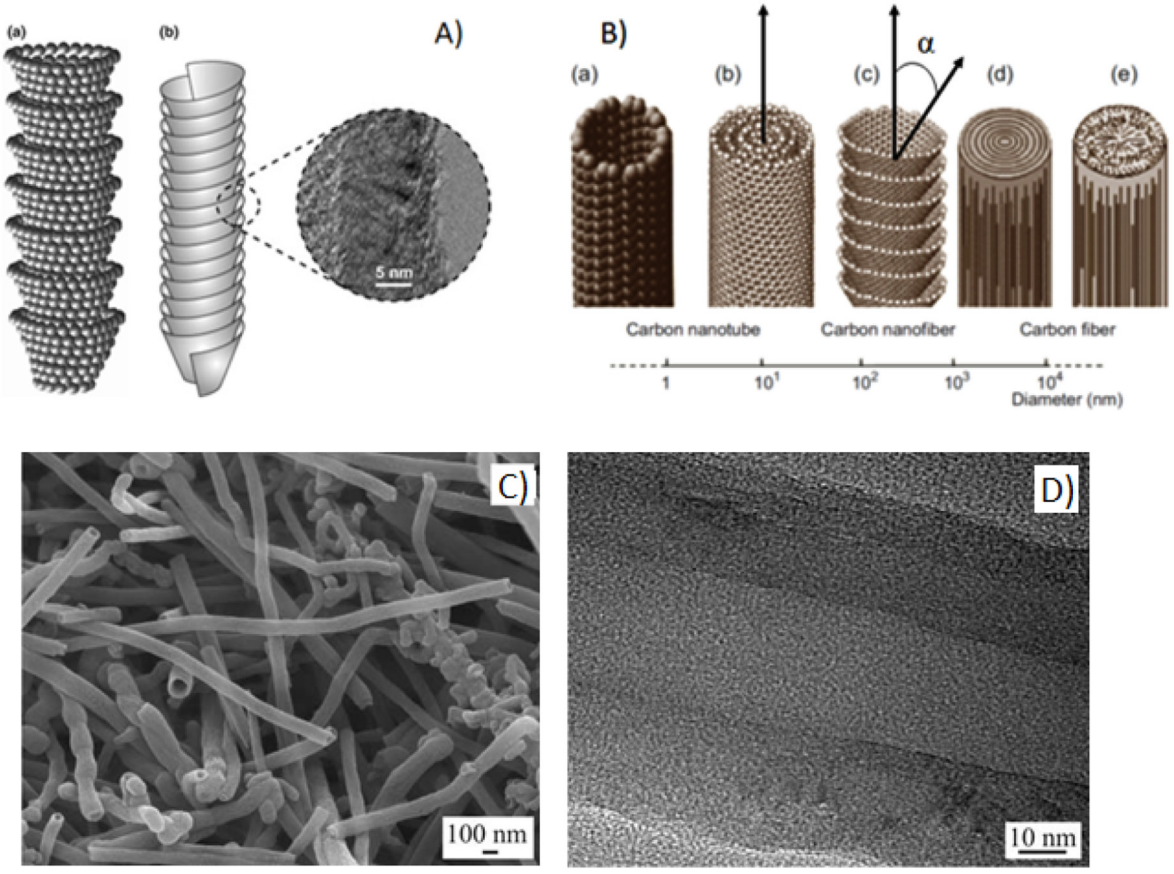


**Fig. 30.** Panel A): (a) 3D representation of cup-stacked graphene layers in a single CNF, and (b) Simplified schematic of stacked-cup carbon nanofiber helical structure with inset showing TEM image of inclined orientation of grapheme planes along the side of structure with respect to nanofiber axis. Image taken from [167]. Courtesy of Elsevier. Panel B): Schematic of size and morphology distribution of various nanotubular structures that shows the main difference in the structure between carbon nanofibers and carbon nanotubes; (a) single wall carbon nanotube, (b) multi walled carbon nanotube, (c) carbon nanofiber, (d and e) carbon fibers of different complexity. Reprinted from [166]. Panel C): SEM Morphology smooth CNF of small diameter and Panel D): HRTEM of a cylindrical nanofiber with the wall thickness of approximately 28 nm and hole diameter of approximately 30 nm. The interlayer spacing of the graphite layers is approximately 0.35 nm. Reprinted from [168].

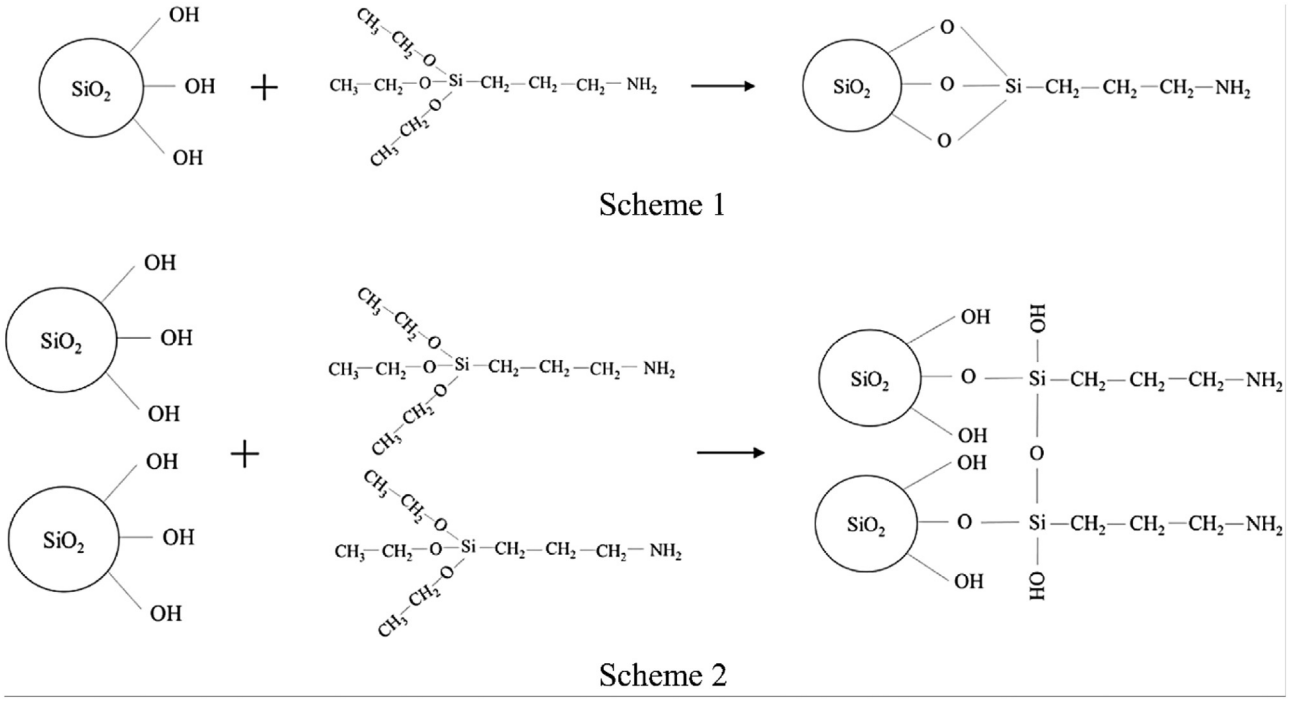


**Fig. 31.** Possible reactions between silica nanoparticles and APTES., speculated by Karnati et al. [121]. Scheme 1: surface functionalization with small amount of APTES; Scheme 2: surface functionalization with large amount of ATPES.

obtained with MWNTs/CCVD dosed at 1% by weight. In fact, the sol-transition temperature increases by only about 5 °C in the case of bitumen modified with the commercial product, while the increase it is about 20 °C for the sample modified with MWNTs / CCVD compared to the neat bitumen.

Moreover, for this latter sample, the curve of loss tangent shows a sort of viscoelastic buffering, with a flat trend in a long temperature range. Loise et al. concluded by assuming that the defects present on the surface of the MWNTs / CCVD may favour the formation of a large network, acting as a "bridge" to connect asphaltenes, this could explain the greater hardening observed for the modified bitumen.

In an interesting study published this year, Yang et al. [162] explored the potential of carbon nanotube (CNT) sponges as modifiers to improve bitumen performance. The CNT sponges, obtained by chemical vapor deposition, are formed by self-assembled and randomly distributed porous CNT skeletons. Sponges have excellent elastic properties, but at the same time they are robust structures [163]. The bitumen used for this research was a 92 mm penetration, and the pore size of the CNT sponges was around 80 nm while the outer diameter of the CNTs that form the sponges were 40 nm. In this study, a particular approach was used for sample preparation. In fact, while generally the CNTs are added to the hot bitumen and the compound is then mixed with a mechanical stirrer for a more or less long time at a given temperature, in this case the sponge has been immersed in the heated bitumen so that the sponge can by capillarity impregnate with bitumen. In the sponge / bitumen CNT matrix thus prepared, the percentage of CNT is approximately 0.5%. The authors highlight how this process, which allows the bitumen to penetrate the porous structure of the sponge, does not cause any collapse of the structure of the CNTs thanks to the high stability of the sponge itself. The images acquired by scanning electron microscope show the structure of the sponge before and after being impregnated with bitumen. The images acquired by scanning electron

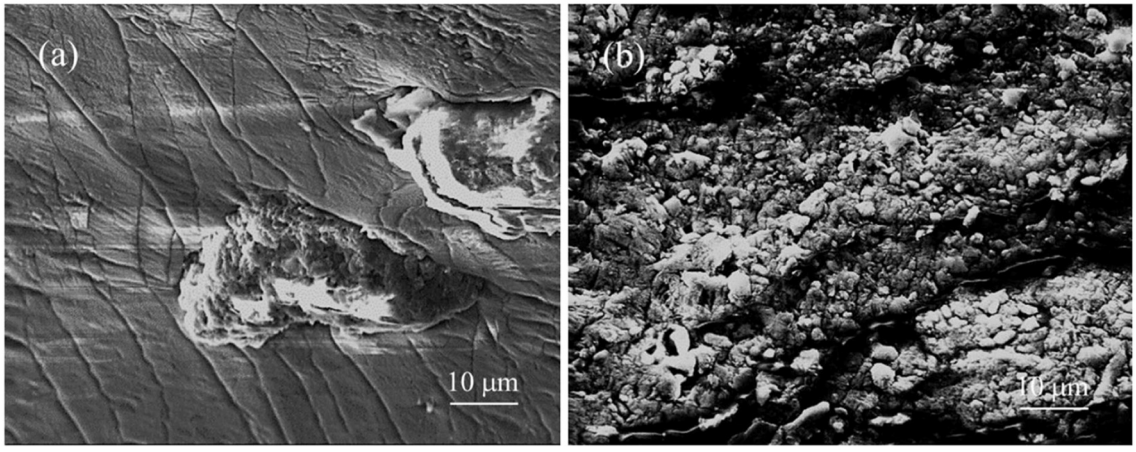


**Fig. 32.** SEM images of (a) pristine SNPs and (b) modified silica nanoparticles in the bitumen, acquired by Karnati et al. [121].

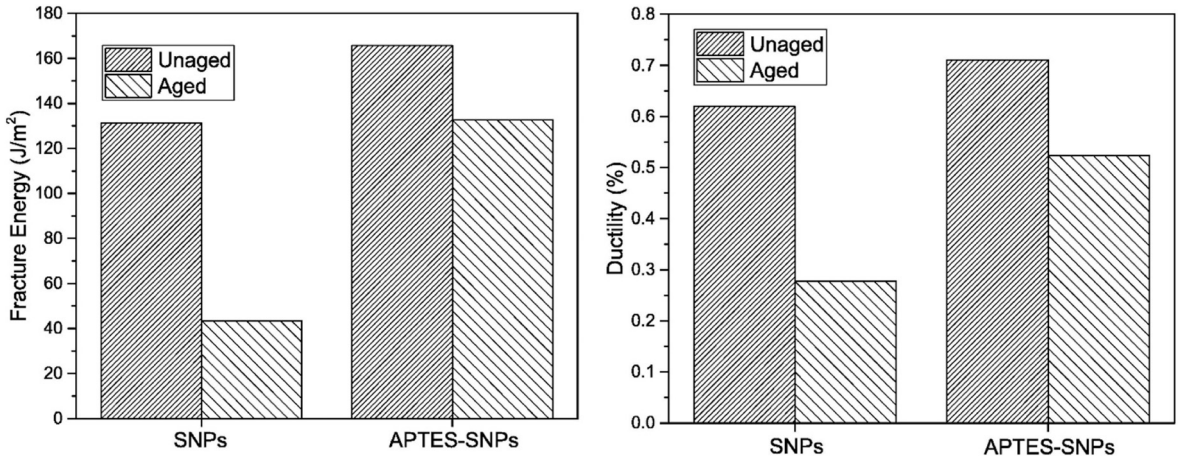


**Fig. 33.** Fracture energy and ductility of unaged and aged bitumen modified with 4 wt% pristine SNPs and with 4 wt% APTES-SNPs, analysed by Karnati et al. [121].

microscope show the structure of the sponge before and after being impregnated with bitumen. Fig. 29 b shows the self-assembled structure of CNTs, while Fig. 29 c shows the homogeneous dispersion of the structure itself in the CNT sponge/bitumen matrix.

Yang et al. accurately analysed the thermal properties of the samples through differential scanning calorimetry (DSC) and through thermal gravimetric analysis (TGA). Through DSC measurements, the glass transition temperature, Tg (low Tg values indicate better resistance to cracking at low temperatures) and the value of endothermic energy, Δcp, were assessed. The value of the endothermic energy is given by the difference in heat exchanged before and after the Tg, that is, the quantity of energy useful to modify the collective state of the unit mass of the bitumen [164]. Furthermore, the lower this value the greater the bitumen crosslinking density, i.e. the density of the chains or segments that connect two infinite parts of the CNT sponge/bitumen network [165]. The analyses showed an increase in the Tg value of about 2 °C in the impregnated sponge sample, showing a slight decrease in cracking resistance at low temperatures. On the contrary, the Δcp value of the CNT sponge/bitumen sample is lower compared to the neat bitumen, thus improving the three-dimensional structure of the network. The thermogram obtained through TGA shows a markedly higher thermal stability for the CNT sponge / bitumen sample. The sponge, in fact, having created a strong network with bitumen would allow to delay thermal decomposition by limiting the evaporation of the most volatile compounds. The authors also investigated the rheological properties of the CNT sponge/bitumen sample by comparing them with those of the neat bitumen. The trend of the master curve shows how the sample containing CNT is more influenced by temperature. Furthermore, its values of the complex modulus are higher than those of the neat bitumen in the high and intermediate temperatures, indicating a better resistance to rutting at high temperatures. Moreover, the master curve built for the phase angle reveals that the CNT sponge / bitumen sample has greater elastic recovery capacity than the neat bitumen, this behaviour is due to the elasticity of the CNT network. Finally, by measuring the rutting parameter as a function of temperature, a better resistance to permanent deformation is shown for the sample containing CNT compared to the neat bitumen. However, it must be emphasized that there is hardly any mixture testing available to directly probe the improvement of the permanent deformation behaviour

*6.6.2.3. Carbon nanofibers.* Carbon nanofibers (CNFs) can be defined as $sp^2$-based linear, noncontinuous filaments with a diameter of about 100 nm and a length of about 200 μm. They differ from carbon fibers, which are continuous with diameter of several micrometers (see Fig. 30 panel B). Carbon nanofibers can be produced via catalytic chemical vapor deposition (CVD) as well as the combination of electrospinning of organic polymer and thermal treatment. For the high specific area, flexibility, and high mechanical strength, CNFs are mainly used in tough composites for vehicle, aerospace applications, biosensors, electrodes and supercapacitors, bone tissue scaffolds, etc. As it

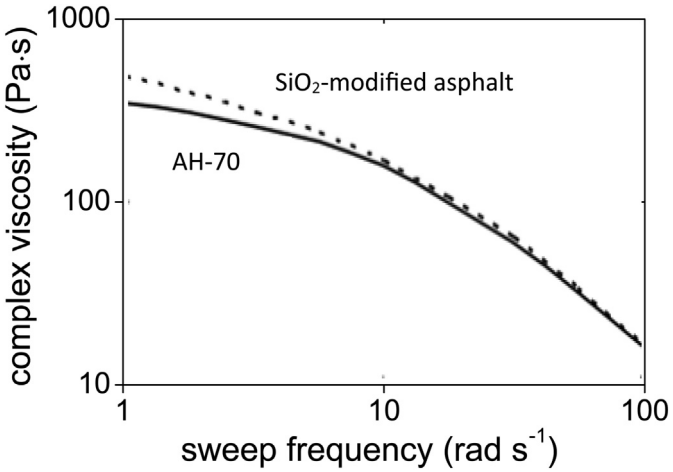


**Fig. 34.** Complex viscosity as a function of sweep frequency as found by Sun et al. ref. [174].

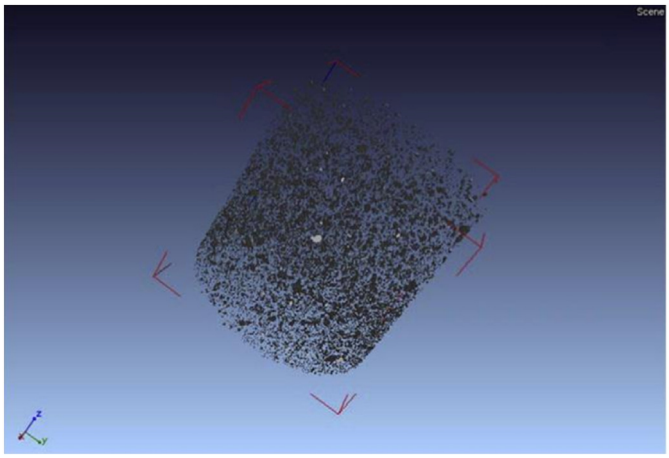

**Fig. 35.** 3D distribution image of Na + Mt. particles in the bitumen.

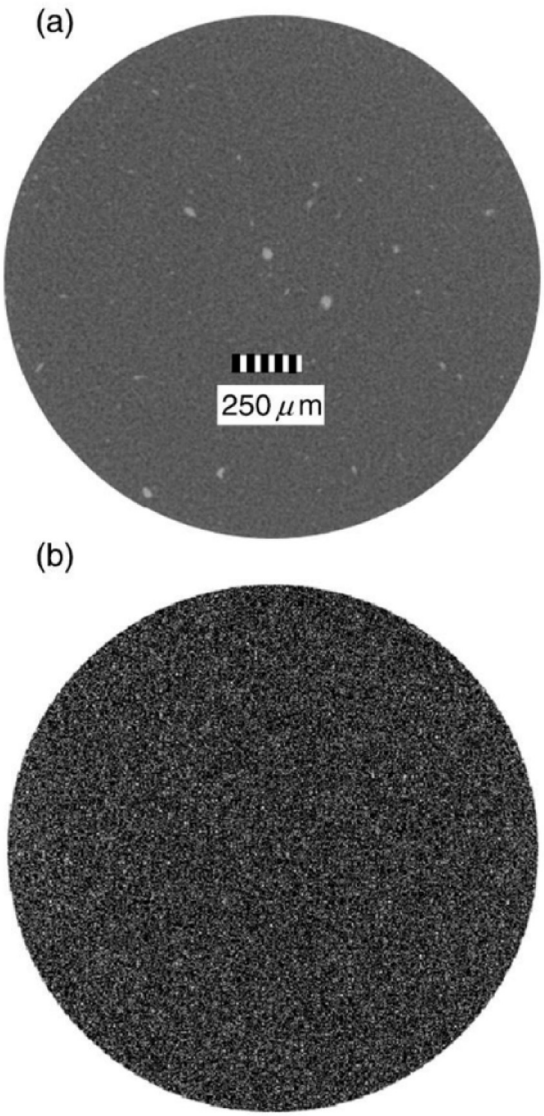


**Fig. 36.** 2D segment images of bitumens (a) with $Na^+$ Mt. and (b) with $OTAC^+$ Mt., at the same resolution (1 μm).

can be seen from Fig. 30 (panel B), CNFs are geometrically different from CNTs; indeed, CNFs have regularly stacked, truncated conical or planar layers along the fiber length. Furthermore, because of the cup-stacked structure, CNFs carry semiconducting behaviour and because both inner and outer surfaces are chemically active, they are well suited for catalysts, reinforcing fillers in composites, photochemical cells, etc. [166].

Khattak et al. [169] investigated the effects of dry process and wet process mixing procedure of various percentages carbon nanofibers (CNFs) with three types of bitumen: AC5 (PG52-22), AC30 (PG64-22) and polymer modified PAC30 (PG70-28), by studying the viscoelastic and fatigue characteristics of neat and CNF-modified AC binders.

According to the authors the homogenous dispersion of CNF produces good viscoelastic and fatigue characteristics of CNF modified bitumens. However, as authors highlighted, the main drawback of the preliminarily dispersion of CNFs into an opportune solvent is due to the use of a large quantity of solvent to disperse a small amount of CNF as well as the scalability for industrial applications. The authors recommended to further explore other mixing techniques to add higher percentages of CNF, with a minimum amount of solvent, without a significant increase in the modified binder viscosity at mixing and compaction temperatures of hot mix asphalt mixtures (HMA). In their work Khattak et al. have shown that regardless of mixing process, the fatigue life of CNF modified bitumens was 2–3 times the unmodified bitumens. According to the authors this is due mainly to crack bridging mechanism by CNF. Indeed, they believe that the CNF network may have bridged across the micro-cracks developed due to dynamic shear loading thus causing hindrance in their growth and consequently increasing the fatigue life of the CNF modified bitumen. Furthermore, it has been noticed that, while, the dry mixing process increased the$G^*/\sin\delta$ (the rutting parameter) up to 47%, the wet mixing process blends showed a slightly lower $G^*/\sin\delta$ at higher frequencies and higher values at lower frequency. The AC5 bitumen modified with CNF using the dry process exhibited $G^*/\sin\delta$ improvement up to 22% at 60 °C, while AC30 and PAC30 binders modified with CNF through a wet process have shown an improvement of the rutting parameter of 42%. The authors have also shown that the CNF wet modified bitumen at frequency $\leq 1Hz$ and in the temperature range from 25 to 64 °C has an average increase of $G^*/\sin\delta$ of about 2.5% - in contrast to the value of about 35% for PAC30 bitumen – while the average increase is 15% at frequency levels higher than 1 Hz and as temperature range from 20 to 1 °C. It has to be said that to our knowledge the only works on the topic of bitumen modification by carbon nanofibers are that by Khattak research group [169–171].

### 6.7. Functionalized nanoparticles: another solution to increase nanoparticles-bitumen affinity

Modifying the nanoparticles surface can cause higher compatibility between the matrix and the modifier thus avoiding agglomeration phenomena. The aim would be to functionalize the nanoparticle surface to change its hydrophobicity towards values more similar to the amphiphilic compounds present in the bitumen.

In this context, Karnati et al. [121] showed that the functionalization of silica nanoparticles can favour their dispersion within the bituminous matrix, and consequently improve their performance.

For this purpose, they modified an asphalt binder, PG 64–22, with silica nanoparticles (SNPs) whose surface had been functionalized with (3-aminopropyl) triethoxysilane (APTES)

FTIR demonstrated the correct functionalization of the nanoparticles, whereas fluorescence absorption and the DLS showed that the optimum is reached when a ratio of 1.6 is reached. In fact, from fluorescence absorption, it is possible to note as the amount of amine group generally increases with the increase of APTES, until saturation level at ratio 1.6. On the other hand, from the DLS they noted that the trend of the average size increase in value as the mass ratio increase, but this trend does not involve the sample with ratio 1.6.

Karnati et al. speculate that eventual increase in size takes place, due to an agglomeration phenomenon due to the hydrolysis of large quantities of APTES and the self-condensation reaction on the surface of the silica nanoparticles. On the contrary, with small amount of APTES these phenomena do not occur and correct functionalization occurs. Fig. 31 Scheme 1 shows the chemical reaction.

A Field Emission Scanning Electron Microscope (FESEM) analysis showed that modified nanoparticles are better distributed (Fig. 32) in bitumen with respect to the unmodified. In the figure panel a shows also evident agglomeration due to the presence of hydrophilic Si – OH groups, which are not very compatible with the hydrophobic components of bitumen. According to the authors, the amine functional group on the surface of modified nanosilica can create hydrogen bond or dipole-dipole interaction with polar group in the binder, favouring the stabilization of these nanoparticles within the bituminous matrix and disadvantaging their aggregation.

In order to evaluate the effect of modified and unmodified nanoparticles on the aging of asphalt binders, Karnati et al. analysed long-term aging samples. These samples were prepared according to ASTM D21.

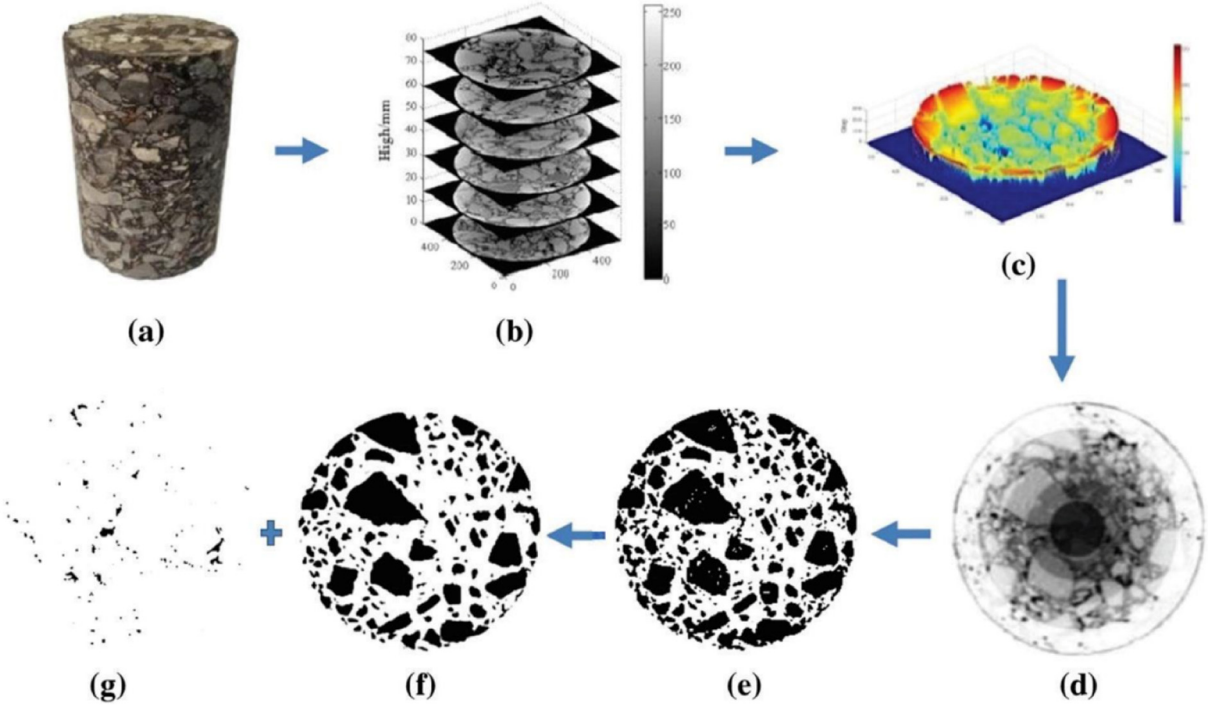


**Fig. 37.** Extraction of the area of interest using CT scan technology [190].

The mechanisms (hydrogen bond, dipole-dipole interaction) that stabilize the modified nanoparticles inside the binder could be the same that allow a 50% reduction of the VAI index (eq. 6) of the samples containing APTES/SNP compared to the samples with neat SNPs. Moreover, the surface functionalization of the nanosilica leads to a reduction of about 7% and 72% of the chemical aging index (CAI) for carbonyl and sulfoxide groups respectively. The CAI are obtained from eq. 12 and 13:

$$CAI_{Carbonyl} = \frac{Carbonylagingindex\ (agedsample) - carbonylagedindex\ (unagedsample)}{Carbonylagedindex\ (unagedsample)} \quad (12,)$$

$$CAI_{Sulfoxide} = \frac{Sulfoxideagingindex\ (agedsample) - Sulfoxideagedindex\ (unagedsample)}{Sulfoxideagedindex\ (unagedsample)} \quad (13,)$$

where *Carbonyl index* and *Sulfoxide index* are from Eq. 4 and eq. 5 respectively.

This notable difference in the reduction of the indices is justified by the authors considering that sulphur has greater electronegativity than carbon and the sulfoxide group is more polar than carbonyl. This would further favour dipole-dipole interactions and hydrogen bonds between the sulphur-containing functional groups of the binder and the modified nanoparticles. The rheological aging index (RAI) allows estimating the effect of modified and un-modified nanoparticles on the rheological properties of the asphalt binder.

APTES/SNPs shows, once again, better resistance to aging than SNPs with a decrease of about 42%.

An evaluation of the resistance to rutting and fatigue cracking can be carried out by calculating two different parameters $G^*/\sin\delta$ and

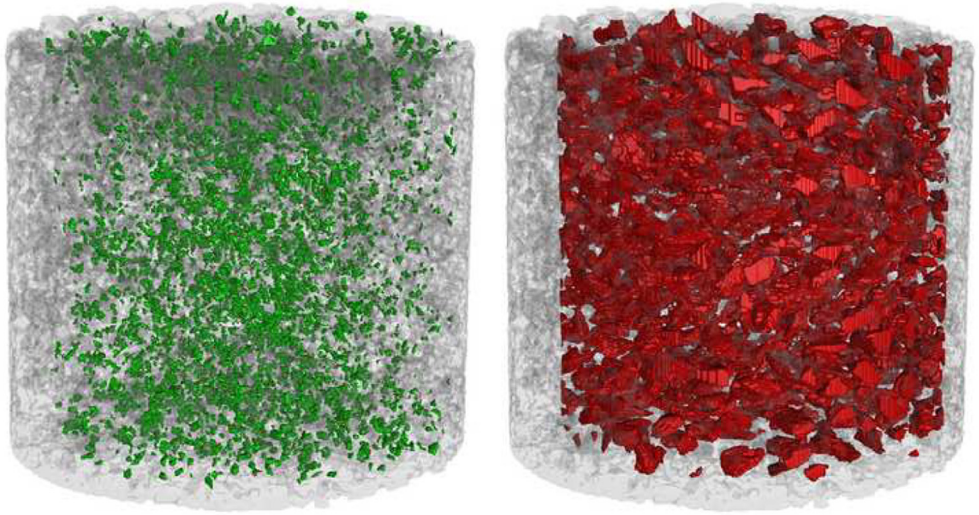

**Fig. 38.** 3D images of the whole cylinder, acquired by Rinaldini et al. [189], as discussed in the text. The spatial distribution inside the sample of the large virgin and small RAP aggregates is shown with different colors (red and green, respectively).

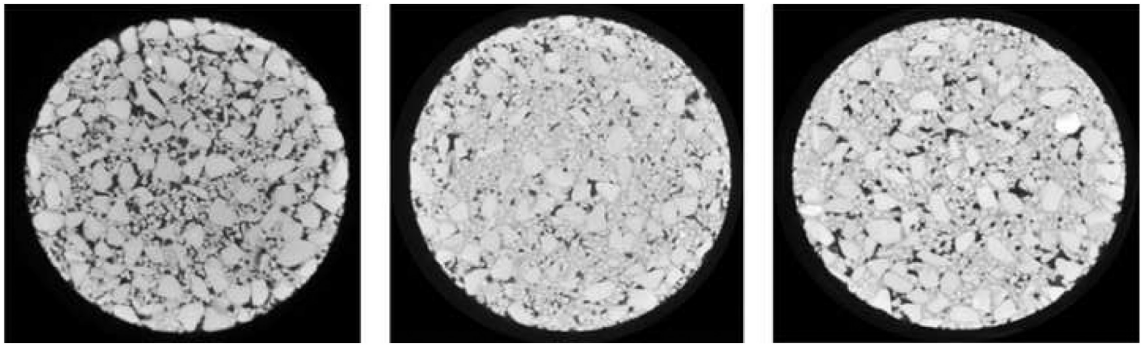

**Fig. 39.** Three cross-section images at three different heights: top, middle and bottom, from left to right, acquired by Rinaldini et al. [189].

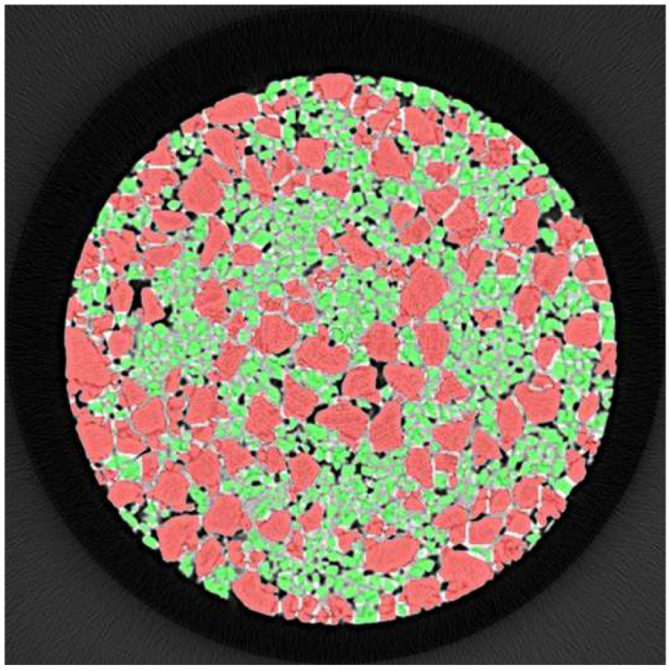

**Fig. 40.** Typical distribution of the mineral aggregates in a slide (see text for details), acquired by Rinaldini et al. [189].

$G^* \times sin\delta$. In general, samples exhibiting high $G^*/\sin\delta$ value should have a greater resistance to permanent deformation (rutting). However, it must be emphasized that it must be pointed out that there is hardly any mixture testing available to directly confirm the improvement of the permanent deformation behaviour. Conversely, samples exhibiting low $G^* \times sen\delta$ value should have a greater resistance to fatigue cracking. The sample containing the modified nanoparticles has the highest rutting parameter and the lowest cracking parameter. These results are obviously in line with those obtained previously, in fact the deformation and the formation of cracks inside the material is strictly linked to the aging of the material itself.

One of the main causes of deterioration of the road surface is cracking at low temperatures, which occurs both in cold regions and in regions that experience large temperature changes between day and night or between seasons of the year [172,173]. For this reason, fracture energy and ductility were measured in order to evaluate low temperature performance (Fig. 33). Both the unaged and aged samples modified with APTES/SNP increase fracture energy and ductility respect to unaged and aged sample modified with SNP. In more detail, the unaged samples have energy greater than about 26% and ductility of about 15%. While the aged samples show an increase in energy of about 205% and ductility of about 89%. Again, the authors justify the increase in fracturing energy thanks to the formation of hydrogen bonds and dipole-dipole interactions between the binder molecule and APTES/SNP. This would improve the interfacial bonding between the matrix and the modifier.

In another study, instead, Zhang et al. [110] used three different kinds of inorganic nanoparticles to improve UV aging resistance of bitumen. The authors used nano-$SiO_2$, nano-$TiO_2$ and nano-ZnO, with diameter between 20 and 50 nm, as such and treated with toluene containing

**Table 20**
Physical properties of the bitumen modified with different nanoparticles, analysed by Sun et al. [174].

| Dispersing condition (170 °C; 5.000 rpm; 30 min) | 25 °C penetration/ 0.1 mm | Softening point (°C) | 10 °C ductility (cm) | 60 °C viscosity (Pa s) |
|---|---|---|---|---|
| AH-70 | 64.5 | 49.7 | 18.1 | 299 |
| AH-70 + 5% $SiO_2$ | 61.2 | 55.8 | 10.5 | 667 |
| AH-70 + 5% $CaCO_3$ | 68.3 | 51.9 | 11.3 | 346 |
| AH-70 + 5% montmorillonite | 66.2 | 51.8 | 10.2 | 381 |
| AH-70 + 5% $TiO_2$ | 66.2 | 52.6 | 9.9 | 358 |
| AH-70 + 5% $Fe_2O_3$ | 62.1 | 51.6 | 10.2 | 361 |
| AH-70 + 5% ZnO | 63.4 | 51.0 | 10.4 | 345 |
| AH-70 + 5% bentonite | 61.6 | 53.5 | 10.0 | 380 |

**Table 21**
Test Physical properties of $SiO_2$ nanoparticle–modified bitumen using different coupling agents, analysed by Sun et al. [174].

| Dispersing condition (170 °C; 5.000 rpm; 30 min) | 25 °C penetration/ 0.1 mm | Softening point (°C) | 10 °C ductility (cm) | 60 °C viscosity (Pa s) |
|---|---|---|---|---|
| AH-70 | 64.5 | 49.7 | 18.1 | 299 |
| AH-70 + 5% $SiO_2$ | 61.2 | 55.8 | 10.5 | 667 |
| AH-70 + 5% $SiO_2$ + 1% K-1 | 53.5 | 55.3 | 7.7 | 630 |
| AH-70 + 5% $SiO_2$ + 2% K-1 | 61.7 | 56.8 | 9.0 | 778 |
| AH-70 + 5% $SiO_2$ + 3% K-1 | 61.2 | 55.6 | 8.3 | 745 |
| AH-70 + 5% $SiO_2$ + 4% K-1 | 65.0 | 55.5 | 10.9 | 650 |
| AH-70 + 5% $SiO_2$ + 1% K-2 | 65.4 | 54.0 | 13.2 | 443 |
| AH-70 + 5% $SiO_2$1.5%K-2 | 62.9 | 55.0 | 11.9 | 568 |
| AH-70 + 5% $SiO_2$2%K-2 | 68.2 | 53.3 | 11.3 | 170 |
| AH-70 + 5% $SiO_2$3%K-2 | 60.6 | 54.5 | 12.3 | 530 |
| AH-70 + 5% $SiO_2$3%K-3 | 61.3 | 53.4 | 12.1 | 638 |
| AH-70 + 5% $SiO_2$5%K-3 | 60.0 | 54.9 | 12.3 | 679 |
| AH-70 + 5% $SiO_2$7%K-3 | 54.7 | 55.1 | 12.4 | 745 |
| AH-70 + 5% $SiO_2$9%K-3 | 56.1 | 55.7 | 14.6 | 650 |

**Table 22**
summarizing scheme of the materials used to modify bitumens and asphalts with nanoparticles, together with the techniques used for their characterization the corresponding references (in chronological order) and the clues.

| Research | Materials | Size (nm) | Analysis/Techniques (Normative reference) | Matrix | Results |
|---|---|---|---|---|---|
| Jahromi et al. (2009) [101] | Clay (closite and nanofil) | See Tab. | Physical characterization** (ASTM: D113, D36, D5), Rheology (D7175), XRD | Fresh bitumen, Short-term aged, Long-term aged | - increased stiffness and resistance against aging as well as improved elastic properties;<br>- intercalation or exfoliation of the nanoclay |
| Wu et al. (2009) [104] | Clay (montmorillonite) | | XRD, Limiting oxygen index methods (ASTM D2863-77), DSC, Rheology (D7175), Physical characterization** (ASTM: D36, D5) | Fresh bitumen, Short-term aged (D2872), Long-term aged (D6521) | - montmorillonite and organically-modified montmorillonite (OMMT) are used to improve the rheological properties of bitumen and also to reduce its flammability;<br>- bitumen changes from being "fuel" to a "self-extinguishing" material;<br>- treated bitumen produced less smoke than the neat bitumen while burning |
| Ghasemi et al. (2012) [84] | $SiO_2$, SBS | 15 ± 3 | Physical characterization** (ASTM: D113, D36, D5), Marshall stability, Flow test (D1559), ITS (D4867), ITSM | Fresh bitumen, HMA | - indirect tensile strength progressively increases with nanoparticle content |
| Zhang et al. (2015) [137] | ZnO, EVMT | 15–25 | Physical characterization** (ASTM D36, D113, D5), Rotational viscosity (ASTM D4402), XRD, FTIR, UV spectroscopy, AFM | Fresh bitumen, Long-term aged (D6521), UV aged | - structural changes of asphaltenes clusters probably due to nucleating effect of inorganic nanoparticles, favouring a heterogeneous nucleation/crystallization of asphaltenes;<br>- thermo-oxidative aging is contrasted by EVMt, photo-oxidative aging is contrasted by nano-ZnO thanks to its semiconductor nature |
| Du et al. (2015) [116] | ZnO | 15–25 | Physical characterization** (ASTM: D5, D36, D113), Rheology (JTG E 20-T 0628–2011), Rotational viscosity (ASTM D4402), AFM, FTIR | Fresh bitumen, Short-term aged, UV-aged bitumens | - nano-ZnO changes morphology, increases the viscosity and reduces ultraviolet (UV) aging of bitumens;<br>- the effect of nano-ZnO depends on the bitumen nature |
| Arabani et al. (2015) [157] | Carbon nanotubes | 10–20*** | ITSM (ASTM D4123), Repeated load axial test, ITF (ASTM D4123), SEM, | HMA | - improvement of the mechanical performance of the hot mix asphalt (HMA);<br>- CNTs gives stiffness increase and strain decrease regardless of the stress applied |
| Li et al. (2015) [109] | ZnO | | FTIR, SEM, Physical characterization** (ASTM: D5, D36, D113), Rotational viscosity (ASTM D4402), Compatibility test (JTG E 20-T 0661–2011), UV spectroscopy | Fresh bitumen, Short-term aged, UV aged | - ZnO nanoparticles are used for increasing resistance of bitumen to ultraviolet aging;<br>- better dispersion of the nanoparticles inside the bitumen is achieved if nanoparticles are surface silano-modified |
| Zhang et al. (2015) [110] | $SiO_2$, $TiO_2$, ZnO | 20–50 | Storage stability, Physical characterization** (ASTM: D5, D36, D113), UV spectroscopy | Fresh bitumen, UV aged | - nanoparticle surface modification improves their dispersion and gives greater effect on the shielding of UV radiation;<br>- same arguments as in Chen et al. 2015 [133] |
| Galooyak et al. (2015) [86] | $SiO_2$, Sasobit | 20–30 | Physical characterization** (ASTM: D113, D36, D5), Rheology, ITS (ASTM D6931), Resilient modulus test (ASTM D4123), Rutting in Wheel Tracking (AASTHO T324) | Fresh bitumen, WMA | - decrease in penetration and ductility and increase in softening point with the nanoparticle content;<br>- modified bitumen has better resistance against rutting at heavy loading condition;<br>- resilient modulus increases as a function of the nanosilica content;<br>- fatigue life of the WMA is higher for samples containing nanoparticles;<br>- direct relationship between the nanosilica content and the number of loading cycles required for cracking |
| Chen et al. (2015) [133] | $SiO_2$, $TiO_2$, ZnO, EVMT | 15–20 | Rheology (ASTM D7175), XRD | Fresh bitumen, Short-term aged (ASTM D1754), Long-term aged (ASTM D6521), UV aged | - modified samples have better resistance to fatigue and higher thermal stability;<br>- nano-$TiO_2$ and nano-ZnO show better anti-aging effect;<br>- nano-$TiO_2$ has antiaging effect even in the case of photo oxidation |
| Le et al. (2016) [146] | Graphene, SBS | | Rheology (AASHTO T315-12), Creep stiffness (AASHTO T313-12), Strength test | Fresh bitumen, Short-term aged (AASHTO T240), Long-term aged (AASHTO R28-12), asphalt mixture | - the addition of graphene affects only a small part of G * and does not affect the relaxation properties of the bitumen;<br>- - the creep stiffness of the asphalt mixture treated with grapene is strongly influenced by the analysis temperature and by the temperature at which the aspahlt mixture is compacted |
| Brcic (2016) [151] | Graphene | | Rheology, Creep stiffness (D7-405–10a), PG (ASTM D6373-07) | Fresh bitumen, Short-term aged, Long-term aged | - graphene modified binder is stiffer than the fresh bitumen;<br>- $\frac{G^+}{sen\delta}$ and $G^+ sen\delta$ are affected by dispersion and mixing time; |

**Table 22** (*continued*)

| Research | Materials | Size (nm) | Analysis/Techniques (Normative reference) | Matrix | Results |
|---|---|---|---|---|---|
| | | | | | - increase in *E*-modulus depending on the mixing time and the percentage of graphene |
| Hamedi et al. (2016) [111] | ZnO | 20 | ITS (AASHTO T283), Surface free energy | Fresh bitumen, HMA | - nano-ZnO improves the adhesion between bitumen and aggregates (antistripping) especially in the case of moisture--conditioned samples;<br>- nanoparticles lower the acidity of the bitumen, favouring the adhesion between the bitumen itself and acid aggregates (i.e. granite) |
| Taherkani et al. (2016) [88] | $SiO_2$ | 11–13 | SEM, Physical characterization** (ASTM: D113, D36, D5) | Fresh bitumen | - strong tendency to form a network of aggregates responsible for the mechanical properties of the modified binder |
| Nejad et al. (2016) [107] | $TiO_2$, ZnO, $Al_2O_3$, $Fe_2O_3$ | 10–25, 10–30, 20, 40 | Physical characterization** (ASTM: D36, D5, D113), Rotational viscosity (ASTM D4402), Flash point (ASTM D 3143), SEM, Static creep test | Fresh bitumen, HMA | - comparison of different inorganic nanoparticles: finding specificities of nanoparticles in creep rate and strain modulus values of Hot Mix Asphalt at various loads |
| Jeoffroy et al. (2016) [131] | $\Upsilon$-$Fe_2O_3$, $Fe_3O_4$, Oleic acid | 20–40, 20–30 and 50–100 | XRD, SEM, ATR-FTIR, TGA, DLS, Magnetization measurements, Thermal response under an alternating magnetic field | Fresh bitumen | - viscosity reduction of bitumen;<br>- closing of micro-cracks |
| Mubaraki et al. (2016) [117] | $Al_2O_3$, Acrylate Styrene Acrylonitrile (ASA) | 13 | Rotational viscosity, Storage stability, Rheology | Fresh bitumen | - increase in viscosity, softening point temperatures, storage stability and resistance against rutting by addition of Nano-$Al_2O_3$ |
| Zeng et al. (2017) [176] | Graphene Oxide | | Rheology, Physical characterization** (ASTM D564, ASTM D3626), Pyrolysis-gas chromatography test | Fresh bitumen, Short-term aged (ASTM D1754), Long-term aged (ASTM D6521) | - improve high-temperature property by showing higher $G^*$and lower phase angle<br>- improve low-temperature property by exhibiting smaller complex modulus and larger phase angle;<br>- increase anti-aging property but not so obvious;<br>- 1% GO performs better than 3% GO in terms of low temperature and cost; CO2 is released when mixing at 115 °C |
| Ali et al. (2017) [119] | $Al_2O_3$ | 13 | Physical characterization** (ASTM D5, D36, D113), Rotational viscosity (ASTM D4402), Storage stability, FE-SEM, FTIR, XRD, Rheology | Fresh bitumen | - penetration decreases and softening point increases;<br>- nanoparticle can give better elastic recovery, better resistance to rutting and increased failure temperature, increased resistance to permanent deformation, decrease of the compliance |
| Sun et al. (2017) [174] | $SiO_2$, $TiO_2$, $CaCO_3$, ZnO, Montmorillonite, Bentonite, $Fe_2O_3$ | 15, 35, 30, 30, 25, 25, 20 | Physical characterization** (JTJ 052–2000), Rheology, SEM, FTIR, Creep stiffness, Direct tension test, GPC, DSC, | Fresh bitumen, asphalt mixture | - nanoparticles modification gives softening point and viscosity general increase and parallel decrease in ductility;<br>- best improvement of high temperature performance by nano-siclica;<br>- attention focused on this modifier |
| Nejad et al. (2017) [95] | $SiO_2$, $TiO_2$, $CaCO_3$ | 20–30, 20, 10–45 | DSC, Rheology | Fresh bitumen | - comparative study among $SiO_2$, $TiO_2$ and $CaCO_3$;<br>- increase in the transition glass temperature with the nanoparticle content |
| Sadeghnejad et al. (2017) [91] | $SiO_2$, $TiO_2$ | 80, 30 | Physical characterization** (ASTM: D5, D36), Kinematic viscosity (ASTM D2170), Rheology (ASTM D7175) | Fresh bitumen | - comparison between nano-silica and nano-titania;<br>- difference in chemical compatibility between nanoparticles and bitumens |
| Hussein et al. (2017) [96] | Ceramic powders | 16 | XRF, TEM, XRD, FTIR, Physical characterization** (ASTM: D5, D36), Rheology, AFM, TCLP (EPA SW846-1311) | Fresh bitumen | - reuse of waste from ceramic materials industries as possible modifiers for bitumen;<br>- the high surface energy and strong surface tension of ultrafine nanoparticles favour the agglomeration of nanoparticles |
| Shafabakhsh et al. (2018) [124] | CuO | 40 | FE-SEM, Rheology (ASTM D7175), Creep stiffness (AASHTO T313) | Fresh bitumen, Short-term aged (ASTM D1754), Long-term aged (ASTM D6521) | - nano-CuO addition to bitumen and to aged bitumens enhances their resistance to rutting deformations but only at temperatures lower than 64 °C;<br>- nano-CuO enhances the fatigue cracking of the virgin bitumen |
| Li et al. (2018) [177] | Graphene Oxide | 10–50 μm | FTIR, XRD, TG test, GC–MS test, Physical properties** (ASTM: D5, D36, D113), Rheology, Rotational Viscosity (ASTM D4402) | Fresh bitumen, SBS modified bitumen | - increase $G^*$, reduce phase angle slightly;<br>- increase resistance to plastic deformation by higher elasticity;<br>- increase cracking risk due to brittleness;<br>- faster heat transfer at 0.5% dosage, the effect remains constant |

(*continued on next page*)

**Table 22** (*continued*)

| Research | Materials | Size (nm) | Analysis/Techniques (Normative reference) | Matrix | Results |
|---|---|---|---|---|---|
| Nazari et al. (2018) [92] | $SiO_2$, $TiO_2$, $CaCO_3$ | 20–30, 30, 10–45 | XRD, SEM, FTIR, Rheology (TP101-14) | Fresh bitumen, Short-term aged bitumen (AASTHO T240), Long-term aged bitumen (AASTHO R28) | - comparative study among $SiO_2$, $TiO_2$ and $CaCO_3$;<br>- silica are the particles giving greatest fatigue resistance;<br>- detected a possible antioxidant effect attributable to nano-$TiO_2$ and nano-$CaCO_3$ |
| Crucho et al. (2018) [85] | $SiO_2$, Zero-Valent Iron, Clay | 70, 50, 1–2 | Affinity test (EN 12,697–11), Stiffness test (EN 12697–26), Fatigue test (EN 1269–24), Wheel Tracking test (EN 1269–22), ITS (EN 1269–23) | Fresh bitumen, asphalt mixture | - hydrophilic bentonite and zero-valent nano-iron have better affinity with bitumens; |
| Liu et al. (2018) [178] | Graphene Oxide, Sasobit, Waste Cooking Oil | | Rheology, MSCR (AASHTO T316-13), FTIR, DSC, Rotational viscosity (AASHTO T316-13) | Fresh Bitumen, HMA, WMA | - improve rutting resistance, failure temperature, creep/recovery behaviour |
| Moreno-Navarro et al. (2018) [148] | Graphene | | Raman spectroscopy, XPS, Optical microscopy, Rheology, Softening point test (EN 1427), Thermal conductivity | Fresh bitumen | - graphene addition to the neat bitumen modifies the typical shape of bee structures;<br>- graphenes give stiffer bitumens with improved elastic behaviour |
| Loise et al. (2019) [160] | Carbon nanotubes | 17–20 and 50–120 | TEM, XRD, Raman spectroscopy, Rheology, TGA | Fresh bitumen | - higher defectiveness in MWNTs gives better improvement of the rheological properties, with probable formation of networks bridged by MWNTs defects |
| Karnati et al. (2019) [121] | $SiO_2$ | 12 | FE-SEM, FTIR, Hydrodynamic diameter, Zeta potential, Rotational viscosity (D4402), Rheology (ASTM D7175-15), Direct tension test (ASTM 6723–12) | Fresh bitumen, Long-term aged (ASTM D 2872–13, D6521) | - functionalization of silica nanoparticles can favour their dispersion within the bituminous matrix;<br>- it can improve the rheological performance (reduction of the chemical aging index for carbonyl and sulfoxide groups);<br>- higher rutting parameter and lower cracking parameter;<br>- mechanism is studied: modification of nanoparticles increases the interfacial bonding between matrix and the modifier |
| Zghair et al. (2020) [89] | $SiO_2$ | 11–12 | Physical characterization**, Rotational viscosity test | Fresh bitumen | - penetration value and ductility decrease with the amount of nanosilica;<br>- softening temperature and rotational viscosity increase with the nanosilica content;<br>- the properties of the binder improve with increasing mixing times |
| Yang et al. (2020) [162] | Carbon nanotube sponges | 40 | SEM, DSC, TGA, Rheology, | Fresh bitumen | - good dispersion of CNTs-sponge with the formation of a continuous and highly porous network with bitumen;<br>- improvement of stability at high temperatures;<br>- improvement of rheological properties, resistance to rutting and elastic recovery |
| Sedaghat et al. (2020) [102] | Clay (montmorillonite), Sasobit | 1–2 | XRD, Physical characterization**, Kinematic viscosity, Rheology (ASTM D4402), Creep tests, Rotational viscosity (AASHTO M320), PG | Fresh bitumen, Short-term aged, Long-term aged | - nano-montmorillonite (size 1–2 nm) is tested after organo-modification to make it organophilic for a better dispersion in bitumen |

** Softening point, Ductility, Penetration.
*** Refer to the diameter of the nanotubes.

γ-(2,3-epoxypropoxy) propyltrimethoxysilane as silane coupling agent to modify the nanoparticles surfaces. The bitumen chosen for this research had the following physical properties (Table 19):

The authors noted that while for the unmodified nanoparticles the best compatibility is obtained with nano-$SiO_2$, in the case of the modified nanoparticles the highest compatibility is obtained with nano-ZnO.

The effect of nanoparticles on bitumen subjected to photo oxidation was assessed through the Increment in Softening Point (ISP) and VAI indices. The VAI index was previously defined in Eq. 6, while the ISP index can be calculated using the underlying equation:

$$ISP = Agedsofteningpointvalue - Unagedsofteningpoint\ value \quad (14)$$

In general, the addition of the nanoparticles reduces both indices, especially when nano-ZnO is added.

In particular, the VAI and ISP indices decrease more in the case of modified nanoparticles. This highlights the improvement effect of the surface modification of the nanoparticles on the bitumen resistance to UV aging. Indeed, the surface modification improving the dispersion, making it more uniform, and has a greater effect on the shielding of

**Table 23**
Characteristics of mineral and bitumens used in the study by Rinaldini et al. [189].

| Sample name | Virgin mineral | | | RAP | | | Virgin bitumen | | |
|---|---|---|---|---|---|---|---|---|---|
| | Fraction size (mm) | Amount (g) | Mass (%) | Fraction size (mm) | Amount (g) | Mass (%) | Pen grade | Amount (g) | Mass (%) |
| MxD | 8/11 | 10,000 | 47.17 | 2/4 | 10,000 | 47.17 | 70/100 | 1000 | 4.72 |

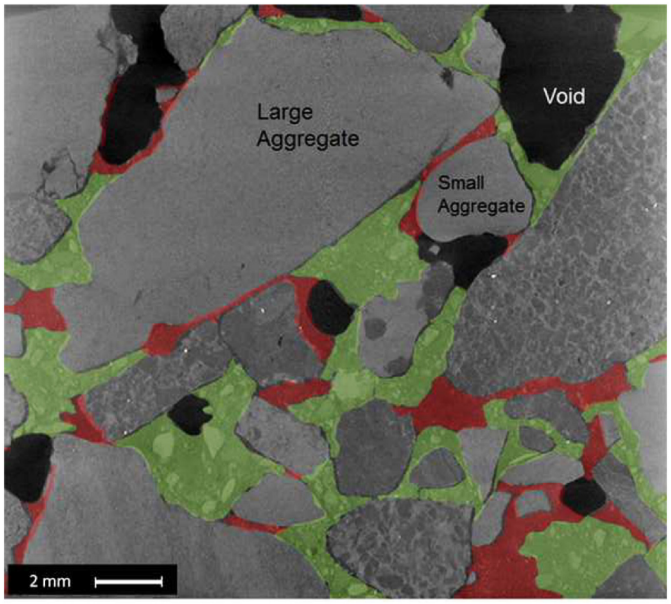


**Fig. 41.** spatial distribution of the virgin and RAP components (higher magnification), acquired by Rinaldini et al. [189].

UV radiation. On the other hand, the same more uniform dispersion of the nanoparticles, causes lesser aggregates thus diminishing scattering of the UV radiation within the samples given by big particles

Self-consistently with the semiconductor nature of the studied nanoparticle, the authors found that nano-ZnO has a greater improvement effect than nano-$TiO_2$ thanks to its longer absorption wavelength (370 nm vs 300 nm of the nano-$TiO_2$) allowing more radiation absorption. Such kind of reasoning have been used in the paragraph 6.6.1. dedicated to organic vermiculite.

Also Sun et al. [174] used modified nanoparticles demonstrating that their modification can give better performances especially at high temperatures. For this purpose, they used three different kinds of coupling agents: silane (K-1); stearic acid (K-2) and polyethylenimmine (K-3), and seven different nanoparticles: $SiO_2$; $CaCO_3$; montmorillonite; $TiO_2$; $Fe_2O_3$; ZnO and bentonite. The particles sizes were 15; 30; 25; 35; 20; 30 and 25 nm respectively.

After having ascertained the softening point and viscosity general increase, parallel to the decrease in ductility (Table 20), as a consequence of nanoparticle addition to the bitumen, the authors noted that the highest effect was given by $SiO_2$ at high temperatures. Being the ultimate goal of this research to improve the performance of the binder at high temperatures, Sun et al. decided to focus only on silica nanoparticles.

So, the authors tested the silica nanoparticles at three different concentrations (3, 5 and 7%) observing a parallel increase in the softening point and viscosity and a decrement of penetration and ductility decrease. The ductility reduction indicates a worsening of physical properties at low temperatures.

Although not specified in the study, the sample containing 5% nano-SiO2 is a good compromise for improving performance at high temperatures without worsening those at low temperatures too much. In fact, the authors have treated only the 5% modified sample with the coupling agents.

Interestingly the authors improved the methodology for surface modification of nanoparticles. The previous procedure involved dosing the coupling agents on the amount of bitumen. Instead, in the new procedure the percentage by weight of coupling agents is calculated with respect to the quantity of nano-$SiO_2$. As can be seen from the table (Table 21), the physical properties are strongly influenced by the type of agent used. Moreover, although the quantity of coupling agents is very low compared to the quantity of binder, their effects are remarkable. 2% K1; 1.5% K2 and 7% K3 are the samples with the greatest improvement in properties. In particular, the sample modified with 2% K1 had a most marked increase in softening point and viscosity respect to AH-70 + 5% $SiO_2$. Consequently, this sample was selected for rheology tests.

The analysis carried out on the sample containing 2% of coupling agent K1 were carried out in accordance with the Superpave system. The low temperature grade was determined through BBR (Bending Beam Rheometer) and DT (Direct Tension) test. Instead, high temperature grade was evaluated through rutting factor, $G^*/\sin\delta$. The addition of modified nanosilica strongly improved the high temperature performance. The authors also carried out a frequency sweep test from 0.1 to 10 Hz, in order to evaluate the ZSV (Zero Shear Viscosity). They used the Cross model proposed by Sybilski [175].

This model involves the calculation of the ZSV, through the fitting of the frequency sweep curves.

$$\left(\eta_0-\eta_\infty\right)\Big/_{\left(\eta-\eta_\infty\right)} = 1+(K\omega)^m \tag{15}$$

Where $\eta$ is the complex viscosity; $\eta_0$is first Newtonian region viscosity (ZSV); $\eta_\infty$ is second Newtonian region viscosity; K is a material parameter; $\omega$ is the frequency and $m$ is a dimensionless material parameter. Through an approximation it is possible to write the Eq. as:

$$\eta = \eta_0\Big/_{1+(K\omega)^m} \tag{16}$$

The authors compared the ZSV value with the viscosity measured through Brookfield apparatus. They noted that in both case the modified sample had a higher viscosity.

From Fig. 34 it is clear a thixotropic behaviour of the asphalt binder. The effect of the modified nano-$SiO_2$ decrease as the frequency increase. In fact, when the frequency exceeds 1 Hz, the trend of the modified asphalt curve's is almost equal to that of the unmodified asphalt. In conclusion, the modified binder will perform better at high temperatures, but, conversely, as the temperature decreases the sample becomes more rigid and cracking phenomena are more likely to occur.

In addition, Sun et al. performed, on asphalt mixtures, rutting test at 60 °C to evaluate the high temperature stability, and bending test at −10 °C in order to assess low temperature crack resistance. Also, the immersion Marshall tests and freeze-thaw split tests were conducted to analyse the water stability of asphalt mixture. From these tests it is possible to note an increasing in the dynamic and residual stability, stiffness modulus and tensile strength ratio with the addition of modified nano-$SiO_2$.

A summarizing scheme of the materials used to modify bitumens and asphalts with nanoparticles, together with the techniques used for their characterization the corresponding references (in chronological order) and the clues is reported in Table 22.

## 7. Perspectives

### 7.1. Vanguard techniques

We have already discussed about promising techniques for bitumen characterization. Recently, we have demonstrated that an accurate use

**Table 24**
Cost evaluation of typical asphalt mixtures.

| Materials | Average Unit Prices (€/ton) |
|---|---|
| Bitumen 35/50 | 350 |
| Natural aggregates | 10 |
| Electric Arc Furnace Steel Slag aggregates | 3 |
| Reclaimed Asphalt Pavement aggregates | 5 |
| Recycled Concrete aggregate | 5 |
| Warm Mix Asphalt additive | 2500 |

**Table 25**
Costs of Carbon Nano Tubes (CNT), Graphene Nano Platelets (GNP) and Graphene Oxide (GO) (obtained from [https://nanografi.com/] [195] and [https://www.us-nano.com/inc/sdetail/494] and slightly implemented with other information taken from bibliography).

| Materials | Purity (%) | Specific Surface Area (SSA) ($m^2/g$) | Unit Price (€) (per gram) |
|---|---|---|---|
| Nano $SiO_2$ | 97 | 50 ÷ 95 | 38 (a) |
| | 97 | 95 ÷ 140 | 40 (a) |
| | 99.5 | 45 ÷ 80 | 26 |
| | | 130–600 | 0.08–0.15 (b) |
| | 98–99.5 | / | 1.59–6.52 (c) |
| Nano Iron | 99.55 | 4.5 ÷ 10 | 17 |
| | 99.55 | / | 4.8 |
| | / | / | 0.1–2.6 (b) |
| $Fe_2O_3$ | / | >55 | 3.4 |
| | / | / | 0.1–0.3 (b) |
| | 98–99.9 | / | 4.42–10.25 (c) |
| $Fe_2O_3$ (5 nm) | 99.9 | / | 11,49 (c) |
| Nano ZnO | 99.99 | 20 ÷ 65 | 1.48 |
| | 99–99.9 | / | 1.23–1.94 (c) |
| Nano CuO | 99.99 | >20 | 2 |
| | 99.995 | 15 | 7.2 |
| | 99–99.95 | / | 1.24–9.8 (c) |
| Nano $Al_2O_3$ (gamma) | 99.55 | 60 | 5.2–9 |
| | 99–99.99 | / | 1.59–6.88 (c) |
| Nano $Al_2O_3$ (alfa) | 99.95 | >10 | 1.8–4.8 |
| | 99–99.99 | / | 1.34–4.94-(c) |
| Nanoclay (800 nm) | 99.9 | / | 1.16 |
| Single Walled CNT (SWCNT) | > 65 | 400 | 65 |
| | >92 | 400 | 90 |
| | >95 | 400 | 159 |
| | >96 | 570 | 195 |
| | >60 - >98 | / | 54.72–263 (c) |
| Double Walled CNT (DWCNT) | > 65 | / | 43 |
| | >60 | / | 51.21 (c) |
| Multiwalled CNT (MWCNT) | >92 | 220 | 1.5–2.1 |
| | >95 | 50 | 33 |
| | >95 | / | 30.90–34.43 (c) |
| | >96 | 50 | 27 |
| | | 220–240 | 29–33 |
| | | 510 | 19 |
| Graphene Nanoplatelets (GNP) | 99.9 | 320–800 | 6–7 |
| | 99.9 | 170 | 9–11 |
| | >99.9 | 135–170 | 7–9 |
| | 95–99.5 | / | 15–114 (c) |
| Graphene Oxide (GO) | 99.8 | ≥420 | 68 |
| | 99.5 (single layer) | / | 165 |
| | 99.3 (single layer) | / | 172.32 (c) |
| Reduced Graphene Oxide (rGO) | / | 1562 | 48 |
| Carbon Nanofibers (CNF) | >96% | 20 | 14 |
| | >95% | / | |
| | | | 65 (c) |

(a) Laser Synthesized; (b) from [193]; (c) from [194].

of rheology [179,180], of X ray scattering [71] and Nuclear Magnetic Resonance [51,52, 181] have proven to be able detailed information both from the structural and from the dynamical point of views.

However, it is strong belief that the synergic use of these different techniques can give an even better comprehension of the complex physical-chemistry involved in these materials [53,54,72,182].

For our considerations and for perspectives the reader is referred to the references just cited.

However, for the characterization of (nano)particles-containing bituminous materials, usually microscopies are used for having a "vision" of the structure. Atomic Force Microscopy can reach strikingly high resolutions and be coupled to quantitative nanomechanics to probe the local mechanical characteristics of the material [183,184].

Scanning Electron Microscopy (SEM) is very versatile and, as it is well known, it can be coupled to Energy Dispersive Spectroscopy (EDS) to probe the chemical composition. However, they are essentially surface methods and therefore they are not fit for probing the inner part of the material.

Given the specific peculiarities of nanoparticles-filled bitumens, we would like to point out the specific use of a modern, emerging technique: nanotomography. Nanotomography, much like its related modalities tomography and microtomography, uses x-rays to create cross-sections from a 3D-object that later can be used to recreate a virtual model [185]. This is a nondestructive technique and can probe the distribution of nanoparticles within the bulk of the whole sample. The term nano is used to indicate that the pixel sizes of the cross-sections are in the nanometer range. In this context, X-ray computed tomography (XCT) acquires radiographic projections from many different viewing angles from 0 to 180 degrees to perform 3D internal structure reconstruction by suitable algorithms. The latest developments have led to XCT systems with nano or submicron resolution. In XCT technique the X-ray beams carry various wavelength and energy (polychromatic). The attenuation μ of these X-rays inside the object is energy-dependent and therefore the parameter μ(E) is not constant. By using X-ray filters, it is possible to reduce the contribution of the parameter μ and finally get approximate information on the density of the object. For most samples, the density will provide an idea of the internal structure. The major difference between Nano Computer Tomography (nano-CT) scanning and other types of X-ray tomography technique is their pixel size in the cross-section images in the nanometer range. The accuracy depends

on the size of the scanned object. As a rough estimation, the size of pixels is approximately 1000 times smaller than the original dimension. For instance, scanning a sample of 0.5 mm diameter can result in 500 nm pixels. Applications for micro- and nano-CT can be found in many areas of research and development like: materials science, geology, biomedical engineering, dentistry, bio-engineering, building engineering – all using the XCT systems all dealing with materials of which the fine internal structure or the changes within the material are of outmost importance to understand the behaviour of the material or to have insights in the processes going on. Nanotomography technique in particular was used by different authors to analyse and reconstruct the 3D structure of bitumen modified with different nanomaterials. Liu et al. [186] for example used nano-CT scanning equipment to investigate the distribution of nano-scale montmorillonite particles in the asphalt system. Fig. 35 presents the 3D distribution image of sodium montmorillonite particles in the bitumen at the maximum resolution (about 1 μm) of the CT scanning equipment and Fig. 36 a is its 2D segment image. It seemed that parts of sodium montmorillonite particles were dispersed in the bitumen like the conventional filler at micrometer scale. This corresponded to the weak change of its XRD curves before and after mixing with bitumen. It was not possible to visualize the octadecyl trimethylammonium montmorillonite ($OTAC^{+}Mt$) particles in Fig. 36 b for its high dispersion in the bitumen.

M. Mohajeri et al. [187] used the XCT technique to study the interaction of the bitumen in a Reclaimed Asphalt Pavement (RAP) and a virgin bitumen used to blend it for new pavement surfacing. In particular, they observed that since density varies due to the type of the binder, the nano-CT scanning can be used for visualizing the interface between two binders of different densities.

However, more commonly the XCT technique is used to study the voids or to know the exact distribution of certain compounds, to understand their effectiveness inside the asphalt concrete. For example, in [188] a rejuvenator for pavement restoration were studied using an industrial CT scan. In many cases, with the assistance of the CT scan, correlations between the mechanical behaviour of the asphalt mix and its internal microstructure are investigated.

For example, Rinaldini et al. [189] used computer tomography (CT), among other techniques, to study the blending of virgin materials (virgin aggregates and bitumen) with reclaimed asphalt pavement (RAP) for new asphalt concrete production. From the structural point of view, being asphalt mixtures heterogeneous materials, composed of aggregates, asphalt, and porous networks their mechanical properties depend on many factors, such as the form and the distribution of the aggregate, the asphalt content, the pore content, pore distribution, and so on. The CT scan is of great assistance, as it generates the exact geometry of the internal structure of the asphaltic mixture as depicted in Fig. 37.

In [189] the authors investigated the nature of blending of virgin materials with reclaimed asphalt pavement (RAP). A small quantity of $TiO_2$ as a tracing agent of the virgin bitumen is used for CT investigation. Characteristics are reported in Table 23.

Samples were mixed by mixing a machine and compacted through a Superpave gyratory compactator to obtain a compacted cylindrical sample of 150 mm diameter x 120 mm height, which was then cut into 8 slices along the cylinder's axis to be analysed by micro-CT measurements and further prepared for electron microscopy.

From the tomographic images of the cylindrical specimen the distribution of the two types of virgin and RAP materials in the compacted mixture can be analysed. Fig. 38 shows 3D images of the whole cylinder, the spatial distribution of the large virgin (shown in red) and small RAP aggregates (shown in green) inside the sample, indicating the existence of the both materials within the sample as a whole.

Fig. 39 instead, shows three cross-section images at three different heights: one from the top, one from the middle and one from the bottom to compare the different compaction degrees.

These images indicate qualitatively that the distribution of the mineral aggregates is not homogeneous and varies according to height and within each slice. Fig. 39 displays visually determined regions of big aggregates (virgin material) very close to each other (highlighted in red) and those of RAP with small aggregates (highlighted in green); suggesting that both materials (virgin and RAP) are not homogeneously mixed. This characteristic appears to be repeated at every height (Fig. 38).

In order to gain more insight into the distribution of the constituents in the micro-scale structure, micro-CT scans were performed on a reduced area (50 mm × 30 mm × 10 mm). As shown in Fig. 40, at this scale, the spatial distribution of the virgin and RAP components can be seen at a higher resolution (Fig. 41).

Red highlighted areas indicate zones dominated by the virgin binder; whereas in green highlighted areas indicate zones dominated by the RAP binder. This distinction is done due to the fact that the RAP material includes filler and other small aggregates whereas the virgin binder does not. It is clearly possible to observe that the virgin and RAP materials are grouped in homogenous but distinct clusters. These cluster are a few millimeters in size. From these images however it is not possible to verify if blending between the virgin and RAP binders occurred. It can be seen that around the large aggregates there are both chunks of RAP components and of virgin bitumen. This phenomenon was noticed during the mixing process as the large aggregates were partially dark after being mixed with RAP aggregates even before the virgin binder was added, indicating that a distinct quantity of bitumen from RAP was mobilized and migrated to the virgin aggregates.

Although these results are for a specific mixture some preliminary conclusions can be drawn. The blending degree commonly estimated and used in practice is an average value not representing local physical properties such as local lack of adhesion between the old and new material and existence of micro-cracks that could lead to material failure. In order to obtain a complete picture of the compacted materials' behaviour it is beneficial to use a multi-scale approach. The CT images give information on the laboratory scale samples that are used for standard material characterization, whereas the micro-CT and ESEM provide a snapshot of particular locations and allow more detailed investigations.

### 7.2. Cost evaluation

Use of nanoparticles implies costs, so few words about the costs involved in asphalt pavement construction are due. They depend on different factors as depicted by Martinho et al. [191]. From their work we report some essential data in the Table 24, redirecting the curious reader to the original paper. In particular the authors analysed the costs of a typical asphalt mixture with and without recycled aggregates, to evaluate the expected influence of incorporating for example artificial aggregates come from the modification of materials subjected to processes that may involve physical and/or chemical changes, like the electric arc furnace steel slag (EAFS), the reclaimed asphalt pavement (RAP), the reclaimed concrete aggregates (RCA) as non-conventional aggregates, as well as equipment, labor, profits and so on.

Compared to the typical costs of production of asphalt concrete reported in Table 22, the cost of nanomaterials, as asphalt additives, is relatively high, due to the highly controlled materials synthesis, to their high purity levels (≥ 98%), the use of expensive equipment and technology and the highly qualified personal involved and so on.

When considering their high cost, however, it must be taken into account for the amount of nanoparticles contained in asphalt concrete: the nanoparticle content in bitumen is 1–5% *w*/w and the bitumen content in asphalt concrete is of the same order of magnitude as shown in Fig. 1. It turns out that any ton of asphalt concrete contains ~1 kg of nanoparticles

Generally, the price of the nanomaterials is highly dependent on the particle's size range specific surface area and/or other structural properties which, in turn, depend on the complexity of the apparatus involved in their production as well as the skill of the people involved. Products

with high purity and narrow size range and high specific surface may demand higher processing efforts, thus having higher final costs. However, it is very difficult to assess very accurate prices for these nanomaterials due to the numerous variables involved in their production. As an example, even the container bag can cause price variations as reported for example in [192] where Si nanoparticles / nanopowder (Silicon, 98 + %, 30–50 nm, Laser Synthesized, Polycrystalline Structure) in in anti-static aluminium bag has a price about 5 times higher than if the sample is sold in a common bottle.

In the following, we report some common mean prices as it can be found on sellers' websites keeping in mind that lower or higher prices can be found as highlighted above. To help the reader, in Table 24 are collected the costs of the various bitumens and asphalts discussed in this review, while Table 25 presents the main characteristics (purity and specific surface area) and the costs of some representative nanomaterials as obtained from NanoGrafi (https://nanografi.com/) and the web site https://www.us-nano.com/inc/sdetail/494 and slightly implemented with other information taken from bibliography.

The prices for nanosilica particles can vary from 80 €/kg to 1500 €/kg according to the size and, above all, size polidispersity. Nanosilica modifications obviously increase the overall costs, depending on the kind of modification and the substrate. Silane modified silica nanoparticles can cost between 180 €/kg to 450 €/kg. Raw nanoclays with natural hydrophilic behaviour are cheap, but their organic modifications are expensive due to the additional surface treatment process.

A bit more expensive, as expected, are nanoiron particles (range 100 €/kg - 2600 €/kg, depending on purity level and size range). As an example, the zero-valent nanoiron (50 nm) can cost nearly 120 €/kg.

Regarding the group of the most studied nanomaterials (nanosilica, and nanoclays) the cost analysis suggests that nanosilica may be more promising as it had the lowest cost, more easily justifiable by the improvements obtained in mechanical performance and aging resistance.

Speaking about carbon family nanomaterials, their costs are dependent on the complexity of the manufacturing process and material properties, namely purity, specific surface area and other structural properties (diameters, lengths etc.…), but they have generally very high costs. High cost is the main obstacle for their application in asphalt industry. For example, Single Walled Nanotubes (SWCNT) cost can span from 65 €/g to about 200 €/g, Multiwalled Carbon Nanotubes (MWCNT) are cheaper ranging from about 2 €/g up to 40 €/g and so are Graphene Nanoplatelets whose price hardly exceeds 15 €/g (for high purity material). Graphene Oxide costs can easily increase up to 165–170 €/g, depending on oxygen content, as well as purity, specific surface area and so forth.

However, Carbon Nanofibers together with Nanoplatelets are the cheapest carbon nanoparticles whose price stands below 15 €/g.

We believe that with an increasing market of carbon and graphene families and with specialized technology development, their unit price can decrease. This would render such kind of materials more appealing for bitumens and asphalt modification. However, so far, inorganic nanoparticles are still preferable.

It is expected that the production of nanoparticles in bulk quantity and the use of alternative sources will significantly reduce the costs. For example, rice husk ash, an abundant waste biomass with high content of silica was identified as a potential low-cost resource for the production of nanosilica particles [196]. At current prices, for the nanomodifications to be cost effective, a significant improvement in durability has to be attained.

In this respect, to understand whether the cost implied in the use of nanoparticles can be justified by parallel long-term economic advantages, a different analysis should be made taking into account for the total cost of facility ownership including all costs of acquiring, owning, and disposing of the road (life cycle assessment). Higher initial costs may be counterbalanced by lower costs of maintenance and longer life, giving net savings.

However, such studies are quite complex and take into account for economic and engineering aspects, which go beyond the scope of this work. However, the eager reader can be redirect to the guidelines by Stanford University for a general view [197] or to some work specifically dealing with Nano-Silica-Modified Asphalt Mixtures [198].

Therefore, it is necessary to carry out economic, ecological and environmental evaluations of nano-modified asphalt before a large-scale application in practical engineering.

## 8. Conclusions

Nanoparticle have unique properties and the recent progresses in nanotechnology allowed their preparation and modification even at the atomic level.

Two approaches for nanoparticle production can be followed. There are: (i) top-down approaches, which starts from bulk materials to get nano-sized particles through mainly physical process (ball milling is a cheap and quick method) and (ii) bottom-up approaches, which get nanoparticles from atomic and molecular precursors by their self-assembly. The use of nanoparticles in bitumens must be scalable and cheap, so the former can be preferred.

From recent works present in the literature it turns out that nanoparticle surface has a pivotal importance in their embedding into the bitumen matrix. The behaviour of filler, i.e. those particles with size <75 μm usually added to bitumen to enhance its overall mechanical properties and its adhesion to aggregates, can be taken as a good example: although it can be expected that the chemical nature of the filler can influence the filler-bitumen interaction giving, in accordance, different types of bonds/strengths, actually it has been concluded that the adsorption of the bitumen elements is proportional to the surface area of the filler and it is not affected by the chemical composition [33].

In this framework we point out that the specific surface can be greatly enhanced if mesoporous materials, like zeolites, are used: modern protocols [199] individuate different stages in their growth so different morphologies can be obtained. In addition, surface manipulation allows nanoparticle functionalization to increase their affinity towards the bitumen apolar nature.

Nanoparticle inclusion in bitumens and asphalts can greatly enhance their properties. Viscosity, stiffness, elasticity, fatigue cracking, resistance to aging are increased, for instance, but other new/novel important properties can be conferred. In this case, resistance to UV radiation is the most appealing to our eyes, because it grants higher stability at longer times.

All this has a cost, not only economic but also in the general sense of resources (time, availability of instruments, know-how…). The question at what extent it is worth of can be therefore spontaneously arise. To answer this question, we want to point out first that there are already some brilliant solutions to reuse nanoparticles from wastes, like that of Hussein et al. [96]. This is a strategy we strongly support for environmental concerns and for sustainable economy, which has also the parallel advantage to cut off the costs for nanoparticles supplying. Another observation is that the costs for some kinds of nanoparticles (nanosilica, nano-clays) are affordable. Of course, at the moment the costs are generally high for a lot of other materials for which the utilization is not yet convenient. There are other solutions to modify bitumens at lower costs: for example, polymer modifiers have proven to confer enhanced properties [200]. Being also compatible with recycling strategies [201].

However, in our opinion, the high costs involved in nanoparticle uses is due to the fact that the use of nanoparticles in bitumens is quite recent, so we expect that with the development of technology the costs will be lower to trigger increase in demand. We believe that the discoveries in nanotechnology field, which have been always confined in small-quantities applications, can be beneficial also in large-scale applications like road pavement, in the next future. This is probably the biggest challenge in modern technology but we are confident that it will be achieved

soon in the field of bitumen, since the intelligent incorporation of nanoparticles can give, as it has been shown, novel properties of extremely added value.

## Declaration of Competing Interest

The authors declare that they have no known competing financial interests or personal relationships that could have appeared to influence the work reported in this paper.

## Acknowledgements

This research did not receive any specific grant from funding agencies in the public, commercial, or not-for-profit sectors.

## References

[1] Lesueur D. The colloidal structure of bitumen: consequences on the rheology and on the mechanisms of bitumen modification. Adv Colloid Interface Sci 2009;145:42–82.
[2] European Commetee for standardization EN 12597. Bitumen and Bituminous Binders-Terminology; 2000.
[3] Petrauskas D, Saleem U. The Shell bitumen handbook. In: Read J, Whiteoak D, editors. The Shell bitumen handbook. Thomas Telford; 2003. p. 29 (ISBN 072773220X).
[4] Paliukaitė M, Vaitkus A, Zofka A. Evaluation of bitumen fractional composition depending on the crude oil type and production technology. 9th Int Conf Environ Eng ICEE; 2014. p. 2014.
[5] Porto M, Caputo P, Loise V, Eskandarsefat S, Teltayev B, Oliviero Rossi C. Bitumen and bitumen modification: a review on latest advances. Appl Sci 2019;9:742.
[6] Thurston RR, Knowles EC. Asphalt and its constituents. Oxidation at service temperatures. Ind Eng Chem 1941;33:320–4.
[7] Calandra P, Caputo P, De Santo M, Todaro L, Liveri V, Oliviero C. Effect of additives on the structural organization of asphaltene aggregates in bitumen. Construct Build Mater 2018;199:288–97.
[8] Loise V, Caputo P, Porto M, Calandra P, Angelico R, Rossi CO. A review on bitumen rejuvenation: mechanisms, materials, methods and perspectives. Appl Sci 2019;9.
[9] Calandra P, Longo A, Ruggirello A, Turco Liveri V. Physico-chemical investigation of the state of Cyanamide confined in AOT and lecithin reversed micelles. J Phys Chem B 2004;108:8260–8.
[10] Calandra P, Giordano C, Ruggirello A, Turco Liveri V. Physicochemical investigation of acrylamide solubilization in sodium bis(2-ethylhexyl)sulfosuccinate and lecithin reversed micelles. J Colloid Interface Sci 2004;277:206–14.
[11] Calandra P, Di Marco G, Ruggirello A, Liveri VT. Physico-chemical investigation of nanostructures in liquid phases: nickel chloride ionic clusters confined in sodium bis(2-ethylhexyl) sulfosuccinate reverse micelles. J Colloid Interface Sci 2009;336:176–82.
[12] Longo A, Calandra P, Casaletto MP, Giordano C, Venezia AM, Liveri VT. Synthesis and physico-chemical characterization of gold nanoparticles softly coated by AOT. Mater Chem Phys 2006;96:66–72.
[13] Petersen Claine J. A review of the fundamentals of asphalt oxidation: chemical, physicochemical, physical property, and durability relationships. Transp Res Circ 2009;E-C140,:7–26.
[14] Calandra P, Turco Liveri V, Riello P, Freris I, Mandanici A. Self-assembly in surfactant-based liquid mixtures: Octanoic acid/Bis(2-ethylhexyl)amine systems. J Colloid Interface Sci 2012;367:280–5.
[15] Calandra P, Ruggirello A, Mele A, Liveri VT. Self-assembly in surfactant-based liquid mixtures: Bis(2-ethylhexyl)phosphoric acid/bis(2-ethylhexyl)amine systems. J Colloid Interface Sci 2010;348:183–8.
[16] Calandra P, Mandanici A, Liveri VT. Self-assembly in surfactant-based mixtures driven by acid–base reactions: bis(2-ethylhexyl) phosphoric acid–n-octylamine systems. RSC Adv 2013;3:5148–55.
[17] Calandra P, Nicotera I, Rossi CO, Liveri VT. Dynamical properties of self-assembled surfactant-based mixtures: triggering of one-dimensional anomalous diffusion in bis(2-ethylhexyl)phosphoric acid/n-octylamine systems. Langmuir 2013;29:14848–54.
[18] Calandra P, Mandanici A, Turco Liveri V, Pochylski M, Aliotta F. Emerging dynamics in surfactant-based liquid mixtures: Octanoic acid/bis(2-ethylhexyl) amine systems. J Chem Phys 2012;136:064515.
[19] D'Melo D, Taylor R. Constitution and structure of Bitumens. The Shell Bitumen Handbook. London: ICE Publishing; 2015. p. 47–62 (ISBN 978-0-7277-5837-8).
[20] Laukkanen O. Low-temperature rheology of bitumen and its relationship with chemical and thermal properties; 2015; 186.
[21] Erkens S, Porot L, Glaser R, Glover CJ. Aging of bitumen and asphalt concrete: Comparing state of the practice and ongoing developments in the United States and Europe. Proceedings of the Transportation Research Board 95th Annual Meeting; Washington; 2016.
[22] Apostolidis P, Liu X, Kasbergen C, Scarpas AT. Synthesis of asphalt binder aging and the state of the art of Antiaging technologies. Transp Res Rec 2017;2633:147–53.
[23] Oliviero C. Adhesion promoters in bituminous road materials: a review. Appl Sci 2017;7:524.
[24] Taborda EA, Franco CA, Ruiz MA, Alvarado V, Cortés FB. Experimental and theoretical study of viscosity reduction in heavy crude oils by addition of nanoparticles. Energy Fuel 2017;31:1329–38.
[25] Steyn W. Applications of nanotechnology in road pavement engineering. Nanotechnology in Civil Infrastructure – A paradigm shift. Berlin Heidelberg: Berlin: Springer-Verlag; 2011. p. 49–84 (ISBN 978-3-642-16656-3).
[26] Gong X, Dong Z, Wang H, Ma X, Yu H, Hu K. Rheological characterization of asphalt fine aggregate matrix using dynamic shear rheometer. Polymers (Basel) 2019;11.
[27] Wang H, Al-Qadi IL, Faheem AF, Bahia HU, Yang SH, Reinke GH. Effect of mineral filler characteristics on asphalt mastic and mixture rutting potential. Transp Res Rec 2011;5:33–9.
[28] Caputo P, Ranieri GA, Godbert N, Aiello I, Tagarelli A, Rossi CO. Investigation of new additives to reduce the fume emission of bitumen during asphalt concrete processing. Mediterr J Chem 2018;7:259–66.
[29] Krishnan JM, Rao CL. Mechanics of air voids reduction of asphalt concrete using mixture theory. Int J Eng Sci 2000;38:1331–54.
[30] Rahman A, Ali SA, Adhikary SK, Hossain QS. Effect of fillers on bituminous paving mixes: an experimental study. J Eng Sci 2012;3:121–7.
[31] Zhambolova A, Vocaturo AL, Tileuberdi Y, Ongarbayev Y, Caputo P, Aiello I, et al. Functionalization and modification of bitumen by silica nanoparticles. Appl Sci 2020;10.
[32] Ashimova S, Teltayev B, Oliviero Rossi C, Caputo P, Eskandarsefat S. Organic-based recycling agents for road paving applications in cold-climate regions. Int J Pavement Eng 2020:1–9.
[33] Clopotel C, Bahia H. The effect of bitumen polar groups adsorption on mastics properties at low temperatures. Road Mater Pavement Des 2013;14:38–51.
[34] No Title Available online: http://www.its.caltech.edu/~feynman/plenty.html.
[35] Taniguchi N. On the basic concept of nanotechnology. Proceedings of the International Conference on Production Engineering; Tokyo; 1974. p. 18–23.
[36] Drexler KE. Molecular engineering: an approach to the development of general capabilities for molecular manipulation. Proc Natl Acad Sci U S A 1981;78:5275–8.
[37] Zhu W, Bartos P, Porro A. Application of nanotechnology in construction. Mater Struct 2004;37:649–58.
[38] Sahoo SK, Parveen S, Panda JJ. The present and future of nanotechnology in human health care. Nanomedicine 2007;3:20–31.
[39] Salerno M, Landoni P, Verganti R. Designing foresight studies for Nanoscience and nanotechnology (NST) future developments. Technol Forecast Soc Change 2008;75:1202–23.
[40] Roduner E. *Nanoscopic Materials Size-Dependent Phenomena*; 1 st. RSC; 2006 (ISBN 10: 085404857X).
[41] Sanchez F, Sobolev K. Nanotechnology in concrete - a review. Construct Build Mater 2010;24:2060–71.
[42] Cao G. Nanostructures and Nanomaterials synthesis, properties, and applications. . 1st ed.London: Imperial Colleg Press; 2004 [1-86094-415-9].
[43] Islam N, Miyazaki K. An empirical analysis of nanotechnology research domains. Technovation 2010;30:229–37.
[44] Pacheco-Torgal F, Jalali S. Nanotechnology: advantages and drawbacks in the field of construction and building materials. Construct Build Mater 2011;25:582–90.
[45] Steyn WJvdM. Research and application of nanotechnology in transportation. Proceedings of the 27th Southern African Transport Conference (SATC); Pretoria; 2008. p. 345–53.
[46] Kroto HW, Heath JR, O'Brien SC, Curl RF, Smalley RE. C60: Buckminsterfullerene. Nature 1985;318:162–3.
[47] Malsch I. Nanotechnology in Europe: scientific trends and organizational dynamics. Nanotechnology 1999;10:1–7.
[48] Correia A. PHANTOMS: nanotechnology network for information processing and storage*. Nanotechnology 2001;12:89–90.
[49] European Commission European Commission. Recommendation of 18 October 2011 on the definition of nanomaterial, 2011/696/EU. Off J Eur Union 2011;54(275):38–40.
[50] Donegà C. The Nanoscience Paradigm: Size Matters. In: Donega C, editor. Nanoparticles: Workhorses of Nanoscience. Berlin Heidelberg: Berlin: Springer-Verlag; 2014. p. 1–12.
[51] Caputo P, Porto M, Loise V, Teltayev B, Rossi CO. Analysis of mechanical performance of bitumen modified with waste plastic and rubber (SBR) additives by rheology and PGSE NMR experiments. Eurasian Chem J 2019;21:235–9.
[52] Caputo P, Loise V, Ashimova S, Teltayev B, Vaiana R, Oliviero Rossi C. Inverse Laplace transform (ILT)NMR: a powerful tool to differentiate a real rejuvenator and a softener of aged bitumen. Colloids Surfaces A Physicochem Eng Asp 2019;574.
[53] Rossi, C.O.; Caputo, P.; Loise, V.; Ashimova, S.; Teltayev, B.; Sangiorgi, C. *A new green rejuvenator: Evaluation of structural changes of aged and recycled bitumens by means of rheology and NMR*; 2019; Vol. 20;.
[54] Oliviero C, Caputo P, Ashimova S, Fabozzi A, D'Errico G, Angelico R. Effects of natural antioxidant agents on the bitumen aging process: an EPR and rheological investigation. Appl Sci 2018;8:1405.
[55] Walenta E. In: Glatter O, Kratky O, editors. Small angle x-ray scattering. London: Academic Press Inc. Ltd.; 1982 (ISBN 0-12-286280-5. X, 515 Seiten, geb. £ 43,60; US $ 81.00. Acta Polym 1985, 36, 296).
[56] Chu B, Hsiao BS. Small-angle X-ray scattering of polymers. Chem Rev 2001;101:1727–62.
[57] Nozue Y, Shinohara Y, Amemiya Y. Application of microbeam small- and wide-angle X-ray scattering to polymeric material characterization. Polym J 2007;39:1221–37.

[58] Calandra P, Turco Liveri V, Ruggirello AM, Licciardi M, Lombardo D, Mandanici A. Anti-Arrhenian behaviour of conductivity in octanoic acid–bis(2-ethylhexyl) amine systems: a physico-chemical study. J Mater Chem C 2015;3:3198–210.
[59] Lombardo D, Munaò G, Calandra P, Pasqua L, Caccamo MT. Evidence of pre-micellar aggregates in aqueous solution of amphiphilic PDMS–PEO block copolymer. Phys Chem Chem Phys 2019;21:11983–91.
[60] Liveri V, Lombardo D, Pochylski M, Calandra P. Molecular association of small amphiphiles: origin of ionic liquid properties in dibutyl phosphate/propylamine binary mixtures. J Mol Liq 2018;263.
[61] Hyland LL, Taraban MB, Yu YB. Using small-angle scattering techniques to understand mechanical properties of biopolymer-based biomaterials. Soft Matter 2013; 9:10218–28.
[62] Ochbaum G, Bitton R. 14 - Using small-angle X-ray scattering (SAXS) to study the structure of self-assembling biomaterials. In: Azevedo HS, Silva RMP, editors. Self-assembling Biomaterials. Woodhead Publishing Series in BiomaterialsWoodhead Publishing; 2018. p. 291–304 (ISBN 978-0-08-102015-9).
[63] Kiselev MA, Lombardo D. Structural characterization in mixed lipid membrane systems by neutron and X-ray scattering. Biochim Biophys Acta - Gen Subj 2017;1861: 3700–17.
[64] Lombardo D, Calandra P, Magazù S, Wanderlingh U, Barreca D, Pasqua L, et al. Soft nanoparticles charge expression within lipid membranes: the case of amino terminated dendrimers in bilayers vesicles. Colloids Surfaces B Biointerfaces 2018;170: 609–16.
[65] Lombardo D, Calandra P, Bellocco E, Laganà G, Barreca D, Magazù S, et al. Effect of anionic and cationic polyamidoamine (PAMAM) dendrimers on a model lipid membrane. Biochim Biophys Acta 2016;1858:2769–77.
[66] de Moor P-PEA, Beelen TPM, van Santen RA, Tsuji K, Davis ME. SAXS and USAXS investigation on Nanometer-scaled precursors in organic-mediated zeolite crystallization from Gelating systems. Chem Mater 1999;11:36–43.
[67] Bonaccorsi L, Calandra P, Kiselev MA, Amenitsch H, Proverbio E, Lombardo D. Self-assembly in poly(dimethylsiloxane)-poly(ethylene oxide) block copolymer template directed synthesis of Linde type a zeolite. Langmuir 2013;29:7079–86.
[68] Ingham B. X-ray scattering characterisation of nanoparticles. Crystallogr Rev 2015; 21:229–303.
[69] Fratzl P. Small-angle scattering in materials science - a short review of applications in alloys, ceramics and composite materials. J Appl Cryst 2003;36:397–404.
[70] Rossi CO, Caputo P, De Luca G, Maiuolo L, Eskandarsefat S, Sangiorgi C. 1H-NMR spectroscopy: a possible approach to advanced bitumen characterization for industrial and paving applications. Appl Sci 2018;8.
[71] Calandra P, Liveri VT, Caputo P, Teltayev B, Rossi CO. Wide angle X-ray scattering as a technique of choice to probe Asphaltene hierarchical structures. J Nanosci Nanotechnol 2020;20:4574–9.
[72] Caputo P, Loise V, Crispini A, Sangiorgi C, Scarpelli F, Oliviero Rossi C. The efficiency of bitumen rejuvenator investigated through powder X-ray diffraction (PXRD) analysis and T <inf>2</inf> -NMR spectroscopy. Colloids Surfaces A Physicochem Eng Asp 2019;571.
[73] Cretu C, Maiuolo L, Lombardo D, Szerb EI, Calandra P. Luminescent supramolecular nano- or micro-structures formed in aqueous media by amphiphiles-noble metals complexes. J Nanomater 2020;2020:5395048.
[74] Bartolotta A, Calandra P. Indication of local phase separation in polyimide/silica hybrid polymers. Macromol Chem Phys 2010;211:1784–92.
[75] Pochylski M, Oliviero C, Nicotera I, Liveri V, Calandra P. Nano-demixing as a novel strategy for magnetic field responsive systems: the case of Dibutyl phosphate/bis (2-ethylhexyl) amine systems. RSC Adv 2016;6.
[76] Calandra P, Loise V, Porto M, Rossi CO, Lombardo D, Caputo P. Exploiting nanoparticles to improve the properties of bitumens and asphalts: at what extent is it really worth it? Appl Sci 2020;10.
[77] Sohnel O, Garside J. Precipitation: Basic principles and industrial applications. Oxford: Butterworth-Heinemann; 1992 (ISBN 0750611073).
[78] Ludwig FP, Schmelzer J. Cluster formation and growth in segregation processes with constant rates of supply of monomers. Zeitschrift für Phys Chemie 1995; 192:155–67.
[79] Napierska D, Thomassen LCJ, Lison D, Martens JA, Hoet PH. The nanosilica hazard: another variable entity. Part Fibre Toxicol 2010;7:1–32.
[80] Li R, Xiao F, Amirkhanian S, You Z, Huang J. Developments of nano materials and technologies on asphalt materials – a review. Construct Build Mater 2017;143: 633–48.
[81] Singh LP, Karade SR, Bhattacharyya SK, Yousuf MM, Ahalawat S. Beneficial role of nanosilica in cement based materials - a review. Construct Build Mater 2013;47: 1069–77.
[82] Enieb M, Diab A. Characteristics of asphalt binder and mixture containing nanosilica. Int J Pavement Res Technol 2017;10:148–57.
[83] Yang J, Tighe SA. Review of advances of nanotechnology in asphalt mixtures. Procedia – Soc Behav Sci 2013;96:1270–2.
[84] Ghasemi M, Marandi M, Tahmooresi M, Jalal Kamali R, Taherzade R. Modification of stone matrix asphalt with Nano-SiO 2. J Basic Appl Sci Res 2012;2:1338–44.
[85] Crucho JML, das Neves JMC, Capitão SD, de Picado-Santos LG. Mechanical performance of asphalt concrete modified with nanoparticles: Nanosilica, zero-valent iron and nanoclay. Construct Build Mater 2018;181:309–18.
[86] Galooyak SS, Palassi M, Goli A, Farahani HZ. Performance evaluation of Nano-silica modified bitumen. *Int*. J Transp Eng 2015;3:55–66.
[87] Oliviero Rossi C, Caputo P, Loise V, Miriello D, Teltayev B, Angelico R. Role of a food grade additive in the high temperature performance of modified bitumens. Colloids Surfaces A Physicochem Eng Asp 2017;532.
[88] Taherkhani H, Afroozi S. The properties of nanosilica-modified asphalt cement. Pet Sci Technol 2016;34:1381–6.
[89] Zghair HH, Jony H, Hassan M. Rheological characteristics of Nano silica modified asphalt binder material. 2019 Int Eng Conf 2020:79–84.
[90] Firoozifar SH, Foroutan S, Foroutan S. The effect of asphaltene on thermal properties of bitumen. Chem Eng Res Des 2011;89:2044–8.
[91] Sadeghnejad M, Shafabakhsh G. Experimental study on the physical and rheological properties of bitumen modified with different Nano materials (Nano SiO2 & Nano TiO2). *Int*. J Nanosci Nanotechnol 2017;13:253–63.
[92] Nazari H, Naderi K, Moghadas Nejad F. Improving aging resistance and fatigue performance of asphalt binders using inorganic nanoparticles. Construct Build Mater 2018;170:591–602.
[93] Tanaka R, Sato E, Hunt JE, Winans RE, Sato S, Takanohashi T. Characterization of Asphaltene aggregates using X-ray diffraction and small-angle X-ray scattering. Energy Fuel 2004;18:1118–25.
[94] Calandra P, Caputo P, De Santo MP, Todaro L, Turco Liveri V, Oliviero Rossi C. Effect of additives on the structural organization of asphaltene aggregates in bitumen. Construct Build Mater 2019;199:288–97.
[95] Nejad FM, Nazari H, Naderi K, Karimiyan Khosroshahi F, Hatefi Oskuei M. Thermal and rheological properties of nanoparticle modified asphalt binder at low and intermediate temperature range. Pet Sci Technol 2017;35:641–6.
[96] Hussein AA, Jaya RP, Abdul Hassan N, Yaacob H, Huseien GF, Ibrahim MHW. Performance of nanoceramic powder on the chemical and physical properties of bitumen. Construct Build Mater 2017;156:496–505.
[97] Dhara S, Giri PK. Size dependent anisotropic strain and optical properties of strained Si nanocrystals. J Nanosci Nanotechnol 2011;11:9215–21.
[98] Uddin F. Clays, Nanoclays, and Montmorillonite minerals. Metall Mater Trans A 2008;39:2804–14.
[99] No Title Available online: tulane.edu/~sanelson/eens211/phyllosilicates.htm.
[100] You Z, Mills-Beale J, Foley JM, Roy S, Odegard GM, Dai Q, et al. Nanoclay-modified asphalt materials: preparation and characterization. Construct Build Mater 2011; 25:1072–8.
[101] Jahromi SG, Khodaii A. Effects of nanoclay on rheological properties of bitumen binder. Construct Build Mater 2009;23:2894–904.
[102] Sedaghat B, Taherrian R, Hosseini SA, Mojtaba Mousavi S. Rheological properties of bitumen containing nanoclay and organic warm-mix asphalt additives. Construct Build Mater 2020;243:118092.
[103] Jamshidi A, Hamzah M, Aman M. Effects of Sasobit (R) content on the rheological characteristics of Unaged and aged asphalt binders at high and intermediate temperatures. Mater Res 2012;15:628–38.
[104] Wu S, Zhang Y, Wang J. A novel potential flame-retarded bitumen nanoclay modified bitumen. Road Mater Pavement Des 2009;10:115–28.
[105] Fenimore CP, Martin FJ. Flammability of polymers. Combust Flame 1966;10:135–9.
[106] John MJ. Chapter 2 - Flammability performance of biocomposites. In: Koronis G, Silva ABT, editors. Woodhead Publishing Series in Composites Science and Engineering. Woodhead Publishing; 2019. p. 43–58 (ISBN 978-0-08-102177-4).
[107] Nejad FM, Tanzadeh R, Tanzadeh J, Hamedi GH. Investigating the effect of nanoparticles on the rutting behaviour of hot-mix asphalt. Int J Pavement Eng 2016;17: 353–62.
[108] Tam WO, Solaimanian M, Kennedy TW, River R. Development and Use of Static Creep Test to Evaluate Rut Resistance of Superpave Mixes (FHWA-TX-1250-4), 7; 2000.
[109] Li R, Pei J, Sun C. Effect of nano-ZnO with modified surface on properties of bitumen. Construct Build Mater 2015;98:656–61.
[110] Zhang H, Zhu C, Yu J, Shi C, Zhang D. Influence of surface modification on physical and ultraviolet aging resistance of bitumen containing inorganic nanoparticles. Construct Build Mater 2015;98:735–40.
[111] Hamedi GH, Nejad FM, Oveisi K. Estimating the moisture damage of asphalt mixture modified with nano zinc oxide. Mater Struct 2016;49:1165–74.
[112] Brown ER, Kandhal PS. Performance Testing For By; 2001.
[113] Katman HY, Ibrahim MR, Matori MY, Norhisham S, Ismail N, Omar RC. Tensile strength of reclaimed asphalt pavement. Int J Civ Environ Eng 2012;12:14–9.
[114] Park S-J, Seo M-K. Chapter 2 - solid-gas interaction. In: Park S-J, Seo M, editors. Interface Science and Composites. Elsevier; 2011. p. 59–145 (ISBN 1573–4285).
[115] Rapp BE. Chapter 22 - measuring surface tension and free surface energy. In Micro and Nano Technologies; Rapp Mechanics and Mathematics, B.E.B.T.-M.M., Ed. Oxford: Elsevier; 2017. p. 453–65 (ISBN 978-1-4557-3141-1).
[116] Du P, Ke N, Zhang H. Effect of Nano-zinc oxide on the morphology and ultraviolet aging properties of various Bitumens. Pet Sci Technol 2015;33:1110–7.
[117] Mubaraki M, Ali SIA, Ismail A, Yusoff NIM. Rheological evaluation of asphalt cements modified with ASA polymer and Al2O3 nanoparticles. Procedia Eng 2016; 143:1276–84.
[118] Navarro FJ, Partal P, Martínez-Boza F, Gallegos C. Thermo-rheological behaviour and storage stability of ground tire rubber-modified bitumens. Fuel 2004;83: 2041–9.
[119] Ali SIA, Ismail A, Karim MR, Yusoff NIM, Al-Mansob RA, Aburkaba E. Performance evaluation of Al 2 O 3 nanoparticle-modified asphalt binder. Road Mater Pavement Des 2017;18:1251–68.
[120] Calandra P, Caponetti E, Chillura Martino D, D'Angelo P, Minore A, Turco Liveri V. FT-IR and dielectric study of water/AOT liquid crystals. J Mol Struct 2000;522: 165–78.
[121] Karnati SR, Oldham D, Fini EH, Zhang L. Surface functionalization of silica nanoparticles to enhance aging resistance of asphalt binder. Construct Build Mater 2019; 211:1065–72.
[122] Szabolcs B, Tejash G, Serji A. Midrange temperature rheological properties of warm asphalt binders. J Mater Civ Eng 2009;21:316–23.

[123] Brooks JJ. 3 - Dimensional stability and cracking processes in concrete. In: Page CL, Page MMBT-D, editors. Woodhead Publishing Series in Civil and Structural Engineering. Woodhead Publishing; 2007. p. 45–85 (ISBN 978-1-85573-940-6).
[124] Shafabakhsh GH, Sajadib SR. Evaluation of rheological behavior of bitumen modified with Nano copper oxide. Int J Eng Technol 2018;7:13–8.
[125] Colombo C, Palumbo G, Ceglie A, Angelico R. Characterization of synthetic hematite (α-Fe2O3) nanoparticles using a multi-technique approach. J Colloid Interface Sci 2012;374:118–26.
[126] Colombo C, Palumbo G, Di Iorio E, Song X, Jiang Z, Liu Q, et al. Influence of hydrothermal synthesis conditions on size, morphology and colloidal properties of hematite nanoparticles. Nano-Structures & Nano-Objects 2015;2:19–27.
[127] Di Iorio E, Colombo C, Cheng Z, Capitani G, Mele D, Ventruti G, et al. Characterization of magnetite nanoparticles synthetized from Fe(II)/nitrate solutions for arsenic removal from water. J Environ Chem Eng 2019;7:102986.
[128] Magro M, Vianello F. Bare Iron oxide nanoparticles: surface tunability for biomedical, sensing and environmental applications. Nanomaterials 2019;9:1608.
[129] White SR, Sottos NR, Geubelle PH, Moore JS, Kessler MR, Sriram SR, et al. Autonomic healing of polymer composites. Nature 2001;409:794–7.
[130] Stuart MAC, Huck WTS, Genzer J, Müller M, Ober C, Stamm M, et al. Emerging applications of stimuli-responsive polymer materials. Nat Mater 2010;9:101–13.
[131] Jeoffroy E, Koulialias D, Yoon S, Partl MN, Studart AR. Iron oxide nanoparticles for magnetically-triggered healing of bituminous materials. Construct Build Mater 2016;112:497–505.
[132] Aristizábal Fontal JE, Cortés F, Franco Ariza C. Viscosity reduction of extra heavy crude oil by magnetite nanoparticle-based ferrofluids. Adsorpt Sci Technol 2017; 36 (026361741770430.
[133] Chen Z, Zhang H, Zhu C, Zhao B. Rheological examination of aging in bitumen with inorganic nanoparticles and organic expanded vermiculite. Construct Build Mater 2015;101:884–91.
[134] Serpone N, Lawless D, Khairutdinov R. Size effects on the Photophysical properties of colloidal Anatase TiO2 particles: size quantization versus direct transitions in this indirect semiconductor? J Phys Chem 1995;99:16646–54.
[135] Calandra P, Ruggirello A, Pistone A, Turco Liveri V. Structural and optical properties of novel surfactant coated TiO2–ag based nanoparticles. J Clust Sci 2010;21: 767–78.
[136] Calandra P, Lombardo D, Pistone A, Liveri V, Trusso S. Structural and optical properties of novel surfactant-coated Yb@TiO2 nanoparticles. J Nanopart Res 2011;13: 5833–9.
[137] Zhang HB, Zhang HL, Ke NX, Huang JH, Zhu CZ. The effect of different nanomaterials on the long-term aging properties of bitumen. Pet Sci Technol 2015;33:388–96.
[138] Oliviero C, Ashimova S, Calandra P, De Santo M, Angelico R. Mechanical resilience of modified bitumen at different cooling rates: a rheological and atomic force microscopy investigation. Appl Sci 2017;7:779.
[139] Zhang HL, Wang HC, Yu JY. Effect of aging on morphology of organo-montmorillonite modified bitumen by atomic force microscopy. J Microsc 2011; 242:37–45.
[140] Novoselov KS, Geim AK, Morozov SV, Jiang D, Zhang Y, Dubonos SV. Electric Field Effect in Atomically Thin Carbon Films, 306; 2016; 666–9.
[141] Cataldi P, Athanassiou A, Bayer I. Graphene nanoplatelets-based advanced materials and recent progress in sustainable applications. Appl Sci 2018;8:1438.
[142] Young RJ, Kinloch IA, Gong L, Novoselov KS. The mechanics of graphene nanocomposites: a review. Compos Sci Technol 2012;72:1459–76.
[143] Le J-L, Du H, Pang SD. Use of 2D Graphene Nanoplatelets (GNP) in cement composites for structural health evaluation. Compos Part B Eng 2014;67:555–63.
[144] Du H, Pang SD. Enhancement of barrier properties of cement mortar with graphene nanoplatelet. Cem Concr Res 2015;76:10–9.
[145] Du H, Pang SD. In: Sobolev K, Shah SP, editors. Mechanical Response and Strain Sensing of Cement Composites Added with Graphene Nanoplatelet Under Tension BT - Nanotechnology in Construction. Cham: Springer International Publishing; 2015. p. 377–82.
[146] Le J, Marasteanu M, Turos M. Graphene nanoplatelet (GNP) reinforced asphalt mixtures: a novel multifunctional pavement material. IDEA Progr Final Rep NCHRP 2016;173:1–28.
[147] Lu S-N, Xie N, Feng L-C, Zhong J. Applications of nanostructured carbon materials in constructions: the state of the art. J Nanomater 2015;2015:807416.
[148] Moreno-Navarro F, Sol-Sánchez M, Gamiz F, Gámez M. Mechanical and thermal properties of graphene modified asphalt binders. Construct Build Mater 2018; 180:265–74.
[149] Aravind S, Isac AJ, Aparajith S. Construction of porous asphalt pavement using graphene. Int J Recent Trends Eng Res 2018;4:475–81.
[150] Le J-L, Marasteanu MO, Turos M. Mechanical and compaction properties of graphite nanoplatelet-modified asphalt binders and mixtures. Road Mater Pavement Des 2019:1–16.
[151] Brcic H. Investigation of the rheological properties of asphalt binder containing Graphene Nanoplatelets. Nor. Univ. Sci. Technol. Dep. Civ. ad Transp. Eng; 2016.
[152] Radushkevich LV. Lukyanovich, V.M. the structure of carbon forming in thermal decomposition of carbon monoxide on an Iron catalyst. Russ J Phys Chem 1952;26: 88–95.
[153] Iijima S. Helical microtubules of graphitic carbon. Nature 1991;354:56–8.
[154] Harris PJF. Carbon nanotube composites. Int Mater Rev 2004;49:31–43.
[155] Vidu R, Rahman M, Mahmoudi M, Enachescu M, Poteca TD, Opris I. Nanostructures: a platform for brain repair and augmentation. Front Syst Neurosci 2014;8:91.
[156] Abouelsayed A, Eisa WH, Dawy M, Shabaka A. Ultraviolet and infrared studies of the single-walled and multi-walled carbon nanotube films with different thickness. Phys B Condens Matter 2016;483:8–12.
[157] Arabani M, Faramarzi M. Characterization of CNTs-modified HMA's mechanical properties. Construct Build Mater 2015;83:207–15.
[158] Nwakaire CM, Yap SP, Yuen CW, Onn CC, Koting S, Babalghaith AM. Laboratory study on recycled concrete aggregate based asphalt mixtures for sustainable flexible pavement surfacing. J Clean Prod 2020;262:121462.
[159] Hussan S, Kamal MA, Hafeez I, Ahmad N. Comparing and correlating various laboratory rutting performance tests. Int J Pavement Eng 2019;20:1239–49.
[160] Loise V, Vuono D, Policicchio A, Teltayev B, Gnisci A, Messina G, et al. The effect of multiwalled carbon nanotubes on the rheological behaviour of bitumen. Colloids Surfaces A Physicochem Eng Asp 2019;566.
[161] Singh CB, Biswas P, Sarkar S, Singh V, Kumar S, Ram S. Raman spectroscopy study of growth of multiwalled carbon nano-tubes using plasma enhanced chemical vapour depositon. Proc Int Conf Nanosci Eng Technol ICONSET 2011;2011.
[162] Yang Q, Li X, Zhang L, Qian Y, Qi Y, Kouhestani HS, et al. Performance evaluation of bitumen with a homogeneous dispersion of carbon nanotubes. Carbon N Y 2020; 158:465–71.
[163] Gui X, Wei J, Wang K, Cao A, Zhu H, Jia Y, et al. Carbon nanotube sponges. Adv Mater 2010;22:617–21.
[164] Guo W, Guo X, Chang M, Dai W. Evaluating the effect of hydrophobic Nanosilica on the viscoelasticity property of asphalt and asphalt mixture. Materials (Basel) 2018; 11:2328.
[165] Wool RP. In: Wool RP, Sun XSBT, editors. 7 - Properties of triglyceride-based thermosets. Burlington: Academic Press; 2005. p. 202–55 (ISBN 978-0-12-763952-9).
[166] Springer Handbook of Nanomaterials; Vajtai, R., Ed.; 1st ed.; Springer-Verlag Berlin Heidelberg, 2013; (ISBN 978-3-642-20594-1).
[167] Palmeri MJ, Putz KW, Ramanathan T, Brinson LC. Multi-scale reinforcement of CFRPs using carbon nanofibers. Compos Sci Technol 2011;71:79–86.
[168] Puchý V, Tatarko P, Dusza J, Morgiel J, Bastl Z, Mihaly J. Characterization of carbon nanofibers by SEM, TEM, ESCA and Raman spectroscopy. Kov Mater 2010;48: 379–85.
[169] Khattak MJ, Khattab A, Rizvi HR, Zhang P. The impact of carbon nano-fiber modification on asphalt binder rheology. Construct Build Mater 2012;30:257–64.
[170] Jamal Khattak M, Khattab A, Rizvi R. H. Characterization of carbon nano-fiber modified hot mix asphalt mixtures. Construct Build Mater 2013;40:738–45.
[171] Rizvi HR, Khattak MJ, Madani M, Khattab A. Piezoresistive response of conductive hot mix asphalt mixtures modified with carbon nanofibers. Construct Build Mater 2016;106:618–31.
[172] Isacsson U, Zeng H. Low-temperature cracking of polymer-modified asphalt. Mater Struct Constr 1998;31:58–63.
[173] Das PK, Tasdemir Y, Birgisson B. Low temperature cracking performance of WMA with the use of the Superpave indirect tensile test. Construct Build Mater 2012; 30:643–9.
[174] Sun L, Xin X, Ren J. Inorganic nanoparticle-modified asphalt with enhanced performance at high temperature. J Mater Civ Eng 2017;29:1–9.
[175] Sybilski D. Zero-shear viscosity of bituminous binder and its relation to bituminous Mixture's rutting resistance. Transp Res Rec 1996;1535:15–21.
[176] Zeng W, Wu S, Pang L, Sun Y, Chen Z. The utilization of Graphene oxide in traditional construction materials: asphalt. Mater (Basel, Switzerland) 2017;10.
[177] Li Y, Wu S, Amirkhanian S. Investigation of the graphene oxide and asphalt interaction and its effect on asphalt pavement performance. Construct Build Mater 2018; 165:572–84.
[178] Liu K, Zhang K, Wu J, Muhunthan B, Shi X. Evaluation of mechanical performance and modification mechanism of asphalt modified with graphene oxide and warm mix additives. J Clean Prod 2018;193:87–96.
[179] Porto M, Caputo P, Loise V, De Filpo G, Oliviero Rossi C, Calandra P. Polysaccharides-reinforced Bitumens: specificities and universality of rheological behavior. Appl Sci 2019;9:5564.
[180] Caputo P, Porto M, Calandra P, De Santo MP, Oliviero Rossi C. Effect of epoxidized soybean oil on mechanical properties of bitumen and aged bitumen. Mol Cryst Liq Cryst 2018;675:68–74.
[181] Oliviero C, Caputo P, Luca G, Maiuolo L, Eskandarsefat S, Sangiorgi C. 1H-NMR spectroscopy: a possible approach to advanced bitumen characterization for industrial and paving applications. Appl Sci 2018;8.
[182] Caputo P, Loise V, Ashimova S, Teltayev B, Vaiana R, Oliviero Rossi C. Inverse Laplace transform (ILT)NMR: a powerful tool to differentiate a real rejuvenator and a softener of aged bitumen. Colloids Surfaces A Physicochem Eng Asp 2019;574: 154–61.
[183] Rashid F, Hossain Z, Bhasin A. Nanomechanistic properties of reclaimed asphalt pavement modified asphalt binders using an atomic force microscope. Int J Pavement Eng 2019;20:357–65.
[184] Nahar S, Schmets A, Schitter G, Skarpas A. Quantitative nanomechanical property mapping of bitumen micro-phases by peak-force atomic force. Microscopy 2014; 2 (ISBN 978-1-138-02693-3).
[185] Nanotomography. Available online: https://en.wikipedia.org/wiki/Nanotomography. (accessed on Sep 16, 2020).
[186] Liu G, Wu S, Ven M, Yu J, Molenaar A. Influence of sodium and organo-montmorillonites on the properties of bitumen. Appl Clay Sci 2010;49:69–73.
[187] Mohajeri M, Molenaar AAA, Van de Ven MFC. Experimental study into the fundamental understanding of blending between reclaimed asphalt binder and virgin bitumen using nanoindentation and nano-computed tomography. Road Mater Pavement Des 2014;15:372–84.
[188] Zhang Y, Verwaal willem, Ven MFC, Molenaar A, Wu S. Using high-resolution industrial CT scan to detect the distribution of rejuvenation products in porous asphalt concrete. Construct Build Mater 2015;100(1–10).

[189] Rinaldini E, Schuetz P, Partl M, Tebaldi G, Poulikakos L. Investigating the blending of reclaimed asphalt with virgin materials using rheology, electron microscopy and computer tomography. Compos Part B Eng 2014;67:579–87.
[190] Hu J, Qian Z, Wang D, Oeser M. Influence of aggregate particles on mastic and air-voids in asphalt concrete. Construct Build Mater 2015;93.
[191] Martinho F, Picado-Santos L, Capitão S. Feasibility assessment of the use of recycled aggregates for asphalt mixtures. Sustainability 2018;10:1737.
[192] No Title Available online: https://www.us-nano.com/inc/sdetail/494.
[193] Crucho J, Picado-Santos L, Neves J, Capitao S. A review of nanomaterials' effect on mechanical performance and aging of asphalt mixtures, 9; 2019 (ISBN 3512184197).
[194] No Title Available online: https://www.us-nano.com/inc/sdetail/50544.
[195] No Title Available online: https://nanografi.com.
[196] Karahancer S, Saltan M, Morova N, Serin S, Terzi S. Evaluation of rice husk ash as filler in hot mix asphalt concrete. Construct Build Mater 2013;48:390–7.
[197] Guidelines for Life Cycle Cost Analysis. Available online https://sustainable.stanford.edu/sites/default/files/Guidelines_for_Life_Cycle_Cost_Analysis.pdf. (accessed on Sep 28, 2020).
[198] Sackey S, Lee DE, Kim BS. Life cycle assessment for the production phase of nano-silica-modified asphalt mixtures. Appl Sci 2019;9.
[199] Bonaccorsi L, Calandra P, Amenitsch H, Proverbio E, Lombardo D. Growth of fractal aggregates during template directed SAPO-34 zeolite formation. Microporous Mesoporous Mater 2013;167:3–9.
[200] Azarhoosh A, Hamedi GH, Azarhoosh MJ. The influence of cohesion and adhesion parameters on the moisture sensitivity of modified asphalt mixtures with polymer additive. J Adhes 2020:1–23.
[201] Daryaee D, Ameri M, Mansourkhaki A. Utilizing of waste polymer modified bitumen in combination with rejuvenator in high reclaimed asphalt pavement mixtures. Construct Build Mater 2020;235:117516.

Journal of Molecular Liquids 339 (2021) 116742

Contents lists available at ScienceDirect

Journal of Molecular Liquids

journal homepage: www.elsevier.com/locate/molliq

# Additives on aged bitumens: What probe to distinguish between rejuvenating and fluxing effects?

Valeria Loise [a], Pietro Calandra [c,*], Abraham A. Abe [a], Michele Porto [a,*], Cesare Oliviero Rossi [a], Mariano Davoli [b], Paolino Caputo [a]

[a] Department of Chemistry and Chemical Technologies, University of Calabria, Via P. Bucci, Cubo 14D – 87036 Rende, Italy
[b] Department of Biology, Ecology and Earth Sciences, University of Calabria, 87036 Rende, Italy
[c] CNR-ISMN, National Research Council – Institute for the Study of Nanostructured Materials, Via Salaria km 29.300, 00015 Monterotondo Stazione (RM), Italy

ARTICLE INFO

*Article history:*
Received 11 March 2021
Revised 8 June 2021
Accepted 14 June 2021
Available online 17 June 2021

*Keywords:*
Bitumen
Tritolil Phosphate Isomers (TPI)
Soy oil
Rejuvenators
Dynamic Shear Rheometer (DSR)
Atomic
Force Microscopy (AFM)
Infrared Spectroscopy (IR)
Optical Microscopy

ABSTRACT

Bitumen is a complex material used for road pavement throughout the world. During paving and pavement service life loss of more volatile compounds and oxidization takes place. Hence, asphaltene micelles become larger so that the fluidity of the system is reduced; the material becomes rigid, stiff and brittle so needing replacement. Once removed, it can be processed to restore its original properties and used for Reclaimed Asphalt Pavement (RAP). For such a process, additives called "rejuvenators" are used: they act on the chemical structure of aged bitumen to restore its physical properties to a state very similar to virgin bitumen. Alternatively, softening agents can be used to restore only the physical properties. An additive conferring regenerating characteristic on the asphalt mix increases the longevity of asphalt pavements due to the fact that it brings the bitumen back to its initial state; on the other hand, softening agents render the aged bitumen more workable but road pavements remain rigid and eventually break in the course of use. At the moment, methods that can distinguish a regenerating effect from a fluxing effect are not known. This study aims at evaluating the different effects of the additives on aged bitumen. For this purpose, we used a commercial additive (tritolyl poly phosphate, TPI) working as rejuvenator and a softening agent (soy oil) which is a well-known fluxing agent. The effects of the additives on aged bitumen have been investigated through Dynamic Shear Rheometer, Atomic Force Microscopy, Optical Microscopy and Infrared Spectroscopy.

© 2021 Elsevier B.V. All rights reserved.

## 1. Introduction

The general problem affecting bitumen and asphalt concretes is their aging, a process giving ever increasing viscosity and stiffness with time thus implying losing of performances.

Under ageing, bitumen molecules and their aggregates become less and less mobile to flow under the applied stress. So, cracking or fracture can take place [1] in the bulk material. Ageing is a complex mechanism, which can be considered as the overall result of several and somehow interconnected spontaneous processes, each of them characterized by its own timescale:

1. volatilization of light components in the maltene taking place even during asphalt construction [2,3];
2. oxidation of bitumen constituents by atmospheric oxygen. This gives oxidized molecules which being more polar can give enhanced self-assembly [4];
3. evaporation of low-molecular weight components: this causes not only a change of bitumen composition, but also an overall reduction light component (at least those with higher vapour pressure) [5];
4. chemical reactions causing polymerization and formation of a bigger structures within the bitumen (thixotropy) [6].

After ageing, the original physical properties of bitumen can be restored essentially in two main ways:

1. by simply restoring the original ductility/viscosity through addition of softening (usually called fluxing) agents like flux oil, lube stock, slurry oil, soy oil etc. [7,8];

* Corresponding authors.
*E-mail addresses:* pietro.calandra@cnr.it (P. Calandra), michele.porto@unical.it (M. Porto).

https://doi.org/10.1016/j.molliq.2021.116742
0167-7322/© 2021 Elsevier B.V. All rights reserved.

2. by restoring the original chemistry of the pristine bitumen and its original inter-molecular structure [9]: this would imply a more sophisticated/complex action (rejuvenation) being able to push back the oxidations, agglomerations and self-assembly processes occurred during the whole aging.

Whatever the mechanisms, it must be stressed that, in general, the resources needed to modify the bitumens (costs, skills and technology involved) must be somehow justified. So, it can happen that cheaper additives, which can exert only a simple fluxing effect, can be sometimes preferred due to their low cost and accessibility. For example, in this ambit, recent trends based on the re-utilization of wastes to modify/restore bitumens in a circular economy approach, are drawing particular attention for environmental issues [10].

On the other hand, although probably the latter mechanism (rejuvenation) is more complex and harder to achieve, it can guarantee a better effect with more prolonged benefits at longer times [11].

For this reason recent research, both academic and industrial, are starting considering the production of additives as real rejuvenators [12,13] with an obvious attention to environmental concerns [14] and, consequently, to the development of green additives [15].

Of course, different efforts are being made to distinguish between these two mechanisms [16]. In the present work the effects of two different additives on aged bitumen were investigated. One of these two additives (soy oil) being a bare fluxing agent, the other one (tritolyl poly phopshate, TPI) behaving as real rejuvenator.

## 2. Experimental

### 2.1. Materials

The base bitumen was kindly supplied by Loprete Costruzioni Stradali (Italy) and was used as fresh standard. Its penetration grade (50/70) was measured by the usual standardized procedure [17], in which a standard needle is loaded with a weight of 100 g and the length traveled into the bitumen specimen is measured in tenths of a millimeter for a known time, at fixed temperature.

TPI (Tritolyl Phosphate Isomers) was supplied by KimiCal s.r.l. (Rende (CS) – Italy) and soy oil by Loprete Costruzioni Stradali (Italy).

### 2.2. Sample preparation

A weighted amount of additive (1 g of additive in 20 g of bitumen giving a final content of 4.76% wt/wt), was added separately to a fully flowing hot bitumen (150 ± 10 °C) and stirred at 500–700 rpm by a mechanical stirrer (IKA RW20, Königswinter, Germany) for 30 min at the same temperature to allow homogenization of the blend. Previous studies showed that such conditions assure the preparation of homogeneous samples: at lower rpm samples homogenization is not effective, while above 700 rpm the bitumen can become oxidized with consequent change in the rheological properties. This method is quite standard and also other authors use analogous procedure [18].

After mixing, the resulting bitumen was poured into a small sealed can and then stored in a dark chamber at 25 °C to retain the desired morphology. Due to the sensitivity of such kind of materials to the annealing time [19], and due to the comparative spirit of our work, we took care that all our samples had the same temperature cooling rate (5 °C $min^{-1}$) and annealing time (15 min).

A standard additive-free bitumen sample was used as reference, hereafter labelled as "ref".

The bitumen samples were artificially aged by means of the Rolling Thin Film Oven Test (RTFOT) using a variation of the ASTM D1754 standard. In this respect a thermal treatment of 225 min at 163 °C was used in order to reproduce the behavior of a Recycled Pavement Asphalt (RAP)

### 2.3. Atomic Force Microscopy AFM

Atomic Force Microscopy (AFM) was carried out by a Nanoscope VIII, Bruker microscope operating in tapping mode (150 kHz). When the tip is brought close to the surface, the vibration of the cantilever is influenced by the tip–sample interaction: shifts in the phase angle of vibration of the cantilever, implying energy dissipation in the tip-sample ensemble, are due to the specific mechanical properties of the sample. Cantilever with nominal tip radius of curvature 10 nm were used. Both topographic and phase images were recorded and they usually match.

### 2.4. Rheology

The complex shear modulus G* = G' + i G" [20] was measured in the regime of small amplitude oscillatory shear at 1 Hz as a function of temperature (temperature controlled by a Peltier element, uncertainty ± 0.1 °C) by dynamic stress-controlled rheometer (SR5, Rheometric Scientific, Piscataway, NJ, USA) equipped with a parallel plate geometry (gap 2 mm; diameter 25 mm for high temperature range and 8 mm for low temperature) [21]. Conditions were chosen after preliminary stress-sweep tests to guarantee linear viscoelastic conditions in all measurements.

The real and imaginary parts define the in-phase (storage, measure of the reversible elastic energy) and the out-of-phase (loss, irreversible viscous dissipation of the mechanical energy) moduli, respectively [22].

Rheology temperature-sweep tests from room temperature (RT, 25 °C) to high (up to 120 °C) and to low (down to −30 °C) temperatures were performed monitoring the elastic modulus (G′) during each temperature ramp at a constant heating rate (1 °C/min) and at a frequency of 1 Hz.

### 2.5. Optical microscopy

Sample were examined with a Leica DMLP polarising microscope equipped with a Leica DFC280 camera and a CalCTec (Italy) heating stage. Samples were inserted in a double microscope glass slide (sandwich model) and a temperature ramp was carried out with a starting temperature of 120° C and a heating rate of 5° C per minute. After any 5° C increase, photos were taken. After reaching the desired temperature at each point, the samples were left to stay for one minute to ensure total melting of the whole sample.

### 2.6. Fourier transforn infrared spectroscopy (FT-IR)

Fourier Transform Infrared (FT-IR) analysis was carried out on the KBr asphalthene pellets samples in the mid-infrared area (4000–400 $cm^{-1}$) with a Perkin Elmer Spectrum 100 FT-IR spectrometer.

## 3. Results and discussions

### 3.1. Rheological tests

Interesting information can be derived from the temperature dependence of G' and G" for the studied samples. A clearly

increasing trend is observed as a function of temperature in accordance with the typical bitumen behaviour. At a deeper sight, the trend shows two regions which correspond to two different regimes [23,24].

At low temperature, in fact, all samples exhibit a viscoelastic response typical of strong gel-like materials where G' > G'' but, when increasing temperature, G' decreases faster than G'' so a crossover temperature (Tcross, at which G' equals G'') takes place (see Fig. 1). So, for T > Tcross, samples typically behave as pseudo-plastic fluids. Tcross is therefore to be considered as the transition temperature from a glassy elastic solid to a viscoelastic liquid. At this temperature, the sample changes from solid-like, with a mainly elastic response [25] but generally more susceptible to cracks [26], to viscoelastic, with a higher mechanical plasticity [27,28].

It can be seen that ageing shifts the Tcross value from 7.8 to 17.2 °C, as expected for a process making the material stiffer and more rigid. This is reasonably due to the oxidation of the aromatic components of the bitumen during the aging process. However, both additives can shift back Tcross quite efficiently, but it is worth of note that the effect exerted by soy oil is a bit more marked than TPI.

When increasing temperatures, the material is progressively softened (see the typical behaviour of G' and G'' at high

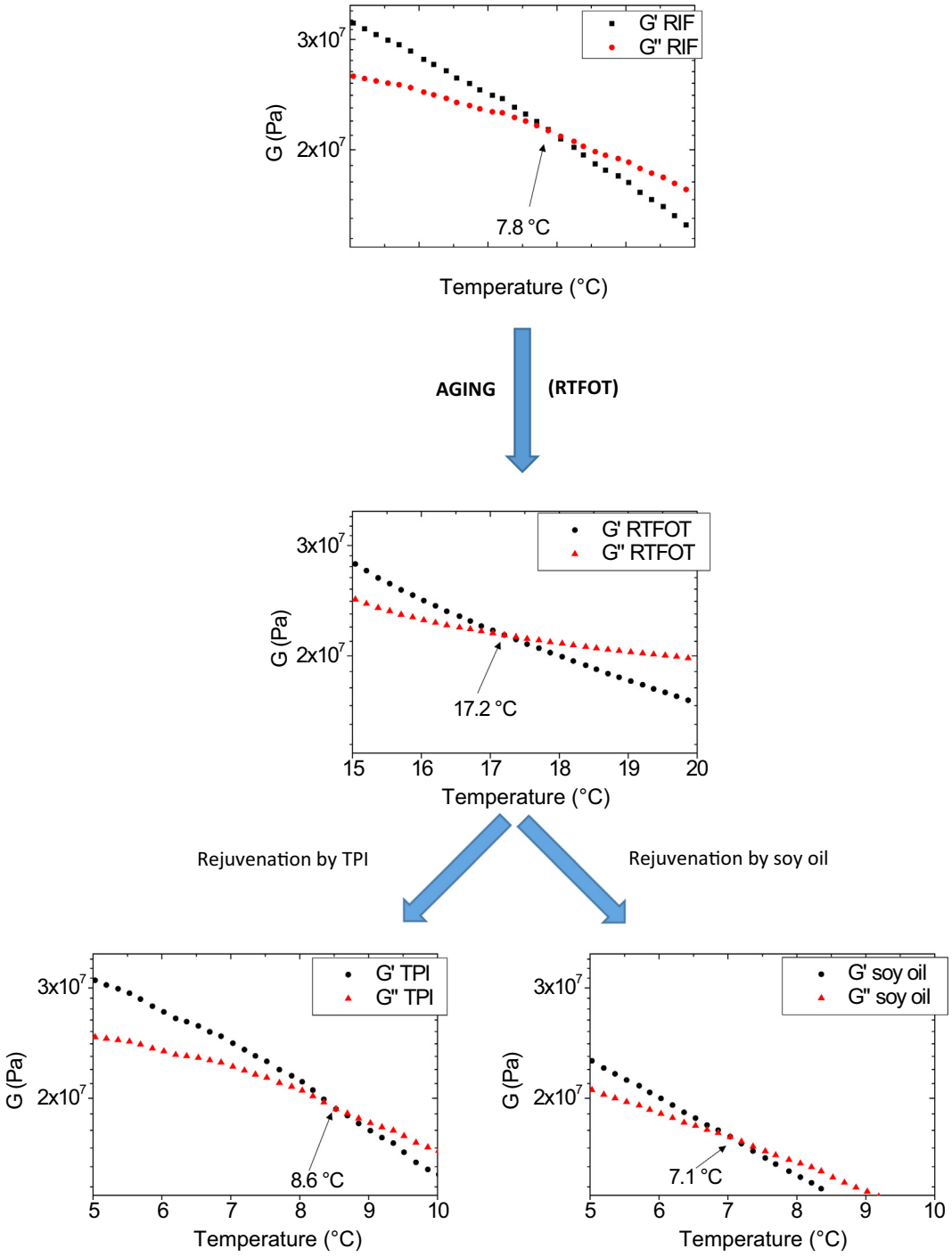


**Fig. 1.** G' and G'' (at 1 Hz) as a function of temperature (lower temperatures) for the studied samples.

temperatures in Fig. 2). The value of G' at 50 °C (G' @ 50 °C) can be seen as an indicator of the rigidity of the material under usage conditions as made in previous papers [29,30]. The values of G' @ 50 °C are reported in the same Fig. 2: for these values the same considerations as those made for Tcross hold, i.e. the ageing shifts the G' @ 50 °C value from 1760 Pa s to 24500 Pa, as expected, and both additives can shift back the value quite efficiently (to 4220 and 3120 Pa for TPI and soy oil, respectively) with a more pronounced effect exerted by soy oil.

At even higher temperatures, a transition from a viscoelastic material to a viscous liquid can be observed. In fact, when temperature is further increased at a certain point G' drops (Tmelt). From the microscopic point of view Tmelt can be intended as the temperature at which the thermal motion is sufficiently high to completely destroy the intermolecular network. This means that, for temperatures higher than Tmelt, no elastic response (storage of mechanical energy) is anymore present in the material under an applied stress; in few words, the bitumen behaves now as a Newtonian fluid. The values of Tmelt are reported in the same Fig. 2; for these, the same considerations as Tcross hold: ageing causes an obvious increase of Tmelt (from 62 to 75 °C) which can be partially restored by addition of TPI or soy oil (shift back to 66 and 67 °C, respectively), with a scarce difference between the two additives.

Therefore, as resulting from the rheological analyses, it seems it was not possible to clearly evaluate the effectiveness of the regenerating additive as it is not possible to differentiate the regeneration effect of the additive from the fluxing effect of the oil. This, in our opinion, can be due to the fact that rheology is a bulk technique, synthetically probing the overall behavior of a material. So, different microscopic structures can give rise to the same rheological behavior, although with subtle but important differences in some intermolecular interactions (polar inter-asphaltene interactions). In the specific, due to its microscopic structure, a bitumen can be described by the so-called weak-gel model, according to the theory of Bohlin [31] and Winter [32] which has been applied to several colloidal complex systems [33].

It is defined as a complex system characterized by a cooperative arrangement of flow units connected by weak physical interactions that cooperatively ensure the stability of the structure. In the analyzed samples, the asphaltene oxidation and the consequent self-assembly/aggregation of its units, as well as the loss of volatile maltene fractions, is counterbalanced, from the rheological point of view, by oil addition into the matrix (maltene). Residual differences between aged-and-additivated and pristine bitumens support this interpretation.

### 3.2. Light Microscopy

Fig. 3 reports the microscopy analysis of the asphaltenic fraction of the bitumen under increasing temperatures. These images have been recorded after the standard procedure for asphaltene isolation from bitumen, IP 143/01 [34] as recently implemented in ref [35].

It must be stressed that conventional methods for measuring melting point of organic solids, (heating sample in a capillary tube), rely on its physical state observation under relatively low heating rates, which prevents application to reactive materials such as asphaltenes. An alternative for qualitative observations of physical behavior is to rapidly heat tiny samples of asphaltenes, as described in [36] with in situ observation by a camera. The heating rate of 5 °C/min adopted in the present work was chosen following this criterion in accordance to the specificities of the instrumentation used.

The presence of micro-meter sized particles can be observed. The presence of aggregates larger than those usually observed in suspension [37], is ascribed to ripening/coalesce/agglomeration phenomena triggered by the progressive increase in nanoparticle concentration occurring during sample preparation (sample filtration and drying) [38]. It can be observed, in panel A, that the asphaltene clusters of the pristine (unaged) bitumen begin to melt around 150 °C and are completely liquid at 160 °C. This temperature range is in accordance with the fact that, as a complex mixture of components, asphaltenes generally do not display a distinct melting point. The melting temperature range found agrees with those found by other Authors. For example, Zhang et al [39] have indications, by visual observations, that softening and melting take place in their samples in the temperature range 150–230 °C.

The asphaltenes aggregates of aged bitumen (see Fig. 3 panel B) begin to melt at higher temperatures (around 165 °C) and are completely liquid at 180 °C. The increased temperature as compared to

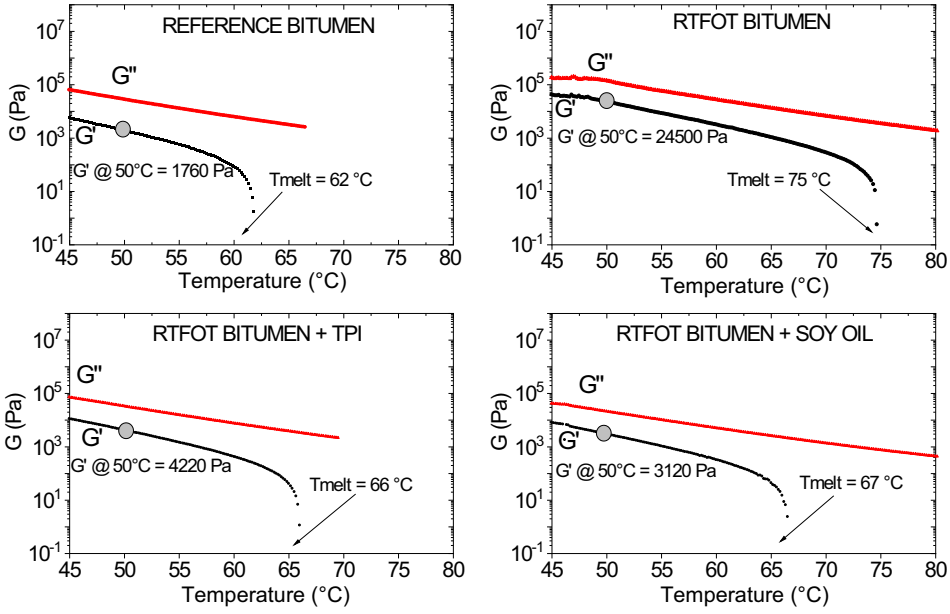


**Fig.2.** G' and G" (at 1 Hz) as a function of temperature (higher temperatures) for the studied samples.

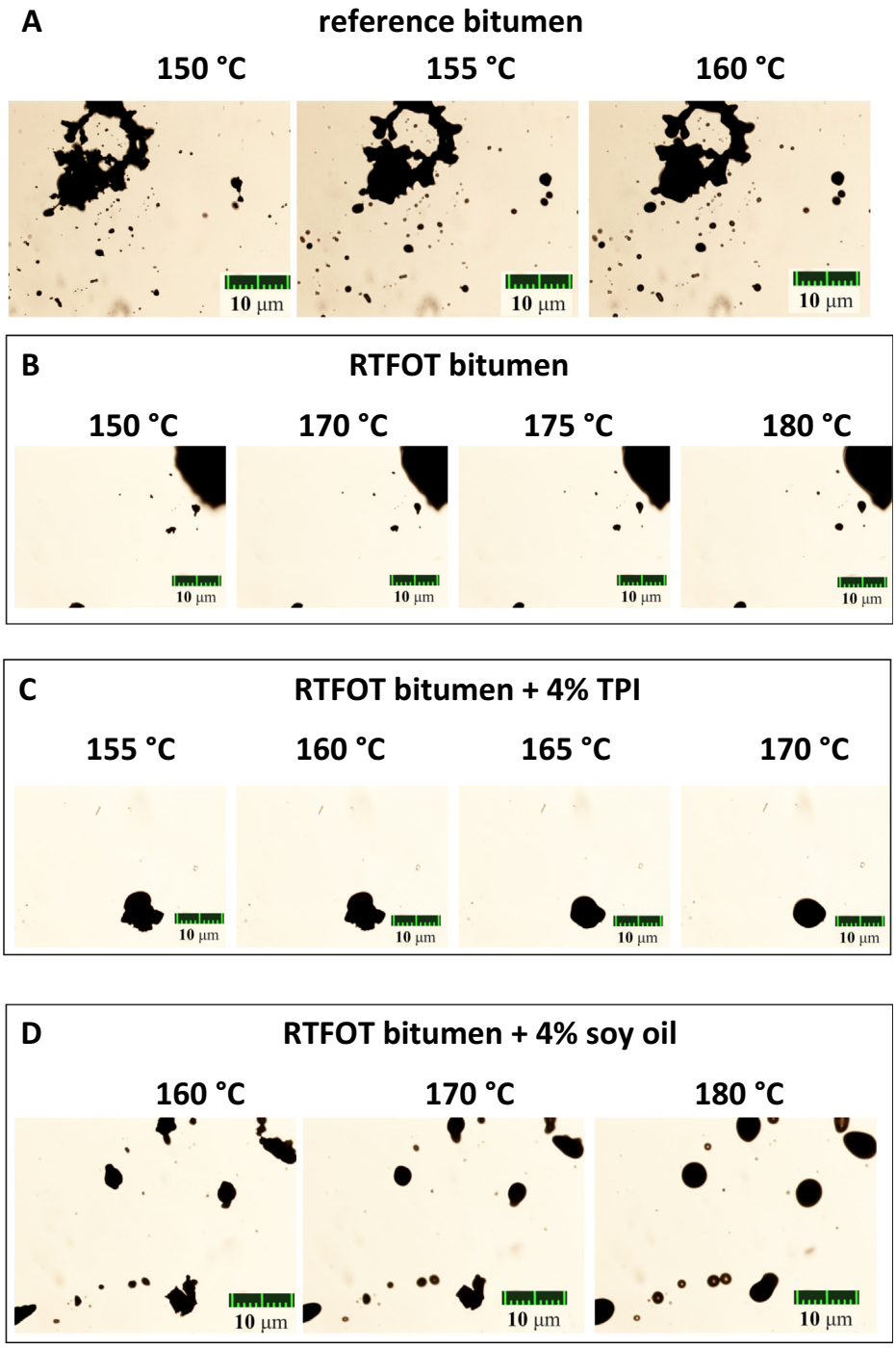


**Fig. 3.** Images from optical microscopy of the various samples at the temperatures shown.

that of pristine bitumen is obviously due to the fact that asphaltenes are more oxidized and therefore are characterized by stronger intermolecular interactions, giving a tighter cluster with higher lattice energy.

It is interesting now to observe significant differences in the images of asphaltenes derived from the aged bitumen modified with soya oil or TPI. In fact, the asphaltenes derived from the bitumen with 4% TPI begin to melt at 155 °C and are completely liquid at 170 °C (see Fig. 3 panel C), showing a behaviour very similar to those derived from non-aged bitumen. Those derived from aged bitumen added with 4% soy oil, instead, show values similar to those recorded for asphaltenes of aged pristine bitumen (160–180 °C, see panel D).

Thus, it can be claimed that the regenerating additive (TPI) has chemically interacted with the asphaltenic part of the bitumen, restoring it almost completely to its initial state. On the other hand, it is clear that this is not true for soy oil, for which only a simple improvement of the flow in aged bitumen can be claimed (see rheological analysis), without any strict chemical interaction with asphaltenic part of the bitumen. It is confirmed, therefore, that the soy oil effect is to be individuated in the maltenic fraction, probably due to its mostly apolar structure allowing only apolar

interactions. On the other hand, TPI, thanks to the phosphate group, allows more polar interactions, effectively binding the asphaltenes clusters. Due to the wide scenario of possible interactions among asphaltene and their clusters, a complex structural pattern, taking place at different lengthscales and characterized by different strengths with hierarchical structures [9], is present. Longer-range structures are expected to be hold up by weaker interactions, which can be broken simply by a temperature increase: small-angle neutron scattering experiments on asphaltenes, indeed, show that the large-scale asphaltene aggregates progressively disperse over a temperature range from 50 to 400 °C [40,41].

Moreover, due to the multiplicity of structures and interactions involved, it is hard to understand the exact localization of TPI-asphaltene interactions. For this, a theoretical approach based on computational chemistry, or ad-hoc experiments, are needed. Here, however, this aspect is not relevant, since what is important, for the purposes of this the research, is TPI stabilization effect towards the single asphaltene molecules, hindering their assembly and giving the overall decrease in melting point of their fraction. It can be concluded that optical microscopy, coupled with thermal treatment, directly probing the melting point of asphaltene clusters, is a good technique to distinguish a mere fluxing effect from a real rejuvenating effect. It is interesting to note that this technique focuses on the specific part of a bitumen (asphaltenes and their clusters/aggregates) directly involved in ageing, an aspect that can be, in our opinion, at the basis of the effectiveness of the technique.

Another interesting observation is that the exploitation of optical microscopy is a very simple approach which involves the use of scientific instrumentation present in almost all research laboratories and which has relatively low costs, both for maintenance and for purchase. This technique will allow the quality of the additives to be used as regenerants for bitumen to be assessed quickly and effectively. Furthermore, given the rapid sample preparation and test execution times, it will speed up the search for new regenerating additives and above all will allow the bodies responsible for quality control during the drafting of bituminous conglomerates (such as ANAS in Italy, NCAT and NAPA in U.S.A., AIA in U.K., etc.) for the construction of road pavements, an immediate verification of the final product (conglomerate) thus providing the possibility to intervene on the composition of the conglomerates in real time, avoiding future maintenance work.

### 3.3. Atomic Force Microscopy (AFM)

Atomic Force Microscopy (AFM) has been proven to be suitable probe to study bitumens morphology at the microscopic level [42]. Furnishing the imaging of the mechanical characteristics of the observed parts [43] and giving information on the supramolecular self-assembly in this kind of material [44].

In Fig. 4, the topography (first column) and phase (second column) images of the studied samples (different rows) are shown.

As it can be seen, the topography and phase images usually match. In the pristine bitumen, elongated clusters of 1–2 μm, with a rippled interior with sub-nanometers edges and dispersed in a quite uniform matrix, can be clearly seen. These aggregates can be safely considered to be made of asphaltene molecules organized in a hierarchical aggregation pattern and in accordance with previous structural observations [45]. This feature is quite well known in the literature, being dealt with as "bee structure" [46] and has been already observed in previous papers [19].

Although in aged bitumen, the domain sizes are similar as compared to those observed in pristine bitumens, the interconnection of the domains appears to be greater in the case of the aged bitumen.

This justifies the increased viscosity and stiffness in this sample. In the soy oil and TPI – containing samples, the domains appear to be larger but in the case of the TPI, they seem to be less connected than in the soy oil case.

In the phase images it is observed that the soft part of the sample (dark part) covers a higher surface fraction in reference bitumen than in aged bitumen where the clear part (hard areas) prevails. This is due to the oxidation of the bitumen during the aging process.

The right column of Fig. 4 reports the relative abundance (percentage) of the phase values. Two bands are clearly visible: one is centred at lower phase values and connected to the soft, maltenic, faction, and the other one is centred at higher phase values and connected to the harder, asphaltenic, part of the sample.

It is worth noting, first, that in the various samples the bands are centred at different phase angles, that means that the hardness itself of the two regions is different. In aged bitumen, indeed, the peaks are shifted to higher phase angles with respect to the pristine bitumen, meaning that both soft and hard regions are harder than the corresponding soft and hard regions of the reference bitumens. This can be somehow expected after an ageing process, since it causes an increase in the fraction of the hard region which hinders the dynamics of the remaining softer part obliging it to a tighter packing and consequently to a higher hardness. In the images relating to the samples with the addition of the regenerating additive TPI, an increase in the fraction of the soft areas is observed as well as a shift back to lower phase angles which resembles the images for non-aged bitumen. Samples with soy oil, instead, showed very similar images to those recorded for aged bitumen.

A different visualization, obtained with the 3D reconstruction, is also reported (third column).

As a conclusion, AFM analysis seems to be able to distinguish the rejuvenating effect from a mere fluxing one. In fact, AFM probes a structural aspect directly connected to the polarity of the asphaltene molecules, therefore catching changes in the chemistry of the material under study. These effects can be justified considering for the chemical nature of the two additives: soy oil is essentially an apolar fluid, so it is expected that it will be localized within the more apolar part of the bitumen (maltene); on the other hand, TPI has a phosphate headgroup which can establish stronger (polar) interactions. The possibility to establish strong interaction of molecules possessing a phosphate group has been recently pointed out [47].

In these systems, the simultaneous presence of a polar phosphate group and an apolar molecular moiety, renders organic phosphates truly amphiphilic molecules, for which particular self-assembly is expected. In particular, a specific localization with the phosphate group strictly interacting with the asphaltene polar domains can be safely hypothesized, with the rest of the molecules pointing towards the apolar (maltene) region, most probably interacting with nearby resins since these ones are located at the same asphaltene/maltene interfaces. However, it is to be considered essential that if several amphiphiles are close to each other they can give rise to peculiar self-assemblies [48] with unexpected emerging properties and dynamics [49,50] up to the formation of ionic liquids [51]. Consequently, the characteristic effect of the TPI is due not only to its peculiar structure, but also to the combined action with the other stabilising amphiphiles naturally present in the bitumens.

The complex self-assembly of amphiphiles has been recently highlighted for specific applicative purposes in various applications of inorganic, organic and pharmaceutical fields [52–59] and this clearly shows the enormous potentialities of such strategy. So, in the specific, we strongly support research in this direction to easily find additives for bitumens with high added-value.

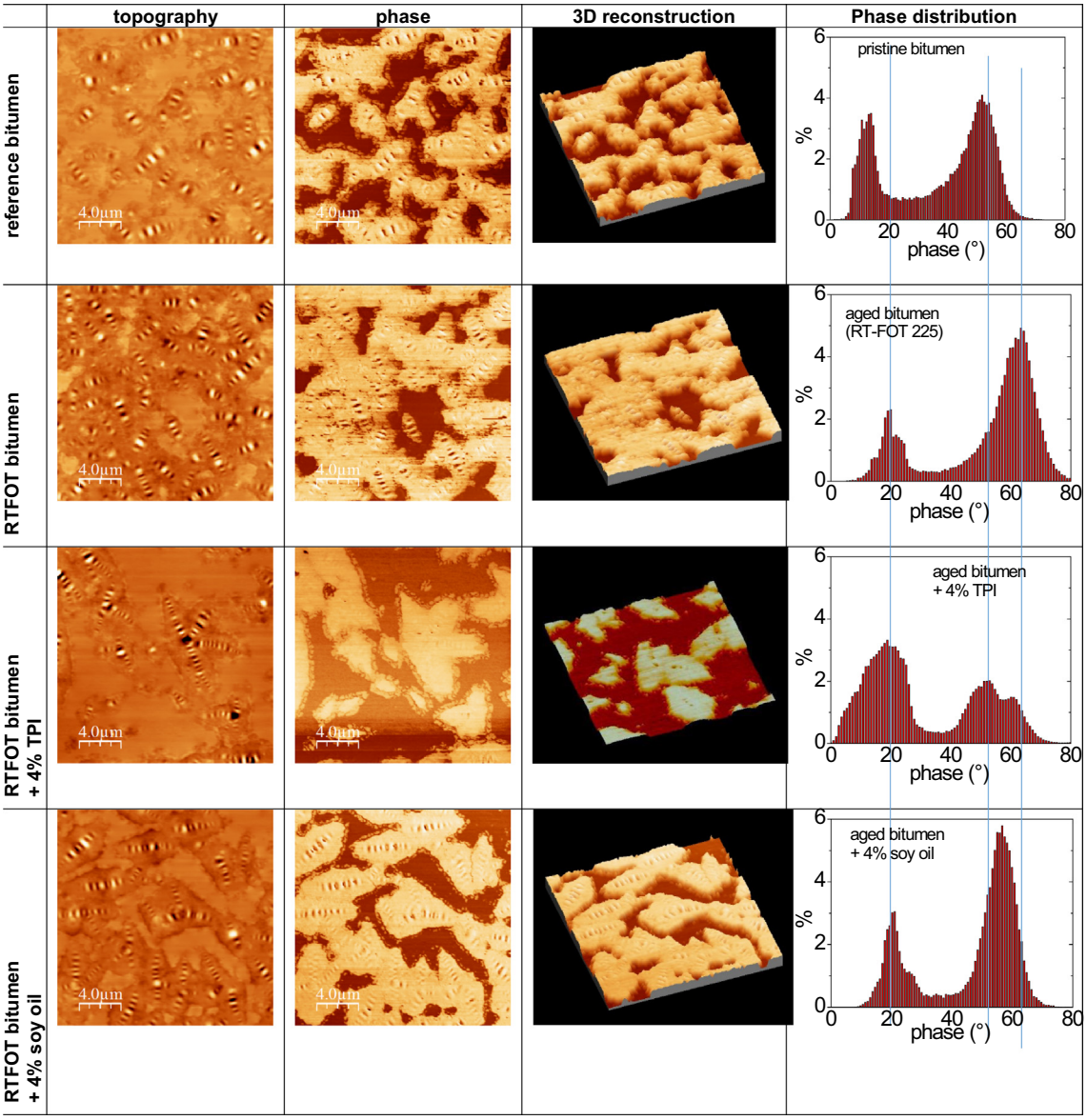


**Fig. 4.** AFM images of the studied sample. Each panel, reports in clockwise order, the topographic, the phase image and the 3D (black background) reconstruction.

This methodology will also make it possible to establish, by means of sampling (coring) in situ and extraction of the binder, both the degree of aging of a road so as to be able to plan any maintenance interventions, and to verify, in cases where the road pavement has been built with a certain fraction of recycled material (Recycled Asphalt Pavement, RAP), the quality of the conglomerate and the successful regeneration of the bitumen can be ascribed to the RAP. In fact, the bodies proposed for quality control (such as ANAS in Italy, NCAT and NAPA in U.S.A., AIA in U.K., etc.) currently do not have laboratory methods capable of distinguishing whether an aged bitumen has actually been regenerated or simply softened so as to make it workable during the production of the conglomerate but not suitable for supporting the traffic loads of a road in when it will continue to have glassy properties due to oxidation of the binder. For example, in the ANAS Special Tender Specifications there are not the standards or methods to distinguishing whether an aged bitumen has actually been regenerated or simply softened but there are only standards or methods to evaluate the performance of the physical properties of the binder/conglomerate/road pavement [60].

### 3.4. Infra-Red spectroscopy (IR)

FTIR is a well-known method for investigating the chemical changes in bitumen due to aging as it probes different functional groups and molecular bonds [61].

As it can be seen from perusal of Fig. 5, where the absorbance spectra of the studied samples are reported, marked differences can be highlighted. Of particular interest are:

1. the peak around 750 $cm^{-1}$, which can be assigned to the C-S stretching;
2. the peak around 1215, which can be assigned to the stretching of C-O-C in ethers and/or of S = O in sulfonic acids;
3. the peak occurring around 1460 $cm^{-1}$o the peaks related to the asymmetric vibration of $CH_2$ and $CH_3$ [62];

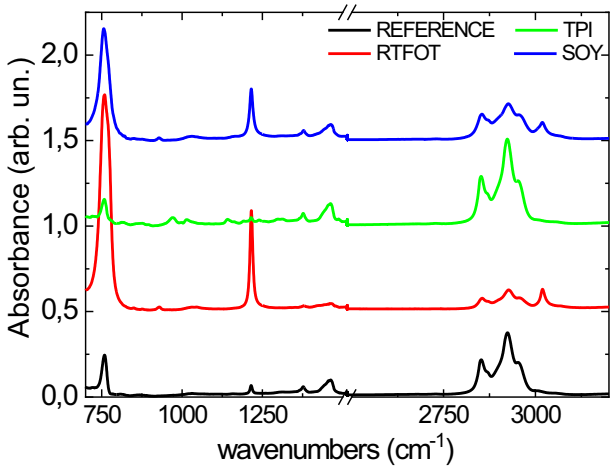


**Fig. 5.** IR spectra for the studied samples. Spectra are vertically shifted for clarity sake.

4. the multiplet in the 2750–3050 range ($CH_2$ and $CH_3$ symmetric and antisymmetric stretching) hereafter referred to as 3000 $cm^{-1}$, for simplicity.

It should be emphasized that in the literature some peaks attributions are non-univocal and sometimes also questionable, probably due to the complexity of the material under investigation. So, in these cases, we referred to classical academic textbooks [63]. It is also important, for this investigation, to stress that the first two peaks are attributed to oxidized parts of asphaltenes, whereas the other two (peak # 3 and #4) are attributed to the hydrocarbonaceous part of the bitumen.

Since the IR spectra have been recorded on samples prepared by weighing the same amount of the respective bitumens, some qualitative comments from the visual inspection of the variations in peaks intensity can already be made. It can clearly be seen that ageing causes an increase of the peak at 750 and 1215 and a reduction of the other two signals. This is ascribed to the ageing, in which oxidation causes a chemical towards the formation of oxidized functional groups. Self-consistently, the addition of soy oil causes a moderate return of the intensity of each of these peaks to its pristine value. More markedly, TPI causes a return to values comparable to the pristine ones.

To make a more quantitative analysis, the ratio of the intensity of a peak (peak #1 or #2) attributed to an oxidized part of the material over the intensity of a peak (peak #3 or #4) attributed to a hydro-carbonaceous part was calculated.

Being ratios of different peaks they would show *relative* intensities, a strategy adopted in the literature [64–66] to face the fact that the absolute intensity of an IR peak can be hardly be treated quantitatively.

The obtained ratios are reported in Table 1. In this table, the subscripted numbers report the wavenumbers of the peaks under consideration; for example, the $I_{750}/I_{3000}$ ratio represents the intensity of the peak at 750 $cm^{-1}$ over the intensity of the peak at 3000 $cm^{-1}$.

**Table 1**
Peak intensity ratios discussed in the text.

| Sample | I760/ I1460 | I760/ I3000 | I1215/ I1460 | I1215/ I3000 |
|---|---|---|---|---|
| Reference bitumen | 2.5 | 0.7 | 1.0 | 0.3 |
| RTFOT bitumen | 25.4 | 9.8 | 11.8 | 4.5 |
| RTFOT bitumen + 4 %TPI | 1.1 | 0.3 | 0.4 | 0.1 |
| RTFOT bitumen + 4 %soy oil | 6.9 | 3.1 | 3.2 | 1.4 |

Let's take into consideration any of them: it can be seen that this ratio markedly increases with aging as a result of the formation of oxidized functional groups at the expenses of C-H aliphatic groups. Soy oil is able to reduce the value but it is not able to restore it to its pristine value. On the other hand, TPI exerts a stronger effect pushing back the value to the pristine one, and even lower. Self- consistently, the same consideration can be made if all the other ratios are considered.

This analysis clearly shows that the changes made by ageing can be partially cancelled by soy oil, but TPI shows a stronger power being able to restore the chemistry of pristine bitumen. FTIR seems, therefore, to be able to distinguish a rejuvenating additive from a mere fluxing agent. In fact, FTIR is able to probe the functional groups of the material under study, therefore catching changes in its chemistry. IR spectroscopy is already used in the road paving sector to identify the presence of some additives such as adhesion promoter within the bitumen used for bituminous conglomerates. Therefore, a methodology based on the use of an instrumentation already present in the various technical annexes, specifications, etc. made by the bodies responsible for the construction of road pavements, will facilitate its diffusion within the sector and will allow all laboratories involved in the quality control of bituminous conglomerates (such as ANAS, NCAT, NAPA, etc.) to be able to introduce further information, relating to the rejuvenation of bitumen, without having to make investments on equipment or qualified personnel.

## 4. Conclusions

Given the now well-established difference between a simple fluxing agent and a real rejuvenator to restore the mechanical properties of an aged bitumen to the pristine performances, we have investigated the capability of the techniques most common in bitumen analysis to distinguish between the two.

We have shown that oscillatory rheometry is not fit for this purpose, whereas optical and atomic force microscopies and infrared spectroscopy can be.

The possibility to make this distinction with instrumentation available in common laboratories will introduce further information on to the rejuvenation of bitumen, allowing the quick and effective quality control of the additives to be used as regenerants for bitumen and without further investments on equipment or qualified personnel.

## Declaration of Competing Interest

The author declare that there is no conflict of interest.

## References

[1] J.C. Petersen, Chemical composition of asphalt as related to asphalt durability: State of the art Transport, Transp. Res. Rec. 999 (1984) 13–30.
[2] F. Deygout, Volatile emissions from hot bitumen storage tanks, Environ. Prog. Sustain. Energy 30 (2011) 102–112, https://doi.org/10.1002/ep.10444.
[3] G. Boczkaj, A. Przyjazny, M. Kamiński, Characteristics of volatile organic compounds emission profiles from hot road bitumens, Chemosphere 107 (2014) 23–30, https://doi.org/10.1016/j.chemosphere.2014.02.070.
[4] H. Soenen, X. Lu, O.V. Laukkanen, Oxidation of bitumen: molecular characterization and influence on rheological properties, Rheol Acta 55 (2016) 315–326, https://doi.org/10.1007/s00397-016-0919-6.
[5] V.V. Vasilyev, E.V. Salamatova, N.V. Maidanova, M.V. Kalinin, V.M. Strakhov, Change in properties of roadmaking bitumen on oxidation, Coke Chem. 63 (2020) 307–314, https://doi.org/10.3103/S1068364X20060083.
[6] F.L. Roberts, P.S. Kandhal, E.R. Brown, D.Y. Lee, T.W. Kennedy, Hot Mix Asphalt Materials, Mixture Design and Construction. 2th ed. NAPA: Lanham, MD, USA; n.d.
[7] H. Asli, E. Ahmadinia, M. Zargar, M.R. Karim, Investigation on physical properties of waste cooking oil – rejuvenated bitumen binder, Constr. Build. Mater. 37 (2012) 398–405, https://doi.org/10.1016/j.conbuildmat.2012.07.042.

[8] C.D. Dedene, Z. You, The performance of aged asphalt materials rejuvenated with waste engine oil, Int. J. Pavement Res. Technol. 7 (2014) 145–152, https://doi.org/10.6135/ijprt.org.tw/2014.7(2).145.

[9] P. Calandra, P. Caputo, M. De Santo, L. Todaro, V. Liveri, C. Oliviero, Effect of additives on the structural organization of asphaltene aggregates in bitumen, Constr. Build. Mater. 199 (2018) 288–297, https://doi.org/10.1016/j.conbuildmat.2018.11.277.

[10] P. Caputo, M. Porto, V. Loise, B. Teltayev, C.O. Rossi, Analysis of mechanical performance of bitumen modified with waste plastic and rubber (SBR) additives by rheology and PGSE NMR experiments, Eurasian Chem. J. 21 (2019) 235–239, https://doi.org/10.18321/ectj864.

[11] P. Caputo, V. Loise, A. Crispini, C. Sangiorgi, F. Scarpelli, Rossi C. Oliviero, The efficiency of bitumen rejuvenator investigated through Powder X-ray Diffraction (PXRD) analysis and T <inf>2</inf> -NMR spectroscopy, Colloids Surfaces A Physicochem. Eng. Asp 571 (2019), https://doi.org/10.1016/j.colsurfa.2019.03.059.

[12] F. Pahlavan, A. Rajib, S. Deng, P. Lammers, E.H. Fini, Investigation of balanced feedstocks of lipids and proteins to synthesize highly effective rejuvenators for oxidized asphalt, ACS Sustain. Chem. Eng. 8 (2020) 7656–7667, https://doi.org/10.1021/acssuschemeng.0c01100.

[13] Samieadel A, Islam Rajib A, Phani Raj Dandamudi K, Deng S, Fini EH. Improving recycled asphalt using sustainable hybrid rejuvenators with enhanced intercalation into oxidized asphaltenes nanoaggregates. Constr Build Mater 2020;262:120090. https://doi.org/https://doi.org/10.1016/j.conbuildmat.2020.120090.

[14] L. Gungat, N.A. Ispal, N.C. Hiong, M.O. Hamzah, Recycled Materials and Warm Mix Asphalt Technology: A Green Approach in Pavement Modification BT - Advances in Waste Processing Technology. In: Yaser AZ, editor., Singapore: Springer Singapore; 2020, p. 195–218. https://doi.org/10.1007/978-981-15-4821-5_13.

[15] C.O. Rossi, P. Caputo, V. Loise, S. Ashimova, B. Teltayev, C. Sangiorgi, A new green rejuvenator: evaluation of structural changes of aged and recycled bitumens by means of rheology and NMR. vol. 20. 2019. https://doi.org/10.1007/978-3-030-00476-7_28.

[16] P. Caputo, V. Loise, S. Ashimova, B. Teltayev, R. Vaiana, Rossi C. Oliviero, Inverse Laplace Transform (ILT)NMR: a powerful tool to differentiate a real rejuvenator and a softener of aged bitumen, Colloids Surfaces A Physicochem Eng Asp 574 (2019) 154–161, https://doi.org/10.1016/j.colsurfa.2019.04.080.

[17] D. Petrauskas, U. Saleem, The Shell bitumen handbook. Read, J., Whiteoak, D. (2003). Shell Bitum. handbook. Thomas Telford., 2003, p. 29. https://doi.org/10.1680/sbh.32200.

[18] E. Shaffie, A.K. Arshad, A. Alisibramulisi, J. Ahmad, W. Hashim, Z. Abd Rahman, et al., Effect of mixing variables on physical properties of modified bitumen using natural rubber latex, Int. J. Civ. Eng. Technol. 9 (2018) 1812–1821.

[19] C. Oliviero, S. Ashimova, P. Calandra, M. De Santo, R. Angelico, Mechanical resilience of modified bitumen at different cooling rates: a rheological and atomic force microscopy investigation, Appl. Sci. 7 (2017) 779, https://doi.org/10.3390/app7080779.

[20] R. Hunter, A. Self, J. Read, The Shell Bitumen Handbook. 6th ed. ICE Publishing, London, 2015.

[21] E. Remišová, V. Zatkaliková, F. Schlosser, Study of rheological properties of bituminous binders in middle and high temperatures, Civ. Environ. Eng. 12 (2018) 13–20, https://doi.org/10.1515/cee-2016-0002.

[22] Barnes H, Hutton JF, Walters K. An introduction to rheology, 1989.

[23] R.G. Larson, The structure and rheology of complex fluids. New York (N.Y.) : Oxford university press; 1999.

[24] L. Zanzotto, J. Stastna, O. Vacin, Thermomechanical properties of several polymer modified asphalts, Appl. Rheol. 10 (2000) 185–191, https://doi.org/10.1515/arh-2000-0012.

[25] H. Jahanbakhsh, M. Karimi, Nejad F. Moghadas, B. Jahangiri, Viscoelastic-based approach to evaluate low temperature performance of asphalt binders, Constr Build Mater 2016;128:384–98. https://doi.org/https://doi.org/10.1016/j.conbuildmat.2016.10.073.

[26] B. Hill, D. Oldham, B. Behnia, E. Fini, W. Buttlar, H. Reis, Evaluation of low temperature viscoelastic properties and fracture behavior of bio-asphalt mixtures, Int. J. Pavement Eng. (2016) 1–8, https://doi.org/10.1080/10298436.2016.1175563.

[27] X.-Y. Wang, X.-M. Xie, L.-Q. Wang, J.-F. Su, Y.-D. Guo, R. Mu, Rheological behaviour of bitumen blending with self-healing microcapsule: effects of physical and chemical interface structures, Colloids Surfaces A Physicochem Eng Asp 586 (2020), https://doi.org/10.1016/j.colsurfa.2019.124212 124212.

[28] J. Zhou, X. Chen, G. Xu, Q. Fu, Evaluation of low temperature performance for SBS/CR compound modified asphalt binders based on fractional viscoelastic model, Constr. Build. Mater. 214 (2019) 326–336, https://doi.org/10.1016/j.conbuildmat.2019.04.064.

[29] P. Caputo, M. Porto, P. Calandra, M.P. De Santo, Rossi C. Oliviero, Effect of epoxidized soybean oil on mechanical properties of bitumen and aged bitumen, Mol. Cryst. Liq. Cryst. 675 (2018) 68–74, https://doi.org/10.1080/15421406.2019.1606979.

[30] M. Porto, P. Caputo, V. Loise, G. De Filpo, C. Oliviero Rossi, P. Calandra, Polysaccharides-reinforced Bitumens: specificities and universality of rheological behavior, Appl Sci 9 (2019) 5564, https://doi.org/10.3390/app9245564.

[31] L. Bohlin, A theory of flow as a cooperative phenomenon, J. Colloid Interface Sci. 74 (1980) 423–434, https://doi.org/10.1016/0021-9797(80)90211-8.

[32] H.H. Winter, Can the gel point of a cross-linking polymer be detected by the G′ – G″ crossover?, Polym. Eng. Sci. 27 (1987) 1698–1702, https://doi.org/10.1002/pen.760272209.

[33] D. Gabriele, B. de Cindio, P. D'Antona, A weak gel model for foods, Rheol. Acta 40 (2001) 120–127, https://doi.org/10.1007/s003970000139.

[34] (ASTM) M. D 6560-00; IP 143/01: Standard Test Method for Determination of Asphaltenes (heptaine Insolubles) in Crude Petroleum and Petroleum Products. ASTM; 2000.

[35] C. Oliviero, P. Caputo, G. Luca, L. Maiuolo, S. Eskandarsefat, C. Sangiorgi, 1H-NMR spectroscopy: a possible approach to advanced bitumen characterization for industrial and paving applications, Appl. Sci. 8 (2018), https://doi.org/10.3390/app8020229.

[36] M.R. Gray, G. Assenheimer, L. Boddez, W.C. McCaffrey, Melting and fluid behavior of asphaltene films at 200–500 °C, Energy Fuels 18 (2004) 1419–1423, https://doi.org/10.1021/ef049923w.

[37] X. Li, Y. Guo, Q. Sun, W. Lan, A. Liu, X. Guo, Experimental study for the impacts of flow rate and concentration of asphaltene precipitant on dynamic asphaltene deposition in microcapillary medium, J. Pet. Sci. Eng. 162 (2018) 333–340, https://doi.org/10.1016/j.petrol.2017.12.031.

[38] S.C. Michaelides, editor., Precipitation: Advances in Measurement, Estimation and Prediction. Springer-Verlag Berlin Heidelberg; 2008.

[39] Y. Zhang, T. Takanohashi, S. Sato, I. Saito, R. Tanaka, Observation of glass transition in asphaltenes, Energy Fuels 18 (2004) 283–284, https://doi.org/10.1021/ef0301147.

[40] P. Thiyagarajan, J.E. Hunt, R.E. Winans, K.B. Anderson, J.T. Miller, Temperature-dependent structural changes of asphaltenes in 1-methylnaphthalene, Energy Fuels 9 (1995) 829–833, https://doi.org/10.1021/ef00053a014.

[41] R. Tanaka, J.E. Hunt, R.E. Winans, P. Thiyagarajan, S. Sato, T. Takanohashi, Aggregates structure analysis of petroleum asphaltenes with small-angle neutron scattering, Energy Fuels 17 (2003) 127–134, https://doi.org/10.1021/ef020019i.

[42] J.-F. Masson, V. Leblond, J. Margeson, Bitumen morphologies by phase-detection atomic force microscopy, J Microsc 221 (2006) 17–29, https://doi.org/10.1111/j.1365-2818.2006.01540.x.

[43] P.K. Das, N. Kringos, V. Wallqvist, B. Birgisson, Micromechanical investigation of phase separation in bitumen by combining atomic force microscopy with differential scanning calorimetry results, Road Mater. Pavement Des. 14 (2013) 25–37, https://doi.org/10.1080/14680629.2013.774744.

[44] Y.A. Golubev, O.V. Kovaleva, N.P. Yushkin, Observations and morphological analysis of supermolecular structure of natural bitumens by atomic force microscopy, Fuel 87 (2008) 32–38, https://doi.org/10.1016/j.fuel.2007.04.005.

[45] R. Tanaka, E. Sato, J.E. Hunt, R.E. Winans, S. Sato, T. Takanohashi, Characterization of asphaltene aggregates using X-ray diffraction and small-angle X-RAY Scattering, Energy Fuels 18 (2004) 1118–1125, https://doi.org/10.1021/ef034082z.

[46] A. Jäger, R. Lackner, C. Eisenmenger-Sittner, R. Blab, Identification of microstructural components of bitumen by means of atomic force microscopy (AFM), PAMM 4 (2004) 400–401, https://doi.org/10.1002/pamm.200410181.

[47] P. Calandra, T. De caro, D. Caschera, D. Lombardo, L. Todaro, V. Liveri, Spectroscopic and structural characterization of pure and FeCl3-containing tri-n-butyl phosphate. Colloid Polym Sci 2014;293:597–603. https://doi.org/10.1007/s00396-014-3439-x.

[48] P. Calandra, A. Ruggirello, A. Mele, V.T. Liveri, Self-assembly in surfactant-based liquid mixtures: Bis(2-ethylhexyl)phosphoric acid/bis(2-ethylhexyl) amine systems, J Colloid Interface Sci 348 (2010) 183–188, https://doi.org/10.1016/j.jcis.2010.04.031.

[49] P. Calandra, I. Nicotera, C.O. Rossi, V.T. Liveri, Dynamical properties of self-assembled surfactant-based mixtures: triggering of one-dimensional anomalous diffusion in bis(2-ethylhexyl)phosphoric acid/n-octylamine systems, Langmuir 29 (2013) 14848–14854, https://doi.org/10.1021/la403522q.

[50] P. Pitzalis, R. Angelico, O. Soderman, M. Monduzzi, Structural investigation of CaAOT/water/oil microemulsions, Langmuir 16 (2000) 442–450, https://doi.org/10.1021/la990656.

[51] V. Turco Liveri, D. Lombardo, M. Pochylski, P. Calandra, Molecular association of small amphiphiles: origin of ionic liquid properties in dibutyl phosphate/propylamine binary mixtures, J. Mol. Liq. 263 (2018) 274–281, https://doi.org/10.1016/j.molliq.2018.05.003.

[52] A.E. Somers, P.C. Howlett, D.R. MacFarlane, M. Forsyth, A review of ionic liquid lubricants, Lubr 1 (2013), https://doi.org/10.3390/lubricants1010003.

[53] L. Maiuolo, V. Algieri, F. Olivito, A. De Nino, Recent developments on 1,3-dipolar cycloaddition reactions by catalysis in green solvents, Catal 10 (2020), https://doi.org/10.3390/catal10010065.

[54] L. Maiuolo, B. Russo, V. Algieri, M. Nardi, M.L. Di Gioia, M.A. Tallarida, et al., Regioselective synthesis of 1,5-disubstituted 1,2,3-triazoles by 1,3-dipolar cycloaddition: Role of Er(OTf)3, ionic liquid and water, Tetrahedron Lett 60 (2019) 672–674, https://doi.org/10.1016/j.tetlet.2019.01.053.

[55] R.D. Falcone, N.M. Correa, J.J. Silber, Amphiphilic ionic liquids as sustainable components to formulate promising vesicles to be used in nanomedicine, Curr. Opin. Green Sustain. Chem. 26 (2020), https://doi.org/10.1016/j.cogsc.2020.100382 100382.

[56] B. Yoo, J.K. Shah, Y. Zhu, E.J. Maginn, Amphiphilic interactions of ionic liquids with lipid biomembranes: a molecular simulation study, Soft Matter 10 (2014) 8641–8651, https://doi.org/10.1039/C4SM01528B.

[57] P. Calandra, On the physico-chemical basis of self-nanosegregation giving magnetically-induced birefringence in dibutyl phosphate/bis(2-ethylhexyl) amine systems, J. Mol. Liq. 310 (2020), https://doi.org/10.1016/j.molliq.2020.113186 113186.
[58] R. Angelico, A. Ceglie, F. Cuomo, Reaction mixtures based on the CTAB-Dodecyl Epoxide-water microemulsion for the synthesis of novel Nucleo-Lipids, Colloids Surf., B 70 (2009) 68–75, https://doi.org/10.1016/j.colsurfb.2008.12.015.
[59] R. Angelico, L. Ambrosone, A. Ceglie, I. Losito, G. De Zio, F. Palmisano, Complementary amphiphilic ribonucleotides confined into nanostructured environments, Phys. Chem. Chem. Phys. 12 (2010) 7977–7987, https://doi.org/10.1039/c001781g.
[60] ANAS. Special Tender Specification. In Road Paving; Technical Standard; 2009.
[61] M. Zargar, E. Ahmadinia, H. Asli, M.R. Karim, Investigation of the possibility of using waste cooking oil as a rejuvenating agent for aged bitumen, J. Hazard Mater. 233–234 (2012) 254–258, https://doi.org/10.1016/j.jhazmat.2012.06.021.
[62] P. Marsac, N. Piérard, L. Porot, W. Van den bergh, J. Grenfell, V. Mouillet, et al., Potential and limits of FTIR methods for reclaimed asphalt characterisation, Mater. Struct. 2014;47:1273–86. https://doi.org/10.1617/s11527-014-0248-0.
[63] D.L. Pavia, G.M. Lampman, G.S. Kriz, Introduction to Spectroscopy. 3rd ed., Harcourt College, 2001.
[64] P. Nayak, U.C. Sahoo, Rheological, chemical and thermal investigations on an aged binder rejuvenated with two non-edible oils, Road Mater Pavement Des 18 (2017) 612–629, https://doi.org/10.1080/14680629.2016.1182058.
[65] C. Roche, M. Ven, W. Van den bergh, T. Gabet, V. Dubois, J. Grenfell, et al. Development of a laboratory bituminous mixtures ageing protocol. Adv. Test. Charact. Bitum. Mater., 2009. https://doi.org/10.1201/9780203092989.ch33.
[66] J. Lamontagne, P. Dumas, V. Mouillet, J. Kister, Comparison by Fourier transform infrared (FTIR) spectroscopy of different ageing techniques: application to road bitumens, Fuel 80 (2001) 483–488, https://doi.org/10.1016/S0016-2361(00)00121-6.

applied sciences

MDPI

*Article*

# Stability of Bituminous Emulsion Induced by Waste Based Bio-Surfactant

**Michele Porto, Paolino Caputo *, Abraham A. Abe, Valeria Loise * and Cesare Oliviero Rossi**

Department of Chemistry and Chemical Technologies, University of Calabria, Via P. Bucci, Cubo 14/D, 87036 Rende, Italy; michele.porto@unical.it (M.P.); abraham.abe@unical.it (A.A.A.); cesare.oliviero@unical.it (C.O.R.)

* Correspondence: paolino.caputo@unical.it (P.C.); valeria.loise@unical.it (V.L.)

**Abstract:** In the asphalt industry, bituminous emulsions are widely used in road pavement operations and in building/construction processes such as cold mix asphalt and waterproofing processes, respectively. A very important fact to keep in mind is that not all types of bitumen are suitable for the realization of bituminous emulsions. This is largely due to the variation in their chemical nature and the different cracking processes carried out on the bitumen during the fractional distillation process in the petroleum industry. The objective of this study is to identify the underlying causes of the non-emulsionability of bitumen using Nuclear Magnetic Resonance (NMR) and Dynamic Shear Rheology (DSR) analysis. NMR analysis aims at identifying the fundamental chemical components that are responsible for the emulsionability of the bitumen binder and how important their role is in this phenomenon. On the other hand, the DSR analysis is aimed at determining if the rheological (viscoelastic) behavior of bitumen is implicated in its emulsionability. The indications gotten from the data produced by these techniques, enable us as soon as the analyzed bitumen is deemed non-emulsionable to identify what type of additive can be used to modify the bitumen and alleviate its non-emulsionability until a point where its chemical components become ideal for the realization of bituminous emulsions. In this research work, a model bitumen (labelled as Cimar) which is known for its excellently high emulsionability in the production of anionic bituminous emulsions was used as the reference sample. Two bitumens (labelled as Adriatica and Alma) which from preliminary testing were deemed non-emulsionable were alongside the additives selected and subjected to the aforementioned techniques for analysis on their emulsionability. The NMR data obtained allowed the identification of the chemical nature of the components of the analyzed bitumens and the design of the right additive which improves the bitumen and makes it suitable for the preparation of emulsions. In addition to these, a largely uncommon however effective method of acid number determination of bitumen gave indications on an underlying factor which largely influences the emulsionability of bitumen. An aliphatic and an aromatic surfactant were identified thanks to the spectroscopic findings in this study.

**Keywords:** bituminous emulsion; rheological properties; nuclear magnetic resonance (NMR) spectroscopy

check for updates

**Citation:** Porto, M.; Caputo, P.; A. Abe, A.; Loise, V.; Oliviero Rossi, C. Stability of Bituminous Emulsion Induced by Waste Based Bio-Surfactant. *Appl. Sci.* **2021**, *11*, 3280. https://doi.org/10.3390/app11073280

Academic Editor: Bettina Wolf

Received: 11 February 2021
Accepted: 31 March 2021
Published: 6 April 2021

**Publisher's Note:** MDPI stays neutral with regard to jurisdictional claims in published maps and institutional affiliations.

**Copyright:** © 2021 by the authors. Licensee MDPI, Basel, Switzerland. This article is an open access article distributed under the terms and conditions of the Creative Commons Attribution (CC BY) license (https://creativecommons.org/licenses/by/4.0/).

## 1. Introduction

Bitumen is a viscoelastic material derived from the petroleum industry and for this reason its chemical composition is hugely dependent on the initial crude oil and the cracking process carried out on it. It is not miscible with water and this feature is fundamental for the production of emulsions. From a chemico–physical point of view, the emulsification process involves the dispersion of a fluid in another provided that the two are not miscible with each other. When this phenomenon occurs, one of the two fluids breaks into drops, while the other exists as a continuous medium. Generally, emulsions are of two types: water in oil or oil in water, depending on whether the dispersing part (continuous medium)

is water or oil [1,2]. Emulsions of this type are thermodynamically unstable systems; in fact, their free energy decreases over time [3]. However, it is possible to stabilize an emulsion with the use of emulsifiers [4,5].

The latter are surfactants, i.e., molecules with a polar (hydrophilic) head and a non-polar (lipophilic) tail. Thanks to their amphiphilic nature, surfactants are adsorbed at the interface of the two phases, arranging themselves with the polar head in the aqueous phase, and with the non-polar tail in the organic phase. This mechanism facilitates the reduction of the interfacial tension between the droplets and the dispersing phase [6]. Bituminous emulsion is a worldwide technology, and its first application was patented in the early 1900s [7] being mainly used for pavement maintenance and road repair. Bituminous emulsions are oil-in-water emulsions in which droplets of bitumen are dispersed in the continuous aqueous phase. In order to reduce the interfacial tension and prevent coalescence phenomena, ionic surfactants are used. The salt form of the fine surfactant is solubilized in water before its addition to the bitumen. The two fluids are poured simultaneously into a colloidal mill, whose rotation speed is between 1000 and 6000 rpm. This speed causes the breaking of the bitumen into small droplets, typically between 1 and 10 µm in diameter, readily covered by the emulsifier [8–10]. The main uses of bitumen emulsions are in road building, roofing and waterproofing [11–14].

Bituminous emulsions are commonly studied in terms of stability, asphalt performance, breaking times [15–17]. Emulsions can be identified according to their chemical nature, basicity or acidity.

The innovative endpoint of the research work behind this article is to make bitumens emulsifiable or rather to understand why some bitumens are not emulsifiable. In this work, only basic emulsions are investigated, without compromising the generality of the proposed methodological approach. Not all types of bitumen used in the road paving sector are emulsifiable under basic conditions. This work therefore aims to identify the chemico–physical causes of the non-emulsifiability of the aforementioned bitumens and to find suitable additives capable of making them emulsifiable [14].

## 2. Materials and Methods

### 2.1. Chemicals and Materials

Three pristine bitumens from different sources are tested in this work: one with a penetration grade of 70/100 from Venezuela (labelled as Cimar), used as the reference sample, the second one with a penetration grade of 70/100 from an Italian refinery—Alma Petroli S.p.A. (labelled as Alma) and the third one also from an Italian refinery—Adriatica Bitumi S.p.A. (labelled as Adriatica). All three bitumens were supplied by Cimar Produzione S.r.l. (Italy); more information is reported in Table 1. A commercial wax (SASOBIT) and a waste from animal fat processing processes supplied by S2A Soluzioni Ambientali in the form of liquid pitches which was labelled as LP were used as additives. Another additive, an aliphatic/aromatic acid surfactant labelled as AS which is used in the field of cosmetics and soap production, supplied by Kimical S.r.l. (Italy) was also used. All of these aforementioned substances were used as additives in this study.

**Table 1.** Physical properties of bitumens used in this study.

| Measured Properties | Standard | Unit | Cimar 70/100 | Adriatica 170/210 | Alma 70/100 |
|---|---|---|---|---|---|
| Penetration at 25 °C | EN 1426 | 0.1 mm | 66 ± 1 | 185 ± 1 | 68 ± 1 |
| Softening point | EN 1427 | °C | 47.8 ± 0.2 | 42.6 ± 0.2 | 47.2 ± 0.2 |
| Flash point | EN 2592 | °C | ≥230 | ≥220 | ≥230 |
| Solubility | EN 12592 | % (m/m) | ≥99 | ≥99 | ≥99 |

### 2.2. Sample Preparations

In general, the emulsions prepared are composed of 50–60% by weight of bitumen and 40–50% of water.

The percentage of emulsifier (1–6%) is weighed based on the total weight of the emulsion. During the emulsion process, the pH was kept stable at 14 thus all the prepared emulsions are basic. This emulsifier was supplied by Cimar Produzione S.r.l. (Italy).

Asphaltene Determination

In a vial, a specific mass of bitumen was dissolved in an equal volume in milliliters of chloroform ($CHCl_3$), for example, 3 g of bitumen in 3 mL of $CHCl_3$. Thereafter, n-pentane which was forty times the $CHCl_3$ volume was added to the solution (in the case of 3 mL of $CHCl_3$, 120 mL of n-pentane would be added). The solution was left in a dark chamber for two hours with occasional homogenization of the solution. The asphaltenes which were precipitated were then filtered using a filter paper (Whatman 42 ashless) in a funnel under vacuum conditions. The residue gathered on the filter paper was then washed several times with n-pentane until the solvent became clear and colorless, thus evidencing the absence of any other component other than the asphaltenes. Finally, the filter paper was dried in an oven at 80 °C for three hours and then the residue of the solvent was removed in vacuum for two hours. Just for further facultative analysis, the filtrate containing the maltene fraction was then evaporated to dryness with a rotary evaporator under reduced pressure and the residual solvent was removed under a vacuum pump [18]. This maltene sample was stored for further analysis.

### *2.3. Rheological Characterization*

Dynamic Shear Rheological (DSR) measurements on bitumen samples were carried out using a controlled shear stress rheometer (SR5, Rheometric Scientific, Piscataway, NJ, USA) equipped with a parallel plate geometry (gap 2 mm, φ = 25 mm within the temperature range 25–150 °C) and a Peltier system (±0.1 °C) for temperature control [19].

### *2.4. NMR Measurement*

The $^1$H-NMR spectra were recorded at room temperature on a high-resolution Bruker Avance 500 MHz spectrometer (11.74 T) (Bruker, Rheinstetten, Germany) equipped with a 5-mm TBO probe (Triple Resonance Broadband Observe) and a standard variable-temperature unit BVT-3000. The $^1$H-NMR experiments were performed on bitumen diluted in Carbon Tetrachloride ($CCl_4$), in order to avoid overlapping with a possible proton signal of the solvent. All three analyzed bitumens showed four different peaks referable to protons as reported by Oliviero Rossi et al. [18].

### *2.5. Bitumen Acidic Number Determination Method*

This is a thermometric catalytic titration method carried out according to ASTM D8045 standards. It was used to determine the end point of a chemical reaction (in this case between bitumen in solution and KOH) through the use of a temperature measuring probe and the addition of a chemical to enhance the detection of the endpoint.

## 3. Results and Discussion

Before examining the chemical composition of the bitumen, we calculated the acid number of each sample correlating the values obtained to the emulsionability of each bitumen. A relatively simple method known as Catalytic Thermometric Titration (as described in Section 2.5) was used to determine the acid number of the bitumen samples used for this study. The main advantage of this method is that it is relatively easy to carry out and this method can be adopted by industries who need to determine if a certain bitumen to be used for the production of emulsions is up to emulsionable standards.

As mentioned earlier, this procedure can be carried out in any laboratory and by any technician who understands the basic principle of titration. As per instrumentation, only basic titration apparatus and a temperature measuring probe are needed. In Table 2, we show the results obtained.

**Table 2.** Acid number for each sample.

| Bitumen | Acid Number (mg/g KOH) |
|---|---|
| Cimar | 22.7 |
| Alma | 13.5 |
| Adriatica | 14.7 |

As expected, making the emulsion as indicated in Section 2.2, we observed that the Cimar bitumen is the only one among the three analyzed bitumen samples to be emulsionable. The high acidity of Cimar bitumen (the only emulsionable one) helps us to understand how this parameter could govern the process of bituminous emulsion formation. Hence, the acidity can be used as a key role to evaluate the tendency of a generic bitumen sample to produce a stable emulsion. We proceeded with the characterization of all samples with the aim of identifying the ideal additives which will make the non-emulsionable bitumen samples emulsionable.

Time cure curves (Figure 1) acquired for the three neat bitumens show that, as expected, the two bitumen samples with the same 70/100 penetration grade have very similar rheological behaviors, while Adriatica bitumen has a lower sol–gel transition temperature of about 10 °C.

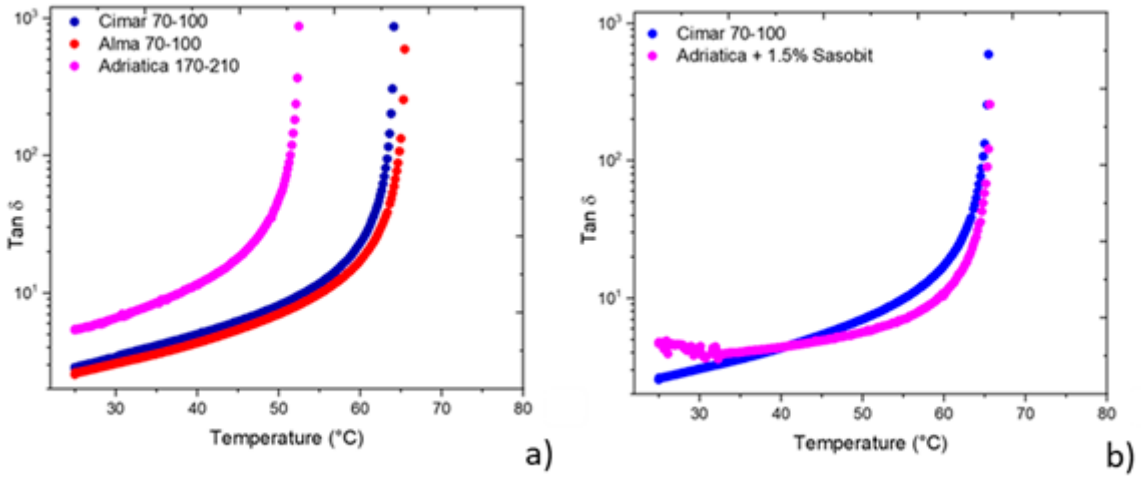


**Figure 1.** (**a**) Time cure test for Cimar 70–100 (blue); Alma 70–100 (red) and Adriatica 170–210. (**b**) Comparison between the time cure test for Cimar and modified Adriatica with 1.5% SASOBIT.

In Table 3, the transition temperature and percentage asphaltene of all the bitumen samples are reported.

**Table 3.** Transition temperature and percentage asphaltene of all bitumen samples.

| Bitumen | Transition Temperature ± 0.1 (°C) | Asphaltene ± 1 (%) |
|---|---|---|
| Cimar | 64.1 | 17 |
| Alma | 64.4 | 31 |
| Adriatica | 52.4 | 19 |

The asphaltene content could play a role in the stability of emulsions; in fact, asphaltenes show an important interfacial activity [20].

Adriatica bitumen shows a different rheological behavior but similar asphaltene concentration to the reference bitumen. Therefore, in order to obtain a mechanical behavior similar to that of the reference bitumen, only the Adriatica bitumen was treated with several modifier additives. On the market, there are several types of modifying additives

with only some of them chemically interacting with the bitumen [21–25]; others simply impart their own chemico–physical properties to it [26–33].

The criteria on which the additive was chosen was its ability to increase the transition temperature without increasing the viscosity of the binder at high temperatures [34–36].

This commercial additive is a wax-based additive called SASOBIT. In fact, at temperatures above 100 °C it acts as a fluxing agent, lowering the viscosity of the binder thus favoring the emulsion process. This additive was added to the Adriatica bitumen in different dosages. In Figure 1b, we reported only the time cure of the best sample obtained with 1.5% additive. This modified bitumen was treated according to the reference experimental conditions for emulsion production. Nevertheless, even in this case, no stable emulsion was obtained proving that the mechanical behavior does not play a decisive role in the formation of bituminous emulsions.

Therefore, having established that the mechanical properties do not significantly affect the emulsifiability of the bitumen, a new approach based on the chemical composition of the bitumen was undertaken. Still using Cimar bitumen as reference, NMR analyses were carried out to obtain more information on the chemical composition of all three bitumens analyzed [18,37–39].

The acquisition of the proton NMR spectra (Figure 2) allowed the characterization of the bitumen under examination from a chemical point of view. Table 4 shows the fractional proton distribution obtained from the normalization and integration of the peaks.

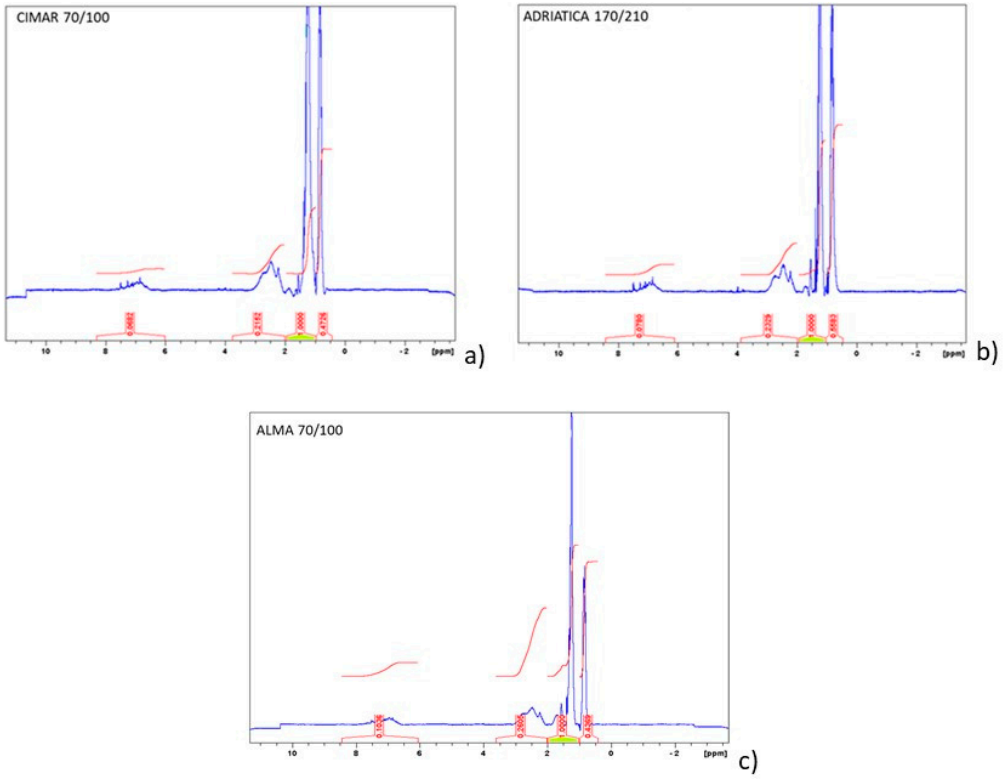


**Figure 2.** $^{1}$H-NMR spectra of Cimar bitumen (**a**), Adriatica bitumen (**b**) and Alma bitumen (**c**).

**Table 4.** Fractional proton distribution of Cimar, Adriatica and Alma bitumens.

| Sample | Hydrogen Distribution ± 0.05 | | | |
|---|---|---|---|---|
| | $H_{ar}$ | $H_{\alpha}$ | $H_{\beta}$ | $H_{\gamma}$ |
| Cimar Bitumen | 3.88 | 12.26 | 56.95 | 26.91 |
| Adriatica Bitumen | 4.17 | 12.46 | 53.50 | 29.87 |
| Alma Bitumen | 5.75 | 14.46 | 55.52 | 24.26 |

By comparing the distribution of the protons of the bitumens analyzed, it emerges that the Cimar bitumen has a similar aromatic character (3.88%) to the Adriatica one (4.17%) while the Alma bitumen has greater aromatic character (5.75) in comparison with the other bitumens. Furthermore, Cimar bitumen is characterized: (i) by having the highest percentage of hydrogens in β compared to the aromatic ring (56.95% against 55.52% and 53.50%); (ii) having a percentage of hydrogens in α (12.26%) in the aromatic ring comparable to that of Adriatica bitumen (12.46%) but lower than that of Alma bitumen (14.46%); (iii) finally, the percentage of methyl hydrogens is intermediate between the percentages of the other two bitumens (26.91% against 24.26% and 29.87%). The major differences correspond to methylene hydrogens in β to the aromatic ring and methyl protons in the γ position. From the information obtained by NMR spectroscopy, it was possible to identify any surfactants that could compensate for the chemical differences between the bitumens.

Adriatica bitumen has a different rheological profile from the reference bitumen, however it has a similar value of percentage asphaltenes and shows values of aromatic components very close to it. This data pointed towards the choice of an additive capable of making the bitumen more acidic without altering the aromatic components, which is an acid aliphatic/aromatic surfactant. In light of this, the commercial additive called "AS" was chosen. This additive is a Brønsted acid surfactant [40,41], consisting of an acid group (polar head), as a substituent of an aromatic ring, and a long hydrophobic chain (lipophilic tail) [42,43]. Thanks to these characteristics, the AS additive has been able to balance both the aromatic and aliphatic components to compensate for the differences with Cimar bitumen.

In fact, once the Adriatica bitumen was modified with AS at different dosages (2.5 to 7.5%), it was possible to proceed with the preparation of the emulsion in accordance with what was done for the emulsion obtained with the Cimar bitumen. This modified bitumen was able to produce stable emulsions and the best emulsion was obtained after modification with 2.5% AS (see Figure 3).

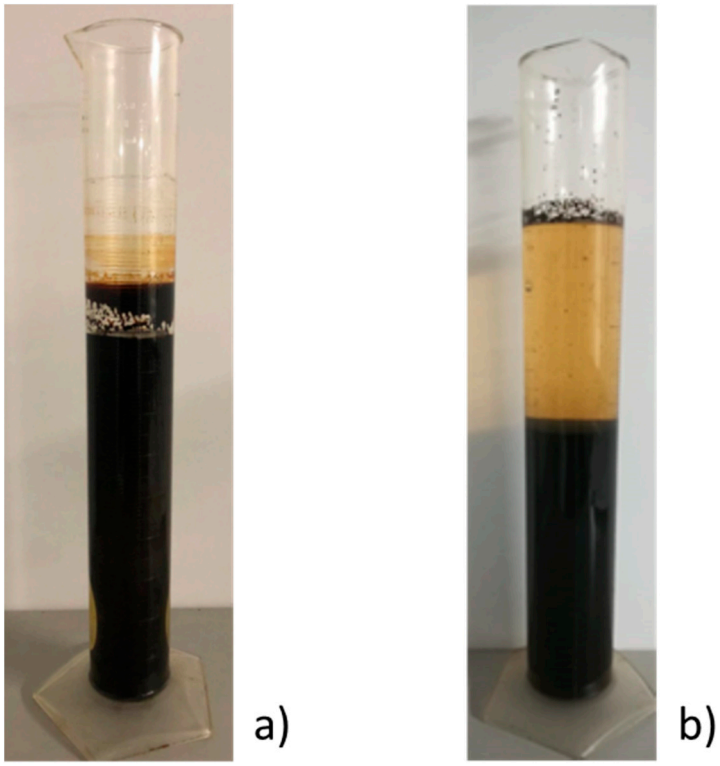


**Figure 3.** Pictorial representation of Adriatica bitumen emulsions obtained with aliphatic/aromatic acid surfactant (AS) additive (**a**), and without AS additive (**b**).

Alma bitumen has a rheological profile very similar to Cimar bitumen (Figure 1a) but has a different percentage of asphaltenes (almost double, see Table 2) [44]. Above all, based on the data obtained by NMR measurements, it is observed that it has a higher aromatic component. Consequently, the function of the additive to be used to make this bitumen more similar to the reference bitumen must be to integrate the maltene part, thus decreasing the asphaltene percentage, lowering the percentage of the aromatic components and also increasing the total acidity of the bitumen with additives. The latter is in fact a central component in the realization of anionic emulsions.

The methodological approach used shows how fundamentally important the chemical nature of bitumen is for the realization of bituminous emulsions. The NMR data obtained give us guidance on the choice of the coadjutant potential of the emulsifier. This step also showed us the importance of determining the acidity of bitumen.

For all these reasons, an aliphatic acidifier called "LP" was identified as a suitable additive. This additive is ecofriendly and facilitates the development and promotion of a circular economy. Its nature is mainly aliphatic and gives an acidic character to the bitumen system and is mainly made up of a mixture of fatty acids (surfactants) [45,46].

The Alma bitumen was modified with LP additive at different dosages (4 to 10%) before proceeding with the preparation of the emulsion in accordance with what was done. This modified bitumen was able to produce stable emulsions and the best emulsion was obtained after modification with 4% LP (see Figure 4).


**Figure 4.** Pictorial representation of Alma bitumen emulsions obtained with liquid pitches (LP) additive (**a**), and without LP additive (**b**).

## 4. Conclusions

There are emulsifiable and non-emulsifiable bitumens on the market and the aim of this study was to identify the type of additive suitable for making non-emulsifiable bitumens emulsifiable.

Two types of approaches were used, one involving the study of the mechanical characteristics and the other a study of the chemical composition of the binders.

The first approach was achieved through rheological analysis and led to the conclusion that the mechanical properties of bitumen do not depict its emulsifiability. In fact, Alma bitumen has a rheological profile similar to that of the reference bitumen but is not emulsifiable. On the other hand, the Adriatica bitumen initially had a different rheological profile from the reference bitumen and was subsequently made similar to the reference through the use of suitable additives. Nevertheless, the Adriatica bitumen remains non-emulsifiable.

The second approach, thanks to the data obtained with NMR measurements, allowed the identification of the problems of the two non-emulsifiable bitumens.

As mentioned earlier, the acid number determination is a useful tool for researchers and most especially for industry personnel to know the acid number of bitumen which they intend to use for production processes. At the moment, we are trying to identify the acid number value limit under which a bitumen sample is non-emulsionable.

In conclusion, we can affirm that, thanks to an approach based on the study of the chemical composition of the various bitumens, it is possible to identify any deficiencies present in the sample and identify additives capable of bridging these gaps which make a non-emulsifiable bitumen suitable for the realization of anionic emulsions.

In the case of the bitumen analyzed in this work, the use of the appropriate additives, LP for Alma bitumen and AS for Adriatica bitumen, made it possible to make both bitumens emulsifiable. Both these additives are eco-friendly and, in the future, have the potential to substitute harmful substances that are used in industrial processes.

**Author Contributions:** Formal analysis (M.P.), investigation, data curation, writing-original draft (P.C.), formal analysis, writing—review & editing (A.A.A.), writing—review & editing (V.L.) supervision, writing—original draft, writing—review & editing (C.O.R.). All authors have read and agreed to the published version of the manuscript.

**Funding:** This research received no external funding.

**Institutional Review Board Statement:** Not applicable.

**Informed Consent Statement:** Not applicable.

**Data Availability Statement:** The data presented in this study are available on request from the corresponding authors.

**Acknowledgments:** Thanks to Cimar Produzione S.r.l. company (Campania, Italy) both for the supply of raw materials and for the contribution and support given for the preparation of the emulsions.

**Conflicts of Interest:** The authors declare no conflict of interest.

## References

1. Leal-Calderon, F.; Schmitt, V.; Bibette, J. *Emulsion Science: Basic Principles*, 2nd ed.; Springer: New York, NY, USA, 2007.
2. Salanger, J.L.; Màrquez, L.; Mira, I.; Pena, A.; Tyrode, E.; Zambran, N.B. Principles of Emulsion Formulation Engineering. In *Adsorption and Aggregation of Surfactants in Solution*; Mittal, K.L., Shah, D.O., Eds.; Marcel Dekker: New York, NY, USA, 2002; pp. 501–523.
3. Kabalnov, A. Thermodynamic and theoretical aspects of emulsions and their stability. *Curr. Opin. Colloid Interface Sci.* **1998**, *3*, 270–275. [CrossRef]
4. Acevedo, S.; Gutierrez, X.; Rivas, H. Bitumen-in-Water Emulsions Stabilized with Natural Surfactants. *J. Colloid Interface Sci.* **2001**, *242*, 230–238. [CrossRef]
5. Villalba, G.U.; Máximo, G.S. Effect of non-homogeneous spatial distributions of surfactants on the stability of high-content bitumen-in-water emulsions. *Interciencia* **2000**, *25*, 415–422.
6. Babchin, A.J.; Schramm, L.L. Osmotic repulsion force due to adsorbed surfactants. *Colloids Surf. B Biointerfaces* **2012**, *91*, 137–143. [CrossRef] [PubMed]
7. Ignatavicius, S.; Kavanagh, A.; Colleran, D.; Brennan, M.J.; Newell, S. Experimental investigation of optimum properties and conditions for use of anionic emulsions in road maintenance applications. In Proceedings of the Civil Engineering Research in Ireland 2020 (CERI 2020), Cork Institute of Technology, Cork, Ireland, 27–28 August 2020; ISBN 978-0-9573957-4-9. Available online: https://sword.cit.ie/monographs/1 (accessed on 6 April 2021).
8. Gingras, J.-P.; Tanguy, P.A.; Mariotti, S.; Chaverot, P. Effect of process parameters on bitumen emulsions. *Chem. Eng. Process. Process. Intensif.* **2005**, *44*, 979–986. [CrossRef]

9. Jair, M. Bitumen Emulsions. In *The Shell Bitumen Handbook*, 6th ed.; Hunter, R.N., Self, A., Read, J., Eds.; ICE Publishing: Westminster/London, UK, 2018; pp. 185–214.
10. International Bitumen Emulsion Federation Publication, Asphalt Emulsions: Beyond Pavement Preservation. Available online: http://www.ibef.net/download/1155/ (accessed on 6 November 2020).
11. Yuliestyan, A.; García-Morales, M.; Moreno, E.; Carrera, V.; Partal, P. Assessment of modified lignin cationic emulsifier for bitumen emulsions used in road paving. *Mater. Des.* **2017**, *131*, 242–251. [CrossRef]
12. Dołżycki, B.; Jaskuła, P. Review and evaluation of cold recycling with bitumen emulsion and cement for rehabilitation of old pavements. *J. Traffic Transp. Eng.* **2019**, *6*, 311–323. [CrossRef]
13. Day, D.; Lancaster, I.M.; McKay, D. Emulsion cold mix asphalt in the UK: A decade of site and laboratory experience. *J. Traffic Transp. Eng.* **2019**, *6*, 359–365. [CrossRef]
14. Ronald, M.; Pumarejo Luis, F. Asphalt emulsions formulation: State-of-the-art and dependency of formulation on emulsions properties. *Constr. Build. Mater.* **2016**, *123*, 162–173. [CrossRef]
15. Yan, Z.; Elliott, J.A.W.; Masliyah, J.H. Roles of Various Bitumen Components in the Stability of Water-in-Diluted-Bitumen Emulsions. *J. Colloid Interface Sci.* **1999**, *220*, 329–337. [CrossRef]
16. Abdelfatah, E.; Chen, Y.; Berton, P.; Rogers, R.D.; Bryant, S.L. Tuning Ionic Liquids for Simultaneous Dilution and Demulsification of Water-In-Bitumen Emulsions at Ambient Temperature. *SPE J.* **2020**, *25*, 759–770. [CrossRef]
17. Ziyani, L.; Gaudefroy, V.; Ferber, V.; Deneele, D.; Hammoum, F. Chemical reactivity of mineral aggregates in aqueous solution: Relationship with bitumen emulsion breaking. *J. Mater. Sci.* **2014**, *49*, 2465–2476. [CrossRef]
18. Rossi, O.; Caputo, P.; de Luca, G.; Maiuolo, L.; Eskandarsefat, S.; Sangiorgi, C. 1H-NMR Spectroscopy: A Possible Approach to Advanced Bitumen Characterization for Industrial and Paving Applications. *Appl. Sci.* **2018**, *8*, 229. [CrossRef]
19. Caputo, P.; Porto, M.; Calandra, P.; de Santo, M.P.; Rossi, C.O. Effect of epoxidized soybean oil on mechanical properties of bitumen and aged bitumen. *Mol. Cryst. Liq.* **2018**, *675*, 68–74. [CrossRef]
20. Gafonova, V.O.; Yarranton, H.W. The Stabilization of Water-in-Hydrocarbon Emulsionsby Asphaltenes and Resins. *J. Colloid Interface Sci.* **2001**, *241*, 469–478. [CrossRef]
21. Samieadel, A.; Fini, E.H. Interplay between wax and polyphosphoric acid and its effect on bitumen thermomechanical properties. *Constr Build Mater.* **2020**, *243*, 118194. [CrossRef]
22. Zieliński, K.; Babiak, M.; Ratajczak, M.; Kosno, J. Impact of chemical and physical modification on thermoplastic characteristics of bitumen. *Procedia Eng.* **2017**, *172*, 1297–1304. [CrossRef]
23. Xia, T.; Chen, X.; Xu, J.; Chen, W.; Zhang, A. Effect of annealing method and chemical reaction on the structure and properties of polyethylene/polyethylene glycol modified bitumen. *Constr. Build. Mater.* **2020**, *269*, 121228. [CrossRef]
24. Cuadri, A.A.; Partal, P.; Navarro, F.J.; García-Morales, M.; Gallegos, C. Bitumen chemical modification by thiourea dioxide. *Fuel* **2011**, *90*, 2294–2300. [CrossRef]
25. Porto, M.; Caputo, P.; Loise, V.; de Filpo, G.; Rossi, C.O.; Calandra, P. Polysaccharides-Reinforced Bitumens: Specificities and Universality of Rheological Behavior. *Appl. Sci.* **2019**, *9*, 5564. [CrossRef]
26. Caputo, P.; Porto, M.; Loise, V.; Teltayev, B.; Rossi, C.O. Analysis of mechanical performance of bitumen modified with waste plastic and rubber (SBR) additives by rheology and PGSE NMR experiments. *Eurasian Chem. Technol. J.* **2019**, *21*, 235–239. [CrossRef]
27. Sengoz, B.; Isikyakar, G. Evaluation of the properties and microstructure of SBS and EVA polymer modified bitumen. *Constr. Build. Mater.* **2008**, *22*, 1897–1905. [CrossRef]
28. Pérez-Lepe, A.; Martínez-Boza, F.J.; Gallegos, C.; González, O.; Muñoz, M.E.; Santamaría, A. Influence of the processing conditions on the rheological behaviour of polymer-modified bitumen. *Fuel* **2003**, *82*, 1339–1348. [CrossRef]
29. Edwards, Y. Influence of Waxes on Bitumen and Asphalt Concrete Mixture Performance. *Road Mater. Pavement Des.* **2009**, *10*, 313–335. [CrossRef]
30. Zhu, J.; Birgisson, B.; Kringos, N. Polymer modification of bitumen: Advances and challenges. *Eur. Polym. J.* **2014**, *54*, 18–38. [CrossRef]
31. Ren, S.; Liu, X.; Fan, W.; Wang, H.; Erkens, S. Rheological properties, compatibility, and storage stability of SBS latex-modified asphalt. *Materials* **2019**, *12*, 3683. [CrossRef]
32. Liang, M.; Sun, C.; Yao, Z.; Jiang, H.; Zhang, J.; Ren, S. Utilization of wax residue as compatibilizer for asphalt with ground tire rubber/recycled polyethylene blends. *Constr. Build. Mater.* **2020**, *230*, 116966. [CrossRef]
33. Lin, P.; Liu, X.; Apostolidis, P.; Erkens, S.; Ren, S.; Scarpas, S.X.T.; Huang, W. On the rejuvenator dosage optimization for aged SBS modified bitumen. *Constr. Build. Mater.* **2021**, *271*, 121913. [CrossRef]
34. Qin, Q.; Farrar, M.J.; Pauli, A.T.; Adams, J.J. Morphology, thermal analysis and rheology of Sasobit modified warm mix asphalt binders. *Fuel* **2014**, *115*, 416–425. [CrossRef]
35. Solouki, A.; Muniandy, R.; Hassim, S.; Kheradmand, B. Rheological Property Investigation of Various Sasobit-modified Bitumen. *Pet. Sci. Technol.* **2015**, *33*, 773–779. [CrossRef]
36. Yousefi, A.; Nowruzi, A.B.A.; Haghshenas, H. Performance evaluation of asphalt mixtures containing warm mix asphalt (WMA) additives and reclaimed asphalt pavement (RAP). *Constr. Build. Mater.* **2020**, *268*, 121200. [CrossRef]
37. Borrego, A.G.; Blanco, C.G.; Prado, J.G.; Díaz, C.; Guillén, M.D. 1H NMR and FTIR Spectroscopic Studies of Bitumen and Shale Oil from Selected Spanish Oil Shales. *Energy Fuel* **1996**, *10*, 77–84. [CrossRef]

38. Caputo, P.; Loise, V.; Ashimova, S.; Teltayev, B.; Vaiana, R.; Rossi, C.O. Inverse Laplace Transform (ILT)NMR: A powerful tool to differentiate a real rejuvenator and a softener of aged bitumen. *Colloids Surf. A* **2019**, *574*, 154–161. [CrossRef]
39. Rossi, C.O.; Caputo, P.; Loise, V.; Ashimova, S.; Teltayev, B.; Sangiorgi, C. A New Green Rejuvenator: Evaluation of Structural Changes of Aged and Recycled Bitumens by Means of Rheology and NMR. In *RILEM 252-CMB 2018, RILEM Bookseries 20*; Poulikakos, L.D., Falchetto, A.C., Wistuba, M., Hofko, B., Porot, L., Di Benedetto, H., Eds.; Springer: Berlin/Heidelberg, Germany, 2018; pp. 177–182.
40. Noda, A.; Susan, M.A.B.H.; Kudo, K.; Mitsushima, S.; Hayamizu, K.; Watanabe, M. Brønsted Acid−Base Ionic Liquids as Proton-Conducting Nonaqueous Electrolytes. *J. Phys. Chem. B* **2003**, *107*, 4024–4033. [CrossRef]
41. Uraguchi, D.; Terada, M. Chiral Brønsted Acid-Catalyzed Direct Mannich Reactions via Electrophilic Activation. *J. Am. Chem. Soc.* **2004**, *126*, 5356–5357. [CrossRef]
42. Wang, J.; Yang, F.; Tan, J.; Liu, G.; Xu, J.; Sun, D. Pickering Emulsions Stabilized by a Lipophilic Surfactant and Hydrophilic Platelike Particles. *Langmuir* **2010**, *26*, 5397–5404. [CrossRef]
43. Kiran, S.K.; Acosta, E.J.; Moran, K. Evaluating the hydrophilic-lipophilic nature of asphaltenic oils and naphthenic amphiphiles using microemulsion models. *J. Colloid Interface Sci.* **2009**, *336*, 304–313. [CrossRef]
44. Calandra, P.; Caputo, P.; de Santo, M.P.; Todaro, L.; Liveri, V.T.; Rossi, C.O. Effect of additives on the structural organization of asphaltene aggregates in bitumen. *Constr. Build. Mater.* **2019**, *119*, 288–297. [CrossRef]
45. Johansson, I.; Svensson, M. Surfactants based on fatty acids and other natural hydrophobes. *Curr. Opin. Colloid Interface Sci.* **2011**, *6*, 178–188. [CrossRef]
46. Holmberg, K. Natural surfactants. *Curr. Opin. Colloid Interface Sci.* **2001**, *6*, 148–159. [CrossRef]

# How Organic Waste Improves Bitumen's Characteristics

**P. Caputo[1], M. Porto[1]*, V. Loise[1]*, A. Abe[1], B. Teltayev[3], P. Calandra[2], C. Oliviero Rossi[1]**

[1]University of Calabria, Via P. Bucci, Cubo 14/D, Rende (CS), 87036, Italy & UdR INSTM della Calabria
[2]CNR-ISMN, National Research Council, Institute of Nanostructured Materials,
Via Salaria km 29.300, 00015, Monterotondo, Italy
[3]Kazakhstan Highway Research Institute Nurpeisova Str. 2a, Almaty 050061, Kazakhstan

**Article info**

*Received:*

*Received in revised form:*

*Accepted:*

**Abstract**

The organic fraction derived from the differentiated collection of urban waste is mainly composed of fatty acids, medium molecular weight hydrocarbons and cellulose. This peculiar composition gave us insight into the possible use of organic waste to improve bitumen's characteristics (possible antioxidant, regenerating and/or viscosifying additive for road pavements). The issue of the disposal of organic waste is a global one and it's constantly of increasing concern. This study looks to alleviate this problem by finding ways for this waste fraction to be utilized for the greater good- in this case, as an additive for bitumen binder in road pavements. The present study is focused on the use of waste as it is and waste treated by the FENTON process (treatment with ferrous sulphate and hydrogen peroxide solution). Dynamic Shear Rheology (DSR) and aging tests (Rolling Thin Film Oven Test, RTFOT) showed that two of the additives tested in this study proved effective: one can be utilised as a viscosifying agent and the other can be used as a filler.

## 1. Introduction

Waste management is a problem of growing concern globally and industrialization amongst other avenues of waste production has contributed significantly to the production of organic waste in recent years. This has led to waste management problems as conventional waste disposal methods are not eco-friendly and are mostly inefficient [1]. About a million tons of waste are produced globally every day and incineration which is arguably the most common conventional waste disposal method is known to produce over 200 different types of toxic compounds such as nitrous oxide, sulphuric acids, fluorides, hydrogen chloride [2, 3]. Research in recent years is drifting towards looking for sustainable ways such as reducing landfill usage to treat and manage the environmental impact brought about by waste products that are produced from human and industrial activities in the 21st century. This has facilitated the drift of research towards the development of green eco-friendly technologies to recycle waste thus creating a circular economy [4–10].

In the road pavement sector, bitumen is used as the binder for preparing asphalt conglomerate. More often than not, conventional bitumen does not have all the performance requirements for road pavement construction. These roads, depending on the geographical location, are increasingly subjected to conditions such as heavy traffic, harsh climatic conditions, oxidation and heavy loads. If the bituminous mixture obtained does not meet these performance requirements, the bitumen binder needs to be modified with additives to improve its performance thereby improving the performance of the asphalt conglomerate as a whole [11–13]. Most additives on the market are not eco-friendly and research in this field keeps looking for more eco-friendly and sustainable ways to improve asphalt performance. Bitumen is a viscoelastic complex mixture of organic compounds derived from the heavy petroleum fractionation process in the refinery. It is a

*Corresponding author.
E-mail: michele.porto@unical.it

© 2021 Eurasian Chemico-Technological Journal.
This is an open access article under the CC BY license (http://creativecommons.org/licenses/by/4.0/).

substance used to bind inorganic conglomerates in road pavement preparation. This binder is mixed with the aggregates at high temperatures, and the presence of oxygen causes the bitumen to undergo strong oxidation which is a detrimental process reducing its mechanical characteristics.

In order to limit oxidation, specific additives are added to the bitumen before the mixing process. On the market, there are no eco-friendly additives [14, 15] and so recent attention is being paid to ecological additives with high performance in order to reduce the oxidation process [16–18].

Since further oxidation can take place also after paving in a slower process called ageing which also involves loss of more volatile components and structural aggregations [19], the same problem holds also for longer times. For this, additives, usually based on strong acids or bases, are present on the market [20–22], but eco-friendly additives are recently being studied [23–28].

The idea to use eco-friendly substances can be extended to eco-friendly processes such as the recycling of aged road pavements (the so-called Recycled Asphalt Pavement – RAP) to be partially reused in new road pavements while maintaining the performance and duration of the latter over time [29–31]. Also in this case, specific (regenerating) additives, generally based on amines, surfactants, oils, etc. are used [32–34].

To make the whole cycle entirely eco-friendly, research in recent years has focused on the use of recycled material from wastes to create new environmentally friendly additives for improving road pavement characteristics, with obvious advantages in terms of environment protection and safeguarding of human health [35–37].

Furthermore, the problem of the disposal of organic waste exists all over the world and so the purpose of this work is to identify possible reuse of this type of waste as an additive for road pavements in accordance with a circular economy facilitated by circular chemistry practices which are constantly gaining widespread acceptance in the industrial research sector [38–41]. One major limiting factor of organic waste is that there is never a homogeneous composition. This composition changes according to the nation, the geographical area, the number of inhabitants, ethnic culture, etc. To further improve the quality of the waste, it was chemically pre-treated (FENTON process) in the laboratory. On the final samples, rheological measurements were performed and to evaluate the performance of the additives as an antioxidant, the aging process in the plant was simulated in the laboratory using Rolling Thin Film Oven Test.

## 2. Experimental part

Waste was obtained in the ambit of the project "RESIFAC" (realization and experimentation of pilot plants for fast composting of civil and industrial organic waste). In the present study our attention is focused on the organic fraction of municipal solid waste, which includes food residues or food preparations and assimilable fractions, and which constitutes more than 30% of the total weight of municipal solid waste. Such residues were collected through a sampling procedure lasting 12 days. On each of these days, waste was taken from a group of four different families, each day a different one. The waste collected on each sampling day (about 5 kg) was mixed and milled to a millimeter size by means of a steel blender. The resulting minced material was stored at -20 °C for 12 days. After this time, all the daily rates were defrosted and mixed; the material obtained was divided into bags of 200 g, re-frozen and then used after heat treatment at 110 °C. This was the starting matrix for the oxidative treatment. The oxidation reaction [42] was carried out using a laboratory-scale glass reactor apparatus. The compounds which are mainly oxidized by Fenton reagent are aromatic and aliphatic hydrocarbons. The details are reported in the work by Salvino et al. [43] which gives details on the whole oxidation process. The sample of organic material, 200 g, was placed into the glass reactor and the Fenton reagents were added: 10 mL of a $FeSO_4$ solution followed by the addition of 10 mL of hydrogen peroxide ($H_2O_2$) solution. The mixture was kept under stirring conditions, the reactor was placed in a water bath, and the internal temperature was kept at 60 °C for the duration of the reaction. The pH of the mixture, initially at 4.5, changed to 3.0 during the reaction. The samples used were collected during the phases of oxidation procedure and were differentiated according to the different percentages of $H_2O_2/FeSO_4$ used [43]. Six samples were prepared at different concentrations of $FeSO_4$ and $H_2O_2$ as shown in Table 1. Sample 1 is the reference sample and was not treated with either $FeSO_4$ or $H_2O_2$. Samples 2, 3 and 4 had the same percentage of $FeSO_4$, 0.05%wt, but different concentrations of $H_2O_2$, i.e., 0.002%wt, 0.015%wt, and 0.02%wt respectively while for samples 5 and 6, $FeSO_4$ was added in the percentage of 0.04% and 0.03% respectively and the $H_2O_2$ percentage was constant at 0.002%.

**Table 1**
Different percentages of $H_2O_2$ and $FeSO_4$ used for treating the waste samples in FENTON process

| Sample | % $FeSO_4$ | % $H_2O_2$ |
|---|---|---|
| CD1 | / | / |
| CD2 | 0.05 | 0.002 |
| CD3 | 0.05 | 0.015 |
| CD4 | 0.05 | 0.02 |
| CD5 | 0.04 | 0.002 |
| CD6 | 0.03 | 0.002 |

Dynamic rheological analysis, including viscosity measurements (steady state), Time cure and Frequency Sweep experiments, were recorded from room temperature up to 120 °C.

All rheological measurements were carried out using an SR5000 rheometer (Rheometrics, Piscataway, NJ, USA) controlled by shear stress and equipped with plate geometry (2 mm gap, 25 mm diameter).

## 3. Results and discussion

Bitumen with a penetration grade of 50/70 was used and this bitumen was aged by means of standardized oxidative processes Rolling thin film ovens (RTFOT) according to the EN 12607-1 standard [44]. This was done in order to create an "aged" reference to be treated with the additives

Both additives were added to the aged bitumen at a dosage of 2% by weight of the binder [45, 46]. This percentage was used because it appears to be the one commonly used for the regenerating additives available on the market. The resulting samples were analysed by dynamic and stationary rheological measurements to understand the effects on the mechanical properties and also on the structural and morphological variations induced by the single additives on the bitumen itself.

### *3.1. Viscosity tests*

The rheological analysis was done more thoroughly by recording the mechanical spectra.

To study the effect of the various additives on the rheological behaviour of bitumens, viscosity measurements were carried out at different temperatures for all the samples. Figure 2 shows the viscosity values for the various samples at the temperatures of 60, 80, 100, 120 °C. First of all, it must be noted that the general sharp decreasing of the viscosity with temperature is expected. This is the consequence of the disordering effect of temperature in soft matter since the thermal motion can easily loosen the bonds hold up by weaker interaction, which are quite common in soft matter and complex systems. As it can be seen, the only sample that brings a significant increase in viscosity and consequently shows good capabilities as a viscosifier is the CD2 sample. Its values appear to be higher while all the other samples show small variations with respect to the reference systems. It worthy to note that this speculation is valid at different temperatures (60, 80, 100, 120 °C).

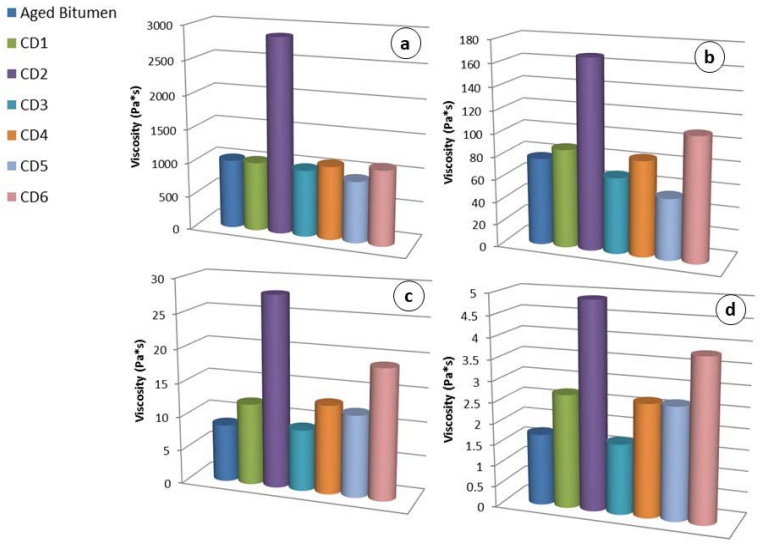


Fig. 1. Viscosity (steady state) of all the samples at different temperatures: a) 60 °C, b) 80 °C, c) 100 °C and d)120 °C.

As a consequence of this finding, CD 2 will be selected as the representative of all the FENTON-treated samples in the other tests.

We can try to give an interpretation of why the relative influence of the different additives does changes with temperature. We think that the lower amount of hydrogen peroxide in CD2 sample can guarantee disruption of bigger molecules (fat, proteins) into small components (fatty acids, peptides, alcohols) which are responsible for the observed behaviour (see for example the effect of polysaccharides [25]) preserving their integrity without further molecular fragmentations. Further oxidation would further deteriorate the organic waste to smaller chemical species with no action in the bitumen structure. Of course, due to the heterogeneities of the organic materials involved, the reaction pattern is complex with many chemical species involved, and this justifies why the relative influence of the different additives change with temperature.

### *3.2. Anti-aging tests*

The effect of an anti-aging agent is evaluated by observing the plastic-fluid transition temperature as probed by rheometry [47–50]. Upon increasing temperature, G' monotonously decreases, but at a certain temperature it suddenly drops. This is the temperature at which the binder can be considered almost as a Newtonian fluid, so from the microscopic point of view, it can be intended as the temperature at which the thermal motion is sufficiently high to destroy the whole structure and therefore no storage of energy can be afforded by the sample.

Now, aging generally causes an increase in the transition temperature due to the oxidation of components; an additive must limit this phenomenon, maintaining the transition temperature, after aging, very similar to that of non-aged bitumen.

From Table 2, it can be seen that the organic waste did not bring any significant improvement compared to the starting bitumen leaving the transition temperature almost unchanged. The additive obtained from FENTON treated organic waste, CD2, at the same concentration 2% demonstrated a stricter interaction with bitumen, increasing the transition temperature of the unaged bitumen as well as the aged bitumen. However, the increase in the transition temperature when passing from unaged to aged bitumen (about 6 °C) is about of the same magnitude as in the case of non-additivated bitumen and the CD1- additivated bitumen (4 °C).

**Table 2**
Transition temperatures (in °C) for unaged and aged bitumens with and without CD1 and CD2

| Additive | Unaged | Aged bitumen |
|---|---|---|
| --- | 74.2 | 78.3 |
| CD1 2% | 74.3 | 78.6 |
| CD2 2% | 78.3 | 84.2 |

The tests were carried out using RT-FOT for 75 min due to the fact that road pavement administration agencies (such as ANAS in Italy, NCAT and NAPA in U.S.A., AIA in U.K., etc.) recommend that the difference between unaged bitumen and bitumen aged with RT-FOT be monitored closely and so there would have been no need to age the bitumen for 225 min with RT-FOT [51]. The test highlights that no anti-aging effect has been revealed but CD2 can be used to increase the resistance of bitumen to temperature.

### *3.3. Regeneration Tests*

Regenerating agents are additives to be added to recycled asphalt (RAP), allowing its reuse in the production of new road pavements with a partial recovery of the pristine characteristics. To evaluate this effect, a 50/70 bitumen was aged by RTFOT for 225 min, and then 2% of CD1 or CD2 was added to the bitumen under stirring at 150 °C and left to mix for 15 min.

Time cure tests were carried out on these samples and the pseudoplastic-to-fluid transition temperatures were recorded. They are shown in Table 3.

Table 3 shows that the addition of CD1 or CD2 at 2% brings no regeneration to the oxidized bitumen since their addition does not bring the transition temperature value of the aged bitumen closer to the value of the pristine bitumen (74.2 °C).

**Table 3**
Transition temperatures for unaged and aged bitumens

| Sample | Transition temperature (±0.5 °C) Bitumen 50/70 |
|---|---|
| Bitumen 50/70 | 74.2 |
| Bitumen 50/70 RTFOT 225 | 85.5 |
| Bitumen 50/70 RTFOT 225 +2% CD1 | 85.0 |
| Bitumen 50/70 RTFOT 225 +2% CD2 | 90.0 |

### *3.4. Frequency sweep tests*

To understand whether the added compounds are engaged in effective interactions with the components of the bitumen thus stabilizing or destabilizing the supramolecular network, frequency sweep tests have been made and analyzed in the framework of the colloidal gel model.

According to the theory of Bohlin [52] and Winter [53], widely reported in literature as the "weak-gel model" [54], which can be applied in the context of the study of viscoelastic materials like bitumen [55], the material is characterized by a cooperative arrangement of flow units connected by weak physical interactions that cooperatively ensure the stability of the structure. This model matches also the complex inter-molecular structure typical of bitumen, where molecules are arranged together to form assemblies at various levels of aggregation and complexity [56], which are held up by weak interactions. In this model, the number of flow units interacting with each other to give the observed flow response z, can be derived by the use of the following equation:

$$|G^*(\omega)| = \sqrt{G'(\omega)^2 + G''(\omega)^2} = A\omega^{\frac{1}{z}}$$

where A is a proper constant related to the overall stiffness or resistance to deformation of the material within the linear viscoelastic region at an angular frequency of 1 rad/s, and G' and G'' are the real and imaginary parts of complex modulus (G*) which are derived by rheological measurements. G' represents the elastic response of the material (storage of energy) under oscillation, and G'' represents the inelastic contribution (dissipation of energy) during the same deformation.

In few words, A represents the force of interaction between the rheological units and z the coordination number, i.e. the number of rheological units interacting with a reference unit.

The derived values, calculated from the non-linear fitting of viscoelastic data to equation, are reported in Fig. 2. The figure shows a higher impact of CD2 on both A and z parameters, which confirms its more effective interactions with the structure of the bitumen.

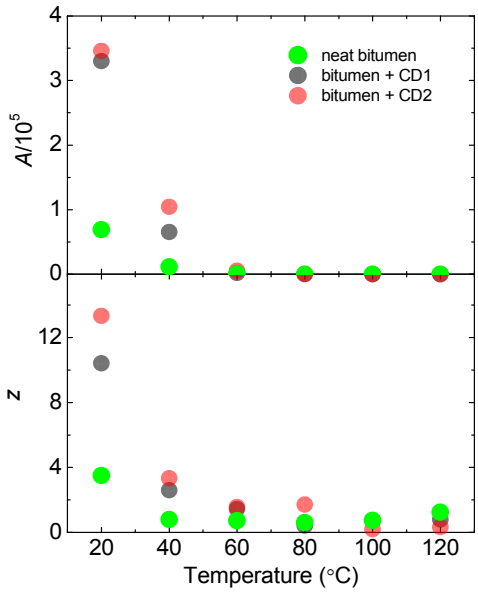


Fig. 2. A and z values as derived through equation for the neat bitumen, and that additivated by CD1 and CD2. The uncertainty associated to the values is of the same order of the symbol size.

## 4. Conclusions

Organic waste materials can be used in bitumen and asphalt concrete production with great benefits, providing better asphalt pavements and helping to develop proper and efficient waste management technology. The present study was prompted by the need of safeguarding the environment through a circular, eco-friendly and sustainable economy. We showed, by rheology, bare organic waste cannot be used as an anti-aging additive or as a regenerator of "aged" bitumen but could be used, instead, as a possible filler in bituminous conglomerates since it does not modify its characteristics/performance. We also showed that the FENTON-treated waste with low amounts of hydrogen peroxide can be used very suitable as a viscosifying agent, with a high capability of interacting with the complex structure of the bitumen.

FENTON-treated waste with high amounts of hydrogen peroxide can be used, instead, as filler in bituminous conglomerates, like the un-treated waste. These effects can be used for industrial applications for which further studies are needed to quantify the scaling-up convenience.

## Acknowledgments

The Authors acknowledge financial support from the Italian Ministero dello Sviluppo Economico (MISE), through the Project "RESIFAC": Realization and experimentation of pilot plants for fast composting of civil and industrial organic waste (Project No. CUP: B28I17000070008, "Horizon 2020" – PON I&C 2014-2020).

## References


[1]. M. Batayneh, I. Marie, I. Asi, *Waste Manage.* 27 (2007) 1870–1876. DOI: 10.1016/j.wasman.2006.07.026

[2]. J. Bolden, T. Abu-Lebdeh, E. Fini, *Am. J. Environ. Sci.* 9 (2013) 14–24. DOI: 10.3844/ajessp.2013.14.24

[3]. M.T. Rahman, A. Mohajerani, F. Giustozzi, *Materials* 13 (2020) 1495. DOI: 10.3390/ma13071495

[4]. C. Oliviero Rossi, P. Caputo, V. Loise, D. Miriello, B. Teltayev, R. Angelico, *Colloid. Surface. A* 532 (2017) 618–624. DOI: 10.1016/j.colsurfa.2017.01.025

[5]. R. Cremiato, M.L. Mastellone, C. Tagliaferri, L. Zaccariello, P. Lettieri, *Renew. Energ.* 124 (2018) 180–188. DOI: 10.1016/j.renene.2017.06.033

[6]. T. Kuhlman, J. Farrington, *Sustainability* 2 (2010) 3436–3448. DOI: 10.3390/su2113436

[7]. M.M.A. Aziz, M.T. Rahman, M.R. Hainin, W.A. Bakar WA, Constr. Build. Mater. 84 (2015) 315–319. DOI: 10.1016/j.conbuildmat.2015.03.068

[8]. T. Abu-Lebdeh, S. Hamoush, W. Heard, B. Zornig, *Constr. Build. Mater.* 25 (2011) 39–46. DOI: 10.1016/j.conbuildmat.2010.06.059

[9]. M.N. James, W. Choi, T. Abu-Lebdeh, *Am. J. Eng. Appl. Sci* 4 (2011) 201–208. DOI: 10.3844/ajeassp.2011.201.208

[10]. S. Hamoush, T. Abu-Lebdeh, M. Picornell, S. Amer, *Constr. Build. Mater.* 25 (2011) 4006–4016. DOI: 10.1016/j.conbuildmat.2011.04.035

[11]. G. King, H. King, R. Pavlvoich, A. Epps, P. Kandhal, Additives in asphalt, AAPT, 68A (1986) 32–69.

[12]. Y. Xue, H. Hou, S. Zhu, J. Zha, *Constr. Build. Mater.* 23 (2009) 989–996. DOI: 10.1016/j.conbuildmat.2008.05.009

[13]. N.S. Mashaan, A. Rezagholilou, H. Nikraz, A. Chegenizadeh, *International Journal of Advances in Science, Engineering and Technology* 7 (2019) 58–60.

[14]. R. Tauste, F. Moreno-Navarro, M. Sol-Sánchez, M.C. Rubio-Gámez, *Constr. Build. Mater.* 192 (2018) 593–609. DOI: 10.1016/j.conbuildmat.2018.10.169

[15]. O. Sirin, D.K. Paul, E. Kassem, *Adv. Civil Eng.* 2018, Article ID 3428961. DOI: 10.1155/2018/3428961

[16]. I. Gawel, F. Czechowski, J. Kosno, *Constr. Build. Mater.* 110 (2016) 42–47. DOI: 10.1016/j.conbuildmat.2016.02.004

[17]. M.H. Nahi, I.B. Kamaruddin, N. Madzlan, *Appl. Mech. Mater.* 567 (2014) 539–544. DOI: 10.4028/www.scientific.net/amm.567.539

[18]. C. Oliviero Rossi, P. Caputo, S. Ashimova, G. D'Errico, R. Angelico, *Appl. Sci.* 8 (2018) 1405. DOI: 10.3390/app8081405

[19]. J. Claine Petersen, *Developments in Petroleum Science* 40 (2000) 363–399. DOI: 10.1016/S0376-7361(09)70285-7

[20]. A. Behnood, J. Olek, *Constr. Build. Mater.* 157 (2017) 635–646. DOI: 10.1016/j.conbuildmat.2017.09.138

[21]. R. Ghabchi, S. Rani, M. Zaman, S. Ashik Ali, *Int. J. Pavement Eng.* 22 (2021) 418–431. DOI: 10.1080/10298436.2019.1614584

[22]. A. Bocoum, S. Hosseinnezhad, E.H. Fini. Investigating effect of amine based additives on asphalt rubber rheological properties. In Asphalt Pavements – Proceedings of the International Conference on Asphalt Pavements, ISAP 2014 (pp. 921–931). (Asphalt Pavements – Proceedings of the International Conference on Asphalt Pavements, ISAP 2014; Vol. 1). DOI: 10.1201/b17219-113

[23]. C.O. Rossi, P. Caputo, V. Loise, S. Ashimova, B. Teltayev, C. Sangiorgi (2019) A New Green Rejuvenator: Evaluation of Structural Changes of Aged and Recycled Bitumens by Means of Rheology and NMR. In: Poulikakos L., Cannone Falchetto A., Wistuba M., Hofko B., Porot L., Di Benedetto H. (eds) RILEM 252-CMB Symposium, 2018. RILEM Bookseries, vol 20. Springer, Cham. DOI: 10.1007/978-3-030-00476-7_28

[24]. A.A. Abe, C. Oliviero Rossi, P. Caputo, M. P. De Santo, N. Godbert, I. Aiello, *Materials* 14 (2021) 1622. DOI: 10.3390/ma14071622

[25]. M. Porto, P. Caputo, V. Loise, G. De Filpo, C. Oliviero Rossi, P. Calandra, *Appl. Sci.* 9 (2019) 5564. DOI: 10.3390/app9245564

[26]. J.B. Król, K.J. Kowalski, Ł. Niczke, P. Radziszewski, *Constr. Build. Mater.* 114 (2016) 194–203. DOI: 10.1016/j.conbuildmat.2016.03.086

[27]. Y. Cheng, W. Wang, Y. Gong, S. Wang, S. Yang, X. Sun, *Materials* 11 (2018) 2488. DOI: 10.3390/ma11122488

[28]. P. Caputo, M. Porto, P. Calandra, M.P. De Santo, C. Oliviero Rossi, *Mol. Cryst. Liq. Cryst.* 675 (2018) 68–74. DOI: 10.1080/15421406.2019.1606979

[29]. P. Caputo, V. Loise, A. Crispini, C. Sangiorgi, F. Scarpelli, C. Oliviero Rossi, *Colloid. Surface. A* 571 (2019) 50–54. DOI: 10.1016/j.colsurfa.2019.03.059

[30]. V. Loise, P. Caputo, M. Porto, P. Calandra, R. Angelico, C. Oliviero Rossi, *Appl. Sci.* 9 (2019) 4316. DOI: 10.3390/app9204316

[31]. L. Noferinia, A. Simone, C. Sangiorgi, F. Mazzotta, *Int. J. Pavement Res. Technol.* 10 (2017) 322–332. DOI: 10.1016/j.ijprt.2017.03.011

[32]. W. Huang, Y. Guo, Y. Zheng, Q. Ding, C.

Sun, J. Yu, M. Zhu, H. Yu, *Constr. Build. Mater.* 273 (2021) 121525. DOI: 10.1016/j.conbuildmat.2020.121525
[33]. F.J. Ortega, F.J. Navarro, M. Jasso, L. Zanzotto, *Constr. Build. Mater.* 222 (2019) 766–775. DOI: 10.1016/j.conbuildmat.2019.06.117
[34]. G. Pipintakos, H.Y. Vincent Ching, H. Soenen, P. Sjövall, U. Mühlich, S. Van Doorslaer, A. Varveri, W. Van den bergh, X. Lu, *Constr. Build. Mater.* 260 (2020) 119702. DOI: 10.1016/j.conbuildmat.2020.119702
[35]. P. Caputo, M. Porto, V. Loise, B. Teltayev, C. Oliviero Rossi, *Eurasian Chem.-Technol.* J. 21 (2019) 235–239. DOI: 10.18321/ectj864
[36]. J. Baena-González, A. Santamaria-Echart, J.L. Aguirre, S. González, *Waste Manage*. 118 (2020) 139–149. DOI: 10.1016/j.wasman.2020.08.035
[37]. A. Sreeram, Z. Leng, R. K. Padhan, X. Qu, *HKIE Transactions* 25 (2018) 237–247. DOI: 10.1080/1023697X.2018.1534617
[38]. J. Zhu, C. Fan, H. Shi, L. Shi, *J. Ind. Ecol.* 23 (2018) 110–118. DOI: 10.1111/jiec.12754
[39]. Di Maria F. (2020) Circular Economy in Italy. In: Ghosh S. (eds) Circular Economy: Global Perspective. Springer, Singapore. DOI: 10.1007/978-981-15-1052-6_11
[40]. M. Robaina, J. Villar, E.T. Pereira, *Environ. Sci. Pollut. Res.* 27 (2020) 12566–12578. DOI: 10.1007/s11356-020-07847-9
[41]. G. Lonca, P. Lesage, G. Majeau-Bettez, S. Bernard, M. Margni, *Resour. Conserv. Recy.* 162 (2020) 105013. DOI: 10.1016/j.resconrec.2020.105013
[42]. W. Koppenol, *Free Radical Bio. Med.* 15 (1993) 645–651. DOI: 10.1016/0891-5849(93)90168-T
[43]. R.A. Salvino, G. Celebre, G. De Luca, *Appl. Sci.* 11 (2021) 2267. DOI: 10.3390/app11052267
[44]. B. Hofko, A. Cannone Falchetto, J. Grenfell, L. Huber, X. Lu, L. Porot, L.D. Poulikakos, Z. You, *RoadMater. PavementDesign* 18 (2017) 108–117. DOI: 10.1080/14680629.2017.1304268
[45]. A. Ongel, M. Hugener, *Constr. Build. Mater* 94 (2015) 467–474. DOI: 10.1016/j.conbuildmat.2015.07.030
[46]. A. Grilli, M. Iorio Gnisci, M. Bocci, *Constr. Build. Mater* 136 (2017) 474–481. DOI: 10.1016/j.conbuildmat.2017.01.027
[47]. S. Ren, X. Liu, H. Wang, W. Fan, S. Erkens, J. *Clean. Prod.* 253 (2020) 120048. DOI: 10.1016/j.jclepro.2020.120048
[48]. J. Tang, C. Zhu, H. Zhang, G. Xu, F. Xiao, S. Amirkhanian, *Constr. Build. Mater* 194 (2019) 238–246. DOI: 10.1016/j.conbuildmat.2018.11.028
[49]. D. Zhang, Z. Chen, H. Zhang, C. Wei, *Constr. Build. Mater* 188 (2018) 409–416. DOI: 10.1016/j.conbuildmat.2018.08.136
[50]. N. Liu, K. Yan, L. You, M. Chen, *Constr. Build. Mater* 189 (2018) 460–469. DOI: 10.1016/j.conbuildmat.2018.08.206
[51]. ANAS. Special Tender Specification. In Road Paving; Technical Standard 2009.
[52]. L. Bohlin, *J. Colloid Interf. Sci.* 74 (1980) 423–434. DOI: 10.1016/0021-9797(80)90211-8
[53]. H.H. Winter, *Polym. Eng. Sci.* 27 (1987) 1698–1702. DOI: 10.1002/pen.760272209
[54]. D. Gabriele, B. de Cindio, P.A. D'Antona, *Rheol. Acta* 40 (2001) 120–127. DOI: 10.1007/s003970000139
[55]. C. Oliviero Rossi, S. Ashimova, P. Calandra, M.P. De Santo, R. Angelico, *Appl. Sci.* 7 (2017) 779. DOI: 10.3390/app7080779
[56]. P. Calandra, P. Caputo, M.P. De Santo, L. Todaro, V. Turco Liveri, C. Oliviero Rossi, *Constr. Build. Mater* 199 (2019) 288–297. DOI: 10.1016/j.conbuildmat.2018.11.277

La borsa di dottorato è stata cofinanziata con risorse del
Programma Operativo Nazionale Ricerca e Innovazione 2014-2020 (CCI 2014IT16M2OP005),
Fondo Sociale Europeo, Azione I.1 “Dottorati Innovativi con caratterizzazione Industriale”

UNIONE EUROPEA
Fondo Sociale Europeo